

# HANDBOOK OF FUNCTIONALIZED NANOMATERIALS FOR INDUSTRIAL APPLICATIONS

Edited by  
Chaudhery Mustansar Hussain



Micro & Nano Technologies Series

# **Handbook of Functionalized Nanomaterials for Industrial Applications**

This page intentionally left blank

# Handbook of Functionalized Nanomaterials for Industrial Applications

---

Edited by

**Chaudhery Mustansar Hussain**

Department of Chemistry and EVSC, New Jersey  
Institute of Technology, Newark, NJ, United States





Elsevier

Radarweg 29, PO Box 211, 1000 AE Amsterdam, Netherlands  
The Boulevard, Langford Lane, Kidlington, Oxford OX5 1GB, United Kingdom  
50 Hampshire Street, 5th Floor, Cambridge, MA 02139, United States

Copyright © 2020 Elsevier Inc. All rights reserved.

No part of this publication may be reproduced or transmitted in any form or by any means, electronic or mechanical, including photocopying, recording, or any information storage and retrieval system, without permission in writing from the publisher. Details on how to seek permission, further information about the Publisher's permissions policies and our arrangements with organizations such as the Copyright Clearance Center and the Copyright Licensing Agency, can be found at our website: [www.elsevier.com/permissions](http://www.elsevier.com/permissions).

This book and the individual contributions contained in it are protected under copyright by the Publisher (other than as may be noted herein).

### Notices

Knowledge and best practice in this field are constantly changing. As new research and experience broaden our understanding, changes in research methods, professional practices, or medical treatment may become necessary.

Practitioners and researchers must always rely on their own experience and knowledge in evaluating and using any information, methods, compounds, or experiments described herein. In using such information or methods they should be mindful of their own safety and the safety of others, including parties for whom they have a professional responsibility.

To the fullest extent of the law, neither the Publisher nor the authors, contributors, or editors, assume any liability for any injury and/or damage to persons or property as a matter of products liability, negligence or otherwise, or from any use or operation of any methods, products, instructions, or ideas contained in the material herein.

### British Library Cataloguing-in-Publication Data

A catalogue record for this book is available from the British Library

### Library of Congress Cataloging-in-Publication Data

A catalog record for this book is available from the Library of Congress

ISBN: 978-0-12-816787-8

For Information on all Elsevier publications  
visit our website at <https://www.elsevier.com/books-and-journals>

*Publisher:* Matthew Deans

*Acquisitions Editor:* Simon Holt

*Editorial Project Manager:* Isabella C. Silva

*Production Project Manager:* R. Vijay Bharath

*Cover Designer:* Matthew Limbert

Typeset by MPS Limited, Chennai, India



Working together  
to grow libraries in  
developing countries

[www.elsevier.com](http://www.elsevier.com) • [www.bookaid.org](http://www.bookaid.org)

# Contents

List of contributors	xvii
Preface	xxv

## Section 1

### Different kinds of functionalized nanomaterial for industrial use nanomaterials

1. Functionalization of nanomaterials for industrial applications: recent and future perspectives	3
<i>Sukanchan Palit and Chaudhery Mustansar Hussain</i>	
1.1 Introduction	3
1.2 Nanotrends in industrial development	4
1.3 Potential of nanomaterials	4
1.4 What are functionalized nanomaterials?	4
1.5 The use of functionalized nanomaterials in industry	5
1.6 Current research on nanomaterials	6
1.7 Recent scientific research in the field of functionalized nanomaterials	8
1.8 The scientific vision of energy and environmental sustainability	11
1.9 Recent research in environmental protection and industrial ecology	11
1.10 Integrated water resource management and human factor engineering	11
1.11 Groundwater remediation and nanotechnology	12
1.12 Future research trends in nanotechnology and nanomaterials	12
1.13 Conclusion and future perspectives	12
References	12
Further reading	14
2. Mixed-matrix membranes incorporated with functionalized nanomaterials for water applications	15
<i>Woon-Chan Chong, Chai-Hoon Koo and Woei-Jye Lau</i>	
2.1 Introduction	15
2.2 Mixed-matrix membranes incorporated with carbon-based nanomaterials	16

2.3	Mixed-matrix membranes incorporated with titania-based nanomaterials	26
2.4	Mixed-matrix membranes incorporated with other nanomaterials	33
2.5	Adsorptive mixed-matrix membranes for heavy-metal removal	40
2.6	Conclusion and future remarks	47
	References	47

## Section 2

### Functionalized nanomaterial for catalysis industry

3.	Photocatalytic oxygen evolution reaction for energy conversion and storage of functional nanomaterials	55
	<i>K. Kaviyarasu, C. Maria Magdalane, A. Raja, N. Matinise, N. Mayedwa, N. Mongwaketsi, Douglas Letsholathebe, G.T. Mola, Naif Abdullah Al-Dhabi, Mariadhas Valan Arasu, G. Ramalingam, S.B. Mohamed, Abdulgalim B. Isaev, K. Kanimozhi, A.K.H. Bashir, J. Kennedy and M. Maaza</i>	
3.1	Introduction	55
3.2	Conclusion	78
	References	78
4.	Functionalized metal-based nanoelectrocatalysts for water splitting	83
	<i>R.M.P.I. Rajakaruna and I.R. Ariyaratna</i>	
4.1	Introduction	83
4.2	Functionalized nanoelectrocatalysts for HER	88
4.3	OER catalysts	92
4.4	Bifunctional electrocatalysts	96
4.5	Summary	100
	References	102
5.	Functionalized nanographene for catalysis	111
	<i>Santosh Bahadur Singh and Chaudhery Mustansar Hussain</i>	
5.1	Nanographene: an introduction	111
5.2	Functionalization of nanographene	114
5.3	Catalytic properties and applications of functionalized nanographene	114
5.4	Industrial, environmental, and health issues of nanographene	119
5.5	Conclusions and future aspects	124
	References	125

## Section 3

**Functionalized nanomaterials for biomedical, pharmaceutical, agriculture, and agri-food industry**  
**Section Functionalized nanomaterial and biology**

<b>6. Delivery of bioactives using biocompatible nanodelivery technologies</b>	<b>133</b>
<i>H. Turasan and J.L. Kokini</i>	
6.1 Introduction	133
6.2 Fabrication methods of biopolymer-based nanodelivery systems	134
6.3 Conclusions	162
References	163
 <b>7. Biopolymer-based nanomaterials for food, nutrition, and healthcare sectors: an overview on their properties, functions, and applications</b>	 <b>167</b>
<i>Mohammad Reza Kasaa</i>	
7.1 Introduction	167
7.2 Sources, structure, and characteristics	168
7.3 Preparation of biopolymer-based nanomaterials	173
7.4 Applications of biopolymer-based nanomaterials	173
7.5 Conclusions	177
7.6 Future perspectives	178
Funding	178
Conflict of interests	178
References	178
Further reading	184
 <b>8. Surface functionalization of PLGA nanoparticles for drug delivery</b>	 <b>185</b>
<i>Joana A.D. Sequeira, Irina Pereira, António J. Ribeiro, Francisco Veiga and Ana Cláudia Santos</i>	
8.1 Introduction: background and driving forces	185
8.2 Active targeting by surface functionalization of PLGA nanoparticles	188
8.3 Noncovalent functionalization of PLGA nanoparticles	189
8.4 Nucleic acid-functionalized PLGA	195
8.5 Concluding remarks	200
Acknowledgements	200
References	200

<b>9. Biomedical-related applications of functionalized nanomaterials</b>	205
<i>Mafalda R. Almeida, Márcia C. Neves, Sergio Morales-Torres, Mara G. Freire, Joaquim L. Faria, Valéria C. Santos-Ebinuma, Cláudia G. Silva and Ana P.M. Tavares</i>	
9.1 Introduction	205
9.2 Functionalized nanoparticles in the biopharmaceutical sector	206
9.3 Types and synthesis procedures of functionalized nanomaterials	208
9.4 Immobilization of functionalized nanomaterials in membranes	217
9.5 Functionalized nanoparticles as drug delivery systems	220
9.6 Conclusions and future trends	221
Acknowledgments	223
References	224
<b>10. Functionalized nanomaterials for biomedical and agriculture industries</b>	231
<i>P. Chandra Kanth, Sandeep Kumar Verma and Nidhi Gour</i>	
10.1 Introduction	231
10.2 Strategies for functionalization of nanomaterials	232
10.3 Functionalized nanomaterials for biomedical and pharmaceutical applications	236
10.4 Application of functionalized nanomaterials in agriculture and agroindustry	248
10.5 Conclusion	252
References	253
Further reading	264
 <b>Section 4</b>	
<b>Functionalized Nanomaterials for Electronics, Electrical and Energy Industry</b>	
<b>11. Functionalized nanomaterials for electronics and electrical and energy industries</b>	269
<i>Shrabani De and Rashmi Madhuri</i>	
11.1 Introduction	269
11.2 Industrial applications	278
11.3 Conclusion	291
Author declaration	291
References	291

## Section 5

**Functionalized nanomaterial in environmental industry**

<b>12. Functionalization of graphene oxide with metal oxide nanomaterials: synthesis and applications for the removal of inorganic, toxic, environmental pollutants from water</b>	299
<i>Shraban Ku Sahoo and G. Hota</i>	
12.1 Introduction	299
12.2 Preparation of metal oxides functionalized GO nanocomposites	302
12.3 Removal of inorganic pollutants from water using metal oxide-functionalized GO—nanosubstrates	311
12.4 Conclusions	321
References	321
 <b>13. Remediation of organic pollutants by potential functionalized nanomaterials</b>	327
<i>Manviri Rani and Uma Shanker</i>	
13.1 Introduction	327
13.2 Environmental concern of organic pollutants	333
13.3 Green synthesis in FNMs	349
13.4 Necessity of functionalization of NMs for remediation of organic contaminants	350
13.5 Working mechanism of FNPs	350
13.6 Importance of green synthesis in FNMs	351
13.7 Organic dyes	356
13.8 Degradation of Organophosphorus (OP) pesticides by FNMs	365
13.9 Toxicity and functionalized nanoparticles	371
13.10 Conclusions and future perspectives	377
References	378
Further Reading	395
 <b>14. Implications of surface coatings on engineered nanomaterials for environmental systems: status quo, challenges, and perspectives</b>	399
<i>Ndeke Musee, Samuel Leareng, Lemme Kebaabetswe, Gosaitse Tubatsi, Ntombikayise Mahaye and Melusi Thwala</i>	
14.1 Introduction	399
14.2 Implications of coatings for engineered nanomaterial transformation in environmental systems	401
14.3 Influence of engineered nanomaterial coatings on cellular organisms toxicity	405

14.4	Molecular approaches to toxicity of engineered nanomaterials: effects of coatings	409
14.5	Concluding remarks and perspectives	410
	References	411
<b>15.</b>	<b>Functionalized halloysite nanotubes: an “ecofriendly” nanomaterial in environmental industry</b>	<b>417</b>
	<i>Gaurav Pandey, Maithri Tharmavaram and Deepak Rawtani</i>	
15.1	Introduction	417
15.2	Functionalization techniques for halloysite nanotubes	418
15.3	Applications of functionalized halloysite nanotubes in environmental industry	421
15.4	Conclusion and future prospects	429
	References	429
<b>16.</b>	<b>Functionalized nanomaterials for chemical sensor applications</b>	<b>435</b>
	<i>Sing Muk Ng</i>	
16.1	Introduction	435
16.2	General characteristics of NMs for chemical-sensing applications	437
16.3	The engineering aspects for functionalization of NMs	446
16.4	Sensing applications	457
16.5	Summary and future perspectives	468
	References	469
<b>17.</b>	<b>Porous nanocomposites for water treatment: past, present, and future</b>	<b>479</b>
	<i>Xiaolin Zhang, Zhixian Li, Ziniu Deng and Bingcai Pan</i>	
17.1	Introduction	479
17.2	Nanocomposite adsorbents	480
17.3	Nanocomposite membranes for water purification	493
17.4	Nanocomposite catalysts	496
17.5	Summary and perspectives	497
	References	498
<b>18.</b>	<b>Impact of functionalized nanomaterials towards the environmental remediation: challenges and future needs</b>	<b>505</b>
	<i>Aashima and S.K. Mehta</i>	
18.1	Introduction	505
18.2	Implementation of functionalized nanomaterial: water pollution remediation	509

18.3	Implementation of functionalized nanomaterial: air pollution remediation	514
18.4	Implementation of functionalized nanomaterial: soil pollution remediation	515
18.5	Conclusion	517
18.6	Future scope and challenges	517
18.7	Acknowledgment	518
	References	518

## Section 6

### **Functionalized nanomaterial in surfaces and coatings (consumer products)**

19.	Natural-based consumer health nanoproducts: medicines, cosmetics, and food supplements	527
	<i>Ana Henriques Mota, Alexandra Sousa, Mariana Figueira, Mariana Amaral, Bruno Sousa, João Rocha, Elias Fattal, António José Almeida and Catarina Pinto Reis</i>	
19.1	Natural sources	527
19.2	Nanotechnology in medicines	528
19.3	Nanoproducts in food supplements	548
19.4	Natural products, nanotechnology, and skin	555
19.5	Conclusions	564
	References	567

## Section 7

### **Functionalized nanomaterial in textiles industry**

20.	Functional nanofibers: fabrication, functionalization, and potential applications	581
	<i>Nabil A. Ibrahim, Moustafa M.G. Fouda and Basma M. Eid</i>	
20.1	Introduction	581
20.2	Electrospinning	581
20.3	Fabrication steps	582
20.4	Polymers used in electrospun NFs	583
20.5	Functional NFs	584
20.6	Potential applications	590
20.7	Future trends	590
	Abbreviations	598
	References	598



<b>21. Nanoengineered textiles: from advanced functional nanomaterials to groundbreaking high-performance clothing</b>	<b>611</b>
<i>Clara Pereira, André M. Pereira, Cristina Freire, Tânia V. Pinto, Rui S. Costa and Joana S. Teixeira</i>	
21.1 Nanotechnology on textiles	611
21.2 Nanoengineered textiles: functionalization processes	614
21.3 Functional nanomaterials@textiles: from production to textile applications	636
21.4 Future trends and prospects	691
Acknowledgments	692
References	693

## Section 8

### Functionalized nanomaterial in cosmetics industry

<b>22. Functional nanomaterials for the cosmetics industry</b>	<b>717</b>
<i>Suman Singh*, Satish Kumar Pandey* and Neelam Vishwakarma</i>	
22.1 Introduction	717
22.2 Cosmetics: performance enhancement using nanotechnology	718
22.3 Nanocosmetics: types and applications	718
22.4 Classification of nanocosmetics on the basis of formulation technologies	718
22.5 Nanocosmetics: some popular categories	722
22.6 Nanotechnology for UV protection	723
22.7 Formulation and manufacturing aspects	724
22.8 Guidance documents on nanomaterials in cosmetics	725
22.9 Safety assurance	725
22.10 Impurity profiling	726
22.11 Evaluation of nanomaterial toxicology	726
22.12 Toxicity testing	727
22.13 Conclusions	728
Acknowledgment	729
References	729
<b>23. Naturally derived pyroxene nanomaterials: an ore for wide applications</b>	<b>731</b>
<i>Gerardo Vitale, Ghada Nafie, Afif Hethnawi and Nashaat N. Nassar</i>	
23.1 Introduction	731
23.2 Synthesis of iron–silicate-based nanomaterials by the hydrothermal method	734
23.3 Conclusions	764
References	766

<b>24. Nanomaterial-based cosmeceuticals</b>	<b>775</b>
<i>Pravin Shende, Drashti Patel and Anjali Takke</i>	
24.1 Introduction	775
24.2 Nanomaterials in cosmeceuticals	775
24.3 Classification of nanocosmeceuticals	781
24.4 Penetration of nanoparticles	782
24.5 Toxicity of nanocosmeceuticals	782
24.6 Safety of nanocosmeceuticals	782
24.7 Regulations of nanocosmeceuticals	784
24.8 Conclusions and future perspectives	788
References	788
Further reading	791

## Section 9

### **Functionalized nanomaterials for aerospace, vehicle and sports industry**

<b>25. Functionalized nanomaterials for the aerospace, vehicle, and sports industries</b>	<b>795</b>
<i>Sadaf Abbasi, M.H. Peerzada, Sabzoi Nizamuddin and Nabisab Mujawar Mubarak</i>	
25.1 Introduction	795
25.2 Types of nanomaterials	796
25.3 Properties of functional nanomaterials	802
25.4 Applications of functional nanomaterials	812
25.5 Benefits and challenges	818
25.6 Conclusion	820
References	820

## Section 10

### **Functionalized nanomaterial in construction industry**

<b>26. Nanomaterials for enhancement of thermal energy storage in building applications</b>	<b>829</b>
<i>Teng Xiong and Kwok Wei Shah</i>	
26.1 Introduction	829
26.2 Nanometal enhancer	833
26.3 Nanometal oxide enhancer	844
26.4 Nanocarbon enhancer	852
26.5 Conclusions	858
References	860

<b>27. Application of functionalized nanomaterials in asphalt road construction materials</b>	<b>865</b>
<i>Henglong Zhang, Chongzheng Zhu, Chuanwen Wei, Haihui Duan and Jianying Yu</i>	
27.1 Introduction	865
27.2 Application of organic layered silicate in asphalt	866
27.3 Application of surface modification inorganic nanoparticles in asphalt	880
27.4 Applications of multidimensional nanomaterials in asphalt	892
27.5 Future trends in research of functionalized nanomaterial-modified asphalt	906
References	906

## Section 11

### **Functionalized nanomaterial in wood & paper-related applications**

<b>28. Functional rubber–clay nanotube composites with sustained release of protective agents</b>	<b>911</b>
<i>Ye Fu, Liqun Zhang and Yuri Lvov</i>	
28.1 Introduction	911
28.2 Encapsulation and sustained release of chemical agents	912
28.3 Functional halloysite rubber nanocomposites	917
28.4 Conclusions	939
References	939

## Section 12

### **Environmental, Legal, Health and Safety Issues of Functionalized Nanomaterials**

<b>29. Handbook of surface-functionalized nanomaterials: safety and legal aspects</b>	<b>945</b>
<i>Neil John Hunt</i>	
29.1 Introduction	945
29.2 Different types of surface modification	946
29.3 Effect of surface on biological mechanisms	948
29.4 Substance-specific examples	952
29.5 Allotropes of carbon	952
29.6 Polymeric nanomaterials	953
29.7 Quantum dots	954
29.8 Inorganic elements and oxides	954

29.9	Regulatory and legal issues that impact surface-functionalized nanomaterials	956
29.10	Current REACH situation with nanomaterials	956
29.11	Board of appeal review	957
29.12	Amendments to the annexes of REACH (2019)	958
29.13	Other EU regulations	965
29.14	Other national regulations that impact nanomaterials	969
29.15	Conclusion	971
	References	971
<b>30.</b>	<b>Functional nanomaterials: selected legal and regulatory issues</b>	<b>983</b>
	<i>Md. Ershadul Karim</i>	
30.1	Introduction	983
30.2	Functional nanomaterials: an overview	984
30.3	Functionalized nanomaterials: applications, human health, and environmental concerns	985
30.4	Functionalized nanomaterials: legal and regulatory aspects	986
30.5	Functionalized nanomaterials: highlights of legal and regulatory initiatives	987
30.6	Discussion	989
30.7	Conclusion	991
	References	991
<b>31.</b>	<b>Functional nanomaterials: selected occupational health and safety concerns</b>	<b>995</b>
	<i>Md. Ershadul Karim</i>	
31.1	Introduction	995
31.2	ENMs and OHS concerns	996
31.3	ENMs and OHS laws: an overview	997
31.4	Initiatives taken by the stakeholders	999
31.5	Evaluation	1000
31.6	Conclusion	1002
	References	1003
	Index	1007

This page intentionally left blank

# List of contributors

**Aashima** Department of Chemistry and Centre of Advanced Studies in Chemistry,  
Panjab University, Chandigarh, India

**Sadaf Abbasi** School of Engineering, RMIT University, Melbourne, VIC, Australia

**Naif AbdullahAl-Dhabi** Addiriyah Chair for Environmental Studies, Department of  
Botany and Microbiology, College of Science, King Saud University, Riyadh,  
Saudi Arabia

**António José Almeida** iMEDULisboa, Research Institute for Medicines, Faculty of  
Pharmacy, Avenida Prof. Gama Pinto, Universidade de Lisboa, Lisboa, Portugal

**Mafalda R. Almeida** CICECO-Aveiro Institute of Materials, Department of  
Chemistry, University of Aveiro, Aveiro, Portugal

**Mariana Amaral** iMEDULisboa, Research Institute for Medicines, Faculty of  
Pharmacy, Avenida Prof. Gama Pinto, Universidade de Lisboa, Lisboa, Portugal

**Mariadhas Valan Arasu** Addiriyah Chair for Environmental Studies, Department of  
Botany and Microbiology, College of Science, King Saud University, Riyadh,  
Saudi Arabia

**I.R. Ariyaratna** Department of Chemistry and Biochemistry, Auburn University,  
Auburn, AL, United States

**A.K.H. Bashir** UNESCO-UNISA Africa Chair in Nanosciences/Nanotechnology  
Laboratories, College of Graduate Studies, University of South Africa (UNISA),  
Pretoria, South Africa; Nanosciences African Network (NANOAFNET),  
Materials Research Department (MRD), iThemba LABS-National Research  
Foundation (NRF), Western Cape Province, South Africa

**P. Chandra Kanth** Department of Science, School of Technology, Pandit Deendayal  
Petroleum University, Gandhinagar, India

**Woon-Chan Chong** Department of Chemical Engineering, Lee Kong Chian Faculty  
of Engineering and Science, Universiti Tunku Abdul Rahman, Kajang, Malaysia

**Rui S. Costa** REQUIMTE/LAQV, Chemistry and Biochemistry Department, Faculty  
of Sciences, University of Porto, Porto, Portugal; IFIMUP, Institute of Physics for  
Advanced Materials, Nanotechnology and Photonics, Physics and Astronomy  
Department, Faculty of Sciences, University of Porto, Porto, Portugal

**Shrabani De** Department of Applied Chemistry, Indian Institute of Technology  
(Indian School of Mines), Dhanbad, Jharkhand, India

- Ziniu Deng** State Key Laboratory of Pollution Control and Resource Reuse, School of Environment, Nanjing University, Nanjing, P.R. China
- Haihui Duan** Key Laboratory for Green & Advanced Civil Engineering Materials and Application Technology of Hunan Province, College of Civil Engineering, Hunan University, Changsha, P.R. China
- Basma M. Eid** Textile Research Division, National Research Centre, Giza, Egypt
- Joaquim L. Faria** Laboratory of Separation and Reaction Engineering-Laboratory of Catalysis and Materials (LSRE–LCM), Faculdade de Engenharia, Universidade do Porto, Porto, Portugal
- Elias Fattal** Institut Galien Paris-Sud, Faculté de Pharmacie, Université Paris-Saclay, Malabry, France
- Mariana Figueira** iMEDULisboa, Research Institute for Medicines, Faculty of Pharmacy, Avenida Prof. Gama Pinto, Universidade de Lisboa, Lisboa, Portugal
- Moustafa M.G. Fouda** Textile Research Division, National Research Centre, Giza, Egypt
- Cristina Freire** REQUIMTE/LAQV, Chemistry and Biochemistry Department, Faculty of Sciences, University of Porto, Porto, Portugal
- Mara G. Freire** CICECO-Aveiro Institute of Materials, Department of Chemistry, University of Aveiro, Aveiro, Portugal
- Ye Fu** School of Materials Science and Mechanical Engineering, Beijing Technology and Business University, Beijing, P.R. China; State Key Laboratory of Organic-Inorganic Composites, Beijing University of Chemical Technology, Beijing, P.R. China
- Nidhi Gour** Department of Chemistry, Indrashil University, Rajpur, Kadi, India
- Afif Hethnawi** Department of Chemical and Petroleum Engineering, University of Calgary, Calgary, Alberta, Canada
- G. Hota** Department of Chemistry, NIT, Rourkela, Odisha, India
- Neil John Hunt** Risk Assessment Services Yordas Group, Lancaster, United Kingdom
- Chaudhery Mustansar Hussain** Department of Chemistry and Environmental Science, New Jersey Institute of Technology, Newark, NJ, United States
- Nabil A. Ibrahim** Textile Research Division, National Research Centre, Giza, Egypt
- Abdulgalim B. Isaev** Department of Environmental Chemistry and Technology, Dagestan State University, Makhachkala, Russian Federation
- K. Kanimozhi** Department of Chemistry, Auxilium College (Autonomous), Vellore, India
- Md. Ershadul Karim** Faculty of Law, University of Malaya, Kuala Lumpur, Malaysia; Bangladesh Supreme Court, Dhaka, Bangladesh
- Mohammad Reza Kasaai** Department of Food Science and Technology, Sari Agricultural Sciences and Natural Resources University, Sari, Iran

- K. Kaviyarasu** UNESCO-UNISA Africa Chair in Nanosciences/Nanotechnology Laboratories, College of Graduate Studies, University of South Africa (UNISA), Pretoria, South Africa; Nanosciences African Network (NANOAFNET), Materials Research Department (MRD), iThemba LABS-National Research Foundation (NRF), Western Cape Province, South Africa
- Lemme Kebaabetswe** Department of Biological Sciences and Biotechnology, Botswana International University of Science and Technology, Palapye, Botswana
- J. Kennedy** UNESCO-UNISA Africa Chair in Nanosciences/Nanotechnology Laboratories, College of Graduate Studies, University of South Africa (UNISA), Pretoria, South Africa; National Isotope Centre, GNS Science, Lower Hutt, New Zealand
- J.L. Kokini** Department of Food Science, Purdue University, West Lafayette, IN, United States
- Chai-Hoon Koo** Department of Civil Engineering, Lee Kong Chian Faculty of Engineering and Science, Universiti Tunku Abdul Rahman, Kajang, Malaysia
- Woei-Jye Lau** Advanced Membrane Technology Research Centre (AMTEC), Universiti Teknologi Malaysia, Skudai, Malaysia
- Samuel Leareng** Emerging Contaminants Ecological Risk Assessment (ECERA) Group, Department of Chemical Engineering, University of Pretoria, Pretoria, South Africa
- Douglas Letsholathebe** Department of Physics, University of Botswana, Gaborone, Botswana
- Zhixian Li** State Key Laboratory of Pollution Control and Resource Reuse, School of Environment, Nanjing University, Nanjing, P.R. China
- Yuri Lvov** Institute for Micromanufacturing, Louisiana Tech University, Ruston, LA, United States
- M. Maaza** UNESCO-UNISA Africa Chair in Nanosciences/Nanotechnology Laboratories, College of Graduate Studies, University of South Africa (UNISA), Pretoria, South Africa; Nanosciences African Network (NANOAFNET), Materials Research Department (MRD), iThemba LABS-National Research Foundation (NRF), Western Cape Province, South Africa
- Rashmi Madhuri** Department of Applied Chemistry, Indian Institute of Technology (Indian School of Mines), Dhanbad, Jharkhand, India
- C. Maria Magdalane** Department of Chemistry, St. Xavier's College (Autonomous), Tirunelveli, India; LIFE, Department of Chemistry, Loyola College (Autonomous), Chennai, India
- Ntombikayise Mahaye** Emerging Contaminants Ecological Risk Assessment (ECERA) Group, Department of Chemical Engineering, University of Pretoria, Pretoria, South Africa
- N. Matinise** UNESCO-UNISA Africa Chair in Nanosciences/Nanotechnology Laboratories, College of Graduate Studies, University of South Africa (UNISA), Pretoria, South Africa; Nanosciences African Network (NANOAFNET), Materials Research Department (MRD), iThemba LABS-National Research Foundation (NRF), Western Cape Province, South Africa



- N. Mayedwa** UNESCO-UNISA Africa Chair in Nanosciences/Nanotechnology Laboratories, College of Graduate Studies, University of South Africa (UNISA), Pretoria, South Africa; Nanosciences African Network (NANOAFNET), Materials Research Department (MRD), iThemba LABS-National Research Foundation (NRF), Western Cape Province, South Africa
- S.K. Mehta** Department of Chemistry and Centre of Advanced Studies in Chemistry, Panjab University, Chandigarh, India
- S.B. Mohamed** Department of Materials Science, Central University of Tamil Nadu, Thiruvavur, India
- G.T. Mola** School of Chemistry Physics, University of KwaZulu-Natal, Pietermaritzburg Campus, Scottsville, South Africa
- N. Mongwaketsi** UNESCO-UNISA Africa Chair in Nanosciences/Nanotechnology Laboratories, College of Graduate Studies, University of South Africa (UNISA), Pretoria, South Africa; Nanosciences African Network (NANOAFNET), Materials Research Department (MRD), iThemba LABS-National Research Foundation (NRF), Western Cape Province, South Africa
- Sergio Morales-Torres** Carbon Materials Research Group, Department of Inorganic Chemistry, Faculty of Sciences, University of Granada, Granada, Spain
- Ana Henriques Mota** iMEDULisboa, Research Institute for Medicines, Faculty of Pharmacy, Avenida Prof. Gama Pinto, Universidade de Lisboa, Lisboa, Portugal
- Nabisab Mujawar Mubarak** Department of Chemical Engineering, Faculty of Engineering and Science, Curtin University, Sarawak, Malaysia
- Ndeke Musee** Emerging Contaminants Ecological Risk Assessment (ECERA) Group, Department of Chemical Engineering, University of Pretoria, Pretoria, South Africa
- Ghada Nafie** Department of Chemical and Petroleum Engineering, University of Calgary, Calgary, Alberta, Canada
- Nashaat N. Nassar** Department of Chemical and Petroleum Engineering, University of Calgary, Calgary, Alberta, Canada
- Márcia C. Neves** CICECO-Aveiro Institute of Materials, Department of Chemistry, University of Aveiro, Aveiro, Portugal
- Sing Muk Ng** Faculty of Engineering, Computing, and Science, Swinburne University of Technology Sarawak Campus, Jalan Simpang Tiga, Kuching, Malaysia; School of Research, Swinburne University of Technology Sarawak Campus, Jalan Simpang Tiga, Kuching, Malaysia
- Sabzoi Nizamuddin** School of Engineering, RMIT University, Melbourne, VIC, Australia
- Sukanchan Palit** Department of Chemical Engineering, University of Petroleum and Energy Studies, Dehradun, India
- Bingcai Pan** State Key Laboratory of Pollution Control and Resource Reuse, School of Environment, Nanjing University, Nanjing, P.R. China; Research Center for Environmental Nanotechnology (ReCENT), Nanjing University, Nanjing, P.R. China

**Gaurav Pandey** Institute of Research & Development, Gujarat Forensic Sciences University, Gandhinagar, India

**Satish Kumar Pandey** CSIR - Central Scientific Instruments Organisation, Chandigarh, India

**Drashti Patel** Shobhaben Pratapbhai Patel School of Pharmacy and Technology Management, SVKM's NMIMS, Mumbai, India

**M.H. Peerzada** School of Engineering, Swinburne University, Melbourne, VIC, Australia

**André M. Pereira** IFIMUP, Institute of Physics for Advanced Materials, Nanotechnology and Photonics, Physics and Astronomy Department, Faculty of Sciences, University of Porto, Porto, Portugal

**Clara Pereira** REQUIMTE/LAQV, Chemistry and Biochemistry Department, Faculty of Sciences, University of Porto, Porto, Portugal

**Irina Pereira** Department of Pharmaceutical Technology, Faculty of Pharmacy, University of Coimbra, Pólo das Ciências da Saúde, Coimbra, Portugal; REQUIMTE/LAQV, Group of Pharmaceutical Technology, Faculty of Pharmacy, University of Coimbra, Coimbra, Portugal

**Tânia V. Pinto** REQUIMTE/LAQV, Chemistry and Biochemistry Department, Faculty of Sciences, University of Porto, Porto, Portugal

**A. Raja** Department of Physics, Kalasalingam Institute of Technology, Krishnan Koil, India

**R.M.P.I. Rajakaruna** Department of Chemistry and Biochemistry, Auburn University, Auburn, AL, United States

**G. Ramalingam** Department of Nanoscience and Technology, Alagappa University, Karaikudi, India

**Manviri Rani** Department of Chemistry, Malaviya National Institute of Technology, Jaipur, India

**Deepak Rawtani** Institute of Research & Development, Gujarat Forensic Sciences University, Gandhinagar, India

**Catarina Pinto Reis** iMEDULisboa, Research Institute for Medicines, Faculty of Pharmacy, Avenida Prof. Gama Pinto, Universidade de Lisboa, Lisboa, Portugal; IBEB, Biophysics and Biomedical Engineering, Faculty of Sciences, Universidade de Lisboa, Campo Grande, Lisboa, Portugal

**António J. Ribeiro** Department of Pharmaceutical Technology, Faculty of Pharmacy, University of Coimbra, Pólo das Ciências da Saúde, Coimbra, Portugal; I3S, Group Genetics of Cognitive Dysfunction, Institute for Molecular and Cell Biology, Porto, Portugal

**João Rocha** iMEDULisboa, Research Institute for Medicines, Faculty of Pharmacy, Avenida Prof. Gama Pinto, Universidade de Lisboa, Lisboa, Portugal

**Shrabhan Ku Sahoo** Department of Chemistry, NIT, Rourkela, Odisha, India

**Ana Cláudia Santos** Department of Pharmaceutical Technology, Faculty of Pharmacy, University of Coimbra, Pólo das Ciências da Saúde, Coimbra, Portugal; REQUIMTE/LAQV, Group of Pharmaceutical Technology, Faculty of Pharmacy, University of Coimbra, Coimbra, Portugal

**Valéria C. Santos-Ebinuma** Department of Engineering Bioprocess and Biotechnology, School of Pharmaceutical Sciences, UNESP-University Estadual Paulista, Araraquara, Brazil

**Joana A.D. Sequeira** Department of Pharmaceutical Technology, Faculty of Pharmacy, University of Coimbra, Pólo das Ciências da Saúde, Coimbra, Portugal

**Kwok Wei Shah** Department of Building, School of Design and Environment, National University of Singapore, Singapore, Singapore

**Uma Shanker** Department of Chemistry, Dr B R Ambedkar National Institute of Technology, Jalandhar, India

**Pravin Shende** Shobhaben Pratapbhai Patel School of Pharmacy and Technology Management, SVKM's NMIMS, Mumbai, India

**Cláudia G. Silva** Laboratory of Separation and Reaction Engineering-Laboratory of Catalysis and Materials (LSRE-LCM), Faculdade de Engenharia, Universidade do Porto, Porto, Portugal

**Santosh Bahadur Singh** Department of Chemistry, National Institute of Technology Raipur, Raipur, Chhattisgarh, India

**Suman Singh** CSIR - Central Scientific Instruments Organisation, Chandigarh, India

**Alexandra Sousa** iMEDULisboa, Research Institute for Medicines, Faculty of Pharmacy, Avenida Prof. Gama Pinto, Universidade de Lisboa, Lisboa, Portugal

**Bruno Sousa** ULHT, Lisboa, Portugal; Health Service of the Autonomous Region of Madeira, Funchal, Portugal

**Anjali Takke** Shobhaben Pratapbhai Patel School of Pharmacy and Technology Management, SVKM's NMIMS, Mumbai, India

**Ana P.M. Tavares** CICECO-Aveiro Institute of Materials, Department of Chemistry, University of Aveiro, Aveiro, Portugal

**Joana S. Teixeira** REQUIMTE/LAQV, Chemistry and Biochemistry Department, Faculty of Sciences, University of Porto, Porto, Portugal; IFIMUP, Institute of Physics for Advanced Materials, Nanotechnology and Photonics, Physics and Astronomy Department, Faculty of Sciences, University of Porto, Porto, Portugal

**Maithri Tharmavaram** Institute of Research & Development, Gujarat Forensic Sciences University, Gandhinagar, India

**Melusi Thwala** Water Centre, Council for Scientific and Industrial Research, Pretoria, South Africa

**Gosaitse Tubatsi** Department of Biological Sciences and Biotechnology, Botswana International University of Science and Technology, Palapye, Botswana

**H. Turasan** Department of Food Science, Purdue University, West Lafayette, IN, United States

**Francisco Veiga** Department of Pharmaceutical Technology, Faculty of Pharmacy, University of Coimbra, Pólo das Ciências da Saúde, Coimbra, Portugal; REQUIMTE/LAQV, Group of Pharmaceutical Technology, Faculty of Pharmacy, University of Coimbra, Coimbra, Portugal

**Sandeep Kumar Verma** Institute of Biological Science, SAGE University, Bypass Road, Kailod Kartal, Indore, India

**Neelam Vishwakarma** CSIR - Central Scientific Instruments Organisation, Chandigarh, India

**Gerardo Vitale** Department of Chemical and Petroleum Engineering, University of Calgary, Calgary, Alberta, Canada

**Chuanwen Wei** Key Laboratory for Green & Advanced Civil Engineering Materials and Application Technology of Hunan Province, College of Civil Engineering, Hunan University, Changsha, P.R. China

**Teng Xiong** Department of Building, School of Design and Environment, National University of Singapore, Singapore, Singapore

**Jianying Yu** State Key Laboratory of Silicate Materials for Architectures, Wuhan University of Technology, Wuhan, P.R. China

**Henglong Zhang** Key Laboratory for Green & Advanced Civil Engineering Materials and Application Technology of Hunan Province, College of Civil Engineering, Hunan University, Changsha, P.R. China

**Liqun Zhang** State Key Laboratory of Organic-Inorganic Composites, Beijing University of Chemical Technology, Beijing, P.R. China

**Xiaolin Zhang** State Key Laboratory of Pollution Control and Resource Reuse, School of Environment, Nanjing University, Nanjing, P.R. China; Research Center for Environmental Nanotechnology (ReCENT), Nanjing University, Nanjing, P.R. China

**Chongzheng Zhu** Key Laboratory for Green & Advanced Civil Engineering Materials and Application Technology of Hunan Province, College of Civil Engineering, Hunan University, Changsha, P.R. China

This page intentionally left blank

# Preface

Nanotechnology refers to the categorization, manufacture, and management of structures, devices, or materials that are smaller than 100 nm. Nanomaterials have been used extensively in the biomedical, environmental, textile, construction, and cosmetics industries. In particular, functionalized nanomaterials (FNMs) have been intensively studied in the last several years, and numerous methods have been developed, including covalent or noncovalent alterations. These functionalization identities offer nanomaterials with versatile applications due to the assimilating functional groups or materials onto their surface. Generally, FNMs have different mechanical, absorption, optical, or electrical properties than the original nanomaterials and thus can be used for a variety of applications. In fact, FNMs are predicted to be a main driver of technology and business and are already involved in the recent development of new products in major industrial sectors as this handbook discusses.

In order to cover specific industrial applications of FNMs as well as offer readers a holistic view of FNMs currently used at industrial scale, this handbook is divided into several sections. [Section 1](#) deals with different kinds of FNMs for industrial use (carbon-based nanomaterials, metal-based nanomaterials, composites, biosourced nanomaterials such as biopolymers, nanocellulose, fibers, etc.). [Section 2](#) discusses industrial-scale functionalization strategies for nanomaterials, while [Section 3](#) focuses on FNMs for the catalysis industry. [Section 4](#) covers FNMs for the biomedical, pharmaceutical, agriculture, and agri-food industries. In [Section 5](#), FNMs for the electronics, electrical, and energy industries are discussed. [Section 6](#) is about utilization of FNMs in the environmental industry. [Section 7](#) covers FNMs in surfaces and coatings, while [Section 8](#) focuses on FNMs in the textiles industry. [Section 9](#) discusses FNMs in the cosmetics industry. Finally, [Section 10](#) covers the FNMs uses in the aerospace, vehicle, and sports industries whereas [Section 11](#) describes the environmental, legal, health, and safety issues related to FNMs.

The purpose of this handbook is to provide the most recent advancements of FNMs in key industrial sectors. College and university graduates and industrial professionals along with industrial scientists, industrial engineers, nanotechnologists, materials scientists, chemists, physicists, pharmacists, biologists, chemical engineers, etc., will find this handbook interdisciplinary

and thorough, with its emphasis on key research and guidelines. The editor and authors are well-known researchers, scientists, and FNM experts from academia and industry. On behalf of Elsevier, we thank all the contributors of this handbook. Very special thanks goes to Simon Holt (acquisitions editor) and Isabella Conti Silva (editorial project manager) at Elsevier, for their enthusiastic support and help during this project.

**Chaudhery Mustansar Hussain**  
Editor

## Section 1

# **Different kinds of functionalized nanomaterial for industrial use nanomaterials**



This page intentionally left blank

## Chapter 1

# Functionalization of nanomaterials for industrial applications: recent and future perspectives

Sukanchan Palit<sup>1</sup> and Chaudhery Mustansar Hussain<sup>2</sup>

<sup>1</sup>*Department of Chemical Engineering, University of Petroleum and Energy Studies, Dehradun, India,* <sup>2</sup>*Department of Chemistry and Environmental Sciences, New Jersey Institute of Technology, Newark, NJ, United States*

## 1.1 Introduction

Nanotechnology and nanoengineering are two opposite sides of a visionary coin. On the one hand, scientific revelation, deep scientific provenance and scientific ingenuity are the pivots of scientific research pursuit in nanotechnology and nanomaterials today. Frequent environmental disasters, global climate change, and stringent environmental regulations are challenging the vast scientific fabric of human civilization. In this chapter, we discuss engineering science and technology with a focus on nanomaterials. Nanotechnology is deeply integrated with diverse areas of science and engineering, due, in part, to evergrowing concerns about global warming and climate change. Water purification, drinking water treatment, and industrial wastewater treatment are some of the current applications of nanotechnology. Environmental science, chemical process engineering, and integrated water resource management are highly stressed areas of science and engineering [1]. The vast and varied challenges of water resource management as well as applications of environmental engineering are discussed in this chapter, with an emphasis on functionalized nanomaterial applications in the environmental and energy sectors. Food engineering and food technology are other important sectors of nanomaterial science and engineering today [2].

## 1.2 Nanotrends in industrial development

Today environmental engineering science, petroleum engineering, and chemical process engineering are challenging areas of science and engineering. The authors in this volume focus on the successful applications of nanomaterials in an effort to provide more environmental protection. In particular, environmental remediation, drinking water treatment, industrial wastewater treatment, and integrated water resource management are covered.

Nanotechnology, nanomaterials, and functionalized nanomaterials are at the forefront of science today. Sustainability whether it is energy, environmental, social, or economic is the biggest need of human civilization today [1,2]. Environmental disasters, global warming, and depletion of fossil fuel resources are key challenges that must be addressed. Nanoengineering and nanovision are at the forefront of this research [1,2].

## 1.3 Potential of nanomaterials

Nanomaterials and green materials are the smart materials of the future. In this volume, the authors focus on the ways nanotechnology is used in human society, in particular engineered nanomaterials and functionalized nanomaterials.

Nanomaterials are materials of which a single unit is sized (in at least one dimension) between 1 and 1000 nm but usually it is 1–100 nm (the usual definition of nanoscale). Materials with structure at the nanoscale have unique and important optical, electronic, and mechanical properties. Today, globally nanomaterials are slowly being commercialized and are emerging as key technologies [1,2].

Engineered nanomaterials have been deliberately engineered and manufactured by humans to have some distinct properties. Legacy and visionary nanomaterials are those that were in commercial production prior to the development of nanotechnology as incremental advancements over other colloidal materials. They include carbon black and titanium dioxide nanomaterials. Incidental nanoparticles may be incidentally produced as a by-product of mechanical and industrial processes. Sources of incidental nanoparticles include vehicle exhausts, welding fumes, combustion fumes, and combustion processes from domestic fuel heating and cooking. Incidental atmospheric nanoparticles are ultrafine particles and can contribute to air pollution.

Biological systems often feature natural and functional nanomaterials. Natural inorganic nanomaterials occur through crystal growth in the diverse chemical conditions of the Earth's crust. Fires are complex reactions and can produce pigments, cement, fumed silica, etc.

## 1.4 What are functionalized nanomaterials?

Functionalized nanomaterials and engineered nanomaterials are next-generation smart materials with applications in environmental engineering,

water purification, drinking water treatment, industrial wastewater treatment, and biomedical engineering science. Bionanotechnology is another promising area of science today.

## **1.5 The use of functionalized nanomaterials in industry**

Nanomaterials and functionalized nanomaterials applications are today replete with immense scientific and academic rigor. In this chapter, the authors deeply elucidates the scientific needs, the scientific profundity and the vast scientific divination in the application areas of nanomaterials, engineered nanomaterials and functionalized nanomaterials [1].

### **1.5.1 Food**

Nanomaterials today have immense applications in the food domain. For example, Ghodake et al. [3] discussed nanoengineered systems for biopesticides. “Green revolution” technology and engineering have resulted in remarkable advancements in agricultural productivity by using high-yielding varieties, chemical fertilizers, and pesticides [3]. The authors deeply discussed the current strategies of pest control including the use of pesticides and biopesticides [3]. The authors discussed in detail the application areas and the scientific ethics behind biopesticides, the advantages of biopesticides over chemical pesticides, the mechanism of action of pesticides, and the formulation development of biopesticides.

Shivakumar et al. [4] discussed nanomaterials for smart food packaging. Packaging has played a vital role in protecting food substances from various environmental conditions in the food supply chain [4]. The authors in this chapter describes and discusses intelligent packaging, which refers to packaging that contains an indicator either externally and internally that provides information about the quality of food. Nanosensors, smart materials, and the feasibility and economics of modern packaging are also discussed. Nanomaterials are expected to revolutionize the food packaging industry due to the enforcement of stringent environmental regulations [4].

Kadam et al. [5] described the novel approaches of nanotechnology in the agro and food industries. This chapter deals deeply with applications of nanotechnology in agrofood production chain and the emerging opportunities [5]. Other topics discussed include packaging, food contact material, and food storage and handling. The use of nanotechnology can improve supply chain visibility, tracking and traceability, food authenticity, and also food security [5].

### **1.5.2 Energy and environmental sectors**

The energy and environmental sectors are experiencing rapid growth due nanotechnology applications. Vazquez et al. [6] described the use of

nanomaterials in energy production. According to the International Energy Outlook 2017, there will be a 28% increase in the worldwide energy demand from 2015 to 2040 [6]. In 2015, the World Energy Council reported that 77.1% of energy consumption is covered by fossil fuel sources (oil, coal, and gas) and 4.4% by the nuclear industry [6].

Energy sustainability and energy engineering are two opposite sides of the visionary coin. This chapter focuses on the application of nanotechnology in the energy production sector [6]. The areas covered are fossil fuels, nuclear, wind turbines, fuel cells, and solar cells. Fossil fuels include oil, coal, and natural gas, which supply more than the 80% of our energy needs. Global wind power generation contributed about 4% of total global power generation in 2015. One important area of scientific research today is fuel cells [6]. Fuel cells are used to produce electrical energy. A fuel cell is basically an electrochemical cell that can convert the chemical energy of a fuel into electrical energy through an electrochemical reaction on the electrode/electrolyte interface [6]. Photovoltaic solar cells are devices used for direct conversion of solar radiation into electrical energy. There are silicon and thin film solar cells, multijunction solar cells, organic solar cells, and dye sensitized solar cells.

Pathakoti et al. [7] discussed nanotechnology applications in the environmental industry. Nanotechnology is the manipulation of matter on the nanoscale (1–100 nm) in diverse and far-reaching fields such as chemical process engineering, material science, electrical engineering, computer science, chemistry, and biology [7]. The authors described in detail water and wastewater treatment and application areas such as nanoadsorbents, nanocatalysts, nanomembranes, and remediation. The nanomaterials discussed include nanoscale zerovalent iron, bimetallic nanoparticles, semiconductor nanoparticles, and dendrimers [7].

### 1.5.3 Other applications of engineered nanomaterials

Biomedical engineering, agricultural sciences, biological sciences, medical sciences, and biotechnology are today interdependent on engineered nanomaterials.

## 1.6 Current research on nanomaterials

Nanomaterials are today integrated with every branch of science and engineering. In this well researched treatise, the author deeply relates the need of scientific vision and the scientific ingenuity in the applications of nanomaterials in energy, environment, medical applications and other domains. The status of environment is extremely disastrous and catastrophic today. There is no respite to environmental disasters and global climate change. Also, industrial wastewater treatment is mesmerizing and challenging the true

vision of global science and engineering. Here comes the vast and necessary importance of engineered nanomaterials to human society [1,2].

Palit et al. [8] described engineered nanomaterials for industrial use including carbon nanotubes, dendrimers, fullerenes, graphene sheets, metal oxides, nanoarrays, and nanocrystals.

Palit [9] discussed recent advances in engineered nanomaterials in the environment industry and did a critical review on this far-reaching scientific domain. The author pointedly focuses on the scientific avenues toward advancement of nanomaterials applications, the vast domain of nanotechnology and largely the success of Engineered Nanomaterials applications in environment industry [1,9]. Nanomaterials and environmental industry are today linked with each other by immense scientific might, determination and vision. The authors detailed recent scientific endeavor in the field of nanotechnology. Success of science and vast engineering applications are the pillars of research and development forays in nanotechnology. These factors are detailed in this chapter. Recent scientific endeavor in the field of nanotechnology and environmental protection/ remediation are described in minute details in this chapter [9].

Das et al. [10] discussed the characteristic features and applications of engineered nanomaterials for water treatment and purification, carbon dioxide sequestration, and remediation of radionuclides. The risk factors associated with the use of nanomaterials are also discussed [10]. According to the Organization for Economic Cooperation and Development (OECD), the Environmental Industry is defined as “An environmental industry consists of activities which produce goods and services to measure, prevent, limit and minimize, or correct environmental destruction to water, air and soil, as well as problems related to waste, noise and ecosystem” [10]. The primary objective of the environmental industry is environmental protection [10]. Chemical process engineering and the vast and intricate areas of chemical technology needs to be enhanced along with Environmental Industry. The research work also dealt with characteristic features and applications of engineered nanomaterials [10]. The authors discuss nanomaterial for groundwater remediation, nanostructured metal oxide for wastewater remediation, multifunctional nanocomposite for environmental remediation, nanomaterial-based membrane in remediation, and nanomaterials for carbon dioxide sequestration.

Park et al. [11] discussed engineered nanomaterials for water treatment and environmental remediation including recent developments such as applications in membrane filtration. Applications of engineered nanomaterials for soil, aquifer, and groundwater remediation are also discussed [11]. Engineered nanomaterials have been widely used in environmental engineering science but their high aggregation tendency greatly limits the surface mobility. Recent progress on preparation of Engineered Nanomaterials was the reduction of the band gap and the production of environmentally friendly materials of higher stability, reactivity and multifunctionality [11].

## 1.7 Recent scientific research in the field of functionalized nanomaterials

Functionalized nanomaterials are the smart materials of tomorrow and today stands in the midst of deep scientific vision and scientific forbearance. The needs of human scientific vision and scientific divination are today immense and far-reaching. Scientific and technological validation along with vast scientific motivation are the necessity of human civilization in modern science today. Today in the global scientific scenario, there are vast scientific intricacies which remains unanswered. Technological gaffe and scientific hiatus in the field of environmental engineering science are devastating the global scientific firmament. Science and technology has practically no answers to heavy metal and arsenic groundwater remediation. Here comes the importance of nanotechnology and nanoengineering.

Darwish et al. [12] discussed new solutions to environmental problems due to high surface area (surface to volume ratio) and associated high reactivity on a scale ranging from one to few hundred nanometers that are not observed at the microscopic level [12]. The most attractive nanomaterials for environmental protection are derived from silica, noble metals, semiconductors, metal oxides, polymers, and carbonaceous materials [12] and their use in remediation of contaminated wastewater, groundwater, surface water, and soil are being investigated. Treatment techniques include, adsorption, photocatalytic degradation, nanofiltration, and sensing and monitoring of various pollutants and contaminants [12]. However, there are some challenges that need to be addressed including the potential impacts of nanomaterials on human health and the ecosystem and the limited reusability and activity of nanomaterials [12]. The authors in this treatise deeply elucidated on nano-adsorption, membranes and membrane processes, nanophotocatalysis, nanosensing, methods of nanomaterials functionalization, direct functionalization, postsynthetic functionalization, polymers in functionalization, and nanomaterial- functional groups bonding types [12]. The other areas of research endeavor in this treatise are functionalization and applications of silica-based nanomaterials and the functionalization and applications of carbonaceous nanomaterials [12]. The applications of functionalized carbonaceous nanomaterials and metal and metal compound nanomaterials are described.

Subbiah et al. [13] discussed nanoparticles and functionalization and multifunctional applications in biomedical applications. Rapid innovations in nanomedicine, medical science, and biomedical engineering have increased the likelihood that engineered nanomaterials will veritably come in contact with human and environment. Nanotechnology has created strong interest in many fields such as biomedical sciences and engineering, in particular the development of functionalized nanoparticles [13]. In recent years a variety of chemical methods have been developed to synthesize functionalized nanoparticles for drug delivery, cancer therapy, diagnostics, tissue engineering, and

molecular biology, and the structure–function relationship of these functionalized nanoparticles has been investigated [13]. Nanotechnology is the study of functional systems at the molecular level and it is the fastest growing areas of science and engineering. Work in the field of nanotechnology began in 1959 [13]. The theoretical capability and the basis of building things with immense atomic precision was initially envisioned by the physicist Richard Feynman who stated that “There is plenty room at the bottom” [13]. This visionary statement marked the start of a newer visionary era in the field of science and engineering. Scientific vision and the vast scientific profundity thus emerged into a newer innovative eon. Functionalization of nanoparticles provides an effective link from materials to medicine and back and is becoming highly indispensable to the discovery and research and development endeavor in innovative therapeutic carriers and diagnostic tools. This type of approach utilized various types of materials and their functionalization and connects the molecular mechanisms involved in physiology to drug targets and other biomedical engineering applications such as imaging, drug delivery science and tissue engineering [13].

Predoi et al. [14] discussed advances in functionalized material research. During the last few decades, intense attention has been given by scientific communities to the development of various nanomaterials such as inorganic, organic, polymeric, biological, and polymer composites for diverse applications from biomedical sciences to environmental engineering. Science and engineering of biomedical sciences are today in the path of newer scientific regeneration and vast scientific vision [14]. Of the emerging visionary areas of research, inorganic nanomaterials have been the most investigated as their properties can be changed through functionalization [14]. They can be made multifunctional with the immense ability to incorporate broad categories of functions relevant to biomedicine, nanomedicine and environmental engineering science. The scientific vision of functionalized materials research is thus opening a new door in the field of engineering and science. This paper focuses on current and expected scientific research advances in the areas of functionalized materials research [14]. The areas covered include design and synthesis of functionalized nanomaterials, structural and morphological characterization of newly functionalized compounds, advanced functionalized materials for biomedical and environmental engineering applications, and functionalized materials with magnetic properties [14].

Oliviera et al. [15] discussed protein functionalized carbon nanomaterials for biomedical applications. Since the invention of low-dimensional carbon allotropes, there has been increased interest in using carbon nanomaterials for biomedical science and engineering applications. Carbon nanomaterials have been used bioimaging, chemical sensing, targeting, delivery, therapeutics, catalysis, and energy harvesting [15]. In this paper, the authors review the surface immobilization of biomolecules, including proteins, peptides, and enzymes, and present the recent advances in synthesis and applications of



these conjugates [15]. In this review, the authors discuss different strategies to the immense scientific challenges when using carbon nanomaterials as protein carriers, explore and investigate various immobilization techniques along with characterization methods and vastly presents recent demonstrations of employing these systems for biomedical engineering applications. Recent scientific advances in the science of nanotechnology has provided a wide variety of nanoscale materials, including carbon nanomaterial allotropes, which have been deeply applied in numerous applications owing to their inherent scientific properties [15]. The use of carbon nanomaterials as scaffolds for biomolecules enhances and increases their utilization potential, especially in biomedical engineering applications [15]. The authors cover the main strategies for the protein functionalization of carbon nanomaterials and their applications, especially in biomedical engineering. The forays in science and engineering of nanotechnology are today opening up newer windows of innovation in the field of medical sciences, biomedical engineering, and biological sciences. The authors reviewed the recent developments in the synthesis of proteins, peptides, and enzymes—carbon nanoparticle conjugates, focusing on single-walled carbon nanotubes as well as major characterization tools for studying these chemical complexes. Nanoparticle surface immobilization of proteins and enzymes, carbon nanotubes as protein carriers, and applications of protein—single-walled carbon nanotubes are also discussed [15].

Wang [16] covers functionalization and characterization of carbon-based nanomaterials for electronics, composite, and biomedical applications. Surface functionalization of nanomaterials to combine different materials' properties has created unlimited possibilities in the field of nanotechnology including functionalization of carbon nanotubes for biomedical applications, covalent functionalization of graphene oxide for cement reinforcement, and noncovalent functionalization of graphene for high thermal conductive adhesive [16]. Nanotechnology as an emerging technology is helping continually improve or revolutionize many traditional technologies in diverse areas ranging from electronic packaging to energy conversion and storage, from additives to catalysis, and from sensors to drug delivery and the vast biomedical engineering science applications. This doctoral thesis focuses on developing flexible chemical approaches to functionalize carbon nanotubes and the functional components [16]. These functionalization approaches are divided into covalent functionalization and noncovalent functionalization.

Palit et al. [17] discussed recent and future perspectives for nanomaterials in environmental science. Chemical process engineering, chemical process technology, environmental engineering science, and material science are covered. Destruction of the environment and loss of ecological biodiversity have created increased interest in nanomaterials [1,17].

Adhikari et al. [18] discussed functionally active nanomaterials for environmental remediation including carbon nanomaterials and composites, metal

nanoparticles, metal-oxide nanoparticles, and nanocomposites and other nanoparticles [18]. Functionally active nanomaterials have been explored as highly efficient adsorbents, photocatalysts, and as a sterilizer for water resources [18]. There is also a focus on the risks of environmental nanomaterials and their synthesis via green chemistry and green nanotechnology.

## **1.8 The scientific vision of energy and environmental sustainability**

Human scientific progress and civilization require energy and environmental sustainability. Today global climate change, environmental catastrophes, and groundwater contamination are changing the face of scientific research pursuit.

Kuhlman et al. [19] discussed the meaning of sustainability. Sustainability as a policy concept has its vast origin and initiation in the Brundtland Report of 1987. That document kept a balance between an improved human life and the life's limitations and vision. After the initial deliberations of that report, the world witnessed immense scientific, social, economic and environmental re-construction and revival [19]. This paper argues that this change in meaning (1) redefines the aims of welfare and environmental conservation, (2) the risks reducing the environmental conservation concept, and (3) the vast distinction between social and economic sustainability [19]. Sustainability can be redefined as a natural topic of study for economists and social scientists. The Brundtland report is deeply comprehended as “development that meets the needs of the present without compromising the ability of future generations to meet their own needs.” The author in this paper discusses the concept of “people, planet and profit” and the future of sustainability.

## **1.9 Recent research in environmental protection and industrial ecology**

Industrial ecology is a relatively newer branch of science but recent advances in this area have shown tremendous scientific potential. Today industrial ecology, systems engineering, and human factor engineering are changing the face of human civilization. In this chapter, the author deeply focuses on the scientific needs, the vast scientific stance and the immense scientific ingenuity in the applications of nanotechnology and functionalized nanomaterials to the human progress and the human scientific rigor [1].

## **1.10 Integrated water resource management and human factor engineering**

Systems engineering is an integral part of human factor engineering today [1]. The authors in this chapter discuss both human factor engineering and

integrated water resource management. Global water scarcity is a challenge to human society today [1,20–22]. Groundwater remediation is integrated with integrated water resource management [2,23,24]. This chapter discusses nanotechnology applications in water purification.

### 1.11 Groundwater remediation and nanotechnology

Today nanotechnology has applications in environmental engineering as well as groundwater remediation. Arsenic groundwater contamination is an environmental disaster in many developing and developed nations around the world [1,2,23,24], in particular in South Asia, India, and Bangladesh. Here comes the need of nanotechnology and application areas of functionalized nanomaterials.

### 1.12 Future research trends in nanotechnology and nanomaterials

There is a huge technological and engineering hiatus in the field of application area of nanomaterials, engineered nanomaterials and functionalized nanomaterials [1,25,26]. The health effects of nanomaterials to humans is alarming and at the same time thought provoking. Future research should focus on environmental remediation, groundwater remediation, and drinking water treatment.

### 1.13 Conclusion and future perspectives

Environmental engineering and environmental protection are the other areas of immense concern to human society today. Diverse areas of science and technology such as environmental engineering, nanomaterials, engineered nanomaterials, functionalized nanomaterials, and petroleum engineering science needs to be validated at the earliest utmost.

## References

- [1] Hussain CM. Handbook of nanomaterials for industrial applications. Amsterdam: Elsevier; 2018.
- [2] Hussain CM, Kharisov B. Advanced environmental analysis-application of nanomaterials, vol. 1. Cambridge: The Royal Society of Chemistry; 2017.
- [3] Ghodake VN, Naik SV, Bhukhanwala KN, Kande KV, Bhor NJ, Patravale VB. Nanoengineered systems for biopesticides, Chapter 14. In: Hussain CM, editor. Handbook of nanomaterials for industrial applications. Amsterdam: Elsevier; 2018. p. 243–59.
- [4] Shivakumar N, Madhusudan P, Kiruba Daniel SCG. Nanomaterials for smart food packaging, Chapter 15. In: Hussain CM, editor. Handbook of nanomaterials for industrial applications. Amsterdam: Elsevier; 2018. p. 260–70.

- [5] Kadam DM, Kaur A. Novel approaches of nanotechnology in agro and food processing, Chapter-16. In: Hussain CM, editor. Handbook of nanomaterials for industrial applications. Amsterdam: Elsevier; 2018. p. 271–91.
- [6] Vazquez CI, Inglesias RA. Engineered nanomaterials in energy production industry, Chapter-38. In: Hussain CM, editor. Handbook of nanomaterials for industrial applications. Amsterdam: Elsevier; 2018. p. 713–23.
- [7] Pathakoti K, Manjunath M, Hwang H-M. Nanotechnology applications for environmental industry, Chapter-48. In: Hussain CM, editor. Handbook of nanomaterials for industrial applications. Amsterdam: Elsevier; 2018. p. 894–907.
- [8] Palit S, Hussain CM. Engineered nanomaterial for industrial use, Chapter-1. In: Hussain CM, editor. Handbook of nanomaterials for industrial applications. Amsterdam: Elsevier; 2018. p. 3–12.
- [9] Palit S. Recent advances in the application of engineered nanomaterials in the environment industry-a critical overview and a vision for the future, Chapter 47. In: Hussain CM, editor. Handbook of nanomaterials for industrial applications. Amsterdam: Elsevier; 2018. p. 883–93.
- [10] Das R, Bhattacharjee C. Engineered nanomaterial in environmental industry, Chapter-54. In: Hussain CM, editor. - Handbook of nanomaterials for industrial applications. Amsterdam: Elsevier; 2018. p. 971–85.
- [11] Park CM, Wang D, Su C. Recent developments in engineered nanomaterials for water treatment and environmental remediation, Chapter-46. In: Hussain CM, editor. Handbook of nanomaterials for industrial applications. Amsterdam: Elsevier; 2018. p. 849–82.
- [12] Darwish M, Mohammadai A. Functionalized nanomaterial for environmental techniques, Chapter-10. In: Hussain CM, Mishra AK, editors. Nanotechnology in environmental science. Amsterdam: Elsevier; 2018. p. 315–49.
- [13] Subbiah R, Veerapandian M, Yun KS. Nanoparticles: Functionalization and multifunctional applications in biomedical sciences. *Curr Med Chem* 2010;17:4559–77.
- [14] Predoi D, Motelica-Heino M, Coustumer PL. Advances in functionalized materials research. *J Nanomater* 2018;1–2.
- [15] Oliveira SF, Bisker G, Bakh NA, Gibbs SL, Landry MP, Strano MS. Protein functionalized carbon nanomaterials for biomedical applications. *Carbon* 2018;95:767–79.
- [16] Wang, N., 2017. Functionalization and characterization of carbon based nanomaterials for electronics, composite and biomedical applications [thesis for the Doctor of Philosophy]. Chalmers University of Technology, Goteborg.
- [17] Palit S, Hussain CM. Nanomaterials for environmental science: a recent and future perspective, Chapter-1. *Nanotechnology in environmental science*. Weinheim: Wiley-VCH; 2018. p. 3–18.
- [18] Adhikari S, Eswar NKR, Mishra AK, Sarkar D, Madras G. Functionally active nanomaterials for environmental remediation, Chapter-9. *Nanotechnology in environmental science*. Weinheim: Wiley-VCH; 2018. p. 293–314.
- [19] Kuhlman T, Farrington J. What is sustainability? *Sustainability* 2010;2:3436–48.
- [20] Palit S. Application of nanotechnology, nanofiltration and drinking and wastewater treatment- a vision for the future, Chapter-17. In: Grumezescu AM, editor. *Water purification*. USA: Academic Press; 2017. p. 587–620.
- [21] Palit S. Nanofiltration and ultrafiltration-the next generation environmental engineering tool and a vision for the future. *Int J Chem Tech Res* 2016;9(5):848–56.
- [22] Palit S. Filtration: Frontiers of the engineering and science of nanofiltration-a far-reaching review. In: Ortiz-Mendez U, Kharisova OV, Kharisov BI, editors. *CRC concise encyclopedia of nanotechnology*. Taylor and Francis; 2016. p. 205–14.

- [23] Palit S. Advanced environmental engineering separation processes, environmental analysis and application of nanotechnology- a far-reaching review, Chapter-14. In: Hussain CM, Kharisov B, editors. Advanced environmental analysis- application of nanomaterials, vol. 1. Cambridge: The Royal Society of Chemistry; 2017. p. 377–416.
- [24] Hussain CM. Magnetic nanomaterials for environmental analysis, Chapter-19. In: Hussain CM, Kharisov B, editors. Advanced environmental analysis- application of nanomaterials, vol. 1. Cambridge: The Royal Society of Chemistry; 2017. p. 3–13.
- [25] LeBlanc C. Demystifying climate risk. Industry and infrastructure implications, vol. II. New Castle Upon Tyne: Cambridge Scholars Publishing; 2017.
- [26] Barrow CJ. Environmental management and development. Routledge perspectives on Development. Oxford: Routledge, Taylor and Francis Group; 2005.

## Further reading

<https://www.ncbi.nlm.nih.gov/pubmed/21062250>  
<https://pdfs.semanticscholar.org/.../e5118a27631b8bac6a072667b18eceeda628.pdf>  
<https://www.sciencedirect.com/science/article/pii/S0921883113001556>  
<https://en.wikipedia.org/wiki/Nanoparticle>  
[https://www.nature.com/npj\\_computational\\_materials](https://www.nature.com/npj_computational_materials) > review articles  
<https://pubs.acs.org/doi/10.1021/cm071368z>  
<https://pubs.rsc.org/en/content/articlelanding/2013/nr/c3nr34005h>  
<https://www.intechopen.com/books/functionalized-nanomaterials>  
<https://www.degruyter.com/view/j/ntrev.2013.2.issue-2/.../ntrev-2012-0080.xml>  
<https://www.elsevier.com/books/...functionalized-nanomaterials/.../978-0-323-50878-...>  
[www.insituarsenic.org/](http://www.insituarsenic.org/)  
[www.insituarsenic.org/origin.html](http://www.insituarsenic.org/origin.html)  
[www.insituarsenic.org/details.html](http://www.insituarsenic.org/details.html)  
[www.waterrf.org/Pages/Projects.aspx?PID=4299](http://www.waterrf.org/Pages/Projects.aspx?PID=4299)  
<https://pdfs.semanticscholar.org/e420/20d98afedbea8d91b002cddea2dc6313a432.pdf>  
[https://mpira.ub.uni-muenchen.de/60684/1/MPIRA\\_paper\\_60684.pdf](https://mpira.ub.uni-muenchen.de/60684/1/MPIRA_paper_60684.pdf)  
[https://www.epa.gov/sites/production/files/2015-06/.../arsenic\\_issue\\_paper.pdf](https://www.epa.gov/sites/production/files/2015-06/.../arsenic_issue_paper.pdf)  
[https://www.worstpolluted.org/projects\\_reports/display/76](https://www.worstpolluted.org/projects_reports/display/76)  
[www.thestandrewsprize.com/finalist/arsenic-removal-from-water](http://www.thestandrewsprize.com/finalist/arsenic-removal-from-water)  
<https://dpw.lacounty.gov/wwd/web/Documents/In-situ%20Arsenic%20Removal.pdf>  
<https://www.sciencedirect.com/science/article/pii/S0883292708000887>  
<https://pubs.rsc.org/en/content/articlelanding/2014/cc/c3cc46920d>  
[https://www.researchgate.net/.../26884819\\_A\\_simple\\_chemical\\_free\\_arsenic\\_removal...](https://www.researchgate.net/.../26884819_A_simple_chemical_free_arsenic_removal...)  
<https://conferences.iaea.org/indico/event/49/session/13/contribution/51.pdf>  
<https://iopscience.iop.org/article/10.1143/JJAP.44.7883>  
<https://www.omicsonline.org/.../insitu-phytoremediation-of-arsenic-from-contaminate...>  
[www.nmlindia.org/pollutionmitigation.html](http://www.nmlindia.org/pollutionmitigation.html)

## Chapter 2

# Mixed-matrix membranes incorporated with functionalized nanomaterials for water applications

Woon-Chan Chong<sup>1</sup>, Chai-Hoon Koo<sup>2</sup> and Woei-Jye Lau<sup>3</sup>

<sup>1</sup>*Department of Chemical Engineering, Lee Kong Chian Faculty of Engineering and Science, Universiti Tunku Abdul Rahman, Kajang, Malaysia,* <sup>2</sup>*Department of Civil Engineering, Lee Kong Chian Faculty of Engineering and Science, Universiti Tunku Abdul Rahman, Kajang, Malaysia,* <sup>3</sup>*Advanced Membrane Technology Research Centre (AMTEC), Universiti Teknologi Malaysia, Skudai, Malaysia*

## 2.1 Introduction

Membrane-based technology has emerged as one of the most effective approaches for producing high-quality water from various sources including seawater, brackish water, ground water, surface water, as well as wastewater. The major drawback of conventional-polymeric membranes (i.e., severe surface fouling) has led to the idea of incorporating inorganic nanomaterials as fillers into the membrane matrix for performance enhancement. In recent years, nanomaterials have attracted much attention among researchers worldwide due to their unique ability to improve membrane properties with respect to hydrophilicity, antifouling resistance, permeability/rejection, and adsorption capabilities [1–4]. Some nanomaterials also possess a broad energy band (for photocatalytic activity), antibacterial properties, and low toxicity, making them useful in designing new generations of membranes.

In principle, nanomaterials are described as materials that exist in one-, two-, or three-dimensional structures whose dimensions fall within the nanometer scale (1–100 nm) [5]. Nanomaterials have a very high surface-area-to-volume ratio compared to their bulk counterparts. Their abundance of active adsorption sites makes them chemically compatible with various materials for specific applications [6,7]. Nanomaterials such as carbon nanotubes (CNTs), graphene oxide (GO), titanium oxide (TiO<sub>2</sub>), silicon dioxide (SiO<sub>2</sub>),

metal-organic framework (MOF), silver (Ag), and zinc oxide (ZnO) have been previously used to synthesize advanced functionalized membranes for water treatment [8,9]. Despite their potential, some inherent limitations exist when embedding nanomaterials directly into membranes. These include severe nanomaterial agglomeration, poor compatibility with polymeric membrane, and possible nanoparticle leaching from membrane.

Mixed-matrix membranes (MMMs) are formed by incorporating nanomaterials into a polymeric matrix [10]. The purpose is to produce MMMs of a desirable morphology with higher permeability (without compromising rejection), greater hydrophilicity, and better antifouling behaviors. Over the past decade, numerous studies have been devoted to designing MMMs by incorporating inorganic nanomaterials into polymeric membranes for specific applications. Past studies have demonstrated that incorporation of nanoparticles such as  $\text{TiO}_2$  [11,12], Ag [13,14], and ZnO [15] into various polymeric membranes successfully improved their water permeability and rejection against pollutants. Additionally, nanomaterials, particularly Ag and ZnO, which possess excellent antimicrobial properties, could effectively destroy bacterial cells and inhibit the growth of bacteria in water medium when they are introduced into membrane structure [14,16].

Since discussions concerning the impact of nanomaterials on the properties of microporous membranes can be found elsewhere [17], this chapter will specifically discuss the effects of functionalized nanomaterials (i.e., titanium-based nanomaterials, carbon-based nanoparticles, binary metal oxides, and MOF) on the properties of MMMs with respect to hydrophilicity, morphology, water flux, solute rejection, antifouling, and antibacterial resistance. The potential for using functionalized nanomaterials in adsorptive MMMs fabrication for use in the heavy-metal ion removal process as well as the advantages and disadvantages of the use of MMMs in commercial applications will also be discussed.

## 2.2 Mixed-matrix membranes incorporated with carbon-based nanomaterials

Great efforts have been expended in exploring the potential of carbon-based nanomaterials as fillers used to improve the physicochemical properties and filtration performance of membranes. The ultimate goal of these efforts is to positively impact the commercialization of MMMs. Single-walled carbon nanotubes (SWCNTs), multiwalled-carbon nanotubes (MWCNTs), GO, and carbon quantum dots (CQDs) are among the carbon-based nanomaterials that have been intensively studied in membrane research development. Carbon-based nanomaterials have received worldwide attention due to their large-surface area, excellent mechanical strength, and high thermal stability. They can be easily modified/functionalized to enable introduction of various functional groups onto their surface, which ultimately favorably impacts the

membrane filtration performance. Modification on carbon-based nanomaterials is normally performed by chemical reaction (covalent reaction) or physical attachment (noncovalent) to facilitate homogenous dispersion in polymer solution by improving their compatibility with the polymeric matrices. CQDs are zero-dimensional carbon nanomaterials with carbon cores of less than 10 nm in size. They are primarily used to produce thin-film nanocomposite as reported elsewhere [18]. CNTs and GO are functionalized before being used for microporous membrane fabrication. This section will discuss the utilization of CNTs and graphene for enhancing the properties and performance of MMMs.

### 2.2.1 Carbon nanotubes

CNTs are a unique family of materials with one-dimensional, hollow-tube structure and are normally produced by chemical vapor deposition method. SWCNTs are formed by rolling one sheet of graphene into a seamless cylinder, with typical diameter of 0.8–2 nm. The diameters of MWCNTs range from 5 to 20 nm with multiple sheets of graphene [19].

Fontananova et al. [20] investigated the impact of MWCNTs with different functional groups on the properties of polyvinylidene difluoride (PVDF) membrane. In this study, MWCNTs were functionalized using  $\text{HNO}_3/\text{H}_2\text{SO}_4$ ,  $\text{NH}_3$ , and thionyl chloride/dibutylamine to produce OX-CNT, Am-CNT and thionyl chloride/dibutylamine (AMD)-CNT, respectively. The functional groups contained in the pristine and modified MWCNTs were identified using titration methods and are summarized in Table 2.1. The pristine MWCNTs possessed only the lactonic group. OX-CNT contained carboxylic, phenolic, and lactonic groups. The AMD-CNTs included phenolic and lactonic groups, while the Am-CNTs contained phenolic, lactonic, and aminic groups. The shift of D, G, and D' bands in Raman implied PVDF as electron donor toward  $\pi$  system of the aminated and amidated functionalized

**TABLE 2.1** Functional groups content of the pristine and functionalized MWCNTs [20].

MWCNT	Carboxylic (mmol/g)	Phenolic (mmol/g)	Lactonic (mmol/g)	Aminic (mmol/g)	Total (mmol/g)
Pristine	0	0	$0.86 \pm 0.02$	0	$0.86 \pm 0.02$
OX-CNT	$0.230 \pm 0.003$	$1.40 \pm 0.02$	$1.35 \pm 0.05$	0	$2.98 \pm 0.07$
AMD-CNT	0	$1.83 \pm 0.02$	$0.61 \pm 0.06$	0	$2.44 \pm 0.08$
Am-CNT	0	$0.143 \pm 0.004$	$1.34 \pm 0.03$	$9.04 \pm 0.18$	$10.5 \pm 0.2$



MWCNTs in the MMMs. In addition to the increment of the permeation volume from 140 to 228 L/m<sup>2</sup> at 1 bar in a 5-h filtration test [three cycles of water and two cycles of bovine serum albumin (BSA)], the MMMs also exhibited greater mechanical stability as presented in Table 2.2. The AMD-CNT-incorporated MMMs had the highest tensile strength and thermal stability due to resonance effect of the amidic groups. These groups had a stronger electron donor effect than the carboxylic groups and resulted in better interaction with the PVDF. The tensile stress at break of AMD-CNT incorporated MMMs had the highest improvement (94%) followed by OX-CNT incorporated (88%), and Am-CNT incorporated MMMs (71%) with respect to pristine PVDF membrane. There was no significant difference between the pristine PVDF membrane and MMMs in the thermal stability test.

Ho et al. [21] fabricated MMMs incorporating GO/oxidized MWCNT (OMWCNT) using an in situ colloidal precipitation method for palm-mill effluent (POME) treatment. The MWCNTs were oxidized using sulfonitric acid mixture to form a carboxylate group. The goal was to reduce agglomeration and enhance interaction with the  $\pi$ -conjugated multiple aromatic regions located at the basal planes of GO. The results showed that the use of a small amount of GO could contribute to better dispersion of the hybrid nanomaterials in the membrane matrices. They also showed that the MMMs made of GO/OMWCNT with a ratio of 1:9 exhibited the highest permeability (52.62 L/m<sup>2</sup> h bar) among 16 different types of fabricated membranes. In contrast, high dosage of GO (GO/OMWCNT ratio of 9:1) sheltered the membrane surface, blocking the water molecules from passing through the membrane, thus resulting in lower permeation flux (34.11–36.83 L/m<sup>2</sup> h bar). Fig. 2.1 shows the 3D atomic force microscopy (AFM) images of several MMMs. The M1c membrane with the smoothest surface experienced the lowest flux decline during the POME filtration. In the rejection study, the M1c membrane that contained only OMWCNTs (43.99 L/m<sup>2</sup> h bar) exhibited a high removal rate of total dissolved solid (TDS), phosphorus, hardness, chemical-oxygen demand (COD), chlorine, turbidity, color, and total suspended solid (TSS) of POME. This was due to higher negative surface charge (−22.2 mV) and formation of smaller membrane pore size (8.09 nm mean pore radius).

Functionalizing carboxylic CNTs by plasma treatment to produce electrically conducting poly(vinyl alcohol) (PVA) membrane was also performed by Dudchenko et al. [22]. When an electrical field was applied on the membrane, the surface charge of the membrane was altered to create high-electrostatic force that effectively enhanced fouling resistance. Although the functional groups on CNTs did not contribute to the membrane conductivity, they improved the dispersion in the polymer matrices, thus increasing the overall membrane negative charge. The fouling rate of PVA-CNT membrane at 0 V toward alginate acid (AA) was reduced, recording 5 psi lower than a commercial polysulfone (PSF) membrane (PS-35) after 100-min filtration,

**TABLE 2.2** Performance of MMMs incorporated with carbon-based nanomaterials.

Membrane	Characteristics	Other findings	Reference
PVDF/DMF/LiCl	Pore size = $\sim 37$ nm Permeability = $\sim 30$ L/m <sup>2</sup> h bar (PWF, third cycle)	Rejection (BSA) = 98% (first cycle) and 97% (second cycle) Tensile = 1.7 MPa Elongation = 37%	[20]
PVDF/DMF/LiCl/ 0.13 wt.% AMD-CNT	Pore size = $\sim 40$ nm Permeability = $\sim 52$ L/m <sup>2</sup> h bar (PWF, third cycle)	Rejection (BSA) = 98% (first cycle) and 95% (second cycle) Tensile = 3.3 MPa Elongation = 71%	
PVDF/DMAc/PVP (M0)	Pore radius = 7.44 nm Contact angle = 73.33 degrees Charge = $-12.8$ mV Permeability = 38.66 L/m <sup>2</sup> h bar	Rejection = $\sim 83\%$ (color), $\sim 1.4\%$ (TDS), $\sim 98\%$ (TSS), $\sim 79\%$ (turbidity), $\sim 70\%$ (COD), $\sim 14\%$ (hardness), and $\sim 4.8\%$ (phosphorus) Average roughness = 38.19 nm	[21]
PVDF/DMAc/PVP/0.1 g OMWCNT (M1c)	Pore radius = 8.09 nm Contact angle = 71.77 degrees Charge = $-22.2$ mV Permeability = 43.99 L/m <sup>2</sup> h bar	Rejection = 86.3% (color), 1.5% (TDS), 100% (TSS), 81.9% (turbidity), 75.5% (COD), 21.8% (hardness), and 6.6% (phosphorus) Average roughness = 27.50 nm	
PES/DMAc/1.5 wt.% CNT (M-C-3)	Pore size = $\sim 74$ nm Contact angle = $\sim 82$ degrees Permeability = $\sim 260$ L/m <sup>2</sup> h bar	Rejection = 97% (BSA) FRR = 59.78% Total fouling = $\sim 57\%$ Reversible fouling = $\sim 17\%$ Irreversible fouling = $\sim 41\%$	[23]
PES/DMAc/1.5 wt.% SLS-CNT(M-S-3)	Pore size = $\sim 83$ nm Contact angle = $\sim 70$ degrees Permeability = $\sim 500$ L/m <sup>2</sup> h bar	Rejection = 96% (BSA) FRR = 89.99% Total fouling = $\sim 52\%$ Reversible fouling = $\sim 41\%$ Irreversible fouling = $\sim 10\%$	

(Continued)

**TABLE 2.2 (Continued)**

Membrane	Characteristics	Other findings	Reference
PSF/DMAc/PVP (M1)	Pore radius = 12.53 nm Contact angle = 66.13 degrees Permeability = $\sim 4.2 \text{ L/m}^2 \text{ h bar}$ (PWF), $\sim 2.1 \text{ L/m}^2 \text{ h bar}$ (BSA)	FRR = 57.14% $R_t = \sim 27 \times 10^{-7} \text{ m}^{-1}$ $R_c = \sim 2 \times 10^{-7} \text{ m}^{-1}$ $R_f = \sim 15.5 \times 10^{-7} \text{ m}^{-1}$ $R_m = \sim 2.3 \times 10^{-7} \text{ m}^{-1}$	[24]
PSF/DMAc/PVP/ 0.25 wt.% PEG-CNT (M3)	Pore radius = 21.27 nm Contact angle = $\sim 58$ degrees Permeability = $\sim 17 \text{ L/m}^2 \text{ h bar}$ (PWF), $\sim 11 \text{ L/m}^2 \text{ h bar}$ (BSA)	FRR = 80.33% $R_t = \sim 5.8 \times 10^{-7} \text{ m}^{-1}$ $R_c = \sim 0.8 \times 10^{-7} \text{ m}^{-1}$ $R_f = \sim 3 \times 10^{-7} \text{ m}^{-1}$ $R_m = \sim 0.8 \times 10^{-7} \text{ m}^{-1}$	
PSF/NMP	Pore size = $\sim 19.5 \text{ nm}$ Contact angle = $\sim 91.5$ degrees Charge = $-0.2 \text{ mV}$ Permeability = $\sim 280 \text{ L/m}^2 \text{ h bar}$	Rejection = $\sim 96.5\%$ (BSA) Strength = $\sim 152 \text{ MPa}$	[25]
PSF/NMP/1.3 wt.% GO	Pore size = $\sim 23 \text{ nm}$ Contact angle = $\sim 82.5$ degrees Charge = $-20 \text{ mV}$ Permeability = $\sim 430 \text{ L/m}^2 \text{ h bar}$	Rejection = $\sim 95.9\%$ (BSA) Strength = $\sim 203 \text{ MPa}$	
Commercial PVDF	Pore size = $41 \text{ nm}$ Contact angle = $78.3$ degrees Permeability = $171.12 \text{ kg/m}^2 \text{ h bar}$	—	[26]
PVDF/PVP/DMAc/ 3.0 wt.% GO	Pore size = $89 \text{ nm}$ Contact angle = $60.5$ degrees Permeability = $552.92 \text{ kg/m}^2 \text{ h bar}$	—	

PSF, NMP	Pore size = 2.04 nm Contact angle = ~65 degrees Permeability = ~0.8 L/m <sup>2</sup> h bar	Rejection = 52% (HA) FRR = ~85% Relative flux reduction rate (RFR) = 22%	<a href="#">[28]</a>
PSF/NMP/0.6 wt.% ZnO-GO	Pore size = 4.09 nm Contact angle = 39 degrees Permeability = ~5 L/m <sup>2</sup> h bar	Rejection = 99% (HA) FRR = ~100% RFR = ~20%	
PVDF/DMAc/PVP	Pore size = 24 nm Contact angle = 92.7 degrees Charge = - 10.2 mV Permeability = 91.26 L/m <sup>2</sup> h bar	Rejection = 64% (proteins), 63% (carbohydrates) Reversible fouling = 56.40% Irreversible fouling = 18.35%	<a href="#">[29]</a>
PVDF/DMAc/PVP/ 0.4 wt.% Ag/GO	Pore size = 27 nm Contact angle = 81.7 degrees Charge = - 20.2 mV Permeability = 112.3 L/m <sup>2</sup> h bar	Rejection = 81% (proteins), 82% (carbohydrates) Reversible fouling = 33.49% Irreversible fouling = 38.85%	

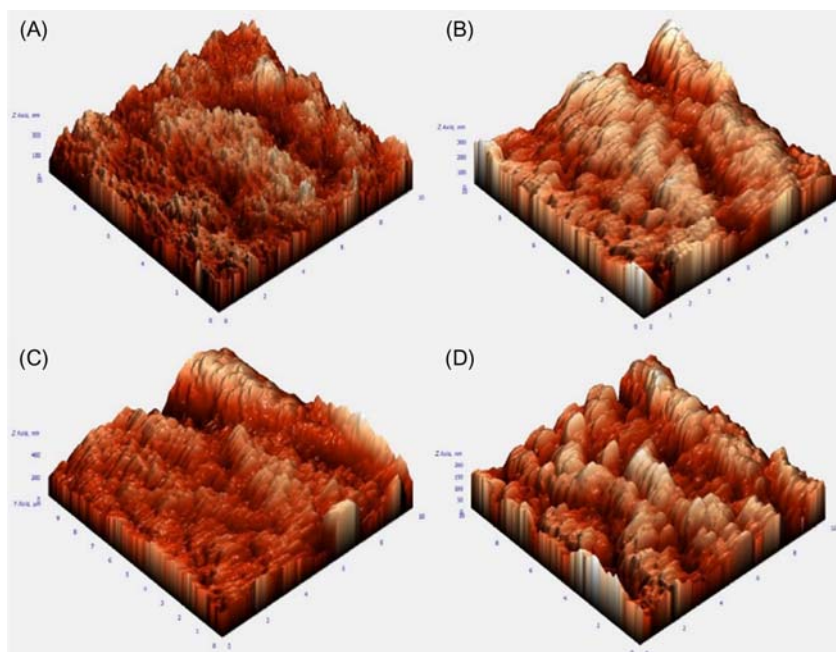


**FIGURE 2.1** 3D AFM images of (A) M0, (B) M1c, (C) M3a, and (D) M5b of membrane. (Note: M0: without nanomaterial; M1c: 0.001 g/L of OMWCNT; M3a: 0.001 g/L of GO/OMWCNT with ratio of 1:9 and M5b: 0.01 g/L of GO/OMWCNT with ratio of 5:5) [21].

as shown in Fig. 2.2A. The applied potential of  $-3$  and  $-5$  V further reduced the final filtration pressure by 33.7% and 51.1%, respectively. A higher fouling rate was observed in Fig. 2.2B when the membranes were tested with synthetic wastewater (SW) containing salt. This resulted because the  $\text{Ca}^{2+}$  ions had caused complexation of AA, thus forming aggregates and deposits on the membrane surface as a gel layer.

Wang et al. [23] functionalized CNTs with sodium lignosulfonate (SLS) using a noncovalent method by grinding CNTs and SLS on a mortar and mixing them via sonication. The functionalized CNTs (f-CNTs) were then blended with polyethersulfone (PES) at different concentrations (0.5–2.5 wt.%). Unlike many other studies showing reduced-membrane contact angle upon the incorporation of hydrophilic nanomaterials, the MMMs (with 1.5 wt.% CNTs) fabricated by Wang et al. [23] showed a higher value (82 degrees) than the pristine membrane ( $\sim 78$  degrees). This is mainly due to severe agglomeration by CNTs on the membrane surface. Using 1.5 wt.% f-CNTs as fillers, the resultant MMMs exhibited greater pure water flux (about onefold higher than the pristine PES membrane) but lower rejection for BSA filtration, owing to larger pore size that reduced the resistance of macromolecules. The MMMs demonstrated an excellent flux recovery rate

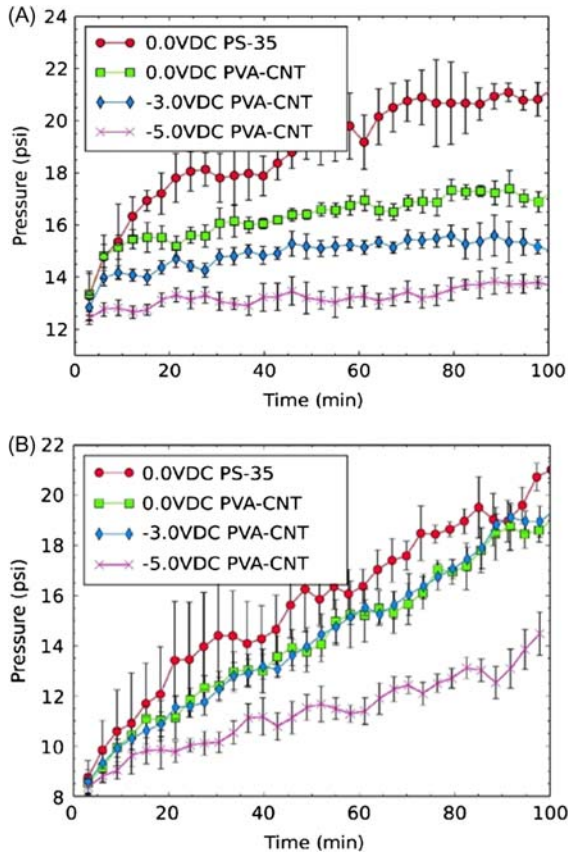


**FIGURE 2.2** (A) Fouling of 5 g/L AA on PS-35 membrane at 0 V and PVA-CNT membranes at 0, -3, and -5 V and (B) fouling of 2.5 g/L of SW-AA on PS-35 at 0 V and 3 g/L of SW-AA on PVA-CNT membranes at 0, -3, and -5 V [22].

(FRR) of 89.99% and lower flux reduction in a three-cycle BSA filtration compared to the pristine membrane. This is probably due to the formation of a hydration layer on the membrane surface, which prevents protein adsorption. Although the SLS has antimicrobial properties, its effect on the MMMs antimicrobial properties was insignificant in this work. The antimicrobial effect of the MMMs was only observed when a weak electrical field was applied on the cross-flow cell. Electron transfer and diffusion occurred rapidly in the CNTs and f-CNTs, accelerating the oxygen reduction reaction and producing large amounts of  $\text{H}_2\text{O}_2$ , which is responsible for the antimicrobial activity.

Khalid et al. [24] prepared polyethylene glycol (PEG)-functionalized CNTs by adding PEG into carboxylic CNTs with the aid of sulfuric acid

( $\text{H}_2\text{SO}_4$ ) (as a catalyst) under 5-h nitrogen atmosphere. The polar groups reduced the Van der Waals forces between the CNTs and improved the membrane hydrophilicity. The PSF-based MMMs with 0.25 wt.% PEG-CNTs showed the highest pure water and BSA permeability with the improvement of around 300% and 400%, respectively, compared to the pristine membrane. This membrane also showed the lowest values of fouling resistance ( $R_f$ ), membrane resistance ( $R_m$ ), cake resistance ( $R_c$ ), and total resistance ( $R_t$ ) among other membranes. Its FRR was recorded at 80.33%, compared to 57.14% shown by the pristine membrane.

### 2.2.2 Graphene oxide

GO can be produced by modified Hummers' method by functionalizing graphite powder with  $\text{H}_2\text{SO}_4$  and potassium permanganate ( $\text{KMnO}_4$ ). The functional groups of GO consisting of epoxy, carbonyl, carboxyl, and hydroxyl are the main factors causing the GO hydrophilic to have high negative surface charge [14]. Over the last decade, many studies have reported the positive results of using GO for improving membrane properties, including permeation flux, rejection, antifouling, antimicrobial, and mechanical strength.

Lee et al. [25] evaluated the self-fabricated GO-embedded membrane in a submerged-membrane bioreactor (MBR) system. They found that even a small amount of embedded GO could greatly affect the membrane pore structure. The membrane pore size increased by 20% with the addition of 1.30 wt.% GO, leading to 45% water flux enhancement. By fixing permeation flux at  $16 \text{ L/m}^2 \text{ h}$  and aeration rate at  $1.5 \text{ L/min}$  in the MBR system, the time taken for transmembrane pressure (TMP) to reach 50 kPa was 10 h for the pristine PSF membrane while it took 50 h for the MMMs (embedded with 1.30 wt.% GO) to achieve the same TMP. This implied that the MMMs lasted five times longer than the pristine membrane.

The reliability of GO-incorporated PVDF membrane was further compared with a commercial PVDF membrane in a long-term submerged-MBR study in the work of Zhao et al. [26]. The MMMs showed great improvement in permeation flux and fouling propensity with 50% increment of critical flux. The tightly bound (TB) proteins and loosely bound (LB) proteins contained in the cake layer of MMMs were only 68.2% and 52% of the commercial membrane, respectively. Moreover, the TB-polysaccharide and LB-polysaccharide content of the MMMs were five times lower than the commercial PVDF membrane. In addition, the thickness of cake layer on the MMMs was  $80 \mu\text{m}$  lower in comparison to the commercial membrane tested under the same condition. You et al. [27] also investigated the effectiveness of GO-incorporated membranes in removing natural organic matters (NOMs) in treated water from a conventional water treatment plant. Results showed that all the GO membranes with different membrane thickness showed 100%

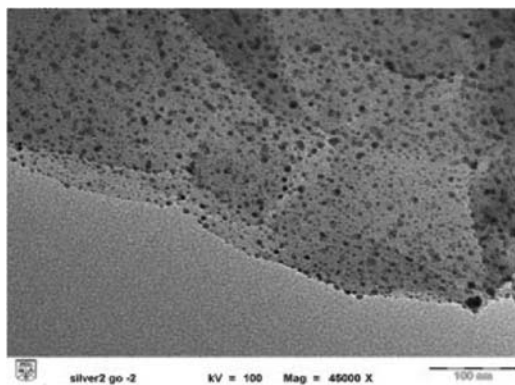


**FIGURE 2.3** Ag nanoparticles deposited on GO [14].

removal of 5 mg/L of NOMs with no fouling observed during the 6-h filtration test.

Because GO contains an abundance of oxygen functional groups, it can be easily functionalized with metal oxides such as ZnO, Ag, and TiO<sub>2</sub> nanoparticles. Fig. 2.3 presents a TEM image of Ag/GO composite in which the GO nanosheet was deposited with Ag nanoparticles. The combination of Ag and GO exhibits the properties of both materials in a new composite. Apart from filtration enhancement, the Ag nanoparticles improve the antibiofouling properties of the MMMs [14]. Chung et al. [28] were the first to blend ZnO-GO into PSF membrane. The MMMs with 0.6 wt.% ZnO-GO were reported to exhibit outstanding performance in humic acid (HA) rejection (99%) while maintaining promising water production rate. Almost 100% FRR was achieved by MMMs due to their reduced surface roughness as confirmed by AFM analysis. Interestingly, the study found that the use of GO in the nanocomposite preparation had reduced the dosage of ZnO nanoparticles in membrane fabrication up to five times while maintaining a similar prepreparation performance.

There are many studies of impregnating different metal oxides into GO for membrane filtration application, but the performance of these modified membranes are rarely compared. For that reason, Chong et al. [29] investigated the effect of different types of modified GO (GO, Ag-GO, and ZnO-GO) on the properties of MMMs in algal organic-matter filtration. All of the fabricated MMMs showed significant improvement in terms of permeation flux and rejections against proteins and carbohydrates compared to the pristine PVDF membrane. The differences among the MMMs were minimal. Nonetheless, the use of Ag-GO and ZnO-GO had significant efficacy on the antimicrobial activity toward *Escherichia coli* as shown in Fig. 2.4. It was believed that the adsorption of surface oxygen on GO, and the rapid electron transfer between the metal oxides and GO had enhanced the generation of



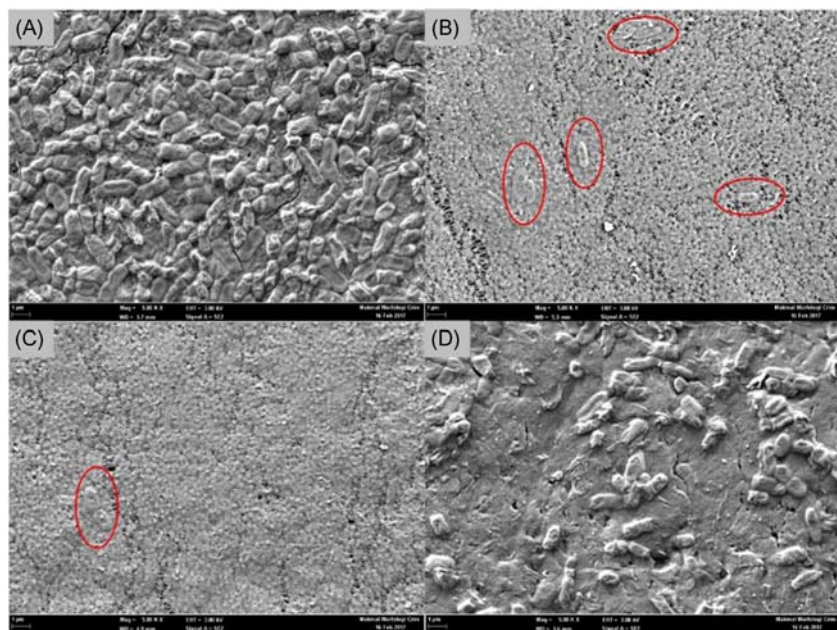


**FIGURE 2.4** Direct observation of *Escherichia coli* growth via FESEM on (A) PVDF, (B) ZnO/GO-PVDF, (C) Ag/GO-PVDF, and (D) GO-PVDF membranes [29].

reactive oxygen species which was responsible for the antimicrobial activity [30]. In another work, Chong et al. [31] further assessed the environmental footprint of Ag/GO MMMs in a microalgae membrane photoreactor (AMPR) using SimaPro (a lifecycle assessment tool). Although the fabrication process of the MMMs showed higher impact on the environment, its application in the AMPR outweighed its fabrication lifecycle results due to higher throughput. Thus the authors claimed that the application of the Ag/GO MMMs in the AMPR was more sustainable in long-term operation due to the improvement of membrane permeability and reduced-membrane fouling. Table 2.2 summarizes the characteristics and performance of MMMs incorporated with functionalized carbon-based nanomaterials for water treatment.

### 2.3 Mixed-matrix membranes incorporated with titania-based nanomaterials

In this section, the potential of various functionalized titania-based nanomaterials such as  $\text{TiO}_2$ , titania nanotubes (TNTs), and nanoporous  $\text{TiO}_2$  for improving the performance of MMMs will be highlighted. Li et al. [11] developed a novel method of preparing PES-based MMMs via the self-assembly of  $\text{TiO}_2$  around the membrane pores. The goal was to improve their

long-term antifouling ability. These  $\text{TiO}_2$  self-assembled MMMs were prepared by introducing tetrabutyl titanate (TBT) of  $\text{TiO}_2$  and triblock copolymer (Pluronic F127) into the PES casting solution via nonsolvent-induced, phase-separation process. The purpose of introducing Pluronic F127, which contains polyethylene oxide (PEO) and polypropylene oxide (PPO) units, into the polymer matrix is to increase the membrane hydrophilicity and fouling-resistant ability. Additionally, segments of Pluronic F127 could act as a binding site for the growth of in situ formed  $\text{TiO}_2$ , leading to a more stable interaction between the  $\text{TiO}_2$  and the polymer matrix and subsequently mitigating the issue of  $\text{TiO}_2$  leaching from the membrane matrix. Fig. 2.5 illustrates the self-assembly of  $\text{TiO}_2$  around the membrane pores, accompanying the synchronous formation of PES membrane during the phase-inversion process.

Li et al. [11] reported that upon addition of 2 mL of TBT and 0.5 g of Pluronic F127 into the PES solution, substantial changes on the MMMs microstructure were observed, whereby larger finger-like pores were formed at the cross section and bottom surface of the MMMs. This enlargement of macrovoids is attributed to the improved demixing process due to incorporation of Pluronic F127-bearing, hydrophilic PEO segments, and TBT containing Ti-OH groups into the casting solution [11]. This finding was further supported by the results of contact angle in which the values of 73.6 and 61.2 degrees were obtained for the pristine and  $\text{TiO}_2$ /F127/PES membranes, respectively. Although the  $\text{TiO}_2$ /F127/PES membrane demonstrated improvement in the pure water flux, its rejection performance against 1.0 g/L BSA solution was not compromised since  $\sim 96\%$  rejection was obtained. In the membrane fouling study, the performance of the  $\text{TiO}_2$ /F127/PES MMMs against BSA solution was found to be obviously improved with the increment of FRR. During the first cycle, the FRR of the tested membranes increased from 62.5% to 83.9% corresponding to the pristine PES and  $\text{TiO}_2$ /F127/PES membranes, respectively. FRR increased from 51.5% to 78.5% during the second cycle. This increase indicated that the modified membranes showed enhanced hydrophilicity, flux, and antifouling performance over the pristine PES membrane. In a separate study done by the same group of researchers [32], the fouling mechanism of the newly developed, self-assembled  $\text{TiO}_2$ /F127/PES MMMs was investigated using sodium alginate (SA), BSA, and HA. They reported that the MMMs exhibited a higher FRR and less fouling after the membrane modification despite incorporation of a lower  $\text{TiO}_2$  loading (0.45 wt.%). In the study, it was concluded that the  $\text{TiO}_2$  self-assembled structure had effectively minimized the formation of a fouling layer on the membrane surface by inhibiting the accumulation of organic foulants inside the membrane pores.

Although  $\text{TiO}_2$  has been found to be effective in mitigating membrane fouling, the issues pertaining to its agglomeration and lower surface charge properties still remain challenging. In 2018, Ayyaru and Ahn [12]

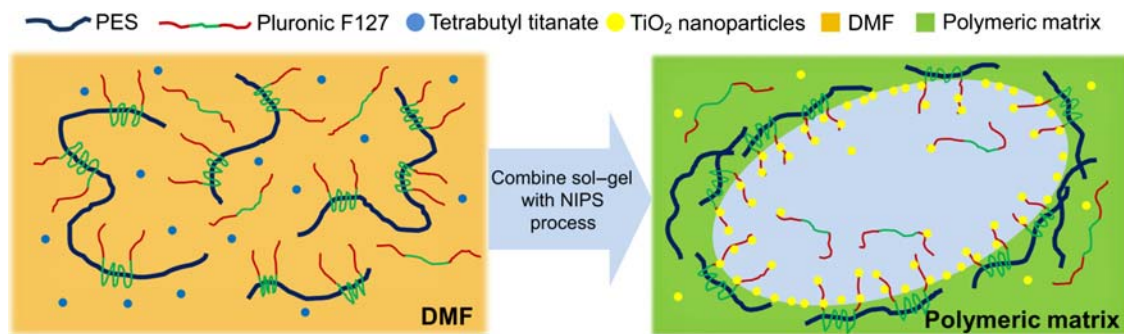


**FIGURE 2.5** Scheme of the self-assembly of  $\text{TiO}_2$  around the membrane pore during the phase-inversion process [11].

synthesized sulfonated  $\text{TiO}_2$  ( $\text{STiO}_2$ ) by modifying  $\text{TiO}_2$  with sulfonic acid ( $-\text{SO}_3\text{H}$ ) group. They hypothesized that the replacement of a hydroxyl group with  $-\text{SO}_3\text{H}$  group in  $\text{TiO}_2$  might help to provide better strategies for combating the problems. This is because the  $-\text{SO}_3\text{H}$  group has stronger hydrophilicity and greater negative charge. Through FTIR analysis, they affirmed that  $-\text{SO}_3\text{H}$  species were successfully attached to the  $\text{TiO}_2$  surface after two extra noticeable peaks at  $1237$  and  $1139\text{ cm}^{-1}$ , which were assigned to the  $\text{S}=\text{O}$  symmetric and asymmetric stretching vibrations, respectively, were observed. Using the functionalized  $\text{TiO}_2$  to fabricate the MMMs, the results showed significant changes in membrane surface roughness, porosity, and pore size compared to the  $\text{TiO}_2/\text{PES}$  MMMs. The  $\text{STiO}_2/\text{PES}$  MMMs exhibited higher water flux ( $650\text{ L/m}^2\text{ h}$ ) than that of  $\text{TiO}_2/\text{PES}$  MMMs ( $522\text{ L/m}^2\text{ h}$ ). Similarly, the  $\text{STiO}_2/\text{PES}$  MMMs showed higher FRR (95.3%) compared to the  $\text{TiO}_2/\text{PES}$  MMMs (76.7%). With the addition of 1 wt.%  $\text{STiO}_2$ , the BSA rejection of  $\text{TiO}_2/\text{PES}$  MMMs increased from 92% to 98.7%. This is because the  $\text{STiO}_2$  could provide higher hydrophilicity and better water permeability and antifouling performance, as well as improved BSA rejection due to the hydrogen bonding force and more electrostatic repulsion properties of  $\text{STiO}_2$ .

In 2017, Lee et al. [33] developed novel membrane architectures containing the fluorosilane-modified  $\text{TiO}_2$  for improving physicochemical properties of PVDF membrane in the application of membrane distillation. In this study, hydrophobic  $\text{TiO}_2$  was functionalized by *1H*, *1H*, *2H*, *2H*-perfluorooctyltriethoxysilane (FTES) before being used as an additive to fabricate the polyvinylidene fluoride-*co*-hexafluoropropylene (PVDF-HFP) electrospun membranes. The FTES was introduced into the  $\text{TiO}_2$  to guarantee proper dispersion and interfacial interaction between the nanomaterials and PVDF polymer matrix as well as to improve its surface wettability. The schematic representation of  $\text{TiO}_2$  functionalization using hydrolyzed FTES is depicted in Fig. 2.6. The fourier transform Infrared (FTIR) spectrum of the F- $\text{TiO}_2$  showed several bands at  $1113$ ,  $1143$ ,  $1191$ , and  $1236\text{ cm}^{-1}$ , referring to the  $\nu(\text{C}-\text{F}_2)$  and  $\nu(\text{C}-\text{F}_3)$  bands, respectively. The bands with a lower intensity

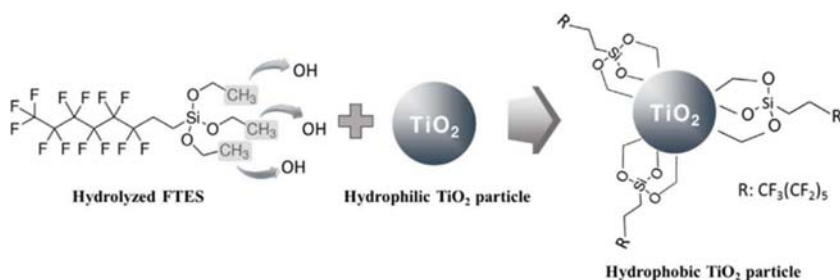


**FIGURE 2.6** Schematic representation of  $\text{TiO}_2$  functionalization using hydrolyzed FTES [33].

at 1056 and 1210  $\text{cm}^{-1}$ , associated with Si-O-Si were observed as evidence of well-coated  $\text{TiO}_2$  with FTES. Upon incorporation of F- $\text{TiO}_2$  into the dope solution of PVDF-HFP for electrospinning, they reported that all F- $\text{TiO}_2$ /PVDF-HFP electrospun membranes achieved higher and more stable water flux of at least 40  $\text{L/m}^2 \text{ h}$  (60°C feed and 20°C permeate) with a 7.0 wt.% NaCl as the feed solution. These membranes also exhibited more antiwetting property while preserving high water flux as well as higher salt rejection (99.99%) than the pristine electrospun membrane.

In a recent study conducted by Gebru and Das [34],  $\text{TiO}_2$  was modified using different amines [i.e., tetraethylenepentamine (TEPA), ethylenediamine (EDA), and hexamethylenetetramine (HMTA)] before blending with cellulose acetate (CA)-dope solution to fabricate ultrafiltration (UF) membranes for Cr(VI) ions removal. As reported elsewhere [35,36], the incorporation of amines into the membrane matrix appeared to be effective in removing heavy-metal ions due to their tendency to develop complex reactions between the heavy-metal ions and the nitrogen atom within the functional groups. The efficiency of Cr(VI) concentration, solution pH, and type of amine on the Cr(VI)-ions removal was investigated. The highest removal of Cr(VI) ion was attained at a low feed concentration of 10 ppm at pH 3.5 due to the availability of excess binding sites for Cr(VI) ions removal by CA/Ti-TEPA. The maximum removal values of the CA/U-Ti (unmodified  $\text{TiO}_2$ ), CA/Ti-HMTA, CA/Ti-EDA and CA/Ti-TEPA membranes against 10 ppm of Cr(VI) ion at pH 3.5 are 47.2%, 86.4%, 93.6%, and 99.8%, respectively.

Rather than  $\text{TiO}_2$ -based nanoparticles, TNTs were utilized in several applications because of their higher specific surface area. Sumisha et al. [37] adopted a facile and ecofriendly method to synthesize functionalized TNTs and used it to modify polyetherimide (PEI) membrane for improved salt rejection. The effect of  $\text{TiO}_2$  and three types of functionalized TNTs, hydrogen trititanate nanotubes (pTNT), nitrogen-doped  $\text{TiO}_2$  nanotubes (N-TNT), and copper ion-exchanged nanotubes (Cu-TNT) on the PEI-based MMMs was investigated. The introduction of functionalized pTNT developed broad finger-like macrovoids in the bottom of the MMMs and the texture of macrovoids became a sponge-like porous structure. The authors claimed that this phenomenon is attributed to decreased interfacial stresses existing between polymer and TNT that were tensed by forming interfacial pores due to growth of the organic phase during the delayed demixing process. Furthermore, extremely large pore size and higher porosity were observed when N-TNT and Cu-TNT were incorporated into the PEI matrix. The PEI/Cu-TNT membrane showed high water flux followed by PEI/N-TNT, PEI/pTNT, PEI/TP, and pristine PEI membranes. This finding is perfectly matched with the observed high hydrophilic nature of the PEI/Cu-TNT MMMs compared to the other MMMs investigated. With respect to separation efficiency, the authors found that the membrane salt rejection rate was increased in the order of  $\text{PEI} < \text{PEI/pTNT} < \text{PEI/N-TNT} < \text{PEI/Cu-TNT}$ .

Several research studies have reported the effect of halloysite-clay incorporation on the  $\text{TiO}_2$  and have used such hybrid nanomaterials to prepare MMMs for enhanced water separation [38–40]. The halloysite nanotubes (HNTs) are incorporated into  $\text{TiO}_2$  due to their excellent hydrophilicity and larger surface area. Zeng et al. [38] attempted to synthesize novel PVDF membranes by blending different contents of titanium-dioxide halloysite nanotube ( $\text{TiO}_2$ -HNTs) composites into the PVDF matrix. The effects of  $\text{TiO}_2$ -HNTs content on membrane performance including hydrophilicity, rejection ratio, and antifouling properties were investigated. The standard hydrophilic tests indicated that the hydrophilicity of membranes was significantly increased with the addition of  $\text{TiO}_2$ -HNTs. The pure water flux of the 3 wt.%  $\text{TiO}_2$ -HNTs/PVDF was increased by 264.8% and 35.6%, respectively, compared with the pristine PVDF and the 3 wt.%  $\text{TiO}_2$ /PVDF membranes. Additionally, these  $\text{TiO}_2$ -HNTs/PVDF MMMs exhibited excellent antifouling performance, which was attributed to the hydrophobic contaminants being resisted by the improved dispersion and hydrophilicity of  $\text{TiO}_2$  via HNTs loading.

In 2017 Mishra et al. [39] modified HNTs with 3-aminopropyl triethoxysilane (APTES) before blending them with titanium(IV) isopropoxide (TIP) solution to form  $\text{TiO}_2$ -Mo.HNTs using sol–gel method. A novel UF hybrid membrane ( $\text{TiO}_2$ -Mo.HNTs/PVC) was prepared by blending  $\text{TiO}_2$ -Mo.HNTs of different concentrations (0, 1, 2, and 3 wt.%) with the 14 wt.% polyvinyl chloride (PVC) matrix by phase-inversion process. The results showed that pure water flux of the hybrid UF membrane increased consistently with increasing nanofiller concentration in the polymeric membrane matrix. The highest pure water flux was achieved by 2 wt.% hybrid UF membrane, recording  $197.5 \text{ L/m}^2 \text{ h}$  at 2 bar. This value was about 81% higher than the pristine PVC membrane ( $109.1 \text{ L/m}^2 \text{ h}$ ). However, a marginal flux reduction was observed in the 3 wt.% hybrid UF membrane ( $179.2 \text{ L/m}^2 \text{ h}$ ) due to lower membrane porosity formed. With respect to BSA and HA rejections, all the hybrid UF membranes demonstrated a significant rejection of  $>80\%$ . In addition, these hybrid UF membranes also exhibited antibacterial properties in which their bacteriostasis rates were recorded at 75%–97.5% (using 3 wt.% hybrid UF membrane) after being tested with *E. coli* culture.

Salimi et al. [40] further explored the compatibility between  $\text{TiO}_2$ -HNTs at different concentrations (0, 0.5, 1, and 2 wt.%) and PSF membrane for natural organic matter (NOM) removal. They discovered that the MMMs with 1 and 2 wt.%  $\text{TiO}_2$ -HNTs had excellent antifouling capacity and could achieve FRR of  $>80\%$ . The increased FRR of these two MMMs, however, was compromised by the decrease in solute rejection. This could be attributed to high loadings of  $\text{TiO}_2$ -HNTs that tended to increase porosity and enlarge pore sizes on the membrane surface, adversely deteriorating the membrane performance.



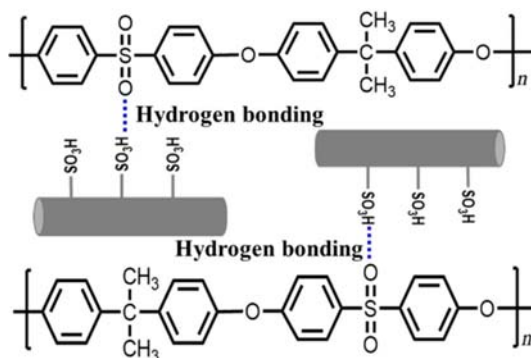


**FIGURE 2.7** Schematic presentation for hydrogen bonds between O = S = O of PSF and -SO<sub>3</sub>H on TNTs in the MMMs [41].

To further improve the antifouling of UF membranes, Alsohaimi et al. [41] modified PSF membrane using sulfonic acid-functionalized TNTs (TNTs-SO<sub>3</sub>H). The TNTs-SO<sub>3</sub>H were first synthesized by performing a coupling reaction between 3-mercaptopropyl trimethoxysilane and hydroxyl groups on TNTs via in situ oxidation using 30 wt.% H<sub>2</sub>O<sub>2</sub> solution. The MMMs containing different concentrations of TNTs-SO<sub>3</sub>H (0, 1, 3, and 5 wt. %) were then prepared from the blend solutions of PSF/TNTs-SO<sub>3</sub>H via phase-inversion method. Fig. 2.7 shows the hydrogen bonds between O = S = O of PSF and -SO<sub>3</sub>H on TNTs in the MMMs. The FRR of the MMMs was found to increase with increasing TNTs-SO<sub>3</sub>H concentration during which the FRR of the MMMs with 5 wt.% TNTs-SO<sub>3</sub>H was 77.4%–90.1%, compared to 60%–67.5% for the membrane, with 1 wt.% TNTs-SO<sub>3</sub>H during BSA and HA solution filtration. The HA rejection efficiency of the TNTs-SO<sub>3</sub>H MMMs was improved with increasing TNTs-SO<sub>3</sub>H concentration, which contradicted the results reported by Salimi et al. [40] on BSA rejection. The contradictory findings can be explained by the fact that the negatively charged HA at pH 7 tends to be better retained by the negatively charged MMMs due to the increase in -SO<sub>3</sub>H groups in the MMMs.

In 2016, Bidsorkhi et al. [42] synthesized novel UF MMMs by incorporating self-synthesized nanoporous TiO<sub>2</sub> into the PSF matrix. The surface of the nanoporous TiO<sub>2</sub> was modified with a silane-based coupling agent to guarantee its proper dispersion in the polymer. The effects of the nanoporous TiO<sub>2</sub> loading on the performance of MMMs were evaluated by conducting UF filtration experiments with BSA solution. The results demonstrated that the pure water flux of the MMMs was found to escalate with added nanoporous TiO<sub>2</sub> loading due to an increase in porosity and the formation of larger pore sizes of the membrane upon addition of nanoporous TiO<sub>2</sub>. The highest pure water flux was achieved by the membrane with 2 wt.% nanoporous TiO<sub>2</sub>, recording ~260 L/m<sup>2</sup> h at 1 bar. This flux value was 53% higher than

the membrane with 0.5 wt.% nanoporous  $\text{TiO}_2$  (170 L/m<sup>2</sup> h). However, the separation efficiency of the MMMs tended to decrease with the nanoporous  $\text{TiO}_2$  loading. The BSA rejection after 70-min filtration of the pristine membrane and the membrane, incorporated with 0.5 wt.% nanoporous  $\text{TiO}_2$ , was 100%. Rejection was slightly affected (99%) for both membranes incorporated with 1 and 2 wt.% nanoporous  $\text{TiO}_2$ . The differences in solute rejection of the MMMs can be explained by the increased membrane pore size as a result of the formation of more macrovoids and thus higher porosity when higher loading of nanoporous  $\text{TiO}_2$  was used.

## 2.4 Mixed-matrix membranes incorporated with other nanomaterials

Tannic acid is a low-cost and environmentally friendly substance which can be extracted from plants. It consists of polyphenol with a number of *o*-dihydroxy and trihydroxy aromatic ring structures that make it easily adhere to various substrates through covalent and noncovalent interactions [43]. Therefore tannic acid has been used to functionalize metals and metal oxides to form inorganic and organic building blocks. The phenolic hydroxyl groups contained in tannic acid could enhance the hydrophilicity of the metals and metal oxides and at the same time improve the composite compatibility and stability in the polymeric matrices.

Fang et al. [44] modified PES membrane by introducing different amounts of hydrophilic iron-tannin framework (ITF) complexes (0.15–0.9 g) into the membrane matrices. The ITF complexes were formed by the reaction of three-galloyl groups from tannic acid with each  $\text{Fe}^{3+}$  ion in the dimethylformamide (DMF) solvent prior to the polymers addition. All of the fabricated MMMs showed simultaneous enhancement of permeability and BSA rejection compared to the pristine membrane even though the membrane pore size was reduced upon incorporation of ITF complexes (see Table 2.3). The ITF complexes were also found to be stable in the PES membranes in a static immersion and dynamic filtration test under neutral aqueous environment. Although the release of  $\text{Fe}^{3+}$  ions was detected at 4.25, 4.18, and 0.43  $\mu\text{g}/\text{cm}^2$  at pH 2, 3, and 4, respectively, no leaching of  $\text{Fe}^{3+}$  ions were noticed at pH > 5, which suggests stability during typical water treatment process with pH ranging from 5 to 8. This strategy was found to be easier, less time-consuming, with higher permeability than the membrane surface-coating method using ITF complexes.

MOFs could also be utilized to modify microporous membranes. They consist of metal ions and organic ligands, forming one-, two-, or three-dimensional structures. The main advantages of MOFs include good compatibility with the soft polymer matrices, high surface area, and controllable porosity [45]. Although MOFs contain organic ligands, they possess the characteristics of an inorganic crystal. They tend to agglomerate in the



**TABLE 2.3** Performance of MMMs incorporated with various functionalized nanomaterials.

Membrane	Characteristics	Other findings	Reference
PES/DMF/PEG	Pore size = 16.1 nm Contact angle = 75 degrees Permeability = 197.8 L/m <sup>2</sup> h bar	Rejection = 25.9% (BSA) FRR = 66.05% (BSA)/70.05% (HA) Reversible fouling = 58.42% (BSA)/ 57.62% (HA) Irreversible fouling = 33.94% (BSA)/ 29.94% (HA)	[44]
PES/DMF/PEG/0.30 wt.% ITF	Pore size = 14.5 nm Contact angle = 57 degrees Permeability = 319.4 L/m <sup>2</sup> h bar	Rejection = 95.9% (BSA) FRR = 88.29% (BSA)/90.81% (HA) Reversible fouling = 77.1% (BSA)/ 52.87% (HA) Irreversible fouling = 11.71 (BSA)/ 9.18% (HA)	
PSF/NMP/2 wt.% ZIF-8 (PSF/Z-2)	Pore size = 59.2 nm Contact angle = 79.8 degrees Permeability = ~250 L/m <sup>2</sup> h bar	Porosity = 59.2% Rejection = ~97.5% (BSA) FRR = 55.9% Irreversible fouling = ~45%	[46]
PSF/NMP/2 wt.% hZIF-8 (PSF/hZ-2)	Pore size = 10.11 nm Contact angle = 62.4 degrees Permeability = 597 L/m <sup>2</sup> h bar	Porosity = 71.4% Rejection = ~98.4% (BSA) FRR = 81.1% Irreversible fouling = 18.7%	
PSF/NMP	Contact angle = 77.1 degrees Permeability = 240 L/m <sup>2</sup> h (0.2 MPa)	Porosity = 63.2% Rejection = ~99% (BSA) FRR = 64.5% Reversible fouling = 45.7%	[47]

PSF/NMP/0.3 wt.% UiO-66-PSBMA	Contact angle = 66.3 degrees Permeability = 602 L/m <sup>2</sup> h (0.2 MPa)	Porosity = 73.4% Rejection = ~98.5% (BSA) FRR = 72.5% Reversible fouling = 58.1%	
PES/NMP/0.6 wt.% pure SBA-15 (SBA@PES)	Contact angle = 64.8 degrees Charge = -36.6 mV Permeability = ~79 L/m <sup>2</sup> h bar	Rejection = ~97.5% (BSA) Reversible fouling = ~1.8 × 10 <sup>12</sup> m <sup>-1</sup> Irreversible fouling = ~1.9 × 10 <sup>12</sup> m <sup>-1</sup> <i>Escherichia coli</i> = ~111 CFU/cm <sup>2</sup>	[48]
PES/NMP/0.6 wt.% silver-loaded SBA-15 (AgSBA@PES)	Contact angle = 64.8 degrees Charge = -36.6 mV Permeability = ~81 L/m <sup>2</sup> h bar	Rejection = ~95.5% (BSA) Reversible fouling = ~2.3 × 10 <sup>12</sup> m <sup>-1</sup> Irreversible fouling = ~3.4 × 10 <sup>12</sup> m <sup>-1</sup> <i>E. coli</i> = < 1 CFU/cm <sup>2</sup> Ag release = ~7.7 µg/g (water)	
PVDF/DMAc/PVP/M-phenylenediamine (MPD)/trimesoyl chloride (TMC)	Contact angle = 80 degrees Initial permeability = ~22.5 L/m <sup>2</sup> h bar (NOM)	Rejection = 73.2% (NOM)	[49]
PVDF/DMAc/PVP/MPD/TMC/NH <sub>2</sub> -MCM-41	Contact angle = 13 degrees Initial permeability = ~58 L/m <sup>2</sup> h bar (NOM)	Rejection = 87.1% (NOM) FRR = 72.5%	
PES/DMAc/PEG 4000	Pore size = 26.6 nm Contact angle = 70.2 degrees Permeability = 554.2 kg/m <sup>2</sup> h	Mean roughness = 8.46 nm FRR = 39.9%	[50]
PES/DMAc/PEG 4000, 0.5 wt.% CuO-NH <sub>2</sub>	Pore size = 39.2 nm Contact angle = ~62 degrees Permeability = 887 kg/m <sup>2</sup> h	Mean roughness = 6.03 nm FRR = ~37%	

membrane matrices, negatively affecting the membrane performance. Therefore MOFs are normally functionalized with hydrophilic substances to ensure homogeneous dispersion in the polymer solution.

Sun et al. [46] synthesized the zeolitic imidazolate framework-8 (ZIF-8) and hydrophilized it with tannic acid to produce hZIF-8 as fillers for membrane fabrication. The porosity and pore size of the membranes were consistent with the thickness of the membranes as seen in Fig. 2.8 and Table 2.3. In PSF/hZ-2 membrane (with 2 wt.% hZIF-8), the hydrophilic fillers increased the exchange rate of solvent and nonsolvent during the phase-inversion process, leading to increased membrane porosity and pore size while reducing skin thickness. However, at higher filler concentration, the hydrogen bonding between the hydroxyl group of hZIF-8, and the sulfonyl and ether groups of the PSF hindered the mobility of the polymer chains, suppressing the mass transfer of solvent and nonsolvent during membrane formation. In a three-cycle, BSA filtration process, the PSF/Z-2 membranes (with 2 wt.% ZIF-8) exhibited the greatest fouling tendency due to the hydrophobicity of the unfunctionalized ZIF-8. Conversely, PSF/hZ-2 membranes demonstrated the highest FRR and the lowest irreversible fouling, resulting from high hydrophilicity and negative charge.

Sun et al. [47] also prepared UiO-66-NH<sub>2</sub> and UiO-66-PSBMA as fillers for PSF membrane fabrication. The functionalization process of the fillers is shown in Fig. 2.9. Poly(sulfobetaine methacrylate) (PSBMA), a zwitterionic polymer possessing cationic and anionic groups, was grafted onto UiO-66-NH<sub>2</sub> (nonfunctionalized MOF) via atom-transfer/radical-polymerization procedure. The grafting of the hydrophilic PSBMA reduced the contact angle and improved the filtration performance of the MMMs (see Table 2.3). The size of water molecule was 2.8 Å while the aperture size of the MOF was around 6.0 Å. The presence of MOFs in the membrane provided additional paths for water to penetrate through the porous structure and tiny interspace. The hydrophilicity of PSBMA further attracted the water molecules passing through the pores and increased the membrane permeability as illustrated in Fig. 2.9. The permeation flux of UiO-66-PSBMA/PSF membrane in cross-flow filtration increased 2.5 and 2 times compared to pristine PSF and UiO-66-NH<sub>2</sub>/PSF membranes, respectively. In the BSA rejection test, the increment of FRR and reduction of reversible and irreversible fouling indicated that the antifouling was mainly contributed by the membrane hydrophilicity rather than surface charge.

The introduction of mesoporous silica has shown potential for enhancing membrane properties in terms of permeability and antifouling resistance. Functionalization of the mesoporous silica followed by incorporation with other materials could further enhance their properties by combining the benefits of different materials. Diez et al. [48] prepared three types of nanomaterials (i.e., pure SBA-15 silica particles, metal-loaded SBA-15, and amine-functionalized SBA-15) for PES-MMM fabrication. The surface free

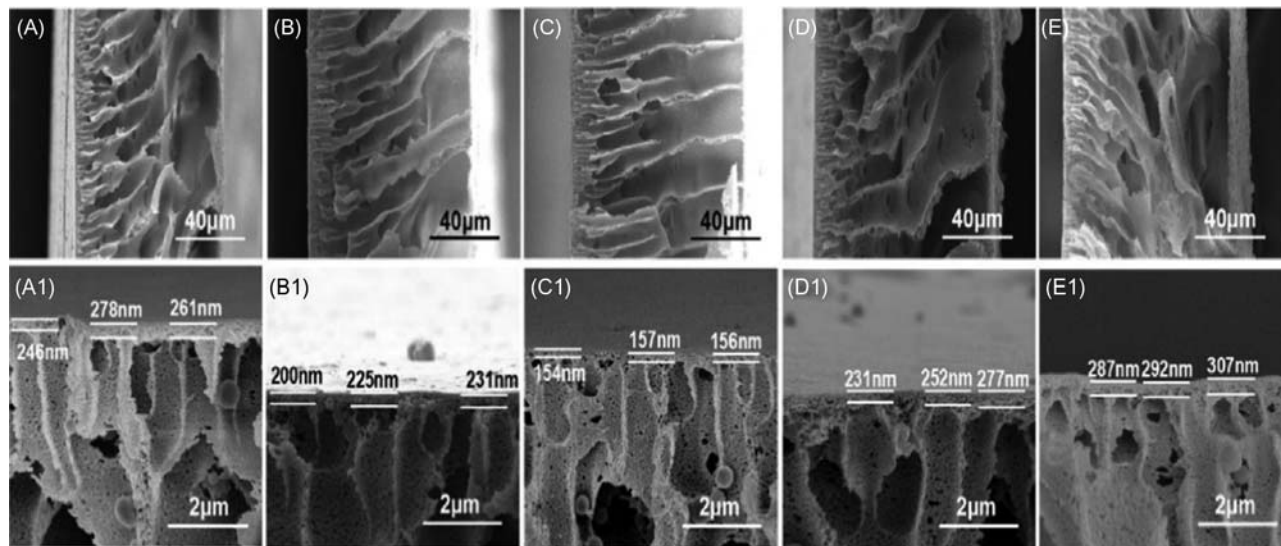


**FIGURE 2.8** The cross-sectional FESEM images of PSF (A, A1), PSF/hZ-1 (B, B1), PSF/hZ-2 (C, C1), PSF/hZ-3 (D, D1), and PSF/Z-2 (E, E1) membranes. (Note: The numbers after hZ and Z refer to the loading (wt.%) of nanomaterials added) [46].

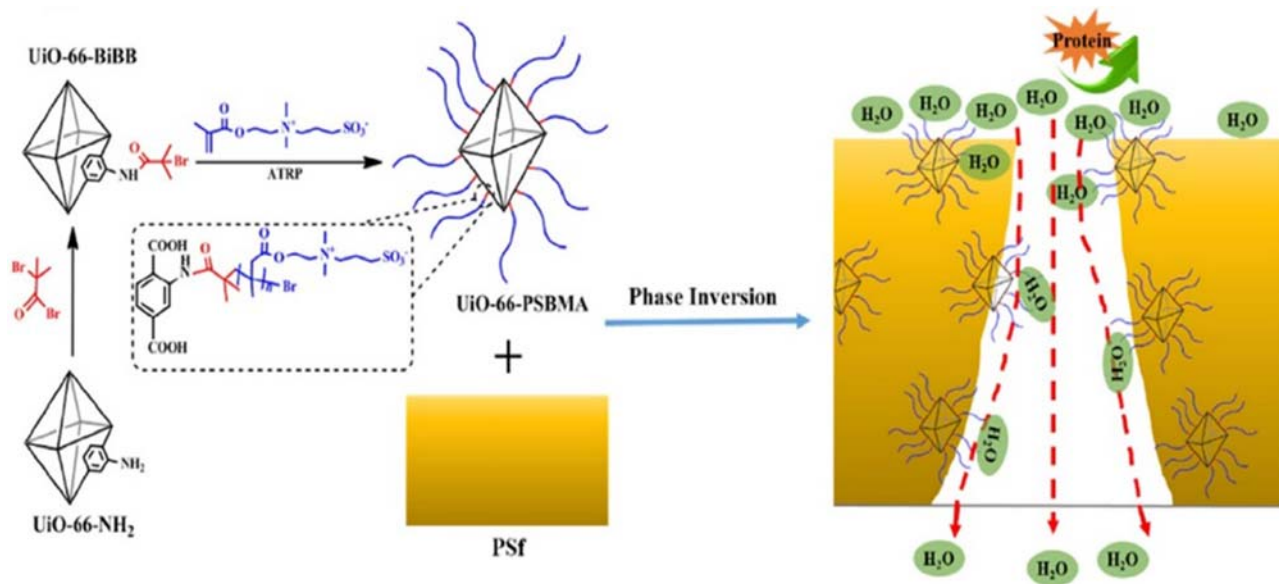


FIGURE 2.9 Illustration of the membrane modification processes using UiO-66-NH<sub>2</sub> and UiO-66-PSBMA [47].

energy,  $\Delta G_{\text{SLS}}$ , of the membranes was determined by measuring the contact angle with water, glycerol, and diiodomethane. All of the membranes showed hydrophilic properties with PES membranes and TriSBA@PES membranes showing the lowest ( $-39.8 \text{ mJ/m}^2$ ) and the highest ( $-20.8 \text{ mJ/m}^2$ ) hydrophilicity, respectively. The MMMs showed higher permeability ( $> 30\%$  higher than PES membrane) owing to the enhanced membrane porosity, thinner skin layer formed, and better pore interconnectivity. The study reported that membrane hydrophilicity and surface charge did not play significant roles in explaining the differential antimicrobial effect. The Ag and Cu-loaded SBA-15 membranes exhibited high antimicrobial activity, with complete removal of bacterial colonies on the membrane surface. In the stability test, the study found that the release of Cu ions from the MMMs was high in nutrient broth (NB) medium after immersion for 24 h, which is attributed to their interaction with organic constituents in the NB medium. Conversely, lower release of Ag ions was detected in the NB medium due to formation of insoluble AgCl in the NB medium, which contained chloride.

MCM-41 is a type of mesoporous silica sieve which possesses well-defined pore size and shape. Bao et al. [49] functionalized MCM-41 with 3-aminopropyltriethoxysilane to form  $\text{NH}_2\text{-MCM-41}$  (amine-functionalized MCM-41). A layer of the  $\text{NH}_2\text{-MCM-41}$  was then grafted onto the PVDF membrane surface (g-PVDF) via interfacial polymerization. The g-PVDF membranes became superhydrophilic with tremendous reduction of contact angle from 80 (c-PVDF, without  $\text{NH}_2\text{-MCM-41}$ ) to 13 degrees. In the filtration of NOM using dead-end cell, the initial permeation flux of the c-PVDF membranes was recorded at around  $22.5 \text{ L/m}^2 \text{ h bar}$  while the c-PVDF membranes was at around  $58 \text{ L/m}^2 \text{ h bar}$ . After 180-min filtration, the permeation flux dropped to around 15 and  $45 \text{ L/m}^2 \text{ h bar}$  for the c-PVDF and g-PVDF, respectively. The g-PVDF membranes showed higher rejection rate and lower flux attenuation rate during the NOM filtration. This was due to the hydrophilic layer of  $\text{NH}_2\text{-MCM-41}$ , which reduced the adsorption of NOM on the membrane surface and also acted as a barrier that hindered the penetration of larger molecules through the membrane pores.

Nasrollahi et al. [50] also used 3-aminopropyltriethoxysilane as an amino precursor to functionalize self-synthesized CuO and ZnO nanoparticles to form  $\text{CuO-NH}_2$  and  $\text{ZnO-NH}_2$ , respectively. The amino-functionalized metal oxides were blended with PES at different concentrations (0.1, 0.2, 0.5, 1, and 2 wt.%). The contact angle of the PES membranes showed the greatest improvement of around 18% and 14% for 2 wt.% of  $\text{CuO-NH}_2$  and  $\text{ZnO-NH}_2$  blended membranes, respectively, due to the presence of amine and oxygenated-hydrophilic groups of the functionalized metal oxides. The surface roughness of the membranes was reduced with the addition of the fillers, with 0.5 wt.% of  $\text{CuO-NH}_2$  showed the smoothest surface. The membranes were further compared with nonfunctionalized CuO and ZnO in terms of flux and antifouling performance. All of the MMMs exhibited

higher pure water flux than that of pristine PES membranes. In addition, the MMMs with 1 wt.% of CuO-NH<sub>2</sub> showed the highest FRR after 90-min BSA filtration. This is likely related to high hydrophilicity and smooth membrane surface. The study concluded that the amino-functionalized CuO showed greater dispersion and hydrophilicity than ZnO-NH<sub>2</sub> which led to better permeability and antifouling of MMMs. Table 2.3 compares the characteristics and performance of MMMs incorporated with various functionalized nanomaterials for water treatment.

## 2.5 Adsorptive mixed-matrix membranes for heavy-metal removal

One of the pioneering works concerning the development of adsorptive membranes for use in heavy-metal removal was conducted by Paul Chen's research group in 2011. Zirconium oxide (ZrO<sub>2</sub>) nanoparticles were embedded within PVDF flat-sheet membranes via direct-blending method for As (V) ion removal [51]. It was reported that in addition to exhibiting excellent pure water flux (177.6 L/m<sup>2</sup> h at 1 psi), the zirconium oxide embedded membrane could achieve 21.5 mg/g of maximum adsorption capability against As (V) ion during batch adsorption experiments. As a comparison, the pristine membrane (without nanoparticle incorporation) showed negligible adsorption capacity.

Many types of nanoparticles have been utilized to fabricate adsorptive membranes and this detailed information can be found elsewhere [52]. Special focus will be given in this section to the surface-functionalized nanomaterials that could show better compatibility with polymeric membrane and exhibit-enhanced adsorption capacity against heavy-metal ions.

In 2013, Shah and Murthy [53] fabricated a series of adsorptive microporous membranes by incorporating different types of surface-functionalized MWNTs ranging from zero to 1.0 wt.% for heavy-metal removals. Three different functionalities were introduced onto the nanotube surface (i.e. oxidized, amide, and azide). The presence of functionalized CNTs reduced the membrane pore sizes (from 0.1 μm in the control membrane to 20–30 nm in the modified membranes) and made them more hydrophilic. Most importantly, it enhanced the membrane's adsorptive nature against heavy-metal ions, particularly Cr(VI) and Cu(II) ions. The results indicated that the membranes incorporated with amide and azide-functionalized CNTs exhibited better metal binding capacity than the membrane incorporated with carboxylic-functionalized CNTs and control membranes. When 1 wt.% amide or azide-functionalized CNTs were embedded within the membrane matrix, Cr(VI) and Cu(II) removal rates as high as 94.2%–94.8% and 93.1%–93.9%, respectively, could be easily obtained. As a comparison, the control membrane and the membrane incorporated with

carboxylic-functionalized CNTs only showed  $\sim 10\%$  and  $80\%$ – $86\%$  removal rates, respectively, for both metal ions.

Using acid-functionalized MWCNTs, Masheane et al. [54] synthesized hybrid MWCNTs by depositing Fe-Ag bimetallic nanoparticles onto the surface of CNTs and using the hybrid nanomaterials for the fabrication of adsorptive PES membranes for Cr(VI) ion removal. The authors confirmed the permanent embedment of Fe-Ag bimetallic nanoparticles onto the CNTs since the detection of Fe and Ag ions in the solution (after prolonged sonication) were well below the detection limits by the analytical instrument. Upon incorporation of hybrid MWCNTs, the resultant membrane demonstrated high removal rates ( $\sim 90\%$ – $100\%$ ) for Cr(VI) ions over a wide range of pH (2–10) in comparison to the poor removal rates ( $<10\%$ ) exhibited by the pristine PES membrane. The enhanced membrane, surface charge property which resulted after the addition of hybrid MWCNTs is also considered an important technique used to assist ions removal via Donnan exclusion mechanism.

The use of functionalized MWCNTs was also reported by Madaeni et al. [55] wherein they embedded oxidized nanomaterials within PVDF-based membrane followed by polyacrylic acid (PAA) surface coating for Ni(II) removal. The mechanism of Ni(II) adsorption using oxidized MWCNTs is illustrated in Fig. 2.10. In contrast to most of the findings that have demonstrated the positive role of nanofillers in improving membrane water flux, the membrane incorporated with oxidized MWCNTs demonstrated the opposite result. The water flux adsorptive membrane was significantly affected, reducing from  $\sim 670 \text{ L/m}^2 \text{ h}$  in the pristine membrane to  $\sim 40 \text{ L/m}^2 \text{ h}$  upon addition  $0.05 \text{ wt.}\%$  oxidized MWCNTs into the membrane. It was explained that in situ polymerization of AA monomer into MWCNTs/PVDF membrane resulted in pore filling in the inter-CNT gaps, which consequently reduced pore void segment in membrane structure. Although the developed membrane aimed to remove Ni(II) ions from aqueous solution, its low adsorption capability (i.e.,  $5.3 \text{ mg/g}$ ) was not adequate for this purpose.

Chitosan's composition includes high contents of amine and hydroxyl groups and is one of the polymeric materials that can be used directly for the fabrication of adsorptive membranes for heavy-metal removal. Although these could be used as the active sites for the sorption of metal ions, the relatively weak mechanical strength and low porosity limit water application [56]. In order to address the issue, Ouyang et al. [57] immobilized different quantities of carboxyl-modified MWCNTs into chitosan-based membranes in order to improve the membrane's mechanical properties. With increasing carboxyl-modified MWCNTs/chitosan, the mass ratio went from zero to  $12 \text{ wt.}\%$ . The tensile strength of the resultant membrane was gradually increased from  $1.16$  to  $2.52 \text{ MPa}$ , owing to the strong interaction between polymer and nanotubes via the formation of hydrogen bonds and the strain-induced alignment of the CNTs in the chitosan membrane. The best



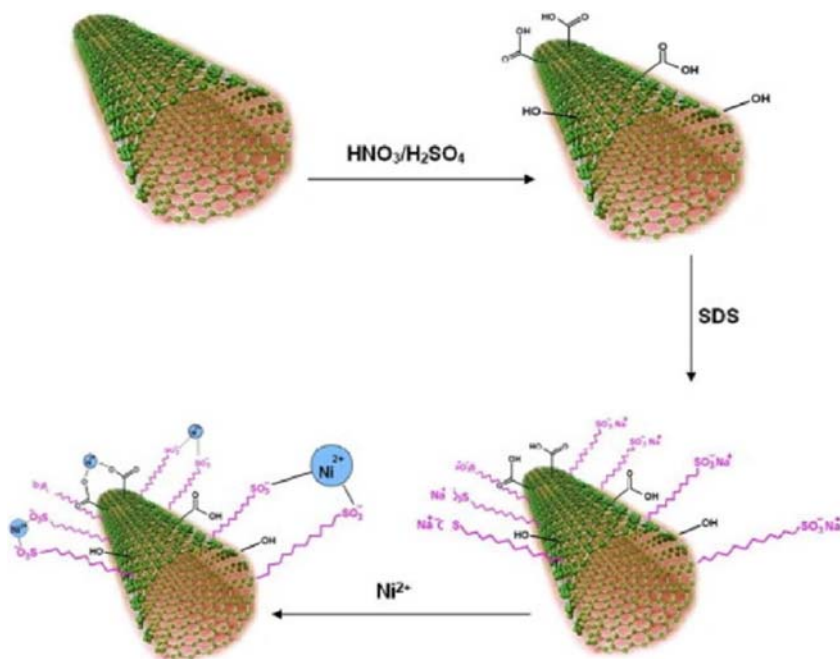


**FIGURE 2.10** Adsorptive mechanism for adsorption of oxidized MWCNTs toward  $\text{Ni}^{2+}$  ions [55].

performing membrane was able to achieve 126.7 mg/g adsorption rate against U(VI), which was significantly higher compared to the pristine chitosan membrane. The authors reported that acidified-ethylenediaminetetraacetic acid (EDTA) solution was an effective agent to regenerate the U(VI)-loaded, carboxyl-modified MWCNTs/chitosan membrane. This type of membrane could be reused for up to five times with less than 15% decrease in sorption capacity.

In addition to CNTs, another type of carbon-based nanomaterial that could also be considered for adsorbing heavy-metal ions is GO nanosheet. Kaleeklak et al. [58] modified PEI-based membranes using different concentrations of carboxylated GO (cGO) (0%, 0.075%, 0.15%, and 0.3%) and then used the developed membranes to remove not only metal ions but also HA. Through a carboxylation process, a substantial amount of  $-\text{COOH}$  group was introduced into the GO sheets, which improved the membrane hydrophilicity (by decrease in contact angle) and water flux upon incorporation. In addition to playing a role in removing metal ions via adsorption mechanism, the cGO was also found to enhance the membrane surface, negative-charge property that created greater repulsion between membrane surface and metal ion and improved removal rate. For the membrane embedded with 0.3%

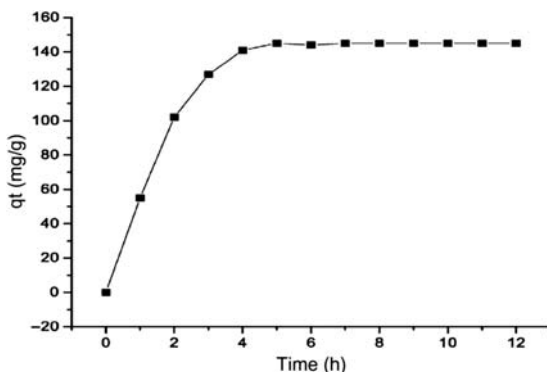


**FIGURE 2.11** Pb(II) ions adsorption of PES membrane incorporated with 0.25 wt.% PANi-coated GO [Initial Pb(II) ion: 200 mg/L and pH: 6] [59].

cGO, the results showed that at least 95.5% Ni(II) and 92.4% Cd(II) removal rates could be achieved. The higher removal rate of Ni(II) ion compared to Cd(II) is likely due to the presence of vacant *d*-orbitals, attributable to higher ligand stability of  $\text{Ni}^{2+}$ .

To further improve the characteristics of GO nanosheet for toxic-metal ion removal, Ghaemi et al. [59] performed in situ polymerization to coat the surface of GO with polyaniline (PANi). PANi is one of the polymeric adsorbents that can efficiently remove metal ions from water. The modification of GO nanosheet with this polymer followed by embedment into the membrane matrix can lead to a higher heavy-metal uptake. Fig. 2.11 presents the Pb(II) adsorption rate of PANi-GO-incorporated membranes as a function of time. As shown, the adsorption capacity of the membrane sharply increased in the first 2 h before the curve was gradually reduced from 2 to 5 h. Its capacity became almost constant after 5 h due to the saturation of adsorption sites of the membrane. The authors also confirmed that the Pb(II) adsorption onto the membrane follows the pseudo first-order kinetics model (i.e., the sorption only occurs on the local sites and the filling rate of the adsorption sites is proportional to the number of vacant sites available on the adsorbent). This sorption behavior is generally reported in other studies that focused on adsorptive membrane development.

Daraei et al. [60] also modified the surfaces of nanomaterials using PANi. The PANi-modified iron oxide ( $\text{Fe}_3\text{O}_4$ ) was then incorporated into PES membrane matrix for Cu(II) ion removal. Upon incorporation of optimum 0.1 wt.% PANi-modified  $\text{Fe}_3\text{O}_4$ , the resultant membranes could remove around 85% and 75% Cu(II) ions when tested with 20 and 5 mg/L  $\text{Cu}(\text{NO}_3)_2$  aqueous solution, respectively. Nevertheless, it must be noted that the equilibrium adsorption of the membrane against Cu(II) ions was extremely low ( $<1.6$  mg/g) and no explanation was given by the authors for the poor adsorption capability.

In a recent study, Koushkbaghi et al. [61] fabricated a new type of dual-layer MMMs in which nanofiber incorporated with aminated  $\text{Fe}_3\text{O}_4$  was established on the top surface of asymmetric-PES membrane. The resultant MMMs showed very promising results toward  $\text{Cr(VI)}$  and  $\text{Pb(II)}$  ions adsorption, recording 509.7 and 525.8 mg/g, respectively at optimum pH of 3 in a binary system. By increasing the thickness of nanofiber from 10 to 30  $\mu\text{m}$ , the metal ion removal rate of membrane could be further improved but with a reduction in water flux. The reusability of the MMMs was also demonstrated since the membrane could maintain high adsorption capability after three sequential runs.

Another type of metal-oxide nanoparticle that can also be used for fabrication of adsorptive microporous membrane is  $\text{TiO}_2$ . It is perhaps the most widely used nanoparticle for modifying the properties of UF membranes for water treatment process, mainly due to its hydrophilic nature and relatively low material cost. In the work conducted by Gebru and Das [34],  $\text{TiO}_2$  was modified using HMTA, EDA, and TEPA in an impregnation process and then used as additive to fabricate adsorptive CA-based membranes for enhanced removal of  $\text{Cr(VI)}$  ions. Fig. 2.12 shows the  $\text{Cr(VI)}$  removal rates of different types of membranes as a function of filtration time. It is clearly observed that the removal of  $\text{Cr(VI)}$  ions by the membranes is increased in the order of  $\text{CA/U-Ti} < \text{CA/Ti-HMTA} < \text{CA/Ti-EDA} < \text{CA/Ti-TEPA}$ . This result may be attributed to the different content and structure of the amine groups ( $\text{NH}_2$ – or  $\text{NH}$ –) within the membranes. CA/Ti-TEPA membrane

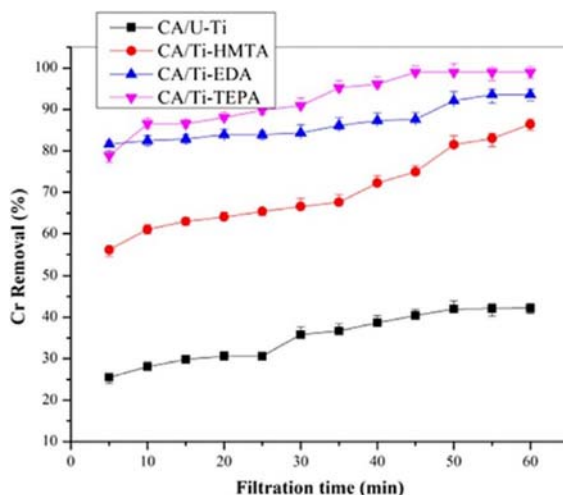


**FIGURE 2.12**  $\text{Cr(VI)}$  removal of CA membranes at pH 3.5 using initial ion concentration of 10 ppm at pressure of 150 kPa. (Note: U-Ti: unmodified  $\text{TiO}_2$ , Ti-HMTA/EDA/TEPA:  $\text{TiO}_2$  modified by HMTA, EDA, and TEPA, respectively) [34].

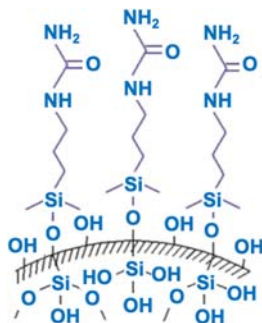


**FIGURE 2.13** Schematic representation of ureido-functionalized PVA/silica nanofiber membranes [62].

generally exhibited better adsorption capability due to the increased active sites that are available for Cr(VI) ions removal.

Instead of using metal-oxide nanoparticles, Zhou et al. [62] utilized non-metal oxide ( $\text{SiO}_2$ ) to synthesize nanofiber membranes for Pb(II) and Cu(II) adsorption. Fig. 2.13 illustrates the surface chemistry of the ureido-functionalized PVA/silica nanofiber membranes. The results indicated that the newly developed membranes possessed high brunauer-emmett-teller surface area of  $\sim 460 \text{ m}^2/\text{g}$  and good Pb(II) adsorption capability of  $\sim 27 \text{ mg/g}$ . However, the membrane capacity for adsorption of Cu(II) was rather poor ( $< 8 \text{ mg/g}$ ) due to the tendency to form chelating complexes with ureido groups.

Research has also shown that functionalized clay could be introduced into the polymeric membranes to improve not only their physicochemical properties (structure, hydrophilicity, water flux, and antifouling resistance) but also adsorption capability against heavy-metal ions. For instance, Hebbar et al. [63] reported that the membrane properties with respect to porosity, hydrophilicity, water flux, and heavy-metal adsorption capacity were improved upon incorporation of acid-activated bentonite clay. It was also shown that the higher the content of the clay in the membrane, the better the membrane flux and rejection. The best results achieved by the membrane incorporating 4 wt.% clay (determined based on the mass ratio of clay to PEI) was 69.3%, 76.2%, and 82.5% rejection for 250 ppm of Cd(II), Ni(II), and Cu(II) ion solutions, respectively. The authors hypothesized that both adsorption and sieving mechanism contributed to the removal of heavy-metal ions.

Using acid-activated montmorillonite, Mahmoudian et al. [64] fabricated a new type of MMMs, which exhibited good selectivity for the elimination of Zn(II) and Ni(II). In this work, the researchers evaluated the membrane performance against four different types of heavy-metal ions. However, the developed membrane only showed good removal rates for

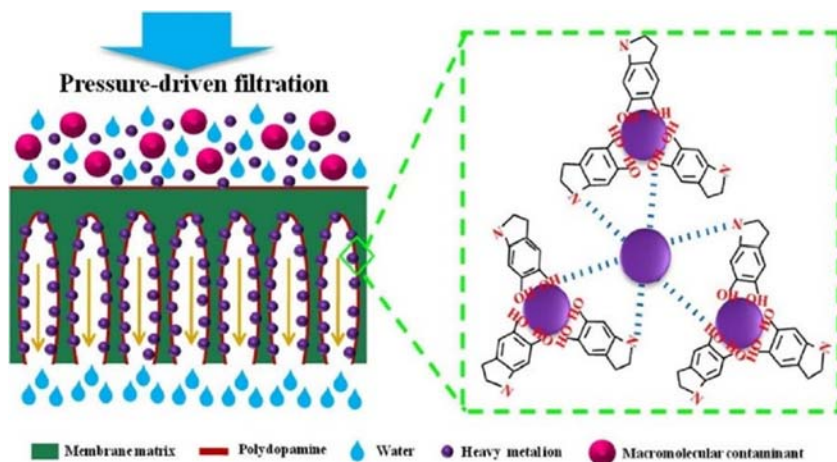


FIGURE 2.14 The possible mechanism of heavy-metal ions adsorbed on PDA membrane [65].

Zn(II) (up to 90%) and Ni(II) ions (75%) in comparison to the Cd(II) ( $\sim 60\%$ ) and Cu(II) ( $\sim 58\%$ ) ions. The findings revealed that the selectivity of adsorptive membrane against heavy-metal ions is strongly dependent on the nature of the adsorbent introduced.

Other functionalized nanomaterials that have also been utilized for fabricating adsorptive membranes are polydopamine (PDA) nanoparticles [65], HNT [66], and zeolite [49]. Fang et al. [65] deposited PDA nanoparticles onto the walls of UF membrane internal pores, aiming to improve membrane adsorption capacities for selective heavy-metal ions. Besides demonstrating ascendant BSA rejection (92.9%) and good pure water flux ( $166 \text{ L/m}^2 \text{ h}$ ), the PDA-incorporated PES membranes also showed reasonably favorable adsorption capacities for Pb(II), Cd(II), and Cu(II), recording 20.23, 17.01, and  $10.42 \text{ mg/g}$ , respectively. Fig. 2.14 illustrates the possible Pb(II) adsorption mechanisms of the developed membrane. The primary mechanisms involved electrostatic attraction between the catechol group and the metal ion, and the N atom in the  $\text{NH}_2$  groups sharing an electron pair to form a metal complex.

Although Bao et al. [49] and Hebbar et al. [66] also attempted to fabricate adsorptive membrane for heavy-metal removal, their findings were not very promising. The adsorption capacities for Cu(II) and Cr(VI) on the membrane incorporating amine-functionalized MCM-41 were only 3.7 and  $2.8 \text{ mg/g}$ , respectively, as reported in the work of Bao et al. [49]. Hebbar et al. [66] were only able to remove 34% Pb(II) and 27% Cd(II) from the feed solution using polydopamine functionalized HNT/PEI membrane. The findings revealed that the selection of nanomaterials is critical during adsorptive membrane fabrication. The ideal nanomaterials should exhibit

high adsorption capacity, large-surface area, and good compatibility with polymeric membrane.

## 2.6 Conclusion and future remarks

Microporous UF membranes have been used for industrial water and wastewater treatment for more than 50 years. Over the past 10 years, we have seen a large number of studies demonstrating the positive impacts of using inorganic nanomaterials for improving the intrinsic properties of UF membranes made of common-polymeric materials such as PES, PSF, PVDF, and PAN. In most cases, it was reported that upon incorporation of nanomaterials into the membrane matrices, the trade-off effect between water permeability and solute rejection of the membranes could be overcome. Depending on the nature of the embedded nanomaterials, additional features such as antifouling properties, antibacterial resistance, and adsorptive capacities were demonstrated. Despite significant progress, more research is still required. To the best of our knowledge, no commercial MMMs are currently available for water treatment applications. Several challenges need to be addressed before such membranes can reach the commercialization level. These include the long-term stability of the nanomaterials embedded within the membrane matrices, manufacturing cost of the MMMs, and their mechanical properties.

## References

- [1] Ng LY, Mohammad AW, Leo CP, Hilal N. Polymeric membranes incorporated with metal/metal oxide nanoparticles: a comprehensive review. *Desalination* 2013;308:15–33.
- [2] Tripathi N, Rath S. Facile synthesis of ZnO nanostructures and investigation of structural and optical properties. *Mater Charact* 2013;86:263–9.
- [3] Hussain CM. *Handbook of nanomaterials for industrial applications*. Elsevier B.V.; 2018.
- [4] Hussain BKCM. *Advanced environmental analysis-application of nanomaterials*. The Royal Society of Chemistry; 2017.
- [5] Malhotra BD, Ali MA, Malhotra BD, Ali MA. Nanomaterials in biosensors: fundamentals and applications. *Nanomater Biosens* 2018;1–74.
- [6] Becaro AA, Jonsson CM, Puti FC, Siqueira MC, Mattoso LHC, Correa DS, et al. Toxicity of PVA-stabilized silver nanoparticles to algae and microcrustaceans. *Environ Nanotechnol, Monit Manag* 2015;3:22–9.
- [7] Murphy M, Ting K, Zhang X, Soo C, Zheng Z. Current development of silver nanoparticle preparation, investigation, and application in the field of medicine. *J Nanomater* 2015;2015:1–12.
- [8] Gray S, Tsuru T, Cohen Y, Lau W-J. *Advanced materials for membrane fabrication and modification*. CRC Press; 2018.
- [9] Lau W-J, Ismail AF, Isloor A, Al-Ahmed A. *Advanced nanomaterials for membrane synthesis and its applications*. Elsevier B.V.; 2019.
- [10] Qadir D, Mukhtar H, Keong LK. Mixed matrix membranes for water purification applications. *Sep Purif Rev* 2017;46:62–80.

- [11] Li X, Fang X, Pang R, Li J, Sun X, Shen J, et al. Self-assembly of TiO<sub>2</sub> nanoparticles around the pores of PES ultrafiltration membrane for mitigating organic fouling. *J Memb Sci* 2014;467:226–35.
- [12] Ayyaru S, Ahn Y. Fabrication and separation performance of polyethersulfone/sulfonated TiO<sub>2</sub> (PES–STiO<sub>2</sub>) ultrafiltration membranes for fouling mitigation. *J Ind Eng Chem* 2018;67:199–209.
- [13] Huang L, Zhao S, Wang Z, Wu J, Wang J, Wang S. In situ immobilization of silver nanoparticles for improving permeability, antifouling and anti-bacterial properties of ultrafiltration membrane. *J Memb Sci* 2016;499:269–81.
- [14] Mahmoudi E, Ng LY, Ba-Abbad MM, Mohammad AW. Novel nanohybrid polysulfone membrane embedded with silver nanoparticles on graphene oxide nanoplates. *Chem Eng J* 2015;277:1–10.
- [15] Chung YT, Ba-Abbad MM, Mohammad AW, Benamor A. Functionalization of zinc oxide (ZnO) nanoparticles and its effects on polysulfone-ZnO membranes. *Desalin Water Treat* 2016;57:7801–11.
- [16] Raghupathi KR, Koodali RT, Manna AC. Size-dependent bacterial growth inhibition and mechanism of antibacterial activity of zinc oxide nanoparticles. *Langmuir* 2011;27:4020–8.
- [17] Ursino C, Castro-Muñoz R, Drioli E, Gzara L, Albeirutty MH, Figoli A. Progress of nanocomposite membranes for water treatment. *Membranes (Basel)*, 8. 2018. p. 1–40.
- [18] Zhao DL, Chung TS. Applications of carbon quantum dots (CQDs) in membrane technologies: a review. *Water Res* 2018;147:43–9.
- [19] De Volder MF, Tawfick S, Baughman R, Hart A. Carbon nanotubes: present and future commercial applications. *Science* 2013;339:535–9.
- [20] Fontananova E, Grosso V, Aljlil SA, Bahattab MA, Vuono D, Pasquale F, et al. Effect of functional groups on the properties of multiwalled carbon nanotubes/polyvinylidene fluoride composite membranes. *J Memb Sci* 2017;541:198–204.
- [21] Ho KC, Teow YH, Ang WL, Mohammad AW. Novel GO/OMWCNTs mixed-matrix membrane with enhanced antifouling property for palm oil mill effluent treatment. *Sep Purif Technol* 2017;177:337–49.
- [22] Dudchenko AV, Rolf J, Russell K, Duan W, Jassby D. Organic fouling inhibition on electrically conducting carbon nanotube – polyvinyl alcohol composite ultra filtration membranes. *J Memb Sci* 2014;468:1–10.
- [23] Wang W, Zhu L, Shan B, Xie C, Liu C, Cui F, et al. Preparation and characterization of SLS-CNT/PES ultrafiltration membrane with antifouling and antibacterial properties. *J Memb Sci* 2018;548:459–69.
- [24] Khalid A, Abdel-Karim A, Ali Atieh M, Javed S, McKay G. PEG-CNTs nanocomposite PSU membranes for wastewater treatment by membrane bioreactor. *Sep Purif Technol* 2018;190:165–76.
- [25] Lee J, Chae H-R, Won YJ, Lee K, Lee C-H, Lee HH, et al. Graphene oxide nanoplatelets composite membrane with hydrophilic and antifouling properties for wastewater treatment. *J Memb Sci* 2013;448:223–30.
- [26] Zhao C, Xu X, Chen J, Wang G, Yang F. Highly effective antifouling performance of PVDF/graphene oxide composite membrane in membrane bioreactor (MBR) system. *Desalination* 2014;340:59–66.
- [27] You Y, Jin XH, Wen XY, Sahajwalla V, Chen V, Bustamante H, et al. Application of graphene oxide membranes for removal of natural organic matter from water. *Carbon N Y* 2018;129:415–19.



- [28] Chung YT, Mahmoudi E, Mohammad AW, Benamor A, Johnson D, Hilal N. Development of polysulfone-nanohybrid membranes using ZnO-GO composite for enhanced antifouling and antibacterial control. *Desalination* 2017;402:123–32.
- [29] Chong WC, Mahmoudi E, Chung YT, Koo CH, Mohammad AW, Kamarudin KF. Improving performance in algal organic matter filtration using polyvinylidene fluoride – graphene oxide nanohybrid membranes. *Algal Res* 2017;27:32–42.
- [30] Chan W, Mahmoudi E, Tao Y, Ba-abbad MM. Polyvinylidene fluoride membranes with enhanced antibacterial and low fouling properties by incorporating ZnO/rGO composites. *Desalination and Water Treatment* 2017;20742.
- [31] Chong WC, Chung YT, Teow YH, Zain MM, Mahmoudi E, Mohammad AW. Environmental impact of nanomaterials in composite membranes: life cycle assessment of algal membrane photoreactor using polyvinylidene fluoride – composite membrane. *J Clean Prod* 2018;202:591–600.
- [32] Li X, Li J, Fang X, Bakzhan K, Wang L, Van der Bruggen B. A synergetic analysis method for antifouling behavior investigation on PES ultrafiltration membrane with self-assembled TiO<sub>2</sub> nanoparticles. *J Colloid Interface Sci* 2016;469:164–76.
- [33] Lee E, Kyoungjin A, Hadi P, Lee S, Chul Y. Advanced multi-nozzle electrospun functionalized titanium dioxide/composite membranes for direct contact membrane distillation. *J Memb Sci* 2017;524:712–20.
- [34] Gebru KA, Das C. Removal of chromium (VI) ions from aqueous solutions using amine-impregnated TiO<sub>2</sub> nanoparticles modified cellulose acetate membranes. *Chemosphere* 2018;191:673–84.
- [35] Najafi M, Yousefi Y, Rafati AA. Synthesis, characterization and adsorption studies of several heavy metal ions on amino-functionalized silica nano hollow sphere and silica gel. *Sep Purif Technol* 2012;85:193–205.
- [36] Hao S, Zhong Y, Pepe F, Zhu W. Adsorption of Pb<sup>2+</sup> and Cu<sup>2+</sup> on anionic surfactant-templated amino-functionalized mesoporous silicas. *Chem Eng J* 2012;189–190:160–7.
- [37] Sumisha A, Arthanareeswarana G, Ismail AF, Kumar DP, Shankar MV. Functionalized titanate nanotube-polyetherimide nanocomposite membrane for improved salt rejection under low pressure nanofiltration. *RSC Adv* 2015;5:39464–73.
- [38] Zeng G, He Y, Yu Z, Zhan Y, Ma L, Zhang L. Preparation and characterization of a novel PVDF ultrafiltration membrane by blending with TiO<sub>2</sub>-HNTs nanocomposites. *Appl Surf Sci* 2016;371:624–32.
- [39] Mishra G, Mukhopadhyay M. Flux improvement, rejection, surface energy and antibacterial properties of synthesized TiO<sub>2</sub>-Mo.HNTs/PVC nanocomposite ultrafiltration membranes. *N J Chem* 2017;41:15049–57.
- [40] Salimi M, Pirouzfard V. Preparation and characterization of a novel MMMs by comprising of PSF–HNT/TiO<sub>2</sub> nanotubes to reduce organic sediments. *Polym Bull* 2018;75:2285–99.
- [41] Alsohaimi IH, Kumar M, Algamdi MS, Khan MA, Nolan K, Lawler J. Antifouling hybrid ultrafiltration membranes with high selectivity fabricated from polysulfone and sulfonic acid functionalized TiO<sub>2</sub> nanotubes. *Chem Eng J* 2017;316:573–83.
- [42] Bidsorkhi H, Riaz H, Emadzadeh D. Preparation and characterization of a novel highly hydrophilic and antifouling polysulfone/nanoporous TiO<sub>2</sub> nanocomposite membrane. *Nanotechnology* 2016;27:415706.
- [43] Hu T, Liu Q, Gao T, Dong K, Wei G, Yao J. Facile preparation of tannic acid-poly(vinyl alcohol)/sodium alginate hydrogel beads for methylene blue removal from simulated solution. *ACS Omega* 2018;3:7523–31.



- [44] Fang X, Li J, Li X, Pan S, Sun X, Shen J, et al. Iron-tannin-framework complex modified PES ultrafiltration membranes with enhanced filtration performance and fouling resistance. *J Colloid Interface Sci* 2017;505:642–52.
- [45] Nayak S, Kobielska PA, Howarth AJ, Farha OK. Metal–organic frameworks for heavy metal removal from water. *Coord Chem Rev* 2018;358:92–107.
- [46] Sun H, Tang B, Wu P. Hydrophilic hollow zeolitic imidazolate framework-8 modified ultrafiltration membranes with significantly enhanced water separation properties. *J Memb Sci* 2018;551:283–93.
- [47] Sun H, Tang B, Wu P. Development of hybrid ultrafiltration membranes with improved water separation properties using modified superhydrophilic metal-organic framework nanoparticles. *ACS Appl Mater Interfaces* 2017;9:21473–84.
- [48] Díez B, Roldán N, Martín A, Sotto A, Perdigón-melón JA. Fouling and biofouling resistance of metal-doped mesostructured silica/polyethersulfone ultrafiltration membranes. *J Memb Sci* 2017;526:252–63.
- [49] Bao Y, Yan X, Du W, Xie X, Pan Z, Zhou J, et al. Application of amine-functionalized MCM-41 modified ultrafiltration membrane to remove chromium (VI) and copper (II). *Chem Eng J* 2015;281:460–7.
- [50] Nasrollahi N, Aber S, Vatanpour V, Mahmoodi NM. The effect of amine functionalization of CuO and ZnO nanoparticles used as additives on the morphology and the permeation properties of polyethersulfone ultrafiltration nanocomposite membranes. *Compos Part B Eng* 2018;154:388–409.
- [51] Zheng YM, Zou SW, Nanayakkara KGN, Matsuura T, Chen JP. Adsorptive removal of arsenic from aqueous solution by a PVDF/zirconia blend flat sheet membrane. *J Memb Sci* 2011;374:1–11.
- [52] W.-J. Lau, D. Emadzadeh, S. Shahrin, P.S. Goh and A.F. Ismail, Chapter 9 – Ultrafiltration membranes incorporated with carbon-based nanomaterials for antifouling improvement and heavy metal removal, *Carbon-Based Polymer Nanocomposites for Environmental and Energy Application*, Elsevier, 2019, 217–232.
- [53] Shah P, Murthy CN. Studies on the porosity control of MWCNT/polysulfone composite membrane and its effect on metal removal. *J Memb Sci* 2013;437:90–8.
- [54] Masheane ML, Nthunya LN, Malinga SP, Nxumalo EN, Mamba BB, Mhlana SD. Synthesis of Fe-Ag/f-MWCNT/PES nanostructured-hybrid membranes for removal of Cr (VI) from water. *Sep Purif Technol* 2017;184:79–87.
- [55] Madaeni SS, Zinadini S, Vatanpour V. Convective flow adsorption of nickel ions in PVDF membrane embedded with multi-walled carbon nanotubes and PAA coating. *Sep Purif Technol* 2011;80:155–62.
- [56] Seo SJ, Kim JJ, Kim JH, Lee JY, Shin US, Lee EJ, et al. Enhanced mechanical properties and bone bioactivity of chitosan/silica membrane by functionalized-carbon nanotube incorporation. *Compos Sci Technol* 2014;96:31–7.
- [57] Ouyang J, Wang Y, Li T, Zhou L, Liu Z. Immobilization of carboxyl-modified multi-walled carbon nanotubes in chitosan-based composite membranes for U(VI) sorption. *J Radioanal Nucl Chem* 2018;317:1419–28.
- [58] Kaleekkal NJ, Thanigaivelan A, Rana D, Mohan D. Studies on carboxylated graphene oxide incorporated polyetherimide mixed matrix ultrafiltration membranes. *Mater Chem Phys* 2017;186:146–58.
- [59] Ghaemi N, Zereshti S, Heidari S. Removal of lead ions from water using PES-based nanocomposite membrane incorporated with polyaniline modified GO nanoparticles: performance optimization by central composite design. *Process Saf Env Prot* 2017;111:475–90.

- [60] Daraei P, Madaeni SS, Ghaemi N, Salehi E, Khadivi MA, Moradian R, et al. Novel polyethersulfone nanocomposite membrane prepared by PANI/Fe<sub>3</sub>O<sub>4</sub> nanoparticles with enhanced performance for Cu(II) removal from water. *J Memb Sci* 2012;415–416:250–9.
- [61] Koushkbaghi S, Zakialamdari A, Pishnamazi M, Ramandi HF, Aliabadi M, Irani M. Aminated-Fe<sub>3</sub>O<sub>4</sub> nanoparticles filled chitosan/PVA/PES dual layers nanofibrous membrane for the removal of Cr(VI) and Pb(II) ions from aqueous solutions in adsorption and membrane processes. *Chem Eng J* 2018;337:169–82.
- [62] Zhou M, Tang W, Luo P, Lyu J, Chen A, Qiao L, et al. Preparation of ureido-functionalized PVA/silica mesoporous fibre membranes via electrospinning for adsorption of Pb<sup>2+</sup> and Cu<sup>2+</sup> in wastewater. *Water Sci Technol* 2017;76:2526–34.
- [63] Hebbar RS, Isloor AM, Ismail AF. Preparation and evaluation of heavy metal rejection properties of polyetherimide/porous activated bentonite clay nanocomposite membrane. *RSC Adv* 2014;4:47240–8.
- [64] Mahmoudian M, Balkanloo PG, Nozad E. A facile method for dye and heavy metal elimination by pH sensitive acid activated montmorillonite/polyethersulfone nanocomposite membrane. *Chin J Polym Sci (Engl Ed)* 2018;36:49–57.
- [65] Fang X, Li J, Li X, Pan S, Zhang X, Sun X, et al. Internal pore decoration with polydopamine nanoparticle on polymeric ultrafiltration membrane for enhanced heavy metal removal. *Chem Eng J* 2017;314:38–49.
- [66] Hebbar RS, Isloor AM, Ananda K, Ismail AF. Fabrication of polydopamine functionalized halloysite nanotube/polyetherimide membranes for heavy metal removal. *J Mater Chem A* 2016;4:764–74.

This page intentionally left blank

## Section 2

# **Functionalized nanomaterial for catalysis industry**

This page intentionally left blank

## Chapter 3

# Photocatalytic oxygen evolution reaction for energy conversion and storage of functional nanomaterials

K. Kaviyarasu<sup>1,2</sup>, C. Maria Magdalane<sup>3,4</sup>, A. Raja<sup>5</sup>, N. Matinise<sup>1,2</sup>,  
N. Mayedwa<sup>1,2</sup>, N. Mongwaketsi<sup>1,2</sup>, Douglas Letsholathebe<sup>6</sup>,  
G.T. Mola<sup>7</sup>, Naif Abdullah Al-Dhabi<sup>8</sup>, Mariadhas Valan Arasu<sup>8</sup>,  
G. Ramalingam<sup>9</sup>, S.B. Mohamed<sup>10</sup>, Abdugali B. Isaev<sup>11</sup>,  
K. Kanimozhi<sup>12</sup>, A.K.H. Bashir<sup>1,2</sup>, J. Kennedy<sup>1,13</sup> and M. Maaza<sup>1,2</sup>

<sup>1</sup>UNESCO-UNISA Africa Chair in Nanosciences/Nanotechnology Laboratories, College of Graduate Studies, University of South Africa (UNISA), Pretoria, South Africa, <sup>2</sup>Nanosciences African Network (NANOAFNET), Materials Research Department (MRD), iThemba LABS-National Research Foundation (NRF), Western Cape Province, South Africa, <sup>3</sup>Department of Chemistry, St. Xavier's College (Autonomous), Tirunelveli, India, <sup>4</sup>LIFE, Department of Chemistry, Loyola College (Autonomous), Chennai, India, <sup>5</sup>Department of Physics, Kalasalingam Institute of Technology, Krishnan Koil, India, <sup>6</sup>Department of Physics, University of Botswana, Gaborone, Botswana, <sup>7</sup>School of Chemistry Physics, University of KwaZulu-Natal, Pietermaritzburg Campus, Scottsville, South Africa, <sup>8</sup>Addiriyah Chair for Environmental Studies, Department of Botany and Microbiology, College of Science, King Saud University, Riyadh, Saudi Arabia, <sup>9</sup>Department of Nanoscience and Technology, Alagappa University, Karaikudi, India, <sup>10</sup>Department of Materials Science, Central University of Tamil Nadu, Thiruvavur, India, <sup>11</sup>Department of Environmental Chemistry and Technology, Dagestan State University, Makhachkala, Russian Federation, <sup>12</sup>Department of Chemistry, Auxilium College (Autonomous), Vellore, India, <sup>13</sup>National Isotope Centre, GNS Science, Lower Hutt, New Zealand

### 3.1 Introduction

Rare earth metal oxides have been used extensively in various applications such as environmental, energy, and biomedical services due to their specific properties such as grain size, elemental configuration, and self-organized structures [1–3]. Current research focuses on cerium oxide nanostructure, due to the low energy bandgap between  $\text{Ce}^{3+}$  and  $\text{Ce}^{4+}$  states in cerium oxide along with their high oxygen mobility and high oxygen storage

capacity [4]. These properties make them suitable for applications in various fields, as gas sensors, optoelectronics, catalysts, fuel cells, and solid-state electrolytes [5]. There is numerous technically projected synthesis of nano-sized ceria such as heterogeneous catalysts by chemical redox reaction, thermal approach, sonochemical method, hydrothermal method, sol-gel process, and self-assembled nanoproceses [6]. Among these, the hydrothermal method is widely used, because of the formation of homogenous nanopowder as the initial product with a fine grain size [7,8]. In general, the photocatalytic efficiency increases by incorporating the heterostructures [9]. Because, heterocomposites prepared can fine tune the electronic properties of the photocatalyst by separating the electron-hole pairs in an efficient manner.

CeO<sub>2</sub> with transitional metal oxide (TMO) have gained much attention because of their attractive optical possessions and photogenerated charge carriers, which may be enhanced in the CeO<sub>2</sub> matrix [10–12]. The exceptional nanostructure morphology and mesoporous nature of cerium with 3d transitional metal ions (TMO) allowed them to become a solar material [13]. When the transition metal ion in lower valance state than 4<sup>+</sup> is collectively dispersed into the ceria matrix, the arrangement of atoms becomes dense and this changes the electronic conductivity of metal ions [14,15]. However, to enhance various properties of CeO<sub>2</sub> nanomaterials, it is desirable to condense the atom size and enhance the growth of the energetic superficial zone [16]. A decrease in particle size augments the electrical conductivity and sensing and catalytic properties of nanomaterials [17]. Here a simple chemical precipitation assisted hydrothermal method without any surfactant has been a cause of stimulation of cerium, cadmium multifaceted nanomaterials with higher surface area and the effective claims [18,19]. This simple method is alternative to the chemical methods with surfactant which are very costly as well as emit hazardous byproducts which can have adverse effect on the environment [20]. Therefore we tried to fabricate CeO<sub>2</sub>/CdO nanomaterials with high active surface area and less particle size using cost effective hydrothermal method [21,22]. In polluted waste waters elimination of organic dye contaminants is necessary, because of the nonbiodegradable nature of the pollutants [23]. Toxic organic dye degradation using semiconducting materials in the existence of UV/visible light studied worldwide [24]. Convention of herbicides, pesticides, and various synthetic dyes are widely polluting the environment [25–28].

The organic pollutant like Rhodamine-B (RhB) dye has been used in productions and in our day-to-day life and the RhB dye produces carcinogens like aminobenzene [29]. The contamination of the physical and biological components of the earth/atmosphere system to such an extent that normal environmental processes are adversely affected [30]. Hence highly carcinogenic organic compounds and their detoxification are critical to the situation and this development converts existing research to preserve human health and security [31]. Thus an efficient method to discard these organic contaminants from the

various waste materials is needed [32]. The photocatalytic degradation (PCD) of toxic organic dyes using catalyst such as  $\text{TiO}_2$ ,  $\text{ZnO}$ ,  $\text{CuO}$ ,  $\text{CeO}_2$ , etc., in UV/visible and xenon beams source is considered a highly effective method [33,34]. Among the various photocatalysts, cerium oxide-containing transition metal oxides have proven to be very efficient. Rare earth/transition metal oxide is easier to recover from aqueous systems due to its higher molecular weight [35]. To understand the formation of heterostructured  $\text{CeO}_2/\text{CdO}$  binary metal oxide nanostructure, it is necessary to examine the influences of the preparation conditions [36]. Since this is not dealt with much in the literature, here we analyze the influence of preparation parameters on the synthesis of heterostructured  $\text{CeO}_2/\text{CdO}$  binary metal oxide nanostructures [37,38]. The exact mechanism of the degradation of dyes by nanostructures is important to understand, but the pathway of decomposition of synthetic dye during the whole process is still not clear and more investigations are needed to characterize the various properties of  $\text{CeO}_2/\text{CdO}$  multilayered nanomaterials [39]. Hence, in this present work, we prepared a binary metal oxide  $\text{CeO}_2/\text{CdO}$  nanostructure with almost uniform size of clusters by hydrothermal technique in different ratios, which were studied for the decomposition of water source and organic dye in aqueous system illuminated with UV/visible light [40]. Also, the synthesized nanomaterial with small grain size and large active surface area was examined against A549 (human lung epithelial cell).

### 3.1.1 Structural investigation of $\text{CeO}_2/\text{CdO}$ nanostructures

The X-ray diffraction (XRD) of the chemical precipitation followed hydrothermal technique synthesized  $\text{CeO}_2$ ,  $\text{CdO}$ , and  $\text{CeO}_2/\text{MO}$  binary metal oxide in 1:1, 2:1, and 1:2 molar ratios correspondingly is shown in Fig. 3.1A. All the peaks can be assigned to either  $\text{CeO}_2$  or  $\text{CdO}$  phase and there are no other new phases. This high-purity binary metal oxides reveal that the major peaks of  $\text{CeO}_2$  has  $2\theta = 28.70, 33.08, 47.51, 56.44, 59.08, 69.47, 76.70$ , and  $79.07$  degrees corresponding to the (111), (200), (220), (311), (222), (400), (331), and (420) planes and has cubic fluorite structure in which each metal cation is surrounded by eight oxygen atoms (space group  $\text{Fm-3m}$  JCPDS Card No. 34-0394).  $\text{CeO}_2$  shows a dominant and high intense peak on (111) plane, which needs high energy to form oxygen vacancies on (111) planes than the less intense peak and they are highly stable. There was no evidence of the presence of  $\text{Ce}_2\text{O}_3$  phase. The diffraction peaks at  $2\theta$  values of  $33.08, 38.43, 55.31, 65.90$ , and  $69.28$  degrees correspond to pure  $\text{CdO}$  matching the (111), (200), (220), (311), and (222) planes with cubic structure (JCPDS Card No. 05-0640), thus indicating the formation of  $\text{CeO}_2/\text{CdO}$  nanostructure with excellent crystalline nature. The strength and locations of the peaks are in perfect arrangement with the literature values. The decrease in the



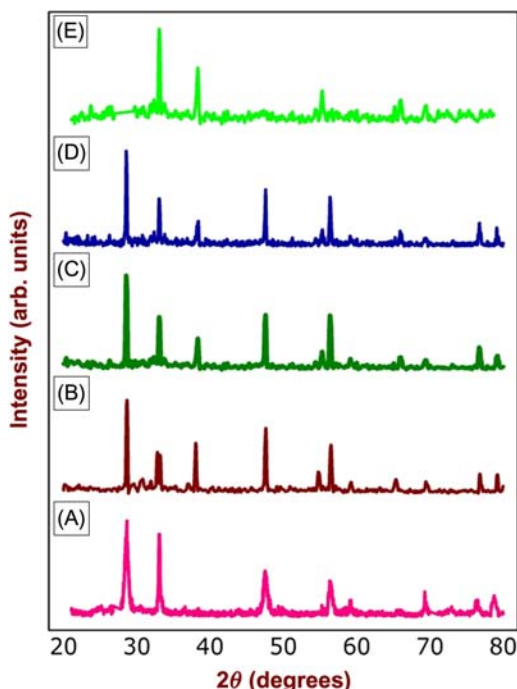


**FIGURE 3.1** X-ray diffraction pattern of synthesized  $\text{CeO}_2/\text{CdO}$  nanostructures: (A) pure ceria (B)  $\text{Ce}_1/\text{Cd}_1$  (C)  $\text{Ce}_2/\text{Cd}_1$  (D)  $\text{Ce}_1/\text{Cd}_2$ , and (E) pure  $\text{CdO}$ .

intensity of  $\text{CdO}$  peaks indicates that  $\text{CeO}_2$  is formed on  $\text{CdO}$  surface and the increase in the ceria peak intensity suggests the larger crystallite sizes.

The XRD pattern of the sample shows no satellite peaks belonging to  $\text{Ce}(\text{OH})_3$  and hexagonal  $\text{Ce}_2\text{O}_3$ , thus indicating a complete conversion of the sample into cubic fluorite ceria. The crystallite size of metal oxides was calculated using Debye–Scherer’s formula  $D = 0.9\lambda/\beta\cos\theta$ , where “ $D$ ” is the crystallite size,  $\lambda$  the wavelength of X-rays,  $\theta$ , the Bragg diffraction angle, and  $\beta$ , the full-width at half-maximum (FWHM) of the diffraction peak. The  $\text{CeO}_2/\text{CdO}$  nanostructures showed only cubic phase, which confirms the composition of  $\text{CeO}_2$  and  $\text{CdO}$  in the heterostructure, and it is in good agreement with early reported work. To establish charge balance, extra positive ions must be introduced into the grain surface. Therefore the  $\text{CeO}_2$  and  $\text{CdO}$  are in the form of composites rather than as solid solution.

### 3.1.2 Fourier transform infrared spectroscopy

The Fourier transform infrared spectrum of  $\text{CeO}_2$  mixed with  $\text{CdO}$  heterostructured binary nanostructures in different ratios (1:1, 1:2, and 2:1) is shown in Fig. 3.2A in the wavelength range of  $3700\text{--}400\text{ cm}^{-1}$ . The extensive band

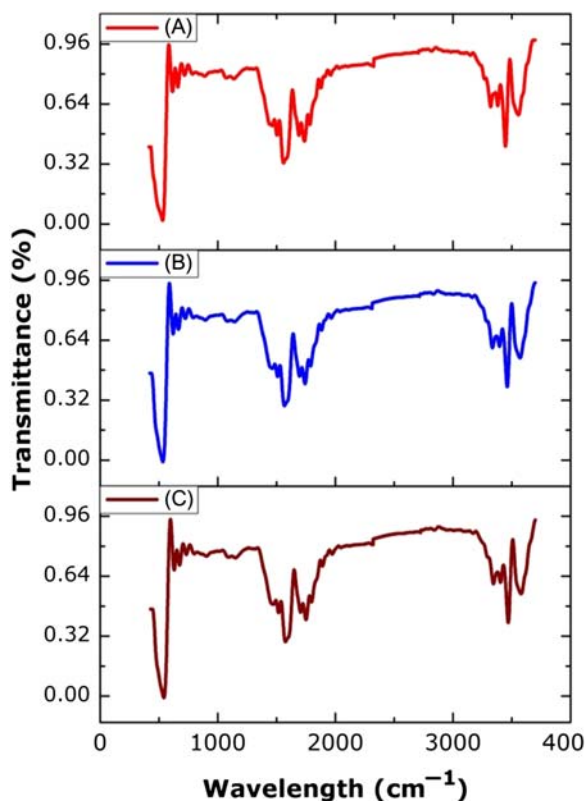


**FIGURE 3.2** FTIR spectra of  $\text{CeO}_2/\text{CdO}$  nanostructures: (A)  $\text{Ce}_1/\text{Cd}_1$  (B)  $\text{Ce}_2/\text{Cd}_1$ , and (C)  $\text{Ce}_1/\text{Cd}_2$ .

in the range of  $3600\text{ cm}^{-1}$  is due to the OH stretching of water molecules [41]. The broad peak at  $450\text{--}700\text{ cm}^{-1}$  is due to the characteristic stretching of Ce—O bond and the frequency is reduced due to the formation of mixed binary metal oxide [42]. The peaks at  $800\text{--}1500\text{ cm}^{-1}$  are assigned to CdO [23,43]. The band at low-frequency regions below  $1400\text{ cm}^{-1}$  corresponds to the formation of doped  $\text{CeO}_2/\text{CdO}$  nanomaterial. The absorption peaks between  $1500$  and  $1700\text{ cm}^{-1}$  are attributed to the twisting vibration of the adsorbed  $\text{H}_2\text{O}$  molecules [44].

### 3.1.3 Field emission scanning electron microscopy studies

The comprehensive superficial morphology and effect of size and shape of  $\text{CeO}_2$  mixed with CdO in different molar ratios (1:1, 1:2, and 2:1) were examined by field emission scanning electron microscopy (FESEM) analysis. All the synthesized samples with different molar ratios form different

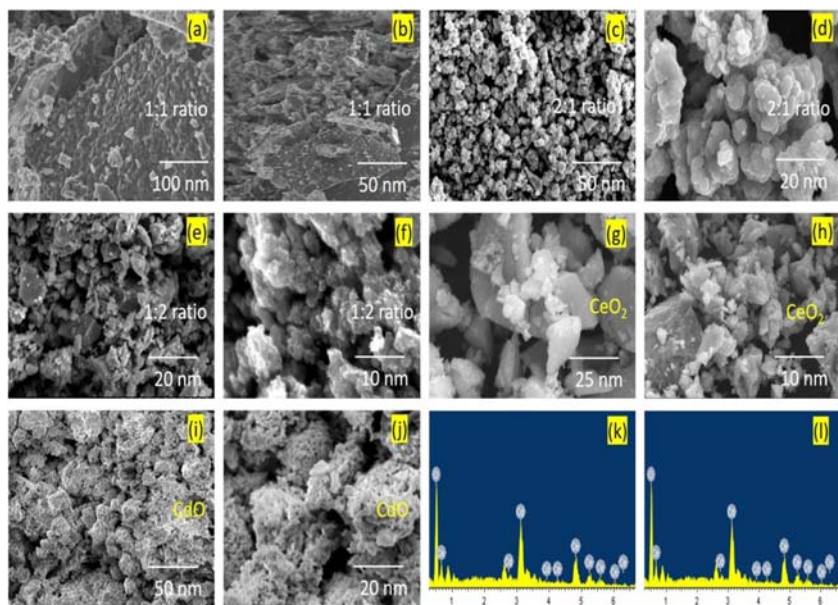


**FIGURE 3.3** Morphology evolution of  $\text{CeO}_2/\text{CdO}$  nanostructures: (A, B)  $\text{Ce}_1/\text{Cd}_1$  (C, D)  $\text{Ce}_2/\text{Cd}_1$  (E, F)  $\text{Ce}_1/\text{Cd}_2$  (G, H) pure ceria (I, J) pure  $\text{CdO}$ , and (K, L) EDX spectrum.

microstructures. Field emission scanning electron micrographs of  $\text{CeO}_2/\text{CdO}$  nanostructures at different magnifications for the prepared samples by hydrothermal method are presented in Fig. 3.3A–L. Fig. 3.3G and H shows that the FESEM images of  $\text{CeO}_2$  are highly porous material with irregular shapes. Fig. 3.3I and J shows the surface morphology of  $\text{CdO}$ , which has agglomerated crystal phases. The FESEM images in Fig. 3.3A and B of binary metal oxide  $\text{Ce}_1/\text{Cd}_1$  nanostructure have spherical and heterogeneous phase distribution with more cavities. The particle size is in the range of 15–40 nm with good porous morphology. Fig. 3.3C and D shows that the FESEM microstructures of  $\text{Ce}_2/\text{Cd}_1$  binary metal oxide have small spherical shape nanoparticles with aggregated morphology. The particle sizes are in the range of 5–30 nm, respectively. A small variation was identified by FESEM and XRD, since FESEM calculations are based on the difference between the visible grain boundaries, whereas XRD calculations measure the extended crystalline region that diffracts X-rays coherently [43]. The FESEM images of  $\text{Ce}_1/\text{Cd}_2$  binary metal oxide show that the particle is aggregated, which is due to the excess of cadmium metal oxide shown in Fig. 3.3E and F. The minimum changes in the particles size could be due to the particle aggregation [45]. Due to the morphological evolution of  $\text{CeO}_2/\text{CdO}$  nano structures with different conditions. Elemental analysis was done along with FESEM using the EDX technique. EDX analysis revealed the

peaks of the elements in the nanostructure. This data helped to ensure that the cerium oxide and cadmium oxide synthesized by various routes resulted in CeO<sub>2</sub>/CdO nanostructures. The EDX spectra showed no other elements, thus confirming the purity of the phase in the composite [46]. It is in good agreement with the XRD analysis.

### 3.1.4 High-resolution transmission electron microscopy studies

The microstructures of the CeO<sub>2</sub>, CdO, and CeO<sub>2</sub>/CdO nanomaterials in different ratios (1:1 and 2:1) were analyzed by high-resolution transmission electron microscope (HRTEM). Pure CeO<sub>2</sub> and CdO metal oxides have an irregular shape as shown in Fig. 3.4A and F. Fig. 3.4G–J shows the HRTEM images of Ce<sub>2</sub>/Cd<sub>1</sub> nanostructure and Fig. 3.4B–E shows the HRTEM images of Ce<sub>1</sub>/Cd<sub>1</sub> nanostructure prepared by hydrothermal method, and the selected area of electron diffraction pattern is shown in Fig. 3.4E and J. The fine particle is the aggregate of nanocrystallites and the shape is spherical, and it reveals the polycrystalline cubic crystal structure [47,48]. Fig. 3.4C shows that the particles are more agglomerated with irregular shape. Fig. 3.4G and H shows that the nanomaterial is monodispersed with the spherical shape. From the HRTEM image it can be seen that the particle diameter is in the range of 25–5 nm, which is consistent with XRD results [49]. There is a slight difference in the average particle size of the samples, which is due to the agglomeration of nanomaterials. Hence, the prepared CeO<sub>2</sub>/CdO nanostructures have a particle size in the range of 5–30 nm using the hydrothermal method [50].

### 3.1.5 Diffuse reflectance spectroscopy studies

The optical possessions of pure CeO<sub>2</sub>, CdO, and mixed heterostructured CeO<sub>2</sub>/CdO metal oxide nanostructures with different ratios (1:1, 1:2, and 2:1) have been studied by UV–visible [diffuse reflectance spectroscopy (DRS)] dimensions; the results are shown in Fig. 3.5A and B. To evaluate the bandgap of the synthesized nanostructures, diffuse reflectance spectroscopy was obtained in the wavelength ranges of 200–800 nm [51]. The bandgap energy is determined by appropriately fitting the data to the shortest transition equation,  $(\alpha h\nu) = A(h\nu - E_g)^n$ , where “ $\nu$ ” is the frequency, “ $A$ ” is a constant, and “ $n$ ” can have values 1/2, 3/2, 2, and 3 depending on the mode of interband transition (i.e., through acceptable and direct forbidden, indirect allowed, and indirect forbidden transitions, respectively). The bandgap of the nanomaterials has been inferred from the altered Kubelka–Munk (K–M) function plots. The reflectance data ( $R$ ) stated as  $F(R)$  have been attained by the submission of the K–M algorithm. In UV, visible diffuse reflectance absorption spectra,  $(F(R)h\nu)^{1/2}$  versus photon energy design gives indirect bandgap and  $(F(R)h\nu)^2$  versus photon energy plot signifies a direct bandgap

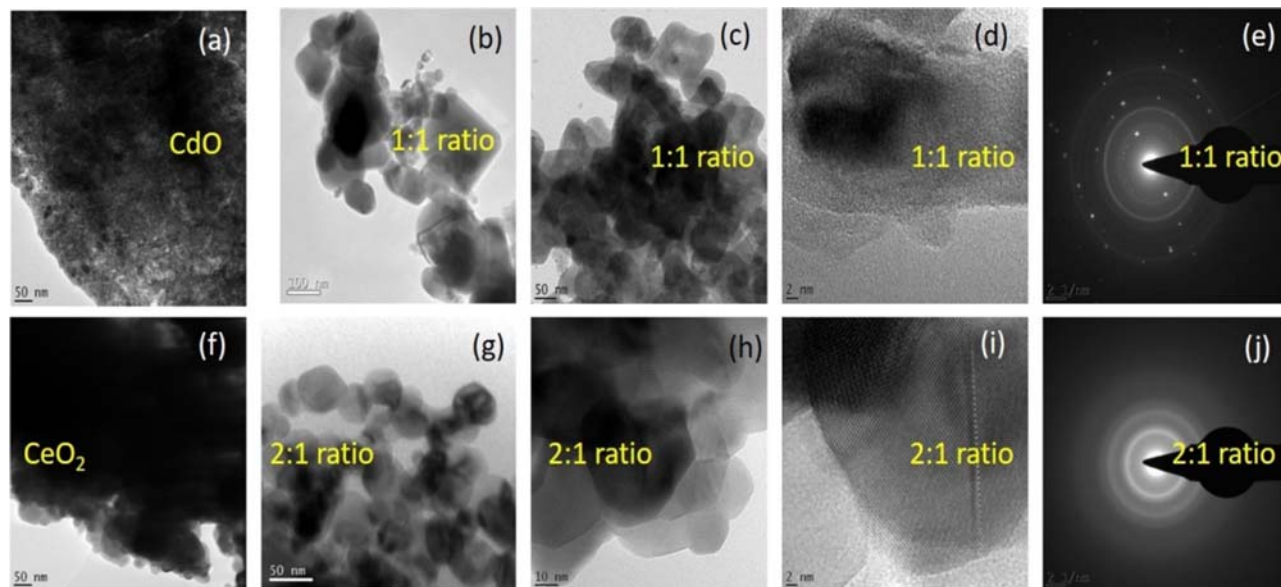


**FIGURE 3.4** HRTEM images of  $\text{CeO}_2/\text{CdO}$  nanostructures: (A) pure  $\text{CdO}$ , (B–E)  $\text{Ce}_1/\text{Cd}_1$ , (F) pure ceria, and (G–J)  $\text{Ce}_2/\text{Cd}_1$ .

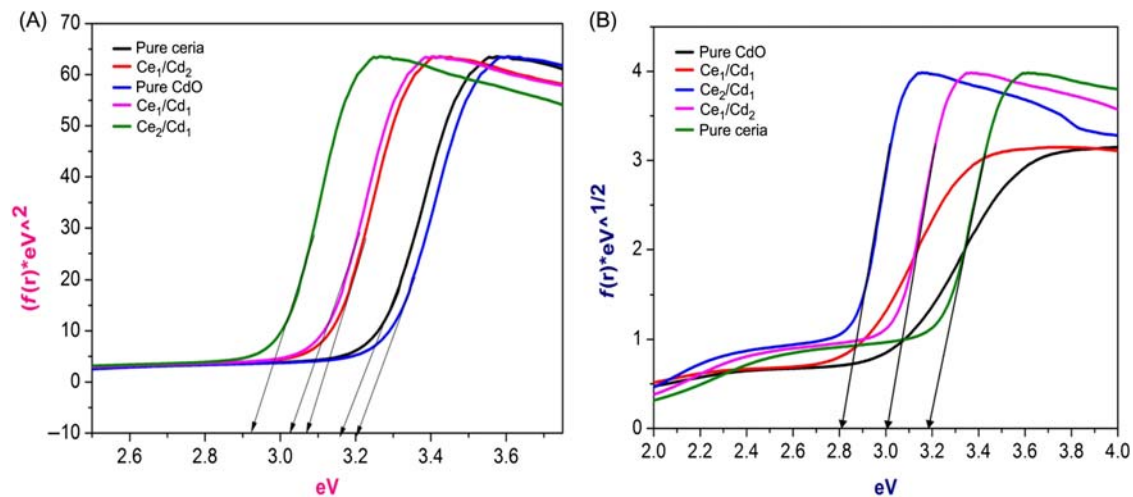


**FIGURE 3.5** DRS spectra: (A) direct bandgap for pure  $CeO_2$ , CdO,  $Ce_1/Cd_1$ ,  $Ce_1/Cd_2$ , and  $Ce_2/Cd_1$ ; (B) indirect bandgap of pure  $CeO_2$ , CdO,  $Ce_1/Cd_1$ ,  $Ce_1/Cd_2$ , and  $Ce_2/Cd_1$  nanostructures.

transition [52]. Both direct and indirect bandgap vitalities are originating to be abridged with the particle size and morphology of nanomaterials, when associated to the discrete metal oxides. Hydrothermally synthesized  $\text{CeO}_2/\text{CdO}$  nanosamples display the bandgap of 3.19, 3.15, 2.98, and 2.89 eV, respectively. The variations in the bandgap energy are due to the different preparation techniques, with average grain values, shape, and structural complaint in the lattice [53]. The optical possession of the absorbance of cerium oxide/cadmium oxide in the UV region proves that it may be used as a respectable entrant for UV absorbing materials [54]. Cadmium oxide with cerium oxide could decrease the bandgap of cerium increasing the growth amount of  $\text{Ce}^{4+}$  states, subsequent to the formation of contained vigor states that are closer to the conduction band. The peak at 400 nm confirms the fluorite cubic structure of nanostructures, revealing the quantum size effect (QSE) of the blue shift modification in the UV–visible spectrum [55]. Hence, there is a transition of electron between the O  $2p$  and Ce  $4f$  states in  $\text{O}^{2-}$  and  $\text{Ce}^{4+}$ .

### 3.1.6 Micro-Raman spectroscopy

To evaluate the molecular motion of nanomaterials, Raman vibrational spectroscopy was used to classify and determine the structural symmetric of the molecules. Raman spectroscopy helps in determining the inelastic scattering of a monochromatic scattered light.  $\text{CeO}_2$  nanoparticles displayed a solid intense band at  $434\text{ cm}^{-1}$ , which represents the  $\text{F}_{2g}$  Raman active mode of fluorite type-like cubic structures [56,57]. The structural characterization of the  $\text{CeO}_2/\text{CdO}$  nanostructures is clearly seen in Fig. 3.6A and B, which shows the broad band at 464 and  $815\text{ cm}^{-1}$  laterally with a weak absorption peak at 300, 370, 500, 605, 734, 780, and  $864\text{ cm}^{-1}$ . The band at  $464\text{ cm}^{-1}$  mostly resembles the  $\text{F}_{2g}$  Raman active mode of cubic fluorite structure, which proves that the synthesized nanomatrix clearly has a crystalline fluorite cubic structure [58,59]. The peaks of the ceria metal oxides occur at higher wave number with high concentration of other metal oxides. The shift in the peak position is due to residual stress and the presence of other  $\text{M}^{2+}$  metal matrix. This also shows that the  $\text{CeO}_2/\text{CdO}$  nanostructure has advanced oxygen defects [60]. Hence, Raman spectroscopy is a promising tool for the structural elucidation of  $\text{CeO}_2/\text{CdO}$  nanostructures can be used to differentiate the different phase modes.

### 3.1.7 Photoluminescence spectra

The photoluminescence (PL) spectra of  $\text{CeO}_2$  and  $\text{CeO}_2/\text{CdO}$  metal oxide nanostructure with different molar ratios 1:1, 1:2, and 2:1 are shown in Fig. 3.7A–D, with an excited wavelength of 290 nm. The captured emission spectra for pure  $\text{CeO}_2$  are in the range of 250 nm for the short wavelength to

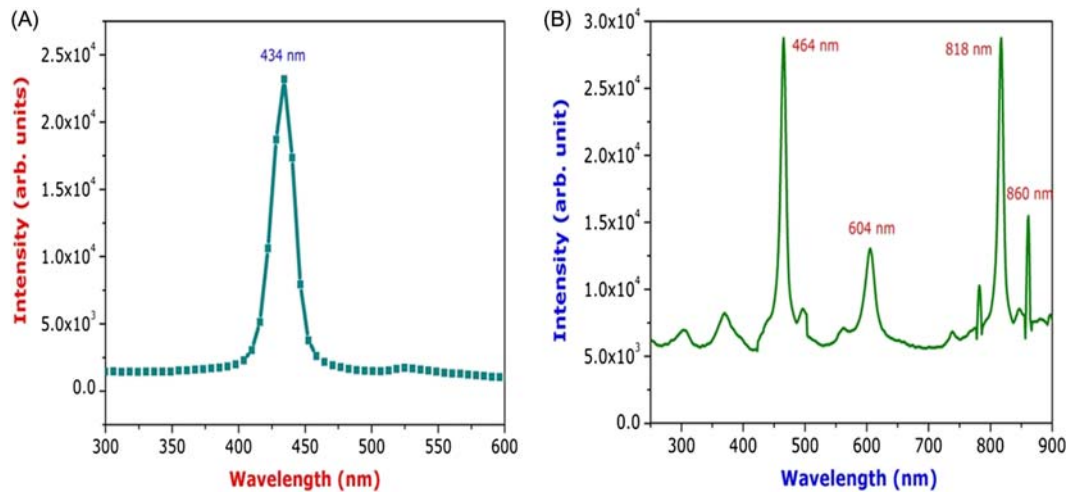


FIGURE 3.6  $\mu$ -Raman spectrum of  $\text{CeO}_2/\text{CdO}$  nanostructures: (A) pure ceria and (B)  $\text{Ce}_2/\text{Y}_1$ .



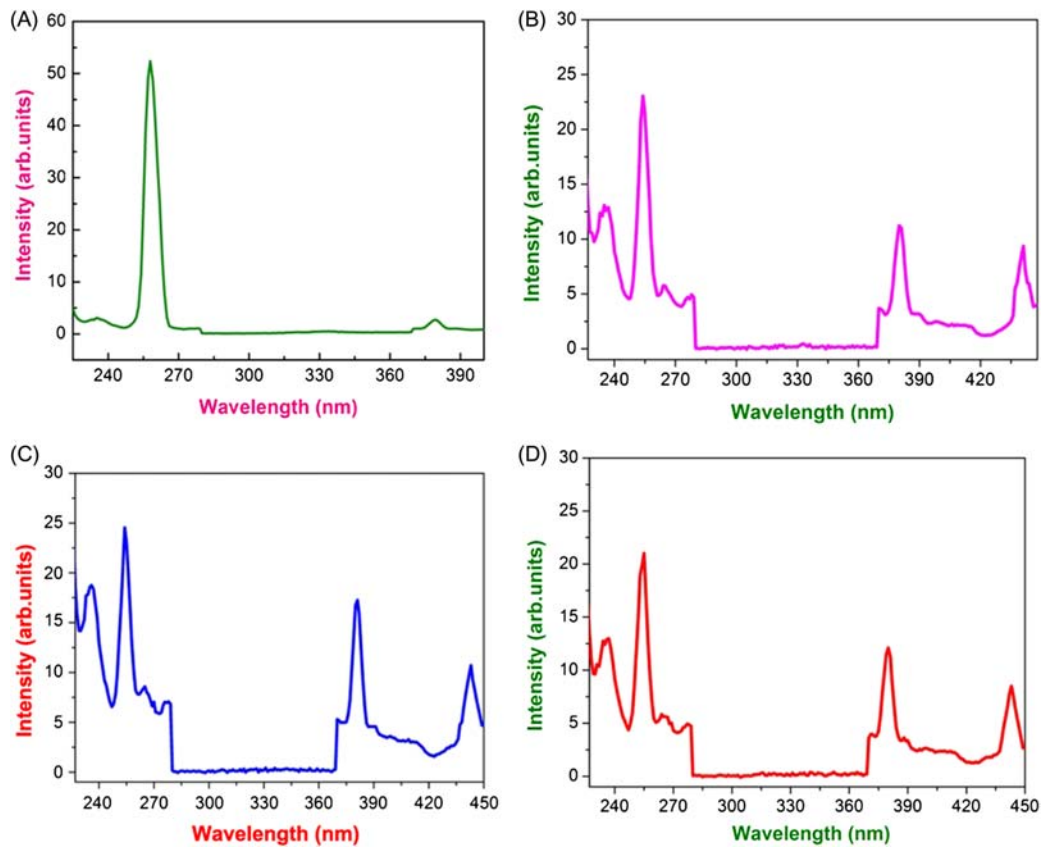
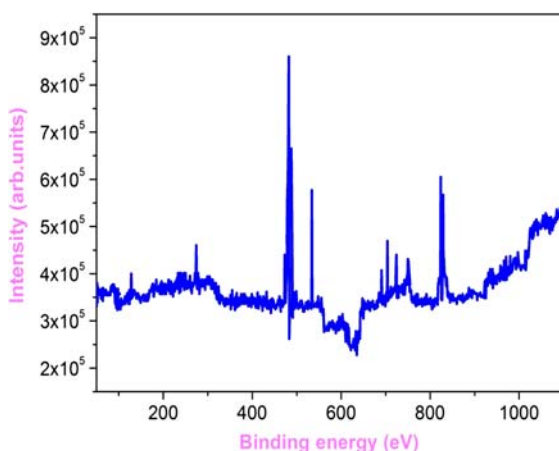


FIGURE 3.7 Photoluminescence (PL) spectrum of CeO<sub>2</sub>/CdO nanostructures: (A) pure ceria, (B) Ce<sub>1</sub>/Cd<sub>1</sub>, (C) Ce<sub>2</sub>/Cd<sub>1</sub>, and (D) Ce<sub>1</sub>/Cd<sub>2</sub>.

400 nm for the long wavelength [61]. By the addition of CdO, the emission peaks appeared at 400–450 nm in the red region spectrum with additional changes in the broadness of the peak positions occurring at room temperature. The emission spectra of  $\text{CeO}_2/\text{CdO}$  were characterized by major peaks near 240, 260, 280, 380, 417, and 445 nm. All emission spectra showed a prominent peak at 445 nm that was attributed to oxygen-related defects in the  $\text{CeO}_2/\text{CdO}$  at microscopy level [62]. The intensity of the emission band at 445 nm increased with increasing CdO content in the  $\text{CeO}_2/\text{CdO}$  nanostructures. The violet band around 402 nm for the  $\text{CeO}_2$  nanostructures initiates from the defect states current widely among the Ce  $4f$  state and O  $2p$  valence band [63]. The two blue emissions at 417 and 445 nm are connected to the plentiful flaws such as displacements, which is supportive for fast oxygen transference. At room temperature, electron transition results mostly from imperfections level to O  $2p$  level [64]. The quantum confinement effect was pragmatic by earnings of PL spectroscopy, which stretches the nearby subbandgap defect states and excitation spectra of the pure nanoparticles. The superficial situations and concentration of defects can modify with the developed circumstances, textural morphology, size, and shapes of nanocrystallites [65].

### 3.1.8 X-ray photoelectron spectroscopy studies

The oxidation state of each element in the sample as well as the composition of the surface functionalization of the  $\text{Ce}_2/\text{Cd}_1$  nanostructure was examined by X-ray photoelectron spectroscopy (XPS). The obtained XPS results show (Fig. 3.8) that the peaks correspond to C (1s), O (1s), Cd, and Ce (3d) for  $\text{CeO}_2$  NPs. The C (1s) signals are mainly expected due to trace quantity of



**FIGURE 3.8** XPS spectrum of  $\text{Ce}_2/\text{Cd}_1$  nanostructure.

surface humidity and absorption of organic contaminants during handling.  $\text{CeO}_2$  nanosphere has the binding energy bands at 872.66, 887.85, 906.14, 922.14, 930.52, 916.34, and 921.33 eV. These spectra were found to be fully consistent with those reported previously [66]. The lower energy level of O (1s) signal at 529.13 eV is attributed to  $\text{O}^{2-}$  ions surrounded by  $\text{Ce}^{4+}$  ions, which corresponds to the Ce–O bond in  $\text{CeO}_2$ . The middle energy level of O (1s) at 533.86 eV can be ascribed to the  $\text{O}^{2-}$  ions in the Ce–O bond where Ce is present in the 3+ state. Finally, the higher energy level of the O (1s) signals located at 531.17 eV are due to OH on the surface and not related to the presence of either  $\text{Ce}^{3+}$  or  $\text{Ce}^{4+}$ .

### 3.1.9 Thermogravimetric analysis

Thermogravimetric (TG) analysis was carried out to quantitatively analyze the presence of impurities and the stability of the nanostructure on its surface level. Samples were interfaced up to  $850^\circ\text{C}$  at a rate of  $5^\circ\text{C min}$  under nitrogen atmosphere and the resulting thermogram is shown in Fig. 3.9. In the sample  $\text{Ce}_2/\text{Cd}_1$  had a weight loss of 10% as observed up to  $850^\circ\text{C}$ . This small reduction in the weight may be due to the removal of hydroxyl group. The weight loss is taken in two parts. (1) The reduction in weight loss is 3% as observed from room temperature to  $200^\circ\text{C}$  due to the release of physically adsorbed water and the water of crystallization from the catalyst's surface. (2) A weight loss of 6% was as observed in TG curve in the temperature range of  $200^\circ\text{C}$ – $500^\circ\text{C}$ , due to solid phase transition or the removal of internal water molecule. The weight loss from  $500^\circ\text{C}$  to  $850^\circ\text{C}$  is due to the loss of mass but is very slight. Similarly, the weight loss in the sample  $\text{Ce}_1/\text{Cd}_1$

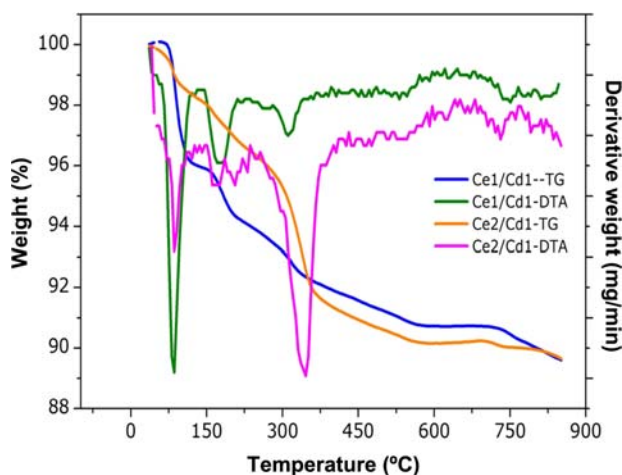


FIGURE 3.9 TG/DTA curve of  $\text{CeO}_2/\text{CdO}$  nanostructures in ratios  $\text{Ce}_1/\text{Cd}_1$  and  $\text{Ce}_2/\text{Cd}_1$ .

is 6% as observed up to 200°C and is due to the release of more surface water molecules. The weight loss of nearly 3% from 200°C to 500°C is due to the removal of chemically combined water molecules. The weight loss is less above 500°C as observed in TG curve. Both the samples are also highly stable on further heating. This confirms that cerium oxide and cadmium oxide are well dispersed with good average crystallite size [67,68].

The differential thermal analysis (DTA) curves of the two CeO<sub>2</sub>/CdO nanostructures prepared in ratios 1:1 and 2:1 (Fig. 3.9) differ slightly. The nanostructure (Ce<sub>2</sub>/Cd<sub>1</sub>) exhibited three endothermic peaks. The first peak is in the range of 70°C–100°C with the minimum value at 85°C. The second endothermic peak is in the range of 151°–214°C with its minimum value located at 178°C. The third endothermic peak is relatively broad in the range of 273°C–362°C with its minimum at 336°C. Likewise, the sample Ce<sub>1</sub>/Cd<sub>1</sub> exhibited three endothermic peaks. The first endothermic peak is broad and in the range of 63°C–113°C with the minimum of 85°C. The second endothermic peak is in the range of 148°C–204°C with a minimum at 180°C. The third endothermic peak is in the range of 293°C–336°C with a minimum at 311°C. The weight loss is probably due to the removal of physisorbed water and interstitially combined H<sub>2</sub>O molecules. The weak peak at 400°C–850°C indicates the transformation of the CeO<sub>2</sub> and CdO oxides phases [69]. The DTA curve did not show the exothermic peak related to crystallization, also indicating the formation of CeO<sub>2</sub>/CdO nanostructures.

### 3.1.10 Photocatalytic activity

The photocatalytic activity of the binary metal oxides was evaluated by taking RhB as the model pollutant. Degradation studies were carried out at both UV light (365 nm) and visible light irradiation. The process conditions were optimized in terms of the following reaction variables:

1. effect of irradiation time on the photodegradation of RhB;
2. effect of pH on the photodegradation of RhB;
3. effect of initial concentration of RhB;
4. effect of catalyst dose;
5. reusability of catalysts; and
6. effect of catalyst on industrial wastewater.

### 3.1.11 Degradation of Rhodamine-B using CeO<sub>2</sub>/CdO heterogeneous catalyst

In this investigation, we chose textile synthetic dye Rhodamine-B as a pollutant due to its high stability. Decomposition was examined using UV light irradiation as shown in Fig. 3.10A–D. The degradation capacity of all the samples with the ratios 1:0, 1:1, 1:2, 2:1, and 0:1 was investigated. The absorption

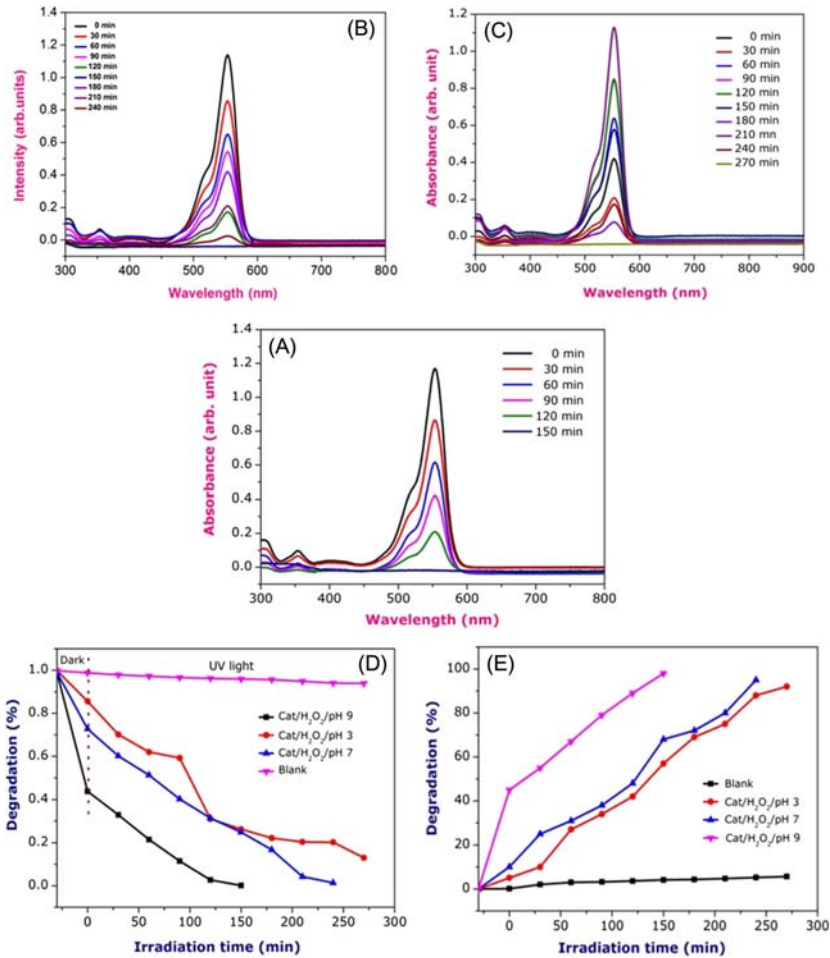


**FIGURE 3.10** Effect of photocatalytic degradation for RhB dye solution in the dark and under UV light irradiation at different time intervals: (A) spectral changes of dye with catalyst–H<sub>2</sub>O<sub>2</sub> at pH 9.0, (B) spectral changes of dye with catalyst–H<sub>2</sub>O<sub>2</sub> at pH 7.0, (C) spectral changes of dye with catalyst–H<sub>2</sub>O<sub>2</sub> at pH 3.0, (D)  $C_t/C_o$  vs time (min) for the photodegradation of dye, and (E) percentage of efficiency, in the presence of catalyst–H<sub>2</sub>O<sub>2</sub> at pH 9.0, pH 7.0, and pH 3.0.

spectrum for decolorization of Rhodamine-B dye with and without CeO<sub>2</sub>/CdO heterogeneous catalyst was recorded with time ( $t$ ) in minutes under UV/visible light irradiation. The absorption peaks at 554 nm were observed for Rhodamine-B, confirming the photodegradation process [70]. The ratios between  $C_t$  (concentration of dye at different time intervals of UV exposure) and  $C_o$  (initial concentration) of the dye were plotted against the time of UV exposure, to compare the efficiency of the degradation under different conditions. The PCD efficiency of the different ratio samples

shows the following order  $2:1 = 1:1 > 1:0 > 1:2 > 0:1$ . It was observed that the  $\text{Ce}_2/\text{Cd}_1$  and  $\text{Ce}_1/\text{Cd}_1$  samples exhibit the best photocatalytic activity compared to all other samples. Both the catalysts have better specific surface area, more reactive sites, mesoporous, higher ability toward absorption of light, and smaller size with high dispersion usually leading to better photodegradation and these features are present in  $\text{CeO}_2/\text{CdO}$  heterogeneous catalyst [71].

### 3.1.12 Photocatalytic degradation of Rhodamine-B dye using $\text{CeO}_2/\text{CdO}$ heterogeneous catalyst ( $\text{Ce}_2/\text{Cd}_1$ ratio)

The PCD activity of the  $\text{CeO}_2/\text{CdO}$  nanostructures was evaluated by decomposition of Rhodamine-B (10 ppm) using 50 mg of photocatalyst. The aqueous solution of the Rhodamine-B synthetic dye was not degraded in the absence of  $\text{CeO}_2/\text{CdO}$  heterogeneous catalyst under UV radiation. But the degradation of Rhodamine-B synthetic dye can be achieved efficiently at 365 nm using  $\text{CeO}_2/\text{CdO}$  dispersions in aqueous medium [72]. The photo-reactor consists of a cylindrical glass reactor with a high-pressure mercury 400 W lamp located in the front of the vessel. The variation of Rhodamine-B absorbance through 30 min was measured at ( $\lambda_{\text{max}} = 365$  nm) using a UV/visible spectrophotometer. The photocatalytic activity was examined against the Rhodamine-B (RhB 99.95% purity). The aqueous Rhodamine-B solution (100 mL) containing 50 mg catalyst was stirred for 30 min, kept in dark conditions to reach the adsorption/desorption equilibrium between the catalyst and RhB molecules, then placed inside the reactor setup and subjected to irradiation by a UV light source ( $\lambda_{\text{max}} = 365$  nm) to induce photochemical reaction; in this process, air was continuously bubbled into the reactor tube. At the end, the dye solution was completely degraded with the color change from pink color solution to colorless solution [73]. The degradation of Rhodamine-B values were calculated as follows: the PCD efficiency ( $\eta$ ) of decolorization was calculated using the expression  $\eta = ((C_o - C_t)/C_o) \times 100$ , where  $C_o$  is the initial concentration of Rhodamine-B and  $C_t$  is the concentration of Rhodamine-B after time “ $t$ .” By using the above formula, the irradiation time (vs) percentage of degradation at different pH values was plotted as shown in Fig. 3.10D.

As can be seen, the degradation percentage increases with time. Degradation of RhB was carried out with catalyst after 210 min of irradiation time at pH 3.0, pH 7.0, pH 9.0, and only  $\text{H}_2\text{O}_2$ , and the dye degradation efficiency was 45%, 48.6%, 52%, and 22.1%, respectively. The percentage of degradation of dye was found to be less in neutral and acidic medium but maximum at pH 9.0. Because at the basic medium the generation of hydroxide ( $\bullet\text{OH}$ ) radical is favored and increases the decomposition of the dye compared to pH 7.0. The results of the PCD spectra of RhB dye evidently prove the gradual decrease in the absorbance with increasing irradiation time, whereas the efficiency of dye degradation was 98.2%, 95.7%, and 92% for

RhB dye using the catalyst and  $\text{H}_2\text{O}_2$  at pH 9.0, pH 7.0, and pH 3.0 in Fig. 3.10E. The results showed that the RhB dye was degraded at 150 min of irradiation time in basic medium whereas in neutral and acidic medium, the dye was degraded after 240 and 270 min, respectively.

The photocatalytic activities of the synthesized heterostructured sample depend on agitation speed, temperature, pH, and ionic strength. The generation of reactive oxygen species (ROS) in the presence of UV light by the catalyst is higher, which is responsible for the decomposition of dyes into small fractions [74]. The possible reason may be that in alkaline medium the hydroxide ion is more easily oxidized to hydroxyl radicals and thus the efficiency of the decomposition of dye is logically increased at pH 9.0. Hence, pH and  $\text{H}_2\text{O}_2$  have more effects on the dye degradation. The concentration of  $\bullet\text{OH}$  radicals in the whole system increases by the addition of  $\text{H}_2\text{O}_2$  with the heterogeneous system.  $\text{H}_2\text{O}_2$  is a better electron acceptor, since it generates more  $\bullet\text{OH}$  radicals and inhibits the exciton recombination process at the same time. When  $\text{H}_2\text{O}_2$  was added to the catalyst solution in basic medium, the maximum degradation was achieved in the first 150 min. Once degradation is completed, the next set of molecules can diffuse immediately on the surface of the catalyst for further degradation [75]. The  $\text{O}_2^\bullet$  and  $\text{OH}^\bullet$  radicals [ROS] can attack the functional group of the dye, which is attached to the surface of the catalysts through *Coulomb interactions*, and degrade the dye to the final products, such as  $\text{CO}_2$ ,  $\text{NO}_3^-$ ,  $\text{H}_2\text{O}$ , and  $\text{H}^+$ . Since RhB dye is a cationic dye, the decomposition is higher in basic media than in acidic and neutral media, which is related to the adsorption capacity of dyes on the surface of the catalyst.

### 3.1.13 Visible light–induced decomposition of Rhodamine-B using $\text{CeO}_2/\text{CdO}$ heterogeneous catalyst ( $\text{Ce}_2/\text{Cd}_1$ )

To evaluate the photocatalytic activities of the synthesized  $\text{CeO}_2/\text{CdO}$  heterogeneous catalyst (2:1), visible light irradiation was used for the decomposition of well-known organic dye RhB. The absorbance spectrum of RhB synthetic dye is presented in Fig. 3.11. The degradation of RhB (10 ppm) was examined in the presence of 50 mg of catalyst–hydrogen peroxide by irradiating visible light at pH 9. The absorption at 554 nm decreases evenly for the decomposition of RhB dye. The pink RhB dye solution becoming colorless in the presence of catalyst is confirmed from the absorption spectra, which are significantly decreased at 554 nm with increase in visible light exposure time (min). The efficiency of the decomposition of dye was found to be 98%, which takes place after 40 min of irradiation of visible light in the presence of synthesized  $\text{CeO}_2/\text{CdO}$  heterogeneous catalyst. Finally, the results clearly indicate that the synthesized  $\text{CeO}_2/\text{CdO}$  heterogeneous catalyst has significant catalytic activity and hence this could be a beneficial photocatalyst for the decomposition of colored dyes.

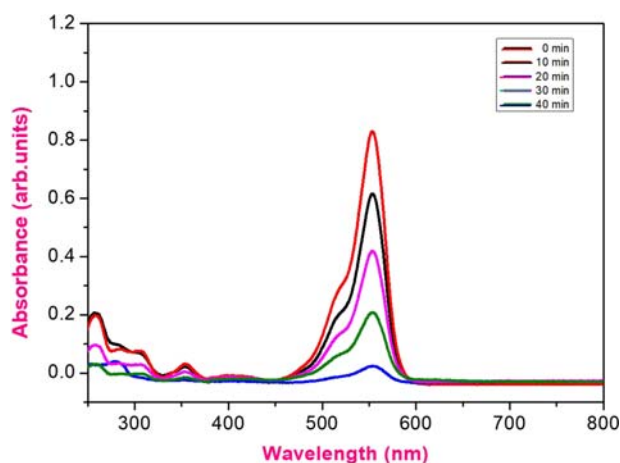
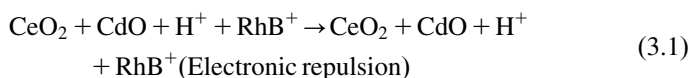


**FIGURE 3.11** Effect of photocatalytic degradation for RhB dye solution with catalyst–H<sub>2</sub>O<sub>2</sub> at pH 9.0 under visible light irradiation at different time intervals.

### 3.1.14 Effect of pH on the photodegradation of Rhodamine-B dye

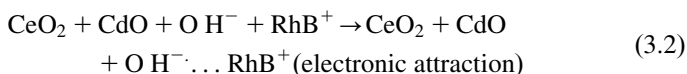
The rate of decomposition of Rhodamine-B synthetic dye was evaluated at different pH as shown in Fig. 3.10A–C. In acidic medium (pH 3), the concentration hydronium ions are higher, proving a positive charge on the surface of the catalyst, as well as a decrease in the number of active sites on the surface of the CeO<sub>2</sub>/CdO heterogeneous binary metal oxide catalyst. However, the substrate adsorbed on the surface of the catalyst, which directly affects the electron transfer between the excited state dye and CeO<sub>2</sub>/CdO heterogeneous catalyst, further influences the rate of the reaction. The absorption of the cationic Rhodamine-B synthetic dyes in the mixture solution by CeO<sub>2</sub>/CdO catalyst becomes poor in the acid medium because of lower concentration of active hydroxyl radicals and hence degradation of the structure of Rhodamine-B synthetic dye into smaller nontoxic molecules is still very slow. The rate of the decomposition process of the dye solution was found to increase along with higher pH value because the heterostructure binary metal oxide surfaces were predominantly negatively charged due to the presence of hydroxyl groups. With higher pH values, the formation of active •OH species is favored, which not only improves transfer of holes to the adsorbed hydroxyls, but also has electrostatic attractive effects between the negatively charged CeO<sub>2</sub>/CdO heterogeneous catalyst particles and the operating cationic dyes [29]. Hence, we propose from our results that the surface of CeO<sub>2</sub>/CdO is negatively charged so that the Rhodamine-B synthetic dye adsorbs on it through the ammonium groups that are positively charged.

In acidic medium





In basic medium



### 3.1.15 Effect of irradiation time on the photodegradation of Rhodamine-B dye

UV light plays a crucial role in the decomposition of Rhodamine-B synthetic dye. The heterostructured binary metal oxide nanomaterials show outstanding PCD with increase in irradiation time. The reason behind this may be due to excitement of valence electrons from the ground state of the metal oxide source to the excited state by illumination of UV light source, which leads to the formation of high energy photoelectron. These photogenerated electrons in the conduction band and the holes in the valence band produce hydroxyl radicals in the whole system, which leads to the decomposition of dye by color change from pink to colorless [76]. The photodegradation efficiency of synthesized nanomaterial with different time intervals was studied to investigate the effect of irradiation time on the photodegradation of Rhodamine-B synthetic dye. This degradation process was carried out at room temperature under UV light irradiation until the degradation process completed. From the above results, we can see that Rhodamine-B synthetic dye is decomposed, which is directly proportional to UV irradiation time as shown in Fig. 3.10A–D. When Rhodamine-B synthetic dye in the presence CdO decorated ceria nanomaterial was irradiated with the UV light at different time intervals, a gradual change in color from pink to colorless occurs, because the CdO decorated ceria nanomaterial decreases the electron/hole recombination effect, improves the charge separation efficiency, and pumps the photogenerated electron of ceria to create a ROS and thus an increase in the degradation of pollutant [77].

### 3.1.16 Effect of catalyst dose on the photodegradation of Rhodamine-B dye

To explore the effect of catalyst loading for the decomposition of RhB dye, a series of batch experiments was carried out with catalyst  $\text{CeO}_2/\text{CdO}$  heterogeneous binary metal oxide nanostructures, in which the loading of catalyst was varied between 40 and 70 mg, and in all the cases we kept dye concentration (10 ppm) and pH 9.0 as constant. The light intensity also remains the same. Fig. 3.12 shows that the decomposition reaction increases up to 50 mg of catalyst in 100 mL of the dye solution due to increase in the reactive sites on the catalyst, beyond which it shows that the degradation process is reduced, which may be due to the scattering of light and weakening in the

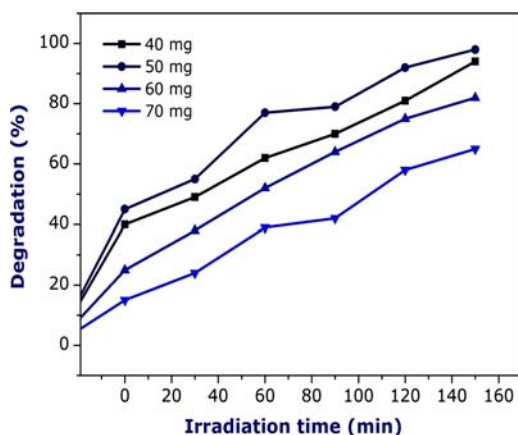


**FIGURE 3.12** Effect of catalyst dose on the photodegradation of Rhodamine-B dye.

penetration of light in the solution for the reaction [78]. At higher amount of catalyst in the dye solution, the high energetic molecules get inactive by collision with fewer energy molecules and the turbidity of the solution medium becomes higher, which decreases the penetration of light, thereby leading to the decrease in the rate of the reaction. Also, the photocatalyst absorbs limited light and the surface area becomes less because of the nanostructure agglomeration at higher concentration of catalyst.

### 3.1.17 Effect of initial concentration of Rhodamine-B dye

PCD of RhB dye was studied for the various concentration of dye for 5, 10, 15, and 20 ppm to identify the effect of initial concentration of RhB synthetic dye. The obtained results are shown in Fig. 3.13 in which the efficiency of decomposition of RhB synthetic dye increases up to 98% for 10 ppm dye concentration and then decreases to 60% for the 15 ppm dye concentration [79]. This may be due to the higher number of dye molecules preferentially adsorbed on the surface of photocatalyst with increase in the dye molecules, whereas the generation of ROS radicals and light irradiation time remain constant. PCD efficiency decreases due to the fewer number of ROS radicals for the decomposition of dye. Also, the penetration of photons becomes poor in high concentration of dye [80]. This investigation reveals that the maximum strength of RhB synthetic dye decomposed by a catalyst dosage up to 10 ppm. To determine the stability of the catalyst, the reusability of the heterostructured binary metal oxide catalyst was examined by separation of the  $\text{CeO}_2/\text{CdO}$  material used. The filtered catalyst was washed with double deionized distilled water and dried at  $120^\circ\text{C}$  in an oven for 2 h; the dried catalyst was then used for the further degradation of dye. In each cycle  $\text{CeO}_2/\text{CdO}$  heterostructured binary metal oxide catalyst showed only

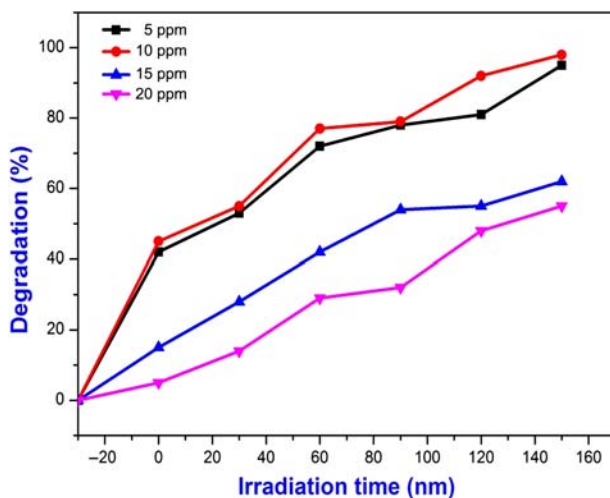


FIGURE 3.13 Effect of initial concentration of Rhodamine-B dye.

minimum changes in the efficiency of dye decomposition. From the result, we found that the degradation efficiency is reduced only by 4% at the end of the three cycles, thus indicating that the  $\text{CeO}_2/\text{CdO}$  heterogeneous binary metal oxide catalyst was highly stable.

### 3.1.18 Removal of Rhodamine-B from urban wastewater

To illustrate the ability of our synthesized  $\text{CeO}_2/\text{CdO}$  heterogeneous nanostructure, the adequate photocatalytic effect for RhB in real wastewater was studied. The PCD experiments were carried out in industrial wastewater by using  $\text{CeO}_2/\text{CdO}$  binary metal oxide catalyst. The industrial wastewater containing Rhodamine-B dye (100 mL) with 50 mg catalyst and  $\text{H}_2\text{O}_2$  at pH 9 was placed inside the photocatalytic reactor setup and subjected to irradiation by a UV light source ( $\lambda_{\text{max}} = 365 \text{ nm}$ ). The absorbance capacity was measured for industrial wastewater with increasing time intervals using a UV–visible spectrophotometer. The absorption value of RhB was decreased consistently (at 552 nm) due to the structural degradation of RhB molecules. From the plot of  $C_t/C_o$  versus irradiation time for the PCD of industrial wastewater, the dye degradation efficiency in wastewater was 89% of RhB dye, which was degraded after 150 min of irradiation time, thus indicating that the potential use of these materials in real wastewater treatment applications. We conclude that the increase in Cd ion concentration on the crystal lattice of  $\text{CeO}_2$  leads to the decrease in crystallite size and maximize the surface area, which is readily available for preferential adsorption of dye molecules over the catalyst surface. Therefore the dye molecules, which are readily adsorbed in the surface of catalyst, will undergo decomposition.

### 3.1.19 Mechanism of photocatalysis

Electrons and holes are created by illumination of UV light on  $\text{CeO}_2/\text{CdO}$  catalyst. The charge transportation processes of  $\text{CeO}_2/\text{CdO}$  nanostructure leads to UV light-driven photocatalytic decomposition of dye as shown in Fig. 3.14. After absorption of UV light, the electron in the valence band of both the binary metal oxide is energized and excited to conduction band, thereby resulting in the separation of electron-hole pairs on the surface of the  $\text{CeO}_2/\text{CdO}$  binary metal oxide NPs. The holes in the valence band are trapped by the  $\text{H}_2\text{O}$  to form active hydroxyl radicals ( $\text{OH}^\bullet$ ), which is the second strongest oxidant having an oxidation potential of 2.8 eV next to fluorine and holes form superoxides ( $\text{O}_2^\bullet$ ,  $\text{HO}_2^\bullet$ ). The photo excitation state of the semiconductor generates electrons in the conduction band, which reacts with oxygen molecule to form superoxide radical anions ( $\text{O}_2^{\bullet-}$ ). Usually the various organic dyes undergoing the PCD under UV light irradiation is attributed to their oxidation by the ROS, which have an ability to oxidize the organic pollutant and yielding  $\text{H}_2\text{O}$ ,  $\text{CO}_2$  molecules. Our results show that  $\text{CeO}_2/\text{CdO}$  binary metal oxide nanostructures act as a good heterocatalysts toward the

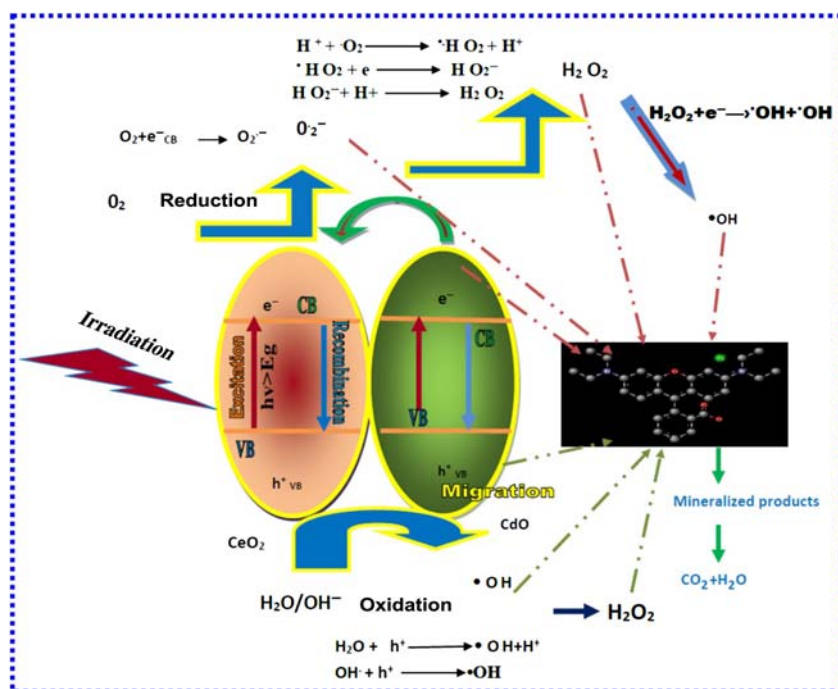
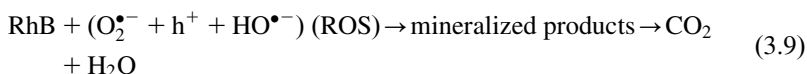
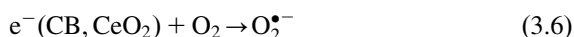
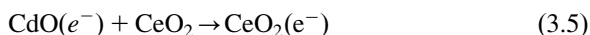
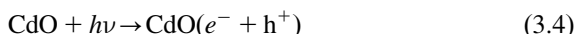
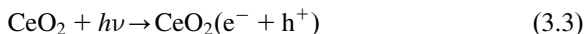


**FIGURE 3.14** Schematic diagram of the charge separation of  $\text{CeO}_2/\text{CdO}$  nanostructures showing photogenerated electron transportation processes leading to UV light-driven photocatalytic degradation of dye.

decomposition of RhB synthetic dye and the dye has a higher affinity toward the synthesized photocatalyst. Therefore due to the presence of synergic effects in between ultrafine CeO<sub>2</sub>/CdO binary metal oxide heterocatalysts lead to the decomposition of the various polluting organics. The complete photodegradation process can be summarized by the following reaction steps:



### 3.2 Conclusion

In this chapter we discussed well-dispersed cerium oxide/cadmium oxide binary metal oxide nanostructures synthesized using the hydrothermal method. The prepared nanostructures were characterized by various studies. The XRD pattern showed that the cerium oxide-cadmium oxide nanostructures were of cubic phase clusters. The morphology of the binary metal oxides was found to be spherical in shape by FESEM and HRTEM analysis. RhB dye was degraded nearly at 150 min of irradiation time in basic medium whereas in neutral and acidic medium, the dye was degraded after 240 and 270 min. The generation of ROS in the presence of UV/visible light by the catalyst was found to be higher, which is responsible for the decomposition of dyes into small fractions. The possible reason is because, in alkaline medium, the hydroxide ion is more easily oxidized to hydroxyl radicals and thus the efficiency of the decomposition of dye is logically increased at pH 9. Hence, pH and H<sub>2</sub>O<sub>2</sub> have more effects on dye degradation. The synthesized nanostructures can be used as an anticancer agent. The different oxidation states of metal oxides can tune the activities of the nanomaterials.

### References

- [1] Zhang YW, Si R, Liao CS, Yan CH. *J Phys Chem B* 2003;107:10159.
- [2] Takami S, Ohara S, Adschiri T, Wakayama Y, Chikyow T. *RSC* 2008;40:5442.

- [3] Sreeremya TS, Krishnan A, Remani KC, Patil KR, Brougham DF, Ghosh S. *ACS Appl Mater Interfaces* 2015;7:8545.
- [4] Cabral AC, Cavalcante LS, Deus RC, Longo E, Simoes AZ, Moura F. *Ceram Int* 2014;40:4445.
- [5] Goharshadi EK, Samiee S, Nancarrow P. *J Colloid Interface Sci* 2011;356:473.
- [6] Khan SB, Faisal M, Rahman MM, Akhtar K, Asiri AM, Khan A, et al. *Int J Electrochem Sci* 2013;8:7284.
- [7] Comini E, Baratto C, Concina I, Faglia G, Falasconi M, Ferroni M, et al. *Sens Actuator B* 2013;179:3.
- [8] Lokesh K, Kavitha G, Manikandan E, Mani GK, Kaviyarasu K, Rayappan JB, et al. *IEEE Sens J* 2016;16:2477.
- [9] Cordeiro MAL, Weng W, Stroppa DG, Kiely CJ, Leite ER. *Chem Mater* 2013;25:2028.
- [10] Kasinathan K, Kennedy J, Manikandan E, Henini M, Maaza M. *Sci Rep* 2016;6:38064.
- [11] Faisal M, Bahadar Khan S, Rahman MM, Jamal A, Akhtar K, Abdullah MM. *J Mater Sci Technol* 2011;27:594.
- [12] Chang K, Mei Z, Wang T, Kang Q, Ouyang S, Ye J. *ACS Nano* 2014;8:7078.
- [13] Gu S, Chen Y, Yuan X, Wang H, Chen X, Liu Y, et al. *RSC Adv* 2015;. Available from: <https://doi.org/10.1039/C5RA16114B>.
- [14] Dutta S, Sahoo R, Ray C, Sarkar S, Jana J, Negishib Y, et al. *Dalton Trans* 2015;44:193.
- [15] Singh K, Ibrahim AA, Umar A, Kumar A, Chaudhary GR, Singh S, et al. *Sens Actuators B Chem* 2014;. Available from: <https://doi.org/10.1016/j.snb.2014.05.11>.
- [16] Taylor HS. A theory of the catalytic surface. *Proc R Soc London, Ser A* 1925;108:105.
- [17] Yates JT. Surface chemistry at metallic defect sites. *J Vac Sci Technol A* 1995;13:1359.
- [18] Esch F, Fabris S, Zhou L, Montini T, Africh C, Fornasiero P, et al. *Science* 2005;309:75.
- [19] Ivanova AS. *Catal* 2009;50:797.
- [20] Reuter K, Scheffler M. *Phys Rev Lett* 2003;90:046.
- [21] Schth F, Henry BE, Schmidt LD. *Adv Catal* 1993;39:51.
- [22] Thangadurai V, Kopp P. *J Power Sources* 2007;168:178.
- [23] Kaviyarasu K, Maria Magdalane C, Anand K, Manikandan E, Maaza M. *Spectrochim Acta, Part A* 2015;142:405.
- [24] Martı'nez-Arias A, Ferna'ndez-Garci'a M, Ballesteros V, Salamanca LN, Conesa JC, Otero C, et al. *Langmuir* 1999;15:4796.
- [25] Kim M, Lee H, Shin YH, Ahn KH, Youn YS, Kim J, et al. *Korean J Chem Eng* 2012;29:1289.
- [26] Kaviyarasu K, Manikandan E, Paulraj P, Mohamed SB, Kennedy J. *J Alloy Compd* 2014;593:67.
- [27] Sherly ED, Judith Vijaya J, John Kennedy L. *J Mol Str* 2015;1099:114.
- [28] Santos CCLD, Farias IAP, De Jesus dos Reis Albuquerque A, Maria de Freitas Silva P, Medeiros da Costa One G, Correia Sampaio F. *BMC Proc* 2014;8:48.
- [29] Negahdary M, Mohseni G, Fazilati M, Parsania S, Rahimi G, Rad S, et al. *Scholars research library. Ann Biol Res* 2012;3:3671.
- [30] Salehi B, Mehrabian S, Ahmadi M. *J Nanobiotechnol* 2014;12:26.
- [31] Wang L, He H, Yu Y, Sun L, Liu S, Zhang C, et al. *J Inorg Biochem* 2014;135:45.
- [32] Gopinathan E, Viruthagiri G, Shanmugam N, Priya SS. *Opt - Int J Light Electron Opt* 2015;. Available from: <https://doi.org/10.1016/j.ijleo.2015.09.014>.
- [33] Elidrisi B, Addou M, Regragui M, Monty C, Bougrine A, Kachouane A. *Thin Solid Films* 2000;379:23.

- [34] Porqueras I, Pearson C, Corbella C, Vives M, Pinyol A, Bertran E. *Solid State Ion* 2003;165:131.
- [35] Conesa JC. *Surf Sci* 1995;339:337.
- [36] Zeng C, Xie S, Yu M, Yang Y, Lu X, Tong Y. *J Pow Source* 2014;247:545.
- [37] Deshpande S, Patil S, Kuchibhatla ST, Seal S. *Appl Phys Lett* 2005;87:276.
- [38] Zawadzki M. *J Alloy Compd* 2008;454:347.
- [39] Hadi A, Yaacob II. *Mater Lett* 2007;61:93.
- [40] Cullity BD. *Elements of X-ray diffraction*. 3rd ed. Reading, MA: Addison-Wesley; 1967.
- [41] Qiu H, Chen G, Fan R, Cheng C, Hao S, Chen D, et al. *Chem Commun* 2011;47:9648.
- [42] Kaviyarasu K, Manikandan E, Nuru ZY, Maaza M. *Lett* 2015;160:61.
- [43] Kaviyarasu K, Manikandan E, Kennedy J, Maaza M. *RSC Adv* 2015;5:82421.
- [44] Jung SH, Oh E, Lee KH, Yang Y, Park CG, Park WJ, et al. *Cryst Growth Des* 2008;8:265.
- [45] Charitidis C, Patsalas P, Logothetidis S. *J Phys Conf Ser* 2005;109:226.
- [46] Sathyamurthy S, Leonard KJ, Dabesani RT, Paranthaman MP. *Nanotechnology* 2005;16:1960.
- [47] Alouche A, Jordan J. *Mech Ind Eng* 2008;2:111.
- [48] Zambare PZ, Girase KD, Murthy KVR, Mahajan OH. *Adv Mater Lett* 2013;4:577.
- [49] Alaya MN, Youssef AM, Roumie A, George R. *J Chem* 2014;7:722.
- [50] Khan SB, Rahman MM, Akhtar K, Asiri AM, Seo J, Han H, et al. *Int J Electrochem Sci* 2012;7:4030.
- [51] Klikovits J. *Phys Rev Lett* 2008;101:266104.
- [52] Kaviyarasu K, Raja A, Devarajan PA. *Spectrochim Acta Part A: Mol Biomol Spectrosc* 2013;114:586–91.
- [53] Kaviyarasu K, Devarajan PA, Xavier SJ, Thomas SA, Selvakumar S. *J Mater Sci Technol* 2012;28:15–20.
- [54] Kaviyarasu K, Devarajan PA. *Adv Appl Sci Res* 2011;2(6):131–8.
- [55] Kaviyarasu K, Devarajan PA. *Scholars research library. Der Pharma Chem* 2011;3(5):248–54.
- [56] Mobeen Amanulla A, Jasmine Shahina SK, Sundaram R, Maria Magdalane C, Kaviyarasu K, Letsholathebe D, et al. *J Photochem Photobiol B: Biol* 2018;183(2018):233–41.
- [57] Raja A, Ashokkumar S, Pavithra Marthandam R, Jayachandiran J, Khatiwada CP, Kaviyarasu K, et al. *J Photochem Photobiol B: Biol* 2018;181:53–8.
- [58] Jesudoss SK, Judith Vijaya J, Iyyappa Rajan P, Kaviyarasu K, Sivachidambaram M, Kennedy LJ, et al. *Photochem Photobiol Sci* 2017;16(5):766–78.
- [59] Iyyappa Rajan P, Judith Vijaya J, Jesudoss SK, Kaviyarasu K, John Kennedy L, Jothiramalingam R, et al. *Mater Res Express* 2017;4(8):085030.
- [60] Judith Vijaya J, Jayaprakash N, Kombaiah K, Kaviyarasu K, John Kennedy L, Ramalingam RJ, et al. *J Photochem Photobiol B: Biol* 2017;177:62–8.
- [61] Kanimozhi K, Basha SK, Kumari VS, Kaviyarasu K. *J Nanosci Nanotechnol* 2018;18(7):4916–22.
- [62] Reddy YS, Magdalane CM, Kaviyarasu K, Mola GT, Kennedy J, Maaza M. *J Phys Chem Solids* 2018;123:43–51.
- [63] Arularasu MV, Anbarasu M, Poovaragan S, Sundaram R, Kanimozhi K, Maria Magdalane C, et al. *J Nanosci Nanotechnol* 2018;18(5):3511–17.
- [64] Kombaiah K, Judith Vijaya J, John Kennedy L, Bououdina M, Kaviyarasu K, Ramalingam R, et al. *Optik* 2017;135:190–9.

- [65] Maria Magdalane C, Kaviyarasu K, Raja A, Arularasu MV, Mola GT, Isaev AB, et al. *J Photochem Photobiol B: Biol* 2018;185:275–82.
- [66] Jayakumar C, Maria Magdalane C, Kanimozhi K, Kaviyarasu K. *J Nanostruct* 2017;7(2):155–64.
- [67] Maria Magdalane C, Kaviyarasu K, Matinise N, Mayedwa N, Mongwaketsi N, Letsholathebe D, et al. *South Afr J Chem Eng* 2018;26:49–60.
- [68] Jesudoss SK, Judith Vijaya J, Kaviyarasu K, Iyyappa Rajan P, Narayanan S, John Kennedy L. *J Photochem Photobiol B: Biol* 2018;186:178–88.
- [69] Iyyappa Rajan P, Judith Vijaya J, Jesudoss SK, Kaviyarasu K, Lee S-C, John Kennedy L, et al. *R Soc Open Sci* 2018;5(3):171430.
- [70] Geetha N, Sivaranjani S, Ayeshamariam A, Siva Bharathy M, Nivetha S, Kaviyarasu K, et al. *J Adv Microsc Res* 2018;13(1):12–19.
- [71] Valsalam S, Agastian P, Arasu MV, Al-Dhabi NA, Ghilan A-KM, Kaviyarasu K, et al. *J Photochem Photobiol B: Biol* 2019;191:65–74.
- [72] Arasu MV, Arokiyaraj S, Viayaraghavan P, Sujin Jeba Kumar T, Duraipandiyan V, Al-Dhabi NA, et al. *J Photochem Photobiol B: Biol* 2019;190:154–62.
- [73] Saravanakkumar D, Abou Oualid H, Brahmi Y, Ayeshamariam A, Karunanaithy M, Mohamed Saleem A, et al. *Open Nano* 2019;4:100025.
- [74] Karunaniithy M, Prabhavathi G, Hameedha Beevi A, Ibraheem BH, Kaviyarasu K, Nivetha S, et al. *J Nanosci Nanotechnol* 2018;18(10):6680–707.
- [75] Kanimozhi K, Khaleel Basha S, Sugantha Kumari V, Kaviyarasu K. *J Nanosci Nanotechnol* 2019;19(5):2493–500.
- [76] Kaviyarasu K, Maria Magdalane C, Kanimozhi K, Kennedy J, Siddhardha B, Subba Reddy E, et al. *J Photochemistry Photobiology B: Biol* 2017;173:466–75.
- [77] Kaviyarasu K, Kanimozhi K, Matinise N, Magdalane CM, Mola GT, Kennedy J, et al. *Mater Sci Engineering: C* 2017;76:1012–25.
- [78] Hussain CM. *Handbook of nanomaterials for industrial applications*. Elsevier; 2018.
- [79] Hussain CM, Kharisov B. *Advanced environmental analysis-application of nanomaterials*. The Royal Society of Chemistry; 2017.
- [80] Magdalane CM, Kaviyarasu K, Vijaya JJ, Siddhardha B, Jeyaraj B. *J Photochem Photobiol B: Biol* 2016;163:77–86.



This page intentionally left blank

## Chapter 4

# Functionalized metal-based nanoelectrocatalysts for water splitting

R.M.P.I. Rajakaruna and I.R. Ariyaratna

*Department of Chemistry and Biochemistry, Auburn University, Auburn, AL, United States*

### 4.1 Introduction

Fossil fuels such as petroleum and coal make up more than 80% of the energy sources used around the world [1]. Although economical and reliable, there are many drawbacks to relying on fossil fuel as the primary source of energy. Fossil fuels are unsustainable and nonrenewable, and burning fossil fuels releases gases that contribute to undesirable phenomena such as the greenhouse effect, which leads to global warming [2]. These limitations have generated increased interest in investigating renewable energy sources to meet the demands for clean energy. Generating hydrogen from water splitting to be used as a source of energy has garnered attention as an economical and sustainable source of energy [3]. Methods like water electrolysis, solar thermochemical water splitting [4], nuclear-powered water splitting [5], photoelectrochemical water splitting [6], natural gas steam reforming [7], and coal gasification are used to generate hydrogen at industrial scales. Out of these methods, solar thermochemical water splitting and nuclear-powered water splitting require high reaction temperatures in the range of 1000°C. Natural gas steam reforming and coal gasification release greenhouse gases. Water electrolysis is considered a desirable method for H<sub>2</sub> generation since it is environmentally benign, economical, and efficient [8].

In this chapter, recent developments in heterogeneous metal-based nano-functionalized electrocatalysts for water splitting will be examined. A brief discussion on the basic electrochemical concepts related to electrocatalysts is also included for the better understanding of the parameters used to evaluate the performance of the described functionalized nanomaterial electrocatalysts.

Water electrolysis was first reported in 1789 [9]. A typical water electrolysis cell consists of an anode and a cathode immersed in an aqueous

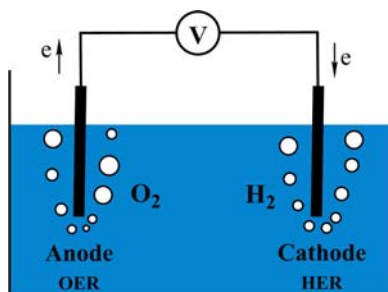
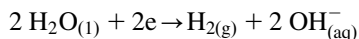


**FIGURE 4.1** A typical scheme of a water electrolysis cell.

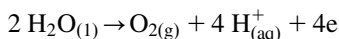
medium. Upon application of adequate potential between the two electrodes, at the cathode hydrogen evolution reaction (HER) takes place while at the anode oxygen evolution reaction (OER) occurs (see Fig. 4.1).

#### 4.1.1 Fundamentals of water electrolysis

Half reaction at the cathode



Half reaction at the anode



Conversion of one mole of  $\text{H}_2\text{O}$  into one mole of  $\text{H}_2$  and a half mole of  $\text{O}_2$  at standard temperature and pressure (298.15K, 1 atm) requires +237.5 kJ/mol of standard Gibbs free energy and the standard enthalpy of water splitting is +286 kJ/mol [10]. Since water splitting is energetically unfavorable, to obtain useful yields of hydrogen, catalysts can be used (Fig. 4.2). The state-of-the-art HER catalysts are Pt based, whereas the OER catalysts are  $\text{IrO}_2$  or  $\text{RuO}_2$  based. However, elemental Pt, Ru, and Ir are not available abundantly and are also expensive. This limits the use of Pt-, Ru-, and Ir-based electrocatalysts at an industrial scale [11].

Electrolysis of water requires a 1.23 V versus RHE. However, in reality a potential higher than 1.23 V is required to drive the reaction to completion at a reasonable rate (see Fig. 4.3) [12]. The extra voltage above 1.23 V required to run the reaction is defined as overpotential ( $\eta$ ) and electrocatalysts are used to lower the  $\eta$  and accelerate the rate of the reaction and therefore increase its efficiency.

Overall operational potential in water electrolysis is given by  $V_{\text{op}} = 1.23 \text{ V} + \eta_a + |\eta_c| + \eta_u$ , where 1.23 V is the ohmic potential of water splitting,  $\eta_a$  and  $|\eta_c|$  are anodic  $\eta$  and cathodic  $\eta$  respectively, and  $\eta_u$  is the excess potential needed to overcome internal resistance. To obtain efficient electrocatalytic activity, it is imperative that the OER and HER catalysts

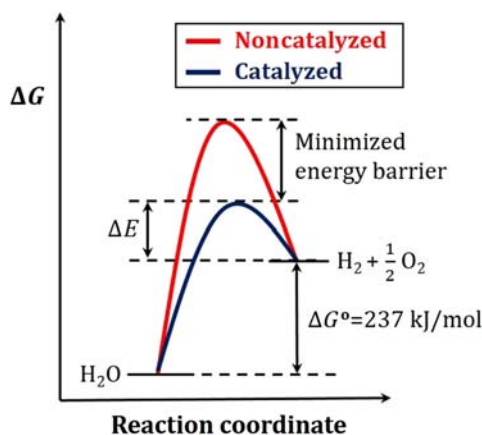


FIGURE 4.2 HER energetics in the absence and presence of a catalyst.

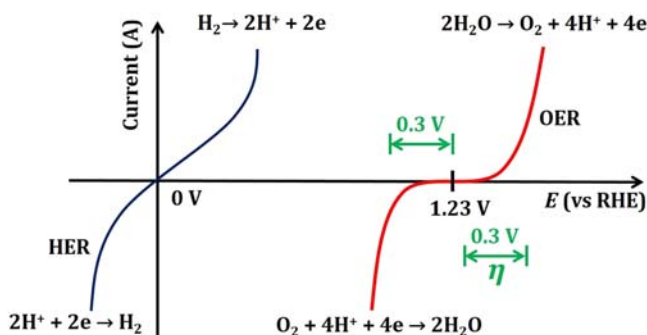


FIGURE 4.3 Representation of the current–potential relationship for hydrogen evolution and oxidation, and for oxygen evolution and reduction.

used at the anode and the cathode have low  $\eta$  so that the overall operational potential for the system is low. To depict the relationship between  $\eta$  and the steady state current density of electrocatalysts, Tafel plots can be used. For the HER process the Tafel equation can be arranged as  $\log(j) = \log(j_0) - (\eta/b)$ , where  $j$  is the catalytic current density and  $j_0$  is the exchange current density ( $\eta > 0.05$  V). For OER the Tafel equation takes the form of  $\log(j) = \log(j_0) + (\eta/b)$ . The Tafel slope  $b$  and exchange current density  $j_0$  are used as markers to evaluate performance of electrocatalysts. Smaller Tafel slopes correspond to better performance in both OER and HER catalysts. Stability, Faradaic efficiency, turnover frequency,  $\eta$ , and current density are other parameters used to evaluate the efficiency of a catalyst [13].

A good electrocatalyst should have a high number of active sites, be stable for extended periods of time (preferably years), be economical to scale industrially, possess good electron transfer ability, and have a high

electrochemically active surface area easily accessible to the reactants and a low  $\eta$  with high catalytic current density, and environmentally safe [13]. To improve the performance of an electrocatalyst one of two major methods is used. The intrinsic activity of the electrocatalytic material could be changed by manipulating its composition or the number of active sites could be improved by changing the morphology of the material.

#### 4.1.2 Functionalized nanomaterials as electrocatalysts

Compared to their bulk counterparts, nanoelectrocatalysts for water splitting introduce increased electrochemically active surface area and reduce the catalyst loading [14]. The porosity of the nanostructures has been found useful for electrocatalysis since it eases the mass transport of reactants. Facile diffusion of reactants and electrolyte is another advantage of utilizing nanostructures as electrocatalysts. Individual nanoparticle electrocatalysts that have poor intrinsic electrical conductivity can be improved by incorporating them in conducting carbon frameworks to synthesize superlattice structures. Traditional nanoscale electrocatalysts for water splitting suffer from several drawbacks. The high surface energies of nanoparticles (NPs) could lead to agglomeration when a high electrical potential is applied. This is detrimental to the catalytic efficiency as agglomeration will inevitably decrease the number of available active catalytic sites [13]. Overoxidation of the catalyst surface is another complication faced by nanoelectrocatalysts. Overoxidation increases the internal resistance of the surface thereby increasing the excess potential required for the reaction to proceed. This phenomenon too would dampen the efficiency of the electrocatalyst. To overcome these obstacles various electrode fabrication methods, which functionalize the nanoelectrocatalytic surface, have been proposed.

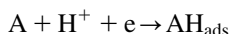
Some of the methods used to obtain better electrocatalytic performance are functionalizing carbon nanomaterials with transition metal NPs to form metal@C core-shell type compounds, and formation of 2D nanostructures, transition metal dichalcogenides, as well as layered double hydroxides (LDH) [13].

Electrochemical deposition, hydrothermal growth, solvothermal growth, chemical vapor deposition, and chemical exfoliation are some techniques used to functionalize nanomaterials for electrocatalysis [15–17].

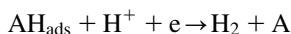
#### 4.1.3 HER process

HER is a two-electron transfer process with  $\text{AH}_{\text{ads}}$  as the intermediate. Here, A is an active site on the electrode surface. In acidic medium, the HER process takes place in either of the two mechanisms: Volmer step followed by Heyrovsky step, or Volmer step followed by Tafel step.

Volmer step:



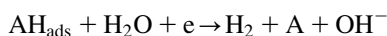
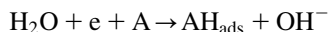
Heyrovsky step:



Tafel step:



Mechanism in alkaline medium



The activation energy required for a electrocatalyst depends on the type of the reaction interface. Since the HER process is a combination of hydrogen adsorption and desorption from the electrode surface, the strength of the bonding between catalytic surface and hydrogen atoms needs to be at an optimal level where it does not strongly favor one step over the other. If the bonding between hydrogen and catalytic surface is weak, adsorption will be inadequate, and the overall efficiency would suffer. On the other hand, if the bonding between hydrogen and the electrocatalytic surface is too strong, it will not desorb from the surface effectively, which would lower the overall efficiency. This phenomenon is described by the Sabatier principle [18]. Therefore the free energy of hydrogen adsorption of  $\Delta G_H$  of the electrocatalyst needs to be considered when selecting a suitable catalyst for HER.

The equation for Nernstian potential required for HER under standard conditions is given by

$$E_{HER} = E_{\left(\frac{H_2}{H^+}\right)}^0 - \frac{RT}{F} \times \ln(a_{H^+}/P_{H_2}^{\frac{1}{2}}) = -0.059 \times \text{pH}; \text{ V vs NHE}$$

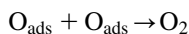
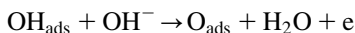
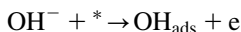
The Nernstian potential for HER is independent of the electrolytes used and depends on the pH of the medium. However, even though the potential required is zero, to obtain the products an activation barrier needs to be created [19]. Therefore in an efficient HER electrocatalyst  $E_{HER} > 0 \text{ V}$ , and sometimes  $>1 \text{ V}$  needs to be applied along with an  $\eta$ . Factors affecting the performance of HER electrocatalysts include hydrogen adsorption free energy, conductivity of the material, accessibility of the electrochemically active sites, and morphology/structure of the electrocatalyst [13]. Out of the two half reactions, HER is kinetically more favorable than the OER process, which is considered to be the bottleneck of the water electrolysis process [3].

### 4.1.4 OER process

The equation for the Nernstian potential required for OER under standard conditions is given by

$$E_{\text{OER}} = E^0_{\left(\frac{\text{O}_2}{\text{H}_2\text{O}}\right)} - \frac{RT}{4F} \times \ln \frac{(a_{\text{H}^+} P_{\text{O}_2} / P^0)}{a_{\text{H}_2\text{O}^2}} = 1.23\text{V} - 0.059 \times \text{pH}; \text{ V vs NHE}$$

OER is a 4e process that involves overcoming a high energy barrier. Therefore OER kinetics are sluggish in nature and require a higher  $\eta$  to be as efficient as the HER process. The OER process may occur through the following mechanism. Here \* denotes an active site on the surface of the electrode.



A low Tafel slope and low  $\eta$  required to reach a certain current density indicates better OER activity.

## 4.2 Functionalized nanoelectrocatalysts for HER

### 4.2.1 Pt-based HER catalysts

Out of all the pure metals, Pt shows the greatest exchange current density and the lowest  $\eta$  for HER. Therefore it is reasonable that Pt is the most commonly used electrocatalyst for HER. Even though various more economical HER catalysts have been proposed, they have not been able to surpass the performance of Pt-based catalysts. To lower the cost of Pt-catalyzed water electrolysis, Pt loading should be decreased and Pt utilization efficiency should be increased [20]. This could be achieved by alloying Pt with first-row transition metals such as Co, Ni, and Fe, which may also enhance the electrocatalytic performance of Pt. In addition to the improved electronic features, this method introduces other valuable properties to the electrocatalyst depending on the metal used for the alloying process. For example, Ni atoms on the surface are capable of desorption of poisoning intermediates, which is beneficial for electrocatalysis. Feng and coworkers have reported a one-pot solvothermal synthesis for melamine-assisted PtNi nanodendrites that can be employed as HER catalysts. The presence of melamine, defects incorporated in the structure, and the stairstepped atoms of these nanodendrites generate a highly efficient electrocatalyst due to an accelerated interfacial catalytic reaction. One important characteristic of this catalyst is its ability to function in both acidic and alkaline media. In 0.5 M KOH, 45 mV applied

potential is necessary at  $10 \text{ mA/cm}^2$ . The electrocatalyst shows HER activity in  $0.5 \text{ M H}_2\text{SO}_4$  medium as well [21].

Another Ni-incorporated Pt-based electrocatalyst nanostructure that is exceptionally efficient at HER was introduced by Huang et al. They decorated the  $\{111\}$  facet of PtNi NPs with NiO; the PtNi–O/C was obtained via annealing PtNi/C in air (see Fig. 4.4). In  $1 \text{ M KOH}$ , PtNi–O/C displayed a  $38.9 \text{ mV } \eta$  at  $10 \text{ mA/cm}^2$ . Formation of atomic layers of  $\text{Ni(OH)}_2$  at the  $\{111\}$  of PtNi–O/C improved the poor water dissociation displayed by other Pt-based HER catalysts, and this is thought to be a major cause of the impressive HER catalytic performance of PtNi–O/C nanostructures [22].

Pt-based electrocatalysts have also been alloyed with Ag to lower Pt loading as well as to improve catalytic activity. AgPt hollow nanostructures have high surface-to-volume ratios in addition to abundant catalytically active sites, which make them attractive candidates for electrocatalysts. Synthesis of hollow  $\text{Ag}_{44}\text{Pt}_{56}$  nanotube bundles with impressive HER activity in acidic media has been recently reported. These nanotube bundles are generated in a one-pot synthesis that is environmentally benign. The presence of the two metals, Ag and Pt, leads to synergistic effects and enhances the catalytic activity [23].

Pt loading of the HER catalysts can be also decreased by designing Pt nanostructure-loaded carbon supports. This introduces several advantageous traits into the electrocatalyst. First, the isolation of Pt NPs by the carbon support prevents the particle aggregation. Also, carbon supports improve electronic conductivity of the catalyst. Furthermore, the interactions between the support and the NPs generate synergistic effects beneficial for HER catalysis. An HER active electrocatalyst made of Pt supported on mesoporous nitrogen-doped carbon was reported by Li and coworkers. This Pt-based catalyst requires low Pt loading of  $\sim 7.20 \text{ wt\%}$ . The intrinsic activity of Pt is enhanced by nitrogen doping as well as the high exposed active surface area. The catalyst showed  $-7 \text{ mV } \eta$  at  $10 \text{ mA/cm}^2$  and 20 h of catalytic activity with negligible loss of performance [24].

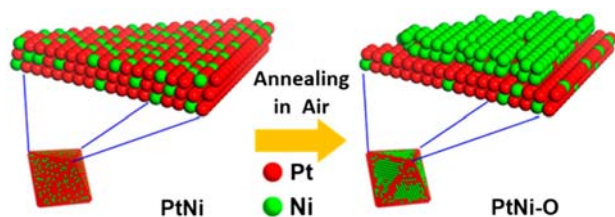


**FIGURE 4.4** Air annealing conversion of PtNi/C to PtNi–O/C [22]. Adapted with permission from Zhao Z, Liu H, Gao W, Xue W, Liu Z, Huang J, et al. Surface-engineered PtNi–O nanostructure with record-high performance for electrocatalytic hydrogen evolution reaction. *J Am Chem Soc* 2018;140:9046–9050. Available from: <https://doi.org/10.1021/jacs.8b04770>. Copyright 2019 American Chemical Society.



### 4.2.2 Nonnoble metal carbides and oxides

Mo-based electrocatalysts are pragmatic alternatives to the state-of-the-art Pt-based HER electrocatalysts due to their availability, cost effectiveness as well as favorable performance. The nitrogen-doped ultrathin Mo<sub>2</sub>C nanosheets synthesized by Chen et al. is one such electrocatalyst. The MoO<sub>2</sub> nanosheets have a thickness of  $\sim 1.1$  nm and the N–Mo<sub>2</sub>C nanosheets are of  $\sim 1.0$  nm thickness. The observed HER activity of 99 mV versus RHE at 10 mA/cm<sup>2</sup> current density is attributed to the high electrochemical area of the 2D N–Mo<sub>2</sub>C nanosheets, which leads to facile diffusion between the electrocatalyst and the electrolyte. Furthermore, the specific crystalline phase of N–Mo<sub>2</sub>C nanosheets has exposed more Mo active sites making the catalyst more efficient [25].

Even though WO<sub>3</sub> is preferable to Pt-based HER catalysts due to their low cost, performance of most reported WO<sub>3</sub> electrocatalysts for water splitting are inferior to Pt-based catalysts due to poor intrinsic activity. Zeng and coworkers used liquid exfoliation to synthesize WO<sub>3</sub> nanosheets with incorporated oxygen vacancies the inclusion of which elevates WO<sub>3</sub> to a degenerate semiconductor with improved conductivity. These modified WO<sub>3</sub> nanosheets display efficient HER activity with 38 mV  $\eta$  at 10 mA/cm<sup>2</sup> [26].

### 4.2.3 Nonnoble metal dichalcogenides and phosphides

Efficient hydrodesulfurization agents such as transition metal dichalcogenides and phosphides have been explored for their HER catalytic activity due to the similarity of the mechanisms of hydrodesulfurization and HER. Both the processes consist of reversible surface adsorption and desorption of hydrogen atoms. The electronegativity of the heteroatoms P and S allow for attraction of electron density from metal atoms, creating a negatively charged environment around the hetero atom. This negative environment is beneficial for trapping protons during HER [27].

Transition metal phosphides are synthesized by doping the transition metal crystal lattices with phosphorous [27]. Phosphorous doping leads to lowered hydrogen adsorption energy at the active sites, as well as improved hydrogen desorption from active sites. One example for an efficient transition metal phosphide HER catalyst is the mixed transition metal Ni–Co–P holey nanosheet, which has a low Tafel slope, 58 mV  $\eta$  at 1.56 V applied potential, and 10 mA/cm<sup>2</sup>. In addition to the favorable effects of P doping, this structure benefits from the synergistic effects between Ni and Co atoms. The catalyst has also shown long-term durability [28].

Transition metal dichalcogenide crystals consist of layers of metal each sandwiched between two layers of chalcogenide and bound by weak van der Waals interactions. In the 2D layered crystal structures of MoS<sub>2</sub>, though the edges show good electrocatalytic activity, the basal plane sites do not.

Therefore when designing MoS<sub>2</sub> catalysts care is taken to expose edge sites. This is achieved by engineering various porous MoS<sub>2</sub> nanostructures including nanosheets, nanodots, and monolayer nanosheets. Creating sulfur vacancies in the basal planes also helps optimize the active edge sites. A MoS<sub>2</sub> nanomesh with defects distributed evenly throughout the mesh has been found to display efficient HER catalytic activity with 160 mV  $\eta$  at 10 mA/cm<sup>2</sup> current density in 0.5 M H<sub>2</sub>SO<sub>4</sub>. The defects and holes have yielded optimal active edge sites, optimal hydrogen adsorption energy as well as good conductivity to the electrocatalyst [29].

To further improve MoS<sub>2</sub> electrocatalytic activity, a 2D electrocatalyst where Co(OH)<sub>2</sub> NPs are confined in MoS<sub>2</sub> have been synthesized in alkaline media. These NPs exhibit excellent HER activity and stability with 89 mV  $\eta$  at 10 mA/cm<sup>2</sup> current density. The stability of the catalyst is mainly due to the confinement of Co(OH)<sub>2</sub> in 2D MoS<sub>2</sub> nanosheets, which helps prevent aggregation (Fig. 4.5) [30].

In addition to doping or alloying MoS<sub>2</sub>-based copounds, formation of core-shell nanostructures could improve electrocatalytic performance of MoS<sub>2</sub>. Core-shell nanostructures would minimize aggregation of the nanocomponents of the catalyst and also, the electronic interactions between the core and shell materials could create synergistic effects. MoSe<sub>2</sub>@MoS<sub>2</sub> core-shell nanocomposites synthesized by a two-step hydrothermal method have been reported as an efficient HER catalyst. This core-shell structure shows improved electrocatalytic performance compared to single MoS<sub>2</sub> and MoSe<sub>2</sub> the core and shell materials used [31]. Also, MoS<sub>2</sub> hollow nanospheres encapsulated by controllable MoS<sub>2</sub> hollow microspheres have been

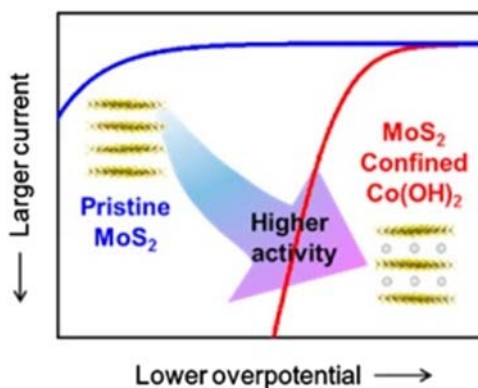


**FIGURE 4.5** The effect of confining Co(OH)<sub>2</sub> in 2D MoS<sub>2</sub> nanosheets [30]. Adapted with permission from Luo Y, Li X, Cai X, Zou X, Kang F, Cheng H-M, et al. Two-dimensional MoS<sub>2</sub> confined Co(OH)<sub>2</sub> electrocatalysts for hydrogen evolution in alkaline electrolytes. *ACS Nano* 2018;12:4565–4573. Available from: <https://doi.org/10.1021/acsnano.8b00942>. Copyright 2019 American Chemical Society.

synthesized and tested for HER activity. The structure allows for improved active sites and electronic conductivity. The catalyst is stable in acidic media, with a  $\eta$  of 112 mV at 10 mA/cm<sup>2</sup> [32].

#### 4.2.4 Other transition metal nanostructures

Surface nanostructuring enhances electrocatalytic performance by increasing the electrochemically active surface area. One complication of HER of water electrolysis is the adhesion of air bubbles on the electrode surface. Electrocatalysts engineered with nanostructure surfaces geared toward facilitating detachment of air bubbles have been designed. Electrodeposited alloy Ni–Co nanocones grown on copper substrate have been employed as HER electrocatalysts in 1.0 M KOH. Nanocones have nanosteps on their surface that lead to increased active surface area compared to nanowire, nanosheet structures. Also, these nanosteps introduce rough-edge active sites that enhance the rate of mass transportation. Furthermore, the Ni–Co alloy nanocones showed strong durability and HER activity at  $\eta$  107 mV to reach 10 mA/cm<sup>2</sup> current density [33]. Selected examples for HER nanoelectrocatalysts for water-splitting are listed in the Table 4.1.

### 4.3 OER catalysts

#### 4.3.1 Noble-metal nanocatalysts

Ru NPs are one of the most active OER electrocatalysts. One major drawback of using Ru NPs as OER catalysts is their oxidation in to various  $\text{Ru}^{x>4+}$  cations, and dissolution in the reaction media, which considerably shortens the lifetime of the catalyst. To slow down the dissolution of  $\text{Ru}^{x>4+}$ , and thereby improve OER activity of the catalyst, NP surfaces with low index facets are used. Gloag et al. successfully engineered bimetallic NPs with 3D branches that are also faceted using *fcc*-Au seeds and *hcp*-Ru branches. These Au–Ru branched NPs boast of a 1.45 V  $\eta$  at 10 mA/cm<sup>2</sup> in 0.1 M HClO<sub>4</sub>. In Au–Ru core-shell NPs this  $\eta$  limits the catalytic current density to 2.44 mA/cm<sup>2</sup> [50].

Kundu et al. synthesized a series of interconnected nanochain networks of Ru<sup>0</sup> NPs at temperatures 30°C, 45°C, and 60°C, which they named Ru-30, Ru-45, and Ru-60. These nanochain networks are synthesized without any surfactant present. In 0.1 M NaOH, all three of the nanochain networks show OER catalytic ability. The Ru<sup>0</sup> atoms on the surface undergo anodization and form RuO<sub>2</sub> during water electrolysis. This newly formed RuO<sub>2</sub> catalyzes OER process. Ru-30, Ru-45, and Ru-60 are reported to require an  $\eta$  of (308 ± 2) mV to yield a current density of 10 mA/cm<sup>2</sup> [51].

**TABLE 4.1** Summary of the performance of some HER electrocatalysts.

Material	Electrolyte	$\eta$ at current density	Tafel slope (mV/dec)	Reference
Porous Ni–CNT nanocone composite	1.0 M KOH	– 82 mV at – 10 mA/cm <sup>2</sup>	120	[34]
Mo <sub>2</sub> C on graphite oxide	0.5 M H <sub>2</sub> SO <sub>4</sub>	– 280 mV at – 5 mA/cm <sup>2</sup>	N/A	[35]
CoSe <sub>2</sub> /WSe <sub>2</sub> /WO <sub>3</sub> nanowires on carbon cloth	1.0 M KOH	– 115 mV at – 10 mA/cm <sup>2</sup>	121	[36]
Ni-doped FeP NPs on TiN nanowire arrays	1.0 M KOH	– 75 mV at – 10 mA/cm <sup>2</sup>	73	[37]
Ni <sub>2(1-x)</sub> Mo <sub>2x</sub> P nanowire arrays	1.0 M KOH	– 72 mV at – 10 mA/cm <sup>2</sup>	46.4	[38]
MoP@P-doped carbon NPs in CNTs	0.5 M H <sub>2</sub> SO <sub>4</sub>	– 75 mV at – 10 mA/cm <sup>2</sup>	55.9	[39]
WP nanostructures on carbon fibers	0.5 M H <sub>2</sub> SO <sub>4</sub>	– 137 mV at – 10 mA/cm <sup>2</sup>	69	[40]
Ni <sub>3</sub> S <sub>2</sub> –NiOOH nanocomposite on Ni foam	1.0 M NaOH	– 160 mV at – 10 mA/cm <sup>2</sup>	92	[41]
Pt–Ni NPs on N-doped porous nanostructure carbon	1.0 M KOH	– 42 mV at – 10 mA/cm <sup>2</sup>	82	[42]
CeO <sub>2</sub> –CoP–C nanostructure	0.5 M H <sub>2</sub> SO <sub>4</sub>	– 71 mV at – 10 mA/cm <sup>2</sup>	53	[43]
Co <sub>6</sub> Mo <sub>6</sub> C nanocrystals on graphene oxide	0.5 M H <sub>2</sub> SO <sub>4</sub>	– 64 mV at – 10 mA/cm <sup>2</sup>	44	[44]
CoP–CNT composite microparticles	0.5 M H <sub>2</sub> SO <sub>4</sub>	– 119 mV at – 10 mA/cm <sup>2</sup>	64	[45]
Co <sub>3</sub> Se <sub>4</sub> nanosheets embedded on N–CNT	1.0 M KOH	– 174 mV at – 10 mA/cm <sup>2</sup>	73.2	[46]
Co <sub>3</sub> Se <sub>4</sub> nanosheets embedded on N–CNT	0.5 M H <sub>2</sub> SO <sub>4</sub>	– 240 mV at – 10 mA/cm <sup>2</sup>	43.8	[46]
Cobalt/nitrogen-doped carbon	1.0 M KOH	– 224 mV at – 10 mA/cm <sup>2</sup>	88	[47]
Fe–MnO nanocubes on reduced GO nanoflakes	0.5 M H <sub>2</sub> SO <sub>4</sub>	– 721 mV (vs Ag/AgCl) at – 300 mA/cm <sup>2</sup>	107	[48]
3D MoS <sub>2</sub> –rGO@Mo nanohybrids	1.0 M KOH	– 123 mV at – 10 mA/cm <sup>2</sup>	62	[49]

*CNT*, carbon nanotube; *CF*, carbon fiber; *GO*, graphene oxide.

### 4.3.2 Nonnoble metal nanocatalysts

Tunable electronic structure, high number of active edges, and high specific area make 2D nanocatalysts attractive candidates for efficient electrocatalysts. The OER catalytic ability of NiPS<sub>3</sub> nanosheets layered with graphene was studied by Ren et al. As a result of synergistic effect these ultrathin composites show efficient OER activity demanding only an  $\eta$  of 294 mV for a catalytic current density 10 mA/cm<sup>2</sup> [52]. Due to their excellent electrical conductivity transition metal carbides are used as electrocatalysts. Ni/Ni<sub>3</sub>C core/shell hierarchical nanospheres have been shown to be efficient OER catalysts with 350 mV  $\eta$  at 10 mA/cm<sup>2</sup> in 0.1 M KOH solutions. This catalyst is environment friendly and has long-term durability [53].

Yan et al. modified the active site of a Cu-based OER electrocatalyst by metal doping. The goal of this exercise was to improve electron transfer between the electrocatalytic active site and the electrode. They synthesized Cu<sub>7</sub>S<sub>4</sub> nanodisks doped with Co and determined the OER activity in alkaline solutions. The  $\eta$  displayed by Co-doped Cu<sub>7</sub>S<sub>4</sub> nanodisks was 270 mV at 10 mA/cm<sup>2</sup>. Apart from the improved electron transfer due to Co doping, Co-induced phase transition improves OER kinetics [54].

In alkaline medium, by immobilizing Co<sub>2</sub>B and Co NPs in B- and N-doped carbon, an electrocatalyst was synthesized that has shown OER activity at 1.53 V at 10 mA/cm<sup>2</sup> and HER activity at 220 mV at 10 mA/cm<sup>2</sup>. The catalyst displayed multiple synergistic effects among its components [55]. Furthermore, a composite capable of catalyzing OER in alkaline medium was synthesized by Huang and coworkers with carbon-coated and nitrogen-doped CoP particles/CNTs. The CoP NPs are derived from Co-based metal organic frameworks. Being attached to CNT has ensured that the catalyst has high conductivity, and the porous structure has increased active surface area, and active sites that are exposed. These factors contribute to the low  $\eta$  required to achieve 10 mA/cm<sup>2</sup> OER catalytic current density. At 251 mV the CNT–NC–CoP composite reaches 10 mA/cm<sup>2</sup> [56].

Functionalized multiwall CNTs functionalized with nitrogen-rich emeraldine salt (ES) have been used to improve the electrocatalytic activity of magnetic maghemite ( $\gamma$ -Fe<sub>2</sub>O<sub>3</sub>). This stable electrocatalyst has shown efficient OER performance in 0.1 M NaOH of 1.52 V at 10 mA/cm<sup>2</sup>. In addition, these multiwall CNTs have proven to be durable with the catalyst being stable even after 5000 cycles of OER [57].

Co<sub>3</sub>O<sub>4</sub> NPs, which have high surface-to-volume ratio, have gained considerable interest as OER catalysts. However, due to high surface energy, as is the general tendency for NPs, these Co<sub>3</sub>O<sub>4</sub> NPs suffer from aggregation, which negatively impact catalytic activity. Moreover, poor conductivity limits the use of Co<sub>3</sub>O<sub>4</sub> NPs as electrocatalysts. Both of these complications could be overcome by incorporating the Co<sub>3</sub>O<sub>4</sub> NPs in a conductive carbon structure like graphene. Qiu et al. have used a Janus

architecture made with graphite and graphene to stabilize  $\text{Co}_3\text{O}_4$  NPs using electrochemical activation and hydrothermal hybridization techniques.  $\text{Co}_3\text{O}_4$  NPs are uniformly distributed in the architecture. The OER activity of this catalyst is 301 mV  $\eta$  at 10 mA/cm<sup>2</sup> [58].  $\text{Co}_3\text{O}_4$  porous nanosheets with exposed {112} high-index facets and oxygen vacancies have exhibited OER activity with 314 mV  $\eta$  at 10 mA/cm<sup>2</sup>. In addition, these nanosheets have been shown to be extremely durable with little effect on the  $\eta$  even after 14 h long testing. The porosity of the structure and the high number of exposed active sites are thought to be the reasons for the improved OER efficiency [59].

OER catalytic activity can be enhanced by surface amorphization. Chen et al. used fluoride surface engineering to improve a cobalt oxide/oxyhydroxide OER catalyst in alkaline media. Due to the high electronegativity of fluoride, Co centers become more ionized and therefore more hydrophilic. This improves the electron transfer abilities of the catalytic system and also facilitates optimal adsorption of the reactive species to the surface of the catalyst. OER activity of the ultrathin nanosheets of F–CoOOH/NF catalyst is 270 mV at 10 mA/cm<sup>2</sup> in basic medium [60].

Zhao et al. reported an OER catalyst synthesized by an anion exchange reaction where  $\text{Co}_4\text{Mn}_1$  LDH nanosheets were selenated to get Mn-modulated cobalt selenide nanosheets ( $\text{CoMnSe}_2$ ). This catalyst has abundant active sites, strategically engineered atomic disorder, and tuned electronic structure. In 1.0 M KOH  $\text{CoMnSe}_2$  requires an  $\eta$  of 0.27 V at a catalytic current density 10 mA/cm<sup>2</sup> [61].

Introduction of very small amounts of Au or Ag into transition-metal-based water-splitting catalysts has been found to improve their electrocatalytic ability due to the synergistic effects between the active catalytic sites and the metal centers. This principle has been applied to nanocomposites synthesized by embedding iron cobalt sulfides in N-doped carbon, where addition of the metallic Ag has improved its OER activity so that 37 mV less  $\eta$  is required to reach 10 mA/cm<sup>2</sup> catalytic current density compared to the non-Ag loaded Fe–Co–S/N-doped carbon nanocomposites in 1.0 M KOH. This enhancement of OER electrocatalytic activity is attributed to the increase of active electrochemical surface due to Ag loading [62].

Even though its availability and low toxicity along with demonstrated catalytic activity render  $\text{MnO}_2$  a desirable candidate for OER catalysis, poor conductivity and inadequate amount of exposed active sites limit its performance as a water-splitting catalyst. The poor conductivity could be remedied by inclusion of Al, Fe, Co, or Ni cations into  $\text{MnO}_2$ -based catalysts. This technique was used to synthesize  $\text{MnO}_2$  nanosheets doped with cobalt with added oxygen vacancies. These nanosheets were supported on carbon nanofibers functionalized with cobalt and nitrogen. In addition to improving conductivity, Co ions also participate in synergistic effects, which leads to improved catalytic performance. In 1 M KOH, this catalyst shows excellent durability and

279 mV  $\eta$  at 10 mA/cm<sup>2</sup> current density [63]. Selected examples for OER nano-electrocatalysts for water-splitting are listed in the Table 4.2.

## 4.4 Bifunctional electrocatalysts

For efficient water splitting, both HER and OER processes require catalysts. The state-of-the-art Pt-based HER catalysts perform better in acidic media. In contrast, metal oxides such as RuO<sub>2</sub>, which are most commonly used as OER catalysts, are unstable in acidic media and undergo deactivation. They have better performance in strong alkaline solutions. This mismatch of pH for the catalysts of the two half reactions makes it difficult to design bifunctional catalysts that are efficient for the overall water-splitting process. Bifunctional water-splitting electrocatalysts are applied as both anode and cathode in a typical water electrolysis cell.

### 4.4.1 Noble metal nanocatalysts

RuO<sub>2</sub>-based electrocatalysts have been successfully used for OER catalysis in both acidic and alkaline media. However, due to the tendency of RuO<sub>2</sub> to oxidize into RuO<sub>4</sub>, which dissolves in the electrolyte solution, maintaining catalytic activity for extended periods is challenging. One-dimensional RuO<sub>2</sub> nanorods (NR) synthesized by calcinating a carbon slurry containing Ru<sup>3+</sup> ions at 500°C have shown to retain its performance for 500 continuous cycles. These RuO<sub>2</sub> NRs are formed without using any stabilizers and have OER activity in 1.0 M NaOH and good HER activity in 0.5 M H<sub>2</sub>SO<sub>4</sub>. The 1D morphology of the catalyst has rendered a high surface-to-volume ratio, which leads to efficient electrocatalytic activity [74].

### 4.4.2 Nonnoble metal nanocatalysts

Ni-based compounds with metallic characteristics have gained interest for catalysis of water splitting due to their abundant availability, cost effectiveness, as well as environmental friendliness. Since they have both proton acceptor and hydride acceptor centers, in alkaline media nickel phosphides are used as both HER and OER catalysts. To improve their performance, surface engineering or inclusion of other metal species is carried out. Yan and coworkers have employed both these techniques to create vanadium-doped oxygen plasma Ni<sub>2</sub>P nanosheets for efficient overall water splitting. This bifunctional catalyst requires 1.56 V  $\eta$  to reach 10 mA/cm<sup>2</sup> current density when it is used as both the cathode and the anode [75]. Also, Ni<sub>x</sub>P<sub>y</sub> type electrocatalysts have been employed for activating both OER and HER processes. The Ni<sub>x</sub>P<sub>y</sub> with the richest Ni<sub>5</sub>P<sub>4</sub> phase at 350°C (Ni<sub>x</sub>P<sub>y</sub> – 350) displayed an efficient HER catalytic activity in both acidic and alkaline media. Furthermore, excellent overall water splitting with Ni<sub>x</sub>P<sub>y</sub> – 350) yielding

**TABLE 4.2** Summary of the performance of some OER electrocatalysts.

Material	Electrolyte	$\eta$ at current density	Tafel slope (mV/dec)	Reference
CoMnSe <sub>2</sub> nanosheets	1.0 M KOH	270 mV at 10 mA/cm <sup>2</sup>	39	[61]
FeNiPs in N-doped carbon nanofiber	1.0 M KOH	300 mV at 10 mA/cm <sup>2</sup>	47	[64]
Fe-doped Co <sub>9</sub> S <sub>8</sub> nanomicrospheres on Ni foam	1.0 M KOH	270 mV at 10 mA/cm <sup>2</sup>	70	[65]
NiFeS <sub>2</sub> NPs on graphene	1.0 M KOH	320 mV at 10 mA/cm <sup>2</sup>	61	[66]
Ni/Co-based nanosheet arrays	1.0 M KOH	247 mV at 10 mA/cm <sup>2</sup>	35	[67]
DNA@IrO <sub>2</sub> NPs	0.1 M NaOH	312 mV at 10 mA/cm <sup>2</sup>	90	[68]
NiCoSe <sub>2</sub> @NiO@CoNi <sub>2</sub> S <sub>4</sub> @CoS <sub>2</sub> on Ni foam	1.0 M KOH	310 mV at 30 mA/cm <sup>2</sup>	159.1	[69]
FeOOH@Ni <sub>3</sub> Si <sub>4</sub> O <sub>10</sub> (OH) <sub>2</sub> .5H <sub>2</sub> O hybrid nanospindle	1.0 M KOH	234 mV at 10 mA/cm <sup>2</sup>	56	[70]
Co <sub>3</sub> ZnC/Co@N-doped carbon	1.0 M KOH	366 mV at 10 mA/cm <sup>2</sup>	81	[71]
CoP/Carbon dots	1.0 M KOH	400 mV at 10 mA/cm <sup>2</sup>	N/A	[72]
Pore-rich FeP nanorods on carbon nanotube	1.0 M KOH	300 mV at 10 mA/cm <sup>2</sup>	53	[73]



10 mA/cm<sup>2</sup> catalytic current density at 1.57 V applied potential in strongly alkaline media has been reported [76]. A bifunctional catalyst for both HER and OER of water splitting has been proposed using Ni<sub>8</sub>P<sub>3</sub> carbon-coated 3D nanosheet array. The bifunctionality is suggested to arise from high conductivity of the electrocatalyst and the high number of active sites present in the 3D nanosheet array. This catalyst is HER active in both acidic and alkaline media. To reach a current density of 10 mA/cm<sup>2</sup>, it requires an  $\eta$  of 267 mV. Development of the heterojunction of Ni<sub>8</sub>P<sub>3</sub>/NiO<sub>x</sub> creates a synergistic effect, which leads to efficient OER activity. This 3D carbon-coated Ni<sub>8</sub>P<sub>3</sub> nanosheet array has an overall water-splitting ability with 1.65 V  $\eta$  at 10 mA/cm<sup>2</sup> [77].

#### 4.4.3 Intermetallic nonnoble nanocatalysts

Vanadium-doped NiS<sub>2</sub> nanosheets have been reported as highly active electrode for water splitting. Ni complexes with semiconductor properties are known to be poor catalysts for water splitting due to their inefficiency in electron transportation. Here, doping of semiconductor NiS<sub>2</sub> with vanadium introduces metallic characteristics to the catalyst and reconfigures the electronic structure of NiS<sub>2</sub> thus improving the electron transportation ability to facilitate good catalytic efficiency. These vanadium-doped NiS<sub>2</sub> nanosheets display 290 mV  $\eta$  for OER and 110 mV for HER at 10 mA/cm<sup>2</sup> (Fig. 4.6) [78].

An OER efficient heterostructure was designed by combining NiFe<sub>2</sub>O<sub>4</sub> NPs and LDH of NiFe on Ni foam. This heterostructure is capable of driving 1000 mA/cm<sup>2</sup> current density at 265 mV. The HER activity of this electrocatalyst is equally impressive with current density of 750 mA/cm<sup>2</sup> driven at 314 mV. Combination of NiFe<sub>2</sub>O<sub>4</sub> NPs with the Ni(LDH) nanosheets

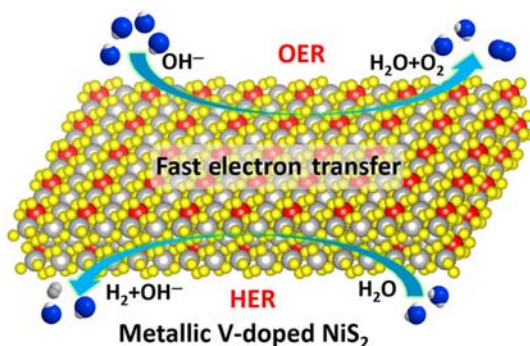


**FIGURE 4.6** Illustration of overall water splitting by vanadium-doped NiS<sub>2</sub> nanosheets [78]. Adapted with permission from Liu H, He Q, Jiang H, Lin Y, Zhang Y, Habib M, et al. Electronic structure reconfiguration toward pyrite NiS<sub>2</sub> via engineered heteroatom defect boosting overall water splitting. *ACS Nano* 2017;11:11574–11583. Available from: <https://doi.org/10.1021/acs-nano.7b06501>. Copyright 2019 American Chemical Society.

improves the charge transfer ability as well as increases the electrochemically active surface area. When the heterostructure array is used as both anode and cathode, the overall water-splitting ability is reported to be 1.535 V  $\eta$  at 10 mA/cm<sup>2</sup> [79].

Electrospun cobalt NPs embedded in porous carbon nanofibers doped with nitrogen (Co–PNCNFs) have high OER activity in alkaline medium due to the porosity of the structure as well as the strong synergistic effect due to nitrogen doping and encapsulated metallic Co NPs. The system also displays HER activity. Overall, when Co–PNCNFs are used as the anode and the cathode, the  $\eta$  required is 1.66 V to reach a catalytic current density of 10 mA/cm<sup>2</sup> [80].

Metallic Co and Ni active sites have low hydrogen adsorption energies. Heterostructures of NiCo–NiCoO<sub>2</sub> embedded in carbon doped with nitrogen are reported to be an efficient bifunctional electrocatalysts for overall water splitting in alkaline media. This heterostructure retains its performance for at least 50 h. The carbon encapsulation of NiCo–NiCoO<sub>2</sub> NPs have ensured that this catalytic system is stable for extended periods of time. Also, this bimetallic thin-film electrocatalyst benefits from the synergistic effects between Ni and Co as well as between Ni and Ni oxide and Co and Co oxide. When this heterostructure is used for both anode and cathode for overall water splitting 1.44 V  $\eta$  is required to achieve a current density of 20 mA/cm<sup>2</sup> [81].

Another stable Ni Co intermetallic catalyst efficient in catalyzing both HER and OER in neutral pH (1 M PBS, pH 7) is Ni<sub>0.1</sub>Co<sub>0.9</sub>P porous nanosheets on carbon fiber paper. These nanosheets were used as both cathode and anode with ~100% Faradaic efficiency where 1.89 V  $\eta$  was required to reach 10 mA/cm<sup>2</sup>. A 2:1 ratio of H<sub>2</sub>:O<sub>2</sub> was obtained from this system [82].

An efficient catalyst for both HER and OER in alkaline media was reported by Sun and coworkers. Nickel diselenide NPs electrodeposited on Ti plate (NiSe<sub>2</sub>/Ti) in 1.0 M KOH behave as a stable and efficient bifunctional catalyst with 96 mV  $\eta$  at 10 mA/cm<sup>2</sup> for HER and 295 mV at 20 mA/cm<sup>2</sup> for OER. Another advantage of this bifunctional catalyst is its low cost, which greatly enhances the scalability of the catalyst for industrial use [83]. Moreover, by electrodepositing a Co nanosheet array, which functions as the HER electrocatalyst, and a CoFeBO nanosheet array, which is the OER electrocatalyst, a bifunctional catalytic system was grown on Ni foam electrodes. This system is reported to have better performance than the current state-of-the-art Pt/C and IrO<sub>2</sub> electrocatalysts used for water splitting at  $\eta$ s greater than 50 mV. In addition, this catalyst retains its activity over an extended period in 1.0 M KOH. For the HER process, an  $\eta$  of 20 mV was required to achieve a current density of 10 mA/cm<sup>2</sup>. This high efficiency is due to the large number of active sites present in Co nanosheet array. For OER an  $\eta$  of 245 mV was required to achieve a current density of 10 mA/cm<sup>2</sup> [84].

$\text{Ni}_3\text{S}_2$  nanorods doped with Mo have been grown on 3D Ni foam and tested for their overall water-splitting electrocatalytic ability. This catalyst has high active surface area and uniform growth due its structure, as well as high charge transfer ability. These factors lead to high electrocatalytic performance. In 1.0 M KOH, HER activity requires  $\eta$  of 278 and 180 mV for OER to reach 100 mA/cm<sup>2</sup> current density [85]. Also,  $\text{CoSn}_2$  tetragonal nanocrystals grown on fluorine-doped tin oxide (FTO) were synthesized by Menezes et al. In 1 M KOH, Co from  $\text{CoSn}_2$  oxidizes and Sn is lost from the crystal lattice. This results in highly disordered  $\text{CoO}_x(\text{H})$ , which acts as a catalyst for OER. The OER process displays an  $\eta$  of 299 mV at 10 mA/cm<sup>2</sup>. The catalyst also showed HER activity with current density 10 mA/cm<sup>2</sup> at  $\eta$  50 mV. For the HER process, the  $\text{Co}^0$  is the active site [86]. Selected examples for bifunctional nano-electrocatalysts for water-splitting are listed in the Table 4.3

## 4.5 Summary

In this chapter we discussed recent developments in metal-based nanofunctionalized electrocatalysts for HER and OER processes and for overall water splitting. Dependence on nonrenewable fossil fuels as the primary source of energy has led to an energy crisis as well as harmful effects on the environment. To reduce the dependence on fossil fuel as an energy source,  $\text{H}_2$  production by water electrolysis can be used. Water electrolysis is a sustainable, scalable, and environmentally friendly process with high energy storage density to obtain  $\text{H}_2$ . For efficient  $\text{H}_2$  production by water electrolysis catalysts need to be used. Pt-based electrocatalysts for HER and  $\text{RuO}_2$  and  $\text{IrO}_2$  for OER require very low  $\eta$  and show excellent activity. However, the scarcity and cost of these catalysts as well as the issues with stability have encouraged the use of more economical noble metal-based catalysts as well as development of earth abundant and cost-effective transition metal oxides, carbides, sulfides, and phosphides for HER and transition metal oxides and hydroxides and bimetallic or trimetallic compounds of Co, Ni, and Mn as OER catalysts. However, many improvements and structural tweaks are required to match the catalytic performance of industrially used OER and HER catalysts.

To decrease Pt-loading, Pt-based nanostructures have been alloyed with first row transition metals such as Fe, Co, and Ni, and also electrocatalysts with Pt nanostructure-loaded carbon supports have been designed.

In order to improve catalytic activity of transition metal-based electrocatalysts various techniques have been employed. Poor charge transfer ability is improved by doping and alloying with other metals. To increase the number of exposed active sites in TMDs, various porous nanostructures have been designed. Doping transition metal nancatalysts with heteroatoms to lower hydrogen adsorption energy at active sites. For increased active

**TABLE 4.3** Summary of the performance of some bifunctional water-splitting electrocatalysts.

Material	Electrolyte	OER activity $\eta$ at current density	HER activity, $\eta$ at current density	Two electrode system $\eta_{10}$ (V)	Reference
Ni <sub>5</sub> P <sub>4</sub> on Ni foam	1.0 M KOH	182 mV at 10 mA/cm <sup>2</sup>	64 mV at 10 mA/cm <sup>2</sup>	N/A	[87]
Carbon-encapsulated NiFe NPs	1.0 M KOH	274 mV at 10 mA/cm <sup>2</sup>	195 mV at 10 mA/cm <sup>2</sup>	1.575	[88]
S, N codoped CNT-encapsulated core-shelled CoS <sub>2</sub> @Co	1.0 M KOH	157 mV at 10 mA/cm <sup>2</sup>	112 mV at 10 mA/cm <sup>2</sup>	1.633	[89]
3D networked Ni <sub>2</sub> P/Ni <sub>3</sub> S <sub>2</sub> heteronanoflake arrays on Ni foam	1.0 M KOH	210 mV at 10 mA/cm <sup>2</sup>	80 mV at 10 mA/cm <sup>2</sup>	1.45	[90]
Zeolitic imidazolate framework@LDH on Ni foam	1.0 M KOH	318 mV at 10 mA/cm <sup>2</sup>	106 mV at 10 mA/cm <sup>2</sup>	1.59	[91]
FeCo <sub>2</sub> S <sub>4</sub> NSAs on Ni Foam	1.0 M KOH	270 mV at 50 mA/cm <sup>2</sup>	132 mV at 10 mA/cm <sup>2</sup>	1.56	[92]
Ni <sub>3</sub> FeN/CC	1.0 M KOH	190 mV at 10 mA/cm <sup>2</sup>	105 mV at 10 mA/cm <sup>2</sup>	N/A	[93]
Ni <sub>1.85</sub> Fe <sub>0.15</sub> P NSAs on Ni Foam	1.0 M KOH	270 mV at 20 mA/cm <sup>2</sup>	106 mV at 10 mA/cm <sup>2</sup>	1.61	[94]
P–CoMoS/CC	1.0 M KOH	260 mV at 10 mA/cm <sup>2</sup>	66 mV at 10 mA/cm <sup>2</sup>	1.54	[95]
NiCoFe <sub>x</sub> P/CC	1.0 M KOH	275 mV at 50 mA/cm <sup>2</sup>	39 mV at 10 mA/cm <sup>2</sup>	1.51	[96]
3D Ni <sub>3</sub> S <sub>2</sub> on Ni Foam	1.0 M KOH	242 mV at 10 mA/cm <sup>2</sup>	89 mV at 10 mA/cm <sup>2</sup>	1.577	[97]
Carbon-coated Ni <sub>8</sub> P <sub>3</sub> NSAs	1.0 M KOH	267 mV at 10 mA/cm <sup>2</sup>	110 mV at 10 mA/cm <sup>2</sup>	1.65	[77]

LDH, layered double hydroxide; CC, carbon cloth; NSA, nanosheet array.

surface area compared to nanosheets and nanowires, transition metal nanocubes have been synthesized.

Nanofunctionalization allows water-splitting electrocatalysts to achieve increased active surface area, introduce disorder and porosity to the structures, enhance electrical conductivity, gain increased stability by forgoing polymer binders, as well as create synergistic effects by doping nanomaterials with metals. All these modifications aid the design of economical, robust, and efficient electrocatalysts.

## References

- [1] Nuclear Power in the World Today 2018. <<http://www.world-nuclear.org/information-library/current-and-future-generation/nuclear-power-in-the-world-today.aspx>>.
- [2] Dresselhaus MS, Thomas IL. Alternative energy technologies. *Nature* 2001;414:332–7. Available from: <https://doi.org/10.1038/35104599>.
- [3] Armaroli N, Balzani V. The future of energy supply: challenges and opportunities. *Angew Chem Int Ed* 2007;46:52–66. Available from: <https://doi.org/10.1002/anie.200602373>.
- [4] Ishida T, Gokon N, Hatamachi T, Kodama T. Kinetics of thermal reduction step of thermochemical two-step water splitting using CeO<sub>2</sub> particles: MASTER-plot method for analyzing non-isothermal experiments. *Energy Procedia* 2014;49:1970–9. Available from: <https://doi.org/10.1016/j.egypro.2014.03.209>.
- [5] Orhan M, Dincer I, Rosen M. Energy and exergy assessments of the hydrogen production step of a copper–chlorine thermochemical water splitting cycle driven by nuclear-based heat. *Int J Hydrog Energy* 2008;33:6456–66. Available from: <https://doi.org/10.1016/j.ijhydene.2008.08.035>.
- [6] Kirner JT, Finke RG. Water-oxidation photoanodes using organic light-harvesting materials: a review. *J Mater Chem A* 2017;5:19560–92. Available from: <https://doi.org/10.1039/C7TA05709A>.
- [7] Chen Y, Wang Y, Xu H, Xiong G. Efficient production of hydrogen from natural gas steam reforming in palladium membrane reactor. *Appl Catal B Env* 2008;81:283–94. Available from: <https://doi.org/10.1016/j.apcatb.2007.10.024>.
- [8] Li X, Hao X, Abudula A, Guan G. Nanostructured catalysts for electrochemical water splitting: current state and prospects. *J Mater Chem A* 2016;4:11973–2000. Available from: <https://doi.org/10.1039/C6TA02334G>.
- [9] Li J, Zheng G. One-dimensional earth-abundant nanomaterials for water-splitting electrocatalysts. *Adv Sci* 2017;4:1600380. Available from: <https://doi.org/10.1002/advs.201600380>.
- [10] Morales-Guio CG, Stern L-A, Hu X. Nanostructured hydrotreating catalysts for electrochemical hydrogen evolution. *Chem Soc Rev* 2014;43:6555. Available from: <https://doi.org/10.1039/C3CS60468C>.
- [11] Wang H, Lee H-W, Deng Y, Lu Z, Hsu P-C, Liu Y, et al. Bifunctional non-noble metal oxide nanoparticle electrocatalysts through lithium-induced conversion for overall water splitting. *Nat Commun* 2015;6:7261. Available from: <https://doi.org/10.1038/ncomms8261>.
- [12] Bajdich M, García-Mota M, Vojvodic A, Nørskov JK, Bell AT. Theoretical investigation of the activity of cobalt oxides for the electrochemical oxidation of water. *J Am Chem Soc* 2013;135:13521–30. Available from: <https://doi.org/10.1021/ja405997s>.

- [13] Anantharaj S, Ede SR, Sakthikumar K, Karthick K, Mishra S, Kundu S. Recent trends and perspectives in electrochemical water splitting with an emphasis on sulfide, selenide, and phosphide catalysts of Fe, Co, and Ni: a review. *ACS Catal* 2016;6:8069–97. Available from: <https://doi.org/10.1021/acscatal.6b02479>.
- [14] Seh ZW, Kibsgaard J, Dickens CF, Chorkendorff I, Nørskov JK, Jaramillo TF. Combining theory and experiment in electrocatalysis: insights into materials design *Science* 2017;80, 355:eaad4998. Available from: <https://doi.org/10.1126/science.aad4998>.
- [15] Voiry D, Yamaguchi H, Li J, Silva R, Alves DCB, Fujita T, et al. Enhanced catalytic activity in strained chemically exfoliated WS<sub>2</sub> nanosheets for hydrogen evolution. *Nat Mater* 2013;12:850–5. Available from: <https://doi.org/10.1038/nmat3700>.
- [16] Chang Y-H, Lin C-T, Chen T-Y, Hsu C-L, Lee Y-H, Zhang W, et al. Highly efficient electrocatalytic hydrogen production by MoS<sub>x</sub> grown on graphene-protected 3D Ni foams. *Adv Mater* 2013;25:756–60. Available from: <https://doi.org/10.1002/adma.201202920>.
- [17] Zhan Y, Liu Z, Najmaei S, Ajayan PM, Lou J. Large-area vapor-phase growth and characterization of MoS<sub>2</sub> atomic layers on a SiO<sub>2</sub> substrate. *Small* 2012;8:966–71. Available from: <https://doi.org/10.1002/sml.201102654>.
- [18] Sabatier P. Hydrogénations et déshydrogénations par catalyse. *Berichte Der Dtsch Chem Ges* 1911;44:1984–2001.
- [19] Liang Y, Li Y, Wang H, Dai H. Strongly coupled inorganic/nanocarbon hybrid materials for advanced electrocatalysis. *J Am Chem Soc* 2013;135:2013–36. Available from: <https://doi.org/10.1021/ja3089923>.
- [20] Cheng N, Stambula S, Wang D, Banis MN, Liu J, Riese A, et al. Platinum single-atom and cluster catalysis of the hydrogen evolution reaction. *Nat Commun* 2016;7:13638. Available from: <https://doi.org/10.1038/ncomms13638>.
- [21] Huang X-Y, Wang A-J, Zhang L, Fang K-M, Wu L-J, Feng J-J. Melamine-assisted solvothermal synthesis of PtNi nanodendrites as highly efficient and durable electrocatalyst for hydrogen evolution reaction. *J Colloid Interface Sci* 2018;531:578–84. Available from: <https://doi.org/10.1016/j.jcis.2018.07.051>.
- [22] Zhao Z, Liu H, Gao W, Xue W, Liu Z, Huang J, et al. Surface-engineered PtNi-O nanostructure with record-high performance for electrocatalytic hydrogen evolution reaction. *J Am Chem Soc* 2018;140:9046–50. Available from: <https://doi.org/10.1021/jacs.8b04770>.
- [23] Zhu X-Y, Zhang L, Yuan P-X, Feng J-J, Yuan J, Zhang Q-L, et al. Hollow Ag<sub>44</sub>Pt<sub>56</sub> nanotube bundles with high electrocatalytic performances for hydrogen evolution and ethylene glycol oxidation reactions. *J Colloid Interface Sci* 2018;532:571–8. Available from: <https://doi.org/10.1016/j.jcis.2018.08.016>.
- [24] Yin Y, Liu T, Liu D, Wang Z, Deng Q, Qu D, et al. Confining nano-sized platinum in nitrogen doped ordered mesoporous carbon: an effective approach toward efficient and robust hydrogen evolution electrocatalyst. *J Colloid Interface Sci* 2018;530:595–602. Available from: <https://doi.org/10.1016/j.jcis.2018.06.096>.
- [25] Jia J, Xiong T, Zhao L, Wang F, Liu H, Hu R, et al. Ultrathin N-doped Mo<sub>2</sub>C nanosheets with exposed active sites as efficient electrocatalyst for hydrogen evolution reactions. *ACS Nano* 2017;11:12509–18. Available from: <https://doi.org/10.1021/acsnano.7b06607>.
- [26] Zheng T, Sang W, He Z, Wei Q, Chen B, Li H, et al. Conductive tungsten oxide nanosheets for highly efficient hydrogen evolution. *Nano Lett* 2017;17:7968–73. Available from: <https://doi.org/10.1021/acs.nanolett.7b04430>.
- [27] Shi Y, Zhang B. Recent advances in transition metal phosphide nanomaterials: synthesis and applications in hydrogen evolution reaction. *Chem Soc Rev* 2016;45:1529–41. Available from: <https://doi.org/10.1039/C5CS00434A>.

- [28] Fang Z, Peng L, Qian Y, Zhang X, Xie Y, Cha JJ, et al. Dual tuning of Ni–Co–A (A = P, Se, O) nanosheets by anion substitution and holey engineering for efficient hydrogen evolution. *J Am Chem Soc* 2018;140:5241–7. Available from: <https://doi.org/10.1021/jacs.8b01548>.
- [29] Li Y, Yin K, Wang L, Lu X, Zhang Y, Liu Y, et al. Engineering MoS<sub>2</sub> nanomesh with holes and lattice defects for highly active hydrogen evolution reaction. *Appl Catal B Env* 2018;239:537–44. Available from: <https://doi.org/10.1016/j.apcatb.2018.05.080>.
- [30] Luo Y, Li X, Cai X, Zou X, Kang F, Cheng H-M, et al. Two-dimensional MoS<sub>2</sub> confined Co(OH)<sub>2</sub> electrocatalysts for hydrogen evolution in alkaline electrolytes. *ACS Nano* 2018;12:4565–73. Available from: <https://doi.org/10.1021/acsnano.8b00942>.
- [31] Ren X, Wei Q, Ren P, Wang Y, Chen R. Synthesis of flower-like MoSe<sub>2</sub>@MoS<sub>2</sub> nanocomposites as the high efficient water splitting electrocatalyst. *Mater Lett* 2018;231:213–16. Available from: <https://doi.org/10.1016/j.matlet.2018.08.049>.
- [32] Guo B, Yu K, Li H, Song H, Zhang Y, Lei X, et al. Hollow structured micro/nano MoS<sub>2</sub> spheres for high electrocatalytic activity hydrogen evolution reaction. *ACS Appl Mater Interfaces* 2016;8:5517–25. Available from: <https://doi.org/10.1021/acsami.5b10252>.
- [33] Darband GB, Aliofkhazraei M, Rouhaghdam AS, Kiani MA. Three-dimensional Ni-Co alloy hierarchical nanostructure as efficient non-noble-metal electrocatalyst for hydrogen evolution reaction. *Appl Surf Sci* 2019;465:846–62. Available from: <https://doi.org/10.1016/j.apsusc.2018.09.204>.
- [34] Barati Darband G, Aliofkhazraei M, Sabour Rouhaghdam A. Three-dimensional porous Ni-CNT composite nanocones as high performance electrocatalysts for hydrogen evolution reaction. *J Electroanal Chem* 2018;829:194–207. Available from: <https://doi.org/10.1016/j.jelechem.2018.10.012>.
- [35] Kim SK, Qiu Y, Zhang Y-J, Hurt R, Peterson A. Nanocomposites of transition-metal carbides on reduced graphite oxide as catalysts for the hydrogen evolution reaction. *Appl Catal B Env* 2018;235:36–44. Available from: <https://doi.org/10.1016/j.apcatb.2018.04.032>.
- [36] Lv Y, Liu Y, Liu Y, Chen Z, Zhang M. CoSe<sub>2</sub>/WSe<sub>2</sub>/WO<sub>3</sub> hybrid nanowires on carbon cloth for efficient hydrogen evolution reaction. *J Alloy Compd* 2018;768:889–95. Available from: <https://doi.org/10.1016/j.jallcom.2018.07.285>.
- [37] Peng X, Qasim AM, Jin W, Wang L, Hu L, Miao Y, et al. Ni-doped amorphous iron phosphide nanoparticles on TiN nanowire arrays: an advanced alkaline hydrogen evolution electrocatalyst. *Nano Energy* 2018;53:66–73. Available from: <https://doi.org/10.1016/j.nanoen.2018.08.028>.
- [38] Yu L, Mishra IK, Xie Y, Zhou H, Sun J, Zhou J, et al. Ternary Ni<sub>2(1-x)</sub>Mo<sub>2x</sub>P nanowire arrays toward efficient and stable hydrogen evolution electrocatalysis under large-current-density. *Nano Energy* 2018;53:492–500. Available from: <https://doi.org/10.1016/j.nanoen.2018.08.025>.
- [39] Li J-S, Wang X-R, Li J-Y, Zhang S, Sha J-Q, Liu G-D, et al. Pomegranate-like molybdenum phosphide@phosphorus-doped carbon nanospheres coupled with carbon nanotubes for efficient hydrogen evolution reaction. *Carbon N Y* 2018;139:234–40. Available from: <https://doi.org/10.1016/j.carbon.2018.06.058>.
- [40] Xu K, Fu X, Li H, Peng Z. A novel composite of network-like tungsten phosphide nanostructures grown on carbon fibers with enhanced electrocatalytic hydrogen evolution efficiency. *Appl Surf Sci* 2018;456:230–7. Available from: <https://doi.org/10.1016/j.apsusc.2018.06.106>.



- [41] Wang X, Liu R, Zhang Y, Zeng L, Liu A. Hierarchical Ni<sub>3</sub>S<sub>2</sub>-NiOOH hetero-nanocomposite grown on nickel foam as a noble-metal-free electrocatalyst for hydrogen evolution reaction in alkaline electrolyte. *Appl Surf Sci* 2018;456:164–73. Available from: <https://doi.org/10.1016/j.apsusc.2018.06.107>.
- [42] Nadeem M, Yasin G, Bhatti MH, Mehmood M, Arif M, Dai L. Pt-M bimetallic nanoparticles (M = Ni, Cu, Er) supported on metal organic framework-derived N-doped nanostructured carbon for hydrogen evolution and oxygen evolution reaction. *J Power Sour* 2018;402:34–42. Available from: <https://doi.org/10.1016/j.jpowsour.2018.09.006>.
- [43] Xiong L, Bi J, Wang L, Yang S. Improving the electrocatalytic property of CoP for hydrogen evolution by constructing porous ternary CeO<sub>2</sub>-CoP-C hybrid nanostructure via ionic exchange of MOF. *Int J Hydrog Energy* 2018;43:20372–81. Available from: <https://doi.org/10.1016/j.ijhydene.2018.09.117>.
- [44] He C, Zhang S, Tao J, Qiu Y. Ultrafine Co<sub>6</sub>Mo<sub>6</sub>C nanocrystals on reduced graphene oxide as efficient and highly stable electrocatalyst for hydrogen generation. *Int J Hydrog Energy* 2018;43:20323–31. Available from: <https://doi.org/10.1016/j.ijhydene.2018.09.019>.
- [45] Kim JK, Park S-K, Kang YC. Structure-optimized CoP-carbon nanotube composite microspheres synthesized by spray pyrolysis for hydrogen evolution reaction. *J Alloy Compd* 2018;763:652–61. Available from: <https://doi.org/10.1016/j.jallcom.2018.05.357>.
- [46] Bose R, Patil B, Rajendiran Jothi V, Kim T-H, Arunkumar P, Ahn H, et al. Co<sub>3</sub>Se<sub>4</sub> nanosheets embedded on N-CNT as an efficient electroactive material for hydrogen evolution and supercapacitor applications. *J Ind Eng Chem* 2018;65:62–71. Available from: <https://doi.org/10.1016/j.jiec.2018.04.013>.
- [47] Chen X, Zhen X, Gong H, Li L, Xiao J, Xu Z, et al. Cobalt and nitrogen codoped porous carbon as superior bifunctional electrocatalyst for oxygen reduction and hydrogen evolution reaction in alkaline medium. *Chin Chem Lett* 2018;. Available from: <https://doi.org/10.1016/j.cclet.2018.09.017>.
- [48] Rezaei B, Taghipour Jahromi AR, Ensafi AA. Porous magnetic iron- manganese oxide nanocubes derived from metal organic framework deposited on reduced graphene oxide nanoflake as a bi-functional electrocatalyst for hydrogen evolution and oxygen reduction reaction. *Electrochim Acta* 2018;283:1359–65. Available from: <https://doi.org/10.1016/j.electacta.2018.07.105>.
- [49] He B, Chen L, Jing M, Zhou M, Hou Z, Chen X. 3D MoS<sub>2</sub>-rGO@Mo nanohybrids for enhanced hydrogen evolution: the importance of the synergy on the Volmer reaction. *Electrochim Acta* 2018;283:357–65. Available from: <https://doi.org/10.1016/j.electacta.2018.06.168>.
- [50] Gloag L, Benedetti TM, Cheong S, Li Y, Chan X-H, Lacroix L-M, et al. Three-dimensional branched and faceted gold-ruthenium nanoparticles: using nanostructure to improve stability in oxygen evolution electrocatalysis. *Angew Chem Int Ed* 2018;57:10241–5. Available from: <https://doi.org/10.1002/anie.201806300>.
- [51] Anantharaj S, Jayachandran M, Kundu S. Unprotected and interconnected Ru<sup>0</sup> nano-chain networks: advantages of unprotected surfaces in catalysis and electrocatalysis. *Chem Sci* 2016;7:3188–205. Available from: <https://doi.org/10.1039/C5SC04714E>.
- [52] Xue S, Chen L, Liu Z, Cheng H-M, Ren W. NiPS<sub>3</sub> nanosheet–graphene composites as highly efficient electrocatalysts for oxygen evolution reaction. *ACS Nano* 2018;12:5297–305. Available from: <https://doi.org/10.1021/acsnano.7b09146>.
- [53] Qin Q, Hao J, Zheng W. Ni/Ni<sub>3</sub>C core/shell hierarchical nanospheres with enhanced electrocatalytic activity for water oxidation. *ACS Appl Mater Interfaces* 2018;10:17827–34. Available from: <https://doi.org/10.1021/acsaami.8b00716>.



- [54] Li Q, Wang X, Tang K, Wang M, Wang C, Yan C. Electronic modulation of electrocatalytically active center of  $\text{Cu}_7\text{S}_4$  nanodisks by cobalt-doping for highly efficient oxygen evolution reaction. *ACS Nano* 2017;11:12230–9. Available from: <https://doi.org/10.1021/acsnano.7b05606>.
- [55] Liu X, Wang Y, Chen L, Chen P, Jia S, Zhang Y, et al.  $\text{Co}_2\text{B}$  and Co nanoparticles immobilized on the N–B-doped carbon derived from nano- $\text{B}_4\text{C}$  for efficient catalysis of oxygen evolution, hydrogen evolution, and oxygen reduction reactions. *ACS Appl Mater Interfaces* 2018;10:37067–78. Available from: <https://doi.org/10.1021/acsami.8b13359>.
- [56] Wang X, Ma Z, Chai L, Xu L, Zhu Z, Hu Y, et al. MOF derived N-doped carbon coated CoP particle/carbon nanotube composite for efficient oxygen evolution reaction. *Carbon* N Y 2019;141:643–51. Available from: <https://doi.org/10.1016/j.carbon.2018.10.023>.
- [57] Davodi F, Mühlhausen E, Tavakkoli M, Sainio J, Jiang H, Gökce B, et al. Catalyst support effect on the activity and durability of magnetic nanoparticles: toward design of advanced electrocatalyst for full water splitting. *ACS Appl Mater Interfaces* 2018;10:31300–11. Available from: <https://doi.org/10.1021/acsami.8b08830>.
- [58] Liu Z, Yu C, Niu Y, Han X, Tan X, Huang H, et al. Graphite-graphene architecture stabilizing ultrafine  $\text{Co}_3\text{O}_4$  nanoparticles for superior oxygen evolution. *Carbon* N Y 2018;140:17–23. Available from: <https://doi.org/10.1016/j.carbon.2018.08.023>.
- [59] Wei R, Fang M, Dong G, Lan C, Shu L, Zhang H, et al. High-index faceted porous  $\text{Co}_3\text{O}_4$  nanosheets with oxygen vacancies for highly efficient water oxidation. *ACS Appl Mater Interfaces* 2018;10:7079–86. Available from: <https://doi.org/10.1021/acsami.7b18208>.
- [60] Chen P, Zhou T, Wang S, Zhang N, Tong Y, Ju H, et al. Dynamic migration of surface fluorine anions on cobalt-based materials to achieve enhanced oxygen evolution catalysis. *Angew Chem Int Ed* 2018;57:15471–5. Available from: <https://doi.org/10.1002/anie.201809220>.
- [61] Zhao X, Li X, Yan Y, Xing Y, Lu S, Zhao L, et al. Electrical and structural engineering of cobalt selenide nanosheets by Mn modulation for efficient oxygen evolution. *Appl Catal B Env* 2018;236:569–75. Available from: <https://doi.org/10.1016/j.apcatb.2018.05.054>.
- [62] Li X, Zhu G, Xiao L, Liu Y, Ji Z, Shen X, et al. Loading of Ag on Fe-Co-S/N-doped carbon nanocomposite to achieve improved electrocatalytic activity for oxygen evolution reaction. *J Alloy Compd* 2019;773:40–9. Available from: <https://doi.org/10.1016/j.jallcom.2018.09.269>.
- [63] Zhao Y, Zhang J, Wu W, Guo X, Xiong P, Liu H, et al. Cobalt-doped  $\text{MnO}_2$  ultrathin nanosheets with abundant oxygen vacancies supported on functionalized carbon nanofibers for efficient oxygen evolution. *Nano Energy* 2018;54:129–37. Available from: <https://doi.org/10.1016/j.nanoen.2018.10.008>.
- [64] Mo R, Wang S, Li H, Li J, Yang S, Zhong J. Electrochimica acta graphene layers-wrapped FeNiP nanoparticles embedded in nitrogen-doped carbon nano fiber as an active and durable electrocatalyst for oxygen evolution reaction. *Electrochim Acta* 2018;290:649–56. Available from: <https://doi.org/10.1016/j.electacta.2018.08.118>.
- [65] Gao W, Qin J, Wang K, Yan K, Liu Z, Lin J, et al. Facile synthesis of Fe-doped  $\text{Co}_9\text{S}_8$  nano-microspheres grown on nickel foam for efficient oxygen evolution reaction. *Appl Surf Sci* 2018;454:46–53. Available from: <https://doi.org/10.1016/j.apsusc.2018.05.099>.
- [66] Liu C, Ma H, Yuan M, Yu Z, Li J, Shi K, et al.  $(\text{NiFe})\text{S}_2$  nanoparticles grown on graphene as an efficient electrocatalyst for oxygen evolution reaction. *Electrochim Acta* 2018;286:195–204. Available from: <https://doi.org/10.1016/j.electacta.2018.08.015>.

- [67] Li Y, Hu L, Zheng W, Peng X, Liu M, Chu PK, et al. Ni/Co-based nanosheet arrays for efficient oxygen evolution reaction. *Nano Energy* 2018;52:360–8. Available from: <https://doi.org/10.1016/j.nanoen.2018.08.010>.
- [68] Anantharaj S, Karthik PE, Kundu S. Self-assembled IrO<sub>2</sub> nanoparticles on a DNA scaffold with enhanced catalytic and oxygen evolution reaction (OER) activities. *J Mater Chem A* 2015;3:24463–78. Available from: <https://doi.org/10.1039/C5TA07075A>.
- [69] Xu Z, Pan H, Lin Y, Yang Z, Wang J, Gong Y. Constructing a hexagonal copper-coin-shaped NiCoSe<sub>2</sub>@NiO@CoNi<sub>2</sub>S<sub>4</sub>@CoS<sub>2</sub> hybrid nanoarray on nickel foam as a robust oxygen evolution reaction electrocatalyst. *J Mater Chem A* 2018;6:18641–8. Available from: <https://doi.org/10.1039/C8TA06084C>.
- [70] Feng Y, Xu C, Hu E, Xia B, Ning J, Zheng C, et al. Construction of hierarchical FeP/Ni<sub>2</sub>P hollow nanospindles for efficient oxygen evolution. *J Mater Chem A* 2018;6:14103–11. Available from: <https://doi.org/10.1039/C8TA03933J>.
- [71] Su J, Xia G, Li R, Yang Y, Chen J, Shi R, et al. Co<sub>3</sub>ZnC/Co nano heterojunctions encapsulated in N-doped graphene layers derived from PBAs as highly efficient bi-functional OER and ORR electrocatalysts. *J Mater Chem A* 2016;4:9204–12. Available from: <https://doi.org/10.1039/C6TA00945J>.
- [72] Zhu M, Zhou Y, Sun Y, Zhu C, Hu L, Gao J, et al. Cobalt phosphide/carbon dots composite as an efficient electrocatalyst for oxygen evolution reaction. *Dalt Trans* 2018;47:5459–64. Available from: <https://doi.org/10.1039/C7DT04291D>.
- [73] Yan Y, Zhao B, Yi SC, Wang X. Assembling pore-rich FeP nanorods on the CNT backbone as an advanced electrocatalyst for oxygen evolution. *J Mater Chem A* 2016;4:13005–10. Available from: <https://doi.org/10.1039/C6TA05317C>.
- [74] Nazir R, Basak U, Pande S. Synthesis of one-dimensional RuO<sub>2</sub> nanorod for hydrogen and oxygen evolution reaction: an efficient and stable electrocatalyst. *Colloids Surf A Physicochem Eng Asp* 2019;560:141–8. Available from: <https://doi.org/10.1016/j.colsurfa.2018.10.009>.
- [75] Dinh KN, Sun X, Dai Z, Zheng Y, Zheng P, Yang J, et al. O<sub>2</sub> plasma and cation tuned nickel phosphide nanosheets for highly efficient overall water splitting. *Nano Energy* 2018;54:82–90. Available from: <https://doi.org/10.1016/j.nanoen.2018.10.004>.
- [76] Li J, Li J, Zhou X, Xia Z, Gao W, Ma Y, et al. Highly efficient and robust nickel phosphides as bifunctional electrocatalysts for overall water-splitting. *ACS Appl Mater Interfaces* 2016;8:10826–34. Available from: <https://doi.org/10.1021/acsami.6b00731>.
- [77] Yu J, Li Q, Chen N, Xu C-Y, Zhen L, Wu J, et al. Carbon-coated nickel phosphide nanosheets as efficient dual-electrocatalyst for overall water splitting. *ACS Appl Mater Interfaces* 2016;8:27850–8. Available from: <https://doi.org/10.1021/acsami.6b10552>.
- [78] Liu H, He Q, Jiang H, Lin Y, Zhang Y, Habib M, et al. Electronic structure reconfiguration toward pyrite NiS<sub>2</sub> via engineered heteroatom defect boosting overall water splitting. *ACS Nano* 2017;11:11574–83. Available from: <https://doi.org/10.1021/acsnano.7b06501>.
- [79] Wu Z, Zou Z, Huang J, Gao F. NiFe<sub>2</sub>O<sub>4</sub> nanoparticles/NiFe layered double-hydroxide nanosheet heterostructure array for efficient overall water splitting at large current densities. *ACS Appl Mater Interfaces* 2018;10:26283–92. Available from: <https://doi.org/10.1021/acsami.8b07835>.
- [80] Zhao Y, Zhang J, Li K, Ao Z, Wang C, Liu H, et al. Electrospun cobalt embedded porous nitrogen doped carbon nanofibers as an efficient catalyst for water splitting. *J Mater Chem A* 2016;4:12818–24. Available from: <https://doi.org/10.1039/C6TA04244A>.
- [81] Xiao Y, Zhang P, Zhang X, Dai X, Ma Y, Wang Y, et al. Bimetallic thin film NiCo–NiCoO<sub>2</sub>@NC as a superior bifunctional electrocatalyst for overall water splitting in alkaline media. *J Mater Chem A* 2017;5:15901–12. Available from: <https://doi.org/10.1039/C7TA03629A>.

- [82] Wu R, Xiao B, Gao Q, Zheng Y-R, Zheng X, Zhu J, et al. A Janus Nickel cobalt phosphide catalyst for high-efficiency neutral-pH water splitting. *Angew Chem Int Ed* 2018;57:15445–9. Available from: <https://doi.org/10.1002/anie.201808929>.
- [83] Pu Z, Luo Y, Asiri AM, Sun X. Efficient electrochemical water splitting catalyzed by electrodeposited nickel diselenide nanoparticles based film. *ACS Appl Mater Interfaces* 2016;8:4718–23. Available from: <https://doi.org/10.1021/acsami.5b12143>.
- [84] Liu B, Zhang N, Ma M. Cobalt-based nanosheet arrays as efficient electrocatalysts for overall water splitting. *J Mater Chem A* 2017;5:17640–6. Available from: <https://doi.org/10.1039/C7TA04248E>.
- [85] Cui Z, Ge Y, Chu H, Baines R, Dong P, Tang J, et al. Controlled synthesis of Mo-doped  $\text{Ni}_3\text{S}_2$  nano-rods: an efficient and stable electro-catalyst for water splitting. *J Mater Chem A* 2017;5:1595–602. Available from: <https://doi.org/10.1039/C6TA09853C>.
- [86] Menezes PW, Panda C, Garai S, Walter C, Guiet A, Driess M. Structurally ordered inter-metallic cobalt stannide nanocrystals for high-performance electrocatalytic overall water-splitting. *Angew Chem Int Ed* 2018;57:15237–42. Available from: <https://doi.org/10.1002/anie.201809787>.
- [87] Lai C, Liu X, Deng Y, Yang H, Jiang H, Xiao Z, et al. Rice-shape nanocrystalline  $\text{Ni}_3\text{P}_4$ : a promising bifunctional electrocatalyst for hydrogen evolution reaction and oxygen evolution reaction. *Inorg Chem Commun* 2018;97:98–102. Available from: <https://doi.org/10.1016/j.inoche.2018.09.024>.
- [88] Park S-W, Kim I, Oh S-I, Kim J-C, Kim D-W. Carbon-encapsulated NiFe nanoparticles as a bifunctional electrocatalyst for high-efficiency overall water splitting. *J Catal* 2018;366:266–74. Available from: <https://doi.org/10.1016/j.jcat.2018.08.016>.
- [89] Wang J-Y, Ouyang T, Li N, Ma T, Liu Z-Q, S, N co-doped carbon nanotube-encapsulated core-shelled  $\text{CoS}_2/\text{Co}$  nanoparticles: efficient and stable bifunctional catalysts for overall water splitting. *Sci Bull* 2018;63:1130–40. Available from: <https://doi.org/10.1016/j.scib.2018.07.008>.
- [90] Zeng L, Sun K, Wang X, Liu Y, Pan Y, Liu Z, et al. Three-dimensional-networked  $\text{Ni}_2\text{P}/\text{Ni}_3\text{S}_2$  heteronanoflake arrays for highly enhanced electrochemical overall-water-splitting activity. *Nano Energy* 2018;51:26–36. Available from: <https://doi.org/10.1016/j.nanoen.2018.06.048>.
- [91] Tang Y, Fang X, Zhang X, Fernandes G, Yan Y, Yan D, et al. Space-confined earth-abundant bifunctional electrocatalyst for high-efficiency water splitting. *ACS Appl Mater Interfaces* 2017;9:36762–71. Available from: <https://doi.org/10.1021/acsami.7b10338>.
- [92] Hu J, Ou Y, Li Y, Gao D, Zhang Y, Xiao P.  $\text{FeCo}_2\text{S}_4$  nanosheet arrays supported on Ni foam: an efficient and durable bifunctional electrocatalyst for overall water-splitting. *ACS Sustain Chem Eng* 2018;6:11724–33. Available from: <https://doi.org/10.1021/acssuschemeng.8b01978>.
- [93] Liu Z, Tan H, Xin J, Duan J, Su X, Hao P, et al. Metallic intermediate phase inducing morphological transformation in thermal nitridation:  $\text{Ni}_3\text{FeN}$ -based three-dimensional hierarchical electrocatalyst for water splitting. *ACS Appl Mater Interfaces* 2018;10:3699–706. Available from: <https://doi.org/10.1021/acsami.7b18671>.
- [94] Wang P, Pu Z, Li Y, Wu L, Tu Z, Jiang M, et al. Iron-doped nickel phosphide nanosheet arrays: an efficient bifunctional electrocatalyst for water splitting. *ACS Appl Mater Interfaces* 2017;9:26001–7. Available from: <https://doi.org/10.1021/acsami.7b06305>.
- [95] Ray C, Lee SC, Sankar KV, Jin B, Lee J, Park JH, et al. Amorphous phosphorus-incorporated cobalt molybdenum sulfide on carbon cloth: an efficient and stable electrocatalyst for enhanced overall water splitting over entire pH values. *ACS Appl Mater Interfaces* 2017;9:37739–49. Available from: <https://doi.org/10.1021/acsami.7b11192>.

- [96] Ray C, Lee SC, Jin B, Kundu A, Park JH, Jun SC. Stacked porous iron-doped nickel cobalt phosphide nanoparticle: an efficient and stable water splitting electrocatalyst. *ACS Sustain Chem Eng* 2018;6:6146–56. Available from: <https://doi.org/10.1021/acssuschemeng.7b04808>.
- [97] Zhang J, Li Y, Zhu T, Wang Y, Cui J, Wu J, et al. 3D coral-like Ni<sub>3</sub>S<sub>2</sub> on Ni foam as a bifunctional electrocatalyst for overall water splitting. *ACS Appl Mater Interfaces* 2018;10:31330–9. Available from: <https://doi.org/10.1021/acsami.8b09361>.

This page intentionally left blank

# Functionalized nanographene for catalysis

Santosh Bahadur Singh<sup>1</sup> and Chaudhery Mustansar Hussain<sup>2</sup>

<sup>1</sup>*Department of Chemistry, National Institute of Technology Raipur, Raipur, Chhattisgarh, India,*

<sup>2</sup>*Department of Chemistry and Environmental Science, New Jersey Institute of Technology, Newark, NJ, United States*

## 5.1 Nanographene: an introduction

Nanomaterials have unique characteristics and thus have versatile applications in industries, environmental analysis, catalysis, energy, medicine, environmental remediation, etc. [1,2]. Among various nanomaterials, two-dimensional (2D) carbon allotrope (i.e., nanographene) have received significant attention as metal-free and green nanomaterials.

Nanographene (carbon allotrope) is made of 2D one-atom-thick carbon sheets. Each graphene sheet acts as a single molecule and is composed of C-atoms linked in hexagonal shapes with each other and covalently bonded to three adjacent carbon atoms. Graphene has close resemblance with carbon nanotubes as carbon atoms are linked in hexagonal pattern, but graphene is flat rather than cylindrical. Due to the presence of covalently bonded carbon atoms, graphene has very good tensile strength. Since graphene has a flat structure rather than a cylindrical one all the atoms are accessible from both sides. Thus there is more interaction with the surrounding molecules. Further, graphene molecules have the capability to bond with a fourth atom because each carbon atom in a graphene sheet is bonded to only three adjacent carbon atoms. This special capability along with its great tensile strength and high surface-to-volume ratio make it very useful among other nanomaterials or composite materials [3–7].

Catalysis plays a significant role in commercialization of chemical science knowledge for material synthesis and is also widely used in environmental protection, energy, organic synthesis, etc. Due to the high cost, toxicity, environmental issues, and low efficiency of conventional catalysts (i.e., metal and metal oxides), there is an urgent need to replace conventional catalysts with nonconventional ones (green and environmentally benign).

The unique characteristics of graphene make it attractive for development of new metal-free green heterogeneous catalysts. This chapter gives a brief review of the graphene chemistry and functionalization of graphene and catalytic applications with special focus on the industrial, environmental, and health issues of graphene.

### 5.1.1 Interest in nanographene

Special interest in nanographene as catalyst is due to its stability and the ability to alter/functionalize its morphology, synthetic approaches, catalytic performance and mechanisms, etc. [8]. A brief overview of current interest in nanoscale graphene is given in Fig. 5.1.

### 5.1.2 Chemistry of nanographene

Graphene is a single atomic sheet of conjugated  $SP^2$ -hybridized carbon atoms. Three atomic orbitals of carbon, namely  $2s$ ,  $2p_x$ , and  $2p_y$ , undergo hybridization to form  $SP^2$  orbitals. These hybridized orbitals form covalent sigma-bond with the neighboring three carbon atoms, with thickness 0.34 nm and a carbon–carbon bond distance 0.142 nm [5].  $SP^2$  hybridization in

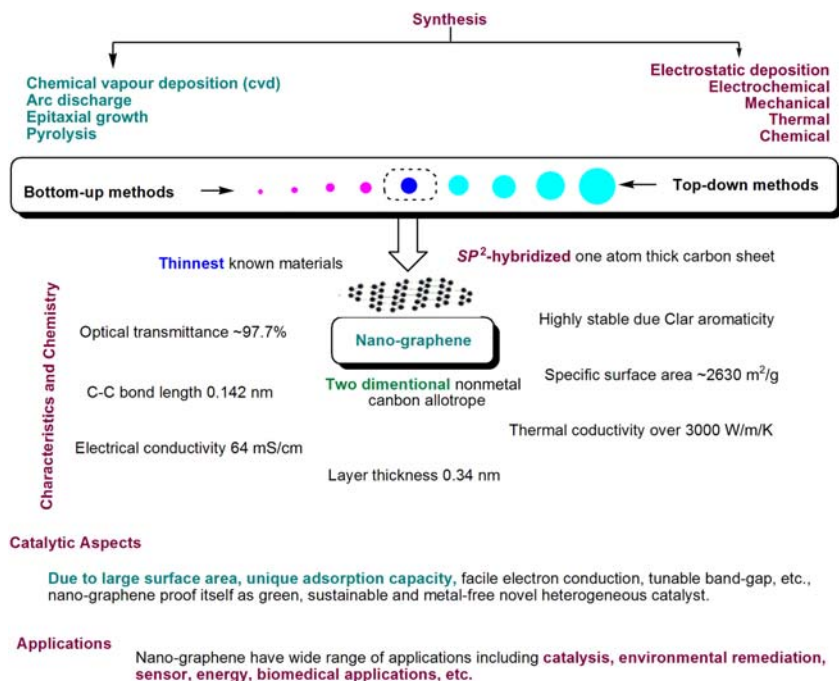


FIGURE 5.1 Nanographene: an overview.

graphene leads to a hexagonal planar structure, referred to as “honeycomb lattice.” The remaining  $2p_z$  orbital is oriented perpendicular (out-of-plane) to the planar structure and forms a  $\pi$ -bond. These  $\pi$ -bonds are delocalized over all the carbon atoms and subsequently form the  $\pi$ -band. The  $\sigma$ -bonds are mainly responsible for the excellent toughness of the graphene lattice structure, while the  $\pi$ -band contributes to the electrical conductivity of graphene [4,5,9]. Graphene is an analog of a giant aromatic polymolecule. Due to its sheet structure, graphene has a wide open two-sided surface, which provides a large specific surface area of  $\sim 2630 \text{ m}^2/\text{g}$  [10]. Graphene has excellent electrical ( $\sigma = 64 \text{ mS/cm}$ ) and thermal conductivity ( $k = 5 \times 10^3 \text{ W/m/K}$ ) making it attractive for developing new photocatalysts and electrocatalysts. It also has high electrochemical, chemical, optical and thermal stability, high mechanical strength (Young’s modulus,  $\sim 1100 \text{ GPa}$ ), and elasticity [11–13].

### 5.1.3 Synthetic methods

Selection of an appropriate synthetic route for nanographene synthesis plays an important role in tuning the characteristics/properties of nanographene for multidimensional applications. There are a number of methods frequently used in graphene synthesis, which may be broadly categorized as (1) top-down methods and (2) bottom-up methods [7,14,15]. The top-down method of nanographene synthesis basically includes the exfoliation of graphite via mechanical, thermal, chemical synthesis, electrochemical expansion, electrostatic deposition, etc. Other important top-down methods are microwave synthesis, chemical and/or thermal reduction of graphene oxide, direct sonication of graphite, super acid dissolution, etc. On the other hand, the bottom-up method of nanographene synthesis includes chemical vapor deposition (CVD), epitaxial growth, pyrolysis, arc discharge, electrochemical reduction of carbon mono- and dioxide, confined self-assembly, etc. Among the various top-down methods chemical reduction of graphene oxide is more commonly used for large-scale and economical production of nanographene. Overall, top-down methods have superiority over bottom-up methods with respect to cheaper and high-quality nanographene production.

#### 5.1.4 Characterization tools

Synthesized nanographene- and graphene-based nanocatalysts can be characterized by various advanced instrumental techniques [4,7,9] including Raman spectroscopy, X-ray photoelectron spectroscopy (XPS), X-ray diffraction (XRD), scanning tunneling microscopy (STM), diffuse reflectance Fourier transform infrared spectroscopy (DRFT-IRS), X-ray absorption near edge structure (XRANES) analysis, X-ray absorption fine structure (XRAFS) analysis, etc. Raman spectroscopy is a quick, facile, and powerful analytical tool



to investigate the structure, quality, quantity, and especially catalytic performance of graphene-based nanomaterials. XPS is the best technique to study surfaces, especially the modified surface of graphene-based nanomaterials, which is crucial for catalysis. Number of layers, crystallinity, and size of graphene-based nanomaterials can be determined by XRD analysis. Morphology and the presence of any defects on graphene due to doping or preparation methods can be detected by STM. DRFT–IRS is used to determine the Bronsted and Lewis acid active sites, two of the most significant characteristics of graphene nanocatalysts.

### 5.1.5 Applications

Graphene and its derivatives attract a lot of attention from researchers due to its unique properties and a wide range of applications including catalysis [8], energy storage and generation [16], sensing platforms [17], molecular imaging [18], drug delivery [19], environmental remediation [15,20], etc.

## 5.2 Functionalization of nanographene

In order to develop modified graphene (chemically active) from pure graphene (chemically inert), the electronic structure must be altered by tuning the distribution of electronic states and increasing the density of states (DOS) around the Fermi level [21–23]. Functionalization of nanographene is discussed based on the (1) nature of the materials used in functionalization, and (2) preparation methods.

In the first category, Ref. [24] provides a bottom-up account encompassing the functionalization of graphene to design nanographene and its derivatives with the highest achievable properties for their specific applications based on material functionalization of nanographene [24]. Functionalization of nanographene with organics, proteins, molecular linkers, etc., as soft matter and solid inorganic metals at nanoscale, semiconductors, etc., as hard matter are the most important methods for fabricating high-performance nanographene-based catalytic materials. Fig. 5.2 shows a schematic summary of nanographene functionalization based on the nature of the materials used.

Method-based functionalization of nanographene is summarized in Fig. 5.3, which includes thermal, hydrothermal, mechanical, and chemical functionalization of nanographene [25]. Methods to prepare modified and functionalized nanographene summarized in Fig. 5.3.

## 5.3 Catalytic properties and applications of functionalized nanographene

Uses of catalysts in any chemical processes are better movement toward sustainable world by decreasing the environmental impact of processes

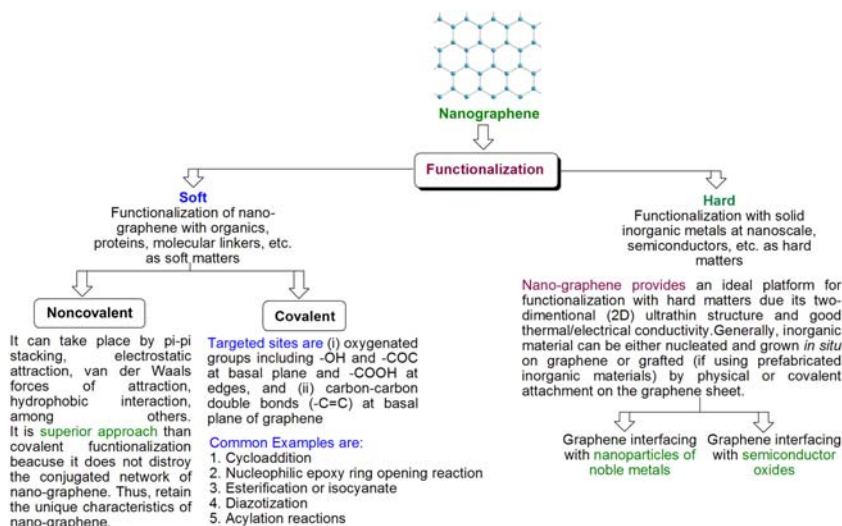


FIGURE 5.2 Schematic outline of nanographene functionalization.

The formation of folds by **thermal treatment, electrostatic interactions or mechanical methods** on the graphene surface, resulting in distortion of the electronic distribution at the surface by destroying 2D structure of graphene. For band-structure engineering of graphene and might render it suitable for catalysis, this method can be used.

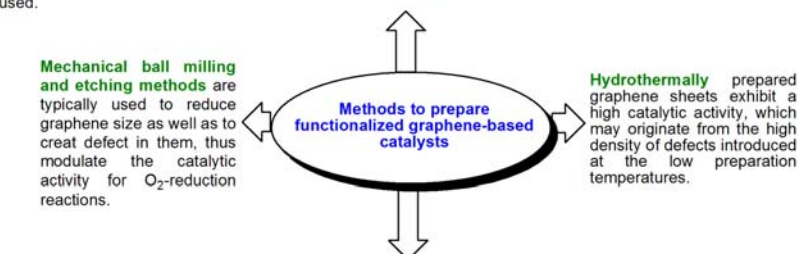
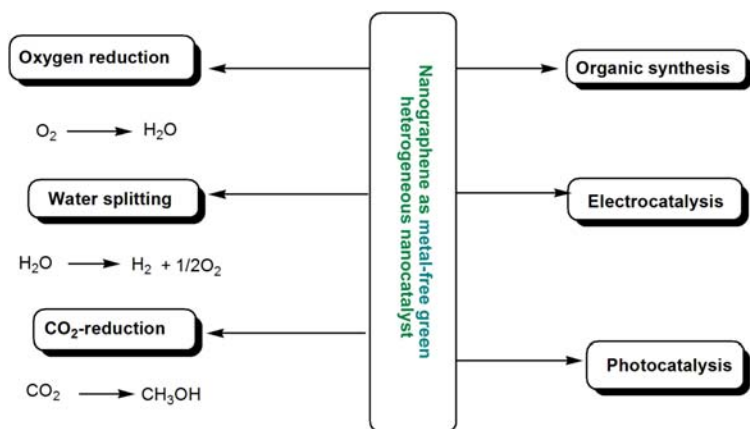


FIGURE 5.3 Methods to prepare functionalized graphene-based catalysts.

involved in chemical and material sciences. Catalyzed reactions are green, energy efficient, economical, and environment benign in comparison to non-catalyzed reactions. Thus catalysis helps to conserve natural resources. Catalysts have a wide range of applications including organic synthesis, pharmaceuticals, energy, sensor, oil refinery, and remediation of natural resources (air, water, and soil), etc. Recently, graphene has gained the attention of researchers as a heterogeneous, metal-free, and green catalyst to



Graphene-based catalysts have great potential to act as metal-free green heterogeneous nanocatalysts due to its unique characteristics. **Graphene** is a non-metal carbon allotrope. It is a two-dimensional(2-D),  $\text{SP}^2$ -hybridized single layer carbon sheet. Due to presence of  $\text{SP}^2$ -hybridized carbon atoms, graphene has both the C-C sigma bond in-plane and pi-bond out-of-plane, which facilitate electron conduction (delocalization) through graphane sheet. **Large specific surface area, 2-D structure, facile decoration, easy electron conduction, tunable band-gap, high adsorption capacity, etc. are unprecedented characteristics of graphene-based nanomaterials, which make it noble metal-free green heterogeneous nanocatalyst.**

**FIGURE 5.4** Graphene as metal-free, green, heterogeneous catalyst and its applications.

replace conventional catalysts (metal-based homogeneous and heterogeneous catalysts) or as supporting material for improving the performance of catalysts [5,19,26–31]. High cost, toxicity, low efficiency, and environmental impact of conventional catalyst limited its application. The unique characteristics of graphene make it a more attractive green catalyst for various advanced catalytic processes. Fig. 5.4 gives an overview of catalytic applications of nanographene.

### 5.3.1 Catalytic properties

Nanographene has various advantages including high surface area, economical, electron mobility, and thermal, chemical, electrochemical, optical stabilities, etc., to synthesize new catalysts. Graphene has the highest surface area ( $2600 \text{ m}^2/\text{g}$ ) among other carbon allotropes. Due to its superior electron mobility that facilitates electron transfer during the catalytic processes, nanographene imparts better catalytic performance. The high thermal, optical, chemical, and electrochemical stabilities of graphene improve the lifetime of graphene-based catalysts [31–41]. Chemically modified graphenes (CMGs) are the most promising catalysts for various catalytic processes (chemical, optical, and electrochemical reactions) and are also attractive materials for fabricating new catalysts and as support for loading catalysts of enzymes,

oxides, metals, other carbon nanomaterials, etc. [32,33]. The future of graphene-based catalysis is bright due to its affordability and sustainability compared to metal-based catalysts [42]. The catalytic activities of graphene-based catalysts can be tuned by doping with hetero atoms (nitrogen, boron, or sulfur), which provide efficient active sites and also tune the band gaps [43].

### 5.3.2 Catalytic applications

Graphene-based nanomaterials have a wide range of catalytic applications, that is, organic synthesis [42], advanced catalysis including photocatalysis [41], electrocatalysis [44,45], carbocatalysis [46], environmental remediation [47], etc.

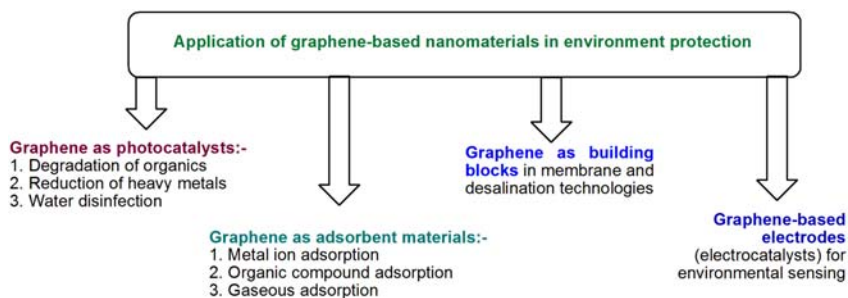
Graphene-based nanocatalysts have good capability to catalyze the redox reactions. Redox reactions are one of the fundamental reactions frequently used in clean operating electrochemical conversion and storage technologies such as rechargeable metal-air batteries and polymer electrolyte fuel cells. These devices are promising components for sustainable, clean and clean energy generate on in coming future. Same time they have some technical and economical issues, which can be solve by using graphene-based catalysts. Graphene-based materials due to the unique tunable surface chemistry and very high surface area are very attractive materials for electrocatalysis community [48]. Ref. [48] gives a critical review of the importance of graphene and its derivatives in the redox reaction electrocatalysis. Graphene couples a highly graphitic characteristics with excellent surface areas, which are important properties for enhancing the electrochemical stability and activity of platinum nanoparticle supported catalysts. Surface tuning of graphene either by chemical functionalization or heteroatom doping processes provides beneficial catalyst support interactions resulting in improvement in activity and stability. Under both acidic and alkaline conditions, the 2D structure of graphene-based materials has shown very promising performance as a host to support catalytically active inorganic nanoparticle catalysts [48]. Ref. [45] reviews the electrocatalytic application of graphene-based materials as a catalyst support in low-temperature fuel cells [45]. Low-temperature fuel cells are among the most promising technologies for efficient and reliable conversion of alcohol or hydrogen into electric energy in distributed power generation, automotive, and portable electronic applications at large scale. The electrocatalysts play a vital role in these devices and improve overall reaction efficiency, cost, and durability. Using graphene sheets as a support, the obtained metal particle size is very low in comparison to the particle size obtained by using other carbon materials as supports. Low particle size favors the high metal loadings on graphene nanosheets (GNS). The graphene oxide (GO) contains oxygen-containing functional groups (i.e., hydroxyl, carboxyl, and epoxy onto each side of the sheet), which improves

electrocatalytic activity by functionalization of graphene, giving rise to higher and more homogeneous metal dispersion [49,50].

Environmental degradation is one of the biggest problems the world is facing today. With explosive increases in the human population and related development activities our environment is being contaminated, with adverse effects on all living things. Thus there is an urgent need to move all our developmental/technological/scientific activities toward greener approaches for sustainable development to protect the environment as well as life on the earth. Graphene-based nanomaterials as novel materials for environmental applications have gained increased attention from research communities. Graphene-based nanomaterials may be used as building blocks for next-generation water treatment and desalination membranes, as adsorbent or photocatalysts for environmental remediation, and as electrode materials (electrocatalysts) for pollutant monitoring or removal [20]. Fig. 5.5 briefly summarizes the various environmental applications of graphene-based nanomaterials [51–69].

Graphene-based nanomaterials in combination with well-known photocatalytic materials such as  $\text{TiO}_2$  have created new possibilities in the field of photocatalyzed environmental remediation due to their flexible structure, large surface area, high electrical and thermal conductivities, mobility of charge carriers at room temperature, and high chemical stability [15].

The term carbocatalyst mainly refers to catalysts containing carbon—a nonmetal element as the active constituent. The term carbocatalysis refers to the acceleration of chemical transformation by addition of a carbon containing organic compound as catalyst. Due to its efficiency as well as selectivity, carbocatalysis has been increasingly studied in recent years. In the construction of complex molecular moieties, carbocatalysis may play an important role [42,46]. Replacing transition metal-based homogeneous and



**The 21<sup>st</sup> century has been termed the Century of the Environment.** The growing world population and intensification of agricultural and industrial activities resulted as contamination of three fundamental elements essential for life i.e air, soils and water, as global climate change, and other environmental issues are become biggest challenges that the world is facing today.

**FIGURE 5.5** Application of nanographene in environmental remediation.

heterogeneous catalysts with alternative renewable resources such as carbon is a part of moving toward more sustainable and greener science. From a commercial point of view, carbon-based catalysts are economical in comparison to metal catalysts due to the considerably high feedstock of carbon materials.

Graphene-based catalysts are widely used in photocatalytic processes including  $\text{H}_2\text{O}$  splitting to generate clean and renewable energy hydrogen ( $\text{H}_2$ ), selective organic transformations and degradation of environmental pollutants [41]. Nanographene has a synergic effect and can improve the catalytic performance of metal photocatalysts in terms of better adsorption capacity, lighter adsorption range, specific surface area, electron conductivity, etc. Similarly, graphene oxide also shows synergistic effects and can enhance catalytic conversion in organic dyes via charge transfer across the graphene interface to facilitate photosensitization [70]. Ref. [71] reported nanographene as an electron-transfer medium during photocatalysis that can store as well as transport the electrons through a stepwise electron transfer process [71].

## **5.4 Industrial, environmental, and health issues of nanographene**

### **5.4.1 Industrial issues**

According to a recent markets analysis report, the global graphene market is expected to reach USD 278.47 million by 2020, with a growth rate of 42.8% from 2015 to 2020 [72]. This report was based on the type of graphene (graphene oxide, graphene nanoplatelets, and others) and its applications mainly in electronics, catalysts, energy, coating, sensors, composites, and other sectors. The commercial-scale production of graphene-based nanomaterials aimed at industrial applications has grown significantly in recent years, especially since many companies in China have entered the market [73]. Compared with large-scale production of graphene, the use of thin graphene sheets are very low. Almost all graphene manufacturers use these materials in composites, energy storage, and functional coatings for electronics. China is one of the biggest lithium-ion battery manufacturers in the world. In the manufacturing of lithium-ion batteries, small graphene sheets are used as a conductive additive in electrodes or as current-collector coatings. Applications of small graphene sheets have also been extended for use as anticorrosion and antistatic coatings, due to their unique characteristics (2D structure, high electrical conductivity, and impermeability). Another application of small graphene is mobile phones and light-emitting diodes.

BCC Research estimates that the global graphene-based products market was worth \$1.5 million in 2015. The market is expected to grow from \$310.4 million in 2020 to \$2.1 billion by 2025, with a compound annual



growth rate (CAGR) of 46.3% [74]. This report includes an overview of the global markets for graphene technologies and commercial applications of graphene-based materials/products in communications, solar cells, data storage, thermal management, sensing and imaging, displays, capacitors, structural materials, and others industrial sectors. Analyses mainly consider the global market trends, with data from 2014, estimates for 2015, and projections of compound annual growth rates (CAGRs) through 2020 and through 2025. The economic aspects of any material depends on their large-scale production and commercialization. A number of issues need to be addressed to advance the commercial application of graphene-based nanomaterials. For example, the cost/performance ratio of graphene is a big concern for industries deciding whether graphene can be used in their products. The cost of graphene is a big challenge. Along with the economical challenges, improvement in techniques/processes used in synthesis of graphene are need to prepare uniform graphene sheets with requisite properties. To extent application of graphene in other emerging fields, methods for modification, doping methods, dispersion methods, and functionalization processes are require improvements/advancements. Graphene is expected to find large-scale commercial utilization in the future, but no material can do everything [73].

#### 5.4.2 Toxicity

Graphene-based nanomaterials, especially those involving cellular interactions, must first prove to be biocompatible before they can expect to reach their full potential for various bioapplications [25]. Nanographene because of its extraordinary and noble characteristics has attracted great interest as a promising nanomaterial for various bioapplications ranging from the biosensing applications for a host of medical conditions to the delivery of chemotherapeutics for treatment of cancers and even for the differentiation and imaging of stem cells [75–78]. Despite the recent increase in the popularity of graphene-based nanomaterials, there are still health and safety concerns. Guo and Mei recently reported the toxicological effects of graphene-based nanomaterials in mammalian cells, bacteria, and animal models [79]. Graphene and its derivatives including GO and reduced graphene oxide (rGO) show toxic effects under both in vivo and in vitro conditions. Surface modifications have great potential to reduce its toxic effects by altering its interaction with living systems. Its toxicity depends on its shape, size, or surface coating, which determines the interactions with the intracellular uptake, cell membranes, and clearance pathways. Russier et al. performed a comparative study to examine the size effect of nanographene and found that smaller particles are more cytotoxic than bigger ones and also cause apoptosis due to the direct cellular membrane destruction [80]. Fig. 5.6 illustrates the various health and safety concerns including biocompatibility of graphene-based nanomaterials [81,82].

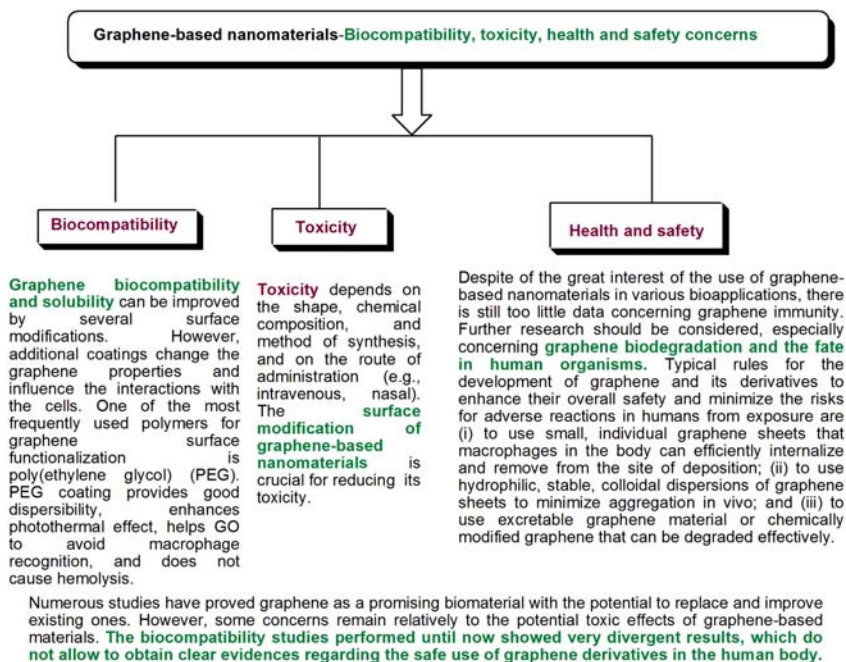


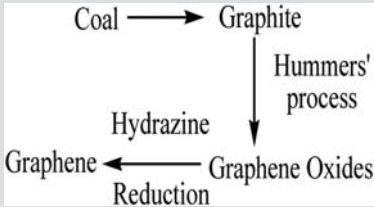
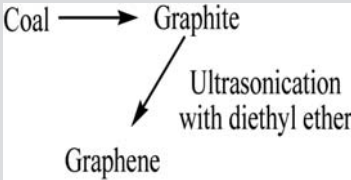
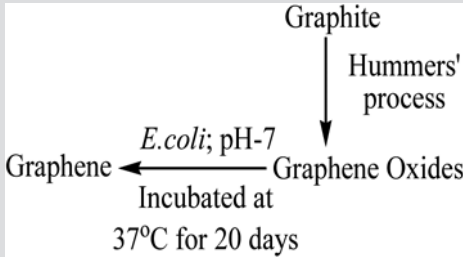
**FIGURE 5.6** Health and safety concerns of graphene-based nanomaterials.

### 5.4.3 Biocompatibility

Biocompatibility of nanographene is discussed in this section in terms of lifecycle assessment (LCA). LCA is a process used to measure the environmental impacts of the processes used to fabricate new materials. LCA of graphene is used to study the effects of different nanographene synthetic methods on the environment. Thus the EIA (environmental impact assessment) of graphene-based nanomaterials is conducted by LCA. Ref. [83] describes the environmental impacts of synthesized nanographene via chemical and sonication methods using LCA [83], while Ref. [84] used LCA to compare synthesized nanographene via biotechnological method (using bacteria *Escherichia coli*) and by chemical method (Hummers' method) focusing on energy consumption and environment [84]. Arvidsson et al. compared both production routes for in-solution graphene using a cradle-to-gate LCA focusing on potential differences in blue water footprint, energy use, ecotoxicity, and human toxicity and concluded that the blue water footprint and energy use were approximately doubled in the chemical reduction method compare to the ultrasonication method. While ultrasonication had the largest human toxicity impact both methods had the same ecotoxicity impact. The sensitivity analysis showed that solvent recovery is important to decrease the blue water footprint of chemical reduction method and also reduce the



**TABLE 5.1** Life cycle assessment (LCA) of graphene synthesis routes: chemical reduction method (CRM), ultrasonication method (USM), and biotechnological method (BTM).

Parameters	Synthetic routes		
	Chemical reduction method (CRM)	Ultrasonication method (USM)	Biotechnological method (BTM)
Synthesis procedure	 <pre> graph TD     Coal --&gt; Graphite     Graphite -- "Hummers' process" --&gt; GO[Graphene Oxides]     GO -- "Hydrazine Reduction" --&gt; Graphene           </pre>	 <pre> graph TD     Coal --&gt; Graphite     Graphite -- "Ultrasonication with diethyl ether" --&gt; Graphene           </pre>	 <pre> graph TD     Graphite -- "Hummers' process" --&gt; GO[Graphene Oxides]     GO -- "E.coli; pH-7 Incubated at 37°C for 20 days" --&gt; Graphene           </pre>
Ecotoxicity	Less toxic than USM	Toxic	Less toxic than CRM
Physiochemical properties	Thicker and lower the C/O ratio than USM	Thinner graphene sheet and higher C/O ratio	Thinner and higher C/O ratio than CRM
Human toxicity	Less toxic than USM	Toxic	—

Energy requirement	1642 Wh	About 1/2 of CRM energy requirement	5 Wh
Blue water footprint	Double of blue water footprint (consumption of surface- and groundwater for a particular process/ activity) of USM	—	—
Summary	Based on various LCA parameters, CRM is not suitable for graphene synthesis from environmental point of view.	High recovery of solvent (diethyl ether) observed in USM, which lowers the combined negative impacts of USM compared to CRM. Thus USM is more environmentally benign than CRM.	In regard to the less negative effects on the marine aquatic ecotoxicity, the photochemical ozone creation potential, global warming, etc. biotechnological method may be considered as green method for graphene production.

impacts of almost all considered environmental impact categories in the ultrasonication route. The results explore the possibility of using LCA based mainly on information from patents and scientific articles, enabling the study of products at early stages of technological development. Khanam et al. concluded that the Hummers' method (chemical reduction process) has higher energy consumption ( $\sim 1642$  Wh) than the energy consumption of the biotechnological reduction process ( $\sim 5$  Wh). The biotechnological method is a green technique for the production of graphene, especially given the reduction in the negative effects on global warming, abiotic depletion, the photochemical ozone creation potential, and the marine aquatic ecotoxicity potential in comparison to the chemical reduction method. Table 5.1 lists the synthetic routes of the chemical reduction method (CRM), ultrasonication method (USM), and biotechnological method (BTM).

#### 5.4.4 Sustainability

As graphene is just a carbon material (thin layer of graphite), it is a natural material and has fewer negative effects on the environment from a sustainability point of view. Graphene-based nanomaterials meet a number of needs of modern society. For example, graphene can be used as the circular top of a Coca Cola bottle to prevent microbial growth, as most promising material for targeted treatment of cancer, and as building material for preparation cloths used in bomb diffusing. However, there is little known about the toxicity of graphene and due to its high cost it is not affordable for everyone [85].

### 5.5 Conclusions and future aspects

Functionalization of nanographene is of crucial importance for its catalytic and other applications. Nanographene functionalization is based on two different approaches: the nature of the materials used and the methods of functionalization. Both the surface as well as the basal plane of nanographene can be modified or functionalized by using soft and hard functionalization methods. Further, catalytic applications of functionalized nanographene include in redox processes, organic synthesis, water splitting, oxygen reduction, carbon dioxide reduction, environmental remediation, etc., as discussed in this chapter. The industrial, economical, health, biocompatibility, and sustainability issues of nanographene were also discussed. As we know nanographene is carbon allotrope and thus has fewer negative effects on the environment than other materials.

Currently, synthesis of active/functionalized nanographene directly from graphite has attracted significant research interest. Therefore further research is needed on functionalization of nanographene in order to improve its synthetic route, yields (mass production), electrical and thermal conductivity, etc., without compromising its positive inherent properties.

## References

- [1] Hussain CM. *Handbook of nanomaterials for industrial applications*. Elsevier; 2018.
- [2] Hussain CM, Kharisov B. *Advanced environmental analysis-application of nanomaterials*, vol. 1. Royal Society of Chemistry; 2017.
- [3] Ahn JH. Things you could do with graphene. *Nat Nanotechnol* 2014;9:737. Available from: <https://doi.org/10.1038/nnano.2014.245>.
- [4] Cooper DR, D'Anjou B, Ghattamaneni N, Harack B, Hilke M, Horth A, et al. Experimental review of graphene. *ISRN Condens Matter Phys* 2012;2012:1–56. Available from: <https://doi.org/10.5402/2012/501686>.
- [5] Geim AK, Novoselov KS. The rise of graphene. *Nat Mater* 2007;6:183–91.
- [6] Allen MJ, Tung VC, Kaner RB. Honeycomb carbon: a review of graphene. *Chem Rev* 2010;110:132–45. Available from: <https://doi.org/10.1021/cr900070d>.
- [7] Hu M, Yao Z, Wang X. Graphene-based nanomaterials for catalysis. *Ind Eng Chem Res* 2017;56:3477–502. Available from: <https://doi.org/10.1021/acs.iecr.6b05048>.
- [8] Singh SB, Hussain CM. Nano-graphene as groundbreaking miracle material: catalytic and commercial perspectives. *ChemistrySelect* 2018;3:9533–44. Available from: <https://doi.org/10.1002/slct.201802211>.
- [9] Lee HC, Liu W-W, Chai S-P, Mohamed AR, Aziz A, Khe C-S, et al. Review of the synthesis, transfer, characterization and growth mechanisms of single and multilayer graphene. *RSC Adv* 2017;7:15644–93. Available from: <https://doi.org/10.1039/C7RA00392G>.
- [10] Stoller MD, Park S, Zhu Y, An J, Ruoff RS. Graphene-based ultracapacitors. *Nano Lett* 2008;8:3498–502. Available from: <https://doi.org/10.1021/nl802558y>.
- [11] Lee C, Wei X, Kysar JW, Hone J. Measurement of the elastic properties and intrinsic strength of monolayer graphene. *Science* 2008;321:385–8. Available from: <https://doi.org/10.1126/science.1157996>.
- [12] Park S, Ruoff RS. Chemical methods for the production of graphenes. *Nat Nanotechnol* 2009;4:217–24. Available from: <https://doi.org/10.1038/nnano.2009.58>.
- [13] Stankovich S, Dikin DA, Dommett GHB, Kohlhaas KM, Zimney EJ, Stach EA, et al. Graphene-based composite materials. *Nature* 2006;442:282–6. Available from: <https://doi.org/10.1038/nature04969>.
- [14] Bhuyan MSA, Uddin MN, Islam MM, Bipasha FA, Hossain SS. Synthesis of graphene. *Int Nano Lett* 2016;6:65–83. Available from: <https://doi.org/10.1007/s40089-015-0176-1>.
- [15] Giovannetti R, Rommozzi E, Zannotti M, D'Amato CA. Recent advances in graphene based TiO<sub>2</sub> nanocomposites (GTiO<sub>2</sub>Ns) for photocatalytic degradation of synthetic dyes. *Catalysts* 2017;7:305. Available from: <https://doi.org/10.3390/catal7100305>.
- [16] Brownson DAC, Metters JP, Banks CE. Graphene for energy production and storage applications. *Nanotechnology for the energy challenge*. KGaA, Weinheim, Germany: Wiley-VCH Verlag GmbH and Co; 2013. p. 133–70. Available from: <https://doi.org/10.1002/9783527665105.ch5>.
- [17] Mao HY, Laurent S, Chen W, Akhavan O, Imani M, Ashkarran AA, et al. Graphene: promises, facts, opportunities, and challenges in nanomedicine. *Chem Rev* 2013;113:3407–24. Available from: <https://doi.org/10.1021/cr300335p>.
- [18] Li J-L, Tang B, Yuan B, Sun L, Wang X-G. A review of optical imaging and therapy using nanosized graphene and graphene oxide. *Biomaterials* 2013;34:9519–34. Available from: <https://doi.org/10.1016/J.BIOMATERIALS.2013.08.066>.

- [19] Goenka S, Sant V, Sant S. Graphene-based nanomaterials for drug delivery and tissue engineering. *J Control Rel* 2014;173:75–88. Available from: <https://doi.org/10.1016/J.JCONREL.2013.10.017>.
- [20] Perreault F, Fonseca de Faria A, Elimelech M. Environmental applications of graphene-based nanomaterials. *Chem Soc Rev* 2015;44:5861–96. Available from: <https://doi.org/10.1039/C5CS00021A>.
- [21] Deng D, Pan X, Yu L, Cui Y, Jiang Y, Qi J, et al. Toward N-doped graphene via solvothermal synthesis. *Chem Mater* 2011;23:1188–93. Available from: <https://doi.org/10.1021/cm102666r>.
- [22] Deng D, Yu L, Pan X, Wang S, Chen X, Hu P, et al. Size effect of graphene on electrocatalytic activation of oxygen. *Chem Commun* 2011;47:10016. Available from: <https://doi.org/10.1039/c1cc13033a>.
- [23] Yu L, Pan X, Cao X, Hu P, Bao X. Oxygen reduction reaction mechanism on nitrogen-doped graphene: a density functional theory study. *J Catal* 2011;282:183–90. Available from: <https://doi.org/10.1016/J.JCAT.2011.06.015>.
- [24] Gong X, Liu G, Li Y, Yu DYW, Teoh WY. Functionalized-graphene composites: fabrication and applications in sustainable energy and environment. *Chem Mater* 2016;28:8082–118. Available from: <https://doi.org/10.1021/acs.chemmater.6b01447>.
- [25] Yin PT, Shah S, Chhowalla M, Lee K-B. Design, synthesis, and characterization of graphene–nanoparticle hybrid materials for bioapplications. *Chem Rev* 2015;115:2483–531. Available from: <https://doi.org/10.1021/cr500537t>.
- [26] Cho JS, Lee J-K, Kang YC. Graphitic carbon-coated FeSe<sub>2</sub> hollow nanosphere-decorated reduced graphene oxide hybrid nanofibers as an efficient anode material for sodium ion batteries. *Sci Rep* 2016;6:23699. Available from: <https://doi.org/10.1038/srep23699>.
- [27] Georgakilas V, Perman JA, Tucek J, Zboril R. Broad family of carbon nanoallotropes: classification, chemistry, and applications of fullerenes, carbon dots, nanotubes, graphene, nanodiamonds, and combined superstructures. *Chem Rev* 2015;115:4744–822. Available from: <https://doi.org/10.1021/cr500304f>.
- [28] Park GD, Cho JS, Lee J-K, Kang YC. Na-ion storage performances of FeSe<sub>x</sub> and Fe<sub>2</sub>O<sub>3</sub> hollow nanoparticles-decorated reduced graphene oxide balls prepared by nanoscale Kirkendall diffusion process. *Sci Rep* 2016;6:22432. Available from: <https://doi.org/10.1038/srep22432>.
- [29] Patel SKS, Choi SH, Kang YC, Lee J-K. Eco-friendly composite of Fe<sub>3</sub>O<sub>4</sub>-reduced graphene oxide particles for efficient enzyme immobilization. *ACS Appl Mater Interfaces* 2017;9:2213–22. Available from: <https://doi.org/10.1021/acsami.6b05165>.
- [30] Rabti A, Raouafi N, Merkoçi A. Bio(Sensing) devices based on ferrocene–functionalized graphene and carbon nanotubes. *Carbon N Y* 2016;108:481–514. Available from: <https://doi.org/10.1016/J.CARBON.2016.07.043>.
- [31] Zhu Y, Murali S, Cai W, Li X, Suk JW, Potts JR, et al. Graphene and graphene oxide: synthesis, properties, and applications. *Adv Mater* 2010;22:3906–24. Available from: <https://doi.org/10.1002/adma.201001068>.
- [32] Huang C, Li C, Shi G. Graphene based catalysts. *Energy Env Sci* 2012;5:8848. Available from: <https://doi.org/10.1039/c2ee22238h>.
- [33] Huang X, Qi X, Boey F, Zhang H. Graphene-based composites. *Chem Soc Rev* 2012;41:666–86. Available from: <https://doi.org/10.1039/C1CS15078B>.
- [34] Kauffman DR, Star A. Graphene versus carbon nanotubes for chemical sensor and fuel cell applications. *Analyst* 2010;135:2790. Available from: <https://doi.org/10.1039/c0an00262c>.

- [35] An X, Yu JC. Graphene-based photocatalytic composites. *RSC Adv* 2011;1:1426. Available from: <https://doi.org/10.1039/c1ra00382h>.
- [36] Krishnamoorthy K, Mohan R, Kim S-J. Graphene oxide as a photocatalytic material. *Appl Phys Lett* 2011;98:244101. Available from: <https://doi.org/10.1063/1.3599453>.
- [37] Loh KP, Bao Q, Ang PK, Yang J. The chemistry of graphene. *J Mater Chem* 2010;20:2277. Available from: <https://doi.org/10.1039/b920539j>.
- [38] Pumera M. Carbon nanotubes contain residual metal catalyst nanoparticles even after washing with nitric acid at elevated temperature because these metal nanoparticles are sheathed by several graphene sheets. *Langmuir* 2007;23(11):6453–8. Available from: <https://doi.org/10.1021/LA070088V>.
- [39] Tran PD, Wong LH, Barber J, Loo JSC. Recent advances in hybrid photocatalysts for solar fuel production. *Energy Env Sci* 2012;5:5902. Available from: <https://doi.org/10.1039/c2ee02849b>.
- [40] Bai S, Shen X. Graphene–inorganic nanocomposites. *RSC Adv* 2012;2:64–98. Available from: <https://doi.org/10.1039/C1RA00260K>.
- [41] Zhang N, Zhang Y, Xu Y-J. Recent progress on graphene-based photocatalysts: current status and future perspectives. *Nanoscale* 2012;4:5792. Available from: <https://doi.org/10.1039/c2nr31480k>.
- [42] Navalon S, Dhakshinamoorthy A, Alvaro M, Garcia H. Carbocatalysis by graphene-based materials. *Chem Rev* 2014;114:6179–212. Available from: <https://doi.org/10.1021/cr4007347>.
- [43] Liu H, Liu Y, Zhu D. Chemical doping of graphene. *J Mater Chem* 2011;21:3335.
- [44] Antolini E. Graphene as a new carbon support for low-temperature fuel cell catalysts. *Appl Catal B Env* 2012;123–124:52–68. Available from: <https://doi.org/10.1016/J.APCATB.2012.04.022>.
- [45] Martínez-Huerta MV, Lázaro MJ. Electrocatalysts for low temperature fuel cells. *Catal Today* 2017;285:3–12. Available from: <https://doi.org/10.1016/J.CATTOD.2017.02.015>.
- [46] Su C, Loh KP. Carbocatalysts: graphene oxide and its derivatives. *Acc Chem Res* 2013;46:2275–85. Available from: <https://doi.org/10.1021/ar300118v>.
- [47] Lü M, Li J, Yang X, Zhang C, Yang J, Hu H, et al. Applications of graphene-based materials in environmental protection and detection. *Chin Sci Bull* 2013;58:2698–710. Available from: <https://doi.org/10.1007/s11434-013-5887-y>.
- [48] Higgins D, Zamani P, Yu A, Chen Z. The application of graphene and its composites in oxygen reduction electrocatalysis: a perspective and review of recent progress. *Energy Env Sci* 2016;9:357–90. Available from: <https://doi.org/10.1039/C5EE02474A>.
- [49] Gao W, Wu G, Janicke MT, Cullen DA, Mukundan R, Baldwin JK, et al. Ozonated graphene oxide film as a proton-exchange membrane. *Angew Chem Int Ed* 2014;53:3588–93. Available from: <https://doi.org/10.1002/anie.201310908>.
- [50] Wu G, Santandreu A, Kellogg W, Gupta S, Ogoke O, Zhang H, et al. Carbon nanocomposite catalysts for oxygen reduction and evolution reactions: from nitrogen doping to transition-metal addition. *Nano Energy* 2016;29:83–110. Available from: <https://doi.org/10.1016/J.NANOEN.2015.12.032>.
- [51] Chen Z, Liu S, Yang M-Q, Xu Y-J. Synthesis of uniform CdS nanospheres/graphene hybrid nanocomposites and their application as visible light photocatalyst for selective reduction of nitro organics in water. *ACS Appl Mater Interfaces* 2013;5:4309–19. Available from: <https://doi.org/10.1021/am4010286>.
- [52] Chowdhury I, Duch MC, Mansukhani ND, Hersam MC, Bouchard D. Interactions of graphene oxide nanomaterials with natural organic matter and metal oxide surfaces. *Env Sci Technol* 2014;48:9382–90. Available from: <https://doi.org/10.1021/es5020828>.

- [53] Cohen-Tanugi D, McGovern RK, Dave SH, Lienhard JH, Grossman JC. Quantifying the potential of ultra-permeable membranes for water desalination. *Energy Env Sci* 2014;7:1134–41. Available from: <https://doi.org/10.1039/C3EE43221A>.
- [54] Akhavan O, Choobtashani M, Ghaderi E. Protein degradation and RNA efflux of viruses photocatalyzed by graphene–tungsten oxide composite under visible light irradiation. *J Phys Chem C* 2012;116:9653–9. Available from: <https://doi.org/10.1021/jp301707m>.
- [55] Dua V, Surwade SP, Ammu S, Agnihotra SR, Jain S, Roberts KE, et al. All-organic vapor sensor using inkjet-printed reduced graphene oxide. *Angew Chem Int Ed* 2010;49:2154–7. Available from: <https://doi.org/10.1002/anie.200905089>.
- [56] Fang Y, Guo S, Zhu C, Zhai Y, Wang E. Self-assembly of cationic polyelectrolyte-functionalized graphene nanosheets and gold nanoparticles: a two-dimensional hetero-structure for hydrogen peroxide sensing. *Langmuir* 2010;26:11277–82. Available from: <https://doi.org/10.1021/la100575g>.
- [57] Ghosh A, Subrahmanyam KS, Krishna KS, Datta S, Govindaraj A, Pati SK, et al. Uptake of H<sub>2</sub> and CO<sub>2</sub> by graphene. *J Phys Chem C* 2008;112:15704–7. Available from: <https://doi.org/10.1021/jp805802w>.
- [58] Huang Z-H, Zheng X, Lv W, Wang M, Yang Q-H, Kang F. Adsorption of lead(II) ions from aqueous solution on low-temperature exfoliated graphene nanosheets. *Langmuir* 2011;27:7558–62. Available from: <https://doi.org/10.1021/la200606r>.
- [59] Joshi RK, Gomez H, Alvi F, Kumar A. Graphene films and ribbons for sensing of O<sub>2</sub>, and 100 ppm of CO and NO<sub>2</sub> in practical conditions. *J Phys Chem C* 2010;114:6610–13. Available from: <https://doi.org/10.1021/jp100343d>.
- [60] Liu X, Pan L, Lv T, Lu T, Zhu G, Sun Z, et al. Microwave-assisted synthesis of ZnO–graphene composite for photocatalytic reduction of Cr(vi). *Catal Sci Technol* 2011;1:1189. Available from: <https://doi.org/10.1039/c1cy00109d>.
- [61] Liu X, Pan L, Lv T, Zhu G, Sun Z, Sun C. Microwave-assisted synthesis of CdS–reduced graphene oxide composites for photocatalytic reduction of Cr(VI). *Chem Commun* 2011;47:11984. Available from: <https://doi.org/10.1039/c1cc14875c>.
- [62] Ning G, Xu C, Mu L, Chen G, Wang G, Gao J, et al. High capacity gas storage in corrugated porous graphene with a specific surface area-lossless tightly stacking manner. *Chem Commun* 2012;48:6815. Available from: <https://doi.org/10.1039/c2cc31785k>.
- [63] Arsat R, Breedon M, Shafiei M, Spizziri PG, Gilje S, Kaner RB, et al. Graphene-like nano-sheets for surface acoustic wave gas sensor applications. *Chem Phys Lett* 2009;467:344–7. Available from: <https://doi.org/10.1016/j.cplett.2008.11.039>.
- [64] Schedin F, Geim AK, Morozov SV, Hill EW, Blake P, Katsnelson MI, et al. Detection of individual gas molecules adsorbed on graphene. *Nat Mater* 2007;6:652–5. Available from: <https://doi.org/10.1038/nmat1967>.
- [65] Sitko R, Turek E, Zawisza B, Malicka E, Talik E, Heimann J, et al. Adsorption of divalent metal ions from aqueous solutions using graphene oxide. *Dalt Trans* 2013;42:5682. Available from: <https://doi.org/10.1039/c3dt33097d>.
- [66] Yan H, Tao X, Yang Z, Li K, Yang H, Li A, et al. Effects of the oxidation degree of graphene oxide on the adsorption of methylene blue. *J Hazard Mater* 2014;268:191–8. Available from: <https://doi.org/10.1016/J.JHAZMAT.2014.01.015>.
- [67] Zhao G, Li J, Ren X, Chen C, Wang X. Few-layered graphene oxide nanosheets as superior sorbents for heavy metal ion pollution management. *Env Sci Technol* 2011;45:10454–62. Available from: <https://doi.org/10.1021/es203439v>.

- [68] Zhao G, Ren X, Gao X, Tan X, Li J, Chen C, et al. Removal of Pb(II) ions from aqueous solutions on few-layered graphene oxide nanosheets. *Dalt Trans* 2011;40:10945. Available from: <https://doi.org/10.1039/c1dt11005e>.
- [69] Bhunia SK, Jana NR. Reduced graphene oxide-silver nanoparticle composite as visible light photocatalyst for degradation of colorless endocrine disruptors. *ACS Appl Mater Interfaces* 2014;6:20085–92. Available from: <https://doi.org/10.1021/am505677x>.
- [70] Lonkar SP, Abdala AA. Applications of graphene in catalysis. *J Thermodyn Catal* 2014;5. Available from: <https://doi.org/10.4172/2157-7544.1000132>.
- [71] Lightcap IV, Kosel TH, Kamat PV. Anchoring semiconductor and metal nanoparticles on a two-dimensional catalyst mat. storing and shuttling electrons with reduced graphene oxide. *Nano Lett* 2010;10:577–83. Available from: <https://doi.org/10.1021/nl9035109>.
- [72] Markets and Markets report 2018. Graphene market-Global trends and forecasts to 2020. <<https://www.marketsandmarkets.com/PressReleases/graphene.asp>> [accessed 18.10.2018.]
- [73] Ren W, Cheng H-M. The global growth of graphene. *Nat Nanotechnol* 2014;9:726–30. Available from: <https://doi.org/10.1038/nnano.2014.229>.
- [74] McWilliams A. Graphene: technologies, applications, and markets. Wellesley, MA: BCC Research Market Forecasting; 2016.
- [75] Lee WC, Lim CHYX, Shi H, Tang LAL, Wang Y, Lim CT, et al. Origin of enhanced stem cell growth and differentiation on graphene and graphene Oxide. *ACS Nano* 2011;5:7334–41. Available from: <https://doi.org/10.1021/nn202190c>.
- [76] Pumera M. Graphene in biosensing. *Mater Today* 2011;14:308–15. Available from: [https://doi.org/10.1016/S1369-7021\(11\)70160-2](https://doi.org/10.1016/S1369-7021(11)70160-2).
- [77] Shao Y, Wang J, Wu H, Liu J, Aksay IA, Lin Y. Graphene based electrochemical sensors and biosensors: a review. *Electroanalysis* 2010;22:1027–36. Available from: <https://doi.org/10.1002/elan.200900571>.
- [78] Sun X, Liu Z, Welsher K, Robinson JT, Goodwin A, Zaric S, et al. Nano-graphene oxide for cellular imaging and drug delivery. *Nano Res* 2008;1:203–12. Available from: <https://doi.org/10.1007/s12274-008-8021-8>.
- [79] Guo X, Mei N. Assessment of the toxic potential of graphene family nanomaterials. *J Food Drug Anal* 2014;22:105–15. Available from: <https://doi.org/10.1016/J.JFDA.2014.01.009>.
- [80] Russier J, Treossi E, Scarsi A, Perrozzi F, Dumortier H, Ottaviano L, et al. Evidencing the mask effect of graphene oxide: a comparative study on primary human and murine phagocytic cells. *Nanoscale* 2013;5:11234. Available from: <https://doi.org/10.1039/c3nr03543c>.
- [81] D'Souza F, Kadish KM. Handbook of carbon nano materials, world scientific series on carbon nanoscience. World Scientific; 2014. Available from: <https://doi.org/10.1142/8979>.
- [82] Goncalves G, Marques P, Vila M. Graphene-based materials in health and environment: new paradigms. Springer; 2016.
- [83] Arvidsson R, Kushnir D, Sandén BA, Molander S. Prospective life cycle assessment of graphene production by ultrasonication and chemical reduction. *Env Sci Technol* 2014;48:4529–36. Available from: <https://doi.org/10.1021/es405338k>.
- [84] Khanam PN, Popelka A, Alejji M, AlMaadeed MA. Biotechnological production process and life cycle assessment of graphene. *J Nanomater* 2017;2017:1–10. Available from: <https://doi.org/10.1155/2017/5671584>.
- [85] Zhang B, Misak H, Dhanasekaran PS, Kalla D, Asmatulu R. Environmental impacts of nanotechnology and its products. Fairmount, Wichita: Wichita State University; 2011.



This page intentionally left blank

## Section 3

**Functionalized  
nanomaterials  
for biomedical,  
pharmaceutical,  
agriculture, and  
agri-food industry**  
**Section Functionalized  
nanomaterial and biology**

This page intentionally left blank

## Chapter 6

# Delivery of bioactives using biocompatible nanodelivery technologies

H. Turasan and J.L. Kokini

*Department of Food Science, Purdue University, West Lafayette, IN, United States*

### 6.1 Introduction

Biocompatible nanodelivery systems and fabrication methods are becoming increasingly important for the encapsulation and delivery of bioactive compounds and drugs. Encapsulating bioactive drugs in polymeric nanoparticles improves their targeted and timely delivery, especially regarding less potent drugs, which are administered through oral routes and therefore lose part of their effects through the gastrointestinal tract [1]. The polymeric coating surrounds the bioactive drug and provides hindrance from the harmful effects of the gastrointestinal tract. This hindrance increases when the polymer has longer chains. Synthetic polymers have longer chains than natural polymers, and so generally provide higher encapsulation efficiencies. However, administering synthetic polymers involves risk of accumulation in tissues, which could lead to serious side effects.

Natural polymers, on the other hand, have minimal side effects in the human body, due to their nontoxic and edible nature. They are also abundantly available, inexpensive, and biocompatible. Depending on application, a natural polymer to be nanoparticulated for drug delivery could be from a plant origin (zein, kafirin, gliadin, starch, pectins, gums, etc.), or an animal source (bovine serum albumin (BSA), ovalbumin, or gelatin). Depending on the desired properties of the delivery systems, the particles could be protein-based, polysaccharide-based, or a combination of both polymers. Protein utilization is more advantageous than polysaccharides, since protein zeta potentials can be tuned easily with pH alteration, to optimize electrostatic attraction between the polyelectrolytes. The most common methods of delivery system fabrication are nanoprecipitation/desolvation, complex coacervation, and layer-by-layer (LbL) assembly. This chapter summarizes recent

studies on fabrication of biobased delivery systems for the delivery of bioactives and drug compounds, as well as fundamental studies that can aid in comprehension of the thermodynamic mechanisms of nanoparticle formation.

## 6.2 Fabrication methods of biopolymer-based nanodelivery systems

### 6.2.1 Nanoprecipitation/desolvation

Nanoprecipitation, also referred to as solvent displacement or desolvation, is a simple technique wherein two miscible solvents are used to particulate the polymer, which acts as the coating material for the delivered bioactive [2]. The solvent that the polymer is dissolved in, which is often referred to as “the solvent” or “the good solvent,” is dropwise added to the other solution, which is usually a “nonsolvent” or “bad solvent” for the polymer [3,4]. The lack of polymer solubility in the nonsolvent changes the conformation of the polymer, leading to a rapid nucleation and aggregation of the polymer molecules, and eventually to nanoparticles. The properties of the encapsulated bioactives (i.e., hydrophilicity/hydrophobicity, solvent type, solvent-to-nonsolvent ratio, temperature, or pH) can be varied. These parameters play a significant role in the size, size distribution, shape, and morphology of the nanoparticles, as well as their ability to efficiently encapsulate bioactive compounds.

#### 6.2.1.1 Nanoprecipitation/desolvation of proteins

The ability to change the charge on protein molecules through pH tuning makes proteins advantageous biomolecules for nanoparticle fabrication. Therefore many researchers are exploring ways to fabricate protein-based nanodelivery systems with higher encapsulation efficiencies, and better bioactive nutraceutical or drug release properties.

BSA, an animal-based protein, was nanoparticulated using the nanoprecipitation technique to encapsulate curcumin [5], which is a polyphenolic bioactive compound that has antiinflammatory, antioxidative and cancer chemopreventative properties [6]. The effects of two nonsolvents, acetone and ethanol, were analyzed on the nanoparticulation efficiency of BSA with four solvent ratios: 100:0, 70:30, 50:50, and 0:100, ethanol-to-acetone. The nanoparticulation efficiency of BSA was highest at 99.2%, when acetone was used alone as the nonsolvent. Ethanol alone exhibited a nanoparticulation efficiency of 95%, and the mixtures of ethanol and acetone displayed nanoparticulation efficiencies ranging between 75% and 97%. The smallest BSA nanoparticles were fabricated when ethanol was used alone as the nonsolvent, and the largest nanoparticles were obtained with acetone solely. The highest curcumin encapsulation efficiency was achieved when the

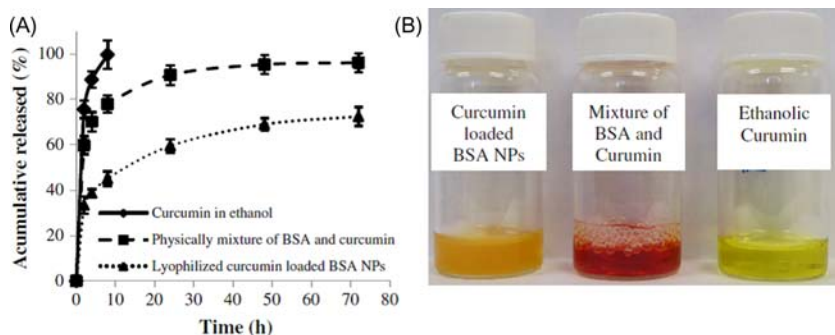


**FIGURE 6.1** In vitro release profiles of curcumin (A), and images of solutions (B). Reprinted from Sadeghi R, Moosavi-Movahedi AA, Emam-jomeh Z, Kalbasi A, Razavi SH, Karimi M, et al. The effect of different desolvating agents on BSA nanoparticle properties and encapsulation of curcumin. *J Nanopart Res* 2014;16(9):2565. Available from: <https://doi.org/10.1007/s11051-014-2565-1> with permission from Springer Nature.

curcumin-to-BSA molar ratio was 1.5, and when ethanol was used as the nonsolvent. Increasing the curcumin-to-BSA ratio increased the particle size of the nanoparticles, while crosslinking the nanoparticles with glutaraldehyde led to smaller particles and higher polydispersity index. Crosslinking also increased the stability of the BSA nanoparticles. The curcumin release study proved that BSA nanoparticles are able to control the release of encapsulated curcumin, when compared to free curcumin in ethanol, or mixtures of BSA and curcumin (Fig. 6.1).

Pristine kafirin nanoparticles, as well as kafirin/carboxymethyl chitosan nanoparticles fabricated through nanoprecipitation method, were also used to encapsulate curcumin, where 80% ethanol was used as the solvent and water as the nonsolvent [7]. In the loaded samples, curcumin was added to the kafirin solution, prior to nanoprecipitation. Further addition of carboxymethyl chitosan increased the size of the particles from 200 to 236 nm, and the polydispersity index from 0.186 to 0.235. Introducing carboxymethyl chitosan also increased the encapsulation efficiency from 55% to 86% and the loading efficiency from 5% to 6%, due to additional hydrogen bonding between the carboxylic hydroxy groups in carboxymethyl chitosan and carbonyl groups on kafirin, which led to a more stable nanoparticle formation and higher retention of curcumin. Encapsulating curcumin in pristine kafirin, or kafirin/carboxymethyl chitosan nanoparticles, improved its photostability significantly, with higher stability in the latter. Additionally, the dissolution of curcumin, both in simulated gastric fluid and in simulated intestinal fluid, increased significantly. In another study, the same group encapsulated curcumin in kafirin nanoparticle-stabilized pickering emulsions [8]. Kafirin nanoparticles were prepared by a nanoprecipitation method using acetic acid as the solvent and water as the nonsolvent, which were then used to

homogenize different ratios of curcumin dissolved in vegetable oil to form emulsions. Increasing temperature and pH yielded less stable kaffirin nanoparticle-stabilized pickering emulsions. The stability of curcumin against UV radiation was higher when kaffirin nanoparticle-stabilized emulsions were used to encapsulate curcumin, compared to bulk oil or Tween 80-stabilized emulsions, and lipid oxidation rates of kaffirin nanoparticle-stabilized emulsions were slower than Tween 80-stabilized emulsions. However, kaffirin nanoparticle-stabilized emulsions did not maintain stability through gastric digestion process, due to pepsin hydrolysis.

Curcumin was also successfully encapsulated in soy protein isolate nanoparticles, fabricated with the desolvation method, where water was used as the solvent for the protein and ethanol was the nonsolvent, containing ethanol-soluble curcumin [9]. The use of ethanol and crosslinker concentrations had a strong impact on the particle size and zeta potential of nanoparticles. A minimum of 80% ethanol and 75% crosslinker was found necessary to form stable nanoparticles, with a negative zeta potential of above  $-36$  mV and particle size around 200 nm. The highest encapsulation efficiency of curcumin, 97.2%, was achieved with a curcumin-to-protein ratio of 1%, which also led to the highest amount of released curcumin: 78% over an 8 h period in PBS/Tween 20 solution (Fig. 6.2) [9].

Ovalbumin (OVA) and  $\alpha$ -lactalbumin ( $\alpha$ -LA) were also nanoparticulated using the desolvation method [10]. Effects of methanol, ethanol, and acetone as the nonsolvents were tested on the nanoparticle sizes, polydispersity indexes, and zeta potentials of the nanoparticles. The smallest nanoparticles

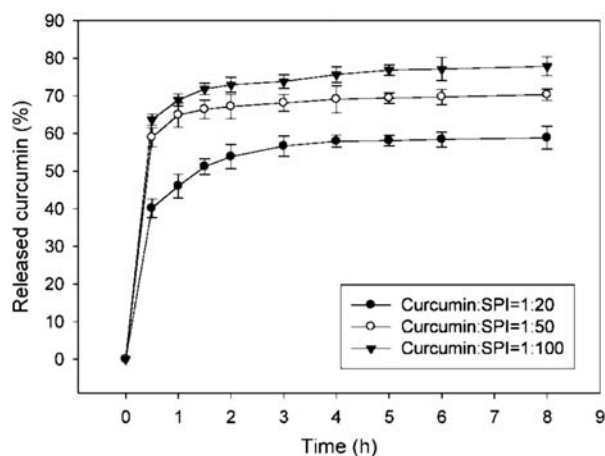


**FIGURE 6.2** Release profile of curcumin from soy protein isolate nanoparticles fabricated with nanoprecipitation method. Reprinted from Teng Z, Luo Y, Wang Q. Nanoparticles synthesized from soy protein: preparation, characterization, and application for nutraceutical encapsulation. *J Agric Food Chem* 2012;60(10):2712–20. Available from: <https://doi.org/10.1021/jf205238x> with permission from ACS.

DA <sup>a</sup>	T <sup>b</sup> (°C)	PS <sup>c</sup> (nm)	PDI <sup>d</sup>	ZP <sup>e</sup> (mv)
Ethanol	80	118.5 ± 1.9	0.166 ± 0.033	-33.9 ± 1.1
Ethanol	50	143.9 ± 0.3	0.196 ± 0.007	-33.5 ± 1.6
Ethanol	25	218.6 ± 5.4	0.050 ± 0.018	-35.3 ± 1.2
Acetone	80	288.5 ± 1.0	0.220 ± 0.030	-35.5 ± 0.8
Acetone	50	202.5 ± 1.0	0.023 ± 0.014	-38.3 ± 1.1
Acetone	25	217.8 ± 4.3	0.041 ± 0.030	-35.9 ± 1.3
Methanol	80	103.0 ± 0.8	0.075 ± 0.022	-36.6 ± 0.5
Methanol	50	116.1 ± 0.3	0.067 ± 0.021	-34.5 ± 1.5
Methanol	25	162.2 ± 3.7	0.062 ± 0.017	-34.6 ± 0.8

DA <sup>a</sup>	T <sup>b</sup> (°C)	PS <sup>c</sup> (nm)	PDI <sup>d</sup>	ZP <sup>e</sup> (mv)
Ethanol	80	59.0 ± 5.2	0.292 ± 0.018	-22.1 ± 0.8
Ethanol	50	48.5 ± 3.0	0.342 ± 0.009	-19.8 ± 2.3
Ethanol	25	80.3 ± 2.8	0.231 ± 0.010	-24.8 ± 4.3
Acetone	80	53.8 ± 4.2	0.211 ± 0.006	-27.0 ± 2.7
Acetone	50	86.4 ± 2.1	0.094 ± 0.014	-24.5 ± 3.7
Acetone	25	96.8 ± 12.2	0.196 ± 0.034	-22.6 ± 5.9
Methanol	80	58.6 ± 8.4	0.217 ± 0.031	-19.2 ± 1.3
Methanol	50	64.1 ± 2.7	0.204 ± 0.048	-24.1 ± 0.6
Methanol	25	60.5 ± 7.8	0.224 ± 0.004	-15.8 ± 7.1

**FIGURE 6.3** Effect of desolvating agent (a, DA) and temperature (b, T) on particle size (c, PS), polydispersity index (d, PSI), and zeta potential (e, ZP) of  $\alpha$ -LA (top table) and OVA (bottom table) nanoparticles. Reprinted from Etorki AM, Gao M, Sadeghi R, Maldonado-Mejia LF, Kokini JL. Effects of desolvating agent types, ratios, and temperature on size and nanostructure of nanoparticles from  $\alpha$ -lactalbumin and ovalbumin. *J Food Sci* 2016;81(10):E2511–20. Available from: <https://doi.org/10.1111/1750-3841.13447> with permission from John Wiley & Sons.

of both OVA and  $\alpha$ -LA nanoparticles were obtained when methanol was used as the nonsolvent, due to its shortest aliphatic chain and therefore highest polarity among the three solvents. OVA nanoparticles had diameters ranging between 60 and 160 nm, and those of  $\alpha$ -LA nanoparticles ranged between 150 and 230 nm. While different ratios of solvent-to-nonsolvent did not have a significant effect on the particle sizes of either of these proteins, heat treatment above their denaturation temperatures generally reduced particle diameters (Fig. 6.3). Crosslinking the proteins with glutaraldehyde during nanoparticulation increased the stability of both OVA and  $\alpha$ -LA nanoparticles. This is due to bond formation between the amine groups of proteins and the aldehyde group of glutaraldehyde, leading to tighter junctions and a more stable network [11]. After 30 days of refrigeration, there was no significant change in the particle sizes or the polydispersity indexes of both OVA and  $\alpha$ -LA nanoparticles, indicating that OVA and  $\alpha$ -LA are good candidates for biopolymer-based nanodelivery systems.

Casein nanoparticles were also fabricated using nanoprecipitation techniques, to encapsulate an anticancer drug: doxorubicin [12]. Water was used as the solvent for sodium caseinate and  $\text{CaCl}_2$  solution was used as the nonsolvent, to provide  $\text{Ca}^{+}$  ions. For drug encapsulation, doxorubicin was added to the sodium caseinate solution prior to the nanoprecipitation step. Excess  $\text{Ca}^{+}$  ions provided by  $\text{CaCl}_2$  solution led to packing of casein molecules and



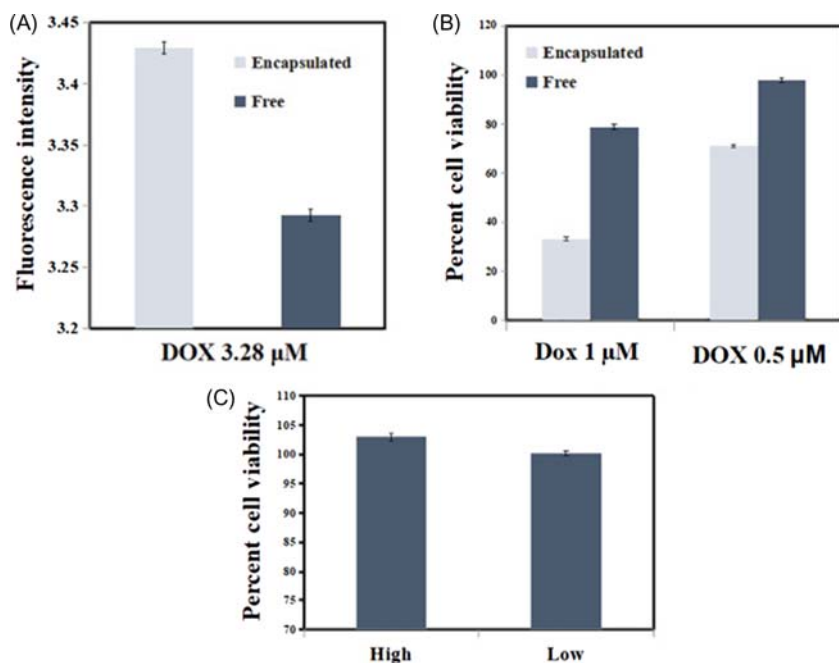


**FIGURE 6.4** (A) Cell uptake assay of casein-bound DOX and an equivalent amount of free DOX (cell line, PANC-1). (B) Cytotoxicity assay of two concentrations of DOX in particles and an equivalent amount of free DOX. (C) Cytotoxicity assay of blank nanoparticles, high = 1.4 mg/mL and low = 0.5 mg/mL. Reprinted from Gandhi S, Roy I. Doxorubicin-loaded casein nanoparticles for drug delivery: preparation, characterization and in vitro evaluation. *Int J Biol Macromol* 2019;121:6–12. Available from: <https://doi.org/10.1016/j.ijbiomac.2018.10.005> with permission from Elsevier.

micelle formation, which then were used to encapsulate doxorubicin. Casein formed spherical nanoparticles with diameters in the range of 100–300 nm, and a polydispersity index of 0.334. Doxorubicin release from the nanoparticles was faster in acidic pH (pH = 1) than physiological pH (pH = 7.4), possibly due to disintegration of casein micelles. It was concluded that these nanoparticles are more likely to dissolve in the stomach, and would be more suitable for delivery of targeted gastric cancer drugs. Cellular uptake of both free doxorubicin, and doxorubicin encapsulated in casein nanoparticles, was tested with human pancreatic carcinoma cells. Encapsulating doxorubicin in casein nanoparticles significantly increased its cellular uptake and reduced cancer cell viability, due to the high biocompatibility of casein with cell structure (Fig. 6.4).

Whey protein is another dairy protein nanoparticulated with the desolvation method, using ethanol as the desolvating agent [13]. Whey protein nanoparticles were immediately diluted in solutions having pH = 3 and pH = 7

after nanoprecipitation, to test their stability. While in the pH = 7 solution, the dairy protein aggregates disintegrated and sizes decreased below 10 nm, showing that the particles were not stable at this pH. On the other hand, pH = 3 did not affect particle sizes. Increase in the ethanol-to-water volumetric ratio from 0 to 5 during nanoprecipitation, increased the particle size from 2.9 to 35.8 nm. Increasing the temperature of freshly nanoprecipitated samples widened their particle size distributions, and increased the average particle sizes significantly. Nanoparticles heated to 90°C exhibited the highest particle size: 4294 nm. The same group also studied zinc incorporation into whey protein nanoparticles [14]. ZnCl<sub>2</sub> solution was added to the protein solution prior to desolvation. Similar to their previous study, ethanol was used as the desolvating agent and ethanol-to-water volume ratios of 0, 1, 2, and 3 were tested. Increasing zinc concentration caused larger particle formations, especially at higher ethanol-to-water ratios. The largest particles fabricated with 1 mM zinc exhibited average diameters of 100 nm, while 5- and 10-mM zinc resulted in particles as large as 1 μm. When 10 mM zinc was added to the protein solutions before nanoprecipitation, zinc loading to the nanoparticles was higher than the 5 mM zinc addition. One week of storage did not significantly affect the diameter of zinc-incorporated whey protein nanoparticles.

Modified nanoprecipitation methods were developed for the fabrication of biopolymer nanoparticles [15]. The flash nanoprecipitation technique (FNP) is a modified version of a nanoprecipitation technique, wherein the biopolymer dissolved in a good solvent, and the desolvating agent (nonsolvent), are injected into a mixing chamber simultaneously. This creates an instantaneous diffusion of the good solvent into the poor solvent, leading to instant and continuous formation of biopolymer nanoparticles [15]. For the fabrication of zein nanoparticles with FNP technique, aqueous ethanol solution and water, with or without sodium caseinate, were used as the good solvent and the nonsolvent, respectively [16]. The effects of flow rate, zein and ethanol concentrations, and the presence of sodium caseinate on the particle sizes and  $\xi$  potentials were analyzed. Increasing zein solution flow rate was found to decrease the size of the particles in both the absence and presence of sodium caseinate, beyond which no significant difference was found between particle sizes. In the absence of sodium caseinate, zein nanoparticle sizes were not affected by increasing zein concentration, and remained at about 130–140 nm up to 5% (w/v). Higher zein concentration (7.5% w/v) increased the particle size to 205 nm. In the presence of sodium caseinate, increasing zein concentration steadily increased the particle size. This difference was attributed to the neutralizing pH of the mixture with sodium caseinate (6.4–6.95), which is close to the isoelectric point of zein, and therefore eliminates the positive charges on zein molecules that usually prevent aggregation of zein in acidic environments (Fig. 6.5) [16]. The smallest zein nanoparticles were fabricated when 60% and 70% aqueous ethanol was used as

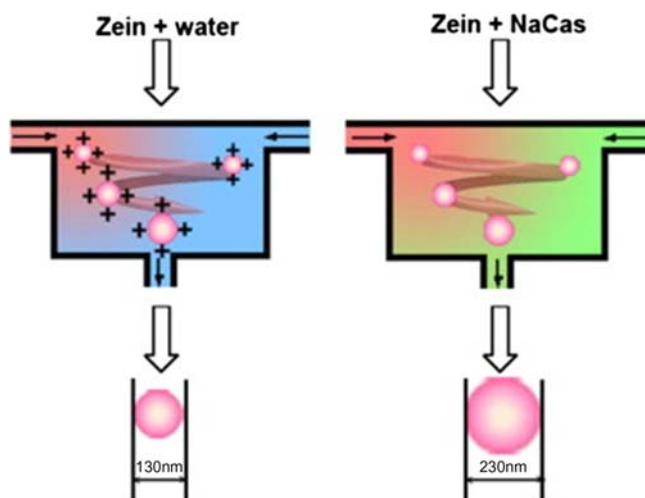


**FIGURE 6.5** The effect of sodium caseinate on the particle size of zein nanoparticles. Positively charged zein molecules at acidic pH in the absence of sodium caseinate lead to smaller nanoparticles (left); neutralizing solution with sodium caseinate eliminates positive charges of zein molecules, leading to aggregation and bigger nanoparticles. Reprinted from Li K-K, Zhang X, Huang Q, Yin S-W, Yang X-Q, Wen Q-B, et al. Continuous preparation of zein colloidal particles by Flash NanoPrecipitation (FNP). *J Food Eng* 2014;127:103–110. Available from: <https://doi.org/10.1016/j.jfoodeng.2013.12.001> with permission from Elsevier.

the good solvent, rather than 80–90% ethanol solution, both in the absence and presence of sodium caseinate.

Microparticles fabricated from wheat gluten proteins soluble in ethanol (gliadins), using the nanoprecipitation technique, were loaded with urea and analyzed for their controlled release of urea, to test their potential as prolonged-release fertilizers [17]. Water was used as the nonsolvent and ethanol was used as the good solvent for the proteins. Gliadin microparticles, having diameters ranging between 900 nm and 1.7  $\mu\text{m}$ , released 50% of the loaded urea during the first hour of direct contact with the aqueous medium, which was attributed to the urea that was on the surface of the microparticles. A slow and gradual release of urea was observed until arrival at equilibrium in 12 h. Equilibrium was reached at 88% release of total urea, when the urea concentration inside of the microparticles was equal to the urea concentration in the aqueous medium. Gliadin was also nanoparticulated using 62% ethanol as the solvent, and aqueous solutions such as NaCl and Pluronic F68 [18]. Zeta potential of gliadin nanoparticles reached a maximum of 23 when the pH was 5, and decreased to  $-25$  as the pH was increased to 9. The highest zeta potential at pH = 5 and the lowest zeta potential at pH = 9 exhibited the most stable gliadin nanoparticles. As the water-to-ethanol ratio increased, the diameters of gliadin nanoparticles decreased from 340 to 235 nm.

Increasing the mixing speed and NaCl concentration significantly increased the particle diameters. Increasing the concentration of Pluronic F68 as a surfactant, or increasing the temperature (especially from 40°C to 60°C), decreased the size of gliadin nanoparticles. Introduction of 2-Mercaptoethanol and dithiothreitol separately, as reducing agents, also decreased the particles sizes, with 2-Mercaptoethanol leading to smaller particles. Curcumin loading to the gliadin nanoparticles resulted in an encapsulation efficiency of 68%, with a slight increase of particle size (from 296 to 378 nm) and an elevated polydispersity index, indicating a less homogenous particle size distribution.

Gelatin nanoparticles encapsulating fluorescein-isothiocyanate-dextran as the model drug were fabricated, with the addition of surfactants and crosslinkers (Fig. 6.6) [19]. Among Poloxamer 407, Poloxamer 188, polysorbate 80, polysorbate 20 and TritonX-100, only Poloxamer 407 and 188 enabled stable nanoparticle formation, at a minimum concentration of 7%. Isopropyl alcohol, acetone, and acetonitrile were poor nonsolvents for nanoparticle formation, but ethanol and methanol aided the formation of nanoparticles, with mean particle sizes of 250 and 280 nm, respectively. The solvent-to-nonsolvent ratio was also found to have a significant effect on particle size, especially in the higher range. Crosslinking provided a slower release profile

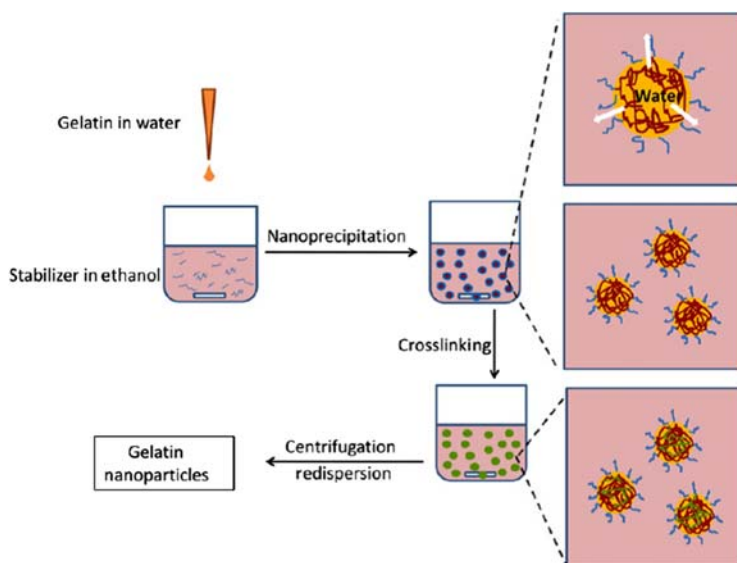


**FIGURE 6.6** Fabrication of gelatin nanoparticles using desolvation/nanoprecipitation method with the addition of surfactant/stabilizer and crosslinker. Reprinted from Khan SA, Schneider M. Improvement of nanoprecipitation technique for preparation of gelatin nanoparticles and potential macromolecular drug loading. *Macromol Biosci* 2013;13(4):455–463. Available from: <https://doi.org/10.1002/mabi.201200382> with permission from John Wiley & Sons.

of the drug from the nanoparticles, such that in the initial 120 h, only 20% of the drug was released. With the addition of a digestive enzyme, trypsin, 80% of the encapsulated drug was released within the hour of addition.

### 6.2.1.2 Nanoprecipitation/desolvation of carbohydrates

Due to their low toxicity, abundance, and high biocompatibility, carbohydrate-based biopolymers have also been extensively studied for nanoparticulation and nanodelivery of bioactive nutraceuticals and drugs. Starch nanoparticles were fabricated for the encapsulation of curcumin [4]. Effects of amylopectin-to-amylose ratios were investigated using four types of corn starch: native normal corn starch (~25% amylose), amioca starch (> 99% amylopectin), Hylon V (55% amylose), and Hylon VII (70% amylose). Ethanol, methanol, and acetone were tested as nonsolvents for all the starch types. Ethanol led to the smallest particle sizes for all types of starch, as low as 98 nm particles, while acetone produced the largest nanoparticles, as high as 475 nm particles. All four types of corn starch were successfully used in fabricating nanoparticles, with normal corn starch leading to the most uniform particles (Fig. 6.7). Encapsulation of curcumin in starch nanoparticles was proven to increase the stability of curcumin significantly.

In a similar study, different starch types with a greater variety of amylose content (i.e., waxy corn starch [0.8%], tapioca starch [18.9%], sweet potato starch [20.6%], normal corn starch [26.5%], potato starch [28%], pea starch [40%] and high amylose corn starch [69.0%]) [20] were used to fabricate nanoprecipitates. Smaller particle sizes were obtained, compared to the first study mentioned [4], with mean particle diameters ranging between 75 and 30 nm for all types of starches. Potato starch resulted in the largest nanoparticles, and high amylose starch resulted in the smallest. The amylose content of the starch was found to have a linear correlation with the crystallinity of starch nanoparticles. The starch polymers, amylose and amylopectin, were also used separately for fabrication of nanoparticles [21,22].

Chitosan, obtained from deacetylation of chitin, is a commonly nanoparticulated polysaccharide for bioactive nutraceutical and drug delivery. Chitosan is insoluble in water, and therefore acidic aqueous solutions or other solvents are often necessary to solubilize it [23]. Two techniques were used to fabricate lime essential oil-loaded chitosan nanoparticles: nanoprecipitation and nanoencapsulation. For nanoprecipitation of chitosan, acetic acid and methanol were used as the solvent and nonsolvent respectively, where lime essential oil was dissolved in the nonsolvent. For the nanoencapsulation, lime essential oil was dissolved in a mixture of acetone, ethanol, and lecithin, which later was added to the chitosan solution. Average particle size of control chitosan nanoparticles was found to be 4.7 nm, while lime essential oil-loaded chitosan nanoparticles were 6.1 nm. Nanocapsules had slightly larger sizes than their corresponding nanoparticles, such that control

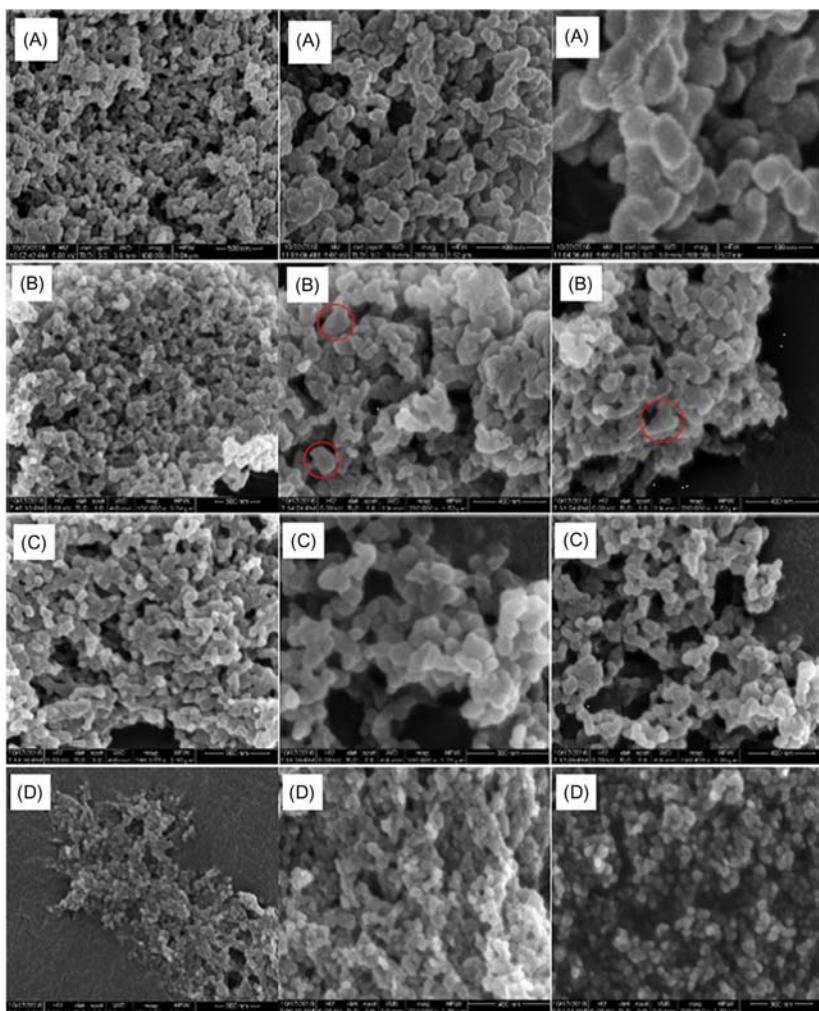


**FIGURE 6.7** Nanoparticles fabricated using desolvation method using normal corn starch (A), Amioca (B), Hylon V (C), and Hylon VII (D) with ethanol as the nonsolvent. *Reprinted from Sadeghi R, Daniella Z, Uzun S, Kokini J. Effects of starch composition and type of non-solvent on the formation of starch nanoparticles and improvement of curcumin stability in aqueous media. J Cereal Sci 2017;76:122–30. Available from: <https://doi.org/10.1016/j.jcs.2017.05.020> with permission from Elsevier.*

chitosan Nanocapsules were 5.8 nm and lime oil-loaded nanocapsules were 6.1 nm in size. With the encapsulation of lime oil, zeta potential of chitosan nanoparticles decreased from 20.2 to 10.0 mV, and nanocapsules from 61.1 to 57.0 mV due to the reduction in the number of available  $-\text{NH}_3^+$  sites of chitosan, as a result of interaction with lime oil. The antibacterial activities

of nanoparticles and nanocapsules were tested on *Staphylococcus aureus*, *Listeria monocytogenes*, *Shigella dysenteriae*, and *Escherichia coli*. Nanoparticles fabricated with the nanoprecipitation method had a higher antimicrobial effect on the bacteria than the nanocapsules. The highest inhibition was seen when lime oil-encapsulated chitosan nanoparticles were used against *S. dysenteriae*.

Nanoprecipitated chitosan nanoparticles were also loaded with citral, another antimicrobial compound [24]. *N*-(methylsulfonic acid) and acetic acid were used as solvents and methanol and water were used as nonsolvents. Smaller chitosan nanoparticles were obtained when chitosan concentration was decreased or when nonsolvent-to-solvent ratio was increased. Larger particles were fabricated when acetic acid was used as the solvent, compared to *N*-(methylsulfonic acid), and when water was used as the nonsolvent, instead of methanol. The highest encapsulation efficiency of 88% was reached when methanol was used as the nonsolvent and acetic acid as the solvent. The loading capacity of the chitosan nanoparticles was 38%, which indicates that 38% of nanoparticles were the encapsulated citral, by weight.

Nanoprecipitation of locust bean gum was achieved by depolymerization of the gum and solubilization of a citrate phosphate buffer, which was then mixed with the nonsolvent isopropanol and boric acid solution. Allicin, an antiinflammatory and antioxidant compound found in garlic, was encapsulated in locust bean gum nanoparticles, which increased the particle sizes above 100 nm. Allicin-loaded locust bean gum nanoparticles were stable for 12 h at pH 7.4. The nanoparticles were also tested for their cellular toxicity, after which it was concluded that allicin-loaded locust bean gum nanoparticles are safe for cells and therefore good candidates for edible drug and bioactive delivery systems.

Cellulose, another naturally abundant polysaccharide, has also been nanoprecipitated into nanoparticles for bioactive and drug delivery. Cellulose, extracted from cotton fibers with NaOH/thiourea/urea treatment and filtration, was nanoprecipitated using NaOH/thiourea/urea mixture as the solvent and ethanol as the nonsolvent [25]. Methylene blue was used as the model bioactive encapsulated in the cellulose nanoparticles and was dissolved in the NaOH/thiourea/urea solution with chitosan prior to nanoprecipitation. Even though the cellulose particles are used as bioactive delivery systems, it has to be noted that the solvent mixture used in this nanoprecipitation method is considered toxic, having possible carcinogenic effects. Spherical nanoparticles were fabricated, especially when cellulose concentration was increased in the solution (Fig. 6.8). Increasing cellulose concentration increased the particle size, and decreasing the solvent-to-nonsolvent ratio decreased the particle size, significantly. The smallest particles, fabricated with 1:60 v/v NaOH/thiourea/urea-to-ethanol ratio, had a mean particle size of 70 nm. Encapsulation efficiency of methylene blue was highest for the



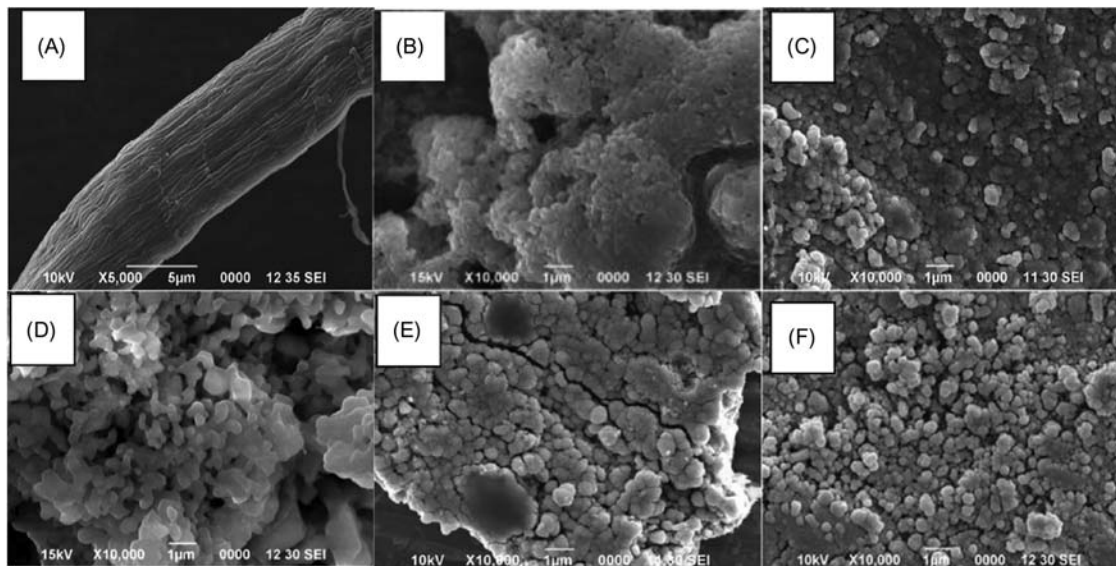


**FIGURE 6.8** Cellulose fiber extracted from cotton, cellulose nanoparticles fabricated with nanoprecipitation using 0.001 w/v % (A), 0.005 w/v % (B), 0.01 w/v % (C), 0.03 w/v % (D), and 0.1 w/v % (E) cellulose. Reprinted from Chin SF, Jimmy FB, Pang SC. Size controlled fabrication of cellulose nanoparticles for drug delivery applications. *J Drug Deliv Sci Technol* 2018;43:262–6. Available from: <https://doi.org/10.1016/j.jddst.2017.10.021> with permission from Elsevier.



smallest cellulose nanoparticles (89%), and decreased to 56% as the particle size increased. Release kinetics of methylene blue was tested in PBS solutions under constant stirring. The smallest cellulose nanoparticles, 70 nm in diameter, exhibited the highest release rate of 38.5%, while the largest nanoparticles showed 11.7% release of methylene blue in the first 12 h. Complete release of methylene blue was slower, as the diameter of the cellulose nanoparticles increased.

Natural gums from different origins can be nanoparticulated alone, or coparticulated with other polymers to form nanoparticles. Carboxymethyl/guar gums were conanoparticulated with the assistance of ultrasonication, where water was used as the solvent and acetone as the nonsolvent [26]. The particles were spherical, with sizes ranging between 12 and 30 nm and a few clusters of 70 nm. Locust bean gum nanoparticles fabricated with the nanoprecipitation method were larger than carboxymethyl/guar gum nanoparticles [27].

Another common technique to improve nanoparticle performance and functionality involves fabrication of a nanoparticle using a polysaccharide, and then coating it with another polysaccharide. For example, a hydrophobic nanoparticle can be coated with a hydrophilic polysaccharide to improve its solubility in water. Active polysaccharides from tea, pumpkin, and balsam pear were encapsulated in maltodextrin nanoparticles, which were fabricated with the nanoprecipitation method to enhance their bioavailability for absorption in the gastrointestinal tract [28]. Maltodextrin dissolved in water was nanoprecipitated with ethanol, followed by investigation of the effects of three emulsifiers (SDS, Span 80, and Tween 80) and variants in the solvent-to-nonsolvent ratio. Tween 80 emulsifier yielded the highest maltodextrin nanoparticle encapsulation (85.3%), followed by Span 80 (80.2%) and SDS (78.6%), at a ratio of 1:10 solvent-to-nonsolvent. Increasing solvent-to-nonsolvent ratio from 1:8 to 1:10 decreased the nanoparticle sizes. However, further increase in the solvent-to-nonsolvent ratio to 1:12 increased the particle sizes. Maltodextrin nanoparticles fabricated with SDS and Span 80 exhibited particle sizes in the range of 40–180 nm, while Tween 80 resulted in smaller nanoparticles (30–140 nm), due to its longer hydrophilic head group and higher interaction with maltodextrin. Balsam pear polysaccharide loading resulted in the largest nanoparticles, with a mean particle size of 116 nm, followed by pumpkin polysaccharide (86 nm), and tea polysaccharide (81 nm). Polysaccharide loading increased the zeta potentials of maltodextrin nanoparticles, resulting in higher stability. While pristine maltodextrin nanoparticles had an average zeta potential of  $-7.8$ , particles loaded with balsam pear, pumpkin, and tea polysaccharides had zeta potentials of  $-20.7$ ,  $-28.4$ , and  $-32.8$ , respectively. Tea polysaccharide-loaded maltodextrin nanoparticles had the highest loading efficiency of 72.1%. Polysaccharide loading improved the stability of nanoparticles against an increasing NaCl concentration, up to 500 mM. The stability of nanoparticles

also increased against pH treatment with a polysaccharide addition. The most stable particles against pH values 1.2 and 7.4 were tea polysaccharide-loaded particles, and the least stable loaded particles were obtained with balsam pear polysaccharide loading.

Pullulan, a natural polysaccharide formed by the fungi *Aureobasidium pullulans*, can also be nanoprecipitated in the form of a copolymer [29]. First, the copolymer pullulan-g-poly(*N*-isopropylacrylamide) was synthesized through free radical polymerization, and then nanoprecipitated using dimethylformamide as the solvent and water as the nonsolvent. The antiinflammatory drug Indomethacin was added into pullulan-g-poly(*N*-isopropylacrylamide) solution prior to nanoprecipitation. Pullulan-g-poly(*N*-isopropylacrylamide) nanoparticles were also fabricated with the dialysis method and compared with nanoprecipitated nanoparticles. Particles fabricated with the nanoprecipitation method exhibited smaller diameters than the ones fabricated with the dialysis method. Increasing the drug-to-polymer ratio to 1:1 (w/w) reduced the particle sizes of nanoparticles prepared with both methods. The highest drug entrapment efficiency of 80% was achieved with 1:1 (w/w) drug-to-polymer ratio and 10 g/L polymer concentration, which yielded mean particle diameter of 247 nm, when particles were formed with nanoprecipitation. The particles' polydispersity index grew with increasing drug-to-polymer ratios. Drug in vitro % release was found to increase with a change in drug-to-polymer ratio from 0.33:1 to 1:1 (Fig. 6.9). While complete release occurred in PBS solution at pH = 7.4, only 60%–80% release occurred in acetate solution at pH = 5. Increasing temperature from 25°C to 37°C also increased % drug release (Fig. 6.9).

### 6.2.2 Coacervation

Particulation through complex coacervation uses the principle of ionic attraction between two polyelectrolytes that are oppositely charged. The attraction between two polymers forms soluble or insoluble nano- or microparticles in the solution, and often precipitates or remains as a suspension [30,31]. Weaker interactions, such as hydrogen bonding or hydrophobic interactions, can also contribute to complex coacervation. Stability of the coacervate complex depends on the magnitude of the charge difference between the two polyelectrolytes. It is therefore crucial to select the appropriate polyelectrolytes, the solvent, and pH conditions in coacervation for maximum attraction between the polyelectrolytes. The interaction between polyelectrolytes is also effective on the resulting nanoparticle structure, texture, and encapsulation efficiency [32].

Complex coacervation of biopolymers has been the focus of many leading groups. For example, Huang's group's focus has been mainly on understanding the mechanism of complex coacervation of many edible polyelectrolytes (from food and agricultural sources), and investigating the

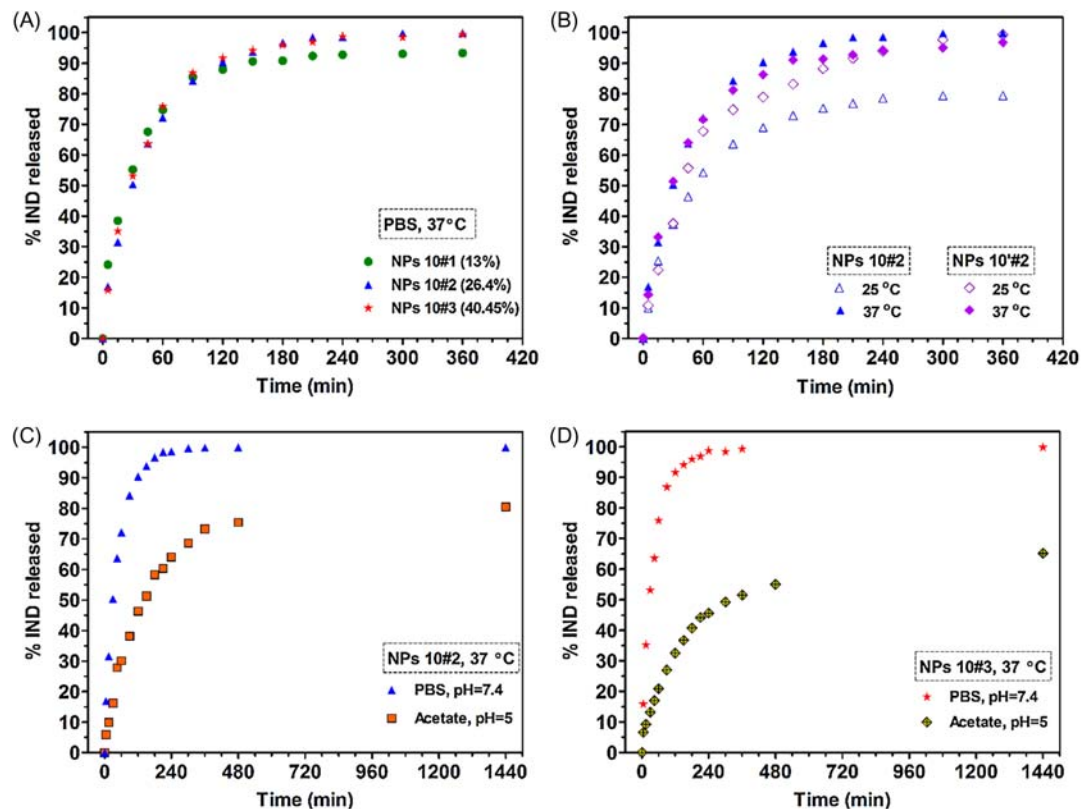


**FIGURE 6.9** In vitro release profiles of indomethacin from pullulan-g-poly(*N*-isopropylacrylamide) nanoparticles fabricated with nanoprecipitation method. (A) Release of indomethacin from nanoparticles with different drug loading content, (B) Release of indomethacin from nanoparticles at different temperatures, (C) and (D) Release of indomethacin from two types of nanoparticles with different drug loading contents at pH 5 and pH 7.4. Reprinted from Constantin M, Bucătaru S, Stoica I, Fundueanu G. Smart nanoparticles based on pullulan-g-poly(*N*-isopropylacrylamide) for controlled delivery of indomethacin. *Int J Biol Macromol* 2017;94:698–708. Available from: <https://doi.org/10.1016/j.ijbiomac.2016.10.064> with permission from Elsevier.

effects of salt concentration, polyelectrolyte ratios, and protein self-association on the coacervates [33,34]. Their recent studies include the encapsulation and delivery of natural antioxidants in complex coacervates of biopolymers, using the double emulsion technique [35,36]. Other groups have also investigated the effects of these same parameters. Tirrell's group focused on looking at the effects of polypeptide ratio, salt concentration, total polymer concentration, molecular weight, pH, and temperature [37]. Sample turbidity was used as the complex formation indicator, as well as optical microscopy imaging; phase diagrams were established to distinguish coacervate to solution boundaries. Their study confirmed the importance of ionic strength on the complex formation, since salt can screen the charged groups. Temperature was also found to be more effective on coacervate formation when total polymer concentration was increased. Olsen's group investigated complex coacervation of supercharged proteins with polyelectrolytes, using succinic anhydride treatment to explore the effects of protein charge on coacervation [38]. Their study showed that chemically supercharging the proteins is more effective in inducing phase separation, leading to complex coacervate formation, compared to changing the pH. This is because coacervates were formed at lower charges, when the proteins were supercharged.

Complex coacervation is specifically advantageous for encapsulation and delivery of bioactives and drugs in the gastrointestinal tract, wherein the particle needs to remain stable at the low pH environment of the stomach, and needs to disintegrate in the pH = 6 environment of the intestinal tract. Therefore the selection of polymers that have the highest attraction to one another at acidic pHs need to be coupled with the collapse of that attraction at pH = 6. Due to their edible nature and low toxicity, natural proteins or carbohydrate-based biopolymers are useful for coacervation. This section summarizes examples of recent studies wherein different pairs of biopolymer polyelectrolytes were used for coacervation.

For a successful complex coacervation, an understanding of the thermodynamic mechanism between polyelectrolytes is integral. The thermodynamics of the interaction between sodium alginate and chitosan was studied using isothermal titration calorimetry (ITC) [39]. The effects of pH on the zeta potentials, the effect of the order of addition, and molar charge ratios of the polyelectrolytes on particle size, size distribution, and stability were investigated. Sodium alginate had a stable negative zeta potential with varying pH, but chitosan was positively charged below pH = 8, and negatively charged above pH = 8. pH = 4 was the optimum pH value for coacervation, since the difference in zeta potentials was highest (Fig. 6.10).

The overall enthalpy of the reaction between sodium alginate and chitosan was higher (−3207 kJ/mol) when chitosan solution was added to sodium alginate solution, than when sodium alginate solution was added into chitosan solution (−1683 kJ/mol). Higher reaction enthalpy showed stronger

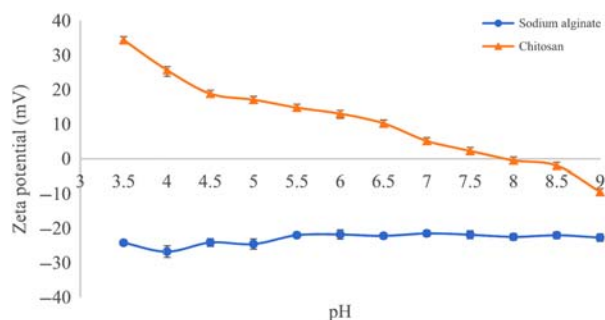


**FIGURE 6.10** Zeta potentials of sodium alginate and chitosan with varying pH values. Reprinted from Yilmaz T, Maldonado L, Turasan H, Kokini J. Thermodynamic mechanism of particulation of sodium alginate and chitosan polyelectrolyte complexes as a function of charge ratio and order of addition. *J Food Eng* 2019;254:42–50. Available from: <https://doi.org/10.1016/j.jfoodeng.2019.03.002> with permission of Elsevier.

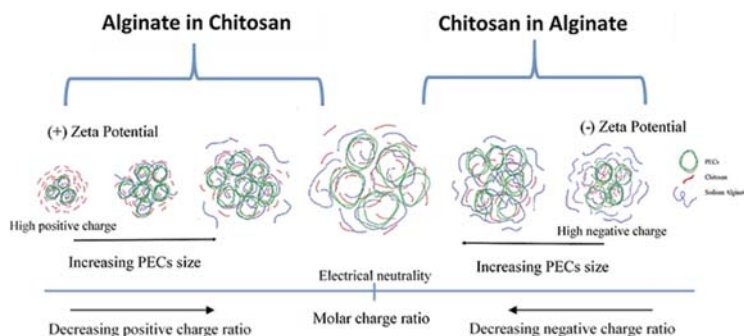


**FIGURE 6.11** Schematic mechanism of PEC formation as a function of the order of addition and charge ratio. Reprinted from Yilmaz T, Maldonado L, Turasan H, Kokini J. Thermodynamic mechanism of particulation of sodium alginate and chitosan polyelectrolyte complexes as a function of charge ratio and order of addition. *J Food Eng* 2019;254:42–50. Available from: <https://doi.org/10.1016/j.jfoodeng.2019.03.002> with permission from Elsevier.

interaction between the polyelectrolytes when sodium alginate was added into chitosan. Sodium alginate addition into chitosan also yielded a higher entropy change, which is another indicator of a higher order of polyelectrolyte coacervation. Addition of sodium alginate into chitosan formed smaller nanoparticles, and increasing their molar charge ratio led to a sharper transition in zeta potential and the enthalpy of reaction, than when chitosan solution was added into sodium alginate solution. The effect of molar charge ratios in two orders of addition can be seen more clearly in Fig. 6.11. When alginate was added into chitosan, the initial positive zeta potential approached electrical neutrality, and the positive charge ratio decreased, resulting in an increase in PEC sizes. When chitosan was added into alginate,

the initial negative zeta potential approached electrical neutrality; negative charge ratio decreased. PECs formed this way also increased in size, with decreasing negative charge ratio. However, the particles were larger when chitosan was added into alginate. Sodium alginate into chitosan coacervates were more stable during storage, when molar charge ratios were below 0.85. Chitosan into sodium alginate coacervates were stable at charge ratios below 0.67. Sodium alginate into chitosan coacervates were more stable than chitosan into sodium alginate coacervates. This study clearly shows the importance of the order of polyelectrolyte addition in coacervation.

The ITC analysis showed that when chitosan solutions were added to buffers, exothermic reactions occurred due to the protonation of the amine groups. When sodium alginate was added to the buffer solution, endothermic reactions occurred due to hydration of hydrogen bonds in mannuronic and guluronic acid [39]. While both alginate into chitosan and chitosan into alginate reactions were exothermic, after saturation, alginate into chitosan showed further endothermic reactions, due to dilution of hydrogen bonds; chitosan into alginate exhibited an exothermic reaction, due to further protonation of amine groups.

Nanoparticles were formed from coacervation of BSA and poly-D-lysine (PDL), and were tested for possible effects of molecular weight of PDL, mass and molar ratios of the polyelectrolytes, salt, and crosslinker concentrations on the nanoparticles [30]. BSA had a positive charge below  $\text{pH} = 5$  and a negative charge above  $\text{pH} = 5$ . Both high molecular weight (HMW) and low molecular weight (LMW) PDL exhibited positive zeta potential below  $\text{pH} = 11$ .  $\text{pH} = 7$  was chosen as the optimum  $\text{pH}$  to form coacervates, since the highest zeta potential difference occurred at this  $\text{pH}$  for both pairs of polyelectrolytes. Smallest PEC nanoparticles for both HMW PDL-BSA and LMW PDL-BSA were formed at  $\text{pH} = 7$ , due to the highest electrostatic attraction. LMW PDL-BSA nanoparticles had spherical shapes, and the smallest of them were obtained at a mass ratio of 2 (BSA: PDL) and a molar ratio of 7, with a particle diameter of 212 nm. HMW PDL-BSA nanoparticles had nonspherical shapes, the smallest being obtained at a mass ratio of 2.5 (BSA: PDL) and at a molar ratio of 15.6 with a particle diameter of 310 nm. In general, HMW PDL-BSA coacervates were larger in diameter than LMW PDL-BSA coacervates. Addition of salt decreased particle sizes for both HMW PDL-BSA and LMW PDL-BSA nanoparticles, and the smallest particles of HMW PDL-BSA were fabricated at 0.4 M salt concentration, while for LMW PDL-BSA were formed at 0.1 M. LMW PDL-BSA nanoparticles were loaded with curcumin (the model bioactive compound). The highest encapsulation efficiency (60%), and the highest loading capacity (22  $\mu\text{g}/\text{mg}$ ) was achieved at a curcumin-to-BSA ratio of 10.

Whey protein isolate (WPI) and chitosan can also form PEC nano/microparticles through complex coacervation [40]. Three types of chitosan were studied, with varying degrees of deacetylation (83%, 94%, and 96%) and

chitosan-to-WPI mass ratio on the coacervation yield, zeta potential, and rheology of the coacervates. Among the three types of chitosan, 96% deacetylated chitosan generally gave the highest coacervation yield with WPI. The highest yield was observed at a chitosan-to-WPI mass ratio of 0.2:1. Rheological tests proved that coacervates of WPI and 96% deacetylated chitosan had the most compact and strongest internal structures. This is due to the higher number of free  $-\text{NH}_3^+$  sites of 96% deacetylated chitosan, which can interact more with the  $-\text{COO}^-$  groups of WPI, ultimately leading to a stronger complex formation. The degree of deacetylation did not cause a statistically significant change in the zeta potential of chitosan alone. However, when complex coacervations were formed with WPI, chitosan (83%)/WPI, chitosan (94%)/WPI, and chitosan (96%)/WPI had zeta potentials of  $-6.67$ ,  $-9$ , and  $-9.93$ , respectively. The highest zeta potential magnitude of 96% deacetylated chitosan/WPI coacervates also explains the higher stability and strongest internal structure of this complex. Microparticles were loaded with garlic extract as the model drug, and the highest total bioactive retention efficiency of 61.40% was achieved with 96% deacetylated chitosan, followed by 94% (54.45% retention) and 83% (51.04% retention) deacetylated chitosan, respectively.

WPI and chitosan complex coacervates were also fabricated to encapsulate pure ergosterol and *Agaricus bisporus* L. extract [41]. Heat treating the loaded microparticles at  $55^\circ\text{C}$  led to more spherical and better-defined shapes than  $95^\circ\text{C}$  heat treatment. Between 0.5 and 10.5 WPI-to-chitosan ratios, the 0.5 ratio exhibited higher encapsulation efficiencies in general. The optimal performance of these particles was found to be 75% microencapsulation yield, 100% encapsulation efficiency, and 12% loading with RSM.

Microparticles fabricated from gelatin and gum arabic using complex coacervation were used to encapsulate ascorbic acid [42]. The effects of gelatin and gum arabic concentrations, wall-to-core ratios, and pH on the particle size encapsulation efficiency, stability, and release profiles of particles were investigated. Encapsulation efficiencies ranged between 27.3% and 93.8%, depending on the gelatin, gum arabic, and ascorbic acid concentrations, the highest of which was reached with a 1:1 gelatin-to-gum arabic ratio (7.5% w/v concentrations each) and 1:0.5 wall-to-core (w/w) ratio. The smallest particles had a mean diameter of  $7.7\ \mu\text{m}$  and formed with a wall-to-core ratio of 1:0.5 and 5% gelatin and 5% gum arabic concentrations; the largest particles had a mean diameter of  $12.4\ \mu\text{m}$ , fabricated with a wall-to-core ratio of 1:0.75 with 5% gelatin and 5% gum arabic. Loaded nanoparticles showed higher stability during storage at  $20^\circ\text{C}$ , compared to pure ascorbic acid. The nanoparticles with the highest encapsulation efficiency (93.8%) also had the highest storage stability (Fig. 6.12). Release of ascorbic acid from microparticles was generally slower near neutral pH values (7.6). At  $\text{pH} = 1$  or  $\text{pH} = 12.0$ , the release of ascorbic acid was fastest (almost complete release within the first 2 h).



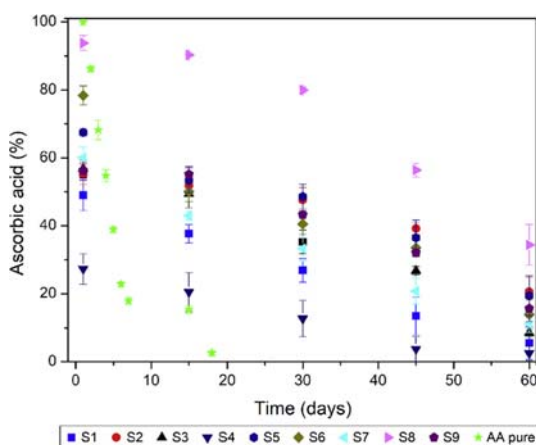


**FIGURE 6.12** Stabilities of pure ascorbic acid and ascorbic acid encapsulated in coacervates. Sample S8 (right-pointing triangle) has 7.5% (w/v) gelatin solution concentration, 7.5% (w/v) gum Arabic solution concentration and 1:0.5 wall-to-core (w/w) ratio. For further information, please see the original source. Reprinted from Rodrigues da Cruz MC, Andreotti Dagostin JL, Perussello CA, Masson ML. Assessment of physicochemical characteristics, thermal stability and release profile of ascorbic acid microcapsules obtained by complex coacervation. *Food Hydrocoll* 2019;87:71–82. Available from: <https://doi.org/10.1016/j.foodhyd.2018.07.043> with permission from Elsevier.

Gelatin and pectin are another pair of polyelectrolytes used for fabrication of coacervates [43]. The zeta potentials of gelatin and two types of pectin, high methyl and low methyl, were analyzed with changing pH in the range of 3–6. Both types of pectin had negative zeta potentials, with low methyl pectin having the lowest. Gelatin was positively charged below pH 4.75 and negatively charged above pH 4.75. Zeta potentials of coacervates were also measured with varying pH and polymer ratios. Regarding gelatin-to-low methoxyl pectin coacervates, neutrality could only be reached at gelatin-to-pectin ratios of 2:1 and higher, while gelatin-to-high methoxyl pectin coacervates exhibited neutral charges between pH = 3.5 and 4.25 at all ratios. The highest particulation yields for gelatin-to-low methoxyl pectin (65%) and gelatin-to-high methyl pectin (67%) were achieved with 6:1 and 3:1 gelatin-to-pectin ratios, respectively. Particles were loaded with cinnamaldehyde and gelatin-to-high methoxyl pectin particles exhibited higher encapsulation yield (93%) and encapsulation efficiency (89%), compared to low methoxyl pectin. Encapsulation of cinnamaldehyde increased the particle size and polydispersity index of gelatin-to-low methoxyl pectin particles more than gelatin-to-high methyl pectin particles (Fig. 6.13). Thermogravimetric analysis showed that encapsulation in coacervates improved thermal stability of cinnamaldehyde significantly, as evident by comparison between coacervates and cinnamaldehyde-gelatin-pectin physical mixtures. Coacervates also retarded the release of cinnamaldehyde more than physical mixtures in hot



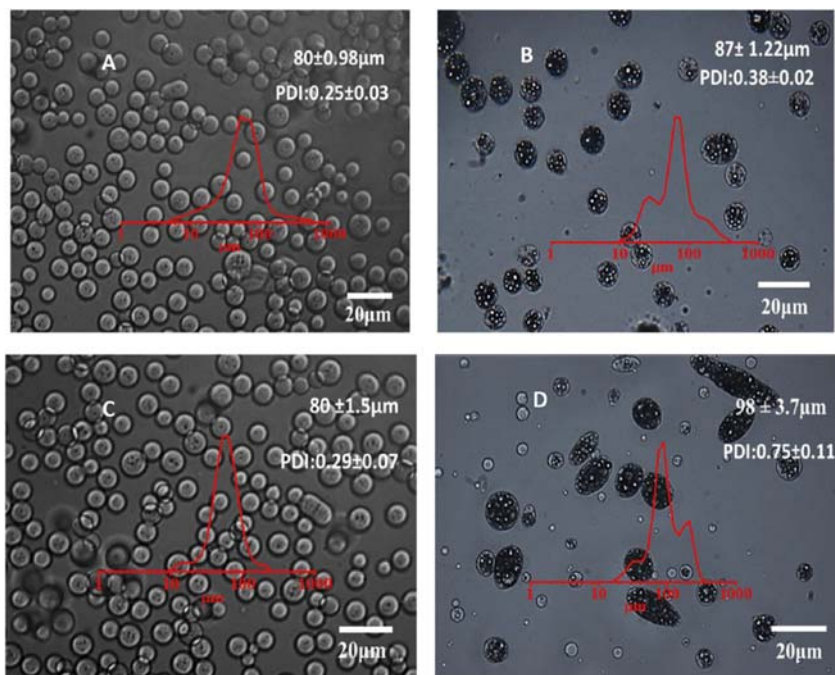


**FIGURE 6.13** Microscope images of gelatin: high methyl pectin (A, B), and gelatin-to-low methyl pectin (C, D) particles unloaded (A, C) and loaded (B, D) with cinnamaldehyde. Reprinted from Muhoza B, Xia S, Cai J, Zhang X, Duhoranimana E, Su J. Gelatin and pectin complex coacervates as carriers for cinnamaldehyde: effect of pectin esterification degree on coacervate formation, and enhanced thermal stability. *Food Hydrocoll* 2019;87:712–22. Available from: <https://doi.org/10.1016/j.foodhyd.2018.08.051> with permission from Elsevier.

water. Gelatin-to-high methyl pectin coacervates had the lowest cinnamaldehyde release (around 32%) in 2 h.

Thermodynamic interactions between low methoxyl pectin and sodium caseinate during complex formation were studied using ITC, along with the effects of pH, ionic strength, and temperature on the coacervates [44]. At pH = 5 and 7, there were no interactions between the polymers, evident from almost no enthalpy change, due to their negative charges at this pH. Because of their opposite charges at pH = 3, an exothermic interaction occurred between the polymers. Addition of NaCl prevented electrostatic interactions between sodium caseinate and pectin, and a temperature change from 25°C to 65°C increased the enthalpy change of the reaction, indicating a stronger interaction between the polymers, possibly caused by the dissociation of low methoxyl pectin at higher temperatures. Increasing temperature from 25°C to 65°C also decreased the entropy of reaction, which indicates the existence of hydrophobic interactions between pectin and sodium caseinate molecules.

In another study, high methoxyl citrus pectin was chemically modified to produce pectins with four degrees of esterification (DE) (8.6%, 41.9%, 72.3% and unmodified [88.4%]) which were then used to form complex coacervates with pea protein isolate [45]. As the pea protein isolate-to-pectin ratio was increased from 1:1 to 15:1, the pH value where complex coacervates formed shifted to higher ranges. The optimum pea protein isolate-to-pectin ratios for coacervate formation were found to be 8:1, 10:1, 10:1, and 15:1, for unmodified citrus pectin (with 88.4% DE), pectin with 72.3% DE, 41.9% DE, and 8.6% DE, respectively. At these optimum polymer ratios, the pH range wherein maximum interactions occurred was 3.70–3.85. DE was also found to be effective on the critical pH value (the pH where the first detectable interactions between polymers occur) for complex formation: pectin with 8.9% DE began forming complexes with pea protein isolate around pH 7.1, while for pectins with 41.9% DE and 72.3% DE, this value was around 6.6, and around 6.4 with unmodified pectin (88.4%). This is due to increasing the number of galacturonic acid residues with lower percentage of DE, leading to more interaction with pea protein isolate molecules. The rigidity of the pectin rod-shaped molecules was affected by DE. Pectin with 8.9% DE had the most rigid molecules, evident from intrinsic viscosity measurements; unmodified pectin exhibited the least rigid molecules. Increasing pectin rigidity was found to increase hydrogen bonding, and therefore the strength of interaction between pea protein isolate and pectin.

Lastly, cress seed mucilage and sodium caseinate were microparticulated using complex coacervation, and utilized as a delivery system for curcumin [46]. A study of the effects of pH on coacervation yield resulted in pH = 4 as giving the highest absorbance value and coacervation yield, making it the optimum pH value for the highest interaction between cress seed mucilage and sodium caseinate. Increasing the mucilage-to-caseinate ratio from 1:1 to 4:1 increased the coacervation yield, but further increasing the ratio to 5:1, decreased the yield slightly. Between spray drying and freeze drying, spray drying was found to more effectively encapsulate curcumin in the coacervates. While increasing curcumin concentration from 10% to 30% decreased encapsulation efficiency, regardless of drying method or biopolymer concentration, increasing the biopolymer concentration from 0.2 to 0.6 significantly increased encapsulation efficiency—for both spray-dried and freeze-dried particles. Encapsulation load was also similarly affected by increasing biopolymer concentration and the drying method, however, unlike encapsulation efficiency, encapsulation load increased by increase of curcumin concentration. Release profiles of curcumin from spray-dried and freeze-dried microcapsules showed that spray drying delayed the curcumin release more than freeze drying. After 480 min, 80.26% of curcumin was released from freeze-dried particles, while 63.47% of curcumin was released from the spray-dried particles.

The studies summarized here indicate that coacervation is a powerful method of polyelectrolyte biopolymer particulation that can be used as drug and bioactive carrier systems. They also exhibit the importance of tailoring fabrication parameters to modify, make, and design particles with the desired properties and functionality.

### 6.2.3 Layer-by-layer deposition

LbL deposition is another interesting method of fabricating nanoparticles from polyelectrolyte biopolymers. The principle of LbL deposition consists of the formation of alternating thin layers of oppositely charged polyelectrolytes to form a layered particle [3]. These particles can be spherical or tubular, and they can be hollow, offering a great deal of flexibility. After the deposition of the first layer of a polyelectrolyte polymer on a solid template, another oppositely charged polyelectrolyte polymer solution is added into the system. This catalyzes electrostatic interactions, thereby forming a second layer of polymer that is strongly bonded to the first. One pair of polyelectrolyte layers is often referred to as a “bilayer.” This process can be repeated until the desired number of bilayers is reached. Each polymer may also exhibit additional properties (e.g., hydrophobicity, porosity, surface roughness, etc.), and depending on which polymer is deposited last, the functionality and properties of the particle changes. The material to be delivered can either be encapsulated in the core of the nanoparticles, within bilayers, or between bilayers [47].

#### 6.2.3.1 Spherical particle formation through layer-by-layer deposition

The LbL technique has been used in the fabrication of hollow and solid kafirin nanoparticles [48]. Regarding the solid kafirin nanoparticles, the nanoprecipitation method was used, with ethanol as the solvent and water as the nonsolvent for kafirin. Hollow kafirin nanoparticles were formed by a sacrificial template, consisting of  $\text{NaCO}_3$ . First, the sacrificial cores were prepared by adding aqueous sodium carbonate solution in ethanol, to reach a final ethanol concentration of 70%. Kafirin in aqueous ethanol (70%) was dropwise added to a sodium carbonate dispersion in ethanol, allowing kafirin nanoparticles to form layers on sodium carbonate particles. These served as nuclei for the precipitation of kafirin, and resulted in a kafirin coat surrounding the sodium carbonate particles (sacrificial template). Redispersion of this solution in water helped sodium carbonate leach out of their kafirin coatings and dissolve in water, resulting in hollow kafirin nanoparticles. Dextran sulfate and chitosan were used to form layers surrounding kafirin, and form a likewise surrounding LBL particle. During this process, solid or hollow kafirin nanoparticles were mixed with dextran sulfate solutions at  $\text{pH} = 4$ ,

where kafirin particles have a positive zeta potential and dextran sulfate molecules have a negative zeta potential. After the formation of the first dextran sulfate layer, the solution containing negatively charged particles was mixed with a positively charged chitosan solution, forming a second layer on top of the dextran sulfate. This procedure was repeated twice, to form two bilayers on the solid and hollow kafirin nanoparticles (Fig. 6.14).

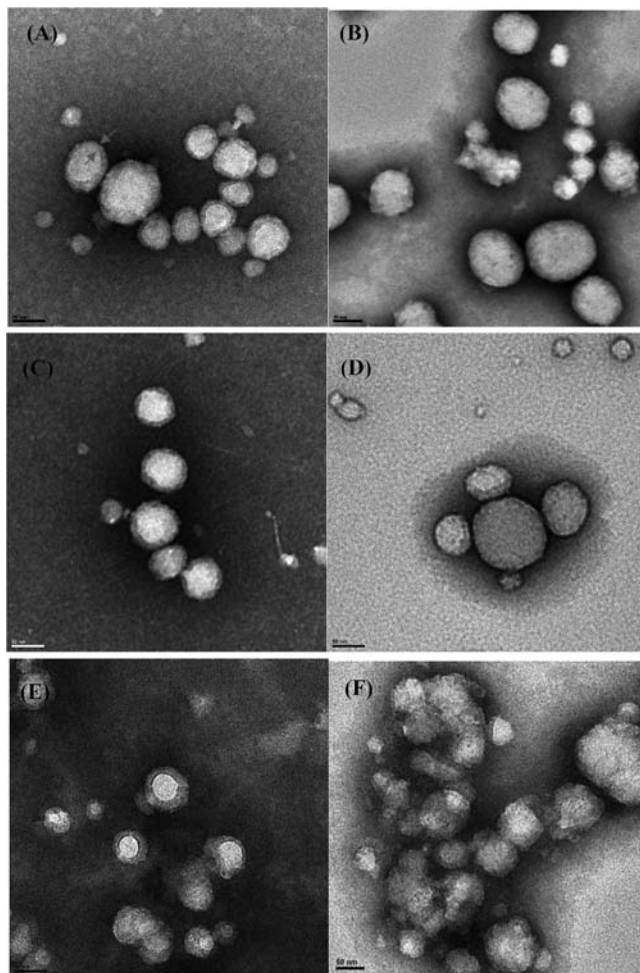


**FIGURE 6.14** TEM images of hollow (A, C, E) and solid (B, D, F) kafirin nanoparticles; unloaded (A, B), curcumin-loaded (C, D), and curcumin-loaded LbL-assembled (E, F) kafirin nanoparticles. Reprinted from Li X, Maldonado L, Malmr M, Rouf TB, Hua Y, Kokini J. Development of hollow kafirin-based nanoparticles fabricated through layer-by-layer assembly as delivery vehicles for curcumin. *Food Hydrocoll* 2019;96:93–101. Available from: <https://doi.org/10.1016/j.foodhyd.2019.04.042> with permission from Elsevier.

Curcumin was selected as the model bioactive compound, and was added to the kafirin ethanolic solutions for the loaded nanoparticles.

The hollow kafirin nanoparticles exhibited zeta potentials between  $-40$  and  $-47$  mV, indicating good particle stability. Neither the ratio of sodium carbonate-to-kafirin, nor the presence of sodium carbonate, affected the stability of the kafirin nanoparticles. Particle diameters were not affected by the encapsulation of curcumin; however, the addition of dextran sulfate/chitosan bilayers increased the diameters of the kafirin nanoparticles from  $60\text{--}70$  to  $200$  nm, as expected. The ratio of curcumin-to-kafirin, as well as the structure of the nanoparticles (solid or hollow), significantly affected encapsulation efficiency: the lowest encapsulation efficiency (42%) was achieved with LbL solid kafirin nanoparticles with a curcumin-to-kafirin ratio of 1:5, and the highest encapsulation efficiencies (94–95%) were achieved with LbL hollow nanoparticles with curcumin-to-kafirin ratios between 1:15 and 1:30. LbL assembly of nanoparticles improved curcumin dissolution in the gastrointestinal tract, compared to native curcumin, wherein LbL hollow nanoparticles exhibited slower release kinetics compared to LbL solid kafirin nanoparticles [48].

Solid lipid nanoparticles using LbL method were fabricated using soya lecithin, sodium caseinate, pectin, and Compritol ATO 888, which is a glyceride [49]. The LbL nanoparticles were designed by surface response methodology. The first layer of the nanoparticles was formed by combining lecithin with the lipid in a mixture of acetone and ethanol, where lecithin forms a layer around the lipid molecule. The second layer surrounding core lipid nanoparticles was fabricated by nanoprecipitating the lipid/lecithin mixture in a sodium caseinate mixture. For the third layer, an aqueous pectin solution was added to the mixture. Effects of four different pH values (4, 4.5, 5, and 6), two pectin concentrations (45 or 60 mg), and the effect of heat treatment ( $80^{\circ}\text{C}$ ) were tested (Fig. 6.15), to ensure an electrostatic interaction between pectin and sodium caseinate.

Addition of the pectin layer increased the particle sizes from  $317$  to  $437$  nm and  $438$  nm in low and high pectin concentrations, respectively. A decrease in particle size was observed in both pectin concentrations,

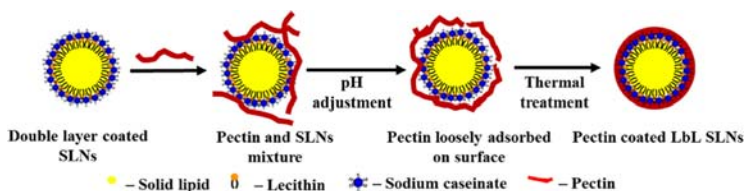


**FIGURE 6.15** Layer-by-layer assembly of solid lipid nanoparticles. Reprinted from Wang T, Hu Q, Zhou M, Xia Y, Nieh M-P, Luo Y. Development of “all natural” layer-by-layer redispersible solid lipid nanoparticles by nano spray drying technology. *Eur J Pharm Biopharm* 2016;107:273–85. Available from: <https://doi.org/10.1016/j.ejpb.2016.07.022> with permission from Elsevier.

when pH was dropped from 6.8 (initial pH) to 6, and remained stable at pH = 5 and 4.5. When pH was further decreased to 4, the size of nanoparticles with low pectin concentration only increased by the addition of heat treatment. For high concentration pectin nanoparticles, decreasing the pH to 4 increased the particle sizes, regardless of heat treatment. The zeta potentials of the nanoparticles decreased with the pH values for both pectin concentrations. Heat treatment aided the formation of more spherical nanoparticles. The optimal conditions for fabrication of ultrafine nanoparticle powders, with spherical particle shapes and good redispersibility, were determined as pH 5 with 80°C heat treatment, and at higher (60 mg) pectin concentration (since higher pectin concentration prevented lipid agglomeration). The redispersed LbL-assembled solid lipid nanoparticles also exhibited good stability.

### 6.2.3.2 Nanotube formation through layer-by-layer deposition

With the choice of the right template, tubular nanoparticles can be fabricated using LbL deposition [50]. Nanotubes from two biopolymers, BSA and PDL, using a track-etched polycarbonate membrane as the templates were fabricated. The optimum interaction pH of the polymers was determined with zeta potential measurements. At pH = 7.4 the highest absolute opposite charges were observed between positively charged PDL and negatively charged BSA, which is necessary for maximum attraction. To fabricate the nanotubes, positively charged PDL solution was run through the negatively charged polycarbonate membrane to form the first outer layer by electrostatic attraction of PDL to polycarbonate. The second layer of nanotubes was formed by running negatively charged BSA solution after PDL. Two and three bilayers of BSA/PDL were formed by repeating the same steps. The polycarbonate template was then dissolved in *N,N*-dimethylformamide solution. Three bilayered nanotubes were the strongest, with defined nanotube structures after drying. The average wall thickness was 61 nm (Fig. 6.16A). Curcumin was loaded to the nanotubes in two ways: by mixing the already prepared nanotubes with curcumin solution, or by mixing curcumin into the ethanolic BSA solution prior to nanotube formation. For the first loading method, curcumin encapsulation was higher when the interior wall of the nanotubes were hydrophobic with BSA [50]. The highest encapsulation efficiency (45%) and the highest loading capacity of (0.27 g/g) nanotubes were obtained with three bilayered nanotubes. The second encapsulation technique only allowed formation of two bilayers, after which the hydrophobic environment of the interior blocked the PDL solution from passing for the third time through the template. These nanotubes had bigger cavities than the nanotubes fabricated with the first method, and were more deformed than the three bilayered nanotubes (Fig. 6.16B).



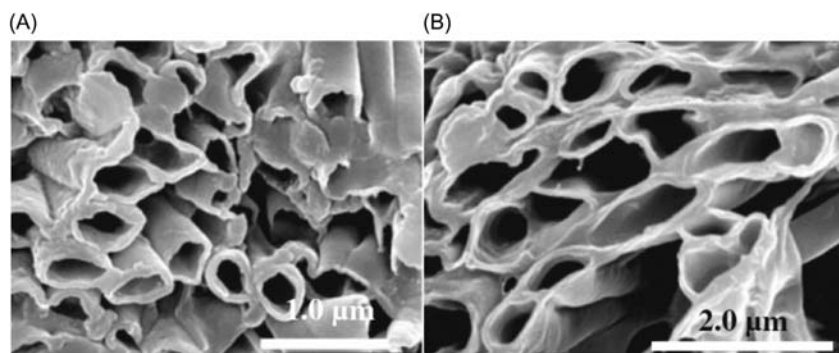


**FIGURE 6.16** BSA/PDL nanotubes with three bilayers (A) and BSA-curcumin/PDL nanotubes with two bilayers (B). Reprinted from Sadeghi R, Kalbasi A, Emam-jomeh Z, Razavi SH, Kokini J, Moosavi-Movahedi AA. Biocompatible nanotubes as potential carrier for curcumin as a model bioactive compound. *J Nanopart Res* 2013;15(11):1931. Available from: <https://doi.org/10.1007/s11051-013-1931-8> with permission from Springer Nature.

Curcumin entrapment was also tested in LbL bionanotubes formed with either chitosan (CHI) and  $\alpha$ -lactalbumin (LAC), or BSA and  $\kappa$ -carrageenan (CAR), using the same polycarbonate template technique [51]. During the tests with CHI and LAC, the highest absolute zeta potential differences with opposite charges occurred at pH = 7; the same, regarding BSA and CAR, occurred at pH = 4. The mechanisms of interactions were analyzed with ITC, and both were found to be exothermic and driven by coulombic interactions with an enthalpy of  $-0.494$  kJ/g (LAC and CHI) and  $-6.14$  kJ/g (BSA and CAR). For both pairs of polyelectrolytes, three types of templates with 400, 600, and 800 nm pore sizes were tested. While 4 bilayers could be deposited with a 400 nm template, 600 and 800 nm templates allowed deposition of 5 bilayers. The average wall thickness of LAC and CHI nanotubes were 81, 97, and 118 nm fabricated with 400, 600, and 800 nm templates, respectively (Fig. 6.17). BSA and CAR interaction resulted in thinner walled nanotubes of 60, 67, and 76 nm with 400, 600, and 800 nm templates, respectively (Fig. 6.17).

Atomic force microscopy imaging and force mapping revealed that BSA/CAR nanotubes were more robust than CHI/LAC nanotubes [51]. The higher strength of BSA/CAR nanotubes was due to their stronger interaction, evident from their larger absolute zeta potential difference and higher enthalpy differences. Stability tests indicated that CHI/LAC nanotubes were more stable than BSA/CAR nanotubes in PBS solution, due to a more suitable pH for the interaction between polyelectrolytes. Curcumin loading was accomplished by mixing the dried nanotubes in curcumin buffer solutions. BSA/CAR nanotubes exhibited higher encapsulation efficiency (46.7%) and loading capacity (0.175 mg/mg nanotube) than CHI/LAC nanotubes (36.9% encapsulation efficiency and 0/14 mg/mg nanotube loading capacity).

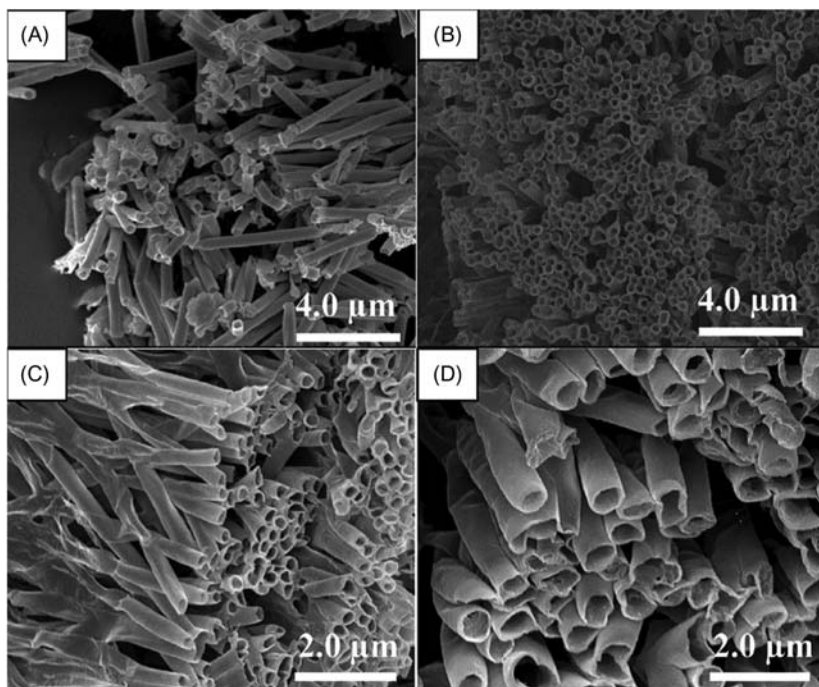


**FIGURE 6.17** CHI/LAC (A, B) and BSA/CAR (C, D) nanotubes fabricated with 400 nm (A, C) and 800 nm (B, D) pore-sized templates. Reprinted from Maldonado L, Chough S, Bonilla J, Kim KH, Kokini J. Mechanism of fabrication and nano-mechanical properties of  $\alpha$ -lactalbumin/chitosan and BSA/ $\kappa$ -carrageenan nanotubes through layer-by-layer assembly for curcumin encapsulation and determination of in vitro cytotoxicity. *Food Hydrocoll* 2019;93:293–307. Available from: <https://doi.org/10.1016/j.foodhyd.2019.02.040> with permission from Elsevier.

The release of curcumin from nanotubes was tested with PBS solution. BSA/CAR nanotubes showed a faster release profile than CHI/LAC nanotubes, which is similarly due to the pH of the buffer solution (7.5), which favors the interaction between CHI and LAC more than BSA and CAR. Therefore BSA/CAR nanotubes experienced a “burst” release of curcumin, with almost 100% release within the first 24 h, while a near complete release occurred after 48 h in the case of CHI/LAC nanotubes. The cytotoxicity of free and loaded nanotubes was tested with HeLa cells. While free BSA/CAR and CHI/LAC nanotubes did not exhibit any toxicity on HeLa cells, curcumin-loaded nanotubes showed concentration-dependent toxicity on the cells, regardless of the polyelectrolyte pairs. The highest cell viability values reached 65% with 60  $\mu\text{g/mL}$  curcumin loading.

Polycarbonate membrane templates were also used for the fabrication of LbL human serum albumin (HSA) and polyethylenimine (PEI) nanotubes [52]. First, positively charged PEI solution was passed through the negatively



charged polycarbonate template, followed by negatively charged HSA solution. The total number of bilayers deposited on the polycarbonate template was 5.5, indicating an additional layer of PEI deposition on the 5 bilayers of PEI/HSA. The average outer and inner diameters of the LbL nanotubes were 455 and 275 nm, respectively, with an average wall thickness of 151 nm. To study the adsorption of LbL nanotubes onto DNA (PolyA<sub>25</sub>), nanotubes were mixed with DNA solution. Due to the negative charges of DNA chains, there occurred an electrostatic interaction between the DNA chains and the positively charged PEI inner and outer walls of nanotubes. As the pH was increased from 4.7 to 11, the adsorption percentage decreased from 94.8% to 87.0%, due to the decreasing positive charges of PEI with an increase in pH. This reduction resulted in less interaction between positively charged PEI and negatively charged DNA. The adsorption kinetics of DNA to LbL nanotubes were found to fit pseudo-second order kinetics. The release of DNA from the LbL nanotubes were analyzed by dissolving the complexes in phosphate buffer solutions at two pH values, 7.4 and 5.7. In the absence of NaCl, no release was observed, and increasing NaCl concentration in the buffer solution increased the release of DNA from the nanotubes. At pH = 5.7, more DNA was released from the nanotubes compared to pH = 7.4.

### 6.3 Conclusions

In this chapter is summarized recent studies which utilized various nanoparticulation techniques to fabricate edible and safe biobased nanodelivery systems. Also, through the summary of fundamental studies, the chapter has detailed the importance of understanding the mechanism of polymer interactions and thermodynamics on the optimization of nanodelivery systems. The effects of many parameters (i.e., pH, zeta potentials, temperature, ionic strength through salt addition, order of addition, etc.) on the size, distribution, encapsulation efficiency, and stability of the nanodelivery systems have also been covered. Collectively, these studies show that: it is crucial to select polyelectrolyte pairs at optimum zeta potential difference for maximum attraction; choosing the optimum solvents for polyelectrolytes affects the particle size, morphology, and stability of the particles; and the ionic strength of environment and temperature is effective on the type of the interaction between the polyelectrolytes, leading to a more stable system. The molecular weight of the polyelectrolytes, the mass and charge ratios, and the order of polyelectrolyte addition were also proven to affect significantly the reaction mechanism and bioactive encapsulation efficiency. All these parameters should be carefully explored and studied in detail, to fabricate and design nanodelivery systems efficiently, and with better release profiles.

## References

- [1] George A, Shah PA, Shrivastav PS. Natural biodegradable polymers based nano-formulations for drug delivery: a review. *Int J Pharm* 2019;561:244–64. Available from: <https://doi.org/10.1016/j.ijpharm.2019.03.011>.
- [2] Bilati U, Allémann E, Doelker E. Development of a nanoprecipitation method intended for the entrapment of hydrophilic drugs into nanoparticles. *Eur J Pharm Sci* 2005;24(1):67–75. Available from: <https://doi.org/10.1016/j.ejps.2004.09.011>.
- [3] Sadeghi R, Chuacharoen T, Sabliov C, Moraru C, Karimi M, Kokini J. Chapter 2: advances in nanotechnology of food materials for food and non-food applications. *Handbook of food engineering*. 3rd ed. CRC Press; 2018. p. 153–224.
- [4] Sadeghi R, Daniella Z, Uzun S, Kokini J. Effects of starch composition and type of non-solvent on the formation of starch nanoparticles and improvement of curcumin stability in aqueous media. *J Cereal Sci* 2017;76:122–30. Available from: <https://doi.org/10.1016/j.jcs.2017.05.020>.
- [5] Sadeghi R, Moosavi-Movahedi AA, Emam-jomeh Z, Kalbasi A, Razavi SH, Karimi M, et al. The effect of different desolvating agents on BSA nanoparticle properties and encapsulation of curcumin. *J Nanopart Res* 2014;16(9):2565. Available from: <https://doi.org/10.1007/s11051-014-2565-1>.
- [6] Kunnumakkara AB, Guha S, Krishnan S, Diagaradjane P, Gelovani J, Aggarwal BB. Curcumin potentiates antitumor activity of gemcitabine in an orthotopic model of pancreatic cancer through suppression of proliferation, angiogenesis, and inhibition of nuclear factor-kappaB-regulated gene products. *Cancer Res* 2007;67(8):3853–61. Available from: <https://doi.org/10.1158/0008-5472.CAN-06-4257>.
- [7] Xiao J, Nian S, Huang Q. Assembly of kafirin/carboxymethyl chitosan nanoparticles to enhance the cellular uptake of curcumin. *Food Hydrocoll* 2015;51:166–75. Available from: <https://doi.org/10.1016/j.foodhyd.2015.05.012>.
- [8] Xiao J, Li C, Huang Q. Kafirin nanoparticle-stabilized pickering emulsions as oral delivery vehicles: physicochemical stability and in vitro digestion profile. *J Agric Food Chem* 2015;63(47):10263–70. Available from: <https://doi.org/10.1021/acs.jafc.5b04385>.
- [9] Teng Z, Luo Y, Wang Q. Nanoparticles synthesized from soy protein: preparation, characterization, and application for nutraceutical encapsulation. *J Agric Food Chem* 2012;60(10):2712–20. Available from: <https://doi.org/10.1021/jf205238x>.
- [10] Etorki AM, Gao M, Sadeghi R, Maldonado-Mejia LF, Kokini JL. Effects of desolvating agent types, ratios, and temperature on size and nanostructure of nanoparticles from  $\alpha$ -lactalbumin and ovalbumin. *J Food Sci* 2016;81(10):E2511–20. Available from: <https://doi.org/10.1111/1750-3841.13447>.
- [11] Turasan H, Barber EA, Malm M, Kokini JL. Mechanical and spectroscopic characterization of crosslinked zein films cast from solutions of acetic acid leading to a new mechanism for the crosslinking of oleic acid plasticized zein films. *Food Res Int* 2018;108:357–67. Available from: <https://doi.org/10.1016/j.foodres.2018.03.063>.
- [12] Gandhi S, Roy I. Doxorubicin-loaded casein nanoparticles for drug delivery: preparation, characterization and in vitro evaluation. *Int J Biol Macromol* 2019;121:6–12. Available from: <https://doi.org/10.1016/j.ijbiomac.2018.10.005>.
- [13] Gülsüren İ, Fang Y, Corredig M. Whey protein nanoparticles prepared with desolvation with ethanol: characterization, thermal stability and interfacial behavior. *Food Hydrocoll* 2012;29(2):258–64. Available from: <https://doi.org/10.1016/j.foodhyd.2012.03.015>.

- [14] Gülseren İ, Fang Y, Corredig M. Zinc incorporation capacity of whey protein nanoparticles prepared with desolvation with ethanol. *Food Chem* 2012;135(2):770–4. Available from: <https://doi.org/10.1016/j.foodchem.2012.04.146>.
- [15] Barreras-Urbina CG, Ramírez-Wong B, López-Ahumada GA, Burrueal-Ibarra SE, Martínez-Cruz O, Tapia-Hernández JA, et al. Nano- and micro-particles by nanoprecipitation: possible application in the food and agricultural industries. *Int J Food Prop* 2016;19(9):1912–23. Available from: <https://doi.org/10.1080/10942912.2015.1089279>.
- [16] Li K-K, Zhang X, Huang Q, Yin S-W, Yang X-Q, Wen Q-B, et al. Continuous preparation of zein colloidal particles by Flash NanoPrecipitation (FNP). *J Food Eng* 2014;127:103–10. Available from: <https://doi.org/10.1016/j.jfoodeng.2013.12.001>.
- [17] Barreras-Urbina CG, Rodríguez-Félix F, López-Ahumada GA, Burrueal-Ibarra SE, Tapia-Hernández JA, Castro-Enríquez DD, et al. Microparticles from wheat-gluten proteins soluble in ethanol by nanoprecipitation: preparation, characterization, and their study as a prolonged-release fertilizer [Research article]; 2018. <<https://doi.org/10.1155/2018/1042798>>.
- [18] Turasan H, Bonilla J, Bozkurt F, Maldonado L, Li X, Yilmaz T, et al. Comparison of the fabrication methods, formation dynamics, structure and delivery performance of solid nanoparticles and hollow layer-by-layer (LbL) edible/biodegradable nanodelivery systems. *J Food Process Eng* 2019. Available from: <https://doi.org/10.1111/jfpe.13413>.
- [19] Khan SA, Schneider M. Improvement of nanoprecipitation technique for preparation of gelatin nanoparticles and potential macromolecular drug loading. *Macromol Biosci* 2013;13(4):455–63. Available from: <https://doi.org/10.1002/mabi.201200382>.
- [20] Qin Y, Liu C, Jiang S, Xiong L, Sun Q. Characterization of starch nanoparticles prepared by nanoprecipitation: influence of amylose content and starch type. *Ind Crop Products* 2016;87:182–90. Available from: <https://doi.org/10.1016/j.indcrop.2016.04.038>.
- [21] Qiu C, Qin Y, Zhang S, Xiong L, Sun Q. A comparative study of size-controlled worm-like amylopectin nanoparticles and spherical amylose nanoparticles: their characteristics and the adsorption properties of polyphenols. *Food Chem* 2016;213:579–87. Available from: <https://doi.org/10.1016/j.foodchem.2016.07.023>.
- [22] Chang Y, Yan X, Wang Q, Ren L, Tong J, Zhou J. Influence of ultrasonic treatment on formation of amylose nanoparticles prepared by nanoprecipitation. *Carbohydr Polym* 2017;157:1413–18. Available from: <https://doi.org/10.1016/j.carbpol.2016.11.019>.
- [23] Sotelo-Boyás ME, Correa-Pacheco ZN, Bautista-Baños S, Corona-Rangel ML. Physicochemical characterization of chitosan nanoparticles and nanocapsules incorporated with lime essential oil and their antibacterial activity against food-borne pathogens. *LWT* 2017;77:15–20. Available from: <https://doi.org/10.1016/j.lwt.2016.11.022>.
- [24] Luque-Alcaraz AG, Lizardi-Mendoza J, Goycoolea FM, Higuera-Ciupara I, Argüelles-Monal W. Preparation of chitosan nanoparticles by nanoprecipitation and their ability as a drug nanocarrier. *RSC Adv* 2016;6(64):59250–6. Available from: <https://doi.org/10.1039/C6RA06563E>.
- [25] Chin SF, Jimmy FB, Pang SC. Size controlled fabrication of cellulose nanoparticles for drug delivery applications. *J Drug Deliv Sci Technol* 2018;43:262–6. Available from: <https://doi.org/10.1016/j.jddst.2017.10.021>.
- [26] Gupta AP, Verma DK. Preparation and characterization of carboxymethyl guar gum nanoparticles. *Int J Biol Macromol* 2014;68:247–50. Available from: <https://doi.org/10.1016/j.ijbiomac.2014.05.012>.
- [27] Soumya RS, Sherin S, Raghu KG, Abraham A. Allicin functionalized locust bean gum nanoparticles for improved therapeutic efficacy: an in silico, in vitro and in vivo approach.

- Int J Biol Macromol 2018;109:740–7. Available from: <https://doi.org/10.1016/j.ijbiomac.2017.11.065>.
- [28] Qiu C, Qin Y, Jiang S, Liu C, Xiong L, Sun Q. Preparation of active polysaccharide-loaded maltodextrin nanoparticles and their stability as a function of ionic strength and pH. LWT - Food Sci Technol 2017;76:164–71. Available from: <https://doi.org/10.1016/j.lwt.2016.10.053>.
- [29] Constantin M, Bucătariu S, Stoica I, Fundueanu G. Smart nanoparticles based on pullulan-g-poly(*N*-isopropylacrylamide) for controlled delivery of indomethacin. Int J Biol Macromol 2017;94:698–708. Available from: <https://doi.org/10.1016/j.ijbiomac.2016.10.064>.
- [30] Maldonado L, Sadeghi R, Kokini J. Nanoparticulation of bovine serum albumin and poly-D-lysine through complex coacervation and encapsulation of curcumin. Colloids Surf B: Biointerfaces 2017;159:759–69. Available from: <https://doi.org/10.1016/j.colsurfb.2017.08.047>.
- [31] Piacentini E. Coacervation. In Drioli E, Giorno L, editors. Encyclopedia of membranes; 2016. p. 422–424. <[https://doi.org/10.1007/978-3-662-44324-8\\_2019](https://doi.org/10.1007/978-3-662-44324-8_2019)>.
- [32] Timilsena YP, Akanbi TO, Khalid N, Adhikari B, Barrow CJ. Complex coacervation: principles, mechanisms and applications in microencapsulation. Int J Biol Macromol 2019;121:1276–86. Available from: <https://doi.org/10.1016/j.ijbiomac.2018.10.144>.
- [33] Li Y, Huang Q. Influence of protein self-association on complex coacervation with polysaccharide: a Monte Carlo Study. J Phys Chem B 2013;117(9):2615–24. Available from: <https://doi.org/10.1021/jp309135m>.
- [34] Ru Q, Wang Y, Lee J, Ding Y, Huang Q. Turbidity and rheological properties of bovine serum albumin/pectin coacervates: effect of salt concentration and initial protein/polysaccharide ratio. Carbohydr Polym 2012;88(3):838–46. Available from: <https://doi.org/10.1016/j.carbpol.2012.01.019>.
- [35] Shaddel R, Hesari J, Azadmard-Damirchi S, Hamishehkar H, Fathi-Achachlouei B, Huang Q. Double emulsion followed by complex coacervation as a promising method for protection of black raspberry anthocyanins. Food Hydrocoll 2018;77:803–16. Available from: <https://doi.org/10.1016/j.foodhyd.2017.11.024>.
- [36] Shaddel R, Hesari J, Azadmard-Damirchi S, Hamishehkar H, Fathi-Achachlouei B, Huang Q. Use of gelatin and gum Arabic for encapsulation of black raspberry anthocyanins by complex coacervation. Int J Biol Macromol 2018;107:1800–10. Available from: <https://doi.org/10.1016/j.ijbiomac.2017.10.044>.
- [37] Priftis D, Tirrell M. Phase behaviour and complex coacervation of aqueous polypeptide solutions. Soft Matter 2012;8(36):9396–405. Available from: <https://doi.org/10.1039/c2sm25604e>.
- [38] Obermeyer AC, Mills CE, Dong X-H, Flores RJ, Olsen BD. Complex coacervation of supercharged proteins with polyelectrolytes. Soft Matter 2016;12(15):3570–81. Available from: <https://doi.org/10.1039/c6sm00002a>.
- [39] Yilmaz T, Maldonado L, Turasan H, Kokini J. Thermodynamic mechanism of particulation of sodium alginate and chitosan polyelectrolyte complexes as a function of charge ratio and order of addition. J Food Eng 2019;254:42–50. Available from: <https://doi.org/10.1016/j.jfoodeng.2019.03.002>.
- [40] Tavares L, Zapata Noreña CP. Encapsulation of garlic extract using complex coacervation with whey protein isolate and chitosan as wall materials followed by spray drying. Food Hydrocoll 2019;89:360–9. Available from: <https://doi.org/10.1016/j.foodhyd.2018.10.052>.

- [41] Rudke AR, Heleno SA, Fernandes IP, Prieto MA, Gonçalves OH, Rodrigues AE, et al. Microencapsulation of ergosterol and *Agaricus bisporus* L. extracts by complex coacervation using whey protein and chitosan: optimization study using response surface methodology. LWT 2019;103:228–37. Available from: <https://doi.org/10.1016/j.lwt.2019.01.018>.
- [42] Rodrigues da Cruz MC, Andreotti Dagostin JL, Perussello CA, Masson ML. Assessment of physicochemical characteristics, thermal stability and release profile of ascorbic acid microcapsules obtained by complex coacervation. Food Hydrocoll 2019;87:71–82. Available from: <https://doi.org/10.1016/j.foodhyd.2018.07.043>.
- [43] Muhoza B, Xia S, Cai J, Zhang X, Duhoranimana E, Su J. Gelatin and pectin complex coacervates as carriers for cinnamaldehyde: effect of pectin esterification degree on coacervate formation, and enhanced thermal stability. Food Hydrocoll 2019;87:712–22. Available from: <https://doi.org/10.1016/j.foodhyd.2018.08.051>.
- [44] Wang J, Dumas E, Gharsallaoui A. Low methoxyl pectin/sodium caseinate complexing behavior studied by isothermal titration calorimetry. Food Hydrocoll 2019;88:163–9. Available from: <https://doi.org/10.1016/j.foodhyd.2018.10.006>.
- [45] Pillai PKS, Stone AK, Guo Q, Wang Q, Nickerson MT. Effect of alkaline de-esterified pectin on the complex coacervation with pea protein isolate under different mixing conditions. Food Chem 2019;284:227–35. Available from: <https://doi.org/10.1016/j.foodchem.2019.01.122>.
- [46] Kavousi HR, Fathi M, Goli SAH. Novel cress seed mucilage and sodium caseinate micro-particles for encapsulation of curcumin: an approach for controlled release. Food Bioprod Process 2018;110:126–35. Available from: <https://doi.org/10.1016/j.fbp.2018.05.004>.
- [47] Bastarrachea LJ, Denis-Rohr A, Goddard JM. Antimicrobial food equipment coatings: applications and challenges. Annu Rev Food Sci Technol 2015;6(1):97–118. Available from: <https://doi.org/10.1146/annurev-food-022814-015453>.
- [48] Li X, Maldonado L, Malmr M, Rouf TB, Hua Y, Kokini J. Development of hollow kafirin-based nanoparticles fabricated through layer-by-layer assembly as delivery vehicles for curcumin. Food Hydrocoll 2019;96:93–101. Available from: <https://doi.org/10.1016/j.foodhyd.2019.04.042>.
- [49] Wang T, Hu Q, Zhou M, Xia Y, Nieh M-P, Luo Y. Development of “all natural” layer-by-layer redispersible solid lipid nanoparticles by nano spray drying technology. Eur J Pharm Biopharm 2016;107:273–85. Available from: <https://doi.org/10.1016/j.ejpb.2016.07.022>.
- [50] Sadeghi R, Kalbasi A, Emam-jomeh Z, Razavi SH, Kokini J, Moosavi-Movahedi AA. Biocompatible nanotubes as potential carrier for curcumin as a model bioactive compound. J Nanopart Res 2013;15(11):1931. Available from: <https://doi.org/10.1007/s11051-013-1931-8>.
- [51] Maldonado L, Chough S, Bonilla J, Kim KH, Kokini J. Mechanism of fabrication and nano-mechanical properties of  $\alpha$ -lactalbumin/chitosan and BSA/ $\kappa$ -carrageenan nanotubes through layer-by-layer assembly for curcumin encapsulation and determination of in vitro cytotoxicity. Food Hydrocoll 2019;93:293–307. Available from: <https://doi.org/10.1016/j.foodhyd.2019.02.040>.
- [52] Jiao P, Guo Y, Niu A, Kang X. Layer-by-layer assembled protein nanotubes with high DNA affinity. RSC Adv 2015;5(47):37130–7. Available from: <https://doi.org/10.1039/C5RA04725K>.

## Chapter 7

# Biopolymer-based nanomaterials for food, nutrition, and healthcare sectors: an overview on their properties, functions, and applications

Mohammad Reza Kasaai

*Department of Food Science and Technology, Sari Agricultural Sciences and Natural Resources University, Sari, Iran*

### 7.1 Introduction

A variety of wastes are generated in both agriculture and marine fields [1–5]. Their accumulation on this planet results in several environmental and health difficulties [6]. Converting different wastes into value-added products, by respecting environmental demands, is an effective pathway to reduce environmental difficulties, and improve economic sustainability of wastes processing. This recycling approach is beneficial not only to the environments, but also to industries, from economical point of view [6,7]. Biopolymers make up a fraction of agriculture, forestry, and marine wastes. Biopolymers are alternatives to synthetic polymers made from petroleum, however, their use has faced several major problems, including low degradation temperatures, poor mechanical properties, and high water vapor and gas permeabilities [8,9]. Surface modification of biopolymers and introduction of ionic groups, functional compounds, and fillers into biopolymers could solve these problems [10,11]. The properties of biopolymers can be improved by adding nanosized filler compounds to form composites. The latter materials (biocomposites) have been fabricated using nanotechnology, in order to improve stability of conventional polymeric matrices [12,13]. Various

biopolymers and nanosized fillers have been used to form bionanocomposite materials [14].

This chapter provides a review compiled from available literature on: (1) fabrication of four biopolymer-based nanomaterials consisting of three polysaccharides (cellulose, starch, and chitosan), and a protein (zein) using surface modification or introducing additives, ionic groups, and functional compounds into the polymer matrices, and (2) employing nanoscience and nanotechnology to overcome limitations and to achieve desirable products.

## 7.2 Sources, structure, and characteristics

Biopolymers (cellulose, starch, chitosan, zein) are naturally occurring materials that are available in large quantities [14–20]. Renewable biopolymers can be isolated from agricultural and forestry biomass.

Cellulose is the most available renewable polymer on the planet that we live on. Its annual production is estimated to be over  $7.5 \times 10^{10}$  tons [17]. Cellulose is present in various plants as a principal component of cell walls, microorganisms, and land and marine animals. It is widely distributed in higher plants and annual crops. Wood (consisting of up to 50% cellulose) is the most important raw material source for cellulose [17,21,22]. It is comprised of beta-(1, 4)-D-glucopyranosyl units and forms a linear chain through many inter- and intramolecular hydrogen bonding [23–25].

Starch occurs in many higher plants, especially cereals (grains), legumes, and most tubers, as discrete particles called granules [26–29]. It is a principal food reserve polysaccharide and serves as the predominant storage carbohydrate in plants—a mixture of linear and branched  $\alpha$ -D-glucans (amylose and amylopectin). Starch granules consist of amylose and amylopectin and usually contain small amounts of proteins and lipids [30]. The ratio of amylose to amylopectin, size, particle size distribution, shape, appearance, and properties of starches vary considerably with sources and species. These variations could make starches viable in several field applications [18,31–33].

Next to cellulose, chitin is the second most abundant polysaccharide found in nature. Chitin occurs naturally, as a support system in plants and animals, hard skeleton of shellfish and marine invertebrate (i.e., crab, shrimp, lobster, prawn, krill, clams, oysters, and squid) [34–37]. It is generally isolated from crustacean shells, and is considered a cellulose derivative. The chemical structure of chitin is similar to cellulose. The difference between the chemical structures of cellulose and chitin, is that the 2-hydroxy groups of cellulose have been replaced with *N*-acetyl groups, resulting in beta-(1–4)-2-acetarnido-2-deoxy-D-glucopynnosic structural units (GlcNAc) [37]. Chitin is not soluble in most common organic and inorganic solvents. Deacetylation of chitin results in chitosan, which consists of  $\beta$  (1  $\rightarrow$  4) linked

**TABLE 7.1** Abbreviations appeared in this chapter.

Abbreviation	Expression, term
BBB	Blood–brain barrier
CLC	Cross-linked cellulose
CNC	Cellulose nanocrystal
CNCs	Cellulose nanocrystals
DLS	Dynamic light scattering
DNA	Deoxy nucleic acid
FDA	Food and Drug Administration
GIT	Gastrointestinal tract
MRI	Magnetic resonance imaging
NFC	Nanofibrillated cellulose
NP	Nanoparticle
NPs	Nanoparticles
O/W	Oil/water
PEG	Polyethylene glycol
SPIO	Superparamagnetic iron oxide
UV	Ultraviolet
ZCCPs	Zein/chitosan colloid particles

D-glucosamine residues [1,7,38]. This results in an improvement in its solubility and promotes processing, thereby widening its practical applications. Chitosans are used for both partially and completely deacetylated chitosans [1,39]. Abbreviations and their corresponding expressions, resources, and characteristics of biopolymers in general, and the characteristics of each biopolymer (cellulose, starch, chitosan, and zein) are provided in Tables 7.1–7.3, respectively.

Zein is the major storage protein in corn [40,41]. It consists of four components (alpha, beta, gamma, and delta) with varying peptide chains, molecular sizes, and solubilities. The most abundant protein in commercial zeins is the alpha, which possesses complex groups of prolamines with molecular weights of 19 and 22 kDa [42], and comprises 70%–85% of the whole zein [41,43]. Zein with a significant amount of nonpolar amino acids (about 50% of total amino acids residues in zein), is a hydrophobic protein [43,44]. Zein is generated as a coproduct, when corn grains are processed for food, feed, agriculture products, and fuels [45].



**TABLE 7.2** Resources, characteristics, properties, and functions of biopolymers (cellulose, starch, chitosan, zein).

Item	Conventional and large sized biopolymers	Nanomaterials
Resources	Agriculture, forestry and marine (naturally occurring materials and available in large quantities)	The same as the conventional biopolymer counterparts
Characteristics	Hydrophilic characters (generally possesses hydrophilic groups) for cellulose, starch, and chitosan, both hydrophilic/hydrophobic characters for zein	At least with one dimension in nanometer- scale (1–100 nm)
Properties	Biodegradable and biocompatible, poor water vapor and gas barrier and mechanical properties, film-forming	A large surface area per volume; and at least a property that deviates from the value of the equivalent bulk materials having the same composition; superior (physical, chemical, and thermal) properties compared to traditional counterparts
Functions	Biopolymers having functional groups are able to interact with functional compounds	Nano-carriers; nanocomposites
Applications	Food, nutrition, pharmaceuticals, medicals, cosmetics, health care	Food, nutrition, pharmaceuticals, medicals, cosmetics, health care

### 7.2.1 Properties and functions of biopolymers

Biopolymers (cellulose, starch, chitosan, zein) are biodegradable and bio-compatible [18–21,38,46–48]. The biopolymers have poor water vapor, oxygen and other gas barriers, mechanical, and thermal properties [14,16,49]. The use of materials with barrier properties results in a shelf life extension, by protecting food and drugs products from oxidative and microbial deteriorations [50]. Properties of biopolymers, and properties of each biopolymer (cellulose, starch, chitosan and zein) are given in [Tables 7.2 and 7.3](#), respectively.

Cellulose and its derivatives exhibit film- and fiber-forming properties (Kaplan, 1998a,b) [21,48]. The linearity of cellulose makes it easy for the molecules to produce parallel arrays and cause a high degree of crystallinity

**TABLE 7.3** Characteristics, properties, and applications of biopolymers.

Biopolymers	Characteristics and properties	Functions and applications of biopolymer-based nanomaterials
Cellulose	High hydrophilic characters, film forming, fiber forming; high degree of crystallinity, highly absorbent, and binding to water properties	Nanofibers, nanopapers, nanocomposites
Starch	High hydrophilic characters; film forming	Nanocomposites, starch nanocrystals can be used to improve mechanical and barrier properties
Chitosan	Cationic nature, film forming, fiber forming; antibacterial and antifungal properties	As antioxidant and antimicrobial compounds in food, nutrition, and medicine sectors; as a core of encapsulation system for nutrient and drug releases
Zein	Amphiphilic (hydrophobic/hydrophilic) character; film forming, fiber forming; antioxidant properties and oil resistance	As a shell of encapsulation system in nutrient and drug releases; nanocomposite in food coating and packaging

[23,25]. Cross-linked cellulose (CLC), a highly absorbent with disintegration and binding properties, was used as a tablet excipient in pharmaceuticals.

Starch exhibits film-forming properties, however, the film is tough and rigid [51]. Mechanical and barrier properties of the starch films can be reinforced and improved by adding other polymers, functional compounds, and organic or inorganic fillers to the starch matrix [51]. Mechanical, barrier, and physico-chemical properties of the starch films exhibited a great variability, depending on the compounds added to the matrix and the processing method. The modified materials were employed in active packaging for foods and drugs [52].

Chitosan is the only cationic polysaccharide, and its cationic nature in acidic medium is especially unique among polysaccharides. Chitosan is very sensitive to the presence of anionic substances in its solutions [31,39,53]. Chitosan with film-forming, antibacterial and antifungal properties, and having the ability of removing of harmful heavy metal ions from polluted water is a good and qualified candidate for food, nutrition and biomedical applications. However, its poor water vapor and gas barrier, and mechanical properties limit its uses [39,49,53,54].

Zein, having an amphiphilic (hydrophobic/hydrophilic) character, exhibits film- and fiber-forming and antioxidant properties, and oil resistance. Fiber-

like structures for the zein–starch system were also observed [52]. The functions of zein nanomaterials are multiple: food or nutrient components, bioactive compounds, cores of nanoencapsulated systems, shells of encapsulated bioactive components, carriers of delivery systems, or fractions of assembly systems [55]. Zein as a sole material cannot be used in food packing for two major reasons: (1) it is brittle, and (2) has no sufficient water barrier properties. A solution for these problems is the use of additives (plasticizers and hydrophobic materials), to improve flexibility and moisture barrier properties [43,56,57]. A possibility to increase barrier properties of zein polymers is treatment with stable silicates (montmorillonite, hectorite, and saponite) [43,57].

### 7.2.2 Properties and functions of nanomaterials

Materials with the following characteristics create novel properties and phenomena: “one dimension in nanometer-length scale (1–100 nm), a large surface area, a large surface area per volume, and at least one property that deviates from the value of the equivalent bulk materials having the same composition” create novel properties and phenomena [13,58]. The greater the surface area, the greater the surface area of nanoparticles (NPs) per mass unit; greater surface area-to-volume ratio for nanomaterials yields an enhancement in their biological activities, in comparison with bulk and larger sized particles. NPs can be used as bioactive compounds in functional foods [59,60]. At the nanometer level, some material properties are affected by the laws of atomic physics, rather than behaving as traditional bulk materials do. In fact, their extremely small features size is of the same scale as the critical size for some physical phenomena, such as light [24]. Properties of synthetic polymers and biopolymers are closely related to their molecular weights and sizes [61–63]. Generally, the amount of raw materials with nanosized dimensions, in comparison with larger counterparts, in a desired application can be reduced, whereas the properties and biological activities of nanomaterials were improved [64]. The number of particles available per square unit of area in a nanosystem is higher than that of a micron-sized system [60,65]. Polymer nanocomposites exhibit superior physical, chemical, and thermal properties, compared to traditional composites [24,50].

Nanoscience and nanotechnology are growing in various fields of science, technology, and engineering, and could result in significant changes in the world in the near future. The properties of nanomaterials enhance their performances and applications. NPs (nutrients and drugs) can enter the human body, including vital organs such as the brain, much easier than larger particles [64]. Different research topics including preparations, properties, characterizations and applications of nanomaterials in vitro and in vivo are now under investigation [13,58,66].

### 7.2.3 Safety and toxicity of biopolymer-based nanomaterials

The three polysaccharides (cellulose, starch, chitosan) are environmentally friendly compounds, safe, and nontoxic—or exhibit low toxicity [15,18,67–69]. The toxicity of materials depends on their sizes, morphologies, and surfaces [55,62,70,71]. Toxicity is the major disadvantage of nanoscale materials for food, nutrition, medical, and healthcare applications [13]. NPs can migrate from packaging/containers to food, nutrient, and drug components [13]. Each new product prepared by nanotechnology must be examined for toxicity before marketing [64].

Cellulose-based nanomaterials such as cellulose nanocrystals (CNCs) have very low toxicity in several models (in vivo, in vitro) [71]. Starch is nontoxic and edible [18,28,29]. It is a favored compound for oral drug delivery systems [72,73]. Chitosan is nontoxic, or exhibits a low toxicity [74,75]. Zein has been approved for oral use by the Food and Drug Administration (FDA). Zein is recognized as safe for food applications [76]. However, the toxicity of zein nanocomposites and zein-based NPs has not been investigated yet [55,56]. The toxicity of nanostarches and nanochitosans have not yet been investigated.

## 7.3 Preparation of biopolymer-based nanomaterials

Hydrophilic nature of biopolymers leads to poor water vapor, oxygen, and other gas barriers, and poor mechanical properties. Surface modification, and introduction of ionic groups thereon, makes the surface more hydrophobic and leads to improvements in various mechanical and barrier properties [10,11,77]. The properties and efficiencies of the biopolymer films can be alternatively modified via making a blend as well as a nano-composite [a mixture of polymer and a filler (a non-sized component such as nano-clay or nano-sized silica) [10,11,77]. In coating and packaging technology, the modification results in shelf life extensions of food, nutrients, and drugs [56,70]. Biocomposite materials have been fabricated using nanotechnology, in order to improve stability of conventional polymeric matrices [13]. The composites can be constructed via electrostatic interactions of oppositely charged counterparts. CNCs are produced from a variety of renewable sources, and they can be chemically modified [78,79]. Chitosan is a suitable material to construct NPs. Because of its reactive amino groups, it is more easily chemically modified using various ligands or antibodies [67].

## 7.4 Applications of biopolymer-based nanomaterials

Natural materials have been used as food, nutrient, pharmaceuticals, and cosmetic compounds [80,81]. These materials can be used in agricultural practices, food coatings, and packaging to reduce environmental harms [7,82,83].

Reinforced fillers have been used in polymer composites for a wide variety of food, hygiene, cosmetic, and medical products [84]. The properties of natural materials, as well as biopolymers (cellulose, starch, chitosan, and zein), can be enhanced by adding nanosized fillers to form biocomposites [14,16,85,86]. Bionanocomposites consist of well-dispersed nanofillers (having a minimum of one dimension within the nanometer range) into biopolymeric matrices. The incorporation of bioactive compounds, such as vitamins, probiotics, antioxidants, or other bioactive compounds, provides a way to develop novel nutrients, drugs, and functional foods. The new materials may have physiological advantages and could diminish the probability of diseases [55,64].

### 7.4.1 Cellulose

Enormous amounts of cellulose and its derivatives are consumed annually in a wide variety of products, for example, fiber, textile, paper, and membranes (Kaplan, 1998a,b) [21,48,87]. The hydrophilic and polar natures of cellulosic fibers lead to two types of agglomerations: (1) that of nanofibrillated cellulose (NFC) during mixing with a hydrophobic compound, and (2) irreversible agglomeration of NFC during a drying process [10]. Cellulose has been applied in a variety of surface modifications such as silylation [88], acetylation [89], and carboxymethylation [90], to overcome hydrophilic properties of cellulose. The effects of various drying processes were also studied, for the efficient use of NFC with superior properties [11]. Drying affects the size and properties of nanofibers. The modified NFC can be also used to improve the transparency and tensile strength of nanopapers [10,11,91].

Surface modification and conjugation with therapeutic nanomaterials makes CNCs suitable as nanocarriers, and facilitates development of new nanocomposites for drug delivery applications [71,78,79]. It is highly desirable to develop controllable methods for chemical or physical modification of the CNC surface, preferably by using mild or green conditions [71]. Chemical treatments to modify the surface of cellulose are employed by the introduction of hydrophobic moieties. Nanocellulose has been employed as a reinforcement agent in polymer matrices. The major difficulty is to achieve a homogeneous dispersion of nanocellulose in hydrophobic polymers [92]. Low-molecular-weight polymers, or oligomers, are adsorbed on the surface of nanocellulose to achieve hydrophobicity. The surface modification of nanocellulose presents several advantages, as it can enhance the interfacial adhesion between nanocellulose and a polymer matrix, as well as the overall performance of nanocomposites [93]. Cellulose in composite systems provides excellent physical and chemical features. This, together with environmentally friendly capabilities, make them ideal materials for long-term practical applications. Nanocellulose (nanocrystals and NFC) with different properties matrices is potentially useful for a large number of industrial applications [24,84].

### 7.4.2 Starch

Starch has been used as a drug carrier in pharmacy and as a thin film coating layer in food and drug packaging technology, because of its biocompatibility, biodegradability, and nontoxicity [18,28,29]. Superparamagnetic iron oxide (SPIO) as a core, and starch as a coating layer with suitable biocompatible properties, have been used in medicine, particularly in magnetic resonance imaging (MRI), tissue engineering, and drug delivery systems [18,60]. Starch-coated Superparamagnetic iron oxide nanoparticles (SPION) exhibit biocompatibility, and can be transported in the extracellular space and internalized in nerve cells [18]. X-ray powder diffraction was used to confirm the magnetite phase of the SPION.

A fresh starch film made by a casting method is thermoplastic, whereas a stored starch film is rigid, and less elastic [51]. Comparison of mechanical properties of starch fresh films and stored films reveals that recrystallization occurs during the storage period. The rigidity effect can be inhibited, by adding organic or inorganic fillers, functional compounds, or other polymers to the starch matrix. Different physicochemical properties of the starch films depend on which compound is added to the matrix, and the processing method. Physical or chemical modification of native starch yields an increase in its possible applications [47,94]. Starch/clay nanocomposite films with superior barrier properties, in comparison with bulk counterparts are suitable coating materials for food and drug coatings and packaging applications.

Silver-coated starch exhibited antimicrobial properties. The presence of silver particles on the starch was confirmed by UV spectra. Inhibitions tests were performed for three types of bacteria on starch, coated by AgNPs. The inhibition results were 25  $\mu\text{g/mL}$  for *Staphylococcus aureus*, and *Salmonella typhi*, and 12.5  $\mu\text{g/mL}$  for *Escherichia coli*. The surface-modified nanostarch with AgNPs shows a potential application for active food coating and packaging [95]. The main interest of starch, in addition to being low cost is that the raw material is relatively pure and does not need intensive purification procedures, such as lingo-cellulosic materials [7,50]. The reinforcing of starch nanocrystals is limited, compared to CNCs, and a higher amount of the former is necessary to attain similar reinforcing effects. However, other interesting properties can be obtained from their platelet-like morphology, such as barrier properties [50]. Starch nanocrystals create a tortuous diffusion pathway for water and oxygen molecules to pass through. This suggests that nanostarch plays the same role as nanoclays do, presumably due to the hydrophilic nature of starch nanocrystals. Nanoclays have been used to improve water and gas barrier properties [50].

### 7.4.3 Chitosan and zein

Chitosan and its blends with other components (i.e., natural polymers, essential oils, and fillers) have been used for food protection [49]. Cationic amino groups of chitosan can form complexes with negatively charges of drug/deoxy nucleic acid (DNA) through strong electrostatic interactions [96]. Chitosan forms NPs through ionic gelation, and can be used in pharmaceutical preparations as a coating agent, tablet binder, gel former, in various drug delivery systems, and mucoadhesive polymers to enhance drug permeation and bioavailability [97]. It also exhibits potential as a nanocarrier. Chitosan has been incorporated into a number of NPs formulations and has been critical in improving delivery of many drugs, since it exhibits better drug bioavailability, stability, and targeted delivery (at the exact site). Cytostatic activity was also increased over a long duration.

Chitosan conjugated with different contents of folic acid was used to prepare chitosan NPs. The average particle size of NPs was between 120 and 140 nm, which is small enough to be up-taken by cancer cells via folate receptor-mediated endocytosis [67]. The zeta potential was around 20 mV and loading efficiency was about 60% [67]. A bioassay was performed on chitosan conjugated with folic acid, which was loaded with indigo carmine. The bioassay results revealed that the quantity of particles that which adhered onto cells increased with incubation time, and the higher-conjugated ratio of folic acid particles had a better adhesion effect. Based on the above-mentioned results, a novel detection system was made to enhance the accuracy of endoscopic diagnosis for colorectal cancer [67].

Zein with positive charges is suitable for delivery of negatively charged drugs, foods, and nutrients. The wide range of isoelectric points for zein is an appropriate condition for delivery of different nutrients and drugs into the body. Incorporating NPs with zein-based compounds expands their number of possible applications. Composites of zein films [40,98], and zein nanocomposites films have been used for food packaging [56]. A layer of silica deposited on the zein particles resulted in an improvement in their properties [99]. Because of the several advantages of zein, in comparison with other proteins, efforts have been made to explore the possibilities of utilizing zein NPs for food and nutrition applications [45].

Vitamin D<sub>3</sub> has been incorporated into zein coated with carboxymethyl chitosan [100–102]. The nanocomplex can protect the embedded compound against heat or light-induced degradation. NPs of carboxymethyl chitosan–zein mixed were prepared, and then vitamin D<sub>3</sub> was incorporated into the combined biopolymers [101]. A nutrient delivery system was fabricated in chitosan NPs as hydrophilic core, and zein as a hydrophobic shell. Selenite (a form of selenium, a key trace element for human health), was encapsulated into zein-chitosan mixed and formed a nano delivery system [103]. Zein-chitosan core–shell NPs with a combined hydrophilic/

hydrophobic character had a higher encapsulation efficiency and a slower release rate in the gastrointestinal tract, in comparison with chitosan NPs without any zein coatings. The hydrophobic zein shell prevented chitosan dissolution in the acidic conditions of the stomach, reduced the rate of releasing, and prolonged the release of hydrophilic selenite. Zein/chitosan colloid particles (ZCCPs) were shown to be effective pickering emulsifiers [104]. The resulting emulsions were highly resistant to coalescence over a 9-month storage period. Food-grade ZCCPs stabilized pickering emulsions have potential applications as emulsifiers to prepare edible pickering emulsions. Nanosized ( $<100$  nm) zein spheres were employed for fabrication of a series of fish oil/water (O/W) pickering emulsions (Soltani and Madadlou, 2016). The NPs of chitosan/DNA were made and then encapsulated into zein using a O/W emulsion technique [19]. The resulting system exhibited tunable loading, high encapsulation efficiencies, good protection properties within gastric conditions, and intestinal enzyme-mediated release of transfection-competent. The encapsulation of various compounds in zein, as well as their coating particles with zein, has been shown to decrease the release profile under simulated gastric conditions [19].

## 7.5 Conclusions

In this chapter, an effort was made to provide a review from some available literature information on properties, functions, efficiencies, and applications of biopolymer-based (cellulose, starch, chitosan, and zein) nanomaterials. This chapter provided an up-to-date evaluation of the existing development on the abovementioned biopolymer-based nanomaterials, and implication of nanoscience and nanotechnology. Biocompatibility, biodegradability, natural and abundant availability, and non- or low toxicity make biopolymers excellent candidates for food, nutrition, and healthcare applications (i.e., pharmaceutical and biomedical, medicine, cosmetics). The biopolymers exhibit coating and film-forming properties. In addition, cellulose, chitosan, and zein also exhibit fiber-forming properties.

The mechanical and barrier properties of biopolymers can be improved by introduction of fillers, functional compounds, or other biopolymers into the biopolymer matrix. The new products (as nanocomposites) can be used for food, drug coating, and packaging. Use of nanomaterials in food and drug coating and packaging results in a longer shelf life in comparison to bulk counterparts. Biopolymer-based nanomaterials can be constructed via electrostatic interactions of opposite charges of biopolymers and additives. NPs as foods, nutrients, and drugs are more efficient and more active than that of bulk counterparts, and thus can enter easier into the human organs much easier than larger particles.

Nanoscience and technology enables fabrication of nanomaterials with better qualities, characteristics, and functionalities, in comparison with bulk



and larger counterparts. The efficiency, rate of delivery, and controlled release of food, nutrition, and drug nanomaterials have been enhanced. Chitosan and zein with positive charges are suitable for delivery of negatively charged foods, nutrients, and drugs. Nanocellulose and nanostarch can be employed as nanofillers, also. Nanofillers show potential in certain applications to improve gas and water vapor barrier properties of other materials.

## 7.6 Future perspectives

Biopolymers with renewable and green resources that exhibit non- or low toxicity and good biocompatibility are promising materials for food, nutrition, medical, and healthcare applications. Investigation in the new area of research “biopolymer-based nanomaterials” would result in better quality of life, and prolonged period of living. However, the toxicity of biopolymer-based nanomaterials must be examined before marketing, in order to eliminate various risks of possible diseases.

## Funding

This research did not receive any specific grant from funding agencies in the public, commercial, or not-for-profit sectors.

## Conflict of interests

The author of this manuscript declares that there is no conflict of interests regarding the publication of this manuscript.

## References

- [1] Van Luyen D, Houngh DM. Chitin and derivatives. In: Salamone JC, editor. *Polymeric materials encyclopedia*, vol. 2. Boca Raton, FL: CRC Press; 1996. p. 1208–17.
- [2] Hettenhaus J. Agricultural residues. In: Nelson P, Hood E, Powell R, editors. *Plant biomass conversion*. New York: John Wiley & Sons Inc; 2011. p. 21–50. Chapter 2.
- [3] Liu DHF, Liptak BG, Bouis PA, editors. *Environmental engineers handbook*. 2nd ed. Boca Raton, FL: Lewis Publishers; 1997.
- [4] Pfaffin JR, Ziegler EN. *Encyclopedia of environmental science and engineering*. Libraries Australia: Gordon and Breach Science Publisher Press; 1998. p. 861–914.
- [5] Schiefelbein GF, Sealock LJ, Ergun S. Thermochemical conversion of biomass to fuels and feed-stocks An overview of R & D activities funded by the Department of Energy ACS Symposium Series, 130. Washington, DC: American Chemical Society; 1980. p. 13–26Chapter 2. Available from: <https://doi.org/10.1021/bk-1980-0130.ch002>.
- [6] Taherzadeh MJ, Karimi K. Pretreatment of lignocellulosic wastes to improve ethanol and biogas production: a review. *Int J Mol Sci* 2008;9(9):1621–51.
- [7] Kasaai MR. Conversion of renewable and food wastes into useful products with environmental perspectives. In: Maleque MA, editor. *Encyclopedia of renewable and sustainable*

- materials. Amsterdam: Elsevier; 2018. Available from: <https://doi.org/10.1016/B978-0-12-803581-8.11250-0>.
- [8] Hernandez-Sanchez H, Gutierrez-Lopez GF. Introduction. In: Hernandez-Sanchez H, Gutierrez-Lopez GF, editors. Food nano-science and nanotechnology. New York: Springer; 2015. Chapter 1.
  - [9] Sanchez-Garcia MD, Lagaron JM. Nano-composites for food packaging. In: Kirk-Othmer, editor. Encyclopedia of chemical technology. New York: John Wiley Inc; 2010. p. 1–11.
  - [10] Eyholzer C, Bordeanu N, Lopez-Suevos F, Rentsch D, Zimmermann T, Oksman K. Preparation and characterization of water-re-dispersible nano-fibrillated cellulose in powder form. *Cellulose* 2010;17(11):19–30.
  - [11] Peng Y, Gardner DJ, Han Y. Drying cellulose nanofibrils: in search of a suitable method. *Cellulose* 2012;19(1):91–102.
  - [12] Hussain CM, Mishra AK. New polymer nanocomposites for environmental remediation. Elsevier; 2018.
  - [13] Silvestre C, Duraccio D, Cimmino S. Food packaging based on polymer nanomaterials. *Prog Polym Sci* 2011;36:1766–82.
  - [14] Othman SH. Bio-nanocomposite materials for food packaging applications: types of biopolymer and nano-sized filler. In: 2nd international conference on agricultural and food engineering, CAFEi2014. Agriculture and Agricultural Science Procedia 2014;2:296–303.
  - [15] Nano-size polymers preparation, properties, applications. In: Fakirov S, editor. Nano-size polymers. Auckland: Springer; 2016.
  - [16] Ghanbarzadeh B, Oleyaei A, Almasi H. Nanostructured materials utilized in biopolymer-based plastics for food packaging applications. *Crit Rev Food Sci Nutr* 2015;55(12):1699–723.
  - [17] Habibi Y, Lucia LA, Rojas OJ. Cellulose nanocrystals: chemistry, selfassembling, and applications. *Chem Rev* 2010;110:3479–500.
  - [18] Kim DK, Mikhaylova M, Wang FH, Kehr J, Bjelke B, Zhang Y, et al. Starch-coated superparamagnetic nanoparticles as MR contrast agents Chemistry of Materials *Chem Mater* 2003;15:4343–51.
  - [19] Liu W, Misra M, Askeland P, Drzal LT, Mohanty AK. ‘Green’ composites from soy based plastic and pineapple leaf fiber: fabrication and properties evaluation. *Polymer* 2005;46:2710–21.
  - [20] Muratore G, Del Nobile MA, Buanocore GG, Lanza CM, Asmundo CN. The influence of using biodegradable packaging films on the quality decay kinetic of plum tomato. *J Food Eng* 2005;67:393–9.
  - [21] Gilbert RD, Kadla JF. Polysaccharides- cellulose. In: Kaplan DL, editor. Biopolymers from renewable resource. Berlin: Springer-Verlag; 1998. p. 47–95. Chapter 3.
  - [22] Klemm D, Kramer E, Sebastian Moritz S, Lindström T, Ankerfors M, Gray D, et al. Nanocelluloses: a new family of nature-based materials. *Angew Int Ed Chem* 2011;50(24):5438–66.
  - [23] Walton AG, Blackwell J. Biopolymers. New York: Academic; 1973. Chapter 11.
  - [24] Brinchi L, Cotana F, Fortunati E, Kenny JM. Production of nanocrystalline cellulose from lignocellulosic biomass: technology and applications. *Carbohydr Polym* 2013;94:154–69.
  - [25] Kondo T. In: Dumitriu S, editor. Polysaccharides, structural diversity and functional versatility. New York: Marcel Dekker; 1998. p. 131–71.
  - [26] Englyst KN, Englyst HN, Hudson GJ, Cole TJ, Cummings JH. Rapidly available glucose in foods: an in vitro measurement that reflects the glycemic response. *Am J Clin Nutr* 1999;69:448–54.

- [27] Englyst HN, Kingman SM, Hudson GJ, Cummings JH. Measurement of resistant starch in vitro and in vivo. *Br J Nutr* 1996;75:749–55.
- [28] Englyst KN, Hudson GJ, Englyst HN. Starch analysis in food. In: Meyers RA, editor. *Encyclopedia of analytical chemistry: applications, theory and instrumentation*, vol. 5. New York: John Wiley and Sons, Ltd.; 2000. p. 4246–62.
- [29] Fennema OR. *Food chemistry*. 3rd ed. New York: Marcel Dekker, Inc; 1996.
- [30] Belitz H-D, Grosch W, Schieberle P. *Food chemistry*. 4th ed. Berlin: Springer-Verlag; 2009. p. 290–6 (p. 807–861).
- [31] Sorlier P, Denuzière A, Viton C, Domard A. Relation between the degree of acetylation and the electrostatic properties of chitin and chitosan. *Bio-macromolecules* 2001;2:765–72.
- [32] Kasaai MR. A comparative study of molecular structure, solution properties and food application for three branched polysaccharides: amylopectin, glycogen, and dextran. *Curr Trends Polym Sci* 2012;16:49–63.
- [33] Kasaai MR. Studies on depolymerization, fragmentation and degradation of a food polymer, starch. In: Wythers MC, editor. *Advances in materials science research*, vol. 12. New York: Nova Publishers; 2011. p. 163–83.
- [34] Blair HS, Guthrie J, Law T, Turkington P. Chitosan and Modified chitosan membranes 1. Preparation and characterization. *J Appl Polym Sci* 1987;33(64):1–656.
- [35] Alwarappan S, Cissel K, Dixit S, Mohapatra S, Li CZ. Chitosan-modified graphene electrodes for DNA mutation analysis. *J Electro-Anal Chem. Lausanne Switz* 2012;686:69–72.
- [36] Knorr D. Use of chitinous polymers in food. *Food Technol* 1984;38(1):85–97.
- [37] McCormick CL, Bock J, Schulz DN. Water-soluble polymers. In: Mark HM, Bikales N, Overberger CG, Manners G, Kroschwitz J, editors. *Encyclopedia of polymer science and engineering*, vol. 17. New York: John Wiley & Sons; 1989. p. 752–3.
- [38] Hudson SM, Smith C. Polysaccharides: chitin and chitosan: chemistry and technology of their use as structural materials. In: Kaplan DL, editor. *Biopolymers from renewable resource*. Berlin: Springer-Verlag; 1998. p. 98–118. Chapter 4.
- [39] Kasaai MR. Various methods for determination of the degree of N-acetylation of chitin and chitosan: a review. *J Agric Food Chem* 2009;57:1667–76.
- [40] Y. Guo, Z. Liu, H. An, M. Li, J. Hu, Nano-structure and properties of maize zein studied by atomic force microscopy. *J Cereal Sci.* 2005;41:277–281.
- [41] Hudson SM. The spinning of silk-like proteins into fibers. In: McGrath K, Kaplan D, editors. *Protein-based materials*. Boston, MA: Birkhauser; 1997. Chapter 10.
- [42] Parris N, Dickey LC, Tomasula PM, Coffin DR, Vergano PJ. Films and coatings from commodity agro-proteins. In: Gross RA, Scholz C, editors. *Biopolymers from polysaccharides and agro-proteins*, 786. Washington, DC: ACS Publishers; 2001. p. 118–31. ACS Symposium Series.
- [43] Shukla R, Cheryan M. Zein: the industrial protein from corn. *Ind Crop Products* 2001;13:171–92.
- [44] Wang Y, Padua GW. Nanoscale characterization of zein self-assembly. *Langmuir* 2012;28:2429–35.
- [45] Reddy N, Yang Y. Potential of plant proteins for medical applications. *Trends Biotechnol* 2011;29:490–8.
- [46] Butler MM, McGrath KP. Protein-based materials. In: Kaplan DL, editor. *Biopolymers from renewable resource*. Berlin: Springer-Verlag; 1998. p. 177–94. Chapter 7.

- [47] Shogren RL. Starch: properties and materials applications. In: Kaplan DL, editor. *Biopolymers from renewable resource*. Berlin: Springer-Verlag; 1998. p. 30–46. Chapter 2.
- [48] Utracki LA. *Commercial polymer blends*. New York: Chapman & Hall; 1998. Chapter 2.
- [49] Elsabee MZ, Abdou ES. Chitosan based edible films and coatings: *a review*. *Mater Sci Eng C* 2013;33(4):1819–41.
- [50] Le Corre D, Bras J, Dufresne A. Starch nano-particles: a review. *Bio-macromolecules* 2010;11:1139–53.
- [51] Jiménez A, Fabra MJ, Talens P, Chiralt A. Edible and biodegradable starch films: a review. *Food Bioprocess Technol* 2012;5:2058–76. Available from: <https://doi.org/10.1007/s11947-012-0835-4>.
- [52] Smith BM, Bean SR, Selling G, Sessa D, Aramouni FM. Effect of salt and ethanol addition on zein–starch dough and bread quality. *J Food Sci* 2017;82:613–21.
- [53] Sandford PA, Hutchings GP. Chitosan- a natural, cationic biopolymer: commercial applications. In: Yalpani M, editor. *Industrial polysaccharides, genetic engineering, structure/property relations and applications*. Amsterdam: Elsevier Science; 1987. p. 363–75.
- [54] Allan GG, Altman LC, Bensinger RE, Ghosh DK, Hirabayashi Y, Neogi AN, et al. Biomedical applications of chitin and chitosan. In: Zikakis JP, editor. *Chitin, chitosan and related enzymes*. New York: Academic Press; 1984. p. 119–33.
- [55] Kasaai MR. Zein and zein -based nano-materials for food and nutrition applications: a review. *Trends Food Sci Technol* 2018;79:184–97. Available from: <https://doi.org/10.1016/j.tifs.2018.07.015>.
- [56] Kasaai MR. Zein and zein-based nanoparticles for food packaging applications: a global view. *Adv Sci Eng Med* 2017;9(6):439–44.
- [57] Lai HM, Padua GW. Water barrier properties of zein films plasticized with oleic acid. *Cereal Chem* 1998;75:194–8.
- [58] Nalwa HS, editor. *Encyclopedia of nano-science and nanotechnology*, vols. 1–10. Stevenson Ranch, CA: American Scientific Publishers; 2004. General Reference.
- [59] Chau CF, Wu SH, Yen GC. The development of regulations for food nanotechnology. *Trends Food Sci Technol* 2007;18:269–80.
- [60] Papazoglou E, Parthasarathy A. *Bio-nanotechnology*. New York: Morgan and Claypool Publishers; 2007. p. 47–66. Chapter 3.
- [61] Kasaai MR. Comparison of various solvents for determination of intrinsic viscosity and viscometric constants for cellulose. *J Appl Polym Sci* 2002;86(9):2189–93.
- [62] Kasaai MR. Molecular weight and molecular weight distribution for biopolymers. *Advances in physicochemical properties of biopolymers*. CW Soest, The Netherlands: Bentham Science Publishers; 2017. p. 21–45. Part 1.
- [63] Kasaai MR. Molecular weight distribution for biopolymers: a review. *J Polym Biopolym Phys Chem* 2018;6(1):39–44. Available from: <https://doi.org/10.12691/jpbpc-6-1-5>.
- [64] Kuo P-C. The application of nanotechnology to functional foods and nutraceuticals to enhance their bioactivities. In: Bagchi D, Lau FC, Ghosh DK, editors. *Biotechnology in functional foods and nutraceuticals*. Boca Raton, FL: CRC, Taylor and Francis Group; 2010. p. 447–84. Chapter. 24.
- [65] Hussain CM. *Handbook of nano-materials for industrial applications*. Elsevier; 2018.
- [66] Hussain CM, Mishra AK. *Nanotechnology in environmental science*. Wiley-VCH; 2018.
- [67] Yang S-J, Chen J-W, Shieh M-J. Colorectal cancer cell detection by chitosan nanoparticles conjugated with folic acid. *Technical proceedings of the 2008 Nano Science and*

- Technology Institute (NSTI) Nanotechnology Conference and Trade Show. Boca Raton, FL: CRC Press, Taylor & Francis Group; 2008. p. 22–5. Boston, June 1–5, 2008.
- [68] Arai K, Kinumaki T, Fujitta T. Toxicity of chitosan. *Bull Tokai Reg Fish Res Lab* 1968;56:89–94.
  - [69] Aspden JJ, Mason JD, Jones NS, Lowe J, Skaugrud O, Illum L. Chitosan as a nasal delivery system: the effect of chitosan solution in vitro and in vivo- muco-ciliary transport rates in human turbinates and volunteers. *J Pharm Sci* 1997;86:509–13.
  - [70] Kasaai MR. Nano-sized particles of silica and its derivatives for applications in various branches of food and nutrition sectors. *J Nanotechnol* 2015; (Hindawi, ID 852394), 2015, 6 pp.
  - [71] Seabra AB, Bernardes JS, Fávoro WJ, Paulae AJ, Durán N. Cellulose nanocrystals as carriers in medicine and their toxicities: a review. *Carbohydr Polym* 2018;181:514–27.
  - [72] Chebli C, Cartilier L, Harman NG. Substituted amylose as a matrix for sustained-drug release: a biodegradation study. *Int J Pharm* 2001;222:183–9.
  - [73] Kost J, Shefer S. Chemically-modified polysaccharides for enzymatically controlled oral drug delivery. *Biomaterials* 1990;11(9):695–8.
  - [74] Jayakumar R, Menon D, Manzoor K, Naira SV, Tamura H. Biomedical applications of chitin and chitosan based nanomaterials - a short review. *Carbohydr Polym* 2010;82:227–32.
  - [75] Shukla SK, Mishra AK, Arotiba OA, Mamba BB. Chitosan-based nanomaterials: a state-of-the-art review. *Int J Biol Macromol* 2013;59:46–58.
  - [76] Weissmueller NT, Lu HD, Hurley A, Prud'homme RK. Nanocarriers from GRAS zein proteins to encapsulate hydrophobic actives. *Bio-macromolecules* 2016;17:3828–37.
  - [77] Alexandre M, Dubois P. Polymer-layered silicate nano-composites: preparation, properties and uses of a new class of materials. *Mater Sci Eng* 2000;28:1–63.
  - [78] Eyley S, Thielemans W. Surface modification of cellulose nanocrystals. *Nano-scale* 2014;6:7764–79.
  - [79] Mondal S. Preparation: properties and applications of nanocellulosic materials. *Carbohydr Polym* 2017;163:301–16.
  - [80] Corradini E, Curti PS, Meniqueti AB, Martins AF, Rubira AF, Muniz EC. Recent advances in food-packing, pharmaceutical and biomedical applications of zein and zein-based materials. *Int J Mol Sci* 2014;15:22438–70. Available from: <https://doi.org/10.3390/ijms151222438>.
  - [81] Gibbs BF, Kermasha S, Alli I, Mulligan CN. Encapsulation in the food industry: a review. *Int J Food Sci Nutr* 1999;50:213–24.
  - [82] Hussain CM, Kharisov B. Advanced environmental analysis-application of nanomaterials. The Royal Society of Chemistry; 2017.
  - [83] Kasaai MR, Moosavi A. Treatment of Kraft paper with citrus wastes for food packaging applications: water and oxygen barrier properties improvement. *Food Packaging Shelf Life* 2017;12:59–65.
  - [84] Endes C, Camarero-Espinosa S, Mueller S, Foster EJ, Petri-Fink A, Rothen- Rutishauser B, et al. A critical review of the current knowledge regarding the biological impact of nanocellulose. *J Nano-biotechnol* 2016;14. Available from: <https://doi.org/10.1186/s12951-016-0230-9> 78 (14 pp.).
  - [85] El Miri N, Abdelouahdi K, Barakat A, Zahouily M, Fihri A, Solhy A, et al. Bio-nanocomposite films reinforced with cellulose nanocrystals: rheology of film-forming solutions, transparency, water vapor barrier and tensile properties of films. *Carbohydr Polym* 2015;129:156–67.

- [86] Arora A, Padua GW. Review: nanocomposites in food packaging. *J Food Sci* 2010;75:43–9.
- [87] Kennedy JF, Knill CJ, Taylor DW. In: Dumitriu S, editor. In polysaccharides, structural diversity and functional versatility. New York: Marcel Dekker; 1998. p. 835–49.
- [88] Andresen M, Leena-Sisko Johansson L-S, Tanem BS, Stenius P. Properties and characterization of hydrophobized microfibrillated cellulose. *Cellulose* 2006;13(6):665–77.
- [89] Bulota M, Kreitsmann K, Hughes M, Paltakari J. Acetylated microfibrillated cellulose as a toughening agent in poly (lactic acid). *J Appl Polym Sci* 2012;126(S1):E449–58.
- [90] Siro I, Plackett D, Hedenqvist M, Ankerfors M, Lindstrom T. Highly transparent films from carboxymethylated microfibrillated cellulose: the effect of multiple homogenization steps on key properties. *J Appl Polym Sci* 2011;119(5):2652–60.
- [91] Abdul Khalil HPS, Davoudpour Y, Islam MN, Mustapha A, Sudesh K, Dungani R, et al. Production and modification of nanofibrillated cellulose using various mechanical processes: a review. *Carbohydr Polym* 2014;99:649–65.
- [92] Chirayil CJ, Mathew L, Thomas S. Review of recent research in nano cellulose preparation from different lignocellulose fibers. *Rev Adv Mater Sci* 2014;37:20–8.
- [93] Kumar Mishra R, Thomas S, Karikal N. Micro and nano fibrillar composites (MFCs and NFCs) from polymer blends. Amsterdam: Elsevier; 2017. Available from: <https://doi.org/10.1016/B978-0-08-101991-7.09989-1>.
- [94] BeMiller JN. 2nd ed. Starch, Modification Encyclopedia of Food Grains, vols. 3–4. Amsterdam: Elsevier; 2015. p. 282–6.
- [95] Amirsoleimani M, Khalilzadeh MA, Sadeghifar F, Sadeghifa H. Surface modification of nanostarch using nano silver: a potential antibacterial for food package coating. *J Food Sci Technol* 2018;55(3):899–904.
- [96] Kennedy JC, Pottier RH, Ross DC. Photodynamic therapy with endogenous protoporphyrin IX; Basic Principles and present clinical experience. *J Photochem Photobiol B Biol* 1990;6:143–8.
- [97] Denkbuss EB, Ottenbrite RM. Perspectives on: chitosan drug delivery systems based on their geometries. *J Bioact Compat Polym* 2006;21(4):351–68.
- [98] Guo H, Shi Y. A novel zein-based dry coating tablet design for zero-order release. *Int J Pharm* 2009;370:81–6.
- [99] Baars RJ, van Leeuwen YM, Hendrix Y, Velikov KP, Kegel VK, Philipse AP. Morphology-controlled functional colloids by hetero-coagulation of zein and nanoparticles. *Colloids Surf A* 2015;483:209–15.
- [100] Teng Z, Luo Y, Wang Q. Carboxymethyl chitosan–soy protein complex nanoparticles for the encapsulation and controlled release of vitamin D<sub>3</sub>. *Food Chem* 2013;141:524–32.
- [101] Luo Y, Teng Z, Wang Q. Development of zein nanoparticles coated with carboxymethyl chitosan for encapsulation and controlled release of vitamin D<sub>3</sub>. *J Agric Food Chem* 2012;60:836–43.
- [102] Luo Y, Wang Q. Zein-based micro- and nano-particles for drug and nutrient delivery: a review. *J Appl Polym Sci* 2015;131. Available from: <https://doi.org/10.1002/APP.40696> (12 pp.).
- [103] Luo YC, Zhang BC, Cheng WH, Wang Q. Preparation, characterization and evaluation of selenite-loaded chitosan/TPP nanoparticles with or without zein coating. *Carbohydr Polym* 2010;82:942–51.
- [104] Wang L-J, Yin S-W, Wu L-Y, Qi J-R, Guo J, Yang X-Q. Fabrication and characterization of Pickering emulsions and oil gels stabilized by highly charged zein/chitosan complex particles (ZCCPs). *Food Chem* 2016;213:462–9. Available from: <https://doi.org/10.1016/j.foodchem.2016.06.119>.

## Further reading

- Faridi Esfanjania A, Jafaria SM. Biopolymer nano-particles and natural nano-carriers for nano-encapsulation of phenolic compounds. *Colloids Surf B: Bio-interfaces* 2016;146:532–43.
- Kamide K, Iijima H. In: Gilber RD, editor. *Cellulosic polymers, blends and composites*. New York: Hanser; 1994. p. 189–206.
- Luo Y, Zhang B, Whent M, Yu L, Wang Q. Preparation and characterization of zein/chitosan complex for encapsulation of  $\alpha$ -tocopherol, and its in vitro controlled release study. *Colloids Surf B* 2011;85:145–52.
- Nitta SK, Keiji Numata K. Biopolymer-based nanoparticles for drug/gene delivery and tissue engineering. *Int J Mol Sci* 2013;14:1629–54. Available from: <https://doi.org/10.3390/ijms14011629>.
- Sanchez-Garcia MD, Lagaron JM. Nanocomposites packaging materials. In: Yam KL, editor. *Encyclopedia of packaging technology*. 3rd ed. New York: John Wiley & Sons; 2009. p. 807–13.
- Wang Y, Padua GW. Formation of zein spheres by evaporation-induced self-assembly. *Colloid Polym Sci* 2012;290:1593–8.

## Chapter 8

# Surface functionalization of PLGA nanoparticles for drug delivery

Joana A.D. Sequeira<sup>1</sup>, Irina Pereira<sup>1,2</sup>, António J. Ribeiro<sup>1,3</sup>,  
Francisco Veiga<sup>1,2</sup> and Ana Cláudia Santos<sup>1,2</sup>

<sup>1</sup>Department of Pharmaceutical Technology, Faculty of Pharmacy, University of Coimbra, Pólo das Ciências da Saúde, Coimbra, Portugal, <sup>2</sup>REQUIMTE/LAQV, Group of Pharmaceutical Technology, Faculty of Pharmacy, University of Coimbra, Coimbra, Portugal, <sup>3</sup>I3S, Group Genetics of Cognitive Dysfunction, Institute for Molecular and Cell Biology, Porto, Portugal

## 8.1 Introduction: background and driving forces

### 8.1.1 Nanoparticles as novel drug delivery systems

Nanoparticles are among the novel drug delivery systems—one of the most extensively exploited, due to their unique properties related to their size [1], capacity of drug protection [2], and controlled drug release [3].

Nanoparticles are colloidal carriers, varying in terms of particle size between 10 and 1000 nm, being typically smaller than 200 nm [4]. Their attributes comprise controlled drug release [5] and protection [2], which is particularly important for inherently unstable drugs like therapeutic proteins and peptides [6]. Such applicability is due to their capacity to target organs and tissues, provide drug delivery in a sustained manner without increasing the effective dose, and improve patient compliance [7] by reducing the number of administrations, particularly regarding diseases that require chronic therapeutic regimens [8]. Parenteral nanoparticles, in particular, have been studied to deliver cancer drugs and to treat central nervous diseases, since by attaining a size smaller than 100 nm facilitates the intracellular delivery of drugs, the accumulation in tumor sites, and the permeation of the blood–brain barrier (BBB) [9,10].

### 8.1.2 Poly(D,L-lactide-co-glycolide) nanoparticles

Poly(D,L-lactide-co-glycolide) (PLGA) polymers are biodegradable, biocompatible [11], and approved for medical use by the US Food and Drug



Administration (FDA), and the European Medicines Agency (EMA) [12]. They first appeared as bioresorbable sutures in the 1970s [13] paving the way for PLGA use as biodegradable drug release systems. In the late 1980s Astra Zeneca introduced Zoladex an implant for prostate and breast cancer still on the market today. The implant releases goserelin, a synthetic peptide blocker of a luteinizing hormone-releasing hormone (LH–RH) receptor, in a controlled release manner, and is aimed at reducing testosterone, or estradiol production [14]. More recently, PLGA microspheres for subcutaneous administration were marketed as Bydureon, from Astra Zeneca, for once-weekly administration of exenatide, a glucagon-like peptide-1 receptor GLP-1R agonist, targeted to treat adults with type 2 diabetes [15].

Research on PLGA has been done extensively with several patents [16] and research papers still emerging, which illustrates that PLGA is regarded as a very promising polymer with current pharmaceutical interest and challenges for researchers to overcome. However, modern PLGA research has placed more emphasis on nanoparticles, rather than microparticles or macro-implants, to deliver drugs in a controlled release and targeted manner [17].

### 8.1.3 Structure and properties of PLGA polymers

PLGAs are aliphatic polyesters, composed of monomeric units of lactic acid and glycolic acid that are connected by ester linkages [18]. Their chemical structure is represented in Fig. 8.1. They are considered relatively stable when in a dry state, but when exposed to moisture or an aqueous environment (e.g., in vivo) [13,19], the polymer chains are broken down to small oligomers, and then to monomers, by a process of hydrolytic chain scission [20,21]. Their final degradation products, the monomers glycolic acid and lactic acid, are eliminated from the body through the Krebs Cycle [18]. There is extensive clinical and toxicological data to sustain the biocompatibility and biodegradability of these polymers [11].

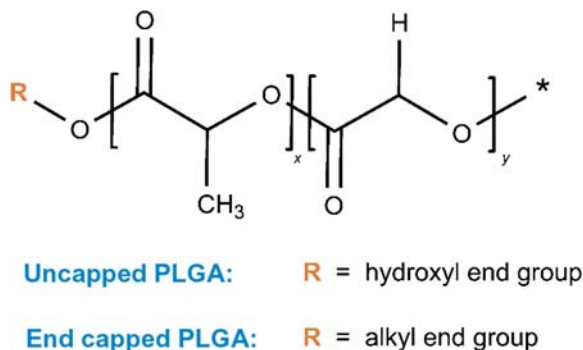


**FIGURE 8.1** Chemical structure of PLGA. “x” and “y” refer to the relative amounts of lactide and glycolide units.

Since lactic acid is more hydrophobic than glycolic acid, PLGA copolymers with higher ratios of lactic acid in their composition are expected to be less hydrophilic, leading to their slower degradation [13,22]. The chemical and physical properties of PLGA impact the release behavior of drugs loaded in PLGA delivery devices. It is possible to tailor the drug release profile of a drug by the type of PLGA carrier, with the right physical chemical characteristics [23].

PLGA nomenclature is related to an important feature of their chains, called the terminus group or end-group (Fig. 8.1). PLGA carrying free carboxylic end groups are known as “uncapped PLGA” [24]. They are more hydrophilic and absorb more water, which leads to a higher degradation rate when compared to the end-capped polymers [25]. End-capped PLGAs have esterified carboxyl groups at the end of the chains [24].

The  $pK_a$  of lactic and glycolic acid carboxyl groups is 3.86 and 3.83, respectively, and at around a physiological  $pH = 7.4$ , these groups are negatively charged [16]. Regarding uncapped PLGA, there is also a negative charge contribution from the terminal free carboxylic end groups. The sum of these negatively charged groups at physiological  $pH$  contribute for the negative surface charge usually present in PLGA nanoparticles.

#### 8.1.4 PLGA nanoparticles production techniques

There are three classical techniques, well-described in the literature, for PLGA nanoparticle preparation [17]: nanoprecipitation (also called solvent displacement or interfacial deposition) [26], emulsion–diffusion, and double emulsification [27]. In the nanoprecipitation technique, PLGA is solubilized, along with the drug and a lipophilic emulsifier (e.g., triglycerides) in a solvent (e.g., acetone), constituting the solvent phase or organic phase. This solvent phase is added dropwise to a nonsolvent phase or aqueous phase, comprised of a PLGA nonsolvent (e.g., water) or a buffer with a surfactant, usually poloxamer 188 [26,27]. This technique is the first option to encapsulate hydrophobic drugs in PLGA nanoparticles.

The emulsion–diffusion and double emulsification techniques allow the incorporation of both lipophilic and hydrophilic drugs in PLGA nanoparticles. In the emulsion–diffusion technique, if the drug is hydrophobic, it is dissolved into an organic phase together with a polymer, and an oil in an organic solvent that is partially miscible with water (e.g., ethyl acetate). Using this technique, three phases are required to produce nanoparticles: an organic phase, an aqueous phase, and a dilution of both phases [2,27]. The organic phase is emulsified under vigorous agitation into the aqueous phase, taking advantage of the high energy rotation of an ultra-turrax.

To incorporate hydrophilic drugs, instead of hydrophobic ones, with this technique, the inner and outer phases are swapped. The aqueous phase is the inner phase, and contains the drug with a stabilizing agent, such as poly

(vinyl alcohol) (PVA) or poly(vinylpyrrolidone) (PVP). The organic phase is the outer phase and is composed of PLGA and an organic solvent (e.g., methylene chloride or acetone) [27].

There are two types of double emulsion techniques: water–oil–water emulsion (w/o/w) and oil–water–oil emulsion (o/w/o). W/o/w allows for higher encapsulation efficiency of hydrophilic drugs, to produce drugs-loaded PLGA nanoparticles. Double emulsions are prepared in a two-step process, using a hydrophobic and a hydrophilic surfactant to stabilize the interface of the w/o internal emulsion, and the external interface of the oil globules in w/o/w emulsions, respectively. The principle and solvents used are the same as stated for single emulsions [2,27].

## 8.2 Active targeting by surface functionalization of PLGA nanoparticles

As previously stated, nanoparticles are an efficient delivery system that allows for controlled release of drugs for a prolonged period. This is especially beneficial for drugs with low therapeutic index (like cancer drugs), with reduced half-lives (like therapeutic proteins) or with poor water solubility and stability. Notwithstanding their promising characteristics, PLGA nanoparticles evidences some intrinsic drawbacks, which impair their role as a novel drug delivery system/drug vector [2]. The nanoparticles' small size allow their accumulation in organs and tissues. A size smaller than 50 nm can allow them to evade the reticulo-endothelial system (RES) [28]. In fact, size determines the biological fate of nanoparticles, however, many times the accumulation is not targeted to the desired tissue or organ where the drug should act, resulting in adverse effects.

After intravenous administration, PLGA nanoparticles are rapidly removed from systemic circulation due to opsonization by the enhanced permeation and retention (EPR) effect, unless the target tissue is a tumor. In this case, the nanoparticles tend to accumulate due to leaky vasculature [29,30].

Also, the *in vivo* blood circulation time of nanoparticles, and the extent to which they are taken up by cells, are affected by various factors, especially the nanoparticles' surface charge. PLGA nanoparticles display a negative charge at the surface due to the chemistry of their chains. A change in surface charge to positive values is sometimes desirable to achieve PLGA nanoparticles with better clinical responses, such as enhanced cellular uptake and opening tight junctions. PLGA nanoparticles are not uptaken by viable cells, and they cannot pass through the BBB, which impairs their use as a drug carrier to the brain [31]. Apart from their small nano size, once in the body, the fate of PLGA nanoparticles is, among other factors, determined by surface characteristics that govern the interaction of the nanoparticles and the biological environment [16] (i.e., body fluids, cells, proteins, and salts).

In fact, once PLGA nanoparticles are parenterally delivered and reach the systemic circulation, the adsorption of proteins present in the blood starts immediately, causing the formation of the protein corona [32], which may change the surface charge of the nanoparticles. PLGA is negatively charged at physiological pH, and together with its hydrophobic moieties, attracts plasma proteins, most of which are cationic at this pH. The biodistribution of the nanoparticles is believed to be determined to a major extent by the binding of plasma proteins (opsonines) on the particles' surfaces, making them recognized by the immune system as antigens. This eventually leads to a reduction of nanoparticles' blood circulation times [33,34].

These are among the rationales behind surface functionalization of nanoparticles. By actively targeting the particles, nanoparticles could be directed to accumulate in specific sites. Active targeting is achieved by surface functionalization of nanoparticles with recognized molecules, in order to enhance intracellular delivery and to increase their retention in cells or tissues, which improves their *in vivo* performance [16,35].

Functionalization of PLGA nanoparticles relies on the introduction of ligands on the surface of the particle, usually taking advantage of the PLGA carboxyl end groups [31]. These introductions can be performed by noncovalent interactions or by covalent conjugations [16,35]; the latter makes use of chemical reactions, forming new bonds between PLGA and ligands. Nevertheless, achieving functionalization of PLGA nanoparticles by performing conjugation reactions is not within the scope of this chapter. This chapter deals exclusively with surface functionalization of PLGA nanoparticles by noncovalent interactions.

Surface functionalization of PLGA nanoparticles by noncovalent interactions is particularly interesting due to their simplicity and spontaneity, allied with the fact that these noncovalent interactions prevent ligand degradation. This factor should be considered when the ligand is a very viable molecule, like an antibody. Also, even PLGA is reported to suffer from transamination and hydrolysis reactions under very mild conditions. The major reported drawbacks associated with these noncovalent interactions are linked to their inherent weak chemical interaction.

### 8.3 Noncovalent functionalization of PLGA nanoparticles

Among the strategies to make PLGA nanoparticles stealth to the RES, two are most reliable: (1) coating with hydrophilic nonionic polymers/surfactants [33], and (2) altering the surface charge by coating the nanoparticles with polyelectrolytes of opposite charge [36].

As previously mention, there are two types of PLGA polymers (Fig. 8.1): chains with a free carboxyl end group known as uncapped PLGA, and chains terminated with alkyl ester end groups or end-capped PLGA [16]. PLGA particles allowing surface functionalization by noncovalent interactions mostly

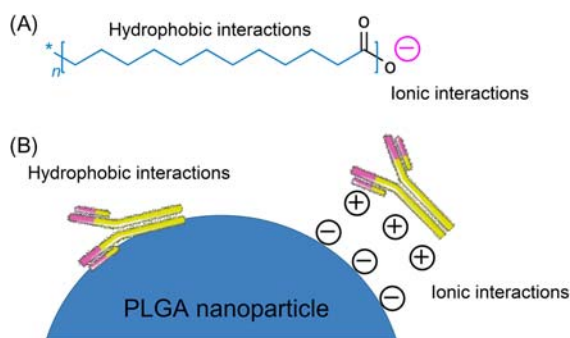


**FIGURE 8.2** Two ways for exploiting noncovalent interactions on a PLGA polymer chain (A); and on the surface of a PLGA nanoparticle (B). The drawings are only demonstrative.

make use of uncapped PLGA in their fabrication process [16], since by exploiting the particles' negative charge, it is possible to form ionic interactions between the PLGA exposed carboxylic end groups and positively charged molecules (Fig. 8.2B). Another approach for noncovalent surface modification relies on exploiting the hydrophobicity of both types of PLGA chains. The hydrophobicity increases with the length of the chain [37]. This type of surface functionalization is not as strong as the ionic one, and is performed under uncontrolled conditions that may allow loss of coating molecules during the fabrication method washing steps [16]. In general, the adsorption of amphiphilic molecules for a specific surface modification is a rapid and convenient method not deleterious for the ligands—if the interaction is strong enough to resist premature desorption. Considering the physicochemical characteristics of a preformed PLGA nanoparticle, the surface carboxylate groups of uncapped PLGA allow for covalent and electrostatic conjugation of ligands, whereas the hydrophobicity of the PLGA matrix can be exploited for adsorption of hydrophobic, or even amphiphilic, ligands (Fig. 8.2A).

This section provides examples of functionalization approaches that take advantage of ligand characteristics and the right conditions to create noncovalent interactions between a ligand and PLGA. It highlights some biological effects *in vitro* and *in vivo*, as well as their potential for therapeutic applications.

### 8.3.1 PEGylated PLGA nanoparticle

PEGylation technology can improve the aqueous stability and solubility minimizing aggregation by steric stabilization, decrease immunogenicity, and prolong the systemic circulation of nanoparticles or other poly(ethylene glycol) PEG-containing products [38,39]. PEG polymers have been extensively employed for the modification of PLGA nanoparticles.

Due to their inherent hydrophobicity and surface negative charge, PLGA nanoparticles are recognized by the RES system and rapidly cleared from the

blood systemic circulation time. Coating the nanoparticles with a layer of PEG has been shown to improve their time of residence in the body [9,40]. When attached to a particle surface, PEG ether groups can bind water molecules via hydrogen bonding, introducing a highly hydrated hydrophilic coating layer around the particle, which tricks the plasma cells to recognize the nanoparticle as only water [41].

Adding to that benefit, coating nanoparticles with a layer of PEG facilitates passive targeting of tumor tissue through EPR effect [42].

PEGylation is more often achieved by conjugating PEG to PLGA, by using a chemical reaction prior to nanoparticle fabrication [43,44], or by using block copolymers that already possess PEG moieties [31]. However, regarding PLGA, this can be achieved by hydrophobic interactions using PEG as a surfactant [16].

PLGA nanoparticles were produced and surface-coated with cationic diblock copolymer, poly(L-lysine)–poly(ethylene glycol)–folate (PLL–PEG–FOL) by ionic interactions in an aqueous phase, to enhance nanoparticles' site-specific intracellular delivery against folate receptor overexpressing cancer cells [45]. The nanoparticles showed improved cellular uptake to folate receptor overexpressing cells (KB) of human epidermal carcinoma, suggesting that they were mainly taken up by folate receptor-mediated endocytosis. This demonstrated an enhanced cellular uptake, achieved both by introducing a receptor ligand, and by improving the circulation time with PEG-coated nanoparticles. Using the same rationale, cell-specific homing moieties at the protein-repellent surface layer, have been the focus of a study to deliver docetaxel (Dtxl). Dtxl-encapsulated PLGA nanoparticles formulated with poly(D,L-lactic-co-glycolic acid)-block-poly(ethylene glycol) (PLGA-b-PEG) copolymer and surface functionalized with A10 2'-fluoropyrimidine RNA aptamers were developed to recognize the extracellular domain of the prostate-specific membrane antigen (PSMA) [46]. In this study, 100% of mice survived after being treated with the formulation.

### 8.3.2 Surfactant PLGA nanoparticles

Nonionic stabilizers/surfactants can be employed to coat PLGA nanoparticles. Due to PLGA's hydrophobic nature, hydrophobic or amphiphilic molecules, polymers, and other substances could be adsorbed via hydrophobic interactions. This is the principle followed by adsorbing amphiphilic molecules like surfactants, polymers, or even proteins. However, regarding the latter, electrostatic interactions are the major determinant for complexation with particle surfaces [16]. Surface adsorption of surfactants via hydrophobic interactions has an impact on the stability of nanoparticle suspensions, ensuring repulsion between nanoparticles, and thus minimizing aggregation [47]. Among the most used are anionic surfactant sodium dodecyl sulfate (SDS), nonionic poly(vinyl alcohol) (PVA) [48], and nonionic polysorbates [49].

For toxicity reasons, nonionic poloxamers and PEG [36,49] are the common choice; they are biocompatible and EMA and FDA approved. Poloxamers (also known as Pluronics) are amphiphilic and arranged in an ABA manner: triblock copolymers consisting of a hydrophobic poly(propylene glycol) (PPG) middle block and two hydrophilic PEG outer blocks. This mode of adsorption leaves the hydrophilic PEG side-arms in a mobile state, which extend outward from the particle surface [49,50], and (as discussed in Section 8.3.1) the extension of PEG chains results in a coating that ensures stealth properties, once the PEGylated nanoparticles reach the systemic circulation.

Saturated chains of phospholipids, such as 1,2-didecanoylphosphatidylcholine (DDPC) or 1,2-dipalmitoylphosphatidylcholine (DPPC), have been proposed as efficient emulsifiers toward the preparation of PLGA nanospheres [16]. Another approach is the use of d- $\alpha$ -tocopheryl polyethylene glycol 1000 succinate (TPGS), which offers several possible advantages over other types of stabilizing agents. TPGS is amphiphilic and water soluble, and is formed by conjugations of vitamin E and PEG. It is used for reversing or preventing vitamin E deficiency, due to its good oral bioavailability, and is also employed as a solubility and absorption enhancer as well as a vehicle for drug delivery. Adding to these beneficial features, vitamin TPGS also inhibits P-glycoprotein active transport carrier (P-gp), which effluxes drugs effectively in the duodenum, avoiding accumulation and, subsequently, its further absorption [51]. Moreover, it is a very good surfactant that is able to stabilize particles [47].

Win and coworkers, prepared coumarin-6 loaded PLGA nanoparticles using a modified solvent extraction/evaporation technique with a fluorescent marker, to visualize the nanoparticles cellular uptake in colon cells, Caco-2 cell monolayers, either with PVA or TPGS as emulsifier. TPGS as emulsifier-based nanoparticles were better internalized in the cells. The TPGS coating of the nanoparticles insures a better cellular uptake, compared with PVA-coated PLGA nanoparticles, making the former particles an oral delivery alternative for anticancer drugs [52].

### 8.3.3 Polyelectrolyte—PLGA nanoparticles

The extracellular face of the cell membrane is composed of anionic phospholipids, which are responsible for the membrane's negative charge. Although the surface charge of PLGA nanoparticles is negative, if a polyelectrolyte interacts with the particles' surface, forming a positive charge coat by electrostatic interactions, cell binding to these coated particles may improve the particles' cell internalization rate and intracellular processing.

Chitosan is a biodegradable, biocompatible, hydrophilic polymer, positively charged at the physiological pH, that presents relatively low immunogenicity and is able to interact with anionic components (i.e., cell

membranes and polymers, like PLGA) [31]. Chitosan has free amino groups in its glucosamine monomeric unit with a  $pK_a$  value of 6.3, which means that at a pH lower than this  $pK_a$ , its primary amino groups are protonated and they can interact with hydroxyl groups of PLGA. Based on these desirable characteristics, chitosan can be used to coat PLGA nanoparticles and develop targeted delivery systems.

Epirubicin (Epi)-loaded PLGA nanoparticles with (Epi-PLGA-CS-Apt) and without aptamer, (Epi-PLGA-CS) for parenteral delivery with a particle size of 222.7 and 183.2 nm and zeta potentials of +10.2 and +18 mV, respectively, were produced by double emulsion/solvent evaporation [53]. The obtained nanoparticles were coated with chitosan by promoting interaction between the negative charge of PLGA and the positively charged chitosan. The aptamer was electrostatically attached to the surface of Epi-PLGA-CS nanoparticle and confirmed by the increase in particle size and decrease in zeta potential.

The *in vitro* cytotoxicity study, performed to assess the affinity of these positively charged nanoparticles to the cell membranes, was successful, since Epi-PLGA-CS-Apt were internalized in the cells. Also, *in vivo* results in BALB/c mice with C26 colon carcinoma presented a remarkable reduction in tumor growth, on account of the targeting provided by the 5TR1 aptamer attached to the CS-modified Epi-loaded PLGA nanoparticles.

In another study, chitosan was also used to change the surface charge of PLGA to improve its interaction with negative charged nucleotides. To improve cell internalization, DNA-loaded PLGA nanoparticles, with zeta potential of +10 mV at pH 7.4 and size under 200 nm, were produced by a new emulsion-diffusion-evaporation technique using a PVA-chitosan blend to stabilize the final obtained nanoparticles [54]. Following the preparation of the blank PLGA nanoparticles coated with chitosan, nanoparticle-DNA complexes were prepared by mixing the nanoparticles with plasmid at a concentration of 10  $\mu\text{g/mL}$  in 25 mM Hepes (pH 7.4), and in deionized water (pH 6.0), at room temperature. This procedure yielded an efficient electrostatic complexation of the negatively charged DNA to the cationic PLGA nanospheres.

### 8.3.4 Cell target ligands coupled on the surface of PLGA nanoparticles

By taking advantage of PLGA hydrophobic and electrostatic interactions, a cell target ligand can be exposed at the surface of the PLGA nanoparticles, making the particles specific.

Lectins are molecules that recognize cells and are capable of promoting cellular uptake of a cargo. They possess a binding affinity for glycosylated components present in cell membranes. Once lectins are attached to the surface of nanoparticles, they can specifically target the particles to cells and



promote their cellular uptake [55], redirecting the nanoparticle cargo. Mannan-decorated PLGA nanoparticles were produced as vaccine carriers to dendritic cells; the *in vitro* uptake cell study demonstrated that decorated nanoparticles were twice as efficiently internalized in bone marrow-derived dendritic cells as the nondecorated PLGA ones [56].

PLGA carboxyl end-groups can be conjugated with biotin-NH<sub>2</sub>. As biotin has a high affinity to avidin and analogues (e.g., streptavidin), the noncovalent interaction between biotinylated PLGA particles and avidin–ligand conjugates can be achieved. Coupling of biotin–PEG–NH<sub>2</sub> to PLGA nanoparticles was also developed as a strategy to transform nanoparticles in cell-recognizable ligands [57]. The same rational approach is behind the attachment of targeting ligands like antibodies to PLGA nanoparticles [31] and will be addressed in more detail in Section 8.3.5.

The receptors for glycoprotein transferrin are overexpressed in many tumors. In a study, PLGA nanoparticles produced by nanoprecipitation were coated with transferrin by adsorption. The results evidence a greater uptake of transferrin–PLGA nanoparticles by glioma cells, confirming the benefits of specific targeting. In the same way, albumin-loaded PLGA nanoparticles revealed a longer systemic half-life [58], following their injection in mice and rats, proving that protein coating prevents interactions between serum and nanoparticles.

### 8.3.5 Antibody-directed PLGA nanoparticles

Nanoparticles coated with proteins and antibodies can bind to cell surface receptors, providing targeted delivery [1]. The surface of nanoparticles is often combined with monoclonal antibodies (mAb) to improve their targeting efficiency. mAbs can be attached to the nanoparticles either by physical adsorption or conjugation. However, being a protein, the structure of the mAb could be impaired due to the harsh conditions of conjugation reactions, losing its integrity. Physical adsorption of proteins on the nanoparticle surface relies on a combination of hydrophobic and electrostatic interactions, providing some strength to the chemical interaction.

In a study by Obermajer and coworkers, anticytokeratin monoclonal IgG was bound to the surface of PLGA nanoparticles by adsorption, with its biological activity preserved, which was demonstrated by its high binding capacity to breast cancer cell lysates (MCF-7 and MCF-10A neoT cell lines). The same mAb was covalently bound to the nanoparticles using 1-ethyl-3-(3-dimethylaminopropyl) carbodiimide hydrochloride as a bifunctional reagent, but the biological activity of the mAb could not be preserved after this conjugation reaction [59].

The affinity of proteins to PLGA depends on their isoelectric points and media pH conditions. Under a physiological medium with pH around 7.4, a therapeutic protein with a pI close to 7.4 will behave as uncharged,

and therefore more capable to establish hydrophobic electrostatic interactions. On the contrary, a protein with pI below 7.4, at physiological pH, will exhibit positive charge and, consequently, will be more appropriate for interaction with negative charged PLGA nanoparticles. The impact of adsorbing therapeutic proteins at the surface of PLGA nanoparticles by ionic interactions also results in the momentarily shifting to zero of the surface charge of PLGA, loss of electrostatic repulsion, and possible aggregation of the particles [16]. Also, one must account for the shifts in pH and ionic strength, as well as competitive absorption of plasma proteins, after administration of the formulation [16].

## 8.4 Nucleic acid-functionalized PLGA

The functionalization of the negatively charged surface of PLGA nanoparticles with nucleic acid-based ligands is mainly achieved by resorting to non-covalent chemical bonds, namely by electrostatic interactions between PLGA and positively charged materials (polymers or lipids) used for nanoparticle surface coating [60,61]. The surface modification is crucial for the subsequent complexation of the anionic macromolecules (i.e., the nucleic acid-based ligands), since, without this modification, the PLGA nanoparticles surface would repel the negative nucleic acid molecules, thereby hindering their complexation. For that purpose, cationic polymers, such as chitosan [53,62], polyethyleneimine (PEI) [60,63,64], as well as cationic lipids, such as 1,2-di-*O*-octadecenyl-3-trimethylammonium propane (DOTMA) [61], were used as coatings in several studies concerning PLGA nanoparticles surface functionalization with nucleic acid-based ligands.

Thus far, the surface of modified PLGA nanoparticles has been electrostatically coupled with (Fig. 8.3): (1) antisense oligonucleotides—synthetic single-stranded oligodeoxynucleotides which impair RNA processing, specifically the translation, and modify the protein expression [62,65]; (2) small interfering RNAs (siRNAs), which are noncoding RNA double-stranded molecules with 21–23 nucleotides and therapeutic activity (since siRNAs can target messenger RNA (mRNA) upon transcription to induce specific gene silencing) [64,66]; (3) plasmid DNA (pDNA), so-called expression vectors, are extrachromosomal circular double-stranded DNA molecules with c. 3 kb size, that encode genes through genetic engineering processes (transgenes), which, upon transport to the nucleus, will be transcribed and translated into proteins by the host cell [60,63,67]; (4) aptamers, which are single-stranded molecules of nucleic acids (DNA or RNA) organized in tertiary conformations (helices or loops) that exhibit a selective target binding [53,68]; (5) mRNA, which encodes an amino acid sequence conveying the genetic information from the complementary DNA (present in the nucleus) to the ribosome (in the cytoplasm), where the translation process, the last step of protein synthesis, occurs [61,69]. Regarding the nucleic acids

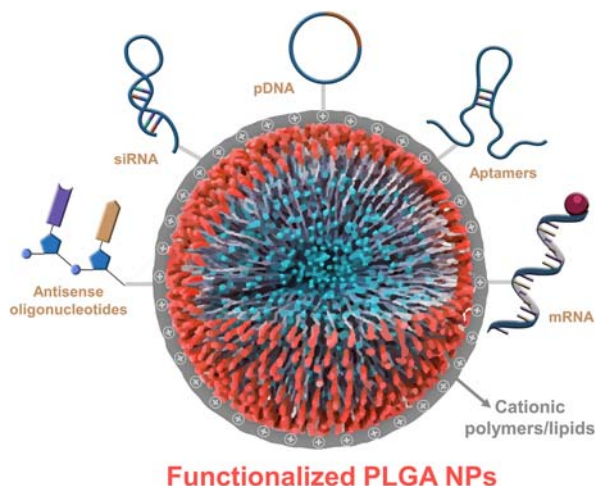


**FIGURE 8.3** Schematic representation of the nucleic acid-based ligands hitherto conjugated with surface modified-PLGA nanoparticles.

formerly cited, antisense oligonucleotides, siRNA, pDNA, and mRNA have essentially a therapeutic activity, whereas aptamers, besides acting as therapeutics, also enable a direct targeted therapy, due to the selectivity to cell specific protein or nucleic acid receptors [68]. The surface functionalization of PLGA nanoparticles with nucleic acid-based ligands is a promising technology, endowed with high therapeutic potential. It enhances the effective delivery of these molecules by surpassing their limitations in permeating biological membranes, notably, their negative charge, hydrophilic nature, and short half-life, which is due to nucleic acids' proneness to enzymatic degradation [62,68].

For instance, in a study by Taetz and coworkers, chitosan-modified PLGA nanoparticles produced by the emulsion–diffusion–evaporation technique coupled with antisense 2'-*O*-methyl-RNA, a human telomerase inhibitor sequence, demonstrated to be as effective as commonly used lipid-based transfection reagents (e.g., *N*-[1-(2,3-Dioleoyloxy) propyl]–*N,N,N*-trimethylammonium methyl–sulfate, also known as, DOTAP) [62]. The nanocomplexes displayed a homogeneous polydispersity, despite the increase in particle size (175 nm), when compared to the bare PLGA nanoparticles (135 nm). This was mainly attributed to the coating assembled in the nanoparticles' surface. In terms of binding efficiency, the group noticed that high concentrations of chitosan led to a higher antisense 2'-*O*-methyl-RNA coupling. The uptake was visualized in two human lung cancer cell lines, A549 and Calu-3, as well as in a nonneoplastic human alveolar epithelial cell line, hAEpC. In the lung cancer cell lines, the nanocomplexes penetrate inside the cell, being, therefore internalized after 24 and 48 h. In contrast, the nanocomplexes in the nonneoplastic hAEpC cell line were observed in the cell

membrane and no internalization occurred after 24 and 48 h, mainly due to the defective endocytosis machinery of these cells. The antisense 2'-*O*-methyl-RNA-chitosan-PLGA nanoparticles proved to exert their action effectively, thus reducing the telomerase activity and, consequently, the telomere shortening in A549 lung cancer cells, with only a slight decrease in cell viability [62].

Wang and collaborators, similarly to Jeon and collaborators, modified PLGA nanoparticles with PEI in order to bind therapeutic siRNA molecules [60,64]. In their study, the Wang group coupled S1 siRNA, which targets the open reading frame (ORF) of the hepatitis B virus (HBsAg) genome, to the modified cationic PLGA nanoparticles, and compared two different polymeric coatings, PEI and chitosan [64]. The PEI–PLGA nanocomplexes were produced by the nanoprecipitation method, while the chitosan–PLGA nanocomplexes were produced by solvent evaporation, since the nanoprecipitation method yielded particles with larger sizes (between 500 and 800 nm). As expected, the coating increased the particle size of the nanoparticles, when compared to bare PLGA nanoparticles; in this case, a c. 50–70 nm increase was observed. The obtained chitosan–PLGA nanocomplexes evidenced a particle size of 261 nm, a polydispersity index (PI) of 0.2, and a zeta potential of +28.7 mV. In comparison, the PEI–PLGA nanocomplexes demonstrated a smaller particle size and PI, 200 nm and 0.1, respectively, and a superior zeta potential, +35.9 mV. The transfection efficacy of PEI–PLGA and chitosan–PLGA nanocomplexes was evaluated in a human liver cell line (PLC/PRF/5) infected with the hepatitis B virus. A significant reduction of HBsAg expression was noticed, however, among chitosan–PLGA and PEI–PLGA nanocomplexes, the latter entailed a higher transfection efficiency, albeit the reduction in HBsAg expression was more pronounced when lipofectamine, a typical transfection reagent, was used. Notwithstanding, when compared to lipofectamine, the PEI–PLGA and chitosan–PLGA nanocomplexes were less toxic (cell viability was 92.9% after exposition to the nanocomplexes vs 72.4% after exposition to lipofectamine) [64].

In turn, Jeon and collaborators developed PLGA nanospheres, by the water-in-oil-in-water solvent evaporation technique, which were further coated by PEI and complexed with the transcription factor SOX9 pDNA, plus the core-binding factor alpha-1 (Cbfa-1) siRNA [60]. SOX9 pDNA was determined to enhance the expression of the SOX9 transcription factor, a protein responsible for chondrogenesis, whereas Cbfa-1 siRNA targets the *Cbfa-1* gene, which is responsible for osteogenic differentiation. Therefore the aim of the Jeon et al. study was to enhance the protein expression of SOX9, and silence the protein expression of Cbfa-1 in order to increase the production of cartilage. PEI–PLGA nanoparticles proved to be a more effective and less cytotoxic pDNA and siRNA transfection system than PEI itself. Several techniques of molecular biology, namely reverse transcription polymerase chain reaction (RT–PCR) and Western Blot, allied with

immunohistochemistry and immunofluorescence, indicated that the *in vitro* (by using human mesenchymal stem cells, hMSCs cell line) and *in vivo* (by using BALB/c mice subcutaneously injected with mesenchymal stem cells) cotransfection of SOX9 pDNA and Cbfa-1 siRNA promoted by the PEI-modified PLGA nanoparticles enhances the expression levels of the *SOX9* gene, and other genes involved in the formation of extracellular matrix (ECM) components (e.g., collagen type IIa1, COL IIa1), as well as reduces the expression of *Cbfa-1* gene, thus promoting chondrogenic differentiation [60].

Similarly, in Park and coworkers' study, PEI-modified PLGA nanoparticles were coupled with pDNA-containing *SOX* trio transgenes (*SOX5*, *SOX6*, and *SOX9* genes) to promote the delivery of these macromolecules to human mesenchymal stem cells (hMSCs) and thus promote chondrogenic differentiation and chondrogenesis [63]. To that aim, PLGA nanospheres were produced by the water-in-oil-in-water solvent evaporation technique and, subsequently, coated with PEI. The expression vectors pEGFP-*SOX5*, pEYFP-*SOX6*, and pRed-*SOX9* were prepared, by recombinant genetic engineering. The pDNA-PEI-PLGA nanocomplexes exhibited a particle size of 82 nm. Western Blot demonstrated that the transfection efficiency of the three pDNA complexed with the PEI-PLGA nanospheres was greater, when compared to lipofectamine and PEI as a gene delivery system. A quantitative real-time polymerase chain reaction (PCR) revealed that, in hMSCs, the transfection of the three pDNA (pEGFP-*SOX5*, pEYFP-*SOX6*, and pRed-*SOX9*) led to a higher expression of chondrocyte-related proteins, enhancing chondrogenesis and being therefore more effective than the transfection of single pDNA [63].

Direct targeted delivery enhances the therapeutic effects of commonly used chemotherapeutic agents, and may be obtained by the surface functionalization of polymeric nanoparticles, constituting an innovative and promising strategy for the treatment of cancer by reducing chemotherapy off-target adverse effects [53]. For that purpose, Taghavi and colleagues encapsulated an anthracycline, epirubicin (Epi), a known conventional chemotherapy agent, in chitosan-modified PLGA nanoparticles. Subsequently, a mucin 1 (MUC1) aptamer (5TR1 aptamer) was electrostatically coupled to the chitosan-PLGA nanoparticles in order to target MUC1 receptors, which are overexpressed in breast cancer cells (e.g., in the MCF7 cell line). The MTT assay showed that the 5TR1 aptamer-chitosan-PLGA nanoparticles loaded with Epi significantly reduced the viability in the MCF7 cells (34.2% cell viability), while cell viability reduction in chinese hamster ovary cells (CHO cell line), which do not overexpress MUC1 receptors, was negligible (92.4% cell viability). *In vitro*, 5TR1 aptamer-chitosan-PLGA nanoparticles loaded with Epi were rapidly internalized by the cancer cells. The acidic tumor environment subsequently led to the rapid degradation of chitosan and PLGA, stimulating the release of Epi, which caused cancer cell viability

reduction and ultimately enhanced Epi therapeutic efficacy. Such effects essentially occurred due to the fact that the nanocomplexes were not absorbed by the extracellular space and healthy cells. C26 colon carcinoma cells, which overexpress MUC1 receptors, were intravenously injected in BALB/c mice. The administration of a single dose of 5TR1 aptamer–chitosan–PLGA nanoparticles loaded with Epi (2 mg/kg of Epi) in the colon cancer-bearing mice model reduced the tumor growth, in comparison with the controls. Such output proved that the functionalization of PLGA nanoparticles with aptamers may be associated with the successful delivery of conventional chemotherapeutic agents, by enhancing their therapeutic efficacy, and thus constituting a potential cancer therapy approach [53].

Quite recently, a hybrid nanosystem was produced using PLGA nanoparticles as the core, and cationic lipids (DOTMA) as the shell [61]. These nanosystems were designated as lipid–polymer hybrid nanoparticles (LPNs) and were prepared by double-emulsion solvent evaporation [61,70]. The LPNs were coupled with mRNA–mCherry, which encodes the mCherry fluorescent protein [61]. The mRNA–LPNs nanocomplexes were produced at different mRNA-to-LPNs ratios (1:10; 1:20 and 1:30) and compared with the same ratios of mRNA–chitosan–modified PLGA nanocomplexes. The mRNA–chitosan–PLGA nanocomplexes (< 176 nm) exhibited a smaller particle size when compared to the mRNA–LPNs nanocomplexes (< 322 nm), although the pI of the mRNA–chitosan–PLGA nanocomplexes was slightly higher (< 0.3) than the pI of mRNA–LPNs nanocomplexes (< 0.2). The zeta potential of mRNA–chitosan–PLGA nanocomplexes and mRNA–LPNs nanocomplexes was positive, except in the mRNA–LPNs nanocomplexes at a ratio of 1:10, where the zeta potential was neutral (0 mV), suggesting the instability of the system. Nevertheless, in the bone marrow-derived murine dendritic cell line (DC2.4 cell line), the mRNA–LPNs nanocomplexes—at a ratio of 1:10—achieved a transfection rate of c. 40%, exhibiting higher transfection efficiency and protein translation at higher w/w mRNA-to-LPNs ratios (1:20 and 1:30, c. 80%). Still, the transfection efficiency and protein translation were higher with mRNA–LPNs nanocomplexes than with mRNA–chitosan–PLGA nanocomplexes (c. 5%). The same was observed in lung cancer cells (A549 cell line), in which the transfection of mRNA–LPNs at a ratio 1:30 was c. 60%. Additionally, according to the gel retardation assay, the transfection kinetics is quick (i.e., the mRNA is released from the mRNA–LPNs after 15 min incubation with heparin). The higher transfection efficiency and kinetics may be related to the additional hydrophobic interactions that DOTMA establishes with the PLGA surface. This data suggests the functionalized mRNA hybrid nanosystems proposed by Yasar and coworkers may constitute a novel and compelling strategy for gene-based vaccines [61].

Overall, the delivery of nucleic acids through the surface functionalization of nanoparticles enables, first and foremost, a rapid release of kinetics,

which blocks the enzymatic degradation of these unstable macromolecules, enhances their stability, and circumvents the exposure of themolecules to the stringent conditions of nanoparticle production.

In gene-based therapies, nanoparticles have shown higher transfection efficiency rates than conventional transfection agents and polymers. Polymeric nanoparticles are emphasized as eligible candidates for genetic material delivery, chiefly due to their biodegradable biocompatible natures, their propensity for scale-up, and easy functionalization through the use of noncovalent interactions [64]. Nevertheless, the application of polymeric nanoparticles, such as PLGA nanoparticles, in gene-based therapies is still evolving and further in vivo experiments are needed to corroborate the in vitro findings obtained so far.

## 8.5 Concluding remarks

Following recognition of PLGA nanoparticles as effective novel delivery systems, targeting these particles has opened new pathways for providing customized, safer, and thereby more effective treatments to patients. Surface modification of PLGA nanoparticles by means of noncovalent surface interactions is feasible, and although not as robust as covalent modification, could be an interesting field to explore for improving the delivery of biomacromolecules.

## Acknowledgements

J. A. D. S. gratefully acknowledges Fundação para a Ciência e a Tecnologia (FCT) and Tecnimede-S.A. for the PhD research grant PD/BDE/135148/2017.

I. P. acknowledges the Ph.D. research grant SFRH/BD/136892/2018 funded by Fundação para a Ciência e a Tecnologia (FCT) and Programa Operacional Capital Humano (POCH).

## References

- [1] Mout R, et al. Surface functionalization of nanoparticles for nanomedicine. *Chem Soc Rev* 2012;41(7):2539–44.
- [2] Kumari A, Yadav SK, Yadav SC. Biodegradable polymeric nanoparticles based drug delivery systems. *Colloids Surf B Biointerfaces* 2010;75(1):1–18.
- [3] Zhang J, Saltzman M. Engineering biodegradable nanoparticles for drug and gene delivery. *Chem Eng Prog* 2013;109(3):25–30.
- [4] Rizvi SAA, Saleh AM. Applications of nanoparticle systems in drug delivery technology. *Saudi Pharm J SPJ Off Publ Saudi Pharm Soc* 2018;26(1):64–70.
- [5] Wang X-Q, Zhang Q. pH-sensitive polymeric nanoparticles to improve oral bioavailability of peptide/protein drugs and poorly water-soluble drugs. *Eur J Pharm Biopharm Off J Arbeitsgemeinschaft fur Pharmazeutische Verfahrenstechnik eV* 2012;82(2):219–29.
- [6] Fu K, Klibanov AM, Langer R. Protein stability in controlled-release systems. *Nat Biotech* 2000;18(1):24–5.



- [7] Musthaba SM, et al. Status of novel drug delivery technology for phytotherapeutics. *Expert Opin Drug Delivery* 2009;6(6):625–37.
- [8] Ajazuddin, Saraf S. Applications of novel drug delivery system for herbal formulations. *Fitoterapia* 2010;81(7):680–9.
- [9] Peer D, et al. Nanocarriers as an emerging platform for cancer therapy. *Nat Nanotechnol* 2007;2(12):751–60.
- [10] Danhier F, et al. PLGA-based nanoparticles: an overview of biomedical applications. *J Controlled Release Off J Controlled Rel Soc* 2012;161(2):505–22.
- [11] Witt C, Mäder K, Kissel T. The degradation, swelling and erosion properties of biodegradable implants prepared by extrusion or compression moulding of poly(lactide-*co*-glycolide) and ABA triblock copolymers. *Biomaterials* 2000;21(9):931–8.
- [12] Sharma S, et al. PLGA-based nanoparticles: a new paradigm in biomedical applications. *TrAC Trends Anal Chem* 2016;80:30–40.
- [13] Jain RA. The manufacturing techniques of various drug loaded biodegradable poly(lactide-*co*-glycolide) (PLGA) devices. *Biomaterials* 2000;21:2475–90.
- [14] Kleiner LW, Wright JC, Wang Y. Evolution of implantable and insertable drug delivery systems. *J Controlled Rel* 2014;181(1):1–10.
- [15] Lee S, Lee DY. Glucagon-like peptide-1 and glucagon-like peptide-1 receptor agonists in the treatment of type 2 diabetes. *Ann Pediatric Endocrinol Metab* 2017;22(1):15–26.
- [16] Ratzinger G, et al. The role of surface functionalization in the design of PLGA micro- and nanoparticles. *Crit Rev Therapeutic Drug Carr Syst* 2010;.
- [17] Kamaly N, et al. Degradable controlled-release polymers and polymeric nanoparticles: mechanisms of controlling drug release. *Chem Rev* 2016;116(4):2602–63.
- [18] Sequeira JAD, et al. Poly(lactic-*co*-glycolic acid) (PLGA) matrix implants. In: Grumezescu AM, editor. *Nanostructures for the engineering of cells, tissues and organs*. Oxford: Elsevier; 2018. p. 375–402 (Chapter 10).
- [19] Stevenson CL, Rhodes CA, Prestrelski SJ. Delivery of peptides and proteins via long acting injections and implants. In: Jeremy C, Wright JC, Burgess DJ, editors. *Long acting injections and implants*. New York: Springer; 2012. p. 409–27 (Chapter 20).
- [20] Alexis F. Factors affecting the degradation and drug-release mechanism of poly(lactic acid) and poly[(lactic acid)-*co*-(glycolic acid)]. *Polym Int* 2005;54(1):36–46.
- [21] Lao LL, et al. Modeling of drug release from bulk-degrading polymers. *Int J Pharm* 2011;418(1):28–41.
- [22] Kapoor DN, et al. PLGA: a unique polymer for drug delivery. *Therap Delivery* 2015;6(1):41–58.
- [23] Hines DJ, Kaplan DL. Poly(lactic-*co*-glycolic) acid-controlled-release systems: experimental and modeling insights. *Crit Rev Therap Drug Carr Syst* 2013;30(3):257–76.
- [24] Gentile P, et al. An overview of poly(lactic-*co*-glycolic) acid (PLGA)-based biomaterials for bone tissue engineering. *Int J Mol Sci* 2014;15(3):3640–59.
- [25] Yeo Y, Park K. Control of encapsulation efficiency and initial burst in polymeric micro-particle systems. *Arch Pharmacol Res* 2004;27(1):1–12.
- [26] Fessi H, et al. Nanocapsule formation by interfacial polymer deposition following solvent displacement. *Int J Pharm* 1989;55(1):R1–4.
- [27] Mora-Huertas CE, Fessi H, Elaissari A. Polymer-based nanocapsules for drug delivery. *Int J Pharm* 2010;385(1–2):113–42.
- [28] Nie S. Understanding and overcoming major barriers in cancer nanomedicine. *Nanomed (London, Engl)* 2010;5(4):523–8.



- [29] Song G, et al. Nanoparticles and the mononuclear phagocyte system: pharmacokinetics and applications for inflammatory diseases. *Curr Rheumatol Rev* 2014;10(1):22–34.
- [30] Storm G, et al. Surface modification of nanoparticles to oppose uptake by the mononuclear phagocyte system. *Adv Drug Deliv Rev* 1995;17(1):31–48.
- [31] Sah H, et al. Concepts and practices used to develop functional PLGA-based nanoparticle systems. *Int J Nanomed* 2013;8:747–65.
- [32] Tenzer S, et al. Rapid formation of plasma protein corona critically affects nanoparticle pathophysiology. *Nat Nanotechnol* 2013;8(10):772–81.
- [33] Heinz H, et al. Nanoparticle decoration with surfactants: molecular interactions, assembly, and applications. *Surf Sci Rep* 2017;72(1):1–58.
- [34] Sempf K, et al. Adsorption of plasma proteins on uncoated PLGA nanoparticles. *Eur J Pharm Biopharm Off J Arbeitsgemeinschaft fur Pharmazeutische Verfahrenstechnik eV* 2013;85(1):53–60.
- [35] Thamake SI, et al. Surface functionalization of PLGA nanoparticles by non-covalent insertion of a homo-bifunctional spacer for active targeting in cancer therapy. *Nanotechnology* 2011;22(3):035101.
- [36] Oliveira CL, et al. Characterization of polymeric nanoparticles for intravenous delivery: focus on stability. *Colloids Surf B, Biointerfaces* 2017;150:326–33.
- [37] Xu Y, et al. Polymer degradation and drug delivery in PLGA-based drug-polymer applications: a review of experiments and theories. *J Biomed Mater Res Part B, Appl Biomater* 2017;105(6):1692–716.
- [38] Knop K, et al. Poly(ethylene glycol) in drug delivery: pros and cons as well as potential alternatives. *Angew Chem (Int ed Engl)* 2010;49(36):6288–308.
- [39] Veronese FM, Mero A. The impact of PEGylation on biological therapies. *BioDrugs Clin Immunotherap Biopharm Gene Ther* 2008;22(5):315–29.
- [40] Gref R, et al. Poly(ethylene glycol)-coated nanospheres: potential carriers for intravenous drug administration. *Pharm Biotechnol* 1997;10:167–98.
- [41] Vonarbourg A, et al. Parameters influencing the stealthiness of colloidal drug delivery systems. *Biomaterials* 2006;27(24):4356–73.
- [42] Petros RA, DeSimone JM. Strategies in the design of nanoparticles for therapeutic applications. *Nat Rev Drug discovery* 2010;9(8):615–27.
- [43] Li Y, et al. PEGylated PLGA nanoparticles as protein carriers: synthesis, preparation and biodistribution in rats. *J Controlled Release Off J Controlled Rel Soc* 2001;71(2):203–11.
- [44] Venkatraman SS, et al. Micelle-like nanoparticles of PLA-PEG-PLA triblock copolymer as chemotherapeutic carrier. *Int J pharmaceutics* 2005;298(1):219–32.
- [45] Kim SH, et al. Target-specific cellular uptake of PLGA nanoparticles coated with poly(L-lysine)-poly(ethylene glycol)-folate conjugate. *Langmuir: ACS J Surf colloids* 2005;21(19):8852–7.
- [46] Farokhzad OC, et al. Targeted nanoparticle-aptamer bioconjugates for cancer chemotherapy in vivo. *Proc Natl Acad Sci USA* 2006;103(16):6315–20.
- [47] McCall RL, Sirianni RW. PLGA nanoparticles formed by single- or double-emulsion with vitamin E-TPGS. *J Visualized Exp JoVE* 2013;51015 (December).
- [48] Niwa T, et al. Preparations of biodegradable nanospheres of water-soluble and insoluble drugs with D,L-lactide/glycolide copolymer by a novel spontaneous emulsification solvent diffusion method, and the drug release behavior. *J Controlled Rel* 1993;25:89–98.
- [49] Swider E, et al. Customizing poly(lactic-co-glycolic acid) particles for biomedical applications. *Acta Biomater* 2018;73:38–51.

- [50] Moghimi SM, Hunter AC. Poloxamers and poloxamines in nanoparticle engineering and experimental medicine. *Trends Biotechnol* 2000;18(10):412–20.
- [51] Mu L, Seow PH. Application of TPGS in polymeric nanoparticulate drug delivery system. *Colloids Surf B, Biointerfaces* 2006;47(1):90–7.
- [52] Win KY, Feng S-S. Effects of particle size and surface coating on cellular uptake of polymeric nanoparticles for oral delivery of anticancer drugs. *Biomaterials* 2005;26(15):2713–22.
- [53] Taghavi S, et al. Chitosan-modified PLGA nanoparticles tagged with 5TR1 aptamer for in vivo tumor-targeted drug delivery. *Cancer Lett* 2017;400:1–8.
- [54] Ravi Kumar MNV, Bakowsky U, Lehr CM. Preparation and characterization of cationic PLGA nanospheres as DNA carriers. *Biomaterials* 2004;25(10):1771–7.
- [55] Sharon N, Lis H. History of lectins: from hemagglutinins to biological recognition molecules. *Glycobiology* 2004;14(11):53R–62R.
- [56] Ghotbi Z, et al. Active targeting of dendritic cells with mannan-decorated PLGA nanoparticles. *J Drug Target* 2011;19(4):281–92.
- [57] Weiss B, et al. Coupling of biotin-(poly(ethylene glycol))amine to poly(D,L-lactide-co-glycolide) nanoparticles for versatile surface modification. *Bioconjugate Chem* 2007;18(4):1087–94.
- [58] Chang J, et al. Transferrin adsorption onto PLGA nanoparticles governs their interaction with biological systems from blood circulation to brain cancer cells. *Pharm Res* 2012;29(6):1495–505.
- [59] Obermajer N, et al. Immunonanoparticles--an effective tool to impair harmful proteolysis in invasive breast tumor cells. *FEBS J* 2007;274(17):4416–27.
- [60] Jeon SY, et al. Co-delivery of SOX9 genes and anti-Cbfa-1 siRNA coated onto PLGA nanoparticles for chondrogenesis of human MSCs. *Biomaterials* 2012;33(17):4413–23.
- [61] Yasar H, et al. Kinetics of mRNA delivery and protein translation in dendritic cells using lipid-coated PLGA nanoparticles. *J Nanobiotechnol* 2018;16(1):72.
- [62] Taetz S, et al. The influence of chitosan content in cationic chitosan/PLGA nanoparticles on the delivery efficiency of antisense 2'-O-methyl-RNA directed against telomerase in lung cancer cells. *Eur J Pharm Biopharm Off J Arbeitsgemeinschaft fur Pharmazeutische Verfahrenstechnik eV* 2009;72(2):358–69.
- [63] Park JS, et al. Chondrogenesis of human mesenchymal stem cells mediated by the combination of SOX trio SOX5, 6, and 9 genes complexed with PEI-modified PLGA nanoparticles. *Biomaterials* 2011;32(14):3679–88.
- [64] Wang J, et al. Evaluation of cationic nanoparticles of biodegradable copolymers as siRNA delivery system for hepatitis B treatment. *Int J Pharm* 2010;400(1–2):194–200.
- [65] Rinaldi C, Wood MJA. Antisense oligonucleotides: the next frontier for treatment of neurological disorders. *Nat Rev Neurol* 2018;14(1):9–21.
- [66] Lam JKW, et al. siRNA versus miRNA as therapeutics for gene silencing. *Mol Ther Nucleic acids* 2015;4(9) pp. e252–e252.
- [67] Watson JD, et al. Nucleic acids convey genetic information. *Molecular biology of the gene*, 41. Pearson Education, Inc; 2014. p. 33–5.
- [68] Silva AC, et al. Nucleic acids delivery systems: a challenge for pharmaceutical technologists. *Curr Drug Metab* 2015;16(1):3–16.
- [69] Watson JD, et al. Techniques of molecular biology. *Molecular biology of the gene*. Pearson Education, Inc; 2014. p. 154–5.
- [70] Jensen DK, et al. Design of an inhalable dry powder formulation of DOTAP-modified PLGA nanoparticles loaded with siRNA. *J Controlled Release Off J Controlled Rel Soc* 2012;157(1):141–8.

This page intentionally left blank

## Chapter 9

# Biomedical-related applications of functionalized nanomaterials

Mafalda R. Almeida<sup>1</sup>, Márcia C. Neves<sup>1</sup>, Sergio Morales-Torres<sup>2</sup>,  
Mara G. Freire<sup>1</sup>, Joaquim L. Faria<sup>3</sup>, Valéria C. Santos-Ebinuma<sup>4</sup>,  
Cláudia G. Silva<sup>3</sup> and Ana P.M. Tavares<sup>1</sup>

<sup>1</sup>CICECO-Aveiro Institute of Materials, Department of Chemistry, University of Aveiro, Aveiro, Portugal, <sup>2</sup>Carbon Materials Research Group, Department of Inorganic Chemistry, Faculty of Sciences, University of Granada, Granada, Spain, <sup>3</sup>Laboratory of Separation and Reaction Engineering-Laboratory of Catalysis and Materials (LSRE–LCM), Faculdade de Engenharia, Universidade do Porto, Porto, Portugal, <sup>4</sup>Department of Engineering Bioprocess and Biotechnology, School of Pharmaceutical Sciences, UNESP-University Estadual Paulista, Araraquara, Brazil

### 9.1 Introduction

The area of nanomaterial research has continued to grow due to the materials' unique properties at the nanoscale, which make nanoparticles (NPs) a promising tool for developing innovative, bio-based technologies within the biomedical field. Accordingly the number of scientific papers related to NPs in this field has also been continuously increasing through the years (Fig. 9.1) illustrating how NPs may be used in the design, process, action and delivery disposition of drugs. NPs can be prepared from a wide variety

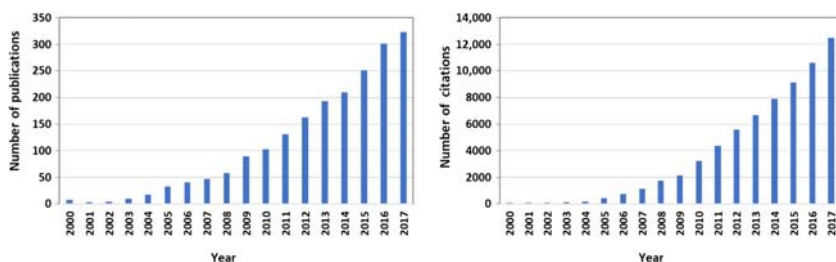


**FIGURE 9.1** Number of publication entries and total citations referring to keywords “functionalized nanoparticles and drugs” from 2006 to 2017 (search on the ISI Web of Knowledge, November 2018).

of materials and modified with various functional groups or ligands, allowing them to display specific properties and to be applied in a range of applications.

This chapter provides an overview on the use of NPs in the biomedical sector, including the methods to functionalize them and their applications in the biomedical field. This book chapter is useful to graduates, postgraduates, senior researchers, educators, and scientists working in biomedicine, pharmacy, biotechnology, nanotechnology, and related areas.

## 9.2 Functionalized nanoparticles in the biopharmaceutical sector

Biopharmaceuticals are products derived from biological sources used as therapeutic and medical solutions to treat diseases and pathological conditions, while pharmaceuticals are products derived from the synthesis of chemical compounds [1]. According to a report by Mordor Intelligence, it is expected that the pharmaceutical market will present a compound annual growth rate (CAGR) of 8.5% from 2018 to 2023, reaching a market value of USD 341.16 billion in 2023 [2]. The biopharmaceuticals market growth results from the high efficacy and safety of these drugs and their ability to improve the quality of life and reduce death rates in patients with chronic diseases [2]. Although there are several studies focusing on the development of biopharmaceutical production processes (upstream and downstream processes) [1,3,4], an important challenge for the biopharmaceutical industry is to expand the use of these compounds. Fig. 9.2 summarizes the related applications of functionalized nanomaterials in biomedicinal and pharmaceutical areas. NPs and functionalized NPs have been used in fields such as drug- and gene-delivery, separation and purification of biological molecules and cells, biodetection of pathogens, and detection of proteins.

NPs have been used in different industrial applications [6], such as in the separation and purification processes of bio-based therapeutics. For instance, Mesgari-Shadi et al. [7] used nanozeolite microspheres to purify scFv antibodies produced by *Escherichia coli* HB2151 cells, achieving a scFv purity of 90% with a purification yield of 60%. Magnetic NPs are another type of nanomaterial commonly used to extract and purify bioproducts, according to a study by Gädke et al. [8]. Gold nanoparticles were functionalized with the papain enzyme with the goal of producing a heterogenous biocatalyst, which has been used in bionalysis and biopharmaceutical analysis [9].

One of the most relevant and frequently researched applications of functionalized materials in the biomedical field is their use as drug delivery systems (DDS) where NPs act as carriers protecting the specific drug from degradation and releasing it in the target tissue/cell, while improving the drug bioavailability [5]. It is important to note that the material used for the pharmaceuticals' delivery must be biocompatible and biodegradable, or at



**FIGURE 9.2** Functionalized nanomaterials and their biomedical-related applications. *Adapted from Robles-García MA, Rodríguez-Félix F, Márquez-Ríos E, Aguilar JA, Barrera-Rodríguez A, Aguilar J, et al. Applications of nanotechnology in the agriculture, food, and pharmaceuticals J Nanosci Nanotechnol 2016;16(8):8188–8207 [5].*

least able to be totally eliminated from the body since it will have intimate contact with biological systems and an immunogenic reaction must be avoided [5,10].

Several functionalized NPs have been used as DDS. For example, carbon nanomaterials such as carbon nanotubes (CNT), carbon nanohorns (CNH), graphene oxide (GO), and surface functionalized silica (silicon dioxide), and silicon-based particles have been proposed for delivering pharmaceuticals through oral administration [11]. More details on the preparation of these materials are given below. Carbon nanomaterials have been specifically researched for their use in the delivery of anticancer drugs [12]. The major advantages of carbon nanomaterials include their ease of fabrication, chemically inert properties, and tailorable physicochemical properties [11,13]. Metallic carrier systems also have been considered to deliver drugs. For example, Unamuno et al. [14] studied Fe and Zr-carboxylated metal–organic frameworks (nanoMOFs) to encapsulate the aminoglycoside antibiotic Gentamicin, demonstrating that this system preserved the antibiotic characteristics under the intestinal conditions [14]. Other metal particles such as gold-NPs [15] and supramagnetic metal oxides (iron oxides:  $\text{Fe}_2\text{O}_3$  or  $\text{Fe}_3\text{O}_4$ ) [16] have also been studied for oral delivery applications.

Due to their great capacity for increasing photoelectric interactions at lower energy levels, functionalized gold-NPs have been studied for radiosensitizing and imaging cancer cells. These materials are able to enhance the impacts of radiotherapy by increasing the energy deposition in tumor tissues [17]. Since DDS are the main application of functionalized NPs, a specific section devoted to this topic is presented after the description of the NPs types and their synthesis.

## 9.3 Types and synthesis procedures of functionalized nanomaterials

### 9.3.1 Metal-based nanoparticles

Metal-based nanoparticles (metal-NPs) have captured the attention of many scientists for over a century due to their unique properties, which allow them wide applications in biomedical and pharmaceutical sciences, in biotechnology, and in engineering. Metal-NPs can be used in magnetic separation, pre-concentration of target analytes, targeted drug- and gene-delivery, and diagnostic imaging [18]. Metal-NPs can also be synthesized and modified with several chemical functional groups, allowing them to specifically bind to antibodies, ligands, drugs, and other related biomolecules [18].

Metal-NPs are made simply through metal precursors, and all stable metals can be used to synthesize nanoparticles [19]. However some noble metal-NPs, such as silver and gold, have been gaining more attention due to their unique properties and diversity of applications [20]. Although the most widely used nanoparticles are silver-NPs, due to their antimicrobial and antifungal properties gold-NPs have also gained a lot of interest because they can be easily functionalized with various targeting ligands [20]. It is advisable in pharmaceutical applications to functionalize the metal-NPs surface because this helps maintain properties such as stability, adsorption characteristics, therapeutic efficacy, and targeting ability. Additionally, functionalizing the metal-NPs surface can also help with other challenges, such as in in vivo environment (e.g., reticulo-endothelial system) detection, adsorption of antibodies, cells, thiols and proteins, and cell uptake processes [21]. There are many metal-NPs surface functionalization methods including PEGylation (i.e., the process of attaching metal-NPs surfaces with engrafted polymer chains, such as polyethylene glycol (PEG)) [21], thiol functionalization, layer by layer (LbL) assembly, coating with biomolecules, and silica coating [21].

PEGylation is a commonly applied method because it can customize the surface properties of metal-NPs, allowing the targeting moieties to covalently bond to the free ends of tethered chains, making metal-NPs that specifically and firmly bind to receptors on the surface of the diseased cell [22,23]. After selecting the proper PEG, the next step is annealing it to the metal-NP

surface. Both covalent and noncovalent methods can be used. For solid NPs such as gold, thiol binding is the classic approach where a sulfhydryl-capped PEG chain adheres to the gold surface [24].

Thiol functionalization involves thiolate monolayers assembled on different bulk surfaces such as silver, gold, or platinum [25]. The thiol monolayers are covalently linked to the surfaces by the reaction of the metal-NPs surfaces with the respective thiols, and, for some metals, by their reaction with disulfides [25]. For gold-NPs surfaces, two different mechanisms for thiol functionalization are applied [26,27]. One mechanism involves the reduction by thiol of the gold's upper surface oxide sublayer, establishing a gold-thiolate bond, while the other mechanism involves hydrogen evolution by the gold-mediated reduction of the thiol protons, which could lead to the gold-thiolate bonding. The formation of the gold-thiolate bond in the presence of disulfide is a redox process, where the gold surface is oxidized by disulfide and the disulfide bond is cloven [25–27].

The LbL method is the most widely used method for metal-NPs surface functionalization due to the easy coating and good control over the resulting biofilm's thickness [21]. Alternate adsorption of cationic and/or anionic polyelectrolytes on the metal-NPs surfaces results in polyelectrolyte multilayers. Although most of the reported LbL films are driven by electrostatic interactions, other interactions such as hydrogen bonding are also used in LbL assembly [28]. Availability of various polyelectrolytes provides the option to vary the surface charge of metal-NPs from positive to negative, and that might play a key role in biological applications [29].

The metal-NPs functionalization with biomolecules is vital in developing biocompatible platforms with minimal toxicity for various biopharmaceutical applications. Molecules such as folic acid, DNA, proteins, and oligonucleotides can be used in surface functionalization of metal-NPs [21]. For instance, there are three ways to functionalize gold-NPs with functional groups or biomolecules: (1) by binding with functional groups of self-assembled monolayer (SAMs); (2) by direct deposition of gold colloid onto the electrode surface; and (3) by co-modification of mixed gold colloid with other components in the composite electrode matrix [30]. Proteins or enzymes can readily be immobilized on colloid gold by dipping a protein solution onto the colloid, gold-modified, electrode surface. The electrostatic interaction between the negatively charged citrate surface of colloidal gold and positively charged groups of the protein leads to the adsorption of protein onto the electrode surface. SAMs can provide a simple way to tailor surfaces with well-defined compositions, structures, and thickness, which can then be employed as specific functionalized surfaces for the immobilization of gold nanoparticles and enzymes [30]. Gold-NPs-modified electrode surfaces can be prepared by covalently binding gold-NPs with surface functional groups ( $-\text{CN}$ ,  $-\text{NH}_2$ , or  $-\text{SH}$ ) of SAMs-modified solid surfaces [30]. Short-chain molecules, such as cysteamine (Cyst) and



3-mercaptopropionic acid (MPA), can be self-assembled on the gold disk electrode for further binding of gold-NPs.

Metal-NPs covered with silica have become increasingly important in the last decade for many promising catalytic and biomedical applications [31]. This type of material exhibits colloidal stability, as well as low level nonspecific binding with biological matrices and molecules. In the late 1960s Stöber et al. developed the sol-gel chemistry (i.e., a method based on the hydrolysis of tetra-alkyl silicate in a homogeneous alcoholic medium, using ammonia as a catalyst) of silicon alkoxides for growing monodisperse, spherical, silica nanoparticles in basic aqueous solutions containing different alcohols, such as methanol, ethanol, or isopropanol [32].

Based on the well-established Stöber method, gold colloid nanoparticles were developed by Liz-Marzán et al. [33]. The method includes the weak surface attachment of the bifunctional (3-aminopropyl) trimethoxysilane in aqueous solution. The  $\text{-NH}_2$  groups are bound to the gold surface, and  $\text{-Si(OEt)}_3$  groups are extended outward for hydrolysis and condensation with sodium silicate to deposit a thin surface-protective silica layer, so as to be transferred into alcohols to form a stable water/alcohol solution of gold-NPs [33]. Then, thicker silica shells can be grown on surface-stabilized gold-NPs by further hydrolysis/condensation of tetraethyl orthosilicate, a typical precursor of silicon alkoxides [33] (see Fig. 9.3). By modifying the silica-coating with a variety of functional groups using silane and silane-coupling agents, the intrinsic surface properties of silica-coated metal-NPs can be easily manipulated according to the intended application [21]. Prior to silica-coating, numerous surface-attachment strategies have been developed in

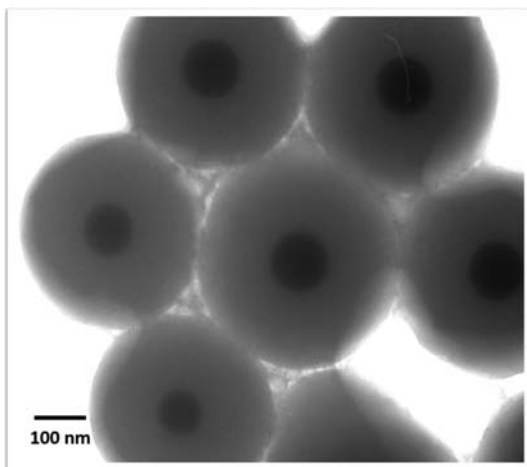


**FIGURE 9.3** Scanning electron microscopy (SEM) of gold-NPs (core) covered with silica (shell) by the Stöber method.

aqueous solutions using bifunctional molecules by means of strong surface-coordination or electrostatic interaction onto metal-NPs for creating colloiddally stable, surface-protected NPs in alcoholic solutions. This surface-protected NPs interface needs to have reactive hydroxyl groups to facilitate the hydrolysis/condensation of tetraethyl orthosilicate [31].

### 9.3.2 Silica nanoparticles

Silica is a commonly used material due to its excellent thermal and mechanical properties, and it is currently used in a wide variety of areas, such as paints and coatings, electrical and thermal insulation, moisture and flame retardants, catalysis, chromatography, and in the cosmetic, pharmaceutical, and food industries [34]. There is also solid scientific knowledge about silica and its derivatives regarding the preparation of silica colloids and NPs of different sizes in the nanometric range [34]. The synthesis of silica is based on relatively simple methods that deliver high purity samples and narrow size distributions. Beyond these advantages, the raw materials' low cost and the process of silica fabrication has boosted the use of silica NPs in several industrial applications [34]. Silica nanomaterials have been synthesized and functionalized in order to be applied in controlled release, purification and synthesis, coatings, catalysis, and sensing [35]. Due to the high tunability of silica NPs, they have been specifically engineered for drug delivery, including genes for gene therapy [35].

Silica NPs are usually obtained from alkoxy silanes through hydrolysis followed by condensation reactions involving oligomeric species, with tetraethoxysilane (TEOS) as one of the most used precursors. The most common method to prepare silica NPs, the Stöber, or sol-gel, method [32], allows the control of the particles' dimensions down to spherical submicrometric silica particles by varying the reaction parameters. An example of the morphology of silica NPs is given in Fig. 9.4. These particles have a narrow size distribution, with size ranging from tens to hundreds of nanometers [32]. Due to the existence of silanol (Si-OH) groups on the surface of the silica particles, their reactivity can be altered by thermal treatments, and covalent bonds can be established through these groups [36].

With improved properties, mesoporous silica nanoparticles (MSN) have emerged in recent decades. These porous materials have high thermal and chemical stability, high hydrophilicity, enriched surface by silanol groups, easy surface modifications, high surface area, and tunable pore size and pore volume. These improved characteristics make these materials suitable for drug delivery, transport of therapeutics, and/or encapsulation of target molecules [37–40].

MSN can be synthesized by several methods, one of them being the sol-gel method. A common synthetic route to obtain MSN is a modified Stöber synthesis based on the use of templates that act as structure directing agents

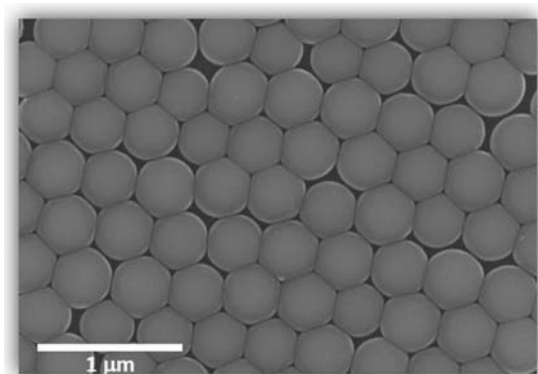


**FIGURE 9.4** Scanning electron microscopy (SEM) of spherical silica particles obtained by the Stöber method.

[41,42]. The most common are surfactants (such as cetyltrimethylammonium bromide (CTAB) and dodecyltrimethylammonium bromide (DTAB)) and/or micelle forming agents or polymers. The concentrations and compositions of silica sources, template-agents, temperature, and stirring conditions produce materials with different properties in terms of particle size, pore size, pore volume, and shape [37]. The surfactant content constrains the particle morphology since it changes the hydrolysis of the alkoxide and the micellization of the surfactant [41,43]. Vazquez et al. [41] studied the synthesis of several MSN that could be used as drug deliverable containers. These particles were produced by the sol-gel method with TEOS as the alkoxide precursor and CTAB as the surfactant. By fixing the molar ratio of TEOS/EtOH to 1/20 and by varying the molar ratio of  $\text{H}_2\text{O}/\text{NH}_3 \cdot \text{H}_2\text{O}/\text{CTAB}$ , the particle morphology changed from dispersed nanospheres to agglomerates [41]. No pore size changes were observed, and particles were obtained with pore diameters from 2.5 to 2.8 nm [41]. Although MSN size and shape have a large influence on the NPs' behavior, the surface modifications have an even more relevant impact.

One of the most common ways of obtaining functionalized silica materials is through reaction with alkoxy silanes. This type of functionalization not only allows for functionalized materials with different functional groups, but also for the ability to use these molecules as a bridge to connect to others. The silica surface can be chemically functionalized with silicon alkoxides, such as methyltriethoxysilane (Me-TES), 3-mercaptopropyltriethoxysilane (SH-PTES), 3-glycidoxypyltriethoxysilane (Gly-PTES), 3-chloropropyltriethoxysilane (Cl-PTES), phenyltriethoxysilane (Ph-TES), 3-(2-(2-aminoethylamino)ethylamino)propyltrimethoxysilane (NHNH<sub>2</sub>-PTMS) or amino propyl trimethoxysilane (NH<sub>2</sub>-PTMS) [38,42–45].

Regarding the functionalization of already synthesized silica materials, silica and the silane-coupling reagent are added to toluene, and the mixture

is heated and refluxed [46]. Depending on the size of the silica materials, the solid is collected by centrifugation or by filtration, and the precipitate washed with toluene and other solvents such as ethanol, water, and methanol, and then dried at room temperature. The composition of silica materials can be controlled by hydrolysis/condensation of the organosilane compounds or by co-condensation of silica precursors [46].

As mentioned above, in some cases, the functionalization with the alkoxy silane is an intermediate step in which this molecule acts as a bridge for other molecules. MSN organo-functionalized with g-glycidoxypolytrimethoxysilane (–Gly), phenyltriethoxysilane (–Ph) and 3-mercaptopropyltrimethoxysilane (–SH) were further functionalized with protein-A by its addition to a phosphate buffer (pH 7.4) dispersion with the previous prepared MSN [44]. An additional example is related to the preparation of  $\text{SiO}_2\text{-SH/IDA-Ni}^{2+}$ . In this case, after the synthesis of silica functionalized with thiol groups ( $\text{SiO}_2\text{-SH}$ ) by a hydrothermal method, a second functionalization is performed with 3-glycidoxypolytriethoxysilane-iminodiacetic acid (IDA), achieving  $\text{SiO}_2\text{-SH/IDA}$ , followed by a third step related to the chelation of  $\text{Ni}^{2+}$  [47]. The compound (3-glycidylxypropyl)trime-thoxysilane (GPTMS) was used as a bridge to link MSN and chitosan, loaded with doxorubicin hydrochloride (DOX) [48]. By an acid-catalyzed amino-oxirane addition reaction, chitosan reacts with  $\text{SiO}_2\text{-Gly}$  [49]. Curcumin (CCM) amino-functionalized silica ( $\text{CCM/SiO}_2\text{-NH}_2$ ) was prepared by ammonia-catalyzed hydrolysis of TEOS, in the presence of CCM, and then functionalized with 3-(aminopropyl)-triethoxysilane (APTES). This material was further functionalized with folate using water-soluble carbodiimides (EDC) and *N*-hydroxysuccinimide (NHS). The carboxyl groups of folic acid were activated with EDC in the presence of NHS and reacted with the amino groups of  $\text{CCM/SiO}_2\text{-NH}_2$  by forming stable amide bonds, leading to  $\text{CCM/SiO}_2\text{-FO}$  [49].

Silica NPs can also be modified with enzyme molecules (glutamate dehydrogenase (GDH) and lactate dehydrogenase (LDH)) [45]. According to the authors, after getting the amino-functionalized silica with 3-(2-(2-aminoethylamino) ethylamino) propyltrimethoxysilane ( $\text{NHNH}_2\text{-PTMS}$ ) the particles are treated with succinic anhydride in dimethylformamide solution, resulting in carboxylate modified particles. The nanoparticles were then treated with GDH or LDH in phosphate buffer solutions [45]. Anti-IgG was also immobilized on the surface of silica materials after the functionalization with methyltriethoxysilane (Me-TES), 3-mercaptopropyltriethoxysilane (SH-PTES), 3-glycidoxypolytriethoxysilane (Gly-PTES), or 3-aminopropyltriethoxysilane ( $\text{NH}_2\text{-PTES}$ ) [43].

Silica functionalization with ionic liquids (ILs) has also been reported in which, in an intermediate step, the silica surface hydroxyl groups react with a functional alkoxy silane, namely 3-chloropropyltriethoxysilane [50].  $\text{SiO}_2\text{-Cl}$  is then refluxed in toluene with the molecule that originates the cation of

the IL: imidazole, 1-methylimidazole, and 2-ethyl-4-methylimidazole [50]. The material obtained is washed with toluene, ethanol, and methanol, and dried to obtain a supported IL silica material [51].

The LbL technique, as previously described, can also be used to functionalize MSN with polyelectrolytes (see Fig. 9.5), given that polyelectrolytes are commonly used as blocking materials in pH-responsive drug delivery. The number of layers of the polycation, that is, polyallylamine hydrochloride (PAH), and of the polyanion, that is, polystyrene sulfonate (PSS), onto the surface of MSN influences the release profiles of the target molecule [52].

In summary, modified silica NPs have several applications in the biopharmaceutical and biomedical field, for which specific examples are given in Table 9.1.

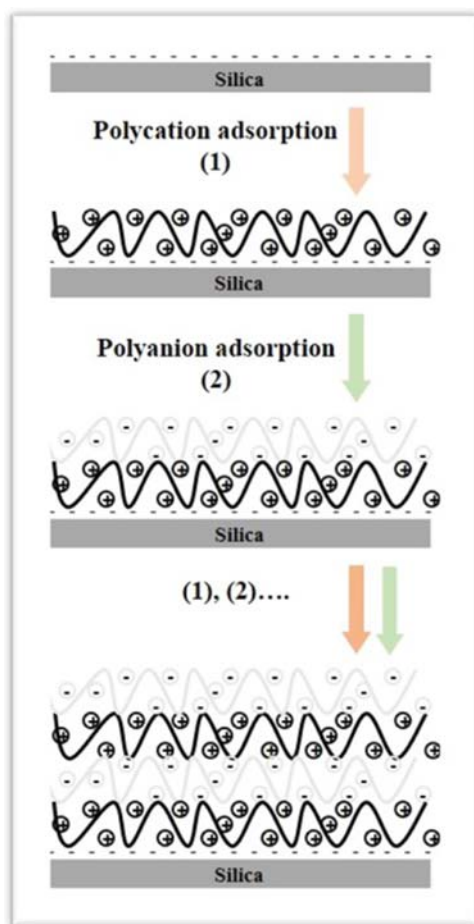


FIGURE 9.5 Scheme of polyelectrolyte assembly on silica surface.

**TABLE 9.1** Applications of modified silica nanoparticles in the biopharmaceutical and biomedical field.

Applications of modified silica nanoparticles	Reference
Stimuli-responsive drug delivery	[39]
Nucleic acid delivery	[53]
Drug delivery and biomedical applications	[54]
Molecular imaging	[55]
Biodistribution and toxicology	[56]
Biomedical imaging	[56]
Cancer theranostics	[57]

### 9.3.3 Carbon nanomaterials

Carbon-based nanomaterials, including CNT, nanohorns, fullerenes, and graphene derivatives, have gained significant interest in the scientific community due to their unique physicochemical properties. These properties are highly promising in many biomedical-related fields. In particular their low cytotoxicity, achieved when properly functionalized, along with the possibility to link multiple bioactive molecules reinforces their potential in the biopharmaceutical field.

Graphene has become one of the most interesting objects of research in the last decade. Single layer graphene possesses an extended honeycomb network—the basic building block of other important allotropes. Graphene can be stacked to form 3D graphite, rolled to form 1D CNTs, wrapped to form 0D fullerenes, and shaped as conical nanotubes to form nanohorns, as depicted in Fig. 9.6.

Although all these carbon allotropes have been explored for biomedical applications, active research in this field is mostly devoted to the use of CNTs and graphene derivatives as drug delivery vehicles, biosensors, nanoprobes for biomedical imaging and, in certain circumstances, as nanodrugs by themselves [58–60].

As for any nanomaterial to be used in living organisms, water solubility and biocompatibility need to be achieved. Different carbon nanomaterials require different strategies of surface functionalization to make them soluble in an aqueous environment and compatible with cells and tissues. Carbon-based materials present many challenges regarding their use in clinical applications. Graphene and pristine CNTs are hydrophobic materials, thus easy to aggregate in aqueous medium including proteins, salts, or other ions, which can lead to toxicity. This happens due to the screening

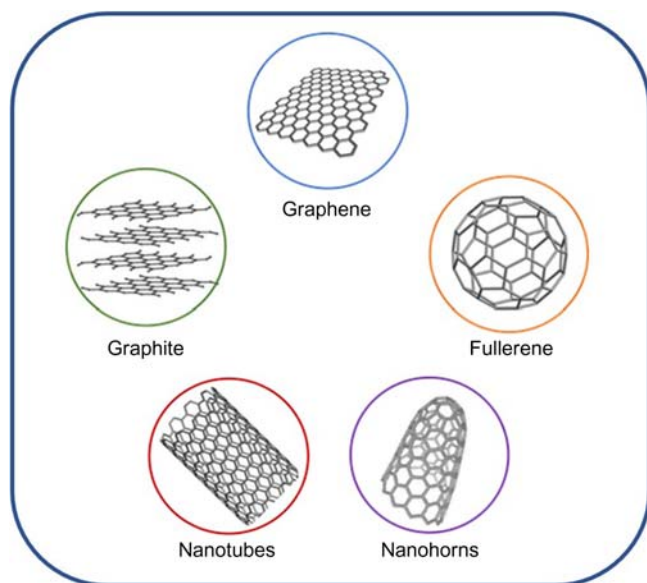


**FIGURE 9.6** Examples of carbon allotropes used in biomedical applications.

electrostatic charges and nonspecific interactions between charged carbon nanomaterials and proteins. For these reasons carbon nanomaterials' surface normally requires chemical functionalization or modification to obtain the desired properties [61].

Surface functionalization of carbon nanomaterials may be carried out through covalent or noncovalent routes. Covalent functionalization involves chemical reactions and the formation of bonds at the surface of the carbon nanomaterials, while noncovalent functionalization creates favorable interactions between the hydrophobic domains of an amphiphilic molecule and the surface of the nanomaterial.

Surface oxidation is the most common technique used to functionalize carbon nanomaterials. Nitric acid is commonly used as an oxidizing agent. During thermal oxidation, oxygen groups such as carboxylic acids, phenols, anhydrides, and lactones are formed at the surface of the carbon materials [62]. Further modification can be achieved by attaching hydrophilic polymers such as PEG to oxidized CNTs, resulting in CNT-polymer conjugates that are stable in biological environments, which have been used in both in vitro and in vivo applications [63]. Apart from PEG there are many other molecules that can be used for nanocarbon functionalization, namely folic acid, DNA, chitosan, poly(vinyl alcohol), polyethylenimine (PEI), sulfonic groups, and polyacrylic acid [58].

Noncovalent surface functionalization occurs through supramolecular interactions between the pristine carbon nanomaterials and the coating

molecules/polymers, which impart minimum structural damage and disturbance to the intrinsic properties of the functionalized materials. Carbon nanomaterials are known to noncovalently interact with various molecules through weak interactions, such as  $\pi$ – $\pi$  stacking interactions, electrostatic interactions, hydrogen bonding, and Van der Waals forces [64–66]. These noncovalent methods increase water miscibility, reducing their toxic effect; however, there are some disadvantages related to noncovalent functionalization, including vulnerability to the external environment. Many biomolecules, polymers, and surfactants have been used for the noncovalent functionalization of carbon nanomaterials to obtain better biocompatibility. For instance, interactions between proteins and CNTs may occur by  $\pi$ – $\pi$  stacking between CNTs and aromatic residues (Trp, Phe, Tyr) of proteins, enhancing their adsorptivity and biocompatibility, rendering them less toxic as compared to pristine CNTs [67,68]. CNT-protein bioconjugates have been applied in biosensor fabrication, drug delivery, and cancer therapy. Some of the proteins that have been immobilized onto CNTs through covalent linkages include chymotrypsin, ferritin, fibrinogen, hemoglobin, and streptavidin. Several researchers have reported the covalent immobilization of proteins onto CNTs using 1-ethyl-3-(3-dimethylaminopropyl) carbodiimide (EDC) as the crosslinking agent [62,69]. CNTs functionalized with DNA have actually been shown to enhance DNA stability. DNA can bind to single-walled CNTs, forming tight helices around them, or they can form noncovalent conjugates with CNTs [70]. DNA-functionalized CNTs can be used as biological transporters and also as biosensors [70].

The hydrophobic interactions,  $\pi$ – $\pi$  stacking, and electrostatic interactions between carbon-based nanomaterials and drugs can be used for efficient drug- or gene-loading. Based on this concept, modified carbon nanomaterials are used to deliver a drug or gene to improve its therapeutic effect and reduce its severe adverse effects [71]. CNTs and graphene-based materials possess a high photothermal conversion coefficient, making them suitable for photothermal therapy. In addition, photosensitizers can be loaded onto the surface of carbon-based materials allowing them for being used in photodynamic therapy [72].

## **9.4 Immobilization of functionalized nanomaterials in membranes**

The immobilization of functionalized nanomaterials in structured supports (e.g., monoliths, films beads, fibers, membranes) has many advantages, such as an easy material recovery from the reaction media, low leaching, enhanced mechanical strength, and prolonged reusability. An ideal support should be stable during the application, offer a high specific surface area, and a strong adherence for the material NPs, as well as a high affinity towards target substances (e.g., pharmaceuticals). The use of porous



membranes also allows the process scale-up in continuous operation and an easy regeneration procedure using simple cleaning with solvents (e.g., hot distilled water) [73,74].

The successful application of membranes in biopharmaceutical-related processes depends on several membrane properties: a desired pore size and a narrow pore size distribution, which control the molecular transport; a high porosity and low membrane thickness, which favor a high permeate flux; a certain mechanical strength; and sufficient thermal and chemical stability. Furthermore, biocompatibility and resistance to biofouling are vital to in vivo applications in order to avoid a negative immunological response and loss of functionality [75]. A membrane typically acts as a physical barrier separating two different phases, but it may also be applied to immobilize enzymes [62,76–78], liposomes [79–81], microspheres [82,83], and NPs [84–86]. Inorganic membranes provide high chemical resistance, but they are expensive, less available, and offer limited mass transfer. On the other hand, polymer membranes are cheaper and more suitable to be prepared with different shapes (flat-sheet, fibers, beads) and a wide variety of functionalities.

The immobilization of NPs in polymer membranes can be achieved by several techniques (Fig. 9.7), which are divided into three main categories: (1) chemical methods, where covalent bonds are established between NPs and the polymer matrix; (2) physical methods, where weaker and noncovalent interactions take place; and (3) entrapment, where particles are retained or entrapped in the membrane pores [75]. The membrane's porous structure and the surface hydrophilicity can be tuned by adding different amounts of these nanomaterials, as well as their dispersion, interaction, and distribution in the polymer chains that can define the membrane's overall performance and stability. More typical polymers such as PEG, poly(lactic-co-glycolic acid) (PLGA), poly(vinyl-2-pyrrolidone) (PVP), polyvinylalcohol (PVA), cellulose, alginate, and chitosan have been researched as well as other less frequently used polymers such as polyvinylidene fluoride (PVDF), polypropylene (PP), polyamide (PA), polyamidoamine (PAMAM), polyacrylonitrile (PAN), polyethylene (PE), PEI, and polyethersulfone (PES). These membranes were studied in drug- and gene-delivery, cancer therapies or other

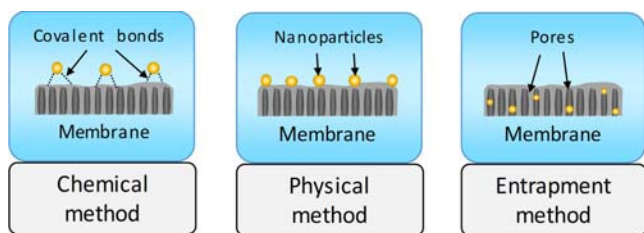


**FIGURE 9.7** Scheme of the different techniques to immobilize nanoparticles in membranes.

diseases, detection of proteins, biosensing and immunoisolation [84,86–91]. Some examples are described in Table 9.2.

Using the chemical method, nanomaterials can be linked by covalent bindings to specific functional groups (e.g.,  $-\text{COOH}$ ,  $-\text{CHO}$ ,  $-\text{OH}$ ,  $-\text{CN}$ , and  $-\text{NH}_2$ ), which are created in the membrane by different pretreatments. Some of these functional groups include epoxies, anhydrides, aldehydes, carboxylic, amides, and amines. The chemical methods of preparation generally allow a strong and stable immobilization of NPs, which are usually carried out by immersing the membrane in the corresponding solution containing the NPs or even by filtrating this solution through the membrane [74]. In certain cases an external energy source like UV irradiation can be used to start the binding reaction [92]. In general, NPs covalently bonded to membranes possess good resistance to variations in pH, ionic strength, desirable temperature, good reusability, and low leaching.

In the physical method, NPs are linked to the membrane by different non-covalent interactions such as Van der Waals forces, H-bonding, and hydrophobic-hydrophilic, or electrostatic interactions. In general, these methods lead to weaker interactions than those established by chemical methods and, consequently, a larger amount of leaching is expected. Adsorption is one of the most simple and common mechanisms used to noncovalently bind NPs to a membrane [74,93]. The surface chemistry of the nanomaterial plays an important role in this aspect because NPs with a different point of zero charge ( $\text{pH}_{\text{PZC}}$ ) lead to more intense interactions in the membrane due to the formation of electrostatic interactions. Furthermore the charge of the membrane can be negatively (e.g., carboxyl groups) or positively (e.g., protonated amino groups) charged depending on the isoelectric point of the polymer and the pH of the media.

**TABLE 9.2** Nanoparticle and polymers used in biopharmaceutical and biomedical processes.

Nanoparticle type	Polymer type	Application	Reference
Nano- $\text{MnO}_2$	Chitosan	Immunosensor for CEA <sup>a</sup>	[84]
Nano- $\text{CeO}_2$	PLGA–PEG	Cerebral ischemic therapy	[86]
CNT/graphene	Chitosan	Detection of EBNA-1	[87]
Gold	PEG	Delivery of anticancer drug	[88]
Graphene oxide	PEG–PEI	Gene delivery	[89]
Platinum	PLGA–PEG	Delivery of cisplatin	[90]
$\text{SiO}_2$	PAMAM	Drug delivery	[91]

<sup>a</sup>CEA, carcinoembryonic antigen; EBNA-1, Epstein Barr virus nuclear antigen 1.

In the entrapment category, NPs are not bound, but entrapped or retained, in membranes. This approach does not require any modification of the surface chemistry of both NPs and membranes, and the immobilization can be achieved following two different strategies: (1) NPs are incorporated into the membrane during the fabrication step; and (2) a solution containing NPs is filtered through the membrane with the NPs being retained in the pores [75]. The first method possesses the advantage of a low amount of leaching, although the activity of the resulting membrane should be lower because some NPs cannot be accessible to target substances. In contrast the second approach creates membranes with a higher activity but also higher amounts of leaching.

## 9.5 Functionalized nanoparticles as drug delivery systems

The use of NPs as DDS in the biopharmaceutical or biomedical field is well explored, and therefore is discussed in more detail. The increasing need for more efficient and less invasive methods to treat disease is stimulating the development of modified NPs to be applied in DDS. In fact, in terms of the health care market, nanotechnology for developing DDS is estimated to be around \$300 billion [94]. The main challenge in the development of DDS using NPs is the achievement of perfect biological activity with high stability, while being able to maintain the drug levels in the body and minimize side effects [95]. In the pharmaceutical sector this type of system is considered a nanopharmaceutical or nanomedicine [96]. The NPs used can be from either organic or inorganic materials, with sizes ranging between 1 and 100 nm [97].

Drug administration routes can be oral, parenteral, transdermal, inhalational, or subcutaneous injection among others [98]. Accordingly drugs must be loaded into NPs without leakage or catabolism by enzymes to recognize and access the specific target tissue or cell [98]. The functionalization of NPs by targeting ligands (drugs, biomolecules, and other chemical moieties) able to identify a specific biological target is entirely possible, promoting the drug delivery to a specific type of cell [96]. Modified NPs usually offer better transport properties and pharmacokinetic profiles and can penetrate deeper into tissues through fine capillaries and epithelial linings, resulting in a more efficient delivery of therapeutic agents to target sites [99].

Compared to traditional pharmaceuticals, formulations, and administration routes, DDS carrying the active pharmaceutical ingredient (API) offer notable advantages, including: (1) improved delivery of drugs that are poorly soluble in water; (2) delivery of a high dose of the therapeutic agent; (3) improved protection of a drug from harsh environments; (4) decrease of dosing regularity; (5) controlled and precise release of a drug; and (6) prevention of side effects if a proper DDS is used [95,96]. However some disadvantages can be also found, such as a material's toxicity, product

degradation, a drug's rapid release, and high cost [95]. All these advantages and disadvantages depend on the material type and functionalization. Thus there is an urgent need to experiment and design improved biomaterials to be used as DDS that can provide more efficient loading and controlled release of APIs [96].

Recently the surface modification design for advanced DDS has allowed for the development of new treatment strategies [11]. There are a number of carriers, including organic- and inorganic-based, or a hybrid combination of the organic and inorganic compounds, that can be used to produce a DDS. Inorganic nanoplateforms include metallic nanostructures, silica nanoparticles, and QD, while organic nanocarriers include polymeric, lipid-based (e.g., liposomes and nanoemulsions), dendrimers, and carbon-based materials. Hybrid combinations include colloidal gold encapsulated in liposomes or superparamagnetic iron oxide particles encapsulated in polymeric nanoparticles [100].

Regarding the optimal ligand design, surface properties must be controlled for a precise material 3D structure and chemical composition of specific functional groups that can interact with the API. The most used method of nanoparticle modification is through the attachment of PEG, minimizing the risks of opsonization and the immunological barriers (phagocytic) of NPs [20]. Hydrophilic coatings, such as PEG, can also reduce interactions with plasma proteins [24] and reduce agglomeration of the nanoparticles, avoiding a higher cytotoxicity [101,102]. Other types of ligands are described in Table 9.3.

Examples of most common functionalized nanoparticles as drug carriers and their applications are presented in Table 9.3. For more information about the incorporation of nanoparticles into drug delivery applications, current databases such as the Nanomaterial Registry (<https://www.nanomaterialregistry.com/>) and CaNanoLab (<https://cananolab.nci.nih.gov/>) can be easily accessed and are recommended. A general scheme on the properties and characteristics of modified nanoparticles as DDS is presented in Fig. 9.8.

## 9.6 Conclusions and future trends

NPs represent a bridge from materials to the biopharmaceutical and medicinal fields, where they have a remarkable role as therapeutic carriers and diagnostic tools. Several materials have been reviewed, together with a range of functionalization methods and functional groups. This chapter briefly described the several materials used, types of functionalization and preparation, and the related biomedical applications of these NPs. The design of nanostructures by controlling their surface properties is the main strategy to achieve improved responses of each type of application. The chapter also briefly described the synthesis and functionalization of metal-based, silica, and carbon NPs that have been mainly used in diagnosis, biosensing and

**TABLE 9.3** Examples of functionalized nanoparticles and their applications as drug delivery systems.

Material	Functionalization	Application	Reference
Chitosan	DNA	Peanut allergy vaccine	[103]
Dextran	<i>N, N'</i> -carbonyldiimidazole	Inflammatory	[104]
Magnetite	Anthracendion derivative mitoxantrone	Tumor angiogenesis	[105]
Magnetite	Poly(ethylene glycol)	Breast cancer	[106]
Silica	2-Devinyl-2-(1-hexyloxyethyl) pyropheophorbide	Cancer	[107]
Mesoporous Silica	Folic acid <sup>a</sup> ; mannose; glycerol-derived polyol-based silanes, orthosilicic acid, sodium metasilicate, tetraethyl orthosilicate (TEOS); tetramethoxysilane (TMOS); tetrakis (2-hydroxyethyl) orthosilicate.	Cancer	[108]
Gold	Amino acids and peptides	Gene delivery vector	[109]
Gold	Amine	Prostate carcinoma	[110]
Gold	Peptide	Adjuvants for vaccine delivery	[111]
CNT <sup>b</sup>	Adsorption of phospholipid with poly(ethylene glycol) (PL-PEG 2000) chains and terminal amine or maleimide groups (PL-PEG-NH <sub>2</sub> or PL-PEG-maleimide)	Intracellular delivery of siRNA	[112]
CNT	Polyethylenimine-grafted	Delivery of DNA	[113]
Graphene	Peptide-silica coated	Glioma therapy	[114]

<sup>a</sup>Review article: some examples of surface ligand are given.<sup>b</sup>CNT, carbon nanotubes.

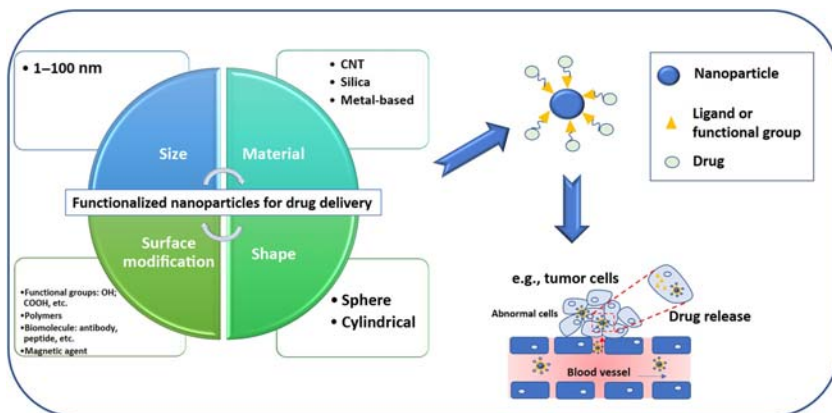


**FIGURE 9.8** General scheme highlighting the properties, characteristics, and way of action of modified nanoparticles to be used as DDS.

bioimaging, and as DDS. The work that has been conducted in this field so far has provided a better understanding of the NPs relevance and has brought significant contributions to the biomedical field. However, there is still a need to find materials with improved efficacy and low cytotoxicity where bio-based materials and bio-inspired functional groups may play a significant role. NPs that respond to stimuli such as temperature, pH, and light, and that are aimed at improving drug release and diagnosis performance must also be more deeply investigated.

## Acknowledgments

This work was financially supported by the project POCI-01-0145-FEDER-031268, funded by FEDER through COMPETE2020—Programa Operacional Competitividade e Internacionalização (POCI), and by national funds (OE) through FCT/MCTES. This work was developed within the scope of the project CICECO-Aveiro Institute of Materials, UIDB/50011/2020 & UIDP/50011/2020, financed by national funds through the FCT/MEC and when appropriate co-financed by FEDER under the PT2020 Partnership Agreement; and financially co-supported by Base Funding—UIDB/50020/2020 of the Associate Laboratory LSRE-LCM—funded by national funds through FCT/MCTES (PIDDAC). Ana P. M. Tavares and Cláudia G. Silva acknowledge the FCT Investigator Programme (IF/01634/2015 and IF/00514/2014, respectively) and Exploratory project with financing from the European Social Fund (ESF) and the Human Potential Operational Programme. Márcia C. Neves acknowledges FCT, I.P. for the research contract CEECIND/00383/2017 under the CEEC Individual 2017. S. Morales-Torres acknowledges the financial support from University of Granada (Reincorporación Plan Propio) and the Project ref. RTI2018-099224-B-I00 (AEI/FEDER, UE). Valeria C. Santos-Ebinuma acknowledges the financial support from FAPESP (São Paulo Research Foundation Brazil) through the project 2018/06908-8.

## References

- [1] dos Santos NV, de Carvalho Santos-Ebinuma V, Pessoa Junior A, Pereira JFB. Liquid-liquid extraction of biopharmaceuticals from fermented broth: trends and prospects. *J Chem Technol Biotechnol* 2018;93(7):1845–63.
- [2] Biopharmaceuticals Market – Segmented by products (monoclonal antibodies, recombinant growth factors, purified proteins, recombinant proteins, recombinant hormones, synthetic immunomodulators, vaccines), by application, by geography- growth, trends, and forecast (2018–2023). 2018 Available from: <<https://www.mordorintelligence.com/industry-reports/global-biopharmaceuticals-market-industry>>.
- [3] Jozala AF, Geraldles DC, Tundisi LL, Feitosa V de A, Breyer CA, Cardoso SL, et al. Biopharmaceuticals from microorganisms: from production to purification. *Braz J Microbiol* 2016;47(Suppl. 1):51–63.
- [4] Hong MS, Severson KA, Jiang M, Lu AE, Love JC, Braatz RD. Challenges and opportunities in biopharmaceutical manufacturing control. *Comput Chem Eng* 2018;110:106–14.
- [5] Robles-García MA, Rodríguez-Félix F, Márquez-Ríos E, Aguilar JA, Barrera-Rodríguez A, Aguilar J, et al. Applications of nanotechnology in the agriculture, food, and pharmaceuticals. *J Nanosci Nanotechnol* 2016;16(8):8188–207.
- [6] Hussain CM. *Handbook of nanomaterials for industrial applications*. 1st ed. Elsevier; 2018.
- [7] Mesgari-Shadi A, Sarrafzadeh M-H, Divband B, Barar J, Omid Y. Batch adsorption/desorption for purification of scFv antibodies using nanozeolite microspheres. *Microporous Mesoporous Mater* 2018;264:167–75.
- [8] Gädke J, Thies J-W, Kleinfeldt L, Schulze T, Biedendieck R, Rustenbeck I, et al. Selective manipulation of superparamagnetic nanoparticles for product purification and microfluidic diagnostics. *Eur J Pharm Biopharm* 2018;126:67–74.
- [9] Liu S, Höldrich M, Sievers-Engler A, Horak J, Lämmerhofer M. Papain-functionalized gold nanoparticles as heterogeneous biocatalyst for bioanalysis and biopharmaceuticals analysis. *Anal Chim Acta* 2017;963:33–43.
- [10] Chakoli AN, Sadeghzadeh M. Recent trends in biomedical and pharmaceutical industry due to engineered nanomaterials. In: Hussain CM, editor. *Handbook of nanomaterials for industrial applications micro and nano technologies*. Elsevier; 2018. p. 499–519.
- [11] Araújo F, das Neves J, Martins JP, Granja PL, Santos HA, Sarmiento B. Functionalized materials for multistage platforms in the oral delivery of biopharmaceuticals. *Prog Mater Sci* 2017;89:306–44.
- [12] Bianco A, Kostarelos K, Prato M. Making carbon nanotubes biocompatible and biodegradable. *Chem Commun* 2011;47(37):10182.
- [13] Araújo F, Shrestha N, Granja PL, Hirvonen J, Santos HA, Sarmiento B. Safety and toxicity concerns of orally delivered nanoparticles as drug carriers. *Expert Opin Drug Metab Toxicol* 2015;11(3):381–93.
- [14] Unamuno X, Imbuluzqueta E, Salles F, Horcajada P, Blanco-Prieto MJ. Biocompatible porous metal-organic framework nanoparticles based on Fe or Zr for gentamicin vectorization. *Eur J Pharm Biopharm* 2018;132:11–18.
- [15] Hillyer JF, Albrecht RM. Gastrointestinal persorption and tissue distribution of differently sized colloidal gold nanoparticles. *J Pharm Sci* 2001;90(12):1927–36.
- [16] Kumari M, Rajak S, Singh SP, Murty USN, Mahboob M, Grover P, et al. Biochemical alterations induced by acute oral doses of iron oxide nanoparticles in Wistar rats. *Drug Chem Toxicol* 2013;36(3):296–305.

- [17] Borran AA, Aghanejad A, Farajollahi A, Barar J, Omid Y. Gold nanoparticles for radio-sensitizing and imaging of cancer cells. *Radiat Phys Chem* 2018;152:137–44.
- [18] Mody VV, Siwale R, Singh A, Mody HR. Introduction to metallic nanoparticles. *J Pharm Bioallied Sci* 2010;2(4):282–9.
- [19] Khan I, Saeed K, Khan I. Nanoparticles: properties, applications and toxicities. *Arab J Chem* 2017;2:908–31.
- [20] Thota S, Crans DC. Metal nanoparticles: synthesis and applications in pharmaceutical sciences. Wiley Ed, 2018.
- [21] Paramasivam G, Kayambu N, Rabel AM, Sundramoorthy AK, Sundaramurthy A. Anisotropic noble metal nanoparticles: synthesis, surface functionalization and applications in biosensing, bioimaging, drug delivery and theranostics. *Acta Biomater* 2017;49:45–65.
- [22] Niidome T, Yamagata M, Okamoto Y, Akiyama Y, Takahashi H, Kawano T, et al. PEG-modified gold nanorods with a stealth character for in vivo applications. *J Control Rel* 2006;114(3):343–7.
- [23] Liopo A, Conjuteau A, Tsybouski D, Ermolinsky B, Kazansky A, Oraevsky A. Biocompatible gold nanorod conjugates for preclinical biomedical research. *J Nanomed Nanotechnol* 2012;S2:001.
- [24] Jokerst JV, Lobovkina T, Zare RN, Gambhir SS. Nanoparticle PEGylation for imaging and therapy. *Nanomedicine* 2011;6(4):715–28.
- [25] Katz E, Shipway AN, Willner I. Chemically functionalized metal nanoparticles. *Nanoscale materials*. Boston, MA: Kluwer Academic Publishers; 2004. p. 5–78.
- [26] Bard AJ, Rubinstein I. *Electroanalytical chemistry. Volume 19: a series of advances*. M. Dekker; 1996.
- [27] Xu J, Li H-L. The chemistry of self-assembled long-chain alkanethiol monolayers on gold. *J Colloid Interface Sci* 1995;176(1):138–49.
- [28] Sundaramurthy A, Vergaalen M, Maji S, Auzély-Velty R, Zhang Z, De Geest BG, et al. Hydrogen bonded multilayer films based on poly[2-oxazoline]s and tannic acid. *Adv Healthc Mater* 2014;3(12):2040–7.
- [29] Gole A, Murphy CJ. Polyelectrolyte-coated gold nanorods: synthesis, characterization and immobilization. *Chem Mater* 2005;17:1325–30.
- [30] Pantano P. Nanomaterials for biosensors. *Nanotechnologies for nanotechnologies for life sciences*. *J Am Chem Soc* 2007;129:10963.
- [31] Liu S, Han M-Y. Silica-coated metal nanoparticles. *Chem Asian J* 2009;5(1):36–45.
- [32] Stöber W, Fink A, Bohn E. Controlled growth of monodisperse silica spheres in the micron size range. *J Colloid Interface Sci* 1968;26(1):62–9.
- [33] Liz-Marzán LM, Giersig M, Mulvaney P. Synthesis of nanosized gold – silica core – shell particles. *Langmuir* 1996;12:4329–35.
- [34] Iler RK. *The chemistry of silica: solubility, polymerization, colloid and surface properties, and biochemistry*. Wiley; 1979. 866 p.
- [35] Pagliaro M. *Silica-based materials for advanced chemical applications*. Cambridge: Royal Society of Chemistry; 2009.
- [36] Nozawa K, Gailhanou H, Raison L, Panizza P, Ushiki H, Sellier E, et al. Smart control of monodisperse stöber silica particles: effect of reactant addition rate on growth process. *Langmuir* 2005;21(4):1516–23.
- [37] Watermann A, Brieger J. Mesoporous silica nanoparticles as drug delivery vehicles in cancer. *Nanomaterials* 2017;7(7):189.



- [38] Zhou Y, Quan G, Wu Q, Zhang X, Niu B, Wu B, et al. Mesoporous silica nanoparticles for drug and gene delivery. *Acta Pharm Sin B* 2018;8(2):165–77.
- [39] Song Y, Li Y, Xu Q, Liu Z. Mesoporous silica nanoparticles for stimuli-responsive controlled drug delivery: advances, challenges, and outlook. *Int J Nanomed* 2017;12:87–110.
- [40] Hao N, Li L, Tang F. Shape matters when engineering mesoporous silica-based nanomedicines. *Biomater Sci* 2016;4(4):575–91.
- [41] Vazquez NI, Gonzalez Z, Ferrari B, Castro Y. Synthesis of mesoporous silica nanoparticles by sol–gel as nanocontainer for future drug delivery applications. *Boletín la Soc Española Cerámica y Vidr* 2017;56(3):139–45.
- [42] Zhao P, Liu M, Lin H, Sun X, Li Y, Yan S. Synthesis and drug delivery applications for mesoporous silica nanoparticles. *J Med Biotechnol* 2017;1(1):1–8.
- [43] Hikosaka R, Nagata F, Tomita M, Kato K. Optimization of pore structure and particle morphology of mesoporous silica for antibody adsorption for use in affinity chromatography. *Appl Surf Sci* 2016;384:27–35.
- [44] Nakanishi K, Tomita M, Nakamura H, Kato K. Specific binding of immunoglobulin G to protein A-mesoporous silica composites for affinity column chromatography. *J Mater Chem B* 2013;1:6321–8.
- [45] Qhobosheane M, Santra S, Zhang P, Tan W. Biochemically functionalized silica nanoparticles. *Analyst* 2001;126(8):1274–8.
- [46] Li B, Zou X, Zhao Y, Sun L, Li S. Biofunctionalization of silica microspheres for protein separation. *Mater Sci Eng C* 2013;33(5):2595–600.
- [47] Yin Y, Wei G, Zou X, Zhao Y. Functionalized hollow silica nanospheres for His-tagged protein purification. *Sens Actuat B Chem* 2015;209:701–5.
- [48] Hu X, Wang Y, Peng B. Chitosan-capped mesoporous silica nanoparticles as pH-responsive nanocarriers for controlled drug release. *Chem Asian J* 2014;9(1):319–27.
- [49] de Oliveira LF, Bouchmella K, Gonçalves K de A, Bettini J, Kobarg J, Cardoso MB. Functionalized silica nanoparticles as an alternative platform for targeted drug-delivery of water insoluble drugs. *Langmuir* 2016;32(13):3217–25.
- [50] Bi W, Row KH. Comparison of different silica-based imidazolium stationary phases for LC in separation of alkaloids. *Chromatographia* 2010;71(1–2):25–30.
- [51] Soares B, Passos H, Freire C, Coutinho JAP, Silvestre AJD, Freire MG. Ionic liquids in chromatographic and electrophoretic techniques: toward additional improvements on the separation of natural compounds. *Green Chem* 2016;18:4582–604.
- [52] Feng W, Zhou X, He C, Qiu K, Nie W, Chen L, et al. Polyelectrolyte multilayer functionalized mesoporous silica nanoparticles for pH-responsive drug delivery: layer thickness-dependent release profiles and biocompatibility. *J Mater Chem B* 2013;1(43):5886–98.
- [53] Kamegawa R, Naito M, Miyata K. Functionalization of silica nanoparticles for nucleic acid delivery. *Nano Res* 2018;11(10):5219–39.
- [54] Wang Y, Zhao Q, Han N, Bai L, Li J, Liu J, et al. Mesoporous silica nanoparticles in drug delivery and biomedical applications. *Nanomed Nanotechnol Biol Med* 2015;11(2):313–27.
- [55] Shirshahi V, Soltani M. Solid silica nanoparticles: applications in molecular imaging. *Contrast Media Mol Imaging* 2015;10(1):1–17.
- [56] Liberman A, Mendez N, Trogler WC, Kummel AC. Synthesis and surface functionalization of silica nanoparticles for nanomedicine. *Surf Sci Rep* 2014;69(2–3):132–58.
- [57] Feng Y, Panwar N, Tng DJH, Tjin SC, Wang K, Yong K-T. The application of mesoporous silica nanoparticle family in cancer theranostics. *Coord Chem Rev* 2016;319:86–109.

- [58] Zhang B, Wang Y, Zhai G. Biomedical applications of the graphene-based materials. *Mater Sci Eng C* 2016;61:953–64.
- [59] Battigelli A, Ménard-Moyon C, Bianco A. Carbon nanomaterials as new tools for immunotherapeutic applications. *J Mater Chem B* 2014;2(37):6144–56.
- [60] Madni A, Noreen S, Maqbool I, Rehman F, Batool A, Kashif PM, et al. Graphene-based nanocomposites: synthesis and their theranostic applications. *J Drug Target* 2018;26(10):858–83.
- [61] Vardharajula S, Ali SZ, Tiwari PM, Ero lu E, Vig K, Dennis VA, et al. Functionalized carbon nanotubes: biomedical applications. *Int J Nanomed* 2012;7:5361–74.
- [62] Costa JB, Lima MJ, Sampaio MJ, Neves MC, Faria JL, Morales-Torres S, et al. Enhanced biocatalytic sustainability of laccase by immobilization on functionalized carbon nanotubes/polysulfone membranes. *Chem Eng J* 2019;355:974–85.
- [63] Bottini M, Rosato N, Bottini N. PEG-modified carbon nanotubes in biomedicine: current status and challenges ahead. *Biomacromolecules* 2011;12(10):3381–93.
- [64] Azevedo RM, Costa JB, Serp P, Loureiro JM, Faria JL, Silva CG, et al. A strategy for improving peroxidase stability via immobilization on surface modified multi-walled carbon nanotubes. *J Chem Technol Biotechnol* 2015;90(9):1570–8.
- [65] Silva CG, Tavares APM, Dražić G, Silva AMT, Loureiro JM, Faria JL. Controlling the surface chemistry of multiwalled carbon nanotubes for the production of highly efficient and stable laccase-based biocatalysts. *Chempluschem* 2014;79(8):1116–22.
- [66] Tavares APM, Silva CG, Dražić G, Silva AMT, Loureiro JM, Faria JL. Laccase immobilization over multi-walled carbon nanotubes: kinetic, thermodynamic and stability studies. *J Colloid Interface Sci* 2015;454:52–60.
- [67] Ge C, Du J, Zhao L, Wang L, Liu Y, Li D, et al. Binding of blood proteins to carbon nanotubes reduces cytotoxicity. *Proc Natl Acad Sci USA* 2011;108(41):16968–73.
- [68] Nagaraju K, Reddy R, Reddy N. A review on protein functionalized carbon nanotubes. *J Appl Biomater Funct Mater* 2015;13(4):301–12.
- [69] Gao Y, Kyratzis I. Covalent immobilization of proteins on carbon nanotubes using the cross-linker 1-Ethyl-3-[3-dimethylaminopropyl]carbodiimide - a critical assessment. *Bioconjug Chem* 2008;19(10):1945–50.
- [70] Chenguo H, Yiyi Z, Gang B, Yuelan Z, Meilin L, Zhong LW. DNA functionalized single-walled carbon nanotubes for electrochemical detection. *J Phys Chem B* 2005;109:20072–6.
- [71] Liu Z, Tabakman S, Welscher K, Dai H. Carbon nanotubes in biology and medicine: in vitro and in vivo detection, imaging and drug delivery. *Nano Res* 2009;2(2):85–120.
- [72] Wang L, Shi J, Liu R, Liu Y, Zhang J, Yu X, et al. Photodynamic effect of functionalized single-walled carbon nanotubes: a potential sensitizer for photodynamic therapy. *Nanoscale* 2014;6(9):4642–51.
- [73] Silva TLS, Morales-Torres S, Figueiredo JL, Silva AMT. Polymer membranes for water desalination and treatment. Nanostructured polymer membranes. Hoboken, NJ: John Wiley & Sons, Inc; 2016. p. 251–86.
- [74] Jochems P, Satyawali Y, Diels L, Dejonghe W. Enzyme immobilization on/in polymeric membranes: status, challenges and perspectives in biocatalytic membrane reactors [BMRs]. *Green Chem* 2011;13(7):1609–23.
- [75] Adiga SP, Jin C, Curtiss LA, Monteiro-Riviere NA, Narayan RJ. Nanoporous membranes for medical and biological applications. *Wiley Interdiscip Rev Nanomed Nanobiotechnol* 2009;1(5):568–81.

- [76] Gupta S, Bhattacharya A, Murthy CN. Tune to immobilize lipases on polymer membranes: techniques, factors and prospects. *Biocatal Agric Biotechnol* 2013;2(3):171–90.
- [77] Yotova LK, Hassaan A, Yaneva S. Covalent immobilization of peroxidase onto hybrid membranes for the construction of optical biosensor. *Int J Bioautomation* 2015;19:177–86.
- [78] Datta S, Christena LR, Rajaram YRS. Enzyme immobilization: an overview on techniques and support materials. *Biotech* 2013;3(1):1–9.
- [79] Torchilin VP, Shtilman MI, Trubetskoy VS, Whiteman K, Milstein AM. Amphiphilic vinyl polymers effectively prolong liposome circulation time in vivo. *Biochim Biophys Acta Biomembr* 1994;1195(1):181–4.
- [80] Tarn D, Ashley CE, Xue M, Carnes EC, Zink JJ, Brinker CJ. Mesoporous silica nanoparticle nanocarriers: biofunctionality and biocompatibility. *Acc Chem Res* 2013;46(3):792–801.
- [81] Ahmed F, Discher DE. Self-porating polymersomes of PEG–PLA and PEG–PCL: hydrolysis-triggered controlled release vesicles. *J Control Rel* 2004;96(1):37–53.
- [82] Sapin A, Garcion E, Clavreul A, Lagarce F, Benoit JP, Menei P. Development of new polymer-based particulate systems for anti-glioma vaccination. *Int J Pharm* 2006;309(1–2):1–5.
- [83] Stsiapura V, Sukhanova A, Artemyev M, Pluot M, Cohen JHM, Baranov AV, et al. Functionalized nanocrystal-tagged fluorescent polymer beads: synthesis, physicochemical characterization, and immunolabeling application. *Anal Biochem* 2004;334(2):257–65.
- [84] Ling S, Yuan R, Chai Y, Zhang T. Study on immunosensor based on gold nanoparticles/chitosan and MnO<sub>2</sub> nanoparticles composite membrane/Prussian blue modified gold electrode. *Bioprocess Biosyst Eng* 2009;32(3):407–14.
- [85] Gulati NM, Stewart PL, Steinmetz NF. Bioinspired shielding strategies for nanoparticle drug delivery applications. *Mol Pharm* 2018;15(8):2900–9.
- [86] Gao Y, Chen X, Liu H. A facile approach for synthesis of nano-CeO<sub>2</sub> particles loaded copolymer matrix and their colossal role for blood-brain barrier permeability in Cerebral Ischemia. *J Photochem Photobiol B Biol* 2018;187:184–9.
- [87] Song C, Xie G, Wang L, Liu L, Tian G, Xiang H. DNA-based hybridization chain reaction for an ultrasensitive cancer marker EBNA-1 electrochemical immunosensor. *Biosens Bioelectron* 2014;58:68–74.
- [88] Sun X, Zhang G, Keynton RS, O'Toole MG, Patel D, Gobin AM. Enhanced drug delivery via hyperthermal membrane disruption using targeted gold nanoparticles with PEGylated Protein-G as a cofactor. *Nanomed Nanotechnol Biol Med* 2013;9(8):1214–22.
- [89] Feng L, Yang X, Shi X, Tan X, Peng R, Wang J, et al. Polyethylene glycol and polyethylenimine dual-functionalized nano-graphene oxide for photothermally enhanced gene delivery. *Small* 2013;9(11):1989–97.
- [90] Dhar S, Gu FX, Langer R, Farokhzad OC, Lippard SJ. Targeted delivery of cisplatin to prostate cancer cells by aptamer functionalized Pt[IV] prodrug-PLGA-PEG nanoparticles. *Proc Natl Acad Sci* 2008;105(45):17356–61.
- [91] Radu DR, Lai C-Y, Jeftinija K, Rowe EW, Jeftinija S, Lin VS-Y. A polyamidoamine dendrimer-capped mesoporous silica nanosphere-based gene transfection reagent. *J Am Chem Soc* 2004;126(41):13216–17.
- [92] Bora U, Sharma P, Kannan K, Nahar P. Photoreactive cellulose membrane-A novel matrix for covalent immobilization of biomolecules. *J Biotechnol* 2006;126(2):220–9.
- [93] Hanefeld U, Gardossi L, Magner E. Understanding enzyme immobilisation. *Chem Soc Rev* 2009;38(2):453–68.

- [94] Kumar CSSR. Nanotechnology tools in pharmaceutical R & D. *Mater Today* 2010;12 (Suppl. 1):24–30.
- [95] Coelho JF, Ferreira PC, Alves P, Cordeiro R, Fonseca AC, Góis JR, et al. Drug delivery systems: advanced technologies potentially applicable in personalized treatments. *EPMA J* 2010;1(1):164–209.
- [96] Couvreur P. Nanoparticles in drug delivery: past, present and future. *Adv Drug Deliv Rev* 2013;65(1):21–3.
- [97] Sun T, Zhang YS, Pang B, Hyun DC, Yang M, Xia Y. Engineered nanoparticles for drug delivery in cancer therapy. *Angew Chem Int Ed* 2014;53(46):12320–64.
- [98] Subbiah R, Veerapandian M, Yun KS. Nanoparticles: functionalization and multifunctional applications in biomedical sciences. *Curr Med Chem* 2010;17(36):4559–77.
- [99] Panyam J, Labhasetwar V. Biodegradable nanoparticles for drug and gene delivery to cells and tissue. *Adv Drug Deliv Rev* 2003;55(3):329–47.
- [100] Brannon-Peppas L, Blanchette JO. Nanoparticle and targeted systems for cancer therapy. *Adv Drug Deliv Rev* 2004;56(11):1649–59.
- [101] Grossman JH, Crist RM, Clogston JD. Early development challenges for drug products containing nanomaterials. *AAPS J* 2017;19(1):92–102.
- [102] Dobrovolskaia MA. Pre-clinical immunotoxicity studies of nanotechnology-formulated drugs: challenges, considerations and strategy. *J Control Rel* 2015;220:571–83.
- [103] Mao H-Q, Roy K, Troung-Le VL, Janes KA, Lin KY, Wang Y, et al. Chitosan-DNA nanoparticles as gene carriers: synthesis, characterization and transfection efficiency. *J Control Rel* 2001;70(3):399–421.
- [104] Hornig S, Bunjes H, Heinze T. Preparation and characterization of nanoparticles based on dextran–drug conjugates. *J Colloid Interface Sci* 2009;338(1):56–62.
- [105] Jurgons R, Seliger C, Hilpert A, Trahms L, Odenbach S, Alexiou C. Drug loaded magnetic nanoparticles for cancer therapy. *J Phys Condens Matter* 2006;18(38):893–902 (Suppl. 2).
- [106] Zhang Y, Sun C, Kohler N, Zhang M. Self-assembled coatings on individual monodisperse magnetite nanoparticles for efficient intracellular uptake. *Biomed Microdevices* 2004;6(1):33–40.
- [107] Roy I, Ohulchanskyy TY, Pudavar HE, Bergey EJ, Oseroff AR, Morgan J, et al. Ceramic-based nanoparticles entrapping water-insoluble photosensitizing anticancer drugs: a novel drug–carrier system for photodynamic therapy. *J Am Chem Soc* 2003;125(26):7860–5.
- [108] Bharti C, Nagaich U, Pal AK, Gulati N. Mesoporous silica nanoparticles in target drug delivery system: a review. *Int J Pharm Investig* 2015;5(3):124–33.
- [109] Ghosh PS, Kim C-K, Han G, Forbes NS, Rotello VM. Efficient gene delivery vectors by tuning the surface charge density of amino acid-functionalized gold nanoparticles. *ACS Nano* 2008;2(11):2213–18.
- [110] Lee SH, Bae KH, Kim SH, Lee KR, Park TG. Amine-functionalized gold nanoparticles as non-cytotoxic and efficient intracellular siRNA delivery carriers. *Int J Pharm* 2008;364(1):94–101.
- [111] Bastús NG, Sánchez-Tilló E, Pujals S, Farrera C, Kogan MJ, Giralt E, et al. Peptides conjugated to gold nanoparticles induce macrophage activation. *Mol Immunol* 2009;46(4):743–8.
- [112] Kam NWS, Liu Z, Dai H. Functionalization of carbon nanotubes via cleavable disulfide bonds for efficient intracellular delivery of siRNA and potent gene silencing. *J Am Chem Soc* 2005;127(36):12492–3.

- [113] Liu Y, Wu D-C, Zhang W-D, Jiang X, He C-B, Chung TS, et al. Polyethylenimine-grafted multiwalled carbon nanotubes for secure noncovalent immobilization and efficient delivery of DNA. *Angew Chem Int Ed* 2005;44(30):4782–5.
- [114] Wang Y, Wang K, Zhao J, Liu X, Bu J, Yan X, et al. Multifunctional mesoporous silica-coated graphene nanosheet used for chemo-photothermal synergistic targeted therapy of glioma. *J Am Chem Soc* 2013;135(12):4799–804.

## Chapter 10

# Functionalized nanomaterials for biomedical and agriculture industries

P. Chandra Kanth<sup>1</sup>, Sandeep Kumar Verma<sup>2</sup> and Nidhi Gour<sup>3</sup>

<sup>1</sup>*Department of Science, School of Technology, Pandit Deendayal Petroleum University, Gandhinagar, India,* <sup>2</sup>*Institute of Biological Science, SAGE University, Bypass Road, Kailod Kartal, Indore, India,* <sup>3</sup>*Department of Chemistry, Indrashil University, Rajpur, Kadi, India*

### 10.1 Introduction

There is a strong drive to design innovative nanoparticles (NPs) because they possess exceptional properties and bridge the gap between bulk materials and atomic or molecular structures [1]. A bulk material has constant properties because it adheres to the laws of classical physics. At the nanoscale, the material follows the laws of quantum mechanics, wherein the nanomaterials have exceptional surface properties leading to the effective entrapment of drugs and providing a larger surface area for interaction with the cells [2]. Hence, nanomaterials serve as extraordinary carriers for drugs and active organic ingredients (AOI) in animal and plant cells. There is also a great interest in developing groundbreaking strategies for functionalization of nanomaterials, because this improves the therapeutic efficiency of these carriers and allows drugs or AOI to reach the desired site avoiding unspecific interactions. In this context, different classes of nanomaterials like carbon nanotubes (CNTs), metal-NPs, magnetic NPs, and polymeric carriers are suitably functionalized with therapeutic or target-specific moieties like si-RNA, aptamers, hydrophobic drugs, folic acid, etc., to enable a site-specific targeting [3]. Functionalized nanomaterials have immense applications in biomedicine and healthcare beginning with the diagnosis of a disease to its therapeutic remedy [4]. Ultrasensitive biosensor devices have been designed that can detect disease-specific biomarkers at a very low concentration, enabling early diagnosis of diseases like cancer, AIDS, Alzheimer's, etc. [5]. Additionally, smart drug delivery systems have been designed that enable

drugs to be carried for prolonged circulation time without degradation and for site-specific release without affecting healthy cells [6].

Similarly, functionalized nanomaterials have been widely used in agriculture for encapsulation and entrapment of agrochemicals such as fertilizers, pesticides, herbicides, plant growth regulators, and other active substances [7–12]. These nanocarriers enable controlled and slow release of agrochemicals, which in turn allow the slow uptake of active ingredients. Hence, the effectiveness of agrochemicals is increased because they can bind firmly to the plant surface, reducing the amount of agrochemical waste that enters the environment [13]. This chapter gives an overview of the various strategies employed to design and synthesize innovative functional materials, and illustrates their potential applications in biomedical, pharmaceutical, agriculture and agri-food industries, along with their challenges.

## 10.2 Strategies for functionalization of nanomaterials

Functionalization of nanomaterials has exponentially gained interest due to their wide spread applications in biomedical, drug delivery, sensors, agriculture and other industrial applications. The plasmonic properties of NPs are vulnerable to their size, shape, and composition [14]. So stabilizing NPs is a crucial step in preserving their desired properties. Most nanomaterials without any surface functionalization generally tend to aggregate or show undesired toxicity. Surface functionalization is a process that incorporates suitable materials on to the NPs' surface in order to improve their applicability and reduce toxicity [15]. Numerous kinds of materials, including small organic molecules, dyes, polymers, inorganic materials, and biomolecules, are used to functionalize nanomaterial surfaces [3]. Fig. 10.1 shows the various types of functionalization possible over nanomaterial surfaces.

Functionalization of nanomaterials can be performed by several methods including pre and postsynthesis methods. In presynthesis or in situ synthesis methods, desired functional materials are directly added to the reaction while nanomaterials formation. Reduction of auric chloride to synthesize gold NPs with cysteine and tyrosine use this method [14]. Most of the surface functionalization will only be done by postsynthesis. This gives full control over the surface modification of nanomaterials. These postsynthesis methods can generally be classified into the following categories: covalent, noncovalent functionalization, grafting, and physical adsorption methods [17]. These methods ensure the coating or grafting of desired material on the NPs surface while maintaining their stability and native properties. Fig. 10.2 illustrates the various opportunities for nanomaterial functionalization.

*Covalent functionalization:* In covalent functionalization, the selected group will be attached using strong binding groups by performing organic coupling reactions. One of the functional groups is first attached to the NP surface, then it is coupled with selected functional material by performing

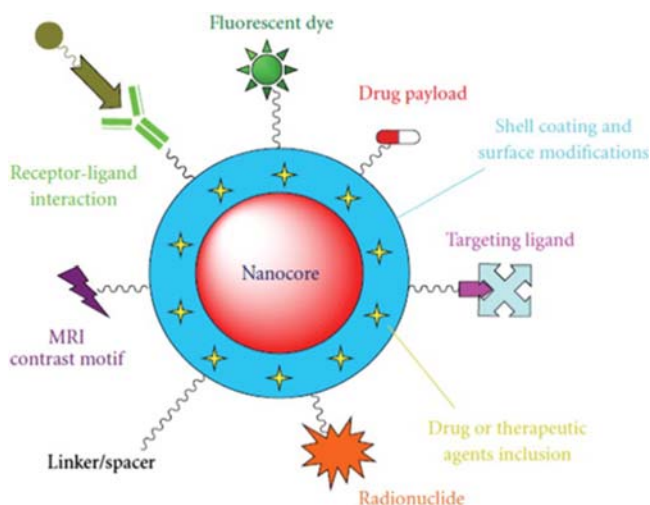


**FIGURE 10.1** NPs with various surface functionalization. Reproduced with permissions from Chatterjee K, Sarkar S, Jagajjanani Rao K, Paria S. Core/shell nanoparticles in biomedical applications. *Adv Colloid Interface Sci* 2014;209:8–39. <https://doi.org/10.1016/j.cis.2013.12.008> [16]. Copyright Elsevier Inc.

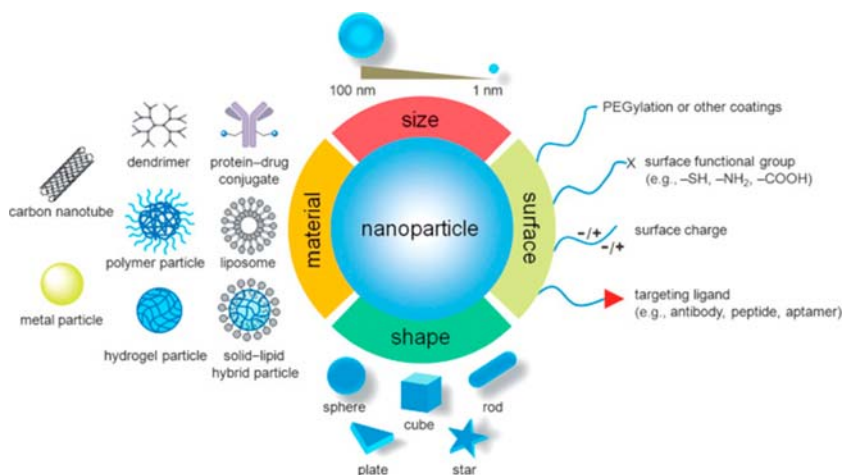


**FIGURE 10.2** Strategies for NP functionalization. Reproduced with permissions from Sun T, Zhang YS, Pang B, Hyun DC, Yang M, Xia Y. Engineered nanoparticles for drug delivery in cancer therapy. *Angewandte Chemie International Edition*. 2014;53(46):12320–12364. <https://doi.org/10.1002/anie.201403036> [18]. Copyright John Wiley & Sons, Inc.

organic reactions. This method further divided into indirect and direct methods. The indirect method refers to the formation of oxygen-containing groups on the surface, then coupling with the desired material [19]. The direct



method makes use of the surface charge associated with NPs to form strong covalent bonds such as thiol functionalization of gold nanomaterials [20].

*Noncovalent functionalization:* Noncovalent functionalization utilizes the surface charge of the nanomaterial as well as functional moiety. In this method, functional material is attached or wrapped on to the NP surface by using noncovalent interactions such as hydrogen bonding, Van der Waal's interactions, electrostatic interactions, and  $\pi$ – $\pi$  stacking [21]. Polymer or surfactant-coated nanomaterials are the best examples of this type of functionalization [5]. In another strategy, supramolecules are used to functionalize the surface of the nanomaterials, and they serve as a host to derive further desired materials [22].

*Grafting:* Grafting is a covalent functionalization technique generally used to introduce polymers on to the surface of nanomaterials to synthesize polymer brush-coated NPs for sensing and adsorption applications [23]. Chemical grafting techniques are basically classified as “grafting onto” and “grafting from” approaches. The “grafting from” approach begins by attaching monomeric groups on the NP surface, followed by in situ polymerization [24,25]. Organo-functional silanes, like nipam, are widely used for “grafting from” processes since they can be polymerized easily. A variety of polymerization techniques, including free radical, cationic, anionic, ring opening, and controlled radical polymerizations, have been used for the growth of polymer chains on NP surfaces [18]. “Grafting onto” approaches are another effective method which involves the reaction of functional end groups of polymers with the reactive groups of NPs or electrostatic interaction with its charged surface. In this method, the polymer is bound with the NP surface by utilizing one of the reactive functional moieties present in the polymer. Grafting of biomolecules, such as DNA and photo-reactive polymers such as polydopamine OR polyaniline, are coated using this strategy [26–28] (Fig. 10.3).

*Physical methods:* Physical methods are similar to noncovalent functionalization methods where only the natural affinity of the molecules are used to coat over the NP surface by physisorption. Polymers are generally coated by physisorption methods providing a passive layer and preventing NP aggregation. Polyelectrolyte materials are coated layer-by-layer using this method. First, one polyelectrolyte is physisorbed on the NP surface which binds to the surface utilizing columbic interactions, then other, oppositely charged material is coated over the primary layer by controlling thickness [20,21,29].

Other unconventional methods are also used for NP functionalization. Most of these methods use specific affinity of the functional groups to modify the NP surface. For example, facet-selective conjugation of DNA molecules onto upconversion NPs via ligand competition reaction was introduced to graft biomolecules over upconversion NPs [28]. Ligand exchange methods are often used to replace small molecules attached to the NP surface by exchanging it with another strong affinity molecule in order to induce the desired properties. This method is also used to interchange the NP surface

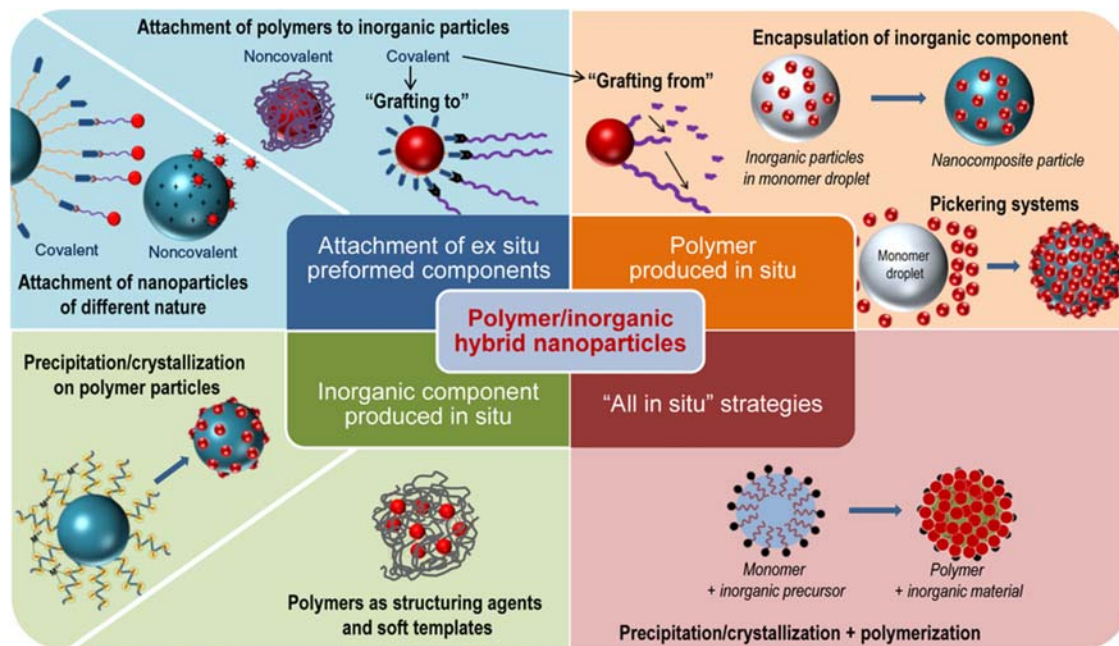


**FIGURE 10.3** NP functionalization with polymers. Reprinted with permissions from Hood M, Mari M, Muñoz-Espí R. Synthetic strategies in the preparation of polymer/inorganic hybrid nanoparticles. *Mater (Basel)*. 2014;7:4057–4087. <https://doi.org/10.3390/ma7054057>. Copyright MDPI journals.

from hydrophilic to hydrophobic and vice versa. Grinding induced covalent functionalization was used to graft carbon-based materials on to the NP surface is a straightforward green method [30]. Encapsulation is another method to functionalize metal-NPs where inorganic or organic material is coated over the surface of NPs to create core shell-type materials [31].

Non-metal nanomaterials like carbon dots and graphene are generally functionalized using covalent modification strategies. These materials often possess conjugation or reactive sites where other molecules can bind through a covalent bond [32,33]. Functionalization of metallic NPs have wide spread applications and there are number of strategies to functionalize the surface depending upon their application. These materials are convenient to functionalize either by noncovalent functionalization using their surface charge or by using metal coordination bonds, or via covalent functionalization by introducing small ligands on to the surface.

*Functionalization of magnetic nanoparticles:* Magnetic NPs (MNPs) are interesting materials with potential use in biomedical applications, but they often fail to deliver due to their toxic nature. The major issues associated with MNPs are their hydrophobicity, toxicity, and poor binding ability with defined target molecules. The successful utilization of MNPs for biological applications requires that surface functionalization should ideally impart the following properties to MNPs [34]. They must be free from aggregation and have increased hydrophilic nature [18]. Capping agents must eliminate the toxicity of MNPs and give control over their magnetic nature. Surface functionalization of MNPs should also prevent their self-association and agglomeration. Functional moieties should be carefully selected to achieve these capabilities, including water compatibility and stability, while at the same time surface functionalization should not adversely affect the magnetic properties of the materials (Fig. 10.4).

## 10.3 Functionalized nanomaterials for biomedical and pharmaceutical applications

### 10.3.1 Functionalized carbon-based materials for biomedical and pharmaceutical applications

Due to their unique physic-chemical properties and exceptional ability to penetrate cell membranes, carbon-based materials like CNTs and graphene are attractive tools for drug delivery [36,37]. Carbon-based materials are also useful in other biomedical fields like biosensing [38], tissue engineering, [39] and gene therapy [40]. Surface functionalization of a suitable ligand to carbon-based material can impart advanced hydrophobic/hydrophilic properties, cell penetrating properties, and site-specific targeting abilities (Fig. 10.5). Such functionalizations are also useful for solubilization of hydrophobic drugs, and its efficient entrapment further allows controlled

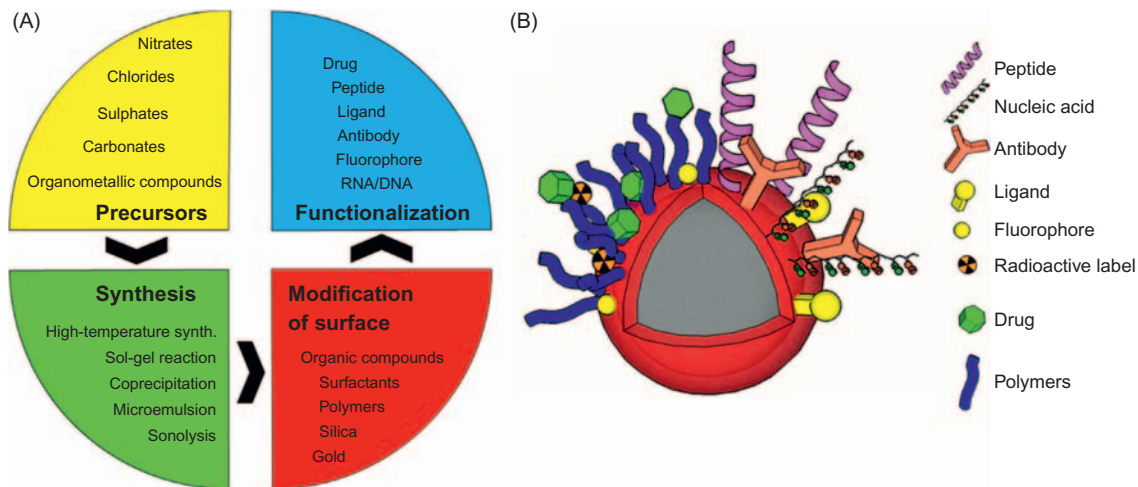


**FIGURE 10.4** Systematic functionalization of MNPs. Reproduced with permissions from Kudr J, Haddad Y, Richtera L, Heger Z, Cernak M, Adam V, et al. *Magnetic nanoparticles: from design and synthesis to real world applications*. *Nanomaterials* 2017;7:243. <https://doi.org/10.3390/nano7090243> [35]. Copyright MDPI journals.

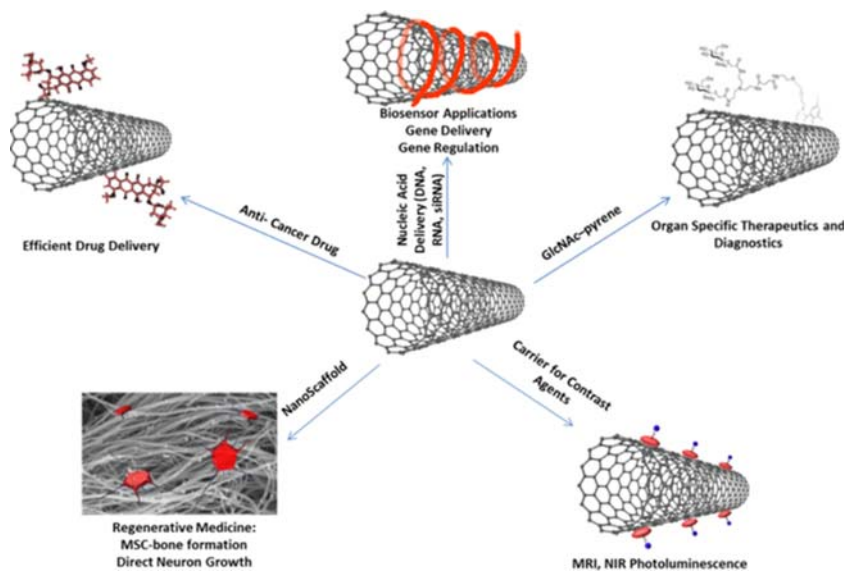


**FIGURE 10.5** Schematic illustration showing the different applications of CNTs such as drug delivery, diagnostics, biosensors, biomedical imaging, as well as tissue engineering and regenerative medicine. *Reproduced with permission. Copyright 1994, ACS.*

release of the drug only to specific disease cells [41]. Several recent studies have shown that single-walled carbon nanotubes (SWNTs) have been functionalized with different bioactive and therapeutic ligands to make them a more effective drug delivery system [42,43]. SWNTs have a large surface area and a workable dimension due to surface modification, which is relatively easy to achieve [44]. A variety of carriers like peptides, proteins, siRNA, therapeutic DNA, and drug molecules can effectively be delivered with high efficiency and potency through functionalized SWCNTs due to their ability to traverse the cell membrane.

Several studies have recently been published on the application of functionalized CNTs. Both SWCNTs and multiwall carbon nanotubes (MWCNT) have been functionalized for various biomedical applications (Fig. 10.5). Guest molecules, like drugs, nucleic acid, siRNA, and metal-NPs, can be effectively attached to CNTs due to the reactive surface sites. Attachment of such ligands imparts biocompatibility and enhances their application as drug carriers. CNTs can also be feasibly modified with peptides, organic molecules, carbohydrates, and polymers, and, as a result, effective drug delivery systems can be designed [45]. Using this method, anticancer drugs and genes were delivered to human gastric cancer cells via polyethylenimine-functionalized carbon nanotubes tagged with AS1411 aptamer. The carboxyl group present SWCNTs surface were first modified with a polyethylene glycol (PEG) linker and then a modified branched polyethylenimine (PEI 10 kDa)

was grafted to create a vehicle for siRNA delivery. Next, an AS1411 aptamer (nucleolin ligand) was covalently attached to SWNT-PEG-PEI conjugate to facilitate drug delivery to the tumor cells overexpressing nucleolin receptors on their surface. Cell viability assays confirmed that the functional SWCNT with doxorubicin intercalated in it could effectively selectively target gastric cancer cells that were overexpressing nucleolin [46]. CNTs have also recently been used to effectively deliver anticancer herbal molecules with improved therapeutic efficacy and safety [47]. In another study, covalent functionalization of the CNTs was done using PEG chains terminated by folic acid fragments. Such functional CNTs hold doxorubicin inside their inner core at a neutral pH, while unloading the drug in a slightly acidic environment. These constructs may serve as excellent carriers of doxorubicin because tumor microenvironments are slightly acidic due to hypoxia, as well the overexpression of folic acid receptors on the surface of cancer cells [48]. The functionalization of both SWCNTs and MWCNTs may be done suitably to allow their complex formation with DNA so CNTs can also potentially be used as gene carriers [27]. MWCNTs have also been functionalized with magneto-fluorescent carbon QDs. As a result, these nanocomposites possess high heat-generating ability, pH and NIR responsive drug delivery, and heat-induced high drug release capacity. Therefore targeting doxorubicin (Dox) through such nanocomposites is very effective and could kill cancer cells at very low concentrations [49]. Liu et al. reported functionalization of carboxylated SWCNT with hydroxypropyl- $\beta$ -Cyclodextrin (HP- $\beta$ -CD) for improving the biocompatibility and reducing the toxicity of CNTs. These functionalized CNTs served as an excellent delivery vehicle for the anticancer drug formononetin (FMN) [50]. In another study Singh et al. used SWCNTs functionalized with polysaccharides, such as alginate (ALG) and chitosan (CHI), as a delivery vehicle for the anticancer drug curcumin [51]. MWCNT functionalized with chitosan-folate has been used for the targeted delivery of docetaxel to lung cancer cells [31]. Chitosan-folate conjugated MWCNT were found to be biocompatible and effectively target docetaxel to lung cancer cells overexpressing the folic acid receptor. The  $IC_{50}$  values indicated that docetaxel loaded inside chitosan-folate conjugated MWCNT was 89-fold more effective than docetaxel delivered alone to human lung cancer cells (A549 cells). A combination approach of targeting anticancer drugs with NPs that are NIR responsive and generate hyperthermia has delivered encouraging results in the treatment of problematic cancers. Recently Wang et al. reported a multimodal MWCNT formed via layer-by-layer deposition of polypyrrole and gold NPs onto the surface of MWCNT. This material was used as an effective carrier of doxorubicin and killed cancer cells effectively via photothermal therapy combined with the drug's anticancer effects [52].

CNT functionalization has also been performed to treat diseases apart from cancer. Nerve growth factor functionalized MWCNT exhibits

neuroprotective effects for prolonged periods in an *in vitro* model of ischemic stroke and could be potentially used for treating neurological disorders [53]. CNTs possess exceptional properties like mechanical strength, optical transparency, and good biocompatibility. These qualities make the materials excellent candidates for treating several pathologies in ophthalmology and excellent therapeutic tools for corneal biomechanic enhancement [54]. MWCNT were functionalized with recombinant Dengue envelope (DENV3E) proteins have also been used as a vaccine against Dengue because it induced significant and specific immune response in mice [55]. The therapeutic efficiency of CNT drug carriers can be further improved by adopting various strategies like optimization of length [56], modulating hydrophilicity of CNTs by PEG functionalization [57], and synthesizing CNT composites with chitosan/gelatine [58].

Apart from CNTs, graphene/grapheme oxide possesses unique physiochemical properties like exceptional mechanical strength, electrical and thermal conductivities, and optical transmittance [59]. Functionalization of the grapheme surface imparts it with more biocompatibility, water solubility, and makes it useful as an excellent drug delivery system (Fig. 10.7). The surface properties of the grapheme-based materials are exceptionally superior due to their nanosize, which in turn leads to a large surface area for interaction with cells. As a result of this, graphene-based nanomaterials can be used for a plethora of biomedical applications including drug and gene delivery, tissue engineering, bioimaging, and biomedical devices [60] (Fig. 10.6).

Several recently published studies demonstrate the application of grapheme-based materials in drug delivery. Wang et al. functionalized the surface of graphene oxide with PEI and PEG. The PEG/PEI modified graphene revealed enhanced cellular uptake and low toxicity in raw264.7 macrophages [61]. Deb et al. designed a chitosan functionalized nanobiocomposite of graphene oxide for the codelivery of two anticancer drugs: camptothecin (CPT) and 3,3'-Diindolylmethane (DIM). The data from *in vivo* studies revealed that drugs carried by these functionalized CNTs showed better biodistribution/bioavailability, low toxicity, and enhanced therapeutic efficiency [62]. Oz et al. reported functionalization of reduced graphene oxide via thiol–maleimide “click” chemistry for easy attachment with the thiol-containing molecules [63]. In another work, a targeted drug delivery system based on nano-graphene oxide was designed by functionalization with dopamine and preparing an aptamer decorated, dextran coated nano-graphene oxide [29]. Xie et al. reported surface modification of graphene oxide (GO) nanosheets by protamine sulfate/sodium alginate for anticancer drug delivery. Such functionalization enables enhanced dispersibility and stability to drug-loaded GO under neutral conditions and drug release only in acidic medium [64]. Functionalization of grapheme oxide with folic acid, tea polyphenols, and AuNPs enable them to act as excellent drug delivery vehicles for curing tumors. Folic acid conjugation leads to targeted



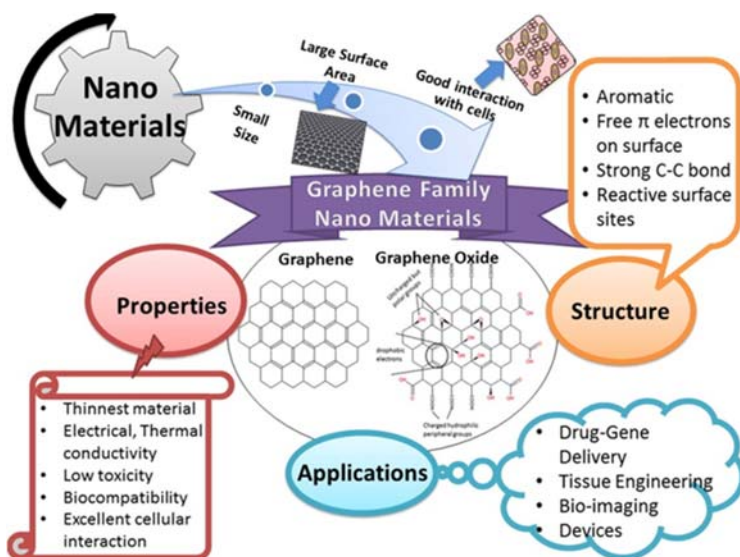


**FIGURE 10.6** Biomedical application of graphene-based materials. *Reproduced with permission from Goenka S, Sant V, Sant S. Graphene-based nanomaterials for drug delivery and tissue engineering. J Control Rel 2014;173:75–88. <https://doi.org/10.1016/j.jconrel.2013.10.017>. Copyright 2014, Elsevier Inc.*

delivery because folic acid receptors are overexpressed in cancerous cells [65]. Functionalization of graphene-based materials with tea polyphenols leads to excellent antioxidant and anti-inflammatory properties and also induce apoptosis in cancerous cells [66]. Functionalization with AuNPs, gold nano shell, and ultrasmall fluorinated graphene shows high NIR absorbance, creating drug delivery systems that could kill tumors by NIR photothermal therapy [67,68].

### 10.3.2 Functionalized metal nanoparticles for biomedical applications

Metal-NPs have immense applications in the biomedical field as molecular probes for cell imaging as drug delivery vehicles and as therapeutic and diagnostic tools [69]. Due to their nanosize, NPs have exceptional optical and electronic properties as compared to bulk metals. For example, bulk gold is inert while gold NPs (AuNPs) are used as a catalyst; bulk gold is yellow, while the color of nanosized gold ranges from wine red to blue due to surface plasmon resonance. Due to these exceptional properties metal-NPs derived from gold and silver are extensively used as sensors and diagnostic tools for identifying biomarkers related to diseases [70]. Different kinds of ligands like aptamers, peptides, oligonucleotides antibodies, and enzymes,



etc. can be readily functionalized on the surface of AuNPs to effectively use them as probes. Oligonucleotides conjugated to AuNPs can be used for detecting complementary DNA; [71] aptamer functionalized AuNPs can bind to target receptors; [72] and enzyme conjugated AuNPs can detect the presence of specific substrates, which may be biomarkers for the disease [73]. AuNPs are being used extensively for developing diagnostic tools for the early detection of cancer [74]. AuNPs-based immunoassay are highly sensitive and can detect cancer-specific biomarkers at very minute concentrations [75]. In these conditions, Kavosi et al. designed ultrasensitive electrochemical immunosensors using AuNPs/PAMAM (Polyamidoamine) dendrimer loaded with an enzyme-linked aptamer as an integrated triple signal amplification strategy for detection of PSA (Prostate specific antigen) biomarkers in prostate cancer cells [76]. Similarly, an electrochemical aptamer/antibody (Apt/Ab) sandwich immunosensor for selective and sensitive detection of epidermal growth factor receptor EGFR, a biomarker for cancer has also been designed [77]. AuNPs are also used effectively in cancer radiotherapy due to their high x-ray absorption and superior chemical, optical, and electrical properties [78].

Apart from the application of AuNPs in the diagnosis of cancer, they can also be used as a therapeutic tool for killing tumors [79]. The therapeutic agents can be efficiently integrated with the engineered NPs of optimal sizes, shapes, and surface properties to prolong their circulation time, increase solubility and biodistribution, and reduce their immunogenicity [80]. AuNPs also serve as an excellent delivery system for drugs, nucleic acid [81], and Si-RNA [82]. The use of these functionalized AuNPs is immense in cancer therapy. Due to the enhanced permeability of cancer cells, AuNPs and their payload can selectively deposit in cancer cells without effecting healthy cells [83]. AuNPs also have exceptional abilities to absorb near infrared (NIR) light. When NIR is shined on them, the AuNPs that are embedded in the cancer cell will absorb NIR leading to heat generation. This process is known as hyperthermia [84]. Hyperthermia drugs will be released from AuNPs, and a combination of the drug, as well as heat, will rupture cancer cells without affecting healthy cells [85]. Thus the applications of functionalized AuNPs for photothermal therapy (PTT) of cancer are of great interest [86]. Due to low toxicity, facile synthesis, easy functionalization, and superior optical properties, AuNPs are the most extensively studied metal-NPs for biomedical applications [87]. The different applications of functionalized AuNPs are shown in Fig. 10.7.

Silver NPs have excellent antibacterial and antimicrobial properties. The functionalization of silver NPs is ideal for targeting a broad spectrum of microbial diseases and to prevent infections. Recently antibacterial properties of both functionalized gold and silver have been extensively illustrated [88]. Functionalization of antimicrobial peptides and polymers may be further executed to enhance the antimicrobial activities of these NPs [89].

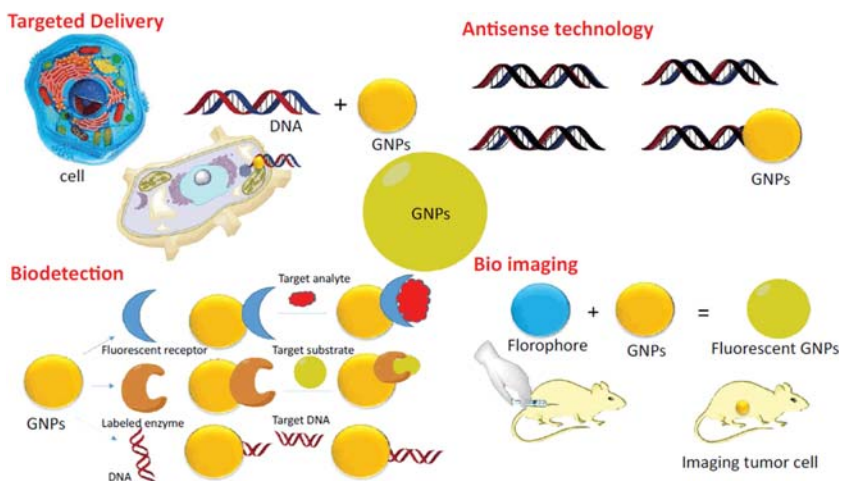


**FIGURE 10.7** Different applications of functionalized AuNPs. *Reproduced with permissions from Tiwari P, Vig K, Dennis V, Singh S. Functionalized gold nanoparticles and their biomedical applications. Nanomaterials 2011;1:31–63. <https://doi.org/10.3390/nano1010031>. Copyright MDPI journals.*

### 10.3.3 Functionalized magnetic nanoparticles for biomedical applications

Magnetic NPs (MNPs), as the name suggests, are nanosized particles with magnetic properties formed by metals like iron, cobalt, and nickel [90]. Due to the unique magnetic properties and ability to interact with the biological system at the cellular and molecular level, MNPs have attracted considerable attention for applications in biomedicine as contrast agents for magnetic resonance imaging (MRI) and as carriers for drug delivery [91]. MNPs can be suitably functionalized with a wide variety of ligands using modern nanotechnology tools and their properties greatly improved [92,93]. However, the safety and efficacy of MNPs are always of great concern. To improve the biocompatibility of MNPs, organic and inorganic polymers like RGD peptides, dextran, chitosan, and fibronectin can be used to coat the magnetic core [15]. Such functionalization greatly improves their biocompatibility by modulating solubility and interaction properties and reducing toxicity [94]. For the biomedical application of MNPs, it is vital that they be biocompatible and have some specified criteria to reduce the risk of any toxicity associated with them [91]. The main criteria that MNPs should possess for successful biomedical applications are biocompatibility, biodegradability, amenability to surface modification, physical and chemical stability, and effectiveness in minimal doses [95]. Fig. 10.8 illustrates the functionalization strategies adopted to make MNPs more biocompatible and accessible for biomedical applications [96].

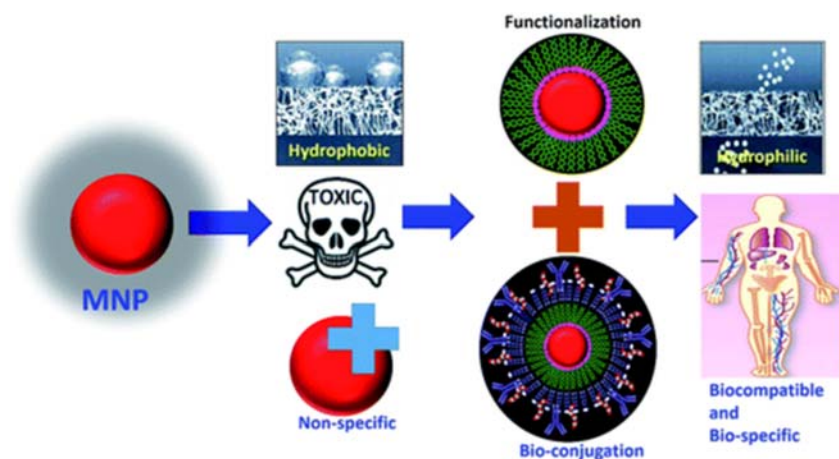


**FIGURE 10.8** Strategies for bridging the gap between MNPs and their successful implementation in healthcare and pharmacy industries. Reproduced with permissions from Markides H, Rotherham M, El Haj AJ. Biocompatibility and toxicity of magnetic nanoparticles in regenerative medicine. *J Nanomater* 2012;2012:1–11. <https://doi.org/10.1155/2012/614094>.

It is desirable that MNPs should have superparamagnetic properties. Superparamagnetic iron oxide NPs (SPIOs) are the most commonly used MNPs for biomedical application because iron is present in the human body naturally in the form of ferritin. Thus the iron-containing NPs are extremely biocompatible because they can be easily metabolized in the body. SPIONs are very small sized MNPs, typically less than 30 nm, and are coated with either a biocompatible organic or inorganic polymer with the core formed by magnetite ( $\text{Fe}_3\text{O}_4$ ) or maghemite ( $\gamma\text{-Fe}_2\text{O}_3$ ). At sizes below 30 nm, magnetite ( $\text{Fe}_3\text{O}_4$ ) or maghemite ( $\gamma\text{-Fe}_2\text{O}_3$ ) acquire superparamagnetism, making the particles ideal for pharmaceutical use because they will not have the tendency to self-agglomerate [97]. A wide variety of biomedical applications are offered by MNPs, like their utility as MRI contrast agents, for magnetic labeling, for cell sorting, for controlled drug release, for killing tumors by hyperthermia, and as biosensors [98]. The functionalization of MNPs ensures that there are controllable interactions with the living cells and no undesired response is elicited. The functionalization strategies also tune the coatings in such a way that the MNPs are best suited for the application envisioned [99].

The most widely used biomedical application of MNPs is as MRI contrast agents. The magnetic particles can penetrate deeply inside cells and produce magnetic signals which can differentiate between diseased and normal cells [100]. The use of iron oxide MNPs has also been approved by the US Food and Drug Administration due to their excellent biocompatibility and low toxicity [101]. Recently multimodal imaging tools have also been designed by functionalizing MNPs to optical and fluorescent probes [102,103]. Another

important application of MNPs is as labeling agents for biological entities like DNA, peptide, and protein cells. Labeling biomolecules with MNPs allow them superior biosensing applications as compared to other fluorescent and optical probes. Many recent studies demonstrate that biomolecules labeled with MNPs are used for biosensing applications, especially in cancer diagnosis. Stem cells could also be labeled by MNPs and their growth and differentiation tracked inside the body [104,105]. MNPs are widely used in regenerative medicine because they have the potential to track the long term fate of the implants and monitor stem cell differentiation [106].

Another important application of MNPs is in controlled drug release [107]. Functionalization of biocompatible nanocarriers with MNPs ensures the drug loaded inside the carrier is released only at the target site [108]. The drug delivery system functionalized via MNPs can be transported to the desired site by the application of a magnetic field. The drug loaded inside a MNP-decorated delivery vehicle can be reliably released at the target site, and its therapeutic efficacy will be enhanced several fold [109]. Another interesting property of MNPs is that they are heated by the application of time, varying by magnetic field, so the local heat generated by this process can be used for killing cancer cells using a combination of chemotherapy and hyperthermia [110]. Due to the enhanced permeation and retention of cancer cells, MNPs can penetrate and become embedded inside cancer cells without going inside normal cells [111]. Cancer cells are also more sensitive to high temperatures as compared to healthy cells, so they burn under these conditions while there is no deterioration in healthy cells. It is also important that the localized magnetic hyperthermia should be produced at a very low concentration of MNPs, and this can be done by modulating the amplitude and frequency of the applied magnetic field [112]. There are several examples in the supporting literature where this combined therapeutic approach has been used for successfully combating cancer [103,113].

### 10.3.4 Functionalized polymer-based nanomaterials for biomedical and pharmaceutical applications

The biodegradable and biocompatible polymers are an excellent scaffold for the design of cutting edge drug carriers because they could help with the effective entrapment and controlled release of the drug only to the target site [114–116]. Functionalization of polymeric nanostructures such as hyper-branched polymers [117], dendrimers, [118] and polymeric micelles [119] are of great interest due to their immense potential in drug delivery. Different types of biodegradable polymers are functionalized with bioactive moiety like folic acid, aptamer, and cell penetrating peptides to utilize their full potential in targeted drug delivery. Using this approach, a variety of multifunctional nanocarriers (e.g., NPs, micelles, polymersomes) for the delivery of molecules like vitamins, hormones, peptides, proteins, si-RNA, nucleic

acid, etc., as well as therapeutic drugs are synthesized [114,120]. The different functionalization strategies adopted for the modification of polymers and their biomedical applications are illustrated in Fig. 10.9.

Polymeric micelles are synthesized via functionalizing hydrophilic segments to hydrophobic biodegradable block polymers. Polymeric micelles (PMs), due to their nanometric size, high stability, (low critical association concentrations (CMC)), and core shell arrangement, serve as excellent drug delivery vehicles [122]. Such PMs could serve as excellent carriers for hydrophobic drugs like doxorubicin since its amphipathic nature will allow the drugs to get solubilized and entrapped and reach the target site without degradation [123,124]. A hydrophobic drug like doxorubicin can also be grafted on a hydrophilic block polymer to make a drug polymer conjugate, which will enhance the therapeutic efficiency of the drug [125]. Hydrophobic biodegradable polymers can also be functionalized or grafted with therapeutic moiety, that is, hydrophilic aptamers or si-RNA to develop a combination drug delivery system [126,127]. Another interesting class of polymers are the stimulus-responsive polymers. Such polymeric systems exhibit large, sharp changes in response to physical (such as temperature, solvents, or light) and chemical stimuli (such as reactants, pH, ions in solution, or chemical recognition). These polymers are of great use in controlled drug delivery, and they facilitate release of the drug only in response to desired stimuli. In a recent review, Zhou et al. comprehensively covered the advances in the development of stimuli-responsive PMs for drug delivery, imaging, and cancer therapy [128]. Fig. 10.10 illustrates

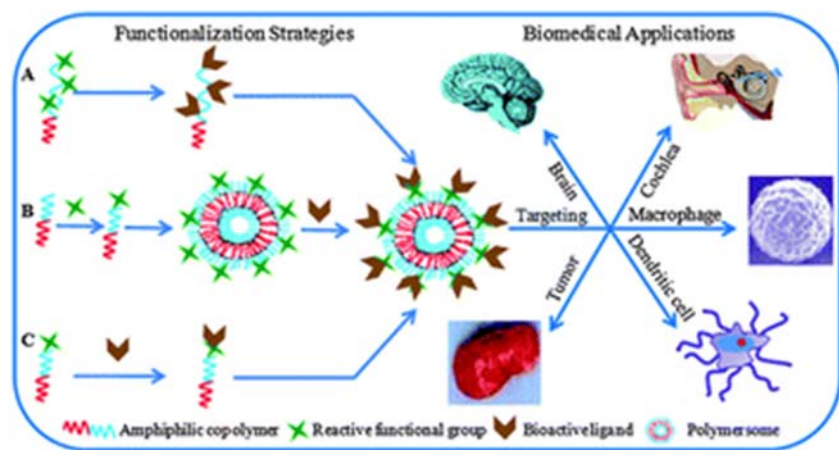


**FIGURE 10.9** Functionalization strategies for biomedical applications. *Reproduced with permissions from Pawar PV, Gohil SV, Jain JP, Kumar N. Functionalized polymersomes for biomedical applications. Polym Chem 2013;4:3160. <https://doi.org/10.1039/c3py00023k> [121]. Copyright Royal Society of Chemistry.*

the different functionalization strategies adopted for effective therapeutic application of PMs.

Apart from micelles, other polymeric nanocarriers used widely for targeted drug delivery include nanocapsules, nanogels, liposomes, dendrimers, and biodegradable and biocompatible hybrid polymer-based NPs [129]. These polymer NPs have been efficiently functionalized to create multifunctional therapeutic vehicles for treatment of a variety of diseases [130]. Recently, several interesting reports on the functionalization of biopolymers and their biomedical applications were published. In one report, Wei et al. conjugated a new tumor-penetrating peptide, cysteine-arginine-glycine-aspartic acid-lysine (CRGDK), onto the surface of doxorubicin encapsulated polymeric micelles (PM). The CRGDK peptide can specifically bind to neuropilin-1 that is overexpressed in cancer, which leads to enhanced cellular uptake and cytotoxicity as assessed by in vitro studies. In vivo studies revealed a high accumulation and penetration of drug-loaded PMs on tumor

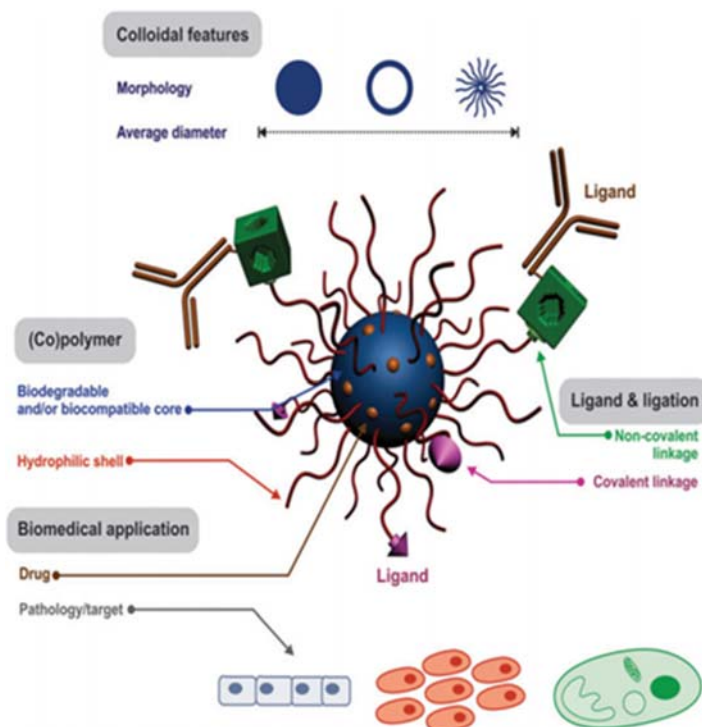


**FIGURE 10.10** Functionalization of PMs for drug delivery. Reprinted with permission from Nicolas J, Mura S, Brambilla D, MacKiewicz N, Couvreur P. Design, functionalization strategies and biomedical applications of targeted biodegradable/biocompatible polymer-based nanocarriers for drug delivery. *Chem Soc Rev* 2013;42:1147–1235. <https://doi.org/10.1039/c2cs35265f> [120]. Copyright Royal Society of Chemistry.



cells leading to their greater therapeutic efficiency [131]. Deng et al. described the design of a biodegradable PMs loaded with doxorubicin that could efficiently suppress tumors by killing circulating tumor cells [132]. Zhu et al. show that cRGD-functionalized biodegradable PMs mediates enhanced doxorubicin (DOX) delivery to U87MG glioma xenografts in vivo [133]. In their comprehensive review, Pang et al. review the recent advances in pH-responsive polymer–drug conjugates with different chemical structures and architectures, and they attempt to clarify their mechanism of action, synthesis, and characterization technology [134]. Cagel et al. presented relevant research outcomes, which revealed polymeric mixed micelles are better drug delivery systems as compared to polymeric pristine micelles [135]. Multifunctional and multimodal therapeutic polymer carriers are also created by adding AuNPs/MNPs and QDs for loading drugs. Such multifunctional carriers are very effective theragnostic tools for targeting diseases cells because they can be used for imaging, diagnosing, and curing the diseased cells [136].

## 10.4 Application of functionalized nanomaterials in agriculture and agroindustry

Nanotechnology permits broad advances in agricultural research, due to the distinct properties of nanomaterials like improved plant disease resistance, efficient nutrient utilization, and enhanced plant growth [8,9]. In addition, nanoscale devices with unique properties make the agricultural systems “smart.” Such devices are capable of responding to different situations by themselves, thus taking appropriate remedial action. These smart systems deliver chemicals in a controlled and targeted manner similar to the proposed use of nanodrug delivery in humans [8,137,138]. Smart delivery systems in agriculture should possess a combination of time controlled, specifically targeted, highly controlled, remotely regulated/preprogramed/self-regulated, and multifunctional characteristics to avoid biological barriers for successful targeting. Agriculture and food system security, innovative delivery systems for disease treatment, new tools for molecular and cellular biology, and new materials for plant pathogen detection are some of the nanotechnological links to agriculture science [9,139].

### 10.4.1 Impact of functionalized nanomaterials in agriculture

The functional carbon-based nanomaterials (fCBNMs) have become very important materials for the agricultural industry due to their distinctive optical properties, high mechanical strength, and electrical and thermal conductivity. The advantage of using fCBNMs, especially carbon nanotubes (CNTs), single-wall carbon nanotubes (SWCNTs), double-wall (DWCNTs), and multiwall (MWCNTs) functionalized with MNPs (fMNPs) (commonly consist of two components, a magnetic material and a chemical component

that has functionality) is that the inner, unoccupied area allows packing of suitable chemicals for plant protection, and fMNPs allow outer control of the movement of nanocarriers inside the plant structure [9,140]. Properly functionalized nanocapsules result in greater piercing via the cuticle and allow for the controlled and slow release of herbicides to reach the target weed. This is a best example for reducing the plant toxicity of herbicides on agricultural crops by controlling parasitical weeds with nanocapsulated active ingredients [141]. Other studies show that amine terminated tetra (ethylene glycol) functionalized honeycomb mesoporous silica NPs (MSNs) with 3-nm pores can transport DNA and chemicals into both plant cells and intact leaves [142]. Surface modified NMs (coating and functionalization) can significantly change and transform the properties for their absorption and accumulation by the plant [143].

Several studies show mixed (positive and negative) results on the plant toxicity of CNMs in plant systems [9]. One suggests that CNMs have some beneficial effects on seed germination, growth, and development, as well as several plant physiological processes, while a second study indicates that CNMs have toxic effect on plants [9]. Cañas et al. [144] reported the root elongation of six different plant species (*Brassica oleracea*, *Daucus carota*, *Cucumis sativus*, *Lactuca sativa*, *Allium cepa*, and *Solanum lycopersicum*) and phytotoxicity after exposure to SWCNTs nonfunctionalized and functionalized with poly-3-aminobenzenesulfonic. The SWCNTs boost the growth of *Cucumis sativus* and *Allium cepa* onion in 24–48 h, while remarkably affecting root elongation of *Brassica oleracea*, *Daucus carota*, *Lactuca sativa*, and *Solanum lycopersicum*. A wide range of concentrations of functionalized SWCNTs (9–1750 µg/mL) were found to have no effect on the physiology and developmental processes of *Brassica oleracea* and *Daucus carota*. However, most of the studies showed that high concentrations of NMs indicated a certain degree of the phytotoxicity. Among the six species tested, the *Lycopersicon esculentum* showed the highest degree of sensitivity to SWCNTs [144]. The researchers showed that fCNTs, especially CNTs, revealed distinct toxic behaviors on plants but generally were less toxic than non-fCNTs. However, how the CNTs were functionalized was not specified. In spite of this, their study focuses on the significance of surface properties of CNTs in determining toxicity in plant species.

Hamdi et al. [145] showed that non-fMWCNTs decreased the root (88%) and shoot (78%) pesticide (chlordane, cis- and trans-chlordane, trans-nonachlor) content in lettuce. The suppression was more modest with amino-fMWCNT, where root decreases were 57%, and shoots were only 23%, relative to controls, after exposure 1000 mg/L non-fMWCNT for 19 days. These findings have implications for food safety and for the use of engineered NMs in agriculture, especially with leafy vegetables [145].

The highest increases in seed germination and enhanced seedling growth were observed for tomato plants exposed to fMWCNTs with stronger



negative groups and well-dispersed MWCNTs. The authors propose that fMWCNTs enhanced the production of water channel protein (WCP) in tomato plants [146]. The exposure of tomato cells to carboxylic-fCNTs could lead to the activation of stress-related genes such as TDR3 and heat shock protein 90 and the gene (*LeAqp2*) for tomato WCP [147]. In Arabidopsis, exposure of carboxyl-groups functionalized CNTs induced a decrease in the defence response, which was partially reversed with the exogenous application of salicylic acid [148]. The activation of root initiation and root elongation was recently observed in in vitro cultures of blackberry treated with fSWCNTs [149].

Chen et al. demonstrated that wheat plant growth was increased under the amine-functionalized graphene (fGO) exposure, and the stem (19.61%) and root (19.27%) lengths were enhanced at high concentrations (2000  $\mu\text{g/mL}$ ). However, the plant tissue structures were not affected, and neither unfunctionalized GO nor fGO were observed to accumulate in the wheat plant root cells [150].

The adhesion strength strongly depended on the functional groups on the NP (three abamectin-loaded poly lactic acid (PLA) NPs ( $\text{CH}_3\text{CO-PLA-NS}$ ,  $\text{HOOC-PLA-NS}$ , and  $\text{H}_2\text{N-PLA-NS}$ ) with various functional groups) surface, and was easily regulated by varying functional groups. These results reveal a route to develop smart pesticide NPs with adhesion regulation through light, heat, or pH for different purposes in crop protection. Using these smart pesticide NPs, it becomes possible that pesticide losses could be substantially lowered and effective utilization efficiency improved, leading to decreased spraying dosage, residue, and pollution in food and the environment [151].

Apart from controlled release, silica NMs have also been proposed as active ingredients against insect pests. Since many insects, such as the *Sitophilus* species that infests agricultural products during storage, have become resistant to a variety of active ingredients, that also remain as residue on the protected crops, Debnath et al. proposed the application of surface functionalized silica NMs as an insecticide [152] to overcome the problem of resistance development to conventional insecticides. In their study [152], regardless of the mechanism of action, silica NM achieved up to 69% mortality of *Sitophilus* adults, whereas the bulk form only reached 23%, indicating the presence of a nonspecific effect.

#### 10.4.2 Impact of surface modified, labeled, and conjugated nanomaterials in agriculture

Nanotechnology is used in the agricultural industry primarily for the development of new materials via different strategies, including coating, labeling, conjugated, and functionalized nanomaterials. To date, nanomaterials have been applied to the following plant species with the indicated impact: *Lemna minor*

(coated ZnO NPs; size: 20 nm; impact on plant: toxicity [153]); *Cucumis sativus* (coated ZnO NPs; size: 75 nm; impact on plant: phytotoxicity [154]); *Pisum sativum* (Fe@ZnO NPs; size: 130 nm; impact on plant: no sign of toxicity [155]); *Gossypium hirsutum* (phycomolecule-coated –ZnO NPs; size 2–54 nm; impact on plant-enhanced growth and biomass [156]); *Zea mays* and *Brassica oleracea* var. capitata (citrate-coated-Ag; size: 11 nm; impact on plant: inhibition of germination and early development [157]); *Lolium multiflorum*, *Panicum virgatum*, *Carex lurida*, *C. scoparia*, *C. vulpinoidea*, *C. lorum*, *Eupatorium fistulosum*, *Phytolacca lorum* s, *Scirpus cyperinus*, *Lobelia cardinalis*, *Juncus lorum* (poly vinyl pyrrolidone (PVP), and gum arabic coated-Ag; size: 21 and 6 nm; impact on plants: indirect and direct effects of NPs [158]); *Actinidia deliciosa* var. *deliciosa* (PVP-coated-AgNPs; size: 10 nm; impact on plant: damaged pollen membranes and inhibited pollen germination [159]); *A. thaliana* (PVP-coated-AgNPs; size: 20 nm; impact on plant: biomass declined [160]); *Eruca sativa* (coated PVP-coated-AgNPs; size: 10 nm; impact on plant: improvement in plant growth [161]); *Arabidopsis* and poplar (carbon-coated and PEG-coated-AgNPs; size: 25 nm and 5, 10 nm; impact on plant: stimulated root elongation, fresh weight [162]); *Ricinus communis* (PVP-coated-AgNPs; size: <100 nm; impact on plant: no effect on seed germination [163]); *Triticum aestivum* (PVP-coated-AgNPs; size: 10 nm; impact on plant: affect the levels of several proteins in multiple cellular compartments and toxicity is driven primarily by released Ag ions [164]); *A. thaliana* (citrate-stabilized AgNPs; size: 20 nm; impact on plant: accumulated in stomatal guard cells [165]); *Spirodela polyrrhiza* (GA-AgNPs; size 6, 20 nm; impact on plant: induced reactive oxygen species accumulation, changed the antioxidant enzymes activities, and NPs also changed the chloroplast ultrastructure [166]); *Nicotiana xanthi* (citrate-capped AuNPs; size: 3.5 and 18 nm; impact on plant: necrotic lesions till 2 weeks and later on no stress [167]); *Oryza sativa*, *Raphanus sativus*, *Cucurbita mixta* cv. *White cushaw*, and *Lolium perenne* L. (functionalized Au NPs; size: 6–10 nm; impact on plant: most efficiently translocated into plant shoots from the roots [168]); *Solanum lycopersicum* (PVP-coated-AuNPs; size: 10, 12, 15, 20, 30, 40, 50, 80, and 100 nm [169]); *Hordeum vulgare* (citrate-stabilized AuNPs; size: 2, 21 nm; impact on plant: translocation [170]); *Allium cepa* (citrate-capped AuNPs; size: 15, 30, 40 nm; impact on plant: phytotoxicity [171]); *Nicotiana tabacum* cv *petite Havana* (mesoporous silica nanoparticles (MSNPs)–Fluorescein isothiocyanate (FITC) labeled; size: 100–200 nm; impact on plant: NPs pores that can transport DNA [142]); *Quercus macdougalii* (citrate-coated Fe<sub>3</sub>O<sub>4</sub>; size: 6–10 nm; impact on plant: improved the germination and growth parameters [172]); *Triticum aestivum* (citric acid–Fe<sub>3</sub>O<sub>4</sub> NPs; size: ~18 nm; impact on plants: exposure did not alter germination, plant growth, and chlorophyll content [173]); *Zea mays* (FITC-conjugated ZnO; size: 15–30 nm; NPs are transported by the apoplastic pathway to the endodermis [174]); *Citrullus lanatus*

(FITC-conjugated  $\gamma$ -Fe<sub>2</sub>O<sub>3</sub>; size: 21.2 nm); *Zea mays* (FITC-conjugated-Fe<sub>2</sub>O<sub>3</sub>; size: 17.7 nm; concentration depended effect [92,93]); *Citrus reticulata* (FITC-conjugated  $\gamma$ -Fe<sub>2</sub>O<sub>3</sub>; size: 82.9 nm; NPs at low concentration contribute to the synthesis of chlorophyll [42,43]); *S. lycopersicum* (citric acid coated-CeO<sub>2</sub>NPs; size: 8231 nm; impact on plant: coated and bare NPs increased stem length, while coated increased CAT activity, total chlorophyll, Chl. a and Chl. b in leaves [175]); *Brassica napus* (PVP-coated-CeO<sub>2</sub>NPs; size: 55.6 nm; impact on plant: enhanced photosynthetic machinery performance and proline synthesis regulation [176]); canola (citrate-coated-CeO<sub>2</sub>; size: 3.5 or 31 nm [177]); Lily (ZnS-coated CdSe QDs; size: 6.3 nm; impact on plant: QDs were utilized for live imaging in plant systems [178]); *Allium fistulosum* (QD565 streptavidin conjugate; size: 15 nm; comparison of QDs with conventional detection systems in immune-labeling experiments demonstrated greater sensitivity than the conventional system [179]); *Zea mays* (water-soluble mercapto-acetic acid (MAA)-coated CdSe/ZnS QDs; QDs caused very low cytotoxicity on maize seed germination and root growth [180]); *Medicago sativa* (mercapto-propanoic acid (MPA) coated CdSe/ZnS QDs; size: 3.6–4.5 nm; impact on plant: cell growth was significantly reduced [181]); *Nicotiana tabacum* (silica/BSA-coated QDs; size: ?; impact on plant: successfully employed Trojan peptoids as vehicles into living tobacco cells [182]); rice (MPA-linked-Oleic acid-CdSe QDs; size: ?; impact on plant: seed germination was arrested with QD [183]); tomato (CNTs-QD conjugates; size: ?; impact on plant: significantly accelerating leaf senescence and inhibiting root formation [184]); *Medicago sativa* (MPA-CdSe/ZnS QDs; size: 13.5 nm; impact on plant: QDs were found to be cytotoxic and genotoxic to plant cells, although not lethal [185]); *Arabidopsis thaliana* [coated CdSe/CdZnS QDs (Coatings: poly(acrylic acid-ethylene glycol) (PAA-EG), polyethylenimine (PEI) and poly(maleic anhydride-alt-1-octadecene)–poly(ethylene glycol) (PMAO–PEG)); size: (data not shown); impact on plant: showed generally uniform distribution in the leaves and more cadmium accumulation [186]. The recent research shows that positively charged AuNPs are most readily taken up by plant roots, while negatively charged AuNPs are most efficiently translocated into plant shoots (including stems and leaves) from the roots [168].

## 10.5 Conclusion

The functionalization of NPs offers several advantages and makes them suitable for a wide range of applications from diagnosis to therapy for controlling plant and animal diseases. The properties of nanomaterials have been tuned via functionalization in order to perform the desired functions. To successfully prepare a functional NP for biomedical or agricultural applications, it is necessary to carefully select and optimize the functionalization strategies. A careful analysis of the physico-chemical and biological properties

should be performed, and the nature of core, shell, and ligands should be carefully tuned. It is also necessary to understand the biological interactions of nanomaterials with plant and animal cells and to address safety concerns for successful implementation in pharma and agro-based applications.

## References

- [1] Vajtai R, editor. Springer handbook of nanomaterials. Berlin, Heidelberg: Springer; 2013. Available from: <https://doi.org/10.1007/978-3-642-20595-8>.
- [2] Filippini L, Sutherland D. Nanotechnologies: principles, applications, implications and hands-on activities. Publ. Off. Eur. Union, Luxemb, 2013.
- [3] Sarmento B, das Neves J. Biomedical applications of functionalized nanomaterials concepts, development and clinical translation, micro and nano technologies. Elsevier Science; 2018.
- [4] Thanh NTK, Green LAW. Functionalisation of nanoparticles for biomedical applications. Nano Today 2010;5:213–30. Available from: <https://doi.org/10.1016/j.nantod.2010.05.003>.
- [5] Holzinger M, Le Goff A, Cosnier S. Nanomaterials for biosensing applications: a review. Front Chem 2014;2. Available from: <https://doi.org/10.3389/fchem.2014.00063>.
- [6] Liu D, Yang F, Xiong F, Gu N. The smart drug delivery system and its clinical potential. Theranostics 2016;6:1306–23. Available from: <https://doi.org/10.7150/thno.14858>.
- [7] Srilatha B. Nanotechnology in agriculture. J Nanomed Nanotechnol 2011;02. Available from: <https://doi.org/10.4172/2157-7439.1000123>.
- [8] Verma SK, Das AK, Patel MK, Sah A, Kumar V, Gantait S. Engineered nanomaterials for plant growth and development: a perspective analysis. Sci Total Environ 2018;630 (C):1413–35. Available from: <https://doi.org/10.1016/j.scitotenv.2018.02.313>.
- [9] Verma SK, Das AK, Gantait S, Kumar V, Gurel E. Applications of carbon nanomaterials in the plant system: a perspective view on the pros and cons. Sci Total Environ 2019;667:485–99. Available from: <https://doi.org/10.1016/j.scitotenv.2019.02.409>.
- [10] Hussain CM, editor. Handbook of nanomaterials for industrial applications. Elsevier; 2018.
- [11] Hussain CM, Kharisov B, editors. Advanced environmental analysis: applications of nanomaterials, Vol. 1. Royal Society of Chemistry; 2016.
- [12] Joseph T, Morrison M. Nanotechnology in agriculture and food science, a nanoforum report. Weinheim, Germany: Wiley-VCH Verlag GmbH & Co. KGaA; 2017. Available from: <https://doi.org/10.1002/9783527697724>.
- [13] Mukhopadhyay SS. Nanotechnology in agriculture: prospects and constraints. Nanotechnol Sci Appl 2014;7:63–71. Available from: <https://doi.org/10.2147/NSA.S39409>.
- [14] Zeng S, Yong KT, Roy I, Dinh XQ, Yu X, Luan F. A review on functionalized gold nanoparticles for biosensing applications. Plasmonics 2011;6:491–506. Available from: <https://doi.org/10.1007/s11468-011-9228-1>.
- [15] Jinhao GAO, Hongwei GU, Bing XU. Multifunctional magnetic nanoparticles: design, synthesis, and biomedical applications. Acc Chem Res 2009;42:1097–107. Available from: <https://doi.org/10.1021/ar9000026>.
- [16] Chatterjee K, Sarkar S, Jagajjanani Rao K, Paria S. Core/shell nanoparticles in biomedical applications. Adv Colloid Interface Sci 2014;209:8–39. Available from: <https://doi.org/10.1016/j.cis.2013.12.008>.

- [17] Imec I, Nanowire GS, Material ACS, Chemicals A, Imec F. Functionalize Nanoparticles for Biomedical Applications 3–4 2007. <https://doi.org/10.1007/s11095-012-0736-2>.
- [18] Sun T, Zhang YS, Pang B, Hyun DC, Yang M, Xia Y. Engineered nanoparticles for drug delivery in cancer therapy. *Angewandte Chemie International Edition* 2014;53(46):12320–64. Available from: <https://doi.org/10.1002/anie.201403036>.
- [19] Zou J, Dai Q, Guda R, Liu X, Worden JG, Goodson T, et al. Controlled chemical functionalization of gold nanoparticles. *ACS Symp Ser* 2008;996:31–40. Available from: <https://doi.org/10.1021/bk-2008-0996.ch003>.
- [20] Chen Y, Xianyu Y, Jiang X. Surface modification of gold nanoparticles with small molecules for biochemical analysis. *Acc Chem Res* 2017;50:310–19. Available from: <https://doi.org/10.1021/acs.accounts.6b00506>.
- [21] Choueiri RM, Galati E, Thérien-Aubin H, Klinkova A, Larin EM, Querejeta-Fernández A, et al. Surface patterning of nanoparticles with polymer patches. *Nature* 2016;538:79–83. Available from: <https://doi.org/10.1038/nature19089>.
- [22] Premkumar T, Geckeler KE. Cucurbit[7]uril as a tool in the green synthesis of gold nanoparticles. *Chem Asian J* 2010;5:2468–76. Available from: <https://doi.org/10.1002/asia.201000338>.
- [23] Hood M, Mari M, Muñoz-Espí R. Synthetic strategies in the preparation of polymer/inorganic hybrid nanoparticles. *Mater (Basel)* 2014;7:4057–87. Available from: <https://doi.org/10.3390/ma7054057>.
- [24] Binder WH, Zirbs R, MacHi D, Gahleitner M. Grafting polyisobutylene from nanoparticle surfaces: concentration and surface effects on livingness. *Macromolecules* 2009;42:7379–87. Available from: <https://doi.org/10.1021/ma900535e>.
- [25] Parda F, Lapinte V, Robin J, Charles I, Montpellier G, Equipe UMRC. Modification of silica nanoparticles by grafting of copolymers containing organosilane and fluorine moieties 12–15, 2009. <https://doi.org/10.1002/pola>.
- [26] Tahir MN. Functionalized surfaces and surface functionalization of nanomaterials. *Single Mol* 2006;1–161.
- [27] Caoduro C, Hervouet E, Girard-Thernier C, Gharbi T, Boulahdour H, Delage-Mourroux R, et al. Carbon nanotubes as gene carriers: focus on internalization pathways related to functionalization and properties. *Acta Biomater* 2017;49:36–44. Available from: <https://doi.org/10.1016/j.actbio.2016.11.013>.
- [28] Liu B, Liu J. Methods for preparing DNA-functionalized gold nanoparticles, a key reagent of bioanalytical chemistry. *Anal Methods* 2017;9:2633–43. Available from: <https://doi.org/10.1039/c7ay00368d>.
- [29] Alibolandi M, Mohammadi M, Taghdisi SM, Ramezani M, Abnous K. Fabrication of aptamer decorated dextran coated nano-graphene oxide for targeted drug delivery. *Carbohydr Polym* 2017;155:218–29. Available from: <https://doi.org/10.1016/j.carbpol.2016.08.046>.
- [30] Kasprzak A, Bystrzejewski M, Koszytkowska-Stawinska M, Poplawska M. Grinding-induced functionalization of carbon-encapsulated iron nanoparticles. *Green Chem* 2017;19:3510–14. Available from: <https://doi.org/10.1039/c7gc00282c>.
- [31] Singh RP, Sharma G, Sonali, Singh S, Bharti S, Pandey BL, et al. Chitosan-folate decorated carbon nanotubes for site specific lung cancer delivery. *Mater Sci Eng C* 2017;77:446–58. Available from: <https://doi.org/10.1016/j.msec.2017.03.225>.
- [32] Namdari P, Negahdari B, Eatemadi A. Synthesis, properties and biomedical applications of carbon-based quantum dots: an updated review. *Biomed Pharmacother* 2017;87:209–22. Available from: <https://doi.org/10.1016/j.biopha.2016.12.108>.

- [33] Ioniță M, Vlăsceanu GM, Watzlawek AA, Voicu SI, Burns JS, Iovu H. Graphene and functionalized graphene: extraordinary prospects for nanobiocomposite materials. *Compos Part B Eng* 2017;121:34–57. Available from: <https://doi.org/10.1016/j.compositesb.2017.03.031>.
- [34] Serrano R, Stafford S. Recent progress in synthesis and functionalization of multimodal fluorescent-magnetic nanoparticles for biological applications. *Appl Sci* 2018;8:172. Available from: <https://doi.org/10.3390/app8020172>.
- [35] Kudr J, Haddad Y, Richtera L, Heger Z, Cernak M, Adam V, et al. Magnetic nanoparticles: from design and synthesis to real world applications. *Nanomaterials* 2017;7:243. Available from: <https://doi.org/10.3390/nano7090243>.
- [36] Liu Z, Robinson JT, Tabakman SM, Yang K, Dai H. Carbon materials for drug delivery & cancer therapy. *Mater Today* 2011;14:316–23. Available from: [https://doi.org/10.1016/S1369-7021\(11\)70161-4](https://doi.org/10.1016/S1369-7021(11)70161-4).
- [37] Alshehri R, Ilyas AM, Hasan A, Arnaout A, Ahmed F, Memic A. Carbon nanotubes in biomedical applications: factors, mechanisms, and remedies of toxicity. *J Med Chem* 2016;59:8149–67. Available from: <https://doi.org/10.1021/acs.jmedchem.5b01770>.
- [38] Zhu Z. An overview of carbon nanotubes and graphene for biosensing applications. *Nano-Micro Lett* 2017;9. Available from: <https://doi.org/10.1007/s40820-017-0128-6>.
- [39] Ku SH, Lee M, Park CB. Carbon-based nanomaterials for tissue engineering. *Adv Healthc Mater* 2013;2:244–60. Available from: <https://doi.org/10.1002/adhm.201200307>.
- [40] Cha C, Shin SR, Annabi N, Dokmeci MR, Khademhosseini A. Carbon-based nanomaterials: multifunctional materials for biomedical engineering. *ACS Nano* 2013;7:2891–7. Available from: <https://doi.org/10.1021/nn401196a>.
- [41] Berlin JM, Leonard AD, Pham TT, Sano D, Marciano DC, Yan S, et al. Effective drug delivery, in vitro and in vivo, by carbon-based nanovectors noncovalently loaded with unmodified paclitaxel. *ACS Nano* 2010;4:4621–36. Available from: <https://doi.org/10.1021/nn100975c>.
- [42] Li Z, de Barros ALB, Soares DCF, Moss SN, Alisaraie L. Functionalized single-walled carbon nanotubes: cellular uptake, biodistribution and applications in drug delivery. *Int J Pharm* 2017;524:41–54. Available from: <https://doi.org/10.1016/j.ijpharm.2017.03.017>.
- [43] Li J, Hu J, Xiao L, Gan Q, Wang Y. Physiological effects and fluorescence labeling of magnetic iron oxide nanoparticles on citrus (*Citrus reticulata*) seedlings. *Water, Air, & Soil Pollution* 2017;228(1):52.
- [44] Beg S, Rahman M, Jain A, Saini S, Hasnain MS, Swain S, et al. Emergence in the functionalized carbon nanotubes as smart nanocarriers for drug delivery applications. *Fullerenes, graphenes and nanotubes*. Elsevier; 2018. p. 105–33. Available from: <https://doi.org/10.1016/B978-0-12-813691-1.00004-X>.
- [45] Mahajan S, Patharkar A, Kuche K, Maheshwari R, Deb PK, Kalia K, et al. Functionalized carbon nanotubes as emerging delivery system for the treatment of cancer. *Int J Pharm* 2018;548:540–58. Available from: <https://doi.org/10.1016/j.ijpharm.2018.07.027>.
- [46] Taghavi S, Nia AH, Abnous K, Ramezani M. Polyethylenimine-functionalized carbon nanotubes tagged with AS1411 aptamer for combination gene and drug delivery into human gastric cancer cells. *Int J Pharm* 2017;516:301–12. Available from: <https://doi.org/10.1016/j.ijpharm.2016.11.027>.
- [47] Jogi H, Maheshwari R, Raval N, Kuche K, Tambe V, Mak KK, et al. Carbon nanotubes in the delivery of anticancer herbal drugs. *Nanomedicine* 2018;13:1187–220. Available from: <https://doi.org/10.2217/nnm-2017-0397>.

- [48] Wolski P, Nieszporek K, Panczyk T. Pegylated and folic acid functionalized carbon nanotubes as pH controlled carriers of doxorubicin. Molecular dynamics analysis of the stability and drug release mechanism. *Phys Chem Chem Phys* 2017;19:9300–12. Available from: <https://doi.org/10.1039/c7cp00702g>.
- [49] Zhang M, Wang W, Wu F, Yuan P, Chi C, Zhou N. Magnetic and fluorescent carbon nanotubes for dual modal imaging and photothermal and chemo-therapy of cancer cells in living mice. *Carbon N Y* 2017;123:70–83. Available from: <https://doi.org/10.1016/j.carbon.2017.07.032>.
- [50] Liu X, Xu D, Liao C, Fang Y, Guo B. Development of a promising drug delivery for formononetin: cyclodextrin-modified single-walled carbon nanotubes. *J Drug Deliv Sci Technol* 2018;43:461–8. Available from: <https://doi.org/10.1016/j.jddst.2017.11.018>.
- [51] Singh N, Sachdev A, Gopinath P. Polysaccharide functionalized single walled carbon nanotubes as nanocarriers for delivery of curcumin in lung cancer cells. *J Nanosci Nanotechnol* 2018;18:1534–41. Available from: <https://doi.org/10.1166/jnn.2018.14222>.
- [52] Wang D, Hou C, Meng L, Long J, Jing J, Dang D, et al. Stepwise growth of gold coated cancer targeting carbon nanotubes for the precise delivery of doxorubicin combined with photothermal therapy. *J Mater Chem B* 2017;5:1380–7. Available from: <https://doi.org/10.1039/c6tb02755e>.
- [53] Hassanzadeh P, Arbabi E, Atyabi F, Dinarvand R. Nerve growth factor-carbon nanotube complex exerts prolonged protective effects in an in vitro model of ischemic stroke. *Life Sci* 2017;179:15–22. Available from: <https://doi.org/10.1016/j.lfs.2016.11.029>.
- [54] Alió JL, editor. Keratoconus, essentials in ophthalmology. Cham: Springer International Publishing; 2017. Available from: <https://doi.org/10.1007/978-3-319-43881-8>.
- [55] Versiani AF, Astigarraga RG, Rocha ESO, Barboza APM, Kroon EG, Rachid MA, et al. Multi-walled carbon nanotubes functionalized with recombinant Dengue virus 3 envelope proteins induce significant and specific immune responses in mice. *J Nanobiotechnology* 2017;15:26. Available from: <https://doi.org/10.1186/s12951-017-0259-4>.
- [56] Farbod M, Zilaie A, Kazeminezhad I. Carbon nanotubes length optimization for preparation of improved transparent and conducting thin film substrates. *J Sci Adv Mater Devices* 2017;2:99–104. Available from: <https://doi.org/10.1016/j.jsamd.2017.02.005>.
- [57] Hadidi N, Kobarfard F, Nafissi-Varcheh N, Aboofazeli R. Optimization of single-walled carbon nanotube solubility by noncovalent PEGylation using experimental design methods. *Int J Nanomed* 2011;6:737–46. Available from: <https://doi.org/10.2147/IJN.S17626>.
- [58] Sharmeen S, Rahman AFMM, Lubna MM, Salem KS, Islam R, Khan MA. Polyethylene glycol functionalized carbon nanotubes/gelatin-chitosan nanocomposite: an approach for significant drug release. *Bioact Mater* 2018;3:236–44. Available from: <https://doi.org/10.1016/j.bioactmat.2018.03.001>.
- [59] Liu J, Cui L, Losic D. Graphene and graphene oxide as new nanocarriers for drug delivery applications. *Acta Biomater* 2013;9:9243–57. Available from: <https://doi.org/10.1016/j.actbio.2013.08.016>.
- [60] Goenka S, Sant V, Sant S. Graphene-based nanomaterials for drug delivery and tissue engineering. *J Control Rel* 2014;173:75–88. Available from: <https://doi.org/10.1016/j.jconrel.2013.10.017>.
- [61] Wang B, Su X, Liang J, Yang L, Hu Q, Shan X, et al. Synthesis of polymer-functionalized nanoscale graphene oxide with different surface charge and its cellular uptake, biosafety and immune responses in Raw264.7 macrophages. *Mater Sci Eng C* 2018;90:514–22. Available from: <https://doi.org/10.1016/j.msec.2018.04.096>.



- [62] Deb A, Andrews NG, Raghavan V. Natural polymer functionalized graphene oxide for co-delivery of anticancer drugs: in-vitro and in-vivo. *Int J Biol Macromol* 2018;113:515–25. Available from: <https://doi.org/10.1016/j.ijbiomac.2018.02.153>.
- [63] Oz Y, Barras A, Sanyal R, Boukherroub R, Szunerits S, Sanyal A. Functionalization of reduced graphene oxide via thiol-maleimide “click” chemistry: facile fabrication of targeted drug delivery vehicles. *ACS Appl Mater Interfaces* 2017;9:34194–203. Available from: <https://doi.org/10.1021/acsami.7b08433>.
- [64] Xie M, Zhang F, Liu L, Zhang Y, Li Y, Li H, et al. Surface modification of graphene oxide nanosheets by protamine sulfate/sodium alginate for anti-cancer drug delivery application. *Appl Surf Sci* 2018;440:853–60. Available from: <https://doi.org/10.1016/j.apsusc.2018.01.175>.
- [65] de Sousa M, Visani de Luna LA, Fonseca LC, Giorgio S, Alves OL. Folic-acid-functionalized graphene oxide nanocarrier: synthetic approaches, characterization, drug delivery study, and antitumor screening. *ACS Appl Nano Mater* 2018;1:922–32. Available from: <https://doi.org/10.1021/acsanm.7b00324>.
- [66] Huang Q, Hao L, Xie J, Gong T, Liao J, Lin Y. Tea polyphenol–functionalized graphene/chitosan as an experimental platform with improved mechanical behavior and bioactivity. *ACS Appl Mater Interfaces* 2015;7:20893–901. Available from: <https://doi.org/10.1021/acsami.5b06300>.
- [67] Assali A, Akhavan O, Adeli M, Razzazan S, Dinarvand R, Zanganeh S, et al. Multifunctional core-shell nanoplatforms (gold@graphene oxide) with mediated NIR thermal therapy to promote miRNA delivery. *Nanomed Nanotechnology, Biol Med* 2018;14:1891–903. Available from: <https://doi.org/10.1016/j.nano.2018.05.016>.
- [68] Gong P, Zhao Q, Dai D, Zhang S, Tian Z, Sun L, et al. Functionalized ultrasmall fluorinated graphene with high NIR absorbance for controlled delivery of mixed anticancer drugs. *Chem - A Eur J* 2017;23:17531–41. Available from: <https://doi.org/10.1002/chem.201702917>.
- [69] Biju V. Chemical modifications and bioconjugate reactions of nanomaterials for sensing, imaging, drug delivery and therapy. *Chem Soc Rev* 2014;43:744–64. Available from: <https://doi.org/10.1039/c3cs60273g>.
- [70] Doria G, Conde J, Veigas B, Giestas L, Almeida C, Assunção M, et al. Noble metal nanoparticles for biosensing applications. *Sensors* 2012;12:1657–87. Available from: <https://doi.org/10.3390/s120201657>.
- [71] Dubertret B, Calame M, Libchaber AJ. Single-mismatch detection using gold-quenched fluorescent oligonucleotides. *Nat Biotechnol* 2001;19:365–70. Available from: <https://doi.org/10.1038/86762>.
- [72] Borghei Y-S, Hosseini M, Dadmehr M, Hosseinkhani S, Ganjali MR, Sheikhejad R. Visual detection of cancer cells by colorimetric aptasensor based on aggregation of gold nanoparticles induced by DNA hybridization. *Anal Chim Acta* 2016;904:92–7. Available from: <https://doi.org/10.1016/j.aca.2015.11.026>.
- [73] Liu D, Yang J, Wang H-F, Wang Z, Huang X, Wang Z, et al. Glucose oxidase-catalyzed growth of gold nanoparticles enables quantitative detection of attomolar cancer biomarkers. *Anal Chem* 2014;86:5800–6. Available from: <https://doi.org/10.1021/ac500478g>.
- [74] Chinen AB, Guan CM, Ferrer JR, Barnaby SN, Merkel TJ, Mirkin CA. Nanoparticle probes for the detection of cancer biomarkers, cells, and tissues by fluorescence. *Chem Rev* 2015;115:10530–74. Available from: <https://doi.org/10.1021/acs.chemrev.5b00321>.
- [75] Viswambari Devi R, Doble M, Verma RS. Nanomaterials for early detection of cancer biomarker with special emphasis on gold nanoparticles in immunoassays/sensors. *Biosens Bioelectron* 2015;68:688–98. Available from: <https://doi.org/10.1016/j.bios.2015.01.066>.



- [76] Kavosi B, Salimi A, Hallaj R, Moradi F. Ultrasensitive electrochemical immunosensor for PSA biomarker detection in prostate cancer cells using gold nanoparticles/PAMAM dendrimer loaded with enzyme linked aptamer as integrated triple signal amplification strategy. *Biosens Bioelectron* 2015;74:915–23. Available from: <https://doi.org/10.1016/j.bios.2015.07.064>.
- [77] Ilkhani H, Sarparast M, Noori A, Zahra Bathaie S, Mousavi MF. Electrochemical aptamer/antibody based sandwich immunosensor for the detection of EGFR, a cancer biomarker, using gold nanoparticles as a signaling probe. *Biosens Bioelectron* 2015;74:491–7. Available from: <https://doi.org/10.1016/j.bios.2015.06.063>.
- [78] Her S, Jaffray DA, Allen C. Gold nanoparticles for applications in cancer radiotherapy: mechanisms and recent advancements. *Adv Drug Deliv Rev* 2017;109:84–101. Available from: <https://doi.org/10.1016/j.addr.2015.12.012>.
- [79] Jain S, Hirst DG, O'Sullivan JM. Gold nanoparticles as novel agents for cancer therapy. *Br J Radiol* 2012;85:101–13. Available from: <https://doi.org/10.1259/bjr/59448833>.
- [80] Blanco E, Shen H, Ferrari M. Principles of nanoparticle design for overcoming biological barriers to drug delivery. *Nat Biotechnol* 2015;33:941–51. Available from: <https://doi.org/10.1038/nbt.3330>.
- [81] Ding Y, Jiang Z, Saha K, Kim CS, Kim ST, Landis RF, et al. Gold nanoparticles for nucleic acid delivery. *Mol Ther* 2014;22:1075–83. Available from: <https://doi.org/10.1038/mt.2014.30>.
- [82] Guo S, Huang Y, Jiang Q, Sun Y, Deng L, Liang Z, et al. Enhanced gene delivery and siRNA silencing by gold nanoparticles coated with charge-reversal polyelectrolyte. *ACS Nano* 2010;4:5505–11. Available from: <https://doi.org/10.1021/nn101638u>.
- [83] Nakamura Y, Mochida A, Choyke PL, Kobayashi H. Nanodrug delivery: is the enhanced permeability and retention effect sufficient for curing cancer? *Bioconjug Chem* 2016;27:2225–38. Available from: <https://doi.org/10.1021/acs.bioconjchem.6b00437>.
- [84] Cherukuri P, Glazer ES, Curley SA. Targeted hyperthermia using metal nanoparticles. *Adv Drug Deliv Rev* 2010;62:339–45. Available from: <https://doi.org/10.1016/j.addr.2009.11.006>.
- [85] Huff TB, Tong L, Zhao Y, Hansen MN, Cheng J-X, Wei A. Hyperthermic effects of gold nanorods on tumor cells. *Nanomedicine* 2007;2:125–32. Available from: <https://doi.org/10.2217/17435889.2.1.125>.
- [86] Riley RS, Day ES. Gold nanoparticle-mediated photothermal therapy: applications and opportunities for multimodal cancer treatment. *Wiley Interdiscip Rev Nanomed Nanobiotechnol* 2017;9:e1449. Available from: <https://doi.org/10.1002/wnan.1449>.
- [87] Tiwari P, Vig K, Dennis V, Singh S. Functionalized gold nanoparticles and their biomedical applications. *Nanomaterials* 2011;1:31–63. Available from: <https://doi.org/10.3390/nano1010031>.
- [88] Li X, Robinson SM, Gupta A, Saha K, Jiang Z, Moyano DF, et al. Functional gold nanoparticles as potent antimicrobial agents against multi-drug-resistant bacteria. *ACS Nano* 2014;8:10682–6. Available from: <https://doi.org/10.1021/nn5042625>.
- [89] Casciaro B, Moros M, Rivera-Fernández S, Bellelli A, de la Fuente JM, Mangoni ML. Gold-nanoparticles coated with the antimicrobial peptide esculentin-1a(1-21)NH<sub>2</sub> as a reliable strategy for antipseudomonal drugs. *Acta Biomater* 2017;47:170–81. Available from: <https://doi.org/10.1016/j.actbio.2016.09.041>.
- [90] Frey NA, Peng S, Cheng K, Sun S. Magnetic nanoparticles: synthesis, functionalization, and applications in bioimaging and magnetic energy storage. *Chem Soc Rev* 2009;38:2532. Available from: <https://doi.org/10.1039/b815548h>.

- [91] Pankhurst QA, Connolly J, Jones SK, Dobson J. Applications of magnetic nanoparticles in biomedicine. *J Phys D Appl Phys* 2003;36:R167–81. Available from: <https://doi.org/10.1088/0022-3727/36/13/201>.
- [92] Li J, Hu J, Ma C, Wang Y, Wu C, Huang J, et al. Uptake, translocation and physiological effects of magnetic iron oxide ( $\gamma$ -Fe<sub>2</sub>O<sub>3</sub>) nanoparticles in corn (*Zea mays* L.). *Chemosphere* 2016;159:326–34.
- [93] Li X, Wei J, Aifantis KE, Fan Y, Feng Q, Cui F-Z, et al. Current investigations into magnetic nanoparticles for biomedical applications. *J Biomed Mater Res Part A* 2016;104:1285–96. Available from: <https://doi.org/10.1002/jbm.a.35654>.
- [94] Wu W, Wu Z, Yu T, Jiang C, Kim WS. Recent progress on magnetic iron oxide nanoparticles: synthesis, surface functional strategies and biomedical applications. *Sci Technol Adv Mater* 2015;16. Available from: <https://doi.org/10.1088/1468-6996/16/2/023501>.
- [95] Lee J-H, Huh Y-M, Jun Y, Seo J, Jang J, Song H-T, et al. Artificially engineered magnetic nanoparticles for ultra-sensitive molecular imaging. *Nat Med* 2007;13:95–9. Available from: <https://doi.org/10.1038/nm1467>.
- [96] Markides H, Rotherham M, El Haj AJ. Biocompatibility and toxicity of magnetic nanoparticles in regenerative medicine. *J Nanomater* 2012;2012:1–11. Available from: <https://doi.org/10.1155/2012/614094>.
- [97] Li L, Jiang W, Luo K, Song H, Lan F, Wu Y, et al. Superparamagnetic iron oxide nanoparticles as MRI contrast agents for non-invasive stem cell labeling and tracking. *Theranostics* 2013;3:595–615. Available from: <https://doi.org/10.7150/thno.5366>.
- [98] Rocha-Santos TAP. Sensors and biosensors based on magnetic nanoparticles. *TrAC Trends Anal Chem* 2014;62:28–36. Available from: <https://doi.org/10.1016/j.trac.2014.06.016>.
- [99] Kang T, Li F, Baik S, Shao W, Ling D, Hyeon T. Surface design of magnetic nanoparticles for stimuli-responsive cancer imaging and therapy. *Biomaterials* 2017;136:98–114. Available from: <https://doi.org/10.1016/j.biomaterials.2017.05.013>.
- [100] Stephen ZR, Kievit FM, Zhang M. Magnetite nanoparticles for medical MR imaging. *Mater Today* 2011;14:330–8. Available from: [https://doi.org/10.1016/S1369-7021\(11\)70163-8](https://doi.org/10.1016/S1369-7021(11)70163-8).
- [101] Wei H, Bruns OT, Kaul MG, Hansen EC, Barch M, Wiśniowska A, et al. Exceedingly small iron oxide nanoparticles as positive MRI contrast agents. *Proc Natl Acad Sci* 2017;114:2325–30. Available from: <https://doi.org/10.1073/pnas.1620145114>.
- [102] Busquets MA, Estelrich J, Sánchez-Martín MJ. Nanoparticles in magnetic resonance imaging: from simple to dual contrast agents. *Int J Nanomed* 2015;1727. Available from: <https://doi.org/10.2147/IJN.S76501>.
- [103] Gobbo OL, Sjaastad K, Radomski MW, Volkov Y, Prina-Mello A. Magnetic nanoparticles in cancer theranostics. *Theranostics* 2015;5:1249–63. Available from: <https://doi.org/10.7150/thno.11544>.
- [104] Zheng B, Vazin T, Goodwill PW, Conway A, Verma A, Ulku Saritas E, et al. Magnetic particle imaging tracks the long-term fate of in vivo neural cell implants with high image contrast. *Sci Rep* 2015;5. Available from: <https://doi.org/10.1038/srep14055>.
- [105] Zhou S, Yin T, Zou Q, Zhang K, Gao G, Shapter JG, et al. Labeling adipose derived stem cell sheet by ultrasmall super-paramagnetic Fe<sub>3</sub>O<sub>4</sub> nanoparticles and magnetic resonance tracking in vivo. *Sci Rep* 2017;7. Available from: <https://doi.org/10.1038/srep42793>.
- [106] Gao Y, Lim J, Teoh S-H, Xu C. Emerging translational research on magnetic nanoparticles for regenerative medicine. *Chem Soc Rev* 2015;44:6306–29. Available from: <https://doi.org/10.1039/C4CS00322E>.

- [107] Sun C, Lee J, Zhang M. Magnetic nanoparticles in MR imaging and drug delivery. *Adv Drug Deliv Rev* 2008;60:1252–65. Available from: <https://doi.org/10.1016/j.addr.2008.03.018>.
- [108] Ulbrich K, Holá K, Šubr V, Bakandritsos A, Tuček J, Zbořil R. Targeted drug delivery with polymers and magnetic nanoparticles: covalent and noncovalent approaches, release control, and clinical studies. *Chem Rev* 2016;116:5338–431. Available from: <https://doi.org/10.1021/acs.chemrev.5b00589>.
- [109] Mou X, Ali Z, Li S, He N. Applications of magnetic nanoparticles in targeted drug delivery system. *J Nanosci Nanotechnol* 2015;15:54–62. Available from: <https://doi.org/10.1166/jnn.2015.9585>.
- [110] Hedayatnasab Z, Abnisa F, Daud WMAW. Review on magnetic nanoparticles for magnetic nanofluid hyperthermia application. *Mater Des* 2017;123:174–96. Available from: <https://doi.org/10.1016/j.matdes.2017.03.036>.
- [111] Wang L, Huang J, Chen H, Wu H, Xu Y, Li Y, et al. Exerting enhanced permeability and retention effect driven delivery by ultrafine iron oxide nanoparticles with T1–T2 switchable magnetic resonance imaging contrast. *ACS Nano* 2017;11:4582–92. Available from: <https://doi.org/10.1021/acsnano.7b00038>.
- [112] Thanh NTK. *Clinical applications of magnetic nanoparticles*. CRC Press; 2018.
- [113] Hayashi K, Nakamura M, Miki H, Ozaki S, Abe M, Matsumoto T, et al. Magnetically responsive smart nanoparticles for cancer treatment with a combination of magnetic hyperthermia and remote-control drug release. *Theranostics* 2014;4:834–44. Available from: <https://doi.org/10.7150/thno.9199>.
- [114] Elsabahy M, Wooley KL. Design of polymeric nanoparticles for biomedical delivery applications. *Chem Soc Rev* 2012;41:2545–61. Available from: <https://doi.org/10.1039/c2cs15327k>.
- [115] Hussain CM, Mishra AK, editors. *Nanotechnology in environmental science, 2 volumes, Vol. 1*. John Wiley & Sons; 2018.
- [116] Hussain CM, Mishra AK, editors. *New polymer nanocomposites for environmental remediation*. Elsevier; 2018.
- [117] Kurniasih IN, Keilitz J, Haag R. Dendritic nanocarriers based on hyperbranched polymers. *Chem Soc Rev* 2015;44:4145–64. Available from: <https://doi.org/10.1039/c4cs00333k>.
- [118] Pandita D, Poonia N, Kumar S, Lather V, Madaan K. Dendrimers in drug delivery and targeting: drug-dendrimer interactions and toxicity issues. *J Pharm Bioallied Sci* 2014;6:139. Available from: <https://doi.org/10.4103/0975-7406.130965>.
- [119] Sutton D, Nasongkla N, Blanco E, Gao J. Functionalized micellar systems for cancer targeted drug delivery. *Pharm Res* 2007;24:1029–46. Available from: <https://doi.org/10.1007/s11095-006-9223-y>.
- [120] Nicolas J, Mura S, Brambilla D, MacKiewicz N, Couvreur P. Design, functionalization strategies and biomedical applications of targeted biodegradable/biocompatible polymer-based nanocarriers for drug delivery. *Chem Soc Rev* 2013;42:1147–235. Available from: <https://doi.org/10.1039/c2cs35265f>.
- [121] Pawar PV, Gohil SV, Jain JP, Kumar N. Functionalized polymersomes for biomedical applications. *Polym Chem* 2013;4:3160. Available from: <https://doi.org/10.1039/c3py00023k>.
- [122] Bae YH, Na K, Lee ES. pH-responsive polymeric micelles for drug delivery. *Curr Pharm Des* 2007;12:4669–84.
- [123] Cabral H, Kataoka K. Progress of drug-loaded polymeric micelles into clinical studies. *J Control Rel* 2014;190:465–76. Available from: <https://doi.org/10.1016/j.jconrel.2014.06.042>.

- [124] Xu W, Ling P, Zhang T. Polymeric micelles, a promising drug delivery system to enhance bioavailability of poorly water-soluble drugs. *J Drug Deliv* 2013;2013:1–15. Available from: <https://doi.org/10.1155/2013/340315>.
- [125] Zhang X, Yao S, Liu C, Jiang Y. Tumor tropic delivery of doxorubicin-polymer conjugates using mesenchymal stem cells for glioma therapy. *Biomaterials* 2015;39:269–81. Available from: <https://doi.org/10.1016/j.biomaterials.2014.11.003>.
- [126] Kedracki D, Filippov SK, Gour N, Schlaad H, Nardin C. Formation of DNA-copolymer fibrils through an amyloid-like nucleation polymerization mechanism. *Macromol Rapid Commun* 2015;36:768–73. Available from: <https://doi.org/10.1002/marc.201400728>.
- [127] Kedracki D, Safir I, Gour N, Ngo KX, Vebert-Nardin C. DNA–polymer conjugates: from synthesis, through complex formation and self-assembly to applications, 2012, pp. 115–149. [https://doi.org/10.1007/12\\_2012\\_181](https://doi.org/10.1007/12_2012_181).
- [128] Zhou Q, Zhang L, Yang TH, Wu H. Stimuli-responsive polymeric micelles for drug delivery and cancer therapy. *Int J Nanomed* 2018;13:2921–42. Available from: <https://doi.org/10.2147/IJN.S158696>.
- [129] Daglar B, Ozgur E, Corman ME, Uzun L, Demirel GB. Polymeric nanocarriers for expected nanomedicine: current challenges and future prospects. *RSC Adv* 2014;4:48639–59. Available from: <https://doi.org/10.1039/c4ra06406b>.
- [130] Sajja H, East M, Mao H, Wang Y, Nie S, Yang L. Development of multifunctional nanoparticles for targeted drug delivery and noninvasive imaging of therapeutic effect. *Curr Drug Discov Technol* 2009;6:43–51. Available from: <https://doi.org/10.2174/157016309787581066>.
- [131] Wei T, Liu J, Ma H, Cheng Q, Huang Y, Zhao J, et al. Functionalized nanoscale micelles improve drug delivery for cancer therapy in vitro and in vivo. *Nano Lett* 2013;13:2528–34. Available from: <https://doi.org/10.1021/nl400586t>.
- [132] Deng S, Wu Q, Zhao Y, Zheng X, Wu N, Pang J, et al. Biodegradable polymeric micelle-encapsulated doxorubicin suppresses tumor metastasis by killing circulating tumor cells. *Nanoscale* 2015;7:5270–80. Available from: <https://doi.org/10.1039/c4nr07641a>.
- [133] Zhu Y, Zhang J, Meng F, Deng C, Cheng R, Feijen J, et al. cRGD-functionalized reduction-sensitive shell-sheddable biodegradable micelles mediate enhanced doxorubicin delivery to human glioma xenografts in vivo. *J Control Release* 2016;233:29–38. Available from: <https://doi.org/10.1016/j.jconrel.2016.05.014>.
- [134] Pang X, Jiang Y, Xiao Q, Leung AW, Hua H, Xu C. PH-responsive polymer-drug conjugates: design and progress. *J Control Release* 2016;222:116–29. Available from: <https://doi.org/10.1016/j.jconrel.2015.12.024>.
- [135] Cagel M, Tesan FC, Bernabeu E, Salgueiro MJ, Zubillaga MB, Moretton MA, et al. Polymeric mixed micelles as nanomedicines: achievements and perspectives. *Eur J Pharm Biopharm* 2017;113:211–28. Available from: <https://doi.org/10.1016/j.ejpb.2016.12.019>.
- [136] Deng H, Dai F, Ma G, Zhang X. Theranostic gold nanomicelles made from biocompatible comb-like polymers for thermochemotherapy and multifunctional imaging with rapid clearance. *Adv Mater* 2015;27:3645–53. Available from: <https://doi.org/10.1002/adma.201501420>.
- [137] Lu J, Choi E, Tamanoi F, Zink JJ. Light-activated nanoimpeller-controlled drug release in cancer cells. *Small* 2008;4(4):421–6.
- [138] Roco MC. Nanotechnology: convergence with modern biology and medicine. *Curr Opin Biotechnol* 2003;14(3):337–46.

- [139] Nair R, Varghese SH, Nair BG, Maekawa T, Yoshida Y, Kumar DS. Nanoparticulate material delivery to plants. *Plant Sci* 2010;179(3):154–63.
- [140] Singh S, Singh BK, Yadav S, Gupta A. Applications of nanotechnology in agricultural and their role in disease management. *Res J Nanosci Nanotechnol* 2015;5(1):1–5.
- [141] Pérez-de-Luque A, Rubiales D. Nanotechnology for parasitic plant control. *Pest Manage Sci Pesticide Sci* 2009;65(5):540–5.
- [142] Torney F, Trewyn BG, Lin VS-Y, Wang K. Mesoporous silica nanoparticles deliver DNA and chemicals into plants. *Nat Nanotechnol* 2007;2(5):295.
- [143] Judy JD, Unrine JM, Rao W, Wirick S, Bertsch PM. Bioavailability of gold nanomaterials to plants: importance of particle size and surface coating. *Environ Sci Technol* 2012;46(15):8467–74.
- [144] Cañas JE, Long M, Nations S, Vadan R, Dai L, Luo M, et al. Effects of functionalized and nonfunctionalized single-walled carbon nanotubes on root elongation of select crop species. *Environ Toxicol Chem* 2008;27(9):1922–31.
- [145] Hamdi H, De La Torre-Roche R, Hawthorne J, White JC. Impact of non-functionalized and amino-functionalized multiwall carbon nanotubes on pesticide uptake by lettuce (*Lactuca sativa* L.). *Nanotoxicology* 2015;9(2):172–80.
- [146] Villagarcia H, Dervishi E, de Silva K, Biris AS, Khodakovskaya MV. Surface chemistry of carbon nanotubes impacts the growth and expression of water channel protein in tomato plants. *Small* 2012;8(15):2328–34.
- [147] Khodakovskaya MV, de Silva K, Nedosekin DA, Dervishi E, Biris AS, Shashkov EV, et al. Complex genetic, photothermal, and photoacoustic analysis of nanoparticle-plant interactions. *Proc Natl Acad Sci* 2011;108(3):1028–33.
- [148] García-Sánchez S, Bernalles I, Cristobal S. Early response to nanoparticles in the Arabidopsis transcriptome compromises plant defence and root-hair development through salicylic acid signalling. *BMC Genom* 2015;16(1):341.
- [149] Flores D, Chacón R, Alvarado L, Schmidt A, Alvarado C, Chaves J. Effect of using two different types of carbon nanotubes for blackberry (*Rubus adenotrichos*) in vitro plant rooting, growth and histology. *Am J Plant Sci* 2014;5(24):3510.
- [150] Chen J, Yang L, Li S, Ding W. Various physiological response to graphene oxide and amine-functionalized graphene oxide in wheat (*Triticum aestivum*). *Molecules* 2018;23(5):1104.
- [151] Yu M, Yao J, Liang J, Zeng Z, Cui B, Zhao X, et al. Development of functionalized abamectin poly (lactic acid) nanoparticles with regulatable adhesion to enhance foliar retention. *RSC Adv* 2017;7(19):11271–80.
- [152] Debnath N, Das S, Seth D, Chandra R, Bhattacharya SC, Goswami A. Entomotoxic effect of silica nanoparticles against *Sitophilus oryzae* (L.). *J Pest Sci* 2011;84(1):99–105.
- [153] Chen X, O'Halloran J, Jansen MA. The toxicity of zinc oxide nanoparticles to *Lemna minor* (L.) is predominantly caused by dissolved Zn. *Aquat Toxicol* 2016;174:46–53.
- [154] Moghaddasi S, Fotovat A, Karimzadeh F, Khazaei HR, Khorassani R, Lakzian A. Effects of coated and non-coated ZnO nano particles on cucumber seedlings grown in gel chamber. *Arch Agron Soil Sci* 2017;63(8):1108–20.
- [155] Mukherjee A, Pokhrel S, Bandyopadhyay S, Mädler L, Peralta-Videa JR, Gardea-Torresdey JL. A soil mediated phyto-toxicological study of iron doped zinc oxide nanoparticles (Fe@ ZnO) in green peas (*Pisum sativum* L.). *Chem Eng J* 2014;258:394–401.
- [156] Priyanka N, Venkatachalam P. Biofabricated zinc oxide nanoparticles coated with phycocyanin as novel micronutrient catalysts for stimulating plant growth of cotton. *Adv Nat Sci Nanosci Nanotechnol* 2016;7(4):045018.

- [157] Pokhrel LR, Dubey B. Evaluation of developmental responses of two crop plants exposed to silver and zinc oxide nanoparticles. *Sci Total Environ* 2013;452:321–32.
- [158] Yin L, Colman BP, McGill BM, Wright JP, Bernhardt ES. Effects of silver nanoparticle exposure on germination and early growth of eleven wetland plants. *PLoS One* 2012;7(10):e47674.
- [159] Speranza A, Crinelli R, Scoccianti V, Taddei AR, Iacobucci M, Bhattacharya P, et al. In vitro toxicity of silver nanoparticles to kiwifruit pollen exhibits peculiar traits beyond the cause of silver ion release. *Environ Pollution* 2013;179:258–67.
- [160] Kaveh R, Li Y-S, Ranjbar S, Tehrani R, Brueck CL, Van Aken B. Changes in *Arabidopsis thaliana* gene expression in response to silver nanoparticles and silver ions. *Environ Sci Technol* 2013;47(18):10637–44.
- [161] Vannini C, Domingo G, Onelli E, Prinsi B, Marsoni M, Espen L, et al. Morphological and proteomic responses of *Eruca sativa* exposed to silver nanoparticles or silver nitrate. *PLoS One* 2013;8(7):e68752.
- [162] Wang J, Koo Y, Alexander A, Yang Y, Westerhof S, Zhang Q, et al. Phytostimulation of poplars and *Arabidopsis* exposed to silver nanoparticles and Ag<sup>+</sup> at sublethal concentrations. *Environ Sci Technol* 2013;47(10):5442–9.
- [163] Yasur J, Rani PU. Environmental effects of nanosilver: impact on castor seed germination, seedling growth, and plant physiology. *Environ Sci Pollution Res* 2013;20(12):8636–48.
- [164] Vannini C, Domingo G, Onelli E, De Mattia F, Bruni I, Marsoni M, et al. Phytotoxic and genotoxic effects of silver nanoparticles exposure on germinating wheat seedlings. *J Plant Physiol* 2014;171(13):1142–8.
- [165] Geisler-Lee J, Brooks M, Gerfen JR, Wang Q, Fotis C, Sparer A, et al. Reproductive toxicity and life history study of silver nanoparticle effect, uptake and transport in *Arabidopsis thaliana*. *Nanomaterials* 2014;4(2):301–18.
- [166] Jiang HS, Qiu XN, Li GB, Li W, Yin LY. Silver nanoparticles induced accumulation of reactive oxygen species and alteration of antioxidant systems in the aquatic plant *Spirodela polyrrhiza*. *Environ Toxicol Chem* 2014;33(6):1398–405.
- [167] Sabo-Attwood T, Unrine JM, Stone JW, Murphy CJ, Ghoshroy S, Blom D, et al. Uptake, distribution and toxicity of gold nanoparticles in tobacco (*Nicotiana xanthi*) seedlings. *Nanotoxicology* 2012;6(4):353–60.
- [168] Zhu Z-J, Wang H, Yan B, Zheng H, Jiang Y, Miranda OR, et al. Effect of surface charge on the uptake and distribution of gold nanoparticles in four plant species. *Environ Sci Technol* 2012;46(22):12391–8.
- [169] Dan Y, Zhang W, Xue R, Ma X, Stephan C, Shi H. Characterization of gold nanoparticle uptake by tomato plants using enzymatic extraction followed by single-particle inductively coupled plasma–mass spectrometry analysis. *Environ Sci Technol* 2015;49(5):3007–14.
- [170] Feichtmeier NS, Walther P, Leopold K. Uptake, effects, and regeneration of barley plants exposed to gold nanoparticles. *Environ Sci Pollut Res* 2015;22(11):8549–58.
- [171] Rajeshwari A, Suresh S, Chandrasekaran N, Mukherjee A. Toxicity evaluation of gold nanoparticles using an *Allium cepa* bioassay. *RSC Adv* 2016;6(29):24000–9.
- [172] Pariona N, Martínez AI, Hernandez-Flores H, Clark-Tapia R. Effect of magnetite nanoparticles on the germination and early growth of *Quercus macdougalii*. *Sci Total Environ* 2017;575:869–75.

- [173] Iannone MF, Groppa MD, de Sousa ME, van Raap MBF, Benavides MP. Impact of magnetite iron oxide nanoparticles on wheat (*Triticum aestivum* L.) development: evaluation of oxidative damage. *Environ Exp Botany* 2016;131:77–88.
- [174] Zhao L, Peralta-Videa JR, Ren M, Varela-Ramirez A, Li C, Hernandez-Viezcas JA, et al. Transport of Zn in a sandy loam soil treated with ZnO NPs and uptake by corn plants: electron microprobe and confocal microscopy studies. *Chem Eng J* 2012;184:1–8.
- [175] Barrios AC, Rico CM, Trujillo-Reyes J, Medina-Velo IA, Peralta-Videa JR, Gardea-Torresdey JL. Effects of uncoated and citric acid coated cerium oxide nanoparticles, bulk cerium oxide, cerium acetate, and citric acid on tomato plants. *Sci Total Environ* 2016;563:956–64.
- [176] Rossi L, Zhang W, Lombardini L, Ma X. The impact of cerium oxide nanoparticles on the salt stress responses of *Brassica napus* L. *Environ Pollution* 2016;219:28–36.
- [177] Hamidat M, Barakat M, Ortet P, Chanéac C, Rose Jr, Bottero J-Y, et al. Design defines the effects of nanoceria at a low dose on soil microbiota and the potentiation of impacts by the canola plant. *Environ Sci Technol* 2016;50(13):6892–901.
- [178] Ravindran S, Kim S, Martin R, Lord EM, Ozkan CS. Quantum dots as bio-labels for the localization of a small plant adhesion protein. *Nanotechnology* 2004;16(1):1.
- [179] Müller F, Houben A, Barker PE, Xiao Y, Käs JA, Melzer M. Quantum dots—a versatile tool in plant science? *J Nanobiotechnol* 2006;4(1):5.
- [180] Hu Y, Li J, Ma L, Peng Q, Feng W, Zhang L, et al. High efficiency transport of quantum dots into plant roots with the aid of silwet L-77. *Plant Physiol Biochem* 2010;48(8):703–9.
- [181] Santos AR, Miguel AS, Tomaz L, Malhó R, Maycock C, Patto MCV, et al. The impact of CdSe/ZnS quantum dots in cells of *Medicago sativa* in suspension culture. *J Nanobiotechnol* 2010;8(1):24.
- [182] Eggenberger K, Frey N, Zienicke B, Siebenbrock J, Schunck T, Fischer R, et al. Use of nanoparticles to study and manipulate plant cells. *Adv Eng Mater* 2010;12(9):B406–12.
- [183] Nair R, Poulouse AC, Nagaoka Y, Yoshida Y, Maekawa T, Kumar DS. Uptake of FITC labeled silica nanoparticles and quantum dots by rice seedlings: effects on seed germination and their potential as biolabels for plants. *J Fluorescence* 2011;21(6):2057.
- [184] Alimohammadi M, Xu Y, Wang D, Biris AS, Khodakovskaya MV. Physiological responses induced in tomato plants by a two-component nanostructural system composed of carbon nanotubes conjugated with quantum dots and its in vivo multimodal detection. *Nanotechnology* 2011;22(29):295101.
- [185] Santos AR, Miguel AS, Macovei A, Maycock C, Balestrazzi A, Oliva A, et al. CdSe/ZnS quantum dots trigger DNA repair and antioxidant enzyme systems in *Medicago sativa* cells in suspension culture. *BMC Biotechnol* 2013;13(1):111.
- [186] Koo Y, Wang J, Zhang Q, Zhu H, Chehab EW, Colvin VL, et al. Fluorescence reports intact quantum dot uptake into roots and translocation to leaves of *Arabidopsis thaliana* and subsequent ingestion by insect herbivores. *Environ Sci Technol* 2014;49(1):626–32.

## Further reading

Joseph T, Morrison M. Nanotechnology in Agriculture and Food. A Nanoforum Report, Institute of Nanotechnology; 2006.

- Pacurari M, Yin XJ, Zhao J, Ding M, Leonard SS, Schwegler-Berry D, et al. Raw single-wall carbon nanotubes induce oxidative stress and activate MAPKs, AP-1, NF- $\kappa$ B, and Akt in normal and malignant human mesothelial cells. *Environ Health Perspect* 2008;116(9):1211.
- Panessa-Warren B, Warren J, Wong S, Misewich J. Biological cellular response to carbon nanoparticle toxicity. *J Phys Condensed Matter* 2006;18(33):S2185.



This page intentionally left blank

## Section 4

# **Functionalized Nanomaterials for Electronics, Electrical and Energy Industry**

This page intentionally left blank

## Chapter 11

# Functionalized nanomaterials for electronics and electrical and energy industries

Shrabani De and Rashmi Madhuri

*Department of Applied Chemistry, Indian Institute of Technology (Indian School of Mines), Dhanbad, Jharkhand, India*

### 11.1 Introduction

Our world is now experiencing different types of environmental issues like high levels of pollution, greenhouse gas effects, and climate change. These environmental issues arise because of industrialization, urbanization, and contamination with different harmful gases and it degrades the environmental balance as well as affects human health [1]. Scientists have for many years been trying to reduce these problems by focusing on different technologies to develop alternative solutions to these environmental issues. On the other hand, industry is a crucial factor for the evolution of our modern society. Most of our needs are fulfilled by the services and product supplied by industries. Thus for long-term improvement, it is very obvious to find some new substances and techniques. Also, the continuously increasing worldwide demand for resources and energy makes it necessary to search for more efficient, economical, environmentally friendly, and sustainable sources of energy.

Nanotechnology is one of the most promising technologies today and plays a very important role in various industries through the use of nanomaterials. In fact, the investigation and application of nanomaterials have become one of the most rapidly emerging research areas. As the name suggests, nanomaterials are ultrafine particles with size in the nanometer range. The definition of nanoparticles is based on the fields, substances, and applications to which they are applied. But in general nanomaterials are viewed as materials with particle size 10–20 nm. In the nanorange size huge changes occur in their physical and chemical properties, in comparison to their parent bulk materials. According to other definitions, particles with size range in between 1 nm and 1  $\mu\text{m}$  or particles with at least one dimension in the 1–100 nm range are called nanomaterials. At this

scale physicochemical characteristics are majorly dependant on the unit shape and size and also their reactivity with biological matrix, since it is different than with large particles. Nanomaterials can be produced naturally through different geological, combustion, and biological processes. Additionally, nanomaterials are manufactured to developed materials with special optical, mechanical, chemical, magnetic, and electrical properties through molecular-level engineering [2].

Although nanomaterials have many advantages, they also have some limitations such as surface reactivity and insolubility in various solvents. Additionally, they can react with substrate, host media, or other individual species, which may limit their use in specific applications. These limitations can be eliminated by functionalizing or modifying the nanomaterials with some specific chemical moieties. The main benefit of functionalization is to tune their required characteristics in a predictable way and fit them in certain applications [3]. Functionalization of nanomaterials has opened up a new scope in the development of improved tools for industrial applications.

In this chapter, we focus on the classifications of nanomaterials, their functionalization, and their role in energy or electrical/electronic industries. Firstly, classification of nanomaterials and requirements of functionalizing nanoparticles are discussed. Then we discuss their applications in the electronics, electrical, and energy industries.

### 11.1.1 Classification of nanomaterials based on dimension

Nanomaterials include a wide range of materials that have size in the nano-scale range and can be prepared mechanically, chemically, physically, or naturally. Different structures of nanomaterials are based on their dimensions: three-dimensional, two-dimensional, one-dimensional, and zero-dimensional nanomaterials.

#### 11.1.1.1 Three-dimensional nanostructures

Three-dimensional nanostructures are associated with three arbitrary dimensions, which are beyond the nanorange ( $> 100$ ). This kind of nanostructure is the combination of multiple nanocrystals, fashioned in various directions. This category of nanomaterials includes foam and honeycomb, fibers and nanotubes, layer skeletons, powdered nanoparticles, and layered composites [4]. Carbon nanobuds, which are made up of a combination of carbon nanotubes (CNTs) and fullerenes, are another member of this category [5].

#### 11.1.1.2 Two-dimensional nanostructures

Nanostructures of this category consist of two dimensions beyond the nanorange ( $> 100$ ) and one dimension in the range of nanometer. Two-dimensional nanomaterials can be:

- Single layered or multilayered
- Crystalline or amorphous

- Metallic, ceramic, or polymeric
- Accumulated on a substrate and can consist of different chemical configurations

Graphene, which is a single graphite layer, is a common example of this class. The structure of graphene is made up with conjugated  $sp^2$  hybridized carbons. It is one type of carbon allotrope with honeycomb structure. Some other examples of two-dimensional nanostructures [6] are nanolayer, nanofiber, nanowall, nanocoating, nanosheet, nanostraw, etc.

### 11.1.1.3 One-dimensional nanostructures

One-dimensional nanostructures are associated with one dimension not enclosed in nanorange and two dimensions that are in nanorange. One-dimensional materials can also be metallic, polymeric, or ceramic; crystalline or amorphous. Examples of nanomaterials that belong to this class [7] are nanotube, nanorod, nanowire, filament, or fiber.

### 11.1.1.4 Zero-dimensional nanostructures

Nanomaterials of this category have all the dimensions in nanorange, which means they must have their size below 100 nm. Common nanomaterials of this category are spherical-shaped materials, but cubes, and nanorods, and polygon-shaped nanostructures can also be included in this class. Some general examples of this class [7] are holospheres, noble metal nanoparticles, metal/metal oxide nanoparticle, core-shell nanomaterials, quantum dots, etc. A schematic representation of the classification of nanomaterials according to their dimensions is given in Fig. 11.1.

## 11.1.2 Classification of nanomaterials according to chemical composition

According to the chemical composition, nanomaterials can be categorized into different classes as follows [7]:

- *Carbonaceous nanomaterials* are derived from carbon-containing materials including fullerene, CNTs, and graphene.
- *Metallic nanomaterials* are derived from noble metal (platinum, gold, and silver nanoparticles), transition metal (iron, zinc, copper, etc.), and metal oxides (alumina, titania, and silica).
- *Highly branched dendrimers* have a branch-like structure with dimensions in the range of nanometer are classified in this category.

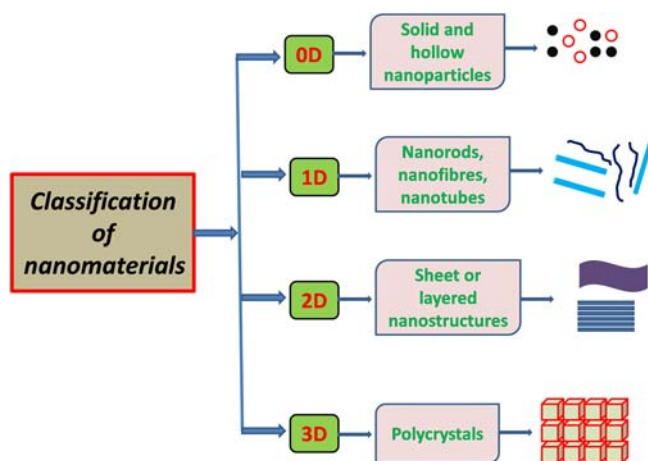


**FIGURE 11.1** Schematic representation of classification of nanomaterials according to their dimension. Redrawn from T.A. Saleh and V.K. Gupta, *Nanomaterial and polymer membranes: synthesis, characterization, and applications*, 2016, Elsevier.

- *Nanocomposites* are nanomaterials formulated by mixing various types of composite materials with at least one of the component with dimension in the nanorange.
- *Quantum dots* are basically nanocrystals, which have a fluorescent property with high photostability and unique optical and chemical properties.

### 11.1.3 Properties of nanomaterials

With decreasing particle size and increasing surface area, the properties of bulk materials start to change. For example, fundamental properties like melting point and dielectric constant may change due to the particle size and these changes are called “size effect.” Therefore, having very small particle size, the nanomaterials have distinctive physical and chemical properties in comparison to their precursors or parent bulk materials.

#### 11.1.3.1 Thermal property

Nanoparticles have lower melting point than the bulk materials because lower energy is required to make them move. As an example, gold as bulk material has a melting point of 1336 K. With decreasing size, the melting point of gold decreases gradually and when size becomes 2 nm the melting point lowers more than 500°C than the bulk material.

#### 11.1.3.2 Structural property

Nanomaterials can easily be absorbed into cell membrane; this phenomenon is called enhanced permeation and retention [8]. Additionally, high surface

area and large surface-to-volume ratio enhance the solubility, reactivity, and sintering performance of nanomaterials.

### *11.1.3.3 Optical property*

Nanomaterials with size in the nanorange absorb light of certain wavelength, because the plasma absorption occurs due to the plasma vibration of the electrons [9]. The color of the transmitted light depends on the particle size and the nature of the material [9]. As a result, we may observe different colors of a same nanomaterial, which depends on the change in particle size. Additionally, materials like germanium and silicon exhibit indirect transition, means they do not produce light as bulk substances, but emit light like direct transition type materials due to the quantum effect of the nanoparticles.

### *11.1.3.4 Electronic property*

Electronic property as well as particle size of nanomaterials is very useful to improve the performance of electronic devices. In the electronic industry, there is a huge need for materials with elevated dielectric constant to produce thin and tiny electronic devices. X-ray diffraction study has confirmed that when particle size decreases to the nanometer range, the dielectric constant increases considerably. For example, the dielectric constant of  $\text{PbTiO}_3$  enhances drastically while particle size reaches in the range of 20 nm. Also, the lowest particle size required to maintain the ferroelectric property changes according to the nature and constitution of nanomaterials. Similarly, the Curie point is the point where ferroelectric material converted to paraelectric material decreases considerably with decreasing particle size of the substance [9].

### *11.1.3.5 Magnetic property*

The superparamagnetic property can be generated when particle size is reduced to nanoscale range. In the Nanoparticles having paramagnetic properties, each single particle has an ferromagnetic property associated with a single magnetic domain. But, In the presence of an external magnetic field, nanoparticles become magnetized and arrange in the same direction as the magnetic field and by removing the magnetic field, magnetization vanishes. Magnetization is dependent on the particle size of the nanomaterials and their paramagnetic nature decreases with increasing the particle size of the material [9].

### *11.1.3.6 Mechanical property*

The mechanical property or hardness of a material enhances with decreasing the size of a material in nanorange. For example, ceramic material shows a special superplastic property in the nanorange, which is enlarged several times than the bulk material at elevated temperature [9].



### 11.1.4 Functionalization of nanomaterials

Modification or functionalization of nanostructured materials is an area of high significance/importance in the field of nanotechnology. The application of nanomaterials in various fields remains limited to some extent due to their insolubility in different solvents and rigidity. The smooth surface of nanomaterials without modification cannot allow any physical or chemical interaction with the matrix or any other material. The unmodified nanoparticles form stable agglomeration due to the intermolecular interaction specially dipole–dipole or Van der Waals interactions, which prevent their dispersion into the solvent [10].

Through surface functionalization, different types of functional groups or chemical species can be introduced on the surface of nanomaterials, which can generate specific active sites according to the requirements. Monitoring the functionalization, a wide range of application of nanomaterials can be controlled and toxicity can also be reduced. Different surface characteristics including their interaction with other materials, solubility, and agglomeration in various solvents can also be tuned by surface modification. Compared with the unmodified nanomaterials, functionalized nanomaterials have opened up several new options in different fields of application due to their excellent surface interaction with other particles [11].

Functionalization can be carried out through covalent or noncovalent interactions (such as electrostatic, van der Waals, and hydrogen bonding interactions) by changing reaction temperature, solvents, and surfactants, which provide opportunities to control the desired functionalities and unique configurations. In covalent types of interactions chemical bonds are formed with the atoms present on the surface of the nanomaterials through chemical reactions. Nanomaterials become hydrophilic due to this type of functionalization and get easily soluble in organic solvents. In noncovalent types of interaction, functionalization is carried out by ionic bonding,  $\pi - \pi$  stacking interaction, hydrogen bonding, or hydrophobic interaction. In this type of interaction, the electronic configuration and properties of the atoms present on the surface remain unaltered [12]. Different functionalization pathways including chemical methods, ligand exchange process, and grafting of synthetic polymer are used to improve the property of nanomaterials including solubility, biocompatibility, and addition of different active sites. In this section, different types of functionalization processes are described.

#### 11.1.4.1 Chemical methods

Chemical methods of functionalization are actually the chemical reactions taking place at the interface of nanomaterials in a specific solution. To improve the reactivity, solubility, hydrophobic interaction, mechanical as well as spectral properties, chemical treatment methods are introduced to functionalize the unmodified nanomaterials. The common chemical treatment

methods are acid treatments (to clean the surface contaminations and oxides), alkali treatments, hydrogen peroxide treatments, heat treatments [13], and treatment with silane coupling agents and metal ethoxides/alkoxides [14]. Here, two very common types of chemical methods, which are treatment with silane coupling agents and metal ethoxides/alkoxides, are described for the functionalization of nanomaterials.

The most popular and simple functionalization of nanomaterials through chemical treatment route is silane modification. Herein, modification of nanomaterials can be carried out by introducing silane coupling agents on the surface through chemical treatment [14]. This method can enhance the dispersion stability of nanoparticles in different solvents and increase the affinity between nanoparticles and polymer surfaces. In Fig. 11.2, a coupling agent 3-methacryloxypropyl trimethoxysilane was used to modify the nanomaterial, and it was observed that the surface of the unmodified nanomaterials is covered with only  $\text{—OH}$  group; on the other hand, after functionalization, the surface of the nanomaterial gets covered with 3-methacryloxypropyl trimethoxysilane. This modification enhances the solubility of nanomaterials in different solvent media.

Similarly, some metal epoxides/alkoxides like aryl or alkyl isocyanates and propylene oxides are also used for surface modification [15]. For

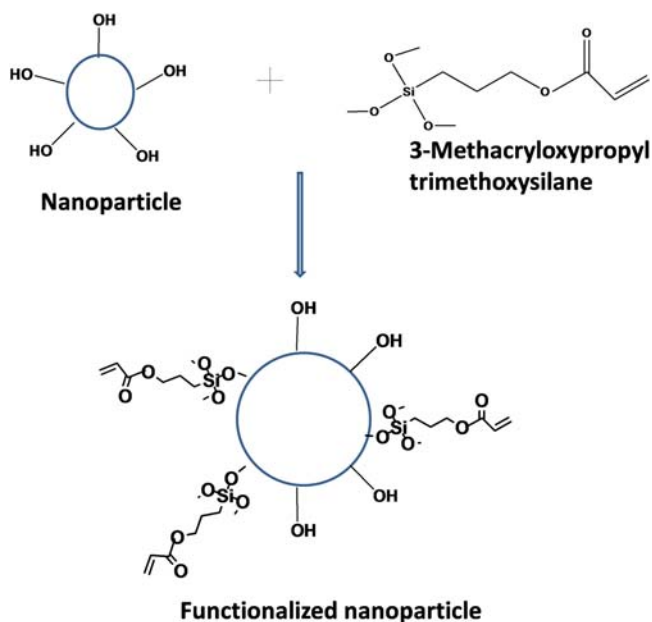


**FIGURE 11.2** Modification of a nanoparticle with 3-methacryloxypropyl trimethoxysilane. Reproduced with permission from S. Kango, S. Kalia, A. Celli, J. Njuguna, Y. Habibi and R. Kumar, *Surface modification of inorganic nanoparticles for development of organic–inorganic nanocomposites—a review*, *Prog Polym Sci* 38 (8), 2013, 1232–1261.

example, Sabzi et al. reported surface functionalization of  $\text{TiO}_2$  nanoparticles using aminopropyl trimethoxysilane, which introduced improvement of the mechanical and UV protective properties of polyurethane composite coating [16]. Ma et al. studied surface modification using KH570 silane coupling agent to improve the dispersion stability of  $\text{ZnO}$  nanoparticles [17]. In another report, surface of  $\text{Al}_2\text{O}_3$  nanoparticles were modified with 3-chloropropyl triethoxysilane and octyltriethoxysilane, which enhance the hydrophobic interaction of nanoparticles with syndiotactic polypropylene matrix [18].

#### 11.1.4.2 Ligand exchange process

To stabilize the nanoparticles in solution and prevent agglomeration, specific organic molecules or polymers are used during the synthesis process. The added materials bind to the surface of the nanoparticles and monitor their shape and size as well as improve their properties. These specific molecules are termed as capping agents, ligands, or surfactants, depending on their chemical composition and role. Some examples of this kind of ligand are trioctylphosphine (TOP), oleylamine (OAm), oleic acid (OA), polyvinyl alcohol (PVA), polyvinyl pyrrolidone (PVP), cetyl trimethyl ammonium bromide (CTAB), ascorbic acid (AA), etc. The capping ligand materials coated on the surface of the nanoparticles act like “organic armor,” resisting the reactant molecules approach to the nanomaterial surface. In the ligand exchange process, ligands bonded at the surface of nanoparticles get interchanged by a competitive interaction process. Through this ligand exchange process, nanomaterials can be decorated widely by various ligands according to the requirements [19].

According to Greenham et al. a ligand layer a few nanometers thick is enough to protect the nanoparticles and to check the movement of electrons among the nanoparticles before the recombination can take place [20]. Commonly, most of the bulky organic ligands do not have any functionally active groups to take part in the charge transfer between the nanoparticles. Thus the removal of synthesis ligands from the nanoparticle surface is required to increase the charge transfer and avoid the recombination loss. This can be obtained by replacing the bulky ligands with more suitable ones. For example, Zhu et al. reported a ligand exchange process to functionalize  $\text{CdSe/ZnS}$  quantum dots [21]. They used different dithiols and thiols as surface ligands and exchanged them with trioctylphosphine oxide/trioctylphosphine (TOPO/TOP). The synthesized quantum dots provided enhanced optical properties [optical stability and photoluminescence (PL) emission intensity] while TOPO/TOP ligand was used.

However, the existence of capping ligands can introduce complexity in the system like uncertain charge transfer and noncovalent interaction between nanomaterials and reactants. The substituted ligand should be easily replaceable by vacuum procedure or thermal annealing to achieve the

improved conductivity and charge separation [22]. Previous studies [23] have described enhanced photocurrent in poly(3-hexylthiophene):CdSe nanorod films after thermal annealing that resulted in a decrease in the number of substitution ligands. After annealing the substitution ligands may be present in the nanofilm, but they should consist of at least one  $\pi$ -electron system, which can provide charge transfer by combining with other nanoparticles. A recent report by Celik et al. [24] described an improved surface functionalization technique for nanoparticles by mixing the benefits of ligand exchange and washing method, which allowed an enhanced solar cell execution with power conversion efficiency values of 3.5%.

#### 11.1.4.3 Grafting of synthetic polymers

Another surface modification technique is grafting of synthetic polymers, which increases the chemical reactivity and changes the surface morphology of nanomaterials. There are three processes of polymer grafting functionalization: grafting-to, grafting-from, and grafting-through. In the grafting-to process, an end-functionalized polymer is bonded directly on the suitable nanomaterial surface. In the grafting-from process, polymer chains are generated from an initiating site of the surface. In the grafting-through process a low-molecular weight monomer is copolymerized with another monomer on the surface of the nanomaterial [25].

Monomers with low molecular weight can penetrate the agglomerated nanoparticles and can react to the active sites of the nanoparticle surface. This will also make the nanoparticle surface hydrophobic, which is an essential criterion for mixing of filler and matrix. Fig. 11.3 shows the dispersion of nanomaterials due to polymer grafting in a polymer matrix [26]. A successful grafting can be obtained by placing the initiating groups on the

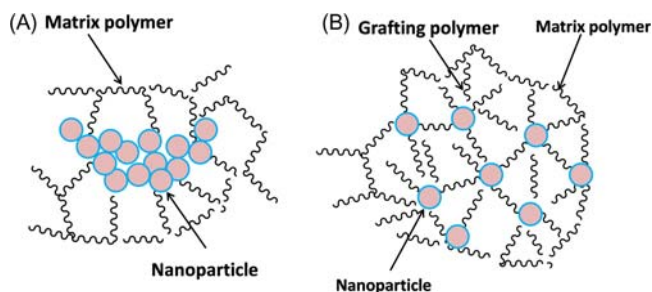


**FIGURE 11.3** Schematic representation of (A) agglomerated nanoparticles in the matrix polymer in the case without grafting polymer and (B) separation of particles due to the presence of grafting polymer. Reproduced with permission from S. Kango, S. Kalia, A. Celli, J. Njuguna, Y. Habibi and R. Kumar, *Surface modification of inorganic nanoparticles for development of organic–inorganic nanocomposites—a review*, *Prog Polym Sci* 38 (8), 2013, 1232–1261.

nanoparticle surfaces. After that, the polymerization reaction (including cationic, anionic, or radical polymerization process) with propagation of the grafter polymers will start from the surface of the nanomaterial [27]. For example, Rong et al. reported the grafting of polyacrylamide and polystyrene on the surface of alumina nanoparticles [28]. Wang et al. proposed a photocatalytic polymerization technique for the fabrication of poly(methyl methacrylate)-grafted  $\text{TiO}_2$  [29]. In the presence of light, poly(methyl methacrylate) chains are grafted directly on the surface of the  $\text{TiO}_2$  nanoparticles present in water.

#### 11.1.4.4 *Miscellaneous methods*

Other surface functionalization methods include in situ surface modification and adsorption of polymeric dispersants on the surface of nanomaterials. In situ surface modification techniques are performed during the nanoparticle synthesis phase. Thermal decomposition of organometallic compound, reverse micelle methods, and polyol methods are examples of in situ surface modification techniques [14,30,31]. To prevent the aggregation, surfactants or capping agents like OA, amines, and TOPOs are dissolved into the reaction solution. On the other hand, anionic or cationic dispersants are used to disperse hydrophilic nanoparticles into highly polar organic solvents. Steric repulsive forces are generated among the polymer chains by the dispersants and enhance the surface charge. This results in improved dispersibility of the nanoparticles. Different types of polycarboxylic acids and their salts are used as anionic surfactants to disperse various types of nanoparticles including  $\text{Al}_2\text{O}_3$ ,  $\text{TiO}_2$ , and  $\text{Fe}_2\text{O}_3$  [32–34].

## 11.2 Industrial applications

Nanotechnology offers cost-effective and sustainable industrial procedures with the ability to design atoms with specific properties by controlling their uniqueness [35]. As described above, nanomaterials are fabricated from various types of molecules or atoms with different shapes and morphologies such as rod, wire, sphere, cube, etc., and are functionalized according to the required surface reactivity and application. Due to the excellent technological and industrial properties of functionalized nanomaterials, significant efforts have been made to design them for different industrial applications. In this section, we focus on the application of functionalized nanomaterials in the electronic, electrical, and energy industries.

### 11.2.1 Applications of functionalized nanomaterials in the electronics industry

In the electronics industry, functional nanomaterials such as semiconductors, metal oxides, noble metals, and alloys are used to develop electrophotonic,

stretchable, and flexible electronics. In the last 5 years, the use of nanomaterials has increased enormously within the electronics industrial sectors. Around 900 companies worldwide have been working to develop advanced nanomaterials and nanodevice invention. Improvement of our modern technology is guided significantly by the tiny version of three-dimensional electronic gadgets with implanted logic circuit to allow diverse applications such as wearable electronics and display device. New-generation electronic devices like flexible and faster electronic storage systems, which consist of millions of nanosized transistors, can go beyond microprocessing and contribute to the development of new electronic devices. The other characteristics of nanodevices are portability, durability, flexibility, miniaturization and easily integrating structure [36].

For example, Zhang et al. reported a new process to synthesize size-controlled copper nanoparticles through an advanced polyol method and used it in flexible printed electronics [37]. After tuning copper nanoparticles with different sizes, it was found that nanoparticles of 50 nm size exhibited better performance. The nanoparticles were used to prepare highly efficient ink by dispersion that was screenprinted on a flexible surface. The conductive ink pattern exhibited very low resistivity of  $16.2 \mu\Omega \text{ cm}$ , when kept under  $\text{N}_2$  atmosphere at  $240^\circ\text{C}$  for 40 min. The nanomaterial showed good oxidation resistance and remained unchanged after 30 days under normal environment. Kang et al. introduced a metamaterial with excellent flexibility and resonance intensified light concentrating property [38]. They used a dual-layered nanometallic absorber to provide nonlinear optical process controlled by the voltage, where second harmonic generation and optical rectification were monitored by the applied voltage.

Among several nanomaterials used in nanodevices and nanoelectronics, CNTs occupy an important position, due to properties like chemical stability, large surface area, and impressive mechanical properties. Usually silicon semiconductors are used in solar cells, but when CNTs are introduced into the semiconductors, they provide much higher electricity than silicon, per square inch. Due to their excellent electron-emitting properties, CNTs are used in producing thinner TVs, paper batteries, and faster computers [36].

Zhong et al. used random, solution-derived CNT film to fabricate top-gate field-effect-transistors (FETs) and integrated circuits, particularly five-stage ring oscillators with oscillation frequency of 5.54 GHz [39]. Generally, CNT network films used in FETs show very poor performance and cannot be used in flexible applications. In their work, they modified the CNT films to obtain enhanced performance as FETs. The prepared transistor showed a high current density of  $0.55 \text{ mA}/\mu\text{m}$  and  $0.46 \text{ mS}/\mu\text{m}$  transconductance at 0.8 V supply voltage. Song et al. introduced ZnO nanorod-deposited graphene as a flexible antireflection array for solar cells [40]. A better performance was obtained from a rough surface of polydimethylsiloxane (PDMS) coated with graphene-tapered ZnO nanorod than the bare PDMS surface.

After different bending experiments, the material exhibited outstanding anti-reflection characteristics on the bouncy surface by combining the antireflection property of ZnO and flexibility of graphene. Kim et al. developed CNT composited with PDMS and found that composite showed high stretchability, elasticity as well as high conductivity than neat PDMS films shown in Fig. 11.4 [41]. Later on, metal-free elastic circuit was prepared by the nano-composite and the material was tested as strain sensor. Additionally, the composite material was used as an electrode for electroencephalogram. In another report, a cost-effective nanoimprinting process was used to fabricate an antireflective nanodome with high packing density and improved transmittance of a flat glass substrate [42]. UV imprinting, one of the most promising procedures of nanomaterial fabrication, was used to fabricate nanodome pattern on glass substrate by a series of UV replication process. The shape of the nanodome was dependant on  $\text{SiO}_2$  layer thickness and the antireflective property of the nanomaterial was analyzed by measuring the optical transmittance. Around 3% enhancement in transmittance was observed compared with the bare glass substrate.

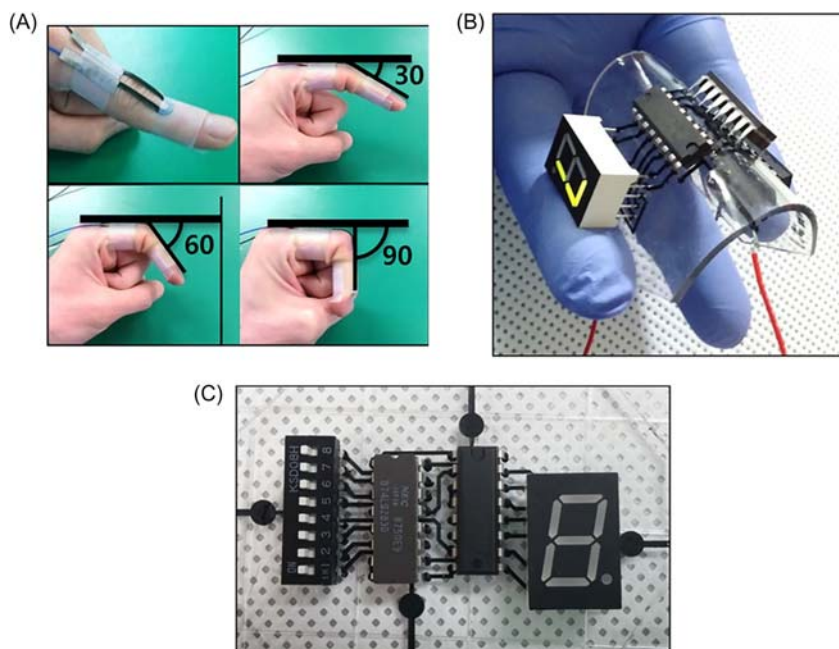


**FIGURE 11.4** Applications using CNT/PDMS composite: (A) Photograph of finger attached to CNT/PDMS sensor, (B) circuit working during bending and (C) assembled flexible electronic circuit. Reproduced from J.H. Kim, J.Y. Hwang, H.R. Hwang, H.S. Kim, J.H. Lee, J.W. Seo, et al., Simple and cost-effective method of highly conductive and elastic carbon nanotube/polydimethylsiloxane composite for wearable electronics, *Sci Rep* 8 (1), 2018, 1375–1385.



Jung et al. synthesized Ag-nanowire network to functionalize PDMS substrate that was found to be a transparent, elastic, and electromagnetic interference (EMI) shielding material [43]. The prepared material exhibited efficient EMI shielding for wireless power transmission set-up and could be used in human skin and biological systems.

### 11.2.2 Application of functionalized nanomaterials in the electrical industry

Recently, there have been a variety of technological improvements in research and development projects associated with nanomaterials and nanotechnology used to enhance the efficiency and reliability of ordinary materials. The electrical industry has taken the benefits of nanotechnology and found different applications such as nanodielectrodes and electrical transformers. In this section we look at the role of nanomaterials in dielectric fluids, insulating materials, outdoor insulators, etc.

Electrical transformers are one of the most common components of electricity generation and distribution network, because any fault in them results interruption in power supply. Actually, electrical transformers are static devices containing several types of inner construction substances like metals or plastics. In dry-cast transformers, polymeric resin is introduced to encapsulate the inner components, and in oil-immersed transformers insulating fluids are incorporated with thermal and dielectric properties [44]. Recently, nanofluids have been regarded as a promising option. The new-generation transformer with insulating nanofluids showed improved cooling capacity. Taha-Tijerina et al. reported a dielectric mineral oil-based nanodiamond fluids as transformer insulating fluid [45]. They reported 70% increase in thermal conductivity using nanodiamond containing thermal fluids than in normal mineral oil. Li et al. presented natural ester-based insulating fluids with  $\text{Fe}_3\text{O}_4$  nanoparticles [46]. Physical, chemical, electrical, and aging properties of the dielectric mineral insulating oil were studied. It was found that the introduction of magnetic  $\text{Fe}_3\text{O}_4$  nanoparticles enhanced the lightning impulse breakdown voltage of natural ester nanofluids.

In electrical transformers, solid insulating materials are a crucial element that increases the lifetime of the instrument. A variety of cellulose-based materials like pressboard and paper are used as solid insulator in power transformers. A cellulose-based solid insulating material was developed by Yuen et al. using montmorillonite (MMT) clay particles to modify the craft papers [47]. The breakdown voltage enhances from 50.3 to 56.9 kV by using kraft MMT-insulating nanopapers. Also, it was observed that the tensile strength of the craft MMT paper was reduced with increasing MMT nanoparticles. Chatterjee et al. reported a gas sensor fabricated by ZnO thin film, which allowed online monitoring of three gases including carbon monoxide, hydrogen, and methane, dissolved in transformer oil [48]. It was found that the sensitivity of the ZnO thin film was enhanced by doping. They fabricated



ZnO-doped manganese film for detecting the three gases at different temperatures so that major defects like overheated cellulose insulation, arcing, and corona could be predicted.

Kruzepa et al. developed electrical transformers in which they replaced commercial copper wire with conducting CNT fibers [49]. Setyawan et al. [50]. reported a magnetic nanoribbon made up with NANOMET alloy of Fe–Co–Si–B–P–Cu using a spinning technique. It was reported that the annealed sample exhibited high flux density of 1.83 T and low coercivity of 5–7 A/m, which made it a better option than commercial copper wire.

### 11.2.3 Energy applications

Energy has become the milestone for continuous growth of society and economy and its increased demand has adverse environmental effects. Therefore research on energy now includes all aspects like generation, harvesting, saving, conversion, and storage of energy with an aim of finding more sustainable and environmentally friendly sources of energy. Nanomaterials exhibit unique properties and have played a significant role in every aspect of recent advancements in energy fields. For example, nanomaterials such as Li-ion batteries, Na-ion batteries, Zn-air batteries, supercapacitors, fuel cells, etc., are used in the field of energy storage. In this section, we focus on electrochemical energy conversion routes along with their applications in the design of batteries.

The most important part of electrochemical energy conversion system is catalyst. The functionalized nanomaterials further allow designing of catalyst materials with improved selectivity, better efficiency, and required electrochemical properties with tuned electrochemical surface area and surface energy. To discuss the role of nanomaterials in energy conversion or storage, here we provide the basic electrochemical conversion reactions (such as oxygen evolution reaction (OER) and hydrogen evolution reaction (HER)) involved in battery supercapacitor and fuel cell applications.

In the electrochemical conversion of energy, two fundamental reactions are very important: OER and HER. They are the central reactions of electrocatalytic water splitting systems, fuel cells, and metal-air batteries. Fabrication of electrocatalyst for splitting of water to the molecular oxygen and hydrogen is very important for huge-scale energy storage systems. In general, fuel cells or metal-air batteries consist of a two-electrode system, where the cathode part involves HER and the anode part involves OER as shown in Fig. 11.5 [51].

#### 11.2.3.1 Role of functionalized nanomaterials in oxygen evolution reaction

OER is a four electron-proton combined reaction, which requires high energy, or in the words, high overpotential, and needed to overcome the

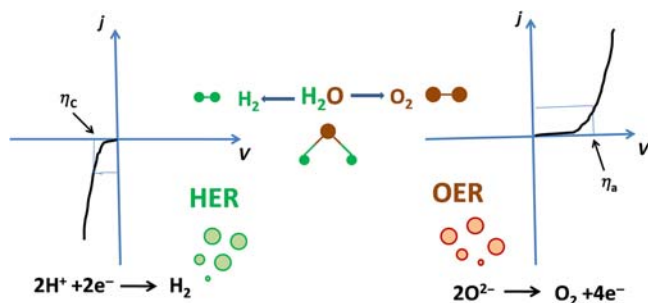


**FIGURE 11.5** Polarization curves for HER (left) and OER (right) and  $\eta_c$  and  $\eta_a$  are the overpotentials for cathode and anode at the same current density ( $j$ ), respectively. Redrawn from N.T. Suen, S.F. Hung, Q. Quan, N. Zhang, Y.J. Xu and H.M. Chen, *Electrocatalysis for the oxygen evolution reaction: recent development and future perspectives*, *Chem Soc Rev* 46 (2), 2017, 337–365.

kinetic energy barrier. In the last few decades, OER has been widely studied and various types of electrocatalysts have been fabricated to enhance electrode kinetics and stability under different electrolyte environments. Theoretical density functional theory (DFT) calculations provide the limiting step of OER, which is the binding strength of oxygen molecules at the electrocatalyst surface [52]. However, highly efficient, inexpensive, and stable electrocatalyst for OER are still not very common. Different electrocatalytic kinetic parameters including onset potential, overpotential, Tafel slop, and exchange current density are used to properly evaluate the activity of electrocatalysts.

Two precious metal oxides,  $\text{RuO}_2$  and  $\text{IrO}_2$ , are generally used as electrocatalysts due to their excellent electrocatalytic activity in both acidic and basic medium [51]. Initially, these two materials were functionalized and applied for OER. For example, Audichon et al. designed core-shell conformation  $\text{IrO}_2@\text{RuO}_2$  to improve the efficiency of  $\text{RuO}_2$  [53]. The modified nanomaterial exhibited excellent efficiency with enhanced stability and low overpotential ( $\sim 300$  mV) than individual  $\text{RuO}_2$  and  $\text{IrO}_2$ . After 1000 cycles, the existing active sites for  $\text{IrO}_2@\text{RuO}_2$ ,  $\text{IrO}_2$ , and  $\text{RuO}_2$  were found to be 96.7%, 87.8%, and 90.8%, respectively. Al-Mamun et al. reported that  $\text{CoCr}_2\text{O}_4$  coupled with carbon nanosheet (CNS) showed better performance than unmodified  $\text{CoCr}_2\text{O}_4$  [54]. Modified  $\text{CoCr}_2\text{O}_4/\text{CNS}$  exhibited sufficiently lower charge transfer resistance even less than commercial  $\text{RuO}_2$ .

It was also reported in the literature that substitution of anions can lead to an alternative way of enhancing OER performance of electrocatalyst. This idea also was proposed by Duan et al. [55]. They fabricated Fe- and O-doped  $\text{Co}_2\text{P}$  phase ( $\text{CoFePO}$ ) grown on Ni-foam and compared it with unmodified  $\text{CoPO}$ ,  $\text{CoO}$ , and Ni-foam. The modified hybrid catalyst allowed impressive OER activity with overpotential value of 274.5 mV at current density of  $10 \text{ mA/cm}^2$ , and the values were found to be smaller than the

CoPO, CoO, and Ni-foam samples. Sun et al. compared different bimetallic systems where Co- and Ni-porphyrin coated on reduced graphene oxide forming a layer-by-layered structure was prepared [56]. They found optimized eight layered compounds, which showed 50 mV/dec Tafel slop with overpotential of  $\sim 330$  mV.

Chen et al. proposed a special 3D architecture by combining nitrogen-doped graphene and CNTs as metal-free electrocatalyst for OER [57]. This 3D electrocatalyst consist of porous structure with high surface area as well as higher active sites and its electrocatalytic activity was compared with non-doped graphene-CNTs. It was observed that nitrogen-doped graphene-CNTs (showed 141 mV/dec Tafel slop and 365 mV overpotential at  $5 \text{ mA/cm}^2$ ) and showed improved OER activity than nondoped graphene-carbon.

### 11.2.3.2 Role of functionalized nanomaterials in hydrogen evolution reaction

In recent decades, hydrogen has been considered as the most suitable energy carrier because of its largest gravimetric energy density, without emission of carbon dioxide [58]. Hydrogen can store energy generated from any sustainable resources in the form of chemical bonds. The stored energy can be transferred to end-users by changing in electrical energy through the metal-air batteries or fuel cells when required. However, hydrogen cannot be obtained in free form; generally it is present as compounds like hydrocarbons and water. Presently, it is generated from hydrocarbon reforming steams, which emit large amounts of greenhouse gases.

Production of hydrogen at industrial scale that is sustainable, cost-effective, and environmentally friendly is still a challenge for researchers. Therefore a sustainable generation of hydrogen through photocatalytic or electrocatalytic water splitting has been proposed, where water molecules can be dissociated to  $\text{H}_2$  and  $\text{O}_2$ , using the renewable solar energy, indirectly or directly [59]. HER is the cathodic part of half-cell reaction of water splitting. It is an important reaction of various energy conversion devices like artificial photosynthetic cell and water electrolyzer. The standard reduction potential of HER is  $E_{\text{H}^+/\text{H}_2\text{O}}^0 = 0\text{V}$  versus reversible hydrogen electrode at  $\text{pH} = 0$ . But the reaction is not easy and electrocatalysts require a certain amount of energy to overcome the potential energy barrier and initiate the HER. Similar to OER electrocatalytic parameters like overpotential, Tafel slop, exchange current density, and onset potential are the parameters used to properly evaluate the HER performance [59].

Noble metals including Pt, Ir, Ru, Pd, and Rh are the ideal electrocatalyst for HER [59]. In order to increase the surface specific activity and decrease the price/cost of platinum group metals, their alloying with some nonprecious metals were also studied. Generally, alloys exhibit distinct characteristics in comparison to the pure metals. For example, Greeley et al. investigated HER

performance of binary alloys, using a computational screening method depending on DFT utilizing more than 700 binary alloys [60]. Among them, the alloy of Pt and Bi was found most impressive. Calculation showed that  $\Delta G$  of BiPt was found  $\sim 0.04$  eV, close to that of Pt, which indicated the comparable or even better HER performance of BiPt than pure Pt. In 2013, another group of scientists proposed the fabrication of tungsten carbide nanocrystals taking mesoporous graphitic  $C_3N_4$  (g- $C_3N_4$ ) as a reactive template with tungsten precursors at high temperature and inert gas environment [61]. The synthesized electrocatalyst allowed better HER performance than unmodified mesoporous g- $C_3N_4$ . Cao et al. reported the triggering effect on HER performance, due to the introduction of Co in molybdenum nitride nanomaterials [62]. Using a two-step solid-state reaction,  $Co_{0.6}Mo_{1.4}N_2$  nanomaterial was synthesized. The electrocatalyst showed a very impressive HER performance (overpotential  $\sim 200$  mV at  $10$  mA/cm<sup>2</sup> current density) compared with Co and MoN. Popczun et al. first synthesized a phosphorus precursor tri-*n*-octylphosphine (TOP) to prepare CoP by a high-temperature solution phase reaction [63]. At the decomposition temperature of  $\sim 320^\circ\text{C}$ , TOP-generated phosphorus with which the preformed metal nanoparticles (Co here) were reacted through a nanorange Kirkendall pathway. It was found that as-prepared hollow cobalt phosphide nanocrystals coated on Ti foil exhibited more efficient electrocatalytic activity toward HER in  $0.5$  M  $H_2SO_4$  medium than the bare Ti electrode. Zheng et al. introduced a metal-free hybrid electrocatalyst by coupling graphitic-carbon nitride on N-doped graphene [64]. The electrocatalytic activity of g- $C_3N_4$ , N-doped graphene, and  $C_3N_4$  coupled N-doped graphene were compared and the latter showed extraordinary HER performance, comparable Tafel slop, and overpotential value with any well-established metal catalyst.

### 11.2.3.3 Role of functionalized nanomaterials in battery design

In last few years, rechargeable batteries have been widely investigated as an important part of portable electronic device and electric vehicles. They are used as a continuous power supply source due to their high efficiency, cyclic stability, impressive specific energy density, low memory, and self-discharge effect [65]. However, these rechargeable batteries still required further advancement to meet the requirements of higher safety, lighter weight, and long-time service.

As we can see in the literature, most of these concerns are directly dependent on the electrode materials used in the design of the battery. Therefore researchers are very actively involved in investigation of a huge range of electrode substances, which can show better electrochemical performance and henceforth improve the overall efficiency of battery. Among the current options, lithium-ion batteries (LIBs) and sodium-ion batteries (SIBs) have established their positions as a worldwide power sources in portable energy

devices. They are used in laptops, smartphones, and in medical devices (pacemakers and prosthetics) as well as in high-power supplying energy storage stations and energy grids [66]. Improvements in battery-related materials have been made possible because of functionalized nanoparticles. We have compiled here some of examples, where functionalized nanomaterials were very well used in the design of batteries. An overview of the functional nanomaterials used in different types of batteries is shown in Fig. 11.6 [65].

Vinayan et al. reported an anode material for LIBs by the fabrication of graphene-multiwalled carbon nanotube (G-MWCNT) hybrid using chemical vapor deposition method [67]. Higher electrical conductivity of MWCNTs triggers the mobility of electrons in the electrode, which makes G-MWCNT a better anode than solar-exfoliated graphene. The initial charge and discharge capacity of G-MWCNT were found to be 912 and 1371 mAh/g, respectively, which was much higher than the charge and discharge capacity of solar-exfoliated graphene (443 and 588 mAh/g, respectively).

Bang et al. prepared two-dimensional  $\text{MoS}_2$  nanosheets composite with reduced graphene oxide (rGO) as an anode material for SIBs [68]. They compared the current capacities of pristine  $\text{MoS}_2$ , exfoliated  $\text{MoS}_2$ , and  $\text{MoS}_2$  composited with rGO. It was found that  $\text{MoS}_2$  composited with rGO exhibited the highest first discharge capacity than the unmodified  $\text{MoS}_2$  nanosheets. Zahoor et al. fabricated  $\alpha$ - and  $\delta$ - $\text{MnO}_2$  nanomaterials with urchin and flower like morphology using a low-temperature hydrothermal process [69]. According to their report, the  $\text{Li-O}_2$  batteries performed better with  $\text{MnO}_2$  catalyst than without any catalyst. Between  $\alpha$ - and  $\delta$ - $\text{MnO}_2$ ,  $\alpha$ - $\text{MnO}_2$  showed improved performance as anode in LIBs and exhibited impressive catalytic activity, good cyclic stability, and high current capacity. Liu et al. fabricated porous  $\text{CoO@C}$  nanohybrid as an anode material of

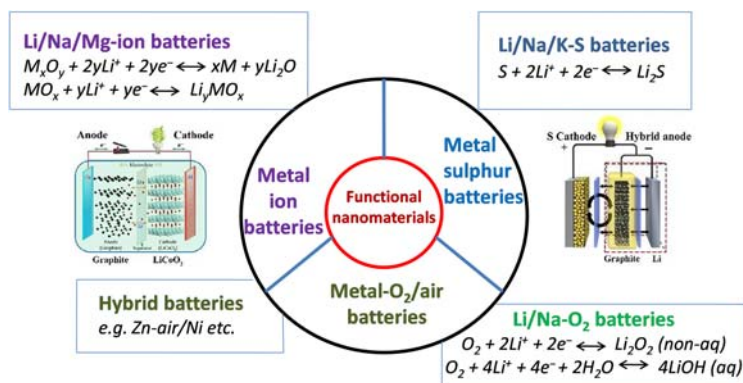


**FIGURE 11.6** Functional nanomaterials used in different types batteries. Reproduced with permission from J. Mei, T. Liao and Z. Sun, Two-dimensional metal oxide nanosheets for rechargeable batteries, *J Energy Chem* 2017.

LIBs [70]. They compared the catalytic activity of the material with bare CoO microsheet anode. CoO@C exhibited good cycling performance and excellent reversible capacity of about 990 mA h/g (after 30 cycles), whereas bare CoO microsheet allowed the reversible capacity of 600 mA h/g only (after 20 cycles). In a recent study, Panda et al. prepared a two-dimensional MoTe<sub>2</sub> nanolayers deposited on reduced graphene oxide to improve the electrochemical performance of MoTe<sub>2</sub> anode [71]. The material used as anode in SIBs and exhibited excellent electrochemical activity of 280 mA h/g at 1.0 A/g current rate for 100 cycles, against sodium metal. In another study, silica nanoparticles (Si-NPs) were double coated by graphene and Li<sub>4</sub>SiO<sub>4</sub> (Si-NPs@graphene@Li<sub>4</sub>SiO<sub>4</sub>) [72]. In addition, Si-NPs, Si@graphene, Si@Li<sub>4</sub>SiO<sub>4</sub>, and Si-NPs@graphene@Li<sub>4</sub>SiO<sub>4</sub> nanomaterials were also prepared and their performance for LIBs was compared to each other. The Si-NPs@graphene@Li<sub>4</sub>SiO<sub>4</sub> material has shown their improved performance as anode material in LIBs than the others. In addition, it has also overcome the lower columbic efficiency generated due to the large volume changes and fast capacity decay.

#### 11.2.3.4 Role of functionalized nanomaterials in supercapacitors

Supercapacitors are very promising energy storage devices consisting of two types of electrode materials [73]: (1) Material store charges via surface adsorption and (2) material store charges applying faradic redox reaction. The supercapacitor made up of first kind of material is known as electrochemical double layer supercapacitors (EDLS), while the supercapacitor with the second kind of electrode material is called a pseudocapacitor. In the EDLS, carbonaceous nanomaterials like CNTs, graphene oxide, activated carbon, and graphene are commonly used for preparation of electrodes. However, in pseudocapacitors different types of conducting polymers, metal oxides, and hydroxides are used as electrode material.

The main key factors to improve the electrochemical energy storage mechanism of supercapacitors are optimization of band gap, structural versatility, charge carrier mobility, and electrical conductivity. It was found that use of modified nanomaterials as EDLS and pseudocapacitive electrode materials increases the energy and power density as well as provides excellent electrochemical performance by increasing the available free charge carriers [73].

Very recently, antimony fabricated by a modification procedure of liquid phase exfoliation was used as electrode material in a supercapacitor [74]. It was found that use of antimony significantly enhanced the energy storage capacities of bare screenprinted electrode in galvanostatic charging as well as cyclic voltammetry. Antimony performed remarkably and showed the capacitance of 1578 F/g and charging current density of 14 A/g. This electrode system showed high power and energy density of 4.8 kW/kg and

20 mW h/kg, respectively. Ensafi et al. proposed a supercapacitor material where adenine was decorated on the surface of reduced graphene oxide (Adenine@rGO) applying diazonium reaction, and this modification enhances the supercapacitive behavior of bare rGO [75]. Adenine was used to modify the surface of reduced graphene oxide and it introduced electrochemical activity as well as pseudocapacitive nature to the final material. The property of EDLC was introduced by reduced graphene oxide to the final electrode and the material achieved 700 F/g specific capacitance at 0.5 A/g current density.

Xie et al. reported the synthesis of cobalt-doped nickel sulfide with high-density active edge sites [76]. Cobalt doping introduced an enhanced activity and capacitive nature to the normal nickel sulfide. The modified electrode material offered impressive electrochemical activity with 2141.9 F/g specific capacitance at 2 A/g current density, due to the presence of active site enriched edges. Xing et al. reported a facile and easy hydrothermal method to synthesize  $\text{Co}_3\text{O}_4$  nanowire@NiO nanosheet structures, which was used as supercapacitor electrode [77]. The nanomaterial exhibited 2018 mF/g specific capacitance at 2 mA/cm<sup>2</sup> current density, which is much higher than the bare NiO nanosheet. It was found that even after 10,000 cycles, the supercapacitor allowed impressive capacity retention of 73.5% at 10 mA/cm<sup>2</sup> current density.

In another report, carbon nanofibers were combined with reduced graphene oxide using spraygun deposition process, which is a fascinating method from an industrial point of view [78]. They reported that combined the final product exhibited better performance than the individual raw materials and the calculated values of capacitance and power were found to be 20 F/g and 40 kW/kg, respectively. Zhang et al. fabricated a  $\text{MoO}_2$ -based superhydrophobic substance with very high contact angles on soft/hard substrate [79]. Tuning the raw  $\text{MoO}_2$ /graphite carbon materials with different structures and functionalities,  $\text{MoO}_2$  nanotubes with carbon exhibited the best supercapacity with impressive cyclic stability and high gravimetric capacitance. Mary et al. reported a hydrothermal synthesis method of  $\text{ZnCo}_2\text{O}_4$  nanocrystal and modified it by changing three different surfactants including oxalic acid, ammonium fluoride, and ethylene glycol [80]. Electrochemical activity was studied using three electrode systems and the best activity was obtained with ethylene glycol surfactant-modified nanomaterial with a specific capacitance of 276.4 F/g at 2 mV/s scan rate. A few energy field applications of functional nanomaterials are summarized in Table 11.1 [81–90].

#### 11.2.3.5 Role of functionalized nanomaterials in fuel cells

Fuel cells are more popular than other energy storage systems because of their high fuel flexibility and electrical efficiency. In fuel cells, electrochemical reactions occur by supplying  $\text{H}_2$  and  $\text{O}_2$ , and factor that influences the electrochemical performance is the electrode material (i.e., cathode and

**TABLE 11.1** Few applications of functional nanomaterials in the field of energy industry [81–90].

S. no.	Material	Application	Substrate	Electrochemical performance	Ref.
1.	CeO <sub>2</sub> /CoSe <sub>2</sub>	OER	GCE	Overpotential 288 mV at 10 mA/cm <sup>2</sup> and Tafel slop 44 mV/dec	[81]
2.	g-C <sub>3</sub> N <sub>4</sub> /graphene	OER	GCE	Overpotential 539 mV at 10 mA/cm <sup>2</sup> and Tafel slop 68.5 mV/dec	[82]
3.	CoNi/ultrathin graphene layer	HER	GCE	Overpotential 142 mV at 10 mA/cm <sup>2</sup> and Tafel slop 105 mV/dec	[83]
4.	Ni/NiO-CNT hybrid	HER	Ni foam	Overpotential 100 mV at 100 mA/cm <sup>2</sup>	[84]
5.	SnO	SIBs	Carbon cloth	Coulombic efficiency ~ 79.1% (first cycle), initial capacity 1072 mAh/g (100 mA/g) and cycling stability 452 mAh/g (1000th cycles at 1.0 A/g)	[85]
6.	NiCo <sub>2</sub> O <sub>4</sub>	LIBs	Ni foam	Coulombic efficiency ~ 71.6% (first cycle), initial capacity 1738 mAh/g (200 mA/g) and cycling stability 1170.1 mAh/g (50th cycles at 0.2 A/g)	[86]
7.	Cu <sub>2</sub> O/CuMnO <sub>4</sub>	SC	—	Specific capacitance 4264 F/g and retention of specific capacitance ~ 73% (10 A/g)	[87]
8.	Fe <sub>3</sub> O <sub>4</sub> @C@PANI	SC	—	Specific capacitance 322.5 F/g and potential window – 0.1 to 0.6 V	[88]
9.	Cu-CeO <sub>2</sub>	SOFC: anode	—	DC conductivity 5200 s/cm with improved electronic conductivity	[89]
10.	Pr <sub>0.7</sub> Sr <sub>0.3</sub> Co <sub>0.9</sub> Fe <sub>0.1</sub> O <sub>3</sub>	SOFC: cathode	—	Conductivity 1236 s/cm at 700°C	[90]

CNT, Carbon nanotube; GCE, glassy carbon electrode; HER, hydrogen evolution reaction; LIBs, lithium ion batteries; OER, oxygen evolution reaction; PANI, polyaniline; SC, supercapacitor; SIB, sodium ion batteries; SOFC, solid oxide fuel cell.



anode). Fuel cells are categorized according to the nature of electrolyte; for example, alkaline fuel cells (with alkali as electrolyte), direct methanol fuel cells (with methanol as electrolyte), phosphoric acid fuel cells (acid as electrolyte), solid-oxide fuel cells (oxide as electrolyte), proton exchange membrane fuel cells, etc. [91]. A schematic representation of a solid-oxide fuel cell is shown in Fig. 11.7. Catalysts used as electrode materials are responsible for speeding up the reactions. Therefore modified nanomaterials offer excellent electrocatalytic activity as the electrode material for fuel cells. Some examples showing the role of functionalized nanomaterials in improvement of fuel cell performance are given in the following.

Wang et al. synthesized nitrogen coordinated single Co atom catalyst through single-step thermal activation from Co-doped metal organic framework [92]. The catalyst exhibited sufficient activity and stability for oxygen reduction reaction (ORR) in acidic medium with a comparable performance with Fe-based catalysts. Fuel cell study confirmed that the catalyst can act as highly efficient cathode in proton exchange membrane fuel cells. Manikandan et al. used a high-temperature solvothermal process to fabricate bimetallic nanoparticles including NiFe-, NiCu-, and NiCo-based alloys with size smaller than 20 nm [93]. The electrocatalytic activity of the nanocatalyst was explored by rotating disk electrode for HOR, and it was used as anode material in alkaline fuel cells.

In another report a Fe-based metal supported on MOF (i.e., FePhen@MOF-ArNH<sub>3</sub>) was prepared and its electrocatalytic activity toward oxygen reduction reaction was compared with Pt/C in phosphoric acid fuel cells [94]. According to the result, the prepared material was a good option to replace Pt/C catalyst. Duan et al. reported Y- and Zr-doped perovskite material as an efficient and stable electrocatalyst [95]. They used the material as a cathode material in solid-oxide fuel cell, which can perform below 500°C.



**FIGURE 11.7** Schematic representation of a solid oxide fuel cell. *Reproduced with permission from A.M. Abdalla, S. Hossain, A.T. Azad, P.M.I. Petra, F. Begum, S.G. Eriksson, et al., Nanomaterials for solid oxide fuel cells: a review, Renew Sust Energ Rev 82, 2018, 353–368.*

### 11.3 Conclusion

Nanotechnology has been revolutionary in fields such as science and engineering. Different nanomaterials have been developed for commercial use [96–97]. Nanomaterials with special characteristics have been fabricated and introduced into various applications. Modification of nanomaterials is essential to prevent agglomeration, improve dispersion stability and reactivity of the surface sites, and for compatibility. Surface functionalization can be carried out by polymer grafting, ligand exchange process, or by introducing small substances like silane coupling agents. Modification enhances the interaction between nanomaterial surfaces with the matrix which results in special optical, electronic, electrical, thermal, mechanical, and chemical properties.

In this chapter, we focused on recent developments of nanomaterials and their application in the electronic, electrical, and energy industries with different modifications according to requirements. Specific surface area, electrical conductivity, and electrocatalytic activity are crucial factors for a high-performance nanomaterial in industrial applications. The enhanced performance, durability, and potential of the modified nanomaterials used in electronic devices offer more opportunities for low-power, portable, and fast nanodigital thin-film devices. Nanomaterials are used as advanced electrocatalysts in various renewable and sustainable energy storage and conversion systems including OER, HER, batteries, supercapacitors, and fuel cells. They play an important role in developing cost-effective, sustainable, durable, and green catalyst materials for several real-time applications in the energy industry. As can be seen, the increasing use of functionalized nanomaterials has a real impact on industrial development as they are commercially available as chemical agents and important materials for various applications.

### Author declaration

Ms. De contributed greatly to the writing of this book chapter along with drawing the figures and tables, securing copyright permissions, etc.

### References

- [1] Arfin T, Tarannum A. Engineered nanomaterials for industrial application: an overview. *Handbook of nanomaterials for industrial applications*. Elsevier; 2018. p. 127–34.
- [2] Richards RM. Introduction to nanoscale materials in chemistry, edition II. *Nanoscale materials in chemistry*. Hoboken, NJ: John Wiley & Sons, Inc; 2009. p. 1–14.
- [3] Neouze MA, Schubert U. Surface modification and functionalization of metal and metal oxide nanoparticles by organic ligands. *Monatsh Chem* 2008;139:183–95.
- [4] Pokropivny VV, Skorokhod VV. Classification of nanostructures by dimensionality and concept of surface forms engineering in nanomaterial science. *Mater Sci Eng C* 2007;27(5–8):990–3.

- [5] Nasibulin AG, Pikhitsa PV, Jiang H, Brown DP, Krashennnikov AV, Anisimov AS, et al. A novel hybrid carbon material. *Nat Nanotechnol* 2007;2(3):156–61.
- [6] Krishnan D, Raidongia K, Shao J, Huang J. Graphene oxide assisted hydrothermal carbonization of carbon hydrates. *ACS Nano* 2013;8(1):449–57.
- [7] Saleh TA, Gupta VK. Nanomaterial and polymer membranes: synthesis, characterization, and applications. Elsevier; 2016.
- [8] Maeda H. The tumor blood vessel as an ideal target for macromolecular anticancer agents. *J Controlled Rel* 1992;19(1–3):315–24.
- [9] Kurokawa Y, Hosoya Y. *Surface* 1996;34(2):100–6.
- [10] Jeon IY, Chang DW, Kumar NA, Baek JB. Functionalization of carbon nanotubes. Carbon nanotubes-polymer nanocomposites. In Tech; 2011.
- [11] Prasad S, Kumar V, Kirubanandam S, Barhoum A. Engineered nanomaterials: nanofabrication and surface functionalization. *Emerg Appl Nanopart Arch Nanostruct* 2018;305–40.
- [12] Georgakilas V, Otyepka M, Bourlinos AB, Chandra V, Kim N, Kemp KC, et al. Functionalization of graphene: covalent and non-covalent approaches, derivatives and applications. *Chem Rev* 2012;112(11):6156–214.
- [13] Liu X, Chu PK, Ding C. Surface modification of titanium, titanium alloys, and related materials for biomedical applications. *Mater Sci Eng R Rep* 2004;47(3–4):49–121.
- [14] Kango S, Kalia S, Celli A, Njuguna J, Habibi Y, Kumar R. Surface modification of inorganic nanoparticles for development of organic–inorganic nanocomposites—a review. *Prog Polym Sci* 2013;38(8):1232–61.
- [15] Lin F. Preparation and characterization of polymer TiO<sub>2</sub> nanocomposites via in-situ polymerization (Master's thesis, University of Waterloo); 2006.
- [16] Sabzi M, Mirabedini SM, Zohuriaan-Mehr J, Atai M. Surface modification of TiO<sub>2</sub> nanoparticles with silane coupling agent and investigation of its effect on the properties of polyurethane composite coating. *Prog Org Coat* 2009;65(2):222–8.
- [17] Ma SR, Shi LY, Feng X, Yu WJ, Lu B. Graft modification of ZnO nanoparticles with silane coupling agent KH570 in mixed solvent. *J Shanghai Univ (Engl Ed)* 2008;12(3):278–82.
- [18] Truong LT, Larsen Å, Holme B, Diplas S, Hansen FK, Roots J, et al. Dispersibility of silane-functionalized alumina nanoparticles in syndiotactic polypropylene. *Surf Interface Anal* 2010;42(6–7):1046–9.
- [19] Merg AD, Zhou Y, Smith AM, Millstone JE, Rosi NL. Ligand exchange for controlling the surface chemistry and properties of nanoparticle superstructures. *Chem Nano Mat* 2017;3(10):745–9.
- [20] Lu Z, Yin Y. Colloidal nanoparticle clusters: functional materials by design. *Chem Soc Rev* 2012;41(21):6874–87.
- [21] Zhu H, Hu MZ, Shao L, Yu K, Dabestani R, Zaman M, et al. Synthesis and optical properties of thiol functionalized CdSe/ZnS (core/shell) quantum dots by ligand exchange. *J Nanomater* 2014;. Available from: <https://doi.org/10.1155/2014/324972>.
- [22] Niu Z, Li Y. Removal and utilization of capping agents in nanocatalysis. *Chem Mater* 2013;26(1):72–83.
- [23] Huynh WU, Dittmer JJ, Libby WC, Whiting GL, Alivisatos AP. Controlling the morphology of nanocrystal–polymer composites for solar cells. *Adv Funct Mater* 2003;13(1):73–9.
- [24] Celik D, Krueger M, Veit C, Schleiermacher HF, Zimmermann B, Allard S, et al. Performance enhancement of CdSe nanorod-polymer based hybrid solar cells utilizing a novel combination of post-synthetic nanoparticle surface treatments. *Sol Energy Mater Sol Cell* 2012;98:433–40.

- [25] Roy D, Semsarilar M, Guthrie JT, Perrier S. Cellulose modification by polymer grafting: a review. *Chem Soc Rev* 2009;38(7):2046–64.
- [26] Rong MZ, Zhang MQ, Zheng YX, Zeng HM, Walter R, Friedrich K. Structure–property relationships of irradiation grafted nano-inorganic particle filled polypropylene composites. *Polymer* 2001;42(1):167–83.
- [27] Tsubokawa N, Kogure A, Sone Y. Grafting of polyesters from ultrafine inorganic particles: copolymerization of epoxides with cyclic acid anhydrides initiated by COOK groups introduced onto the surface. *J Polym Sci A Polym Chem* 1990;28(7):1923–33.
- [28] Rong MZ, Ji QL, Zhang MQ, Friedrich K. Graft polymerization of vinyl monomers onto nanosized alumina particles. *Eur Polym J* 2002;38(8):1573–82.
- [29] Wang X, Song X, Lin M, Wang H, Zhao Y, Zhong W, et al. Surface initiated graft polymerization from carbon-doped TiO<sub>2</sub> nanoparticles under sunlight illumination. *Polymer* 2007;48(20):5834–8.
- [30] Pileni MP. The role of soft colloidal templates in controlling the size and shape of inorganic nanocrystals. *Nat Mater* 2003;2(3):145–50.
- [31] Feldmann C. Polyol-mediated synthesis of nanoscale functional materials. *Adv Funct Mater* 2003;13(2):101–7.
- [32] Sato K, Kondo S, Tsukada M, Ishigaki T, Kamiya H. Influence of solid fraction on the optimum molecular weight of polymer dispersants in aqueous TiO<sub>2</sub> nanoparticle suspensions. *J Am Ceram Soc* 2007;90(11):3401–6.
- [33] Palmqvist L, Holmberg K. Dispersant adsorption and viscoelasticity of alumina suspensions measured by quartz crystal microbalance with dissipation monitoring and in situ dynamic rheology. *Langmuir* 2008;24(18):9989–96.
- [34] Nsib F, Ayed N, Chevalier Y. Dispersion of hematite suspensions with sodium polymethacrylate dispersants in alkaline medium. *Colloids Surf A* 2006;286(1–3):17–26.
- [35] Hussain CM, Hussain CG. Future of industrial development and nanomaterials: (concluding notes). *Handbook of nanomaterials for industrial applications*. Elsevier; 2018. p. 1073–6.
- [36] Lah NA, Zubir MN, Mahendran A, Samykano L. Engineered nanomaterial in electronics and electrical industries. *Handbook of nanomaterials for industrial applications*. Elsevier; 2018. p. 324–64.
- [37] Zhang Y, Cui C, Yang B, Zhang K, Zhu P, Li G, et al. Size-controllable copper nanomaterials for flexible printed electronics. *J Mater Sci* 2018;53(18):12988–95.
- [38] Kang L, Cui Y, Lan S, Rodrigues SP, Brongersma ML, Cai W. Electrifying photonic metamaterials for tunable nonlinear optics. *Nat Commun* 2014;5:4680–6.
- [39] Zhong D, Zhang Z, Ding L, Han J, Xiao M, Si J, et al. Gigahertz integrated circuits based on carbon nanotube films. *Nat Electron* 2018;1(1):40–5.
- [40] Song T. Graphene-tapered ZnO nanorods array as a flexible antireflection layer. *J Nanomater* 2015;12–17.
- [41] Kim JH, Hwang JY, Hwang HR, Kim HS, Lee JH, Seo JW, et al. Simple and cost-effective method of highly conductive and elastic carbon nanotube/polydimethylsiloxane composite for wearable electronics. *Sci Rep* 2018;8(1):1375–85.
- [42] Lim J, Lee SM, Jang HY, Kim SM. Fabrication of an antireflective nanodome array with high packing density for photovoltaic applications. *J Nanomater* 2015;6–11. Available from: <https://doi.org/10.1155/2015/561586>.
- [43] Jung J, Lee H, Ha I, Cho H, Kim KK, Kwon J, et al. Highly stretchable and transparent electromagnetic interference shielding film based on silver nanowire percolation network for wearable electronics applications. *ACS Appl Mater Interfaces* 2017;9(51):44609–16.

- [44] Contreras JE, Rodriguez EA, Taha-Tijerina J. Nanotechnology applications for electrical transformers-a review. *Electr Pow Syst Res* 2017;143:573–84.
- [45] Taha-Tijerina JJ, Narayanan TN, Tiwary CS, Lozano K, Chipara M, Ajayan PM. Nanodiamond-based thermal fluids. *ACS Appl Mater Interfaces* 2014;6(7):4778–85.
- [46] Li J, Liao R, Yang L. Investigation of natural ester based liquid dielectrics and nanofluids. In *High Voltage Engineering and Application (ICHVE)*, September, 2012 International Conference on IEEE, 2012, pp. 16–21.
- [47] Yuan Y, Liao R. A novel nanomodified cellulose insulation paper for power transformer. *J Nanomater* 2014;.
- [48] Chatterjee A, Sarkar R, Roy NK, Kumbhakar P. Online monitoring of transformers using gas sensor fabricated by nanotechnology. *Int T Electr Energy* 2013;23(6):867–75.
- [49] Kurzepa L, Lekawa-Raus A, Patmore J, Koziol K. Replacing copper wires with carbon nanotube wires in electrical transformers. *Adv Funct Mater* 2014;24(5):619–24.
- [50] Setyawan AD, Takenaka K, Sharma P, Nishijima M, Nishiyama N, Makino A. Magnetic properties of 120-mm wide ribbons of high B s and low core-loss NANOMET® alloy. *J Appl Phys* 2015;117(17) 17B715.
- [51] Suen NT, Hung SF, Quan Q, Zhang N, Xu YJ, Chen HM. Electrocatalysis for the oxygen evolution reaction: recent development and future perspectives. *Chem Soc Rev* 2017;46(2):337–65.
- [52] Kolla P, Smirnova A. Catalytically active nanomaterials for electrochemical energy generation and storage. *ACS Symposium Ser* 2015;1213:137–72.
- [53] Audichon T, Napporn TW, Canaff C, Morais C, Comminges C, Kokoh KB. IrO<sub>2</sub> coated on RuO<sub>2</sub> as efficient and stable electroactive nanocatalysts for electrochemical water splitting. *J Phys Chem C* 2016;120(5):2562–73.
- [54] Al-Mamun M, Su X, Zhang H, Yin H, Liu P, Yang H, et al. Strongly coupled CoCr<sub>2</sub>O<sub>4</sub>/carbon nanosheets as high performance electrocatalysts for oxygen evolution reaction. *Small* 2016;12(21):2866–71.
- [55] Duan J, Chen S, Vasileff A, Qiao SZ. Anion and cation modulation in metal compounds for bifunctional overall water splitting. *ACS Nano* 2016;10(9):8738–45.
- [56] Sun J, Yin H, Liu P, Wang Y, Yao X, Tang Z, et al. Molecular engineering of Ni–Co–porphyrin multilayers on reduced graphene oxide sheets as bifunctional catalysts for oxygen evolution and oxygen reduction reactions. *Chem Sci* 2016;7(9):5640–6.
- [57] Chen S, Duan J, Jaroniec M, Qiao SZ. Nitrogen and oxygen dual-doped carbon hydrogel film as a substrate-free electrode for highly efficient oxygen evolution reaction. *Adv Mater* 2014;26(18):2925–30.
- [58] Walter MG, Warren EL, McKone JR, Boettcher SW, Mi Q, Santori EA, et al. Solar water splitting cells. *Chem Rev* 2010;110(11):6446–73.
- [59] Zeng M, Li Y. Recent advances in heterogeneous electrocatalysts for the hydrogen evolution reaction. *J Mater Chem A* 2015;3(29):14942–62.
- [60] Greeley J, Jaramillo TF, Bonde J, Chorkendorff IB, Nørskov JK. Computational high-throughput screening of electrocatalytic materials for hydrogen evolution. In *Materials for sustainable energy: a collection of peer-reviewed research and review articles from Nature Publishing Group*. 2011. p. 280–84.
- [61] Garcia-Esparza AT, Cha D, Ou Y, Kubota J, Domen K, Takanabe K. Tungsten carbide nanoparticles as efficient cocatalysts for photocatalytic overall water splitting. *Chem Sus Chem* 2013;6(1):168–81.

- [62] Cao B, Veith GM, Neuefeind JC, Adzic RR, Khalifah PG. Mixed close-packed cobalt molybdenum nitrides as non-noble metal electrocatalysts for the hydrogen evolution reaction. *J Am Chem Soc* 2013;135(51):19186–92.
- [63] Popezun EJ, Read CG, Roske CW, Lewis NS, Schaak RE. Highly active electrocatalysis of the hydrogen evolution reaction by cobalt phosphide nanoparticles. *Angew Chem Int Ed* 2014;53(21):5427–30.
- [64] Zheng Y, Jiao Y, Zhu Y, Li LH, Han Y, Chen Y, et al. Hydrogen evolution by a metal-free electrocatalyst. *Nat Commun* 2014;5:3783–90.
- [65] Mei J, Liao T, Sun Z. Two-dimensional metal oxide nanosheets for rechargeable batteries. *J Energy Chem* 2017;.
- [66] Wu S, Du Y, Sun S. Transition metal dichalcogenide based nanomaterials for rechargeable batteries. *Chem Eng J* 2017;307:189–207.
- [67] Vinayan BP, Nagar R, Raman V, Rajalakshmi N, Dhathathreyan KS, Ramaprabhu S. Synthesis of graphene-multiwalled carbon nanotubes hybrid nanostructure by strengthened electrostatic interaction and its lithium ion battery application. *J Mater Chem* 2012;22(19):9949–56.
- [68] Bang GS, Nam KW, Kim JY, Shin J, Choi JW, Choi SY. Effective liquid-phase exfoliation and sodium ion battery application of MoS<sub>2</sub> nanosheets. *ACS Appl Mater Interfaces* 2014;6(10):7084–9.
- [69] Zahoor A, Jang HS, Jeong JS, Christy M, Hwang YJ, Nahm KS. A comparative study of nanostructured  $\alpha$  and  $\delta$  MnO<sub>2</sub> for lithium oxygen battery application. *RSC Adv* 2014;4(18):8973–7.
- [70] Liu J, Zhou Y, Liu C, Wang J, Pan Y, Xue D. Self-assembled porous hierarchical-like CoO@C microsheets transformed from inorganic–organic precursors and their lithium-ion battery application. *Cryst Eng Comm* 2012;14(8):2669–74.
- [71] Panda MR, Sarkar A, Bao Q, Mitra S. Electrochemical investigation of MoTe<sub>2</sub>/rGO composite materials for sodium-ion battery application. In: *AIP Conference Proceedings*, AIP Publishing, May 2018; 1961;1:030033–37.
- [72] Ai Q, Zhou P, Zhai W, Ma X, Hou G, Xu X, et al. Synergistic double-shell coating of graphene and Li<sub>2</sub>SiO<sub>4</sub> on silicon for high performance lithium-ion battery application. *Diam Relat Mater* 2018;88:60–6.
- [73] Wang G, Zhang L, Zhang J. A review of electrode materials for electrochemical supercapacitors. *Chem Soc Rev* 2012;41(2):797–828.
- [74] Martínez-Periñán E, Down MP, Gibaja C, Lorenzo E, Zamora F, Banks CE. Antimonene: a novel 2D nanomaterial for supercapacitor applications. *Adv Energy Mater* 2018;8(11):1702606–13.
- [75] Ensafi AA, Alinajafi HA, Rezaei B. Adenine decorated@ reduced graphene oxide, a new environmental friendly material for supercapacitor application. *J Alloy Compd* 2018;735:1010–16.
- [76] Xie S, Gou J, Liu B, Liu C. Synthesis of cobalt-doped nickel sulfide nanomaterials with rich edge sites as high-performance supercapacitor electrode materials. *Inorg Chem Front* 2018;5(5):1218–25.
- [77] Xing L, Dong Y, Hu F, Wu X, Umar A. Co<sub>3</sub>O<sub>4</sub> nanowire@ NiO nanosheet arrays for high performance asymmetric supercapacitors. *Dalton Trans* 2018;47(16):5687–94.
- [78] Bondavalli P, Pogon G, Koumoulos E, Charitidis C. Dynamic air-brush deposition method for the new generation of graphene based supercapacitors. *MRS Adv* 2018;3(1–2):79–84.

- [79] Zhang Y, Yang S, Wang S, Liu HK, Li L, Dou SX, et al. Engineering high-performance MoO<sub>2</sub>-based nanomaterials with supercapacity and superhydrophobicity by tuning the raw materials source. *Small* 2018;1800480–18004.
- [80] Mary AJC, Bose AC. Surfactant assisted ZnCo<sub>2</sub>O<sub>4</sub> nanomaterial for supercapacitor application. *Appl Surf Sci* 2018;449:105–12.
- [81] Zheng YR, Gao MR, Gao Q, Li HH, Xu J, Wu ZY, et al. An efficient CeO<sub>2</sub>/CoSe<sub>2</sub> nanobelt composite for electrochemical water oxidation. *Small* 2015;11(2):182–8.
- [82] Tian J, Liu Q, Asiri AM, Alamy KA, Sun X. Ultrathin graphitic C<sub>3</sub>N<sub>4</sub> nanosheets/graphene composites: efficient organic electrocatalyst for oxygen evolution reaction. *Chem Sus Chem* 2014;7(8):2125–30.
- [83] Deng J, Ren P, Deng D, Bao X. Enhanced electron penetration through an ultrathin graphene layer for highly efficient catalysis of the hydrogen evolution reaction. *Angew Chem Int Ed* 2015;54(7):2100–4.
- [84] Gong M, Zhou W, Tsai MC, Zhou J, Guan M, Lin MC, et al. Nanoscale nickel oxide/nickel heterostructures for active hydrogen evolution electrocatalysis. *Nat Commun* 2014;5:4695–700.
- [85] Zhang F, Zhu J, Zhang D, Schwingenschlög U, Alshareef HN. Two-dimensional SnO anodes with a tunable number of atomic layers for sodium ion batteries. *Nano Lett* 2017;17(2):1302–1311.
- [86] Leng X, Shao Y, Wei S, Jiang Z, Lian J, Wang G, et al. Ultrathin mesoporous NiCo<sub>2</sub>O<sub>4</sub> nanosheet networks as high-performance anodes for lithium storage. *Chem Chem* 2015;80(12):1725–31.
- [87] Du D, Lan R, Xu W, Beanland R, Wang H, Tao S. Preparation of a hybrid Cu<sub>2</sub>O/CuMoO<sub>4</sub> nanosheet electrode for high-performance asymmetric supercapacitors. *J Mater Chem A* 2016;4(45):17749–56.
- [88] Wu Q, Chen M, Chen K, Wang S, Wang C, Diao G. Fe<sub>3</sub>O<sub>4</sub>-based core/shell nanocomposites for high-performance electrochemical supercapacitors. *J Mater Sci* 2016;51(3):1572–80.
- [89] Shaikh SP, Mughtar A, Somalu MR. A review on the selection of anode materials for solid-oxide fuel cells. *Renew Sust Energ Rev* 2015;51:1–8.
- [90] Sun C, Hui R, Roller J. Cathode materials for solid oxide fuel cells: a review. *J Solid State Electrochem* 2010;14(7):1125–44.
- [91] Abdalla AM, Hossain S, Azad AT, Petra PMI, Begum F, Eriksson SG, et al. Nanomaterials for solid oxide fuel cells: a review. *Renew Sust Energ Rev* 2018;82:353–68.
- [92] Wang XX, Cullen DA, Pan YT, Hwang S, Wang M, Feng Z, et al. Nitrogen-coordinated single cobalt atom catalysts for oxygen reduction in proton exchange membrane fuel cells. *Adv Mater* 2018;30(11):1706758.
- [93] Manikandan M, Singh G, Barnett AO, Seland F, Sunde S. Development of Ni-based bimetallic electrocatalysts for hydrogen oxidation reaction in alkaline fuel cells. In: Meeting Abstracts No. 30; Electrochem. Soc. April 2018; 1737.
- [94] Strickland K, Pavlicek R, Miner E, Jia Q, Zoller I, Ghoshal S, et al. Anion resistant oxygen reduction electrocatalyst in phosphoric acid fuel cell. *ACS Catal* 2018;8(5):3833–43.
- [95] Duan C, Hook D, Chen Y, Tong J, O'Hayre R. Zr and Y co-doped perovskite as a stable, high performance cathode for solid oxide fuel cells operating below 500°C. *Energy Environ Sci* 2018;10(1):176–82.
- [96] Hussain CM. Handbook of nanomaterials for industrial applications. Elsevier; 2018.
- [97] Hussain CM, Kharisov B. Advanced environmental analysis-application of nanomaterials. The Royal Society of Chemistry; 2017.

## Section 5

# **Functionalized nanomaterial in environmental industry**



This page intentionally left blank

# Functionalization of graphene oxide with metal oxide nanomaterials: synthesis and applications for the removal of inorganic, toxic, environmental pollutants from water

Shraban Ku Sahoo and G. Hota

*Department of Chemistry, NIT, Rourkela, Odisha, India*

### 12.1 Introduction

Water pollution causes disease and death and is a major global problem [1]. Water contaminants include inorganic pollutants (i.e., arsenic, cadmium, chromium, fluoride, lead, and mercury), organic contaminants (i.e., acrylamide, phenol, benzene hexachloride, and carbon tetrachloride), and different organic dyes (i.e., congo red, methyl blue, and methyl orange) [2–5]. Although inorganic pollutants such as heavy metal ions and fluoride are essential nutrients in proper concentration, the environment and human health are threatened when the proper concentration is exceeded. The maximum-acceptable concentrations of these inorganic pollutants in drinking water have been established by World Health Organization (WHO) and many countries, as shown in Table 12.1. Some toxic metal ions such as Hg (II), Pb(II), Cr(VI), Cd(II), and As(III)/(V) and fluoride( $F^-$ ) are nonbiodegradable and accumulate in the environment and living organisms. Their metabolites are toxic, carcinogenic, and mutagenic, and cause chromosomal fractures and respiratory disorders. The removal of these inorganic contaminants from wastewater effluent before it is discharged into a natural water stream is vital [6–9]. Processes such as reverse osmosis, precipitation, activated carbon filter, membrane separation, ion exchange, photocatalysis, adsorption, solvent extraction, and nanofiltration have been employed.

**TABLE 12.1** Permissible limits of selected inorganic pollutants in drinking water in different countries (mg/L).

Inorganic pollutants	WHO	US	EU	China	Australia	Canada	Japan	India
Arsenic	0.01	0.01	0.01	0.01	0.007	0.025	0.01	0.05
Cadmium	0.003	0.005	0.05	0.005	0.002	0.005	0.01	0.01
Chromium	0.05	0.05	0.005	0.05	0.05	0.05	0.05	0.05
Fluoride	1.5	—	1.5	—	—	1.5	—	1.5
Mercury	0.006	0.002	0.001	0.001	0.001	0.001	0.0005	0.001
Lead	0.01	0.015	0.01	0.01	0.05	0.05	0.01	0.05

Of these, adsorption is the most commonly used method, due to its low cost, simple operation and design requirements, low residual product generation, lack of interaction with toxic substances, and potential for reuse [10–12].

Any materials having dimensions in the range of 1–100 nm are called nanomaterials [13]. They may be zero dimensions (0D), one (1D), two (2D), or three (3D) dimensional materials [14]. Nanomaterials containing nanotubes, nanofibers, nanowires, nanorods, and nanoparticles possess unique properties (i.e., small dimension structure and high aspect ratio), making them useful for application in adsorption, filter media, composite materials, biomedical applications, and nanocatalysis [15–18]. Nanocomposites are the composite systems in which at least one of the constituent phases is in the nanometre range ( $1\text{ nm} = 10^{-9}\text{ m}$ ). During the past 10 years, nanocomposite adsorbents have proven to be a suitable alternative to microcomposites and monolithic adsorbents [19,20].

Their large surface areas and high reactive sites make nanosized metal oxide adsorbents promising for use in removal of inorganic pollutants from aqueous medium [21–23]. Due to being environmentally friendly and cost effective, metal oxide (i.e., aluminum, iron, and magnesium) nanocomposites can be used in the catalyst industry, gas sensors, solar cells, and adsorption [24–28]. They are considered to be promising for use in heavy metals and fluoride removal from aqueous systems. Research has shown that metal oxide nanomaterials are good adsorbents. However, nanosized metal oxide adsorbents aggregate during the adsorption process, which decreases their adsorption capacity. In order to decrease the aggregation behavior of nanomaterials, and improve adsorption capacity, recent research has focused on engineered nanomaterials being mounted onto high surface-area GO nanosheet substrate [29,30].

Graphene is one of the most promising advanced carbon-based nanomaterials. It has a 2D honeycomb  $sp^2$  carbon lattice, large theoretical surface area ( $2630\text{ m}^2/\text{g}$ ), excellent chemical inertness, high transparency, enormous electron mobility, good thermal conductivity, and remarkable elasticity [31–33]. This composition makes graphene a favorable material for various applications including sensors, transistors, catalysis, and environmental pollution treatment. GO is an oxidized derivative of graphene and contains epoxide, hydroxyl, and carboxyl groups. These functional groups lead to the negative charge, hydrophilicity, and easy dispersion of GO in aqueous solutions. These characteristics make GO a potential candidate for the removal of different pollutants by adsorption [34,35]. Due to its large surface area and presence of a large number of functional groups, GO can be used to grow various nanoparticles. Since GO also helps in preventing agglomeration of nanoparticles, it can be effectively used as a template or precursor for the growth of different kinds of nanoparticles. In functionalization of GO with metal oxide nanomaterials, graphene not only serves as a highly conductive support material but also provides a large surface for the dispersion of metal

oxide nanoparticles [7,36,37]. GO can be surface modified by using different organic groups, inorganic groups, or polymer. It has been used for removing inorganic environmental pollutants to achieve high adsorption efficiency. These functional groups can form stable chelates with heavy metal ions. Metal oxide, based on functionalized GO nanocomposites has received more attention in the adsorption field due its achievements of high capacity and electivity in the last few years [38–42].

This chapter summarizes the synthesis of functionalized GO, especially functionalization of GO-based nanosheet substrate with aluminum, iron, and magnesium oxide nanocomposites. The functionalized GO-based nanosheet has been used as nanoadsorbents for the removal of inorganic, toxic, environmental, pollutants (mainly arsenic, chromium, mercury, lead, fluoride, and cadmium) from water. Impregnation of metal oxide nanomaterials onto GO nanosheet substrate may generate novel nanocomposites materials for efficient toxic ion removal and improved adsorption capacity. The adsorption affinity, mechanisms, and factors of sorption capacity are discussed here.

## 12.2 Preparation of metal oxides functionalized GO nanocomposites

### 12.2.1 Preparation of GO using modified Hummer's method

GO was prepared from graphite powder using a modified Hummer's method (shown in Fig. 12.1) by oxidation treatment [43]. Sulfuric acid (98%), graphite powder, and sodium nitrate (1:1 ratio) were dissolved and stirred in an ice bath. Next,  $\text{KMnO}_4$  was added slowly under continuous stirring conditions for another few hours. The temperature of the reaction mixture was increased to  $98^\circ\text{C}$  and continuously stirred for 12 h. The suspension was cooled to room temperature and mixed with distilled water followed by addition of 30%  $\text{H}_2\text{O}_2$  and sonicated for 30 min to molt GO into single layers. The diluted mixture was then centrifuged for 15 min at 10,000 rpm. The solid residue was washed properly with distilled water and  $\text{HCl}(5\%)$  several times for complete neutralization, followed by being vacuum dried at room temperature for 12 h, to obtain GO powder.

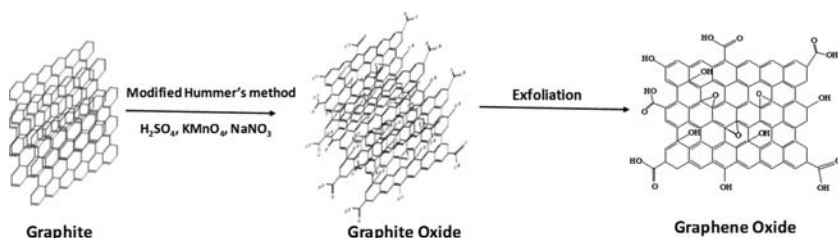


FIGURE 12.1 Synthesis of GO by Hummer's method.

### 12.2.2 Functionalization of GO with metal oxides nanomaterials

GO nanosheets decorated with metal oxide nanoparticles combine the outstanding features of each because of the synergistic effect between them. The synthesis of GO-based composites provides a vital landmark to enhance the application behavior of metal oxide nanomaterials in adsorption fields. These hybrids have versatile and tailor-made properties with performances superior to those of other oxide nanomaterials. Thus considerable efforts have been made to decorate GO with metal oxides nanoparticles [7,35,37]. To date, various kinds of metal oxides have been synthesized and supported on GO for heavy metals and fluoride adsorbents, which include  $\text{TiO}_2$ ,  $\text{Al}_2\text{O}_3$ ,  $\text{SiO}_2$ ,  $\text{MnO}_2$ ,  $\text{Fe}_3\text{O}_4$ ,  $\text{Fe}_2\text{O}_3$ ,  $\text{FeOOH}$ ,  $\text{AlOOH}$ ,  $\text{MgO}$ ,  $\text{MFe}_2\text{O}_4$  ( $\text{M} = \text{Mg}$ ,  $\text{Co}$ ,  $\text{Ni}$ , and  $\text{Mn}$ ), and their mixed binary oxides [35,37]. The size and shape of nanomaterials are important factors affecting their adsorption performance. Efficient synthetic methods to obtain shape-controlled, highly stable, and monodisperse metal oxide nanomaterials have been widely studied during the last decade. For synthesis of these GO-based metal oxides, several methods are used such as chemical precipitation [30,44,45], self-assembly [29,46], sol-gel [47,48], and hydrothermal synthesis [49,50] techniques. In the following section, we will briefly overview the synthesis of graphene–metal oxide composites with a focus on recent developments.

#### 12.2.2.1 Preparation of GO functionalized with iron oxide nanoadsorbents

Iron oxides exist in many forms in nature. Magnetite ( $\text{Fe}_3\text{O}_4$ ), maghemite ( $\gamma\text{-Fe}_2\text{O}_3$ ), and hematite ( $\alpha\text{-Fe}_2\text{O}_3$ ) are the most common. The iron oxide nanomaterials and their mixed-oxide nanocomposites have received much more attention for use in wastewater treatment due to their unique properties, such as extremely small size, high surface-area-to-volume ratio, surface modifiability, excellent magnetic properties, easy preparation, cost effectiveness, and high biocompatibility [23]. Recently, many methods have been developed to synthesize GO-based iron oxide nanocomposites. Here, we will discuss simple and cost-effective methods.

Chandra et al. reported on the development of magnetic graphene hybrids ( $\text{RGO-Fe}_3\text{O}_4$ ) via a simple chemical method using Iron (II) and (III) chloride precursors [44]. The procedure details are shown in Fig. 12.2. This

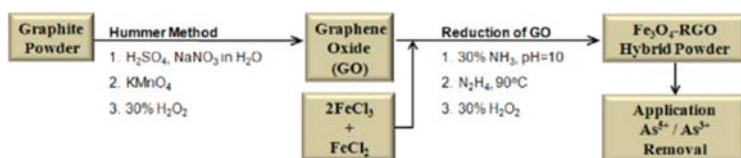


FIGURE 12.2 Synthesis and application of  $\text{Fe}_3\text{O}_4$ –RGO composites [44].

prepared nanocomposite was used to remove the As(III) and As(V) from drinking water in wide areas of South Asia.

Deng et al. used a low-cost coprecipitation method for preparation of GO-based  $\text{Fe}_3\text{O}_4$  nanocomposite [51]. The formation of magnetic iron oxide nanoparticles was achieved by coprecipitation of iron oxide nanoparticles on the surface of GO nanomaterials. In this method 1 g dry GO was dispersed in 100 mL ultrapure water with ultrasonication to form stable suspension. Then, 5.8 g ferrous ammonium sulfate and 10.7 g ammonium ferric sulfate were dissolved in 100 mL ultrapure water to form mixed iron–salt solution under oxygen-free condition. 10 mL aqueous ammonia was rapidly added into the mixed solution to generate iron oxide nanoparticles, followed by slow addition of GO suspension with stirring. The reaction was continued for 45 min at  $85^\circ\text{C}$  with stirring for 45 min and then cooled to room temperature. Ultimately, the desired solid was assembled by a magnet and was washed properly with ultrapure water and anhydrous ethanol three times, respectively, and dried for 12 h at  $70^\circ\text{C}$  in a vacuum oven. GO was functionalized by goethite ( $\text{FeOOH-GO}$ ), which was synthesized via an in situ hydrolysis technique reported by Kuang et al. (shown in Fig. 12.3) [53]. First, GO (0.1 g) was dispersed in 100 mL of water and sonication for 30 min. Then 2.7 g of  $\text{FeCl}_3 \cdot 6\text{H}_2\text{O}$  was added into GO solution. Subsequently, the mixture was put in the water bath at  $80^\circ\text{C}$  and stirred for 4 h. The synthesized precipitate was separated by centrifugation then washed with water and ethanol. They also synthesized  $\text{FeOOH-GO}$  in the presence of 4.1 g anhydrous sodium acetate (called  $\text{FeOOH + Ac-GO}$ ). The morphology and phases of prepared  $\text{FeOOH}$  on GO surface was different, that is, rice spike-like Akaganeite was formed in absence of acetate and spherical goethite quantum dots are formed in presence of acetate ions. Both adsorbents were used for the removal of fluoride ion;  $\text{FeOOH + Ac-GO}$  was more effective.

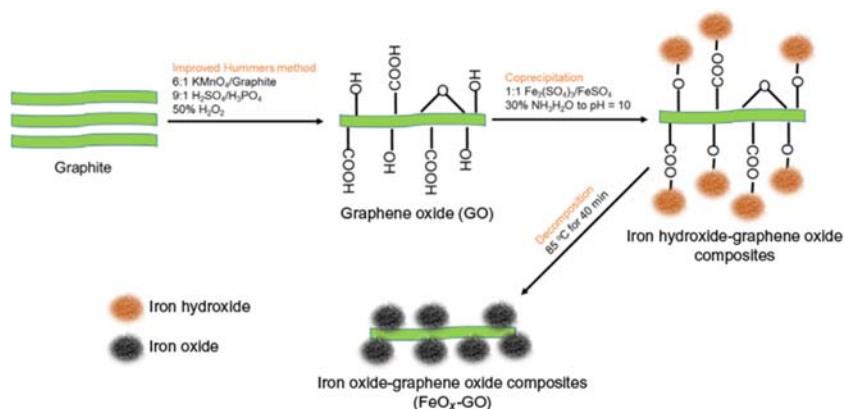


FIGURE 12.3 Schematic synthesis of  $\text{FeO}_x\text{-GO}$  nanocomposites [52].

H. Su et al. reported the synthesis of a new range of iron oxide–GO nanocomposites having different iron oxide content (36–80 wt%). These are high-performance adsorbents for arsenic removal by coprecipitation of iron oxide on GO sheets [52]. The detailed method is shown in Fig. 12.3.

Manganese dioxide/iron oxide/graphene-based magnetic nanocomposites ( $\text{MnO}_2/\text{Fe}_3\text{O}_4/\text{GO}$ ) was synthesized by a simple two-step reaction and implemented for the removal of hexavalent chromium ion from water [54]. In the first step,  $\text{GO}-\text{Fe}_3\text{O}_4$  was synthesized in a one-pot solvothermal method using  $\text{Fe}(\text{acac})_3$  and ethyl glycol as precursor. Then  $\text{MnO}_2$  was coated with  $\text{Fe}_3\text{O}_4/\text{GO}$  by simple immersion into a  $\text{KMnO}_4$  aqueous solution, which is similar to  $\text{MnO}_2$  coated on carbon nanotubes.

Bhunia et al. used a different type of synthetic method for the preparation of porous  $\text{rGO}-\text{Fe}(0)-\text{Fe}_3\text{O}_4$  composites with high surface area for the removal of all toxic heavy metals such as  $\text{Cr}(\text{VI})$ ,  $\text{Hg}(\text{II})$ ,  $\text{Pb}(\text{II})$ ,  $\text{Cd}(\text{II})$ , and  $\text{As}(\text{III})$  [55]. In this procedure, the  $\text{Fe}_3\text{O}_4$  nanoparticles of the  $\text{rGO}-\text{Fe}(0)-\text{Fe}_3\text{O}_4$  composite were assumed to be intercalated in rGO layers and successively converted to  $\text{Fe}(0)$  by thermal annealing at different temperatures in a  $\text{H}_2/\text{Ar}$  atmosphere. At  $400^\circ\text{C}$ , a matrix of  $\text{Fe}(0)-\text{Fe}_3\text{O}_4$  was supported on rGO, whereas at  $600^\circ\text{C}$ ,  $\text{Fe}_3\text{O}_4$  was absolutely converted to  $\text{Fe}(0)$  (Fig. 12.4).

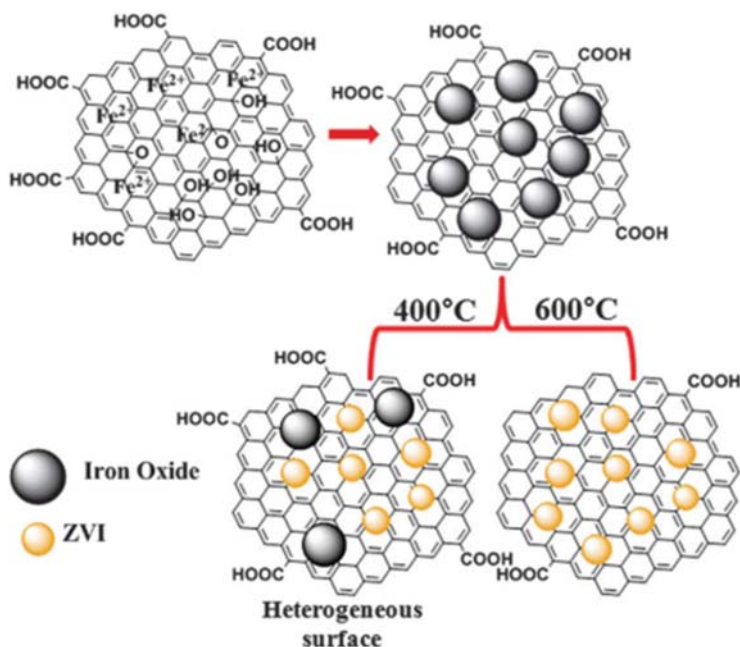


FIGURE 12.4 Synthesis of the porous  $\text{rGO}-\text{Fe}(0)-\text{Fe}_3\text{O}_4$ , and  $\text{rGO}-\text{Fe}(0)$  [55].



Metal ferrites, such as nickel, cobalt, magnesium, and manganese, are more widely used in adsorption due to their spinel structure. They exhibit excellent chemical stability, saturation magnetization, and easy separation. The hydrothermal method is most popular for use in synthesis of metal ferrite structure. Ag–CoFe<sub>2</sub>O<sub>4</sub>–GO nanocomposite was synthesized by hydrothermal method using Co(NO<sub>3</sub>)<sub>2</sub>·6H<sub>2</sub>O, Fe(NO<sub>3</sub>)<sub>3</sub>·9H<sub>2</sub>O, AgNO<sub>3</sub>, and CH<sub>3</sub>COONa in the ethanol suspension of GO, which was used to purify both bacteria and Pb(II) from polluted water. This method was reported by Ma et al. [56]. Lingamdinne et al. synthesized GO-based nickel ferrite (GO–NiFe<sub>2</sub>O<sub>4</sub>) using a simple cost-effective coprecipitation method. This method uses nickel and iron nitrate solution with NaOH as precipitating agent and Pb(III) and Cr(III) as adsorbents [57]. The other recently developed methods used to synthesize functionalized GO with iron oxide-based nanocomposite are summarized in Table 12.2.

#### 12.2.2.2 Preparation of GO functionalized with other metal oxide nanoadsorbents

For adsorption of heavy metals and fluoride from aqueous systems, the most widely studied metal oxides (excluding iron oxides) are manganese oxides, aluminum oxides, magnesium oxide, zirconium oxide, cerium oxide, and titanium oxides. These are cost effective, have large surface area, and are nontoxic [43].

Jin et al. reported the synthesis of amorphous alumina-modified expanded GO (Al<sub>2</sub>O<sub>3</sub>/GO). The composite was prepared via a facile solution method followed by thermal treatment at 450°C for 2 h, which was used to remove trace fluoride ions in aqueous solution [72]. S. Kanrar et al. used a simple coprecipitation method for the synthesis of GO-based iron and aluminum mixed-oxide composite using ammonia solution as precipitating agent [63]. The highly efficient heavy metal adsorbent AlOOH–RGO nanocomposites were synthesized using hydrothermal method, which was reported by C. Gao et al. [73]; 0.57 g of Al(NO<sub>3</sub>)<sub>3</sub>·9H<sub>2</sub>O and 0.27 g of urea were added to 18 mL of 0.5 mg/mL GO aqueous solution under stirring. Finally, it was treated under hydro-thermal condition at 180°C.

Varadwaj et al. synthesized three-dimensional (3D) porous Mg – Al layered double-hydroxide nanocomposites decorated onto the GO surface using coprecipitation technique [74]. GO was fabricated by a modified Hummer's method then layered double-hydroxide nanosheets were homogeneously grown on the surface of the GO sheets by an in situ crystallization approach, using a coprecipitation method. Wen et al. also synthesized the same materials using the hydrothermal method [66]. In this procedure, GO was sonicated in Milli-Q water for 1 h to achieve homogeneous suspensions. A solution of MgCl<sub>2</sub>·6H<sub>2</sub>O, AlCl<sub>3</sub>·6H<sub>2</sub>O, and hexamethylenetetramine with appropriate ratios was added. The resulting solution was stirred and then transferred to a

**TABLE 12.2** Removal of different inorganic pollutants by metal oxide-functionalized GO nanoadsorbents.

Adsorbent	Preparation method	Target metals	Maximum adsorption capacity (mg/g) at pH	Refs
Anionic polypeptide poly ( $\gamma$ -glutamic acid)–functionalized magnetic $\text{Fe}_3\text{O}_4$ –GO–(o–MWCNTs) hybrid nanocomposite	A simple one-pot reaction	Cd(II) Cu(II) Ni(II)	625.00 at 8.0 574.71 at 5.0 384.62 at 5.0	[58]
$\text{Fe}_3\text{O}_4$ –GO	Chemical precipitation in $\text{N}_2$ atmosphere	As(III) As(V)	85.00 at 4 38.00 at 7	[30]
EDTA functionalized magnetic graphene oxide	Hydrothermal method	Pb(II) Hg(II) Cu(II)	508.4 at 4.2 268.4 at 4.1 301.2 at 5.1	[59]
$\text{Ag}/\gamma\text{–Fe}_2\text{O}_3@\text{r–GO}$	Chemical precipitation	Pb(II)	42.9 at 5	[60]
Polypyrrole decorated reduced graphene oxide– $\text{Fe}_3\text{O}_4$	Situ polymerization	Cr(VI)	293.3 at 3	[61]
$\text{MnO}_2/\text{Fe}_3\text{O}_4/\text{GO}$	Solvothermal	Cr(VI)	193.1 at 2 175.4 at 5	[54]
Smart magnetic graphene oxide	Microwave oven under a nitrogen atmosphere	Cr(VI) As(V) Pb(II)	4.86 at neutral pH 3.26 6.00	[62]
Iron–aluminum oxide–graphene oxide	Chemical method	$\text{F}^-$	22.13 at 7	[63]
Hierarchical $\text{AlOOH}@\text{reduced graphene oxide}$	Antisolvent process	$\text{F}^-$	118.7 at 6.5	[64]
Graphene oxide decorated by MgO nanocubes	Precipitation method	Pb(II)	187.9 at 6.5	[65]
Mg – Al layered double hydroxides and graphene oxide	Hydrothermal process	As(V)	180.26 at 5	[66]
Graphene oxide–hydrated manganese oxide	Chemical precipitation	Pb(II)	>553 at 6.5	[67]
Graphene oxide–MgO nanohybrid	Precipitation method	Pb(II)	190 at 6.5	[68]

(Continued)

**TABLE 12.2 (Continued)**

Adsorbent	Preparation method	Target metals	Maximum adsorption capacity (mg/g) at pH	Refs
Functionalization of GO with MgO–MgFe <sub>2</sub> O <sub>4</sub> binary oxides	Hydrothermal	F <sup>–</sup>	34.24 at 6	[43]
Graphene oxide/Fe–Mn composite	Chemical method	Hg(II)	32.9 at 7	[69]
3D graphene/δ–MnO <sub>2</sub> aerogels	Self-assembly	Pb(II) Cd(II) Cu(II)	643.62 at 6 250.31 at 6 228.46 at 6	[46]
MnFe <sub>2</sub> O <sub>4</sub> –graphene composite	Solvothermal process	Pb(II) Cd(II)	100.00 at 5 76.90 at 7	[70]
Graphene oxide-based inverse spinel nickel ferrite	Precipitation method	Pb(II) Cr(III)	25.00 at 5.5 45.50 at 4	[57]
rGO/ZrO <sub>2</sub>	Hydrothermal method	F <sup>–</sup>	46.00 at 7	[50]
SiO <sub>2</sub> –graphene composite	Chemical method	Pb(II)	113.6 at 6	[71]
Magnetic SiO <sub>2</sub> @CoFe <sub>2</sub> O <sub>4</sub> nanoparticles decorated on graphene oxide	solvothermal and sol–gel processes	Cr(VI)	207.91 at 1	[47]
Reduced graphene oxide-supported mesoporous Fe <sub>2</sub> O <sub>3</sub> /TiO <sub>2</sub> nanoparticles	sol–gel route	As(V) As(III)	99.5 at 6 77.7 at 7	[48]
Flower-like TiO <sub>2</sub> on exfoliated graphite oxide	Hydrothermal method	Cd(II) Pb(II)	14.9 at 5 35.6 at 5	[49]

50 mL Teflon-lined stainless-steel autoclave. The autoclave was heated to 140°C and maintained for 12 h. Morphology of both the materials is similar; both are excellent adsorbent for toxic arsenic and lead from aqueous solution.

The GO and magnesium oxide (MgO) nanohybrid (GO–MgO) was prepared by simple precipitation method and has been successfully utilized for the removal of Pb(II) from water. Mg(NO<sub>3</sub>)<sub>2</sub>·6H<sub>2</sub>O was used as a precursor and NaOH as precipitating agent, as reported by Mohan et al. [65]. GO–MgO nanocomposite was also synthesized by Heidarizad et al. using simple sol-gel method with MgCl<sub>2</sub>·6H<sub>2</sub>O metal precursor [75].

Pan et al. synthesized both  $\alpha$  and  $\gamma$  manganese dioxide-decorated GO (GO–MnO<sub>2</sub>). This was accomplished via fixation of crystallographic MnO<sub>2</sub> ( $\alpha$ ,  $\gamma$ ) on the surface of GO. It was then used as an adsorbent material for simultaneous removal of thorium/uranium ions from aqueous solutions [76]. GO– $\alpha$ –MnO<sub>2</sub>, MnCl<sub>2</sub>·4H<sub>2</sub>O (0.1364 g) was added into GO (0.1970 g) and isopropyl alcohol (60 mL) solution and sonicated. An aqueous solution of KMnO<sub>4</sub> (0.077 g KMnO<sub>4</sub>/4 mL H<sub>2</sub>O) was immediately put into the mixture. Then it was refluxed at 87°C with vigorous stirring. In this synthesis 12 mL of water with 0.077 g of KMnO<sub>4</sub>, rather than 4 mL water, was used for converting the  $\alpha$ -phase to  $\gamma$ -phase. The detailed synthetic mechanism is described in Fig. 12.5.

Santhosh et al. synthesized magnetic SiO<sub>2</sub>@CoFe<sub>2</sub>O<sub>4</sub> nanoparticles decorated on GO using solvothermal and sol-gel processes [47]. The prepared nanocomposite materials were used as magnetic adsorbents for the removal of organic and inorganic pollutants (i.e., acid black 1 dye and Cr(VI) ions) from aqueous solution.

The rGO/ZrO<sub>2</sub> nanocomposite was prepared by Mohan et al. using a simple one step hydrothermal method in which ZrOCl<sub>2</sub>·8H<sub>2</sub>O acted as the ZrO<sub>2</sub> precursor and GO as the supporting material [50]. Other recently-developed GO-based metal oxides nanocomposites are presented in Table 12.2.

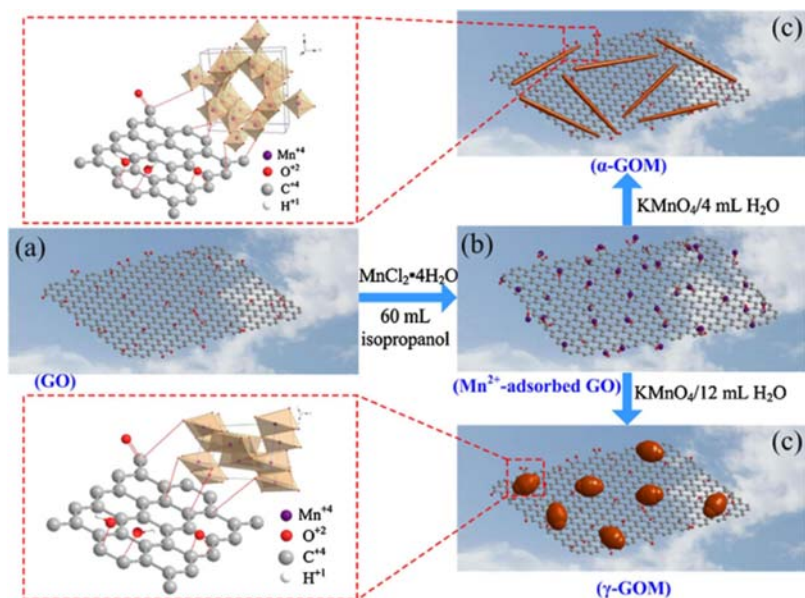


**FIGURE 12.5** Schematic diagram the growth of needle-like  $\alpha$ -MnO<sub>2</sub> or spindle-like  $\gamma$ -MnO<sub>2</sub> on GO: (A) GO, (B) Mn<sup>2+</sup> adsorbed GO, (C) in situ formation of MnO<sub>2</sub> on GO by redox reaction [76].

### 12.2.3 Preparation of surface modified GO metal oxides composite nanoadsorbents

In recent years, researchers have also focused on surface modified GO with organic, inorganic, and polymer molecules and decoration with different types of metal oxides nanomaterials. The main advantages of these types of adsorbent materials include high selectivity and high adsorption capacity because these groups can form stable chelates with heavy metal ions.

Li et al. developed a simple chemical bonding method to synthesize magnetic cyclodextrin–chitosan/GO and tested adsorption behaviors of Cr(VI) in aqueous solution [77]. The results show that with the advantage of large surface area, abundant hydroxyl and amino groups of the material, and the magnetic property of  $\text{Fe}_3\text{O}_4$ , the Cr(VI) can be easily and rapidly extracted from the water by magnetic attraction. In this method, 0.1 M 1-ethyl-3-(3-dimethylaminopropyl) carbodiimide hydrochloride and 0.1 M *N*-hydroxyl succinimide solutions were added to the GO dispersion with continuous stirring in order to activate the carboxyl groups of GO. The pH of the resulting solution was maintained at 7.0 using dilute sodium hydroxide. Magnetic cyclodextrin–chitosan (0.1 g), the activated GO solution, and 5 mL glutaraldehyde were added into a flask and dispersed in distilled water by ultrasonic dispersion for 10 min. After ultrasonic dispersion, the mixed solutions were stirred at  $65^\circ\text{C}$  for 2 h.

Ternary magnetic composite polypyrrole-modified rGO– $\text{Fe}_3\text{O}_4$  nanoparticles (Ppy– $\text{Fe}_3\text{O}_4/\text{rGO}$ ) were fabricated by a simple two-step reaction route, which is shown in Fig. 12.6 [61]. First,  $\text{Fe}_3\text{O}_4/\text{rGO}$  composite was fabricated,

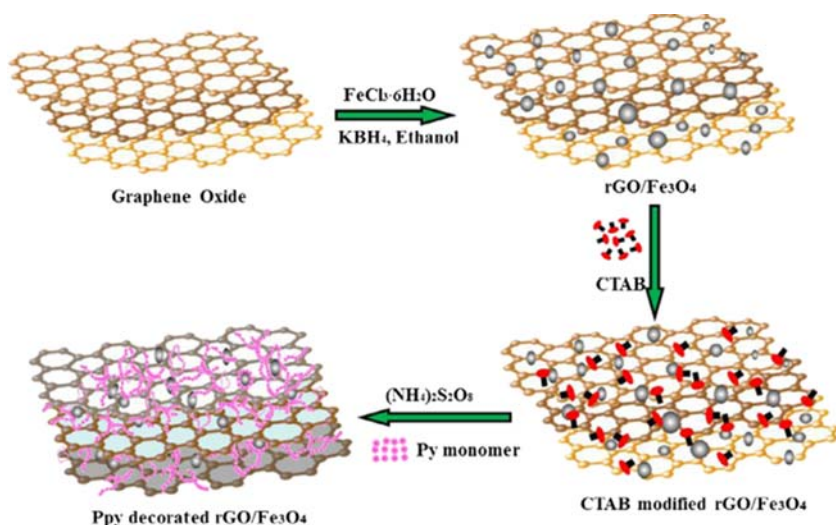


**FIGURE 12.6** Synthetic route for ternary magnetic-composite polypyrrole-modified rGO– $\text{Fe}_3\text{O}_4$  nanoparticles (Ppy– $\text{Fe}_3\text{O}_4/\text{rGO}$ ) [61].

then polypyrrole was decorated on the surface of  $\text{Fe}_3\text{O}_4/\text{rGO}$  composite by in situ polymerization. This was done using ammonium persulfate (APS) as the oxidant. No acid was used.

Cui et al. reported the synthesis of EDTA-functionalized magnetic GO (EDTA-GO- $\text{Fe}_3\text{O}_4$ ) and used it as adsorbent for heavy metal (Pb(II), Hg(II), and Cu(II)). GO was synthesized by modified Hummer's method and  $\text{Fe}_3\text{O}_4$ -nanoparticles were synthesized by hydrothermal method [59]. For the synthesis of magnetic GO (GO- $\text{Fe}_3\text{O}_4$ ), the prepared  $\text{Fe}_3\text{O}_4$  and GO (mass ratio of 1:1) solution was added into the Teflon-lined autoclave and reacted for 8 h at  $200^\circ\text{C}$ . For EDTA-GO- $\text{Fe}_3\text{O}_4$ , 1.0 g GO- $\text{Fe}_3\text{O}_4$  was dispersed in 20 mL of acetic acid (10%) aqueous solution and 6.0 g EDTA was evenly dispersed in 100 mL of methyl alcohol. Next, the mixtures were mixed by mechanical rabbling and reacted at room temperature for 24 h. Zhao et al. established a simple hydrothermal method for preparing ammine-functionalized GO decorated with  $\text{Fe}_3\text{O}_4$  nanoparticles. This was used for selective removal of hexavalent chromium [78]. Here, 0.5 g  $\text{FeCl}_3 \cdot 6\text{H}_2\text{O}$ , 3 g sodium acetate, and 30 mL diethylenediamine were dissolved in GO-ethylene glycol solution at ambient temperature. The mixture was transferred into a Teflon-lined stainless-steel autoclave and reacted at  $200^\circ\text{C}$  for 6 h. Additional materials involving synthetic procedure are listed in Table 12.2.

## 12.3 Removal of inorganic pollutants from water using metal oxide-functionalized GO-nanosubstrates

The interaction between toxic metal and fluoride ions and the surface oxygen-containing groups such as hydroxyl, carboxyl, and epoxy plays an important role in adsorption capacity of heavy metals on GO-based metal oxide nanomaterials. In this section, the effect of adsorption affinity, mechanisms, and factors (such as pH, time, and temperature) on adsorption capacity are discussed.

### 12.3.1 Adsorption of anionic pollutants

The primary anionic-inorganic pollutants present in wastewater are fluoride, nitrates, arsenic, and chromium. In aqueous solution, fluoride is present as  $\text{F}^-$ , arsenic is two formed (i.e., arsenate (As(V)) and arsenite (As(III))), and chromium is also two formed (i.e., Cr(VI) and Cr(III) complex). As(V) is primarily in surface water and As(III) is primarily in groundwater water systems. Among the two arsenic forms, As(III) is present in negative ionic form ( $\text{H}_2\text{AsO}_3^-$ ) in all pH conditions. However As(V) exists mainly as  $\text{H}_3\text{AsO}_4$  at  $\text{pH} < 2.2$ ,  $\text{H}_2\text{AsO}_4^-$  at pH range 2.2–6.98,  $\text{HAsO}_4^{2-}$  at pH 6.98–11.5 and  $\text{AsO}_4^{3-}$  at  $\text{pH} > 11.5$ . For chromium complex, Cr(IV) is more toxic than Cr(III). At low pH, the predominant Cr(VI) form is  $\text{HCrO}_4^-$ , but as the pH

increases, this form converts to  $\text{Cr}_2\text{O}_7^{2-}$  or  $\text{CrO}_4^{2-}$  [47,48,66,78,79]. For these anionic pollutants, a low pH value is required for better adsorption. At low pH the surface of the adsorbent becomes highly protonated and positively charged, which favors the electrostatic interaction between the anionic pollutants and adsorbent surface. Increasing pH of the solution makes the surface negatively charged, greatly weakening the electrostatic attraction between the adsorbent and negatively charged anionic pollutants. This decreases the removal efficiency. At higher pH, there is competition between negative hydroxyl group ( $\text{OH}^-$ ) and anionic contaminants.

### 12.3.1.1 Adsorption of fluoride ( $\text{F}^-$ )

Water contaminated with fluoride ions has become a worldwide problem. The source of the contamination is industrial manufacturing of semiconductors, makeup, ceramics, and aluminum smelting. The presence of higher concentration of fluoride ions in drinking water (more than 1.5 mg/L) causes numerous bone diseases (i.e., skeletal fluorosis, dental fluorosis, arthritis, osteoporosis, and many more) [43]. Thus the urgency to develop a suitable technique for fluoride ion removal.

Anions have been proposed to be adsorbed on adsorbent surface through specific and nonspecific processes. The specific adsorption involves ligand exchange reactions, wherein the anions displace  $-\text{OH}$  groups from the surface. The nonspecific adsorption involves electrostatic forces and mainly depends on the  $\text{pH}_{\text{PZC}}$  (point zero charge) of graphene to adsorb the fluoride ions from water. Research suggests that fluoride adsorption by GO-based metal oxide nanocomposite involves ion exchange between fluoride ions in solution and hydroxyl ions on graphene. Adsorption of fluoride is affected by the pH of the solution and an acidic medium (less pH). Adsorption capacity increases with temperature. Sahoo et al. [43] used GO–MgO– $\text{MgFe}_2\text{O}_4$  magnetic nanocomposite for fluoride removal. They also researched the affect by changing different parameters such as contact time, pH, and temperature. The maximum adsorption capacity is found to be 34 mg/g at pH = 6 with 60 min. The adsorption process followed a pseudo-second-order kinetic equation and the Langmuir isotherm model. The mechanism of fluoride adsorption includes anion exchange, electrostatic interactions, and complex formation, which is shown in Fig. 12.7.

Kanrar, et al. used GO-incorporated iron-aluminium oxide for removal of toxic fluoride ions [63]. The fluoride adsorption was higher at pH below point of zero charge ( $\text{pH}_{\text{ZPC}} = 6$ ; i.e., pH = 5 of the solution). At lower pH, adsorption occurred due to electrostatic interactions between positively charged adsorbent surface and fluoride ions. Increase in adsorption at higher pH was due to an ion-exchange mechanism. It followed the pseudo-second-order kinetics model and was endothermic in nature. The spontaneity of the reaction increased with increasing temperatures. The adsorption data



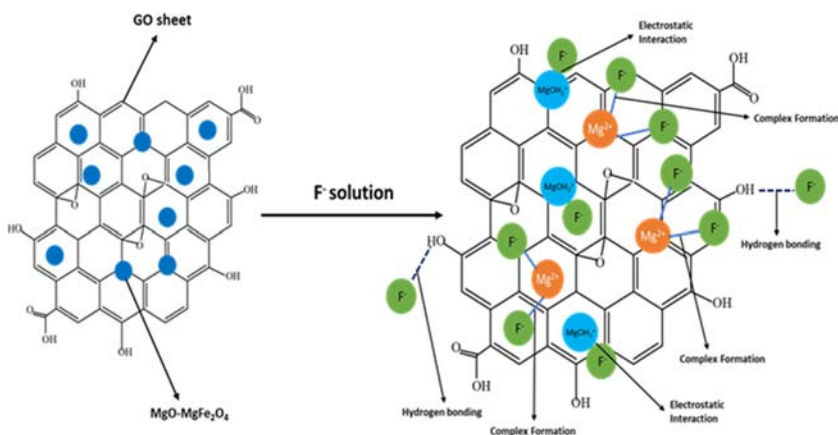


**FIGURE 12.7** Plausible mechanism for  $F^-$  removal on GO-based  $MgO-MgFe_2O_4$  nanocomposite [43].

corresponded with the Langmuir model, which indicates a monolayer adsorption occurred. The maximum adsorption capacity was found to be 27.8 mg/g. Barathi et al. [79] used functionalized GO with  $AlOOH$  for selective fluoride removal. It is possible to treat 2000 mL of 5.0 ppm fluoride solution at pH 7.0. This is possible at the normal pH existing in water. The  $Al-O(OH)$ -decorated GO adsorbent could demonstrate its efficacy for field applications.

### 12.3.1.2 Adsorption of arsenic ( $As(V)$ and $As(III)$ )

Arsenic is one of the common hazardous elements in water. The main sources are biological activity, leakage from minerals or soils, petroleum refining, industrial-waste discharge, mining, and agriculture where arsenic-containing pesticides, herbicides, and fertilizers are used. Drinking of arsenic-contaminated water can cause cancers affecting the bladder, lungs, skin, kidney, liver, and prostate. Arsenic primarily exists in natural water in two stable forms: arsenate  $As(V)$  and arsenite ( $As(III)$ ). Arsenite is more toxic than arsenate. The removal of arsenic from drinking water is a necessity for a safe and healthy environment [30,80].

Yoon et al. [30] have investigated arsenic removal by using GO or reduced GO-based  $Fe_3O_4$  composite. They found that  $Fe_3O_4$ -GO exhibited greater adsorption capacity for both  $As(III)$  and  $As(V)$  than did  $Fe_3O_4$ -rGO. This is due to more surface-functional groups present on GO-based composites compared to rGO-based composites. More  $Fe_3O_4$  nanoparticle formed on GO surface than rGO surface.  $As(III)$  was more adsorbed onto both nanocomposites than was  $As(V)$ . The adsorption of  $As(V)$  mainly occurred due to the electrostatic interaction between the positively charged surface of adsorbents and anionic  $As(V)$  species whereas the adsorption of



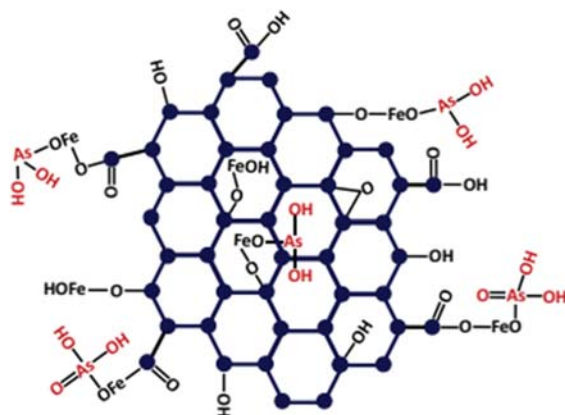


**FIGURE 12.8** Attachment sites of As(III) and As(V) on FeOOH@GO-COOH nanocomposite [80].

As(III) was mostly dependent on surface complexation, rather than electrostatic interactions. According to this journal GO and rGO had no adsorption capacity for arsenic. However, when  $\text{Fe}_3\text{O}_4$  nanoparticles were decorated on GO and rGO, they exhibited adsorption properties toward arsenic, which was due to the reduction process and shows difference properties. This indicates that more  $\text{Fe}_3\text{O}_4$  formed on GO surface because more surface-functional groups were present on GO, which facilitated synthesis with iron. The functional group, including oxygen, supported the composition of the  $\text{Fe}_3\text{O}_4$ .  $\text{GO-Fe}_3\text{O}_4$  shows better adsorption capacity than  $\text{rGO-Fe}_3\text{O}_4$ .

Chen et al. [80] synthesized carboxylic-functionalized GO ( $\text{GO-COOH}$ ) decorated with akaganeite ( $\beta\text{-FeOOH}$ ). It was used as an arsenate and arsenite adsorbent. The adsorption process of arsenite and arsenate was performed within a wide range of pH 3–10, providing high adsorption capacities of 77.5 mg/g for As(III) and 45.7 mg/g for As(V). The attachment sites of As(III) and As(V) on FeOOH@GO-COOH nanocomposites are shown in Fig. 12.8.

The Mg-Al layered-double hydroxides and GO nanocomposites achieved much more adsorption capacity (183.11 mg/g) than other materials with high concentration. The adsorption process followed the Langmuir model, which is indicative of a monolayer adsorption [66].

### 12.3.1.3 Adsorption of Cr(VI)

Chromium (Cr) is one of the highly toxic heavy metals in aqueous medium. It is discharged from electroplating, tanneries, metal refining, and textile industries. Concentration of Cr above the permissible level (0.05 mg/L) is carcinogenic and mutagenic to the ecosystem and humans. It can cause health problems including lung cancer, kidney and liver damage, anemia,

and ulcer formation. In water, chromium primarily exists in two oxidation states (i.e., Cr(VI) and Cr(III)). Between them, Cr(VI) is more toxic, soluble, and carcinogenic than the much less soluble Cr(III). The removal of Cr(VI) is imperative in order to meet safe discharge levels [41,78].

Metal oxides (iron and aluminum magnesium) nanocomposites have been used as effective adsorbent for Cr(VI), which facilitates magnetic and cost-effective removal of Cr(VI). However, bare metal oxide nanoparticles are likely to agglomerate to form larger aggregates in acidic solutions, which decreases adsorption capacity. Decorating these nanoparticles on graphene substrate is an effective method for solving this problem.

Wang et al. [61] used  $\text{Fe}_3\text{O}_4$  nanoparticles decorated on polypyrrole (Ppy)-coated RGO (Ppy- $\text{Fe}_3\text{O}_4/\text{rGO}$ ) to remove Cr(VI) from aqueous solutions. They have also prepared  $\text{Fe}_3\text{O}_4/\text{rGO}$  for comparison study. It was found that polypyrrole-coated nanocomposite shows much higher adsorption capacity (293.3 mg/g) than that of  $\text{Fe}_3\text{O}_4/\text{rGO}$  at pH = 3. The removal process and mechanism depended on pH. Thermodynamic study at different temperatures revealed that the adsorption process was exothermic and spontaneous. The adsorption of Cr(VI) was facilitated through both electrostatic attraction and ion exchange process.

$\text{MnO}_2/\text{Fe}_3\text{O}_4/\text{GO}$  ( $\text{MnO}_2/\text{Fe}_3\text{O}_4/\text{GO}$ ) was the most effective adsorption material for Cr(VI), as reported by Liu et al. [54]. Hexavalent chromium adsorption by  $\text{MnO}_2/\text{Fe}_3\text{O}_4/\text{GO}$  was primarily pH dependent and showed excellent adsorption capacities both at pH 5.0 (maximum adsorption capacity = 175.4 mg/g) and pH 2.0 (maximum adsorption capacity 193.1 mg/g). The adsorption data followed pseudo-second-order kinetic model. It was also stable and easily recovered from water.

Recently, Zhao et al. [78] used both amine-functionalized GO decorated with  $\text{Fe}_3\text{O}_4$  and GO decorated with  $\text{Fe}_3\text{O}_4$  nanocomposites for the removal of Cr(VI) from aqueous solution. It was found that amine-functionalized materials show maximum adsorption capacity (123.4 mg/g). The adsorption process was pH dependent. At pH = 2.0, maximum adsorption was achieved. The mechanism of Cr(VI) adsorption on the adsorbent surface was mainly the electrostatic attraction and reduction process from Cr(VI) to Cr(III) by using pi electrons from GO ring. The Cr(III) complex then chelates with amine groups. The attaching sites for Cr(VI) removal are shown in Fig. 12.9.

### 12.3.2 Adsorption of cationic pollutants (Pb(II), Hg(II), and Cd(II))

Pb(II), Hg(II), and Cd(II) are toxic, cationic, inorganic metals in wastewater. Natural and anthropogenic activities such as mining activities, waste incineration, and oil and coal combustion are the major sources of these toxic heavy metals emissions. Their presence in water causes detrimental effects on humans and the environment. Long-term consumption of these heavy metals will cause serious health problems including anemia, cancer, kidney disease,

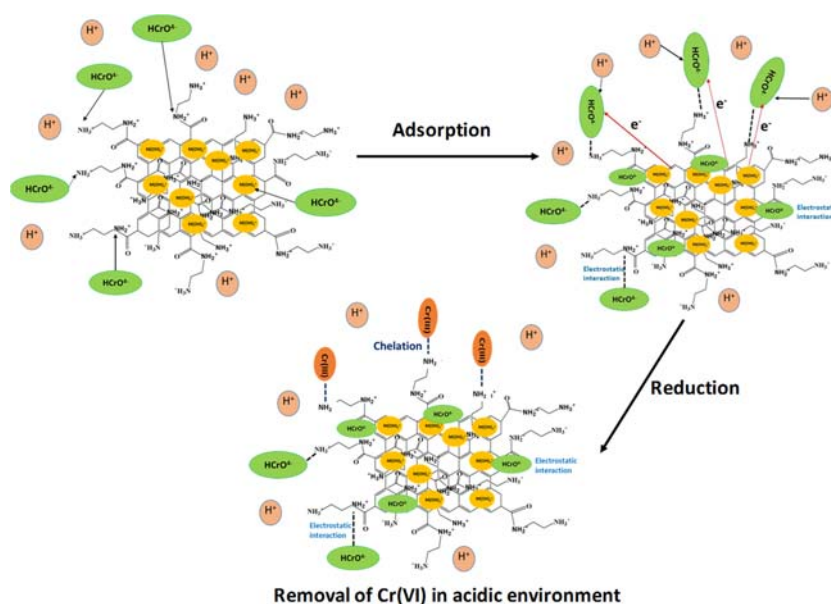


**FIGURE 12.9** Cr(VI) removal on amine-functionalized GO decorated with metal oxide in acidic medium.

mental retardation, renal damage, emphysema, hypertension, cardiovascular disorder, diabetes mellitus, and skeletal malformation. It is necessary to remove these toxic ions from drinking water [49,56,69].

The adsorption of these cationic metal ions on nanocomposite can be achieved by three types of interactions: electrostatic interaction, ion exchange, and complex formation [59,70]. The presence of oxygen-containing groups on GO sheets can be used as attaching sites to bind ions by electrostatic interaction, ion exchange, and coordination. Higher pH value is required for adsorption of these metal ions. At lower pH, there is a competition on carboxylate and phenoxide ( $-\text{COO}^-$  and  $-\text{O}^-$ )—sites of GO between proton and positive metal ions, which will result in a lower adsorption capacity. However, at high pH values, there is a formation more of above groups to carboxylate and phenoxide ions ( $-\text{COO}^-$  and  $-\text{O}^-$ )—and provide electrostatic interaction that are favorable to adsorb cationic species.

Mohan et al. [65] reported the removal of Pb(II) ions from water using GO-based MgO nanocubes (GO–MgO). The maximum adsorption capacity was 187.9 mg/g at pH 6.5 with initial lead concentration of 80 mg/L. They examined the adsorption mechanism of Pb(II) on GO–MgO surface. The adsorption involved two processes: adsorption by GO and ion exchange reaction between Pb(II) and Mg(II), as shown in Fig. 12.10.

Three-dimensional graphene/ $\delta$ -MnO<sub>2</sub> aerogels were used for the removal of heavy metal ions (Pb(II), Cd(II), and Cu(II)). They exhibited a fast

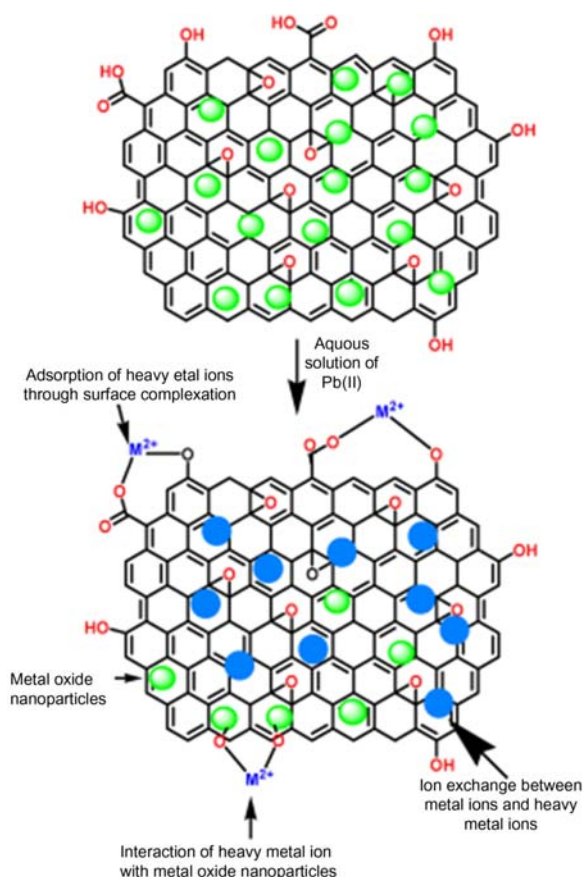


**FIGURE 12.10** Schematic representation of mechanism of Pb(II) removal GO-decorated metal oxide nanoparticles [65].

adsorption kinetic rate and superior adsorption capacity toward heavy metal ions because of their unique structural characteristics [46]. The maximum adsorption capacities of graphene/ $\delta$ -MnO<sub>2</sub> aerogels were as large as 643.62 mg/g for Pb(II), 250.31 mg/g for Cd (II), and 228.46 mg/g for Cu (II). The heavy metal ions could not only adsorb on the surface of graphene/ $\delta$ -MnO<sub>2</sub>, but also inserted into the interlayer gaps of birnessite MnO<sub>2</sub>, which produces the synergistic effect of the static-electrical attraction, surface complexation, and ion exchange.

Tang et al. [69] synthesized GO-based different Fe–Mn oxide nanocomposites for Hg(II) removal. These materials were effective for removal of mercury and reduction of bioavailability. Fe–Mn oxides were coated on the GO surface through oxygen-containing functional groups. They interacted with more *sp*<sup>3</sup> defects and had greater thermal stability than GO. Several

metal oxides ( $\text{FeOOH}$ ,  $\text{Fe}_2\text{O}_3$ ,  $\text{MnO}_2$ ,  $\text{MnOOH}$ , and  $\text{MnO}$ ), when on the surface of  $\text{GO/Fe-Mn}$  and oxygen-containing functional groups of GO can stop mercury through ligand exchange and surface complexation. The adsorption equilibrium is nonideal in nature, i.e., multilayer sorption at low mercury concentrations, while a monolayer adsorption at high concentrations.

EDTA-functionalized GO decorated with magnetic metal oxide ( $\text{EDTA-Fe}_3\text{O}_4\text{-GO}$ ) is a good adsorbent for  $\text{Pb(II)}$ ,  $\text{Hg(II)}$ , and  $\text{Cu(II)}$ , as reported by Cui et al. [59]. The effect of adsorbent dose, contact time, pH, and initial concentration on adsorption process were examined.  $\text{EDT-Fe}_3\text{O}_4\text{-GO}$  showed more adsorption capacities than parent composites ( $\text{EDTA-GO}$ ,  $\text{EDTA-Fe}_3\text{O}_4$ , and  $\text{Fe}_3\text{O}_4\text{-GO}$ ). The adsorption mechanism depends on electrostatic attractions and chelation. Their magnetic properties expedite solid-liquid separation. The adsorption data corresponded to the pseudo-second-order kinetic model and Freundlich and Temkin isotherms models rather than the Langmuir model. The optimum adsorption capacity was 508.4 mg/g for  $\text{Pb(II)}$ , 268.4 mg/g for  $\text{Hg(II)}$ , and 301.2 mg/g for  $\text{Cu(II)}$ . Thermodynamic studies indicate that the adsorption process was endothermic and spontaneous in nature.

Additional recently developed GO-based metal oxide nanomaterials used to remove inorganic pollutants are listed in Table 12.2.

### 12.3.3 Adsorption isotherms, kinetics, and thermodynamics

We will describe the adsorption process using the two most frequently used isotherm models, Langmuir and Freundlich. The Langmuir has monolayer adsorption at homogenous surface and the Freundlich has heterogeneous adsorption due to the diversity of the adsorption sites or the diverse nature of the ions adsorbed [43]. From the reported experimental data [30,44,45,51,61,77], almost all of the adsorption isotherms for GO-based metal oxide nanocomposites follow the Langmuir model rather than the Freundlich. This confirms that a monolayer adsorption occurs in homogenous adsorption sites on GO-based metal oxide nanocomposites.

The kinetics of the adsorption process describes changing the contact time of the adsorption experiments and determining how these changes affect adsorption. The adsorption-kinetic data are typically examined in terms of pseudo-first-order, pseudo-second-order kinetic models. Almost all the adsorption kinetics for GO-based metal oxide nanocomposites followed the pseudo-second-order kinetics [44,45,59,78,79]. This is based on the assumption that the rate-limiting step might be chemical adsorption and the adsorption behavior might involve valence forces through sharing or exchange of electrons between adsorbent and adsorbate [58].

Thermodynamic studies are carried out in order to evaluate the feasibility of the adsorption process. It has been shown that the adsorption process for GO-based metal oxide nanocomposites was spontaneous and endothermic in

nature [42,43,45]. For all GO-based composites, it was found that the change in Gibbs energy ( $\Delta G$ ) value was negative and that both enthalpy ( $\Delta H$ ) and entropy ( $\Delta S$ ) were positive. The negative value of  $\Delta G$  showed the adsorption process was spontaneous. The positive value of  $\Delta H$  showed the adsorption process was endothermic in nature and adsorption capacity increased with increase in temperature. A positive value of  $\Delta H$  also indicated that metal ions dissolved well in water and the hydration cover of metal ion had to be destroyed before its adsorption on the adsorbent. Because this process requires more energy, high temperature is helpful for high adsorption. The positive value of  $\Delta S$  revealed increasing randomness at the solid-liquid interface during the adsorption process.

### 12.3.4 Regeneration of adsorbents

Regeneration (reusability) and desorption studies of adsorbents are important for developing an advanced and cost-effective adsorption process [43]. The graphene-based adsorbent can be defined as an advanced adsorbent. The desorption agents used to regenerate the adsorbent are generally HCl, NaOH, EDTA, and thiourea–HCl solution [51,59,65]. For inorganic catatonic pollutants such as Pb(II), Cd(II), and Hg(II), HCl was used as a desorption agent because the adsorbent surface was completely covered with  $H^+$  ions. After addition of HCl, metal ions could not compete with  $H^+$  for ion-exchange sites and moved away from the solid surface into the solution. This has also occurred with the use of NaOH solution for the desorption of anionic-inorganic pollutants including  $F^-$ , As(V), As(III), and Cr(VI). Fluoride-adsorbed MgO–MgFe<sub>2</sub>O<sub>4</sub>/GO nanoadsorbent was used for the desorption study [43]. The fluoride-adsorbed MgO–MgFe<sub>2</sub>O<sub>4</sub>/GO is produced by adsorbing 10 mg/L fluoride solution on 0.05 g MgO–MgFe<sub>2</sub>O<sub>4</sub>/GO per 100 mL at pH 6. After adsorption, the adsorbents were removed by centrifugation and repeated washing. The adsorbent was then reduced after performing desorption studies at different pH values (8–12) by addition of 0.1 M NaOH solution. Fig. 12.11A shows that up to pH 8, and no fluoride comes into the solution. The desorption efficiency increases to 97% of fluoride as the pH increases to pH 12. The MgO–MgFe<sub>2</sub>O<sub>4</sub>/GO adsorbent performed well after reuse (Fig. 12.11B) with only a slight decrease in its efficiency. The adsorption percentage of fluoride was found to be 91.0%, 87.0%, 77.0%, 67.0%, and 57.0% for the first, second, third, fourth, and fifth cycles of fluoride operation, respectively.

Most of the Pb(II) and Hg(II) adsorbed on EDTA–Fe<sub>3</sub>O<sub>4</sub>–GO surface was easily removed by HCl [59]. After five recycles, EDTA–Fe<sub>3</sub>O<sub>4</sub>–GO still showed good adsorption efficiency (86.4% of Pb(II) and 85.9% of Hg(II)). This suggests that with these metals the nanoadsorbents can show good adsorption capacities after up to five successive cycles.

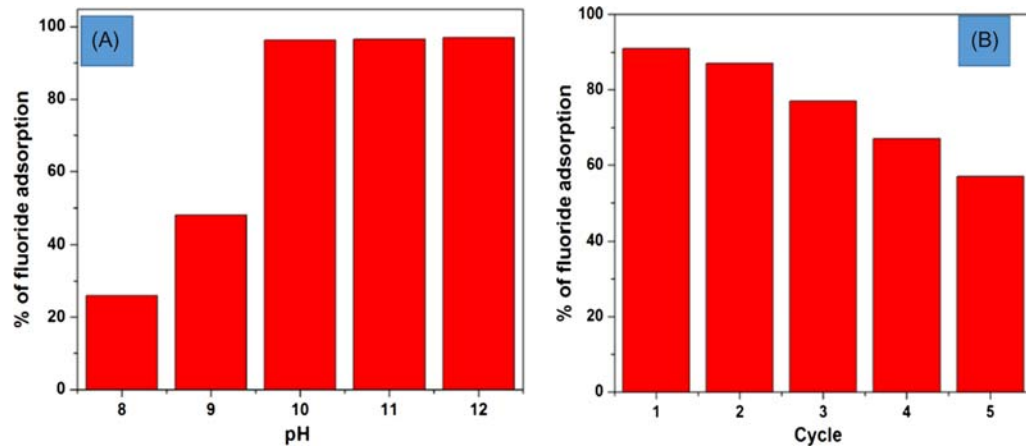


**FIGURE 12.11** (A) Desorption of fluoride from loaded MgO–MgFe<sub>2</sub>O<sub>4</sub>/GO at various pH values; (B) regeneration results for MgO–MgFe<sub>2</sub>O<sub>4</sub>/GO over five cycles [43].

## 12.4 Conclusions

This chapter focused on the adsorption applications of metal oxide nanomaterials and functionalized GO nanoadsorbents for the removal of inorganic pollutants (As, Cd, Hg, Cr, Pb, and F) from water. Due to specific layered-functionality structure, a large number of adsorption-active sites such as carboxyl, hydroxyl, and epoxy functional groups, pi electrons, and the outer surface of the decorated nanoparticles improve adsorption efficiency. The electrostatic interaction and low pH value enable the adsorption of anionic pollutants such as As, Cr, and F. A high pH value favors the adsorption of cationic pollutants such as Cd, Pb, and Hg. Anions have adsorbed on adsorbent surface through specific and/or nonspecific adsorption. Cations are based on the electrostatic interaction, ion exchange, and complex formation. The adsorption kinetics and isotherms can be described by Langmuir and pseudo-second-order model. The adsorption process for GO-based metal oxide nanocomposites is spontaneous and endothermic in nature. The regeneration of adsorbents can be achieved with desorption agents such as HCl or NaOH solution. The adsorption efficiency is found to be decreased by increasing the number of regenerated cycles.

## References

- [1] Hussain CM. *Handbook of nanomaterials for industrial application*. Elsevier; 2018.
- [2] Chowdhury SR, Yanful EK. Arsenic and chromium removal by mixed magnetite e maghemite nanoparticles and the effect of phosphate on removal. *J Environ Manage* 2010;91:2238–47. Available from: <https://doi.org/10.1016/j.jenvman.2010.06.003>.
- [3] Bhaumik M, Maity A, Srinivasu VV, Onyango MS. Enhanced removal of Cr (VI) from aqueous solution using polypyrrole/Fe<sub>3</sub>O<sub>4</sub> magnetic nanocomposite. *J Hazard Mater* 2011;190:381–90. Available from: <https://doi.org/10.1016/j.jhazmat.2011.03.062>.
- [4] Ajmal A, Majeed I, Malik N. Principles and mechanisms of photocatalytic dye degradation on TiO<sub>2</sub> based photocatalysts. *RSC Adv* 2014;37003–26. Available from: <https://doi.org/10.1039/c4ra06658h>.
- [5] Alqadami AA, Naushad M, Abdalla MA, Ahamad T, Alothman ZA, Alsehri SM, et al. Efficient removal of toxic metal ions from wastewater using a recyclable nanocomposite: a study of adsorption parameters and interaction mechanism. Elsevier Ltd.; 2017. Available from: <https://doi.org/10.1016/j.jclepro.2017.04.085>.
- [6] Xu J, Cao Z, Zhang Y, Yuan Z, Lou Z, Xu X, et al. A review of functionalized carbon nanotubes and graphene for heavy metal adsorption from water: preparation, application, and mechanism. *Chemosphere*. 2018;195:351–64. Available from: <https://doi.org/10.1016/j.chemosphere.2017.12.061>.
- [7] Peng W, Li H, Liu Y, Song S. A review on heavy metal ions adsorption from water by graphene oxide and its composites. *J Mol Liq* 2017;230:496–504. Available from: <https://doi.org/10.1016/j.molliq.2017.01.064>.
- [8] Mejias IE, Mangadla JD, Nguyen HN, Advincula RC, Rodrigues DF. Graphene oxide functionalized with ethylenediamine triacetic acid for heavy metal adsorption and antimicrobial applications. *Carbon N Y* 2014;77:289–301. Available from: <https://doi.org/10.1016/j.carbon.2014.05.032>.



- [9] Chem JM, Fan L, Luo C, Sun M, Qiu H. Synthesis of graphene oxide decorated with magnetic cyclodextrin for fast chromium removal. *J Mater Chem* 2012;22:24577–83. Available from: <https://doi.org/10.1039/c2jm35378d>.
- [10] Corte D, Toro-labbe A. Improving As (III) adsorption on graphene based surfaces: impact of chemical doping. *Phys Chem Chem Phys* 2015;17:12056–64. Available from: <https://doi.org/10.1039/C5CP01313E>.
- [11] Duman O, Tunc S, Polat TG, Bozo BK. Synthesis of magnetic oxidized multiwalled carbon application in cationic Methylene Blue dye adsorption. *Carbohydr Polym* 2016;147:79–88. Available from: <https://doi.org/10.1016/j.carbpol.2016.03.099>.
- [12] Online VA, Zhang J, Shi C, Huang J, Yan B, Liu Q, et al. Poly(acrylic acid) functionalized magnetic graphene oxide nanocomposite for removal of methylene blue. *RSC Adv* 2015;5:32272–82. Available from: <https://doi.org/10.1039/c5ra01815c>.
- [13] Hussain CM, Kharisov B. *Advanced environmental analysis-application of nanomaterials*. The Royal Society of Chemistry; 2017.
- [14] Nanoparticles types, classification, characterization, fabrication methods, n.d. Available from: <https://doi.org/10.1007/978-3-319-41129-3>.
- [15] Barreto JA, Malley WO, Kubeil M, Graham B, Stephan H, Spiccia L. Nanomaterials: applications in cancer imaging and therapy. *Adv Healthc Mater* 2011;23:18–40. Available from: <https://doi.org/10.1002/adma.201100140>.
- [16] Lu X, Wang C, Wei Y. One-dimensional composite nanomaterials: synthesis by electrospinning and their applications. *Small*. 2009;5:2349–70. Available from: <https://doi.org/10.1002/smll.200900445>.
- [17] Mauter MS, Elimelech M. Environmental applications of carbon-based nanomaterials. *Environ Sci Technol* 2008;42:5843–59.
- [18] Khot LR, Sankaran S, Mari J, Ehsani R, Schuster EW. Applications of nanomaterials in agricultural production and crop protection: a review. *Crop Prot* 2012;35:64–70. Available from: <https://doi.org/10.1016/j.cropro.2012.01.007>.
- [19] Callister WD, J. Wiley, Materials science, n.d.
- [20] Henrique P, Camargo C, Satyanarayana KG, Wypych F. Nanocomposites: synthesis, structure, properties and new application opportunities. *Mater Res* 2009;12:1–39.
- [21] Kim E, Lee C, Chang Y, Chang Y. Hierarchically structured manganese oxide-coated magnetic nanocomposites for the efficient removal of heavy metal ions from aqueous systems. *ACS Appl Mater Interfaces* 2013;5:9628–34. Available from: <https://doi.org/10.1021/am402615m>.
- [22] Hu BJ, Zhong L, Song W, Wan L. Synthesis of hierarchically structured metal oxides and their application in heavy metal ion removal. *Adv Mater* 2008;20:2977–82. Available from: <https://doi.org/10.1002/adma.200800623>.
- [23] Hua M, Zhang S, Pan B, Zhang W, Lv L, Zhang Q. Heavy metal removal from water/wastewater by nanosized metal oxides: a review. *J Hazard Mater* 2012;211–212:317–31. Available from: <https://doi.org/10.1016/j.jhazmat.2011.10.016>.
- [24] Li Z, Lin Z. Noble metal–metal oxide nanohybrids with tailored nanostructures for efficient solar energy conversion, photocatalysis and environmental remediation. *Energy Environ Sci* 2017;10:402–34. Available from: <https://doi.org/10.1039/c6ee02265k>.
- [25] Ray C, Pal T. Recent advances of metal – metal oxide nanocomposites and their tailored nanostructures. *J Mater Chem A* 2017;5:9465–87. Available from: <https://doi.org/10.1039/c7ta02116j>.

- [26] Korotcenkov G, Cho BK. Metal oxide composites in conductometric gas sensors: achievements and challenges. *Sens Actuators B Chem* 2017;244:182–210. Available from: <https://doi.org/10.1016/j.snb.2016.12.117>.
- [27] Zhong BL, Hu J, Liang H, Cao A, Song W, Wan L. Self-assembled 3D flowerlike iron oxide nanostructures and their application in water treatment. *Adv Mater* 2006;18:2426–31. Available from: <https://doi.org/10.1002/adma.200600504>.
- [28] Song H, Zhang L, He C, Qu Y, Tian Y, Lv Y. Graphene sheets decorated with SnO<sub>2</sub> nanoparticles: in situ synthesis and highly efficient materials for cataluminescence gas sensors. *J Mater Chem* 2011;21:5972–7. Available from: <https://doi.org/10.1039/c0jm04331a>.
- [29] Liu M, Wen T, Wu X, Chen C, Hu J, Li J, et al. Synthesis of porous Fe<sub>3</sub>O<sub>4</sub> hollow microspheres/graphene oxide composite for Cr(vi) removal. *Dalt Trans* 2013;42:14710–17. Available from: <https://doi.org/10.1039/c3dt50955a>.
- [30] Yoon Y, Park WK, Hwang TM, Yoon DH, Yang WS, Kang JW. Comparative evaluation of magnetite-graphene oxide and magnetite-reduced graphene oxide composite for As(III) and As(V) removal. *J Hazard Mater* 2016;304:196–204. Available from: <https://doi.org/10.1016/j.jhazmat.2015.10.053>.
- [31] Wang J, Tsuzuki T, Tang B, Hou X, Sun L, Wang X. Reduced graphene oxide/ZnO composite: reusable adsorbent for pollutant management. *ACS Appl Mater Interfaces* 2012;4:3084–90. Available from: <https://doi.org/10.1021/am300445f>.
- [32] Mandal P, Chattopadhyay AP. Excellent catalytic activity of magnetically recoverable Fe<sub>3</sub>O<sub>4</sub>–graphene oxide nanocomposites prepared by a simple method. *Dalt Trans* 2015;44:11444–56. Available from: <https://doi.org/10.1039/C5DT01260K>.
- [33] Yu S, Wang X, Tan X, Wang X. Sorption of radionuclides from aqueous systems onto graphene oxide-based materials: a review. *Inorg Chem Front* 2015;2:593–612. Available from: <https://doi.org/10.1039/c4qi00221k>.
- [34] Zhu BY, Murali S, Cai W, Li X, Suk JW, Potts JR, et al. Graphene and graphene oxide: synthesis, properties, and applications. *Adv Mater* 2010;22:3906–24. Available from: <https://doi.org/10.1002/adma.201001068>.
- [35] Al-Warthan AA, Tremel W, Khan M, Tahir MN, Adil SF, Khan HU, et al. Graphene based metal and metal oxide nanocomposites: synthesis, properties and their applications. *J Mater Chem A* 2015;3:18753–808. Available from: <https://doi.org/10.1039/c5ta02240a>.
- [36] Boruah PK, Borah DJ, Handique J, Sharma P, Sengupta P, Das MR. Facile synthesis and characterization of Fe<sub>3</sub>O<sub>4</sub> nanopowder and Fe<sub>3</sub>O<sub>4</sub>/reduced graphene oxide nanocomposite for methyl blue adsorption: a comparative study. *J Environ Chem Eng* 2015;. Available from: <https://doi.org/10.1016/j.jece.2015.06.030>.
- [37] Upadhyay RK, Sinha S. Role of graphene/metal oxide composites as photocatalysts, adsorbents and disinfectants in water treatment: a review. *RSC Adv* 2014;4:3823–51. Available from: <https://doi.org/10.1039/c3ra45013a>.
- [38] Wu Y, Luo H, Wang H, Wang C, Zhang J, Zhang Z. Adsorption of hexavalent chromium from aqueous solutions by graphene modified with cetyltrimethylammonium bromide. *J Colloid Interface Sci* 2013;394:183–91. Available from: <https://doi.org/10.1016/j.jcis.2012.11.049>.
- [39] Fang W, Jiang X, Luo H, Geng J. Synthesis of graphene/SiO<sub>2</sub>@polypyrrole nanocomposites and their application for Cr(VI) removal in aqueous solution. *Chemosphere*. 2018;197:594–602. Available from: <https://doi.org/10.1016/j.chemosphere.2017.12.163>.
- [40] Etemadi M, Samadi S, Yazd SS, Jafari P, Yousefi N, Aliabadi M. Selective adsorption of Cr(VI) ions from aqueous solutions using Cr<sup>6+</sup>-imprinted Pebax/chitosan/GO/APTES nanofibrous adsorbent. *Int J Biol Macromol* 2017;95:725–33. Available from: <https://doi.org/10.1016/j.jbiomac.2016.11.117>.

- [41] He C, Yang Z, Ding J, Chen Y, Tong X, Li Y. Effective removal of Cr(VI) from aqueous solution by 3-aminopropyltriethoxysilane-functionalized graphene oxide. *Colloids Surf A Physicochem Eng Asp* 2017;520:448–58. Available from: <https://doi.org/10.1016/j.colsurfa.2017.01.086>.
- [42] Jana M, Saha S, Khanra P, Samanta P, Koo H, Murmu NC, et al. Non-covalent functionalization of reduced graphene oxide using sulfanilic acid azocromotrop and its application as a supercapacitor electrode material. *J Mater Chem A* 2015;3:7323–31. Available from: <https://doi.org/10.1039/c4ta07009g>.
- [43] Sahoo SK, Hota G. Surface functionalization of GO with MgO/MgFe<sub>2</sub>O<sub>4</sub> binary oxides: a novel magnetic nanoadsorbent for removal of fluoride ions. *J Environ Chem Eng* 2018;6:2918–31. Available from: <https://doi.org/10.1016/j.jece.2018.04.054>.
- [44] Chandra V, Park J, Chun Y, Lee JW, Hwang IC, Kim KS. Water-dispersible magnetite-reduced graphene oxide composites for arsenic removal. *ACS Nano* 2010;4:3979–86. Available from: <https://doi.org/10.1021/nn1008897>.
- [45] Fan L, Luo C, Sun M, Li X, Qiu H. Highly selective adsorption of lead ions by water-dispersible magnetic chitosan / graphene oxide composites. *Colloids Surf B Biointerfaces* 2013;103:523–9. Available from: <https://doi.org/10.1016/j.colsurfb.2012.11.006>.
- [46] Online VA, Liu J, Ge X, Ye X, Wang G, Zhang H, et al. 3D graphene/d-MnO<sub>2</sub> aerogels for highly efficient and reversible removal of heavy metal ions. *J Mater Chem A* 2016;4:1970–9. Available from: <https://doi.org/10.1039/c5ta08106h>.
- [47] Santhosh C, Daneshvar E, Kollu P, Peräniemi S, Nirmala A, Bhatnagar A. Magnetic SiO<sub>2</sub>@CoFe<sub>2</sub>O<sub>4</sub> nanoparticles decorated on graphene oxide as efficient adsorbents for the removal of anionic pollutants from water. *Chem Eng J* 2017;322:472–87. Available from: <https://doi.org/10.1016/j.cej.2017.03.144>.
- [48] Babu CM, Vinodh R, Sundaravel B, Abidov A, Peng MM, Cha WS, et al. Characterization of reduced graphene oxide supported mesoporous Fe<sub>2</sub>O<sub>3</sub>/TiO<sub>2</sub> nanoparticles and adsorption of As(III) and As(V) from potable water. *J Taiwan Inst Chem Eng* 2016;62:199–208. Available from: <https://doi.org/10.1016/j.jtice.2016.02.005>.
- [49] Lee Y-C, Yang J-W. Self-assembled flower-like TiO<sub>2</sub> on exfoliated graphite oxide for heavy metal removal. *J Ind Eng Chem* 2012;18:1178–85. Available from: <https://doi.org/10.1016/j.jiec.2012.01.005>.
- [50] Mohan S, Kumar V, Singh DK, Hasan SH. Synthesis and characterization of rGO/ZrO<sub>2</sub> nanocomposite for enhanced removal of fluoride from water: kinetics, isotherm, and thermodynamic modeling and its adsorption mechanism. *RSC Adv* 2016;6:87523–38. Available from: <https://doi.org/10.1039/C6RA15460C>.
- [51] Deng J, Zhang X, Zeng G, Gong J, Niu Q, Liang J. Simultaneous removal of Cd (II) and ionic dyes from aqueous solution using magnetic graphene oxide nanocomposite as an adsorbent. *Chem Eng J* 2013;226:189–200. Available from: <https://doi.org/10.1016/j.cej.2013.04.045>.
- [52] Su H, Ye Z, Hmidi N. High-performance iron oxide – graphene oxide nanocomposite adsorbents for arsenic removal. *Colloids Surf A Physicochem Eng Asp* 2017;522:161–72. Available from: <https://doi.org/10.1016/j.colsurfa.2017.02.065>.
- [53] Kuang L, Liu Y, Fu D, Zhao Y. FeOOH-graphene oxide nanocomposites for fluoride removal from water: acetate mediated nano FeOOH growth and adsorption mechanism. *J Colloid Interface Sci* 2017;490:259–69. Available from: <https://doi.org/10.1016/j.jcis.2016.11.071>.
- [54] Liu Y, Luo C, Yan S. Synthesis of manganese dioxide / iron oxide / graphene oxide magnetic nanocomposites for hexavalent chromium removal. *RSC Adv* 2015;5:54156–64. Available from: <https://doi.org/10.1039/c5ra06455d>.

- [55] Bhunia P, Kim G, Baik C, Lee H. A strategically designed porous iron – iron oxide matrix on graphene for heavy metal adsorption. *Chem Commun* 2012;48:9888–90. Available from: <https://doi.org/10.1039/c2cc35120j>.
- [56] Ma S, Zhan S, Jia Y, Zhou Q. Highly efficient antibacterial and Pb(II) removal effects of Ag-CoFe<sub>2</sub>O<sub>4</sub>-GO nanocomposite. *ACS Appl Mater Interfaces* 2015;7:10576–86. Available from: <https://doi.org/10.1021/acsami.5b02209>.
- [57] Prasanna L, Reddy J, Choi Y. Studies on removal of Pb (II) and Cr (III) using graphene oxide based inverse spinel nickel ferrite nano-composite as sorbent. *Hydrometallurgy*. 2016;165:64–72. Available from: <https://doi.org/10.1016/j.hydromet.2015.11.005>.
- [58] Wang L, Hu D, Kong X, Liu J, Li X, Zhou K, et al. Anionic polypeptide poly ( $\gamma$ -glutamic acid)-functionalized magnetic Fe<sub>3</sub>O<sub>4</sub>-GO-(o-MWCNTs) hybrid nanocomposite for high-efficiency removal of Cd (II), Cu (II) and Ni (II) heavy metal ions. *Chem Eng J* 2018;346:38–49. Available from: <https://doi.org/10.1016/j.cej.2018.03.084>.
- [59] Cui L, Wang Y, Gao L, Hu L, Yan L, Wei Q, et al. EDTA functionalized magnetic graphene oxide for removal of Pb (II), Hg (II) and Cu (II) in water treatment: adsorption mechanism and separation property. *Chem Eng J* 2015;281:1–10. Available from: <https://doi.org/10.1016/j.cej.2015.06.043>.
- [60] Narjes B. Green removal of toxic Pb (II) from water by a novel and recyclable Ag/ $\gamma$ -Fe<sub>2</sub>O<sub>3</sub>@r-GO nanocomposite. *Iran J Chem Chem* 2018;37:29–37.
- [61] Wang H, Yuan X, Wu Y, Chen X, Leng L, Wang H, et al. Facile synthesis of polypyrrole decorated reduced graphene oxide-Fe<sub>3</sub>O<sub>4</sub> magnetic composites and its application for the Cr(VI) removal. *Chem Eng J* 2015;262:597–606. Available from: <https://doi.org/10.1016/j.cej.2014.10.020>.
- [62] Gollavelli G, Chang C, Ling Y. Facile synthesis of smart magnetic graphene for safe drinking water: heavy metal removal and disinfection control. *ACS Sustain Chem Eng* 2013;1:462–72. Available from: <https://doi.org/10.1021/sc300112z>.
- [63] Kanrar S, Debnath S, De P, Parashar K, Pillay K, Sasikumar P, et al. Preparation, characterization and evaluation of fluoride adsorption efficiency from water of iron-aluminium oxide-graphene oxide composite material. *Chem Eng J* 2016;306:269–79. Available from: <https://doi.org/10.1016/j.cej.2016.07.037>.
- [64] Sun R, Zhang H, Qu J, Yao H, Yao J, Yu Z. Supercritical carbon dioxide fluid assisted synthesis of hierarchical AlOOH @ reduced graphene oxide hybrids for efficient removal of fluoride ions. *Chem Eng J* 2016;292:174–82. Available from: <https://doi.org/10.1016/j.cej.2016.02.008>.
- [65] Mohan S, Singh DK, Kumar V, Hasan SH. Modelling of fixed bed column containing graphene oxide decorated by MgO nanocubes as adsorbent for Lead (II) removal from water. *J Water Process Eng* 2017;17:216–28. Available from: <https://doi.org/10.1016/j.jwpe.2017.03.009>.
- [66] Wen T, Wu X, Tan X, Wang X, Xu A. One-pot synthesis of water-swellaable Mg – Al layered double hydroxides and graphene oxide nanocomposites for efficient removal of As (V) from aqueous solutions. *ACS Appl Mater Interfaces* 2013;5:3304–11. Available from: <https://doi.org/10.1021/am4003556>.
- [67] Wan S, He F, Wu J, Wan W, Gu Y, Gao B. Rapid and highly selective removal of lead from water using graphene oxide-hydrated manganese oxide nanocomposites. *J Hazard Mater* 2016;314:32–40. Available from: <https://doi.org/10.1016/j.jhazmat.2016.04.014>.
- [68] Mohan S, Kumar V, Singh DK, Hasan SH. Effective removal of lead ions using graphene oxide-MgO nanohybrid from aqueous solution: isotherm, kinetic and thermodynamic modeling of adsorption. *J Environ Chem Eng* 2017;5:2259–73. Available from: <https://doi.org/10.1016/j.jece.2017.03.031>.

- [69] Tang J, Huang Y, Gong Y, Lyu H, Wang Q, Ma J. Preparation of a novel graphene oxide/Fe-Mn composite and its application for aqueous Hg (II) removal. *J Hazard Mater* 2016;316:151–8. Available from: <https://doi.org/10.1016/j.jhazmat.2016.05.028>.
- [70] Chella S, Kollu P, Komarala EVPR, Doshi S, Saranya M, Felix S, et al. Solvothermal synthesis of MnFe<sub>2</sub>O<sub>4</sub>-graphene composite-investigation of its adsorption and antimicrobial properties. *Appl Surf Sci* 2015;327:27–36. Available from: <https://doi.org/10.1016/j.apsusc.2014.11.096>.
- [71] Hao L, Song H, Zhang L, Wan X, Tang Y, Lv Y. SiO<sub>2</sub>/graphene composite for highly selective adsorption of Pb(II) ion. *J Colloid Interface Sci* 2012;369:381–7. Available from: <https://doi.org/10.1016/j.jcis.2011.12.023>.
- [72] Jin H, Ji Z, Yuan J, Li J, Liu M, Xu C, et al. Research on removal of fluoride in aqueous solution by alumina-modified expanded graphite composite. *J Alloy Compd* 2015;620:361–7. Available from: <https://doi.org/10.1016/j.jallcom.2014.09.143>.
- [73] Gao C, Yu X, Xu R, Liu J, Huang X. AlOOH-reduced graphene oxide nanocomposites: one-pot hydrothermal synthesis and their enhanced electrochemical activity for heavy metal ions. *ACS Appl Mater Interfaces* 2012;4:4672–82. Available from: <https://doi.org/10.1021/am3010434>.
- [74] Varadwaj GBB, Oyeta OA, Rana S, Martincigh BS, Jonnalagadda SB, Nyamori VO. Facile synthesis of three-dimensional Mg–Al layered double hydroxide/partially reduced graphene oxide nanocomposites for the effective removal of Pb<sup>2+</sup> from aqueous solution. *ACS Appl Mater Interfaces* 2017;9:17290–305. Available from: <https://doi.org/10.1021/acsami.6b16528>.
- [75] Heidarizad M, Şengör SS. Synthesis of graphene oxide/magnesium oxide nanocomposites with high-rate adsorption of methylene blue. *J Mol Liq* 2016;224:607–17. Available from: <https://doi.org/10.1016/j.molliq.2016.09.049>.
- [76] Pan N, Li L, Ding J, Li S, Wang R, Jin Y, et al. Preparation of graphene oxide-manganese dioxide for highly efficient adsorption and separation of Th (IV)/ U (VI). *J Hazard Mater* 2016;309:107–15. Available from: <https://doi.org/10.1016/j.jhazmat.2016.02.012>.
- [77] Li L, Fan L, Sun M, Qiu H, Li X, Duan H, et al. Adsorbent for chromium removal based on graphene oxide functionalized with magnetic cyclodextrin-chitosan. *Colloids Surf B Biointerfaces* 2013;107:76–83. Available from: <https://doi.org/10.1016/j.colsurfb.2013.01.074>.
- [78] Zhao D, Gao X, Wu C, Xie R, Feng S, Chen C. Facile preparation of amino functionalized graphene oxide decorated with Fe<sub>3</sub>O<sub>4</sub> nanoparticles for the adsorption of Cr(VI). *Appl Surf Sci* 2016;384:1–9. Available from: <https://doi.org/10.1016/j.apsusc.2016.05.022>.
- [79] Barathi M, Krishna Kumar AS, Kumar CU, Rajesh N. Graphene oxide–aluminium oxyhydroxide interaction and its application for the effective adsorption of fluoride. *RSC Adv* 2014;4:53711–21. Available from: <https://doi.org/10.1039/C4RA10006A>.
- [80] Chen M, Sun Y, Huo C, Liu C, Wang J. Akaganeite decorated graphene oxide composite for arsenic adsorption / removal and its preconcentration at ultra-trace level. *Chemosphere*. 2015;130:52–8. Available from: <https://doi.org/10.1016/j.chemosphere.2015.02.046>.

## Chapter 13

# Remediation of organic pollutants by potential functionalized nanomaterials

Manviri Rani<sup>1</sup> and Uma Shanker<sup>2</sup>

<sup>1</sup>*Department of Chemistry, Malaviya National Institute of Technology, Jaipur, India*

<sup>2</sup>*Department of Chemistry, Dr B R Ambedkar National Institute of Technology, Jalandhar, India*

### 13.1 Introduction

During the last few decades, pollution by organic substances has become a global threat and its level is continuously increasing due to urbanization, rapid development, and lifestyles [1]. The high stability toward heat, light, and oxidizing agents led to the persistence of pollution by organic substances and accumulation in the environment [2]. Accidents related to these pollutants have caused severe damage to the environment (Table 13.1).

Various industries such as the textile, cosmetics, pulp and paper, food processing, pharmaceutical, and pesticide industries discharge untreated effluents to water bodies [4] and exert an enormous hazard to the hydrosphere and living organisms [5–7]. Among the constituents of wastewater (Table 13.2), synthetic dyes, pesticides, amine, phenol and substituted phenols, and polycyclic aromatic hydrocarbons (PAHs) are abundantly present [8]. Like other POPs, they may also be transformed into more toxic byproducts [8–16].

Such pollutants are introduced to humans via contact with air, food, water, soil, and dust (Fig. 13.1). Dyes change the quality of water by just a small concentration (~1 ppm) [17–21]. Azo dyes are used [22] frequently, as are benzidine, and both are carcinogenic. Pesticides released from various industries, anthropogenic activities, and surface excess from agricultural areas are the most abundant pollutants in the wastewaters of growing nations [23–25]. Most of the pollutants are toxic and are allegedly cancer-causing with endocrine disruptor potential [26–29]. Aromatic amines such as benzidine, toluidine, chloroanilines, and many more have been seen in the

**TABLE 13.1** Some important organic pollutants related accidents worldwide (Rani 2012) [3].

Pesticide	Place	Year	Causes	References
Parathion	India	1958	Contaminated food due to leakage	Rani (2012) [3]
	India	1962	Inhalation in manufacturing plant	
HCH	India	1963	Contaminated rice	
Endrin	India	1964	Contaminated food	
HCH	India	1963	Contaminated rice	
Endrin	India	1964	Contaminated food	
DDT	India	1965	Contaminated chutney	
Diazinon	India	1968	Contaminated food	
HCH	India	1976	Mixed with wheat	
Endrin	India	1977	Contaminated crabs in rice field	
Aluminum phosphide	India	1983	Contaminated food grain	
Methyl isocyanate	India	1984	Storage tank leakage	
Cartap hydrochloride	India	1988	Factory workers	
Endosulfan	India	1997	Contamination due to aerial spray	
Phorate	India	2001	Spray drift from banana field	
Endosulfan	India	2002	Contaminated wheat flour	
2,3,7,8-tetrachlorobenzo-10-dioxin (TCDD)	Italy	1976	Air pollution due to poisonous gas	De (2010) [304]
Sarin	Japan	1985–95	Mass poisoning	Nagami (2010) [305]
Pesticides	USA	1968–78	Contaminated food	Laseter (1978)
Phenol	USA	1974	Accidental spillage	Baker et al. (1978) [306]

(Continued)

TABLE 13.1 (Continued)

Pesticide	Place	Year	Causes	References
Phenol	India	1999	Accidental overdose of phenol	Gupta et al. (2008) [307]
Phenol	New Zealand	1980	Absorption of phenol through skin	Lewin and Cleary (1982) [308]
2,4-dinitrophenol	China	2009	Nonoral exposure to workers in a chemical factory	Lu et al. (2011) [309]
2,4-dinitrophenol	USA	1933–38	Poisoning due to weight loss pill	Bartlett et al. (2010) [310]
Phenol	USA	1974	Accidental spillage of 37,900	Baker et al. (1978) [305]
PAHs (Lakeview Gusher)	USA	1910	1200 tons of crude oil released	Rani and Shanker (2018) [102]
PAHs (Kuwaiti oil lakes)	Kuwait	1991	Kuwaiti oil lakes accidental spillage	
PAHs (Kuwaiti oil fires)	Kuwait	1991	136,000 tons of crude oil released	
PAHs	S. Korea	2007	MT <i>Hebei Spirit</i> oil spill	
PAHs	USA	2010	<i>Deep Water Horizon</i> oil spill	
PAHs (Sundarbans oil spill)	Bangladesh	2014	Accidental spillage	
PAHs (Ennore oil spill)	Chennai	2017	Accidental spillage	
PAHs (Lakeview Gusher)	USA	1910	1200 tons of crude oil released	

environment, as degeneration or degradation intermediates of those recalcitrant compounds are extremely noxious [30,31]. Phenol and its derivatives have been designated as priority pollutants with protein-degenerating effects, and they are difficult to degrade in conventional wastewater treatments. Another emerging problem is PAHs released into the atmosphere due to volcanic eruptions, accidental oil spills, inadequate burning of fuel, coal, etc.) [32,33].

During the last few decades, the concentration of PAHs has increased tremendously and can be found everywhere in the ecosystem—air, soil, sediment, water,



**TABLE 13.2** Constituents of wastewater (Henze, 1992).

Type	Components	Effects
Microorganisms	Pathogenic bacteria, virus, etc.	Risk while bathing and eating fish
Organic materials	Oxygen depletion in rivers, lakes, and fjords	Eutrophication, aquatic death, may contain disease-causing microorganisms
Synthetic organic materials	Pesticides, fat, oil and grease, dyes, phenols, amines, PAHs, pharmaceuticals, etc.	Toxic effect, aesthetic inconveniences, bioaccumulation
Nutrients	N, P, ammonium, Ca, Na, Mg, K, etc.	Eutrophication, oxygen depletion, toxic effects
Inorganic materials	Acids, bases, heavy metals (Hg, Pb, Cd, Cr, Cu, Ni)	Corrosion, toxic effect, hardness, aquatic death, bioaccumulation
Radioactivity	Various radioactive elements	Toxic effect, accumulation

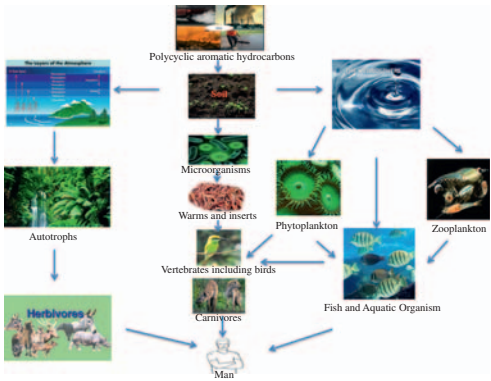


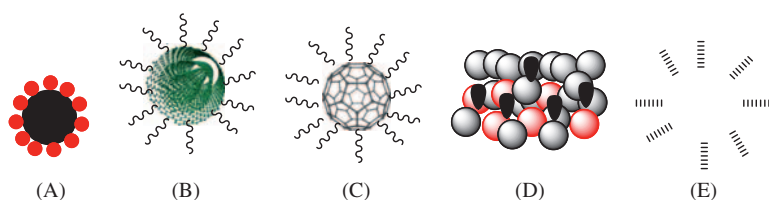
**FIGURE 13.1** Biological transfer of OPs to man via food chain and food web.

oil, tar, and foodstuffs—as well as in the tissues of various aquatic creatures and birds [34–37]. Several researchers have reported that over 80,000 tons of PAHs are being discharged into the bodies of water every year [38,39]. The low water-solubility of PAHs prompted their resistance to degradation, and their toxicity increased with molecular weight [40,41]. Due to extensive contamination, recalcitrant, and potential of persistence (called bioaccumulation), 17 unsubstituted PAHs have been categorized as priority pollutants by the USEPA [42].

Presently, more than 10,000 types of organic dyes, approximately 700,000 tons annually, have been produced as per statistics in the Color Index [43]. China is the world’s largest consumer of organic color pigments, and India

accounts for nearly 10% of the total consumption [44–47]. The largest consumption of pesticides is reported in Europe, and Asia is second. In Asia, China is the leading manufacturer of pesticides, and India stands second with an annual production 100,000 million tons (MT). In fact, India ranks twelfth globally [48]. Out of 415 carcinogenic chemicals, 12% are recognized to be AA [49]. Aniline is listed as a high-priority chemical in the study of wastes from coal-conversion processes [50]. A recent report on aniline estimated that by 2019, the insulation sector will be the largest end user of aniline ( $\sim 46\%$ ), followed by the rubber product sector (11.5%) and consumer transportation sectors (10.3%) worldwide. Due to the sharp increase in automotive and infrastructure industries, aniline consumption was 6.6 MT in the year of 2016 and is expected to reach 8.1 MT in 2019 [51]. Due to their widespread utilization, toxicity, and resistance to degradation, there is a tremendous need right now to develop inexpensive and/or easy-to-handle solutions for the effective removal of such pollutants from the environment [52–54]. NMs are playing a bigger role in the removal of pollutants and remediation of pollutant-affected sites owing to their increased specific surface area, roughness, and enhanced surface properties [55,56]. Investigations on carbonaceous NMs (e.g., fullerenes C60, CNTs, and graphene), metal/moss (e.g., Au, Ag, TiO<sub>2</sub>, ZnO, zero-valent Fe<sup>0</sup>, Ag<sup>0</sup>, and Au<sup>0</sup>), semiconductor quantum dots (QD) (e.g., CdSe, ZnSe, and CdTe), zero-valent metals, and various types of nanocomposites and dendrimers are in progress [55–59]. Additionally, noble metals have shown advanced electrocatalytic or photothermal activities in the near-IR region (1000–2000 nm wavelength), and nanoclusters, nanofibers, nanowires, and nanosheets have also been used [60,61]. ZnO nanostructures have been utilized in the removal of dyes like methylene blue to their photocatalytic efficiency.

Recently, functionalized NMs (Fig. 13.2) have been in demand for diverse high-tech and engineering applications due to the extraordinary transitions in their properties as compared to bare NMs [62,63]. Limitations



Various Functionized Nanomaterials

- (A) Nanomaterials of metal, metal oxides, metal sulfides, etc.
- (B) CNTs based nanomaterials
- (C) Fullerenes based nanomaterials
- (D) Polymer nanocomposites (Metal+Polymers, etc.)
- (E) magnetic core shell based nanomaterials

**FIGURE 13.2** Various functionalized NMs.

(e.g., high aggregation tendency, less surface reactivity, and mobility) of bare NMs can be diminished by surface modification, hybridization of NMs with one or more NM conjugates, and green synthesis [64].

Br-functionalized CNTs were prepared by the vapor-phase bromination method where multiwalled nanotubes (MWNTs) were treated with bromine vapors [65]. Functionalization creates engineered nano-materials with reduced band gap, are environmentally friendly, and have higher stability/reactivity and multifunctionality. Advanced functionalized NMs have been examined for their excellent adsorptive removal ability, chemical reactivity, and antimicrobial activity for water treatment and environmental remediation. The carbonaceous NMs in combination with metal or metallic oxides (e.g., ZnO/graphene/CNTs) showed excellent potential in the removal of recalcitrant from wastewater. The main reason for such high activity was predicted on the basis of alteration in the band gap, grain size, crystal defects, and doping with carbon-based NMs like CNTs, graphene, etc. or the synergistic effect in between CNMs and metal-based NPs. Synthesis of carbonaceous NMs, fullerenes, CNTs, and graphene have been reviewed [66–68]. Fig. 13.3 displaying the extraordinary carbon nanomaterial combinations with other NMs. Recently, nanozerovalent iron (nZVI) and its derivatives have shown excellent removal and degradation capability in in situ nanoremediation of soils, sediment aquifers, and groundwater. Moreover, it was also found that surface modification of nZVI by surfactants, polyelectrolytes, polymers, and macromolecules exhibited higher efficiency and economy.

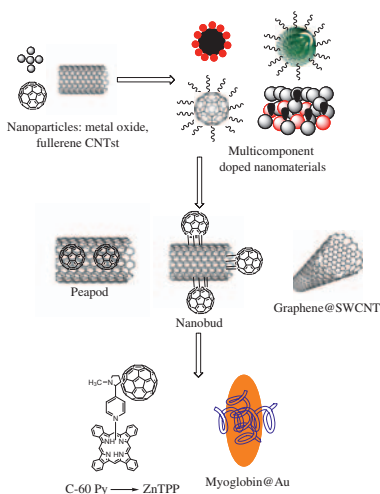


**FIGURE 13.3** Expansion and development of various types NMs conjugations. Inspired from [69] Shanker U, Jassal V, Rani M, Kaith BS. Towards green synthesis of nanoparticles: From bio-assisted sources to benign solvents. A review. *Int J Env Anal Chem* 2016;96:801–835.

## 13.2 Environmental concern of organic pollutants

Growing population, rapid industrialization, modernization of developments, agronomic, and domestic wastes are deteriorating the quality of water and soil around the globe. Synthetic dyes, pesticides, aromatic amines and phenols, and emerging PAHs are entering bodies of water in large quantities. These recalcitrant toxins in the form of secondary waste, persistent and sometimes metabolites [1,3,70,71]. Azo dyes and benzidine are highly carcinogenic, as well as explosive [18]. Their untreated discharge to bodies of water must be prohibited as it might contain carcinogens [20]. The European Commission has disqualified several noxious azo dyes, such as navy blue, used in the leather industry [72]. Presently, China produces 40%–45% of the world's total dye consumption [10]. It has been reported that after processing around 12–20 tons of textiles, 3000 m<sup>3</sup> of water is let out per day [73,74]. Another big problem is the use of pesticides (dispersed off: 85%–90%). It is estimated that pesticide use was  $5.5 \times 10^8$  kg in the United States and  $2.59 \times 10^9$  kg globally in 1995 [9]. Regardless of stern conventions, priority hazardous substances [75] are still found in rivers and seafood indicating their long persistence or current use [76,77]. There have been several cases of pesticide poisoning reported in developing countries like India, and, as a consequence, many lives are lost every year (e.g., between 1997–2002 several farmers died due to endosulfan poisoning) [78].

The 80,000 tons/year of untreated PAHs discharged to the water streams are evolving and, they are documented as ubiquitously present in the environment as carcinogens and mutagens [38,79]. It has been reported that 46%–90% mass of individual PAHs are emitted by motor vehicles in the cities [80,81]. Indoor emission contributions to PAHs include ~16% in United States, 29% in Sweden, and 33% in Poland [82,83]. Individuals expend 80%–93% of their time indoors inhaling PAHs [84]. Oil spills in coastal regions are the main reason PAH pollution has caused loss of various marine lives [85]. A total of 17 unsubstituted PAHs have been identified as priority carcinogens by USEPA [86].

Aromatic phenols and amines are major organic constituents ordinarily found in wastewater (range: 1–100 mg/L) [51,87]. The USEPA has determined that exposure to phenol in drinking water at a concentration of 4 milligrams per liter (mg/L) for up to 10 days is not expected to cause any adverse effects in a child. [88,89]. Phenols are dangerous for the life of aquatic bodies at 9–25 mg/L [90,91]. Consequently, the EPA lists phenols as specific priority pollutants [92,93]. Bisphenol A (BPA) is another common pollutant found in wastewater due to its extensive use and bulk production as a plastic antioxidant. BPA affects marine creatures and distresses physiological functions even at picogram concentrations [94–96]. The annual growth rate of BPA as a pollutant was found to be 4.6% from 2013 to 2019 due to worldwide demand of plastics (e.g., around 6.5 MT) [97].

With these facts in mind, it may be concluded that there has been an increase in concern about the removal of harmful pollutants and toxic metabolites prevalent in the environment. Moreover, these pollutants may also be produced by the degradation of several biocalcitrant substances. A number of reviews have been published on NPs and surface modification and functionalized NMs, including silica-based, carbonaceous, and metal-based, for water treatment and environmental industries application [9,98,99]. It was concluded that functionalization can help to overcome the limitations of bare NPs and provide favorable future prospects for environmental remediation and removal of pollutants like PAHs, dyes, heavy metals, etc., from wastewater. Chemical approaches are better for the NM diversity and ability to outfit them with large number of functionalities [98]. Carbon-based functionalized materials are frequently used as promising adsorbents for treating organic and inorganic wastewater pollutants. Jun et al. [100] reviewed functionalized CNT and graphene for organic pollutant (e.g., organic dye and phenol) removal. Nanoadsorbents-based polymer nanocomposites are more beneficial for environmental sustainability due to their low-energy consumption, large adsorption capacity, ease of operation, high stability, selective sorption, recycling, and biodegradation [101]. Rani et al. [102] discussed the impact of engineered NMs like metal-based nanoparticles (e.g., Ag, Fe, and Zn), MO (TiO<sub>2</sub>, ZnO, and Fe<sub>2</sub>O<sub>3</sub>), CNTs, and nanocomposites for industrial and public health. The present chapter reviews the different synthesis methods for functionalization of various nanoparticles for their application in environmental remediation. The chapter also presents the future challenges, perspectives, and directions in the area of NM functionalization and their utilization.

*Methods of NM Functionalization:* NMs can be mainly functionalized by a direct (co-condensation and in situ) and indirect (grafting) functionalities including organic ligands, inorganic moieties, and surface polymerization. Table 13.3 represents the various methods for the functionalization of NMs.

### 13.2.1 Direct functionalization

Direct functionalization is the modification of NMs by bifunctional ligands containing complex and modifying groups (–COOH, –OH, and –NH<sub>2</sub>) during one-pot synthesis (Fig. 13.4). Homogeneous surfaces, better control over the amount of ligand incorporated in the nanomaterial, and the opportunity of using a wide variety of functional groups are a few advantages of functionalization.

#### 13.2.1.1 Covalent functionalization

Carbon-based NMs and nZVI have been extensively functionalized by covalent mechanisms, including surface oxidation, alkali activation, doping with

**TABLE 13.3** Details of methods for functionalized nanoparticles.

Functionalized NMs	Method of functionalization	Details of method	References
oMWCNTs	Oxidation by sodium hypochlorite	MWCNTs were oxidized by various concentrations of sodium hypochlorite	Yu et al. (2004)
oMWCNTs	Oxidation by 18% H <sub>2</sub> O <sub>2</sub>	MWCNTs (2.0 g) were added to 200 mL solutions of 8 M HNO <sub>3</sub> , 18% H <sub>2</sub> O <sub>2</sub> , and 1 M KMnO <sub>4</sub> (acidified), separately	Salam (2012)
oMWCNTs	Oxidation by concentrated H <sub>2</sub> O <sub>3</sub> : H <sub>2</sub> OSO <sub>4</sub> (1:3,v/v)	50 mg C <sub>60</sub> was dissolved in 50 mL benzene, + of 2 mL of 2 mol/L NaOH, 5 drops of tetra-butyl–ammonium hydroxide (TBAH, 40% in water), and 5 mL 30% H <sub>2</sub> O <sub>2</sub>	Wang et al. (2013) [84]
oMWCNTs	Alkali activated using KOH:CNTs (6:1) + 750°C for 1 h under flowing argon	A mixture of purified CNTs and KOH powder was performed in a stainless steel with weight ratio of KOH to CNTs was 6:1	Ma et al. (2012)
oMWCNTs	Sulfonation by H <sub>2</sub> SO <sub>4</sub> (98%) + MWCNT Covalent functionalization	Sulfonation by H <sub>2</sub> SO <sub>4</sub> (98%) + MWCNT sonication for 30 min, heating to 180°C for 24 h with are flux condensation	Ge et al. (2012)

(Continued)

**TABLE 13.3 (Continued)**

Functionalized NMs	Method of functionalization	Details of method	References
Graphene oxide	Covalent functionalization	Grafting with Diazonium compounds by GO + aryl diazonium salt of sulfanilic acid in an ice bath for 2 h	Zhao et al. (2012)
GO–EDTA	Covalent functionalization	Silylation process; Silylation reaction of N-(trimethoxysilyl propyl) ethylenediamine triacetic acid (EDTA-silane) with GO in ethanol solution	Madadrang et al. (2012)
Carboxylated MWCNTs (C–MWCNTs)	Covalent functionalization	Thiolation; Cysteamine hydrochloride + CMWCNTs in ethanol. Then 1-ethyl (3,3 di-amino-propyl)acetate (EDC) was used for better reaction between C-MWCNTs and cysteamine hydrochloride	Robati et al. (2016)
G–tea polyphenols	Noncovalent functionalization	$\pi$ – $\pi$ stacking between oxidized tea polyphenols and graphene nanosheets	Song et al. (2012)
G–CTAB	Noncovalent	Ionic interactions between the carboxyl group of GO with the ammonium ion of CTAB. CTAB–GO was reduced to form G–CTAB	Wu et al. (2013)

(Continued)

**TABLE 13.3 (Continued)**

Functionalized NMs	Method of functionalization	Details of method	References
GO–poly (amidoamine)	Polymer coated	Grafting-from method Cu <sub>2</sub>	Yuan et al. (2013)
Graphene/ $\delta$ -MnO <sub>2</sub>	Inorganic functionalization	Redox reaction under microwave irradiation	Ren et al. (2011)
MWCNT/Al <sub>2</sub> O <sub>3</sub>	Inorganic functionalization	Pyrolysis of aluminum nitrate on to the surface of oxidized MWCNTs	Gupta et al. (2011) [13]
Au Cu, Ag, Pd S, Sn, Ni, FeC doped with nZVI	Doping	Doping of nZVI was carried out with 1 wt.% Cu, Ag, or Au, freshly made nZVI was introduced to Cu <sub>2</sub> +, Ag +, or Au <sub>3</sub> + solutions separately (the weight ratio of Me/Fe was 1%, Me = Cu <sub>2</sub> +, Ag +, and Au <sub>3</sub> +), and the mixture was ultrasonicated (Crest, USA) for 20 min at 25°C	Su et al. (2014), Devi and Saroha (2015), Jin et al. (2018)
Hollow TiO <sub>2</sub> -doped with Sn and C	Doping	CS (0.4 g) + 20 mL of ethanol and stirred vigorously for 30 min. 5 mL of titanium isopropoxide + 20 mL of ethanol was added drop-by-drop stirred vigorously for 1 h	Ao et al. (2010) [85] Shi et al. (2012) [86]
Fe <sub>3</sub> O <sub>4</sub> @SiO <sub>2</sub> MNPs	Modified by grafting	Fe <sub>3</sub> O <sub>4</sub> @ SiO <sub>2</sub> MNPs were grafted by poly (1vinylimidazole)	Shan et al. (2015)

(Continued)



**TABLE 13.3 (Continued)**

Functionalized NMs	Method of functionalization	Details of method	References
bimetallic oxide NPs	Mixing, covalent bonding	To the one metal salt solution (0.05 M, 100 mL); another metal solution (0.05 M, 100 mL) surfactant ( <i>A. marmelos</i> ) was added dropwise	Rani and Shanker (2018) [10]
Fe <sub>2</sub> O <sub>3</sub> @ZnHCF	Doping, Azarichta indica	Suspension of Fe <sub>2</sub> O <sub>3</sub> was added to Zn(NO <sub>3</sub> ) <sub>2</sub> (0.1 M, 100 mL), K <sub>4</sub> [Fe(CN) <sub>6</sub> ] (0.1 M, 100 mL) and 2 mL of plant extract (molar ratio 1:1:1)	Rachna et al. (2018) [87], Rani and Shanker (2018) [102]
SnO <sub>2</sub> –ZnO	Homogeneous precipitation combined with a hydrothermal treatment	Two steps: 1. synthesis of nanosized SnO <sub>2</sub> and reaction of as-prepared SnO <sub>2</sub> particles with zinc acetate followed by calcination at 500°C. Mesoporous network of aggregated wurtzite ZnO (27 nm) and cassiterite SnO <sub>2</sub> nanocrystallites (4.5 nm)	Uddin et al. (2012)
heterostructured Bi <sub>2</sub> O <sub>3</sub> –ZnO	Hydrothermal–thermal decomposition	XRD: monoclinic lattice phase of Bi <sub>2</sub> O <sub>3</sub> and the hexagonal wurtzite phase of ZnO. HR–SEM: ordered mixture of nanofiber and nanochain structures	Balachandran and Swaminathan (2012)

(Continued)

**TABLE 13.3 (Continued)**

Functionalized NMs	Method of functionalization	Details of method	References
Cadmium sulfide–ferrite nanocomposite	Two-step hydrothermal method	Magnetically recyclable photocatalyst	Xiong et al. (2013)
Cu <sup>2+</sup> –ZnO	Flame spray pyrolysis process	Surface modification by a cocatalyst on ZnO	Kumar et al. (2014) [88]
Zn-doped CdS nanoarchitectures	Simple hydrothermal method with water as the only solvent	Improvement of photocatalytic activity and stability of CdS through the method of metal ion doping	Yang et al. (2012)
Graphene /ZnO	chemical deposition-calcination	Solvent exfoliated graphene (SEG), Zn(NH <sub>3</sub> ) <sub>4</sub> CO <sub>3</sub> , NaOH as a precipitating agent, and poly (vinylpyrrolidone) as an interface linker	Ong et al. (2014)
FeWO <sub>4</sub> @ZnWO <sub>4</sub> /ZnO	Two-step hydrothermal method	Dispersing of FeWO <sub>4</sub> nanoparticles on the surface of ZnWO <sub>4</sub> /ZnO nanorods	Wang et al. (2016)
ZnO as zinc glycerolate	Nonhydrolytic route	Glycerol has been used both as a ligand and as a solvent. This glycerolate precursor has subsequently been converted into the hexagonal phase of zinc oxide	Das and Khushalani (2010)

*(Continued)*

**TABLE 13.3 (Continued)**

Functionalized NMs	Method of functionalization	Details of method	References
ZnIn <sub>2</sub> S <sub>4</sub> microspheres	Hydrothermal method	The specific surface area (SBET) of ZnIn <sub>2</sub> S <sub>4</sub> products declined with increasing synthesis temperature. The 80°C sample had the largest SBET (85.53 m <sup>2</sup> /g)	Chen et al. (2009)
Cu <sub>2</sub> ZnSnS <sub>4</sub> –Pt/Au		Quasispherical Cu <sub>2</sub> ZnSnS <sub>4</sub> nanoparticles with unprecedented narrow size	Yu et al. (2014)
Zn-doped In(OH)γSz	Hydrothermal method.	In(NO <sub>3</sub> ) <sub>3</sub> , thiourea, and Zn (NO <sub>3</sub> ) <sub>2</sub> in an aqueous solution of ethylenediamine	Li et al. (2008)
ZnO-graphene	Hydrothermal process	Hydrothermal method addition of ZnO to graphene under pressure	Malekshoar et al. (2014)
ZnO and Zn/Mg Oxide Nanoparticles	Sol–gel method	Formation of crystal defects by the incorporation of Zn into MgO	Sierra-Fernandez et al. (2017)
TiO <sub>2</sub> coated ZnO	Hydrothermal method	Coating of TiO <sub>2</sub> with ZnO under wet chemical process	Wang et al. (2015)
(Cu–ZnO, Cu–Cu <sub>2</sub> O–ZnO, and Cu <sub>2</sub> O–ZnO)	surface plasmon resonance (SPR) effect	varying the complexing agents; introduced cheap and common Cu and Cu <sub>2</sub> O in ZnO matrix individually and conjointly	Pal et al. (2015)

*(Continued)*

**TABLE 13.3 (Continued)**

Functionalized NMs	Method of functionalization	Details of method	References
Polyacrylamide/ Ni <sub>0.02</sub> Zn <sub>0.98</sub>	In situ mixing	by addition of nanoparticles during polymerization of acrylamide in aqueous medium using ammonium persulfate and N, N'-methylenebis (acrylamide)	Kumar et al. (2014) [88]
CuS/ZnO nanowires	Two-step wet-chemical method	nanowire arrays are compactly/ vertically aligned on stainless steel mesh	Hong et al. (2016)
Graphdiyne–ZnO Nanohybrids	Hydrothermal method	The utility of carbonaceous materials for hybrid semiconductor photocatalysts has been rapidly increasing in recent years	Thangavel et al. (2015)
Zn <sub>1-x</sub> Cd <sub>x</sub> S Nanocrystals	Solvothermal synthesis	Template-free synthesis; using 4,4'-dipyridyldisulfide (DPDS = (C <sub>5</sub> H <sub>4</sub> N) <sub>2</sub> S <sub>2</sub> ) as a new temperature-dependent in situ source of S <sup>2-</sup> ions	Kaur and Nagaraja (2017)
ZnIn <sub>2</sub> S <sub>4</sub> nanocrystals	A one-pot method	[Zn(SC(O)Ph) <sub>2</sub> ] <sub>2</sub> •2 H <sub>2</sub> O reacted with [In(bipy)(SC(O)Ph) <sub>3</sub> ] and decomposed to make the ternary metal indium sulfides	Batabyal et al. (2016)
Multivalent Cu-doped ZnO nanoparticles	Metathesis-based, green-chemical approaches	Synthesis yield of ~ 100%. particle sizes ≥ 50 nm	Jacob et al. (2014)

*(Continued)*

**TABLE 13.3** (Continued)

Functionalized NMs	Method of functionalization	Details of method	References
3D-ZnIn <sub>2</sub> S <sub>4</sub> /PVDF–Poly (MMA-co-MAA)	Hydrothermal process	ZnIn <sub>2</sub> S <sub>4</sub> (ZIS) nanosheets (20 nm) distribute uniformly on surface of nanofiber polymers to form mats	Peng et al. (2012)
SnO <sub>2</sub> /ZnO	Two-step solvothermal	SnO <sub>2</sub> /ZnO sample with a molar ratio of Sn/Zn = 1 is a mesoporous composite material composed of SnO <sub>2</sub> and ZnO	Zheng et al. (2009)
Ag @ ZnO	Solvothermal-assisted heat treatment	AgNPs (diameter: 20–50 nm) were anchored onto the surface of n–ZnO MRs (diameter: 90 to 150 nm and length: 0.5 and 3 μm) by a photoreduction method.	Deng et al. (2012)
ZnO and ZnS	Coprecipitation	Coprecipitation of salt of Zn with alkali	He et al. (2016)
ZnO/Ag <sub>2</sub> S core/shell ZnO/CdS core/shell	Introduction of the core/shell geometry	Band-gap engineered ZnO semiconductor nanorods by introducing a core/shell geometry with Ag <sub>2</sub> S sensitizer as the shell	Khanchandani et al. (2014)
ZnO @ Gold	Solvothermal route	Solvothermal synthesis under pressure using Zn salt as precursor	Xia et al. (2015) [89]

(Continued)

**TABLE 13.3 (Continued)**

Functionalized NMs	Method of functionalization	Details of method	References
(GQD/ZnO NWs)	Electrochemical technique	Different amounts of GQDs (0, 0.2, 0.4, 0.8, and 1.2 wt%) were decorated uniformly on the surface of anodized ZnO NWs	Ebrahimi et al. (2017)
(rGO) embedded ZnO	Bioinspired approach	Mineralization of ZnO nanostructures from zinc nitrate, reduction of graphene oxide (GO), and finally their assembly to form rGO–ZnO composite structures under environmentally benign conditions	Reddy et al. (2015)
Pd/ZnTPyP/Pd/TiO <sub>2</sub> –Py triad hybrid multilayers	Layer-by-layer (LBL) method	Addition of Pd to Zn layer by layer	Ren et al. (2012)
ZnO–TiO <sub>2</sub> nanotube arrays ZnO/TNTs	Two-step anodization combined Pyrolysis strategy	In situ formed ZnO phases were uniformly grafted to TNTs framework giving Rise to hybrid nanostructure, which is ascribed to cooperative interfacial interaction between polar TiO <sub>2</sub> layer and ZnO precursor	Xiao (2012)
ZnO/CdS Core–shell Nanorods arrays		Synthesized with varying shell thickness. Core diameter of	Khanchandani et al. (2012)

(Continued)

**TABLE 13.3 (Continued)**

Functionalized NMs	Method of functionalization	Details of method	References
		100 nm with variable shell thickness (10–30 nm); synthesized by varying the concentration of the citric acid	
ZnO/ $\gamma$ -Fe <sub>2</sub> O <sub>3</sub>	Simple precipitation	Heat treatment of nanocatalysts at 450°C for an hour	Abdullah et al. (2013)
ZnO–Chitosan (CS–ZnONPs)	polymer-based method	In situ addition of ZnO to chitosan	Dehaghi et al. (2014)
ZnO–CeO <sub>2</sub> nanostructures	Simple and efficient low-temperature method	Low-temperature mixing of CeO <sub>2</sub> during ZnO synthesis from salt	Faisal et al. (2011)
CeO <sub>2</sub> –ZnO nano ellipsoids	Hydrothermal process	Low-temperature mixing of CeO <sub>2</sub> during ZnO synthesis from salt	Singh et al. (2014)
ZnO-doped CeO <sub>2</sub> nanoplatelets	Solvothermal route	Doping of CeO <sub>2</sub> by ZnO under pressure	Kaviyarasu et al. (2016)
ZnO/TiO <sub>2</sub>	Tape casting method	TiO <sub>2</sub> content of the plates was sintering temperature of the plates is 700°C	Konyar et al. (2010)
La-doped ZnO 0.8 wt%	Coprecipitation	La <sup>3+</sup> is uniformly dispersed on ZnO nanoparticles as small La <sub>2</sub> O <sub>3</sub> cluster	Anandan et al. (2007)
ZnO/Au and ZnO/Ag	Reverse micelle	Deposition on ZnO surface using hydrazine hydrate as reducing agent	Fageria et al. (2014)
undoped and Er-doped ZnO nanoparticles	sonochemical method	Doping of ZnO by Er under ultrasonicator	TORBATI et al. (2017)

*(Continued)*

TABLE 13.3 (Continued)

Functionalized NMs	Method of functionalization	Details of method	References
CuS/CdIn <sub>2</sub> S <sub>4</sub> /ZnIn <sub>2</sub> S <sub>4</sub>	Microvave-assisted	Simple missing under microwave	Chen et al. (2016)
TiO <sub>2</sub> /ZnO/chitosan	In situ addition	Well-dispersed of TiO <sub>2</sub> /ZnO nanocomposite embedded in chitosan films	Zhu et al. (2012)
ZrO <sub>2</sub>  ZnO	Coprecipitation	Synthesis of nanocomposites using CTAB as surfactant	Quintana et al. (2017)

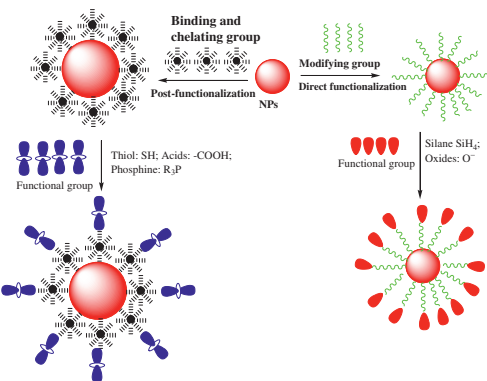
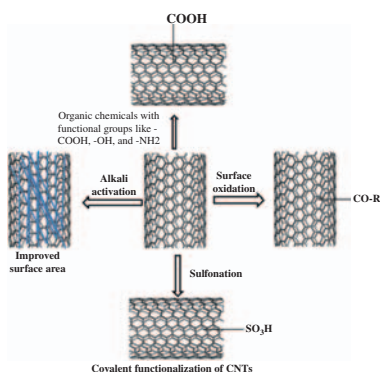


FIGURE 13.4 Schematic representation of functionalization methods. Direct functionalization, which uses a conjugating agent in order to directly attach the chemical moiety, and postfunctionalization, which uses a binding/chelating agent to attach to the NPs and a secondary functional group for covalent attachment of the biomolecule of interest.

heteroatoms, and sulfonation. Fig. 13.5 offers a pictorial representation of covalent functionalization of CNTs. A covalent bond is much stronger and can resist any desorption compared to noncovalent bonds. Yang Xing (2010) reported on the surface oxidation of CNM with oxygen functional groups (e.g., carboxyl, carbonyl, and hydroxyl) by various oxidation treatments utilizing oxidizing gases (e.g., air, O<sub>2</sub>, O<sub>3</sub>, NO<sub>2</sub>, and NO<sub>3</sub>) and oxidizing solutions (e.g., HNO<sub>3</sub>, H<sub>2</sub>O<sub>2</sub>, ClO<sup>-</sup>, S<sub>2</sub>O<sub>8</sub><sup>-2</sup>, MnO<sub>4</sub><sup>-2</sup>, Cr<sub>2</sub>O<sub>7</sub><sup>-2</sup>, and ClO<sub>3</sub><sup>-1</sup>) [103]. The surface oxidation process offers the advantages of an increased acidic property, the removal of mineral elements, an improved hydrophilic nature, and the creation of more surface groups by subsequent functionalization through covalent, electrostatic, and hydrogen bonds [104,105]. CNMs activated via heating with alkali KOH change the surface of carbon-based NMs





**FIGURE 13.5** Pictorial representation of covalent functionalization of CNTs.

to increase the specific surface area and pore volume (i.e., porous carbon). Graphene oxide-derived carbons with a high surface area ( $1900 \text{ m}^2/\text{g}$ ) showed favorable gas adsorption capacities compared to  $10 \text{ m}^2/\text{g}$  of precursors and other high surface area carbons (Srinivas et al., 78). Heating CNMs with ammonia at  $400^\circ\text{C}$ – $900^\circ\text{C}$  can produce basic nitrogen functionalities [106]. Sulfonation of CNM produced potential, environmentally benign, solid acid catalysts that could be substituted for the nonrecyclable traditional liquid acid [107].

nZVI coated with biopolymers (e.g., guar gum, polyacrylic acid, starch, carboxymethyl, and cellulose) is stable and noncorrosive, has decent dispersibility, and exhibits scarcer aggregation in water. Poly(ethylene glycol) (PEG) utilized for safety of the surface passivation of nZVI helped to impart magnetic properties for biomedical application [108] and could control aggregation of nZVI by PEG concentration and its functional group. The Fe NPs were efficiently stabilized in the presence of guar gum (green polymers) demonstrating less aggregation via the electrostatic and steric repulsion in comparison to alginate and potato starch [109]. Rani et al. [110], developed a magnetic nanoadsorbent using covalently bounded polyacrylic acid to the surface of magnetite nanoparticles followed by functionalization of an amino group by diethylenetriamine via carbodiimide activation.

Functionalization of silica-based NMs (e.g., zeolite and mesoporous) is usually performed using organic templates or surfactants [111,112]. Pure inorganic materials have fewer surface groups and limited adsorption capacity and low selectivity of adsorption [113,114]. Consequently, zeolites and mesoporous silica provide better properties like large surface area, uniform pore size distribution, fast mass transport, and, most importantly, surface reactivity, adsorption capacity, enhanced stability, and ease of modification by various desirable functional groups [116,117]. With the use of silanol groups, the hydrophobicity/hydrophilicity of the surface could be tuned. Almost all functional groups such as amino [118], carboxylic acid [119],

thiol [120], and sulfonic acid [121] have been loaded on the surface of silica-based nanomaterials using this reaction.

### 13.2.1.2 *Noncovalent functionalization*

Noncovalent hydrophobic interactions and the interaction of amphiphilic molecules with aromatic surfaces of CNMs in aqueous media have been used to reduce the hydrophobic interface and improve the solubility of CNMs in their polar environment [122,123].

### 13.2.1.3 *Inorganic functionalization*

*Inorganic Functionalization:* Metal and metal compounds have been used for CNM surface modification via mixing and in situ synthesis. Mixing includes solution mixing and melt compounding. In situ synthesis involves the contact between a precursor or solution and the carbon material, followed by nanoparticle formation on the CNM surface [124].

### 13.2.1.4 *Functionalization by heteroatoms doping*

The doped NMs can be synthesized by hydrolysis or heating of a precursor, hydrothermal, and ion implantation [125,126]. Doping of heteroatoms (e.g., N, B, P, and O) introduces catalytic active sites and surges the surface hydrophilicity and electrical conductivity of the doped material [127]. N-doped CNTs were synthesized by mixing hydrocarbon and ammonia [128], hydrocarbon and organic amine, [129] or simply pure organic amine [130] as the carbon and nitrogen source. It was observed that surface doping of pristine nZVI with transition metal ions reduced the aggregation and improved reactivity and adsorption capacity [131,132]. There are several classes of doped materials such as nZVI doped with Pd, Au, Cu, Ag; N–TiO<sub>2</sub> doped by N, F, S, and C or transition metal ions; and N- and P-doped CNMs that will enhance the photocatalytic nature by reducing the wide band gap of the individual functionalized NMs. Doping expedites the generation of reactive oxygen species, which facilitates the degradation of pollutants. Some studies showed that N-doped on anatase TiO<sub>2</sub> enlarged the valence band by 0.140.73 eV, while rutile TiO<sub>2</sub> resulted in the band-gap energy by 0.08 eV by increasing the conduction band (0.05 eV) and reducing VB (0.03 eV) [133]. It was also found that hollow TiO<sub>2</sub> with porous structure have smaller band-gap energy than that of solid structures [134]. The porous structure was doped by several metals like Sn, Ba, Co, Al, Fe, Sn, Bi, and nonmetals (e.g., C, N, S, and F), and with lighter elements [135–142]. Khalid et al. [143] reported that functionalization of TiO<sub>2</sub> with graphene or NMs as cocatalysts inhibited the recombination rate of electron hole [143,144]. For example, Cu (II)- or Fe(III)-doping TiO<sub>2</sub> significantly increased the photocatalytic activity while Ti(III) doping showed inactive photocatalytic behaviors [145].

### 13.2.1.5 Functionalization by immobilization

Immobilization of moss ZnO and  $\text{Fe}_2\text{O}_3$  with laccase enzyme was successfully established and reported [146,147]. Fig. 13.6 represents the immobilization of moss. Pristine nZVI was immobilized by porous supporting materials like resins [148],  $\text{Mg}(\text{OH})_2$  [149], green tea, kaolin [150], bentonite [151], carbon [152], and mesoporous silica microspheres [153], a process that improves reactive sites, available surface area, and stability in order to have enhanced activity.

## 13.2.2 Indirect or postsynthetic functionalization (grafting)

Indirect functionalization is carried out by grafting bifunctional ligands on to the surface of NMs after synthesis. The binding group reacts first, and then the coupling site functional group may be transformed in to the final functional group in the second step. Functionalized mesoporous silica creates an effective support in the synthesis of inorganic-organic hybrid materials by grafting organic chains on to their surface through the silylation process. The Si-OH groups on silica's surface are substituted by chosen organic ligands via a one-step homogeneous method or multisteps like the heterogeneous method attachment [154].

Grafting via oxygen-containing groups is the most common method where preexisting carboxyl groups on CNMs can react with  $\text{SOCl}_2$  to form acylchloride [100]. As a result of carboxamide formation via acylchloride, CNMs were functionalized with aryl amines, aliphatic amines, amino acid derivatives, peptides, and amino group-substituted dendrimers [155]. In addition, the acylchloride-functionalized CNMs will react with alcohol to form an ester functionalized CNMs (e.g., esterification). Thiolation is achieved by consecutive carboxylation, sonication, reduction, chlorination, and thiolation applied to the open ends of CNTs and formed by breaking the tubes through sonochemical activation [156].

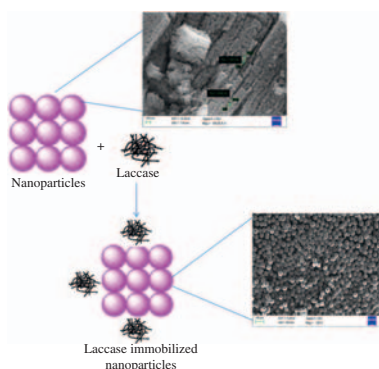


**FIGURE 13.6** Functionalization of MOs via immobilization.

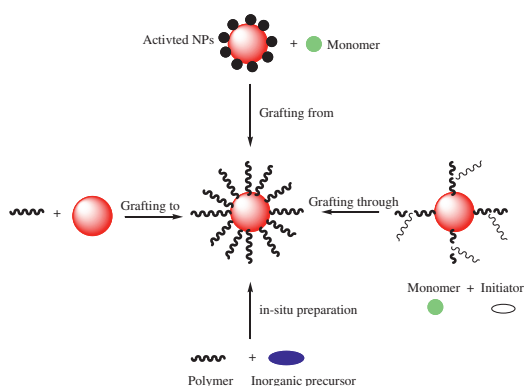


**FIGURE 13.7** Coating of NMs with polymers either noncovalent (polymer wrapping and absorption) and covalent attachment (“grafting to,” “grafting from,” and others).

### 13.2.2.1 Polymer coating

Coating CNM surface with polymers noncovalent (e.g., polymer wrapping and absorption) or covalent attachment processes (“grafting to,” “grafting from,” and others) improved the chemical compatibility, mechanical strength, wettability, conductivity, and adsorption properties [157]. The covalent approach is the preferred method of grafting polymers on to CNM surfaces through  $-\text{COOH}$  and  $-\text{OH}$  groups that serve as anchoring sites. The grafting of CNTs by  $\text{NH}_2$ -containing polymers reacting with acylchloride on the surface has been investigated [158]. Fig. 13.7 presents polymer coating of functionalized NMs.

## 13.3 Green synthesis in FNMs

In order to avoid use of toxic solvents such as DCM, DMF, hydrazine,  $\text{NaBH}_4$ , etc., green tactics employing environmentally benign and renewable materials are preferred. Green technologies are usually more reliable and sustainable, and are bioinspired bottom-up approaches [159,160]. Green synthesis of FNMs has several benefits over traditional methods such as being cheaper, ecofriendly, safe, reusable, easy manipulation of size, morphology, and shape, as well as surface functionality, generation of relative stability, and remarkable biocompatibility and biodegradability [159,161,162]. Intracellular or inner surface biosynthesis modulates the crystal growth and nucleation processes of NP microbial synthesis. During the NP synthesis, reactive enzymes, proteins, and reducing components on the cell surfaces serve as reducing and stabilizing (or capping) agents [163]; however, this method is time consuming ( $\sim 30$  days) and expensive too.

### 13.4 Necessity of functionalization of NMs for remediation of organic contaminants

Several physical (e.g., membrane filtration, adsorption, and coagulation-flocculation), chemical (e.g., catalytic degradation, chemical precipitation, ion exchange, and oxidation), and biological approaches have been used to degrade noxious pollutants [143,144]. Among them all, adsorption was established as the most efficient method due to its simplicity and cost-effective methodology [166–168]. Due to high surface area and reasonable band-gap semiconductors, NMs (e.g.,  $\text{TiO}_2$ ,  $\text{ZnO}$ ,  $\text{CdS}$ ,  $\text{SnO}_2$ ,  $\text{WO}_3$ , and  $\text{Fe}_2\text{O}_3$ ) show superior properties of adsorption with photocatalysis [169–171]. However, their limitations, such as charge-carrier trapping, hole-electron recombination, mediated interfacial charge transfer, and limited accessible surface area, hinder their feasibility. In order to avoid the aforementioned drawbacks, functionalization of NMs via polymer coating, surface oxidation, or deposition of dopants into the original material's framework, etc., is a new method trend [172,173]. Moreover, to evade bioaccumulation and control the enrichment of a particular metallic framework, alternative methods should be promoted.

### 13.5 Working mechanism of FNP

Although similar to NMs, FNPs work in different ways (Fig. 13.8): (1) sorbents (absorb contaminants inside such as sponges, moss); (2) adsorption (absorb contaminants on surface such as CNTs, metal nanoparticles); (3) filtration via membranes; (4) chemical reactions like dechlorination, reduction, oxidation; and (5) finally, photocatalysis where FNPs act as adsorbent/photocatalyst. When these nanocatalysts with small band gap are exposed to a light source (UV or visible) electron-hole pairs are generated that ultimately degrade the OPs into nontoxic products via photooxidation (e.g., change of  $\text{H}_2\text{O}$  or  $\text{H}_2\text{O}_2$  into  $\text{OH}^*$ ) or photoreduction (e.g., change of  $\text{O}_2$  into

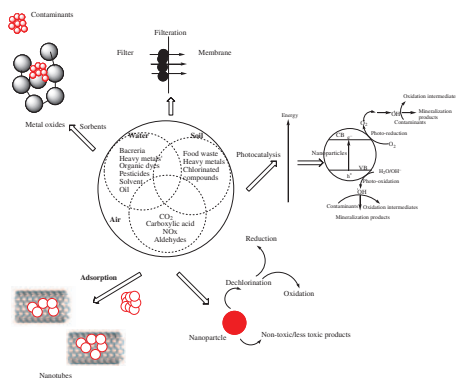


**FIGURE 13.8** Several types of working mechanisms for FNPs.

$O_2^{\bullet -}$  and  $OH^{\bullet}$ ) [174–176]. Doping or coupling prevents the electron-hole recombination due to this  $e^-$ , and  $h^+$  remains longer in the conduction and valence bands, respectively. Doping with other nanoparticles and smaller size NM enhances the rate of degradation. Doping can also tailor the nanocatalyst's band gap, and, consequently, the photooxidation or photoreduction will become easier. Photocatalytic degradation of several pollutants using functionalized nanoparticles is shown in Fig. 13.8. Due to their characteristic destructive nature, they do not involve mass transfer, and the process can be carried out under ambient conditions where atmospheric  $O_2$  is used as oxidant.

### 13.6 Importance of green synthesis in FNMs

Green synthesis employing sunlight or nontoxic environmentally benign and renewable materials such as water, ionic liquids, microbes, plant-based surfactants, or a combination of those can be used on a large scale. Fig. 13.9 represents the various green methodologies used for synthesis of NMs. Functionalized NMs synthesized via green methods are low cost and are effective catalysts for remediation of environmental pollutants. Despite this, they are not used as often as probes for contaminants. RGO-based plasmonic nanohybrids (e.g., Ag–RGO, Au–RGO, and Ag/Au–RGO) synthesized using extracts of baker's yeast showed exceptional photothermal transformation adeptness for waste desalination and purification under visible light [177]. Moreover, Ag–RGO synthesized by means of aqueous extracts of *Psidium guajava* leaves showed a detection capability for methylene blue (MB) even at very low concentrations [178]. A magnetic nanohybrid of Pd–Fe<sub>3</sub>O<sub>4</sub> synthesized by use of Fe(III)-reducing bacterium (*Geobacter sulfurreducens*) converted iodobenzene to ethyl acrylate and styrene through the Heck coupling reaction in 3 h [179]. The bimetallic Pd–Au nanostructures produced by *Shewanella oneidensis* were found to be effective for dehalogenation of many organic impurities including pharmaceutical drugs [180]. Compared to bare Ag or Au, FNPs like Ag–Cu prepared by use of leaf extracts of *Prosopis cineraria* offers advantages of superior antibacterial activity and cytotoxicity against human breast cancer cell lines (MCF-7) [181]. Biofunctionalization of Ag and GO with phenylalanine peptide (i.e., GO-peptide-Ag) nanohybrids showed electrochemical detection of small molecules like H<sub>2</sub>O<sub>2</sub> [182]. The almond shell was applied to conjugate the Ag-almond nanocomposites obtained from *Ruta graveolens* sleeves, which acts as both reducing and stabilizing agents, and was able to degrade 4-nitrophenol, rhodamine B (RhB), and MB [183]. Nanocomposites of GO with crystalline cellulose displayed astonishing adsorption capacity for MB (2630 mg/g) [184]. Additionally, cellulose–Ag nanocomposites have unlimited talent for commercial applications (e.g., catalysis, antibacterial, sensor,



**FIGURE 13.9** Various green strategy for the synthesis of doped metal hexacyanoferrates, bimetallic oxides simple, and doped with PMMA.

and environmental) [185]. Silver nanoparticles with *Amaranthus gangeticus* may be able to remove more than 50% of Congo red dye in 15 min [186].

Anthracene and dyes can be removed via photocatalysis using biosynthesized nanocomposites of ZnO and copper oxide with graphene oxide [187,188]. Fardood and his research group biofabricated several nanocomposites of moss (e.g., Zn, Cu, and Ni) and ferrites (e.g., Ni-Cu-Zn, Ni-Cu-Mg, and Cu-Fe<sub>3</sub>O<sub>4</sub>) by use of gel, gum, or plants, and used them as catalysts for organic synthesis and photocatalysis for removal of OPs [189–192]. In addition, supermagnetic MgFe<sub>2</sub>O<sub>4</sub>@ $\gamma$ -Al<sub>2</sub>O<sub>3</sub> FNP were used for remediation of several reactive dyes [191–193]. Green tea or starch fabricated iron-based FNPs have been considered for photocatalysis [194–196]. Compared to bare ones, green synthesized FNPs showed superior activities: bimetallic Fe/Pd > Fe and Fe<sub>2</sub>O<sub>3</sub>@ZnHCF nanocubes > ZnHCF > Fe<sub>2</sub>O<sub>3</sub> nanoparticles [197–199]. Better catalytic efficiency of green tea–iron nanoparticles than Fe nanoparticles fabricated by borohydride reduction further supported this fact [200].

Shanker and his research group applied several green methods based on sunlight assisted by synthesis and plant extracts (e.g., *A. marmelos*, *S. mukorossi*, *A. indica*) for fabrication of bimetallic oxides, metal hexacyanoferrates, and cobaltates nanostructures for photocatalytic degradation of several OPs [44–46,51,146,147,201–208].

Green synthesized, highly crystalline, sharp metal hexacyanoferrates (KCuHCF > KNiHCF > KCoHCF) (Fig. 13.10) and transition MO nanostructures obtained via the use of sunlight and natural surfactants (*A. marmelos*) were able to photodegrade quantitative (more than 90%) amounts of dyes [146,147,201–204]. Biogenic Ag NPs obtained from different sources like *Polygonum Hydropiper*, *Saccharomyces cerevisiae*, and *Morinda tinctoria* leaf extracts have different degradation ability for dye removal under sunlight irradiation: 100% in 13 min [209], 90% in 6 h [210], and 95% in 72 h [211], respectively.

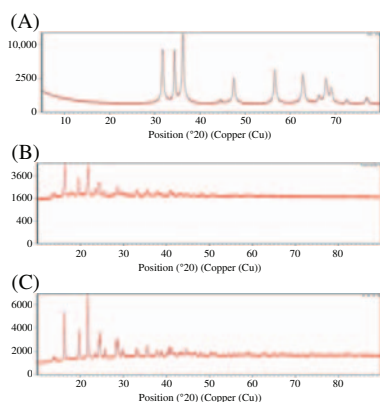


**FIGURE 13.10** PXRD pattern of (A) ZnO, (B) ZnHCF, and (C) ZnO@ZnHCF.

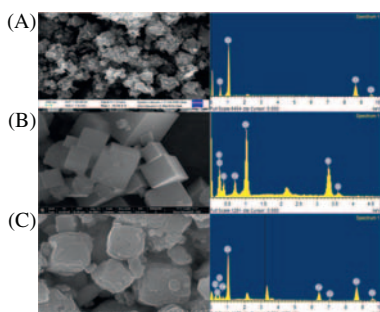


**FIGURE 13.11** FE-SEM image and EDS pattern of (A) ZnO, (B) ZnHCF, and (C) ZnO@ZnHCF.

Metal hexacyanoferrate nanoparticles (10–100 nm) were more effective for removing toxic PAHs under sunlight than under UV light and with dark exposure. Depending upon the size of the rings, molecular weight, and aromaticity, anthracene was initially adsorbed followed by degradation to maximum content over the surface of the photocatalyst more effectively than phenanthrene, fluorine, chrysene, and BaP in water (70%–93%) along with soil (68%–84%) at neutral pH under daylight contact. The XRD pattern, FE-SEM images of zinc oxide, zinc hexacyanoferrate, and their composites are presented in Figs. 13.10 and 13.11. While the photocatalytic degradation of BPA is shown in Fig. 13.12. Their potential was increased by the discovery of minor and less-toxic metabolites that led to mineralization Fig. 13.13.

Crystalline nanocubes of  $\text{Fe}_2\text{O}_3@\text{ZnHCF}$  and  $\text{ZnO}@\text{ZnHCF}$  nanocomposite were synthesized using water and the *A. indica* plant extract, a locally available plant. Phytochemicals like benzoquinones, saponin, and polyphenols have a tendency to regulate particle growth by minimizing interfacial tension. Functionalization with doping improved the surface-to-volume ratio area from 343 to 114  $\text{m}^2/\text{g}$  and band energy from 2.18 to 2.2 eV) as well because of the synergistic effect of both semiconductors, which were moss and ZnHCF. This fact is supported by 3–6 times better adsorption of



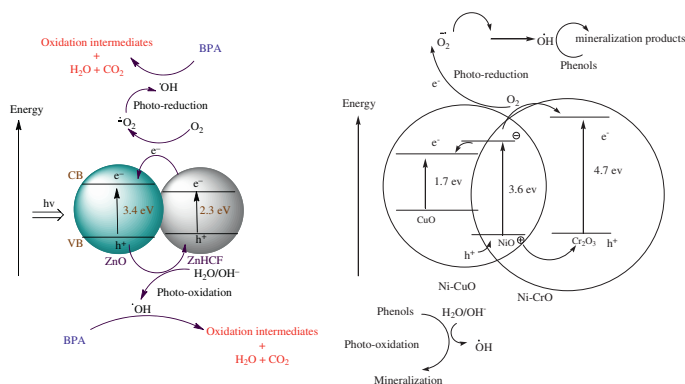


**FIGURE 13.12** Photocatalytic degradation process of various phenols occurring over the surface of encapsulated ZnO@ZnHCF and mixed metal oxides nanocomposites.

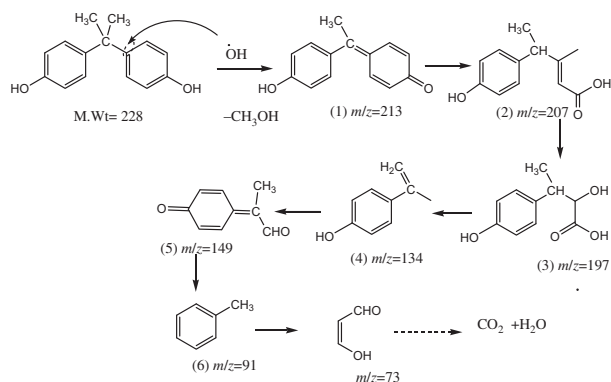


**FIGURE 13.13** Degradation pathways of Bisphenol A over the surface of ZnO@ZnHCF nanocubes (Concentration; 2 mg/L; pH: ~ 7; catalyst dose: 25 mg; natural sunlight).

chrysene ( $X_m = 45.45$  mg/g) by doped nanocubes than bare ZnHCF ( $X_m = 16.22$  mg/g) and  $\text{Fe}_2\text{O}_3$  ( $X_m = 7.348$  mg/g). Here, iron oxides and ZnO were modified via doping with ZnHCF, and doped materials showed enhanced photocatalytic first-order degradation of chrysene and BPA under sunlight, respectively. They initially adsorbed them on their surfaces via the Langmuir adsorption mechanism. A very small amount, 25 mg, of FNPs was able to degrade 92% of 2 mg/L of chrysene [198]. For BPA degradation the trend of ZnO–ZnHCF was highest (97%), followed by ZnHCF (88%) and ZnO (75%). Finally, BPA was converted to minor and small nontoxic oxidative chemicals like malealdehyde, propionic acid, and but-2-ene-1,2,4-triol by countless  $\cdot\text{OH}$  generated by conduction of wrapped nanocomposite. Both of the functionalized catalysts are easily regenerated and used up to ten cycles, emphasizing their high potential for industrial applications.

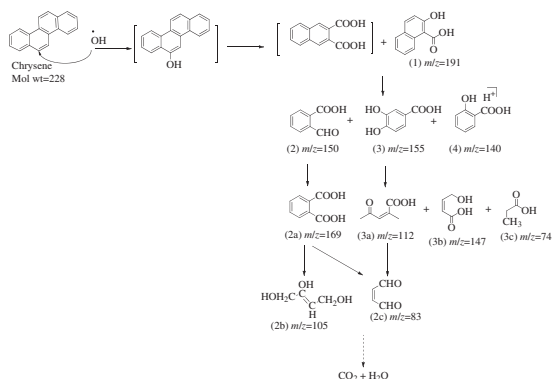


**FIGURE 13.14** Proposed degradation pathway for the degradation of chrysene over  $\text{Fe}_2\text{O}_3@\text{ZnHCF}$  nanocubes (Concentration; 2 mg/L; pH ~ 7; catalyst dose: 25 mg; natural sunlight).

Degradation pathways, along with byproducts of PAHs, have been shown in Figs. 13.14 and 13.15. Functionalization further improved charge separation and prevented the charge carriers' recombination because of the movement of photogenerated electrons from photocatalysts to photosensitizer.

Recently, mixtures of two or more oxides have been reported for photocatalytic efficiency. Green synthesis is commonly used for metal oxides, but is limited for bimetallic and higher forms. Fardood and his research group [212] carried out green functionalization of ZnO with Ce ion or Ag for photocatalytic degradation of OPs. Rani and Shanker fabricated bimetallic oxides (below 50 nm), such as Ni–CuO nanorods,  $\text{CuCr}_2\text{O}_4$  nanoflowers, and  $\text{NiCrO}_3$  nanospheres via use of *A. marmelos* leaf extract consisting of terpenoids, alkaloids, and phenylpropanoids as phytochemicals for controlling the morphology of FNPs. Under optimized conditions of concentration, catalyst dose and pH of solution, FNPs (15 g) were able to degrade a maximum content (87%–97%) of noxious phenols ( $1 \times 10^{-4}$  M). 3-aminophenol was more basic than phenol and 2,4-dinitrophenols, therefore more attracted toward the acidic surface of catalysts and much degraded. The degradation efficiency of bimetallic oxides (BMOs) of Ni–Cu oxide, Ni–Cr oxide, and Cu–Cr oxide are in order of zeta potential, brunauer-emmett-teller surface area, and the uniform distribution of nanoparticles of both oxides involved. The characterization of BMOs via XRD, FE-SEM, and TEM is shown in Figs. 13.16–13.18. The byproduct obtained from degradation (e.g., oxidation and cleavage of benzene-rings) of phenols were oxalic acid, benzoquinone, (Z)-hex-3-enedioic acid, (Z)-but-2-enal, and (Z)-4-oxobut-2-enoic acid (Figs. 13.19–13.21). Moreover, like metal oxide FNPs with ZnHCF, mixtures of metal oxides are less expensive because they use an inexpensive synthesizing process and are reusable ( $n = 10$ ) with an enhanced charge separation.

Different researchers of FNPs observed diverse possibilities for the use of FNPs fabricated from green sources and containing different phytochemicals

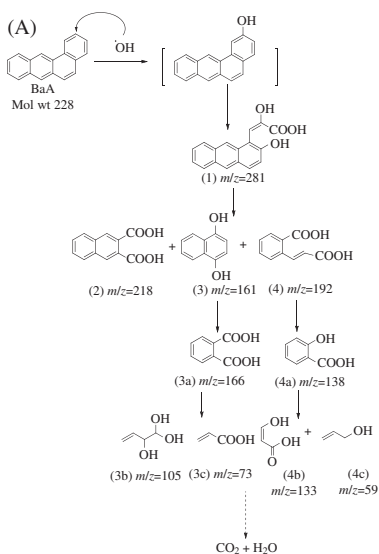
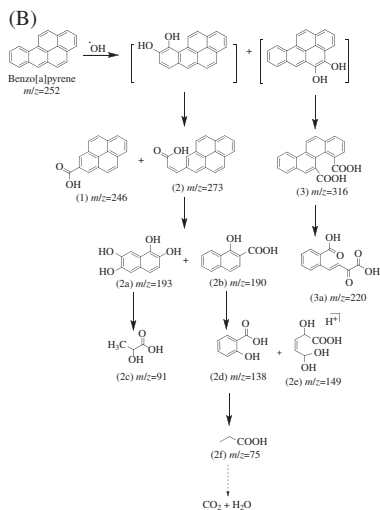


**FIGURE 13.15** Proposed degradation pathway for the degradation of (A) BaA and (B) BaP over  $\text{ZnHCF@ZnO}$  nanocubes (Concentration; 2 mg/L; pH:  $\sim 7$ ; catalyst dose: 25 mg; natural sunlight).



surfactants. Thanks to that research, numerous FNPs of different size and morphology were obtained. Hence, in view of this, commercialization of green synthesized FNPs should be encouraged.

### 13.7 Organic dyes

Among the cheap and highly efficient FNPs,  $\text{TiO}_2$  followed by  $\text{ZnO}$ , iron oxides,  $\text{NiO}_2$  and silica-based NMs (nanocomposites and biocomposites),

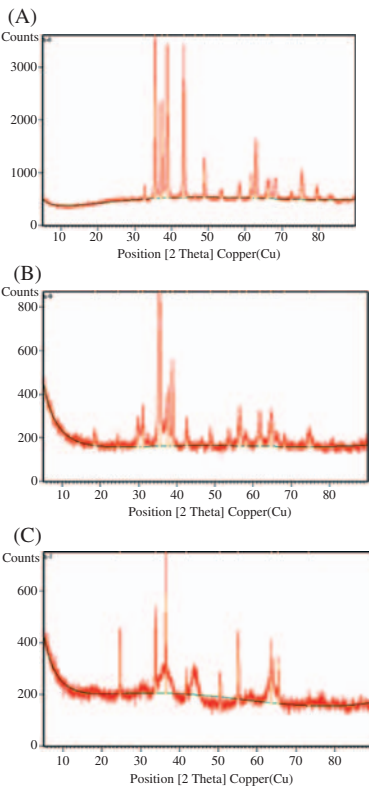


**FIGURE 13.16** PXRD spectra of (A) Ni–CuO, (B) CuCr<sub>2</sub>O<sub>4</sub>, and (C) NiCrO<sub>3</sub> nanoparticles.

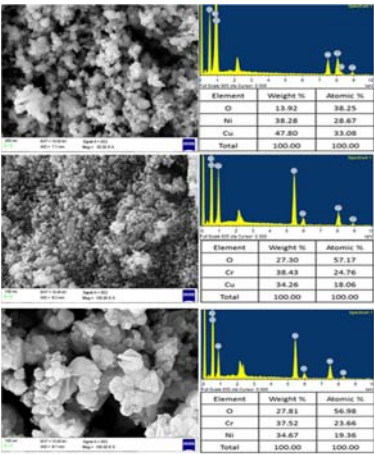


**FIGURE 13.17** FE-SEM images of (A) Ni–CuO, (B) CuCr<sub>2</sub>O<sub>4</sub>, and (C) NiCrO<sub>3</sub> nanoparticles.

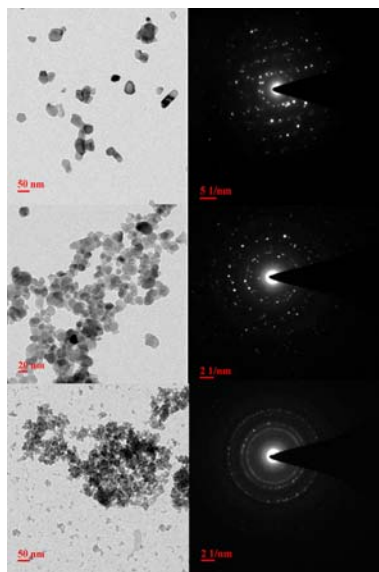


**FIGURE 13.18** TEM images with SAED patterns of (A) Ni–CuO, (B) CuCr<sub>2</sub>O<sub>4</sub>, and (C) NiCrO<sub>3</sub> nanoparticles.

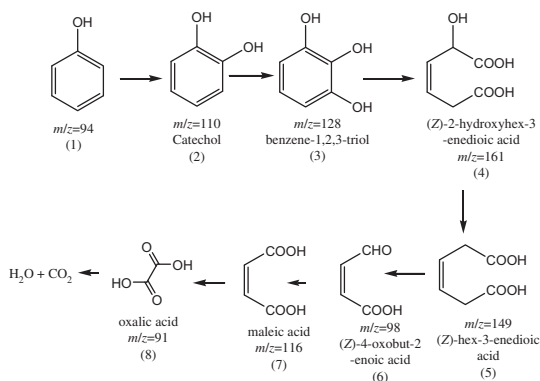


**FIGURE 13.19** proposed degradation pathway of phenol over the surface of bimetallic metal oxides nanoparticles.

along with metals (Fe, Pt and Pd) have been widely fabricated due to their wide band gap, high surface area, and intense performance observed for individual FNPs [213,214]. A commercially available TiO<sub>2</sub> semiconductor is cheap, highly responsive to UV or visible irradiation, and photostable with less toxicity [215–217]. Though TiO<sub>2</sub> needs UV radiation for activation, TiO<sub>2</sub> doped with N-graphene (5 wt%) was able to degrade 60% of dye within 3 h under visible light [218]. Here, doping with N, because it is more electron rich, converted TiO<sub>2</sub> into O–Ti–N, and reduced the binding energy of Ti due to less electronegativity of N over O [219–221]. Graphene provided high surface area for rapid adsorption and quick attachment of organic

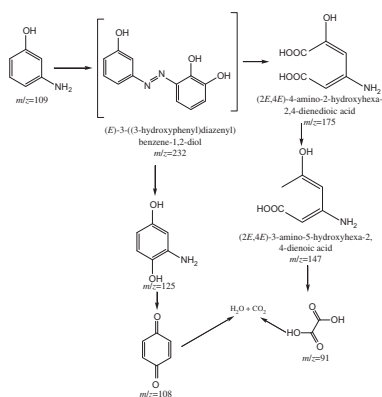


**FIGURE 13.20** proposed degradation pathway of 3-aminophenol over the surface of bimetallic metal oxides nanoparticles.

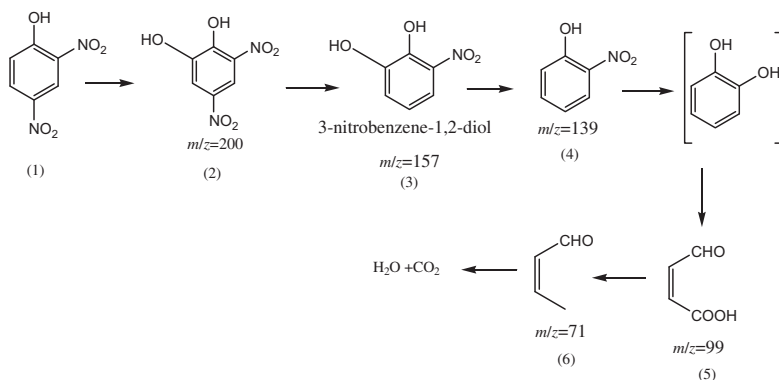


**FIGURE 13.21** Proposed degradation pathway of 2,4-dinitrophenol over the surface of bimetallic metal oxides nanoparticles.

materials to nanocomposites. Doping also introduced the new energy level via the inclusion of metal oxides or electron rich elements and hence, reduced the band gap and shifted the absorption to longer wavelengths. Doped FNPs are more efficient in the removal of most contaminants by formation of nontoxic, unstable byproducts or mineralization in short intervals. The combination of CuO and silver with TiO<sub>2</sub> further reduced the degradation time for dye (100% within 45–160 min) [218,222]. Other examples are Hes–TiO<sub>2</sub> (Hesperidin modified TiO<sub>2</sub>), graphene oxide and TiO<sub>2</sub> doped with Sr<sup>2+</sup> [168,223], and Fe<sup>3+</sup> and Pt<sup>4+</sup> impregnated TiO<sub>2</sub> nanostructures used for the rapid removal of organic colorants [224].

ZnO has gained attention over the past few years because of doping using n-type and p-type conductivity, that has resulted in high transparency, piezoelectricity, and chemical-sensing effects. However, ZnO has the possibility of photocorrosion and a decrease of photocatalytic activity in aqueous

solutions. Methyl orange was massively (95%) removed by Al-doped ZnO (3% of Al) in 2 h [225], but Ag needed 12 h for the same process [226]. Transition metal-doped ZnO nanoparticles converted MO into eleven intermediates [227]. Iron nanoparticles ( $\text{Fe}^0$ ,  $\text{Fe}_3\text{O}_4$ ) removed the organic contaminants (OCs) via redox reaction. Congo red was effectively removed by  $\text{Gd}^{3+}$ -doped cobalt ferrites [228], magnetic  $\text{Sr}_5(\text{PO}_4)_3(\text{OH})/\text{Fe}_3\text{O}_4$  [229,230], sulfanilic acid-modified P25  $\text{TiO}_2$  [231], and bimetallic Fe–Zn nanoparticles [232]. Due to higher extent of  $\cdot\text{OH}$  radicals produced, Alizarin red S (ARS) was removed by polypyrrole-coated  $\text{Fe}_3\text{O}_4$  (60 min) and ZnO/poly (1-naphthylamine) nanoparticles in acidic pH [233]. ARS degraded in to smaller byproducts under microwave radiation using ZnO nanohybrids by Riaz et al. [234].

Introduction of  $-\text{COOH}$  and  $-\text{NH}_2$  group on silica improved its selectivity and adsorption capacity rate due to its high surface areas and robust electrostatic interactions (47–51). The  $-\text{COOH}$  functionalized cubic cage-type KIT-5 mesoporous silica exhibited excellent adsorption capacities for different types of cationic dyes in comparison to pure silica KIT-5. CuI–CuO nanocomposites [235] also exhibited high catalytic efficiency at neutral pH due to lesser ion screening of  $\text{H}^+$  and  $\text{OH}^-$  ions. ZnSe/graphene [236], copper-clay [237], Th(IV) tungstomolybdate [238], ZnS quantum dots (QDs) with  $\text{Fe}^{3+}$  ions [239], BiOBr/montmorillonite composite, Pt-graphene and Pd-graphene [240], and Ta-doped ZnO nanocomposites [241] are also reported for remediation of dye. For cationic dye, the nanographite/ $\text{Fe}_3\text{O}_4$  composite was favored at pH more than 10.0 because of increased negative charges [242]. Ag/ZnO/graphene oxide gave better results (95% degradation in 8 min) for rhodamine B under solar light irradiation [243]. Green synthesized ZnO/GO nanocomposite had better efficiency for Brilliant blue-R, and other dyes than annealed ones (90.64% degradation) [187,244,245]. Table 13.4 represents various NMs used for the degradation of various organic dyes. Recently [102] reported facile green synthesis of various MOs functionalized with PMMA and their use for the degradation of methylene blue dye. Figs. 13.22 and 13.23 represents the FE-SEM images of nanocomposites and the degradation profile of methylene blue. A reusability analysis of nanocomposites for MB degradation also revealed that it was recyclable ten times without significant loss in the activity. Photodegradation of Eriochrome Black T using  $\text{Fe}^{3+}$  and  $\text{Pt}^{4+}$  impregnated  $\text{TiO}_2$  nanostructures was reported. The degradation profile is presented as Fig. 13.24 [246]. The degradation pathway is presented as Fig. 13.25.  $\text{BiVO}_4$  and gold nanoparticles loaded on activated carbon. [247,248],  $\text{Sn}/\text{Al}_2\text{O}_3$  [249], Pd–ZnS/rGO [250], and Pt- and Pd-graphene nanocomposites [240] were also reported as photocatalysts for dye.

**TABLE 13.4** List of various Nanoparticles used for dye degradation.

Nanoparticles	Dye	Remarks	References
Nanocrystalline TiO <sub>2</sub> /activated carbon composite	Chromotrope 2 R	Effective photodegradation under UV irradiation with 80-activated carbon-TiO <sub>2</sub> calcined at 450°C. Initial quantum yield = 1.01%	Wang et al., 2007
Sr <sub>5</sub> (PO <sub>4</sub> ) <sub>3</sub> (OH)/Fe <sub>3</sub> O <sub>4</sub> (0.20 g)	Congo red	89% Adsorption capacit	Zhang et al., 2016 [206]
Bimetallic Fe/Ni–Polyacrylic acid functionalized commercial polyvinylidene fluoride membrane	Methyl orange	More than 80% degradation within 120 min at pH 4.0 due to formation of nickel hydride, which facilitated azo dye adsorption process	Sikhwivhilu and Moutloali, 2015
Intercalated CdS into titanate (0.08 g)	Congo red	Complete removal in 15 min	Sehati and Entezari, 2016
Silver–TiO <sub>2</sub> nanocomposites	Eosin Y	100% degradation with 50% of mineralization in 160 min	Alfaro et al., 2011 [198]
Multielement-doped ZrO <sub>2</sub>	Indigo carmine	Complete photodegradation with Eu, C, N, S-doped ZrO <sub>2</sub> (0.6% Eu) in 150 min	Agorku et al., 2015
Cr-doped titanium oxide	Methyl orange	Nearly 90% of the dye was degraded using 5% mol Cr <sup>3+</sup> -doped TiO <sub>2</sub> nanoparticles in a time period of around 350 min	Hamadianian et al., 2014
Bimetallic Fe/Pd	Orange II	98% Degradation with green synthesized bimetallic nanoparticles and only 16% of the dye removal with Fe nanoparticles	Luo et al., 2016 [177]
Au loaded on activated carbon (0.015 g)	Alizarin red S	More than 95% degradation in 5 min	Roosta et al., 2014 [211]

(Continued)

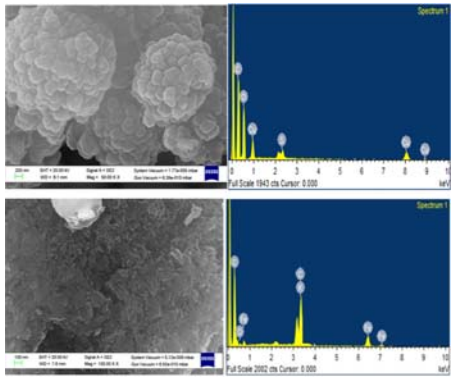


**TABLE 13.4 (Continued)**

Nanoparticles	Dye	Remarks	References
$\text{Cu}_{0.5}\text{Mn}_{0.5}\text{Fe}_2\text{O}_4$ nanospinels	Brilliant green	The adsorption order: $\text{MnFe}_2\text{O}_4 < \text{CuFe}_2\text{O}_4$ $< \text{Mn}_{0.2}\text{Cu}_{0.8}\text{Fe}_2\text{O}_4$ $< \text{Mn}_{0.8}\text{Cu}_{0.2}\text{Fe}_2\text{O}_4$ $< \text{Mn}_{0.4}\text{Cu}_{0.6}\text{Fe}_2\text{O}_4 < \text{Mn}_{0.5}\text{Cu}_{0.5}\text{Fe}_2\text{O}_4(92\%)$	Hashemian et al., 2015
Nanocrystalline $\text{CoFe}_2\text{O}_4$	Brilliant blue-R	65–93% adsorption within 1 min; equilibrium in 60–120 min	Khan et al., 2015
Graphene quantum-dots	New fuchsin (6 mg/L)	95.83% degradation within 110 min	Roushani et al., 2015
CdS embedded on Zeolite A	Crystal violet	80% photodecolorization in 20 min under sunlight	Nezamzadeh-Ejhieh and Banan, 2012
Nanographite/ $\text{Fe}_3\text{O}_4$ composite	Methyl violet	98.9% degradation at pH above 10; adsorption of the dye strongly increased with increasing pH because increased negative charges favors the interaction between cationic dye and negatively charged adsorbent	Li et al., 2014 [220]
1%Ta-doped ZnO	Methylene blue	99% degradation at pH 8.0 with catalyst annealed at 700 °C at low alkaline pH, high hydroxylation of the catalyst surface attracts the cationic dye	Kong et al., 2010 [219]
CuI–CuO nanocomposite	Malachite green	High adsorption capacity = 136.6 mg/g in a time less than 20 min	Nekouei et al., 2016 [214]

### 13.7.1 Degradation of pesticides by functionalized NMs

Like dyes, FNPs based on  $\text{TiO}_2$ , ZnO, and  $\text{Fe}^0$  were reported as being the most economic, rapid, and effective photocatalysts for pesticides (80%–100% removal) under UV irradiation and sunlight. They not only adsorbed



**FIGURES 13.22** FE-SEM & EDS patterns of ZnO–PMMA, Ni<sub>2</sub>O<sub>3</sub>–PMMA, CuO–PMMA, and Fe<sub>2</sub>O<sub>3</sub>–PMMA nanocomposite.

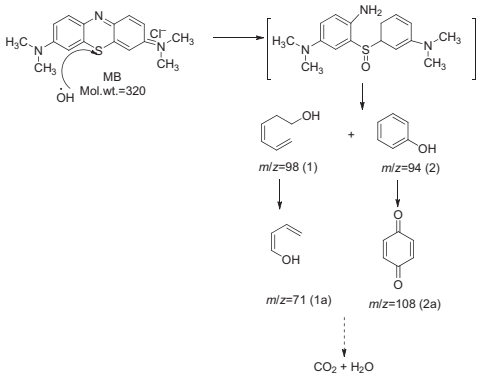


**FIGURE 13.23** Proposed degradation pathway for the degradation of MB over ZnO–PMMA nanocomposite (concentration; 2 mg/L; pH: ~7; catalyst dose: 80 mg; natural sunlight).

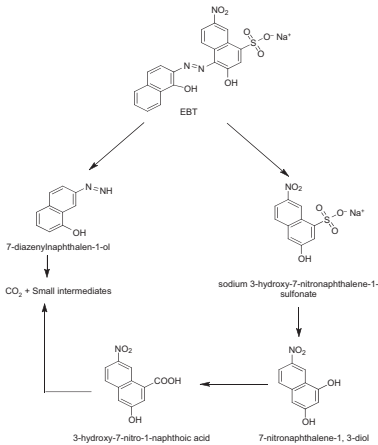


**FIGURE 13.24** Possible pathway for the photo-degradation of Eriochrome Black T using Fe<sup>3+</sup> and Pt<sup>4+</sup> impregnated TiO<sub>2</sub> nanostructures [246].

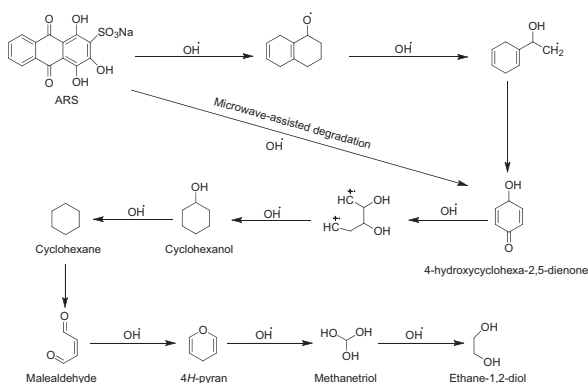


**FIGURE 13.25** Degradation pathway of Alizarin Red S using nanohybrid of ZnO [234].

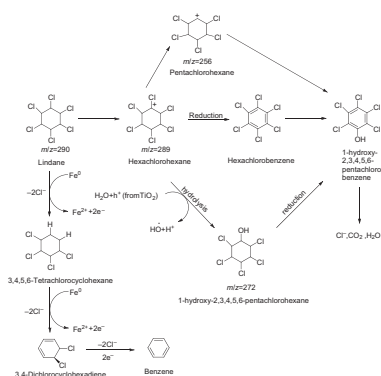


**FIGURE 13.26** Proposed degradation pathway of lindane using N-doped TiO<sub>2</sub> [251] and zero-valent iron [255].

contaminants, but also degraded them via photocatalytic, redox, and reactive methods.  $\text{H}_2\text{O}_2$  further improved their oxidative efficiency with more  $\bullet\text{OH}$  radicals produced. Only the OCs and OPs were frequently degraded by  $\text{ZnO}/\text{clay}$ ,  $\text{Fe}/\text{zeolite}$  and  $\text{TiO}_2/\text{zeolite}$ , and  $\text{TiO}_2/\text{chitosan}$  (e.g., nanobiocomposites with enhanced activity and biocompatibility). Not much attention has been paid to emerging contaminants like carbamates and substituted urea.

Photocatalytic efficiency of TiO<sub>2</sub> doped with nitrogen (1.6:1 molar ratio) is almost double for OCs than that of bare TiO<sub>2</sub> [250], (2008). Lindane was degraded successfully with N-doped TiO<sub>2</sub> (Fig. 13.26) [251] and bimetallic Fe-Pd within 8 h [252]. Bimetallic Ni-Fe nanostructures were found to have potential at weakly acidic or alkaline pH for degradation of DDT [253] (Fig. 13.27). Aldrin, endrin, and lindane were massively adsorbed by Fe<sub>3</sub>O<sub>4</sub>-polystyrene [254]. On the other hand, C-ZnO-CdS combination worked on photocatalysis for 98% removal of 4-chloro phenol [174] (Fig. 13.28).

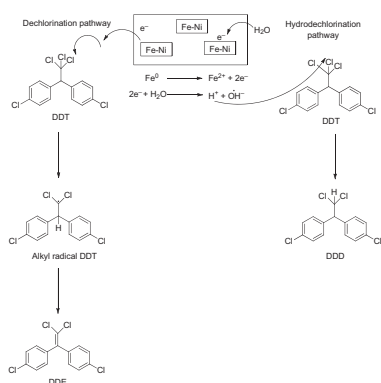


**FIGURE 13.27** Tentative degradation pathway of DDT using Ni/Fe bimetallic nanoparticles [253].

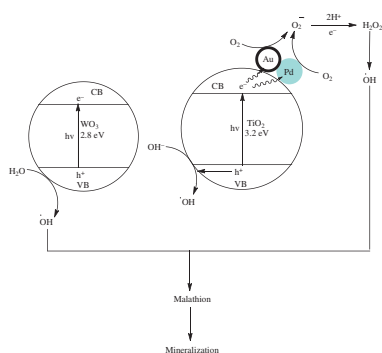


**FIGURE 13.28** Photodegradation of malathion in presence of TiO<sub>2</sub>/WO<sub>3</sub> [256] and Au-Pd-TiO<sub>2</sub> nanofilm [257].

### 13.8 Degradation of Organophosphorus (OP) pesticides by FNM

Comparable OCs, TiO<sub>2</sub>, and iron-based FNP worked as heterogeneous photocatalysts for remediation of commonly used OPs like malathion, chlorpyrifos, and parathion methamidophos [258–263]. Under solar irradiation, malathion was completely removed by photocatalyst 2% WO<sub>3</sub>/TiO<sub>2</sub>, while 47% mineralization was obtained with bare TiO<sub>2</sub> [256]. Doping with two or more transition metals further improved the efficiency, or quantum yield, of surface processes due to an increase in the number of energy levels between CB and VB edge of TiO<sub>2</sub> as well increase in surface area (Malathion removal: 172% with Au-Pd-TiO<sub>2</sub> nanotube film) [257]. Moreover, metal ions facilitated charge parting of e<sup>-</sup> and h<sup>+</sup> and acted as charge-carrier trappers. On the basis of doping identity and concentration, a number of Ti<sup>3+</sup> ion with more surface defects are produced and enable effectual adsorption of atmospheric or moisturized oxygen on a titania surface. Charge transfer transition of electrons occurs between energy levels of dopants and TiO<sub>2</sub>

[264].  $\text{TiO}_2$  functionalized with Ag and Au are effectively employed for the degradation of OPs containing phenols at  $\text{pH} \sim 3$  [265]. Monocrotophos and quinalphos were degraded to their maximum extent using  $\text{ZnO}/\text{TiO}_2$  (7:3 or 8:2) [266]. Monocrotophos with dichlorvos and phoxim were eradicated by doped nanocomposites  $\text{TiO}_2 \cdot \text{SiO}_2$  beads,  $\text{TiO}_2$  supported on zeolite,  $\text{IO}_3 - \text{TiO}_2$ , La– $\text{ZnO}$ , and La-doped  $\text{TiO}_2$  [267,268–270]. Other FNPs used for the treatment of OPs (e.g., dichlorvos, monocrotophos, malathion) are  $\text{ZnO}$ –zeolite,  $\text{CuO}$ –chitosan,  $\text{CuO}$ –montmorillonite–chitosan, and  $\text{CuO}$ –montmorillonite gumghatti nanobiocomposites (biopolymers are good adsorbents) [271–273]. Henych et al., [274] demonstrated reactive degradation of toxic OPs like malathion and parathion methyl with mixed metals and their oxides in organic medium. The efficiency composites order was as follows:  $\text{Ti}/\text{Ce}$  oxides (2:8 and 1:1 molar ratio) > nanotitania;  $\text{TiO}_2/\text{CeO}_2$  > pure  $\text{CeO}_2$ .

Both surface area and porosity were enhanced for OPs due to a solid collaboration of Ti with Ce that resulted in high production of  $\text{Ce}^{3+}$  and formation of  $\text{Ti}^{4+}$  states. A few degradation studies by FNMs are also available on miscellaneous pesticides like carbamate and SU.  $\text{TiO}_2$  functionalized with polyacrylonitrilenanofiber and Fe supported on Zeolite was used for complete oxidation of aldicarb and Methomyl under UV radiation, respectively [273,275]. Gold doped to  $\text{ZnO}$  and  $\text{TiO}_2$  increased the degradation percentage of chloridazone within a shorter time due to prevention of the electron-hole recombination [276]. In similar way,  $\text{FeO}/\text{Fe}_3\text{O}_4$  and  $\text{Fe}_3\text{O}_4/\text{Au}$  composite worked for thiamethoxam and imidacloprid removal at acidic pH from water under irradiation [277]. Depending on the absence or presence of  $\text{H}_2\text{O}_2$ ,  $\text{FeO}/\text{Fe}_3\text{O}_4$  behaved as reducing or as oxidizing catalysts [278]. Ru doped  $\text{TiO}_2$  and Ag/chitosan nanobiocomposite used for 80–98% removal of metsulfuron-methyl and Atrazine [279,280] while only 40% achieved with bare MOss. Further details of various OCs and OPs and other pesticides degraded by FNMs are shown in Table 13.5 and 13.6.

### 13.8.1 Degradation of phenols and BPA by FNMs

Phenols, nitro as well amino, are extensively used in industries as reactants/intermediates for synthesis of dyes and pesticides. Therefore they are found in abundance in the environment due to industrial discharges and breakdown of those organic compounds. They are employed as prototypical for acute estimation of photoactivity of synthesized FNPs. The modified FNPs (e.g., doped, composite, Fenton type) that are used for treatment of dyes and pesticides are almost adapted for degradation of phenols and amines from wastewaters in UV and visible light. For example, Pr– $\text{TiO}_2$  [281], Bi– $\text{TiO}_2$  nanotubes [282],  $\text{TiO}_2$  and  $\text{ZnO}$  composites with graphene (Malekshoar et al., 2014), and  $\text{TiO}_2$  and  $\text{CuO}$  functionalized with  $\text{H}_2\text{O}_2$  [281,283]. FNPs are highly active due to the synergistic effects of their constituents:

**TABLE 13.5** List of various OCs and OPs pesticides degraded using nanoparticles.

Pesticide (/mgL)	Nanoparticles	Brief summary	Mechanism	Reference
Lindane ( $5 \times 10^{-4}$ mmol/L)	Degussa P-25, Anatase TiO <sub>2</sub> , N-doped TiO <sub>2</sub>	Effectively degraded (100%) under visible light, $k = 0.099/\text{min}$ , $0.117/\text{min}$ , $0.007/\text{min}$	Photodegradation	Senthilnathan and Philip, 2010 [225]
Lindane (5)	FeS stabilized by biopolymers	94% of degradation in 8 h	Oxidative degradation	Paknikar et al., 2005
Aldrin, Endrin, Lindane	Fe <sub>3</sub> O <sub>4</sub> supported on polystyrene	24.7 mg/g, 33.5 mg/g, 10.2 mg/g	Adsorption	Jing et al., 2013 [228]
DDT (150 mL of 100 µg/mL)	Bimetallic Ni/Fe	Effective degradation in 4 h with higher efficiency in alkaline or weakly acidic medium, $k = 0.6073/\text{s}$	Redox degradation	Tian et al., 2009 [227]
Lindane (1)	Bimetallic Fe–Pd	Degraded under: aerobic (65%;) and anaerobic (100%)	Redox degradation	Joo et al., 2008
Di and tri chlorophenoxy acetic acid (20)	ZnO/ $\gamma$ -Fe <sub>2</sub> O <sub>3</sub>	55.2 and 57.0%	Photocatalytic degradation	Abdullah et al., 2013
4-Chloro phenol (10)	C/ZnO/CdS	98.0% in 120 min	Photocatalytic degradation	Lavand and Malghe, 2015 [155]
Lindane	Ag-reduced GO	99.9%	Degradation	Gupta et al., 2015
Monocrotophos, dichlorv (20)	TiO <sub>2</sub> –Zeolite	100%	Photocatalysis	Gomez et al., 2015 [241]

*(Continued)*

**TABLE 13.5 (Continued)**

Pesticide (/mgL)	Nanoparticles	Brief summary	Mechanism	Reference
Phoxim (20)	La-doped TiO <sub>2</sub>	Complete mineralization after 4 h	Photocatalysis	Dai et al., 2009 [242]
Monocrotophos, quinalphos	ZnO/TiO <sub>2</sub>	84.2% and 96%, k = 0.00567/min and 0.00199/min	Photocatalysis	Kaur et al., 2013 [238]
Malathion (10) ppm	ZnO, TiO <sub>2</sub> , Au/ZnO	30.0% degradation within 30 min	Photocatalysis	Fouad and Mohamed, 2012 [247]
Malathion (12)	TiO <sub>2</sub> (anatase)/WO <sub>3</sub> (2 wt.%)	Complete degradation after 2 h	Photocatalysis	Ramos-Delgado et al., 2013
Chlorpyrifos, cypermethrin, chlorothalonil	Coating of Fe-granular-activated carbon	With H <sub>2</sub> O <sub>2</sub> (100 mg/L), complete degradation in 1 min K = 0.017 – 0.024/min	Oxidation	Affam et al., 2015
Chloropyrifos (10)	Au and Ag supported on Al	Complete degradation within 3 h	Adsorption	Bootharaju and Pradeep, 2012
Monocrotophos (16)	ZnO supported on Zeolite	100% degradation in 4 h	Photocatalysis	Tomasevic et al., 2010 [245]
Malathion (2)	CuO–Chitosan	99.9% (k = 0.53 g/mg/min)	Adsorption	Jaiswal et al., 2012 [243]
Chlorpyrifos (5)	CoFe <sub>2</sub> O <sub>4</sub> @TiO <sub>2</sub> –reduced G	89.9% in 60 min	Photocatalysis	Gupta et al., 2015
Dichlorvos (20–100)	CuO–MMT	83.2%	Adsorption	Sahithya et al., 2015 [244]

*(Continued)*

**TABLE 13.5 (Continued)**

Pesticide (/mgL)	Nanoparticles	Brief summary	Mechanism	Reference
Dichlorvos (20–100)	CuO–MMT supported on chitosan Gum ghatti and poly lactic acid	93.4, 87.8 and 63.3% removal, respectively	Adsorption	Sahithya et al., 2015 [244]
Parathion methyl (PM)	Titania-iron mixed oxides	Highest degradation (< 70%) with Ti:Fe ratio 0.25)	SN <sub>2</sub>	Henych et al., 2015
PM(100 µL of 10,000 mg/L)	Titania-ceria mixed oxides	Highest degradation at Ti:Ce 2:8 and 1:1 molar ratio	SN <sub>2</sub>	Henych et al., 2016 [246]
Glyphosate	Fe <sub>3</sub> O <sub>4</sub> @SiO <sub>2</sub> @UiO-67	High adsorption capacity (256.54 mg/g), low detection limit (0.093 mg/L) for glyphosate	Synchronous Adsorption/ detection	Yang et al., 2018
Atrazine	Iron oxide nanoparticles and chitosan	Maximum removal of 91.6%–96% removal	Uniform nanoporous ultrafiltration membrane	Mukherjee et al. 2018 [250]



**TABLE 13.6** List of various miscellaneous pesticides (including carbamate and pyrethroid) degraded using nanoparticles.

Pesticide(mg/L)	Bulk/nanoparticles	Brief summary	Mechanism	References
Methomyl(16) (Carbamate)	Fe–zeolite(1or 5 g/L)	100% degradation in 4 h	Photocatalysis	Tomasevic et al., 2010 [245]
<i>Pyridazinone Pesticides:</i> Chloridazon (10)	Au/TiO <sub>2</sub> (10 <sup>-4</sup> , 3 × 10 <sup>-5</sup> , 10 <sup>-5</sup> M)	50% in 30 min	Photocatalysis	Fouad and Mohamed, 2012 [247]
Chloridazon (20)	Fe <sub>3</sub> O <sub>4</sub> and coreshell Fe <sub>3</sub> O <sub>4</sub> @Au (10 <sup>-4</sup> M)	> 90% degradation	Photocatalysis	Fouad and Mohamed, 2011 [248]
Permethrin (25 ml, 0.1 mg/L) (Pyrethroid Pesticide)	ZnO–chitosan (0.5 g)	99%	Adsorption	Dehaghi et al., 2014
<i>Neonicotinoids Pesticides:</i> Imidacloprid, Thiamethoxam, Clothianidin	Immobilized TiO <sub>2</sub>	Mineralized within 2 h with k = = 0.035, 0.019, and 0.021/min, respectively.	Photocatalysis (UV)	Zabar et al., 2012
Imidacloprid, Isoproctum, Phosphamidon (1.14 × 10 <sup>-4</sup> M each)	5 wt% TiO <sub>2</sub> supported on porous nanosilica (3 g/L)	At neutral pH, degradation within 90, 240, and 120 min, respectively.	Photocatalysis (UV)	Sharma et al., 2009
Thiamethoxam (20 mL; 50 mg/L) Imidacloprid (20 mL; 35 mg/L)	Fe/Fe <sub>3</sub> O <sub>4</sub> (0.06 mol/L) with/or H <sub>2</sub> O <sub>2</sub>	> 90% in 30 min, highly efficient in acidic conditions.	Redox degradation	de Urzedo et al., 2009
Atrazine (2 g)	Ag-chitosan (1 L of 1 mg/L)	98% degradation in 65 min.	Adsorption	Saifuddin et al., 2011 [249]

$\text{FeWO}_4@\text{ZnWO}_4/\text{ZnO}$   $\text{ZnWO}_4/\text{ZnO}$  and  $\text{FeWO}_4$  [285] and  $\text{CuO}-\text{Co}_3\text{O}_4@\text{MnO}_2$  activated with peroxymonosulfate  $\text{Cu}@\text{MnO}_2$  and  $\text{Co}@\text{MnO}_2$  alone [286].

BPA is found in industrial and domestic household wastewater, and extensive studies are available on its degradation or removal via selective adsorption and photodegradation (Table 13.8). The examples of catalysts are:  $\text{ZnFe}_2\text{O}_4-\text{ZrO}_2$ , Au deposited on  $\text{TiO}_2$  [287],  $\text{TiO}_2/\text{graphene}/\text{Cu}_2\text{O}$  [288],  $\gamma\text{-C}_3\text{N}_4/\text{BiOBr}$  [289], Pd-mesoporous graphite carbon nitride (Pd/mpg- $\text{C}_3\text{N}_4$ ) [290], and hybrid iron core-shell magnetic catalysts [291], Fenton like catalyst Cu-doped  $\text{AlPO}_4$  with  $\text{H}_2\text{O}_2$  [292]. More details about degradation of phenols and BPA are summarized in Table 13.7 and 13.8.

### 13.8.2 Degradation of PAHs by FNMs

Compared to dyes and pesticides, emerging PAHs are studied less than functionalized NM photocatalysts in assisted degradation. Reasons for this might include less knowledge about PAH standards and their expensiveness. For removal of PAHs  $\text{TiO}_2$ - and  $\text{ZnO}$ -based FNPs were used extensively for complete and quick mineralization. FNPs potential was observed in their lack of toxic byproducts and short-lived metabolites. Ti doped to  $\text{ZnO}-\text{Cr}_2\text{O}_3$  and La/N codoped  $\text{TiO}_2$  supported on activated carbon are employed for quantitative removal of naphthalene within 2–4 h via photo-mechanism [293,294]. In the absence of light, a hybrid, gel-derived  $\text{ZrO}_2$ -acetylacetonate was used for whole mineralization of phenanthrene in wastewater at 30°C [295]. Phenanthrene, being stable, was quickly removed with  $\text{Co}-\text{TiO}_2$  nanotubes compared to that of native  $\text{TiO}_2$ , which took 12 h for its degradation [296]. Chrysene was degraded with curcumin-modified, conjugated  $\text{ZnO}$  ( $\text{Zn}(\text{cur})\text{O}$ ) within 2.2 h [297]. A mixture of  $\text{TiO}_2/\text{Fe}_2\text{O}_3$  rapidly removed BaP in 90 h using only  $\text{TiO}_2$  (363 h), further suggesting the importance of functionalization [298]. Fatty acids coated on  $\text{Fe}_3\text{O}_4$  showed rapid adsorption (5 min) of BaP and indicated excellent adsorbency at room temperature [299]. High-molecular-weight PAHs, such as BP, IP, BKF, and DBA, are presumed to treat environmental pollutants with new, advanced, and more efficient FNPs due to their high stability, longer half-lives, and recalcitrance to biodegradation. Table 13.9 represents various PAHs degraded by some of the FNMs.

## 13.9 Toxicity and functionalized nanoparticles

Functionalized NPs are used as multifunctional tools in nanobiotechnology and medicine [300–302]. Subbiah et al. [303] reviewed the safe and widespread applications of functionalized NPs in biomedicine. FNPs are better than traditional therapeutics and nearly 26 FNP-based medicines are in medical use (Zhang et al., 2008). For example, greater antibacterial characteristics

**TABLE 13.7** Comparison data for degradation of phenols using nanoparticles.

Target	Nanoparticles	Brief summary	Mechanism	References
Phenol	Ultrasound/H <sub>2</sub> O <sub>2</sub> /CuO process	Oxidant: H <sub>2</sub> O <sub>2</sub> , reaction temperature: 29.5°C	Heterogeneous catalyst	Drijvers et al., 1999
Phenol (40 mg/L)	Graphene-based titanium dioxide and zinc oxide composites (TiO <sub>2</sub> -G, ZnO-G)	Complete degradation within 60 min while using coupled ZnO-G/TiO <sub>2</sub> -G photocatalysts	Photocatalytic activity (solar)	Malekshoar et al., 2014
Phenol	FeWO <sub>4</sub> @ZnWO <sub>4</sub> /ZnO	Photocatalytic activity: FeWO <sub>4</sub> @ZnWO <sub>4</sub> /ZnO composite > than FeWO <sub>4</sub> and ZnWO <sub>4</sub> /ZnO; synergetic effect of ZnWO <sub>4</sub> /ZnO and FeWO <sub>4</sub> @ZnWO <sub>4</sub> /ZnO	Visible-light photocatalytic activity	Wang et al., 2016
Phenol	Pr-doped TiO <sub>2</sub> (1 g/L)	Complete degradation in aqueous solutions after 2 h irradiation; 0.072 mol% of Pr(III)	Photocatalytic degradation	Chiou and Juang, 2007
Phenols (30 mg/L)	Peroxymonosulfate activated by CuO-Co <sub>3</sub> O <sub>4</sub> @MnO <sub>2</sub>	Synergistic effect between bi-metallic oxides of Cu and Co; 100%; Efficient 0.5%Cu-2%Co-MnO <sub>2</sub> than 0.5%Cu@MnO <sub>2</sub> or 2%Co@MnO <sub>2</sub> alone	Photocatalytic degradation	Khan et al., 2017
Phenol	Bismuth-doped TiO <sub>2</sub> nanotubes composite	Efficiency: bismuth doped TiO <sub>2</sub> (by a factor of 4) > undoped TiO <sub>2</sub> rate was 5.2 times faster due to OH• and superoxides	Photocatalytic degradation (visible light)	Ali et al., 2017
2,4-dinitrophenol (2,4-DNP) (40 mg/L)	Al <sub>2</sub> O <sub>3</sub> -supported Fe(III)-5-sulfosalicylic acid (ssal) complex 1.0 g/L	pH 2.5; 30 °C; c H <sub>2</sub> O <sub>2</sub> : 5 mmol/L; 100 min	Solar-light-assisted Fenton oxidation	Wang et al., 2010 [126]
(Continued)				

**TABLE 13.7 (Continued)**

Target	Nanoparticles	Brief summary	Mechanism	References
2,4-DNP	Popcorn balls-like ZnFe <sub>2</sub> O <sub>4</sub> –ZrO <sub>2</sub> microsphere	rate of ZnFe <sub>2</sub> O <sub>4</sub> –ZrO <sub>2</sub> photocatalyst (mass ratio of ZnFe <sub>2</sub> O <sub>4</sub> /ZrO <sub>2</sub> = 2:1) was almost 7.4 and 2.4 times higher than those of pure ZnFe <sub>2</sub> O <sub>4</sub> and ZrO <sub>2</sub>	Photocatalytic degradation (simulated solar visible)	Chen et al., 2017
2,4-DNP	Nanosized particles of TiO <sub>2</sub>	At a pH of 8, 70% removal within 7 h	Photocatalytic degradation (UV)	Shukla et al., 2009
2,4-DNP	ε-Bi <sub>2</sub> O <sub>3</sub> /Bi <sub>2</sub> MoO <sub>6</sub> composites	Solar and visible light irradiation	Photocatalytic degradation	Ma et al., 2014
2,4-DNP	Bamboo-inspired hierarchical nanoarchitecture of Ag/CuO/TiO <sub>2</sub> nanotube array	Under simulated solar light irradiation, the 2,4-dinitrophenol (2,4-DNP) photocatalytic degradation rate over Ag/CuO/TiO <sub>2</sub> was about 2.0, 1.5, and 1.2 times that over TiO <sub>2</sub> nanotubes, CuO/TiO <sub>2</sub> and Ag/TiO <sub>2</sub> , respectively	Photocatalytic degradation	Zhang et al., 2016 [206]
3-Aminophenol	Aqueous TiO <sub>2</sub> suspensions	TiO <sub>2</sub> P25 Degussa as the photocatalyst	Photodegradation	San et al., 2001
p-Aminophenol (20 mg/L)	CuO supported Clinoptilolite (2.0 g/L)	H <sub>2</sub> O <sub>2</sub> and potassium bromate considerably increased the rate of degradation at pH 6.0	solar photocatalytic degradation	Nezamzadeh-Ejhieh and Amiri, 2013

**TABLE 13.8** Comparison data for degradation of BPA by several nanoparticles.

Nanoparticles	Brief summary	Mechanism	References
TiO <sub>2</sub> –zeolite sheets	Composite TiO <sub>2</sub> –zeolite sheets > zeolite-free TiO <sub>2</sub> sheets indicated synergistic effect of combined use	Photodecomposition, UV irradiation	Fukahori et al., 2003
CoMnAl	Typically, 10 mg/L of BPA could be completely degraded under the coexistence of 0.02 g/L of CoMnAl–MMO and 0.15 g/L of Oxone within 90 min at 25 C	Catalytic degradation	Li et al., 2015
TiO <sub>2</sub> and platinized TiO <sub>2</sub>	At pH 3, 20 mg/L of BPA, completely mineralized into CO <sub>2</sub> after 120 min of UV illumination. However, only 20–30% of the carbon from the BPA was converted into CO <sub>2</sub> for the same illumination time at pH 10	Photocatalytic degradation (UV) and mineralization	Chiang et al., 2004
Immobilized TiO <sub>2</sub>	UV illumination in a horizontal circulating bed photocatalytic reactor (HCBPR)	Photocatalytic degradation	Wang et al., 2009
Ce–ZnO	Ce-ZnO (2%) achieved 100% BPA degradation and 61% BPA mineralization after 24 h	Photocatalytic degradation	Bechambi et al., 2016
Fe <sub>x</sub> Co <sub>3–x</sub> O <sub>4</sub> nanocages	By activation of peroxymonosulfate	Catalytic degradation	Li et al., 2016
graphite-C <sub>3</sub> N <sub>4</sub> /BiOBr	More efficiency than that of pure BiOBr	Visible light irradiation	Xia et al., 2014 [255]
Au deposited on TiO <sub>2</sub>	Small amount of rutile only beneficial	UV-visible light	Cojocaru et al., 2017 [253]
Cu-doped AlPO <sub>4</sub>	Cu(0.05)-AlPO <sub>4</sub> with Cu/Al molar ratio of 0.05 was highly effective and stable in the presence of H <sub>2</sub> O <sub>2</sub>	Fenton-like catalyst	Zhang et al., 2017 [257]
Pd-doped mesoporous (Pd/mpg-C <sub>3</sub> N <sub>4</sub> )	100% degradation in 360 min OH, h <sup>+</sup> and O <sup>2–</sup> were reason for the degradation while the O <sup>2–</sup> was more predominant	Photocatalytic-simulated solar light irradiation	Chang et al., 2013 [258]
ZnHCF@ ZnO	ZnHCF@ZnO (97%) > ZnHCF (88%), > ZnO (75%)	Sunlight	Rani and Shanker, 2018 [102]

**TABLE 13.9 PAHs degradation by various FNMs.**

PAH	Nanoparticles	Remarks	Mechanism	References
BaP	Fe <sub>3</sub> O <sub>4</sub> coated with fatty acids	Adsorption within 5 min at RT	Adsorption	Liao et al. 2015 [263]
Chrysene	Curcumin conjugated ZnO	100% removal in 2.2 h	Photodegradation	Moussawi and Patra
Naphthalene	La and N co-doped TiO <sub>2</sub> supported on activated carbon	Efficient degradation (93.5%) within 120 min	Photodegradation	Liu et al. 2016 [259]
Phenanthrene	Co-doped titanate nanotubes	98.6% removal in 12 h	Photodegradation	Zhao et al. 2016 [261]
BaA	Fe <sup>3+</sup> + -modified montmorillonite	17% in 6 h		Zhao et al., 2017
Chrysene	Fe <sub>2</sub> O <sub>3</sub> @ZnHCF	92% in 24 h	Photodegradation	Rachna et al. 2018 [87]
BaP BaA	ZnHCF@ZnO (distorted nanocubes) ZnHCF (nanocubes, 108.70 m <sup>2</sup> /g) ZnO (Flower shaped, 12 m <sup>2</sup> /g)	BaP: ZnHCF@ZnO (90%) > ZnHCF 65%) > ZnO (38%) in 24 h BaA: ZnHCF@ZnO (93%) > ZnHCF 70%) > ZnO (46%) in 24 h	Photodegradation	Unpublished data

*(Continued)*

**TABLE 13.9 (Continued)**

PAH	Nanoparticles	Remarks	Mechanism	References
ACN, PHN & FLU	TiO <sub>2</sub> @ZnHCF	96%, 95% and 93% in water & 86%, 84%, 82% in soil samples	Photodegradation	Unpublished data
Phenanthrene	Coupling magnetic-nanoparticle mediated isolation			
Benzo[a]pyrene	Starch nanoparticles	95% of BaP degradation was equivalent to 52.9 µg of BaP degraded per gram of starch used: 2.4 and 1.5-fold	Fenton degradation	Delsarte et al., 2018
Phenanthrene and pyrene	Amorphous ferric Hydroxide in combination with sediment microbial fuel cell	PAHs biodegradation with removal efficiencies of phenanthrene and pyrene reaching to 99.47 ± 0.15% and 94.79 ± 0.63% respectively after 240 days of experiments	Anaerobic degradation	Yan et al., 2012
Benzo[a]pyrene	ZnO nanoparticles in combination with yeast	Maximum BaP degradation was found to be 82.67 ± 0.01 (%) at pH 7.0, temperature 30°C 2 g/L of ZnO nanoparticle	Photodegradation	Mandal et al., 2018
Anthracene	n-ZnO/p-MnO nanocomposites	Photodegradation studies of anthracene in an ethanol:water (1:1, pH 12) solution were performed, showing that anthraquinone is the main product with no photodegrading of ethanol. The results suggest that the junction n-ZnO/p-MnO and materials with high transient time constant (τ), enhance the photocatalytic degradation	Photocatalytic	Martínez-Vargas et al., 2019

have been shown by graphene nanohybrids with biocidal magnetic NMs due to dimensional appearances of their sharp edges. Surface roughness or surface-to-volume ratio (via attrition and rubbing) is also enhanced by the introduction of functional groups like  $-\text{COOH}$  and  $-\text{OH}$ . Due to the inhibition of electron-hole recombination, nanocomposites of grapheme (sheets and plates) with  $\text{Ag}_3\text{PO}_4$ ,  $\text{TiO}_2$ ,  $\text{TiO}_2$ , and  $\text{Bi}_2\text{MoO}_6$  have been found to remove microorganisms and *E. coli* under visible light irradiation. Having antimicrobial properties, metals like Ag, Cu, and Zn attached to the membrane could be used as a nondestructive substitute for chlorine decontamination without any harmful byproducts and reduced operating cost. Though grapheme showed limitations in the areas of size reduction and folding tendency, and, hence, less inactivation of the microorganisms, surface modification has the potential to prevent its aggregation tendency.

### 13.10 Conclusions and future perspectives

Functionalization of NMs (e.g., silica, carbonaceous, and metal-based  $\text{ZnO}$ ,  $\text{TiO}_2$ , Fe, Pt and Pd, and  $\text{NiO}_2$ ) for environmental applications were reviewed in this chapter. Various types of functionalization methods, especially the chemical approach for its diversity and ability to decorate NMs with large number of functionalities, were discussed. High production and wide use of innumerable, perilous manmade organics are considered as the prominent sources of water pollution in Asia and worldwide. FNPs may overcome the principal limitations that hinder wide-scale applications of NPs. Due to functionalization, their working ability is enhanced at a neutral pH under UV or solar radiation. FNPs are used wide-range to exclude or remove their destructive impacts via several processes including oxidation, photocatalysis (i.e., generation of electron-hole pairs), and adsorption. Degradation results in more or less complete removal of environmental toxins through mineralization or transformation to less-toxic chemicals in a short span. Green synthesis-produced FNPs with variable morphology and size depend on different biogenic sources (e.g., plant surfactants, microorganisms). The FNPs obtained may have better efficacy than that of chemically synthesized ones because of the role of surfactants that enter the lattice or are sometimes found dispersed on it. However, more time and focused research is needed to employ FFNPs as a milestone in environmental remediation and other commercial nanotechnology.

While green synthesis may result in less expensive and more effective and sustainable FNPs than the mediated degradation process, the use of biopolymer-based functionalized composites should also be encouraged. More research is needed to explore different NMs on traditional or upcoming OPs, carbamates, and SU to ban or restrict them. FNPs with high potential should also be used to treat persisting OCs. For some pollutants like quintonzene, pentachlorophenol and toxaphene, FNPs have never been used.



## References

- [1] Natarajan TS, Thomas M, Natarajan K, Bajaj HC, Tayade RJ. Study on UV-LED/TiO<sub>2</sub> process for degradation of Rhodamine B dye. *Chem Eng J* 2011;169:126–34.
- [2] Jain R, Sikarwar S. Removal of hazardous dye congo red from waste material. *J Hazard Mater* 2008;152:942–8.
- [3] Rani M. Chapter 1–5 Studies on decay profiles of quinalphos and thiram pesticides. Ph.D Thesis. Roorkee, Uttarakhand, India: Indian Institute of Technology Roorkee; 2012.
- [4] Sahoo C, Gupta AK, Pal A. Photocatalytic degradation of methyl red dye in aqueous solutions under UV irradiation using Ag + doped TiO<sub>2</sub>. *Desalination* 2005;181:91–100.
- [5] Mohan D, Singh KP, Singh G, Kumar. Removal of dyes from wastewater using fly ash, a low-cost adsorbent. *Ind Eng Chem Res* 2002;41:3688–95.
- [6] Safavi A, Momeni S. Highly efficient degradation of azo dyes by palladium/hydroxyapatite/Fe<sub>3</sub>O<sub>4</sub> nanocatalyst. *J Hazard Mater* 2012;201–202:125–31.
- [7] William IV L, Ismail AA, Mazyck DW. Impact of heat treatment and composition of ZnO–TiO<sub>2</sub> nanoparticles for photocatalytic oxidation of an azo dye. *Ind Eng Chem Res* 2008;47:1483–7.
- [8] Henze M. Characterization of wastewater for modelling of activated sludge processes. *Water Sci Technol* 1992;25:1–15.
- [9] Rani M, Shanker U. Advanced treatment technologies. In: Hussain CM, editor. *Handbook of environmental materials management*. Springer International Publishing AG; 2018. p. 2018. Available from: [https://doi.org/10.1007/978-3-319-58538-3\\_33-1](https://doi.org/10.1007/978-3-319-58538-3_33-1).
- [10] Rani M, Shanker U. Remediation of polycyclic aromatic hydrocarbons using nanomaterials. Green adsorbents for pollutant removal. Springer International Publishing AG, part of Springer Nature; 2018. Available from: [https://doi.org/10.1007/978-3-319-92111-2\\_10](https://doi.org/10.1007/978-3-319-92111-2_10).
- [11] Rani M, Shanker U. Degradation of traditional and new emerging pesticides in water by nanomaterials: recent trends and future recommendations. *Int J Env Sci Technol* 2018;15:1347–80.
- [12] Rani M, Shanker U, Jassal V. Recent strategies for removal and degradation of persistent and toxic organochlorine pesticides using nanoparticles: a review. *J Env Manage* 2017;190:208.
- [13] Gupta B, Rani M, Kumar R. Degradation of thiram in water, soil and plants: a study by high-performance liquid chromatography. *Biomed Chromatogr* 2012;26:69–75.
- [14] Gupta B, Rani M, Kumar R, Dureja P. Decay profile and metabolic pathways of quinalphos in water, soil and plants. *Chemosphere* 2011;85:710–16.
- [15] Gupta B, Rani M, Kumar R, Dureja P. Identification of degradation products of thiram in water, soil and plants using LC-MS technique. *J Environ Sci Health Part B* 2012;47:823–31.
- [16] Gupta B, Rani M, Salunke R, Kumar R. In vitro and in vivo studies on degradation of quinalphos in rats. *J Haz Mat* 2012;213–214:285–91.
- [17] Prevot AB, Baiocchi C, Brussino MC, Pramauro E, Savarino P, Augugliaro V, et al. Photocatalytic degradation of acid blue 80 in aqueous solutions containing TiO<sub>2</sub> suspensions. *Env Sci Technol* 2001;35:971–6.
- [18] Ratna, Padhi BS. Pollution due to synthetic dyes toxicity & carcinogenicity studies and remediation. *Int J Env Sci* 2012;3:940–55.
- [19] Bazin I, Hassine AIH, Hamouda YH, Mnif W, Bartegi A, Lopez-Ferber M, et al. Estrogenic and anti-estrogenic activity of 23 commercial textile dyes. *Ecotoxicol Env Saf* 2012;85:131–6.

- [20] San NO, Celebioglu A, Tumas Y, Uyar T, Tekinay T. Reusable bacteria immobilized electrospun nanofibrous webs for decolorization of methylene blue dye in wastewater treatment. *RSC Adv* 2014;4:32249–55.
- [21] Zhang W, Wu CW. Dyeing of multiple types of fabrics with a single reactive azo disperse dye. *Chem Pap* 2014;68:330–5.
- [22] Gregory P. Classification of Dyes by Chemical Structure, Chapter, The Chemistry and Application of Dyes, Part of the series Topics in Applied Chemistry. US: Springer; 1990. p. 17–47.
- [23] Neumann M, Schulz R, Schäfer K, Müller W, Mannheller W, Liess M. The significance of entry routes as point and non-point sources of pesticides in small streams. *Water Res* 2002;36:835–42.
- [24] Cahill MG, Caprioli G, Stack M, Vittori S, James KJ. Semi-automated liquid chromatography– mass spectrometry (LC–MS/MS) method for basic pesticides in wastewater effluents. *Anal Bioanal Chem* 2011;400:587–94.
- [25] Varma R, Varma DR. The Bhopal disaster of 1984. *Bull Sci Technol Soc* 2005;25 (1):37–45.
- [26] Kuroda K, Yamaguchi Y, Endo G. Mitotic toxicity, sister chromatid exchange and recombination assay of pesticides. *Arch Env Contam Toxicol* 1992;23:13–18.
- [27] Rehana Z, Malik A, Ahmad M. Mutagenic activity of the Ganges water with special reference to pesticide pollution in the river between Kachla to Kannauj (UP), India. *Mutat Res* 1995;343:137–44.
- [28] Salazar-Arredondo E, Solis-Heredia M, Rojas-Garcia E, Hernandez- Ochoa I, Quintanilla-Vega B. Sperm chromatin alteration and DNA damage by methyl-parathion; chlorpyrifos and diazinon and their oxon metabolites in human spermatozoa. *Reprod Toxicol* 2008;25:455–60.
- [29] de Flora S, Vigano L, D'Agostini F, Camoirano A, Bagnasco M, Bennicelli C, et al. Multiple genotoxicity biomarkers in fish exposed in situ to polluted river water. *Mutat Res/Gen Toxicol* 1993;319:167–77.
- [30] Palmiotto G, Pieraccini G, Moneti G, Dolara P. Determination of the levels of aromatic amines in indoor and outdoor air in Italy. *Chemosphere* 2001;433:355–61.
- [31] Tang H, et al. Photochemical removal of aniline in aqueous solutions: switching from photocatalytic degradation to photo-enhanced polymerization recovery. *J Hazard Mater* 2010;175:977–84.
- [32] International Agency for Research on Cancer (Wright). Benzo[a]pyrene, polynuclear aromatic compounds, part 1, chemical, environmental and experimental data. *Monogr Eval Carcinogen Risk Chem Hum Polycycl* 1983;32:211–24.
- [33] Menzie CA, Potocki BB, Santodonato J. Exposure to carcinogenic PAHs in the environment. *Env Sci Technol* 1992;26:1278–84.
- [34] Latimer J, Zheng J. The sources, transport, and fate of PAH in the marine environment. In: Douden PET, editor. PAHs: an ecotoxicological perspective. New York: John Wiley and Sons Ltd; 2003.
- [35] Lijinsky W. The formation and occurrence of polynuclear aromatic hydrocarbons associated with food. *Mutat Res* 1991;259:251–62.
- [36] Baklanov A, Hänninen O, Slørdal LH, Kukkonen J, Bjergene N, Fay B. Integrated systems for forecasting urban meteorology, air pollution and population exposure. *Atmos Chem Phys* 2007;7:855–74.
- [37] Freeman DJ, Cattell FCR. Woodburning as a source of atmospheric polycyclic aromatic hydrocarbons. *Env Sci Technol* 1990;24:1581–5.

- [38] Wright DA, Welbourn P. Environmental toxicology. Cambridge: Cambridge University Press; 2002.
- [39] Guo W, He M, Yang Z, Lin C, Quan X, Wang H. Distribution of polycyclic aromatic hydrocarbons in water, suspended particulate matter and sediment from Daliao River watershed. *Chemosphere* 2007;68:93–104.
- [40] Kaushik CP, Haritash AK. Polycyclic aromatic hydrocarbons (PAHs) and environmental health. *Our Earth* 2006;3:1–7.
- [41] Cerniglia CE. Biodegradation of polycyclic aromatic hydrocarbons. *Biodegradation* 1992;3:351–68.
- [42] ATSDR (Agency for Toxic Substances and Disease Registry). Toxicological Profile for Polycyclic Aromatic Hydrocarbons. Acenaphthene, Acenaphthylene, Anthracene, Benzo(a)anthracene, Benzo(a)pyrene, Benzo(b)fluoranthene, Benzo(g,i,h)perylene, Benzo(k)fluoranthene, Chrysene, Dibenzo(a,h)anthracene, Fluoranthene, Fluorene, Indeno(1,2,3-c,d)pyrene, Phenanthrene, Pyrene. Prepared by Clement International Corporation, under Contract No. 205-88-0608. ATSDR/TP-90-20; 1990.
- [43] Moussavi G, Mahmoudi M. Removal of azo and anthraquinone reactive dyes from industrial wastewaters using MgO nanoparticles. *J Hazard Mater* 2009;168:806–12.
- [44] Shanker U, Jassal V, Rani M. Green synthesis of iron hexacyanoferrate nanoparticles: potential candidate for the degradation of toxic PAHs. *J Env Chem Engg* 2017;5:4108–20.
- [45] Shanker U, Jassal V, Rani M. Degradation of toxic PAHs in water and soil using potassium zinc hexacyanoferrate nanocubes. *J Env Manage* 2017;204:337–45.
- [46] Shanker U, Rani M, Jassal V. Degradation of hazardous organic dyes in water by nanomaterials. *Env Chem Lett* 2017;15:623.
- [47] CEH, Chemical Economics Handbook. Color Pigments, 2015, pp. 1–90. <<https://www.ihs.com/products/organic-color-chemical-economics-handbook.html>>.
- [48] Annual Report. Production of selected major chemicals and petrochemicals. Government of India Ministry of Chemicals & Fertilizers Department of Chemicals and Petrochemicals; 2015–6.
- [49] USA National Toxicology Program. 11th report on carcinogens. U.S. Department of Health and Human Services; 2005.
- [50] Harrison FL, Mallon B. Selection of representative organic compounds for in-depth studies of mobility in soil-water systems. Lawrence Livermore National Laboratory: DE84-011 625; UCID-20031, NTIS; 1982.
- [51] Rani M, Shanker U. Removal of carcinogenic aromatic amines by metal hexacyanoferrates nanocubes synthesized via green process. *J Env Chem Eng* 2017;5:5298–309.
- [52] Morasch B, Bonvin F, Reiser H, Grandjean D, de Alencastro LF, Perazzolo C, et al. Occurrence and fate of micropollutants in the vidy bay of Lake Geneva, Switzerland. Part II: micropollutant removal between wastewater and raw drinking water. *Env Toxicol Chem* 2010;29:1658–68.
- [53] Ormad M, Miguel N, Mosteo R, Rodríguez J, Ovelheiro JL. Study of the presence of pesticides in treated urban wastewaters. In: Stoytcheva M, editor. Pesticides in the modern world-risks and benefits, 9. Croatia: InTech; 2011. p. 453–70.
- [54] Pitarch E, Portoles T, Marin JM, Ibanez M, Albarran F, Hernandez F. Analytical strategy based on the use of liquid chromatography and gas chromatography with triple-quadrupole and time-of-flight MS analyzers for investigating organic contaminants in wastewater. *Anal Bioanal Chem* 2010;397(7):2763–76.

- [55] Bystrzejewska-Piotrowska G, Golimowski J, Urban PL. Nanoparticles: their potential toxicity, waste and environmental management. *Waste Manage* 2009;29:2587–95.
- [56] Zweck A, Bachmann G, Luther W, Ploetz C. Nanotechnology in Germany: from forecasting to technological assessment to sustainability studies. *J Clean Prod* 2008;16:977–87.
- [57] Klaine SJ, Alvarez PJ, Batley GE, Fernandes TF, Handy RD, Lyon DY, et al. Nanomaterials in the environment: behavior, fate, bioavailability, and effects. *Env Toxicol Chem* 2008;27:1825–51.
- [58] Oberdörster G, Oberdörster E, Oberdörster J. Nanotoxicology: an emerging discipline evolving from studies of ultrafine particles. *Env Health Perspect* 2005;823–39.
- [59] Rejeski D, Lekas D. Nanotechnology field observations: scouting the new industrial west. *J Clean Prod* 2008;16:1014–17.
- [60] Skrabalak SE, Chen J, Sun Y, Lu X, Au L, Cobley CM, et al. Gold nanocages: synthesis, properties, and applications. *Acc Chem Res* 2008;41:1587–95.
- [61] Cobley CM, Chen J, Cho EC, Wang LV, Xia Y. Gold nanostructures: a class of multifunctional materials for biomedical applications. *Chem Soc Rev* 2011;40:4456–61.
- [62] Hussain CM. Handbook of nanomaterials for industrial applications. Elsevier; 2018.
- [63] Hussain CM, Kharisov B. Advanced environmental analysis-application of nanomaterials. The Royal Society of Chemistry; 2017.
- [64] Yan W, Lien H-L, Koel BE, Zhang W-X. Iron nanoparticles for environmental clean-up: recent developments and future outlook. *Env Sci Process Impacts* 2013;15:63–77.
- [65] Mazov I, Krasnikov D, Stadnichenko A, Kuznetsov V, Romanenko A, Anikeeva O, Tkachev E. Direct Vapor-Phase Bromination of Multiwall Carbon Nanotubes. *Functional Nanomaterials* 2009;2012:1–5.
- [66] Mittal G, Dhand V, Rhee KY, Park S, Lee WR. A review on carbon nanotubes and graphene as fillers in reinforced polymer nanocomposites. *J Indus Eng Chem* 2015;21:11–25.
- [67] Ma P, Naveed S, Gad M, Jang-Kyo K. Dispersion and functionalization of carbon nanotubes for polymer-based nanocomposites: A review. *Compos. Part A Appl Sci Manuf* 2010;41:1345–67.
- [68] Santos CV, Hernández ALM, Fisher FT, Ruoff R, Castan VM. Improvement of Thermal and Mechanical Properties of Carbon Nanotube Composites through Chemical Functionalization. *Chem Mater* 2003;15:4470.
- [69] Shanker U, Jassal V, Rani M, Kaith BS. Towards green synthesis of nanoparticles: From bio-assisted sources to benign solvents. A review. *Int J Env Anal Chem* 2016;96:801–35.
- [70] Rani M, Shanker U. Effective adsorption and enhanced degradation of various pesticides from aqueous solution by Prussian blue nanorods. *J Env Chem Engg* 2018;6:1512–19.
- [71] Ghaedi M, A. Hassanzadeh, S. NasiriKokhdan Multiwalled carbon nanotubes as adsorbents for the kinetic and equilibrium study of the removal of Alizarin Red S and Morin, J. Chem. Eng. Data 2011;56(5):2511–20.
- [72] Chemical Industries Newsletter, SRI Consulting, California, March 2008.
- [73] Kdasi A, Idris A, Saed K, Guan C. Treatment of textile wastewater by advanced oxidation processes-A review. *Glob Nest Int J* 2004;6:222–30.
- [74] Pagga U, Brown D. The degradation of dyestuffs: part II behaviour of dyestuffs in aerobic biodegradation tests. *Chemosphere* 1986;15:479–91.
- [75] EC, 2008. Directive on Environmental Quality Standards (Directive 2008/105/EC).
- [76] Kannan K, Tanabe S, Giesy JP, Tatsukawa R. Organochlorine pesticides and polychlorinated biphenyls in foodstuffs from Asian and Oceanian countries. *Rev Env Contam Toxicol* 1997;152:1–55.

- [77] Navarro A, Tauler R, Lacorte S, Barcelo D. Occurrence and transport of pesticides and alkylphenols in water samples along the Ebro River Basin. *J Hydrol* 2010;383:18–29.
- [78] Rao CHS, Venkateswarlu V, Surender T, Eddleston M, Buckley NA. Pesticide poisoning in south India-Opportunities for prevention and improved medical management. *Trop Med Int Health* 2005;10:581–8.
- [79] IARC Monographs on the Evaluation of the Carcinogenic Risk of Chemicals to Humans, Vol. 35, Polynuclear Aromatic Compounds.
- [80] Dubowsky SD, Wallace LA, Buckley TJ. The contribution of traffic to indoor concentrations of polycyclic aromatic hydrocarbons. *J Expo Anal Env Epid* 1999;9:312–21.
- [81] Rachna M, Rani U. Shanker Sunlight mediated improved photocatalytic degradation of carcinogenic benz[a]anthracene and benzo[a]pyrene by zinc oxide encapsulated hexacyanoferrate nanocomposite. *J Photochem. and Photobiol. A: Chem* 2019;381:111861.
- [82] Li CS, Ro YS. Indoor characteristics of polycyclic aromatic hydrocarbons in the urban atmosphere of Taipei. *Atmos Env* 2000;34:611–20.
- [83] Lung SC, Kao MC, Hu SC. Contribution of incense burning to indoor PM10 and particle-bound polycyclic aromatic hydrocarbons under two ventilation conditions. *Indoor Air* 2003;13:194–9.
- [84] Brunekreef B, Janssen NA, de Hartog JJ, Oldenwening M, Meliefste K, Hoek G, et al. Personal, indoor and outdoor exposures of PM25 and its components for groups of cardiovascular patients in Amsterdam and Helsinki. *Res Rep Health Eff Inst* 2005;127:1–70.
- [85] Reddy MS, Basha S, Joshi HV, Ramachandraiah G. Seasonal distribution and contamination levels of total PHCs, PAHs and heavy metals in coastal waters of the Alang-Sosiya ship scrapping yard, Gulf of Cambay, India. *Chemosphere* 2005;61:1587–93.
- [86] Fu PP, Xia Q, Sun X, Yu H. Phototoxicity and environmental transformation of polycyclic aromatic hydrocarbons (PAHs)-light induced reactive oxygen species, lipid peroxidation, and DNA damage. *J Environ Sci Health* 2012;Part C 30:1–41.
- [87] Rani M, Rachna, Shanker U. Metal hexacyanoferrates nanoparticles mediated degradation of carcinogenic aromatic amines. *Env Nanotechnol Monit Manage* 2018;10:36–50.
- [88] Rani M, Shanker U. Photocatalytic degradation of toxic phenols from water using bimetallic metal oxide nanostructures. *Colloids Surf A* 2018;553:546–61.
- [89] Jadhav DN, Vanjara AK. Removal of phenol from wastewater using sawdust, polymerized sawdust and sawdust carbon. *Indian J Chem Technol* 2004;11:35–41.
- [90] El-Ashtouky SZ, El-Taweel YA, Abdelwahab O, Nassef EM. Treatment of petrochemical wastewater containing phenolic compounds by electrocoagulation using a fixed bed electrochemical reactor. *Int J Electrochem Sci* 2013;8:1534–50.
- [91] Veeresh GS, Kumar P, Mehrotra K. Treatment of phenol and cresols in upflow anaerobic sludge blanket (UASB) process: a review. *Water Res* 2004;39:154–70.
- [92] Babich H, Davis DL. Phenol: a review of environmental and health risks. *Regul Toxicol Pharmacol* 1981;1:90–9.
- [93] Singh A, Kumar V, Srivastava JN. Assessment of bioremediation of oil and phenol contents in refinery waste water via bacterial consortium. *Pet Env Biotechnol* 2013;4:1–4.
- [94] Kang JH, Kondo F, Katayama Y. Human exposure to bisphenol A. *Toxicology* 2006;226:79–89.
- [95] Negri-Cesi P. Bisphenol A interaction with brain development and functions. *Res Int J* 2015;6:1–12.
- [96] Suzuki T, Nakagawa Y, Takano I, Yaguchi K, Yasuda K. Environmental fate of bisphenol A and its biological metabolites in river water and their xeno-estrogenic activity. *Env Sci Technol* 2004;38:2389–96.

- [97] Im J, Löffler FE. Fate of bisphenol A in terrestrial and aquatic environments. *Env Sci Technol* 2016;50:8403–16.
- [98] Darwish M, Mohammadi A. Functionalized nanomaterial for environmental techniques. Nanotechnology in environmental science. Weinheim, Germany: Wiley-VCH Verlag GmbH & Co. KGaA; 2018.
- [99] Rani M, Shanker U. Green synthesis of TiO<sub>2</sub> and its photocatalytic activity, *Handbook of Smart Photocatalytic Materials Fundamentals, Fabrications, and Water Resources Applications* 2020;11–61.
- [100] Jun S, Choi M, Ryu S, Lee H, Ryoo R. Ordered mesoporous carbon molecular sieves with functionalized surfaces. *Stud Surf Sci Catal* 2003;146:37–40.
- [101] Rani M, Shanker U. Promoting sun light-induced photocatalytic degradation of toxic, phenols by efficient and stable double metal cyanide nanocubes. *Environ Sci Pollut Res* 2018;25:23764–79.
- [102] Rani M, Shanker U. Sun-light driven rapid photocatalytic degradation of methylene blue by poly (methyl methacrylate)/metal oxide nanocomposites. *Colloids Surf A* 2018;559:136–47.
- [103] Yang K, Xing B. Adsorption of organic compounds by carbon nanomaterials in aqueous phase: polanyi theory and its application. *Chem Rev* 2010;110(10):5989–6008.
- [104] Hummers WS, Offeman RE. Preparation of graphitic oxide. *J Am Chem Soc* 1958;80(6) 1339–1339.
- [105] Yan Y, Miao J, Yang Z, Xiao FX, Yang HB, Liu B, et al. Carbon nanotube catalysts: recent advances in synthesis, characterization and applications. *Chem Soc Rev* 2015;44 (10):3295–346.
- [106] Mangun CL, Benak KR, Economy J, Foster KL. Surface chemistry, pore sizes and adsorption properties of activated carbon fibers and precursors treated with ammonia. *Carbon* 2001;39(12):1809–20.
- [107] Wang L, Wang D, Zhang S, Tian H. Synthesis and characterization of sulfonated graphene as a highly active solid acid catalyst for the ester exchange reaction. *Catal Sci Technol* 2013;3(5):1194–7.
- [108] Bonder M, Zhang Y, Kiick K, Papaefthymiou V, Hadjipanayis G. Controlling synthesis of Fe nanoparticles with polyethylene glycol. *J Magn Magn Mater* 2007;311:658–64.
- [109] Tiraferri A, Chen KL, Sethi R, Elimelech MJ. Reduced aggregation and sedimentation of zero-valent iron nanoparticles in the presence of guar gum. *Colloid Interface Sci* 2008;324:71–9.
- [110] Rani M, Rachna, Shanker U. Metal oxide-chitosan based nanocomposites for efficient degradation of carcinogenic PAHs. *J. Environ Chem Eng.* 2020;8:103810.
- [111] Lehman SE, Larsen SC. Zeolite and mesoporous silica nanomaterials: greener syntheses, environmental applications and biological toxicity. *Env Sci Nano* 2014;1(3):200–13.
- [112] Sierra I, Perez QD. Heavy metal complexation on hybrid mesoporous silicas: an approach to analytical applications. *Chem Soc Rev* 2013;42:3792–807.
- [113] Mahto TK, Chandra S, Halder C, Sahu SK. Kinetic and thermodynamic study of polyani-line functionalized magnetic mesoporous silica for magnetic field guided dye adsorption. *RSC Adv* 2015;5(59):47909–19.
- [114] Bagheri H, Roostaie A, Babanezhad E. New grafted nanosilica based sorbent for needle trap extraction of polycyclic aromatic hydrocarbons from water samples followed by GC/MS. *Chromatographia* 2011;74(5):429.
- [115] Valtchev V, Tosheva L. Porous nanosized particles: preparation, properties, and applications. *Chem Rev* 2013;113(8):6734–60.

- [116] Ciriminna R, Fidalgo A, Pandarus V, Béland F, Ilharco LM, Pagliaro M. The sol–gel route to advanced silica – based materials and recent applications. *Chem Rev* 2013;113(8):6592–620.
- [117] Gu H, Guo Y, Wong SY, Zhang Z, Ni X, Zhang Z, et al. Study of amino-functionalized mesoporous silica nanoparticles (NH<sub>2</sub>-MSN) and polyamide-6nanocomposites incorporated with NH<sub>2</sub>-MSN and organo-montmorillonite. *Micropor Mesopor Mater* 2013;170:226–34.
- [118] Deka JR, Saikia D, Lai Y-S, Tsai C-H, Chang W-C, Kao H-M. Roles of nanostructures and carboxylic acid functionalization of ordered cubic mesoporous silicas in lysozyme immobilization. *Micropor Mesopor Mater* 2015;213:150–60.
- [119] Liu J-f, Zhao Z-s, Jiang G-b. Coating Fe<sub>3</sub>O<sub>4</sub> magnetic nanoparticles with humic acid for high efficient removal of heavy metals in water. *Env Sci Technol* 2008;42(18):6949–54.
- [120] Usai EM, Sini MF, Meloni D, Solinas V, Salis A. Sulfonic acid functionalized mesoporous silicas: microcalorimetric characterization and catalytic performance toward biodiesel synthesis. *Micropor Mesopor Mater* 2013;179:54–62.
- [121] Georgakilas V, Tiwari JN, Kemp KC, Pernan JA, Bourlinos AB, Kim KS, et al. Noncovalent functionalization of graphene and graphene oxide for energy materials, biosensing, catalytic, and biomedical applications. *Chem Rev* 2016;116(9):5464–519.
- [122] Kumar A, Kaith BS, Gupta B, Shanker U, Lochab SP. A facile strategy to synthesize a novel and green nanocomposite based on gum Salaiguggal - Investigation of antimicrobial activity. *Mat Chem Phy* 2018;219:129–41.
- [123] Bai H, Li C, Shi G. Functional composite materials based on chemically converted graphene. *Adv Mater* 2011;23(9):1089–115.
- [124] Guo Z, Li Y, Pan S, Xu J. Fabrication of Fe<sub>3</sub>O<sub>4</sub>@cyclodextrin magnetic composite for the high-efficient removal of Eu (III). *J Mol Liq* 2015;206:272–7.
- [125] Guo Z, Ren G, Jiang C, Lu X, Zhu Y, Jiang L, et al. High performance heteroatoms quaternary-doped carbon catalysts derived from *Shewanella* bacteria for oxygen reduction. *Sci Rep* 2015;5:17064–74.
- [126] Xue Y, Liu J, Chen H, Wang R, Li D, Qu J, et al. Nitrogen-doped graphene foams as metal-free counter electrodes in highperformance dye-sensitized solar cells. *Angew Chem Int Ed* 2012;51(48):12124–7.
- [127] Chizari K, Vena A, Laurentius L, Sundararaj U. The effect of temperature on the morphology and chemical surface properties of nitrogen doped carbon nanotubes. *Carbon* 2014;68:369–79.
- [128] Adjizian J-J, Leghrib R, Koos AA, Suarez-Martinez I, Crossley A, Wagner P, et al. Boron- and nitrogen-doped multi-wall carbon nanotubes for gas detection. *Carbon* 2014;66:662–73.
- [129] Dong J, Qu X, Wang L, Zhao C, Xu J. Electrochemistry of nitrogen-doped carbon nanotubes (CN<sub>x</sub>) with different nitrogen content and its application in simultaneous determination of dihydroxybenzene isomers. *Electroanalysis* 2008;20(18):1981–6.
- [130] Travlou NA, Seredych M, Rodríguez-Castellón E, Bandoz TJ. Activated carbon-based gas sensors: effects of surface features on the sensing mechanism. *J Mater Chem A* 2015;3(7):3821–31.
- [131] Grubbs RB. Roles of polymer ligands in nanoparticle stabilization. *Polym Rev* 2007;47(2):197–215.
- [132] Valentin D, Finazzi E, Pacchioni G, Selloni A, Livraghi S, Paganini MC, et al. N-doped TiO<sub>2</sub>: theory and experiment. *Chem Phys* 2007;339:4456–63.

- [133] Peng B, Meng X, Tang F, Ren X, Chen D, Ren J. General synthesis and optical properties of monodisperse multifunctional metal-ion-doped TiO<sub>2</sub> hollow particles. *J Phys Chem C* 2009;113:20240–5.
- [134] Chaudhuri RG, Paria S. Visible light induced photocatalytic activity of sulfur doped hollow TiO<sub>2</sub> nanoparticles, synthesized via a novel route. *Dalton Trans* 2014;43:5526–34.
- [135] Nagamine S, Tohyama S, Ohshima M, Iwamoto H, Konishi Y, Tsukui S. Fabrication of hollow N-doped TiO<sub>2</sub> photocatalyst by spray-induced hydrolysis. *J Ceram Soc Jpn* 2009;117:1158–60.
- [136] Wang P, Wu J, Ao Y, Wang C, Hou J, Qian J. Preparation and enhanced photocatalytic performance of Sn ion modified titania hollow spheres. *Mater Lett* 2011;65:3278–80.
- [137] Ao Y, Xu J, Zhang S, Fu D. A one-pot method to prepare N-doped titania hollow spheres with high photocatalytic activity under visible light. *Appl Surf Sci* 2010;256:2754–8.
- [138] Shi J-W, Chen J-W, Cui H-J, Fu M-L, Luo H-Y, Xu B, et al. One template approach to synthesize C-doped titania hollow spheres with high visible-light photocatalytic activity. *Chem Eng J* 2012;195:226–32.
- [139] Zhu Z, He Z, Li J, Zhou J, Wei N, Liu D. Two-step template-free route for synthesis of TiO<sub>2</sub> hollow spheres. *J Mater Sci* 2011;46:931–7.
- [140] Son JE, Chattopadhyay J, Pak D. Electrocatalytic performance of Badoped TiO<sub>2</sub> hollow spheres in water electrolysis. *Int J Hydrog Energy* 2010;35:420–7.
- [141] Xu J, Chen M, Fu D. Study on highly visible light active Bi-doped TiO<sub>2</sub> composite hollow sphere. *Appl Surf Sci* 2011;257:7381–6.
- [142] Chattopadhyay J, Kim HR, Moon SB, Pak D. Performance of tin doped titania hollow spheres as electrocatalysts for hydrogen and oxygen production in water electrolysis. *Int J Hydrog Energy* 2008;33:3270–80.
- [143] Khalid N, Ahmed E, Hong Z, Sana L, Ahmed M. Enhanced photocatalytic activity of graphene–TiO<sub>2</sub> composite under visible light irradiation. *Curr Appl Phys* 2013;13:659–63.
- [144] Wang Y, Shi R, Lin J, Zhu Y. Significant photocatalytic enhancement in methylene blue degradation of TiO<sub>2</sub> photocatalysts via graphene-like carbon in situ hybridization. *Appl Catal, B* 2010;100:179–83.
- [145] Creutz C, Brunschwig BS, Sutin N. Interfacial charge-transfer absorption: 3. Application to semiconductor-molecule assemblies. *J Phys Chem B* 2006;110:25181–90.
- [146] Shanker U, Jassal V, Rani M. Catalytic removal of organic colorants from water using some transition metal oxide nanoparticles synthesized under sunlight. *RSC Adv* 2016;6:94989–9499.
- [147] Shanker U, Jassal V, Rani M, Kaith BS. Toward green synthesis of nanoparticles: from bio-assisted sources to benign solvents. A review. *Int J Env Anal Chem* 2016;96:801.
- [148] Shu H-Y, Chang M-C, Chen C-C, Chen P-E. Using resin supported nano zero-valent iron particles for decoloration of Acid Blue 113 azo dye solution. *J Hazard Mater* 2010;184:499–505.
- [149] Liu M, Wang Y, Chen L, Zhang Y, Lin Z. Mg(OH)<sub>2</sub> supported nanoscale zero valent iron enhancing the removal of Pb(II) from aqueous solution. *ACS Appl Mater Interfaces* 2015;7:7961–9.
- [150] Zhang X, Lin S, Lu X-Q, Chen Z-L. Removal of Pb(II) from water using synthesized kaolin supported nanoscale zero-valent iron. *Chem Eng J* 2010;163:243–8.



- [151] Chen ZX, Jin X-Y, Chen Z, Megharaj M, Naidu R. Removal of methyl orange from aqueous solution using bentonite-supported nanoscale zerovalent iron. *J Colloid Interface Sci* 2011;363:601–7.
- [152] Xiao J, Gao B, Yue Q, Sun Y, Kong J, Gao Y, et al. Characterization of nanoscale zero-valent iron supported on granular activated carbon and its application in removal of acrylonitrile from aqueous solution. *J Taiwan Inst Chem Eng* 2015;55:152–8.
- [153] Qiu X, Fang Z, Liang B, Gu F, Xu Z. Degradation of decabromodiphenyl ether by nano zero-valent iron immobilized in mesoporous silica microspheres. *J Hazard Mater* 2011;193:70–81.
- [154] Quintanilla P, delHierro D, Fajardo IM, Sierra I. Mesoporous silica functionalized with 2-mercaptopyridine: synthesis, characterization and employment for Hg(II) adsorption. *Micropor Mesopor, Mater* 2006;89:58–68.
- [155] Hirsch A, Vostrowsky O. Functionalization of carbon nanotubes. In: Schlüter AD, editor. *Functional molecular nanostructures*. Heidelberg: Springer; 2005. p. 193–237.
- [156] Lim JK, Yun WS, Yoon M-H, Lee SK, Kim CH, Kim K, et al. Selective thiolation of single-walled carbon nanotubes. *Synth Met* 2003;139(2):521–7.
- [157] Choi M, Ryoo R. Ordered nanoporous polymer–carbon composites. *Nat Mater* 2003;2(7):473–6.
- [158] Czerw R, Guo Z, Ajayan PM, Sun Y-P, Carroll DL. Organization of polymers onto carbon nanotubes: a route to nanoscale assembly. *Nano Lett* 2001;1(8):423–7.
- [159] Makarov VV, Love AJ, Sinitsyna OV, Makarova SS, Yaminsky IV, Taliansky ME, et al. “Green” nanotechnologies: synthesis of metal nanoparticles using plants. *Acta Nat* 2014;6:35–44.
- [160] Virkutyte J, Varma RS. *Green synthesis of nanomaterials: environmental aspects. Sustainable nanotechnology and the environment: advances and achievements*. Washington, DC: American Chemical Society; 2013.
- [161] Li X, Xu H, Chen ZS, Chen G. Biosynthesis of nanoparticles by microorganisms and their applications. *J Nanomater* 2011;2011:1–16.
- [162] Virkutyte J, Varma RS. Green synthesis of metal nanoparticles: biodegradable polymers and enzymes in stabilization and surface functionalization. *Chem Sci* 2011;2:837–46.
- [163] Narayanan KB, Sakthivel N. Biological synthesis of metal nanoparticles by microbes. *Adv Colloid Interface Sci* 2010;156:113–20.
- [164] Kuo WS, Ho PH. Solar photocatalytic decolorization of methylene blue in water. *Chemosphere* 2001;45:77–83.
- [165] Galindo C, Jacques P, Kalt A. Photooxidation of the phenylazonaphthol AO20 on TiO<sub>2</sub>: kinetic and mechanistic investigations. *Chemosphere* 2001;45:997–1005.
- [166] Kumar R, Rashid J, Barakat MA. Synthesis and characterization of a starch-AIOOH-FeS<sub>2</sub> nanocomposite for the adsorption of congo red dye from aqueous solution. *RSC Adv* 2014;4:38334–40.
- [167] Sheibani M, Ghaedi M, Marahel F, Ansari A. Congo red removal using oxidized multi-walled carbon nanotubes: kinetic and isotherm study. *Desalin Water Treat* 2015;53:844–52.
- [168] Ghaedi M, Mohammdi F, Ansari A, Dispers C. Gold nanoparticles loaded on activated carbon as novel adsorbent for kinetic and isotherm studies of methyl orange and sunset yellow adsorption. *J Sci Technol* 2015;36:652–9.
- [169] Kleinstreuer C, Li J, Koo J. Microfluidics of nano-drug delivery. *Int J Heat Mass Transf* 2008;51:5590–7.

- [170] Lattuada M, Hatton T. Synthesis, properties and applications of Janus nanoparticles. *Nano Today* 2011;6:286–308.
- [171] Garg A, Visht S, Sharma PK, Kumar N. Formulation, characterization and application on nanoparticle: a review. *Der Pharm Sin* 2011;2:17–26.
- [172] Pozan GS, Isleyen M, Gokcen S. Transition metal coated TiO<sub>2</sub> nanoparticles: synthesis, characterization and their photocatalytic activity. *Appl Catal B Env* 2013;140:537–45.
- [173] Satheesh R, Vignesh K, Suganthi A, Rajarajan M. Visible light responsive photocatalytic applications of transition metal (M = Cu, Ni and Co) doped  $\alpha$ -Fe<sub>2</sub>O<sub>3</sub> nanoparticles. *J Env Chem Eng* 2014;2:1956–68.
- [174] Lavand AB, Malghe YS. Visible light photocatalytic degradation of 4-chlorophenol using C/ZnO/CdS nanocomposites. *J Saudi Chem Soc* 2015;19(5):471–8.
- [175] Yasmima M, Mourad K, Mohammed SH, Khaoula C. Treatment heterogenous photocatalysis; Factors influencing the photocatalytic degradation by TiO<sub>2</sub>. *Energy Procedia* 2014;50:559–66.
- [176] Ahmed S, Rasul MG, Martens WN, Brown R, Hashib MA. Heterogenous photocatalytic degradation of phenols in wastewater: a review on current status and developments. *Desalination* 2010;261:3–18.
- [177] Attia YA, Mohamed YMA, Altalhi TA. Photobiosynthesis of metal/grapheme nanocomposites: new materials for water desalination and purification. *Desalin Water Treat* 2016;57:26014–21.
- [178] Chettri P, Vendamani VS, Tripathi A, Singh MK, Pathak AP, Tiwari A. Green synthesis of silver nanoparticle-reduced graphene oxide using Psidium guajava and its application in SERS for the detection of methylene blue. *Appl Surf Sci* 2017;406:312–18.
- [179] Coker VS, Bennett JA, Telling ND, Henkel T, Charnock JM, van der Laan G, et al. Microbial engineering of nanoheterostructures: biological synthesis of a magnetically recoverable palladium nanocatalyst. *ACS Nano* 2010;4:2577–84.
- [180] De Corte S, Hennebel T, Fitts JP, et al. Biosupported bimetallic Pd-Au nanocatalysts for dechlorination of environmental contaminants. *Environ Sci Technol* 2011;45(19):8506–13.
- [181] Jinu U, Gomathi M, Geetha N, Benelli G, Venkatachalam P. Green engineered biomolecule-capped silver and copper nanohybrids using Prosopis cineraria leaf extract: enhanced antibacterial activity against microbial pathogens of public health relevance and cytotoxicity on human breast cancer cells (MCF-7). *Microb Pathogenesis* 2017;105:8695–9705.
- [182] Wang L, Lin J. Phenylalanine-rich peptide mediated binding with grapheme oxide and bioinspired synthesis of silver nanoparticles for electrochemical sensing. *Appl Sci* 2017;7:160–8.
- [183] Bordbar M. Biosynthesis of Ag/almond shell nanocomposite as a costeffective and efficient catalyst for degradation of 4-nitrophenol and organic dyes. *RSC Adv* 2017;7:180–9.
- [184] Wei X, Huang T, Yang JH, Zhang N, Wang YC, Zhou ZW. Green synthesis of hybrid graphene oxide/microcrystalline cellulose aerogels and their use as supersorbents. *J Hazard Mater* 2017;335:28–38.
- [185] Cao J, Sun X, Zhang X, Lu C. Homogeneous synthesis of Ag nanoparticles-doped water-soluble cellulose acetate for versatile applications. *Macromolecules* 2016;92:167–73.
- [186] Kolya H, Maiti P, Pandey A, Tripathy T. Green synthesis of silver nanoparticles with antimicrobial and azo dye (Congo red) degradation properties using *Amaranthus gangeticus* Linn leaf extract. *J Anal Sci Technol* 2015;6:33–9.

- [187] Lellala K, Namratha K, Byrappa K. Microwave assisted synthesis and characterization of nanostructure zinc oxide-graphene oxide and photo degradation of brilliant blue. *Mater Today Proc* 2016;3:74–83.
- [188] Hassan SSM, Azab WIME, Ali HR, Mansour MSM. Green synthesis and characterization of ZnO nanoparticles for photocatalytic degradation of anthracene. *Adv Nat Sci Nanosci Nanotechnol* 2015;6:1–10.
- [189] Ramazani A, Taghavi Fardood S, Hosseinzadeh Z, Sadri F, Joo SW. Green synthesis of magnetic copper ferrite nanoparticles using tragacanth gum as a biotemplate and their catalytic activity for the oxidation of alcohols. *Iran J Catal* 2017;7:181–5.
- [190] Sorbiun M, Mehr ES, Ramazani A, Fardood ST. Green synthesis of zinc oxide and copper oxide nanoparticles using aqueous extract of Oak Fruit Hull (Jaft) and comparing their photocatalytic degradation of basic violet 3. *Int J Env Res* 2018;12:29–37.
- [191] Fardood ST, Ramazani A, Pegah SM, Asiabi A. Green synthesis of zinc oxide nanoparticles using arabic gum and photocatalytic degradation of direct blue 129 dye under visible light. *J Mater Sci: Mater Electro* 2017;28:13596.
- [192] Fardood ST, Ramazani A, Golfar Z, Joo SW. Green synthesis of Ni-Cu-Zn ferrite nanoparticles using tragacanth gum and their use as an efficient catalyst for the synthesis of polyhydroquinoline derivatives. *Appl Organomet Chem* 2017;31:3823–70.
- [193] Atrak K, Ramazani A, Fardood ST. A novel sol–gel synthesis and characterization of  $\text{MgFe}_2\text{O}_4@ \gamma\text{-Al}_2\text{O}_3$  magnetic nanoparticles using tragacanth gel and its application as a magnetically separable photocatalyst for degradation of organic dyes under visible light. *J Mater Sci: Mater Electron* 2018;29:6702–10.
- [194] Huang L, Weng X, Chen Z, Megharaj M, Naidu R. Synthesis of iron-based nanoparticles using Oolong tea extract for the degradation of malachite green. *Spectrochim Acta A* 2013;117:801–9.
- [195] Madhavi V, et al. Application of phytogenic zerovalent iron nanoparticles in the adsorption of hexavalent chromium. *Spectrochim Acta A* 2013;116:17–27.
- [196] Hoag GE, Collins JB, Holcomb JL, Hoag JR, Nadagouda MN, Varma RS. Degradation of bromothymol blue by ‘greener’ nano-scale zero-valent iron synthesized using tea polyphenols. *J Mater Chem* 2009;19:8671–7.
- [197] Luo F, Yang D, Chen Z, Megharaj M, Naidu R. One-step green synthesis of bimetallic Fe/Pd nanoparticles used to degrade orange II. *J Hazard Mater* 2016;303:145–51.
- [198] Rachna, Rani M, Shanker U. Enhanced photocatalytic degradation of chrysene by  $\text{Fe}_2\text{O}_3@ \text{ZnHCF}$  nanocubes. *Chem Eng J* 2018;348:754–60.
- [199] Smuleac V, Varma R, Sikdar S, Bhattacharyya D. Green synthesis of Fe and Fe/Pd bimetallic nanoparticles in membranes for reductive degradation of chlorinated organics. *J Membr Sci* 2011;379:131–40.
- [200] Shahwan T, Abu Sirriah S, Nairat M, Boyacı E, Eroğlu AE, Scott TB, et al. Green synthesis of iron nanoparticles and their application as a fenton-like catalyst for the degradation of aqueous cationic and anionic dyes. *Chem Eng J* 2011;172:258–68.
- [201] Jassal V, Shanker U, Gahlot S. Green synthesis of some iron oxide nanoparticles and their interaction with 2-Amino, 3-Amino and 4-Aminopyridines. *Mater Today Proc* 2016;3:1874–80.
- [202] Jassal V, Shanker U, Gahlot S, Kaith BS, Kamaluddin, Iqbal MA, et al. Sapindus mukorossi mediated green synthesis of some manganese oxide nanoparticles interaction with aromatic amines. *Appl Phys A* 2016;122:271–80.

- [203] Jassal V, Shanker U, Kaith BS. Aegle marmelos mediated green synthesis of different nanostructured metal hexacyanoferrates: activity against photodegradation of harmful organic dyes. *Scientifica* 2016;2016:1–17.
- [204] Jassal V, Shanker U, Kaith BS, Shankar S. Green synthesis of potassium zinc hexacyanoferrate nanocubes and their potential application in photocatalytic degradation of organic dyes. *RSC Adv* 2015;5:26141–50.
- [205] Rani M, Shanker U. Insight in to the degradation of bisphenol A by doped ZnO@ZnHCF nanocubes: high photocatalytic performance. *J Colloid Interface Sci* 2018;530:16–28.
- [206] Rani M, Shanker U. Promoting sunlight-induced photocatalytic degradation of toxic phenols by efficient and stable double metal cyanide nanocubes. *Env Sci Pollut R* 2018;25:23764–79.
- [207] Rani M, Shanker U. Removal of chlorpyrifos, thiamethoxam, and tebuconazole from water using green synthesized metal hexacyanoferrate nanoparticles. *Env Sci Pollut Res* 2018;25:10878–88.
- [208] Rani M, Shanker U, Chaurasia A. Catalytic potential of laccase immobilized on transition metal oxides nanomaterialsNMs: degradation of alizarin red S dye. *J Env Chem Engg* 2017;5:2730–9.
- [209] Bonnia NN, Kamaruddin MS, Nawawi MH, Ratim S, Azlinae HN, Ali ES. Green biosynthesis of silver nanoparticles using 'polygonum Hydropiper' and study its catalytic degradation of methylene blue. *Procedia Chem* 2016;19:594–602.
- [210] Roy K, Sarkar CK, Ghosh CK. Photocatalytic activity of biogenic silver nanoparticles synthesized using yeast (*Saccharomyces cerevisiae*) extract. *Appl Nanosci* 2015;5:953–9.
- [211] Vanaja M, Paulkumar K, Baburaja M, Rajeshkumar S, Gnanajobitha G, Malarkodi C, Sivakavinesan M, Annadurai G. Degradation of methylene blue using biologically synthesized silver nanoparticles. *Bioinorg Chem App* 2014;2014:742346–53.
- [212] Fardood ST, Ramazani A, Golfar Z, Joo SW. Green synthesis of Ni-Cu-Zn ferrite nanoparticles using tragacanth gum and their use as an efficient catalyst for the synthesis of polyhydroquinoline derivatives. *Appl Organomet Chem* 2017;31:3823–70.
- [213] Priya, Kaith BS, Shanker U, Gupta B. One-pot green synthesis of polymeric nanocomposite: biodegradation studies and application in sorption-degradation of organic pollutants. *J Env Manage* 2019;234:345–56.
- [214] Priya, Kaith BS, Shanker U, Gupta B, Bhatia JK. RSM-CCD optimized In-air synthesis of photocatalytic nanocomposite: application in removal-degradation of toxic brilliant blue. *Reactive Funct Polym* 2018;131:107–22.
- [215] Stamate M, Lazar G. Application of titanium dioxide photocatalysis to create self-cleaning materials, MOCM 13. *Rom Tech Sci Acad* 2007;3:280–5.
- [216] Oncescu T, Stefan MI, Oancea P. Photocatalytic degradation of dichlorvos in aqueous TiO<sub>2</sub> suspensions. *Environ Sci Pollut Res* 2010;17:1158–66.
- [217] Zubieta CE, Messina PV, Schulz PC. Photocatalytic degradation of acridine dyes using anatase and rutile TiO<sub>2</sub>. *J Environ Manag* 2012;101:1–6.
- [218] Liu Y, Pei F, Lu R, Xu S, Cao S. TiO<sub>2</sub>/N-graphene nanocomposite via a facile in-situ hydrothermal sol-gel strategy for visible light photodegradation of eosin Y. *Mater Res Bull* 2014;60:188–94.
- [219] Sathish M, Viswanathan B, Viswanath RP. Characterization and photocatalytic activity of N-doped TiO<sub>2</sub> prepared by thermal decomposition of Ti–melamine complex. *Appl Catal B: Env* 2007;74:307–12.

- [220] Chen X, Burda C. Photoelectron spectroscopic investigation of nitrogen-doped titania nanoparticles. *J Phys Chem B* 2004;108(40):15446–9.
- [221] Cong Y, Zhang J, Chen F, Anpo M. Synthesis and characterization of nitrogen doped TiO<sub>2</sub> nanophotocatalyst with high visible light activity. *J Phys Chem C* 2007;111(19):6976–82.
- [222] Alfaro SO, Rodríguez-González V, Zaldívar-Cadena AA, Lee SW. Sonochemical deposition of silver-TiO<sub>2</sub> nanocomposites onto foamed waste-glass: evaluation of Eosin Y decomposition under sunlight irradiation. *Catal Today* 2011;166:166–71.
- [223] Sood S, Umar A, Mehta SK, Sinha ASK, Kansal SK. Efficient photocatalytic degradation of brilliant green using Sr-doped TiO<sub>2</sub> nanoparticles. *Ceram Int* 2015;41:3533–40.
- [224] Kansal SK, Sood S, Umar A, Mehta SK. Photocatalytic degradation of eriochrome black T dye using well-crystalline anatase TiO<sub>2</sub> nanoparticles. *J Alloy Compd* 2013;581:392–7.
- [225] Lee HJ, Kim JH, Park SS, Hong SS, Lee GD. Degradation kinetics for photocatalytic reaction of methyl orange over Al-doped ZnO nanoparticles. *Ind Eng Chem* 2015;25:199–206.
- [226] Kumar P, Govindaraju M, Senthamilselvi S, Premkumar K. Photocatalytic degradation of methyl orange dye using silver (Ag) nanoparticles from *Ulva lactuca*. *Colloids Surf B: Biointerfaces* 2013;103:658–61.
- [227] Kaur J, Singhal S. Facile synthesis of ZnO and transition metal doped ZnO nanoparticles for the photocatalytic degradation of methyl orange. *Ceram Int* 2014;40:7417–24.
- [228] Zhao X, Wang W, Zhang Y, Wu S, Li F, Liu JP. Synthesis and characterization of gadolinium doped cobalt ferrite nanoparticles with enhanced adsorption capability for congo red. *Chem Eng J* 2014;250:164–74.
- [229] Zhang F, Yin X, Zhang W. Development of magnetic Sr<sub>5</sub>(PO<sub>4</sub>)<sub>3</sub>(OH)/(Fe<sub>3</sub>O<sub>4</sub>) nanorod for adsorption of congo red from solution. *J Alloy Compd* 2016;657:809–17.
- [230] Zhang L, Gu FX, Chan JM, Wang AZ, Langer RS, Farokhzad, et al. Fate of bisphenol A in terrestrial and aquatic environments. *Env Sci Technol* 2016;50:8403–16.
- [231] Guo H, Lin K, Zheng Z, Xiao F, Li S. Sulfanilic acid-modified P25 TiO<sub>2</sub> nanoparticles with improved photocatalytic degradation on congo red under visible light. *Dye Pigment* 2012;92:1278–84.
- [232] Gautam RK, Rawat V, Banerjee S, Sanroman MA, Soni S, Singh SK, et al. Synthesis of bimetallic Fe-Zn nanoparticles and its application toward adsorptive removal of carcinogenic dye malachite green and congo red in water. *J Mol Liq* 2015;212:227–36.
- [233] Gholivand MB, Yamini Y, Dayeni M, Seidi S, Tahmasebi E. Adsorptive removal of alizarin red-S and alizarin yellow GG from aqueous solutions using polypyrrole-coated magnetic nanoparticles. *J Env Chem Eng* 2015;3:529–40.
- [234] Riaz U, Ashraf SM, Budhiraja V, Aleem S, Kashyap J. Comparative studies of the photocatalytic and microwaveassisted degradation of alizarin red using ZnO/poly(1-naphthylamine) nanohybrids. *J Mol Liq* 2016;216:259–67.
- [235] Nekouei F, Noorizadeh H, Nekouei S, Asif M, Tyagi I, Agarwal S, et al. Removal of malachite green from aqueous solutions by cuprous iodide–cupric oxide nano-composite loaded on activated carbon as a new sorbent for solid phase extraction: isotherm, kinetics and thermodynamic studies. *J Mol Liq* 2016;213:360–8.
- [236] Hsieh SH, Chen WJ, Yeh TH. Degradation of methylene blue using ZnSe–graphene nanocomposites under visible-light irradiation. *Ceram Int* 2015;41:13759–66.

- [237] Mekewi MA, Darwish AS, Amin MS, EshaqGh, Bourazan HA. Copper nanoparticles supported onto montmorillonite clays as efficient catalyst for methylene blue dye degradation. *Egypt J Pet* 2016;25(2):269–79.
- [238] Gupta VK, Agarwal S, Pathania D, Kothiyal NC, Sharma G. Use of pectin–thorium (IV) tungstomolybdate nanocomposite for photocatalytic degradation of methylene blue. *Carbohydr Polym* 2013;96:277–83.
- [239] Shamsipur M, Rajabi HR. Study of photocatalytic activity of ZnS quantum dots as efficient nanoparticles for removal of methyl violet: effect of ferric ion doping. *Spectrochim Acta Mol Biomol Spectrosc* 2014;122:260–7.
- [240] Fardood ST, Ramazani A, Golfar Z, Joo SW. Green synthesis of Ni-Cu-Zn ferrite nanoparticles using tragacanth gum and their use as an efficient catalyst for the synthesis of polyhydroquinoline derivatives. *Appl Organomet Chem* 2017;31:3823.
- [241] Kong JZ, Li AD, Li XY, Zhai HF, Zhang WQ, Gong YP, et al. Photo-degradation of methylene blue using Ta-doped ZnO nanoparticle. *J Solid State Chem* 2010;183:1359–64.
- [242] Li C, Dong Y, Yang J, Li Y, Huang C. Modified nano-graphite/Fe<sub>3</sub>O<sub>4</sub> composite as efficient adsorbent for the removal of methyl violet from aqueous solution. *J Mol Liq* 2014;196:348–56.
- [243] Nagaraja R, Kottam N, Girija CR, Nagabhushana BM. Photocatalytic degradation of Rhodamine B dye under UV/solar light using ZnO nanopowder synthesized by solution combustion route. *Powder Technol* 2012;215-216:91–7.
- [244] Kashinath L, Namratha K, Byrappa K. Microwave assisted synthesis and characterization of nanostructure zinc oxide-graphene oxide and photo degradation of brilliant blue. *Mater Today Proc* 2016;3:74–83.
- [245] Sankar R, Manikandan P, Malarvizhi V, Fathima T, Shivashangari KS, Ravikumar V. Green synthesis of colloidal copper oxide nanoparticles using Carica papaya and its application in photocatalytic dye degradation. *Spectrochim Acta Mol Biomol Spectrosc* 2014;121:746–50.
- [246] Bonamali P, Kaur R, Grover IS. Superior adsorption and photodegradation of eriochrome black-T dye by Fe<sup>3+</sup> and Pt<sup>4+</sup> impregnated TiO<sub>2</sub> nanostructures of different shapes. *J Ind Eng Chem* 2016;33:178–84.
- [247] Abraham SD, David ST, Bennie RB, Joel C, Kumar DS. Eco-friendly and green synthesis of BiVO<sub>4</sub> nanoparticle using microwave irradiation as photocatalyst for the degradation of Alizarin Red S. *J Mol Struc* 2016;1113:174–81.
- [248] Roosta M, Ghaedi M, Mohammadi M. Removal of Alizarin Red S by gold nanoparticles loaded on activated carbon combined with ultrasound device: optimization by experimental design methodology. *Powder Technol* 2014;267:134–44.
- [249] Coelho MG, de Lima GM, Augusti R, Maria DA, Ardisson JD. New materials for photocatalytic degradation of indigo carmine-Synthesis, characterization and catalytic experiments of nanometric tin dioxide-based composites. *Appl Catal B* 2010;96:67–71.
- [250] Yu B, Zeng J, Gong L, Zhang M, Zhang L, Chen X. Investigation of the photocatalytic degradation of organochlorine pesticides on a nano-TiO<sub>2</sub> coated film. *Talanta* 2007;72:1667–74.
- [251] Senthilnathan J, Philip L. Photocatalytic degradation of lindane under UV and visible light using N-doped TiO<sub>2</sub>. *Chem Eng J* 2010;161:83–92.
- [252] Joo SH, Zhao D. Destruction of lindane and atrazine using stabilized iron nanoparticles under aerobic and anaerobic conditions: effects of catalyst and stabilizer. *Chemosphere* 2008;70:418–25.

- [253] Tian H, Li J, Mu Z, Li L, Hao Z. Effect of pH on DDT degradation in aqueous solution using bimetallic Ni/Fe nanoparticles. *Sep Purif Technol* 2009;66:84–9.
- [254] Jing L, Yang C, Zongshan Z. Effective organochlorine pesticides removal from aqueous systems by magnetic nanospheres coated with polystyrene. *J Wuhan Univ Technol* 2013;29:168–73.
- [255] Elliott DW, Lien HL, Zhang WX. Degradation of lindane by zero-valent iron nanoparticles. *J Environ Eng* 2009;135:317–24.
- [256] Ramos-Delgado NA, Gracia-Pinilla MA, Maya-Trevino L, Hinojosa-Reyes L, Guzman-Mara JL, Hernandez-Ramirez A. Solar photocatalytic activity of TiO<sub>2</sub> modified with WO<sub>3</sub> on the degradation of an organophosphorus pesticide. *J Hazard Mater* 2013;263:36–44.
- [257] Yu H, Wang X, Sun H, Huo M. Photocatalytic degradation of malathion in aqueous solution using an Au–Pd–TiO<sub>2</sub> nanotube film. *J Hazard Mater* 2010;184:753–8.
- [258] Xu AW, Gau Y, Liu HQ. The preparation, characterization and their photocatalytic activities of rare-earth-doped TiO<sub>2</sub> nanoparticles. *J Catal* 2002;207(2):151–7.
- [259] Doong R, Chang W. Photoassisted titanium dioxide mediated degradation of organophosphorus pesticides by hydrogen peroxide. *J Photochem Photobiol A: Chem* 1997;107:239–44.
- [260] Rani M, Shanker U. Insight in to the degradation of bisphenol A by doped ZnO@ZnHCF nanocubes: High photocatalytic performance. *J Colloid Interf Sci* 2018;530:16.
- [261] Zhang L, Yan F, Wang Y. Photocatalytic degradation of methamidophos by UV irradiation in the presence of nano-TiO<sub>2</sub>. *J Inorg Mater* 2006;42:1379–87.
- [262] Rani M, Shanker U, Jassal V. Recent strategies for removal and degradation of persistent & toxic organochlorine pesticides using nanoparticles: A review. *J. Environ Manag* 2017;190:208.
- [263] Kralj MB, Cernigoj U, Franko M. Comparison of Photocatalysis and photolysis of malathion, isomalathion, malaaxon, and commercial malathion: products and toxicity studies. *Water Res* 2007;41:4504–14.
- [264] Ramacharyulu PVRK, Kumar JP, Prasad GK, Dwivedi K. Photoassisted remediation of toxic chemical warfare agents using titania NMs. *JSIR* 2014;73:308–12.
- [265] Shet A, Shetty VK. Photocatalytic degradation of phenol using Ag core-TiO<sub>2</sub> shell (Ag@TiO<sub>2</sub>) nanoparticles under UV light irradiation. *Env Sci Pollut Res* 2016;23:20055–64.
- [266] Kaur P, Bansal P, Sud D. Heterostructured nanophotocatalysts for degradation of organophosphate pesticides from aqueous streams. *J Korean Chem Soc* 2013;57(3):382–8.
- [267] Anandan C, Nurmatov U, Van Schayck OCP, Sheikh A. Is the prevalence of asthma declining? Systematic review of epidemiological studies. *Eur J Allergy Clin Immunology* 2010;65:152–67.
- [268] Shifu C, Gengyu C. Study on the photocatalytic reduction of dichromate and photocatalytic oxidation of dichlorvos. *Chemosphere* 2005;60:1308–15.
- [269] Gomez S, Marchena CL, Renzini MS, Pizzio L, Pierella L. In situ generated TiO<sub>2</sub> over zeolitic supports as reusable photocatalysts for the degradation of dichlorvos. *Appl Catal B: Env* 2015;162:167–73.
- [270] Dai K, Ping T, Chen H, Liu J, Zan L. Photocatalytic degradation of commercial phoxim over La-Doped TiO<sub>2</sub> nanoparticles in aqueous suspension. *Env Sci Technol* 2009;43:1540–5.

- [271] Jaiswal M, Chauhan D, Sankaramakrishnan N. Copper chitosan nanocomposites: synthesis, characterization, and application in removal of organophosphorous pesticide from agricultural runoff. *Env Sci Pollut R* 2012;19:2005–62.
- [272] Sahithya K, Das D, Das N. Effective removal of dichlorvos from aqueous solution using biopolymer modified MMT-CuO composites: equilibrium, kinetic and thermodynamic studies. *J Mol Liq* 2015;211:821–30.
- [273] Tomasevic A, Kiss E, Petovic S, Mijin D. Study on the photocatalytic degradation of insecticide methomyl in water. *Desalination* 2010;262:228–34.
- [274] Henych J, Janos P, Kormunda M, Tolasz J, Stengl V. Reactive adsorption of toxic organophosphates parathion methyl and DMMP on nanostructured Ti/Ce oxides and their composites. *Arab J Chem* 2016. Available from: <https://doi.org/10.1016/j.arabjc.2016.06.002>.
- [275] Dixit V, Tewari JC, Obendorf SK. Identification of degraded products of aldicarb due to the catalytic behavior of titanium dioxide/polyacrylonitrile nanofiber. *J Chromatogr A* 2009;1216:6394–9.
- [276] Fouad DM, Mohamed MB. Comparative study of the photocatalytic activity of semiconductor nanostructures and their hybrid metal nanocomposites on the photodegradation of malathion. *J Nanomater* 2012;2012:1–8.
- [277] de Urzedo APFM, Nascentes CC, Augusti R. Degradation of the insecticides Thiamethoxam and Imidacloprid in aqueous solution as promoted by an innovative Fe<sub>8</sub>/Fe<sub>3</sub>O<sub>4</sub> composite. *J Braz Chem Soc* 2009;20(1).
- [278] Fouad DM, Mohamed MB. Photodegradation of chloridazon using core-shell magnetic nanocomposites. *J Nanotechnol* 2011;2011:1–7.
- [279] Senthilnathan M, Ho DP, Vigneswaran S, Ngo HH, Shon HK. Visible light responsive ruthenium-doped titanium dioxide for the removal of metsulfuron-methyl herbicide in aqueous phase. *Sep Purif Technol* 2010;75:415–19.
- [280] Saifuddin N, Nian CY, Zhan LW, Ning KX. Chitosan-silver nanoparticles composite as point-of-use drinking water filtration system for household to remove pesticides in water. *Asian J Biochem* 2011;6:142–59.
- [281] Chiou CH, Juang RS. Photocatalytic degradation of phenol in aqueous solutions by Pr-doped TiO<sub>2</sub> nanoparticles. *J Hazard Mater* 2007;149:1.
- [282] Ali I, Aboul-Enein HY. Chiral pollutants: distribution, toxicity and analysis by chromatography and capillary electrophoresis. Chichester, UK: John Wiley & Sons; 2004.
- [283] Chiou CH, Wu CY, Juang RS. Influence of operating parameters on photocatalytic degradation of phenol in UV/TiO<sub>2</sub> process. *Chem Eng J* 2008;139:322.
- [284] Kurt BZ, Durmus Z, Durmus A. Preparation and characterization of platinum (Pt) and palladium (Pd) nanoparticle decorated graphene sheets and their utilization for the elimination of basic fuchsin and indigo carmine dyes. *Solid State Sci* 2016;51:51–8.
- [285] Wang S, Li H. Structure directed reversible adsorption of organic dye on mesoporous silica in aqueous solution. *Micropor Mesopor Mater* 2006;97(1–3):21–6.
- [286] Khan A, Liao Z, Liu Y, Jawad A, Ifthikar J, Chen Z. Synergistic degradation of phenols using peroxymonosulfate activated by CuO-Co<sub>3</sub>O<sub>4</sub>@MnO<sub>2</sub> nanocatalyst. *J Hazard Mater* 2017;329:262.
- [287] Cojocaru B, Andrei V, Tudorache M, Lin F, Cadigan C, Richards R, et al. Enhanced photo-degradation of bisphenol pollutants onto gold-modified photocatalysts. *Catal Today* 2017;284:153–9.
- [288] Yang L, Li Z, Jiang H, Jiang W, Su R, Luo S, et al. Photoelectrocatalytic oxidation of bisphenol A over mesh of TiO<sub>2</sub>/graphene/Cu<sub>2</sub>O. *Appl Catal B* 2016;183:75–85.



- [289] Xia J, Di J, Yin S, Li H, Xu H, Shu H, et al. Solvothermal synthesis and enhanced visible-light photocatalytic decontamination of bisphenol A (BPA) by g-C<sub>3</sub>N<sub>4</sub>/BiOBr heterojunctions. *Mat Sci Semicon Pro* 2014;24:96–103.
- [290] Fürhacker M, Scharf S, Weber H. Bisphenol A: emissions from point sources. *Chemosphere* 2000;41:751–6.
- [291] Nadejde C, Neamtu M, Hodoroaba VD, Schneider RJ, Ababei G, Panne U. Hybrid iron-based core–shell magnetic catalysts for fast degradation of bisphenol A in aqueous systems. *Chem Eng J* 2016;302:587–94.
- [292] Zhang L, Xu D, Hu C, Shi Y. Framework Cu-doped AlPO<sub>4</sub> as an effective Fenton-like catalyst for bisphenol A degradation. *Appl Catal B* 2017;207:9–16.
- [293] Liu D, Wu Z, Tian F, Ye BC, Tong Y. Synthesis of N and La co-doped TiO<sub>2</sub>/AC photocatalyst by microwave irradiation for the photocatalytic degradation of naphthalene. *J Alloy Compd* 2016;676:489–98.
- [294] Xia S, Zhang L, Zhou X, Shao M, Pan G, Ni Z. Fabrication of highly dispersed Ti/ZnO–Cr<sub>2</sub>O<sub>3</sub> composite as highly efficient photocatalyst for naphthalene degradation. *Appl Catal B* 2015;176–177:266–77.
- [295] Sannino F, Pirozzi D, Vitiello G, D'errico G, Aronne A, Fanelli E, et al. Oxidative degradation of phenanthrene in the absence of light irradiation by hybrid ZrO<sub>2</sub>-acetylacetonate gel-derived catalyst. *Appl Catal B* 2014;156–157:101–7.
- [296] Zhao X, Cai Z, Wang T, O'Reilly SE, Liu W, Zhao D. A new type of cobalt-deposited titanate nanotubes for enhanced photocatalytic degradation of phenanthrene. *Appl Catal B* 2016;187:134–43.
- [297] Moussawi RN, Patra D. Nanoparticle self-assembled grain like curcumin conjugated ZnO: curcumin conjugation enhances removal of perylene, fluoranthene, and chrysene by ZnO. *Sci Rep* 2016;6:24565–72.
- [298] Zhang LH, Li PJ, Gong ZQ, Oni AA. Photochemical behaviour of benzo [a] pyrene on soil surface under UV light irradiation. *J Environ Sci* 2006;18:1226–32.
- [299] Liao W, Ma Y, Chen A, Yang Y. Preparation of fatty acids coated Fe<sub>3</sub>O<sub>4</sub> nanoparticles for adsorption and determination of benzo(a)pyrene in environmental water samples. *Chem Eng* 2015;271:232–9.
- [300] Smith B, Uhl K. Drug delivery in the twenty-first century: a new paradigm. *Clin Pharmacol Ther* 2009;85:451–5.
- [301] Wang L, Wang L, Zhu C, Wei X, Kan X. Preparation and application of functionalized nanoparticles of CdS as a fluorescence probe. *Anal Chim Acta* 2002;468:35–41.
- [302] Cegnar M, Kristl J, Kos J. Nanoscale polymer carriers to deliver chemotherapeutic agents to tumours. *Expert Opin Biol Ther* 2005;5:1557–69.
- [303] Subbiah R, Veerapandian M, Yun KS. Nanoparticles: functionalization and multifunctional applications in biomedical sciences. *Curr Med Chem* 2010;17(36):4559–77.
- [304] De AK. *Environmental Chemistry*, Wiley, New Delhi, India. 2010;76.
- [305] Nagami H. Historical perspective of pesticide poisoning in Japan and measures taken by the Japanese Association of Rural Medicine. *J Rural Med* 2010;5(1):129–133.
- [306] Baker EL, Warren MW, Zack M, Bobbin RD, Miles JW, Miller S. Epidemic malathion poisoning in Pakistan malaria workers. *Lancet* 1978;311:31–34.
- [307] Gupta S, Ashrith G, Chandra D, Gupta AK, Finkel KW, Guntupalli JS. Acute phenol poisoning: a life-threatening hazard of chronic pain relief. *Clin Toxicol (Phila)*. 2008; 46(3):250–3.
- [308] Lewin JF, Cleary WT. An accidental death caused by the absorption of phenol through skin. A case report. *Forensic Sci Int* 1982;19:177–179.

- [309] Lu Y, Jiang J, Huang W. Clinical features and treatment in patients with acute 2,4-dinitrophenol poisoning. *J Zhejiang Univ Sci B*. 2011;12(3):189–192.
- [310] Bartlett J., Brunner M., Gough K. Deliberate poisoning with dinitrophenol (DNP): an unlicensed weight loss pill. *Emerg Med J*. 2010;27:159–160.

## Further Reading

- Affam AC, Chaudhuri M. Degradation of pesticides chlorpyrifos, cypermethrin and chlorothalonil in aqueous solution by  $\text{TiO}_2$  photocatalysis. *J Env Manage* 2013;130:160–5.
- Albanis T.A., Hela D.G., Sakellarides T.M., Konstantinou I.K. Pesticide residues in surface water, ground waters and rainfall of Imathia (N. Greece) K.L. Katsifarakis, G.P. Korfiatis, Y.A. Mylopoulos, A.C. Demetracopoulos (Eds.), *Proceedings of an International Conference* (1998), 119–12.
- Al-Fartusie FS, Mohssan SN. Essential trace elements and their vital roles in human body Indian. *J Adv Chem Sci* 2017;5:127–36.
- Arabzadeh N, Khosravi A, Mohammadi A, Mahmoodi NM. Enhanced photodegradation of hazardous tartrazine by composite of nanomolecularly imprinted polymer-nanophotocatalyst with high efficiency. *Desalin Water Treat* 2016;57(7):3142–51.
- Asano M, Sumino S, Jiku F. Decomposition of benzo (a) pyrene on artificial sea water using of UV/photocatalytic oxidation process. *J Env Sci Eng A* 2009;18:195–9.
- Badrudoza AZM, Shawon ZBZ, Tay WJD, Hidajat K, Uddin MS.  $\text{Fe}_3\text{O}_4$ /cyclodextrin polymer nanocomposites for selective heavy metals removal from industrial wastewater. *Carbohydr Polym* 2013;91(1):322–32.
- Baioni AP, Vidotti M, Fiorito PA, Ponzio EA, Cordoba de Torresi S. Synthesis and characterization of copper hexacyanoferrate nanoparticles for building up long-term stability electrochromic electrodes. *Langmuir* 2007;23:6796–800.
- Chang W-C, Deka JR, Wu H-Y, Shieh F-K, Huang S-Y, Kao H-M. Synthesis and characterization of large pore cubic mesoporous silicas functionalized with high contents of carboxylic acid groups and their use as adsorbents. *Appl Catal B* 2013;142–143:817–27.
- Cortes DR, Hites RA. Detection of statistically significant trends in atmospheric concentrations of semivolatile compounds. *Env Sci Tec* 2000;34:2826–9.
- Depang L, Leyuan S, Xili L, Xiance Y. A successful control programme for falciparum malaria in Xinyang. *China Trans, R Soc Trop Med Hyg* 1996;90:100–2.
- Dierick M, Hoorebeke LV, Jacobs P, Masschaele B, Vlassenbroeck J, Cnudde V, et al. The use of 2D pixel detectors in micro-and nano-CT applications. *Nucl Instrum Methods Phys Res Sect A* 2008;591:255–9.
- Du YB, Kyung M, Kim MJ, et al. *Compre Rev Food Sci Food Saf* 2012;11:453–70.
- Fawell JK, Hunt S. The polyaromatic hydrocarbons. *Environmental toxicology: organic pollutants*, 6. West Sussex: Ellis Harwood; 1988. p. 241–69.
- Fromme H, Oddoy A, Piloty M, Krause M, Lahrz T. Polycyclic aromatic hydrocarbons (PAH) and diesel engine emission (elemental carbon) inside a car and a subway train. *Sci Total Env* 1998;217:165–73.
- Fung AKM, Chiu BKW, Lam MHW. Surface modification of  $\text{TiO}_2$  by aruthenium (II) polypyridyl complex via silyl-linkage for the sensitized photocatalytic degradation of carbon tetrachloride by visible irradiation. *Water Res* 2003;37(8):1939–47.
- Gómez J, Bódalo A, Gómez E, Hidalgo A, Gómez M, Murcia M. A transient design model of a continuous tank reactor for removing phenol with immobilized soybean peroxidase and hydrogen peroxide. *Chem Eng J* 2008;145:142–8.

- Hong H-J, Jeong HS, Kim B-G, Hong J, Park I-S, Ryu T, et al. Highly stable and magnetically separable alginate/Fe<sub>3</sub>O<sub>4</sub> composite for the removal of strontium (Sr) from seawater. *Chemosphere* 2016;165:231–8.
- Jarosz P, Du P, Schneider J, Lee S-H, McCamant D, Eisenberg R. Platinum(II) terpyridyl acetylacetonate complexes on platinumized TiO<sub>2</sub>: toward the photogeneration of H<sub>2</sub> in aqueous media. *Inorg Chem* 2009;48(20):9653–63.
- Jeyasubramanian K, Hikku GS, Sharma RK. Photo-catalytic degradation of methyl violet dye using zinc oxide nano particles prepared by a novel precipitation method and its anti-bacterial activities. *J Water Proc Eng* 2015;8:35–44.
- Ji L, Zhou L, Bai X, Shao Y, Zhao G, Qu Y, et al. Facile synthesis of multiwall carbon nanotubes/iron oxides for removal of tetrabromo bisphenol A and Pb (ii). *J Mater Chem* 2012;22(31):15853–62.
- Kim H-R, Jang J-W, Park J-W. Carboxymethyl chitosan modified magnetic-cored dendrimer as an amphoteric adsorbent. *J Hazard Mater* 2016;317:608–16.
- Klaysri R, Tubchareon T, Praserttham P. One- step synthesis of amine-functionalized TiO<sub>2</sub> surface for photocatalytic decolorization under visible light irradiation. *J Ind Eng Chem* 2017;45:229–36.
- Konstantinou IK, Hela DG, Albanis TA. The status of pesticide pollution in surface waters (rivers and lakes) of Greece. Part I. Review on occurrence and levels. *Env Pollut* 2006;141:555–70.
- Kuch HM, Ballschmiter K. Determination of endocrine-disrupting phenolic compounds and estrogens in surface and drinking water by HRGC-(NCI)-MS in the picogram per liter range. *Env Sci Technol* 2001;35:3201–6.
- Kumar R, Kumar G, Akhtar MS, Umar A. Sonophotocatalytic degradation of methyl orange using ZnO nano-aggregates. *J Alloy Compd* 2015;629:167–72.
- Kuo CY, Wu CH, Lin HY. Photocatalytic degradation of bisphenol A in a visible light/TiO<sub>2</sub> system. *Desalination* 2010;256:37–42.
- Kyzas GZ, Lazaridis NK, Mitropoulos AC. Removal of dyes from aqueous solutions with untreated coffee residues as potential low-cost adsorbents: equilibrium, reuse and thermodynamic approach. *Chem Eng J* 2012;189–190:148–59.
- Li J, Zhang S, Chen C, Zhao G, Yang X, Li J, et al. Removal of Cu(II) and fulvic acid by graphene oxide nanosheets decorated with Fe<sub>3</sub>O<sub>4</sub> nanoparticles. *ACS Appl Mater Interfaces* 2012;4(9):4991–5000.
- Ling H, Kim K, Liu Z, Shi J, Zhu X, Huang J. Photocatalytic degradation of phenol in water on as-prepared and surface modified TiO<sub>2</sub> nanoparticles. *Catal Today* 2015;258:96–102.
- Lopes RP, De Urzedo APFM, Nascentes CC, Augusti R. Degradation of the insecticides thiamethoxam and imidacloprid by zero-valent metals exposed to ultrasonic irradiation in water medium: electrospray ionization mass spectrometry monitoring. *Rapid Commun Mass Spectrom* 2008;22:3472–80.
- Mahmoodi NM, Khorramfar S, Najafi F. Amine-functionalized silica nanoparticle: preparation, characterization and anionic dye removal ability. *Desalination* 2011;279(1–3):61–8.
- Maliszewska-Kordybach B. Sources, concentrations, fate and effects of polycyclic aromatic hydrocarbons (PAHs) in the environment. Part A: PAHs in air. *Pol J Env Stud* 1999;8:131–6.
- Manoli E, Samara C. Polycyclic aromatic hydrocarbons in natural waters: sources, occurrence and analysis. *Trends Anal Chem* 1999;18:417–28.
- Matsuoka M, Ide Y, Ogawa M. Temperature-dependent photocatalytic hydrogen evolution activity from water on a dye-sensitized layered titanate. *Phys Chem Chem Phys* 2014;16(8):3520–2.

- Mesdaghinia A, Azari A, Nodehi RN, Yaghmaeian K, Bharti AK, Agarwal S, et al. Removal of phthalate esters (PAEs) by zeolite/Fe<sub>3</sub>O<sub>4</sub>: investigation on the magnetic adsorption separation, catalytic degradation and toxicity bioassay. *J Mol Liq* 2017;233:378–90.
- Michalowicz J. Bisphenol A - sources, toxicity and biotransformation *Environ. Toxicol Pharmacol* 2014;37:738–58.
- Moctezumaa E, Leyva E, Palestino G, de Lasa H. Photocatalytic degradation of methyl parathion: reaction pathways and intermediate reaction products. *J Photochem Photobiol A: Chem* 2007;186:71–84.
- Mukherjee D, Bhattacharya P, Jana A, Bhattacharya S, Sarkar S, Ghosh S, et al. Synthesis of ceramic ultrafiltration membrane and application in membrane bioreactor process for pesticide remediation from wastewater. *Process Saf Env Prot* 2018;116:22–9.
- Murakami Y, Miyauchi Y, Chiashi S, Maruyama S. Direct synthesis of high-quality single-walled carbon nanotubes on silicon and quartz substrates. *Chem Phys Lett* 2003;377(1–2):49–54.
- Kashif N, Ouyang F. Parameters effect on heterogeneous photocatalysed degradation of phenol in aqueous dispersion of TiO<sub>2</sub>. *J Env Sci* 2009;21:527–33.
- Naf C, Broman D, Brunstrom B. Distribution and metabolism of polycyclic aromatic hydrocarbons (PAHs) injected into eggs of chicken (*Gallus domesticus*) and common eider duck (*Somateria mollissima*). *Env Toxicol Chem* 1992;11:1653–60.
- Nair MG, Nirmala M, Rekha K, Anukaliani A. Structural, optical, photocatalytic and antibacterial activity of ZnO and Codoped ZnO nanoparticles. *Mater Lett* 2011;65(12):1797–800.
- Nemerow NL, Dasgupta A. Industrial and hazardous waste treatment. New York, London: Van Nostrand Reinhold Publishing Company; 1991. Elsevier Butterworth-Heinemann.
- P.P. Singh, Ambika Environmental remediation by nanoadsorbents-based polymer nanocomposite, *New Polymer Nanocomposites for Environmental Remediation* 2018, 223–241.
- Pandey A, Kalal S, Ameta C, Ameta R, Kumar S, Punjabi PB. Synthesis, characterization and application of naive and nano-sized titanium dioxide as a photocatalyst for degradation of methylene blue. *J Saudi ChemSoc* 2015;19:528–36.
- Papoulias DM, Tillitt DE, Talykina MG, Whyte JJ, Richter CA. Atrazine reduces reproduction in Japanese medaka (*Oryzias latipes*). *Aquat Toxicol* 2014;154:230–9.
- Sachdeva S, Kumar A. Preparation of nanoporous composite carbon membrane for separation of rhodamine B dye. *J MembrSci* 2009;329:2–10.
- Santos DO, deLourdes Nascimento Santos M, Costa JAS, deJesus RA, Navickiene S, Sussuchi EM, et al. Investigating the potential of functionalized MCM-41 on adsorption of remazolred dye. *Env Sci Pollut Res* 2013;20(7):5028–35.
- Shahrezaei F, Mansouri Y, Zinatizadeh AAL, Akhbari A. Process modeling and kinetic evaluation of petroleum refinery wastewater treatment in a photocatalytic reactor using TiO<sub>2</sub> nanoparticles. *Powder Technol* 2012;221:203–12.
- Stronkhorst J, Ysebaert TJ, Smedes F, Meininger PL, Dirksen S. Contaminants in eggs of some waterbird species from Scheldt Estuary, SW Netherlands. *Mar Pollut Bull* 1993;26:572–8.
- Suzuki TM, Tanaka H, Morikawa T, Iwaki M, Sato S, Sasaki S, et al. Direct assembly synthesis of metal complex-semiconductor hybrid photocatalysts anchored by phosphonate for highly efficient CO<sub>2</sub> reduction. *Chem Commun* 2011;47:8673–5.
- Tanaka A, Fuku K, Nishi T, Hashimoto K, Kominami H. Functionalization of Au/TiO<sub>2</sub> plasmonic photocatalysts with Pd by formation of a core-shell structure for effective dechlorination of chlorobenzene under irradiation of visible light. *J Phys Chem C* 2013;117(33):16983–9.

- Tchobanoglous G, Franklin LB. Wastewater engineering: treatment, disposal and reuse. New York: McGraw Hill, Inc; 1991. p. 1991.
- The Concentration of Organochlorine Pesticides in the Western Australian Population 1966–1991.
- Tonne CC, Whyatt RM, Camann DE, Perera FP, Kinney PL. Predictors of personal polycyclic aromatic hydrocarbon exposures among pregnant minority women in New York City. *Env Health Perspect* 2004;112:754–9.
- Wilson SC, Jones KC. Bioremediation of soils contaminated with polynuclear aromatic hydrocarbons (PAHs): a review. *Env Pollut* 1993;55:329–47.
- Wright DA. P. Welbourn Environmental toxicology. Cambridge: Cambridge University Press; 2002.
- Wu Z, Huang W, Cui K, Gao Z, Wang P. Sustainable synthesis of metals-doped ZnO nanoparticles from zinc-bearing dust for photodegradation of phenol. *J Hazard Mater* 2014;278:91–9.
- Yan Z, Tao S, Yin J, Li G. Mesoporous silicas functionalized with a high density of carboxylate groups as efficient absorbents for the removal of basic dyestuffs. *J Mater Chem* 2006;16(24):2347–53.
- Yang Q, Wang J, Chen X, Yang W, Pei H, Hu N, et al. The simultaneous detection and removal of organophosphorus pesticides by a novel Zr-MOF based smart adsorbent. *J Mat Chem A* 2018;6:2184–92.
- Yasmina M, El-Katori EE, Gharni ZH. Photocatalytic degradation of methylene blue dye using Fe<sub>2</sub>O<sub>3</sub>/TiO<sub>2</sub> nanoparticles prepared by solgel method. *J Alloy Compd* 2013;553:1929–39.
- Yokota H, Tsuruda Y, Maeda M, Oshima Y, Tadokoro H, Nakazono A, et al. Effect of bisphenol a on the early life stage in Japanese medaka (*Oryzias latipes*). *Env Toxicol Chem* 2000;19:1925–30.
- Zhang M, Johnston CP, Dahal G. A comparative evaluation of hexavalent chromium treatment in contaminated soil by calcium polysulfide and green-tea nanoscale zero-valent iron. *J Hazard Mater* 2012;201:33–42.
- Zheng Z, Zhao J, Yuan Y, Liu H, Yang D, Sarina S, et al. Tuning the surface structure of nitrogen-doped TiO<sub>2</sub> nanofibres: an effective method to enhance photocatalytic activities of visible-light-driven green synthesis and degradation. *Chem Eur J* 2013;19(18):5731–41.
- Zhou JL, Maskouki K, Qiu YW, Hong HS, Wang ZD. Polychlorinated biphenyl congeners and organochlorine insecticides in the water column and sediments of Daya Bay. *China Env Pollut* 2001;113:373–84.
- Zhou C, Zhang W, Xia M, Zhou W, Wan Q, Peng K, et al. Synthesis of poly(acrylic acid) coated-Fe<sub>3</sub>O<sub>4</sub> superparamagnetic nanocomposites and their fast removal of dye from aqueous solution. *J Nanosci Nanotech* 2013;13(7):4627–33.
- Zhou Y-T, Nie H-L, Branford-White C, He Z-Y, Zhu LM. Removal of Cu<sup>2+</sup> from aqueous solution by chitosan-coated magnetic nanoparticles modified with  $\alpha$ -ketoglutaric acid. *J Colloid Interface Sci* 2009;330(1):29–37.

# Implications of surface coatings on engineered nanomaterials for environmental systems: status quo, challenges, and perspectives

Ndeke Musee<sup>1</sup>, Samuel Leareng<sup>1</sup>, Lemme Kebaabetswe<sup>2</sup>, Gosaitse Tubatsi<sup>2</sup>, Ntombikayise Mahaye<sup>1</sup> and Melusi Thwala<sup>3</sup>

<sup>1</sup>Emerging Contaminants Ecological Risk Assessment (ECERA) Group, Department of Chemical Engineering, University of Pretoria, Pretoria, South Africa, <sup>2</sup>Department of Biological Sciences and Biotechnology, Botswana International University of Science and Technology, Palapye, Botswana, <sup>3</sup>Water Centre, Council for Scientific and Industrial Research, Pretoria, South Africa

### 14.1 Introduction

During the last two decades there has been expansive growth in the field of nanotechnology, with wide use of engineered nanomaterials (ENMs) in both consumer products and industrial applications [1,2]. Concomitant with this increase are increasing releases into different ecological systems [3–5]. As a result, there are concerns for the potential implications of ENMs on environmental systems. In this chapter, we review and evaluate the influence of surface coating agents used on ENMs and their beneficial and adverse implications for the environment.

Different types and chemistries of coatings have become important in the design of ENMs in the endeavor to optimize consumer products and industrial-application functionalities [6]. Coatings are widely used on ENMs for stabilization purposes in various applications such as catalysis [6] and drug delivery [7]. Frequently used coatings on different models of ENMs are summarized in Dwivedi et al. [8]. We have summarized them here, where specific applications have been discussed. Numerous studies have investigated the implications of ENMs in aquatic systems. where the influence of inherent physicochemical properties (i.e., size, shape, and coatings) and water chemistry (i.e., pH and ionic strength) have been extensively investigated [9,10].

Although research has been conducted on the influence of physicochemical properties such as size and surface charge on the adaptability and toxicity of ENMs in environmental systems [11,12], little has been conducted on the role of coatings. Therefore we will outline how the type and chemistry of ENMs coatings, from synthesis or acquisition, following entry into environmental systems, affects ENM' adaptability and toxicity. Kim et al. [13] reported that the toxicity of silver nanoparticles (nAg) to zebrafish embryos was dependent on surface coating. Polyvinylpyrrolidone (PVP) coated—Ag was more toxic than citrate coated, regardless of particle size (20 or 50 nm). Other research has shown that smaller-sized citrate-coated nAg was more toxic as evidenced by induction of mortality and malformations on zebrafish embryos relative to those coated with PVP [14]. The differences in observed toxicity among the studies [13,14] can be attributed to the agglomeration of ENMs. It has been observed that citrate-coated ENMs are more unstable in exposure media [15]. Therefore the smaller-sized PVP-coated ENMs exhibit higher toxicity.

In Powers et al. [14], the effect of agglomeration on the reported toxicity was not explained, possibly leading to the conclusion that citrate ENMs were more toxic. Such findings are important to consider. Following uptake of ENMs by organisms, the biodistribution of internalized ENMs may potentiate size changes (i.e., aggregation or agglomeration), and subsequently impede the efficacy of ENMs in breaching cell membrane barriers [16,17]. For example, Qui et al. [18] showed that the toxicity of negatively charged mercaptopropionic acid (MPA) and polyallylamine hydrochloride (PAH)-coated nAg to *Shewanella oneidensis* MR-1 and *Daphnia magna* gene-expression patterns was coating-type dependent. These effects were due to differences in electrostatic attractions between the ENM charges and negatively charged organisms. ENMs are known to undergo size-linked transformations, such as dissolution and/or loss of surface coating during biodistribution in organisms [19].

Following release into environmental systems [4,20], ENMs interact with natural organic matter (NOM). This may result in the formation of NOM coating on ENM surfaces [21,22]. This formation, which has been widely reported, leads to the modification of surface properties, dissolution rates [23], and stability [24]. This exerts great influence on ENM adaptability, transport, and toxicity in aquatic systems [25].

In this chapter, we summarize data retrieved from published literature on fate and toxicity of ENMs in environmental systems with specific focus on their coatings. Our goal is to (1) identify the mechanisms by which coating affects fate and ecotoxicity of ENMs, and specific driving factors, (2) summarize challenges associated with accounting for the role of coatings on risk assessment of ENMs in environmental systems, and (3) provide recommendations on how these challenges may be addressed. Specific attention, for example, relates to how different forms and types of coatings influence the life and toxicity of ENMs in different aquatic systems and specific taxa. The range of effects, from

subcellular to whole organism, caused by various coatings on ENMs will be examined. The influences of coating on their future fate and transformation processes in different exposure matrixes (i.e., freshwater and wastewater) will be highlighted. Fate of current knowledge of the implications for ENM coatings on environmental systems, innovative approaches for future design, and risk assessment of ENMs will be outlined.

## 14.2 Implications of coatings for engineered nanomaterial transformation in environmental systems

Relevant literature concerning influences on the transformation of ENM coatings in aquatic systems is outlined. Numerous studies have reported that diverse factors influence ENMs fate and behavior, as controlled by water chemistry matrixes (i.e., pH and NOM). Their inherent physicochemical properties such as size [26,27], shape [28], and surface properties [24] have also been reported. Our discussions will be limited to the fundamental representative studies on fate and behavior of ENMs with specific focus on their engineered coatings [8,29], and coatings formed from interactions between ENMs and environmental macromolecules (in this case NOM) [30].

In environmental systems, ENMs undergo transformation processes that include dissolution, adsorption, aggregation, disaggregation, deposition, photooxidation, and surface alteration. In this chapter, we focus on the two key environmental transformations, dissolution and aggregation [31,32], as schematically illustrated in Fig. 14.1. Both are predominant in natural systems due to the abundance of NOM. Both have been widely investigated [15].

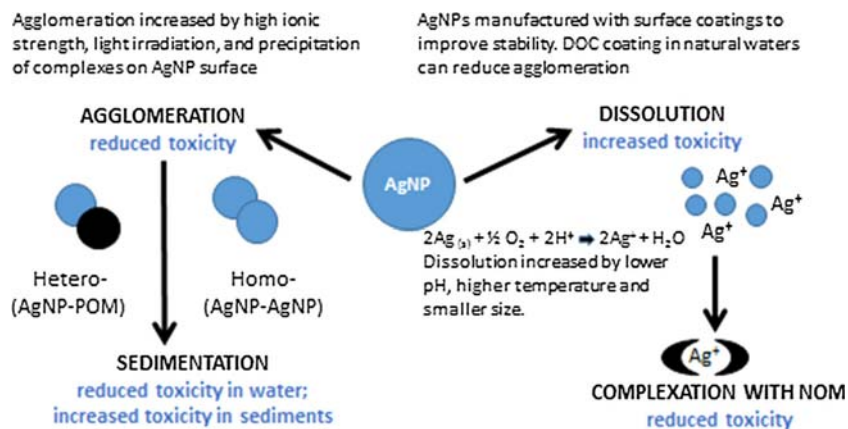


**FIGURE 14.1** Agglomeration and dissolution as key transformations of ENMs in aquatic ecosystems and their effect on fate and toxicity using Ag NPs as an illustrative example. Adapted from Furtado LM, Bundschuh M, Metcalfe CD. Monitoring the fate and transformation of silver nanoparticles in natural waters. *Bull Environ Contamin Toxicol*. 2016;97(4):449–55.



In order to provide a framework by which the fate and behavior of ENMs are linked to their coatings, each process is briefly summarized for both engineered [8,29] and natural-macromolecules (i.e., NOM, proteins, and biological exudates) [21,30] coatings. Such an approach is valuable since coatings exert distinctive influence on dissolution [33], aggregation [34], and toxicity potential (e.g., phytotoxicity) [35].

### 14.2.1 Dissolution

During the design phase of certain ENMs, the dissolution process is essential since it determines their mode of action as antibacterial agents (e.g., surface coatings used in textiles and personal-care products), and medical applications [1,2]. However, they may induce adverse implications when released into environmental systems [36,37]. Parameters influencing the dissolution of ENMs into environmental systems have been extensively reviewed (Refs. [21,22,38], articles cited therein). Metallic ENMs are either soluble (i.e., Ag, CuO, and ZnO), or insoluble (i.e., CeO<sub>2</sub> and TiO<sub>2</sub>) [38,39]. Solubility controls the degree of persistence of ENMs in environmental systems and its hazard potential [21,40]. Many studies have also investigated the parameters that control the dissolution of ENMs, including their inherent physicochemical properties such as size, morphology, and coating as influenced by water chemistry [15]. The coating parameter will be addressed in this chapter.

#### 14.2.1.1 Influence of engineered coatings on dissolution

The nature and type of coating may induce variant dissolution rates as influenced by the exposure media chemistry. For instance, Wu et al. [41] quantified the influence of three different coatings on the dissolution of Ag-NPs, and their consequent uptake and toxicity to organisms. The coatings were polyethylene glycol (PEG-Ag-NPs), silica (Si-Ag-NPs), and aminated silica-coated Ag-NPs (Ami-Si-AgNP). Results showed low dissolution rates of 2.2%, 2.4%, and 5.3% for Ami-Si, PEG, and Si-Ag-NPs, respectively, compared to 1 mg/L Ag-NPs nominal exposure concentration after 120 h. The Si-coated Ag-NPs had the highest dissolution concentration ( $22.4 \pm 1.0 \mu\text{g/L}$ ), followed by PEG-Ag ( $14.4 \pm 0.47 \mu\text{g/L}$ ). Ami-Si-Ag had the least ( $7.3 \pm 0.7 \mu\text{g/L}$ ) [41].

In another study, dissolution of uncoated and coated nAg [using three types of coatings: trisodium citrate, sodium dodecyl sulfate (SDS), and Tween 80 (Tween)] were investigated. Results indicated that the dissolution of nAg-NPs was inhibited by the SDS and Tween coatings, but none was observed under the citrate coating. In chloride-electrolytes media a secondary precipitate of AgCl was observed bridging the individual particles [42]. Thus the published data suggest that coating agents exert significant influence on

the fate of ENMs in aquatic systems as characterized by varying degrees of either enhancing or inhibiting ENM dissolution.

#### 14.2.1.2 *Influence of macromolecules coatings on dissolution*

Extensive studies indicate that the dissolution of ENMs in environmental systems is dependent on macromolecules [21,43,44] and is a surface-controlled reaction [45] wherein the release of ions is influenced by their surface-area and water-chemistry characteristics. This dissolution process is controlled by NOM adsorbing to ENM surfaces [46,47] in three fundamental ways: the coating may act as a barrier for diffusion of ions by blocking the oxidation sites [48], shift of kinetic reactions through chelation of ions by the NOM, thus leading to inhibition of oxidation of ENMs [24,49], and/or occurrence of reversible reaction of released ions to particulates or vice versa (e.g.,  $\text{Ag}^+$  to  $\text{Ag}^0$ ) with humic acid (HA) and fulvic acid (FA) acting as reductants [23].

The formation of organic coatings due to macromolecules adsorption on ENM surfaces through electrostatic and/or static interactions can lead to variant dissolution kinetics in aqueous media. High-molecular weight (MW) macromolecules (i.e., FA (0.5–2 kDa) [50] and HA (1–10 kDa) [50] have been observed to inhibit nAg dissolution coated with citrate [23] and oleic acid [51] in a dose-dependent fashion. The underlying mechanism was attributed to the trapping of nAg sites on a humic acid matrix [23,24]. The released  $\text{Ag}^+$  ions were transformed into nAg with HA/FA acting as reductants, and/or the elimination of  $\text{H}_2\text{O}_2$  oxidant by NOM [52]. Conversely, lower MW macromolecules (i.e., citric acid and oxalic acid) enhanced oxidative dissolution, as observed in nCu linked to surface complex and accelerated oxidation by dissolved oxygen [53].

Similar results on the influence of MW were reported by Miao et al. [54]. For instance, low MW chelating effect of cysteine coating (amino acid with a carboxylate) on nZnO led to an increase in dissolution, which was most likely due to surface complexation-dominated mechanism. However, high MW–FA played an opposite role especially at low concentrations where the dissolution of nZnO was inhibited. Thus FA did not facilitate dispersion of nZnO as expected. It is likely that the formation of coated nZnO following FA adsorption due to electrostatic attraction protected the ENMs from dissolution [54].

The inhibitive effects were less remarkable at higher NOM concentrations in comparison to lower ones, thus exhibiting concentration-dependent dissolution inhibition especially for higher MW macromolecules (function of NOM composition). This points to the dual effects of macromolecules coatings on ENMs. They can inhibit ENM dissolution [52,54] involving the blockage of macropores through the adsorption process [55]. Or, they can induce ENM dissolution through the complexation of metallic ionic species

with NOM [56,57] as controlled by the exposure media pH, as previously observed for nZnO [58] and nCuO [56].

A key question remains as to what happens in the actual environmental systems where ENMs with coatings encounter natural macromolecules (i.e., NOM). Studies show that NOM (FA and HA) can displace existing coatings on ENMs such as  $\beta$ -glucose-coated nAu [59], citrate-coated nAg [30,60] and nZnO [27], and PVP-coated nAg [60]. Depending on the ENM type (e.g., nAg or nZnO), displacement of the engineered coating by NOM may lead to either stabilization or destabilization. For example, acetate coating on nZnO surface was displaced by NOM, consequently contributing to dissolution directly linked to ligand-assisted mechanism [27]. In contrast, is the displacement of nAg capping agents (citrate and PVP) by NOM induced destabilization [60]. There is no evidence of interactions between coatings and NOM, but evidence of displacement. Therefore, the findings should point to outcomes of NOM interactions with ENPs after displacement of coating by NOM.

Yin et al. [61] investigated the interactions of MW-fractionated NOM (Mf–NOM) with Cit, and PVP-coated nAg. Enhanced agglomeration or dispersion of nAg in NOM conditions was found to be dependent on the coating type, and that Mf–NOM fractions exhibited distinctive roles in the aggregation and dispersion processes. For example, high MW–Mf–NOM (> 100 and 30–100 kDa) enhanced aggregation of PVP-coated nAg–NMs. Lower MW–Mf–NOM (10–30, 3–10 and <3 kDa) inhibited the aggregation of PVP–AgNMs [61].

### 14.2.2 Agglomeration

The agglomeration of ENMs is partially due to weak interparticle repulsion since strong repulsion can effectively counter the agglomeration process. During synthesis and functionalization of ENMs, agglomeration potential is controlled by use of electrostatic and sterical coatings in order to retain functional properties [62]. These surface coatings have been observed to exert varied effects on ENM agglomeration in aquatic systems [21,22]. For instance, SDS and nonylphenol ethoxylate surfactants on nZnO were observed to reduce agglomeration and sedimentation under relatively high ionic strength in six different water matrices in variant degrees when compared to nonfunctionalized counterparts [63].

Similarly, Lodeiro et al. observed improved stabilization and reduced agglomeration of nAg when the surfaces were functionalized with natural polysaccharides [64]. Agglomeration kinetics of nAg have been observed elsewhere [42,65] as being dependent on surface coating properties, where the rate of agglomeration was higher in bare nAg compared to citrate and PVP-coated particles. Lower agglomeration of nTiO<sub>2</sub> in aqueous suspension was evident owing to surface coating of the nanoparticles using dodecanyl succinic anhydride and poly acrylic acid [66]. The stabilizing effect of PVP

resulted from steric interparticle repulsion. The surface stabilizer also exerts an influence on the agglomeration of NPs, and this has been well documented with nAg as a model for ENMs. For instance, surface functionalization of nAg with citrate, SDS, and Tween stabilized the nanoparticles sterically although the effect was lesser with the citrate coating [44]. It has been suggested that sterical and electrosterical stabilization are more resistant to destabilization driven by media chemistry in comparison to the electrostatic form when it is readily neutralized by media ions [34].

Generations of free radicals were observed to be dependent on surface coating properties [42], thus illustrating that coatings can be employed as a measure to proactively address the potential environmental risk of ENMs as within the *safety-by-design* principles. Godinez et al. [67] showed that surface coating of nTiO<sub>2</sub> with Triton X-100 induced a reduction in agglomeration size as compared to an uncoated counterpart. Surface coating has received more media attention. Following the exposure of nTiO<sub>2</sub> to NOM, there was reduced agglomeration size and enhanced stability, which was due to the increase of negative charge(s) on nTiO<sub>2</sub> NPs, which delayed the destabilization effect of divalent electrolytes (Ca<sup>2+</sup> and Mg<sup>2+</sup>) [68]. Studies from the Keller research group [69] reported a reduction in the agglomeration of nZnO in the presence of NOM–HA, even under high ionic strength conditions, due to NOM coating on the ENM surface. Thus both electrostatic interaction and steric hindrance of HA inhibited the agglomeration and sedimentation of nZnO.

## 14.3 Influence of engineered nanomaterial coatings on cellular organisms toxicity

### 14.3.1 Cellular organisms

Numerous studies have documented the influence of coatings on the toxicity of ENMs on cellular organisms [70–73]. Findings from these studies have shown that the use of coatings on ENMs induces variations on surface charges, which alters the uptake, translocation to different tissues, and cytotoxicity. Feng and coworkers evaluated the toxicity of three gold NPs (nAu) due to surface coatings. They are anionic MPA–nAu ( $-37 \pm 3.9$  mV), cationic 3-mercaptopropylamine (MPNH<sub>2</sub>)–nAu ( $26.9 \pm 2.5$  mV), and cationic poly (allylamine hydrochloride) (PAH)–nAu ( $35.1 \pm 3.4$  mV). This was performed on gram negatively charged and gram positively charged *S. oneidensis* MR-1 and *Bacillus subtilis* [71]. The results revealed that cationic PAH–nAu had higher affinity for cell membranes on both organisms, which is linked to its high positive charge, thus increasing bacteria cell and ENM interactions (Fig. 14.2).

Results of Qui et al. [18] showed that positively charged PAH-coated nAu was more toxic to *S. oneidensis* MR-1 than the negatively charged MPA-coated nAu. This is due to electrostatic interactions dependent on the

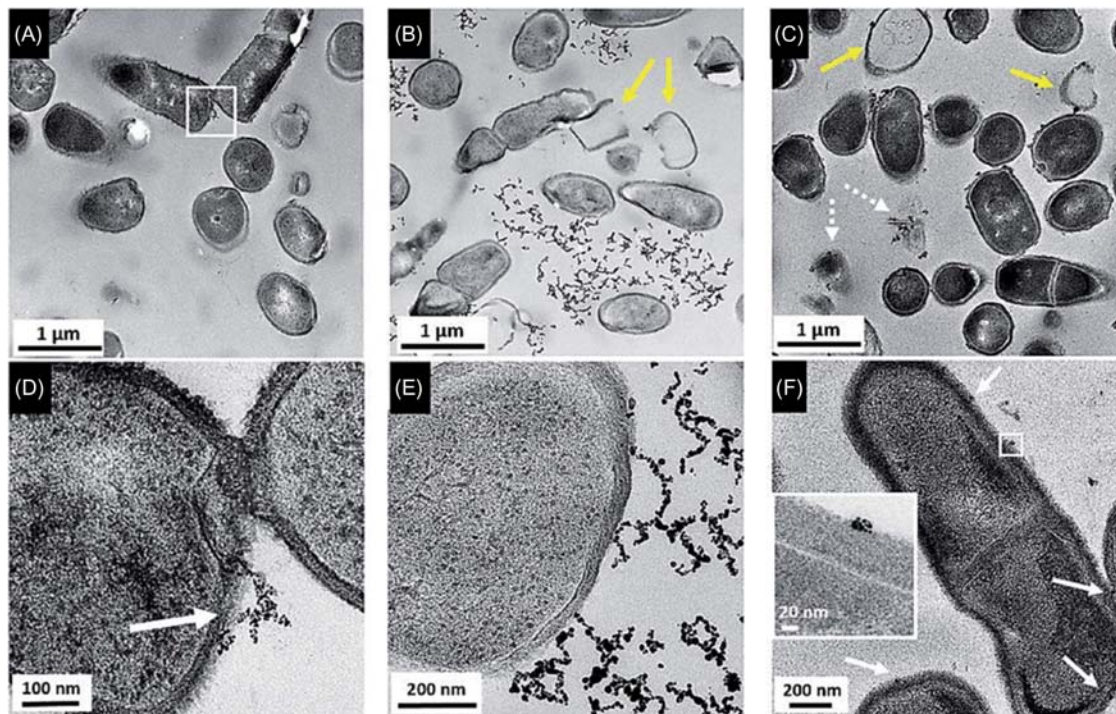


**FIGURE 14.2** TEM images showing the association of 5 mg/mL MPA–AuNPs (A and D), 5 mg/mL MPNH2–AuNPs (B and E), and 0.5 mg/mL PAH–AuNPs (C and F) and bacterial cell walls. Adapted from Feng et al. (2015). Feng ZV, Gunsolus IL, Qiu TA, Hurley KR, Nyberg LH, Frew H, et al. Impacts of gold nanoparticle charge and ligand type on surface binding and toxicity to Gram-negative and Gram-positive bacteria. *Chem Sci* 2015;6 (9):5186–96.

nature of surface charge. The work of Silva and colleagues [74] indicated that surface charge could alter the toxicity of the same ENMs (in this case nAg) on *Escherichia coli*. For instance, branched polyethyleneimine-coated nAg (electrosteric, positively charged) exhibited higher toxicity associated with high attraction forces with cells when compared to citrate–nAg (electrostatic, negatively charged) and PVP–nAg (steric, negatively charged), with the latter two showing the least toxicity.

Surface coatings can also influence dissolution or release of ions from ENMs (Section 14.2.1) when generally soluble ENMs are rendered less soluble by the coating [75]. On bacteria, the toxicity of tetrapolyphosphate (TPP)-coated zerovalent iron (TPP–nZVI) was higher than other forms of nZVIs in deionized water, owing to enhanced dissolution. For TPP–nZVI, toxicity was evidenced by the peaks shift in the protein region of *E. coli* [72]. Fe ions released from TPP–nZVI were considered to interact with the amino acids, inducing alteration of proteins or enzymes [72].

Others have demonstrated that surface charge on quantum dots (QDs)—NPs significantly altered the core material toxicity following coating using mercaptoacetic acid (MMA), dihydrolipoic acid (DHLA), and L-cysteine (L-Cys) [73]. The stabilizers altered the release of Cd ions from the QDs, with higher toxicity observed for L-Cy–CdSe than MMA–CdSe and DHLA–CdSe QDs, which had a similar, insignificant effect on *Photobacterium phosphoreum*. Similar effects of CdSe–QDs were also observed by Mahendra et al [70]. They found that QDs with intact surface coatings reduced the growth rates of *B. subtilis* and *E. coli*, but were not bactericidal. However, under acidic and alkaline conditions, CdSe–QDs significantly increased bactericidal activity due to release of Cd and Se ions following the loss of polyanionic polymaleic anhydride-alt-1-octadecene (PMAO), polycationic polyethylenimine (PEI), and carboxyl coatings.

Studies on the interactions of algae and coated ENMs similarly revealed variant toxicities depending on coating type and form. For example, citrate-stabilized nAg induced enhanced effects of *Chattonella marina* algae on fish gill cells [76]. The addition of citrate-stabilized nAg enhanced the toxicity, which caused a decrease in the viability of the fish-gill cells. The synergistic toxic effects were linked to the production of superoxide, known to induce toxicity in fish-gill cells [77]. Copper oxide NPs (nCuO) coated with poly(styrene-co-butyl acrylate) were found to be toxic to aquatic organisms [78,79].

Evidence of bare and coated nCuO inside algal cells showed marked differences in uptake and disruptions in the cells with greater effects from coated ENMs compared to uncoated ones (Fig. 14.3). As a result, an increase of starch granules and nCuO aggregation in algal cells exposed to coated nCuO was observed [78]. Exposure of nCuO onto *Chlamydomonas reinhardtii* algal cells resulted in the formation of reactive oxygen species (ROS) and enhanced inhibition of PSII [78]. Coated nCuO exhibited higher toxic effects to algal cells compared to bare ones regardless of nominal exposure concentrations.



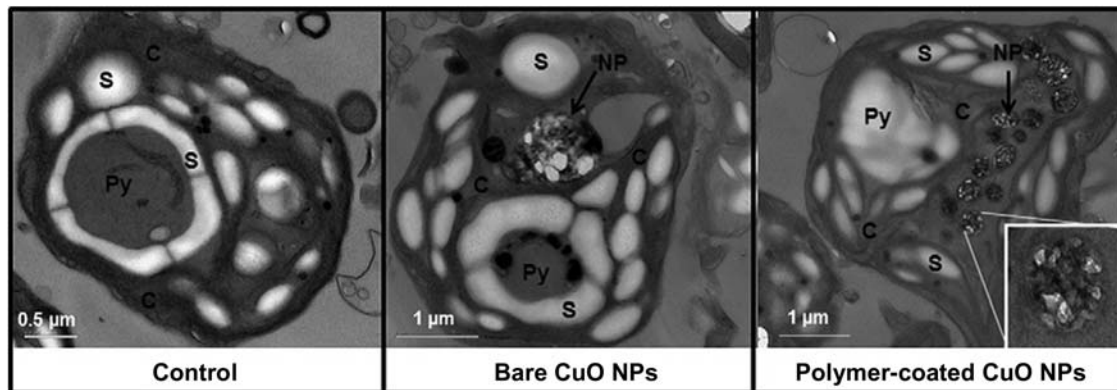


**FIGURE 14.3** TEM Images of *Chlamydomonas reinhardtii* cells after treatment with bare CuO NPs or polymer coated CuO NPs. Cell structures are the pyrenoid (Pyr), chloroplast (C), starch granules (S) and CuO NPs aggregates (NP). Insert (right picture): enlarged view of a NP aggregate. Reprinted from Perreault F, Oukarroum A, Melegari SP, Matias WG, Popovic R. Polymer coating of copper oxide nanoparticles increases nanoparticles uptake and toxicity in the green alga *Chlamydomonas reinhardtii*. *Chemosphere* 2012;87(11):1388–94, with permission from Elsevier.

### 14.3.2 Invertebrates and vertebrates

Surface charges caused by surface functionalization can influence the toxicity of ENMs to invertebrates. For example, Collin et al. [80] showed that positively-charged cerium oxide —NPs (diethylaminoethyl-dextran (DEAE-nCeO<sub>2</sub>)) had higher bioaccumulation and toxicity to the nematode *Caenorhabditis elegans*, than to neutral and negatively charged carboxymethyl dextran (CM-CeO<sub>2</sub>)—nCeO<sub>2</sub>. The authors suggested that the observed differences in the uptake and bioaccumulation of nCeO<sub>2</sub> was due to electrostatic interactions between the positively charged ENMs, and the negatively charged lipid bilayers of *C. elegans* membrane [80]. Surface coatings, however, may not always increase toxicity of ENMs. Ahn and colleagues [81] found that following exposure of nematodes, *C. elegans* with bare and PVP-coated nAg demonstrated that coatings may reduce ion release from nAg. Toxicity due to Ag<sup>+</sup> ions may likely be lower in the coated NPs.

In zebrafish, citrate-coated nAg was shown to accumulate in the embryos [82], an aspect attributed to the downregulation of certain genes involved in cell proliferation, growth, and differentiation [83]. Furthermore, citrate and PVP-coated nAg were shown to induce higher toxicity to Japanese medaka (rice fish) when compared to bare counterparts. A comparison of bare, citrate, and PVP-coated nAg illustrated that even though citrate-coated nAg induced toxicity, the responses of *D. magna* toxicity to the PVP-coated nAg resulted in an upregulation of the metallothionein and DNA damage-repair proteins [84]. The exposure of *Drosophila melanogaster* to mannitol-modified nAg-induced acute toxicity. Prolonged exposure affected the *Drosophila* fertility during their early three-filial generations [29].

In higher organisms like plants, the TPP—ZVI was found to generate H<sub>2</sub>O<sub>2</sub> as toxicity mechanisms in the roots of *Arabidopsis thaliana* seedlings [72]. To study the effects of nAg coating on plants, Liang and colleagues employed *Physcomitrella patens*, a model bryophytes plant [85]. nAg was shown to induce surface-coating-dependent adverse effects at various plant growth stages [85].

The studies briefly highlighted here suggest that the underlying mechanisms or toxicity effects of ENMs are influenced by coating type and form but are also plausibly linked to other factors. Further investigation is needed in order to further comprehensive risk assessment of ENMs in the environment.

## 14.4 Molecular approaches to toxicity of engineered nanomaterials: effects of coatings

The influence of ENM coating on genotoxicity has recently been highlighted [86–88]. Data indicates that coatings can either reduce or enhance ENMs toxicity based on their interaction with the test organism. Poynton et al. [84] investigated the genotoxicity of PVP and citrate-coated nAg on *D. magna*.



PVP-coated nAg was found to induce DNA damage-repair genes. Results for the citrate-coated nAg elicited the least differentially expressed genes (approximately half the number of genes differentially expressed by the PVP-coated nAg or AgNO<sub>3</sub>). Exposure of *Pimephales promelas*, to AgNO<sub>3</sub>, PVP, and citrate-coated nAg for 96 h showed unique transcriptional changes depending on Ag type and coating form. For example, 185, 423, and 615 differentially expressed genes corresponding to AgNO<sub>3</sub>, PVP, and citrate-coated nAg, respectively, were observed relative to the control [89]. Overall, the coating may have no influence on the observed toxic effects. However, they could have contributed to the stabilization effect of ENMs in the exposure media [21], and consequently, the stable ENMs could be easily ingested by organisms [90].

A study compared both cytotoxic and gene-expression profiles. The effects of uncoated iron oxide (nU-Fe<sub>3</sub>O<sub>4</sub>) and starch-coated iron oxide NPs (nOC-Fe<sub>3</sub>O<sub>4</sub>) in zebrafish showed that nU-Fe<sub>3</sub>O<sub>4</sub> was more toxic to fish gills. Coated ENMs were more toxic to the liver. The coating was suggested to mitigate the effects of the ENM in the fish gills while it enhanced the dispersion of ENMs in the liver [88]. Further validation of the findings is necessary.

Studies have applied proteomics approaches to the effects of ENMs on aquatic organisms in order to understand complex nano- and biointeractions [91]. Efforts to understand how coatings influence the proteomics of ENMs and their environmental risk are ongoing. However, the progress has been limited because ENMs are synthesized with different coatings to avoid non-specific interactions with cells [16,75]. Because ENMs are continuously transformed in the environment, their surface coatings and environmental conditions render fully understanding the influence of coating on observed toxicity at the protein level difficult.

Studies have suggested that proteomics-related toxicity is dependent on ENM coating type. Yang et al. [75] reported that the mechanism(s) of toxicity was dependent on ENM surface coating wherein nanospecific release of ROS induced oxidative-stress effects. Wiggington and colleagues [92] assessed the protein and nAg interactions in *E. coli* using bare and carbonate-coated nAg. Their findings revealed that different specific proteins were bound to bare or carbonate-capped nAg. Enzymatic activity was significantly reduced due to protein binding to bare nAg. For example, a reduction of 50% on TNase activity was observed when bound to carbonate-coated nAg, and 90% for bare nAg. The binding of the protein to bare nAg may have sterically blocked access to the active site, altered conformation, and consequently distorted the 3D structure of the protein.

## 14.5 Concluding remarks and perspectives

In this chapter, we have highlighted the influence of ENM coatings on stability and toxicity as well as concomitant implications of their behavior, fate, persistence, bioavailability, and biological interactions in aquatic systems.

However, it is not possible to assess the exposure and hazard of ENMs with unequivocal certainty. Examples presented with respect to the influence of surface coatings illustrate this point (i.e., same-parent ENMs: nAg and nZnO). In considering environmental risks associated with nanotechnology, there is an urgent need for descriptors of environmental behavior and hazards related to ENMs. Further research could enable their grouping in accordance with relative properties, such as coating. The application of surfactants improves the stability of ENMs by reducing their agglomeration potential in aquatic media, but also may increase their toxicity, thus strengthening the case for grouping of ENMs using surface coating application. Further tiered-grouping into coating types would be beneficial.

Molecular-based techniques are critical for understanding the effects of pollutants, particularly in the environment. Presently, there is a gap in knowledge concerning the toxicity of ENMs. The expectation of low concentrations ( $\sim$ ppb level) in the environment [4] raises the need for further research. New techniques will be highly valuable.

Lastly, although current data and knowledge on the implications of ENM coatings is nascent, available studies offer valuable insights for possibilities of designing green ENMs using coating to achieve this objective. Future design for ENM coatings should consider agents that influence the future applicability, behavior, and toxicity differently from some of the case studies reviewed in this chapter. *Safety-by-design* approaches may entail avoidance of cationic coatings since they exacerbate toxicity and persistence of ENMs in the aquatic systems. This is achievable through a multidisciplinary approach wherein potential risks of ENMs are considered at the inception and design phases. Discovering effective, greener, more proactive, and cost-saving alternatives is the goal.

## References

- [1] The Nanodatabase: Jointly Published by: DTU Environment, the Danish Ecological Council and Danish Consumer Council; 2016.
- [2] Vance ME, Kuiken T, Vejerano EP, McGinnis SP, Hochella Jr MF, Rejeski D, et al. Nanotechnology in the real world: redeveloping the nanomaterial consumer products inventory. *Beilstein J Nanotechnol* 2015;6:1769.
- [3] Musee N, Zvimba JN, Schaefer LM, Nota N, Sikhwivhilu LM, Thwala M. Fate and behavior of ZnO- and Ag-engineered nanoparticles and a bacterial viability assessment in a simulated wastewater treatment plant. *J Environ Sci Health, Part A* 2014;49(1):59–66.
- [4] Musee N. A model for screening and prioritizing consumer nanoproduct risks: a case study from South Africa. *Environ Int* 2017;100:121–31.
- [5] Bäuerlein PS, Emke E, Tromp P, Hofman JA, Carboni A, Schooneman F, et al. Is there evidence for man-made nanoparticles in the Dutch environment? *Sci Total Environ* 2017;576:273–83.
- [6] Kainz QM, Reiser O. Polymer- and dendrimer-coated magnetic nanoparticles as versatile supports for catalysts, scavengers, and reagents. *Acc Chem Res* 2014;47(2):667–77.

- [7] Barrow M, Taylor A, Murray P, Rosseinsky MJ, Adams DJ. Design considerations for the synthesis of polymer coated iron oxide nanoparticles for stem cell labelling and tracking using MRI. *Chem Soc Rev* 2015;44(19):6733–48.
- [8] Dwivedi AD, Dubey SP, Sillanpää M, Kwon Y-N, Lee C, Varma RS. Fate of engineered nanoparticles: implications in the environment. *Coord Chem Rev* 2015;287:64–78.
- [9] Suresh AK, Pelletier DA, Doktycz MJ. Relating nanomaterial properties and microbial toxicity. *Nanoscale*. 2013;5(2):463–74.
- [10] Peng C, Zhang W, Gao H, Li Y, Tong X, Li K, et al. Behavior and potential impacts of metal-based engineered nanoparticles in aquatic environments. *Nanomaterials* 2017;7(1):21.
- [11] Jiang J, Oberdörster G, Biswas P. Characterization of size, surface charge, and agglomeration state of nanoparticle dispersions for toxicological studies. *J Nanopart Res* 2009;11(1):77–89.
- [12] Nel AE, Mädler L, Velegol D, Xia T, Hoek EM, Somasundaran P, et al. Understanding biophysicochemical interactions at the nano–bio interface. *Nat Mater* 2009;8(7):543.
- [13] Kim K-T, Truong L, Wehmas L, Tanguay RL. Silver nanoparticle toxicity in the embryonic zebrafish is governed by particle dispersion and ionic environment. *Nanotechnology*. 2013;24(11):115101.
- [14] Powers CM, Slotkin TA, Seidler FJ, Badireddy AR, Padilla S. Silver nanoparticles alter zebrafish development and larval behavior: distinct roles for particle size, coating and composition. *Neurotoxicol Teratol* 2011;33(6):708–14.
- [15] Yin Y, Shen M, Tan Z, Yu S, Liu J, Jiang G. Particle coating-dependent interaction of molecular weight fractionated natural organic matter: impacts on the aggregation of silver nanoparticles. *Environ Sci Technol* 2015;49(11):6581–9.
- [16] Verma A, Stellacci F. Effect of surface properties on nanoparticle–cell interactions. *Small* 2010;6(1):12–21.
- [17] Vijver MG, Zhai Y, Wang Z, Peijnenburg WJ. Emerging investigator series: the dynamics of particle size distributions need to be accounted for in bioavailability modelling of nanoparticles. *Environ Sci: Nano* 2018;5(11):2473–81.
- [18] Qiu T, Bozich J, Lohse S, Vartanian A, Jacob L, Meyer B, et al. Gene expression as an indicator of the molecular response and toxicity in the bacterium *Shewanella oneidensis* and the water flea *Daphnia magna* exposed to functionalized gold nanoparticles. *Environ Sci: Nano* 2015;2(6):615–29.
- [19] Li WM, Wang WX. Distinct biokinetic behavior of ZnO nanoparticles in *Daphnia magna* quantified by synthesizing 65Zn tracer. *Water Res* 2013;47(2):895–902.
- [20] Klaine SJ, Alvarez PJ, Batley GE, Fernandes TF, Handy RD, Lyon DY, et al. Nanomaterials in the environment: behavior, fate, bioavailability, and effects. *Environ Toxicol Chem* 2008;27(9):1825–51.
- [21] Louie SM, Tilton RD, Lowry GV. Critical review: impacts of macromolecular coatings on critical physicochemical processes controlling environmental fate of nanomaterials. *Environ Sci: Nano* 2016;3(2):283–310.
- [22] Lowry GV, Gregory KB, Apte SC, Lead JR. Transformations of nanomaterials in the environment. ACS Publications; 2012.
- [23] Liu J, Hurt RH. Ion release kinetics and particle persistence in aqueous nano-silver colloids. *Environ Sci Technol* 2010;44(6):2169–75.
- [24] Philippe A, Schaumann GE. Interactions of dissolved organic matter with natural and engineered inorganic colloids: a review. *Environ Sci Technol* 2014;48(16):8946–62.

- [25] Yu S, Liu J, Yin Y, Shen M. Interactions between engineered nanoparticles and dissolved organic matter: a review on mechanisms and environmental effects. *J Environ Sci* 2017;63:198–217.
- [26] Diedrich T, Dybowska A, Schott J, Valsami-Jones E, Oelkers EH. The dissolution rates of SiO<sub>2</sub> nanoparticles as a function of particle size. *Environ Sci Technol* 2012;46(9):4909–15.
- [27] Bian S-W, Mudunkotuwa IA, Rupasinghe T, Grassian VH. Aggregation and dissolution of 4 nm ZnO nanoparticles in aqueous environments: influence of pH, ionic strength, size, and adsorption of humic acid. *Langmuir*. 2011;27(10):6059–68.
- [28] S-j Yu, Y-g Yin, J-b Chao, M-h Shen, J-f Liu. Highly dynamic PVP-coated silver nanoparticles in aquatic environments: chemical and morphology change induced by oxidation of Ag<sup>0</sup> and reduction of Ag<sup>+</sup>. *Environ Sci Technol* 2013;48(1):403–11.
- [29] Sharma VK, Siskova KM, Zboril R, Gardea-Torresdey JL. Organic-coated silver nanoparticles in biological and environmental conditions: fate, stability and toxicity. *Adv Colloid Interface Sci* 2014;204:15–34.
- [30] Diegoli S, Manciualea AL, Begum S, Jones IP, Lead JR, Preece JA. Interaction between manufactured gold nanoparticles and naturally occurring organic macromolecules. *Sci Total Environ* 2008;402(1):51–61.
- [31] Urine JM, Colman BP, Bone AJ, Gondikas AP, Matson CW. Biotic and abiotic interactions in aquatic microcosms determine fate and toxicity of Ag nanoparticles. Part 1. Aggregation and dissolution. *Environ Sci Technol* 2012;46(13):6915–24.
- [32] Furtado LM, Bundschuh M, Metcalfe CD. Monitoring the fate and transformation of silver nanoparticles in natural waters. *Bull Environ Contamin Toxicol* 2016;97(4):449–55.
- [33] Zook JM, Long SE, Cleveland D, Geronimo CLA, MacCuspie RI. Measuring silver nanoparticle dissolution in complex biological and environmental matrices using UV–visible absorbance. *Anal Bioanal Chem* 2011;401(6):1993.
- [34] Badawy AME, Luxton TP, Silva RG, Scheckel KG, Suidan MT, Tolaymat TM. Impact of environmental conditions (pH, ionic strength, and electrolyte type) on the surface charge and aggregation of silver nanoparticles suspensions. *Environ Sci Technol* 2010;44(4):1260–6.
- [35] Pereira SP, Jesus F, Aguiar S, de Oliveira R, Fernandes M, Ranville J, et al. Phytotoxicity of silver nanoparticles to *Lemna minor*: surface coating and exposure period-related effects. *Sci Total Environ* 2018;618:1389–99.
- [36] Gunsolus IL, Mousavi MP, Hussein K, Bühlmann P, Haynes CL. Effects of humic and fulvic acids on silver nanoparticle stability, dissolution, and toxicity. *Environ Sci Technol* 2015;49(13):8078–80786.
- [37] Thwala M, Musee N, Sikhvivilu L, Wepener V. The oxidative toxicity of Ag and ZnO nanoparticles towards the aquatic plant *Spirodela punctata* and the role of testing media parameters. *Environ Sci: Process Impacts* 2013;15(10):1830–43.
- [38] Wang Z, Zhang L, Zhao J, Xing B. Environmental processes and toxicity of metallic nanoparticles in aquatic systems as affected by natural organic matter. *Environ Sci: Nano* 2016;3(2):240–55.
- [39] Bondarenko OM, Heinlaan M, Sihtmäe M, Ivask A, Kurvet I, Joonas E, et al. Multilaboratory evaluation of 15 bioassays for (eco) toxicity screening and hazard ranking of engineered nanomaterials: FP7 project NANOVALID. *Nanotoxicology* 2016;10(9):1229–42.
- [40] Ellis LJA, Valsami Jones E, Lead JR, Baalousha M. Impact of surface coating and environmental conditions on the fate and transport of silver nanoparticles in the aquatic environment. *Sci Total Environ* 2016;568:95–106.

- [41] Wu F, Harper BJ, Harper SL. Differential dissolution and toxicity of surface functionalized silver nanoparticles in small-scale microcosms: impacts of community complexity. *Environ Sci: Nano* 2017;4(2):359–72.
- [42] Li Y, Zhang W, Niu J, Chen Y. Surface-coating-dependent dissolution, aggregation, and reactive oxygen species (ROS) generation of silver nanoparticles under different irradiation conditions. *Environ Sci Technol* 2013;47(18):10293–301.
- [43] Liu Z, Wang C, Hou J, Wang P, Miao L, Lv B, et al. Aggregation, sedimentation, and dissolution of CuO and ZnO nanoparticles in five waters. *Environ Sci Pollut Res* 2018;25(31):31240–9.
- [44] Li X, Lenhart JJ, Walker HW. Aggregation kinetics and dissolution of coated silver nanoparticles. *Langmuir* 2011;28(2):1095–104.
- [45] Quik JT, Vonk JA, Hansen SF, Baun A, Van De Meent D. How to assess exposure of aquatic organisms to manufactured nanoparticles? *Environ Int* 2011;37(6):1068–77.
- [46] Misra SK, Dybowska A, Berhanu D, Luoma SN, Valsami-Jones E. The complexity of nanoparticle dissolution and its importance in nanotoxicological studies. *Sci Total Environ* 2012;438:225–32.
- [47] Markiewicz M, Kumirska J, Lynch I, Matzke M, Köser J, Bemowsky S, et al. Changing environments and biomolecule coronas: consequences and challenges for the design of environmentally acceptable engineered nanoparticles. *Green Chem* 2018;20(18):4133–68.
- [48] Dubas ST, Pimpian V. Humic acid assisted synthesis of silver nanoparticles and its application to herbicide detection. *Mater Lett* 2008;62(17–18):2661–3.
- [49] Tso C-p, Zhung C-m, Yang-hsin S, Young-Ming T, Wu S-c, Doong R-a. Stability of metal oxide nanoparticles in aqueous solutions. *Water Sci Technol* 2010;61(1):127.
- [50] Thurman EM, Wershaw R, Malcolm R, Pinckney D. Molecular size of aquatic humic substances. *Org Geochem* 1982;4(1):27–35.
- [51] Chappell MA, Miller LF, George AJ, Pettway BA, Price CL, Porter BE, et al. Simultaneous dispersion–dissolution behavior of concentrated silver nanoparticle suspensions in the presence of model organic solutes. *Chemosphere* 2011;84(8):1108–16.
- [52] Liu X, Wazne M, Han Y, Christodoulatos C, Jasinkiewicz KL. Effects of natural organic matter on aggregation kinetics of boron nanoparticles in monovalent and divalent electrolytes. *J Colloid Interface Sci* 2010;348(1):101–7.
- [53] Mudunkotuwa IA, Pettibone JM, Grassian VH. Environmental implications of nanoparticle aging in the processing and fate of copper-based nanomaterials. *Environ Sci Technol* 2012;46(13):7001–10.
- [54] Miao AJ, Zhang XY, Luo Z, Chen CS, Chin WC, Santschi PH, et al. Zinc oxide–engineered nanoparticles: dissolution and toxicity to marine phytoplankton. *Environ Toxicol Chem* 2010;29(12):2814–22.
- [55] Kang S, Xing B. Humic acid fractionation upon sequential adsorption onto goethite. *Langmuir* 2008;24(6):2525–31.
- [56] Adeleye AS, Conway JR, Perez T, Rutten P, Keller AA. Influence of extracellular polymeric substances on the long-term fate, dissolution, and speciation of copper-based nanoparticles. *Environ Sci Technol* 2014;48(21):12561–8.
- [57] Gelabert A, Sivry Y, Ferrari R, Akrouit A, Cordier L, Nowak S, et al. Uncoated and coated ZnO nanoparticle life cycle in synthetic seawater. *Environ Toxicol Chem* 2014;33(2):341–9.
- [58] Han Y, Kim D, Hwang G, Lee B, Eom I, Kim PJ, et al. Aggregation and dissolution of ZnO nanoparticles synthesized by different methods: influence of ionic strength and humic acid. *Colloids Surf A: Physicochem Eng Asp* 2014;451:7–15.

- [59] Pallem VL, Stretz HA, Wells MJ. Evaluating aggregation of gold nanoparticles and humic substances using fluorescence spectroscopy. *Environ Sci Technol* 2009;43(19):7531–5.
- [60] Lau BL, Hockaday WC, Ikuma K, Furman O, Decho AW. A preliminary assessment of the interactions between the capping agents of silver nanoparticles and environmental organics. *Colloids Surf A: Physicochem Eng Asp* 2013;435:22–7.
- [61] Yin Y, Yang X, Zhou X, Wang W, Yu S, Liu J, et al. Water chemistry controlled aggregation and photo-transformation of silver nanoparticles in environmental waters. *J Environ Sci* 2015;34:116–25.
- [62] Mlambo M, Mdluli PS, Shumbula P, Skepu A, Tshikhudo R, Moloto N. A size-controlled synthesis and characterization of mixed monolayer protected silver-S(CH<sub>2</sub>)<sub>11</sub>-NHCO-coumarin nanoparticles and their Raman activities. *J Mater Res* 2015;30(12):1934–42.
- [63] Li X, Yoneda M, Shimada Y, Matsui Y. Effect of surfactants on the aggregation and sedimentation of zinc oxide nanomaterial in natural water matrices. *Sci Total Environ* 2017;581:649–56.
- [64] Lodeiro P, Achterberg EP, Pampín J, Affatati A, El-Shahawi MS. Silver nanoparticles coated with natural polysaccharides as models to study AgNP aggregation kinetics using UV-Visible spectrophotometry upon discharge in complex environments. *Sci Total Environ* 2016;539:7–16.
- [65] Huynh KA, Chen KL. Aggregation kinetics of citrate and polyvinylpyrrolidone coated silver nanoparticles in monovalent and divalent electrolyte solutions. *Environ Sci Technol* 2011;45(13):5564–71.
- [66] Elbasuney S. Sustainable steric stabilization of colloidal titania nanoparticles. *Appl Surf Sci* 2017;409:438–47.
- [67] Godínez IG, Darnault CJ. Aggregation and transport of nano-TiO<sub>2</sub> in saturated porous media: effects of pH, surfactants and flow velocity. *Water Res* 2011;45(2):839–51.
- [68] Romanello MB, de Cortalezzi MMF. An experimental study on the aggregation of TiO<sub>2</sub> nanoparticles under environmentally relevant conditions. *Water Res* 2013;47(12):3887–98.
- [69] Zhou D, Keller AA. Role of morphology in the aggregation kinetics of ZnO nanoparticles. *Water Res* 2010;44(9):2948–56.
- [70] Mahendra S, Zhu H, Colvin VL, Alvarez PJ. Quantum dot weathering results in microbial toxicity. *Environ Sci Technol* 2008;42(24):9424–30.
- [71] Feng ZV, Gunsolus IL, Qiu TA, Hurley KR, Nyberg LH, Frew H, et al. Impacts of gold nanoparticle charge and ligand type on surface binding and toxicity to Gram-negative and Gram-positive bacteria. *Chem Sci* 2015;6(9):5186–96.
- [72] Yoon H, Pangging M, Jang M-H, Hwang YS, Chang Y-S. Impact of surface modification on the toxicity of zerovalent iron nanoparticles in aquatic and terrestrial organisms. *Ecotoxicol Environ Saf* 2018;163:436–43.
- [73] Wang L, Zheng H, Long Y, Gao M, Hao J, Du J, et al. Rapid determination of the toxicity of quantum dots with luminous bacteria. *J Hazard Mater* 2010;177(1–3):1134–7.
- [74] Silva T, Pokhrel LR, Dubey B, Tolaymat TM, Maier KJ, Liu X. Particle size, surface charge and concentration dependent ecotoxicity of three organo-coated silver nanoparticles: comparison between general linear model-predicted and observed toxicity. *Sci Total Environ* 2014;468:968–76.
- [75] Yang X, Gondikas AP, Marinakos SM, Auffan M, Liu J, Hsu-Kim H, et al. Mechanism of silver nanoparticle toxicity is dependent on dissolved silver and surface coating in *Caenorhabditis elegans*. *Environ Sci Technol* 2011;46(2):1119–27.

- [76] He D, Dorantes-Aranda JJ, Waite TD. Silver nanoparticle-algae interactions: oxidative dissolution, reactive oxygen species generation and synergistic toxic effects. *Environ Sci Technol* 2012;46(16):8731–8.
- [77] Marshall JA, Ross T, Pyecroft S, Hallegraeff G. Superoxide production by marine microalgae. *Mar Biol* 2005;147(2):541–9.
- [78] Perreault F, Oukarroum A, Melegari SP, Matias WG, Popovic R. Polymer coating of copper oxide nanoparticles increases nanoparticles uptake and toxicity in the green alga *Chlamydomonas reinhardtii*. *Chemosphere* 2012;87(11):1388–94.
- [79] Shi J, Abid AD, Kennedy IM, Hristova KR, Silk WK. To duckweeds (*Landoltia punctata*), nanoparticulate copper oxide is more inhibitory than the soluble copper in the bulk solution. *Environ Pollut* 2011;159(5):1277–82.
- [80] Collin B, Oostveen E, Tsyusko OV, Unrine JM. Influence of natural organic matter and surface charge on the toxicity and bioaccumulation of functionalized ceria nanoparticles in *Caenorhabditis elegans*. *Environ Sci Technol* 2014;48(2):1280–9.
- [81] Ahn JM, Eom HJ, Yang X, Meyer JN, Choi J. Comparative toxicity of silver nanoparticles on oxidative stress and DNA damage in the nematode, *Caenorhabditis elegans*. *Chemosphere* 2014;108:343–52.
- [82] Park K, Tuttle G, Sinche F, Harper SL. Stability of citrate-capped silver nanoparticles in exposure media and their effects on the development of embryonic zebrafish (*Danio rerio*). *Arch Pharm Res* 2013;36(1):125–33.
- [83] Kashiwada S, Ariza ME, Kawaguchi T, Nakagame Y, Jayasinghe BS, Gärtner K, et al. Silver nanocolloids disrupt medaka embryogenesis through vital gene expressions. *Environ Sci Technol* 2012;46(11):6278–87.
- [84] Poynton HC, Lazorchak JM, Impellitteri CA, Blalock BJ, Rogers K, Allen HJ, et al. Toxicogenomic responses of nanotoxicity in *Daphnia magna* exposed to silver nitrate and coated silver nanoparticles. *Environ Sci Technol* 2012;46(11):6288–96.
- [85] Liang L, Tang H, Deng Z, Liu Y, Chen X, Wang H. Ag nanoparticles inhibit the growth of the bryophyte, *Physcomitrella patens*. *Ecotoxicol Environ Saf* 2018;164:739–48.
- [86] Mahaye N, Thwala M, Cowan D, Musee N. Genotoxicity of metal based engineered nanoparticles in aquatic organisms: a review. *Mutat Res/Rev Mutat Res* 2017;773:134–60.
- [87] Charles S, Jomini S, Fessard V, Bigorgne-Vizade E, Rousselle C, Michel C. Assessment of the in vitro genotoxicity of TiO<sub>2</sub> nanoparticles in a regulatory context. *Nanotoxicology* 2018;12(4):357–74.
- [88] Zheng M, Lu J, Zhao D. Effects of starch-coating of magnetite nanoparticles on cellular uptake, toxicity and gene expression profiles in adult zebrafish. *Sci Total Environ* 2018;622:930–41.
- [89] Garcia-Reyero N, Thornton C, Hawkins AD, Escalon L, Kennedy AJ, Steevens JA, et al. Assessing the exposure to nanosilver and silver nitrate on fathead minnow gill gene expression and mucus production. *Environ Nanotechnol Monit Manag* 2015;4:58–66.
- [90] Hund-Rinke K, Simon M. Ecotoxic effect of photocatalytic active nanoparticles (TiO<sub>2</sub>) on algae and daphnids (8 pp). *Environ Sci Pollut Res* 2006;13(4):225–32.
- [91] He X, Fu P, Aker WG, Hwang H-M. Toxicity of engineered nanomaterials mediated by nano–bio–eco interactions. *J Environ Sci Health, Part C* 2018;36(1):21–42.
- [92] Wigginton NS, Titta Ad, Piccapietra F, Dobias J, Nesatyy VJ, Suter MJ, et al. Binding of silver nanoparticles to bacterial proteins depends on surface modifications and inhibits enzymatic activity. *Environ Sci Technol* 2010;44(6):2163–8.

# Functionalized halloysite nanotubes: an “ecofriendly” nanomaterial in environmental industry

Gaurav Pandey, Maithri Tharmavaram and Deepak Rawtani

*Institute of Research & Development, Gujarat Forensic Sciences University, Gandhinagar, India*

### 15.1 Introduction

Due to their small size and high surface-to-volume ratio, nanomaterials are different from their bulk counterparts. This difference gives them a high level of application in environmental industries [1]. They have excellent adsorptive and catalytic properties, which are essential for applications such as pollutant remediation from contaminated soil and water, nanofiltration, and monitoring of contaminant levels through sensing [2,3]. These properties can be further enhanced through functionalization. The process allows introduction of specific functional groups or properties onto the surfaces of nanomaterials. This both enhances the intrinsic properties of the nanomaterials and creates new and desirable properties [4–6].

During the last decade, the environmental industry has experienced an upsurge in the use of functionalized nanomaterials fabricated from noble metals, metal oxides, polymers, and semiconducting and conducting materials for different applications. However, nanomaterials synthesized from such materials have certain limitations. The potential impact of these nanomaterials on the environment is unknown. They may be dangerous to aquatic and terrestrial, plant and animal life. The effect of the environment on such nanomaterials is also unknown, which severely limits the ability to identify precautions which should be taken before releasing them. This limits the practical use of these nanomaterials, thereby necessitating the need for newer and more environmentally friendly nanomaterials [4].



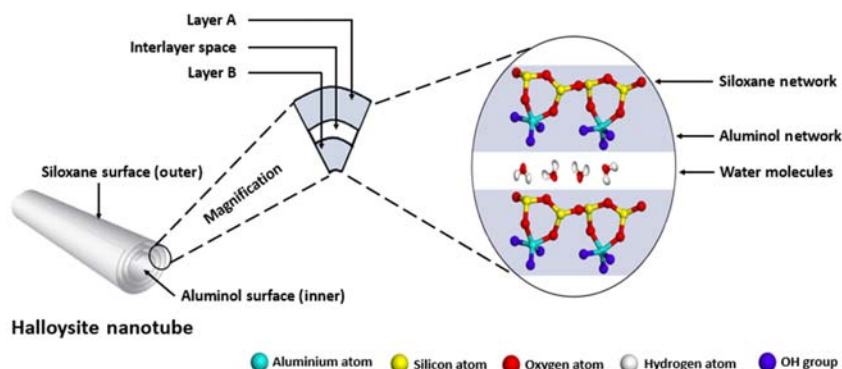


FIGURE 15.1 Structure of halloysite nanotubes [12].

Halloysite nanotubes (HNTs) are naturally occurring clay minerals of aluminosilicate composition. They have a rolled layer-like structure and consist of a definite lumen with interlayer spaces between the rolled kaolinite sheets [7]. Due to such morphology, nanotubes have been utilized as nanocontainers for the controlled loading and release of different functional groups, as adsorbents, as supports for different biochemical compounds, or in the formation of nanocomposites for different applications [8–11]. They are also economical, easily available, nontoxic, and environmentally friendly. These nanotubes are highly suitable for applications in the environmental field.

The rolled-layer structure of HNTs is rich in alumina groups on the inner surface (lumen), while the outer surface contains silica moieties. The alumina groups cause the lumen to be positively charged, while the silica groups cause the outer surface to be negatively charged. HNTs also tend to exist in either hydrated or dehydrated form. In the hydrated form, water molecules are present in the interlayer space, while in the dehydrated form no water molecules are present (Fig. 15.1). The groups, along with their charge disparity, raise the possibility of bond formation with different functional molecules. This enhances their potential as subjects for different functionalization strategies for various applications.

This chapter covers the different approaches for the functionalization of the inner and outer surfaces of HNTs. Applications of the functionalized HNTs in the environmental industry are discussed as well.

## 15.2 Functionalization techniques for halloysite nanotubes

The outer surface of HNTs, as discussed in Section 15.1, is primarily composed of silica groups that cause the surface to be negatively charged. Several functionalization strategies with organosilanes, polymers, biopolymers, nanoparticles, surfactants, and compounds of biological origin have been developed. Organosilanes usually react via a grafting process with

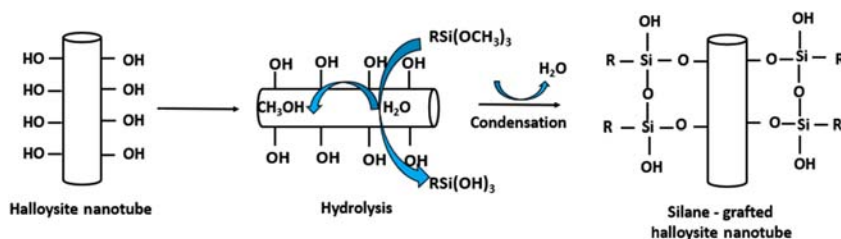


**FIGURE 15.2** Reaction scheme of organosilanes grafting on the surface of halloysite nanotube [12].

the hydroxyl moiety-rich external surfaces of HNTs. Functionalization of HNTs with organosilanes is an excellent technique because of its ease of use, and the attachment of functional groups such as  $-\text{NH}_2$ ,  $-\text{SH}$ , and  $-\text{Cl}$  on their surfaces [13]. Such groups can be introduced by using organosilanes, including 3-aminopropyltriethoxysilane, mercaptopropyltriethoxysilane, and 3-chloropropyltrimethoxysilane. The grafting process of the organosilanes onto HNTs occurs through a series of hydrolysis and condensation reactions (Fig. 15.2). However, grafting with organosilanes requires high specificity to the surfaces of HNTs. Therefore these reactions are usually carried out in nonpolar solvents to prevent self-hydrolysis and self-condensation reactions [14–18].

The outer surfaces of HNTs have also been modified with polymers to attach functional groups. Such modification is usually associated with the advantage of forming a compact network of functional moieties on their surfaces. Functionalization with polymers also has the advantage of imparting properties such as high thermal and mechanical stability. Nanocomposites formed by HNTs and functionalized with polymers have increased mechanical strength, stiffness, and impact resistance, making them useful for different environmental applications [19,20]. Polymers also increase the stability of HNTs in aqueous solutions by preventing their aggregation. Typically, the attachment of a polymer on the external surface of nanotubes is either through polymerization of monomers via oxidizing agents, or by attaching the entire polymer. Polymers such as polyethyleneimine (PEI), poly butylene adipate [21], and polymethyl methacrylate [22] have been utilized for this purpose. Biopolymers such as polysaccharides [23], DNA [24], and polypeptides [25] have also been utilized to functionalize nanotubes. There are advantages to utilizing biopolymers. It is possible to include an abundance of functional groups in their side chains. They are ecofriendly. They possess the capacity to confer antibacterial and thermal properties to the surfaces of HNTs [26,27]. These advantages make them highly suitable for applications in the environmental industry (Fig. 15.3).

Polyphenols, which are compounds primarily extracted from plants, have also been used to functionalize the outer surface of HNTs. Polyphenols such

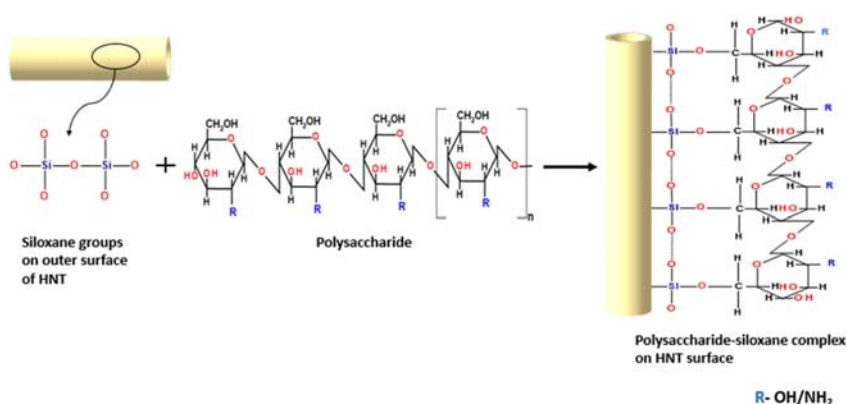


**FIGURE 15.3** Functionalization of the outer surface of HNTs with polysaccharides [12].

as tannic acid have zwitterionic properties that not only allow attachment of a specific functional group onto a surface but also confer zwitterionic properties to the surface of HNTs. Such properties allow HNTs to be used as anti-fouling agents for the treatment of wastewater [28]. In addition to polymers and organosilanes, the exterior surface of HNTs can also be functionalized with surfactants. These compounds consist of a hydrophobic and hydrophilic moiety, which makes them highly dispersable in nonpolar solvents [29,30]. When the outer surfaces are treated with the surfactants, these moieties create steric barriers between the surfaces of the HNTs and the surrounding solvent. The barriers increase the stability of HNTs in solvents. The surfactant could be either cationic or anionic, depending on the head group. Surfactants such as sodium dodecanoate and decyltrimethylammonium bromide (DeTAB) have been used to functionalize the surfaces of HNTs [29]. These specific surfactants can be used to form reverse micelles, which can be later used for release of functional compounds or antibacterial agents for water remediation. Several research groups have also utilized metal or metal oxide nanoparticles for functionalizing the exterior surfaces of nanotubes. The functionalization with nanoparticles can be done in two ways: by reducing the metal or metal oxide precursors on the surface of HNTs, or by adsorbing presynthesized nanoparticles on the surface of HNTs [12]. The nanoporous surface of HNTs acts as a template for the synthesis of the nanoparticles and as a nanoadsorbent for the proper immobilization of nanoparticles [31,32]. Nanoparticles offer the advantage of imparting metal-based properties such as increased conductivity and optoelectronic properties [33,34] to the exterior surfaces of nanotubes. These properties make them suitable as nanosupports for fabricating various electrochemical biosensors. Nanoparticles of silver can be used to impart antibacterial properties to the surfaces of HNTs, thereby making them suitable for environmental applications such as water or soil remediation.

The lumen of HNTs is exclusively composed of aluminol groups. Due to the presence of these groups, the lumen is positively charged. It comprises 10% of the total HNT volume and allows the nanotube to act as a nanocontainer for the loading and release of functional compounds. Organosilanes attach to the internal surface of the nanotube through the grafting mechanism, which is similar to that used with the external surface. The organosilanes undergo hydrolytic and condensation reactions to attach the functional group onto the surface of the lumen. However, the grafting of organosilanes on the lumen requires HNTs of excellent tubular morphology. Poor tubular morphology leads to a drastic decrease in the grafting of the organosilane [35]. The lumen of HNTs have also been functionalized with polymers. As discussed previously, functionalization via polymers forms a compact web of functional moieties on the interior surface (lumen) of the nanotube. This functionalization also empowers HNTs to be utilized as compatibilizer for blending two polymers, and as an interfacial mediator to boost the bonding between the two. Functionalization with polymers in the lumen also increases the affinity of the lumen surface for immobilization of different biomolecules. The lumen can also be modified with biopolymers. However, the presence of alumina groups confers a positive charge to the surface and thereby increases the affinity of the lumen for modification with anionic biopolymers. The internal surface can also be functionalized via biopolymers such as polysaccharides and polypeptides (pectin and polydopamine), in addition to the synthetic polymers discussed earlier [27]. Apart from biopolymers, polyphenols such as curcumin have also been used to functionalize the lumen of HNTs. Functionalization with curcumin conferred antioxidative, metal chelating and anti-inflammatory properties to the nanotube. This functionalization technique makes the nanotube highly ecofriendly, nontoxic, and useful for environmental remediation [36]. The lumen of HNTs have also been functionalized by surfactants. Proper selection of a surfactant delivers the benefit of balancing the total charge stability of HNTs. For instance, functionalization of the positively charged inner lumen with an anionic surfactant balances the overall charge of the nanotube, which in turn increases the stability of the nanotube in aqueous solvents [29]. The head group of the surfactant plays a critical role in the functionalization of the lumen; it determines the amount of hydrophobization. For instance, surfactants with carboxyl headgroup contribute to increased formation of micelles thereby increasing the hydrophobization of the lumen [30].

### 15.3 Applications of functionalized halloysite nanotubes in environmental industry

HNTs functionalized with various agents have been used in different areas of environmental industry, as depicted in Fig. 15.4. Additional environmental

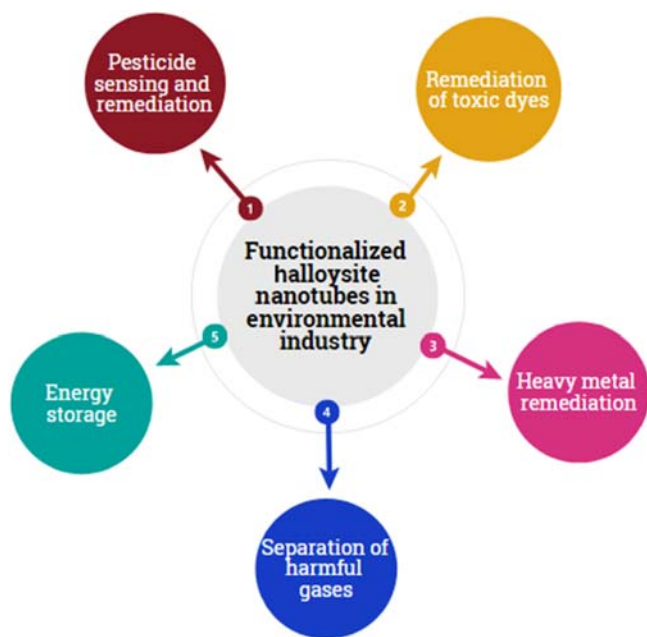


**FIGURE 15.4** Functionalized halloysite nanotubes in environmental industry.

applications utilizing various kinds of surface-functionalized HNTs have also been given in [Table 15.1](#).

### 15.3.1 Pesticide sensing and remediation

Pesticides are generally employed in agriculture or in households for controlling as well as eliminating pests and weeds. These chemicals protect crops and household materials from being damaged by pests. However, only a small portion of the applied pesticide reaches its target, and a major portion of it reaches other destinations such as soil. These pesticides remain in the soil and enter nearby water bodies through rain and agricultural runoffs [37,38]. The presence of pesticides in water bodies is becoming a major concern for the environment industry, since these agrochemicals significantly reduce the quality of water [39]. The adverse effects of pesticides on the environment include destruction of bird habitats [40], declining biodiversity, reduced population of insect pollinators [41], and risks to endangered species [42]. Therefore a major part of environmental research is focused on the sensing and remediation of different pesticides in soil and water. Conventionally, techniques such as gas chromatography–mass spectroscopy and high-performance liquid chromatography have been used for detecting these agrochemicals. However, the necessity of skilled technicians, intensive

**TABLE 15.1** Environmental applications of halloysite nanotubes functionalized with different agents.

S. No.	Environmental Application	Functionalization agent for Halloysite Nanotubes		Target	Reference
		Category	Example		
1	(a) Pesticide sensing	● Enzyme and carbon-based materials	Esterase, graphite and CNT	Carbofuran	[45]
		● Nanoparticle	CNPs	Methyl and ethyl parathion	[46]
	(b) Pesticide remediation	● Metal ion	$\text{Cu}^{2+}$	2,4,6-TCP	[47]
		● Metal oxide	$\text{TiO}_2$	Parathion	[48]
2	Dye remediation	● Biomolecule and organosilane	Dopamine and KH550	Methylene blue	[56]
		● Biopolymer	Polydopamine	Congo red and Methylene blue	[52]
3	Heavy metal removal	● Organosilane	AZPTMS	$\text{Pb}^{2+}$	[66]
		● Metal oxide	Magnetite ( $\text{Fe}_3\text{O}_4$ )	$\text{Cd}^{2+}$	[68]
4	Gas separation	● Alkali and organosilane	NaOH and APTES	$\text{CO}_2$ , $\text{CH}_4$ and $\text{N}_2$	[73]
		● Organosilane	AEAPTMS	$\text{CH}_4$ , $\text{CO}_2$ , $\text{N}_2$ and $\text{O}_2$	[74]
5	Energy storage	● Organosilane	KH590	-	[76]
		● Metal oxide	NiO	-	[77]

CNT: Carbon Nanotubes; CNPs: Carbon Nanoparticles;  $\text{Cu}^{2+}$ : Copper ion;  $\text{TiO}_2$ : Titanium dioxide; KH550: 3-aminopropyltriethoxysilane; AZPTMS: 3-azidopropyl trimethoxysilane;  $\text{Pb}^{2+}$ : Lead ion;  $\text{Cd}^{2+}$ : Cadmium ion; NaOH: Sodium hydroxide; APTES: 3-aminopropyl triethoxysilane; AEAPTMS: N- $\beta$ -(aminoethyl)- $\gamma$ -aminopropyltrimethoxy silane; KH590: 3-mercaptopropyl trimethoxysilane; NiO: Nickel oxide.

sample preparation, and costly equipment are some of the major drawbacks of these techniques [43,44]. In recent years, nanotechnology-based materials, especially ecofriendly HNTs, have emerged as an efficient alternative for the sensing and remediation of various classes of pesticides. HNTs functionalized with different surface-modification agents can be very efficiently used in environmental industry as an ecofriendly nanomaterial for detecting, as well as degrading or removing various pesticides present in soil and water.

Research on sensing of pesticides using functionalized HNTs is in its initial phase. A few studies have reported the use of these clay-based nanotubes for sensing different classes of pesticides. In one case, scientists have utilized esterase-functionalized HNTs for the development of an electrochemical sensor as a detector of carbofuran, a well-known broad-spectrum pesticide. The nanotubes were initially functionalized with esterase through physical adsorption. The enzyme was isolated from *Eupenicillium shearii*, an endophytic fungus. Postfunctionalization with esterase, the nanotubes were further modified with graphite powder and multi-walled carbon nanotubes. The mixture was homogenized in mineral oil to prepare the final paste, which was used for constructing the biosensor. The mechanism of pesticide detection was the inhibition of esterase activity in the presence of carbofuran, using square-wave voltammetry. The developed biosensor performed best at 0.5 U concentration of esterase. The detection limit for the biosensor was 1.69  $\mu\text{g/L}$ , while the quantification limit was 5.13  $\mu\text{g/L}$ . It exhibited excellent reproducibility and repeatability, while remaining stable for a duration of 20 weeks [45]. In another study, halloysite functionalized with carbon nanoparticles (CNPs) was used to modify carbon-paste electrode in order to determine methyl and ethyl parathion in different sample matrices, including soil and water. The detection limit for methyl parathion was  $4.7 \times 10^{-10}$  M, while for ethyl parathion it was  $3.67 \times 10^{-10}$  M. The electrode exhibited advantages such as simple fabrication, high sensitivity, reproducibility, and low detection limits [46].

Functionalized HNTs have also been used in the removal and degradation of pesticides in soil and water. A group of researchers has enhanced the adsorption capacity of HNTs by functionalizing its surface with  $\text{Cu}^{2+}$  ions. This nanoparticle-modified HNT was further used for degradation of the pesticide 2,4,6-trichlorophenol. The positive charge on metal ions generated an attractive force toward the anion of the pesticide, which was ultimately adsorbed on the nanoparticle [47]. In a recent study, HNT functionalized with titanium dioxide ( $\text{TiO}_2$ ) was used to prepare solid-phase microextraction fiber coating. This ecofriendly nanocomposite was used for the extraction of parathion from different sample matrices, including river water and agricultural wastewater. The extracted pesticide was determined using negative corona discharge—ion mobility spectrometer. The detection limit for the pesticide was 0.03  $\mu\text{g/L}$ . The excellent mechanical strength of HNTs in combination with large surface area, durability, and porous structure of  $\text{TiO}_2$

helped with efficient removal of parathion [48]. In another study, HNTs were modified with Rose Bengal, which is a well-known photosensitizer for the removal of *n*-nonylphenol. Rose Bengal was used in a very minute concentration (0.412 mg/g of HNT) to functionalize the HNT surface. The photosensitizer was responsible for the release of singlet oxygen in water, which converted the pesticide into its less-toxic metabolite [49].

### 15.3.2 Remediation of toxic dyes

The rapid increase of industrialization has become a major cause of water pollution [39,50]. Pollutants rich in nitrates, when present in drinking water, may cause serious health problems for humans [51]. Wastewater coming from the textile, cosmetic, paper, and paint industries is polluted with water-soluble organic dyes and usually gets routed into nearby water bodies [12]. Most of the dyes, especially azo dyes, once dumped into the water bodies cannot be biochemically oxidized. The metabolites produced due to anaerobic degradation of these dyes are dangerous due to their carcinogenic and toxic nature [52]. The treatment of such wastewater, which is polluted with toxic dyes, is becoming a major concern for environmental industry. HNT is a good adsorbent, and this property has been utilized for the removal of various dyes from water [53,54]. Functionalization of HNTs with different agents further enhances their efficiency for removing dyes present in wastewater.

The surface-functionalized nanotubes have been used either as free nanocomposite or have been incorporated in membrane for the remediation of dyes. In a recent study, an HNT functionalized with magnetic iron oxide nanoparticles was used to synthesize a nanoadsorbent. The nanoadsorbent was then utilized for the remediation of Naphthol Green B dye. The kinetic studies showed that the Langmuir adsorption isotherm model was more effective than the Freundlich model for the removal of Naphthol Green B, thereby confirming that the dye forms a monolayer on the nanoadsorbent [55]. Functionalization of HNTs with dopamine as well as KH550, a well-known organosilane, was carried out to synthesize a core double-shell magnetic HNT. The HNT was then utilized for the removal of Methylene Blue. The magnetic nature was imparted to nanotubes via modification with magnetic nanoparticles, which expedited the separation of nanotubes post dye removal. The modification with dopamine and KH550 helped increase the number of amine and hydroxyl groups on the HNT surface, thereby considerably increasing the number of adsorption sites. The nanocomposite exhibited high adsorption efficiency (714.29 mg/g) for the dye [56].

Apart from HNT-based nanocomposites, surface-functionalized HNTs have also been incorporated in different membranes for the efficient removal of toxic dyes. In a recent study, nanocomposite of HNT and reduced graphene oxide was functionalized with polydopamine in order to fabricate a membrane.



The membrane was further used for the effective removal of congo red and methylene blue. It showed excellent antifouling properties and displayed high removal efficiency for congo red (99.09%) and methylene blue (99.72%) [57]. Dyes such as Direct Yellow 4, Direct Red 28, and Direct Blue 14 have also been removed using membrane technology by incorporating dopamine-functionalized HNT for enhanced removal and antifouling properties [58]. Membrane prepared through tannic acid functionalized HNT has been used to remove reactive black and reactive orange dyes from aqueous systems [28]. In another study, membrane prepared by introducing organosilane-modified HNT was used to remove Direct Red 80 dye from a mixture of dye and copper ions. The organosilane modification helped in enhancing the dispersion ability of HNTs in the viscous matrix for efficient reinforcement of the nanotubes in the membrane [59].

### 15.3.3 Heavy metal remediation

Pollution due to heavy metals has received a substantial amount of attention in the environmental industry. Industrial as well as agricultural activities, along with vehicular emission are major sources of heavy metal pollution in the environment. In contrast to other organic pollutants, metals are nonbiodegradable and therefore remain in the environment. They accumulate in different ecosystems as well as human bodies, thus causing various health problems [60,61]. High concentrations of metals in water may cause serious health issues to humans [62], and if the water is polluted with heavy metals, the health risks increase. Long-term exposure to heavy metals may damage organs or cause nervous, cardiovascular, or immune system-related disorders [63,64]. During the last decade, myriad nanomaterials have been used for heavy metal removal from soil and water. Clay-based materials, specifically HNTs, have also attracted attention in the environmental industry because they are naturally availability, ecofriendly, and nontoxic [65]. Functionalization of these nanotubes with various functionalization agents increases the specificity of the nanomaterial for different heavy metals.

Recently, a research group used functionalized HNTs with 3-azidopropyl trimethoxysilane for enhancing the removal of lead(II) ions from water. The study involved a comparison of the efficacy between pristine and functionalized HNTs in the removal of  $\text{Pb}^{2+}$  ions. The adsorption ability of both types was studied in the pH range of 3–6. The surface functionalization of HNTs enhanced the removal of  $\text{Pb}^{2+}$  ion by increasing the pH and decreasing the ionic strength [66]. Another group of researchers has also achieved the removal of lead(II) ions from water using a different functionalization strategy for HNTs. Initially, the nanotubes were magnetically modified, followed by functionalization with manganese oxide nanoparticles. This composite was used for removing  $\text{Pb}^{2+}$  ions from aqueous systems. The maximum adsorption capacity for the ions using the nanosorbent was found to be

59.9 mg/g, and the equilibrium data exhibited the best fit for the Langmuir isotherm model. The nanosorbent also displayed excellent reusability and stability [67]. HNT modified with magnetic nanoparticles have also been used as a nanosorbent for the removal of cadmium(II) ions. The nanotubes were functionalized with magnetite ( $\text{Fe}_3\text{O}_4$ ) via chemical precipitation method. Electrostatic interaction between the positively charged cadmium ions and the negatively charged surface of the magnetic HNTs ensured the adsorption of the cadmium ions on the surface. The metal ions were further quantified using flame atomic absorption spectrometry [68]. In another study, an HNT was modified with an organic carbon group in order to attach  $-\text{COOH}$  group onto its surface. This  $-\text{COOH}$ -functionalized HNT was further used to synthesize a magnetic hybrid material to remove chromium(VI) ions. The magnetic property was imparted to the HNT through the immobilization of magnetic nanoparticles. Because of the  $-\text{COOH}$ -functionalization, the HNT played a significant role in removing the heavy metal ions. The magnetic nature of the nanocomposite had the advantage of easy separation after ion removal from the water. The mechanism for the removal of  $\text{Cr(VI)}$  ions was adsorption on the surface of the functionalized HNT [69].

The development of novel functionalization strategies for HNTs can enhance the specificity and selectivity of the nanotubes toward different heavy metal ions. This approach may help the environmental industry tackle the serious issue of heavy metal contamination in water bodies as well as in wastewater from different industries.

#### 15.3.4 Separation of harmful gases

Air pollution has increased due to rapid industrialization and today's ever-increasing population. The emission of toxic gases from vehicles, industries, and households is increasing in the atmosphere, causing various skin and respiratory diseases. There has also been an increase in the concentration of greenhouse gases such as carbon dioxide and methane in the atmosphere. This increase has been the major cause of global warming. Their removal is vital. Since the environmental industry is focusing on the separation of such gases, nanomaterials have emerged as a helpful tool for this purpose. HNTs are environmentally friendly and naturally available, which reduces the cost of gas separation [12].

The process of separating different gases is usually achieved by using mixed-matrix membranes (MMMs). These high-performance membranes are hybrid systems, fabricated by embedding different types of fillers such as zeolites, silica, metal-organic frameworks, and metal oxides into various polymer matrices. This hybrid system synergistically combines the separation properties of fillers with the versatile processing of polymers, creating an excellent separation performance [69–71]. In a recent study, HNTs were modified by alkali etching and 3-aminopropyltriethoxysilane (APTES) was

used as a filler to fabricate MMMs, which was further used for the separation of  $\text{CO}_2$ ,  $\text{CH}_4$ , and  $\text{N}_2$ . The increased roughness of the HNTs after functionalization helped in easy dispersion in the membrane. The etched HNT improved the interfacial affinity, while the silane-grafted HNT contributed to filler dispersion. MMMs containing the etched HNT had higher permeability and selectivity for  $\text{CO}_2$ . On the contrary, silane-grafted HNT only enhanced the permeability of MMM, with no contribution toward enhancing  $\text{CO}_2$  selectivity. Overall, surface etching of HNTs proved to be a better strategy for improving the gas separation [73]. In another study, HNTs functionalized with *N*- $\beta$ -(aminoethyl)- $\gamma$ -aminopropyltrimethoxy silane (AEAPTMS) were used as a filler material in MMMs. The organosilane in this case played the role of a compatibilizer, thereby enhancing the interfacial affinity between the membrane and the nanotubes. The AEAPTMS-functionalized HNTs improved dispersion ability in the membrane, and displayed great selectivity toward the gas mixture containing  $\text{CH}_4$ ,  $\text{CO}_2$ ,  $\text{N}_2$ , and  $\text{O}_2$  [74].

### 15.3.5 Energy storage

Production of clean and green energy-storage devices is a priority for most environmental industries. Most of the conventionally used energy-storage devices are associated with multiple environmental hazards. Leakage of toxic chemicals from energy-storage devices such as batteries has been a concern. The advent of novel nanotechnology-based materials is a favorable beginning for the remediation of energy-storage devices. Several nanomaterials have shown immense potential for applications related to green energy (i.e., catalysts, lithium ion batteries, thermoelectronics, supercapacitors, and hydrogen storage) [75]. HNT use is being considered by researchers working in environmental industries. There is particular interest in its use for energy storage because it is naturally available, cost effective, and ecofriendly.

The generation of supercapacitors using surface-functionalized HNTs has been a growing area of research in the past few years. In one study, an HNT functionalized with 3-mercaptopropyl trimethoxysilane (KH-590) was mixed with nickel sulfide ( $\text{Ni}_3\text{S}_2$ ) to develop an efficient nanohybrid system for energy storage in supercapacitor. Glucose was used as a binder between the nanotubes and  $\text{Ni}_3\text{S}_2$  during a hydrothermal reaction, which helped in depositing CNPs in the composite. The nanocomposite thus formed displayed excellent stability and electrochemical performance due to the synergistic effect between HNT,  $\text{Ni}_3\text{S}_2$ , and CNPs. The developed supercapacitor was subjected to over 2000 cycles of nonstop charging and discharging with the current density maintained at 1 A/g. This supercapacitor exhibited a capacity of 450.4 C/g [76]. In other research, HNTs functionalized with nickel oxide (NiO) nanosheets were used to develop an excellently performing supercapacitor. A simple-precipitation reaction was carried out for functionalizing the nanotubes with NiO. The nanocomposite exhibited excellent charge-storage

capacitance (1047.3 F/g at 5 A/g), with an unwavering cycling performance of 1338 F/g for more than 7200 cycles at a current density of 10 A/g [77]. These environmentally friendly systems can transform the future composition energy-storage devices. This change will decrease the environmental hazards caused by conventionally manufactured devices such as batteries.

## 15.4 Conclusion and future prospects

Nanomaterials have emerged as a promising tool with possibilities for different applications. They can potentially satisfy the present need for ecofriendly nanomaterial usable in different areas of the environmental industry. One important advantage is their natural availability. This drastically reduces cost and increases potential for diverse environmental applications. The need for novel, ecofriendly energy-storage devices grows in relation to ever-increasing pollution. Surface-functionalization strategies for nanotubes assist in targeting more types of pollutants and expand potential areas of development within the environmental industry. The surfaces of HNTs have been functionalized with organosilanes, polymers, biopolymers, nanoparticles, and polyphenols. As discussed in this chapter, functionalized HNTs have been widely used in the environmental industry for the remediation and sensing of pesticides, and removal of pollutants, toxic gases, and heavy metals. Green energy-storage systems have also been developed using functionalized HNTs.

Future functionalization of HNTs with less-explored, nontoxic, and biocompatible biopolymers and biomolecules will enable modification of their surface without harm to the environment. Different modification agents have imparted antimicrobial action to HNTs [12]. Such developing functionalization strategies in combination with existing ones will provide antimicrobial action to the HNT. This property can help in developing antimicrobial membranes reinforced with functionalized HNTs. These membranes will not only remove the pollutants from wastewater, but also disinfect it from different microbes. Development of more novel surface-functionalization strategies may further help in targeting additional types of environmental pollutants.

## References

- [1] Hussain CM, editor. *Handbook of nanomaterials for industrial applications*. Elsevier; 2018.
- [2] Hussain CM, Kharisov B, editors. *Advanced environmental analysis-application of nanomaterials*. The Royal Society of Chemistry; 2017.
- [3] Hussain CM, Mishra AK, editors. *Nanotechnology in environmental science*. Wiley-VCH; 2018.
- [4] Darwish M, Mohammadi A. *Functionalized nanomaterial for environmental techniques*. In: Hussain CM, Mishra AJ, editors. *Nanotechnology in environmental sciences*. Wiley-VCH Verlag GmbH & Co. KGaA; 2018.

- [5] Pandey G, Rawtani D, Agrawal YK. Aspects of nanoelectronics in materials development. In: Kar A, editor. *Nanoelectronics and materials development*, 2016. Croatia: InTech; 2016. p. 23–39.
- [6] Tharmavaram M, Rawtani D, Pandey G. Fabrication Routes for one-dimensional nanostructures via block copolymers. *Nano Conver* 2017;4:12.
- [7] Rawtani D, Agrawal YK. Multifarious applications of halloysite nanotubes: a review. *Rev Adv Mater Sci* 2012;30:282–95.
- [8] Deepak R, Agrawal YK. Study of nanocomposites with emphasis to Halloysite Nanotubes. *Rev Adv Mater Sci* 2012;32:149–57.
- [9] Lvov Y, Wang W, Zhang L, Fakhrulin R. Halloysite clay nanotubes for loading and sustained release of functional compounds. *Adv Mater* 2016;28:1227–50.
- [10] Rawtani D, Agrawal YK. Halloysite as support matrices: a review. *Emerg Mater Res* 2012;1:212–20.
- [11] Pandey G, Mungumbe DM, Tharmavaram M, Rawtani D, Agrawal YK. Halloysite nanotubes-an efficient ‘nano-support’ for the immobilization of  $\alpha$ -amylase. *Appl Clay Sci* 2017;136:184–91.
- [12] Tharmavaram M, Pandey G, Rawtani D. Surface modified halloysite nanotubes: a flexible interface for biological, environmental and catalytic applications. *Adv Colloid Interface Sci* 2018;261:82–101.
- [13] Massaro M, Lazzara G, Milioto S, Noto R, Riela S. Covalently modified halloysite clay nanotubes: synthesis, properties, biological and medical applications. *J Mater Chem B* 2017;5:5867.
- [14] Arkles B. Tailoring surfaces with silanes. *Chem. Tech.* 1977;7:766–778.
- [15] Li C, Liu J, Qu X, Yang Z. A general synthesis approach toward halloysite-based composite nanotube. *J Appl Polym Sci* 2009;112:2647–55.
- [16] Luo P, Zhang J, Zhang B, Wang J, Zhao Y, Liu J. Preparation and characterization of silane coupling agent modified halloysite for Cr(VI) removal. *Ind Eng Chem Res* 2011;50:10246–52.
- [17] Sun P, Liu G, Lv D, Dong X, Wu J, Wang D. Effective activation of halloysite nanotubes by piranha solution for amine modification via silane coupling chemistry. *RSC Adv* 2017;5:52916–25.
- [18] Rawtani D, Pandey G, Tharmavaram M, Pathak P, Akkireddy S, Agrawal YK. Development of a novel ‘nanocarrier’ system based on Halloysite Nanotubes to overcome the complexation of ciprofloxacin with iron: an in vitro approach. *Appl Clay Sci* 2017;150:293–302.
- [19] Liu M, Guo B, Du M, Cai X, Jia D. Properties of halloysite nanotube-epoxy resin hybrids and the interfacial reactions in the systems. *Nanotechnology* 2007;18:455703.
- [20] Liu M, Jia D, Zhou C. Recent Advance in research on halloysite nanotubes-polymer nanocomposite. *Prog Polym Sci* 2014;39:1498–525.
- [21] Yin B, Hakkarainen M. Core-shell nanoparticle-plasticizers for the design of high-performance polymeric materials with improved stiffness and toughness. *J Mater Chem* 2011;21:8670–7.
- [22] C. Liu , Y. F. Luo, Z. X. Jia, B. C. Zhong, S. Q. Li, B. C. Guo, D. M. Jia. 2011. Enhancement of mechanical properties of poly(vinyl chloride) with polymethyl methacrylate-grafted halloysite nanotube. *Express Polymer Letters* 5 (7) (2011) 591–603.
- [23] Fuentes S, Retuert J, Benavente E, Lozano H, González G. Chitosan-siloxane nanocomposites. Formation, structure, and properties of films. *Mol Cryst Liq Cryst* 2008;483:109–19.

- [24] Shamsi MH, Geckeler KE. The first biopolymer-wrapped non-carbon nanotubes. *Nanotechnology* 2008;19:075604.
- [25] Yah WO, Xu H, Soejima H, Ma W, Lvov Y, Takahara A. Biomimetic Dopamine Derivative for selective polymer modification of Halloysite Nanotube Lumen. *J Am Chem Soc* 2012;134:12134–7.
- [26] Crini G. Non-conventional low-cost adsorbents for dye removal: a review. *Bioresour Technol* 2006;97:1061–85.
- [27] Bertolino V, Cavallaro G, Lazzara G, Milioto S, Parisi F. Biopolymer-targeted adsorption onto halloysite nanotubes in aqueous media. *Langmuir* 2017;33:3317–23.
- [28] Ibrahim GPS, Isloor AM, Moslehiani A, Ismail AF. Bio-inspired, fouling resistant, tannic acid functionalized halloysite nanotube reinforced polysulfone loose nanofiltration hollow fiber membranes for efficient dye and salt separation. *J Water Process Eng* 2017;20:138–48.
- [29] Cavallaro G, Lazzara G, Milioto S. Exploiting the colloidal stability and solubilization ability of clay nanotubes/ionic surfactant hybrid nanomaterials. *J Phys Chem C* 2012;116:21932–8.
- [30] Cavallaro G, Lazzara G, Milioto S, Parisi F. Hydrophobically modified halloysite nanotubes as reverse micelles for water-in-oil emulsion. *Langmuir*. 2015;31:7472–8.
- [31] Rawtani D, Agrawal YK. Study the interaction of DNA with halloysite nanotube-gold nanoparticle- based composite. *J Bionanosci* 2012;6:95–8.
- [32] Rawtani D, Agrawal YK, Prajapati P. Interaction behaviour of DNA with halloysite nanotube-silver nanoparticle based composite. *J Bionanosci* 2013;3:73–8.
- [33] Cuenya BR. Synthesis and catalytic properties of metal nanoparticles: size, shape, support, composition, and oxidation state effects. *Thin Sol Film* 2010;518:3127–50.
- [34] Mody VV, Siwale R, Singh A, Mody HR. Introduction to metallic nanoparticles. *J Pharm Bioallied Sci* 2010;2:282–9.
- [35] Yuan P, Southon PD, Liu Z, Kepert CJ. Organosilane functionalization of halloysite nanotubes for enhanced loading and controlled release. *Nanotechnology* 2012;23:375705.
- [36] Sabahi H, Khorami M, Rezayan AH, Jafari Y, Karami MH. Surface functionalization of halloysite nanotubes via curcumin inclusion. *Colloids Surf A Physicochem Eng Asp* 2018;538:834–40. <https://doi.org/10.1016/j.colsurfa.2017.11.038>.
- [37] Khatri N, Tyagi S. Influences of natural and anthropogenic factors on surface and ground-water quality in rural and urban areas. *Front Life Sci* 2015;8:23–39.
- [38] Rawtani D, Khatri N, Tyagi S, Pandey G. Nanotechnology-based recent approaches for sensing and remediation of pesticides. *J Environ Manage* 2018;206:749–62.
- [39] Khatri N, Tyagi S, Rawtani D. Assessment of drinking water quality and its health effects in rural areas of Harij taluka, Patan district of northern Gujarat. *Environ Claims J* 2016;28:223–46.
- [40] Palmer WE, Bromley PT, Brandenburg RL. Wildlife & pesticides - peanuts. North Carolina Cooperative Extension Service; 2007.
- [41] Wells M. Vanishing bees threaten U.S. crops. London: BBC News; 2007. <<http://news.bbc.co.uk/2/hi/americas/6438373.stm>>.
- [42] Miller GT. Sustaining the earth. 6th ed. Pacific Grove, CA: Thompson Learning, Inc; 2004. p. 211–6 [chapter 9].
- [43] Alder L, Greulich K, Kempe G, Vieth B. Residue analysis of 500 high priority pesticides: better by GC-MS or LC-MS/MS? *Mass Spectrom Rev* 2006;25:838–65.
- [44] Stan H. GC-MS. I: basic principles and technical aspects of GC-MS for pesticide residue analysis. In: Fernandez A, editor. *Chromatographic-mass spectrometric food analysis for*

- trace determination of pesticide residues. Almeria: Elsevier; 2005. p. 269–337 [chapter 6].
- [45] Grawe GF, de Oliveira TR, de Andrade Narciso E, Moccellini SK, Terezo AJ, Soares MA, et al. Electrochemical biosensor for carbofuran pesticide based on esterases from *Eupenicillium shearii* FREI-39 endophytic fungus. *Biosens Bioelectron* 2015;63:407–13.
  - [46] Sanghavi BJ, Hirsch G, Karna SP, Srivastava AK. Potentiometric stripping analysis of methyl and ethyl parathion employing carbon nanoparticles and halloysite nanoclay modified carbon paste electrode. *Anal Chim Acta* 2012;735:37–45.
  - [47] Zango ZU, Garba ZN, Abu Bakar NHH, Tan WL, Abu Bakar M. Adsorption studies of  $\text{Cu}^{2+}$ -Hal nanocomposites for the removal of 2,4,6-trichlorophenol. *Appl Clay Sci* 2016;132–133:68–78.
  - [48] Saraji M, Jafari MT, Mossaddegh M. Chemically modified halloysite nanotubes as a solid–phase microextraction coating. *Anal Chim Acta* 2017;964:85–95.
  - [49] Bielska D, Karewicz A, Lachowicz T, Berent K, Szczubiałka K, Nowakowska M. Hybrid photosensitizer based on halloysite nanotubes for phenol-based pesticide photodegradation. *Chem Eng J* 2015;262:125–32.
  - [50] Khatri N, Tyagi S, Rawtani D. Rural environment study for water from different sources in cluster of villages in Mehsana district of Gujarat. *Env Monit Assess* 2017;190:10.
  - [51] Tyagi S, Rawtani D, Khatri N, Tharmavaram M. Strategies for Nitrate removal from aqueous environment using nanotechnology: a review. *J Water Process Eng* 2018;21:84–95.
  - [52] Liu W, Fizir M, Hu F, Li A, Hui X, Zha J, et al. Mixed hemimicelle solid-phase extraction based on magnetic halloysite nanotubes and ionic liquids for the determination and extraction of azo dyes in environmental water samples. *J Chromatogr A* 2018;1551:10–20.
  - [53] Khatri N, Tyagi S, Rawtani D. Removal of basic dyes auramine yellow and auramine O by halloysite nanotubes. *Int J Environ Waste Manag* 2016;17:44–59.
  - [54] Rawtani D, Agrawal YK. A study of the behaviour of HNT with DNA intercalator acridine orange. *BioNanoSci* 2013;3:52–7.
  - [55] Riahi-Madvaar R, Taher MA, Fazelirad H. Synthesis and characterization of magnetic halloysite-iron oxide nanocomposite and its application for naphthol green B removal. *Appl Clay Sci* 2017;137:101–6.
  - [56] Wan X, Zhan Y, Long Z, Zeng G, He Y. Core@double-shell structured magnetic halloysite nanotube nano-hybrid as efficient recyclable adsorbent for methylene blue removal. *Chem Eng J* 2017;330:491–504.
  - [57] Liu Y, Tu W, Chen M, Ma L, Yang B, Liang Q, et al. A mussel-induced method to fabricate reduced graphene oxide/halloysite nanotubes membranes for multifunctional applications in water purification and oil/water separation. *Chem Eng J* 2018;336:263–77.
  - [58] Zeng G, Ye Z, He Y, Yang X, Ma J, Shi H, et al. Application of dopamine-modified halloysite nanotubes/PVDF blend membranes for direct dyes removal from wastewater. *Chem Eng J* 2017;323:572–83.
  - [59] Zeng G, He Y, Zhan Y, Zhang L, Pan Y, Zhang C, et al. Novel polyvinylidene fluoride nanofiltration membrane blended with functionalized halloysite nanotubes for dye and heavy metal ions removal. *J Hazard Mater* 2016;317:60–72.
  - [60] Fan HT, Wu JB, Fan XL, Zhang DS, Su ZJ, Yan F, et al. Removal of cadmium (II) and lead (II) from aqueous solution using sulfur-functionalized silica prepared by hydrothermal-assisted grafting method. *Chem Eng J* 2012;198–199:355–63.
  - [61] Förstner U, Salomons W, Mader P, editors. Heavy metals, problems and solutions. Berlin Heidelberg: Springer-Verlag; 1995.

- [62] Khatri N, Tyagi S, Rawtani D. Recent strategies for the removal of iron from water: a review. *J Water Process Eng* 2017;19:291–304.
- [63] Gidlow DA. Lead toxicity. *Occup Med* 2015;65:348–56.
- [64] Mason LH, Harp JP, Han DY. Pb neurotoxicity: neuropsychological effects of lead toxicity. *Biomed Res Int* 2014;2014:8.
- [65] Dong Y, Liu Z, Chen L. Removal of Zn (II) from aqueous solution by natural halloysite nanotubes. *J Radioanal Nucl Chem* 2012;292:435–43.
- [66] Cataldo S, Lazzara G, Massaro M, Muratore N, Pettignano A, Riela S. Functionalized halloysite nanotubes for enhanced removal of lead (II) ions from aqueous solutions. *Appl Clay Sci* 2018;156:87–95.
- [67] Afzali D, Fayazi M. Deposition of MnO<sub>2</sub> nanoparticles on the magnetic halloysite nanotubes by hydrothermal method for lead (II) removal from aqueous solutions. *J Taiwan Inst Chem Eng* 2016;63:421–9.
- [68] Amjadi M, Samadi A, Manzoori JL. A composite prepared from halloysite nanotubes and magnetite (Fe<sub>3</sub>O<sub>4</sub>) as a new magnetic sorbent for the preconcentration of cadmium (II) prior to its determination by flame atomic absorption spectrometry. *Microchim Acta* 2015;182(9–10):1627–33.
- [69] Tian X, Wang W, Tian N, Zhou C, Yang C, Komarneni S. Cr (VI) reduction and immobilization by novel carbonaceous modified magnetic Fe<sub>3</sub>O<sub>4</sub>/halloysite nanohybrid. *J Hazard Mater* 2016;309:151–6.
- [70] Denny MS, Cohen SM. In situ modification of metal–organic frameworks in mixed-matrix membranes. *Angew Chem Int Ed* 2015;54:9029–32.
- [71] Bae TH, Long JR. CO<sub>2</sub>/N<sub>2</sub> separations with mixed-matrix membranes containing Mg<sub>2</sub>(dobdc) nanocrystals. *Energy Environ Sci* 2013;6:3565–9.
- [72] Rodenas T, Luz I, Prieto G, Seoane B, Miro H, Corma A, et al. Metal–organic framework nanosheets in polymer composite materials for gas separation. *Nat Mater* 2015;14:48–55.
- [73] Ge L, Lin R, Wang L, Rufford TE, Villacorta B, Liu S, et al. Surface-etched halloysite nanotubes in mixed matrix membranes for efficient gas separation. *Sep Purif Technol* 2017;173:63–71.
- [74] Hashemifard SA, Ismail AF, Matsuura T. Mixed matrix membrane incorporated with large pore size halloysite nanotubes (HNT) as filler for gas separation: experimental. *J Colloid Interface Sci* 2011;359:359–70.
- [75] Zhang Q, Uchaker E, Candelaria SL, Cao G. Nanomaterials for energy conversion and storage. *Chem Soc Rev* 2013;42:3127–71.
- [76] Li Y, Zhou J, Liu Y, Tang J, Tang W. Hierarchical nickel sulfide coated halloysite nanotubes for efficient energy storage. *Electrochim Acta* 2017;245:51–8.
- [77] Liang J., Fan Z., Chen S., Ding, S., Guang, Y. Hierarchical NiCo<sub>2</sub>O<sub>4</sub> Nanosheets@halloysite Nanotubes with Ultrahigh Capacitance and Long Cycle Stability As Electrochemical Pseudocapacitor Materials chem. Mater. 2014;26(15):4354–4360.



This page intentionally left blank

## Chapter 16

# Functionalized nanomaterials for chemical sensor applications

Sing Muk Ng<sup>1,2</sup>

<sup>1</sup>Faculty of Engineering, Computing, and Science, Swinburne University of Technology Sarawak Campus, Jalan Simpang Tiga, Kuching, Malaysia, <sup>2</sup>School of Research, Swinburne University of Technology Sarawak Campus, Jalan Simpang Tiga, Kuching, Malaysia

## 16.1 Introduction

Nanomaterials (NMs) are unique in the sense that they can display totally different behavioral, chemical, and physical characteristics as compared to their bulk counterparts even if they consist of identical chemical compositions. This paradoxical behavioral has driven researchers to understand the basic physiology and chemistry behind this group of NMs. The significant increase in the number of publications on the subject is clear evidence that NM research is a growing field. Researchers now have better knowledge and understanding of the nature of NMs, and are leading the way toward producing NMs with intentional properties and functionalities. Their research has created the opportunity to utilize NMs for various applications such as sensing, bioimaging, as catalysts, in cosmetic, drug delivery, and industrial applications, etc. [1]. They are also useful for separation purposes such as in chromatography applications [2] and for environmental protection and remediation [3]. The constant exploration and reporting of new synthesis methods has led to the production of NMs with easier synthesis, greater affordability, consistent quality, and higher yield. These are important factors that make commercialization of NMs for real applications highly possible and realistically achievable.

There are a few distinct properties of NMs that make them suitable for various applications. Most NMs are reported to show a fluorescence property, enabling them to be utilized as optical transducers in sensing applications, as an optical tag for bioimaging, and as a digital screen display panel [4–6]. In most cases, they have the potential to replace the use of existing organic fluorophores that have less stability, require lengthy synthesis methods governed by organic chemistry principles, and use substantial amounts

of organic solvents. Besides the fluorescence property, the unique conductivity feature induced by the change in dimension is also a good candidate for use as sensing transducer. Their naturally small size is suitable for use in vivo application because they have the flexibility to move across membranes and reach into the cellular cells within the biological system. This fits the requirements for cell imaging or as a drug delivery system on targeted sites. Some NMs are reported to be low in toxicity at their initial stage such as carbon dots (CDs) [7], thus having a high potential for real applications especially in the areas of biomedicine and healthcare. In addition, the small dimension of NMs result in a high surface-to-volume ratio compared to the same volume of bulk counterparts. The NM surface property is important because more atoms are at the interface, and their activity is no longer negligible, which means that the chemical property is more reactive. This helps to explain the observed increments in the catalytic activity of nanocatalysts since the reaction occurs at the surface of the materials. The interface interaction is more effective due to the large surface areas, and usually this is a requirement for the success of many applications.

In general, most NM properties are suitable to be employed for chemical-sensing applications. In brief, the sensing mechanism is based on the change—trigger in the initial property of the sensing receptor after interacting with the analyte. Changes can be electrical, optical, or even in the physical dimension. For example, the optical property in the form of fluorescence is used as a sensing signal by monitoring the degree in signal change before and after the interaction with a specific analyte. Properties monitored can be the intensity of change or the shift in the wavelength of the emission peak. The promoted surface chemistry, due to the large surface area, is also favorable to enhancing the sensing sensitivity factor since more effective interaction can occur between the nanoreceptor and the analyte. This strong interaction induces significant disturbance on the original property that, in return, causes huge changes in signal.

While NMs have unique features that suit the general working principle as a chemical-sensing receptor, continuous research and development efforts are needed to bridge the gap from the fundamental knowledge to real sensor application for various fields. Without such effort, the sensing performance will be low and lack of specificity. For instance, stronger interface interaction due to the NMs' small size is good for sensing but generally lacking in specificity and could bind to various analytes of similar nature. This issue requires the design of the raw NMs with specific elements for targeting only the selected analyte. One of the design solution is to functionalize NMs with additional ligands, which serve to compensate for the lack of NMs' selectivity for chemical-sensing applications. Usually the initial physiochemical properties of NMs are not affected by foreign compounds that are present together if they do not have direct interaction. Engineering NMs with additional functionality could add value by coupling a specific ligand with good

binding affinity toward the selected analyte onto the NMs. Using this design, the bound analyte is in proximity of the NMs and can subsequently disturb the NMs' initial properties that eventually can be read as a sensing signal. One such example is capping l-cysteine to CDs enabling a probe to be used for detection of peroxide, glutathione, mercuric ions, tetracycline, and nitrobenzene [8].

This chapter covers some fundamental properties of raw NMs reported in the literature that are suitable for use in chemical-sensing applications. This chapter focuses mainly on those NMs that are formed from the basic building units into homogenous, nanosized structures, rather than those formed from heterogeneous, hybrid materials, such as the entrapment of dyes onto an organic matrix that is of nanometer range. The chapter also discusses the functionalization approaches that can be performed to design NMs with additional functionalities for sensing applications. These approaches include the major engineering techniques that are commonly used craft chemical and biological species onto NMs. In order to have a better understanding of the purpose and significance of performing functionalization, this chapter highlights some real examples of the use of functionalized NMs for the sensing of different species as reviewed in the literature. The emphasis is on the advantages of having the additional functional groups graphed on the NMs as compared to the bare NMs for the purpose of detecting different analyte groups.

## 16.2 General characteristics of NMs for chemical-sensing applications

NMs have several unique properties, including size, shape, and morphology, that are generally suitable for use as chemical-sensing applications and for having effective interaction with analytes. Their nanosized dimension enables unique features such as fluorescence emission and semiconductor electrical properties that are suitable for use as sensing signals. Often a change in a specific property due to interaction with a targeted analyte can be correlated to the identity or quantity of that analyte. In some cases, the change is induced by a change in the microsurroundings (i.e., temperature or pH). Other properties, such as their chemical and biocompatibility nature, are also to be considered when developing specific sensors to ensure they will not harm or contaminate the sample or the testing host. Such considerations definitely apply to biomedical applications such as developing an in situ sensor that is going to operate in the human tissue. The sensors should not create negative side effect or cause serious stress to the cells. This section covers the general characteristics that make NMs suitable for sensing applications.

### 16.2.1 Morphology

The definition of a NM generally refers to a material with at least one dimension that is in the nanometer range, which is within the range of 1–100 nm. However, sometimes there are exceptions when the size might exceed the 100 nm limit, but still be considered a NM as long as it displays the signature properties of a NM. NMs can have different shapes, with the most common being the two-dimension spherical type known as “dots” such as quantum dots (QD) [9] and the cylindrical type known as “rod” such as the well-known carbon nanotube [10]. There are other less commonly encountered shapes like cube [11], flower-like [12], pyramid-shaped [13], hexagonal [14], etc. Using the existing microscopic techniques SEM and TEM and their resolution capability in the nanometer range, the views of raw NMs often show smooth surfaces. However, intentional modification of the surface alters the initial smooth surface accordingly as shown in Fig. 16.1. The image captures the NMs’ rough surface after capping with silica-based materials where the core is made of the NM. The size has grown as compared to the initial morphology, and the capping is used as a size

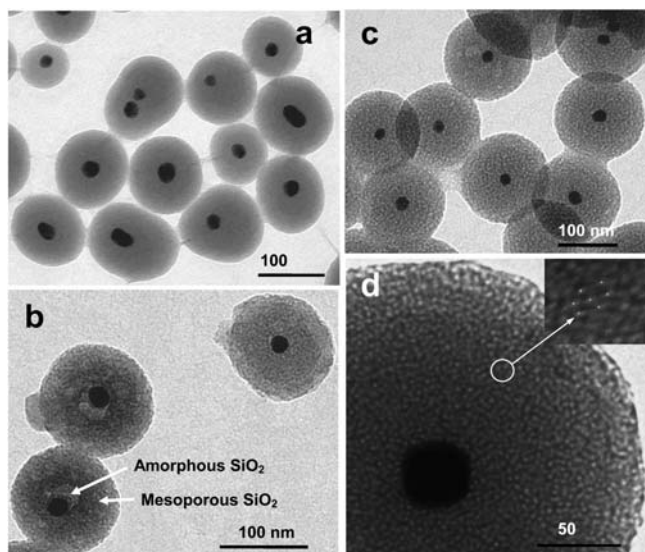


**FIGURE 16.1** (A) Gold nanoparticles encapsulated in amorphous silica nanospheres prepared by Stober’s method; (B, C) Gold mesoporous silica nanoparticles synthesis by pseudomorphic transformation of preformed gold nanoparticles encapsulated with silica at an intermediate state detected at  $t = 15$  min (B) and after complete change (C); and (D) detail of wormhole-like channels of nanomaterial microstructure; the inset shows the local arrangement in hexagonal symmetry. Reproduced from Botella P, Corma A, Navarro MT. Single gold nanoparticles encapsulated in monodispersed regular spheres of mesostructured silica produced by pseudomorphic transformation. *Chem Mater* 2007;19(8):1979–83 [15].

controller by adjusting the thickness according to the amount of capping agent added.

Due to the small size, several physical properties of a solid have become more pronounced and useful for sensing applications. One such property is the elasticity factor that has become more dependent on changes in the microenvironment compared to its bulk format. When integrated into a surface acoustic wave system, any changes in this parameter could be recorded and correlated to the factor causing the change. The elasticity of the indium tin oxide (ITO nanoparticles (NPs)) that were integrated into a layer with a multiguiding structure reported a change in the presence of volatile organic compounds [16]. The change was identified indirectly based on the change in the surface acoustic wave that was resonating with the nanoparticles and was recorded using an oscillator.

NMs have the flexibility to form different arrangements into larger clusters based on their surface chemistry. Their small dimension gives them the mobility to move and interact with the other surrounding species, unlike solids that have fixed lattice arrangements within their building blocks. In view of this, the tuning of surface chemistry controls the clustering behavior, which indirectly alters some of the NMs' initial properties. The changes induced on a property are modeled as a sensing signal. One simple example is the change of surrounding pH value that induces the agglomeration of the nanoparticles. The agglomeration affinity is dependent to the surface chemistry of the NMs. In the work where  $\text{TiO}_2$  NPs were dispersed in aqueous media with different pH conditions, the agglomeration was the most effective at  $\text{pH } 5.0 < \text{pH} < 7.2$  due to the strong destabilization of the individual NPs (Fig. 16.2). Once it is in a cluster format, the self-quenching process is likely

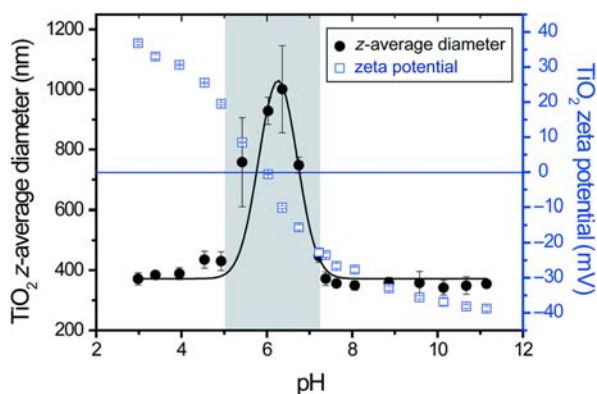


**FIGURE 16.2**  $\text{TiO}_2$  (50 mg/L  $\text{TiO}_2$  dispersion) z-average diameters and  $\zeta$  potential values as function of pH. Reproduced from Loosli F, Stoll S. Effect of surfactants, pH and water hardness on the surface properties and agglomeration behavior of engineered  $\text{TiO}_2$  nanoparticles. *Environ Sci Nano* 2017;4(1):203–11 [17].

to occur and turns off the NPs' fluorescence, as has been observed in many studies [18,19]. Under careful consideration, sensors for monitoring the pH change have been developed by determining the change in the fluorescence intensity as correlated to the surrounding pH. Similar pH sensors have been reported to be used for applications to determine the intercellular pH condition for cells.

NMs also have morphology advantages that allow them to penetrate the membranes of living cells. This feature has enabled various bio-applications to be performed such as bioimaging and usage as an *in vivo* diagnostic tool without the need to operate the host. Some studies have shown that NMs permeate the stratum corneum via a mechanism similar to the adsorption of organic molecules through the skin. This mainly follows the common intercellular pathways via the epidermal lipids [20]. Gold (Au) NPs are one of the examples where the studies using multiphoton tomography and fluorescence lifetime imaging have shown that they have the ability to penetrate the skin layer [21]. The size, exposure time, skin grade, and surface hydrophobicity are some of the significant factors that influence penetration depth and rate. Aside from skin, one study showed that AuNPs could penetrate through human placental coculture microtissues due to their small size and when they have the ideal capping agent with a hydrophilic nature [22]. In some cases, the NMs even showed the ability of cellular penetration. CDs synthesized using eggplant sepals have been found to enter the cellular layer of the living HeLa cells [23]. The CDs entered the cytosol when endocytic processes were blocked, which suggests that passive penetration is taking place through the plasma membrane of the cells. Morphology aspects, in terms of size homogeneity and tunable surface property via NM functionalization, hold the key to the penetration profile.

### 16.2.2 Optical property

Most raw NMs show fluorescence properties. As their size decreases, the material experiences gradual changes in the solid property that also affects the molecular property. During the transition, the material reaches a stage of formation of discrete band states as the physical dimension shrinks. The quantized energy level allows the excitation of the ground level electrons, especially by ultraviolet (UV) light, while the relaxation process generally generates the emission of fluorescence in the visible range. In a specific example of a semiconductor material, the reduction in size from its bulk stage causes the physical dimension to be smaller than the Exciton Bohr radius. Once the reduced size occurs, the electrons experience the confinement effect that leads the splitting of the original energy levels into smaller ones [24]. This effect is explained using the model of particles in a box where typically their dimension is less than 10 nm, and the energy gap changes accordingly with their size. This change gives rise to the property of

fluorescence emission having a wavelength that is dependent on the NMs' size. One common example is QDs, which can display various emissions based on their sizes as shown in Fig. 16.3. Smaller size particles will have larger band gaps, thus showing a blue shift in the emission.

Uniquely, nonsemiconductor NMs have also been shown to possess fluorescence property, although there is no clear band gap structure within the materials. CDs are one example where the origin of fluorescence is still under debate. There are various theories suggesting similar size confinement effects, such as the one describing fluorescence origin of QDs [25], while others postulate that the aggregated aromatic and conjugated derivative clumps that form during the carbonization of organic precursors could also

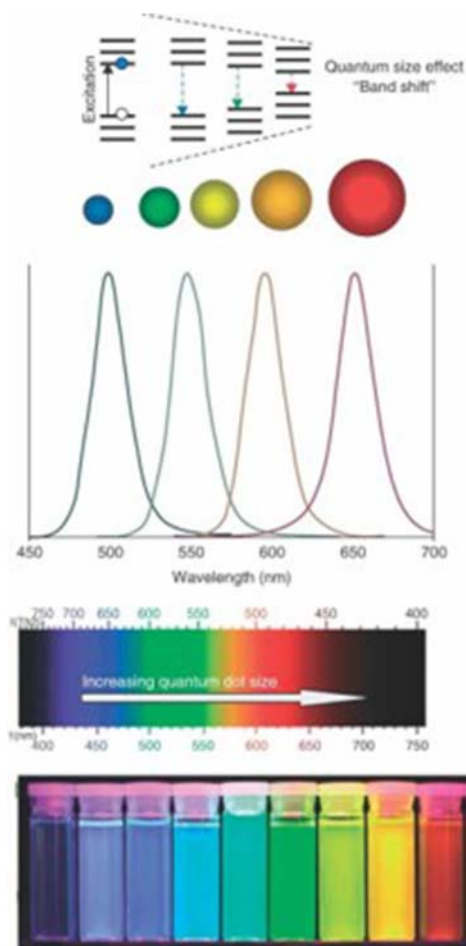


**FIGURE 16.3** QDs of different sizes showing a range of emission wavelengths [9].



promote fluorescence. In this theory the intermediates that are generated during the decomposition stage are highly reactive, forming the organic derivatives, and the fluorescence property is promoted due to the rich aromatic ring and conjugated pi bonds. For instance, the CDs formed by heating a glucose-starting precursor in the presence of phosphoric acid has an orange emission, and the origin has been suggested to be due to the aggregates of the hydroxymethylfurfural derivatives [26]. Another study suggested the fluorescence origins of CDs are from pyridine-derivatives and the presence of defective states [27]. Surface defect is another widely accepted possible explanation of the origin of fluorescence. The defects are created by surface oxidation forming an energy gap and serving as capturing centers of excitons. Specifically, the continuous introduction of the oxidation sites via a longer period of oxidation process narrows down the energy band gap that leads toward the red-shift in the emission profile [28]. The brightness and quantum yield are also observed to be improved under this condition [29]. The other model that offers a possible cause for the NMs' fluorescence is the red-edge effect [30,31].

Another unique optical property of some NMs is their light absorption ability which is caused by the surface plasmon resonance (SPR) mechanism, a feature clearly observed in metallic NPs. The basic principle of this mechanism involves the oscillations of conduction electrons of the free electron on the surface of the NPs being excited by electromagnetic radiation. The amplitude of the oscillation differs with the change in the radiation frequency and usually refer as the SPR when it reaches its maximum. The NP's color is determined by the adsorption of the radiation that falls within the visible range. Of the metallic NPs, those made of noble metal such as Au and silver (Ag) have strong SPR absorbance in the visible range. For AuNPs this resonance often occurs at the 500 nm region, causing them to show an intense red color solution [32,33]. Whereas AgNPs often show a strong band around 400 nm, causing the solution to show a yellow color. Theoretically the SPR frequency depends on various factors such as the metal type, size, shape, composition, dielectric constant, surface chemistry, etc. [34]. A star-shaped AuNPs type has shown multiple SPRs when measured using a single particle spectroscopy. This outcome has resulted in polarization-dependent scattering with multiple spectral peaks as generated by the tips on the star-shaped structure [35]. Another interesting fact is that the change in solution's dielectric can shift of the SPR and the degree of shifting can be used for chemical assay. Different concentrations of chemicals alter the dielectric constant, and this is reflected in the shifting SPR frequency that can be later correlated to the concentration of the chemical species.

### 16.2.3 Toxicity and biocompatibility

One of the advantages of using NMs as sensing probes is that their small size enables them to access various spaces with minimum. Their size makes

them well-suited for biomedical applications, where the probes are introduced to various body parts for diagnostic purposes without the need of physical operation. Therefore issues of NMs' toxicity and biocompatibility become important because any harmful effects need to be avoided during the application stage. However, the interaction mechanisms between NMs and living organisms are very complex and involve multiple parameters, which to date have yet to be fully understood. The changes in the physiochemical properties such as different size, shape, and surface chemistry show different toxicity effects even though the NMs' core is made of the same material [36]. This situation means that hazard identification for NMs is not straightforward and cannot generally be applied to all type of NMs. It would be rather more accurate to focus on the toxicity nature by the classes of NMs. Comparison of NMs' toxicity cannot be directly taken from various reports; although the types of NMs are the same they do not have identical testing systems and conditions. Mostly in vitro assays have been performed for indicating toxicity compared to lesser in vivo assays that are deemed to be far more complex and difficult to quantify. There are various possible causes of toxicity by the NMs, and one cause may be the formation of reactive oxygen species (ROS) by the NMs' photoactivity. Some of the common assays performed to study the cytotoxicity effect in vitro include lactate [lactic] dehydrogenase (LDH) assay of cell membrane integrity, the 3-(4,5-dimethylthiazol-2-yl) - 2,5-diphenyl-tetrazolium bromide (MTT) assay of mitochondrial function, and immunochemistry markers for apoptosis and necrosis [37].

QDs are one of the commonly used NMs for sensing applications due to their superior fluorescence property. However, there is always concern over their toxicity since most QDs content has a toxic precursor such as a heavy metal. These ions are usually found to have a binding tendency with the thiol groups in the mitochondria leading to malfunction of the cell. In this instance, capping with a natural or biological compound on the surface is taken as a measure to encapsulate the core and avoid the leaching of metal ions that cause stress, trigger apoptotic response, and eventual cell death. CdS QDs treated with plant extracts as a capping agent are found to show much lower toxicity effect toward cells as compared to the bare CdS QDs [38]. Capping with a polymeric layer such as polyethyleneimine could also reduce the toxicity of QDs since this layer acts as a protective layer to avoid the Cd reaching the intercellular cell, besides controlling the size that can reduce the uptake by the cells [39]. The coating layer property and the type of coating used sometimes plays an important role in cellular uptake levels that have a direct correlation to the toxicity effect [40]. In vivo toxicity studies have also been carried out on various organs using an animal model. Cd-containing QDs have been shown to persist in the lungs of rats treated for 14 days by intratracheal instillation with saline, and the deposits are difficult to clear from the lung [41]. The liver is another major organ that accumulates

QDs when exposed at acute and chronic levels according to studies that showed significant impairments to the livers of tested mice [42]. QDs could lead to morphological alteration to the hepatic lobules and an increase of oxidative stress. Surprisingly, QDs are found to have induced the production of intracellular ROS, indicated by a significant increase of the malondialdehyde level within hepatocytes.

Carbon-based NMs, such as CDs and carbon nanotubes, garner less concern over their toxicity effect as compared to the QDs. The building blocks of mainly carbon-based NMs do not show high levels of toxicity. Usually the in vitro study is performed using various cell lines as the model depending on the final proposed application. The NMs are added into the cell culture and incubated for a period of time. The cell visibility is checked and compared against a control that is incubated together under identical conditions except for the absence of the NMs. For example, the toxicity of graphene quantum dots (GQDs) has been tested using this method and was found to have low toxicity [43]. HeLa (or A549) cells were used for the study and added accurately with different concentrations of the GQDs in a culture medium and incubated accordingly. After the incubation period, the cell viability, cell apoptosis and necrosis, and LDH and ROS level were examined using the respective assays to evaluate the effect of GQD on cells. Surface functionalization also alters the toxicity effect by changing the cell intake profile that subsequently imposes some oxidative stresses to the cells that leads to death. The capping of CDs with neutral polyethyleneglycol (PEG) has shown low or no toxicity effect on A cell based on in vitro study, but those coated with positively charged polyethylenimine (PEI) showed harmful effects to the cell based on the same testing assay [44]. Since the NM core is made from the same carbon-based building block, the difference in the toxicity effect must be from the capping agent on the surface that varied the CDs physiochemical property when interacting with cells.

Beyond just cell lines, studies have investigated the toxicity of CDs on more complex microorganisms such as microbes and algae. Yeast, a single celled microorganism, has been tested with CDs, and the study found that CDs imposed some toxicity toward the survival of the cells at higher concentration of CDs [45]. The tracking based on the fluorescence imaging revealed that the CDs adsorbed on the surface of yeast, causing the cell to shrink, deform, and eventually killing the cells. Further study also found that the CDs can generate ROS in the presence of light that eventually harms the cells. In the case of algae, the presence of CDs showed to have lower toxicity effect when compared to most of the QDs. This finding means the CDs had little effect on the growth inhibition, and chlorophyll a (Chla) contents, and protein contents, and the activity of enzymatic and metabolites contents on the concentration range tested also suggest a low risk of the CDs contaminating and harming the environment [46]. As for microbes, a study using *Escherichia coli* as a testing candidate found that CDs showed a

concentration dependent effect with a  $LC_{50}$  value recorded at 18.53 mL/L [47]. The CDs were prepared using an acid treatment on CNTs without specific surface modification. The growth inhibition of the microbes observed in this study was thought to be caused by the membrane and oxidative stresses induced by interactions between *E. coli* and CDs at high concentrations.

There have also been toxicity studies performed using an animal model for CDs. The CDs were introduced to animal models, usually mice or rats, via injection and their conditions monitored over the study period. The animal is sacrificed, and various organs are examined for abnormalities, if any, that were caused by the CDs. One such study was performed on CDs prepared from carbon soot that were refluxed with nitric acid and passivated with PEG2000N [48]. The CDs were introduced to the selected mouse and rat groups via injection with the predetermined amount of CDs. After the study period, the test group treated with CDs were sacrificed and no abnormalities or lesions were observed in the major organs. Examination also found that the CDs did not exhibit any gene toxicity, confirming the CDs have good biocompatibility and were nontoxic at the concentration level tested. However, the exposure of CDs on an in vivo system, such as by inhalation of high concentrations, has been shown to cause animal deaths due to the induced injuries in the lung and liver [49]. This is caused by the physical property instead of the chemical property of the CDs. The effects observed after exposure, such as inflammation and necrosis, increase with a dose-dependent and time-dependent manner. Since the CDs have fluorescence, the tracking on the biodistribution could be made directly using fluorescence spectroscopy.

Metal-based NMs such as Ag- or Au-based nanoparticles have been demonstrated to show good potential for use in various sensing applications, including use as in vivo diagnosis tools. Looking at the base building block of metal ions, there are some safety concerns raised over the possible presence of leached metal ions, especially on those that have been proven to show high toxicity in their free ionic format. However, it is also noted that living organisms require trace amounts of metal ions such as iron, magnesium, calcium, cobalt, etc. The implication is that the use of the metal-based NMs at a low concentration should be fine, as the leaching of free metal ions from the NMs' core to the biological environment is expected to be even lower. Mohan et al. demonstrated that free  $Ag^+$  ions showed higher toxicity effect on human THP-1 monocyte cells as compared to the AgNPs capped with starch [50]. Thus rough predictions on the toxicity of metal-based NMs could be linked to the toxicity studies of the free metal ions. Metal ions from the heavy metal class such as  $Hg^{2+}$ ,  $Cd^{2+}$ , and  $Pb^{2+}$  ions are usually classified as very toxic and will avoid being incorporated in the core of NMs. On the other hand, NM cores comprised of  $Fe^{2+}$ ,  $Au^{2+}$ , and  $Pt^{2+}$  ions are frequently observed to be relatively less toxic, which could partly be due to their poor solubility in aqueous media.

Besides referring to the core for toxicity effects, metallic NMs also pose some unique physiochemical properties in their nonsized state, such as the antimicrobial property. AgNPs are one of the commonly reported on antimicrobial agents, and their activity is thought to originate from the partially oxidized  $\text{Ag}^+$  ions species that absorbed on the NPs' surface [51]. The effect is suggested to be similar to free  $\text{Ag}^+$  ions, where NPs interact with the cell wall of the microbes. As for the suggested mechanism, the  $\text{Ag}^+$  ions at the surface are transferred to the microbes directly, and their study found very less leachate in the incubation solution at the time. Similarly, magnesium oxide (MgO) NPs in one of the studies showed the ability to attach to the cell wall, eventually causing damage to the cell membrane [52]. The attachment was due to the phosphate groups present on the surface of the cells, and no sign of ROS formation was detected in the study. Other parameters such as variation in size and shape were also found to have influenced the toxic effect of the metallic NMs. Eventually NPs with smaller sizes were shown to have higher toxic effects as compared to larger size NPs. AgNPs of the size ranging around 10 nm showed to have much higher toxic effects compared to those in the range larger than 50 nm [53]. The effect is associated with the smaller size that allows cellular uptake processes from the cell membranes to the nuclear pores, eventually altering the biological processes of the cells. Metallic NMs often have the property of inducing the production of ROS, which is very harmful to cells. The NPs induce stress in the cells and eventually promote the production of ROS. Iron oxide ( $\text{Fe}_3\text{O}_4$ ) NPs have been shown to induce necrosis-type cell death in lung cancer cells by inducing ROS and autophagy [54]. Other metallic NMs that show a similar property of inducing ROS and promoting toxicity include titanium oxide ( $\text{TiO}_2$ ) [55], zinc oxide (ZnO) [56], copper oxide (CuO) [57], etc.

## 16.3 The engineering aspects for functionalization of NMs

The major aim of functionalizing NMs is to add additional features to the existing unique properties of NMs. The features will often complement the NMs' properties and the conjugated capping agent, and together they achieve better performance as chemical sensors. Functionalization makes the NMs more specific in targeting certain analytes, improves the sensitivity aspect for trace analysis, reduces the noise to signal ratio, and allows for better integration into the other components of the sensor, like the electronic components. Various techniques are employed to achieve functionalization, and some of the common engineering approaches are discussed in this section.

### 16.3.1 Covalent conjugation

Forming a covalent bond as the means of bridging the capping agent to the NMs is a good option to consider because this strong bond reduces the

probability of leaching. Usually the chemical conjugation of NMs is easily achieved via the oxygen-containing groups such as hydroxyl and carboxyl groups on the surface. These groups are introduced naturally during the formation of the NMs during the synthesis of GQDs [58] or can be purposely introduced via chemical treatments such as refluxing the NMs in a strong oxidizing acid like nitric acid [59]. In some cases direct thermal treatment under the presence of oxygen can also introduce these oxygen-rich groups to the NMs' surface [60]. Other specific functional groups like the carboxylic ( $-\text{COOH}$ ) and amine ( $-\text{NH}_2$ ) are introduced using the self-assembled monolayers (SAM) via chemisorption on the NMs.

Amidation is one of the common approaches taken to link functional groups to NMs. The linkage bond is formed between  $-\text{COOH}$  with the  $-\text{NH}_2$  and is known as amide bonding. In order to achieve this bond, the surface of the NMs should have one of these functional groups present that is ready to react with their counterpart. Under normal lab conditions, the reactivity for this type of reaction is considerably low, meaning the process will not occur simultaneously to form the desired product in good yield. Thus an activator is often applied to promote the reaction by increasing the reactivity of these functional groups. One commonly used activator class for the amidation is the carbodiimide-based group. This group targets the  $-\text{COOH}$  group by forming an active intermediate readying it to react with the  $-\text{NH}_2$  group. The condition for this reaction is usually mild and can even be performed at low temperatures. This ability makes them a good candidate for the covalent attachment of biological compounds that are often fragile and can be destroyed under harsh conditions. Most protein can be denatured under high temperature or in high acidic solution. Among the different type of carbodiimide compounds, 1-Ethyl-3-(3-dimethylaminopropyl)carbodiimide (EDC) is one of the most commonly employed to activate the  $-\text{COOH}$  group to form an *O*-acylisourea, an active intermediate that could be easily displaced by a ligand containing an  $-\text{NH}_2$  terminal that is present in the same surrounding. The  $-\text{NH}_2$  group acts as a nucleophile and attack the *O*-acylisourea to form the covalent amide bond. At the same time isourea, a by-product originated from the EDC, is generated after the reaction. The optimum pH is often reported to be at around neutral. In some cases, *N*-hydroxysuccinimide (NHS) is added to the coupling protocols to improve efficiency by creating a dry-stable ( $-\text{NH}_2$ -reactive) ester intermediate. This intermediate is considerably more stable compared to the *O*-acylisourea intermediate and promotes a better efficiency for the later conjugation with  $-\text{NH}_2$ . Under careful control, various ligands are attached to the NMs' surface. This includes the attachment of peptides on the surface of AuNPs [61], horseradish peroxidase enzyme immobilized on GQDs [62], antibodies tagged on QDs [63], etc.

Click chemistry is another method that is gaining more interest for use as a means to covalently attach a ligand to the surface of NMs. Click chemistry

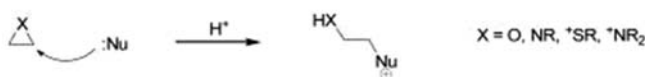
generally refers to a group of organic reactions that are efficient, easy to handle, and produce high yield. Commonly, click chemistry can be divided into few categories as summarized in Fig. 16.4, and among these, the cycloadditions type is the most widely reported. A study has been carried out to demonstrate a flexible functionalization of QDs with a specific ligand via simple click chemistry [65]. A ligand containing the norbornene terminal was first introduced to the QDs' surface, followed by the efficient click

### Cycloadditions

Cu<sup>I</sup>-catalyzed Huisgen 1,3-dipolar cycloadditions of azides and alkynes

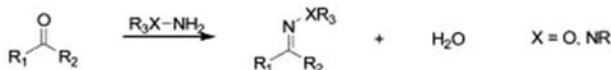


### Nucleophilic Ring-Openings

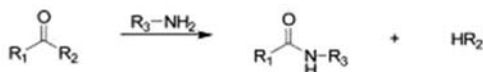


### Non-Aldol Carbonyl Chemistry

Hydrazone/oxime ether formation



Amide/isourea formation



### Carbon Multiple Bond Additions

Formation of various three-member rings



Certain Michael Additions



**FIGURE 16.4** Major classifications of click chemistry reactions, along with corresponding examples. Nu, nucleophile; EWG, electron withdrawing group. *Reproduced from Hein CD, Liu X-M, Wang D. Click chemistry, a powerful tool for pharmaceutical sciences. Pharm Res 2008;25(10):2216–30 [64].*



chemistry to connect with a tetrazine bearing PEG hydrophilic molecule. Similarly, tetrakis(5-hexyn-oxy) Fe(II) phthalocyanine was successfully conjugated on azide-functionalized CdSe/ZnS QDs and was adapted for use in the detection of paraquat [66]. In that particular study, the azide group had first been functionalized using EDC/NHS method via amide bonding as the linker, and azide starting precursors of 4-azidoaniline hydrochloride was tagged to the NMs. In some cases, the click reaction proceeded even without the copper ions as the catalyst [67]. Other reports demonstrated how the click chemistry was adapted to detect viruses [65]. The working principle is based on surface passivation of the QDs with dibenzocyclooctynes on the surface and the azine group labeled onto the virus. The click reaction induces the optical change for the QDs that can be used as sensing signal.

Instead of activating the  $-\text{COOH}$  group, the  $-\text{NH}_2$  group on the NMs can also be activated by using sulfo-succinimidyl 4-(*N*-maleimidomethyl) cyclohexane-1-carboxylate (sulfo-SMCC). A maleimide reactive species forms after the addition of sulfo-SMCC to the NMs containing the  $-\text{NH}_2$  group. In order to incorporate the ligand to the maleimide terminal, the ligand needs to have a thiol group (sometimes known as sulfhydryl group) for the conjugation. A study demonstrated the conjugation of antibody on the surface of  $\text{Fe}_3\text{O}_4$  NPs via this method as shown in Fig. 16.5 [68]. The antibody was first modified with iminothiolane to introduce the sulfhydryl group for the later reaction with the  $\text{Fe}_3\text{O}_4$  NPs modified with sulfo-SMCC having the maleimide group. Similar conjugation was performed to introduce the NMs with various ligands such as enzymes, matrix metalloproteinase [69], and the peptide hormone somatostatin [70].

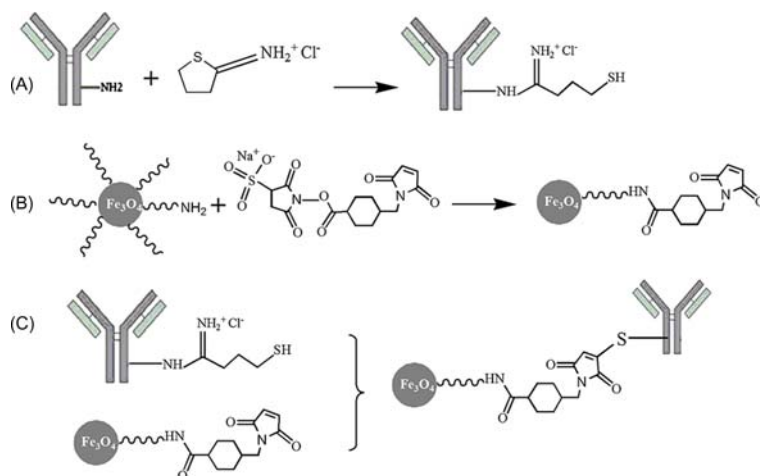


**FIGURE 16.5** Scheme showing the conjugation mechanism using sulfo-SMCC and sulfhydryl groups. Reproduced from Abdolahi M, et al., *Synthesis and in vitro evaluation of MR molecular imaging probes using J591 mAb-conjugated SPIONs for specific detection of prostate cancer. Contrast Media Mol Imaging* 2013;8(2):175–84.



Glutaraldehyde crosslinking chemistry is another method that can be used to surface functionalize the NMs. The reaction is performed at a neutral pH, and glutaraldehyde is water soluble, making it suitable to be used to link bio-compounds to various NMs and matrices containing  $\text{-NH}_2$  groups. The  $\text{-NH}_2$  group undergoes nucleophilic addition on the carbonyl site of the aldehyde molecule to produce carbinolamines, which then dehydrate to create substituted imines. This means the  $\text{-NH}_2$  and aldehyde have combined into one molecule by excluding water as the side product. Since glutaraldehyde contains two aldehyde groups with one at each terminal position, it can link two  $\text{-NH}_2$  groups together. One of these  $\text{-NH}_2$  could be present on the surface of the NMs, while the other on the ligand. NPs coated with a silica layer containing the  $\text{-NH}_2$  group have been successfully conjugated with lipase using glutaraldehyde as the linker [71]. Similarly, the goat anti-human HBsAg antibody was immobilized onto the amino-functionalized silica shell and used as probe for ultrasensitive immunoassays with glutaraldehyde as the spacer [72]. ZnO nanorods have also been reported as being successfully immobilized with antibodies using the glutaraldehyde chemistry [73], while other groups have reported their accomplishments in capping nanocomposite with amino-linked lysozyme aptamer [74].

### 16.3.2 Self-assembly

Capping functional groups onto NMs via the physical adsorption approach is based on attraction forces without any chemical bond. The forces that hold them together are comparatively weaker than covalent bonding. The forces used are hydrogen bonding, polar–polar attractions, induced polar interactions, hydrophobic interactions, and van der Waals forces. This functionalization method is usually straightforward and simple, where the NMs and the intended functional groups are added together to form the self-assembly interaction. When using some of the weaker bonding forces, nonspecific interactions might occur and cause less homogenous orientation, although most of the absorbed species will show their initial activity. This approach has been one of the earliest capping techniques, but the intentions at that point were mostly to stabilize the NMs and to avoid aggregation. As NM development progresses, attempts have been carried out to exchange this layer with other intended capping agents, while some have also attached a secondary capping agent on top of the first layer. The compounds that are often adapted are surfactants [75], polymers [76,77], and simple molecules [78–80]. The ligand selection is determined by the nature of the surface (i.e., hydrophobic NMs will be introduced with hydrophobic type of ligand and vice versa).

The formation of SAM of organic molecules on the surface of the NMs is usually based on adsorption interaction. SAM formation involves the chemisorption of the ligand on a surface of the materials, followed by the spontaneous generation of a two-dimensional, molecularly ordered domain

on the material's surface. The ligand molecule for SAM usually consists of three parts: the head group, the hydrocarbon spacer backbone chain, and the terminal group as shown in Fig. 16.6. The head group is the part that interacts with the substrate, while the backbone type chain group determines the arrangement and property of the two-dimensional domain layer. The terminal group influences the final property of the surface, such as its hydrophilicity, since it is the group located at the interface boundary with the solvent. The terminal group could also be used later to graft other compounds via covalent bonds or adsorption via electrostatic interaction. The noncovalent interactions on the head group with the substrate results in low energy kinetic barriers, allowing the ligand to attain its minimum free energy configuration despite the thermodynamic reduction in number of degrees of freedom when the ligand is packed into a denser phase of the SAM. Ligands containing a sulfur head group (i.e., thiols, dithiols, sulfide and disulfides) are the most commonly employed type, especially with metal or metal oxide-based NMs substrates such as Au and Ag surfaces. The exact mechanism of strong sulphur-metal interaction is still under investigation but the supporting literature has offered good theories about the mechanism [82–84]. Generally, SAM is formed quite easily in liquid media or even in the gas phase. The ligand containing the sulphur head group can be added and the concentration range is commonly controlled around 10–1000  $\mu\text{M}$  in different solvents depending on the solubility of the ligand. Usually the adsorption process time takes around 2–12 h to form a well-ordered SAM. Some ligands might

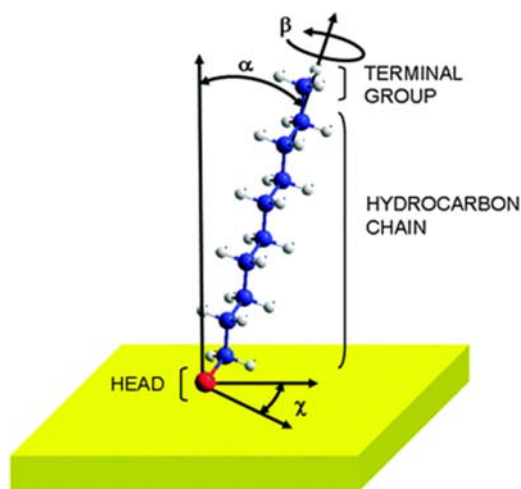


**FIGURE 16.6** Sketch of the major parts of a typical ligand used for forming SAM: head group, backbone spacer, and terminal. Reproduced from Vericat C, et al., *Self-assembled monolayers of thiols and dithiols on gold: new challenges for a well-known system*. *Chem Soc Rev* 2010;39 (5):1805–34.

need a longer time depending on the affinity of the head group and the length of the chain [81]. A study has shown that cysteine SAM has been successfully formed over AuNPs that later modified on a gold electrode for the determination of epinephrine in the presence of sodium dodecyl sulfate [85]. The synthesis was performed by the direct soaking of the substrates in cysteine under an acidic buffer solution for 5 min at room temperature.

Depending of the surface condition and charge of the NMs, the adsorption of their counterpart ligands having the opposite charge is achieved by polar–polar attraction. For example, metal NPs with net surface charges interact with biological species via noncovalent interaction. Larger biological species such as protein and enzymes have lots of chemical terminals of different charges that allow the interactions to occur. Adsorption of protein on the surface of NPs is common and better known as a protein corona. Since proteins are large biomolecules consisting of one or more long chains of amino acid residues, this means that there is a localization of charge points throughout the structure of the protein. The charge of these terminals is dependent on the solution pH, where the charges can change depending on the equilibrium with the protons that are present in the solution. These terminals serve as anchors that interact with the NPs and can be simultaneously influenced by multiple complex attractions, such as hydrophobic interactions, hydrogen bonds, Van der Waals interactions, electrostatic interactions, etc. FeO<sub>4</sub> NPs that have been capped with positive polyethyleneimine (PEI) and negative poly(acrylic acid) have both been shown to have an uptake of protein due to physical attraction, but they display different affinities since their surfaces have the opposite charges [86].

In a more advance design, the adsorption can be controlled to form a multilayer architecture in order to achieve a greater amount of ligands on the surface of the NMs. The mechanism of layer formation is governed by various factors including the composition of the dispersing medium, the structure of the NMs, the property of the ligand, pH, etc. Using protein as an example, the formation of the conjugate layers is achieved by tuning the pH parameter, where the protein grows layer-by-layer as a function of the increase in pH value on the surface of a AuNPs [87]. Besides pH, there is also the possibility of protein layers forming by using an opposite charged matrix in between the layers to induce the interaction with the protein. This means the protein could be loaded on the NMs surface and followed by an agent of opposite charge. The electrostatic interaction leads to the adsorption of the agent on the protein layer, making the outermost layer oppositely charged from the protein. When free protein is loaded again, they would then form the second layer on the matrix surface, creating a sandwich-like architecture. Fe<sub>3</sub>O<sub>4</sub> NPs have been successfully coated with multiple layers of lysozyme using tannic acid. In this case, the lysozyme holds a positive charge and the tannic acid is negatively charged. The opposite charges allow the interaction to occur in forming the layer-by-layer

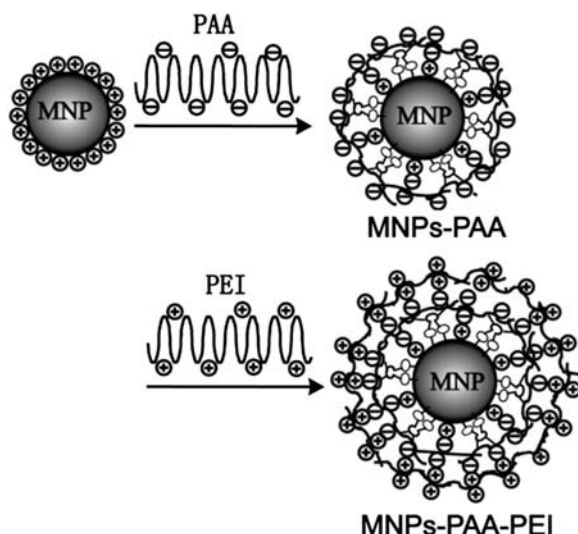


**FIGURE 16.7** The process of layer-by-layer self-assembly of polyaspartate (PAA) and poly(ethyleneimine) (PEI) on magnetic nanoparticles. *Reproduced from Wang S, et al., Layer-by-layer self-assembly of polyaspartate and poly(ethyleneimine) on magnetic nanoparticles: characterization and adsorption of protein. Curr Appl Phys 2011;11(6):1337–42.*

structure when they are added alternately [88]. Based on this similar mechanism, several layers of polymers of opposite charge are first adsorbed on the NMs forming the sandwich structure that is later used to load the protein. Polyaspartate (PAA) and (PEI) are good candidates to form such layers because both have opposite charges on the backbone of the polymers [89]. PAA is negatively charged and PEI is positively charged, and they assemble into a structure as shown in Fig. 16.7 for loading protein into the cavities in between the layers.

Another option for noncovalent linkage is the use of biotin–streptavidin chemistry. Generally, the affinity of streptavidin for biotin is one of the strongest biological interactions known, and it has a low dissociation constant [90]. Each streptavidin monomer has four active binding sites that allow the specific binding of one biotin at each site. The multiple binding sites offer the option to attach different ligands, especially biological compounds, to the surface of the NMs. For instance, the AuNPs can be outfitted with biomolecules such as horseradish peroxidase via the biotin–streptavidin interaction [91]. NPs were first surface modified with the biotin terminal, followed by the addition of horseradish peroxidase modified with streptavidin. Oligonucleotide has also been successfully outfitted on the surface of CdTe QDs following the mechanism proposed in Fig. 16.8 [92]. The QDs were capped with mercaptopropionic acid via in situ approach during synthesis

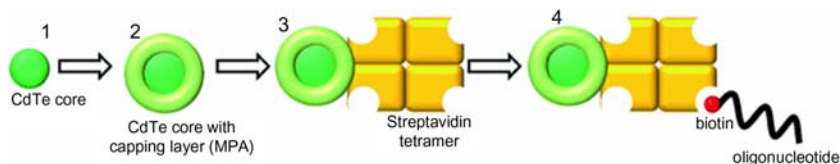


**FIGURE 16.8** Scheme showing the application of oligonucleotide on CdTe QDs via biotin–streptavidin interactions. *Reproduced from Stanisavljevic M, et al., Study of streptavidin-modified quantum dots by capillary electrophoresis. Chromatographia 2013;76(7):335–43.*

and later mixed with streptavidin to allow their adsorption on the surface. The introduction of biotin-modified oligonucleotide then interacts specifically with the streptavidin, outfitting the surface of the QDs with the oligonucleotide.

### 16.3.3 Other capping approaches

Bioaffinity tagging exploits the natural interactions of a biological species with other counterparts or ligands. The affinity is induced by the presence of multiple functional groups of the biological species at a fixed site within the structure. Thus the interaction possesses high specificity due to the formation of binding sites of specific shapes and sizes. Of course, nonspecific binding occurs as well when a functional group has partially bound with a ligand or loosely bound within a cavity of bigger size compared to the ligand. Pretreated spores of *Bacillus subtilis* have demonstrated good binding affinity with CdTe/ZnS QDs, making it possible to outfit the spore with QDs for pH sensing applications [93]. Another example is the use of eggshell membranes to immobilize NMs due to their bioaffinity to attract NMs [94].

The functionality of a secondary species can also be instilled to the NMs using the blending method. This means the NMs and the functional species are added together to form a nanocomposite within an inert matrix. While direct bonding between the NMs and the functional ligands is not guaranteed, given the fixed position within the matrix the likelihood of bonding is high. For instance, a sensitive glucose sensor was developed by blending ZnO NPs and eggshell membrane preimmobilized with glucose oxidase using ionic liquid as the holding matrix on a modified glassy carbon electrode [95]. Cyclic voltammetry was used to detect the activity and used as sensing signal. Such blending morphology was clearly observed using SEM as shown in Fig. 16.9. In other study, ZnO QDs were blended with other sensing components within a three-dimensional nitrogen-doped graphene hydrogel, and an impregnation approach was performed to incorporate horseradish peroxidase as a bioactive compound into the system [96]. The system was used to detect glucose.

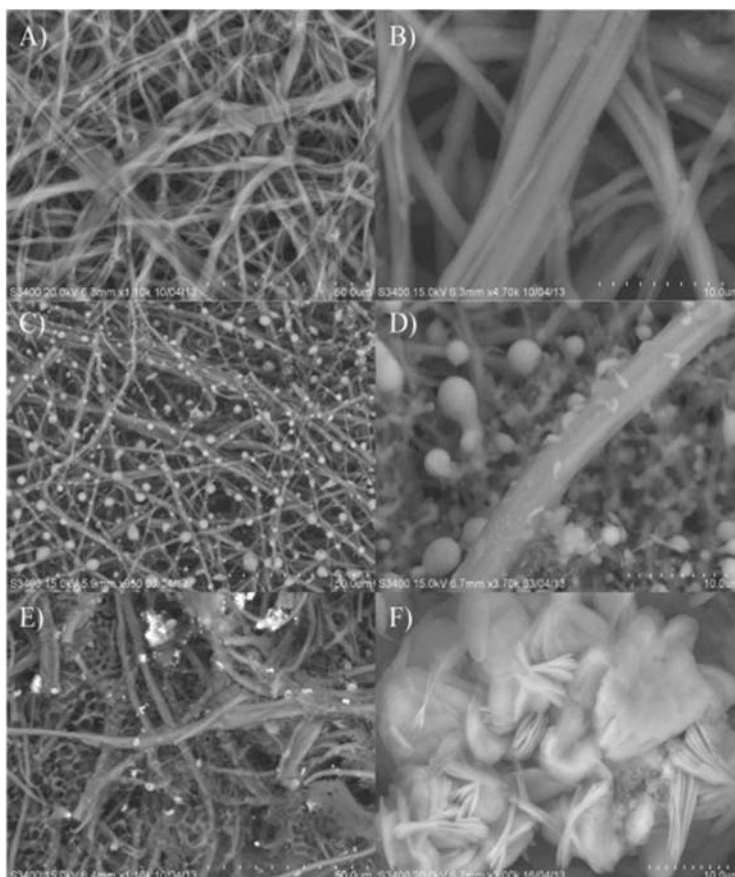


**FIGURE 16.9** A scanning electron micrograph shows different resolution of (A, B) eggshell membrane, (C, D) eggshell membrane immobilized with glucose oxidase, and (E, F) eggshell membrane immobilized with ZnO nanoparticles and glucose oxidase. *Reproduced from Aini BN, et al., Development of glucose biosensor based on ZnO nanoparticles film and glucose oxidase-immobilized eggshell membrane. Sens Bio-Sensing Res 2015;4:46–56.*

Core-shell architecture is another type of surface modification approach used to design NMs for sensing application. Core-shell architecture is mainly used to tune the basic physiochemical properties of NMs; but in some cases, the shell is utilized directly as the sensitive sensing layer for interaction with the analyte. In other cases, the shell is used as a protective layer for the core materials, as they might not be suitable for exposure to surrounding conditions due to biocompatibility and/or toxicity issues. Various materials can be used as the shell, and their selection depends mainly on the intended application. The metal–organic frameworks (MOFs) are one such candidate due their unique characteristics including coordination sites, flexible structure,

tunable permeability, chemical stability, etc. [97]. MOFs are basically crystalline porous materials that form from metal ions' building units that are interconnected with poly-topic organic linkers [98]. Generally, the coating shell layer is made by mixing the core NMs with the precursors used to form the MOFs, and, subsequently, a MOFs layer grows on the surface. Usually the NPs are first modified with chemical groups such as the  $-\text{COOH}$  group and later act as anchors for the MOFs layer that grows. For example, MOFs consisting of MIL-100(Fe) were grown on the surface of  $\text{Fe}_3\text{O}_4$  NPs, where the NPs surface were first treated with citric acid to form  $-\text{COOH}$  group [99]. In situ formation of the NMs' coating using the one-pot approach has also been attempted. A uniform shape of core-shell NPs of  $\text{Au@MOF-5}$  ( $\text{Zn}_4\text{O}(\text{1,4-benzenedicarboxylate})_3$ ) formed directly from their respective starting precursors in a suitable solvent system without first forming the AuNPs [100]. This formation was possible because Au precursors were first reduced to form the NPs on which the MOFs subsequently grew. This nanoprobe has been shown to be sensitive toward carbon dioxide monitoring using the SERs transduction technique.

The core-shell system is commonly used in QD systems to improve photoluminescence efficiency, where different types of semiconductors are blended in layers to form the final core-shell architecture. Different types of QD core-shells are produced and generally categorized into specific groups depending on the band gaps between them as shown in Fig. 16.10. The two semiconductors should eventually have similar crystalline structures, but with some mismatch in the lattice. The synthesis is usually carried out by a two-step or multiple-step process, where the core QDs are produced first via conventional methods and the subsequent shell is then formed on the core particle via different methods. The core structure is isolated and purified

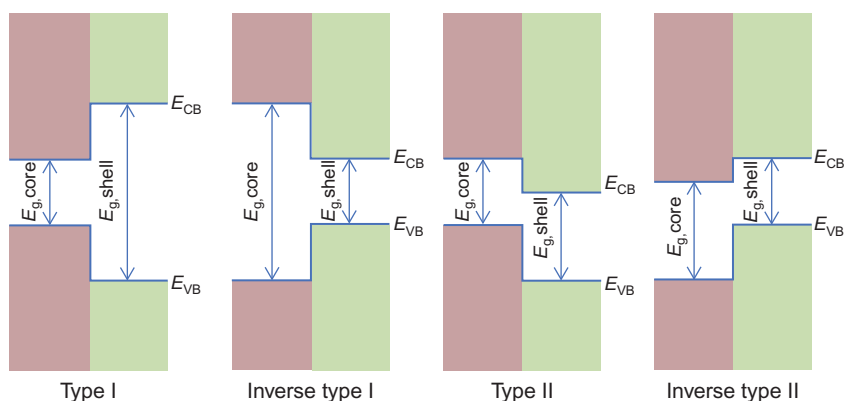


**FIGURE 16.10** Different categories of core-shell QDs. Reproduced from Vasudevan D, et al., Core-shell quantum dots: Properties and applications. *J Alloy Compd* 2015;636:395–404 [101].



from impurities before dispersed in the solution for the coating. In this case, the precursors for forming the shell layer are injected slowly into the solution containing the core NPs under controlled conditions, particularly the temperature. In order to avoid the nucleation that leads to the formation of NPs from the shell precursors, the temperature is usually kept slightly lower than the temperature used during the synthesis of the core NPs. The thickness of the shell is controlled by tuning the number of precursors added during shell formation and is optimized to get the desired luminescence property. For example, CdSe/ZnS core-shell QDs are produced by first forming the CdSe QDs using the conventional synthesis method, which later form the shell layer of ZnS under controlled conditions by slowly adding the Zn and S precursors into the system [102].

The functionalization of NMs by coating molecularly imprinted polymers (MIPs) on the surface has become more important in the recent years. The rise in importance is due to the flexibility offered by this layer in terms of tuning the selectivity toward the needs of the application. MIPs are basically produced by performing a polymerization process in the presence of a template, where the template is then removed from the matrix upon the formation of the polymer. This process leaves behind cavities of specific shapes and sizes that are complementary to the initial template used, allowing recognition in future binding. The result is analogous to the key-lock binding mechanism for enzymes, but the choice of targets that fit the role of key is more diverse. One can select the type of cavity required on the MIPs by choosing the right template, whereas there is no such option when it comes to the selection of enzymes. There are a few approaches to integrate NMs with MIPs to form the final architecture. One method is by directly growing the MIPs layer on the surface of the NMs, where functional groups that can take part in the polymerization are first assembled on the surface of the NMs. For instance, monomer with a thiol group could first be attached on AuNPs as SAM and later take place in the polymerization process to form the MIPs [103]. The polymer layer forms on the surface, and later removal of the template leaves a cavity on this layer. MIPs could also be introduced to NMs via the layer-by-layer self-assembly approach by coating the NMs with the MIPs layer. Usually the NMs are fixed on a substrate before performing the imprinting process using monomers, cross-linkers, and the template. The MIPs layer forms on top of the NMs and upon removal of the template this layer is ready to be used as the sensing receptor for the targeted analyte. CdTe QDs have been successfully functionalized with MIPs using this technique and were successfully used for the detection deltamethrin with high specificity [104].

## 16.4 Sensing applications

The utilization of functionalized NMs has gained a lot of interest for use as chemical-sensing applications, and a great amount of work has been reported



on the success in detecting various analytes. Environmental pollutants are one area where functionalized NMs are being used as chemical sensors [105]. This section covers some of the examples of the applications where nanoparticles are specifically functionalized to target the sensing needs of different categories of the analytes, from simple ions up to complex macromolecules.

### 16.4.1 pH

A solution's pH refers to the concentration of protons ( $H^+$ ) in the negative log scale. Although  $H^+$  is just a small ion species, they play an important role in many biological and chemical processes that are important for supporting life, and they are a part of the ecosystem processes of the environment and the operation processes of various industries. Thus monitoring them is crucial, and development for better options, such as the ability for biological systems to reach difficult to access areas or to have durable sensors for long term monitoring, is still ongoing. The NMs' surface can be functionalized with species that allow protonation and deprotonation according to the change in the surrounding pH. This type of functionalization should eventually induce a measurable change in some of the basic properties of the NMs. Using NMs to sense the pH of intercellular environments is a good example of this type of functionalization. The functionalized NMs offer great advantages because they can reach the inner part of the cell, and no wire connection is required in the case where the sensing signal is harvested from the optical property. AuNPs grafted with 3,5-dimercaptobenzoic acid as the pH reporter receptor have successfully been used to determine the intracellular pH levels inside human induced pluripotent stem cells [106]. The Au acted as the metal scaffold that enhanced the surface-plasmon-resonant (SPR) effect, and the detection technique was based on surface enhanced Raman scattering (SERS). The modifier also played a role as colloidal linker to link the Au into aggregates of controlled sizes in forming the hot-spot that enhanced the signal of SERS.

pH sensing using the fluorescence quenching of NMs is another common technique. In this case, fluorescence NMs are first tagged with the pH sensitive receptor that is able to undergo protonation and deprotonation according to the surrounding pH condition. In some cases, the pH sensitive groups consist of just simple functional groups such as the  $-COOH$ ,  $-NH_2$  and hydroxyl ( $-OH$ ) that formed in situ during the synthesis process. CDs prepared from mushrooms as a starting precursor without further surface modification have been shown to possess the pH responsive ability and have been able to effectively monitor biological samples [107]. There are few factors that were proposed to have caused this pH responsive behavior. One is based on the acceptance of the proton at lower pH by the functional group later being transferred over to the carbon moiety promotes fluorescence intensity.

The formation of a strong hydrogen bond at this stage is another factor thought to contribute to enhancing the intensity. There is also the contribution from electronic transitions of  $\pi-\pi^*$  and  $n-\pi^*$  by refilling or depleting their valence bands due to the protonation and deprotonation activities.

The ratiometric method for pH sensing using NMs is also very popular. The NMs are tagged with another fluorophore having a different emission wavelength that is sensitive to the pH. Once the pH condition of the surrounding changes, the fluorescence signal from the fluorophore will also change accordingly while not for the NMs since they are not pH sensitive. By taking the ratios in the intensity of these two peaks, the pH value is derived and the interference of the background noise from the surrounding is minimized. In one of the studies, CDs tagged with 1,8-naphthalimide derivative displayed this property and were used for the intracellular pH monitoring of living HeLa cells [108]. The fluorescence of the 1,8-naphthalimide derivative became completely quenched under high pH conditions, while the blue fluorescence emitted by the CDs was not affected. The fluorescence of the CDs were taken as baseline, and the signal of the grafted 1,8-naphthalimide derivative was corrected using this baseline to reduce the background fluctuation.

Fluorescent QDs tagged with the (1,3)-oxazine ring have been shown to have their intensity turned off in the presence of hydroxide ions ( $-\text{OH}$ ), allowing them to be used as pH sensors because the concentration of  $-\text{OH}$  is determined by the pH value [109]. The working mechanism is simply the reaction of the  $-\text{OH}$  with the ring to form a new a 4-nitrophenylazophenolate chromophore that later acts as the energy acceptor for the excited QDs. This type of sensor is proposed for use in two-phase systems where the pH aqueous samples, such as an environment sample, can be tested with the modified QDs in the organic phase after vigorous mixing of the two phases. Based on a similar principle, a study has shown that graphene oxide that was covalently tagged with a zwitterionic betaine molecule on the surface has the capability to undergo nonradiative recombination of the tagged group with excited holes. As a result, the fluorescence property of the graphene oxide was observed to be quenched [110]. However, this only happened at a high pH value due to the deprotonation of the tagged group, and the intensity was restored under low pH as protonation causes the group to be pointed outward, halting the nonradiative recombination process from happening (Fig. 16.11).

### 16.4.2 Metal ions

The use of functionalized NMs for sensing metal ions is one of the most frequently reported on applications due to the health and environmental concerns associated with them, especially those in the heavy metals categories. The positively charged nature of metals ions makes them more responsive

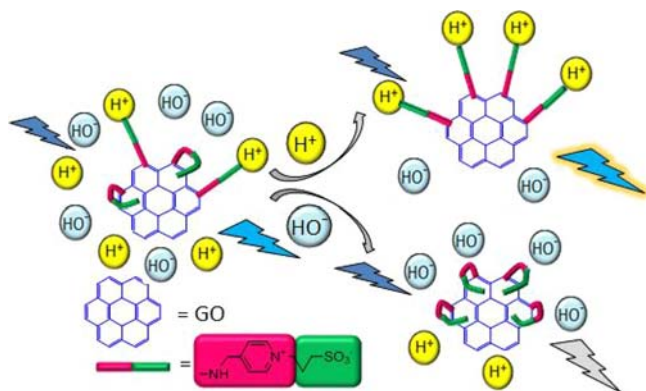


**FIGURE 16.11** Schematic illustration of the pH sensing mechanism for a functionalized graphene oxide. Reproduced from Lu L, et al., *Low toxic fluorescent nanoprobe applicable for sensing pH changes in biological environment. Sens Actuators B: Chem* 2018;257:860–65.

and easier to design a NM to interact with them. In many cases, the synthesis of the NMs in the presence of oxygen, or any oxidizing agent, promotes the generation of oxygen-rich chemical functional groups on the NMs' surface. The negative nature of these groups induces the productive interaction with the metal ions and subsequently changes the initial properties of the NMs. CDs produced from the pyrolysis of sago waste fibers have shown to be rich in alcohol or phenol, alkyl, carboxylic acid, amide, and aromatic groups, which were later found to be responsive to a series of metal ions [60]. The initial fluorescence was quenched when added to the metal ions, and the responses were concentration dependent. Lactose carbonized under thermal conditions in the presence of phosphoric acid produces CDs that emit orange fluorescence. The emission has been demonstrated to show various responses when added to different metal ions [111]. However, these simple functional groups are mostly inducing nonselective binding and thus the selectivity of the sensor will be generally lower and of less potential for real application when used as it is.

In other cases, organic ligands have been used to specifically interact with metal ions. Mercaptosuccinic acid and catechol-terminated thiol adsorbed on AuNPs system have been shown to change their solution color from pinkish to bluish in the presence of  $\text{Cu}^{2+}$  ions [112]. This change can be directly used as calorimetric sensor application for the detection of  $\text{Cu}^{2+}$  ions. In this case, the metal ions serve as the linker to the AuNPs via the capped ligands, causing them to aggregate and subsequently changing the absorbance band. Tris(hydroxymethyl)aminomethane, although just a simple molecule, induces specific binding toward  $\text{Co}^{2+}$  ions when capped on the CDs as compared with the bare CDs as shown in Fig. 16.12. The sensing mechanism is based upon the binding that brings the  $\text{Co}^{2+}$  ions near the CDs

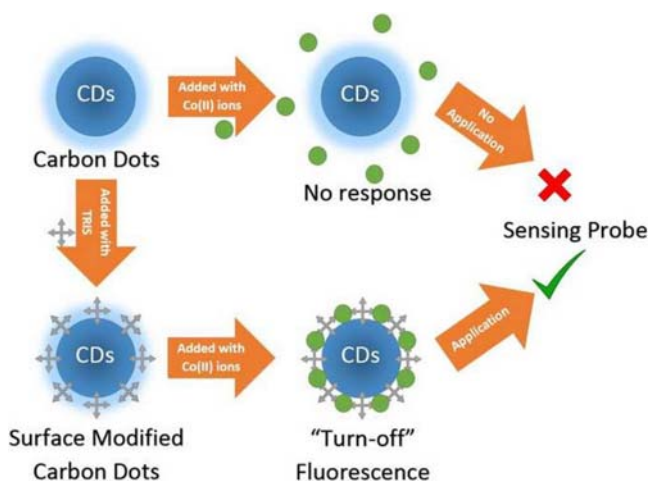


**FIGURE 16.12** Schematic diagram to show the capping agent of tris(hydroxymethyl)amino-methane has induced binding to  $\text{Co}^{2+}$  ions that eventually caused quenching effect of the CDs as compared to the bare CDs. Reproduced from Ng YH, et al., Utilising the interface interaction on tris(hydroxymethyl)aminomethane-capped carbon dots to enhance the sensitivity and selectivity towards the detection of Co(II) ions. *Sens Actuators B: Chem* 2018;273:83–92.

and subsequently promotes the Förster resonance energy transfer (FRET), since the CDs' emission is overlapping with the absorbance of  $\text{Co}^{2+}$  ions [113]. The quenching is dependent on the amount of  $\text{Co}^{2+}$  ions present in the sensing system. Thiolactic acid capped on CdTe QDs has been shown to promote selectivity toward  $\text{Ag}^+$  ion sensing via a fluorescence-quenching sensing mechanism [114]. The study proposed that the attached ligand was a branched molecule with a side methyl group that caused steric effects that hindered the metal ions from binding with the  $-\text{COOH}$  group. This effect created the necessary exclusivity for the  $\text{Ag}^+$  ions to adsorb on the surface of the QDs that eventually lead to the quenching of the fluorescence.

In a more advance setting, the same type of NM could be designed with different capping agents and used as a sensing array for the simultaneous determination of various metal ions with high selectivity. This method is basically adapting the profile recognition for each signal generated from the different capping agents when the mixture of metal ions is introduced to the arrays. For instance, three type of CDs capped with different amino acids have demonstrated the ability to detect and discriminate six different, toxic, heavy metal ions at various concentrations with a detection limit of  $10 \mu\text{M}$  [115]. Each of the differently capped CDs showed different affinities toward the metal ions tested and thus generated a unique signal profile from the sensing array. Discrimination was performed by data analysis using linear discriminate analysis (LDA) to separate the data set based on their signature features into the major components. Other similar work reported on coating

QDs using different amino acids as well as discriminating up to nine different metal ions [116]. More interestingly, the sensing array system demonstrated the ability to discriminate between a concentration of  $\text{Fe}^{2+}$  and  $\text{Fe}^{3+}$  ions mixture into their respective ratio. Besides using different capping agents, the use of CDs synthesized from various starting precursors have also been adapted as sensor arrays to discriminate metal ions accordingly [117]. Usually the different precursors and synthesis conditions generate CDs with specific surface conditions and functional groups, leading to the generation of cross-selectivity on different metal ions based on the binding affinity variation.

### 16.4.3 Simple molecules and organic pollutants

Continuous research is being conducted on diversifying the usage of the functionalized NMs in the detection of some simple molecules such as pesticides, organic pollutants, and traces of drugs. Since most of these species are harmful and highly toxic to living organisms, they are concerning even at very trace levels. Thus there is a need to have a powerful sensor to capture the presence of these species at very low concentrations. The detection limit needs to be low, meaning the interaction of these species with the NMs must induce significant change to the properties of the NMs as a signal. AgNPs that are tagged with L-cysteine have been used to detect cypermethrin, a synthetic pyrethroid used as an insecticide in large-scale commercial agricultural activity [118]. The presence of the  $-\text{COOH}$  group from the L-cysteine has prevented the AgNPs from forming aggregates due to the negatively charged surface terminal. In the presence of cypermethrin, the negative terminal interacts with the positively charged moieties within the pesticide molecules leading to a reduction in the charge density. The more neutral surface has ultimately promoted the formation of aggregates, which are reflected as the color changes from brownish-yellow to clear. Increasing cationic concentrations in the system by simply adding some salt promotes the aggregation and indirectly promotes sensitivity. In a separate study, the CDs produced from the carbonization of sucrose using strong acid interacted with paraoxon-ethyl pesticide and caused quenching of the CDs. A vigorous carbonization process introduced a high density of oxygen content to the surface as recorded by the XPS analysis. The degree of CD quenching was found to be dependent on the concentration of the paraoxon-ethyl pesticide, making it useful to be adapted for use as an analytical probe [119]. The quenching mechanism is proposed to be a nonradiant energy transfer process due to the close distance between the paraoxon-ethyl molecule and the CDs when the two species are interacting. Another functionalization approach is outfitting the NMs with a coupler via a weak interaction that changes the NMs' initial property. The coupler is then removed by the analyte and subsequently restored back to the initial property. In one of the examples, CDs are first quenched by Au

ions and the fluorescence is restored by the thiocholine generated by AChE-catalyzed hydrolysis of acetylthiocholine [120]. However, the presence of organophosphate pesticide inhibits the hydrolysis process, causing a decrease in the restoration ability of the CDs-Au system. The decrease in the fluorescence restoration efficiency is used as the sensing signal to quantify the amount of pesticide available. Besides using metal to first quench the NMs for later restoration, a second type of NMs could be used instead. A study has successfully coupled CdTe QDs capped with thioglycolic acid with AuNPs stabilized with cysteamine (CS-AuNPs), and the design enabled effective FRET to occur between the two systems. When added with the glyphosate pesticide as shown in Fig. 16.13, the aggregation of CS-AuNPs happened due to electrostatic interactions and halting the FRET, resulting in the fluorescence recovery [121].

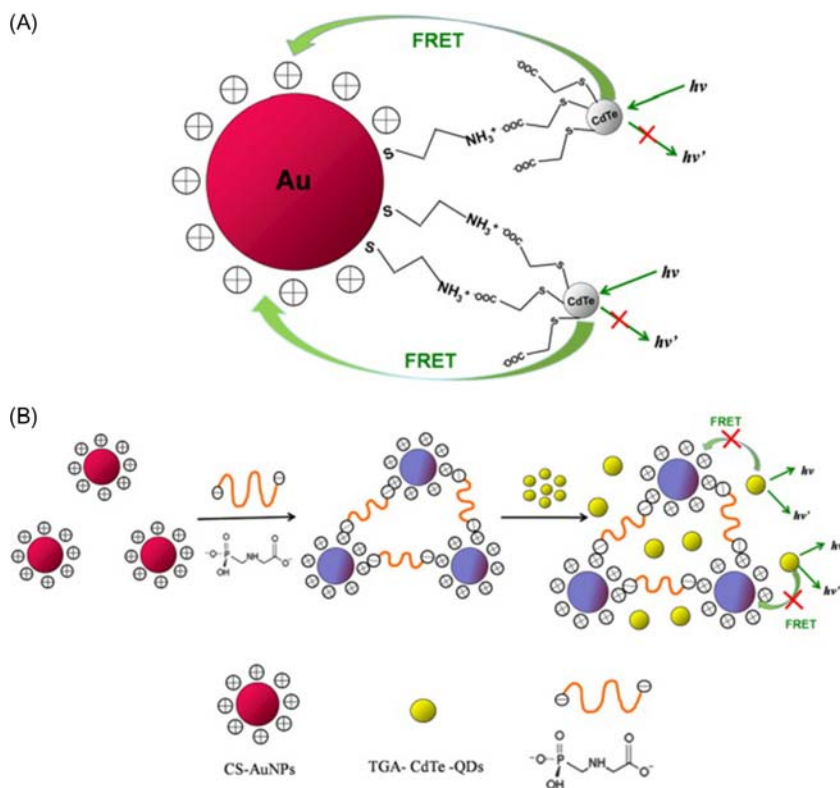


**FIGURE 16.13** Sensing mechanism for glyphosate based on the specifically designed CdTe QDs with AuNPs system. Reproduced from Guo J, et al., *Efficient fluorescence resonance energy transfer between oppositely charged CdTe quantum dots and gold nanoparticles for turn-on fluorescence detection of glyphosate*. *Talanta* 2014;125:385–92.

Another common approach in the area of molecule sensing is functionalizing the NMs with bio-recognition elements such as antibody, enzyme, or aptamer. For instance, a nanoprobe used for the detection of dichlorodiphenyltrichloroethane (DDT), a type of organochlorine pesticide, has been developed by conjugating AuNPs with anti-DDT antibodies (IgY) as the sensing receptor [122]. In this case, the AuNPs-anti-DDT reacted with 1,1,1-trichloro-2,2-bis(chlorophenyl)acetic acid conjugate with bovine serum albumin to form a red, intense immunocomplex. In the presence of free DDT, the AuNPs-anti-DDT is bound on the active sites by the DDT, making it impossible to form the immunocomplex and subsequently leading to the observation of less intense red as the indicator. Paraoxon has also been detected using core-shell QDs that were first surface absorbed with organophosphorus hydrolase [123]. The enzyme's activity was reported to be well-preserved, evenly immobilized on the NMs, and able to hydrolyze the paraoxon. The hydrolysis process has led to the loss of the fluorescence intensity due to conformational changes in the enzyme, which has been confirmed by circular dichroism spectroscopy. The use of a binding-specific aptamer has also been proven to promote the sensing capability of NMs toward specific pesticides. Acetamiprid was detected using an acetamiprid aptamer-modified ZnS:Mn QD probe based on a fluorescence enhancement mechanism [124]. Prior the introduction of the acetamiprid, the probe was first quenched with multiwalled carbon nanotubes (MWCNTs) based on FRET process. Once the acetamiprid was introduced, competitive displacement of the carbon nanotubes occurs due to the higher affinity of acetamiprid to the aptamer, thus destroying the initial FRET and restoring the intensity of the fluorescence. The interference from foreign species was low as the aptamer has very specific binding.

Functionalized NMs have also demonstrated their ability to detect active molecules such as drugs, antioxidants, and dyes. Detection of an analyte of interest occurs directly when it is in close contact with the NMs, or other species are detected and later correlated to generate information on the analyte of interest. CdTe QDs capped with glutathione have been shown to be sensitive toward the presence of hydrogen peroxide and have been used indirectly to detect uric acid [125]. Detection is possible because the uric acid was stoichiometrically converted into hydrogen peroxide and allantoin in the presence of uricase. The detection of hydrogen peroxide concentration was used as input to generate the analytical information regarding the concentration for uric acid. A similar sensing mechanism of using hydrogen peroxide as an indirect signal reporter has been performed to generate analytical information for paraoxon [126].

Direct interaction between the capping agents on the NMs and organic molecules generated analytical meaningful signals as well. Quenching was reported for CDs nanoprobe surface modified with ethylenediamine in the presence of trinitrotoluene (TNT) [127]. TNT is mainly used as an explosive



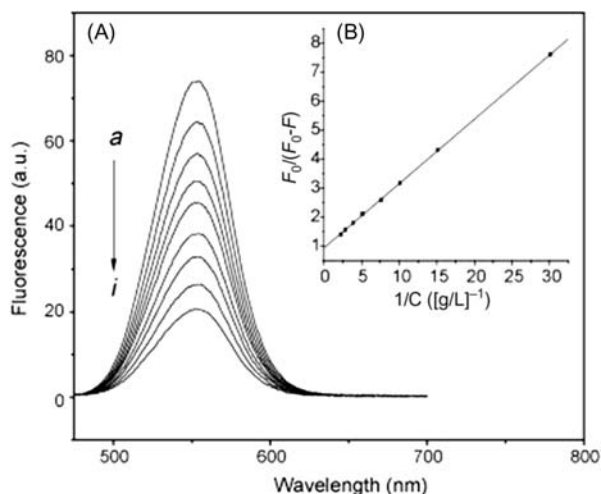


**FIGURE 16.14** The schematic diagram showing the quenching of fluorescence based vitamin B6 probe (with increasing amount of vitamin B6, (A) 0, (B) 33.22, (C) 66.23, (D) 99.00, (E) 131.6, (F) 196.1, (G) 259.7, (H) 353.7, and (I) 445.9  $\mu\text{g/mL}$  added to the QDs). Insert is the linear Stern–Volmer plot for the quenching. *Reproduced from Sun JF, et al., CdTe quantum dots as fluorescence sensor for the determination of vitamin B6 in aqueous solution. Chin Chem Lett 2008;19(7):855–59.*

and has raised environmental concerns since the molecule is relatively stable and poses several health threats to human. A similar quenching mechanism has been adapted for the detection of sulfapyridine, a simple organic molecule having an antibiotic property with a risk of polluting the environment [128]. CdTe QDs capped by thioglycolic acid have demonstrated the capability to induce binding toward vitamin B6. The binding allows the electron transfer mechanism, leading to the decrease of the initial fluorescence intensity of the QDs as illustrated in Fig. 16.14 [129]. In some cases, core-shell QDs also reported better binding results compared to just using the core QDs. Although just another secondary layer and not particularly a functional ligand, the sensitivity of the NMs system was improved. For instance, the sensitivity for the detection of folic acid increased by at least one fold when using a core-shell ZnSe/ZnS instead of just ZnSe QDs [130]. Other simple molecules detected using functionalized NMs include glucose [131–133], toxins [134], phosphate ions [135], pyrophosphate anion [136], etc.

The strong interaction was achieved between a simple organic analyte and the NMs by using MIPs as the active and selective receptor layer. The MIPs layer constructed from phenyl trimethoxysilane as a functional monomer and tetramethoxysilane as cross-linker via the sol–gel technique on palladium (Pd) NPs showed the recognition property toward norepinephrine,



which was the template used during the synthesis stage. The detection of norepinephrine is important due to their biological activity and has been successfully carried out using the PdNPs coated with MIPs via the electrochemical sensing method [137]. Other analytes that have been detected using similar NMs coated MIPs include 1-naphthylamine in drinking water [138], mycotoxin zearalenone in cereal samples [139], cholic acid [103], sulfamethazine [140], etc.

Techniques based on NMs fluorescence enhancement were also explored for the detection of simple organic molecules. CDs outfitted with  $\text{Fe}^{3+}$  ions were used to detect ascorbic acid, where the removal of the  $\text{Fe}^{3+}$  ions by the ascorbic acid restored the initial fluorescence of CDs [141]. In this case, the  $\text{Fe}^{3+}$  ions promoted the nonradiation pathway of the CDs causing the reduction of the fluorescence intensity. However, the presence of ascorbic acid reduced the  $\text{Fe}^{3+}$  ions into  $\text{Fe}^{2+}$  ions and was no longer effective in causing the CDs to quench.

#### 16.4.4 Biomarkers and biomolecules

The general nontoxic nature of some of the functionalized NMs has prompted the utilization of their the sensing system as biomedical diagnostic tools. The NMs are coupled with bio-receptors at the binding site to specifically detect various biomarkers and biomolecules used to diagnose diseases. Biomarkers are generally known as substances generated from a biological system that are used as an indicator to reflect the bioprocesses, especially those related to diseases. Dopamine is one of the important neurotransmitters that plays a significant role in the human metabolism processes. Any abnormality in their concentration may be an indication of diseases such as schizophrenia or Parkinson's. Carbon-based NPs that have been functionalized with L-cysteine were shown to detect the concentration of dopamine using electrochemical method [142]. Other studies used the hexagonal-shaped platelet AgNPs that were surface functionalized with task-specific ionic liquid for colorimetric sensing of dopamine [143]. The change in the color of the solution after the introduction of dopamine is due to the trigger of an etching process that changes the hexagonal shape of the initial AgNPs into round-shaped AgNPs. Another example of a biomarker that has been commonly detected using functionalized NMs are cardiac troponin molecules. AgNPs functionalized with hemin/G-quadruplex DNAzyme has been used to detect the presence of troponin based on a sandwich immunocomplex with capture antibody on a glass slide [144]. The troponin acts as the linker in the sandwich structure that leads to the generation of a chemiluminescence signal due to the reaction of the luminol-p-iodophenol and hydrogen peroxide in the system. Other biomarkers detected using functionalized NMs include volatile organic compounds for tuberculosis [145], arginine for the diagnosis of cancer [146], Ki-67 for the detection of breast cancer [147], etc.

The functionalized NMs are also used to detect macromolecules such as protein. Some of these proteins are used as biomarkers to detect diseases such as Alzheimer's [148] and cancers [149]. Lanthanum carbonate NPs that are surface adsorbed with curcumin via electrostatic interaction into a hard corona system have been shown to attract protein to form soft corona. The interaction was captured by steady-state fluorescence spectroscopy and the enhancement in the fluorescence curcumin was observed to be concentration dependent and able to be used as sensing signals [150]. AuNPs that have been functionalized with aptamer were used to detect thrombin using fluorescence method [151]. Doubled strains aptamer was employed, and one of the strains was tagged with a fluorescence dye. The system was in the quenching stage when the pair strain was in bundle form, but once one of the strains had bound to the thrombin, quenching no longer could happen between the dye and the AuNPs due to the increase in the distance. This eventually caused an increment in the fluorescence intensity of the dye, allowing it to be used as a sensing signal.

#### 16.4.5 Microorganisms

Functionalized NMs potential for sensing has also been extended into the detection of living microorganisms. The focus is on specifically targeting those microorganisms that are pathogenic and that could be harmful to human health when found to be contaminating resources such as foods, water, and the environment. Conventional ways of detection are usually based on the plate counting method and the later confirmation of the species using a polymerase chain reaction. Detection using functionalized NMs offers better options as the sensing can be performed rapidly, easily, and on site. Antibodies have been always a good candidate as a bio-recognition element for interaction with microorganisms. Thus antibodies tagged on NMs could serve as a bridge to bring the NMs closer to the microorganism and trigger sensing signals. Antibody-conjugated Au nanorods have successfully detected the presence of the foodborne pathogenic bacteria, *E. coli* O157: H7 and *Salmonella typhimurium* based on the localized SPR sensing technique. Aptamer is another sensing receptor that has been effectively used to detect microorganisms when bound on NMs. These methods could even be extended for real-time, continuous monitoring, and nondestructive single-cell detection of selected bacteria based on an opto-fluidic particle-sensor system [152]. Reduced graphene oxide tagged with an azophloxine dye nanocomposite and coupled with a label-free DNA aptamer has been employed for the electrochemical detection of *S. typhimurium* [153]. On a less specific end, the NMs' surface that has been capped using polymer can be used to detect microbes based on the electrostatic interactions of the microbes with the functional groups present on the backbone of the polymer [154]. In some cases, the presence of the microorganism is made known by detecting the

spores of these microorganisms. An example of this is an Au/Ag nanocluster capped with MIPs that have been imprinted using dipicolinic acid as template and being used as a probe to detect *Bacillus* spores using the fluorescence-quenching method [155].

## 16.5 Summary and future perspectives

Substantial progress has been made in recent years using NMs in chemical-sensing applications for different analytes, and various studies have demonstrated this progress. But there is still a need for deeper understanding of the fundamental properties of NMs in order to design them with better selectivity and sensitivity to suit the requirements for use in sensor applications. One approach is to functionalize the NMs with capping agents with the intention to introduce additional properties that could improve sensing performance. This method requires special attention to ensure the functionalization process would combine the NMs' properties and the capping agent to create a new hybrid entity. They should complement each other in terms of the functionality instead of interfering with or destroying the original properties. Often the NMs contribute to providing the sensing signal, while the capping agent acts as the recognition site for the binding of the analyte. There are various engineering approaches that can be employed to functionalize the NMs, and the suitability depends on the type of NMs involved, the natural stability of the capping agents, final intended applications, costs, and practicality. Most of the approaches are based on well-established chemistry practices, while only some modifications are required based on case to case basis.

While there is excitement surrounding the potential use of functionalized NMs in chemical-sensing applications, there are still some challenges to be addressed before these systems can be fully developed and commercialized for the market. Because of the numerous types of NMs available and the unlimited possibilities of capping agents, this leads to broad area of research exploration and making it less focusing on just specific application. Besides, the synthesis of NMs and capping agents involves lot of parameters, and each variation of a parameter can lead to a different outcome due to changes in the formation mechanism. This process differs from conventional organic chemistry where fluorophore synthesis for use as sensing receptors has clear mechanisms and steps can be classified clearly. NM functionalization creates hurdles in identifying a standard for benchmarking and for comparison purposes, while also making it difficult to repeat the experiment for the exact expected outcomes.

In many cases, the origin of some of the basic properties of NMs is still unclear, and this makes it difficult to design NMs for the intended chemical-sensing probes. It is well known that NMs have their own unique properties that are different from the bulk format; however, there are still issues to resolve such as discovering what are the exact triggers for these properties

including interface chemistry, optical behavior, and interaction with biological systems. For instance, the debate on the origin of fluorescence for CDs is still ongoing, and various research groups have postulated different mechanisms supported by the results of their study. However, they are not necessarily consistent, and it has been difficult to reach a general conclusion. Clear classification of the mechanism is not possible, and sometimes it is believed to be a combination of different origins within the same NM. Similarly, the interface chemistry sometimes generates observations that are not consistent between different research groups. Additionally, there is still disagreement about what factors govern the selectivity of NMs, especially when introduced to the same class of analyte such as metal ions. Although the use of capping agents helps in promoting selectivity and sensitivity in general, it is difficult to identify the exact binding sites and to understand the micro-condition of the NMs. With regard to toxicity effects, although various toxicity studies have been performed and reported on, it has been acknowledged that the variables involved are huge and interactions with biological systems are complex. Small alterations such as the capping agent, compositions, size, or shape will affect NMs' toxicity. As during real application, the NMs are foreseen to alter over time due to their dynamic surroundings, and effects on the biological surrounding are a big concern. Additional complex study is required in order to discover more information about NM functionalization and toxic effects, and it will definitely take time to accomplish this.

The advantages of NMs are promising, and, although there is still additional work to be accomplished before they are ready for commercialization, this suggests that research and development of NMs for chemical sensing will continue to grow.

## References

- [1] Hussain CM, editor. *Handbook of Nanomaterials for Industrial Applications*. Amsterdam, The Netherlands: Elsevier; 2018.
- [2] Current Trends in Chromatographic Research Technology and Techniques. In: Hussain CM, editor. *Nanomaterials in Chromatography*, Vol. 1. Amsterdam, The Netherlands: Elsevier; 2018. p. 554.
- [3] Hussain CM, Kharisov B, editors. *Advanced Environmental Analysis: Applications of Nanomaterials*, Vol 1. Cambridge, UK: Royal Society of Chemistry; 2017.
- [4] Jiang C, et al. Full-color quantum dots active matrix display fabricated by ink-jet printing. *Sci China Chem* 2017;60(10):1349–55.
- [5] Ng SM, Koneswaran M, Narayanaswamy R. A review on fluorescent inorganic nanoparticles for optical sensing applications. *RSC Adv* 2016;6(26):21624–61.
- [6] Sharma P, et al. Nanoparticles for bioimaging. *Adv Colloid Interface Sci* 2006;123-126:471–85.
- [7] Yan F, et al. Carbon dots serve as an effective probe for the quantitative determination and for intracellular imaging of mercury(II). *Microchim Acta* 2016;183(5):1611–18.
- [8] Han M, et al. High-bright fluorescent carbon dot as versatile sensing platform. *Talanta* 2017;174:265–73.

- [9] Mansur HS. Quantum dots and nanocomposites. Wiley Interdiscip Rev Nanomed Nanobiotechnol 2010;2(2):113–29.
- [10] Eatemadi A, et al. Carbon nanotubes: properties, synthesis, purification, and medical applications. Nanoscale Res Lett 2014;9(1). p. 393–393.
- [11] Park J-E, et al. Highly controlled synthesis and super-radiant photoluminescence of plasmonic cube-in-cube nanoparticles. Nano Lett 2016;16(12):7962–7.
- [12] Lu Y, et al. Fabrication of flower-like silver nanoparticles for surface-enhanced Raman scattering. Chin Chem Lett 2016;27(5):689–92.
- [13] Alivov Y, Fan ZY. A method for fabrication of pyramid-shaped  $\text{TiO}_2$  nanoparticles with a high {001} facet percentage. J Phys Chem C 2009;113(30):12954–7.
- [14] Shaban SM, et al. One step green synthesis of hexagonal silver nanoparticles and their biological activity. J Ind Eng Chem 2014;20(6):4473–81.
- [15] Botella P, Corma A, Navarro MT. Single gold nanoparticles encapsulated in monodispersed regular spheres of mesostructured silica produced by pseudomorphic transformation. Chem Mater 2007;19(8):1979–83.
- [16] Frago-Mora JR, et al. Gas sensors based on elasticity changes of nanoparticle layers. Sens Actuators B: Chem 2018;268:93–9.
- [17] Loosli F, Stoll S. Effect of surfactants, pH and water hardness on the surface properties and agglomeration behavior of engineered  $\text{TiO}_2$  nanoparticles. Environ Sci Nano 2017;4(1):203–11.
- [18] Wang C, et al. A hydrothermal route to water-stable luminescent carbon dots as nanosensors for pH and temperature. Carbon 2015;82:87–95.
- [19] Yu Y, et al. Saccharomyces-derived carbon dots for biosensing pH and vitamin B 12. Talanta 2018.
- [20] Wertz PW. Epidermal lipids and the intercellular pathway. In: Dragicevic N, Maibach HI, editors. Percutaneous penetration enhancers chemical methods in penetration enhancement: drug manipulation strategies and vehicle effects. Berlin, Heidelberg: Springer Berlin Heidelberg; 2015. p. 13–8.
- [21] Labouta HI, et al. Mechanism and determinants of nanoparticle penetration through human skin. Nanoscale 2011;3(12):4989–99.
- [22] Muoth C, et al. Impact of particle size and surface modification on gold nanoparticle penetration into human placental microtissues. Nanomed J Artic 2017;12(10):1119.
- [23] Wang Y, Jiang X. Synthesis of cell-penetrated nitrogen-doped carbon dots by hydrothermal treatment of eggplant sepals. Sci China Chem 2016;59(7):836–42.
- [24] Zorman B, Ramakrishna MV, Friesner RA. Quantum confinement effects in cdse quantum dots. J Phys Chem 1995;99(19):7649–53.
- [25] Bhattacharya A, et al. Size-dependent penetration of carbon dots inside the ferritin nanocages: evidence for the quantum confinement effect in carbon dots. Phys Chem Chem Phys 2015;17(19):12833–40.
- [26] Gude V, et al. Molecular origin of photoluminescence of carbon dots: aggregation-induced orange-red emission. Phys Chem Chem Phys 2016;18(40):28274–80.
- [27] Fang Q, et al. Luminescence origin of carbon based dots obtained from citric acid and amino group-containing molecules. Carbon 2017;118:319–26.
- [28] Bao L, et al. Electrochemical tuning of luminescent carbon nanodots: from preparation to luminescence mechanism. Adv Mater 2011;23(48):5801–6.
- [29] Bao L, et al. Photoluminescence-tunable carbon nanodots: surface-state energy-gap tuning. Adv Mater 2015;27(10):1663–7.

- [30] Cushing SK, et al. Origin of strong excitation wavelength dependent fluorescence of graphene oxide. *ACS Nano* 2014;8(1):1002–13.
- [31] Khan S, et al. Time-resolved emission reveals ensemble of emissive states as the origin of multicolor fluorescence in carbon dots. *Nano Lett* 2015;15(12):8300–5.
- [32] Zou B, et al. Gold nanoparticles based digital color analysis for quinidine detection. *Chin Sci Bull* 2013;58(17):2027–31.
- [33] Majles Ara MH, et al. Diffraction patterns and nonlinear optical properties of gold nanoparticles. *J Quant Spectrosc Radiat Transf* 2012;113(5):366–72.
- [34] Tu MH, Sun T, Grattan KTV. Optimization of gold-nanoparticle-based optical fibre surface plasmon resonance (SPR)-based sensors. *Sens Actuators B: Chem* 2012;164(1):43–53.
- [35] Nehl CL, Liao H, Hafner JH. Optical properties of star-shaped gold nanoparticles. *Nano Lett* 2006;6(4):683–8.
- [36] Suresh AK, Pelletier DA, Doktycz MJ. Relating nanomaterial properties and microbial toxicity. *Nanoscale* 2013;5(2):463–74.
- [37] Sun H, et al. The effects of composition and surface chemistry on the toxicity of quantum dots. *J Mater Chem B* 2013;1(47):6485–94.
- [38] Prasad KS, et al. Synthesis of water soluble CdS nanoparticles and study of their DNA damage activity. *Arab J Chem* 2017; 10: p. S3929-S3935.
- [39] Romoser A, et al. Mitigation of quantum dot cytotoxicity by microencapsulation. *PLoS One* 2011;6(7). p. e22079.
- [40] Manshian BB, et al. Evaluation of quantum dot cytotoxicity: interpretation of nanoparticle concentrations versus intracellular nanoparticle numbers. *Nanotoxicology* 2016;10(9):1318–28.
- [41] Wu T, Tang M. Toxicity of quantum dots on respiratory system. *Inhalation Toxicol* 2014;26(2):128–39.
- [42] Liu W, et al. CdSe quantum dot (QD)-induced morphological and functional impairments to liver in mice. *PLoS One* 2011;6(9):e24406.
- [43] Chong Y, et al. The in vitro and in vivo toxicity of graphene quantum dots. *Biomaterials* 2014;35(19):5041–8.
- [44] Havrdova M, et al. Toxicity of carbon dots – effect of surface functionalization on the cell viability, reactive oxygen species generation and cell cycle. *Carbon* 2016;99:238–48.
- [45] Bagheri Z, et al. Investigation the cytotoxicity and photo-induced toxicity of carbon dot on yeast cell. *Ecotoxicol Environ Saf* 2018;161:245–50.
- [46] Xiao A, et al. Carbon and metal quantum dots toxicity on the microalgae *Chlorella pyrenoidosa*. *Ecotoxicol Environ Saf* 2016;133:211–17.
- [47] Liu W, et al. Microbial toxicity of a type of carbon dots to *Escherichia coli*. *Arch Environ Contamination Toxicol* 2015;69(4):506–14.
- [48] Wang K, et al. Systematic safety evaluation on photoluminescent carbon dots. *Nanoscale Res Lett* 2013;8(1):122.
- [49] Yang Y, et al. Toxicity and bio-distribution of carbon dots after single inhalation exposure in vivo. *Chin Chem Lett* 2018;29(6):895–8.
- [50] Mohan S, et al. Synthesis, antibacterial, cytotoxicity and sensing properties of starch-capped silver nanoparticles. *J Mol Liq* 2016;213:75–81.
- [51] Lok C-N, et al. Silver nanoparticles: partial oxidation and antibacterial activities. *JBIC J Biol Inorg Chem* 2007;12(4):527–34.
- [52] Leung YH, et al. Mechanisms of antibacterial activity of MgO: non-ROS mediated toxicity of MgO nanoparticles towards *Escherichia coli*. *Small* 2014;10(6):1171–83.

- [53] Kim T-H, et al. Size-dependent cellular toxicity of silver nanoparticles. *J Biomed Mater Res Part A* 2012;100A(4):1033–43.
- [54] Khan MI, et al. Induction of ROS, mitochondrial damage and autophagy in lung epithelial cancer cells by iron oxide nanoparticles. *Biomaterials* 2012;33(5):1477–88.
- [55] Shukla RK, et al. ROS-mediated genotoxicity induced by titanium dioxide nanoparticles in human epidermal cells. *Toxicol Vitro* 2011;25(1):231–41.
- [56] Dutta RK, et al. Studies on antibacterial activity of ZnO nanoparticles by ROS induced lipid peroxidation. *Colloids Surf B: Biointerfaces* 2012;94:143–50.
- [57] Fahmy B, Cormier SA. Copper oxide nanoparticles induce oxidative stress and cytotoxicity in airway epithelial cells. *Toxicol Vitro* 2009;23(7):1365–71.
- [58] Zhu S, et al. Investigating the surface state of graphene quantum dots. *Nanoscale* 2015;7(17):7927–33.
- [59] Chin SF, et al. Facile synthesis of fluorescent carbon nanodots from starch nanoparticles. *Mater Lett* 2012;85:50–2.
- [60] Tan XW, et al. Carbon dots production via pyrolysis of sago waste as potential probe for metal ions sensing. *J Anal Appl Pyrolysis* 2014;105:157–65.
- [61] Bartczak D, Kanaras AG. Preparation of peptide-functionalized gold nanoparticles using one pot EDC/Sulfo-NHS coupling. *Langmuir* 2011;27(16):10119–23.
- [62] Muthurasu A, Ganesh V. Horseradish peroxidase enzyme immobilized graphene quantum dots as electrochemical biosensors. *Appl Biochem Biotechnol* 2014;174(3):945–59.
- [63] Zhang B, et al. Improving detection sensitivity by oriented bioconjugation of antibodies to quantum dots with a flexible spacer arm for immunoassay. *RSC Adv* 2016;6(55):50119–27.
- [64] Hein CD, Liu X-M, Wang D. Click chemistry, a powerful tool for pharmaceutical sciences. *Pharm Res* 2008;25(10):2216–30.
- [65] Chen Y, et al. A ligand system for the flexible functionalization of quantum dots via click chemistry. *Angew Chem Int Ed* 2018;57(17):4652–6.
- [66] Nxele SR, Nyokong T. Conjugation of azide-functionalised CdSe/ZnS quantum dots with tetrakis(5-hexyn-oxy) Fe(II) phthalocyanine via click chemistry for electrocatalysis. *Electrochim Acta* 2016;194:26–39.
- [67] Bernardin A, et al. Copper-free click chemistry for highly luminescent quantum dot conjugates: application to in vivo metabolic imaging. *Bioconjugate Chem* 2010;21(4):583–8.
- [68] Abdolahi M, et al. Synthesis and in vitro evaluation of MR molecular imaging probes using J591 mAb-conjugated SPIONs for specific detection of prostate cancer. *Contrast Media & Mol Imaging* 2013;8(2):175–84.
- [69] Li D, et al. Facile functionalization and phase reduction route of magnetic iron oxide nanoparticles for conjugation of matrix metalloproteinase. *Adv Eng Mater* 2010;12(6):B210–14.
- [70] Hafez Abdellatif AA, Abdelhafez WA, Sarhan HA. Somatostatin decorated quantum dots for targeting of somatostatin receptors. *Iran J Pharm Res: IJPR* 2018;17(2):513–24.
- [71] Hu B, et al. Immobilization of *Serratia marcescens* lipase onto amino-functionalized magnetic nanoparticles for repeated use in enzymatic synthesis of Diltiazem intermediate. *Process Biochem* 2009;44(9):1019–24.
- [72] Yang W, et al. Novel fluorescent silica nanoparticle probe for ultrasensitive immunoassays. *Analytica Chim Acta* 2004;503(2):163–9.
- [73] Ibupoto ZH, et al. Development of a disposable potentiometric antibody immobilized ZnO nanotubes based sensor for the detection of C-reactive protein. *Sens Actuators B: Chem* 2012;166-167:809–14.

- [74] Rezaei B, Jamei HR, Ensafi AA. An ultrasensitive and selective electrochemical aptasensor based on rGO-MWCNTs/Chitosan/carbon quantum dot for the detection of lysozyme. *Biosens Bioelectron* 2018;115:37–44.
- [75] Heinz H, et al. Nanoparticle decoration with surfactants: molecular interactions, assembly, and applications. *Surf Sci Rep* 2017;72(1):1–58.
- [76] Medina-Ramirez I, et al. Green synthesis and characterization of polymer-stabilized silver nanoparticles. *Colloids Surf B: Biointerfaces* 2009;73(2):185–91.
- [77] Nagasaki Y, et al. Novel molecular recognition via fluorescent resonance energy transfer using a biotin – PEG/polyamine stabilized CdS quantum dot. *Langmuir* 2004;20(15):6396–400.
- [78] Xiang-Ying S, et al. Synthesis of blue fluorescence CdS quantum dots stabilized by L-cysteine in aqueous phase. *J Nanosci Nanotechnol* 2011;11(8):6810–14.
- [79] Zhang J, et al. Cadmium sulfide quantum dots stabilized by aromatic amino acids for visible light-induced photocatalytic degradation of organic dyes. *N J Chem* 2015;39(9):6951–7.
- [80] Ai X, et al. Photophysics of (CdSe)ZnS colloidal quantum dots in an aqueous environment stabilized with amino acids and genetically-modified proteins. *Photochem Photobiol Sci* 2007;6(9):1027–33.
- [81] Vericat C, et al. Self-assembled monolayers of thiols and dithiols on gold: new challenges for a well-known system. *Chem Soc Rev* 2010;39(5):1805–34.
- [82] Schreiber F. Structure and growth of self-assembling monolayers. *Prog Surf Sci* 2000;65(5):151–257.
- [83] Frank S. Self-assembled monolayers: from 'simple' model systems to biofunctionalized interfaces. *J Phys Condens Matter* 2004;16(28):R881.
- [84] Park CS, et al. Thiol-based self-assembled monolayers: formation, organization, and the role of adsorbate structure. Reference module in materials science and materials engineering. Elsevier; 2016.
- [85] Atta NF, Galal A, El-Ads EH. A novel sensor of cysteine self-assembled monolayers over gold nanoparticles for the selective determination of epinephrine in presence of sodium dodecyl sulfate. *Analyst* 2012;137(11):2658–68.
- [86] Calatayud MP, et al. *The effect of surface charge of functionalized Fe<sub>3</sub>O<sub>4</sub> nanoparticles on protein adsorption and cell uptake*. *Biomaterials* 2014;35(24):6389–99.
- [87] Sotnikov DV, et al. Adsorption of proteins on gold nanoparticles: one or more layers? *Colloids Surf B: Biointerfaces* 2019;173:557–63.
- [88] Wang X, et al. Silver nanoparticle and lysozyme/tannic acid layer-by-layer assembly antimicrobial multilayer on magnetic nanoparticle by an eco-friendly route. *Mater Sci Eng C* 2017;76:886–96.
- [89] Wang S, et al. Layer-by-Layer self-assembly of polyaspartate and Poly(ethyleneimine) on magnetic nanoparticles: characterization and adsorption of protein. *Curr Appl Phys* 2011;11(6):1337–42.
- [90] Chivers CE, et al. How the biotin-streptavidin interaction was made even stronger: investigation via crystallography and a chimaeric tetramer. *Biochem J* 2011;435(1):55–63.
- [91] Lakshmi Priya T, et al. Signal enhancement in ELISA: biotin-streptavidin technology against gold nanoparticles. *J Taibah Univ Med Sci* 2016;11(5):432–8.
- [92] Stanisavljevic M, et al. Study of streptavidin-modified quantum dots by capillary electrophoresis. *Chromatographia* 2013;76(7):335–43.
- [93] Zhang X, et al. A quantum dot-spore nanocomposite pH sensor. *Talanta* 2016;150:184–9.



- [94] Xue G, et al. Highly-sensitive organophosphorus pesticide biosensors based on CdTe quantum dots and bi-enzyme immobilized eggshell membranes. *Analyst* 2016;141(3):1105–11.
- [95] Aini BN, et al. Development of glucose biosensor based on ZnO nanoparticles film and glucose oxidase-immobilized eggshell membrane. *Sens Bio-Sensing Res* 2015;4:46–56.
- [96] Hao N, et al. Three-dimensional nitrogen-doped graphene porous hydrogel fabricated biosensing platform with enhanced photoelectrochemical performance. *Sens Actuators B: Chem* 2017;250:476–83.
- [97] Lei J, et al. Design and sensing applications of metal–organic framework composites. *TrAC Trends Anal Chem* 2014;58:71–8.
- [98] Xuan W, et al. Mesoporous metal–organic framework materials. *Chem Soc Rev* 2012;41(5):1677–95.
- [99] Wu Y, et al. *Metal-organic framework coated Fe<sub>3</sub>O<sub>4</sub> magnetic nanoparticles with peroxidase-like activity for colorimetric sensing of cholesterol*. *Sens Actuators B: Chem* 2017;249:195–202.
- [100] He L, et al. Core–shell noble-metal@metal-organic-framework nanoparticles with highly selective sensing property. *Angew Chem Int Ed* 2013;52(13):3741–5.
- [101] Vasudevan D, et al. Core–shell quantum dots: properties and applications. *J Alloy Compd* 2015;636:395–404.
- [102] Duong HD, Rhee JI. Use of CdSe/ZnS core-shell quantum dots as energy transfer donors in sensing glucose. *Talanta* 2007;73(5):899–905.
- [103] Gültekin A, et al. Preparation of new molecularly imprinted nanosensor for cholic acid determination. *Sens Actuators B: Chem* 2012;162(1):153–8.
- [104] Ge S, et al. Layer-by-layer self-assembly CdTe quantum dots and molecularly imprinted polymers modified chemiluminescence sensor for deltamethrin detection. *Sens Actuators B: Chem* 2011;156(1):222–7.
- [105] Darwish M, Mohammadi A. Functionalized nanomaterial for environmental techniques. In: Hussain CM, Mishra AK, editors. *Nanotechnology in environmental science*. Weinheim, Germany: Wiley-VCH Verlag GmbH & Co. KGaA; 2018.
- [106] Lawson LS, Chan JW, Huser T. A highly sensitive nanoscale pH-sensor using Au nanoparticles linked by a multifunctional Raman-active reporter molecule. *Nanoscale* 2014;6(14):7971–80.
- [107] Wang W-J, et al. Green preparation of carbon dots for intracellular pH sensing and multicolor live cell imaging. *J Mater Chem B* 2016;4(44):7130–7.
- [108] He Y, et al. Ratiometric fluorescent detection of acidic pH in lysosome with carbon nanodots. *Chin Chem Lett* 2017;28(10):1969–74.
- [109] Tomasulo M, Yildiz I, Raymo FM. pH-sensitive quantum dots. *J Phys Chem B* 2006;110(9):3853–5.
- [110] Lu L, et al. Low toxic fluorescent nanoprobes applicable for sensing pH changes in biological environment. *Sens Actuators B: Chem* 2018;257:860–5.
- [111] Tang JLL, Nishi PJ, Ng SM. Synthesis of orange emitting carbon dots as potential optical sensing receptor for metal ions. In 2017 4th IEEE International Conference on Engineering Technologies and Applied Sciences (ICETAS), 2017.
- [112] Ye S, et al. A colorimetric sensor based on catechol-terminated mixed self-assembled monolayers modified gold nanoparticles for ultrasensitive detections of copper ions. *Analyst* 2012;137(14):3365–71.
- [113] Ng YH, et al. Utilising the interface interaction on tris(hydroxymethyl)aminomethane-capped carbon dots to enhance the sensitivity and selectivity towards the detection of Co (II) ions. *Sens Actuators B: Chem* 2018;273:83–92.

- [114] Mahapatra N, et al. Emergence of the selective ultra-sensing of Ag(I): thiolactic acid as efficient capping agent for cadmium chalcogenide quantum dots in modulating photoluminescence and metal reception. *Sens Actuators B: Chem* 2017;240:543–52.
- [115] Wang Z, et al. Fluorescence sensor array based on amino acid derived carbon dots for pattern-based detection of toxic metal ions. *Sens Actuators B: Chem* 2017;241:1324–30.
- [116] Jing W, et al. Fluorescence sensor array based on amino acids-modulating quantum dots for the discrimination of metal ions. *Anal Chim Acta* 2017;985:175–82.
- [117] Wu Y, et al. Differentiation and determination of metal ions using fluorescent sensor array based on carbon nanodots. *Sens Actuators B: Chem* 2017;246:680–5.
- [118] Kodir A, et al. Pesticide colorimetric sensor based on silver nanoparticles modified by L-cysteine. 2016 International Seminar on Sensors, *Instrumentation, Meas Metrology (ISSIMM)*. 2016.
- [119] Chang MMF, Ginjom IR, Ng SM. Single-shot ‘turn-off’ optical probe for rapid detection of paraoxon-ethyl pesticide on vegetable utilising fluorescence carbon dots. *Sens Actuators B: Chem* 2017;242:1050–6.
- [120] Wang M, et al. “Off–On” fluorescent sensing of organophosphate pesticides using a carbon dot–Au(III) complex. *RSC Adv* 2018;8(21):11551–6.
- [121] Guo J, et al. Efficient fluorescence resonance energy transfer between oppositely charged CdTe quantum dots and gold nanoparticles for turn-on fluorescence detection of glyphosate. *Talanta* 2014;125:385–92.
- [122] Lisa M, et al. Gold nanoparticles based dipstick immunoassay for the rapid detection of dichlorodiphenyltrichloroethane: an organochlorine pesticide. *Biosens Bioelectron* 2009;25(1):224–7.
- [123] Ji X, et al. (CdSe)ZnS quantum dots and organophosphorus hydrolase bioconjugate as biosensors for detection of paraoxon. *J Phys Chem B* 2005;109(9):3793–9.
- [124] Lin B, et al. Turn-on sensor for quantification and imaging of acetamiprid residues based on quantum dots functionalized with aptamer. *Sens Actuators B: Chem* 2016;229:100–9.
- [125] Jin D, et al. Quantitative determination of uric acid using CdTe nanoparticles as fluorescence probes. *Biosens Bioelectron* 2016;77:359–65.
- [126] Gao X, Tang G, Su X. Optical detection of organophosphorus compounds based on Mn-doped ZnSe d-dot enzymatic catalytic sensor. *Biosens Bioelectron* 2012;36(1):75–80.
- [127] Tian X, et al. Highly sensitive and selective paper sensor based on carbon quantum dots for visual detection of TNT residues in groundwater. *Sens Actuators B: Chem* 2017;243:1002–9.
- [128] Hu Y, et al. One-pot synthesis of a fluorescent molecularly imprinted nanosensor for highly selective detection of sulfapyridine in water. *Anal Methods* 2018;10(8):884–90.
- [129] Sun JF, et al. CdTe quantum dots as fluorescence sensor for the determination of vitamin B6 in aqueous solution. *Chin Chem Lett* 2008;19(7):855–9.
- [130] Mir IA, et al. ZnSe core and ZnSe@ZnS core-shell quantum dots as platform for folic acid sensing. *J Nanopart Res* 2017;19(7):260.
- [131] Dhara K, Mahapatra DR. Electrochemical nonenzymatic sensing of glucose using advanced nanomaterials. *Microchim Acta* 2017;185(1):49.
- [132] Rathod D, et al. Platinum nanoparticle decoration of carbon materials with applications in non-enzymatic glucose sensing. *Sens Actuators B: Chem* 2010;143(2):547–54.
- [133] Kang X, et al. Glucose oxidase–graphene–chitosan modified electrode for direct electrochemistry and glucose sensing. *Biosens Bioelectron* 2009;25(4):901–5.
- [134] Kumari S, Tiwari M, Das P. Multi format compatible visual and fluorometric detection of SEB toxin in nanogram range by carbon dot-DNA and acriflavine nano-assembly. *Sens Actuators B: Chem* 2019;279:393–9.

- [135] Zhao HX, et al. Highly selective detection of phosphate in very complicated matrixes with an off-on fluorescent probe of europium-adjusted carbon dots. *Chem Commun* 2011;47(9):2604–6.
- [136] Tong L-I, et al. Fluorescent sensing of pyrophosphate anion in synovial fluid based on DNA-attached magnetic nanoparticles. *Biosens Bioelectron* 2015;72:51–5.
- [137] Chen J, et al. A novel composite of molecularly imprinted polymer-coated PdNPs for electrochemical sensing norepinephrine. *Biosens Bioelectron* 2015;65:366–74.
- [138] Valero-Navarro A, et al. Synthesis of a novel polyurethane-based-magnetic imprinted polymer for the selective optical detection of 1-naphthylamine in drinking water. *Biosens Bioelectron* 2011;26(11):4520–5.
- [139] Fang G, et al. A novel molecularly imprinted polymer on CdSe/ZnS quantum dots for highly selective optosensing of mycotoxin zearalenone in cereal samples. *RSC Adv* 2014;4(6):2764–71.
- [140] Tian J, et al. A core-shell-structured molecularly imprinted polymer on upconverting nanoparticles for selective and sensitive fluorescence sensing of sulfamethazine. *Analyst* 2015;140(15):5301–7.
- [141] Fong JFY, Chin SF, Ng SM. A unique “turn-on” fluorescence signalling strategy for highly specific detection of ascorbic acid using carbon dots as sensing probe. *Biosens Bioelectron* 2016;85:844–52.
- [142] Amiri M, Eynaki H, Mansoori Y. Cysteine-anchored receptor on carbon nanoparticles for dopamine sensing. *Electrochim Acta* 2014;123:362–8.
- [143] Rostami S, et al. Colorimetric sensing of dopamine using hexagonal silver nanoparticles decorated by task-specific pyridinium based ionic liquid. *Sens Actuators B: Chem* 2018;271:64–72.
- [144] Zong C, et al. Chemiluminescence immunoassay for cardiac troponin T by using silver nanoparticles functionalized with hemin/G-quadruplex DNAzyme on a glass chip array. *Microchimica Acta* 2017;184(9):3197–204.
- [145] Bhattacharyya D, Sarswat PK, Free ML. Quantum dots and carbon dots based fluorescent sensors for TB biomarkers detection. *Vacuum* 2017;146:606–13.
- [146] Verma N, Singh AK, Saini N. Synthesis and characterization of ZnS quantum dots and application for development of arginine biosensor. *Sens Bio-Sensing Res* 2017;15:41–5.
- [147] Sun G, et al. Targeting breast cancer cells with a CuInS(2)/ZnS quantum dot-labeled Ki-67 bioprobe. *Oncol Lett* 2018;15(2):2471–6.
- [148] Begcevic I, et al. Brain-related proteins as potential CSF biomarkers of Alzheimer’s disease: a targeted mass spectrometry approach. *J Proteom* 2018;182:12–20.
- [149] Nolen BM, Lokshin AE. Protein biomarkers of ovarian cancer: the forest and the trees. *Future Oncol (London, Engl)* 2012;8(1):55–71.
- [150] Srivastava AK, et al. New insight into curcumin tethered lanthanum carbonate nanospheres and protein corona conferring fluorescence enhancement based sensitive detection of Amyloid- $\beta$  aggregates. *Sens Actuators B: Chem* 2018;262:687–95.
- [151] Wang W, et al. Aptamer biosensor for protein detection using gold nanoparticles. *Anal Biochem* 2008;373(2):213–19.
- [152] Chung J, et al. Fast and continuous microorganism detection using aptamer-conjugated fluorescent nanoparticles on an optofluidic platform. *Biosens Bioelectron* 2015;67:303–8.
- [153] Muniandy S, et al. Graphene-based label-free electrochemical aptasensor for rapid and sensitive detection of foodborne pathogen. *Anal Bioanal Chem* 2017;409(29):6893–905.

- [154] Yu Z, Lv H, Tang D. One pot synthesis of water stable ZnO quantum dots with binding ability to microbe. *Mater Lett* 2018;210:207–10.
- [155] Gültekin A, et al. Gold–silver nanoclusters having dipicolinic acid imprinted nanoshell for *Bacillus cereus* spores recognition. *Talanta* 2009;78(4):1332–8.

This page intentionally left blank

# Porous nanocomposites for water treatment: past, present, and future

Xiaolin Zhang<sup>1,2</sup>, Zhixian Li<sup>1</sup>, Ziniu Deng<sup>1</sup> and Bingcai Pan<sup>1,2</sup>

<sup>1</sup>State Key Laboratory of Pollution Control and Resource Reuse, School of Environment, Nanjing University, Nanjing, P.R. China, <sup>2</sup>Research Center for Environmental Nanotechnology (ReCENT), Nanjing University, Nanjing, P.R. China

## 17.1 Introduction

Recent advances in the manipulation of nanomaterials facilitates the application of nanotechnology in water/wastewater treatment. Environmental nanotechnology has gained attention as an important supplement to traditional water treatment techniques [1]. Generally, environmental nanomaterials make good adsorbents and catalysts due to their large, specific surface area and high reactivity. For instance, nanoadsorbents often possess greatly improved capacity and affinity toward target pollutants in comparison with their bulky counterparts [2]. As expected the utilization of nanomaterials in water treatment has been widely accepted as a promising way to enhance the removal of diverse pollutants such as heavy metals, phosphorus, arsenic, fluorine, and organic matters [3].

However, the aggregation of nanoparticles (NPs) is a thermodynamically spontaneous process, and nanosized particles tend to attract each other to reduce the surface free energy [4]. For example, silica NPs (12 nm) are likely to agglomerate together and form much bigger particles (52 nm) in water [5,6]. Once the aggregate of NPs increases to submicron size, the unique characteristics of NPs would be weakened or even disappear. Additionally, the fast development of nanotechnology and widespread application of NPs may result in the possible release of NPs into the environment through various pathways. Among those pathways is the loss of active sites during reaction and recycle processes, which is a thorny problem for metal-based NPs [7,8]. Some studies point to evidence of the release of engineered NPs from commercially available antiodor socks and self-cleaning facade coatings of

buildings [9]. NPs can be discharged into terrestrial and aquatic environments and affect soil organisms in term of activity, biomass, and composition of microbial communities, and they can alter ecosystem productivity and biogeochemistry [10]. In order to address the potentially adverse effects associated with environmental nanotechnology, it is imperative to find a way to minimize the release or mobilization of NPs while maintaining their high reactivity. Among the available methods for reducing the release of NPs into the environment, the incorporation of reactive NPs into porous hosts has shown promise due to the hosts' easy handling, highly efficient, and robust nature [11]. The widely utilized hosts include, but are not limited to, activated carbon (AC) [12], polymer [13,14], and silicates [15].

This chapter summarizes the structure, fabrication, properties, and decontamination reactivity of various porous, nanocomposite adsorbents/catalysts for water purification. Of note is that authentic wastewaters are very complex and variable in contaminant levels and species, solution chemistry, and intended use, thus rendering the application of environmental nanotechnology in water treatment extremely challenging. The perspectives of environmental nanotechnology will be briefly discussed to eventually meet practical demands in water treatment.

## 17.2 Nanocomposite adsorbents

### 17.2.1 Carbon-based nanocomposites

Carbon materials are often utilized to support NPs to achieve enhanced decontamination performance [12]. Three typical carbon-based supports, including AC, carbon nanotube (CNT), and graphene, are the focus of this section.

ACs are widely used to decontaminate water of organic pollutants thanks to cost effectiveness, high capacity, and inert chemistry [16]. The abundant microporous structure allows ACs to possess enough room to accommodate NPs. Some typical AC-based nanocomposite adsorbents are listed in Table 17.1.

Agarwal et al. [17] prepared n-Cu<sub>2</sub>O@AC by depositing Cu<sub>2</sub>O NPs on powder AC and investigated its rapid adsorption toward anionic dyes such as sunset yellow (SY), eosin B (EB), and methylene blue (MB). The dyes interacted with the embedded Cu<sub>2</sub>O NPs through electrostatic attraction and complexation. The maximum capacities toward SY, EB, and MB were 113, 137, and 110 mg/g at pH 5.0 (25°C) respectively. In addition, a low-cost and environmentally friendly adsorbent, n-ZnS:Cu@AC, was prepared by loading ZnS:Cu NPs inside AC for ultrasound-assisted rapid removal of MB and auramine-O (AO) dyes [18]. High removal efficiency (>99.5%) for both dyes could be achieved in 2.2 min at circumneutral pH by using a small quantity (0.40 g/L) of n-ZnS:Cu@AC. Many other reports about AC-based

**TABLE 17.1** Recent applications of AC-based nanocomposites in removal of target pollutants from aqueous solutions.

Adsorbents	NPs	Pollutants	Description	References
Cu <sub>2</sub> O–NP–AC	Cu <sub>2</sub> O	Sunset yellow (SY), eosin B (EB), methylene blue (MB)	The maximum adsorption capacities of SY, EB, and MB were 113, 137, and 110 mg/g, respectively.	[17]
ZnS:Cu–NP–AC	ZnS–Cu	MB, Auramine O (AO)	The adsorption occurred at neutral pH. Maximum capacities: 106.9 mg/g for MB, and 94.2 mg/g for AO.	[18]
Au–NP–AC	Au	Alizarin red S (ARS)	A small amount of adsorbent (0.015 g) was applied for successful removal of 95% ARS in 5 min with the adsorption capacity at 123.4 mg/g.	[19]
CuS–NP–AC	CuS	Methyl orange (MO)	Maximum adsorption capacity: 122 mg/g.	[20]
AC/SiO <sub>2</sub>	SiO <sub>2</sub>	Dichloromethane, trichloromethane, and carbon tetrachloride	The AC/SiO <sub>2</sub> had a higher thermal stability than the AC.	[21]
ZnO:Cr–NPs–AC	ZnO–Cr	Malachite green (MG), eosin yellow (EY), and AO	Maximum adsorption capacities: 214.0 mg/g for MG, 189.7 mg/g for EY and 211.6 mg/g for AO.	[22]
Fe <sup>0</sup> NP/SAC	Zero-valent iron	Pb(II)	Maximum removal was obtained in the pH range 5.5–6.1, and higher adsorbents dosage or iron content, higher capacity. In addition, the water erosion resistance test showed the prepared Fe <sup>0</sup> NPs–SAC was safe when used in drinking water.	[23]
GAC–NSIO	Iron oxide	Cd(II)	The maximum capacity of GAC–NSIO (7.84 mg/g) increased by 700%, over the virgin GAC (0.98 mg/g). The presence of humic acid could greatly promote Cd(II) adsorption at low concentrations (1–10 mg/L) and inhibited adsorption at high concentrations (10–300 mg/L).	[24]

*(Continued)*



**TABLE 17.1 (Continued)**

Adsorbents	NPs	Pollutants	Description	References
Iron and manganese oxides modified activated carbon	Fe <sub>2</sub> MnO <sub>4</sub>	As(V)	The iron impregnation presented an increase in the maximum As(V) capacity from about 4 mg/g of the raw carbon to 11.05 mg/g, while Mn incorporation further increased it to 19.35 mg/g.	<a href="#">[25]</a>
Magnetic carbon nanocompositefabrics	Iron oxide	Cr(VI)	The nanocomposites are highly porous for the removal of Cr(VI) with much higher capacity of 3.74 mg/g than cotton fabrics (0.32 mg/g) and carbon fabrics (0.46 mg/g).	<a href="#">[26]</a>
Nanocomposite activated carbon nanofibers containing metal oxide NPs	MgO, Al <sub>2</sub> O <sub>3</sub>	2-Chloroethyl ethyl sulfide (2-CEES)	The adsorption kinetics of 2-CEES onto the composite ACNFs embedded with MgO and Al <sub>2</sub> O <sub>3</sub> NPs are represented by the pseudo-second order model.	<a href="#">[27]</a>

nanocomposites for dye removal are available, including alizarin red S (ARS) removal by gold NPs loaded on AC (nAu@AC) [19], methyl orange (MO) removal by copper sulfide NPs loaded on activated carbon (nCuS@AC) [20], and malachite green (MG), eosin yellow (EY) and auramine-O (AO) removal by chromium doped zinc oxide NPs loaded on activated carbon (nZnO:Cr@AC) [22].

AC-based nanocomposite adsorbents for inorganic pollutants have also been developed in recent years. Qi et al. [23] synthesized  $n\text{Fe}^0\text{@SAC}$  by immobilizing zero-valent iron NPs ( $n\text{Fe}^0$ ) inside the sintered activated carbon (SAC) to treat lead-bearing wastewater. Erosion resistance tests suggested that  $\text{Fe}^0\text{@SAC}$  was safe for drinking water treatment. Iron oxide NPs loaded within granular AC (GAC) was prepared by Xu et al. [24] and was used for the removal of Cd(II) from aqueous solutions. The nanocomposite adsorbent exhibited superior adsorption toward Cd(II) over GAC, with an increased rate of  $\sim 700\%$  in the maximum capacity. Gallios et al. [25] used iron-modified AC as alternative adsorbent for the removal of As(V) from water and incorporated Mn into the adsorbent to bring out the AC's magnetic properties for easy separation. The maximum adsorption capacity increased from about 4 mg/g of the raw AC to  $\sim 11$  mg/g after iron modification, while the incorporation of Mn further increased it to  $\sim 19$  mg/g.

CNTs, classified as a one-dimensional nanomaterial, are of immense importance in the environmental engineering field because of their strong electrical and thermal conductivities, special adsorption properties, and high strength and stiffness [28]. Owing to its one-dimensional nanostructure and hollow and layered structures, all adsorption sites of CNTs are located on the inner or outer layer surface. Consequently, CNTs can serve as a promising adsorbent in water treatment. CNT was used in adsorptive studies soon after its first report in 1991 [29], and research activity using them has expanded in the past decade. In most adsorption cases of CNTs, several driving forces occur simultaneously, including  $\pi$ - $\pi$  interaction, electron-donor-acceptor interaction, hydrophobic effect, electrostatic attraction, and hydrogen bond formation [28]. In order to improve adsorption capacity toward target pollutants, especially to hydrophilic pollutants, CNTs are often modified by changing the morphology, grafting functional groups, incorporating with metal oxide, etc. Recent studies on various pollutants removal by CNTs are listed in Table 17.2.

In addition to directly serving as adsorbents, CNTs can be utilized as a desirable matrix to embed metal oxide NPs. Li et al. [38] reported a candidate adsorbent for fluoride removal [i.e., amorphous  $\text{Al}_2\text{O}_3$  NPs supported on CNT ( $\text{Al}_2\text{O}_3\text{/CNTs}$ )] whose adsorption capacity toward fluoride was  $\sim 13.5$  times that of ACs, and 4 times higher than that of  $\gamma\text{-Al}_2\text{O}_3$  at the equilibrium concentration of 12 mg/L. Wang et al. [36] synthesized Mn oxide-coated carbon nanotubes ( $\text{MnO}_2\text{/CNTs}$ ) to remove Pb(II) from an aqueous solution. The maximum Pb(II) capacity of  $\text{MnO}_2\text{/CNTs}$  was

**TABLE 17.2** Modified CNTs-based nanomaterial in water treatment for target pollutants.

Adsorbents	Modified methods	Pollutants	Description	References
Opened carbon single-walled nanotubes (o-SWCNTs)	Morphology change	<i>n</i> -Nonane, CCl <sub>4</sub>	Internal adsorption sites of o-SWCNTs were filled first, followed by the groove sites. The adsorption capacities of the nanotube interior and groove sites were directly influenced by molecular packing effects.	[30]
SWCNTs MWCNTs	Morphology change	Zn(II)	The maximum Zn <sup>2+</sup> adsorption capacities are 43.66 mg/g for SWCNTs, 32.68 mg/g for MWCNTs, and 13.04 mg/g for PAC, respectively, at an initial Zn <sup>2+</sup> concentration range of 10–80 mg/L, as calculated by the Langmuir model.	[31]
Aligned carbon nanotubes (ACNTs)	Morphology change	Fluoride	Equilibrium adsorption capacity reached 4.2 mg/g at equilibrium fluoride concentration of 15 mg/L.	[32]
Oxidized multiwalled carbon nanotubes (OMWCNT)	Oxidation treatment	Zn(II), Cd(II)	The carboxyl-carbon sites were over 20 times more energetic for zinc sorption than unoxidized carbon (graphenic-carbon) sites, though both sites are important to sorption.	[33]
OH-functionalized CNTs, COOH-functionalized CNTs	Oxygen-containing functional group functionalized	Cu(II)	OH– (or COOH–) functionalized CNTs have improved adsorption capacity in low copper concentration solutions.	[34]
Graphitized MWCNTs, purified MWCNTs, OH–MWCNTs, COOH–MWCNTs	Oxygen-containing functional group functionalized	Polar and nonpolar organic compounds	The decrease of surface area-normalized adsorption capacity of the organic compound with more polarity and higher adsorption affinity by surface oxidation was less because of the heterogeneous nature of hydrophilic sites of MWCNTs' surface.	[35]
MnO <sub>2</sub> /CNTs	MnO <sub>2</sub> loaded	Pb(II)	Maximum adsorption capacity of MnO <sub>2</sub> /CNTs toward Pb(II) was 78.74 mg/g.	[36]

MnO <sub>2</sub> /MWCNTs	MnO <sub>2</sub> loaded	Pb(II)	The optimum removal was observed at pH 6–7. In the fixed bed system, the higher the layer thickness of MnO <sub>2</sub> /CNT nanocomposite, the more efficient the removal.	[37]
Al <sub>2</sub> O <sub>3</sub> /CNTs	Al <sub>2</sub> O <sub>3</sub> loaded	Fluoride	The adsorption capacity for Al <sub>2</sub> O <sub>3</sub> /CNTs is about 13.5 times higher than that of AC300 carbon, 4 times higher than that of $\gamma$ -Al <sub>2</sub> O <sub>3</sub> at the equilibrium fluoride concentration of 12 mg/L.	[38]
CeO <sub>2</sub> –CNTs	CeO <sub>2</sub> loaded	As(V)	Under natural pH conditions, the coexisting Ca <sup>2+</sup> and Mg <sup>2+</sup> from 0 to 10 mg/L resulted an increase from 10 to 81.9 and 78.8 mg/g for As(V) adsorption. The loaded adsorbent can be efficiently regenerated (the efficiency > 94%) by diluted NaOH (0.1 mol/L).	[39]
Iron oxide coated e-MWCNTs	Iron oxide loaded	As(III)/As(V)	The maximum capacities obtained from Langmuir model for As(V) on e-MWCNT/Fe <sup>2+</sup> and e-MWCNT/Fe <sup>3+</sup> were 23.47 and 13.74 mg/g at 25°C, respectively.	[40]
Ca/Al-LDH@CNTs	Ca/Al layered double hydroxide loaded	U(VI)	The maximum capacity of U(VI) on Ca/Al-LDH@CNTs was 382.9 mg/g at 289.15K.	[41]

78.74 mg/g. Peng et al. [39] developed a new adsorbent for the removal of As(V) from an aqueous solution, which was fabricated by incorporating Ce(OH)<sub>3</sub> particle onto hydroxyl (–OH) and carboxyl (–COOH) functionalized CNTs. CeO<sub>2</sub>–CNTs exhibited satisfactory adsorption performance in As(V) removal, and more significantly, the coexistence of calcium and magnesium in natural water significantly enhanced their adsorption toward As(V). In addition, the As(V) loaded-adsorbent can be efficiently regenerated by NaOH solution for repeated use with constant decontamination efficiency.

Graphene, possessing two-dimensional structure with monoatomic thickness, is an extremely interesting material with excellent thermal, electrical, and mechanical properties [42]. In addition to nanoelectronics, optomechanical devices, and biology, graphene's use has also been widely studied in water decontamination methods including adsorption, catalytic oxidation reduction, and filtration [43]. Graphene can be classified into graphene oxide (GO), which is equipped with various oxygen-containing functional groups, and reduced graphene oxide (RGO). As listed in Table 17.3, graphene employed in adsorption could be improved by morphology change, surface chemical modification, and NP introduction.

The large specific surface area of graphene (> 2000 m<sup>2</sup>/g [44]) makes it possible to provide enough space for NPs to enhance the adsorption reactivity. Guo et al. [49] prepared nano-Fe@graphene composites by reducing Fe<sup>3+</sup>@GO complexes with NaBH<sub>4</sub>. The resultant nanocomposite was used in the removal of methyl blue with high capacities over the bare Fe particles. Ferric hydroxide@GO composite (GO-Fe) [51] was used for As(V) removal at 23.78 mg/g, while the layered double hydroxides@GO [52] performed better with the maximum capacity of 183.11 mg/g. Additionally, a graphene-based magnetic nanocomposite [i.e., manganese-incorporated iron(III) oxide@graphene (IMBO@GR)], as synthesized by Nandi et al. [50], was promising for As(III) removal. IMBO@GR exhibited a higher removal (> 99.9%) than the manganese-incorporated iron(III) oxide particles, resulting in the effluent As(III) below 10 µg/L. For the purpose of heavy metals removal, SiO<sub>2</sub> [53], MnO<sub>2</sub> [54], and TiO<sub>2</sub> [55] NPs were incorporated with graphene. The resultant nanocomposite adsorbents exhibited significantly enhanced adsorption capacity and selectivity toward heavy metals such as Pb(II), Hg(II), and Cd(II), respectively.

### 17.2.2 Polymer-based nanocomposites

Polymeric exchangers are among the most promising host materials for a variety of NPs in terms of high mechanical strength, abundant porous structure, bulky size, and excellent chemical stability [56]. The polymer hosts can also be covalently modified with charged groups to allow preconcentration of target pollutants inside the polymer matrix prior to interacting with the

**TABLE 17.3** Graphene-based nanomaterials for pollutant removal.

Adsorbents	Modified methods	Pollutants	Description	References
AGN	Wrinkles and folds	<i>p</i> -Nitrotoluene, naphthalene and phenanthrene	The maximum capacity of <i>p</i> -nitrotoluene increased from 106.9 mg/g of GNS to 201.0 mg/g of AGN, and similar increase appeared in naphthalene removal (from 146.8 to 216.1 mg/g) and phenanthrene removal (from 268.3 to 316.9 mg/g).	[44]
ED-RGO	Ethylenediamine-reduced	Cr(VI)	An optimal pH around 2.0 was observed and nearly 89% of the total Cr was removed.	[45]
ED-DMF-RGO	GO reduced with ED using DMF as solvent	Cr(VI)	The optimum pH for the total Cr removal was at pH 2.0 with the Cr (VI) removal of 92.15 mg/g for ED-DMF-RGO, ~27 times higher than that of activated carbon and even nearly 4–8 times higher than those of various activated carbons. Both the Cr(VI) adsorption and subsequent reduction of adsorbed Cr(VI) to Cr(III) contributed to the Cr(VI) removal.	[46]
CTAB-graphene	CTAB modified	Cr(VI)	The adsorption was rapid within the first 5 min and reached equilibrium in about 40 min. The adsorption capacity of Cr(VI) on modified graphene inferred from the Langmuir model was 21.57 mg/g at 293K.	[47]
EDTA-GO	EDTA modified	Pb(II)	The adsorption capacity for Pb(II) was $479 \pm 46$ mg/g at pH 6.8, and the adsorption reached equilibrium within 20 min. EDTA-GO could be reused after HCl rinsing, suggesting potential applications in environmental cleanup.	[48]
FGC	Fe loaded	Methyl blue	The removal of FGC was enhanced due to the more adsorption sites in the hybrids than the bare Fe particles, resulting from reducing the Fe NP size and inhibiting aggregation. FGC were environmentally benign and easily separated.	[49]

(Continued)

**TABLE 17.3 (Continued)**

Adsorbents	Modified methods	Pollutants	Description	References
IMBO–GR	Manganese-incorporated iron (III) oxide loaded	As(III)	IMBO–GR exhibited higher adsorption efficiency than IMBO particles, with near-complete As(III) removal and the effluent As(III) below 10 µg/L.	[50]
GO–Fe	Ferric hydroxide loaded	As(V)	The arsenate capacity of GO–Fe was 23.78 mg/g when the initial arsenate concentration was 51.14 mg/L. It decreased as pH increased over 8.	[51]
LDH/GO	Mg–Al LDH loaded	As(V)	The maximum arsenate capacity of 183.11 mg/g (2.44 mmol/g) for LDHs/GO containing 6.0% GO.	[52]
SiO <sub>2</sub> /graphene	SiO <sub>2</sub> loaded	Pb(II)	SiO <sub>2</sub> /graphene composite for highly selective adsorption of Pb(II) ion.	[53]
RGO–metal/metal oxide	Ag/MnO <sub>2</sub> loaded	Hg(II)	RGO–MnO <sub>2</sub> composites enhanced Hg(II) removal over the parent material.	[54]
GO–TiO <sub>2</sub>	TiO <sub>2</sub> loaded	Pb(II), Zn(II), Cd(II)	Flower-like TiO <sub>2</sub> in GO–TiO <sub>2</sub> significantly improved the removal of heavy metals over the colloidal GO (from 30.1 to 88.9 mg/g for Zn <sup>2+</sup> , from 14.9 to 72.8 mg/g for Cd <sup>2+</sup> , from 35.6 to 65.6 mg/g for Pb <sup>2+</sup> ).	[55]

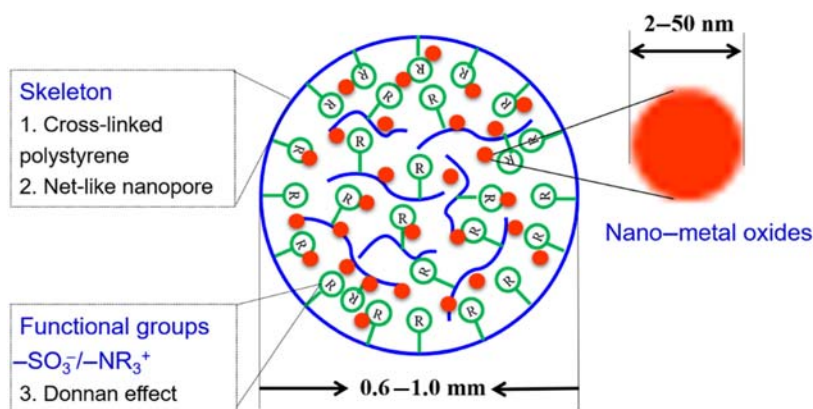


**FIGURE 17.1** Schematic illustration of the structure of polymer-based nanocomposite.

embedded NPs [57]. The structure of a typical polymer-based nanocomposite is schematically illustrated in Fig. 17.1. The hosts are cross-linked polystyrene beads of millimeter size, covalently bound with charged functional groups like sulfonic or quaternary ammonium groups to preconcentrate ionic pollutants. Metal oxide NPs in diameter of 2–50 nm are encapsulated inside the reticular structure of the hosts, rendering the resultant nanocomposites capable of preferentially adsorbing the target pollutants. Some recent studies on the utilization of polymer-based nanocomposites as water purifiers are listed in Table 17.4.

Sengupta et al. used commercially available ion exchangers as host materials for dispersing hydrated ferric oxide (HFO) NPs within the polymer matrix [70]. The resulting polymeric/inorganic hybrid adsorbents were then used for arsenic removal from water. Pan et al. proposed an innovative process to immobilize HFO NPs within a macroporous anion exchange resin D-201 for enhanced removal of arsenic [71] and phosphate [58] from water [72]. In brief, a binary  $\text{FeCl}_3\text{--HCl}$  solution was flushed through a column packed with D-201 beads, where the resulting  $\text{FeCl}_4^-$  anions present in the solution were preferably ion exchanged onto D-201. Afterwards the  $\text{FeCl}_4^-$  ions preloaded on D-201 beads were decomposed and simultaneously in situ precipitated onto the inner-pore surface of D-201 by rinsing the D-201 column with  $\text{NaCl--NaOH}$  solution. Finally, the resultant beads were thermally treated to obtain the nanocomposite adsorbent HFO-201. The resultant HFO-201 possessed two types of adsorption sites for anionic pollutants (arsenate or phosphate) removal: the quaternary ammonium groups bound to the D-201 matrix as well as the loaded HFO NPs. The coexisting sulfate anion strongly competes for quaternary ammonium groups, which interact with target pollutants through electrostatic attraction. Meanwhile, sulfate poses negligible effects on target pollutants adsorption by the loaded HFO NPs, as



**TABLE 17.4** Recent application of polystyrene-supported nanocomposites in pollutants removal.

Adsorbents	Pollutants	Description	References
HFO-201	$\text{PO}_4^{3-}$	Treatment capacity of 800 bed volume (BV) per run (from 2 to <0.5 mg-P/L).	[58]
HFO-201	$\text{SeO}_3^{2-}$	Treatment capacity of 1200 BV per run (from 2 to <10 $\mu\text{g-Se/L}$ ).	[59]
HZO-201	$\text{F}^-$	Treatment capacity of >3000 BV per run for acidic effluent (from 3.3 to <1.5 mg/L).	[60]
HZO-201	$\text{AsO}_4^{3-}$	Capture $\text{AsO}_3^{4-}$ from 100 to <10 $\mu\text{g/L}$ within 2600 BV for simulated groundwater, and from 750 to <50 $\mu\text{g/L}$ within 2900 BV for a real acidic mining effluent.	[61,62]
HZO-201	$\text{PO}_4^{3-}$	Treatment capacity of 1600 BV per run (from 2 to <0.5 mg-P/L).	[61,62]
HMO-001	$\text{Pb}^{2+}$	Maximum adsorption capacity: 395 mg/g.	[63]
HMO-001	$\text{Cd}^{2+}$ , $\text{Zn}^{2+}$	Treatment capacity of >3000 BV per run for $\text{Cd}^{2+}$ (influent $\text{Cd(II)}$ = 5 mg/L) and 350 BV per run for $\text{Zn}^{2+}$ (influent $\text{Zn(II)}$ = 50 mg/L).	[64,65]
HMO-001	$\text{Ti}^+$	Remove $\text{Ti}^+$ from 1–4 $\mu\text{g/L}$ to a value lower than 0.1 $\mu\text{g/L}$ , treatment capacity of 1600 BV per run.	[64,65]
HFO-001	$\text{Pb}^{2+}$ , $\text{Cd}^{2+}$ , $\text{Cu}^{2+}$	Treatment capacity of 6000 BV per run for $\text{Pb}^{2+}$ (from 1 mg/L to 10 $\mu\text{g/L}$ ), treatment capacity of 1100 BV per run for $\text{Cd}^{2+}$ (from 0.1 mg/L to 3 $\mu\text{g/L}$ ) and treatment capacity of 800 BV per run for $\text{Cu}^{2+}$ (from 10 to 1 mg/L).	[66]
HZP	$\text{Pb}^{2+}$ , $\text{Cd}^{2+}$	Treatment capacity of 1700 BV per run for $\text{Pb}^{2+}$ (from 20 to 1 mg/L) and treatment capacity of 280 BV per run for $\text{Cd}^{2+}$ (from 5 to 0.1 mg/L).	[67]

(Continued)

**TABLE 17.4 (Continued)**

Adsorbents	Pollutants	Description	References
HFO@PS-Cl	As(III)	Treatment capacity of >1760 BV per run synthetic groundwater to meet the drinking water standard (from 200 to 10 µg/L).	[68,69]
Zr-MPS	Pb <sup>2+</sup>	Treatment capacity of 2500 BV per run (from 5 mg/L to 10 µg/L).	[68,69]

driven by the formation of the inner-sphere complexes [73]. In the column runs of phosphate or arsenate removal, HFO-201 could treat at least 950 bed volume (BV) and 2000 BV polluted water respectively before a significant breakthrough (0.5 mg/L for phosphate and 0.01 mg/L for arsenate) occurred, while the polymeric exchanger D-201 could only generate ~250 and 10 BV clean water, respectively, under the otherwise identical conditions [58,71]. The exhausted HFO-201 could be steadily regenerated by using NaOH–NaCl binary solution. A continuous 5-cycle adsorption-regeneration cyclic run demonstrated that no significant loss of adsorption capability was observed. Besides, HFO-201 also exhibited improved adsorption selectivity toward  $\text{SeO}_3^{2-}$ . Similarly, two possible mechanisms were involved in selenite removal by HFO-201: the electrostatic interaction from the quaternary ammonium groups bound to the D-201 matrix, and the formation of inner-sphere complexes between the loaded HFO NPs and  $\text{SeO}_3^{2-}$  [59]. Column adsorption tests suggested that satisfactory removal of selenite from 2 to <0.01 mg/L could be achieved by HFO-201, even in the presence of the commonly encountered anionic competition at greater concentration with the treatment capacity of ~1200 BV for each run.

In 2013 Pan et al. developed a unique nanocomposite HZO-201 by encapsulating nanosized hydrous zirconium oxide (HZO) inside D-201 for highly efficient water defluoridation [60]. Similar to HFO-201, HZO-201 has two distinct active sites available for fluoride uptake. One is the positively charged quaternary ammonium groups covalently binding the matrix of D-201, which captures fluoride through a nonspecific electrostatic attraction. The other is HZO NPs exhibiting preferable adsorption toward fluoride through ligand exchange or metal-ligand interaction. HZO-201 could successively treat >3000 BV of the acidic effluent (around 3.5 mg F<sup>−</sup>/L) at pH 3.5 each time. The exhausted HZO-201 could be regenerated by NaOH solution for repeated use without obvious loss in removal efficiency. HZO-201 was also used to remove arsenic [61] and phosphorus [62] from water, exhibiting comparable performance with HFO-201. The major advantage of HZO-201 over HFO-201 was the excellent stability against solution chemistry [58,60].

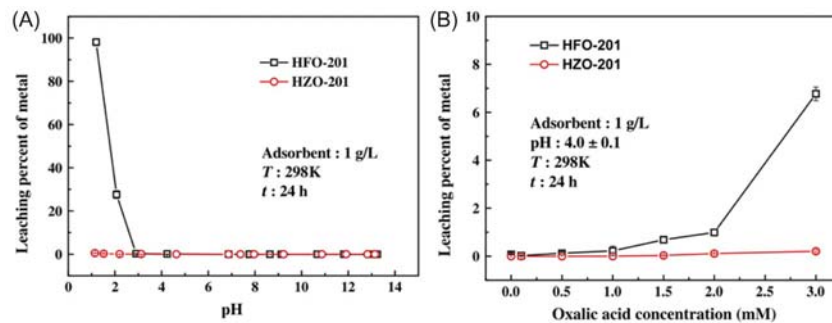


**FIGURE 17.2** Leaching of NPs from HFO-201 and HZO-201 (A) at different pH, and (B) in the presence of oxalic acid [61].

As suggested in Fig. 17.2A, less than 0.5% of HZO NPs were dissolved from HZO-201 at pH 1.2, while over 98% of HFO NPs were dissolved into water under similar conditions. Also, the presence of organic ligands such as oxalate posed negligible effect on HZO-201 stability but obviously facilitated HFO NPs dissolution ( $>6\%$  with 3 mM oxalic acid) from HFO-201 [61].

As for heavy metal cations removal, Su et al. produced the new hybrid adsorbent HMO-001 by impregnating nanosized hydrated manganese dioxide (HMO) onto porous polystyrene cation exchange resin D-001 to enhance the removal of Pb(II) ions from water [63]. Fixed-bed column adsorption of a simulated water indicated that lead retention on HMO-001 resulted in a conspicuous decrease of the toxic metal from 1 to below 0.01 mg/L. The exhausted adsorbent particles were amenable to efficient regeneration by the binary  $\text{CH}_3\text{COONa}-\text{CH}_3\text{COOH}$  solution without significant capacity loss. Also, HMO-001 was utilized to decontaminate water from other heavy metals including Cd(II) and Zn(II) ions [64,65]. Particularly, HMO-001 exhibited satisfactory removal toward Tl(I) even in the presence of massively competitive Ca(II) ions. The adsorbed Tl(I) was partially oxidized into insoluble Tl(III) by HMO at an acidic pH, while negligible oxidation was observed at neutral pHs. The exhausted HMO-001 was responsive to efficient regeneration by binary  $\text{NaOH}-\text{NaClO}$  solution with a constant removal efficiency. In addition, HZO, HFO, and zirconium phosphate NPs were encapsulated inside D-001 to prepare heavy metal scavengers [66–69].

### 17.3 Nanocomposite membranes for water purification

Nanocomposite membranes are expected to play an increasingly important role in water/wastewater treatment. The existing membranes, typically polymer in nature, are still restricted by several challenges including the trade-off between permeability and selectivity, and low resistance to biofouling [74]. The nanocomposite membrane, a new class of membranes fabricated by combining polymeric materials with nanomaterials, is emerging as a promising solution to these challenges. The nanocomposite membranes could be specifically designed by tuning their structure and physicochemical properties (e.g., hydrophilicity, porosity, charge density, and thermal and mechanical stability) and introducing unique functionalities (e.g., antibacterial, photocatalytic, or adsorptive capabilities). Some relevant studies are summarized in Table 17.5.

In one study, a nanocomposite membrane coated with functional NPs like nano- $\text{TiO}_2$  was prepared for oily wastewater treatment.  $\text{TiO}_2$ /carbon membrane was prepared via the sol–gel method and dip-coating technique [75].  $\text{TiO}_2$  sol–gel was synthesized using tetrabutyl titanate as a precursor. The membrane performance was tested by treating oily wastewater. The oil removal rate increased with a decrease in the liquid hourly space velocity (LHSV) through the electrocatalytic membrane reactor. When 200 mg/L oily water was treated, the COD removal was  $\sim 100\%$  with a LHSV of  $7.2 \text{ h}^{-1}$ .

**TABLE 17.5** Recent applications of nanocomposite membranes in water treatment.

Matrix	Nanoparticles	Description	References
Carbon	TiO <sub>2</sub>	The COD removal rate was almost 100% with a LHSV of 7.2 h <sup>-1</sup> and 87.4% with a LHSV of 21.6 h <sup>-1</sup> .	[75]
Thin-film nanocomposite	Graphene oxide	Rejections for Na <sub>2</sub> SO <sub>4</sub> , MgSO <sub>4</sub> , MgCl <sub>2</sub> , and NaCl recorded at 95.2%, 91.1%, 62.1%, and 59.5%.	[76]
Sodium alginate	Pristine graphene oxide and RGO	A separation factor of 1566 and a permeation flux of 1699 g/(m <sup>2</sup> h) was achieved for membrane incorporated with 1.6 wt. % of rGO.	[77]
Polyvinylidene fluoride	ZnO	94.8% water flux recovery after exposure to low-pressure 10 W UV-C mercury lamp irradiation for 30 min.	[78]
Vinylidene fluoride	Al <sub>2</sub> O <sub>3</sub>	The addition of nanosized Al <sub>2</sub> O <sub>3</sub> particles did not affect membrane pore sizes and numbers. Instead, it improved the surface hydrophilicity of the membrane.	[79]
Sandwich-structured polyamide 6	TiO <sub>2</sub>	A pure water flux up to 13.77 L/m <sup>2</sup> /h/bar even under an extremely low external pressure. High flux for common solvents (12.32, 4.91, and 1.26 L/m <sup>2</sup> /h/bar for methanol, ethanol, and NMP).	[80]
Polyethersulfone	Ag	Outstanding antifouling property (> 96% antimicrobial efficiency), high water flux (15.2 LMH for FO mode), and excellent selectivity (low B/A value, 0.12 bar).	[81]

(Continued)

**TABLE 17.5 (Continued)**

Matrix	Nanoparticles	Description	References
Polysulfone	Sulfonated graphene oxide	SGO/PSf membrane containing 1.5 w/w% of SGO nanoparticles exhibited a peak pure water flux value. The BSA rejection of the prepared membranes remained constantly above 98%.	[82]
N-doped carbon	Molybdenum carbide and NiO	Efficient and robust catalytic reduction of toxic Cr(VI) to Cr(III) using FA as a reducing agent.	[83]
Poly( <i>N</i> -isopropylacrylamide)	Ag	At 20°C–45°C, the membrane exhibits both satisfactory thermoresponsive characteristics and catalytic properties. With an increase in the temperature and 4-NP concentration, the conversion of reactant molecules in the penetrating solution decreased.	[84]

and 87.4% with a LHSV of 21.6 h<sup>-1</sup>. Such results indicated that the synergistic effect of electrocatalytic oxidation and membrane separation played a key role in the removal of oil. In addition, an unusual thin film nanocomposite (TFN) membrane was fabricated by incorporating graphene oxide (GO) of different loadings (0–0.5 wt.%) into polysulfone (PSf) microporous substrate [76]. A polyamide layer was formed on top of the neat PSf and PSf–GO substrate to produce TFC and TFN membranes respectively through the interfacial polymerization of piperazine and trimesoyl chloride monomers. The GO-incorporated TFN membranes exhibited high pure water flux and high salt rejection, demonstrating that GO plays an important role in increasing both membrane hydrophilicity and surface negativity.

## 17.4 Nanocomposite catalysts

Catalytic, or photocatalytic oxidation, is an advanced oxidation process for the removal of trace contaminants and microbial pathogens from water. It is

a useful pretreatment method in enhancing the biodegradability of hazardous contaminants. Nanocatalysts of high surface-to-volume ratio showed significantly enhanced catalysis over their bulky counterparts. Additionally, the band gap and crystalline structure of the nanosized semiconductors are size-dependent. Their electron hole redox potential and photogenerated charge distribution varied as the size dropped down. Furthermore, by immobilizing NPs into various substrates, the stability of the nanocatalyst could be improved, and the resultant nanocomposites might be compatible with the existing photoreactor.

CNTs and graphene can be utilized as favorable catalysts and excellent catalyst-supports due to high specific surface area and high electron and thermal conductivity with charge recombination inhibition in loaded NPs [85,86]. Recent studies revealed that CNTs enhanced the photocatalytic oxidation activity of  $\text{TiO}_2$  NPs in CNT/ $\text{TiO}_2$  composites by reducing charge recombination of  $\text{TiO}_2$ , as evidenced by the diminished photoluminescence intensity [87]. In contact with CNTs, electrons were promoted to transfer from the  $\text{TiO}_2$  NPs to the CNT surface, resulting in lower Fermi level of  $\text{TiO}_2$ . As a result, photogenerated electrons were stored by CNTs and the recombination of electrons and holes was inhibited. Numerous reports about CNT/ $\text{TiO}_2$  composites for catalytic degradation of organic pollutants are available. Meanwhile, other NPs supported by CNTs were also prepared for catalytic degradation of organic pollutants, including ZnS [88], CdS [89],  $\text{WO}_3$  [90], and others.

In addition, carbon-based nanocomposites were applied in other advanced oxidation processes including ozone and Fenton (-like) reactions. Recently, Li et al. [91] synthesized RGO modified 3D sea urchin-like  $\alpha\text{-MnO}_2$  architectures ( $\alpha\text{-MnO}_2/\text{RGO}$ ) for removal of bisphenol-A (BPA) by ozone oxidation. Significant promotion of catalytic degradation of  $\alpha\text{-MnO}_2/\text{RGO}$  was observed with the removal of BPA by  $\text{O}_3$  oxidation increasing from 20% to 90%, a much higher amount than by homogeneous  $\alpha\text{-MnO}_2$  (70%) under similar conditions. Efficient catalytic degradation of  $\alpha\text{-MnO}_2/\text{RGO}$  mainly arose from the large surface area and abundant active sites provided by the 3D sea urchin-like  $\alpha\text{-MnO}_2$ , as well as the accelerated electron transfer rate. Note that  $\alpha\text{-MnO}_2/\text{RGO}$  is stable in the catalytic ozonation of BPA, performing much better recyclability than  $\alpha\text{-MnO}_2$ . Some other studies on ozonation of organic matters by using nanocomposite catalysts were carried out in recent years, including magnetic carbon nanospheres ( $\text{Fe}_3\text{O}_4/\text{CS}$  core/shell) [92] and  $\text{FeMgO}/\text{carbon}$  nanotube composite ( $\text{FeMgO}/\text{CNT}$ ) [93] for phenol removal and  $\text{Fe}_3\text{O}_4/\text{multi-wall carbon nanotubes}$  ( $\text{Fe}_3\text{O}_4/\text{MWCNTs}$ ) [94] for dimethyl phthalate removal. As for Fenton reactions, Yang et al. [95] reported that efficient atrazine (ATZ) degradation (> 90%) was achieved in the presence of 20 mg/L functionalized multiwalled carbon nanotubes (FMWCNT-H) with 2.0 mg/L Fe(III) and 170 mg/L  $\text{H}_2\text{O}_2$  at 20°C. Combined with X-ray photoelectron spectroscopy (XPS) analysis, the authors

deemed that the complexation of Fe(III) and carboxyl groups on the surface of FCNT–H played a vital role in efficient Fe(III)/Fe(II) cycling due to the electron migration from Fe(III) to FCNT–H, providing new inspiration for the development of ferric nanocomposites as Fenton catalysts. Xiao et al. [96] synthesized akaganeite ( $\beta$ -FeOOH)/RGO (Ak/rGO) nanocomposites by coprecipitating and reduction. Ak/rGO was applied in oxidative decomposition of 2-chlorophenol (2-CP) by Fenton-like reaction. An ideal 2-CP removal (up to 88%) was achieved in the presence of 100 mM  $\text{H}_2\text{O}_2$  at initial pH 4.0 within 72 h, 2.6 times higher than  $\beta$ -FeOOH. Other studies using nanocomposites to catalyze Fenton-like reactions were also conducted. For example, magnetic cobalt ferrite NPs loaded on RGO ( $\text{CoFe}_2\text{O}_4$ –rGO) were used in a heterogeneous sono-Fenton-like process for the removal of organic dyes (AO7, AR17, BR46, and BY28) [97], graphene oxide–iron oxide ( $\text{Fe}_3\text{O}_4$ –O) was used as a photo-Fenton catalyst in the degradation of phenol [98], and Pb-doped  $\text{BiFeO}_3$  NP grafted on to RGO sheets ( $\text{Pb}$ – $\text{BiFeO}_3$ /rGO) was applied in microwave-Fenton-like process for degradation of perfluorooctanoic acid [99].

## 17.5 Summary and perspectives

The use of functionalized nanomaterials including adsorbents, membranes, and catalysts has increased in water treatment in recent years. Nevertheless, their application in environmental industry is limited by several bottlenecks: (1) most of the functionalized nanomaterials are still in the stage of laboratory research, and are hard to be manufactured in kilogram or even ton-scale for the purpose of industrial utilization; (2) the stability and regeneration of functionalized nanomaterials is far from the requirements of engineering application; (3) the environmental benignity of nanomaterials is not verified, and they may bring potential risks to human health; and (4) the deficiency of process and/or equipment suitable for NPs hinders the conjunction of nanotechnology with existing water treatment processes.

Among the functionalized nanomaterials mentioned above, polymeric nanocomposites have already realized industrial-scale production, and some of them are commercially available. For example, China has achieved ton-scale manufacture of HZO@D201 [100]. Additionally, NPs in the polymeric nanocomposites are protected by the cross-linked matrix, resulting in exceptional stability even under yearlong, successive column adsorption assay [58,68,101]. Though safety assessment of the polymeric nanocomposites under realistic conditions is still unavailable, it seems that iron- or zirconium-based polymeric nanocomposites may be of no concern to human health because the polymer host (i.e., polystyrene) is widely used in drinking water purification systems due to its inert chemistry and high mechanical strength, and a trace iron/zirconium dissolution is harmless to human health. With a millimetric size, polymeric nanocomposite beads can be easily



utilized in flow-through systems such as fixed-bed reactors, imitating a traditional ion exchanger water treatment process, which can be readily integrated into existing water treatment systems [67].

## References

- [1] Zhang Y, Wu B, Xu H, Liu H, Wang M, He Y, et al. Nanomaterials-enabled water and wastewater treatment. *NanoImpact* 2016;3-4:22–39.
- [2] Khin MM, Nair AS, Babu VJ, Murugan R, Ramakrishna S. A review on nanomaterials for environmental remediation. *Energy Environ Sci* 2012;5(8):8075.
- [3] Guo HM, Yang SZ, Tang XH, Li Y, Shen ZL. Groundwater geochemistry and its implications for arsenic mobilization in shallow aquifers of the Hetao Basin, Inner Mongolia. *Sci Total Env* 2008;393(1):131–44.
- [4] Jia Y, Guo H, Jiang Y, Wu Y, Zhou Y. Hydrogeochemical zonation and its implication for arsenic mobilization in deep groundwaters near alluvial fans in the Hetao Basin, Inner Mongolia. *J Hydrol* 2014;518:410–20.
- [5] Amerio E, Fabbri P, Malucelli G, Messori M, Sangermano M, Taurino R. Scratch resistance of nano-silica reinforced acrylic coatings. *Prog Org Coat* 2008;62(2):129–33.
- [6] Hashemi-Nasab R, Mirabedini SM. Effect of silica nanoparticles surface treatment on in situ polymerization of styrene–butyl acrylate latex. *Prog Org Coat* 2013;76(7–8):1016–23.
- [7] Pan B, Xing BS. Applications and implications of manufactured nanoparticles in soils: a review. *Eur J Soil Sci* 2012;63(4):437–56.
- [8] Zhou S, Jin W, Ding Y, Shao B, Wang B, Hu X, et al. In situ intercalation of Au nanoparticles and magnetic gamma-Fe<sub>2</sub>O<sub>3</sub> in the walls of MCM-41 with abundant void defects for highly efficient reduction of 4-nitrophenol and organic dyes. *Dalton Trans* 2018;47:16862–75.
- [9] Benn TM, Westerhoff P. Nanoparticle silver released into water from commercially available sock fabrics. *Environ Sci Technol* 2008;42(11):4133–9.
- [10] Sweet, MJ, Singleton, I. Chapter 5 - Silver Nanoparticles: A Microbial Perspective. Laskin, AI, Sariaslani, S, Gadd, GM, Editors. *Advances in Applied Microbiology*. Academic Press; 2011. Vol. 77, pp 115–133.
- [11] Williamson CB, Nevers DR, Hanrath T, Robinson RD. Prodigious effects of concentration intensification on nanoparticle synthesis: a high-quality, scalable approach. *J Am Chem Soc* 2015;137(50):15843–51.
- [12] Ghosh A, Nayak AK, Pal A. Nano-particle-mediated wastewater treatment: a review. *Curr Pollut Rep* 2016;3(1):17–30.
- [13] Chakrabarty A, Teramoto Y. Recent advances in nanocellulose composites with polymers: a guide for choosing partners and how to incorporate them. *Polymers* 2018;10(5):517.
- [14] Lofrano G, Carotenuto M, Libralato G, Domingos RF, Markus A, Dini L, et al. Polymer functionalized nanocomposites for metals removal from water and wastewater: an overview. *Water Res* 2016;92:22–37.
- [15] Khan TA, Chaudhry SA, Ali I. Thermodynamic and kinetic studies of As(V) removal from water by zirconium oxide-coated marine sand. *Env Sci Pollut Res Int* 2013;20(8):5425–40.
- [16] Foo KY, Hameed BH. An overview of landfill leachate treatment via activated carbon adsorption process. *J Hazard Mater* 2009;171(1–3):54–60.

- [17] Agarwal S, Tyagi I, Gupta VK, Bagheri AR, Ghaedi M, Asfaram A, et al. Rapid adsorption of ternary dye pollutants onto copper (I) oxide nanoparticle loaded on activated carbon: experimental optimization via response surface methodology. *J Environ Chem Eng* 2016;4(2):1769–79.
- [18] Asfaram A, Ghaedi M, Hajati S, Rezaeinejad M, Goudarzi A, Purkait MK. Rapid removal of Auramine-O and Methylene blue by ZnS:Cu nanoparticles loaded on activated carbon: a response surface methodology approach. *J Taiwan Inst Chem Eng* 2015;53:80–91.
- [19] Roosta M, Ghaedi M, Mohammadi M. Removal of Alizarin Red S by gold nanoparticles loaded on activated carbon combined with ultrasound device: optimization by experimental design methodology. *Powder Technol* 2014;267:134–44.
- [20] Mokhtari P, Ghaedi M, Dashtian K, Rahimi MR, Purkait MK. Removal of methyl orange by copper sulfide nanoparticles loaded activated carbon: kinetic and isotherm investigation. *J Mol Liq* 2016;219:299–305.
- [21] Abdelbassit MSA, Alhooshani KR, Saleh TA. Silica nanoparticles loaded on activated carbon for simultaneous removal of dichloromethane, trichloromethane, and carbon tetrachloride. *Adv Powder Technol* 2016;27(4):1719–29.
- [22] Jamshidi M, Ghaedi M, Dashtian K, Hajati S, Bazrafshan AA. Sonochemical assisted hydrothermal synthesis of ZnO: Cr nanoparticles loaded activated carbon for simultaneous ultrasound-assisted adsorption of ternary toxic organic dye: derivative spectrophotometric, optimization, kinetic and isotherm study. *Ultrason Sonochem* 2016;32:119–31.
- [23] He Q, Dai J, Zhu L, Xiao K, Yin Y. Synthesis and lead absorption properties of sintered activated carbon supported zero-valent iron nanoparticle. *J Alloy Compd* 2016;687:326–33.
- [24] Xu Z, Zhang D, Chen W, Li Y, Yuan S. Nanoscale iron oxides loaded granular activated carbon (GAC-NSIO) for cadmium removal. *Desalin Water Treat* 2016;57(8):3559–71.
- [25] Gallios G, Tolkou A, Katsoyiannis I, Stefusova K, Vaclavikova M, Deliyanni E. Adsorption of arsenate by nano scaled activated carbon modified by iron and manganese oxides. *Sustainability* 2017;9(10):1684.
- [26] Zhu J, Gu H, Guo J, Chen M, Wei H, Luo Z, et al. Mesoporous magnetic carbon nanocomposite fabrics for highly efficient Cr(vi) removal. *J Mater Chem A* 2014;2(7):2256–65.
- [27] Dadvar S, Tavanai H, Morshed M, Ghiaci M. A study on the kinetics of 2-chloroethyl ethyl sulfide adsorption onto nanocomposite activated carbon nanofibers containing metal oxide nanoparticles. *Sep Purif Technol* 2013;114:24–30.
- [28] Liu X, Wang M, Zhang S, Pan B. Application potential of carbon nanotubes in water treatment: a review. *J Environ Sci* 2013;25(7):1263–80.
- [29] Mackie EB, Wolfson RA, Arnold LM, Lafdi K, Migone AD. Adsorption studies of methane films on catalytic carbon nanotubes and on carbon filaments. *Langmuir* 1997;13(26):7197–201.
- [30] Kondratyuk P, Yates JT. Desorption kinetic detection of different adsorption sites on opened carbon single walled nanotubes: the adsorption of n-nonane and CCl<sub>4</sub>. *Chem Phys Lett* 2005;410(4–6):324–9.
- [31] Lu C, Chiu H. Adsorption of zinc(II) from water with purified carbon nanotubes. *Chem Eng Sci* 2006;61(4):1138–45.
- [32] Li Y-H, Wang S, Zhang X, Wei J, Xu C, Luan Z, et al. Adsorption of fluoride from water by aligned carbon nanotubes. *Mater Res Bull* 2003;38(3):469–76.
- [33] Cho H-H, Wepasnick K, Smith BA, Bangash FK, Fairbrother DH, Ball WP. Sorption of aqueous Zn[II] and Cd[II] by multiwall carbon nanotubes: the relative roles of oxygen-containing functional groups and graphenic carbon. *Langmuir* 2010;26(2):967–81.

- [34] Rosenzweig S, Sorial GA, Sahle-Demessie E, Mack J. Effect of acid and alcohol network forces within functionalized multiwall carbon nanotubes bundles on adsorption of copper (II) species. *Chemosphere* 2013;90(2):395–402.
- [35] Wu W, Chen W, Lin D, Yang K. Influence of surface oxidation of multiwalled carbon nanotubes on the adsorption affinity and capacity of polar and nonpolar organic compounds in aqueous phase. *Environ Sci Technol* 2012;46(10):5446–54.
- [36] Wang S, Gong W, Liu X, Yao Y, Gao B, Yue Q. Removal of lead(II) from aqueous solution by adsorption onto manganese oxide-coated carbon nanotubes. *Sep Purif Technol* 2007;58(1):17–23.
- [37] Saleh TA, Gupta VK. Column with CNT/magnesium oxide composite for lead(II) removal from water. *Environ Sci Pollut Res* 2012;19(4):1224–8.
- [38] Li YH, Wang SG, Cao AY, Zhao D, Zhang XF, Xu CL, et al. Adsorption of fluoride from water by amorphous alumina supported on carbon nanotubes. *Chem Phys Lett* 2001;350(5–6):412–16.
- [39] Peng X, Luan Z, Ding J, Di Z, Li Y, Tian B. Ceria nanoparticles supported on carbon nanotubes for the removal of arsenate from water. *Mater Lett* 2005;59(4):399–403.
- [40] Veličković Z, Vuković GD, Marinković AD, Moldovan M-S, Perić-Grujić AA, Uskoković PS, et al. Adsorption of arsenate on iron(III) oxide coated ethylenediamine functionalized multiwall carbon nanotubes. *Chem Eng J* 2012;181–182:174–81.
- [41] Chen H, Chen Z, Zhao G, Zhang Z, Xu C, Liu Y, et al. Enhanced adsorption of U(VI) and (241)Am(III) from wastewater using Ca/Al layered double hydroxide@carbon nanotube composites. *J Hazard Mater* 2018;347:67–77.
- [42] Bonaccorso F, Colombo L, Yu G, Stoller M, Tozzini V, Ferrari AC, et al. 2D materials. Graphene, related two-dimensional crystals, and hybrid systems for energy conversion and storage. *Science* 2015;347(6217):1246501.
- [43] Pan M, Zhang Y, Shan C, Zhang X, Gao G, Pan B. Flat graphene-enhanced electron transfer involved in redox reactions. *Environ Sci Technol* 2017;51(15):8597–605.
- [44] Wang J, Chen B, Xing B. Wrinkles and folds of activated graphene nanosheets as fast and efficient adsorptive sites for hydrophobic organic contaminants. *Environ Sci Technol* 2016;50(7):3798–808.
- [45] Ma H-L, Zhang Y, Hu Q-H, Yan D, Yu Z-Z, Zhai M. Chemical reduction and removal of Cr(vi) from acidic aqueous solution by ethylenediamine-reduced graphene oxide. *J Mater Chem* 2012;22(13):5914.
- [46] Zhang Y, Ma H-L, Peng J, Zhai M, Yu Z-Z. Cr(VI) removal from aqueous solution using chemically reduced and functionalized graphene oxide. *J Mater Sci* 2013;48(5):1883–9.
- [47] Wu Y, Luo H, Wang H, Wang C, Zhang J, Zhang Z. Adsorption of hexavalent chromium from aqueous solutions by graphene modified with cetyltrimethylammonium bromide. *J Colloid Interface Sci* 2013;394:183–91.
- [48] Madadran CJ, Kim HY, Gao G, Wang N, Zhu J, Feng H, et al. Adsorption behavior of EDTA-graphene oxide for Pb (II) removal. *ACS Appl Mater Interfaces* 2012;4(3):1186–93.
- [49] Guo J, Wang R, Tjiu WW, Pan J, Liu T. Synthesis of Fe nanoparticles@graphene composites for environmental applications. *J Hazard Mater* 2012;225–226:63–73.
- [50] Nandi D, Gupta K, Ghosh AK, De A, Banerjee S, Ghosh UC. Manganese-incorporated iron(III) oxide-graphene magnetic nanocomposite: synthesis, characterization, and application for the arsenic(III)-sorption from aqueous solution. *J Nanopart Res* 2012;14(12).
- [51] Zhang K, Dwivedi V, Chi C, Wu J. Graphene oxide/ferric hydroxide composites for efficient arsenate removal from drinking water. *J Hazard Mater* 2010;182(1–3):162–8.

- [52] Wen T, Wu X, Tan X, Wang X, Xu A. One-pot synthesis of water-swella-ble Mg-Al layered double hydroxides and graphene oxide nanocomposites for efficient removal of As (V) from aqueous solutions. *ACS Appl Mater Interfaces* 2013;5(8):3304–11.
- [53] Hao L, Song H, Zhang L, Wan X, Tang Y, Lv Y. SiO<sub>2</sub>/graphene composite for highly selective adsorption of Pb(II) ion. *J Colloid Interface Sci* 2012;369(1):381–7.
- [54] Sreepasad TS, Maliyekkal SM, Lisha KP, Pradeep T. Reduced graphene oxide-metal/metal oxide composites: facile synthesis and application in water purification. *J Hazard Mater* 2011;186(1):921–31.
- [55] Lee Y-C, Yang J-W. Self-assembled flower-like TiO<sub>2</sub> on exfoliated graphite oxide for heavy metal removal. *J Ind Eng Chem* 2012;18(3):1178–85.
- [56] Park Y-S, Dmytruk A, Dmitruk I, Kasuya A, Takeda M, Ohuchi N, et al. Size-selective growth and stabilization of small CdSe nanoparticles in aqueous solution. *ACS Nano* 2010;4(1):121–8.
- [57] Pan S, Zhang X, Qian J, Lu Z, Hua M, Cheng C, et al. A new strategy to address the challenges of nanoparticles in practical water treatment: mesoporous nanocomposite beads via flash freezing. *Nanoscale* 2017;9(48):19154–61.
- [58] Pan B, Wu J, Pan B, Lv L, Zhang W, Xiao L, et al. Development of polymer-based nano-sized hydrated ferric oxides (HFOs) for enhanced phosphate removal from waste effluents. *Water Res* 2009;43(17):4421–9.
- [59] Pan B, Xiao L, Nie G, Pan B, Wu J, Lv L, et al. Adsorptive selenite removal from water using a nano-hydrated ferric oxides (HFOs)/polymer hybrid adsorbent. *J Environ Monit* 2010;12(1):305–10.
- [60] Pan B, Xu J, Wu B, Li Z, Liu X. Enhanced removal of fluoride by polystyrene anion exchanger supported hydrous zirconium oxide nanoparticles. *Environ Sci Technol* 2013;47(16):9347–54.
- [61] Pan B, Li Z, Zhang Y, Xu J, Chen L, Dong H, et al. Acid and organic resistant nano-hydrated zirconium oxide (HZO)/polystyrene hybrid adsorbent for arsenic removal from water. *Chem Eng J* 2014;248:290–6.
- [62] Chen L, Zhao X, Pan B, Zhang W, Hua M, Lv L, et al. Preferable removal of phosphate from water using hydrous zirconium oxide-based nanocomposite of high stability. *J Hazard Mater* 2015;284:35–42.
- [63] Su Q, Pan B, Pan B, Zhang Q, Zhang W, Lv L, et al. Fabrication of polymer-supported nanosized hydrous manganese dioxide (HMO) for enhanced lead removal from waters. *Sci Total Environ* 2009;407(21):5471–7.
- [64] Wan S, Zhao X, Lv L, Su Q, Gu H, Pan B, et al. Selective adsorption of Cd(II) and Zn(II) ions by nano-hydrous manganese dioxide (HMO)-encapsulated cation exchanger. *Ind Eng Chem Res* 2010;49(16):7574–9.
- [65] Pan B, Wan S, Zhang S, Guo Q, Xu Z, Lv L, et al. Recyclable polymer-based nano-hydrous manganese dioxide for highly efficient Tl(I) removal from water. *Sci China Chem* 2013;57(5):763–71.
- [66] Pan B, Qiu H, Pan B, Nie G, Xiao L, Lv L, et al. Highly efficient removal of heavy metals by polymer-supported nanosized hydrated Fe(III) oxides: behavior and XPS study. *Water Res* 2010;44(3):815–24.
- [67] Hua M, Jiang Y, Wu B, Pan B, Zhao X, Zhang Q. Fabrication of a new hydrous Zr(IV) oxide-based nanocomposite for enhanced Pb(II) and Cd(II) removal from waters. *ACS Appl Mater Interfaces* 2013;5(22):12135–42.
- [68] Zhang X, Wu M, Dong H, Li H, Pan B. Simultaneous oxidation and sequestration of As (III) from water by using redox polymer-based Fe(III) oxide nanocomposite. *Environ Sci Technol* 2017;51(11):6326–34.

- [69] Zhang Q, Du Q, Hua M, Jiao T, Gao F, Pan B. Sorption enhancement of lead ions from water by surface charged polystyrene-supported nano-zirconium oxide composites. *Environ Sci Technol* 2013;47(12):6536–44.
- [70] Cumbal L, Sengupta AK. Arsenic removal using polymer-supported hydrated iron(III) oxide nanoparticles: role of Donnan membrane effect. *Environ Sci Technol* 2005;39(17):6508–15.
- [71] Zhang Q, Pan B, Chen X, Zhang W, Pan B, Zhang Q, et al. Preparation of polymer-supported hydrated ferric oxide based on Donnan membrane effect and its application for arsenic removal. *Sci China Ser B-Chem* 2008;51(4):379–85.
- [72] Pan, BC, Chen, XQ, Zhang, WM, Pan, BJ, Shen, W, Zhang, QR, et al. Preparation process of resin-based adsorbent for arsenic, Chinese Patent, CN 2005100951775.
- [73] Wan B, Yan Y, Tang Y, Bai Y, Liu F, Tan W, et al. Effects of polyphosphates and orthophosphate on the dissolution and transformation of ZnO nanoparticles. *Chemosphere* 2017;176:255–65.
- [74] Yin J, Deng BL. Polymer-matrix nanocomposite membranes for water treatment. *J Membr Sci* 2015;479:256–75.
- [75] Yang Y, Wang H, Li J, He B, Wang T, Liao S. Novel functionalized nano-TiO<sub>2</sub> loading electrocatalytic membrane for oily wastewater treatment. *Environ Sci Technol* 2012;46(12):6815–21.
- [76] Lai GS, Lau WJ, Goh PS, Ismail AF, Yusof N, Tan YH. Graphene oxide incorporated thin film nanocomposite nanofiltration membrane for enhanced salt removal performance. *Desalination* 2016;387:14–24.
- [77] Cao K, Jiang Z, Zhao J, Zhao C, Gao C, Pan F, et al. Enhanced water permeation through sodium alginate membranes by incorporating graphene oxides. *J Membr Sci* 2014;469:272–83.
- [78] Hong J, He Y. Polyvinylidene fluoride ultrafiltration membrane blended with nano-ZnO particle for photo-catalysis self-cleaning. *Desalination* 2014;332(1):67–75.
- [79] Yan L, Li YS, Xiang CB. Preparation of poly(vinylidene fluoride)(pvdf) ultrafiltration membrane modified by nano-sized alumina (Al<sub>2</sub>O<sub>3</sub>) and its antifouling research. *Polymer* 2005;46(18):7701–6.
- [80] Chen L, Li N, Wen Z, Zhang L, Chen Q, Chen L, et al. Graphene oxide based membrane intercalated by nanoparticles for high performance nanofiltration application. *Chem Eng J* 2018;347:12–18.
- [81] Qiu M, He C. Novel zwitterion-silver nanocomposite modified thin-film composite forward osmosis membrane with simultaneous improved water flux and biofouling resistance property. *Appl Surf Sci* 2018;455:492–501.
- [82] Kang Y, Obaid M, Jang J, Ham MH, Kim IS. Novel sulfonated graphene oxide incorporated polysulfone nanocomposite membranes for enhanced-performance in ultrafiltration process. *Chemosphere* 2018;207:581–9.
- [83] Yao Y, Hu Y, Yu M, Lian C, Gao M, Zhang J, et al. Nitrogen-doped carbon encapsulating molybdenum carbide and nickel nanostructures loaded with PVDF membrane for hexavalent chromium reduction. *Chem Eng J* 2018;344:535–44.
- [84] Xie R, Luo F, Zhang L, Guo SF, Liu Z, Ju XJ, et al. Catalytic membrane with multiscale pores prepared via vapor-induced phase separation. *Small* 2018;14(18):e1703650.
- [85] Pan X, Bao X. The effects of confinement inside carbon nanotubes on catalysis. *Acc Chem Res* 2011;44(8):553–62.
- [86] Zhang H, Fan X, Quan X, Chen S, Yu H. Graphene sheets grafted Ag@AgCl hybrid with enhanced plasmonic photocatalytic activity under visible light. *Environ Sci Technol* 2011;45(13):5731–6.

- [87] Yao Y, Li G, Ciston S, Lueptow RM, Gray KA. Photoreactive  $\text{TiO}_2$ /carbon nanotube composites: synthesis and reactivity. *Environ Sci Technol* 2008;42(13):4952–7.
- [88] Feng S-a, Zhao J-h, Zhu Z-p. The manufacture of carbon nanotubes decorated with ZnS to enhance the ZnS photocatalytic activity. *N Carbon Mater* 2008;23(3):228–34.
- [89] Ma L-L, Sun H-Z, Zhang Y-G, Lin Y-L, Li J-L, Yu KY, et al. Preparation, characterization and photocatalytic properties of CdS nanoparticles dotted on the surface of carbon nanotubes. *Nanotechnology* 2008;19(11).
- [90] Wang S, Shi X, Shao G, Duan X, Yang H, Wang T. Preparation, characterization and photocatalytic activity of multi-walled carbon nanotube-supported tungsten trioxide composites. *J Phys Chem Solids* 2008;69(10):2396–400.
- [91] Li G, Lu Y, Lu C, Zhu M, Zhai C, Du Y, et al. Efficient catalytic ozonation of bisphenol-A over reduced graphene oxide modified sea urchin-like  $\alpha\text{-MnO}_2$  architectures. *J Hazard Mater* 2015;294:201–8.
- [92] Wang Y, Sun H, Ang HM, Tadé MO, Wang S. Magnetic  $\text{Fe}_3\text{O}_4$ /carbon sphere/cobalt composites for catalytic oxidation of phenol solutions with sulfate radicals. *Chem Eng J* 2014;245:1–9.
- [93] Nguyen TT, Trinh TV, Tran DN, Le GT, Le GH, Vu TA, et al. Novel  $\text{FeMgO/CNT}$  nano composite as efficient catalyst for phenol removal in ozonation process. *Mater Res Express* 2018;5(9).
- [94] Bai Z, Yang Q, Wang J. Catalytic ozonation of dimethyl phthalate using  $\text{Fe}_3\text{O}_4$ /multi-wall carbon nanotubes. *Environ Technol* 2017;38(16):2048–57.
- [95] Yang Z, Yu A, Shan C, Gao G, Pan B. Enhanced  $\text{Fe(III)}$ -mediated Fenton oxidation of atrazine in the presence of functionalized multi-walled carbon nanotubes. *Water Res* 2018;137:37–46.
- [96] Xiao F, Li W, Fang L, Wang D. Synthesis of akageneite ( $\beta\text{-FeOOH}$ )/reduced graphene oxide nanocomposites for oxidative decomposition of 2-chlorophenol by Fenton-like reaction. *J Hazard Mater* 2016;308:11–20.
- [97] Hassani A, Celikdag G, Eghbali P, Sevim M, Karaca S, Metin O. Heterogeneous sono-Fenton-like process using magnetic cobalt ferrite-reduced graphene oxide ( $\text{CoFe}_2\text{O}_4\text{-rGO}$ ) nanocomposite for the removal of organic dyes from aqueous solution. *Ultrason Sonochem* 2018;40(Pt A):841–52.
- [98] Yu L, Chen J, Liang Z, Xu W, Chen L, Ye D. Degradation of phenol using  $\text{Fe}_3\text{O}_4\text{-GO}$  nanocomposite as a heterogeneous photo-Fenton catalyst. *Sep Purif Technol* 2016;171:80–7.
- [99] Li S, Zhang G, Zhang W, Zheng H, Zhu W, Sun N, et al. Microwave enhanced Fenton-like process for degradation of perfluorooctanoic acid (PFOA) using  $\text{Pb-BiFeO}_3\text{/rGO}$  as heterogeneous catalyst. *Chem Eng J* 2017;326:756–64.
- [100] Zhang X, Zhang L, Li Z, Jiang Z, Zheng Q, Lin B, et al. Rational design of antifouling polymeric nanocomposite for sustainable fluoride removal from NOM-rich water. *Environ Sci Technol* 2017;51(22):13363–71.
- [101] Nie G, Pan B, Zhang S, Pan B. Surface chemistry of nanosized hydrated ferric oxide encapsulated inside porous polymer: modeling and experimental studies. *J Phys Chem C* 2013;117(12):6201–9.

This page intentionally left blank

# Impact of functionalized nanomaterials towards the environmental remediation: challenges and future needs

Aashima and S.K. Mehta

*Department of Chemistry and Centre of Advanced Studies in Chemistry, Panjab University, Chandigarh, India*

## 18.1 Introduction

The break-neck pace of industrialization and its resulting byproducts have altered the balanced environmental composition by releasing hazardous wastes, poisonous gas fumes, and smoke into the environment, thus, producing harmful effects on living beings. This has created a global menace, and the magnitude of it is proliferating day-by-day leading to environmental pollution. Pesticides, oil spills, particulate matter, heavy metals, herbicides, fertilizers, toxic gases, industrial effluents, sewage, and organic compounds are just a few examples of the numerous dangerous contaminants. Maintaining clean air, pure water, and a healthy environment is a challenging task under these conditions. Fortunately, new technologies have been explored for the remediation of air, soil, and water [1]. The rise of nanotechnology has created huge opportunities and space for the fabrication of nanomaterials (NMs) with desired properties (i.e., large surface-to-volume ratio and unique functionalization) to treat pollutants. Although, the utilization of nanotechnology in the field of electronics and health science is at high rise [2–4], but, its incorporation into other fields of technology is limited. For example, the adaptation of NMs in conventional everyday products (clothes, cosmetics, and dyes) and in industrial, agricultural, and environmental protection processes [5–7] encounters more skepticism based on a huge quantity of demands combined with their high cost. Nanotechnology-based building products have wide range of applications in cement and concrete industry, self cleaning processes, nanocoating and nano glass fabrication to name a few. They are being commercialized to



overcome the persisting problems of high environmental degradation and shelf life of the conventional products [8]. NMs provide more effective and increased physical properties as compared to bulk materials because of their higher surface to volume ratio. Not only are physical properties enhanced, NMs also offer the potential to leverage unique surface chemistry via functionalization or grafting the functional groups, through which a pollutant can be targeted for remediation processes as compared to traditional methods. Tuning physical properties with different functionalization offers remarkable additions to the materials over the traditional methods for addressing environmental issues. Further designing or tuning of NMs (i.e., size, morphology, porosity, shape, and chemical composition) can be done to create additional advantageous characteristics, which indirectly or directly affect the performance of the material. Despite having innumerable advantages NMs are accompanied by some unpredictable contaminations (degradation producted) if not tailored under controlled environment. Once released into the environment, the fate and effects of NMs remains inadequately understood and difficult to predict. Thus, there is a need to carefully design and optimise the NMs to extracts maximum benefits.

Taking into account the advantages that NMs provide, methods are being developed to fabricate hybrid NMs with enhanced efficiency followed by lower environmental toxicity. These combinations will provide more effective, stable, and selective methods as compared to a available ones. For example, attaching nanoparticles (NPs) to a matrix increases the stability of NPs, as aggregation can be minimized, which increases the effectiveness of NPs for remediation processes as compared to NPs used alone. Selectivity can be achieved by employing specific chemical functionalization for targeting certain contaminants. It is also important to keep in mind that materials created for use in remediation processes should not themselves become pollutants when they are employed for the environmental cause. The different NMs employed in environmental remediation are been presented in [Table 18.1](#).

The commercialization of biocompatible materials not only enhance the acceptance of advanced technology but also increases consumer interest and products' acceptability. These modified NMs does not generate waste that needs to be disposed of after treatment, and would offer a greener route for environmental remediation. The advantage of these kind of functionalized NMs is that they are target specific due to presence of particular functional moiety which can bind to a specific molecule or functional group. The study of the literature ([Table 18.1](#)) reveals the potential of NMs in handling toxins present in air, soil, and water.

The present day research is focused on augmenting nanotechnology with chemical surface modifications to obtain materials that can be employed to handle the environmental challenges in the present era. The key points to consider while fabricating these materials are nontoxicity, cost effectiveness, and regeneration after the remediation process. The other important point is

**TABLE 18.1** Summary of NMs employed for the pollutant treatment in environment.

Type of nanomaterial	Target material	References
Ag-doped TiO <sub>2</sub>	Waterborne pathogenic virus in drinking water	[9]
One dimension TiO <sub>2</sub> /Fe-doped TiO <sub>2</sub>	Arsenic (As(V))	[10]
TiO <sub>2</sub> thin film and composite with Al <sub>2</sub> O <sub>3</sub>	Methylene blue (MB), creatinine, biological toxins (microcystin-LR), <i>Escherichia coli</i>	[11]
One dimension (1D) TiO <sub>2</sub>	Lead (Pb(II))	[12]
Ag-doped TiO <sub>2</sub> nanofibres	MB, NO <sub>x</sub> and toluene in air and 2,4,6-Trichlorophenol	[13]
Cu/Fe/Ag-doped TiO <sub>2</sub>	Nitrate	[14]
Ag-doped TiO <sub>2</sub> nanofibres	2,4,6-Trichlorophenol	[15]
Modified jacobsite (MnFe <sub>2</sub> O <sub>4</sub> )	Cr(VI)	[16]
Iron nanoparticles in calcium alginate beads	Cr(VI)	[17]
Magnetic NPs encapsulated by poly(3,4-ethylenedioxythiophene)	Ag(I), Hg(II), Pb(II)	[18]
Magnetite NPs modified with dimercaptosuccinic acid	Hg(II), Co(II), Cu(II), As(V), Ag(I), Cd(II), Ti(III), Pb(II), chromate ions	[19,20]
Maghemite (Fe <sub>2</sub> O <sub>3</sub> )	Mo(VI)	[21]
Superparamagnetic magnetite (Fe <sub>3</sub> O <sub>4</sub> ) with silica functionalization	Hg(II)	[22]
Cubic silica functionalized by SBA-16	Removal of polycyclic aromatic hydrocarbons (PAH), such as pyrene and phenanthrene, and Pb(II), Cd(II), Hg(II), Cr <sub>2</sub> O <sub>7</sub> <sup>2-</sup> from contaminated aqueous solutions	[23]
Amine-Quartz mesoporous adsorbent	Separation of CO <sub>2</sub> from a feed gas mixture of CO <sub>2</sub> and N <sub>2</sub> on porous substrates	[24]
Poly(amidoamine) (PAMAM) dendrimer composite membrane consisting of chitosan and a dendrimer	Separation of CO <sub>2</sub> from fossil fuel emission on porous substrates	[25,26]

(Continued)

**TABLE 18.1 (Continued)**

Type of nanomaterial	Target material	References
Amphiphilic polyurethane NPs	Removal of organic pollutants, such as polycyclic aromatic hydrocarbons, trihalogen methane, pesticides, and methyl-tert-butyl ether	[27]
Gold coated with chitosan polymer	Removal of metal ions from waste water	[28]
CNT with Ag ions and Cu NPs	Removal of <i>E. coli</i> and <i>Staphylococcus aureus</i> from contaminated water	[29]
CNT with TiO <sub>2</sub> NPs and P-25 TiO <sub>2</sub>	Removal of organic dyes, derivatives of phenol, azo substances, and metallic ions from contaminated water	[30–33]
CNT with iron oxide magnetic composites	Removal of Co(II), Sr(II), and Ni (II) from the aqueous solution	[34]
Hybrid diatomite/carbon composites	Removal of polar aromatic compounds ( <i>p</i> -cresol) from aqueous solutions	[35]
Fe <sup>0</sup> /Pd polyacrylic acid/polyvinyl alcohol	Trichloroethylene	[36]
TiO <sub>2</sub> polyaniline	Phenol	[37]
TiO <sub>2</sub> poly (tetrafluoroethylene)	Trichlorobenzene	[38]
Fe <sup>0</sup> polystyrene–divinylbenzene	Nitrate	[39]
TiO <sub>2</sub> poly(3-hexylthiophene)	Methylene orange	[40]
Polyhydroxybutyrate films with TiO <sub>2</sub>	MB	[41]
Fe <sup>0</sup> carboxymethyl cellulose	Cr <sup>6+</sup>	[42]
Fe <sup>0</sup> poly(vinyl pyrrolidone)	Bromate	[43]
Fe <sup>0</sup> /Pd sodium carboxymethyl cellulose	Para-nitrochlorobenzene	[44]
Biosynthesized Cu <sup>0</sup>	Dyes	[45]
Ni/Fe cellulose acetate	Trichloroethylene	[46]
Au/TiO <sub>2</sub> core–shell nanocomposites	Trichloroethylene	[47]
Magnetite montmorillonite	Cr(VI)	[48]

(Continued)

**TABLE 18.1** (Continued)

Type of nanomaterial	Target material	References
Hydrated ferric oxide polymeric anion exchangers	As ions	[49]
Hydrated ferric oxide polymeric cation exchanger	As ions	[50]
Polymer-based nanohydrous manganese dioxide	Thallium removal	[51]
Fe <sub>3</sub> O <sub>4</sub> alginate	MB, methyl orange	[52]
Chitosan-capped gold nanoparticles	Metal ions	[28]
Nanowire polystyrene/polyaniline	Ethanol, acetone	[53]
TiO <sub>2</sub> polyaniline	Trimethylamine	[54]
Iron oxide polypyrrole	CO <sub>2</sub> , N <sub>2</sub> , CH <sub>4</sub>	[55]
Pd polyaniline	Methanol	[56]
Surface plasmon resonance sensor	Zn(II), Cu(II)	[57]

to prevent agglomeration and to increase stability for NMs' under different conditions. This chapter summarizes the present scenario of NMs in literature, their fabrication process, and their ability to target specific pollutants.

## 18.2 Implementation of functionalized nanomaterial: water pollution remediation

Clean water is essential for living beings to lead a healthy and long life. But this basic necessity is becoming scarce and scanty due to incontinent water pollution. Water pollution is the contamination of water bodies (i.e., surface and ground water) due to excessive accumulation of waste products produced by industrialization and environmental degradation [58]. Organic pollutants such as dyes are released from textile, food, cosmetics, paper, and fabric industries into aquatic ecosystems. Dyes found in bodies of water interrupt the incoming sun-rays resulting in decreased photosynthetic activity of aquatic plants [59]. Similarly, the phenolic compounds released by textile, plastics, oil refineries, as well as pharmaceuticals industries [60] are considered a toxic threat to bodies of water and to human beings. Pesticides are another class of water pollutants that are generally used in the agricultural sector for protecting crops from pest damage. Pathogenic bacteria even at

very low concentrations in water causes serious human health issues [61]. The contamination by carcinogenic and toxic inorganic heavy metals ions like Cr, As, Cd, Pd, and Hg, are also degrading the water quality. The aquatic ecosystem has become contaminated from the continuous discharge of these organic, inorganic, and biological pollutants, which are responsible for causing serious health problems such as diarrhea, lung diseases, cancer, lead poisoning, muscle weakness, and many more ailments [62]. NMs are one of the potential solutions being used in water treatment via adsorption and catalysis processes due to their unique and effective surface properties. Functionalization of NMs can further enhance the effectiveness of the treatment by decreasing the process time and augmenting the process efficiency. The various possible ways in which contaminants like inorganic ions, organic compounds, and pathogens can be removed are – adsorption, filtration, degradation into nontoxic components, and photocatalysis. In the next section, the various functionalized NMs and their application in water purification are thoroughly discussed. Further, different pollutants (i.e. bacteria, pesticides, metal ions, solvents and oils) are also reviewed in next sections.

Dyes have become one of the most critical water contaminant issues, and their untreated, effluent discharges into environment have created a big concern for society. The current techniques employed for the removal of dyes fall under three main classes: physical methods (adsorption, surfactants); chemical methods (oxidation method using hydrogen peroxide, Fenton's reagent); and biological methods (algae, bacteria). Over recent years, there has been great interest in development of novel nanoadsorbents having high adsorption capacity. In this regard, adsorption capacity of zero valent iron NPs (biologically/chemically fabricated) for removal of crystal violet (CV) was found to be 99.8% due to functionalization of  $\beta$ -cyclodextrin (Fig. 18.1). The reason for such a high removal percentage is attributed to the increase in number of active sorption sites of nanoadsorbent. The green synthesized  $\text{Fe}^0$  NPs by *Ferula persica* extract displayed better performance than the chemically synthesized, 39.5 versus 14.7%, respectively because of their higher surface area (46.68 vs 34.38  $\text{m}^2/\text{g}$ , respectively) [63].

A new magnetic nanoadsorbent that is polycatechol modified  $\text{Fe}_3\text{O}_4$  NPs ( $\text{Fe}_3\text{O}_4/\text{PCC}$  MNPs) was synthesized using a simple coprecipitation method and showed strong adsorption capacity and a fast adsorption rate [64]. Different cationic dyes, methylene blue, cationic turquoise blue, malachite green (MG), CV, and cationic pink FG were removed from wastewater and various parameters were also optimized (i.e., contact time, ion strength, effect of pH, and temperature) to evaluate the optimum conditions for removal.

Chaudhary *et al.* [65] demonstrated wastewater cleanup by adsorption using surfactant functionalized cerium oxide (Ceria) NPs. The NPs were prepared via coprecipitation method and functionalized using cationic surfactants that showed dye removal efficiencies varying from 112.4 to 171.3  $\text{mg}/\text{g}$  of dye, which is superior to other nanoadsorbents. MG dye was adsorbed

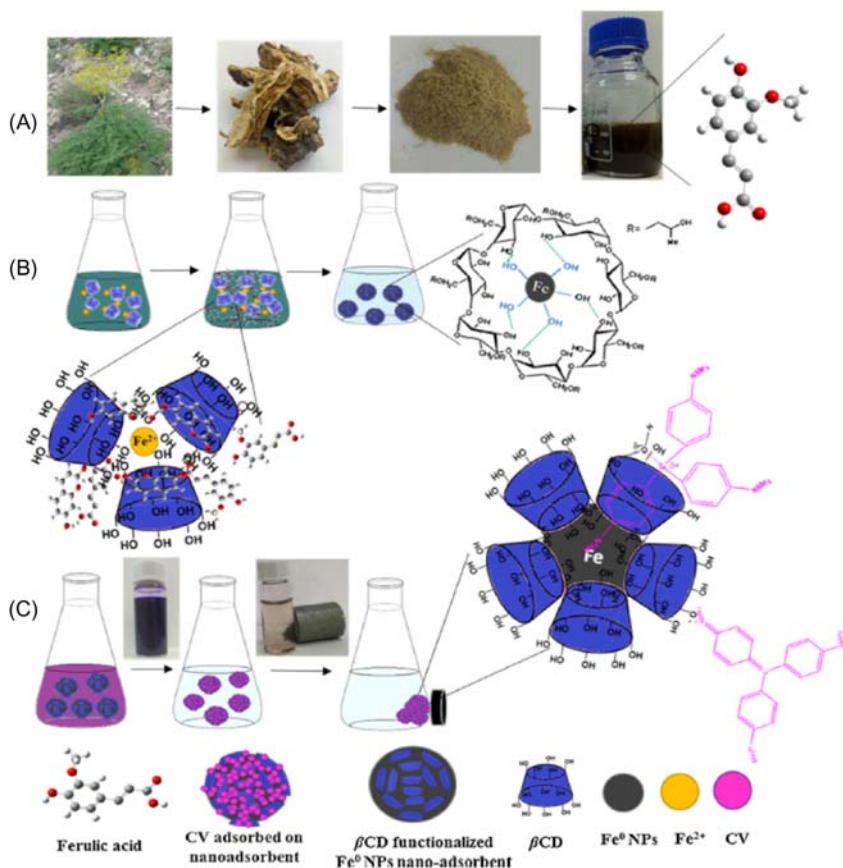


**FIGURE 18.1** Schematic illustration for (A, B) synthesis of biogenic  $\beta$ -cyclodextrin functionalized Fe<sup>0</sup> NPs (5G-Fe<sup>0</sup> NPs/ $\beta$ CD) using *Ferula persica* root extract (C) removal of CV.

over the surface of strontium titanate (SrTiO<sub>3</sub>) NPs at pH = 10 with adsorption efficiency of 98% achieved [66]. The fabricated NPs were more effective as compared to commercially available SrTiO<sub>3</sub> in removing MG dye. Therefore, it was quite evident that functionalized NPs came out as better nano-adsorbent than the bare NPs. Water pollution from heavy metals (e.g.,  $\text{Pb}^{2+}$ ,  $\text{Hg}^{2+}$  and  $\text{Cd}^{2+}$ ) has gained attention because the metals are toxic and carcinogenic, and they pose a serious threat to human health and the environment [67]. Mohmood *et al.* [68] reported the synthesis of dithiocarbamate functionalized silica-coated Fe<sub>3</sub>O<sub>4</sub> NPs for mercury decontamination of saltwater with  $\text{Hg}^{2+}$  and with As and Cd (Fig. 18.2). The results displayed that under highly competitive conditions, the removal of  $\text{Hg}^{2+}$  from seawater using magnetic NPs. The removal efficiency was 98% with concentration ranging from 50 to 500  $\mu\text{g/L}$ .

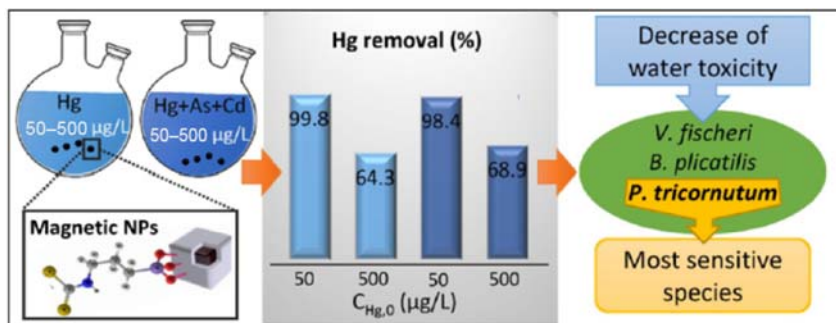


FIGURE 18.2 Magnetic and functionalized NPs for mercury ion sensing.

An environmentally friendly nanosensor with multimodal properties, magnetic as well as fluorescent, was developed via a multistep synthesis procedure for detection and removal of  $\text{Hg}^{2+}$  ions in water. This nanosensor consists of a thin silica shell encapsulating magnetic NPs, a fixed spacer arm, and fluorescent quantum dots (QD) for simultaneous detection and removal [69]. An efficient and selective detection of  $\text{Hg}^{2+}$  ions was done by multifunctional nanocomposites based on magnetite NPs, chitosan NPs, and polythiophene. The synthesized nanocomposites not only showed a complete removal of  $\text{Hg}^{2+}$  ions, but they also displayed higher selectivity in the presence of other metal ions over a wider pH range. The reason for high selectivity was the presence of several functionalities: hydroxyl, amino, sulfur, and phosphate groups in addition to the magnetic property of magnetite NPs [70]. Magnetic NPs can also be functionalized with different organic ligands such as aminopropyl, silane, peptone, and yam—peel biomass. The presence of chemical groups like carboxyl and amino lead to the removal of  $\text{Hg}^{2+}$  ions from water [71]. Among metal ions, lead and cadmium are extensively used in the manufacturing of batteries, metal alloys, ceramics, paints, and pigments, which slowly accumulate in water. Wang *et al.* [72] reported carboxyl functionalized NPs with magnetic core and mesopore carbon shell as absorbent, which can remove 97% of  $\text{Pb}^{2+}$  ions from an acidic aqueous solution. NPs displayed high removal capacities at lower pH value, 3 and treat high concentration of pollutant (100 mg/L). The porous carbon layer and carboxyl functionalization allows the possibility to remove the toxic metal ions from aqueous solution. In another study, Hashemzadeh *et al.* [73] reported the surface modified hematite NPs fabrication *via* hydrothermal method at 250°C. The  $\text{Pb}^{2+}$  ions removal was found to be dependent on pH, adsorbent dose, and contact time. The maximum uptake capacity was estimated to be 111 mg/g and  $R_L$  value of 0.021 which confirmed the favorability of adsorption. Magnetic nanosorbents based on manganese ferrite NPs capped with carboxymethylated biopolymers (starch or cellulose) were shown to remove ~100%  $\text{Pb(II)}$  efficiently from the aqueous solution after 30 min of contact

[74]. Hybrid NPs were also fabricated and utilized as absorbent for the metal ion removal. Silica-calcium phosphate hybrid NPs were synthesized by a facile one-pot method and assessed for  $\text{Cd}^{2+}$  ions removal from aqueous solutions. The experiments demonstrated that silica modified ferrite NPs have a high adsorption capacity due to silanol groups present on the surface, which lead to electrostatic interaction resulting in removal of  $\text{Cd}^{2+}$  ions [75]. Hence, the functionalized NMs are emerging as an efficient adsorbent for the remediation metal ions from wastewater. Researchers are working in this particular area of functionalization as well as in magnetic nanoadsorbents to be utilized at large scale. Organic pollutants consist of a wide range of compounds (i.e., polychlorinated biphenyls, oils, phenols, etc.). Oil spills can cause large scale pollution in very short time; after a spill the oil spreads quickly and forms a film on the water's surface [76]. Vidal-Vidal *et al.* [77] applied a one-pot microemulsion method to produce oleylamine functionalization onto the NMs surface, which resulted in oil removal from water. Activated carbon, a popular adsorbent, was composited with magnetite by in situ coprecipitation method resulting in adsorption efficiency of premium oil (12.93 g/g) and used oil (7.65 g/g), which is more than observed for only activated carbon. Polychlorinated biphenyls are some of the most persistent and pervasive pollutants in the environment. Polyphenolic-based moieties, curcumin and quercetinmultiacrylate, were incorporated with poly(ethylene glycol)-based polymeric shells to create high affinity binding sites for the capture of polychlorinated biphenyls via  $\pi$ - $\pi$  stacking [78].

The growing resistance of antibacterial drugs (i.e. antibiotics) has become more challenging and has created a need to look for alternative solutions. The bacteria have succeeded in developing resistance against conventional antibiotics via various mechanisms [79]. The new emerging antibacterial agents have overcome this problem of resistance without any/reduced side effects. The efficacy of conventional antibiotics can also be enhanced by combining with metal oxide NPs to lower the prevailing side effects prevailing antibiotics. Chitosan functionalized NPs were synthesized via an easy one-step hydrothermal treatment. The pH for synthesis was also varied, and different shaped structures were obtained. They were then tested for antibacterial activity against gram-negative and gram-positive strains. The structure obtained at  $\text{pH} = 5$  was found to be most effective for the antibacterial applications. The reason for the strong antibacterial activity was the release of Ag ions and the soluble nature of the functionalized system [80]. Another report indicated that biogenic stabilized Ag NPs showed enhanced antimicrobial effect. These synthesized Ag NPs were tested on bacterial strains *Staphylococcus aureus* and *Pseudomonas aeruginosa*, and it was found that the bacterial membrane were damaged due to exposure to Ag NPs, which results in antimicrobial action [81]. Biocompatible iron oxide ( $\text{Fe}_2\text{O}_3$  NPs) via *Skimmia laureola* leaf extract and synthesized NPs were evaluated for their antibacterial efficacy against bacterial wilt pathogen *Ralstonia*



*solanacearum* in *in vitro* and in plants. The bacterial cultural media containing 6 mg/mL synthesized NPs drastically inhibit the bacterial growth *in vitro* [82]. The above literature discussion indicates the importance of NMs functionalization in the treatment of wastewater and point to their broader scope in near future.

### 18.3 Implementation of functionalized nanomaterial: air pollution remediation

Air pollution is the alteration of air quality characterized by the assessment of chemical and physical pollutants in the air. It is one of the biggest threats to human life and the environment. Studies have revealed that air pollutants are responsible for various diseases (i.e., lung diseases, heart problems) [83]. Air pollutants associated with adverse conditions of air include ozone, sulfur oxides, carbon monoxide, nitrogen oxides, carbon dioxide and polycyclic aromatic hydrocarbons, and volatile organic compounds (VOCs) [84]. Gas emissions have become incompatible with various policies on climate change, and they have deleterious effects on human health. In the real world emissions are higher than regulations allow, exacerbating air quality problems of various cities. It is necessary to develop innovative techniques that can be employed to detect, perceive, and treat air pollutants at even lower contaminant concentrations. VOC is one of the major air pollutants in indoor air and factories of petrochemical industries. Benzene is one of the major VOC pollutants, and its control emission is a vital matter of concern in industries and the environment.  $\text{TiO}_2\text{--CeO}_2$  nanocomposite under irradiation of an Xe lamp was used for the gas-phase oxidation of benzene with enhanced catalytic activity. The carbon dioxide rate formation of  $\text{TiO}_2\text{--CeO}_2$  nanocomposite with Ti/Ce molar ratio 0.108 under synergetic photothermocatalytic conditions is 36.4 times higher than the rate observed in conventional photocatalytic conditions at room temperature (Fig. 18.3) [85].

An efficient method based on solid phase gas extraction with Schiff base immobilized on multi walled carbon nanotubes (TerphApm@MWCNTs) as a novel sorbent was used for benzene removal from artificial air preloaded in Robson quartz tubes [86]. A clay supported  $\text{TiO}_2$  photocatalyst was reported for the air treatment, and a benchtop photocatalytic flow reactor employing clay-based  $\text{TiO}_2$  system was used for the photocatalytic treatment of toluene. The different parameters (i.e., effect of relative humidity and two UV lamps with varying power) were employed to find a better system as well as conditions [87]. The Au@NiO core shell NPs were used for preparing p-type gas sensors for the detection of ethanol and were found to be efficient as compared to bare NiO NPs. The reason for this behavior was due to the increase of charge carriers in case of Au@NiO [88]. VOC species are precursors of photochemical oxidants that are classified as respiratory toxicants. N-butanol gas was adsorbed on the surface of zinc oxide (ZnO) NPs and Cd

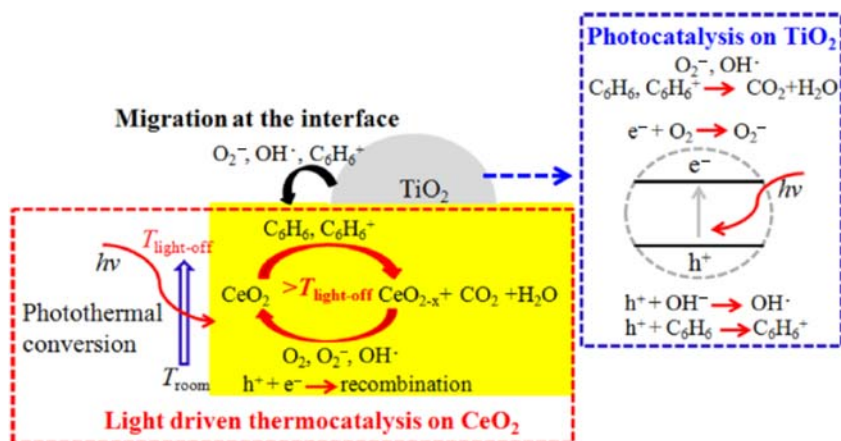


**FIGURE 18.3** Schematic illustration of solar-light-driven thermocatalysis and the synergetic effect between the photocatalysis.

doped ZnONPs. The effect of different concentrations of Cd ion as dopant over the fabrication of ZnONPs was investigated. The particles have displayed significant activity toward the gas sensing field [89].

The comparison of vanadium oxide ( $\text{V}_2\text{O}_5$ ) and  $\text{Sn}-\text{V}_2\text{O}_5$  NPs for the assessment of detection of ammonia (5–50 ppm) gas by employing photoluminescence has been studied. The  $\text{V}_2\text{O}_5$  NPs were doped with Sn (2–6 wt. %) with an increasing concentration of Sn as dopant, and a linear effect on the microstrain of the particles was observed. The UV-visible adsorption profile showed that band gap energy decreases with increasing dopant concentration. These systems were utilized for ammonia sensing [90]. The functionalized NMs were employed extensively in air pollution remediation and found to be efficient in this field.

## 18.4 Implementation of functionalized nanomaterial: soil pollution remediation

Soil is one of the vital components on planet Earth. It is estimated that 25% of the soil worldwide is highly degraded, and 44% of the soil is moderately degraded. The cause of degradation is because of the increasing concentration of metal, metal ions, pesticides, antibiotics, and disinfectants [91]. The human population has been living on earth for about 2 million years. Industrialization has led to great economic developments on the one hand but has also led to greater environmental degradation on the other. The depletion of natural resources, carbon emissions, pollution, and health problems are among the various issues caused by industrialization. Soil pollution is also a major environmental problem, which occurs mainly due to the

presence of toxic chemicals, pollutants, or contaminants in the soil. Some of the major sources of soil pollution include contamination arising from the underground water storage tanks, application of pesticides, oil and fuel dumping, leaching of wastes from landfills, and the direct discharge of industrial wastes into the soil. Silica-coated maghemite functionalized with diethylenetriaminepentacetic acid (DTPA) have been employed for extracting different metals. These types of functionalized materials are able to form complexes with metal resulting in removal of metal ions [92]. These NPs have the ability to extract 80% of metal ions from polluted soil samples. Calcium phosphate NPs (CPNs) were investigated for the remediation process of soil. They were treated with soil samples, and after treatment process the extractable contents of Pb, Cu, and Zn were found to be decreased in soil [93]. Bimetallic Pd/Fe NPs were investigated in removal of hydrodechlorination of polychloroethanes [94]. Biogenic  $\text{Fe}_3\text{O}_4$  and  $\text{Fe}_2\text{O}_3$ , synthesized using *Geobacter metallireducens*, were found to be effective in degrading  $\text{CCl}_4$  to methane [95].  $\text{Fe}_2\text{O}_3$  nanowires containing zero valent iron were used for aerobic oxidation of p-nitrophenol [96]. A commonly known chlorophenol-2,4-dichlorophenol (2,4-DCP) is a broad-spectrum antimicrobial agent used in wood preservation and pesticides, and now is a frequently found pollutant. Calcium peroxide ( $\text{CaO}_2$ ) NPs were utilized for completely degrading 2,4z-DCP, while the conventional one was found to be saturated at 75% degradation rate. The reason for this is that hydroxyl ion generation results in degradation [97]. Bimetallic Pd/Fe systems stabilized via carboxymethyl-cellulose were used for the removal of hexachlorocyclohexane from contaminated soil slurry. The stabilizer has enhanced the efficacy of the bimetallic NPs with 100% removal of pollutants when compared with bare ones. The proposed mechanism initiated with the corrosion of iron is followed by the dissociation of hydrogen gas by Pd. This results in the formation of a strong reducing agent that degrades the pollutant [98]. Li *et al.* [99] reported that complete dechlorination and removal of 70% of pentachlorophenol (PCP) from contaminated soil using Pd/Fe NPs was possible. PCP is converted into phenol by using synthesized NPs and removed thorough electroosmosis from soil. Yuan *et al.* [100] also reported the degradation of PCP into phenol as final product (46.6%) resulting in removal of PCP from soil. In a more recent study, Fan *et al.* [101] laundered polychlorinated biphenyls (PCBs) from contaminated soil using gum-stabilized Pd/Fe NPs. The utilization of surfactants in the procedure enhances the solubility of PCBs and, hence, increases their removal from soil. A nanohetro assembly of superparamagnetic  $\text{Fe}_3\text{O}_4$  and bismuth vanadate assembled into the *Pinus roxburghii*, derived from biochar, were used for the remediation of soil (Fig. 18.4). An emerging pollutant, methylparaben (MeP), was 97.4% degraded in 2 h.

The key takeaway is that the combination of two nanojunctions and ligand functionalization can lead to increased effective soil remediation processes.

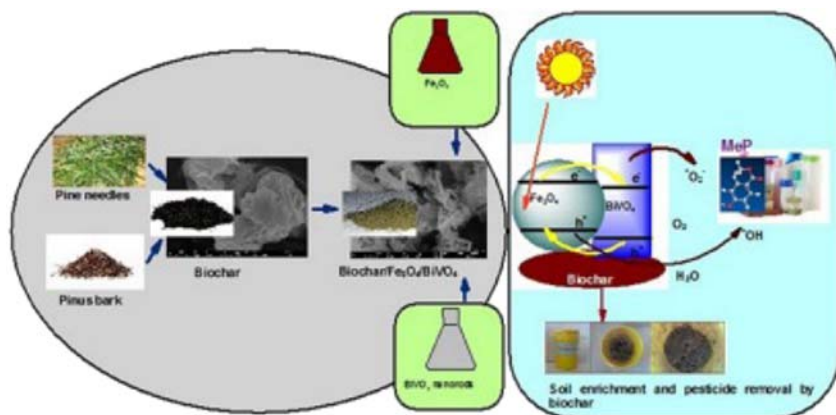


**FIGURE 18.4** Nano-hetro assembly of superparamagnetic  $\text{Fe}_3\text{O}_4$  and bismuth vanadate for pesticide removal.

## 18.5 Conclusion

The metal/metal oxide NPs, bimetallic systems, modified NPs, have demonstrated efficient capability as environmental remediation agents. Different sets of nano based systems have been developed and employed to fight against various types of lethal pollutants. These functionalized systems with advanced features have lower toxicity effects along with improved treatment efficacy. They may overcome the principal limitations that hinder their wide-scale applications. The robustness of these NMs at a wide range of alkaline and acidic conditions, temperature fluctuation, different pollutant concentration have increased their scope in pollutant removal. The shape, morphology, and surface passivation have directly/indirectly influenced their properties. Their selectivity, porosity, magnetic behavior, and recyclability has increased their scope in environmental remediation process in the foreseeable future. Nanotechnology has come up with innovative solutions to manage the mess of degrading surroundings and has great scope in dealing with prevailing global environmental issues. However, the way is still long and full of challenges to reach a milestone in applied environment nanotechnology.

## 18.6 Future scope and challenges

The nanoremediation has great potential to address and resolve environmental issues. Conventional remediation techniques are now being replaced by nanoremediation due to the selectivity, specificity, effectiveness, short time removal, and recyclability they offer for treatment. Chemically powered nanomotors, small autonomous devices capable of performing complex tasks while being self-propelled in fluids are the latest feather in the cap. These smart devices designed for environmental remediation are becoming a part

of the solution for environmental remediation. For instance, self-propelled microjets used for the degradation of organic dyes is 12 times faster than NPs [102]. These types of devices have potential capability for the remediation of contaminated water. The solid waste (i.e., plastics) treatment/conversion into nanosystems will also be a creative alternative on both ends, plastic as well as wastewater treatment [103]. These kinds of upcoming nanosystems have strengthened the positive aspects of nanotechnology usage in environmental remediation. A long-term outlook needs to be evaluated on nanocontamination, and a full risk assessment should be done on new NMs before they are employed in treatment processes. Life cycle analysis should be carried out for the new nanosystems before the utilization in their respective work. The immobilization of nanosystems onto the solid bulk system can reduce the risk of nanosystems entering the food chain. New ab initio models are available that take advantage of increased computing, by means of which the behavior of the material at nanoscale and mechanisms in the engineering of the design process can also be evaluated. An in-depth understanding of the mechanisms that operate at nanoscale, obtained using in situ synchrotron radiation and neutron experimentation, will be critical to generate the knowledge required for the reliable application of NMs in engineering applications and an interesting study to undertake. The awareness of nanodamage mechanisms is also needed as input in simulation models. A thorough risk assessment of nanosystems seems to suggest that they can offer a great solution in the future for waste treatment as well as environmental remediation at a global level.

## 18.7 Acknowledgment

The authors are thankful to DST Purse grant-II. Aashima is grateful to CSIR for Open Senior Research Fellowship (SRF).

## References

- [1] Masciangoli T, Zhang W. Environmental technologies at the nanoscale. *Environ Technol Environ Sci Technol* 2003;37(5):102A.
- [2] Keren K, Berman RS, Buchstab E, Sivan U, Braun E. DNA-templated carbon nanotube field-effect transistor. *Science* 2003;302:1380.
- [3] Taton TA. Nanostructures as tailored biological probes. *Trends Biotechnol* 2002;20(7):277.
- [4] Pankhurst QA, Connolly J, Jones SK, Dobson J. Applications of magnetic nanoparticles in biomedicine. *J Phys D: Appl Phys* 2003;36:167.
- [5] Adelye SA, Conway JR, Garner K, Huang Y, Su Y, Keller AA. Engineered nanomaterials for water treatment and remediation: costs, benefits, and applicability. *Chem Eng J* 2003;286:640.
- [6] Prasad R, Kumar V, Prasad KS. Nanotechnology in sustainable agriculture: present concerns and future aspects. *Afr J Biotechnol* 2014;13:705.

- [7] Gogos A, Knauer K, Bucheli TD. Nanomaterials in plant protection and fertilization: current state, foreseen applications, and research priorities. *J Agric Food Chem* 2012;60:9781.
- [8] Savage N, Diallo MS. Nanomaterials and water purification: opportunities and challenges. *J Nanopart Res* 2005;7:331.
- [9] Liga MV, Bryant EL, Colvin VL, Li Q. Virus inactivation by silver doped titanium dioxide nanoparticles for drinking water treatment. *Water Res* 2011;45(2):535.
- [10] Deedar N, Irfan A, Ishtiaq AQ. Evaluation of the adsorption potential of titanium dioxide nanoparticles for arsenic removal. *J Environ Sci* 2009;21:402.
- [11] Choi H, Antoniou MG, Delacruz AA, Stathatos E, Dionysiou DD. Photocatalytic TiO<sub>2</sub> films and membranes for the development of efficient wastewater treatment and reuse systems. *Desalination* 2006;202:199.
- [12] Giammar DE, Maus CJ, Xie LY. Effects of particle size and crystalline phase on lead adsorption to titanium dioxide nanoparticles. *Environ Eng Sci* 2007;24:85.
- [13] Srisithirakul C, Pongsorarith V, Intasanta N. The potential use of nanosilver-decorated titanium dioxide nanofibers for toxin decomposition with antimicrobial and self-cleaning properties. *Appl Surf Sci* 2011;257:8850.
- [14] Sa J, Aguera CA, Gross S, Anderson JA. Photocatalytic nitrate reduction over metal modified TiO<sub>2</sub>. *Appl Catal, B* 2009;85:192.
- [15] Rengaraj S, Li XZ. Enhanced photocatalytic activity of TiO<sub>2</sub> by doping with Ag for degradation of 2,4,6-trichlorophenol in aqueous suspension. *J Mol Catal A: Chem* 2006;243:60.
- [16] Moore AM, Deleon CH, Young TM. Rate and extent of aqueous perchlorate removal by iron surfaces. *Environ Sci Technol* 2003;37:3189.
- [17] Bezbaruaha AN, Krajangpana S, Chisholmb BJ, Khana E, Bermudez JJ. Entrapment of iron nanoparticles in calcium alginate beads for groundwater remediation applications. *J Hazard Mater* 2009;166:1339.
- [18] Shin S, Jang J. Thiol containing polymer encapsulated magnetic nanoparticles as reusable and efficiently separable adsorbent for heavy metal ions. *Chem Commun* 2007;4230.
- [19] Yantasee W, Warner CL, Sangvanich T, Addleman RS, Carter TG, Wiacek RJ, et al. Removal of heavy metals from aqueous systems with thiol functionalized superparamagnetic nanoparticles. *Environ Sci Technol* 2007;41:5114.
- [20] Hu J, Lo IMC, Chen GH. Performance and mechanism of chromate (VI) adsorption by  $\delta$ -FeOOH-coated maghemite ( $\gamma$ -Fe<sub>2</sub>O<sub>3</sub>) nanoparticles. *Sep Purif Technol* 2007;58:76.
- [21] Afkhami A, Norooz-Asl R. Removal, preconcentration and determination of Mo(VI) from water and wastewater samples using maghemite nanoparticles. *Colloids Surf, A* 2009;346:52.
- [22] Girginova PI, Daniel-da-Silva AL, Lopes CB, Figueira P, Otero M, Amaral VS, et al. Silica coated magnetite particles for magnetic removal of Hg<sup>2+</sup> from water. *J Colloid Interface Sci* 2010;345:234.
- [23] Tsai CH, Chang WC, Saikia D, Wu CE, Kao HM. Functionalization of cubic mesoporous silica SBA-16 with carboxylic acid via one-pot synthesis route for effective removal of cationic dyes. *J Hazard Mater* 2016;309:236.
- [24] Son WJ, Choi JS, Ahn W-S. Adsorptive removal of carbon dioxide using polyethyleneimine-loaded mesoporous silica materials. *Microporous Mesoporous Mater* 2008;113:31.
- [25] Leal O, Bolívar C, Ovalles C, García JJ, Espidel Y. Reversible adsorption of carbon dioxide on amine surface-bonded silica gel. *Inorg Chim Acta* 1995;240:183.

- [26] Kouketsu T, Duan S, Kai T, Kazama S, Yamada K. PAMAM dendrimer composite membrane for CO<sub>2</sub> separation: formation of a chitosan gutter layer. *J Membr Sci* 2007;287:51.
- [27] Tungtittiplakorn W, Lion LW, Cohen C, Kim JY. Engineered polymeric nanoparticles for soil remediation. *Environ Sci Technol* 2004;38:1605.
- [28] Sugunan A, Thanachayanont C, Dutta J, Hilborn JG. Heavy-metal ion sensors using chitosan-capped gold nanoparticles. *Sci Technol Adv Mater* 2005;6:335.
- [29] Hyung H, Fortner JD, Hugues JB, Kim JH. Antimicrobial nanomaterials for water disinfection and microbial control: potential applications and implications. *Env Sci Technol* 2007;41:179.
- [30] Koo Y, Littlejohn G, Collins B, Yun Y, Shanov VN, Schulz M, et al. Synthesis and characterization of Ag–TiO<sub>2</sub>–CNT nanoparticle composites with high photocatalytic activity under artificial light. *Compos Part B: Eng* 2014;57:105.
- [31] Silva CG, Faria JL. Photocatalytic oxidation of phenolic compounds by using a carbon nanotube-titanium dioxide composite catalyst. *ChemSusChem* 2010;3:609.
- [32] Dalt SD, Alves AK, Bergmann CP. Photocatalytic degradation of methyl orange dye in water solutions in the presence of MWCNT/TiO<sub>2</sub> composites. *Mater Res Bull* 2013;48:1845.
- [33] Sampaio MJ, Silva CG, Marques RRN, Silva AMT, Faria JL. Carbon nanotube–TiO<sub>2</sub> thin films for photocatalytic applications. *Catal Today* 2011;161:91.
- [34] Chen C, Hu J, Shao D, Li J, Wang X. Adsorption behavior of multiwall carbon nanotube/iron oxide magnetic composites for Ni(II) and Sr(II). *J Hazard Mater* 2009;164:923.
- [35] Hadjar H, Hamdi B, Ania CO. Adsorption of p-cresol on novel diatomite/carbon composites. *J Hazard Mater* 2011;188:304.
- [36] Huguet MR, Marshall WD. Reduction of hexavalent chromium mediated by micro- and nano-sized mixed metallic particles. *J Hazard Mater* 2009;169:1081.
- [37] Tennakone K, Kottegoda IRM. Photocatalytic mineralization of paraquat dissolved in water by TiO<sub>2</sub> supported on polythene and polypropylene films. *J Photochem Photobiol* 1996;93:79.
- [38] Qian Y, Chi L, Zhou W, Yu Z, Zhang Z, Zhang Z, et al. Fabrication of TiO<sub>2</sub>-modified polytetrafluoroethylene ultrafiltration membranes via plasma-enhanced surface graft pretreatment. *Appl Surf Sci* 2016;360:749.
- [39] Ratnayake SY, Ratnayake AK, Schild D, Maczka E, Jartych E, Luetzenkirchen J, et al. Chemical reduction of nitrate by zerovalent iron nanoparticles adsorbed radiation-grafted copolymer matrix. *NUKLEONIKA* 2017;62(4):269.
- [40] Wang DS, Zhang J, Luo Q, Guo R, Li XY, Duan Y, et al. Characterization and photocatalytic activity of poly(3-hexylthiophene)-modified TiO<sub>2</sub> for degradation of Methyl orange under visible light. *J Hazard Mater* 2009;169:546.
- [41] Yew SP, Tang HY, Sudesh K. Photocatalytic activity and biodegradation of polyhydroxybutyrate films containing titanium dioxide. *Polym Degrad Stab* 2006;91:1800.
- [42] Wang Q, Qian HJ, Yang YP, Zhang Z, Naman C, Xu X. Reduction of hexavalent chromium by carboxymethyl cellulose-stabilized zero-valent iron nanoparticles. *J Contam Hydrol* 2010;114:35.
- [43] Xu X, Wang Q, Choi H, Kim YH. Encapsulation of iron nanoparticles with PVP nanofibrous membranes to maintain their catalytic activity. *J Membr Sci* 2010;348:231.
- [44] Xu X, Zhou H, He P, Wang D. Catalytic dechlorination kinetics of p-dichlorobenzene over Pd/Fe catalysts. *Chemosphere* 2005;58(8):1135.



- [45] Ismail M, Gul S, Khan MI, Khan MA, Asiri AM, Khan SB. Green synthesis of zerovalent copper nanoparticles for efficient reduction of toxic azo dyes congo red and methyl orange. *Green Process Synth* 2019;8:135.
- [46] Tee YH, Gurlke E, Bhattacharyya D. Role of Ni/Fe nanoparticle composition on the degradation of trichloroethylene from water. *Ind Eng Chem Res* 2005;44:7062.
- [47] Ren W, Zhou Z, Irudayaraj JM. Trichloroethylene sensing in water based on SERS with multifunctional Au/TiO<sub>2</sub> core-shell nanocomposites. *Analyst* 2015;140:6625.
- [48] He YT, Traina SJ. Cr(VI) Reduction and immobilization by magnetite under alkaline pH conditions: the role of passivation. *Environ Sci Technol* 2005;39:4499.
- [49] Martin BD, Parsons SA, Jefferson B. Removal and recovery of phosphate from municipal wastewaters using a polymeric anion exchanger bound with hydrated ferric oxide nanoparticles. *Water Sci Technol* 2009;60(10):2637.
- [50] Cumbal L, Sengupta AK. Arsenic removal using polymer-supported hydrated iron(III) oxide nanoparticles: role of Donnan membrane effect. *Environ Sci Technol* 2005;39:6508.
- [51] Pan BC, Wan SL, Zhang SJ, Guo QW, Xu ZC, Lv L, et al. Recyclable polymer-based nano-hydrous manganese dioxide for highly efficient Ti(I) removal from water. *Sci China Chem* 2014;57:763.
- [52] Rocher V, Siaugue JM, Cabuil V, Bee A. Removal of organic dyes by magnetic alginate beads. *Water Res* 2008;42:1290.
- [53] Gu F, Yin X, Yu H, Wang P, Tong L. Polyaniline/polystyrene single-nanowire devices for highly selective optical detection of gas mixtures. *Opt Express* 2009;17:11230.
- [54] Mikhaylov S, Ogurtsov N, Noskov Y, Redon N, Coddeville P, Wojkiewicz JL, et al. Ammonia/amine electronic gas sensors based on hybrid polyaniline–TiO<sub>2</sub> nanocomposites. The effects of titania and the surface active doping acid. *RSC Adv* 2015;5:20218.
- [55] Suri K, Annapoomi S, Sarkar AK, Tandon RP. Gas and humidity sensors based on iron oxide–polypyrrole nanocomposites. *Sens Actuators B: Chem* 2002;81:277.
- [56] Athawale AA, Bhagwat SV, Katre PP. Nanocomposite of Pd–polyaniline as a selective methanol sensor. *Sens Actuators B: Chem* 2006;114:263.
- [57] Forzani ES, Zhang H, Chen W, Tao N. Detection of heavy metal ions in drinking water using a high-resolution differential surface plasmon resonance sensor. *Environ Sci Technol* 2005;39:1257.
- [58] Chen L, Ji T, Mu L, Shi Y, Brisbin L, Guo Z, et al. Facile synthesis of mesoporous carbon nanocomposites from natural biomass for efficient dye adsorption and selective heavy metal removal. *RSC Adv* 2016;6:2259.
- [59] Zhu S, Jiao S, Liu Z, Pang G, Feng S. High adsorption capacity for dye removal by CuZn hydroxyl double salts. *Environ Sci Nano* 2014;1:172.
- [60] Chen MY, Lee DJ, Ren NQ. Degradation of phenol by acinetobacter strain isolated from aerobic granules. *Chemosphere* 2007;67:1566.
- [61] Lewis D, Gattie D. Pathogen risks from applying sewage sludge to land. *Environ Sci Technol* 2002;36:286.
- [62] Al-Ghouthi MA, Khraisheh MAM, Allen SJ, Ahmad MN. The removal of dyes from textile wastewater: a study of the physical characteristics and adsorption mechanisms of diatomaceous earth. *J Environ Manage* 2003;69:229.
- [63] Nasiria J, Motamedib E, Naghavia MR, Ghafooria M. Removal of crystal violet from water using  $\beta$ -cyclodextrin functionalized biogenic zero-valent iron nanoadsorbents synthesized via aqueous root extracts of *Ferula persica*. *J Hazard Mater* 2019;36:325.



- [64] Hua Y, Xiao J, Zhang Q, Cui C, Wang C. Facile synthesis of surface-functionalized magnetic nanocomposites for effectively selective adsorption of cationic dyes. *Nanoscale Res Lett* 2018;13:99.
- [65] Chaudhary S, Sharma P, Singh D, Umar A, Kumar R. Chemical and pathogenic cleanup of wastewater using surface-functionalized CeO<sub>2</sub> nanoparticles. *ACS Sustain Chem Eng* 2017;5:6803.
- [66] Bhagya NP, Prashanth PA, Raveendra RS, Sathyanarayani S, Ananda S, Nagabhushana BM, et al. Adsorption of hazardous cationic dye onto the combustion derived SrTiO<sub>3</sub> nanoparticles: kinetic and isotherm studies. *J Asian Ceram Soc* 2016;4:68.
- [67] Huang CC, Chang HT. Parameters for selective colorimetric sensing of mercury(II) in aqueous solutions using mercaptopropionic acid-modified gold nanoparticles. *Chem Commun* 2007;0:1215.
- [68] Mohmood I, Lopes CB, Lopes I, Tavares DS, Soares AMVM, Duarte AC, et al. Remediation of mercury contaminated saltwater with functionalized silica coated magnetite nanoparticles, *Sci Total Environ* 2016;557–558:712.
- [69] Satapathi S, Kumar V, Chini MK, Rajesh B, Halder KK, Patra A. Highly sensitive detection and removal of mercury ion using multimodal nanosensor. *Nano-Structures Nano-Objects* 2018;16:120.
- [70] Morsi RE, Al-Sabagh AM, Moustafa YM, ElKholy SG, Sayed MS. Polythiophene modified chitosan/magnetite nanocomposites for heavy metals and selective mercury removal. *Egypt J Pet* 2018;27:1077.
- [71] Bolívar WM, Benítez LT, Herrera AP. Removal of mercury (II) from water using magnetic nanoparticles coated with amino organic ligands and yam peel biomass. *Environ Nanotechnol Monit Manag* 2018;10:486.
- [72] Wang H, Yu YF, Chen QW, Cheng K. Carboxyl-functionalized nanoparticles with magnetic core and mesopore carbon shell as adsorbents for the removal of heavy metal ions from aqueous solution. *Dalton Trans* 2011;40:559.
- [73] Hashemzadeh M, Nilchi A, Hassani AH. Synthesis of novel surface-modified hematite nanoparticles for lead ions removal from aqueous solution. *Mater Chem Phys* 2019;227:279.
- [74] Perez T, Pasquini D, Lima ADF, Rosa EV, Sousa MH, Cerqueira DA, et al. Efficient removal of lead ions from water by magnetic nanosorbents based on manganese ferrite nanoparticles capped with thin layers of modified biopolymers. *J Environ Chem Eng* 2019;7:102892.
- [75] He Y, Luo L, Liang S, Long M, Xu H. Synthesis of mesoporous silica-calcium phosphate hybrid nanoparticles and their potential as effective adsorbent for cadmium ions removal from aqueous solution. *J Colloid Interface Sci* 2018;9797(18):30422.
- [76] Zhu Q, Tao F, Pan QM. Fast and selective removal of oils from water surface via highly hydrophobic core-shell Fe<sub>2</sub>O<sub>3</sub> @C nanoparticles under magnetic field. *ACS Appl Mater Interface* 2010;2:3141.
- [77] Vidal-Vidal J, Rivas J, López-Quintela M,A. Synthesis of monodisperse maghemite nanoparticles by the microemulsion method. *Colloid Surf A* 2006;288:44.
- [78] Raj KG, Joy PA. Coconut shell based activated carbon-iron oxide magnetic nanocomposite for fast and efficient removal of oil spills. *J Environ Chem Eng* 2015;3:2068.
- [79] Dibrov P, Dzioba J, Khoosheh K, Hase C. Chemiosmotic mechanism of antimicrobial activity of Ag<sup>+</sup> in *Vibrio cholera*. *J Antimicrob Agents Chemother* 2002;46:2668.

- [80] Biao L, Tan S, Wang Y, Guo X, Fua Y, Xu F, et al. Synthesis, characterization and anti-bacterial study on the chitosan-functionalized Ag nanoparticles. *Mater Sci Eng C* 2017;76:73.
- [81] Shahverdi A, Fakhimi A, Shahverdi H, Minaian S. Synthesis and effect of silver nanoparticles on the antibacterial activity of different antibiotics against *Staphylococcus aureus* and *Escherichia coli*. *Nanomedicine* 2007;3:168.
- [82] Alama T, Khanb RAA, Alic A, Sherc H, Ullah Z, Ali M. Biogenic synthesis of iron oxide nanoparticles via *Skimmia laureola* and their antibacterial efficacy against bacterial wilt pathogen *Ralstonia solanacearum*. *Mater Sci Eng C* 2019;98:101.
- [83] Buoli M, Grassi S, Caldiroli A, Carnevali GS, Mucci F, Iodice S, et al. Is there a link between air pollution and mental disorders? *Environ Int* 2018;118:154.
- [84] Yu BF, Hu ZB, Liu M, Yang HL, Kong QX, Liu YH. Review of research on air-conditioning systems and indoor air quality control for human health. *Int J Refrig* 2009;32:3.
- [85] Zeng M, Li Y, Mao M, Bai J, Ren L, Zhao X. Synergetic effect between photocatalysis on TiO<sub>2</sub> and thermocatalysis on CeO<sub>2</sub> for gas-phase oxidation of benzene on TiO<sub>2</sub>/CeO<sub>2</sub> nanocomposites. *ACS Catal* 2015;5:3278.
- [86] Abadi MBH, Shirkhanloo H, Rakhtshah J. Air pollution control: the evaluation of TerphApm@MWCNTs as a novel heterogeneous sorbent for benzene removal from air by solid phase gas extraction. *Arab. J. Chem* 2020;13:1741.
- [87] Kibanova D, Cervini-Silva J, Destailats H. Efficiency of clay-TiO<sub>2</sub> nanocomposites on the photocatalytic elimination of a model hydrophobic air pollutant. *Environ Sci Technol* 2009;43:1500.
- [88] Majhi SM, Naik GK, Lee HJ, Song HG, Lee CR, Lee IH, et al. Au@NiO core-shell nanoparticles as a P-type gas sensor: novel synthesis, characterization, and their gas sensing properties with sensing mechanism. *Sens Actuator B Chem* 2018;268:223.
- [89] Zhao R, Li K, Wang Z, Xing X, Wang Y. Gas-sensing performances of Cd-doped ZnO nanoparticles synthesized by a surfactant-mediated method for n-butanol gas. *J Phys Chem Solids* 2018;112:43.
- [90] Singh N, Umar A, Singh N, Fouad H, Alothman OY, Haque FZ. Highly sensitive optical ammonia gas sensor based on Sn doped V<sub>2</sub>O<sub>5</sub> nanoparticles. *Mater Res Bull* 2018;108:266.
- [91] Tripathi V, Fraceto LF, Abhilash PC. Sustainable clean-up technologies for soils contaminated with multiple pollutants: plant-microbe-pollutant and climate nexus. *Ecol Eng* 2015;82:330.
- [92] Hughes DL, Afsar A, Laventine DM, Shaw EJ, Harwood LM, Hodson ME. Metal removal from soil leachates using DTPA functionalised maghemite nanoparticles, a potential soil washing technology. *Chemosphere* 2018;209:480.
- [93] Lago AD, Seijo AR, Vila ML, Couce A, Vega FA. Using Ca<sub>3</sub>(PO<sub>4</sub>)<sub>2</sub> nanoparticles to reduce metal mobility in shooting range soils. *Sci Total Environ* 2016;571:1136.
- [94] Lien HL, Zhang W. Hydrochlorination of chlorinated ethanes by nanoscale Pd/Fe bimetallic particles. *J Environ Eng* 2005;131:4.
- [95] McCormick ML, Adriaens P. Carbon tetrachloride transformation on the surface of nano-scale biogenic magnetite nanoparticles. *Environ Sci Technol* 2004;38:1045.
- [96] Ai Z, Gao Z, Zhang L, He W, Yin JJ. Core-shell structure dependent reactivity of Fe@Fe<sub>2</sub>O<sub>3</sub> nanowires on aerobic degradation of 4-chlorophenol. *Environ Sci Technol* 2013;47:5344.

- [97] Qian Y, Zhang J, Zhang Y, Chen J, Zhou X. Degradation of 2,4-dichlorophenol by nano-scale calcium peroxide: implication for groundwater remediation. *Sep Purif Technol* 2016;166:222.
- [98] Singh R, Misra V, Mudiam MKR, Chauhan LKS, Singh RP. Degradation of HCH spiked soil using stabilized Pd/Fe<sup>0</sup> bimetallic nanoparticles: pathways, kinetics and effect of reaction conditions. *J Hazard Mater* 2012;237–238:355.
- [99] Li Z, Yuan S, Wan J, Long H, Tong M. A combination of electrokinetics and Pd/Fe PRB for the remediation of pentachlorophenol-contaminated soil. *J Contam Hydrol* 2011;124:99.
- [100] Yuan S, Long H, Xie W, Liao P, Tong M. Electrokinetic transport of CMC-stabilized Pd/Fe nanoparticles for the remediation of PCP-contaminated soil. *Geoderma* 2012;185:18.
- [101] Fan G, Cang L, Qin W, Zhou C, Gomes HI, Zhou D. Surfactants-enhanced electrokinetic transport of xanthan gum stabilized nanoPd/Fe for the remediation of PCBs contaminated soils. *Sep Purif Technol* 2013;114:64.
- [102] Soler L, Magdanz V, Fomin VM, Sanchez S, Schmidt OG. Self-propelled micromotors for cleaning polluted water. *ACS Nano* 2013;7(11):9611.
- [103] Assis GCD, Skovroinski E, Leite VD, Rodrigues MO, Galembeck A, Alves MCF, et al. Conversion of “waste plastic” into photocatalytic nanofoams for environmental remediation. *ACS Appl Mater Interfaces* 2018;10(9):8077.

## Section 6

# **Functionalized nanomaterial in surfaces and coatings (consumer products)**

This page intentionally left blank

# Natural-based consumer health nanoproducts: medicines, cosmetics, and food supplements

Ana Henriques Mota<sup>1</sup>, Alexandra Sousa<sup>1</sup>, Mariana Figueira<sup>1</sup>, Mariana Amaral<sup>1</sup>, Bruno Sousa<sup>2,3</sup>, João Rocha<sup>1</sup>, Elias Fattal<sup>4</sup>, António José Almeida<sup>1</sup> and Catarina Pinto Reis<sup>1,5</sup>

<sup>1</sup>iMEDULisboa, Research Institute for Medicines, Faculty of Pharmacy, Avenida Prof. Gama Pinto, Universidade de Lisboa, Lisboa, Portugal, <sup>2</sup>ULHT, Lisboa, Portugal, <sup>3</sup>Health Service of the Autonomous Region of Madeira, Funchal, Portugal, <sup>4</sup>Institut Galien Paris-Sud, Faculté de Pharmacie, Université Paris-Saclay, Malabry, France, <sup>5</sup>IBEB, Biophysics and Biomedical Engineering, Faculty of Sciences, Universidade de Lisboa, Campo Grande, Lisboa, Portugal

## 19.1 Natural sources

In recent years, interest in plants or parts of plants (roots, leaves, flowers, and fruits) has been increasing due to their biologically active compounds and subsequent use in the pharmaceutical, cosmetic, and food industries [1]. The use of plant-based products has advantages, such as being safe and having low cost, having efficiency to prevent or to help in treatment of some diseases, and helping to maintain good health, as this is the case for cosmetics and food supplements [2,3]. These advantages and their easy accessibility have led to their widespread use by a great part of population (mainly for a primary health care) [3,4]. In fact, a large number of natural products are obtained from parts of plants (e.g., fruits and leaves, due to their abundance in phytochemical compounds) [5].

Natural products appear to play an important role in photo-aging prevention and management (e.g., green tea, olive oil, soy, and coffee berry). The topical application of antioxidants (e.g., vitamins C and E) have shown to provide efficient protection of skin against UV-mediated damage, as was reported in a study by Mota *et al.* [2]. Some studies suggest a correlation between the polyphenol content with antioxidant activity (AA) and reduction

in skin damage caused by sun exposure and pollution, among other aggressors. In addition, natural products were shown to play a key role against some diseases due to their potential in modulating human metabolism, being useful for prevention of chronic and degenerative disorders [5,6]. Among such phytochemicals, monoterpenoids, diterpenoids, triterpenoids, sesquiterpenoids, phenolics, flavonoids, esters, alcohols, aldehydes, alkaloids, and tannins are described in literature as the most important bioactive plant extracts [3,7,8]. Table 19.1 shows some examples of plants used in traditional medicine and/or phytotherapy.

Moreover, some of these phytochemicals are already being studied in combination with nanotechnology approaches (Table 19.2).

## 19.2 Nanotechnology in medicines

Nanotechnology has become an excellent platform with many applications in different fields of science, allowing to control and manipulate matter at the nanoscale by designing and engineering new systems [86,87]. The application of nanotechnology for medical purposes is called nanomedicine.



Nanomedicine uses selective targeting technologies to define where the drug should be released. The main goal is to obtain complex molecular particles with functional properties for medical application. Beyond that, nanomedicine promises control over physical and chemical processes and their intensification and enhancement in precision [88]. It includes nanopharmaceuticals, nanodiagnostics, nanotheranostics, and nanobiomaterials [88–92]. Today, nanopharmaceuticals represent 75% of the market share of approved nanomedicines [92].

According to the European Medicines Agency (EMA), nanopharmaceuticals are systems designed for clinical applications with at least one component at the nanoscale, resulting in reproducible properties and characteristics for a specific route of administration and dose, and associated with the clinical advantages of nanoengineering [89]. There are underlying criteria for a drug to be classified as a nanomedicine. Nanoengineering is required to play a role in the manufacturing process and the nanomaterial used must be essential for its therapeutic purpose or provide advantageous characteristics to it [93].

Nanotechnology offers many advantages including integrating molecules that otherwise could not be used due to their toxicity; exploiting multiple mechanisms of action, maximizing efficacy and reducing dose and toxicity; providing drug targeting, controlled, and site-specific release; favoring a preferential distribution within the body; and improved transport across biological barriers [89].

Nanomaterials have different properties when compared with big-scale materials, giving them some advantages. Many biological mechanisms in the human body work at the nanoscale, making nanopharmaceuticals effective when crossing natural barriers, entering new tissues, and interacting with





**TABLE 19.1** Some examples of plants used in traditional medicine and/or phytotherapy.





Plant	Major Compounds	Main properties	Uses	References
<p><i>Sambucus nigra</i></p> 	<p><math>\alpha</math>-terpineol, lectin, anthocyanins, flavonols, and phenolic acids.</p>	<p>Cardiovascular, anti-inflammatory, immune-stimulatory, diaphoretic and hemostatic.</p>	<p>Cancer, diabetes, feverish catarrhal affections, laxative, purgative, against cold, coughs, flu, insect repellent, analgesic, sedative effects, antihemorrhoid, antiprotozoa, antibacterial, burns, infected wounds, oedema, eczema, colic, diarrhea, bronchitis, sinusitis, chronic nasal catarrh, neuralgia, sciatica, and rheumatism.</p>	<p>[9–18]</p>
<p><i>Plectranthus amboinicus</i></p> 	<p>Monoterpenes, sesquiterpenes, 3-methyl-4-isopropyl phenol, carvacrol, squalene, (Z)-caryophyllene, carvacrol, and flavonoids.</p>	<p>Anti-inflammatory, bronchodilator, antiviral, antifungal, antileptospiral, nephroprotective, antioxidant, and antiaging.</p>	<p>Dyspepsia, indigestion, diarrhea, carminative, burns, wounds, sores, insect bites, allergies, furuncles, antidandruff, cuts, skin allergy, superficial mycoses, diaper rash, itching, antiseptic dressing, ulcerations (<i>Leishmania braziliensis</i>), chronic coughs, asthma, bronchitis, catarrhal infections, sore, relieve kidney troubles, treat vaginal discharges, stiff neck, antimicrobial infections, antiviral infections, and pain.</p>	<p>[3,19–29]</p>

(Continued)







**TABLE 19.1 (Continued)**




Plant	Major Compounds	Main properties	Uses	References
<i>Plectranthus barbatus</i> 	Eugenol, (Z)-caryophyllene, germacrene D, thymol, viridiflorol, carvacrol, $\beta$ -caryophyllene, cyclosativene, 1,2 $\alpha$ -copaene, $\alpha$ -pinene, forskolin, rosmarinic acid, luteolin, and apigenin.	Acetylcholinesterase inhibitor, antidyspeptic, antiulcerous, antiaging, anti-inflammatory, antibacterial, antiviral, antifungal, cytotoxic and antitumor promoting activity.	Glaucoma, prostatism, hypertension, aid for weight loss, inotropic action in myocardium, gastritis, intestinal spasms, teeth and gum disorders, nausea, liver complaints, burns, wounds, and ringworms.	<a href="#">[22,23,25,29–37]</a>
<i>Plectranthus ecklonii</i> 	Rosmarinic acid, parvifloron D (PvD), sugiol, $\beta$ -sitosterol, stigmasterol, ursolic acid, oleanolic acids, and flavones.	Acetylcholinesterase inhibitor, antioxidant, and antibacterial.	Skin infections and cancer.	<a href="#">[38–42]</a>
<i>Plectranthus fruticosus</i> 	Apigenin-7-4'-dimethyl ether, genkwanin, salvigenin, cirsimaritin, eupatorine, ursolic acid, and oleanolic acid.	Healing.	Burns.	<a href="#">[29,41,43]</a>
<i>Plectranthus hadiensis</i> 	Flavonoids, alkaloids, phenols, tannins, proteins, carbohydrates, saponins, glycosides, cardiac glycosides, phenol acids, and quercetin.	Antioxidant and antimicrobial.	Antiseptic, hemostatic, digestive disorders, skin and respiratory diseases.	<a href="#">[4,7,22,29,44]</a>

<p><i>Plectranthus hereroensis</i></p> 	<p>Horminone and abietane diterpenoids.</p>	<p>Antimicrobial.</p>	<p>Digestive disorders.</p>	<p>[29,45,46]</p>
<p><i>Plectranthus madagascarensis</i></p> 	<p>Rosmarinic acid, Abietanes, and coleon U quinone.</p>	<p>Antibacterial and insect antifeedant.</p>	<p>Scabies, small wounds, colds, cough, chest complaints and asthma.</p>	<p>[29,31,47,48]</p>
<p><i>Plectranthus strigosus</i></p> 	<p>Parvifloron D, ferulic acid, fatty alcohols, fatty acids, salvigenin, ursolic acid, parvifloron F, and hinokiol.</p>	<p>Anti-inflammatory, antioxidant, antitumor, and hepatoprotective.</p>		<p>[49–51]</p>
<p><i>Ananas comosus</i></p> 	<p>Bromelain, L-ascorbic acid, carotenoids, citric acid, malic acid, tartaric acid, ferulic acid, and chlorogenic acid.</p>	<p>Anti-inflammatory, antioxidant, and anticancer.</p>	<p>Skin's wound healing, oedema, bruising and pain.</p>	<p>[1,52–54]</p>




(Continued)



**TABLE 19.1 (Continued)**

Plant	Major Compounds	Main properties	Uses	References
<i>Corylus avellane</i> 	Phenols, tannins, flavan-3-ols, flavonoids, and gallic acid.	Antioxidant, astringent, vasoprotective, antimicrobial, and antioedema.	Hemorrhoids, varicose veins, phlebitis and oedema.	<a href="#">[55–57]</a>
<i>Rosmarinus officinalis</i> 	1,2-cineole, $\alpha$ -pinene, apigenin, botulin, betulinic acid, caffeic acid, camphor, carnosic acid, limonene, thymo,l and ursolic acid.	Antioxidant, antibacterial, antifungal, antimutagenic, anti-inflammatory, antidiabetic, neuroprotective, antineuropathic, and cardioprotective.	Antispasmodic, inflammatory diseases, atherosclerosis, ischemic heart disease, and diabetes.	<a href="#">[50,58–61]</a>
<i>Olea europaea</i> 	Triglycerides, $\alpha$ -tocopherol, carotenoids, squalene, oleic acid, linoleic acid, and linolenic acid.	Antioxidant.	Acne, psoriasis, seborrhea, photo-aging, and eczema.	<a href="#">[2,62]</a>
<i>Matricaria chamomilla</i> 	$\alpha$ -bisabolol, apigenin, luteolin, patuletin, and quercetin.	Anti-inflammatory, antiphlogistic, antiseptic, analgesic, antioxidant, antiparasitic, anticancer, immunoregulatory, thrush, mucositis, gingivitis, antimicrobial.	Inflamed skin sunburn, rashes, and eye inflammations.	<a href="#">[63–65]</a>

<p><i>Mentha piperita</i></p> 	<p>Menthol menthone limonene <math>\beta</math>-pinene eucalyptol rosmarinic acid cinnamic acid and caffeic acid.</p>	<p>Carminative, gastric stimulant, analgesic, anaesthetic, antiseptic, antispasmodic, mentally stimulant, vasoconstrictive, decongestant, and expectorant.</p>	<p>[66–68]</p>
<p><i>Castanea sativa</i></p> 	<p>Castalagin, vescalagin, castalin, vescalin, glucosidic tannins, rutin, quercetin, apigenin, oleic acid, linoleic acid, and palmitic acid.</p>	<p>Antioxidant and anti-inflammatory.</p>	<p>[8,69,70]</p>
<p><i>Ficus carica</i></p> 	<p>Phenolics, vitamin E, and anthocyanins.</p>	<p>Antioxidant, antimutagenic, anti-inflammatory and antimicrobial.</p>	<p>[35,71–73]</p>
<p>(Continued)</p>			

**TABLE 19.1** (Continued)

Plant	Major Compounds	Main properties	Uses	References
<i>Aloe Vera</i> 	Salicylic acid, anthraquinones, and arachidonic acid.	Anti-inflammatory, antiseptic, and antibacterial.	Arthritis, asthma, candida, chronic fatigue syndrome, atonic constipation, irritable bowel syndrome, Crohn's disease, ulcerative colitis, lupus erythematoses, eczema, psoriasis, acne, burns, athlete's foot, cold sores, frostbite sports injuries, gout, constipation, and ulcers.	<a href="#">[74–77]</a>
<i>Curcuma longa</i> 	Curcumin.	Anticancer, therapeutic for Alzheimer's disease.	Hangovers, erectile dysfunction, baldness, hirsutism, fertility booster, and contraceptive.	<a href="#">[78,79]</a>
<i>Vitis vinifera</i> 	Resveratrol.	Anticancer, cardioprotective, neuroprotective, and antioxidant.		<a href="#">[80,81]</a>

<p><i>Solanum lycopersicum</i></p> 	<p>Lycopene.</p>	<p>Antioxidant, prostatic hyperplasia, prostate cancer, atherosclerosis, acute and chronic coronary syndromes, male fertility, osteoporosis, and radiation protection.</p>		<p><a href="#">[82]</a></p>
<p><i>Vaccinium</i> ssp.</p> 	<p>Ascorbic acid flavonoids, procyanidins, kaempferol, quercetin, myricetin, and phenolic acids.</p>	<p>Anti-inflammatory, anticarcinogenic, and antioxidant.</p>	<p>Diminish the risk of coronary diseases, atherosclerosis.</p>	<p><a href="#">[83]</a></p>

**TABLE 19.2** Some examples of phytochemicals (extracts or isolated compounds) used in association with particulate carrier systems, including macro-, micro- and nanotechnology approaches.

Plant or compound	Macro-, micro- or nanoparticles (NPs)	Uses for	Year	References
<i>Plectranthus ecklonii</i> (rosmarinic and caffeic acids)	Beads	Acetylcholinesterase inhibitor and antioxidant.	2014	[41]
<i>Plectranthus madagascarensis</i> (rosmarinic acid)	Polymeric beads	Activity against <i>S. epidermidis</i> and Antioxidant.	2014	[84]
<i>Ananas comosus</i>	Silver NPs (AgNPs)	Antioxidant	2012	[52]
<i>Ananas comosus</i> (leaf extract)		Antimicrobial activity against <i>S. aureus</i> , <i>S. pneumoniae</i> , and <i>E. coli</i> .	2014	[85]
<i>Olea europaea</i> (olive oil)	Alginate beads	Acne, psoriasis, seborrhoea eczema, photoprotection, and hydration.	2018	[2]

them [91]. Due to their small size, nanomaterials have a high specific surface area in relation to volume. Consequently, nanomaterials are much more reactive and able to adsorb biomolecules when in contact with biological fluids [89].

Nanomedicine could potentially provide improved and cost-effective healthcare, allowing availability and affordability [91]. The advances in nanoscience and nanotechnology contributed to overcome the formulation problems of classical pharmaceutical systems [94].

### 19.2.1 Some key concepts

The term “nanoparticles” is a simplified way to refer to nanomaterials in general when no functionality of said nanomaterials is specified. Herein, NPs are considered three-dimensional, solid, submicron-sized drug delivery systems ranging from 1 to 1000 nm. They can interact with many functions in the cell and can be used as drug delivery systems, imaging agents, and photothermal probes, among others [87,95].

NPs are designed to maximize the benefit/risk ratio [91]. Besides improving the solubility and stability of active compounds, NPs can extend a formulation's action and successfully combine active substances with different degrees of hydrophilicity [91,94,96]. Their targeting abilities to deliver drugs directly to the affected organs and tissues are another advantage of these systems that can be used in medicine [94,97]. Drug delivery systems based on NPs can improve pharmacokinetics, bio-distribution, solubility and stability, controlled and targeted release, and site-specific delivery of therapeutic agents [98–101]. Nanocarriers can therefore improve the efficiency of drugs by changing body distribution, decreasing acute toxicity, and increasing their dissolution rate and *in vivo* stability concerning the risk of metabolism and degradation [94,96]. NPs offer several advantages including higher intracellular uptake, stability in biologic fluids since their size makes the preparations suitable for parenteral administration, and sustained release in a specific organ or target [102]. NPs can protect a drug from degradation and promote pharmacokinetic modification with absorption enhancement and distribution improvement [103,104].

However, there also are some challenges associated with nanomedicine. There is a need for a better characterisation and understanding of toxicity issues. The industry is still facing lack of specific regulation and the cost/benefit ratio needs to be considered and analysed in each case [97,105]. There also is a challenge in the scale-up of NPs manufacturing due to the variety of possible formulations and combinations of nanomaterials [105]. When it comes to toxicity, the wide range of possibilities for NPs composition and development is responsible for a variety of immune reactions that might not be desirable. Thus a balance should be obtained. It is required to



have NPs that can either improve drug delivery of therapeutic agents without resulting in toxicity or causing unwanted interactions with the immune system [106]. The major barrier with toxicological studies of nanopharmaceuticals is the absence of validated *in vitro* tests and reference standards [107].

For several years, the EMA and the US Food and Drug Administration (FDA) have been deciding on a “case-by-case” basis, regarding the approval of nanopharmaceuticals. For every specific formulation, an analysis of benefits and risk is generally made [107]. In 2006, the first regulatory reflection paper was prepared and published with information regarding essential aspects to take in account when developing nanopharmaceuticals for human use [107,108]. In 2009, EMA created a working group with the purpose of addressing quality, safety, and efficacy of nanopharmaceuticals—the European Nanomedicines Expert Group. Through this group, the EMA has been working along with the FDA and Japan’s regulatory entities (PDMA/MHLW) to achieve a common ground in the future of nanomedicine and its future perspectives [105,108]. Furthermore, an internationally agreed upon set of guidelines (Q8, Q9, Q10, Q11, and Q12) has been published by the International Council of Harmonization (ICH), which are being applied to the testing of pharmaceuticals and other products for human use [105,109].

Three generations of NPs can be identified. The first generation is the simple combination of a carrier and an active compound where the targeting is passive. The second generation can target a specific tissue or organ through antibodies and other molecules. The third generation is capable of more complex functions such as time-controlled release through different types of barriers and targets [88].

There are different types of NPs, divided in two main categories: organic and inorganic (Fig. 19.1). Organic NPs include polymeric NPs and lipid-based NPs; inorganic NPs include metallic NPs, ceramic NPs, and silica NPs. The clinically approved formulations include lipid NPs, metallic NPs, polymeric NPs, and protein NPs [90,104].

### 19.2.1.1 Lipid-based nanoparticles

Lipid NPs include liposomes, phytosomes, or ethosomes, and matrix-based nanostructured systems, such as solid lipid nanoparticles (SLNs), nanostructured lipid carriers (NLCs), and lipid–drug conjugates (LDCs), etc. [92].

Being administered through oral, parenteral, or topical routes, lipid NPs allow drug targeting and the delivery of poorly water-soluble molecules [110]. Lipid NPs have been reported to offer advantages compared to polymeric NPs, when it comes to biocompatibility and toxicity, cost and scalability, and encapsulation efficiency of lipophilic compounds [110].

Liposomes are spherical lipid vesicles of about 50–1000 nm. They appear to be an ideal drug delivery system due to their morphology being similar to cellular membranes (phospholipids and cholesterol) and due to

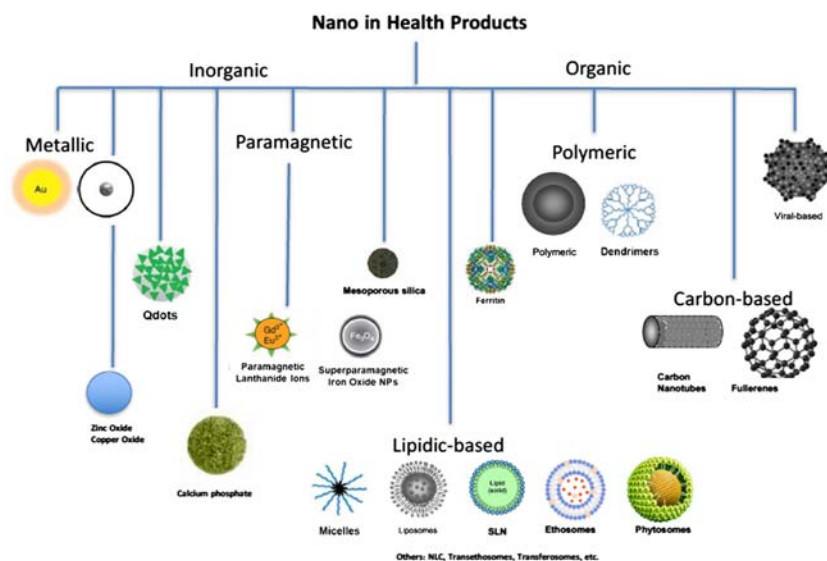


**FIGURE 19.1** Nanotechnology in health products.

their ability to incorporate biologically active compounds [87,111–113]. This characteristic provides biocompatibility and biodegradability, making them a safe choice as a drug delivery system [111,112]. In addition, their structure provides the entrapment of drugs having a wide range of molecular weights, which promotes versatility to their use [92,111,112]. Another important advantage is the protection guaranteed to the drug and to healthy tissue. The lipid bilayer protects the drug from enzymatic degradation and chemical inactivation, while minimizing exposure of healthy tissues to the encapsulated drug. Liposomes store, protect, and transfer substantial amount of drug, and are well tolerated in patients. It is therefore possible to obtain an improved biopharmaceutical profile with reduced toxicity, favorable pharmacokinetic behavior, and enhanced therapeutic effects [111]. Parenteral administration is the route that benefits the most from these characteristics but topical administration is also frequently used [87,111,112,114]. Currently, anticancer delivery and gene therapy are the main focuses of liposome formulations [87]. Besides conventional liposomes (mainly composed by phospholipids, phosphatidylcholine, and/or sphingomyelin), there are pH-sensitive liposomes, immune liposomes, and long circulating liposomes [112,114]. Each one of these categories includes different surface ligands or bilayer constituents specific for the required purpose [112]. It is also possible to make anionic and cationic liposomes. Anionic liposomes are less stable and more susceptible to opsonization by other side, cationic ones are generally used for gene delivery [111,112]. Liposomes offer a wide

protection to DNA as well as being able to carry amounts correspondent to chromosomes [112].

Other variables are taken into account to further categorize liposomes. Phytosomes, for example, come from an interaction between phospholipids with an extract or polyphenolic compounds, where the active herbal compounds remain protected within. As another category, ethosomes are lipid-based systems that due to their higher ethanol percentage can provide greater skin permeation [92,114]. Many others are arising, being the base mechanism and structure very similar to the well-known liposomes.

SNLs are colloidal particles composed of lipids solid at both room and body temperatures as a nucleus with an outer shell composed of an amphiphilic surfactant. With the same size range as liposomes, SLNs appear to be preferable since the mobility of the drug in a solid lipid matrix is lower than in a liquid one [92,115]. It is possible to encapsulate both hydrophilic and hydrophobic drugs while protecting them from degradation and allowing sustained release [92,115,116]. In addition, SLNs are biocompatible and biodegradable, provide increased drug stability, lack organic solvents, and are easy to scale-up [92,116]. Many classes of drugs have been considered for SLN delivery, such as antibacterial, antioxidant, anticancer, hormones, genetic material, and plant extracts with therapeutic uses, among others [92,115]. Vaccine delivery, drug targeting, and gene delivery are also successful uses [92]. Parenteral delivery remains the most common administration route used along with oral, ocular, and topical administrations [92,116]. NLCs were developed from SLNs with the addition of liquid lipids, and they appear to provide better drug loading, stability during storage, and drug release modulation [92,117].

### 19.2.1.2 Polymeric nanoparticles

Polymeric NPs are solid, submicron-sized drug carriers that may or may not be biodegradable. Their diameter is around 300 nm but when encapsulating drugs, the range can go from 1 to 1000 nm [99,102,114]. Having high surface-to-volume ratio, polymeric NPs show an ability to modify the bioactivity of drugs [99]. Polymeric NPs appear to be the simplest type of NPs due to their easy synthesis and wide applicability across all aspects of the field [118]. They allow better drug stability, specific targeting, and controlled release [87,119]. Depending on the physicochemical characteristics of the drug, it is possible to choose the best method and polymer for efficient entrapment of the drug [102].

Natural polymers such as chitosan, alginate, dextran, and proteins like albumin and gelatin, and synthetic polymers such as polylactic acid (PLA), copolymers of lactic and glycolic acid (PLGA) and poly- $\epsilon$ -caprolactone (PCL), among others, are often used to prepare polymeric NPs [87,92,114,120,121]. Sometimes, synthetic polymers are preferable to use

instead of natural polymers, which lack purity and often require cross-linking [87]. Nevertheless, both types can be biocompatible and biodegradable providing stability in many environments, slow release of the drug, and versatility in use [92,122]. Natural hydrophilic polymers have proved to be efficient when used for NPs production since they allow better drug-loading capacity, biocompatibility, and less opsonization [104]. Generally, synthetic polymers have more homogenous compositions and higher purity than natural polymers, which leads to a more reproducible preparation. Natural polymers have a higher variety in purity and require cross-linking and other modifications to improve stability [123].

Chitosan is a polysaccharide with unique mucoadhesive, antimicrobial, antiviral, immunoadjuvant, and potential antitumor properties [123]. It has been widely considered in drug delivery systems in the form of NPs as promising vehicles for oral drug sustained-release formulations [124]. The products of chitosan degradation are nontoxic, making them appropriate for drug delivery [123]. Beyond that, its mucoadhesive properties increase NPs uptake and prolong the retention time in targeted locations [125]. Some functional groups can also be chemically modified to improve particle properties.

Dextran and alginate also belong to the polysaccharide family, and are similar to chitosan in some properties [126,127]. The three of them are frequently referred to as a delivery system for oral insulin administration [127].

Protein NPs are an example of natural polymeric NPs with many advantages. Proteins are an excellent candidate for polymers due to their amphiphilicity that allows interaction with both the drug and solvent [128]. Made of proteins like albumin and gelatin, they show biocompatibility, biodegradability, are easy to prepare, and allow attachment of targeting ligands [104,128–130]. Proteins also have the advantage of good absorbability and metabolism [104,128]. Protein-based NPs have the capacity to bind to different kinds of drugs in a relatively nonspecific manner due to their surface charge and polymeric matrix [128,129]. The application of albumin as an effective drug carrier is motivated by multiple factors [98]. Albumin is the most abundant protein in blood plasma and is a versatile protein carrier for drug delivery, since it is biocompatible, biodegradable, and nontoxic [104,131,132]. Albumin NPs are easy to prepare and have reactive surface groups such as amino and carboxylic groups on the surface of the NPs, allowing covalent bonds to be formed with targeting ligands [128,133]. Additionally, albumin exhibits unique active targeting potential, which enhances cellular uptake, promoting the effective release of therapeutic compound to the cellular environment while coupling with the proteolytic degradation of albumin and avoiding enzymatic degradation and endocytic recycling [98,131,132]. With the advantage of also having low cost, it is an ideal material to produce NPs [131]. Gelatin is regarded as a safe compendial excipient, with a long history of safe use in the preparation of capsules [128]. However, its applications can be widened. Gelatin is a natural protein

with low toxicity, biodegradable, easy to cross-link and inexpensive [123,128]. In addition, the presence of ionizable groups such as carboxyl, amino, phenol, guanidine, and imidazole allows chemical modifications and conjugation [128]. Another important property of gelatin is the ability to form a thermally reversible gel in water under a variety of pH, temperature, and solute conditions [126]. Cross-linking agents such as glutaraldehyde provide stability, shape, and increased circulation time, which determine the release of the drug from the NPs [128].

PLGA is approved by the FDA and EMA for several therapeutic applications due to its biodegradability, biocompatibility, and sustained release properties [134]. This polymer is one of the most successfully used [135]. It has high purity. Being made from copolymers, it is more stable against hydrolytic cleavage. Its surface is also easily modified to obtain functionalization and targeting [123]. They are also biodegradable since their hydrolysis results in the formation of both lactic and glycolic acids, which are biodegradable [123,135]. In addition, it is low toxic and immunogenicity [134]. Similar to PLGA, there is PLA, which is another synthetic polymer that is biodegradable and biocompatible. This group of polymers also includes PCL, which is especially used in the preparation of long-term implantable devices due to its degradation being slower than that of PLA [135].

### 19.2.1.3 *Metallic NPs*

Many metal elements can form nanostructures [136]. Metallic NPs have a larger surface area and area-to-volume ratio, special optical and physical properties, and are easy to prepare [87,92,136]. The surface of the particles can also be modified and functionalized due to its simple surface chemistry [87,92]. All these characteristics can be very useful for cancer treatment, among other conditions [92,137]. Other areas include imaging, analytical processes, and sensors as signal-amplification reagents and photothermal applications [87,92]. There has been increasing concern about these types of particles regarding their release into the environment and associated potential effects on ecological systems [137].

Silver NPs are commonly used for their antimicrobial and anti-inflammatory properties [114,136]. They are one of the most extensively studied types of nanomaterials for their unique sensing, catalytic, optical, and antimicrobial properties as efficient probes for detecting various biomolecules and monitoring biotransformation [138].

Gold NPs are fit for imaging, with colloidal NPs being used in the immune labeling of samples to be viewed using transmission electron microscopy (TEM). Drug delivery systems with gold NPs have also been studied [136]. Gold NPs are also exploited in cancer therapy and diagnostics, chemical and biological imaging, catalysis and sensors [114,138].

Iron oxide NPs (IONP) can include magnetite, maghemite, or a nonstoichiometric combination of the two, being the original compounds the most commonly used. Both magnetite and maghemite have nearly identical properties. Nevertheless, magnetite possesses Fe(II) ions have larger radius than maghemite Fe(III) ions. Both oxides display superparamagnetic behaviors. Beyond that, they have chemical stability under physiological conditions, low toxicity, and are highly magnetic [139]. IONPs can be utilized as contrast agents due to their superparamagnetic properties. Superparamagnetic IONPs (SPIONPs) display therapeutic properties through hyperthermia leading to the apoptosis desired in cancer cells and allowing targeted drug delivery [137]. IONPs have also been studied *in vitro* and *in vivo* for tracking stem cells [136].

#### 19.2.1.4 Targeting and sustained release

A great advantage of using NPs in drug delivery of natural compounds is the possibility to target specific tissues or organs [140]. Targeting can improve drug bioavailability by increasing the fraction of drug that reaches the site of interest, while reducing toxic side effects [140]. Two main categories are considered: passive targeting requires the NPs to reach the targeted area without specific chemical interaction, relying only on physical transport of the NPs according to its own properties like charge, size, and shape; active targeting relies on specific interaction between ligands attached to the surface of the NPs and cell markers [103,140,141].

The use of ligands allows the recognition of certain markers or receptors, improving NPs uptake, enhancing drug delivery and therapeutic effect [142]. Small molecules like folate (FA) and hyaluronic acid (HA) can be used as well as ligands [142–144]. FA is not immunogenic, and has a specific interaction with the correspondent receptor overexpressed in some tumors [143]. It has been demonstrated that NPs conjugated with FA can be actively internalized via receptor-mediated endocytosis and effectively directed to folate receptor-positive cancer cells [144]. HA is biocompatible, nontoxic, and has many functional groups for chemical modification [143]. Thus it appears to be the polymer of choice for the development of drug delivery vehicles against CD44 overexpressing tumors [143].

Antibodies show excellent target affinity and specificity [142]. The use of antibody fragments is also believed to be an interesting choice for the targeting of NPs due to their smaller size, good expression, solubility, and stability as well as specificity and affinity [144]. A variety of peptides and aptamers can also be used for the same purpose [142,144]. Site-specific conjugation, low immunogenicity, low toxicity, and versatility are some of the advantages of these molecules [144].

Polymer coatings are alternatives to small molecule ligands [145]. Polyethylene glycol (PEG) is the most frequently used surface coating for

NPs [142,145]. It allows a decrease and delay in plasma protein opsonization and immune clearance while increasing circulation time [142,145]. Besides bringing many advantages by itself, PEG also allows the addition of ligands to its surface to further optimize targeting and sustained release [145]. As seen in Table 19.3, other hydrophilic polymers can be used, such as natural polysaccharides and synthetic polymers [142].

19.2.1.5 Examples of NPs made from natural products

Drug delivery technology is accomplished with the right polymer choice for the control of drug release. Natural polymers are of considerable importance for their general biocompatibility, biodegradability, low toxicity, and low immunogenicity [147]. As mentioned above, natural polymers can be either polysaccharides or proteins.

Chitosan has been widely used and there are many examples of studied formulations with this polymer. Tamoxifen-loaded chitosan NPs have been shown to increase the accumulation of drug in tumor cells through the enhanced permeability and retention (EPR) effect and induce apoptosis.

TABLE 19.3 Some examples of patented formulations with surface functionalization.			
Formulation	NP type	Therapeutic area	Patent number
Functional PLA–PEG copolymers	PLA–PEG NPs	Cancer treatment and imaging	WO2013127949 A1
Human recombinant epidermal growth factor (hrEGF)-modified cisplatin-loaded polymeric NPs	mPEG–PLGA–PLL NPs	Cancer treatment	CN102793671 A
Antibody fragment-targeted immunoliposomes	Immunoliposome	Gene therapy and cancer treatment	US20090191331 A1
Chitosan-modified methazolamide SLNs	SLNs	Glaucoma treatment	CN102793672 A
Liposomal delivery system	PEGylated liposome	Delivery of therapeutic agents and imaging	WO2013135892 A1
Source: Adapted from Martins P, Rosa D, Fernandes AR, Baptista PV. Recent Pat Nanomed 3 (2013) [146].			



Paclitaxel-loaded chitosan NPs also displayed a prolongation in circulation time, less macrophage recognition, and lower liver accumulation [124]. Insulin is another compound that can benefit from chitosan NPs, being especially characterized by optimized intestinal absorption [127].

Being hydrophilic and biodegradable, alginate has been found safe to use as a polymer for drug delivery systems [126,148]. Alginate has been studied for the encapsulation of many compounds, such as curcumin and resveratrol, for prostate cancer treatment. In both cases, cytotoxic effects were obtained and there was no sign of hemolysis, which guaranteed safety for intravenous administration [148].

Gelatin NPs have the capacity of carrying out controlled drug delivery through either bursts or controlled-release mechanisms [123]. Gelatin NPs coated with mannan were formulated to enhance the macrophage uptake and distribution of the HIV drug didanosine, leading to higher uptake of the drug. Another example is the encapsulation of ibuprofen sodium into PEGylated gelatin NPs, which resulted in improved plasma half-life of the drug [149].

#### 19.2.1.6 *Natural products encapsulated in NPs*

The chemical complexity of natural products is one of the major challenges for their encapsulation. The application of NPs to natural products has been extensively cited by many authors due to their promotion of sustained release of the drug with the fulfilment of other important required criteria [94]. Many compounds have been studied with different formulations.

Curcumin is a polyphenol that has shown potent antitumor and neuroprotective properties [94,150]. Starting with liposomes and going through PLGA NPs and chitosan NPs, among others, curcumin-loaded NPs were developed to enhance curcumin's characteristics, such as solubility, stability, bioavailability, sustained release, and targeted delivery [100,151,152]. An extended absorption capacity can be obtained when using lipid NPs with curcumin due to a slower drug release. This improved pharmacokinetic comes without any adverse effects, which is another advantage. When using PLGA, particle size can be controlled, and surface functionalization can be added to target curcumin to a specific tissue, frequently tumor tissue. PLGA encapsulation has also enhanced the half-life of curcumin in the cerebral cortex and hippocampus leading to increased retention time values and therefore to improved therapeutic effects [151,152]. However, despite these advantages there are no curcumin nanoproducts approved by any regulatory entity.

The natural polyphenol resveratrol has also proved interesting for cancer therapy [153]. However, its poor bioavailability, low solubility, and lack of targeting specificity must be addressed. Chitosan, alginate albumin, gelatin, and lipids are possible polymers for this purpose, demonstrating protection against degradation, improvement in toxicity, and enhanced activity against tumor growth due to an enhancement in the cellular uptake [100,153].



Resveratrol is a great example of a compound that clearly benefits from nanotechnology showing results at a specific target [153].

Quercetin is a natural flavonoid and many NPs have been developed to increase its bioavailability, aqueous solubility, and antitumor activity [116]. Quercetin seems to be more effective when incorporated into lipid NPs, having enhanced cytotoxic effects [94,100,153]. PLGA has also showed potential as a polymer for the delivery of quercetin since it led to apoptosis in a breast cancer context [153]. Nonetheless, no quercetin formulation has been approved yet.

PvD is a diterpenoid that has shown potential for cancer therapy, especially with nanotechnology. PvD is a lipophilic compound, and is difficult for drug delivery since it does not dissolve well. Having low bioavailability, encapsulation is a solution to this [140]. A recent published study shows results from PvD encapsulated into NPs as a potential treatment against melanoma [154]. PvD was encapsulated in NPs made of oleic acid, PCL with addition of HA and a peptide ligand,  $\alpha$ -melanocyte stimulating hormone ( $\alpha$ -MSH). These NPs were able to promote cell death of melanoma cells. Thus these nanosystems appear to be promising platforms for long-term drug release, presenting the desired structure and robust performance for a targeted and local antitumor therapy in cutaneous melanoma *in situ* [154].

Lycopene is an unsaturated carotenoid with strong antioxidant activity and the ability to reduce oxidative damage to somatic cells [155]. However, lycopene's poor water solubility and instability require the use of NPs to improve solubility and prevent degradation [156]. Recently, lycopene encapsulation into liposomes showed preventive action in brain damage induced by transient ischemia. It was evident that the liposomal drug delivery system was crucial for enhanced protection and efficient delivery of the drug [155]. Besides liposomes, other options have been studied. Core-shell lycopene/oligomerized epigallocatechin-3-*O*-gallate/chitosan NPs were efficient to encapsulate lycopene allowing it to escape degradation and improve pharmacokinetic parameters, showing promising characteristics for drug delivery applications [156].

Cannabinoids such as  $\Delta$ 9-tetrahydrocannabinol (THC) and cannabidiol (CBD) have received great attention lately due to their therapeutic advantages [157,158]. Recently, Hoffman *et al.* studied the encapsulation of these compounds in piperine-pro-nanolipospheres (PPNs) as a novel oral delivery system, where piperine works as an absorption enhancer [157,158]. PPNs appear to improve the oral bioavailability of these poorly water-soluble compounds since they inhibit first-pass intestinal metabolism and allow better delivery of the compounds [157,158].

### 19.2.1.7 Approved nanopharmaceuticals containing natural products

Over the last 30 years, nanomedicine has matured from the lab to the market. At the moment, the nanopharmaceuticals market is anticipated to grow over

**TABLE 19.4** Approved nanopharmaceuticals made of natural products.

Product name	Company	Drug & formulation	Therapeutic area	FDA/EMA Approval
Doxil/Caelyx	Jansen—Cilag	Doxorubicin Liposomes	Cancer	1995/1996
Myocet	Teva B.V.	Doxorubicin Liposomes	Cancer	—/2000
Marquibo	Talon Therapeutics Inc.	Vincristine Sulfate Liposomes	Cancer	2012/—
Abraxane	Celgene Corporation	Paclitaxel Albumin NPs	Cancer	2005/2008
Taxol	Bristol—Myers Squibb	Micelles	Cancer	1992/—

\$79.29 billion by 2026, according to the BIS Research Report on Global Nanopharmaceutical Drugs Market (2018-2026).

Today, the approval of nanopharmaceuticals in humans is regulated by national regulatory agencies like the FDA, the EMA, and the PDMA/MHLW [105,108,118]. Table 19.4 shows the most representative approved nanopharmaceuticals made from natural products.

As seen, clinical application of nanotechnology is broad, but its focus is generally on cancer [88]. Many NPs-based products have been approved for the treatment of various tumors, some of them still in various phases of clinical trials [99]. Approved by the FDA (1995) and the EMA (1996), Doxil was the first liposomal-encapsulated doxorubicin formulation. This anticancer drug showed superior clinical performance in a variety of neoplasms due to its pharmacokinetics and biodistribution, having reduced adverse side effects and improved overall patient compliance and quality of life [160]. This formulation contains PEG chains on the liposomal surface. This characteristic increases the longevity of the liposomes in the circulation system [93].

Another example of a NPs-based anticancer drug is Marquibo (vincristine sulfate liposomal injection). In this formulation approved by the FDA (2012), vincristine was encapsulated in sphingomyelin and cholesterol NPs to overcome dosing and pharmacokinetic problems of vincristine. It was designed to ease the loading and retention of vincristine, increasing its circulation time and exposure to tumor cells. These characteristics result in a higher concentration of drug in the target tissues and enhanced activity [161].

Approved by the FDA (2005) and the EMA (2008), Abraxane<sup>®</sup> is seen as one of the biggest successes in the development of nanomedicines [159].

**TABLE 19.5** Some examples of patented formulations containing natural products and NPs.

NP type	Therapeutic area	Patent number
Gelatin and PLGA NPs	Cancer treatment	CN102697737 A
Curcumin NPs and Chitosan-bound curcumin NPs	Various	US 2011/0190399 A1
Curcumin Liposomes	Cancer	US 7,968,115 B2
Chitosan-modified methazolamide SLNs	Glaucoma treatment	CN102793672 A
Paclitaxel, albumin NPs, and Bevacizumab	Cancer	US 2010/01 12077 A1

*Source:* Adapted from Martins P, Rosa D, Fernandes, AR, Baptista PV. Recent Pat Nanomed 3 (2013) and Jadhav NR, Powar T, Shinde S, Nadaf S. Asian J Pharm (2014) [164].

The paclitaxel-protein bound NPs formulation was developed to substitute paclitaxel formulation Taxol. This formulation consists of micelles made of paclitaxel in organic solvents of polyoxyethylated castor oil (Cremophor EL<sup>®</sup>) and dehydrated ethanol (50/50, v/v) [162,163]. Cremophor EL<sup>®</sup> was proved to be toxic so substitute formulations were required [162,163]. Besides fulfilling this purpose, Abraxane has also improved pharmacokinetics and enhanced tumor inhibition [118,159]. Therefore, Abraxane has exemplified protein–drug NPs as excellent solutions for improvement of toxicity and passive delivery to a target [118].

The patents regarding NPs with natural products are mainly for cancer therapy, but it is not the only area of interest [146] (Table 19.5).

### 19.3 Nanoproducts in food supplements

A food supplement is an isolated or purified product coming from food, usually sold in a pharmaceutical form, that demonstrates a physiologic benefit or that provides protection against diseases [165]. A dietary supplement is considered a product that has one (or more) of the following ingredients: a vitamin, a mineral, an amino acid, a medical herb or other botanical, a dietary substance to supplement the diet through increase of total daily intake, or a concentrate, metabolite, constituent, extract, or combination of these elements [166]. They can be used to delay the aging process, to increase life expectancy, etc. The interest in food supplements has been a field of increasing biomedical research [167].

### 19.3.1 Food supplement and its clinical usage

The use of food supplements goes back many years, where some plants were used for preventive or therapeutic purposes. It is based on knowledge of pharmacological activities of natural compounds followed by clinical evidence of safety and efficacy. The majority of food supplements possess multiple properties, and are used in conditions like neurological and cardiovascular diseases, cancer, and diabetes. In these conditions, plenty of redox reactions are involved, and a large part of food supplements have antioxidant properties that act against these reactions.

### 19.3.2 Neurodegenerative diseases

There is a large spectrum of neurodegenerative diseases that are complex and multifactorial [168], and are usually associated with mutated genes, accumulation of abnormal proteins, increased reactive oxygen species (ROS), or destruction of the neurons in a specific part of the brain [169–173]. Neurodegenerative diseases include Alzheimer's disease (AD), Parkinson's disease (PD), Huntington's disease (HD), multiple sclerosis (MS), and amyotrophic lateral sclerosis (ALS), which are some of the most debilitating conditions [168].

The chronic use of the currently available therapeutic agents against neuronal damage leads to several adverse effects, being one of their major disadvantages. Food supplements have the ability to act on multiple cellular pathways and consequently appear to be promising candidates for long-term consumption as required for management of chronic illnesses like the neurodegenerative disorders mentioned above [168].

Some potent antioxidants like lycopene, resveratrol, coenzyme Q10 (ubiquinone),  $\beta$ -carotene,  $\alpha$ -lipoic acid, astaxanthin, and curcumin have showed beneficial effects against many diseases by neutralizing oxidative stress, boosting the endogenous antioxidant levels, and stabilizing mitochondrial functions [174–180].

The major pathways involved in neuronal damage that lead to neurodegenerative diseases are mitotoxicity,  $\text{Ca}^{2+}$  overload, oxidative stress, and inflammation. Knowing these pathways, there are some natural products that have neural effects. Curcumin restores homeostasis of the inflammatory system, boosts the heart shock system in order to increase toxic aggregates clearance, scavenges free radicals, and induces elements with antioxidant response. It also binds to and limits the aggregation of  $\beta$ -sheet conformation of the amyloid characteristic of many neurodegenerative diseases [181]. The  $\alpha$ -lipoic acid is also a potent mitochondrial stabilizer that also improves mitochondrial functions and physiology, protecting neurons against chemotherapy, hypoxia,  $\text{A}\beta$ , and other neurotoxicity induced by other toxics [182–187]. Another example is astaxanthin, a carotenoid with various health

benefits, including anti-inflammatory, antiapoptotic, antioxidant effects, the potential to promote and maintain neural plasticity [188], mitochondria protection, and a boost of energy production without increasing ROS [189,190]. Coenzyme Q10 is a powerful antioxidant that might prevent mitochondrial functions in stroke, epilepsy, and other neurodegenerative disorders, thus protecting neuronal cells. It may prevent cell membranes from being damaged by free radicals through peroxyl radicals scavenge, therefore preventing lipid, protein, and DNA oxidation. L-sulforaphane isothiocyanate decreases accumulation of ROS and protects oxidative stress induced by  $H_2O_2$  [168] and blueberries have anthocyanins that possess neuroprotective effects through inhibition of phospholipase A2 [191]. A blueberry diet shows neuroprotection through modulation of gene expression involved in inflammation [192]. They are also reported to have other activities like antioxidant [193–203], anti-inflammatory [195,204–206], antiproliferative [207–209], antiobesity properties [210–212], and neuroprotective actions [213–215]. Moreover, resveratrol is a phenol that has a neuroprotective effect through antioxidant properties and its capacity to modulate  $A\beta$  processing [216]. It has also shown beneficial potential with Alzheimer's [217–223]. It can be found in mulberries, red grapes, peanuts, tea, and wine [224]. Another example is rosmarinic acid that has a neuroprotective action by scavenging ROS. Moreover, vitamins like vitamin D have shown to modulate some inflammatory markers in patients with MS, PD, and AD [225]. Vitamin E is associated with a lower risk of Alzheimer's development [226–228]. Caffeine can be found in coffee or tea and, when administered regularly, has beneficial effects in acute and chronic neurological disturbances, including stroke, dementia, and AD [229]. Finally, selenium is a nutrient that is essential in the diet due to the presence of selenocysteine in selenoproteins, which are known to provide protection from cell damage induced by ROS, whose mechanisms involve the glutathione peroxidase family and selenoprotein P. This last one is synthesized in the brain and protects it from oxidative damage, and is the most important selenoprotein for cerebral functions. Therefore, selenium may affect the rate of disease through ROS protection as an antioxidant or by improving metabolism.

### 19.3.3 Cardiovascular diseases

The cardiovascular disease spectrum includes coronary heart disease, peripheral vascular diseases, cerebrovascular disease (stroke), hypertension, and heart failure. Similarly to other diseases, there are food supplements that can be used to prevent the harmful consequences of these conditions. Resveratrol is a polyphenolic compound known for its antioxidant and anti-inflammatory properties and the ability to upregulate endothelial NO synthase (eNOS) and scavenge peroxyl radicals, which can limit the processes of lipid peroxidation. Resveratrol also induces vasorelaxation and cardioprotective effects.

Additionally, flavonoids that are present in various vegetables (onions, cruciferous), fruits (pomegranate, apples, grapefruit, cherries, berries), red wine [230–232], and garlic prevent and improve the treatment of these cardiovascular diseases by blocking the angiotensin-converting enzyme, the cyclooxygenase enzymes that break down prostaglandins, thus preventing platelet aggregation [233]. They can decrease the risk of hypertension and ischemic heart disease [234,235]. Garlic extracts also show antihypertensive and antiapoptotic properties [236]. Phytosterols compete with cholesterol stemming from the diet, blocking cholesterol uptake, and facilitating its excretion at the same time. They are present in most plants and can be found in lipid-rich foods such as nuts, peanuts, and also chickpea, vegetables, and fruits [165]. Sulforaphane is present in broccoli and protects against inflammation and also the myocardium from ischemic reperfusion by upregulating phase II detoxification enzymes involved in clearance of ROS [237,238]. Tea contains Epigallocatechin-3-gallate (EGCG) and theanine (amino acid) that diminish blood pressure. Tea also contains flavonoids with antioxidant properties that improves vascular function, produces NO, and enhances platelet activity and leukocyte adhesion. Furthermore, it has anti-inflammatory activities. It also affects lipid and lipoprotein levels, potentially lowers cholesterol, and reduces LDL/HDL ratio. CoQ10 improves cardiovascular function through the lowering of blood pressure, improvement of ventricular ejection fraction, and reducing arrhythmias. It is an electron carrier in the mitochondrial synthesis of ATP. CoQ10 improves mitochondrial energy production, decreases the inactivation of NO to peroxynitrite, and diminishes the oxidative damage to LDL. It has been found that in heart disease a deficiency of CoQ10 is present. It can be found in meat, fish, nuts, and also a little in dairy products, fruits, and vegetables. Again, curcumin reduces intracellular ROS. It has anti-inflammatory properties and it lowers triglycerides, LDL, and lipid peroxides [239]. Omega-3 fatty acid, eicosapentaenoic acid (EPA), and docosahexaenoic acid (DHA) lower triglycerides and are recommended for hypertriglyceridemia. They also function as antiarrhythmic through prevention of calcium overload in cardiac myocytes during stress. Lycopene lowers LDL oxidation [240] and has antioxidant properties that reduce blood pressure [241]. Lycopene inhibits cholesterol synthesis by inhibiting the activity of an enzyme involved in that synthesis [236]. Lycopene is present in red fruits, watermelons, and tomato juice. Carnitine prevents lactic acid formation in heart muscles that damages the myocardium in failing hearts. During myocardial infarction a reduction of 40% carnitine content is detected. Carnitine is found in meat, nuts, and vegetables. Finally, soy contains isoflavone phytoestrogens that bind to estrogen receptor [242] and improve vascular functions [243] by estrogenic mechanisms [244,245]. Isoflavones also inhibit LDL oxidation and therefore exert antiatherogenic effects [246]. Soy lowers mean blood pressure, reducing also systolic and diastolic pressure [247].

### 19.3.4 Cancer

Chemoprevention is the use of natural or synthetic chemicals to suppress, reverse, or prevent carcinogenesis process. A plant-based diet has been shown to have positive effects on cancer development and its progression, and those aspects have been attributed to its elevated amount of antioxidants. Again, curcumin is known for its anti-inflammatory, antioxidant, and anti-cancer properties [248]. Carotenoids have antioxidant activities and therefore are effective in cancer prevention. There is also interest in lycopene, which acts through a decrease in oxidative stress and damage to DNA. Regarding prostate cancer, plants rich in daidzen, biochanin, isoflavones, and genistein are interesting compounds as they inhibit cell growth. Isoflavones possess prevention properties regarding cancer. They are present in soybeans and appear to offer protection when it comes to breast, uterine, lung, colorectal, and prostate cancer [249]. Saponins are an example of phytochemicals reported to have antitumor activity, thus preventing cancer. They are found in soybeans, some herbs, peas, tomatoes, potatoes, and spinach [250]. Tannins are used as anticarcinogenics, due to their ability to search harmful free radicals and detoxify carcinogens. They are present in grapes, berries (blackberries, cranberries, and blueberries), tea, and lentils. Pecans, walnuts, strawberries, cranberries, pomegranates, and red raspberry seeds contain ellagic acid, which is also an anticancer agent [250]. Pectin acts against cancer metastasis by inhibiting the cancer cells from adhering to other cells in the body. It is found in apples, and there are several studies that show that pectin also decreases cholesterol levels [251]. Glucosinolates and their hydrolysis products include indoles and isothiocyanates, that along with a high intake of cruciferous vegetables, have been associated with a lowering of the risks of these cancers. Those hydrolysis products block the enzymes that promote tumor growth, especially regarding the lung and colorectal cancer [252]. EGCG has antitumor properties on a variety of cancer cell lines from the more common to more rare tumors, such as malignant mesothelioma and anaplastic thyroid carcinoma, and is found in green tea. Resveratrol may also help in cancer due to its anticancer, anticarcinogenesis, and anti-inflammatory properties, having chemopreventive properties and has shown therapeutic potential in patients with cancer.

### 19.3.5 Diabetes

There are two main types of diabetes: Type 1, caused by an autoimmune destruction of pancreatic  $\beta$  cells that are normally responsible for insulin production; and type 2 diabetes, which happens due to deficient insulin production or insulin resistance. The lack of insulin leads to high plasma levels of glucose that can harm various organs [253]. Examples of food supplements or food components with clinical use in diabetes are isoflavones, which are

in the group of phytoestrogens and have similar structure and function as human estrogen. Soy isoflavones intake has been moderately studied and those studies have shown an association between their intake and the lower incidence and mortality of type II diabetes, heart disease, osteoporosis, and certain types of cancer [254].

Lipoic acid has also shown effectiveness as a long-term dietary supplement for protection of complications in diabetics [255]. In addition, psyllium has been extensively used as pharmacological supplements and food ingredients, and for glucose control in diabetics [256]. Cinnamon and aqueous extract fraction and cinnamaldehyde are also used for diabetes modulation. The clinical studies supporting the antihyperglycemic effect of cinnamon are limited and the efficacy in humans is not yet well established [236]. In addition, bitter melon has strong antihyperglycemic properties in animals and clinical trials [257]. There are several reports published describing antihyperglycemic and hypolipidemic properties [258], and in type 2 diabetics it is considered a supplement with moderate effect for managing glucose levels [236]. Again, resveratrol causes metabolic changes [259–261] and protection from diabetes consequences [262–267]. Another example is ginger; several studies support its efficacy in managing hyperglycemia in patient with diabetes, and include preclinical/animal studies [268–270] and clinical studies [271–273]. Raw ginger aqueous extract (intraperitoneal) demonstrated hypoglycemic and hypolipidemic effects [268]. Another study, also performed in animals, showed a decrease in blood glucose levels, as well as a lipid-lowering and antioxidant effect [269]. Information compiled [270] has shown ginger to be helpful in diabetes and other metabolic diseases.

### 19.3.6 Nanotechnology and food supplements

One of the main disadvantages of natural products as food supplements is their low absorption. The low absorption associated with their poor solubility in the gastrointestinal fluids (causing their incomplete absorption) or due to their first-pass metabolism leads to a diminution in their biological activity, which is a major concern. In order to address this issue, nanotechnology has been used for the efficient delivery of these natural products. Here, some parameters must be considered. For instance, low gastric residence time, low permeability, and/or solubility within the gut and instability in the gastrointestinal (GI) tract can limit their activity [274]. Other aspects like chemical instability and crystallization before incorporating these bioactive molecules into commercial food products must be considered. By using nanotechnology, it is possible to create new formulations where the solubility, stability, and delivery of bioactives from foods are overcome.

Several works have already successfully described the *in vitro* improvement of the absorption of various phytochemicals through nanoproducts. Safety aspects and toxicity potential of those nanoproducts are still being



researched [95]. The GI tract is well adapted to facilitate the uptake of certain materials but to date, little research has been undertaken on the impact, behavior, and interaction of nanomaterials in the GI tract. In contrast, a significant amount of research has taken place on the effects of nanomaterials on the lung [95]. Understanding of the factors that determine the pattern of the accumulation and distribution of NPs within the body is fundamental. In addition, the long-term effects are more difficult to detect than immediate toxic impacts.

There is enormous interest in developing nanostructured colloidal delivery systems to encapsulate, protect, and deliver food products. One of the NPs-based colloidal delivery systems suitable for food industry are microemulsions, which are thermodynamically stable [275]. They can be oil-in-water (O/W), composed of surfactant and oil molecules dispersed in water. Surfactant molecules are generally arranged in a way that makes nonpolar tails gathered in a hydrophobic interior, opposing the polar head, which are located in the hydrophilic exterior, in contact with water. Oil molecules can form a separate hydrophobic core or be located between surfactant molecules and nonpolar tails. Lipophilic bioactive molecules can be solubilized in the hydrophobic interior. The hydrophobic effect is the driving force for microemulsion formation [276].

In addition, there are small liposomes (nanometric range) made from phospholipids, constituted with a polar group (head) and two nonpolar tails [277]. They have a tendency to self-assemble into bilayer structures having layers of phospholipid molecules united head-to-head and tail-to-tail. Polar bioactives can be trapped in the hydrophilic region and nonpolar in the hydrophobic part.

Additionally, there are nanoemulsions, which are colloidal dispersions that are thermodynamically unstable and made with oil, emulsifier, and water. O/W nanoemulsions consist of small particles rich in lipids dispersed in water, with a nonpolar core formed by lipid molecules covered with a layer of emulsifier molecules: surfactants, phospholipids, particles, polysaccharides, or proteins. In the lipid core of nanoemulsion droplets, it is possible to solubilize lipophilic bioactives.

As mentioned in the previous section, SLNs are small crystalline lipid particles dispersed in water made by creating an O/W nanoemulsion at elevated temperatures, followed by cooling it with a lower temperature than the crystallization point of the lipid phase. Their solid core can limit molecular diffusion inside the particle, making it an advantage when compared to liquid lipid NPs (LLNs), and helping to prevent undesirable effects like the release of encapsulated components or chemical degradation reactions. The transition from solid to liquid phase can also be used as a trigger mechanism for the lipophilic nutraceutical to be released.

Finally, biopolymer NPs and nanogels can be made from different types of proteins and polysaccharides using different fabrication methods [278].

These particles consist of strongly packed biopolymer molecules, whereas biopolymer nanogels contain more elevated quantities of water trapped in a biopolymer network [276].

Table 19.6 presents some examples of nanoproducts with food supplements.

### 19.3.7 Advances in Patents

In terms of Patents in Food Supplements and Nanotechnology, the Patent WO2017060916 (A1) relates to pharmaceutical composition/s comprising of at least one metallic NPs either alone or in combination and at least one drug from the category such as antiseizure, antiepileptic, antioxidants, or nutraceuticals or other therapeutic class having the potential to be used in such disorders. Another example of patent regarding NPs relates to the preparation and methodology of silk fibroin NPs (US2011305765 (A1)). This invention uses NPs sizing 1 nm to about 500 nm for delivery of drugs and/or nutraceuticals that include a fibroin polypeptide and a drug or nutraceutical. The NPs may further include a chitosan, or a proteoglycan such as decorin. Finally, US2011038942 (A1) describes colloidally stable dispersions of NPs comprising beta-lactoglobulin and a polysaccharide, which are useful as delivery vehicles of hydrophobic nutraceuticals and fat-soluble vitamins, for enrichment of food products, especially of transparent beverages and other nonfat or low fat foods and drinks.

## 19.4 Natural products, nanotechnology, and skin

The skin has three major layers: epidermis, dermis, and hipodermis [114,309,310]. The cells that form the skin are renewed every 21–30 days [311]. The skin is able to absorb various substances, including chemicals and xenobiotics. It works as a selective barrier mainly due to the presence of the *stratum corneum*. To penetrate this barrier, different pathways can be used, such as the intercellular route, where the substance passes in between the keratinocytes; the intracellular route, where the substance is able to diffuse past the lipid matrix; or through the ducts of sweat and sebaceous glands and hair follicles [114,311,312]. The permeability of the skin varies according to different factors, such as age, gender, skin thickness and vascularity, density of hair follicles, mechanical trauma (integrity of the skin), and diseases [312]. Hair follicles may act as reservoirs for substances, including NPs. The substances that are stored in the hair follicle may be continuously diffused and can ultimately reach the blood system [312,313].

Some characteristics of NPs are important for better skin permeation, both in dermatological and cosmetic applications. Physicochemical parameters found to interfere with skin diffusion are size, surface charge, surface chemistry, and nanodispersion when in contact with the skin. Moreover,

**TABLE 19.6** Nanoproducts with food supplements.

Ingredient	Activity	Formulation	Main achievements	References
Anthocyanins		SLNs	Increased stability against high pH	<a href="#">[281]</a>
$\beta$ -caroteno, folic acid, curcumin, and ergocalciferol	Antioxidant activity	Protein–polysaccharide soluble nanocomplex	Increased activity	<a href="#">[282]</a>
Caffeine		SLNs	Enhanced skin permeation	<a href="#">[283]</a>
	Antimicrobial activity	Nanohydrogels	Improved antimicrobial activity	<a href="#">[284]</a>
		NPs	Increased dopaminergic neurons endurance, fibre outgrowth, and prolonged expression of tyrosine hydroxylase (TH)	<a href="#">[285]</a>
Carotenoids		Lipid nanocarriers	New delivery systems for lipophilic plant extracts	<a href="#">[286]</a>
CoQ10		Lipid free nanoformulation	Enhanced bioavailability of CoQ10	<a href="#">[287]</a>
CoQ10 and long chain fatty acids		Nanoemulsion	Delivery systems that improve oral bioavailability	<a href="#">[288]</a>
	Antimalarial	HPMC and PVP NPs loaded with curcumin		<a href="#">[289]</a>
	Anti-inflammatory	Nanotransfersomes of curcumin and diclofenac diethylamine	Enhanced permeation and high bioavailability	<a href="#">[290]</a>
	Anti-inflammatory and antioxidant	NPs loaded with curcumin and celecoxib (pH sensitive)	Enhanced efficacy for ulcerative colitis	<a href="#">[291]</a>

Curcumin	Anti-inflammatory	Nanocarrier transdermal gel with curcumin and diclofenac diethylamine	Targeted effect with enriched biological activity	<a href="#">[292]</a>
	Antimicrobial activity and wound healing	Hydrogel NPs	Increased activity	<a href="#">[293]</a>
	Oxygen scavengeing activity	SNLs		<a href="#">[294]</a>
		Nanoemulsion	Controlled lipid digestion rate and free fatty acid adsorption	<a href="#">[295]</a>
Curcumin and temozolomide	Anticancer and antitumor activity	Magnetic NPs loaded with curcumin and temozolomide	Cell death pathway stimulation (increased anticancer activity)	<a href="#">[296]</a>
Glycyrrhizic acid	Anti-inflammatory activity	Polymeric NPs	Enhanced activity	<a href="#">[297]</a>
	Antibacterial activity	Polymeric NPs	Improved activity	<a href="#">[298]</a>
Green tea extract	Antioxidant activity	Nanostructured lipid carriers	Increased activity	<a href="#">[299]</a>
Lutein		Polymeric NPs	Enhanced solubility	<a href="#">[300]</a>
		Polymeric NPs	Improved chemical stability	<a href="#">[301]</a>
Melatonin		Polymeric NPs	Sustained release	<a href="#">[302]</a>
	Wound epithelialization	Polymeric NPs	Improved activity	<a href="#">[303]</a>
(Continued)				

**TABLE 19.6 (Continued)**

Ingredient	Activity	Formulation	Main achievements	References
Omega-3-fatty acids and oil soluble vitamins		Biopolymeric nanogels	Protection of bioactives	[278]
Quercetin	Antioxidant activity	NPs	Prolonged quercetin release and improved antioxidant activity	[304]
		Polymeric NPs	Enhanced pharmacological effects of quercetin with increased liver targeting	[305]
		SLNs and NLC	Validated for trans-resveratrol protection, stabilization, and intestinal permeability	[306]
Resveratrol	Cytotoxicity against C6 glioma cells	SLNs	Significantly higher cytotoxicity than free resveratrol	[307]
	Oxidative stress	Polymeric NPs	Improvement in treatment of oxidative stress	[308]

Source: Adapted from Gopi S, Amalraj A. J Nanomed Biotherap Discov 6 (2016) 1–8 and Kumar S, Joginder G, Duhan S, Kumar R, Priyanka S, Kumar S, et al. Advances in animal biotechnology and its applications. Springer Singapore, Singapore, 2018 [279,280]).

formulation, concentration of both drug and NPs, and time of exposure were also found to be important for good skin permeation [313].

### 19.4.1 Nanoparticles in Dermatology and Cosmetics

Concerning dermatological products, dermal delivery of drugs can be done through two different mechanisms: transdermal or topical drug delivery [313]. Transdermal drug delivery is a process in which the drug formulation has to permeate the different layers of the skin, including the *stratum corneum*. Drugs administrated through this route normally enter systemic circulation in order to act. This administration allows drugs to have an extended period of action and to reduce the frequency of administration [314]. Furthermore, transdermal route also surpasses the first-pass metabolism [315].

In topical administrations the drug acts locally, keeping the levels of the drug in circulation at a minimum [311] As previously reported for the transdermal administration, topical administration is not affected by the first-pass metabolism [315].

The permeability of the skin can be altered with mechanical or chemical enhancers. Different types of NPs are broadly used in cosmetics and dermatological fields, and various applications have been explored [316,317,318].

For these formulations to act, they need to reach their target, deliver a compound or perform a therapy, and be cleared from the system. Many types of NPs are not able to penetrate the healthy skin barrier, when it is not compromised. Some characteristics of NPs can be engineered for better skin permeation, such as surface charge. Furthermore, NPs skin permeation may be improved by using physical techniques and/or chemical compounds, as was previously mentioned [318]. Hair follicles seem to be able to act as a reservoir for NPs [319].

NPs are commonly used in cosmetic products as they are able to increase stability of the ingredients (such as fatty acids, vitamins, and antioxidant compounds) present in cosmetic formulations, increase permeability of these compounds, and can make the product more visually pleasant [316].

There are several examples of NPs applied to the skin delivery as cosmetics or as dermatological products. One example of application of polymeric NPs is Hydrogel (Carbopol<sup>®</sup> Ultrez 10 NF) with dexamethasone to treat psoriasis. Through these, the active compound is released at a controlled rate, and is able to diffuse and permeate the skin [9]. Another example of applications of polymeric NPs for topical delivery is the use of chitosan-based NPs with retinol [320] for the treatment of acne, in the dermatological field, and its applications in antiwrinkle cream, in cosmetics. By nanoencapsulating retinol, its toxicity is diminished and it irritates the skin less [315].

Carbon nanotubes are cylindrical-shaped carbon NPs with a hollow core that usually have diameters of 100 nm. Carbon nanotubes are of interest due to its antioxidant potential and cytoprotective effect [317]. These type of nanocarriers have applications in the diagnosis of chronic skin diseases and infections, and early stage skin cancer by constituting highly sensitive suborganelles biomarkers due to its high conductivity. It can also be applied to the cosmetic field in rejuvenating products, such as moisturizers, make-up, and sunscreens [317].

Fullerenes are made of carbon atoms and their shape (spherical, ellipsoid, and cylindrical) can vary according to the organization of the atoms. The most common form of these NPs, and also the smallest, is Fullerene C<sub>60</sub>, a fullerene composed of 60 carbon atoms organized in a spherical shape. Derivates of this fullerene can and are being developed, such as Fullerene C<sub>70</sub> and Fullerene C<sub>84</sub> [321]. These NPs have limited solubility in polar solvents and are hydrophobic. These limitations can be surpassed by attributing various groups to its surface. If the attached molecules are organic compounds, the fullerenes formed are organofullerenes. Organofullerenes show better solubility, which is an advantage in comparison to Fullerene C<sub>60</sub> [321]. Fullerene C<sub>60</sub> has different characteristics of interest, such as its antioxidant effect exerted by the scavenging ROS, free radicals, and reactive nitrogen species, and by increasing the activity of superoxide dismutase. The aging of the skin is due to increased oxidation in the cells and consequent cell apoptosis. Thus fullerenes are of interest for antiaging cosmetic products as they seem to be able to fight, or at least slow down, oxidation in keratinocytes and therefore skin aging [321].

As mentioned, lipid-based NPs are the most commonly studied NPs for topical applications and encompass a broad spectrum of NPs.

Lipid-based NPs have been studied in order to improve the treatment of various skin disorders. Some of these include acne, atopic eczema, psoriasis, and inflammations [316]. One example application of lipid NPs is the usage of nanosized HA to improve HA skin permeation, a formulation under development [317]. Topical formulations containing liposomes have been used in cosmetics for antiaging creams, lotions, and other products by many brands, including Christian Dior SE, France [316].

Another example, are SLNs, which can have active compounds incorporated into their solid core, since they can carry active substances [322]. They are of interest in this field as they are able to hydrate, whiten, and lubricate the skin [323]. Furthermore, SLNs are being used in sunscreens and UV blocker formulations [323,324] due to their higher load and slower drug release. Thus the amount of the active compound/sunscreen released over time is diminished in these formulations. SLNs are also able to scatter light, including UV radiation, having UV blocking abilities of their own [323]. Formulations combining these NPs and many compounds used in cosmetic products have been produced, such as CoQ10, ascorbyl palmitate,

tocopherol, and retinol [316]. These NPs also have applications in the dermatological field. One example of these applications is the use of SLNs for topical delivery of drugs, such as clotrimazole, prednicarbate, and betamethasone 17-valerate [324].

Transfersomes, like liposomes, are vesicles produced with phospholipids and edge activators. In contrast to liposomes, transfersomes are elastic vesicles, which gives them the ability to penetrate through pores and spaces much smaller than the NPs size [325,326]. Due to its deformability transfersomes improve skin permeation of different drugs through a mechanism not totally understood. Drug formulations with these elastic vesicles can permeate both compromised and intact skin, *in vitro* and *in vivo* [324,325]. Transfersomes have been used in order to better skin penetration of active compounds such as triamcinolone acetonide and estradiol, for example [327]. An example of topical formulations using transfersomes is Diractin<sup>®</sup>, but it did not get in to the market [328].

Ethosomes are another subtype of lipid-based NPs. Like transfersomes, ethosomes are able to penetrate the *stratum corneum*, delivering drugs past this barrier due to its deformability. Ethosomes are very effective in delivering higher quantities of drugs into deeper layers of the skin [311,326,329]. Formulations containing ethosomes have been used to treat skin infections (ethosomes containing bacitracin and erythromycin, for example), provide pain relief (ethosomes and ibuprofen formulations), and to reduce inflammation (ethosomes and ammonium glycyrrhizinate formulations) [330].

Niosomes are formed by hydrated nonionic surfactants and cholesterol, or its derivatives. Hydrophilic substances can be adsorbed on the surface of the bilayer or trapped in the vesicles aqueous core. Lipophilic substances are encapsulated in between the layers of the lipid bilayer [331]. Niosomes are more chemically stable than liposomes, but stiffer than transfersomes and liposomes [324]. These hydrolysis-susceptible NPs are also able to aggregate and fuse together [311]. Furthermore, niosomes size, shape, and flow ability can be engineered and the nonionic surfactants present in the structures of these NPs act as enhancers of skin permeation [311]. Niosomes-based formulations have been used for antiaging products by brands such as L'Oreal Paris [316]. The first applications of niosomes were in cosmetic formulations, but now these NPs also have different dermatological applications, such as in the treatment of acne and psoriasis, for example [311].

In addition, phytosomes are able to form a link to the polar heads of the phospholipids present on the vesicular membrane of these NPs through chemical bonds, carrying the active compounds in its membrane. Phytosomes have different applications due to the properties of the herbal extracts used, which include anti-inflammatory properties. They can also be used for transdermal formulations as they can penetrate the *stratum corneum* and enter the systemic circulation. These systems have good skin penetration due to their high lipid profile, and thus are appropriate for skin applications,



including in the cosmetics and dermatological fields [332–334]. These plant extract-based NPs have been used in cosmetic formulations of sunscreens, skin moisturizers, and in antiaging creams and products [335].

### 19.4.2 Applications of Natural Nanoproducts in Dermatology and Cosmetics

Natural nanoproducts with dermatological applications can be one of two types: NPs produced with natural materials; or NPs carrying natural compounds, such as plant extracts or phytochemicals.

Table 19.7 shows some of the many nanoproducts produced with natural materials available on the market with dermatological applications that are administered topical or transdermally.

Besides the marketed formulations, many other nanoproducts made with natural materials with dermatological applications and nanoproducts have been produced. Table 19.8 summarizes some examples of these formulations.

As previously mentioned, NPs carrying natural compounds are also considered natural nanoproducts. Table 19.9 summarizes some examples of inorganic NPs delivering natural compounds.

In order to improve the efficacy of transdermal formulations, such as improving the cellular uptake of the compounds, the NPs surface can be modified. These modifications in the surface of the NPs can be achieved by employing different methods, which include adding ligands to the NPs surface or coating the NPs surface with polymers, such as PEG [356]. Furthermore, these surface functionalizations are important for targeted delivery and specificity of the NPs, as well as for reducing degradation [357].

Surface functionalization can be achieved with different methods according to the goal [340]. Polymer NPs and liposomes can be coated with chitosan or avidin–biotin in order to improve binding capacity [358]. Polymeric NPs may also be coated with a second polymer with or without functional groups, creating a barrier for skin diffusion enabling sustained release over a long period of time [340]. Surface charges can be altered with a polymer coating, which can also be beneficial for different applications in transdermal formulations [359].

An example of transdermal formulations of NPs with modified surfaces is chitosan NPs in Carbopol 940<sup>®</sup> gel containing aceclofenac, which were coated with egg albumin in order to create a polyelectrolyte complex and improve transdermal drug delivery [359].

Similar to dermatological nanoproducts, interest in cosmetic applications of NPs has increased in recent years. This is due to NPs allowing deeper skin penetration, more durability of effects, and improved appearance of products. For example, some large particles make a product opaque, but the

**TABLE 19.7** Selected examples of marketed dermatological nanoproducts (as encapsulant natural material) and its applications.

Commercial name	Drug	Formulation	Application	References
Estrasorb™	Estradiol Topical Emulsion	Liposomes	Menopausal symptoms	<a href="#">[336]</a>
Nanominox®	Minoxidil 4%	Ethosomes	Hair growth promoter	<a href="#">[337]</a>
Pevaryl Lipogel®	Econazole	Liposomes	Treatment of dermatomycosis	<a href="#">[338]</a>
Diclac® Lipogel	Diclofenac	Liposomes	Topical treatment of osteoarthritis	<a href="#">[339]</a>
Daylong Actinica	Methoxycinnamates butyl-methoxydibenzoylmethane	Liposomes	Prophylaxis of actin keratosis	<a href="#">[338]</a>
Transfersulin	Insulin	Transfersomes	Delivery of insulin	<a href="#">[339]</a>

**TABLE 19.8** Selected examples of formulations for dermatological applications of natural-based nanoproducts (mainly as encapsulant material) under study.

Drug	Formulation	References
Podophyllotoxin	Solid Lipid NPs	[340]
Cyclosporin A	Liposomes	
Methotrexane	Liposomes	
Psoralen	Liposomes	
Clotrimazole	Liposomes	
Retinol	Polymeric	[315]
Methotrexate	Other Lipid NPs	[341]
Fluconazole	Ethosomes	[342]
Paclitaxel	Ethosomes	[343]
Minoxidil	Ethosomes	[344]
Aciclovir	Ethosomes	
Testosterone	Ethosomes	
Lidocaine hydrochloride	Niosomes	[345]
Dithranol	Niosomes	
pMEL34	Niosomes	
Sertraline hydrochloride	Niosomes	[346]
Ovalbumin	Polymeric	[347]
Tretinoin	Polymeric	

same compound nanoformulated can contribute to transparency [360]. Big cosmetic and skincare brands have used NPs for their formulations, such as Christian Dior SE, L'Óreal Paris, Chanel S.A., and La Prairie, Switzerland [308]. Some of these examples and other cosmetic products containing NPs and their applications are presented in Table 19.10.

Besides the marketed cosmetic products shown in Table 19.10, Table 19.11 shows selected examples of nanoformulations produced with phytocompounds or plant extracts for cosmetic applications.

## 19.5 Conclusions

The use of natural compounds for health conditions is expanding and is receiving growing attention. However, these natural products have some

**TABLE 19.9** Selected examples of formulations for dermatological applications under study, carrying natural compounds obtained from plant extracts.

Plant extract	Formulation	Applications	References
<i>Sambucus nigra</i>	Silver NPs	Psoriasis	[348]
<i>Plectranthus amboinicus</i>	Zinc oxide NPs	Antifungal	[349]
<i>Olea europaea</i>	Nanoemulsions	Antimicrobial, eczema, psoriasis, ulcers, burns, and skin infections	[350], [351]
<i>Aloe vera</i>	Polymeric NPs	Burn wound treatment	[352]
<i>Iresine herbstii</i>	Silver NPs	Eczema and antimicrobial	[353]
<i>Coriandrum sativum</i>	Silver NPs	Antiacne and antidandruff	[354]
<i>Pistacia integerrima</i>	Gold NPs	Antiinflammatory and psoriasis	[355]

limitations such as low water solubility, low *in vivo* stability, and low permeability across biological barriers. Here, nanotechnology may be considered a suitable strategy to overcome those issues. This chapter showed that functionalized or not functionalized nanotechnology has demonstrated its capability to manipulate particles in order to target specific areas of the body and control the release of bioactive compounds (as isolated compounds or as extracts). It is evident that nanotechnology can create new products, contributing to knowledge and innovation. In a very near future, there will be access to more and more safe and practical products.

Despite the many benefits of applying nanotechnology for better delivery of natural products, there are still some concerns that face the development of nanoproducts with natural products, one of the leading ones being the transition from bench to bedside. The difficulty of reproducing NPs synthesis on a scale needed for commercialization, the lack of understanding of how NPs interact with biosurface, and insufficient knowledge about the fate of NPs and potential NPs toxicity also need to be further investigated, especially if these systems are to be used to prevent and to treat diseases. At the end, nanotechnology research, development and commercialization of the nanoproducts must ensure that these products undergo to the market with no risk (or minimal risk). The balance between benefit and risk must be always critically analysed, fully characterized and clearly favorable.

**TABLE 19.10** Selected examples of marketed cosmetic nanoproducts (mainly based on natural encapsulant materials).

Product	Brand	Formulation	Application	References
Capture	Christian Dior	Liposomes	Antiaging	<a href="#">[361]</a>
Efect du Soleil	L'Óreal	Liposomes	Promotes tanning	
Future Perfect Skin Gel	Estée Lauder	Liposomes	Antiaging	
Eye PerfeCTOR	Avon	Liposomes	Sooths eye irritation	
Decorin cream	Genome Cosmetics, Pennsylvania, US	Ethosomes	Antiaging, skin repair, reduces hyperpigmentation	<a href="#">[362]</a>
Zelens Fullerene C-60 Night Cream	Zelens	Fullerene C <sub>60</sub>	Antiaging	<a href="#">[363]</a>
Primordiale Optimum Lip	Lancôme	Phytosomes	Lip treatment	
Intensive Serum Nano Repair Q10	Dr. Rimpler	Solid Lipid NPs	Antiaging	
Swiss Cellular White Illuminating Eye Essence	La Prairie	Solid Lipid NPs	Skin brighter and skin whitener	<a href="#">[364]</a>
Sericoside	Indena	Phytosomes	Antiwrinkler and improves skin	<a href="#">[365]</a>
PA2	Indena	Phytosomes	UV protector, trophodermic and firming cream	
Curbilene	Indena	Phytosomes	Matting cream	

**TABLE 19.11** Selected examples of formulations for cosmetic applications under study, formulated with phytochemicals or herbal extracts.

Phytochemical/plant extract	Formulation	Applications	References
<i>Lavandula stoechas ssp</i>	Polymeric NPs	Antioxidant and antiaging	[366]
<i>Rosmarinus officinalis</i>	Lipid NPs	Antioxidant	[367]
<i>Aloe Vera</i>	Liposomes	Improves collagen production and keratinocytes proliferation	[368]
Lutein	Lipid NPs	Antioxidant and photo-damage protector	[369]
<i>Curcuma longa</i>	Lipid NPs	UV protector and hydration	[370]
Resveratrol	SLNs, SLCs	UV-B protector	[371]
<i>Camellia sinensis</i>	Fullerene	Antiaging	[372]

## References

- [1] Freitas A, Moldão-Martins M, Costa HS, Albuquerque TG, Valente A, Sanches-Silva A. J Sci Food Agric 2015;95:44–52.
- [2] Mota AH, Silva CO, Nicolai M, Baby A, Palma L, Rijo P, et al. Pharm Dev Technol 2018;23:794–805.
- [3] Arumugam G, Swamy M, Sinniah U. Molecules 2016;21:369.
- [4] Menon DB, Sasikumar JM, Latha K. Indian J Nat Prod Resour 2012;3:359–65.
- [5] Mota AH. Int J Pharmacogn Phytochem Res 2016;8:572–91.
- [6] Kozłowska M, Laudy AE, Przybył JL, Ziarno M, Majewska E. Acta Pol Pharm Drug Res 2015;72:757–67.
- [7] Menon DB, Sasikumar JM. Int J Pharm Pharm Sci 2011;3:300–4.
- [8] Braga N, Rodrigues F, Beatriz M, Oliveira PP. Nat Prod Res 2015;29:1–18.
- [9] Beaux D, Fleurentin J, Mortier F. Phyther Res 1999;13:222–5.
- [10] Committee on Herbal Medicinal Products. Eur Med Agency 2013;44:1–26.
- [11] Daryani A, Ebrahimzadeh MA, Sharif M, Ahmadpour E, Edalatian S, Esboei BR, et al. Int J Trop Biol Conserv 2015;63:7–12.
- [12] Ercisli S, Tosun M, Akbulut M. Pharmacogn Mag 2009;5:320.
- [13] Gray AM, Abdel-Wahab YHA, Flatt PR. J Nutr 2000;130:15–20.
- [14] Harokopakis E, Albzreh MH, Haase EM, Scannapieco FA, Hajishengallis G. J Periodontol 2006;77:271–9.
- [15] Ho GTT, Ahmed A, Zou Y-F, Aslaksen T, Wangenstein H, Barsett H. Carbohydr Polym 2015;125:314–22.
- [16] Kite GC, Larsson S, Veitch NC, Porter EA, Ding N, Simmonds MSJ. J Agric Food Chem 2013;61:3501–8.

- [17] Krawitz C, Mraheil MA, Stein M, Imirzalioglu C, Domann E, Pleschka S, et al. *BMC Complement Altern Med* 2011;11:16.
- [18] Simonyi A, Chen Z, Jiang J, Zong Y, Dennis Y, Gu Z, et al. *N Prog A Sci Life Sci* 2015;128:30–8.
- [19] Chang JM, Cheng CM, Hung LM, Chung YS, Wu RY. Evidence-based complement. *Altern Med* 2010;7:115–20.
- [20] De Oliveira FFM, Torres AF, Gonçalves TB, Santiago GMP, De Carvalho CBM, Aguiar MB, et al. *Evid Based Complement Altern Med* 2013;2013.
- [21] Ravikumar VR, Dhanamani M, Sudhamani T. *Anc Sci Life* 2009;28:7–9.
- [22] Rice LJ, Brits GJ, Potgieter CJ, Van Staden J. *South Afr J Bot* 2011;77:947–59.
- [23] Dos Santos NO, Mariane B, Lago JHG, Sartorelli P, Rosa W, Soares MG, et al. *Molecules* 2015;20:8440–52.
- [24] Chen YS, Yu HM, Shie JJ, Cheng TJR, Wu CY, Fang JM, et al. *Bioorg Med Chem* 2014;22:1766–72.
- [25] Galvão Rodrigues FF, Costa JGM, Rodrigues FFG, Campos AR. Evidence-based complement. *Altern Med* 2013;2013.
- [26] Gurgel APAD, da Silva JG, Grangeiro ARS, Oliveira DC, Lima CMP, da Silva ACP, et al. *J Ethnopharmacol* 2009;125:361–3.
- [27] Koti BC, Gore A, Thippeswamy AH, Swamy AV, Kulkarni R. *Indian J Pharmacol* 2011;43:286–90.
- [28] Kuo Y-S, Chien H-F, Lu W. *Evid Based Complement Altern Med* 2012;2012:418679.
- [29] Lukhoba CW, Simmonds MSJ, Paton AJ. *J Ethnopharmacol* 2006;103:1–24.
- [30] Falé PLV, Ascenso L, Serralheiro MLM, Haris PI. *Spectroscopy* 2011;26:79–92.
- [31] Reis AC, Viccini LF, de Sousa SM. *Comp Cytogenet* 2015;9:451–63.
- [32] Alasbahi R, Melzig M. *Planta Med* 2010;76:653–61.
- [33] Alasbahi R, Melzig M. *Planta Med* 2010;76:753–65.
- [34] Santos Veríssimo R, Lins T, Assis Bastos M, Albuquerque Sarmiento P, Alvino V, Silva Araujo M, et al. *BMC Proc* 2014;8:P264.
- [35] Du Toit R, Volsteedt Y, Apostolides Z. *Toxicology* 2001;166:63–9.
- [36] Chen J, Hammell DC, Spry M, D'Orazio JA, Stinchcomb AL. *J Nat Prod* 2009;72:769–71.
- [37] da Cunha AP. *Plantas e Prod Veg Em Fitoter* 2006;246–7.
- [38] Burmistrova O, Perdomo J, Simões MF, Rijo P, Quintana J, Estévez F. *Phytomedicine* 2015;22:1009–16.
- [39] Figueiredo NL, de Aguiar SRMM, Falé PL, Ascensão L, Serralheiro MLM, Lino ARL. *Food Chem* 2010;119:664–8.
- [40] Grayer RJ, Eckert MR, Lever A, Veitch NC, Kite GC, Paton AJ. *Biochem Syst Ecol* 2010;38:335–41.
- [41] Rijo P, Falé PL, Serralheiro ML, Simões MF, Gomes A, Reis C. *Meas J Int Meas Confed* 2014;58:249–55.
- [42] Simões MF, Rijo P, Duarte A, Matias D, Rodriguez B. *Phytochem Lett* 2010;3:234–7.
- [43] Gaspar-Marques C, Simões MF, Rodríguez B. *J Nat Prod* 2004;67:614–21.
- [44] Mothana RAA, Abdo SAA, Hasson S, Althawab FMN, Alaghbari SAZ, Lindequist U. Evidence-Based Complement. *Altern Med* 2010;7:323–30.
- [45] Batista O, Duarte A, Nascimento J, Simões MF, de la Torre MC, Rodríguez B. *J Nat Prod* 1994;57:858–61.
- [46] Batista O, Fátima Simões M, Duarte A, Luisa Valdeira M, de la Torre MC, Rodríguez B. *Phytochemistry* 1995;38:167–9.

- [47] Ascensao L, Figueiredo AC, Barroso JG, Pedro LG, Schripsema J, Deans SG, et al. *Int J Plant Sci* 1998;159:31.
- [48] Kubínová R, Pořízková R, Navrátilová A, Farsa O, Hanáková Z, Bačinská A, et al. *J Enzyme Inhib Med Chem* 2014;6366:1–4.
- [49] Gaspar-Marques C, Simões MF, Valdeira ML, Rodríguez B. *Nat Prod Res* 2008;22:167–77.
- [50] Miroddi M, Calapai G, Isola S, Minciullo PL, Gangemi S. *Allergol Immunopathol (Madr)* 2014;42:616–19.
- [51] Wang Y-W, Yang C-T, Gong C-L, Chen Y-H, Chen Y-W, Wu K-C, et al. *Pharmacol Rep* 2015;67:1049–54.
- [52] Ahmad N, Sharma S. *Green sustain. Chem* 2012;02:141–7.
- [53] Baumann LS. *Dermatol Ther* 2007;20:330–42.
- [54] da Cunha AP. *Plantas e Prod. Veg. Em Fitoter.* 2006. p. 116–7.
- [55] Alasalvar C, Karamać M, Kosińska A, Rybarczyk A, Shahidi F, Amarowicz R. *J Agric Food Chem* 2009;57:4645–50.
- [56] Cerulli A, Masullo M, Montoro P, Hošek J, Pizza C, Piacente S. *J Pharm Biomed Anal* 2018;160:168–78.
- [57] Del Rio D, Calani L, Dall'Asta M, Brighenti F. *J Agric Food Chem* 2011;59:9935–41.
- [58] Grissa I, Ezzi L, Chakroun S, Mabrouk A, Ben Saleh A, Braham H, et al. *Env Sci Pollut Res* 2017;24:12474–83.
- [59] Neves JA, Neves JA, de R, Oliveira CM. *Expert Opin Ther Pat* 2018;28:399–413.
- [60] Valones MAA, Higino JS, Souza PRE, Crovella S, de A, Júnior FC, et al. *Braz Dent J* 2016;27:497–501.
- [61] Nicolai M, Pereira P, Vitor RF, Reis CP, Roberto A, Rijo P. *Meas J Int Meas Confed* 2016;89:328–32.
- [62] Smaoui Slim. *Afr J Biotechnol* 2012;11:9664–71.
- [63] Batista ALA, Diógenes Alves Uchôa Lins R, de Souza Coelho R, do Nascimento Barbosa D, Moura Belém N, Alves Celestino FJ. *Complement Ther Clin Pract* 2014;20:93–8.
- [64] Singh O, Khanam Z, Misra N, Srivastava M. *Pharmacogn Rev* 2011;5:82.
- [65] Srivastava JK, Shankar E, Gupta S. *Mol Med Rep* 2010;3:895–901.
- [66] Herro E, Jacob S. *Dermat Contact Atopic Occup Drug* 2010;21:327–9.
- [67] Loolaie M, Moasefi N, Rasouli H, Adibi H. *Arch Clin Microbiol* 2017;8.
- [68] Oh JY, Park MA, Kim YC. *Toxicol Res (Camb)* 2014;30:297–304.
- [69] Aires A, Carvalho R, José M. *Waste Manag* 2016;48:457–64.
- [70] Durazzo A, Turfani V, Azzini E, Maiani G, Carcea M. *Food Chem* 2013;140:666–71.
- [71] Eberhardt MV, Lee CY, Liu RH. *Nature* 2000;405:903–4.
- [72] Silva RH, Abílio VC, Takatsu AL, Kameda SR, Grassl C, Chehin AB, et al. *Neuropharmacology* 2004;46:895–903.
- [73] Solomon A, Golubowicz S, Yablowicz Z, Grossman S, Bergman M, Gottlieb HE, et al. *J Agric Food Chem* 2006;54:7717–23.
- [74] Eshun K, He Q. *Crit Rev Food Sci Nutr* 2004;44:91–6.
- [75] Klein AD, Penneys NS. *J Am Acad Dermatol* 1988;18:714–20.
- [76] Shelton RM. *Int J Dermatol* 1991;30:679–83.
- [77] Vogler BK, Ernst E. *Br J Gen Pract* 1999;49:823–8.
- [78] Lestari MLAD, Indrayanto G. *Curcumin*, 2014.
- [79] Nelson KM, Dahlin JL, Bisson J, Graham J, Pauli GF, Walters MA. *J Med Chem* 2017;60:1620–37.



- [80] Hosseini SM, Bahramnejad B, Douleti Baneh H, Emamifar A, Goodwin PH. *World J Microbiol Biotechnol* 2017;33:1–10.
- [81] Nawaz W, Zhou Z, Deng S, Ma X, Ma X, Li C, et al. *Nutrients* 2017;9.
- [82] Barreiro C. *Microbial carotenoids*, 2018.
- [83] Michalska A, Łysiak G. *Int J Mol Sci* 2015;16:18642–63.
- [84] Rijo P, Matias D, Fernandes A, Simões M, Nicolai M, Reis C. *Polym (Basel)* 2014;6:479–90.
- [85] Emeka EE, Ojiefoh OC, Aleruchi C, Hassan LA, Christiana OM, Rebecca M, et al. *Micron* 2014;57:1–5.
- [86] Rebelo A, Molpeceres J, Rijo P, Pinto Reis C. *Curr Drug Metab* 2017;18:346–59.
- [87] Mallick S, Choi JS. *J Nanosci Nanotechnol* 2014;14:755–65.
- [88] Riehemann K, Schneider SW, Luger TA, Godin B, Ferrari M, Fuchs H. (2009) 872–897.
- [89] Soares S, Sousa J, Pais A, Vitorino C. 6 (2018) 1–15.
- [90] Wolfram J, Zhu M, Yang Y, Shen J, Gentile E, Paolino D, et al. 16 (2016) 1671–1681.
- [91] Chang EH, Harford JB, Eaton MAW, Boisseau PM, Dube A, Hayeshi R, et al. *Biochem Biophys Res Commun* 2015;.
- [92] Mishra DK, Shandilya R, Mishra PK. *Nanomed Nanotechnol Biol Med* 2018;.
- [93] Weissig V, Pettinger TK, Murdock N. *Int J Nanomed* 2014;9:4357–73.
- [94] Bonifácio BV, da Silva PB, Aparecido dos Santos Ramos M, Maria Silveira Negri K, Maria Bauab T, Chorilli M. *Int J Nanomed* 2013;9:1–15.
- [95] Lord Haskel, Lord Warner, Lord Mitchell, Lord Haskel, *Sci. Technol. Comm. I* (2010).
- [96] Kouchakzadeh H, Shojaosadati SA, Maghsoudi A, Vasheghani Farahani E. *AAPS PharmSciTech* 2010;11:1206–11.
- [97] Ventola CL. 42 (2017) 742–755.
- [98] Blanco E, Shen H, Ferrari M. *Nat Biotechnol* 2015;33:941–51.
- [99] Ud Din F, Aman W, Ullah I, Qureshi OS, Mustapha O, Shafique S, et al. *Int J Nanomed* 2017;12:7291–309.
- [100] Chuan L, Jia Z, Yu-jiao Z, Shu-fang N, Jun C, Qian W, et al. *B Park, HHS Public Access* 2017;13:641–52.
- [101] Reis CP, Martinho N, Rosado C, Fernandes AS, Roberto A. *Drug Dev Ind Pharm* 2014;40:409–17.
- [102] Pinto Reis C, Neufeld RJ, Ribeiro AJ, Veiga F. *Nanomed Nanotechnol Biol Med* 2006;2:8–21.
- [103] Havel H, Finch G, Strode P, Wolfgang M, Zale S, Bobe I, et al. *AAPS J* 2016;18:1373–8.
- [104] Elzoghby AO, Samy WM, Elgindy NA. *J Control Rel* 2012;157:168–82.
- [105] Matos AI, Peres C, Zupanc E, Moura L, Sainz V, Silva LC, et al. 468 (2015) 504–510.
- [106] David CAW, Owen A, Neill J. (2016).
- [107] Wacker MG. (2014) 777–784.
- [108] Pita R, Ehmann F, Papaluca M. *AAPS J* 2016;.
- [109] Wacker M. *Int J Pharm* 2013;457:50–62.
- [110] Carbone C, Leonardi A, Cupri S, Pignatello R. 3 (2014) 199–215.
- [111] Bozzuto G. (2015) 975–999.
- [112] Daraee H, Etemadi A, Kouhi M, Alimirzalu S, Akbarzadeh A. (2014) 1–11.
- [113] Almeida AJ, Souto E. *Adv Drug Deliv Rev* 2007;59:478–90.
- [114] Mota AH, Rijo P, Molpeceres J, Reis CP. *Int J Pharm* 2017;532:710–28.
- [115] Geszke-Moritz M, Moritz M. 68 (2016) 982–994.

- [116] Kathe N, Henriksen B, Chauhan H. 9045 (2014) 1–11.
- [117] Beloqui A, Solinís MÁ, Rodríguez-Gascón A, Almeida AJ, Préat V. *Nanomed Nanotechnol Biol Med* 2015;.
- [118] Bobo D, Robinson KJ, Islam J, Thurecht KJ, Corrie SR. *Pharm Res* 2016;33:2373–87.
- [119] Reis CP, Gomes A, Rijo P, Candeias S, Pinto P, Baptista M, et al. *Microsc Microanal* 2013;19:1141–50.
- [120] Reis CP, Damgé C. *Methods Enzymol* 2012;508:271–94.
- [121] Reis CP, Silva C, Martinho N, Rosado C. *Ther Deliv* 2013;4:251–65.
- [122] Reis CP, Figueiredo IV, Carvalho RA, Jones J, Nunes P, Soares AF, et al. *Nanotoxicology* 2008;2:205–17.
- [123] Lai P, Daear W, Löbenberg R, Prenner EJ. *Colloids Surf B Biointerfaces* 2014;118:154–63.
- [124] Prabakaran M. *Int J Biol Macromol* 2014;1–10.
- [125] Abbaspour-Aghdam MAGF, Anarjan N, Berenjian A. (2014).
- [126] Hudson D, Margaritis A. (2012) 1–19.
- [127] Fonte P, Araújo F, Silva C, Pereira C, Reis S, Santos HA, et al. *Biotechnol Adv* 2015;33:1342–54.
- [128] Lohcharoenkal W, Wang L, Chen YC, Rojanasakul Y. **2014** (2014).
- [129] Kouchakzadeh H, Safavi MS, Shojaosadati SA. *Efficient delivery of therapeutic agents by using targeted albumin nanoparticles*. 1st ed. Elsevier Inc; 2015.
- [130] Estrada LPH, Champion JA. (2015).
- [131] Yu X, Jin C. *J Mater Sci Mater Med* 2016;27:1–10.
- [132] Yu X, Di Y, Xie C, Song Y, He H, Li H, et al. *Int J Nanomed* 2015;10:6825–34.
- [133] Karimi M, Bahrami S, Ravari SB, Zangabad PS, Mirshekari H, Bozorgomid M, et al. *Expert Opin Drug Deliv* 2016;13:1609–23.
- [134] Kapoor DN, Kaur R, Sharma R, Dhawan S. 6 (2015) 41–58.
- [135] Kumari A, Yadav SK, Yadav SC. *Colloids Ans Surf B Biointerfaces* 2010;75:1–18.
- [136] Edmundson MC, Capeness M, Horsfall L. *N Biotechnol* 2014;31:572–8.
- [137] Sharma H, Mishra PK, Talegaonkar S, Vaidya B. *Drug Discov Today* 2015;.
- [138] Sharma VK, Filip J, Zboril R, Varma RS. *Chem Soc Rev* 2015;.
- [139] Estelrich J, Escribano E, Queralt J, Busquets MA. (2015) 8070–8101.
- [140] Watkins R, Wu L, Zhang C, Davis RM, Xu B. *Int J Nanomed* 2015;10:6055–74.
- [141] Gaspar DP, Faria V, Quintas JP, Almeida AJ. *Curr Org Chem* 2017;21:2360–75.
- [142] Ellah NHA, Abouelmagd SA. 5247 (2016).
- [143] Li J, Wang F, Sun D, Wang R. *J Drug Target* 2016;.
- [144] Adam RL, Friedman D, Sarah E. *Claypool Curr Pharm Des* 2014;19:6315–29.
- [145] Rotello VM, Mout R, Moyano DF. *Subinoy Rana Chem Soc Rev* 2014;41:2539–44.
- [146] Martins P, Rosa D, Fernandes AR, Baptista PV. *Recent Pat Nanomed* 2013;3.
- [147] Anwunobi AP, Emeje MO. (2011) 2–7.
- [148] Saralkar P, Dash AK. (2017).
- [149] Foxx M, Zilberman M. (2015) 8–10.
- [150] Faridi Esfanjani A, Mahdi Jafari S. *Colloids Surf B Biointerfaces* 2016;146:532–43.
- [151] Yallapu MM, Jaggi M, Chauhan SC. *Drug Discov Today* 2012;17:71–80.
- [152] Yallapu SC, Murali M, Jaggi M. Chauhan, 19 (2013) 1994–2010.
- [153] Aras A, Khokhar AR, Qureshi MZ, Silva F, Sobczak-Kupiec A, Alfonso E, et al. 15 (2014) 3865–3871.
- [154] Silva CO, Molpeceres J, Batanero B, Fernandes AS, Saraiva N, Costa JG, et al. *Ther Deliv* 2016;7:521–44.

- [155] Zhao Y, Xin Z, Li N, Chang S, Chen Y, Geng L, et al. Nano-liposomes of lycopene reduces ischemic brain damage in rodents by regulating iron metabolism. Elsevier B.V; 2018.
- [156] Mousa SA. *J Control Rel* 2017;.
- [157] Cherniakov I, Izgelov D, Barasch D, Davidson E, Domb AJ, Hoffman A. 266 (2017) 1–7.
- [158] Cherniakov I, Izgelov D, Domb AJ, Hoffman A. *Eur J Pharm Sci* 2017;.
- [159] Ragelle H, Danhier F, Préat V, Langer R, Anderson G. *Expert Opin Drug Deliv* 2017;14:851–64.
- [160] Barenholz Y. *J Control Rel* 2012;160:117–34.
- [161] Silverman JA, Deitcher SR. *Cancer Chemother Pharmacol* 2013;71:555–64.
- [162] Ma P, Mumper RJ. *J Nanomed Nanotechnol* 2013;4:1–35.
- [163] Bernabeu E, Cagel M, Lagomarsino E, Moretton M, Chiappetta DA. *Int J Pharm* 2017;526:474–95.
- [164] Jadhav NR, Powar T, Shinde S, Nadaf S. *Asian J Pharm* 2014;.
- [165] Nasri H, Baradaran A, Shirzad H, Rafieian-Kopaei M. *Int J Prev Med* 2014;5:1487–99.
- [166] Zeisel SH. *Science* 1999;285:1853–5.
- [167] Fernandes A. *Investigação Clínica Com Nutracêuticos* 2016;.
- [168] Dadhania VP, Trivedi PP, Vikram A, Tripathi DN. *Curr Neuroparmacol* 2016;14:627–40.
- [169] Fu X-Y, Yang M, Cao M-Z, Li D-W, Yang X-Y, Sun J, et al. *Mol Neurobiol* 2016;53:369–78.
- [170] Keber U, Kliez M, Carlsson T, Oertel WH, Weihe E, Schäfer MK-H, et al. *Neuroscience* 2015;298:302–17.
- [171] Kumar A, Leinisch F, Kadiiska MB, Corbett J, Mason RP. *Mol Neurobiol* 2016;53:2983–94.
- [172] Mattson MP, Magnus T. *Nat Rev Neurosci* 2006;7:278–94.
- [173] Zindo FT, Joubert J, Malan SF. *Future Med Chem* 2015;7:609–29.
- [174] Tripathi DN, Jena GB. *Mutat Res Toxicol Env Mutagen* 2010;696:69–80.
- [175] Trivedi PP, Jena GB. *Food Chem Toxicol* 2013;59:339–55.
- [176] Trivedi PP, Jena GB. *Eur J Nutr* 2015;54:639–52.
- [177] Dadhania VP, Tripathi DN, Vikram A, Ramarao P, Jena GB. *Chem Biol Interact* 2010;183:85–97.
- [178] Kumar A, Sharma SS. *Biochem Biophys Res Commun* 2010;394:360–5.
- [179] Prakash A, Kumar A. *Eur J Pharmacol* 2014;741:104–11.
- [180] Soto-Urquieta MG, López-Briones S, Pérez-Vázquez V, Saavedra-Molina A, González-Hernández GA, Ramírez-Emiliano J. *Biol Res* 2014;47:74.
- [181] Hu S, Maiti P, Ma Q, Zuo X, Jones MR, Cole GM, et al. *Expert Rev Neurother* 2015;15:629–37.
- [182] Jalali-Nadoushan M, Roghani M. *Brain Res* 2013;1505:68–74.
- [183] Melli G, Taiana M, Camozzi F, Triolo D, Podini P, Quattrini A, et al. *Exp Neurol* 2008;214:276–84.
- [184] Müller U, Kriegelstein J. *J Cereb Blood Flow Metab* 1995;15:624–30.
- [185] Prehn JHM, Karkoutly C, Nuglisch J, Peruche B, Kriegelstein J. *J Cereb Blood Flow Metab* 1992;12:78–87.
- [186] Salinthon S, Yadav V, Bourdette DN, Carr DW. *Endocr Metab Immune Disord Drug Targets* 2008;8:132–42.

- [187] Zhang L, Xing GQ, Barker JL, Chang Y, Maric D, Ma W, et al. *Neurosci Lett* 2001;312:125–8.
- [188] Grimmig B, Kim S-H, Nash K, Bickford PC, Douglas Shytle R. *GeroScience* 2017;39:19–32.
- [189] Kim J-H, Choi W, Lee J-H, Jeon S-J, Choi Y-H, Kim B-W, et al. *J Microbiol Biotechnol* 2009;19:1355–63.
- [190] Lu Y-P, Liu S-Y, Sun H, Wu X-M, Li J-J, Zhu L. *Brain Res* 2010;1360:40–8.
- [191] Frisardi V, Panza F, Solfrizzi V, Seripa D, Pilotto A. *J Am Geriatr Soc* 2010;58:2429–30.
- [192] Shukitt-Hale B, Lau FC, Carey AN, Galli RL, Spangler EL, Ingram DK, et al. *Nutr Neurosci* 2008;11:172–82.
- [193] Borges G, Degeveve A, Mullen W, Crozier A. *J Agric Food Chem* 2010;58:3901–9.
- [194] Faria A, Oliveira J, Neves P, Gameiro P, Santos-Buelga C, de Freitas V, et al. *J Agric Food Chem* 2005;53:6896–902.
- [195] Wang H, Nair MG, Strasburg GM, Chang Y-C, Booren AM, Gray JJ, et al. *J Nat Prod* 1999;62:294–6.
- [196] Kähkönen MP, Heinonen M. *J Agric Food Chem* 2003;51:628–33.
- [197] Kalt W, Ryan DAJ, Duy JC, Prior RL, Ehlenfeldt MK, Vander Kloet SP. *J Agric Food Chem* 2001;49:4761–7.
- [198] Mazza G, Kay CD, Cottrell T, Holub BJ. *J Agric Food Chem* 2002;50:7731–7.
- [199] Prior RL, Wu X, Gu L, Hager T, Hager A, Wilkes S, et al. *Mol Nutr Food Res* 2009;53:1406–18.
- [200] Tsuda T, Horio F, Kitoh J, Osawa T. *Arch Biochem Biophys* 1999;368:361–6.
- [201] Tsuda T, Ohshima K, Kawakishi S, Osawa T. *Lipids* 1996;31:1259–63.
- [202] Tsuda T, Watanabe M, Ohshima K, Norinobu S, Choi S-W, Kawakishi S, et al. *J Agric Food Chem* 1994;42:2407–10.
- [203] Tsuda T, Ueno Y, Aoki H, Koda T, Horio F, Takahashi N, et al. *Biochem Biophys Res Commun* 2004;316:149–57.
- [204] DeFuria J, Bennett G, Strissel KJ, Perfield JW, Milbury PE, Greenberg AS, et al. *J Nutr* 2009;139:1510–16.
- [205] Karlsen A, Paur I, Bøhn SK, Sakhi AK, Borge GI, Serafini M, et al. *Eur J Nutr* 2010;49:345–55.
- [206] Schreckinger ME, Wang J, Yousef G, Lila MA, Gonzalez de Mejia E. *J Agric Food Chem* 2010;58:8966–76.
- [207] Faria A, Pestana D, Teixeira D, de Freitas V, Mateus N, Calhau C. *Phyther Res* 2010;24:1862–9.
- [208] Li L, Adams LS, Chen S, Killian C, Ahmed A, Seeram NP. *J Agric Food Chem* 2009;57:826–31.
- [209] Pacheco-Palencia LA, Mertens-Talcott SU, Talcott ST. *Food Chem* 2010;119:1071–8.
- [210] Meydani M, Hasan ST. *Nutrients* 2010;2:737–51.
- [211] Tsuda T, Ueno Y, Kojo H, Yoshikawa T, Osawa T. *Biochim Biophys Acta - Mol Cell Biol Lipids* 2005;1733:137–47.
- [212] Vuong T, Benhaddou-Andaloussi A, Brault A, Harbilas D, Martineau LC, Vallerand D, et al. *Int J Obes* 2009;33:1166–73.
- [213] Andres-Lacueva C, Shukitt-Hale B, Galli RL, Jauregui O, Lamuela-Raventos RM, Joseph JA. *Nutr Neurosci* 2005;8:111–20.
- [214] Barros D, Amaral OB, Izquierdo I, Geracitano L, do Carmo Bassols Raseira M, Henriques AT, et al. *Pharmacol Biochem Behav* 2006;84:229–34.

- [215] Joseph JA, Arendash G, Gordon M, Diamond D, Shukitt-Hale B, Morgan D, et al. *Nutr Neurosci* 2003;6:153–62.
- [216] Pocernich CB, Lange MLB, Sultana R, Butterfield DA. *Curr Alzheimer Res* 2011;8:452–69.
- [217] Torres-Lista V, Parrado-Fernández C, Alvarez-Montón I, Frontiñán-Rubio J, Durán-Prado M, Peinado JR, et al. *Behav Brain Res* 2014;271:140–6.
- [218] Porquet D, Casadesús G, Bayod S, Vicente A, Canudas AM, Vilaplana J, et al. *Age (Omaha)* 2013;35:1851–65.
- [219] Calliari A, Bobba N, Escande C, Chini EN. *Exp Neurol* 2014;251:91–100.
- [220] Feng X, Liang N, Zhu D, Gao Q, Peng L, Dong H, et al. *PLoS One* 2013;8:e59888.
- [221] Rege SD, Geetha T, Broderick TL, Babu JR. *Curr Alzheimer Res* 2015;12:147–56.
- [222] Turner RS, Thomas RG, Craft S, van Dyck CH, Mintzer J, Reynolds BA, et al. *Neurology* 2015;85:1383–91.
- [223] Du L-L, Xie J-Z, Cheng X-S, Li X-H, Kong F-L, Jiang X, et al. *Age (Omaha)* 2014;36:613–23.
- [224] Tellone E, Galtieri A, Russo A, Giardina B, Ficarra S. *Oxid Med Cell Longev* 2015;2015:1–14.
- [225] Gianforcaro A, Hamadeh MJ. *CNS Neurosci Ther* 2014;20:101–11.
- [226] Morris MC, Evans DA, Tangney CC, Bienias JL, Wilson RS, Aggarwal NT, et al. *Am J Clin Nutr* 2005;81:508–14.
- [227] Morris MC, Evans DA, Bienias JL, Tangney CC, Bennett DA, Aggarwal N, et al. *JAMA* 2002;287:3230–7.
- [228] Morris MC, Evans DA, Bienias JL, Tangney CC, Wilson RS. *Arch Neurol* 2002;59:1125–32.
- [229] Panza F, Solfrizzi V, Barulli MR, Bonfiglio C, Guerra V, Osella A, et al. *J Nutr Health Aging* 2015;19:313–28.
- [230] Gharipour M, Ramezani MA, Sadeghi M, Khosravi A, Masjedi M, Khosravi-Boroujeni H, et al. *J Res Med Sci* 2013;18:467–72.
- [231] Khosravi-Boroujeni H, Mohammadifard N, Sarrafzadegan N, Sajjadi F, Maghroun M, Khosravi A, et al. *Int J Food Sci Nutr* 2012;63:913–20.
- [232] Khosravi-Boroujeni H, Sarrafzadegan N, Mohammadifard N, Sajjadi F, Maghroun M, Asgari S, et al. *J Health Popul Nutr* 2013;31:252–61.
- [233] Asgari S, Kelishadi R, Rafieian-Kopaei M, Najafi S, Najafi M, Sahebkar A. *Pediatr Cardiol* 2013;34:1729–35.
- [234] Mikaili P, Maadirad S, Moloudizargari M, Aghajanshakeri S, Sarahroodi S. *Iran J Basic Med Sci* 2013;16:1031–48.
- [235] Hara Y, Noda A, Miyata S, Minoshima M, Sugiura M, Kojima J, et al. *Exp Anim* 2013;62:305–10.
- [236] Anadón A, Martínez-Larrañaga MR, Ares I, Martínez MA. *Nutraceuticals*. Elsevier; 2016. p. 757–75.
- [237] Mukherjee S, Lekli I, Ray D, Gangopadhyay H, Raychaudhuri U, Das DK. *Br J Nutr* 2010;103:815.
- [238] Jeffery E, Araya M. *Phyther Rev* 2009;8:283–98.
- [239] Khurana S, Venkataraman K, Hollingsworth A, Piche M, Tai T. *Nutrients* 2013;5:3779–827.
- [240] Rao AV. *Exp Biol Med* 2002;227:908–13.
- [241] Slavin JL, Lloyd B. *Adv Nutr* 2012;3:506–16.
- [242] Babiker F. *Cardiovasc Res* 2002;53:709–19.

- [243] Lichtenstein AH. *J Nutr* 1998;128:1589–92.
- [244] Nestel P. *Arterioscler Thromb Vasc Biol* 2002;22:1743–4.
- [245] Teede HJ, Dalais FS, Kotsopoulos D, Liang Y-L, Davis S, McGrath BP. *J Clin Endocrinol Metab* 2001;86:3053–60.
- [246] Anthony MS, Clarkson TB, Williams JK. *Am J Clin Nutr* 1998;68:1390S–3S.
- [247] Rivas M, Garay RP, Escanero JF, Cia P, Cia P, Alda JO. *J Nutr* 2002;132:1900–2.
- [248] Wang K, Tan S-L, Lu Q, Xu R, Cao J, Wu S-Q, et al. *Am J Chin Med* 2018;46:1357–68.
- [249] Thomasset SC, Berry DP, Garcea G, Marczylo T, Steward WP, Gescher AJ. *Int J Cancer* 2007;120:451–8.
- [250] Li H, Wang Z, Liu Y. *Zhong-Yao-Cai* 2003;26:444–8.
- [251] Rafieian-Kopaei M, Nasri H, Sahinfard N, Rafieian M, Rafieian S, Shirzad M. *J HerbMed Pharmacol* 2014;3:5–8. *J HerbMed Pharmacol*.
- [252] Higdon J, Delage B, Williams D, Dashwood R. *Pharmacol Res* 2007;55:224–36.
- [253] Abdali D, Samson SE, Grover AK. *Med Princ Pract* 2015;24:201–15.
- [254] Tavafi M. *J Nephropathol* 2013;2:20–7.
- [255] Coleman MD, Eason RC, Bailey CJ. *Env Toxicol Pharmacol* 2001;10:167–72.
- [256] Singh B. *Int J Pharm* 2007;334:1–14.
- [257] Ojewole JAO, Adewole SO, Olayiwola G. *Cardiovasc J S Afr* 2006;17:227–32.
- [258] Chaturvedi P. *J Med Food* 2012;15:101–7.
- [259] Rivera L, Morón R, Zarzuelo A, Galisteo M. *Biochem Pharmacol* 2009;77:1053–63.
- [260] Bhatt JK, Thomas S, Nanjan MJ. *Nutr Res* 2012;32:537–41.
- [261] Timmers S, Konings E, Bilet L, Houtkooper RH, van de Weijer T, Goossens GH, et al. *Cell Metab* 2011;14:612–22.
- [262] Yaylali A, Ergin K, Çeçen S. *Anal Quant Cytopathol Histopathol* 2015;37:243–51.
- [263] Wang H, Guan Y, Karamercan MA, Ye L, Bhatti T, Becker LB, et al. *Shock* 2015;44:173–80.
- [264] Bagul PK, Deepthi N, Sultana R, Banerjee SK. *J Nutr Biochem* 2015;26:1298–307.
- [265] Zeng K, Wang Y, Yang N, Wang D, Li S, Ming J, et al. *Mol Neurobiol* 2017;54:4000–14.
- [266] Liu S, Lin Y, Liu X. *Exp Ther Med* 2016;11:257–62.
- [267] Yang Q, Wang H, Liu Y, Gao C, Sun L, Tao L. *J Cardiovasc Pharmacol* 2016;68:304–12.
- [268] Al-Amin ZM, Thomson M, Al-Qattan KK, Peltonen-Shalaby R, Ali M. *Br J Nutr* 2006;96:660–6.
- [269] Bahadur Singh A, Singh N, Maurya R, Kumar Srivastava A. *Int J Med Med Sci* 2009;1:536–44.
- [270] Rahmani AH, Al Shabirmi FM, Aly SM. *Int J Physiol Pathophysiol Pharmacol* 2014;6:125–36.
- [271] Arablou T, Aryaeian N, Valizadeh M, Sharifi F, Hosseini A, Djalali M. *Int J Food Sci Nutr* 2014;65:515–20.
- [272] Mozaffari-Khosravi H, Talaei B, Jalali B-A, Najarzadeh A, Mozayan MR. *Complement Ther Med* 2014;22:9–16.
- [273] Mahluji S, Attari VE, Mobasseri M, Payahoo L, Ostadrahimi A, Golzari SE. *Int J Food Sci Nutr* 2013;64:682–6.
- [274] Bell LN. *Handb Nutraceuticals Funct Foods* 2001;501–16.
- [275] Flanagan J, Singh H. *Crit Rev Food Sci Nutr* 2006;46:221–37.

- [276] Zeeb B, McClements DJ. *Nanotechnol. Agric. Food Sci.* Weinheim, Germany: Wiley-VCH Verlag GmbH & Co. KGaA; 2017. p. 135–52.
- [277] Reza Mozafari M, Johnson C, Hatziantoniou S, Demetzos C. *J Liposome Res* 2008;18:309–27.
- [278] Matalanis A, Jones OG, McClements DJ. *Food Hydrocoll* 2011;25:1865–80.
- [279] Gopi S, Amalraj A. *J Nanomed Biotherap Discov* 2016;6:1–8.
- [280] Kumar S, Joginder G, Duhan S, Kumar R, Priyanka S, Kumar S, et al. *Advances in animal biotechnology and its applications*. Singapore, Singapore: Springer; 2018.
- [281] Ravanfar R, Tamaddon AM, Niakousari M, Moein MR. *Food Chem* 2016;199:573–80.
- [282] Hosseini SMH, Emam-Djomeh Z, Sabatino P, Van der Meer P. *Food Hydrocoll* 2015;50:16–26.
- [283] Puglia C, Offerta A, Tirendi GG, Tarico MS, Curreri S, Bonina F, et al. *Drug Deliv* 2016;23:36–40.
- [284] Bourbon AI, Cerqueira MA, Vicente AA. *J Food Eng* 2016;180:110–19.
- [285] Singhal NK, Agarwal S, Bhatnagar P, Tiwari MN, Tiwari SK, Srivastava G, et al. *J Biomed Nanotechnol* 2015;11:2211–22.
- [286] Lacatusu I, Badea N, Niculae G, Bordei N, Stan R, Meghea A. *Eur J Lipid Sci Technol* 2014;116:1708–17.
- [287] Zhou H, Liu G, Zhang J, Sun N, Duan M, Yan Z, et al. *Biomed Res Int* 2014;2014:1–9.
- [288] Cho HT, Salvia-Trujillo L, Kim J, Park Y, Xiao H, McClements DJ. *Food Chem* 2014;156:117–22.
- [289] Dandekar PP, Jain R, Patil S, Dhumal R, Tiwari D, Sharma S, et al. *J Pharm Sci* 2010;99:4992–5010.
- [290] Chaudhary H, Kohli K, Kumar V. *Int J Pharm* 2013;454:367–80.
- [291] Gugulothu D, Kulkarni A, Patravale V, Dandekar P. *J Pharm Sci* 2014;103:687–96.
- [292] Chaudhary H, Kohli K, Kumar V. *Int J Pharm* 2014;465:175–86.
- [293] Krausz AE, Adler BL, Cabral V, Navati M, Doerner J, Charafeddine RA, et al. *Nanomed Nanotechnol Biol Med* 2015;11:195–206.
- [294] Jourghanian P, Ghaffari S, Ardjmand M, Haghighat S, Mohammadnejad M. *Adv Pharm Bull* 2016;6:17–21.
- [295] Joung HJ, Choi M-J, Kim JT, Park SH, Park HJ, Shin GH. *J Food Sci* 2016;81:N745–53.
- [296] Dilnawaz F, Sahoo SK. *Eur J Pharm Biopharm* 2013;85:452–62.
- [297] Bernela M, Ahuja M, Thakur R. *Eur J Pharm Biopharm* 2016;105:141–7.
- [298] Rani R, Dilbaghi N, Dhingra D, Kumar S. *Int J Biol Macromol* 2015;78:173–9.
- [299] Manea A-M, Vasile BS, Meghea A. *Comptes Rendus Chim* 2014;17:331–41.
- [300] Hong DY, Lee J-S, Lee HG. *Int J Biol Macromol* 2016;85:9–15.
- [301] Chaiyasan W, Srinivas SP, Tiyaaboonchai W. *Int J Pharm Pharm Sci* 2016;8:261–6.
- [302] Altındal DÇ, Gümüşderelioğlu M. *J Microencapsul* 2016;33:53–63.
- [303] Blažević F, Milekić T, Romić MD, Juretić M, Pepić I, Filipović-Grčić J, et al. *Carbohydr Polym* 2016;146:445–54.
- [304] Antônio E, Khalil NM, Mainardes RM. *J Nanosci Nanotechnol* 2016;16:1346–53.
- [305] Guan X, Gao M, Xu H, Zhang C, Liu H, Lv L, et al. *Drug Deliv* 2016;23:3307–18.
- [306] Neves A, Martins S, Segundo M, Reis S. *Nutrients* 2016;8:131.
- [307] Vijayakumar MR, Kumari L, Patel KK, Vuddanda PR, Vajanthri KY, Mahto SK, et al. *RSC Adv* 2016;6:50336–48.
- [308] Kim J-H, Park E-Y, Ha H-K, Jo C-M, Lee W-J, Lee SS, et al. *Asian-Austr J Anim Sci* 2015;29:288–98.

- [309] Venus M, Waterman J, McNab I. *Surg* 2010;28:469–72.
- [310] Lane ME. *J Microencapsul* 2011;28:709–16.
- [311] Antunes A, Pereira P, Reis C, Rijo P, Reis C. *Curr Drug Metab* 2017;18:412–25.
- [312] Larese Filon F, Mauro M, Adami G, Bovenzi M, Crosera M. *Regul Toxicol Pharmacol* 2015;72:310–22.
- [313] Alvarez-Román R, Naik A, Kalia YN, Guy RH, Fessi H. *J Control Rel* 2004;99:53–62.
- [314] Guy RH. In: Schafer-Korting M, editor. *Handb. Exp. Pharmacol.* Berlin, Heidelberg: Springer; 2010. p. 399–410.
- [315] Zhang Z, Tsai P-C, Ramezanli T, Michniak-Kohn BB. *Wiley Interdiscip Rev Nanomed Nanobiotechnol* 2013;5:205–18.
- [316] Mu L, Sprando RL. *Pharm Res* 2010;27:1746–9.
- [317] Gupta S, Gupta S, Jindal N, Jindal A, Bansal R. *Indian Dermatol Online J* 2013;4:267.
- [318] El-Sayed N, El-Khourdagui L, Schneider M. *Nanoscience Dermatology*. Elsevier; 2016. p. 99–113.
- [319] DeLouise LA. *J Invest Dermatol* 2012;132:964–75.
- [320] Kim D, Jeong Y, Choi C, Roh S, Kang S, Jang M, et al. *Int J Pharm* 2006;319:130–8.
- [321] Lens M. *Recent Pat Biotechnol* 2009;3:118–23.
- [322] Radtke M, Wissing SA. *I* (2002) 131–155.
- [323] Morabito K, Shapley NC, Steeley KG, Tripathi A. *Int J Cosmet Sci* 2011;33:385–90.
- [324] Liu J, Hu W, Chen H, Ni Q, Xu H, Yang X. *Int J Pharm* 2007;328:191–5.
- [325] Duangjit S, Opanasopit P, Rojanarata T, Ngawhirunpat T. *J Drug Deliv* 2011;2011:1–9.
- [326] Rattanapak T, Young K, Rades T, Hook S. *J Pharm Pharmacol* 2012;64:1560–9.
- [327] Schaferkorting M, Mehner W, Korting H. *Adv Drug Deliv Rev* 2007;59:427–43.
- [328] Rother M, Seidel EJ, Clarkson PM, Mazgareanu S, Vierl U, Rother I. *Drug Des Devel Ther* 2009;3:143–9.
- [329] Shen L-N, Zhang Y-T, Wang Q, Xu L, Feng N-P. *Int J Pharm* 2014;460:280–8.
- [330] Ainbinder D, Paolino D, Fresta M, Touitou E. *J Biomed Nanotechnol* 2010;6:558–68.
- [331] Ali I, Madan J, Kaushik D, Sardana S, Shankar R, Ali A. (n.d.) 774–782.
- [332] Awasthi R, Kulkarni GT, Pawar VK. *Int J Pharm Pharm Sci* 2011;3:2–4.
- [333] Kidd PM. *Altern Med Rev* 2009;14.
- [334] Bhattacharya S. *Int J Heal Res* 2009;2:223–32.
- [335] Chanchal D, Swarnlata S. *J Cosmet Dermatol* 2008;7:89–95.
- [336] Naunton M, Al Hadithy AFY, Brouwers JRB, Archer DF. *Menopause* 2006;13:517–27.
- [337] Uchechi O, Ogbonna JDN, Attama AA. *Appl. Nanotechnol. Drug Deliv. InTech*; 2014.
- [338] Korting HC, Schäfer-Korting M. In: Schäfer-Korting M, editor. *Am. J. Respir. Crit. Care Med.* Berlin, Heidelberg: Springer Berlin Heidelberg; 2010. p. 435–68.
- [339] Cevc G, Gebauer D, Stieber J, Schätzlein A, Blume G. *Biochim Biophys Acta Biomembr* 1998;1368:201–15.
- [340] Papakostas D, Rancan F, Sterry W, Blume-Peytavi U, Vogt A. *Arch Dermatol Res* 2011;303:533–50.
- [341] Pinto MF, Moura CC, Nunes C, Segundo MA, Costa Lima SA, Reis S. *Int J Pharm* 2014;477:519–26.
- [342] Bhalaria MK, Naik S, Misra AN. *Indian J Exp Biol* 2009;47:368–75.
- [343] Paolino D, Celia C, Trapasso E, Cilurzo F, Fresta M. *Eur J Pharm Biopharm* 2012;81:102–12.
- [344] Touitou E, Godin B, Weiss C. *Drug Dev Res* 2000;50:406–15.
- [345] Rahimpour Y, Hamishehkar H. *Recent Adv Nov Drug Carr Syst* 2012;140–64.
- [346] Rajendran V. *J Sci Innov Res* 2016;5:138–43.



- [347] Rancan F, Blume-Peytavi U, Vogt A. *Clin Cosmet Investig Dermatol* 2014;33:23.
- [348] David L, Moldovan B, Vulcu A, Olenic L, Perde-Schrepler M, Fischer-Fodor E, et al. *Colloids Surf B Biointerfaces* 2014;122:767–77.
- [349] Tiwari N, Pandit R, Gaikwad S, Gade A, Rai M. *IET Nanobiotechnol* 2017;11:205–11.
- [350] Ruiz A, Arias JL, Gallardo V. *Skin Creams Made with Olive Oil*. Elsevier Inc; 2010.
- [351] Maqbool Q, Nazar M, Naz S, Hussain T, Jabeen N, Kausar R, et al. *Int J Nanomed* 2016;11:5015–25.
- [352] Pereira GG, Guterres SS, Balducci AG, Colombo P, Sonvico F. *Biomed Res Int* 2014;2014.
- [353] Dipankar C, Murugan S. *Colloids Surf B Biointerfaces* 2012;98:112–19.
- [354] Sathishkumar P, Preethi J, Vijayan R, Mohd Yusoff AR, Ameen F, Suresh S, et al. *J Photochem Photobiol B Biol* 2016;163:69–76.
- [355] Islam NU, Jalil K, Shahid M, Muhammad N, Rauf A. *Arab J Chem* 2015;.
- [356] Dingler A, Blum RP, Niehus H. *J Microencapsul* 1999;16:751–67.
- [357] Pardeike J, Hommoss A, Müller RH. *Int J Pharm* 2009;366:170–84.
- [358] Gref R, Couvreur P, Barratt G, Mysiakine E. *Biomaterials* 2003;24:4529–37.
- [359] Jana S, Manna S, Nayak AK, Sen KK, Basu SK. *Colloids Surf B Biointerfaces* 2014;114:36–44.
- [360] Raj S, Sumod U, Jose S, Sabitha M. *J Pharm Bioallied Sci* 2012;4:186.
- [361] Laouini A, Jaafar-Maalej C, Limayem-Blouza I, Sfar S, Charcosset C, Fessi H. *J Colloid Sci Biotechnol* 2012;1:147–68.
- [362] Tyagi LK, Kumar S, Maurya SS, Kori ML. *Bull Pharm Res* 2013;3:6–13.
- [363] Lohani A, Verma A, Joshi H, Yadav N, Karki N. *ISRN Dermatol* 2014;2014:1–14.
- [364] Shukla T, Upmanyu N, Prakash Pandey S, Gosh D. *Lipid Nanocarriers Drug Target*. Elsevier; 2018. p. 1–47.
- [365] Bhagyashree HAP. *J Bioanal Biomed* 2015;07:6–12.
- [366] Pereira F, Baptista R, Ladeiras D, Madureira AM, Teixeira G, Rosado C, et al. *Meas J Int Meas Confed* 2015;74:170–7.
- [367] Lacatusu I, Badea N, Murariu A, Nichita C, Bojin D, Meghea A. *Mol Cryst Liq Cryst* 2010;523 260/[832]-272/[844].
- [368] Takahashi M, Kitamoto D, Asikin Y, Takara K, Wada K. *J Oleo Sci* 2009;58:643–50.
- [369] Mitri K, Shegokar R, Gohla S, Anselmi C, Müller RH. *Int J Pharm* 2011;414:267–75.
- [370] Kaur CD, Saraf S. *J Cosmet Dermatol* 2011;10:260–5.
- [371] Gokce E, Korkmaz, Deller, Sandri, Bonferoni, Ozer O. *Int J Nanomed* 2012;1841.
- [372] Ganesan P, Choi DK. *Int J Nanomed* 2016;1987.

## Section 7

# **Functionalized nanomaterial in textiles industry**

This page intentionally left blank

# Functional nanofibers: fabrication, functionalization, and potential applications

Nabil A. Ibrahim, Moustafa M.G. Fouda and Basma M. Eid

*Textile Research Division, National Research Centre, Giza, Egypt*

## 20.1 Introduction

The increasing demand for high-quality, functional, and value-added nano-based functional materials with unique properties for numerous potential applications [1–7] without adversely affecting human health and environment has led to the adoption and application of innovative technologies especially advanced nanotechnology. This chapter addresses the current state of the art in the area of fabrication, functionalization, and potential applications of functionalized nanofibers (NFs). Future trends are also highlighted in brief.

## 20.2 Electrospinning

Electrospinning process is one of the most promising, efficient, and scalable techniques to fabricate NFs with entirely unique properties, like nanoporous surface morphology, large surface area-to-volume ratio, innovative physico-chemical, and biological properties along with high functionality in the range from submicron to nanoscale fiber diameter. Fabrication of solid NFs from polymeric solution, natural and/or synthetic, with or without proper additives is accomplished by application of electric force [8,9].

A typical electrospinning setup has the following units (Fig. 20.1):

- High-voltage power supply to provide an electrostatic field for electrospinning of polymer solution
- A spinneret, single or multi, with or without a flow control pump, which affects both the constructed form as well as productivity
- A fiber collector, either a stationary plate or a rotating drum, to provide different NF assemblies according to the actual needs and final applications [10–12]

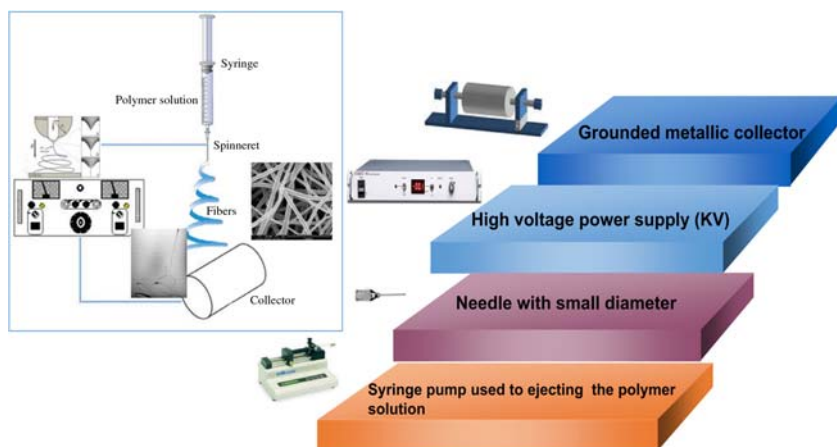


FIGURE 20.1 Electrospinning setup units.

### 20.3 Fabrication steps

Generally, the main steps to construct and fabricate natural and/or synthetic polymers NFs comprise [10,12]:

- Preparing a polymer solution of specific viscosity by using a proper solvent
- Charging the polymer solution into a syringe followed by pumping through a thin nozzle with an inner diameter range from 100  $\mu\text{m}$  to 1 nm
- Cone-jet formation
- Formation of a continuous ultrathin fiber under electric field
- Evaporation of the used solvent in the polymer jet before reaching the collector
- Deposition of NF layer-by-layer polymer onto the collecting target, followed by the formation of nonwoven NF mat

The main parameters affecting the fabrication of NFs using electrospinning techniques include [12–15]:

- Polymer: molecular weight, solution viscosity, charge density, surface tension, conductivity, etc.
- Processes conditions: field strength, tip-to-collector distance, flow rate, needle tip design, collector composition and geometry, etc.
- Environmental conditions: temperature, humidity, air velocity, etc.

Both solution viscosity and conductivity play important roles in determining the efficiency of fiber formation during the electrospinning process. On the other hand, the obtained electrospun fiber diameter is governed by the applied voltage, solution concentration, and tip-to-collector gap. An increase in the applied voltage results in a decrease in fiber diameter along with rapid

evaporation of the used solvent from the NFs. A lower flow rate is desirable to ensure high solvent evaporation. Additionally, decreasing the tip-to-collector distance enables the fabrication of flatter or smaller NFs. Meanwhile, increasing this distance gives rounder NFs. Moreover, decreasing solution viscosity at high temperature favors the formation of finer NFs during the electrospinning process, and high humidity may positively affect discharge of electrospun [10,11,14,15].

Generally, using the simple electrospinning technique brings about randomly oriented NF type, while aligned NF type can be formed by using numerous approaches such as a combination of mechanical and electrostatic tools, electrostatic steering of the NFs at collector or by using a rotating collector [15,16].

## 20.4 Polymers used in electrospun NFs

The most commonly used natural and/or synthetic polymers with remarkable potential for the fabrication of NFs using electrospinning are listed in Table 20.1.

NFs based on a broad range of natural biopolymers such as gelatin, chitosan, collagen, cellulose, modified starch, etc., are preferred over NFs based on synthetic ones especially for biomedical applications like pharmaceuticals

**TABLE 20.1** Most commonly studied natural and/or synthetic polymers for fabrication of electrospun NFs.

Natural polymer [12,15–21]	Synthetic polymers [12,16,22,23]	Combination [12,14,20,24–27]
<ul style="list-style-type: none"> <li>● Cellulose derivatives</li> <li>● Starch and modified starch</li> <li>● Chitin &amp; chitosan</li> <li>● Alginate</li> <li>● Gelatin &amp; collagen</li> <li>● Aloe vera</li> <li>● Silk fibron</li> <li>● Hyaluronic acid</li> <li>● Gelatin/chitosan</li> <li>● Cellulose/chitosan</li> <li>● Gelatin/keratin</li> </ul>	<ul style="list-style-type: none"> <li>● Poly(lactic acid), PLA</li> <li>● Polyvinyl alcohol, PVOH</li> <li>● Polyvinyl acetate, PVAC</li> <li>● Poly(amide), PA</li> <li>● Poly(acrylonitrile), PAN</li> <li>● Poly(ethylene) oxide, PEO</li> <li>● Poly(ethylene) glycol, PEG</li> <li>● Poly(urethane), PU</li> <li>● Poly(ethyleneterephthalate), PET</li> <li>● Poly(caprolactone), PCL</li> <li>● Poly(lactide-co-glycolide), PLGA</li> <li>● Aromatic poly(imide), PIs</li> </ul>	<ul style="list-style-type: none"> <li>● Starch/PCL</li> <li>● Starch/PVOH</li> <li>● Starch/PLA</li> <li>● Starch/PLGA</li> <li>● Gelatin/PVOH</li> <li>● Chitin/PET or Chitosan/PET</li> <li>● Chitosan/PVOH</li> <li>● Gelatin/PCL</li> <li>● Cellulose/PVOH</li> <li>● Cellulose/PEO</li> <li>● Dextran/PVOH</li> <li>● Dextran/PLA</li> <li>● Wool keratin/PEO</li> </ul>

and drug release and in wound healing, vascular grafts, and tissue-engineering scaffolds. Biopolymers are commercially available, naturally abundant, biocompatible, biodegradable, and nonimmunogenic. However, natural polymers are more difficult to fabricate in comparison with synthetic ones most probably due to their complex chemical structure, molecular weight, limited solubility, high surface tension, poor mechanical properties as well as rapid biodegradability. One of the most effective approaches to overcome and solve the abovementioned problems and drawbacks is to blend them with proper biocompatible synthetic polymers that can be easily electrospun and successfully can be help form NFs of natural polymers [20,28,29], or by a postcross-linking process with proper cross-linkers [14].

## 20.5 Functional NFs

Various approaches have been devoted to fabricating functional NFs with highly demanded functional properties for advanced potential applications. Particular attention has been given to:

### 20.5.1 Fabrication of structural functional NFs

Using electrospinning technique, with different morphologies such as core-sheath, aligned, porous, and gradient structures, to impart excellent properties such as very large specific area, excellent mechanical performance via fiber orientation, and loading capacity [30,31]. Recent studies have proved that using miscible solvents for preparing polymer solution or emulsion electrospinning could help the formation of core-shell fabric structure (Fig. 20.2) [32–34]. Additionally, using a rotating fiber collector along with a field controllable electrode brings about highly aligned/oriented NFs with superior mechanical properties for a wide range of potential applications in such fields [35]. Furthermore, electrospun porous NFs could be successfully prepared by using highly volatile solvents, like methylene chloride thereby facilitating formation of pores during electrospinning, by employing bicomponent spinning, or by thermal treatment under different atmospheric conditions (e.g., carbon or inorganic porous NFs) [30,36]. On the other hand, fabrication of gradient NFs with desirable mechanical performance facilitates their use in a wide range of engineering applications (e.g., mechanical, filtration, photoelectric, and tissue engineering) [37,38].

### 20.5.2 Development of new composite functional NFs with multifunctional capabilities and enhanced physicochemical properties

Composite functional NFs include polymer/polymer, polymer/nanoparticles, and polymer/inorganic salt composite NFs [39]. Electrospinning of polymer

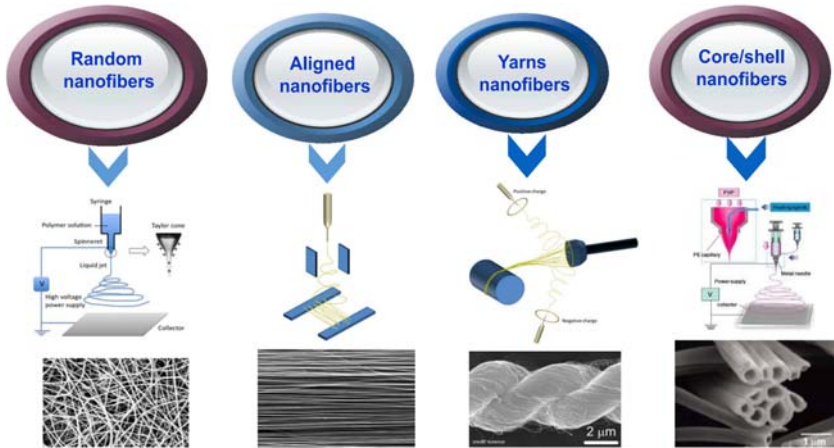


**FIGURE 20.2** Different NF morphologies.

blends such as chitosan and PVOH or PEO polymer result in the formation of composite NFs with improved mechanical and functional properties [40,41]. Polymer/nanocomposite NFs can be produced by (1) postimmersing of the prefabricated NFs into a nanoparticulate containing composite solution followed by thermal or chemical treatment to enhance the extent of fixation of the loaded NPs onto the NFs, and by (2) direct electrospinning of a polymer solution containing the selected NPs (e.g., montmorillonite, Ag, ZnO, SiO<sub>2</sub>, TiO<sub>2</sub>, Cu, Fe<sub>3</sub>O<sub>4</sub> NPs, etc.) as a one-step procedure [28,39,42–47].

Additionally, fabrication of polymer/inorganic salt composite NFs, such as PAN/ZnCl<sub>2</sub> and PAN/FeCl<sub>3</sub> NFs, have potential uses for new applications like optical and catalysis materials, environmental protection, and human health [48–50].

### 20.5.3 Production of inorganic NFs with different styles and various functions

The production methods of inorganic NFs include: (1) Mixing the nominated inorganic precursors with proper polymers for electrospinning followed by subsequent calcination at high temperature, and (2) by controlling both the reaction velocity and precursor solution viscosity for direct electrospinning [51]. Combined sol–gel and electrospinning techniques for processing inorganic NFs have several advantages including simplicity, applicability, and low cost [52]. The combination of sol–gel and electrospinning techniques has been successfully used to fabricate TiO<sub>2</sub> inorganic NFs [51] using the Ti (OC<sub>4</sub>H<sub>9</sub>)<sub>4</sub> solution as precursor. Recently, selected dopants based on metal or nonmetal materials have been doped with inorganic NFs to enlarge their application areas and upgrade their functional properties [51].



### 20.5.4 Surface modification and functionalization of polymer NFs

Different technologies such as physical, chemical, and/or biotechnology are used in order to impart the desired surface and functional properties for opening up a variety of technical applications (Fig. 20.3) [53,54].

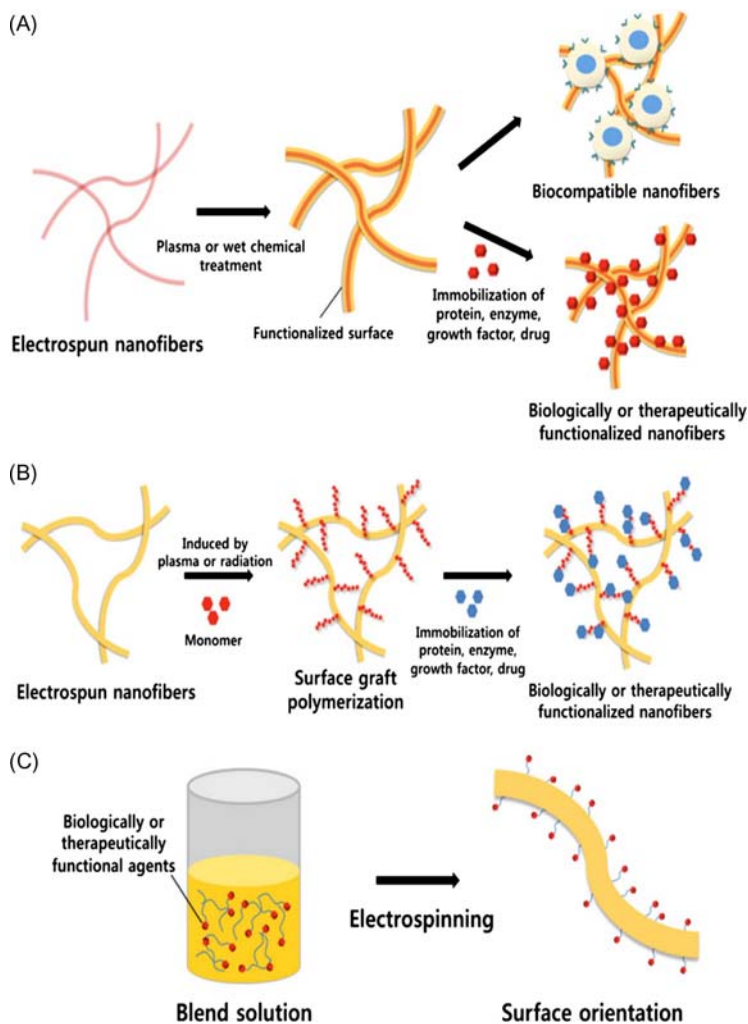


**FIGURE 20.3** Surface modification techniques of electrospun NFs. (A) Plasma treatment or wet chemical method. (B) Surface graft polymerization. (C) Coelectrospinning. *Reprinted with permission from Cai Y, Wang Q, Wei Q, You Q, Huang F, Song L, et al. Structure, thermal, and antibacterial properties of polyacrylonitrile/ferric chloride nanocomposite fibers by electrospinning. Int J Polym Anal Charact. 2010;15(2):110–118 [50]. Copyright (2009) Elsevier.*

### 20.5.4.1 Using physical technologies

Plasma treatment, as an ecofriendly tool, results in remarkable physicochemical surface modification of NFs as a direct consequence of generation of active species (e.g., free radicals, electrons, etc.) without adversely affecting the bulk properties of the treated substrate [55–59]. Surface modification of PA6–NFs with cold plasma results in a significant improvement in their surface wettability [60]. On the other hand, treatment of cellulose triacetate, CTA, and electrospun mat with CF<sub>4</sub>–plasma imparts superhydrophobicity to the CTA fibrous mat [61]. Additionally, plasma-induced grafting has also been used to upgrade the hydrophilicity of poly(lactic-co-glycolic acid), PLGA–NFs using O<sub>2</sub> or ammonia gas as a direct consequence of the creation of polar groups onto NFs [62]. Moreover, using a physical vapor deposition (PVD) coating process that includes evaporation and metallic sputter coating results in significant improvement in electrical properties and surface conductivity [63]. Also modification of the mechanical properties of PVOH–NFs can be achieved by using a broad energy ion beam implementation [64].

### 20.5.4.2 Using chemical technologies

Surface modification and functionalization of NFs using chemical technologies can be categorized into surface grafting, chemical cross-linking, chelation as well as surface chemical deposition [53].

Pretreatment of poly(carpolactone)–PCL–NFs with air plasma to create –COOH groups on NFs surface followed by covalent grafting of gelation using water-soluble carbodiimide as coupling agent enhanced compatibility and spreading of endothelial cells (ECs) and orientation along the fabricated NFs for potential application as blood vessels [65].

On the other hand, cross-linking of PVOH–NFs using glutaraldehyde as a cross-linker in acetone results in remarkable improvement in the obtained NF water resistance along with improvement in their mechanical properties [66].

Additionally, modified amido-oxime-polyacrylonitrile (AOPAN–NFs) by metal chelation were fabricated by pretreatment with hydroxylamine hydrochloride to introduce adsorption sites for chelation of metal ions [53].

Moreover, surface functionalization of PA6–NFs by electroless deposition of a wide range of metals such as Au, Cu, and Ni was carried out by pre-O<sub>2</sub>–plasma treatment at low temperature (Fig. 20.4) [67].

### 20.5.4.3 Using nanotechnologies

A wide range of options have been developed to fabricate nanostructured and functional NFs using nanotechnology for specific applications [53].

The sol–gel technique has been widely used to develop functional coatings on a wide range of materials [57,68]. Postdeposition of ZnO onto

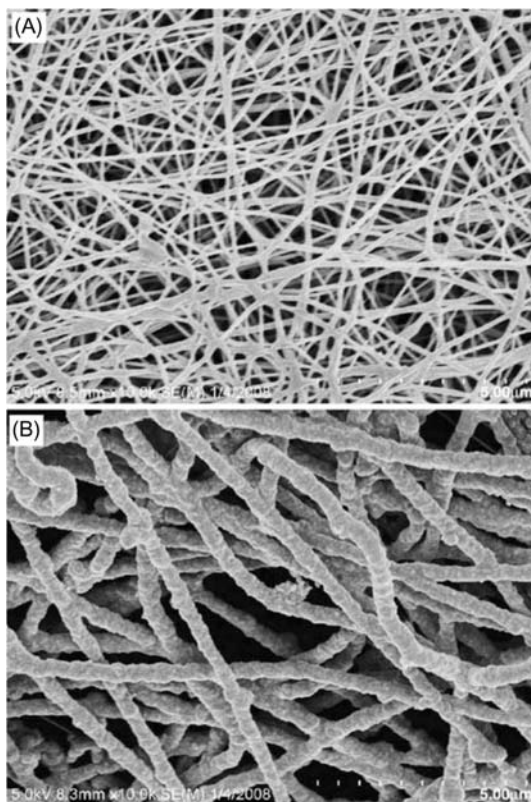


**FIGURE 20.4** SEM images of the electrospun PA6 fibers before and after Cu deposition: (A) as spun and (B) after Cu deposition. Reprinted with permission from Wei Q, Tao D, Gao W, Huang Y. *Scanning electron microscopy and atomic force microscopy of composite nanofibres. Microscopy Anal* 2008;22(2):11–12. Copyright (2008) Springer Nature.

PVAc-NFs using sol–gel technique followed by carbonization results in the formation of functional carbon NFs [45,69]. On the other hand, combining sol–gel process with electrospinning technique can be used to get PVAc/TiO<sub>2</sub> Hybrid Nanofibers [47]. Moreover, Al<sub>2</sub>O<sub>3</sub> sol–gel coating of nonwoven PET fabrics results in a significant improvement in the wettability of the modified surface [70].

Modification of surface properties of polymer NFs has also been studied [71] via doping of Ag NPs into PAN–NF film by in situ reduction of Ag ions using N<sub>2</sub>H<sub>5</sub>OH as a reductant.

On the other hand, multilayer coating using layer-by-layer (LbL) deposition has many attractive advantages over the monolayer counterpart [72]. Combination of electrospinning technique along with LbL technology enables fabrication of hybrid multilayered hollow NFs based on

TiO<sub>2</sub>/polyacrylate [73]. Also, LbL technology has been used to fabricate homogenous and ultrathin films of carbon NFs using chitosan as a binding agent [74].

#### 20.5.4.4 Using biotechnology

Immobilization of bioactive molecules on the surface of NFs is an option to obtain biologically functionalized NFs essential for utilization in specific applications such as drug delivery, tissue engineering as a well as biosensors [53].

Enzyme immobilization approaches include physical adsorption and chemical binding and by entrapment [75,76]. Immobilization of catalases onto AOPAN–NF membrane increased its storage stability as well as reusability for a wide range of applications such as synthesis pharmaceutical chemicals, bioremediation, biosensors fabrication, and food processing [53,77] (Fig. 20.5) [55].

#### 20.5.5 Molecular imprinting

Recently many attempts have been made to fabricate molecularly imprinted NF membranes as novel functional materials for potential technical applications [53,78]. Many trials have been developed to introduce imprinting recognition sites on the membrane surface via surface photografting [79], surface

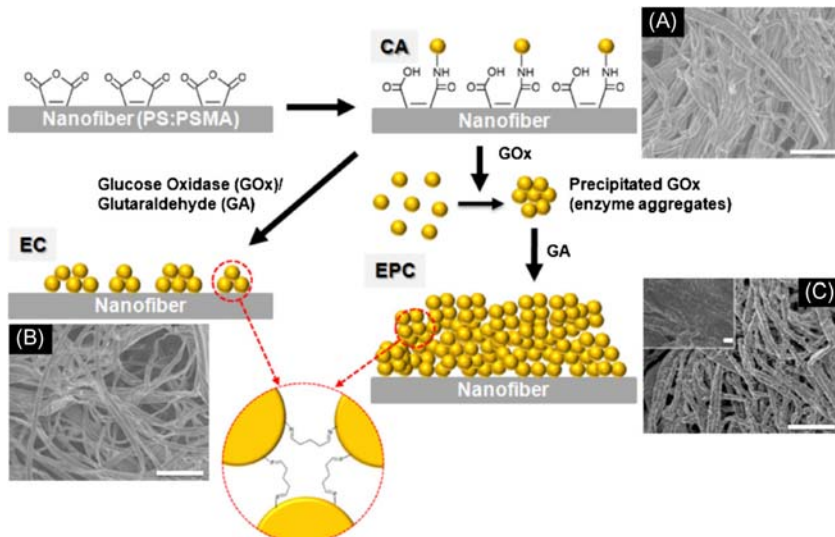


**FIGURE 20.5** Schematic illustration of three different approaches to GOx immobilization on NFs, together with SEM images of (A) covalent attachment (CA–GOx), (B) enzyme coating (EC–GOx), and (C) enzyme precipitate coating (EPC–GOx). Reprinted with permission from Park JH, Kim BS, Yoo YC, Khil MS, Kim HY. Enhanced mechanical properties of multilayer nano-coated electrospun nylon 6 fibers via a layer-by-layer self-assembly. *J Appl Polym Sci*. 2008;107(4):2211–2216. Copyright (2011) Elsevier.

deposition [80] as well as emulsion polymerization [81]. The extent of adoption of the abovementioned approaches is determined by simplicity in preparation, imprinted efficiency and binding capacity, media of imprinting process, in aqueous or nonaqueous, as well as the size of imprinting molecules.

## 20.6 Potential applications

Table 20.2 lists some functionalized NFs and their potential applications.

## 20.7 Future trends

Additional RST efforts are expected in the future to improve NFs formulation, scale up both the fabrication and functionalization processes taking in consideration the cost-benefit analysis and environmental concerns, as well as to upgrade both performance and functional properties of the produced NFs construct for diverse and novel areas of applications.

The possible future trends in fabrication, functionalization, and new applications of NFs will be focused on:

- Cutting down the drawbacks of the used polymeric materials, harsh solvent, active ingredients, and chemicals, as well as fabrication and post-processing technologies to develop highly functional NFs construct with superior properties comply with a wide range of applications.
- Adoption of environmentally sound and sustainable emerging technologies to fabricate NFs construct with innovative functionalities.
- Enabling the translation of emerging technologies for fabrication and functionalization of NFs construct from research stage to the full commercialization and deployment stage taking in consideration the economy and ecology aspects as well as social responsibility.
- Fabrication of multifunctional NFs, composite NFs, membranes and filters, etc., by using physical, chemical, nano-, and/or biotechnologies for highly demanded and novel applications such as tissue engineering, wound dressing, drug delivery, water and air filtration and purification, in protective clothing, sound absorption, and in the food industry, which is still a challenge and will be one of the hot topics and highly demanded targets in the future.

On the other hand, to achieve a breakthrough in the field of fabrication and potential applications of the functional NFs structure as well as to avoid or minimize the potential risk of nanoscale products and their overall negative impacts on humans and environment, extensive collaboration and integration of researchers in different fields including material sciences, chemistry, engineering, biology, environment, and industrialists are needed in the near future.

**TABLE 20.2** Some functional NFs and their potential applications.

Potential application	Type of functionalized nanofiber (FNFs)	References
<b>Encapsulation</b>	Chitosan nanobead encapsulation of quantum dots (QDs)	[82]
	Polyphenolic antioxidants/zein/gelatin shell core fibers	[83]
<b>Transdermal</b>	Gellan/polyvinyl alcohol (PVOH) NFs	[84]
<b>Antibacterial</b>	Carboxymethyl dandelions (CPD)/polyethylene oxide (PEO) NF matrix	[85]
	Benzyl triethylammonium chloride (BTEAC) functionalized poly(vinyl alcohol) (PVOH) NFs	[86]
	Aloe vera polyvinylpyrrolidone (Av/PVP) and aloe vera acetate-polyvinylpyrrolidone (AvAc/PVP) electrospun fibers	[87]
	Monolaurin-loaded electrospun shellac NFs	[88]
	Silver NP-loaded poly(vinyl alcohol)–lignin electrospun NFs	[89]
	Cross-linked pectin NFs with well-dispersed Ag NPs	[90]
	Lignin-decorated thin multiwalled carbon nanotubes in poly(vinyl alcohol) nanocomposites	[91]
	Polycaprolactone/gelatin/hydroxyapatite NPs-loaded doxycycline	[92]
<b>Bone regeneration</b>	Hydroxyapatite/peptide scaffolds NFs	[93]
<b>Hydrogel</b>	Chitosan/TEMPO-oxidized cellulose NFs	[94]
<b>Stem cell</b>	End-functional Poly(lactide); PLLA/peptide Tyr-Ile-Gly-Ser-Arg (YIGSR) NFs	[95]
<b>Immune sensor</b>	Carboxylated multiwalled carbon nanotube (MWCNT) doped nylon 6 (PA6) composite NFs (MWCNT-PA6)	[96]
<i>(Continued)</i>		

**TABLE 20.2 (Continued)**

Potential application	Type of functionalized nanofiber (FNFs)	References
<b>Biosensor</b>	The functional NFs composites (PG/GR/CS/PPy). (PG, the graphene (GR) doped polycaprolactam 6 (PA6) were prepared via one-step electrospinning), graphene (GR) and chitosan (CS) were served as the nanosized backbones for pyrrole (Py) electropolymerization	[97]
	Carbon nanotubes (MWCNTs) doped chitosan (CTS)	[98]
<b>Scaffolds</b>	Graphene–NF hybrid (Fig. 20.6)	[99]
	Blend NFs of polycaprolactone CA/PCL	[100]
	Poly( $\epsilon$ -caprolactone)/amino-functionalized tannin electrospun	[101]
	Polycaprolactone PCL/zein/gum arabic electrospun nanocomposite scaffold	[102]
<b>Biomedical</b>	Tinidazole (TNZ) functionalized biodegradable chitosan/poly( $\epsilon$ -caprolactone) (PCL) mucoadhesive hybrid NF membrane (TNZ–PCHNF)	[103]
	Auxetic polycaprolactone (PCL) based NF membranes	[104]
	Casein NFs with silver NPs	[105]
	Hydroxypropyl methylcellulose/polyethylene oxide blend NFs	[106]
	Electrospun nonwovens of poly( $\epsilon$ -caprolactone)/quaternized chitosan	[107]
	Honey bee propolis-loaded cellulose acetate NFs	[108]
<b>Gas sensing</b>	WO <sub>3</sub> NFs functionalized by RuO <sub>2</sub> NPs loaded by apoferritin	[109]
	WO <sub>3</sub> –Au NFs has been fabricated	[110]
<b>Glucose sensing</b>	MnO <sub>2</sub> NPs and carbon NF nanocomposites	[111]
<b>Drug delivery</b>	Cellulose acetate electrospun NFs	[23]
	Immobilization of the antibiotic gentamicin sulfate (GS) in electrospun fiber mats composed of poly(lactic acid) (PLA), poly( $\epsilon$ -caprolactone) (PCL), and the copolymer poly(lactic-co-glycolic acid) (PLGA)	[112]
	Biocompatible PCL–NFs modified by COOH–anhydride plasma polymers and gentamicin immobilization	[113]
	Poly(ethylene terephthalate) for encapsulation and delivery of anionic antibiotics	[114]

<b>Wound dressing/ healing</b>	Beta-glucan ( $\beta$ G)-loaded NF wound dressing	[115]
	Starch-based NF	[116]
	Chitosan/polyvinyl alcohol/zinc oxide nanofibrous mats	[117]
	Fibronectin NFs	[118]
	Curcumin-loaded electrospun poly(3-hydroxy butyric acid-co-3-hydroxy valeric acid) (PHBV) NFs	[119]
	Poly(caprolactone) (PCL) nanofibrous membranes functionalized with biosynthesized Maillard reaction products (MRPs)	[120]
	Poly(vinyl alcohol) incorporated with functionally active silk sericin	[121]
	Poly(caprolactone)—chitosan—poly(vinyl alcohol) (PCL: Cs: PVA) nanofibrous blend scaffolds	[122]
	Electrospun chitosan/polycaprolactone-hyaluronic acid bilayered scaffold	[123]
	Electrospun polycaprolactone coated with gelatin—silver NPs	[124]
	Electrospun poly( $\epsilon$ -caprolactone)/gelatin micro/NFs	[125]
	Ciprofloxacin-loaded sodium alginate/poly(lactic-co-glycolic acid) electrospun fibrous	[126]
	Nanochitosan—poly- $\epsilon$ -caprolactone electrospun	[127]
	Silver nanoparticle/bacterial cellulose nanocomposite	[128]
	Chitosan/poly(vinyl alcohol)/graphene oxide composite	[129]
	Cross-linked electrospun cartilage acellular matrix/poly(caprolactone-co-lactide-co-glycolide) NF	[130]
<b>Vascular graft</b>	Eugenol-loaded electrospun membranes of poly( $\epsilon$ -caprolactone)/gelatin incorporated with REDV	[131]
<b>Tissue Engineering</b>	Polyurethane/poly(glycerol sebacate) hybrid scaffolds	[132]
	Multiwalled carbon nanotubes on electrospun poly(3-hydroxybutyrate) scaffold	[133]
<b>Packaging industry</b>	Pullulan (PL) and lysozyme NFs (LNFs) nanocomposite films	[134]
	$\epsilon$ -poly-lysine/chitosan NFs	[135]
	Thyme essential oil/gelatin NFs	[136]
(Continued)		



**TABLE 20.2 (Continued)**

Potential application	Type of functionalized nanofiber (FNFs)	References
	Nisin-loaded NPs	[137]
	Poly(ethylene oxide) NFs containing tea tree oil/beta-cyclodextrin	[138]
	Gelatin-glycerin- $\epsilon$ poly-lysine NF	[139]
	$\epsilon$ -Poly-lysine/chitosan NFs	[135]
	Chitosan-adsorbed cellulose NF (CNF) films	[140]
	Chitosan and (2-carboxyethyl)- $\beta$ -cyclodextrin onto polylactic acid (PLLA)	[141]
<b>Pollutant/dye removal</b>	Novel bromopropyl functionalized silica NF films. The mixture of tetraethylorthosilicate (TEOS) and polyvinyl alcohol (PVA) followed by calcination and subsequent surface modification with 3-bromopropyl trichlorosilane (BPTCS)	[142]
	Cyclodextrin functionalized cellulose NF composites	[143]
	Polyacrylonitrile NFs functionalized with EDTA	[144]
	PAN–CNT/TiO <sub>2</sub> –NH <sub>2</sub> NFs using electrospinning technique followed by chemical modification of TiO <sub>2</sub> NPs	[145]
	Polyacrylonitrile NFs (oPAN@C) through preoxidation and hydrothermal carbonization	[146]
	Nanosheet of Mo/N-codoped TiO <sub>2</sub> nanorods immobilized on carbon NFs	[147]
	Polyacrylonitrile NFs/biogenic silica composite NFs	[148]

	Malachite green dye via surface modified polyacrylonitrile NFs/biogenic silica composite NFs	[148]
	Polyethersulfone nanofibrous membranes	[149]
	Chitosan composite adsorbent functionalized with EDTA	[150]
	Cellulose acetate/graphene oxide composite NFs	[151]
<b>Protective clothing</b>	Electrospun NFs in protective clothing	[152]
	Nanofibrous mats of polyamide 6 (PA6) were deposited onto a nonwoven viscose substrate by electrospinning technique	[153]
	Electrospun polyurethane fiber web layered on spunbonded nonwoven were developed	[154]
	Polyurethane electrospun NF membranes for protective clothing	[155]
	Polyurethane (TPU) and a hydrophilic poly(vinyl alcohol) (PVA) electrospun NF mats	[156]
	ZnO/Nylon 6 NF	[157]
	Polyurethane (TPU) tree-like NF membrane was fabricated via one-step electrospinning by adding a small amount of tetrabutylammonium chloride (TBAC)	[158]
<b>Ion-exchange membranes</b>	Poly(acrylic acid) (PAA) was grafted to the surfaces of individual NFs that had been modified with poly(glycidyl methacrylate)	[159]
	Ion-exchange zirconium sorption by functionalized carbon NFs	[160]
<b>Super capacitor</b>	Functionalized graphene oxide-reinforced electrospun carbon NFs	[161]
	Graphene-polyaniline/polypyrrole/activated carbon/carbon nanotube	[162]
(Continued)		

**TABLE 20.2 (Continued)**

Potential application	Type of functionalized nanofiber (FNFs)	References
<b>Filtration</b>	Polyacrylonitrile (PAN)/polyaniline (PANI)—nylon core-shell NF membrane	[163]
	Nylon 6 & nylon 6,6 NF membranes (Fig. 20.7)	[164,165]
	Poly(vinyl alcohol) NFs containing benzyl triethylammonium chloride	[166]
	Soy protein isolate (SPI)/polyvinyl alcohol (PVA) system	[167]
	Graphene oxide-embedded titanate NF membranes	[168]
	Lignin—zeolite composite NFs	[169]
	PAN—PVC nonwoven mats	[170]
	Iron-doped electrospun chitosan NF mat	[171]
	Cellulose/polyacrylonitrile electrospun composite fiber	[172]
	Functionalized with cellulose nanofibrils/CdTe quantum dots	[173]
	TiO <sub>2</sub> incorporated polyacrylonitrile electrospun NFs	[174]
	Metallo—Terpyridine-modified cellulose NF	[175]
<b>Biotechnology</b>	Fabrication of Starch NFs	[176]

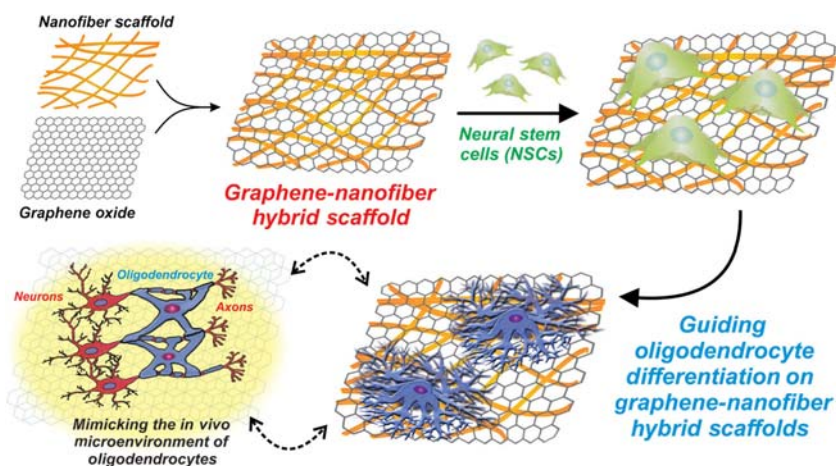


**FIGURE 20.6** Graphene–NF hybrid scaffold fabrication and application. Polymeric NFs, based on polycaprolactone, generated using electrospinning were subsequently coated with graphene oxide (GO) and seeded with neural stem cells (NSCs). Reprinted with permission from Smith Callahan LA, Xie S, Barker IA, Zheng J, Reneker DH, Dove AP, et al. Directed differentiation and neurite extension of mouse embryonic stem cell on aligned poly(lactide) nanofibers functionalized with YIGSR peptide. *Biomaterials*. 2013;34(36):9089–9095. Copyright (2014) John Wiley & Sons.

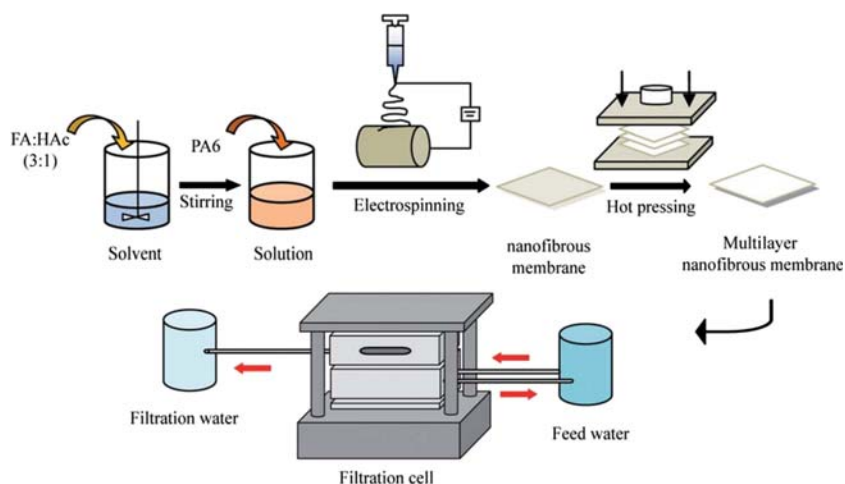


**FIGURE 20.7** Preparation of PA6 multilayer nanofibrous membranes and filtration cell setup for dye filtration. Reprinted with permission from Yu Y, Ma R, Yan S, Fang J. Preparation of multi-layer nylon-6 nanofibrous membranes by electrospinning and hot pressing methods for dye filtration. *RSC Adv*. 2018, 8, 12173 Published by The Royal Society of Chemistry. This article is licensed under a Creative Commons Attribution-NonCommercial 3.0 Unported Licence.

## Abbreviations

<b>AOPAN</b>	amido-oxime-polyacrylonitrile
<b>BTEAC</b>	benzyl triethylammonium chloride
<b>CNF</b>	cellulose nanofiber
<b>CNT</b>	carbon nanotube
<b>CPD</b>	carboxymethyl dandelions
<b>CS</b>	chitosan
<b>CTA</b>	cellulose triacetate
<b>CTS</b>	chitosan
<b>ECs</b>	endothelial cells
<b>EDTA</b>	ethylenediaminetetraacetic acid
<b>GOx</b>	graphite oxide
<b>GR</b>	graphene
<b>LbL</b>	layer-by-layer
<b>NFs</b>	nano-nanofibers
<b>NPs</b>	nanoparticles
<b>PA</b>	poly(amide)
<b>PA6</b>	polyamide 6
<b>PAN</b>	poly(acrylonitrile)
<b>PCL</b>	poly(caprolactone)
<b>PEG</b>	poly(ethylene) glycol
<b>PEO</b>	poly(ethylene) oxide
<b>PET</b>	poly(ethyleneterephthalate)
<b>PG</b>	the graphene (GR) doped polycaprolactam 6 (PA6)
<b>PIs</b>	poly(imide)
<b>PLA</b>	poly (lactic acid)
<b>PLGA</b>	poly(lactide- <i>co</i> -glycolide)
<b>PLLA</b>	poly(lactide)
<b>PU</b>	poly(urethane)
<b>PVAC</b>	polyvinyl acetate
<b>PVD</b>	physical vapor deposition
<b>PVOH</b>	polyvinyl alcohol
<b>PVP</b>	polyvinylpyrrolidone
<b>Py</b>	pyrrole
<b>QDs</b>	quantum dots
<b>REDV</b>	a short active peptide,
<b>TEMPO</b>	2,2,6,6-tetramethylpiperidine-1-oxyl radical
<b>TNZ</b>	tinidazole
<b>YIGSR</b>	Tyr-Ile-Gly-Ser-Arg peptide

## References

- [1] Gleiter H. Nanostructured materials: basic concepts and microstructure. *Acta Mater* 2000;48(1):1–29.
- [2] Noor-Evans F, Peters S, Stingelin N. Nanotechnology innovation for future development in the textile industry. In: Horne L, editor. *New product development in textiles*. Woodhead Publishing; 2012. p. 109–31.

- [3] Ibrahim NA. Nanomaterials for antibacterial textiles. In: Rai M, Kon K, editors. *Nanotechnology in diagnosis, treatment and prophylaxis of infectious diseases*. Boston, MA: Academic Press; 2015. p. 191–216.
- [4] Palit S, Hussain CM. Nanomaterials for environmental science: a recent and future perspective. In: Hussain CM, Mishra AK, editors. *Nanotechnology in environmental science*. Wiley-VCH Verlag GmbH & Co; 2018. p. 3–18.
- [5] Palit S, Hussain CM. Chapter 1 - Engineered nanomaterial for industrial use. In: Mustansar Hussain C, editor. *Handbook of nanomaterials for industrial applications*. Elsevier; 2018. p. 3–12.
- [6] Kecili R, Hussain CM. Mechanism of adsorption on nanomaterials. In: Hussain CM, editor. *Nanomaterials in chromatography*. Elsevier; 2018. p. 89–115.
- [7] Palit S. Chapter 14 advanced environmental engineering separation processes, environmental analysis and application of nanotechnology: a far-reaching review. *Advanced environmental analysis: applications of nanomaterials*, vol. 1. The Royal Society of Chemistry; 2017. p. 377–416.
- [8] Bhardwaj N, Kundu SC. Electrospinning: a fascinating fiber fabrication technique. *Biotechnol Adv* 2010;28(3):325–47.
- [9] Subbiah T, Bhat GS, Tock RW, Parameswaran S, Ramkumar SS. Electrospinning of nanofibers. *J Appl Polym Sci* 2005;96(2):557–69.
- [10] Wei Q, Tao D, Xu Y. Nanofibers: principles and manufacture. In: Wei Q, editor. *Functional nanofibers and their applications*. Woodhead Publishing; 2012. p. 3–21.
- [11] Qiao Z, Shen M, Xiao Y, Zhu M, Mignani S, Majoral J-P, et al. Organic/inorganic nanohybrids formed using electrospun polymer nanofibers as nanoreactors. *Coord Chem Rev* 2018;372:31–51.
- [12] Moheman A, Alam MS, Mohammad A. Recent trends in electrospinning of polymer nanofibers and their applications in ultra thin layer chromatography. *Adv Colloid Interface Sci* 2016;229:1–24.
- [13] Kenry, Lim CT. Nanofiber technology: current status and emerging developments. *Prog Polym Sci* 2017;70:1–17.
- [14] Liu G, Gu Z, Hong Y, Cheng L, Li C. Electrospun starch nanofibers: recent advances, challenges, and strategies for potential pharmaceutical applications. *J Controlled Rel* 2017;252:95–107.
- [15] Thakkar S, Misra M. Electrospun polymeric nanofibers: new horizons in drug delivery. *Eur J Pharm Sci* 2017;107:148–67.
- [16] Panthi G, Park M, Kim H-Y, Park S-J. Electrospun polymeric nanofibers encapsulated with nanostructured materials and their applications: a review. *J Ind Eng Chem* 2015;24:1–13.
- [17] Qian Y-F, Zhang K-H, Chen F, Ke Q-F, Mo X-M. Cross-linking of gelatin and chitosan complex nanofibers for tissue-engineering scaffolds. *J Biomater Sci Polym Ed* 2011;22(8):1099–113.
- [18] Krieger C, Arrechi A, Kit K, McClements DJ, Weiss J. Fabrication, functionalization, and application of electrospun biopolymer nanofibers. *Crit Rev Food Sci Nutr* 2008;48(8):775–97.
- [19] Babitha S, Rachita L, Karthikeyan K, Shoba E, Janani I, Poornima B, et al. Electrospun protein nanofibers in healthcare: a review. *Int J Pharm* 2017;523(1):52–90.
- [20] Rezaei A, Nasirpour A, Fathi M. Application of cellulosic nanofibers in food science using electrospinning and its potential risk. *Comp Rev Food Sci Food Saf* 2015;14(3):269–84.

- [21] Yao C-H, Lee C-Y, Huang C-H, Chen Y-S, Chen K-Y. Novel bilayer wound dressing based on electrospun gelatin/keratin nanofibrous mats for skin wound repair. *Mater Sci Eng C* 2017;79:533–40.
- [22] Ding Y, Hou H, Zhao Y, Zhu Z, Fong H. Electrospun polyimide nanofibers and their applications. *Prog Polym Sci* 2016;61:67–103.
- [23] Khoshnevisan K, Maleki H, Samadian H, Shahsavari S, Sarrafzadeh MH, Larijani B, et al. Cellulose acetate electrospun nanofibers for drug delivery systems: applications and recent advances. *Carbohydr Polym* 2018;198:131–41.
- [24] Yang C, Wu X, Zhao Y, Xu L, Wei S. Nanofibrous scaffold prepared by electrospinning of poly(vinyl alcohol)/gelatin aqueous solutions. *J Appl Polym Sci* 2011;121(5):3047–55.
- [25] Maslaci NN, Ulusoy S, Uygun E, Çevikbaş H, Oksuz L, Can HK, et al. Ibuprofen and acetylsalicylic acid loaded electrospun PVP-dextran nanofiber mats for biomedical applications. *Polym Bull* 2017;74(8):3283–99.
- [26] Li B, Huang C, Yang X. Preparation and characterization of electrospun wool keratin/polyethylene oxide nanofibers for air filtration applications. *Dig J Nanomaterials & Biostructures (DJNB)* 2017;12(2):293–301.
- [27] Sathish Kumar Y, Unnithan AR, Sen D, Kim CS, Lee YS. Microgravity biosynthesized penicillin loaded electrospun polyurethane–dextran nanofibrous mats for biomedical applications. *Colloids Surf A: Physicochem Eng Asp* 2015;477:77–83.
- [28] Li D, Xia Y. Electrospinning of nanofibers: reinventing the wheel? *Adv Mater* 2004;16(14):1151–70.
- [29] Lee KY, Jeong L, Kang YO, Lee SJ, Park WH. Electrospinning of polysaccharides for regenerative medicine. *Adv Drug Deliv Rev* 2009;61(12):1020–32.
- [30] Wei Q, Xia X. Types and processing of structured functional nanofibers: core-shell, aligned, porous and gradient nanofibers. In: Wei Q, editor. *Functional nanofibers and their applications*. Woodhead Publishing; 2012. p. 22–37.
- [31] Fang J, Niu H, Lin T, Wang X. Applications of electrospun nanofibers. *Chin Sci Bull* 2008;53(15):2265.
- [32] Li X, Shen J, Wan M, Chen Z, Wei Y. Core–shell structured and electro-magnetic functionalized polyaniline composites. *Synth Met* 2007;157(13):575–9.
- [33] Xiaoqiang L, Yan S, Rui C, Chuanglong H, Hongsheng W, Xiumei M. Fabrication and properties of core-shell structure P(LLA-CL) nanofibers by coaxial electrospinning. *J Appl Polym Sci* 2008;111(3):1564–70.
- [34] Angeles M, Cheng H-L, Velankar SS. Emulsion electrospinning: composite fibers from drop breakup during electrospinning. *Polym Adv Technol* 2008;19(7):728–33.
- [35] Lee H, Yoon H, Kim G. Highly oriented electrospun polycaprolactone micro/nanofibers prepared by a field-controllable electrode and rotating collector. *Appl Phys A* 2009;97(3):559.
- [36] Zou L, Gan L, Lv R, Wang M, Huang Z-H, Kang F, et al. A film of porous carbon nanofibers that contain Sn/SnOx nanoparticles in the pores and its electrochemical performance as an anode material for lithium ion batteries. *Carbon*. 2011;49(1):89–95.
- [37] Matsuda T, Kawahara D. Electrospinning fabrication of high-trackable catheter tip with gradually graded or gradient flexibility. *J Biomed Mater Res Part B: Appl Biomater* 2008;87B(1):35–41.
- [38] Wen S, Liu L, Zhang L, Chen Q, Zhang L, Fong H. Hierarchical electrospun SiO<sub>2</sub> nanofibers containing SiO<sub>2</sub> nanoparticles with controllable surface-roughness and/or porosity. *Mater Lett* 2010;64(13):1517–20.
- [39] Cai Y, Wei Q, Huang F. Processing of composite functional nanofibers. In: Wei Q, editor. *Functional nanofibers and their applications*. Woodhead Publishing; 2012. p. 38–54.

- [40] Li L, Hsieh Y-L. Chitosan bicomponent nanofibers and nanoporous fibers. *Carbohydr Res* 2006;341(3):374–81.
- [41] Nguyen TTT, Tae B, Park JS. Synthesis and characterization of nanofiber webs of chitosan/poly(vinyl alcohol) blends incorporated with silver nanoparticles. *J Mater Sci* 2011;46(20):6528–37.
- [42] Drew C, Liu X, Ziegler D, Wang X, Bruno FF, Whitten J, et al. Metal oxide-coated polymer nanofibers. *Nano Lett* 2003;3(2):143–7.
- [43] Lim J-M, Moon JH, Yi G-R, Heo C-J, Yang S-M. Fabrication of one-dimensional colloidal assemblies from electrospun nanofibers. *Langmuir*. 2006;22(8):3445–9.
- [44] Chen R, Zhao S, Han G, Dong J. Fabrication of the silver/polypyrrole/polyacrylonitrile composite nanofibrous mats. *Mater Lett* 2008;62(24):4031–4.
- [45] Shao D, Wei Q, Zhang L, Cai Y, Jiang S. Surface functionalization of carbon nanofibers by sol–gel coating of zinc oxide. *Appl Surf Sci* 2008;254(20):6543–6.
- [46] Huang Z-M, Zhang YZ, Kotaki M, Ramakrishna S. A review on polymer nanofibers by electrospinning and their applications in nanocomposites. *Compos Sci Technol* 2003;63(15):2223–53.
- [47] Wu N, Shao D, Wei Q, Cai Y, Gao W. Characterization of PVAc/TiO<sub>2</sub> hybrid nanofibers: from fibrous morphologies to molecular structures. *J Appl Polym Sci* 2009;112(3):1481–5.
- [48] Bai J, Li Y, Yang S, Du J, Wang S, Zhang C, et al. Synthesis of AgCl/PAN composite nanofibres using an electrospinning method. *Nanotechnology*. 2007;18(30):305601.
- [49] Thavasi V, Singh G, Ramakrishna S. Electrospun nanofibers in energy and environmental applications. *Energy Environ Sci* 2008;1(2):205–21.
- [50] Cai Y, Wang Q, Wei Q, You Q, Huang F, Song L, et al. Structure, thermal, and antibacterial properties of polyacrylonitrile/ferric chloride nanocomposite fibers by electrospinning. *Int J Polym Anal Charact* 2010;15(2):110–18.
- [51] Wu N, Wei Q. Inorganic functional nanofibers: processing and applications. In: Wei Q, editor. *Functional nanofibers and their applications*. Woodhead Publishing; 2012. p. 71–91.
- [52] Shao C, Kim H, Gong J, Lee D. A novel method for making silica nanofibres by using electrospun fibres of polyvinylalcohol/silica composite as precursor. *Nanotechnology*. 2002;13(5):635–7.
- [53] Huang F, Wei Q, Cai Y. Surface functionalization of polymer nanofibers. In: Wei Q, editor. *Functional nanofibers and their applications*. Woodhead Publishing; 2012. p. 92–118.
- [54] Yoo HS, Kim TG, Park TG. Surface-functionalized electrospun nanofibers for tissue engineering and drug delivery. *Adv Drug Deliv Rev* 2009;61(12):1033–42.
- [55] El-Zawahry MM, Ibrahim NA, Eid MA. The impact of nitrogen plasma treatment upon the physical-chemical and dyeing properties of wool fabric. *Polym Technol Eng* 2006;45(10):1123–32.
- [56] Ibrahim NA, El-Hossamy M, Hashem MM, Refai R, Eid BM. Novel pretreatment processes to promote linen-containing fabrics properties. *Carbohydr Polym* 2008;74(4):880–91.
- [57] Ibrahim NA, Eid BM, Hashem MM, Refai R, El-Hossamy M. Smart options for functional finishing of linen-containing fabrics. *J Ind Text* 2010;39(3):233–65.
- [58] Ibrahim NA, Eid BM, Abdel-Aziz MS. Green synthesis of AuNPs for eco-friendly functionalization of cellulosic substrates. *Appl Surf Sci* 2016;389:118–25.



- [59] Ibrahim NA, Eid BM, Abdel-Aziz MS. Effect of plasma superficial treatments on antibacterial functionalization and coloration of cellulosic fabrics. *Appl Surf Sci* 2017;392:1126–33.
- [60] Wei QF, Gao WD, Hou DY, Wang XQ. Surface modification of polymer nanofibres by plasma treatment. *Appl Surf Sci* 2005;245(1):16–20.
- [61] Yoon YI, Moon HS, Lyoo WS, Lee TS, Park WH. Superhydrophobicity of cellulose triacetate fibrous mats produced by electrospinning and plasma treatment. *Carbohydr Polym* 2009;75(2):246–50.
- [62] Park H, Lee KY, Lee SJ, Park KE, Park WH. Plasma-treated poly(lactic-co-glycolic acid) nanofibers for tissue engineering. *Macromol Res* 2007;15(3):238–43.
- [63] Wei Q, Tao D, Gao W, Huang Y. Scanning electron microscopy and atomic force microscopy of composite nanofibres. *Microscopy Anal* 2008;22(2):11–12.
- [64] Wong KKH, Hutter JL, Zinke-Allmang M, Wan W. Physical properties of ion beam treated electrospun poly(vinyl alcohol) nanofibers. *Eur Polym J* 2009;45(5):1349–58.
- [65] Ma Z, He W, Yong T, Ramakrishna S. Grafting of gelatin on electrospun poly(caprolactone) nanofibers to improve endothelial cell spreading and proliferation and to control cell orientation. *Tissue Eng* 2005;11(7-8):1149–58.
- [66] Wang X, Chen X, Yoon K, Fang D, Hsiao BS, Chu B. High flux filtration medium based on nanofibrous substrate with hydrophilic nanocomposite coating. *Environ Sci Technol* 2005;39(19):7684–91.
- [67] Tao D, Wei Q, Cai Y, Xu Q, Sun L. Functionalization of polyamide 6 nanofibers by electroless deposition of copper. *J Coat Technol Res* 2008;5(3):399–403.
- [68] Ibrahim NA, Refaie R, Ahmed AF. Novel approach for attaining cotton fabric with multifunctional properties. *J Ind Text* 2010;40:65–83.
- [69] Liu Z, Jin Z, Li W, Liu X. Ordered porous ZnO thin films formed by dip-coating method using PS templates. *J Sol-Gel Sci Technol* 2006;40(1):25–30.
- [70] Xiao X, Chen F, Wei Q, Wu N. Surface modification of polyester nonwoven fabrics by Al<sub>2</sub>O<sub>3</sub> sol–gel coating. *J Coat Technol Res* 2009;6(4):537.
- [71] Wang Y, Yang Q, Shan G, Wang C, Du J, Wang S, et al. Preparation of silver nanoparticles dispersed in polyacrylonitrile nanofiber film spun by electrospinning. *Mater Lett* 2005;59(24):3046–9.
- [72] Park JH, Kim BS, Yoo YC, Khil MS, Kim HY. Enhanced mechanical properties of multilayer nano-coated electrospun nylon 6 fibers via a layer-by-layer self-assembly. *J Appl Polym Sci* 2008;107(4):2211–16.
- [73] Pan C, Dong L, Ge L-Q, Wang J, Gu Z-Z. Highly active TiO<sub>2</sub>/polyelectrolytes hybrid multilayered hollow nanofibrous photocatalyst prepared from electrospun fibers using electrostatic layer-by-layer technique. *J Macromol Sci Part B* 2009;48(1):92–105.
- [74] Murphy MA, Wilcox GD, Dahm RH, Marken F. Electrochemical characterisation of ultrathin carbon nanofiber-chitosan multi-layer films. *Indian Journal of Chemistry Section a-Inorganic Bio-Inorganic Physical Theoretical & Analytical Chemistry*. 2005;44(5):924–931.
- [75] Xu Z-K, Huang X-J, Wan L-S. Surface engineering of polymer membranes. Springer Science & Business Media; 2009.
- [76] Kim BC, Zhao X, Ahn H-K, Kim JH, Lee H-J, Kim KW, et al. Highly stable enzyme precipitate coatings and their electrochemical applications. *Biosens Bioelectron* 2011;26(5):1980–6.

- [77] Jia H, Zhu G, Vugrinovich B, Kataphinan W, Reneker DH, Wang P. Enzyme-carrying polymeric nanofibers prepared via electrospinning for use as unique biocatalysts. *Biotechnol Prog* 2002;18(5):1027–32.
- [78] Alexander C, Andersson HS, Andersson LI, Ansell RJ, Kirsch N, Nicholls IA, et al. Molecular imprinting science and technology: a survey of the literature for the years up to and including 2003. *J Mol Recognit* 2006;19(2):106–80.
- [79] Ulbricht M, Yang H. Porous polypropylene membranes with different carboxyl polymer brush layers for reversible protein binding via surface-initiated graft copolymerization. *Chem Mater* 2005;17(10):2622–31.
- [80] González MB, Wu A, Vilarinho PM. Influence of solvents on the microstructure and dielectric properties of  $\text{Ba}_{0.5}\text{Sr}_{0.5}\text{TiO}_3$  thin films prepared by a diol-based sol – gel process. *Chem Mater* 2006;18(7):1737–44.
- [81] Han M, Kane R, Goto M, Belfort G. Discriminate surface molecular recognition sites on a microporous substrate: a new approach. *Macromolecules*. 2003;36(12):4472–7.
- [82] Tan WB, Zhang Y. Multifunctional quantum-dot-based magnetic chitosan nanobeads. *Adv Mater* 2005;17(19):2375–80.
- [83] Torkamani AE, Syahariza ZA, Norziah MH, Wan AKM, Juliano P. Encapsulation of polyphenolic antioxidants obtained from *Momordica charantia* fruit within zein/gelatin shell core fibers via coaxial electrospinning. *Food Biosci* 2018;21:60–71.
- [84] Vashisth P, Srivastava AK, Nagar H, Raghuwanshi N, Sharan S, Nikhil K, et al. Drug functionalized microbial polysaccharide based nanofibers as transdermal substitute. *Nanomed Nanotechnol Biol Med* 2016;12(5):1375–85.
- [85] Lin L, Zhu Y, Li C, Liu L, Surendhiran D, Cui H. Antibacterial activity of PEO nanofibers incorporating polysaccharide from dandelion and its derivative. *Carbohydr Polym* 2018;198:225–32.
- [86] Park J-A, Kim S-B. Anti-biofouling enhancement of a polycarbonate membrane with functionalized poly(vinyl alcohol) electrospun nanofibers: permeation flux, biofilm formation, contact, and regeneration tests. *J Membr Sci* 2017;540:192–9.
- [87] Aghamohamadi N, Sanjani NS, Majidi RF, Nasrollahi SA. Preparation and characterization of Aloe vera acetate and electrospinning fibers as promising antibacterial properties materials. *Mater Sci Eng C* 2019;94:445–52.
- [88] Chinatangkul N, Limmatvapirat C, Nunthanid J, Luangtana-Anan M, Sriamornsak P, Limmatvapirat S. Design and characterization of monolaurin loaded electrospun shellac nanofibers with antimicrobial activity. *Asian J Pharm Sci* 2018;13(5):459–71.
- [89] Aadil KR, Mussatto SI, Jha H. Synthesis and characterization of silver nanoparticles loaded poly(vinyl alcohol)-lignin electrospun nanofibers and their antimicrobial activity. *Int J Biol Macromol* 2018;120:763–7.
- [90] Li K, Cui S, Hu J, Zhou Y, Liu Y. Crosslinked pectin nanofibers with well-dispersed Ag nanoparticles: preparation and characterization. *Carbohydr Polym* 2018;199:68–74.
- [91] Lee E-S, Kim Y-O, Ha Y-M, Lim D, Hwang JY, Kim J, et al. Antimicrobial properties of lignin-decorated thin multi-walled carbon nanotubes in poly(vinyl alcohol) nanocomposites. *Eur Polym J* 2018;105:79–84.
- [92] Ramírez-Agudelo R, Scheuermann K, Gala-García A, Monteiro APF, Pinzón-García AD, Cortés ME, et al. Hybrid nanofibers based on poly-caprolactone/gelatin/hydroxyapatite nanoparticles-loaded doxycycline: effective anti-tumoral and antibacterial activity. *Mater Sci Eng C* 2018;83:25–34.
- [93] He B, Zhao J, Ou Y, Jiang D. Biofunctionalized peptide nanofiber-based composite scaffolds for bone regeneration. *Mater Sci Eng C* 2018;90:728–38.

- [94] Nguyen THM, Abueva C, Ho HV, Lee S-Y, Lee B-T. In vitro and in vivo acute response towards injectable thermosensitive chitosan/TEMPO-oxidized cellulose nanofiber hydrogel. *Carbohydr Polym* 2018;180:246–55.
- [95] Smith Callahan LA, Xie S, Barker IA, Zheng J, Reneker DH, Dove AP, et al. Directed differentiation and neurite extension of mouse embryonic stem cell on aligned poly(lactide) nanofibers functionalized with YIGSR peptide. *Biomaterials*. 2013;34(36):9089–95.
- [96] Wang X, Gao C, Shu G, Wang Y, Liu X. The enzyme electrocatalytic immunosensor based on functional composite nanofibers for sensitive detection of tumor suppressor protein p53. *J Electroanal Chem* 2015;756:101–7.
- [97] Wang X, Wang Y, Shan Y, Jiang M, Jin X, Gong M, et al. A novel and sensitive electro-generated chemiluminescence biosensor for detection of p16INK4a gene based on the functional paste-like nanofibers composites-modified screen-printed carbon electrode. *J Electroanal Chem* 2018;823:368–77.
- [98] Wang X, Wang Y, Jiang M, Shan Y, Jin X, Gong M, et al. Functional electrospun nanofibers-based electrochemiluminescence immunosensor for detection of the TSP<sub>53</sub> using RuAg/SiO<sub>2</sub>NPs as signal enhancers. *Anal Biochem* 2018;548:15–22.
- [99] Shah S, Yin PT, Uehara TM, Chueng S-TD, Yang L, Lee K-B. Guiding stem cell differentiation into oligodendrocytes using graphene-nanofiber hybrid scaffolds. *Adv Mater* 2014;26(22):3673–80.
- [100] Xu T, Liang Z, Ding B, Feng Q, Fong H. Polymer blend nanofibers containing polycaprolactone as biocompatible and biodegradable binding agent to fabricate electrospun three-dimensional scaffolds/structures. *Polymer*. 2018;151:299–306.
- [101] Martins AF, Facchi SP, da Câmara PCF, Camargo SEA, Camargo CHR, Popat KC, et al. Novel poly( $\epsilon$ -caprolactone)/amino-functionalized tannin electrospun membranes as scaffolds for tissue engineering. *J Colloid Interface Sci* 2018;525:21–30.
- [102] Pedram Rad Z, Mokhtari J, Abbasi M. Fabrication and characterization of PCL/zein/gum arabic electrospun nanocomposite scaffold for skin tissue engineering. *Mater Sci Eng C* 2018;93:356–66.
- [103] Khan G, Yadav SK, Patel RR, Kumar N, Bansal M, Mishra B. Tinidazole functionalized homogeneous electrospun chitosan/poly( $\epsilon$ -caprolactone) hybrid nanofiber membrane: development, optimization and its clinical implications. *Int J Biol Macromolecules* 2017;103:1311–26.
- [104] Bhullar SK, Rana D, Lekesiz H, Bedeloglu AC, Ko J, Cho Y, et al. Design and fabrication of auxetic PCL nanofiber membranes for biomedical applications. *Mater Sci Eng: C* 2017;81:334–40.
- [105] Selvaraj S, Thangam R, Fathima NN. Electrospinning of casein nanofibers with silver nanoparticles for potential biomedical applications. *Int J Biol Macromol* 2018;120:1674–81.
- [106] Aydogdu A, Sumnu G, Sahin S. A novel electrospun hydroxypropyl methylcellulose/polyethylene oxide blend nanofibers: morphology and physicochemical properties. *Carbohydr Polym* 2018;181:234–46.
- [107] dos Santos DM, Leite IS, Bukzem ADL, de Oliveira Santos RP, Frollini E, Inada NM, et al. Nanostructured electrospun nonwovens of poly( $\epsilon$ -caprolactone)/quaternized chitosan for potential biomedical applications. *Carbohydr Polym* 2018;186:110–21.
- [108] Sharaf S, El-Naggar ME. Eco-friendly technology for preparation, characterization and promotion of honey bee propolis extract loaded cellulose acetate nanofibers in medical domains. *Cellulose*. 2018;25(9):5195–204.

- [109] Kim K-H, Kim S-J, Cho H-J, Kim N-H, Jang J-S, Choi S-J, et al. WO<sub>3</sub> nanofibers functionalized by protein-templated RuO<sub>2</sub> nanoparticles as highly sensitive exhaled breath gas sensing layers. *Sens Actuators B: Chem* 2017;241:1276–82.
- [110] Yang X, Salles V, Kaneti YV, Liu M, Maillard M, Journet C, et al. Fabrication of highly sensitive gas sensor based on Au functionalized WO<sub>3</sub> composite nanofibers by electrospinning. *Sens Actuators B: Chem* 2015;220:1112–19.
- [111] Zhang L, Chen Q, Han X, Zhang Q. MnO<sub>2</sub> nanoparticles and carbon nanofibers nanocomposites with high sensing performance toward glucose. *J Clust Sci* 2018;29(6):1089–98.
- [112] Coimbra P, Freitas JP, Gonçalves T, Gil MH, Figueiredo M. Preparation of gentamicin sulfate eluting fiber mats by emulsion and by suspension electrospinning. *Mater Sci Eng C* 2019;94:86–93.
- [113] Permyakova ES, Polčák J, Slukin PV, Ignatov SG, Gloushankova NA, Zajíčková L, et al. Antibacterial biocompatible PCL nanofibers modified by COOH-anhydride plasma polymers and gentamicin immobilization. *Mater Des* 2018;153:60–70.
- [114] Liu S, Fukushima K, Venkataraman S, Hedrick JL, Yang YY. Supramolecular nanofibers self-assembled from cationic small molecules derived from repurposed poly(ethylene terephthalate) for antibiotic delivery. *Nanomed Nanotechnol Biol Med* 2018;14(1):165–72.
- [115] Grip J, Engstad RE, Skjæveland I, Škalko-Basnet N, Isaksson J, Basnet P, et al. Beta-glucan-loaded nanofiber dressing improves wound healing in diabetic mice. *Eur J Pharm Sci* 2018;121:269–80.
- [116] Waghmare VS, Wadke PR, Dyawanapelly S, Deshpande A, Jain R, Dandekar P. Starch based nanofibrous scaffolds for wound healing applications. *Bioact Mater* 2018;3(3):255–66.
- [117] Ahmed R, Tariq M, Ali I, Asghar R, Noorunnisa Khanam P, Augustine R, et al. Novel electrospun chitosan/polyvinyl alcohol/zinc oxide nanofibrous mats with antibacterial and antioxidant properties for diabetic wound healing. *Int J Biol Macromol* 2018;120:385–93.
- [118] Chantre CO, Campbell PH, Golecki HM, Buganza AT, Capulli AK, Deravi LF, et al. Production-scale fibronectin nanofibers promote wound closure and tissue repair in a dermal mouse model. *Biomaterials*. 2018;166:96–108.
- [119] Mutlu G, Calamak S, Ulubayram K, Guven E. Curcumin-loaded electrospun PHBV nanofibers as potential wound-dressing material. *J Drug Deliv Sci Technol* 2018;43:185–93.
- [120] Simões D, Miguel SP, Correia IJ. Biofunctionalization of electrospun poly(caprolactone) fibers with Maillard reaction products for wound dressing applications. *Reactive Funct Polym* 2018;131:191–202.
- [121] Gilotra S, Chouhan D, Bhardwaj N, Nandi SK, Mandal BB. Potential of silk sericin based nanofibrous mats for wound dressing applications. *Mater Sci Eng C* 2018;90:420–32.
- [122] Gholipour-Kanani A, Samadikuchaksaraei A, Mohsenzadegan M, Fayyazi M. Nanofibrous scaffolds from chitosan and poly(caprolactone) for excision wound healing application in canine model. *Mater Today Proc* 2018;5(7, Part 3):15629–34.
- [123] Chanda A, Adhikari J, Ghosh A, Chowdhury SR, Thomas S, Datta P, et al. Electrospun chitosan/polycaprolactone-hyaluronic acid bilayered scaffold for potential wound healing applications. *Int J Biol Macromol* 2018;116:774–85.

- [124] Tra Thanh N, Ho Hieu M, Tran Minh Phuong N, Do Bui Thuan T, Nguyen Thi Thu H, Thai VP, et al. Optimization and characterization of electrospun polycaprolactone coated with gelatin-silver nanoparticles for wound healing application. *Mater Sci Eng C* 2018;91:318–29.
- [125] Shi R, Geng H, Gong M, Ye J, Wu C, Hu X, et al. Long-acting and broad-spectrum antimicrobial electrospun poly( $\epsilon$ -caprolactone)/gelatin micro/nanofibers for wound dressing. *J Colloid Interface Sci* 2018;509:275–84.
- [126] Liu X, Nielsen LH, Kłodzińska SN, Nielsen HM, Qu H, Christensen LP, et al. Ciprofloxacin-loaded sodium alginate/poly(lactic-co-glycolic acid) electrospun fibrous mats for wound healing. *Eur J Pharm Biopharm* 2018;123:42–9.
- [127] Cr R, Ps S, O M, Pp S, A S. Nanochitosan enriched poly- $\epsilon$ -caprolactone electrospun wound dressing membranes: a fine tuning of physicochemical properties, hemocompatibility and curcumin release profile. *International Journal of Biological Macromolecules*. 2018;108:1261–72.
- [128] Jalili Tabaei M, Emtiazi G. Transparent nontoxic antibacterial wound dressing based on silver nano particle/bacterial cellulose nano composite synthesized in the presence of tri-polyphosphate. *J Drug Deliv Sci Technol* 2018;44:244–53.
- [129] Yang S, Lei P, Shan Y, Zhang D. Preparation and characterization of antibacterial electrospun chitosan/poly(vinyl alcohol)/graphene oxide composite nanofibrous membrane. *Appl Surf Sci* 2018;435:832–40.
- [130] Lee JW, Park JY, Park SH, Kim MJ, Song BR, Yun H-W, et al. Cross-linked electrospun cartilage acellular matrix/poly(caprolactone-co-lactide-co-glycolide) nanofiber as an anti-adhesive barrier. *Acta Biomater* 2018;74:192–206.
- [131] Li Z, Zhou P, Zhou F, Zhao Y, Ren L, Yuan X. Antimicrobial eugenol-loaded electrospun membranes of poly( $\epsilon$ -caprolactone)/gelatin incorporated with REDV for vascular graft applications. *Colloids Surf B: Biointerfaces* 2018;162:335–44.
- [132] Jiang L, Jiang Y, Stiadle J, Wang X, Wang L, Li Q, et al. Electrospun nanofibrous thermoplastic polyurethane/poly(glycerol sebacate) hybrid scaffolds for vocal fold tissue engineering applications. *Mater Sci Eng C* 2019;94:740–9.
- [133] Zarei M, Karbasi S. Evaluation of the effects of multiwalled carbon nanotubes on electrospun poly(3-hydroxybutyrate) scaffold for tissue engineering applications. *J Porous Mater* 2018;25(1):259–72.
- [134] Silva NHCS, Vilela C, Almeida A, Marrucho IM, Freire CSR. Pullulan-based nanocomposite films for functional food packaging: exploiting lysozyme nanofibers as antibacterial and antioxidant reinforcing additives. *Food Hydrocoll* 2018;77:921–30.
- [135] Lin L, Xue L, Duraianarasan S, Haiying C. Preparation of  $\epsilon$ -polylysine/chitosan nanofibers for food packaging against *Salmonella* on chicken. *Food Packaging Shelf Life* 2018;17:134–41.
- [136] Lin L, Zhu Y, Cui H. Electrospun thyme essential oil/gelatin nanofibers for active packaging against *Campylobacter jejuni* in chicken. *LWT* 2018;97:711–18.
- [137] Cui H, Wu J, Li C, Lin L. Improving anti-listeria activity of cheese packaging via nanofiber containing nisin-loaded nanoparticles. *LWT Food Sci Technol* 2017;81:233–42.
- [138] Cui H, Bai M, Lin L. Plasma-treated poly(ethylene oxide) nanofibers containing tea tree oil/beta-cyclodextrin inclusion complex for antibacterial packaging. *Carbohydr Polym* 2018;179:360–9.
- [139] Lin L, Gu Y, Cui H. Novel electrospun gelatin-glycerin- $\epsilon$ -poly-lysine nanofibers for controlling *Listeria monocytogenes* on beef. *Food Packaging Shelf Life* 2018;18:21–30.

- [140] Deng Z, Jung J, Zhao Y. Development, characterization, and validation of chitosan adsorbed cellulose nanofiber (CNF) films as water resistant and antibacterial food contact packaging. *LWT Food Sci Technol* 2017;83:132–40.
- [141] Andrade-Del Olmo J, Pérez-Álvarez L, Hernáez E, Ruiz-Rubio L, Vilas-Vilela JL. Antibacterial multilayer of chitosan and (2-carboxyethyl)- $\beta$ -cyclodextrin onto polylactic acid (PLLA). *Food Hydrocoll* 2019;88:228–36.
- [142] Yue X, Feng S, Li S, Jing Y, Shao C. Bromopropyl functionalized silica nanofibers for effective removal of trace level dieldrin from water. *Colloids Surf A: Physicochem Eng Asp* 2012;406:44–51.
- [143] Yuan G, Prabakaran M, Qilong S, Lee JS, Chung I-M, Gopiraman M, et al. Cyclodextrin functionalized cellulose nanofiber composites for the faster adsorption of toluene from aqueous solution. *J Taiwan Inst Chem Eng* 2017;70:352–8.
- [144] Chaúque EFC, Dlamini LN, Adelodun AA, Greyling CJ, Ngila JC. Electrospun polyacrylonitrile nanofibers functionalized with EDTA for adsorption of ionic dyes. *Phys Chem Earth Parts A/B/C* 2017;100:201–11.
- [145] Mohamed A, Osman TA, Toprak MS, Muhammed M, Uheida A. Surface functionalized composite nanofibers for efficient removal of arsenic from aqueous solutions. *Chemosphere*. 2017;180:108–16.
- [146] Zhao X, Ma X, Zheng P. The preparation of carboxylic-functional carbon-based nanofibers for the removal of cationic pollutants. *Chemosphere*. 2018;202:298–305.
- [147] Qiu J, Liu F, Yue C, Ling C, Li A. A recyclable nanosheet of Mo/N-doped TiO<sub>2</sub> nanorods decorated on carbon nanofibers for organic pollutants degradation under simulated sunlight irradiation. *Chemosphere*. 2019;215:280–93.
- [148] Mohamed A, Ghobara MM, Abdelmaksoud MK, Mohamed GG. A novel and highly efficient photocatalytic degradation of malachite green dye via surface modified polyacrylonitrile nanofibers/biogenic silica composite nanofibers. *Sep Purif Technol* 2019;210:935–42.
- [149] Xu Y, Bao J, Zhang X, Li W, Xie Y, Sun S, et al. Functionalized polyethersulfone nanofibrous membranes with ultra-high adsorption capacity for organic dyes by one-step electrospinning. *J Colloid Interface Sci* 2019;533:526–38.
- [150] Chen B, Zhao H, Chen S, Long F, Huang B, Yang B, et al. A magnetically recyclable chitosan composite adsorbent functionalized with EDTA for simultaneous capture of anionic dye and heavy metals in complex wastewater. *Chem Eng J* 2019;356:69–80.
- [151] Aboamara NM, Mohamed A, Salama A, Osman TA, Khatlab A. An effective removal of organic dyes using surface functionalized cellulose acetate/graphene oxide composite nanofibers. *Cellulose*. 2018;25(7):4155–66.
- [152] Gorji M, Bagherzadeh R, Fashandi H. 21 - Electrospun nanofibers in protective clothing. In: Afshari M, editor. *Electrospun nanofibers*. Woodhead Publishing; 2017. p. 571–98.
- [153] Faccini M, Vaquero C, Amantia D. Development of protective clothing against nanoparticle based on electrospun nanofibers. *J Nanomaterials* 2012;2012:9.
- [154] Lee S, Obendorf SK. Use of electrospun nanofiber web for protective textile materials as barriers to liquid penetration. *Text Res J* 2007;77(9):696–702.
- [155] Gorji M, Jeddi AAA, Gharehaghaji AA. Fabrication and characterization of polyurethane electrospun nanofiber membranes for protective clothing applications. *J Appl Polym Sci* 2012;125(5):4135–41.
- [156] Akduman C, Oğlakcıoğlu N, Kumbasar PA A, Sarı B. Investigation of thermal comfort properties of electrospun nanofiber mats. *J Fash Technol Text Eng* 2018;(4) <https://doi.org/10.4172/2329-9568.s4-015>.

- [157] Vitchuli N, Shi Q, Nowak J, Kay K, Caldwell JM, Breidt F, et al. Multifunctional ZnO/Nylon 6 nanofiber mats by an electrospinning–electrospraying hybrid process for use in protective applications. *Sci Technol Adv Mater* 2011;12(5):055004.
- [158] Ju J, Shi Z, Deng N, Liang Y, Kang W, Cheng AB. Designing waterproof breathable material with moisture unidirectional transport characteristics based on a TPU/TBAC tree-like and TPU nanofiber double-layer membrane fabricated by electrospinning. 2017;7:32155–32163.
- [159] Chitpong N, Husson SM. Polyacid functionalized cellulose nanofiber membranes for removal of heavy metals from impaired waters. *J Membr Sci* 2017;523:418–29.
- [160] Van Nguyen H, Luu ST, Rakov EG. Ion-exchange zirconium sorption by functionalized carbon nanofibers. *Inorg Mater* 2012;48(2):128–31.
- [161] Chee WK, Lim HN, Andou Y, Zainal Z, Hamra AAB, Harrison I, et al. Functionalized graphene oxide-reinforced electrospun carbon nanofibers as ultrathin supercapacitor electrode. *J Energy Chem* 2017;26(4):790–8.
- [162] Kandasamy SK, Kandasamy K. Recent advances in electrochemical performances of graphene composite (graphene-polyaniline/polypyrrole/activated carbon/carbon nanotube) electrode materials for supercapacitor: a review. *J Inorg Organomet Polym Mater* 2018;28(3):559–84.
- [163] Almasian A, Giahi M, Chizari Fard G, Dehdast SA, Maleknia L. Removal of heavy metal ions by modified PAN/PANI-nylon core-shell nanofibers membrane: filtration performance, antifouling and regeneration behavior. *Chem Eng J* 2018;351:1166–78.
- [164] Bilad MR, Azizo AS, Wirzal MDH, Jia Jia L, Putra ZA, Nordin NAHM, et al. Tackling membrane fouling in microalgae filtration using nylon 6,6 nanofiber membrane. *J Environ Manag* 2018;223:23–8.
- [165] Yu Y, Ma R, Yan S, Fang J. Preparation of multi-layer nylon-6 nanofibrous membranes by electrospinning and hot pressing methods for dye filtration. *RSC Adv* 2018;8(22):12173–8.
- [166] Park J-A, Kim S-B. Antimicrobial filtration with electrospun poly(vinyl alcohol) nanofibers containing benzyl triethylammonium chloride: immersion, leaching, toxicity, and filtration tests. *Chemosphere*. 2017;167:469–77.
- [167] Fang Q, Zhu M, Yu S, Sui G, Yang X. Studies on soy protein isolate/polyvinyl alcohol hybrid nanofiber membranes as multi-functional eco-friendly filtration materials. *Mater Sci Eng B* 2016;214:1–10.
- [168] Xu C, Wang C, He X, Lyu M, Wang S, Wang L. Processable graphene oxide-embedded titanate nanofiber membranes with improved filtration performance. *J Hazard Mater* 2017;325:214–22.
- [169] Bahi A, Shao J, Mohseni M, Ko FK. Membranes based on electrospun lignin-zeolite composite nanofibers. *Sep Purif Technol* 2017;187:207–13.
- [170] Namsaeng J, Panyodom W, Worajittiphon P. Synergistic effect of welding electrospun fibers and MWCNT reinforcement on strength enhancement of PAN–PVC non-woven mats for water filtration. *Chem Eng Sci* 2019;193:230–42.
- [171] Min L-L, Yang L-M, Wu R-X, Zhong L-B, Yuan Z-H, Zheng Y-M. Enhanced adsorption of arsenite from aqueous solution by an iron-doped electrospun chitosan nanofiber mat: preparation, characterization and performance. *J Colloid Interface Sci* 2019;535:255–64.
- [172] Karki HP, Kafle L, Ojha DP, Song JH, Kim HJ. Cellulose/polyacrylonitrile electrospun composite fiber for effective separation of the surfactant-free oil-in-water mixture under a versatile condition. *Sep Purif Technol* 2019;210:913–19.

- [173] Li X, Hu Y. Luminescent films functionalized with cellulose nanofibrils/CdTe quantum dots for anti-counterfeiting applications. *Carbohydr Polym* 2019;203:167–75.
- [174] Haddad MY, Alharbi HF, Karim MR, Aijaz MO, Alharthi NH. Preparation of TiO<sub>2</sub> incorporated polyacrylonitrile electrospun nanofibers for adsorption of heavy metal ions. *J Polym Res* 2018;25(10):218.
- [175] Hassan M, Hassan E, Fadel SM, Abou-Zeid RE, Berglund L, Oksman K. Metallo-terpyridine-modified cellulose nanofiber membranes for papermaking wastewater purification. *J Inorg Organomet Polym Mater* 2018;28(2):439–47.
- [176] Ashraf R, Sofi HS, Malik A, Beigh MA, Hamid R, Sheikh FA. Recent trends in the fabrication of starch nanofibers: electrospinning and non-electrospinning routes and their applications in biotechnology. *Applied Biochemistry and Biotechnology* 2019;187:47–74.



This page intentionally left blank

# Nanoengineered textiles: from advanced functional nanomaterials to groundbreaking high- performance clothing

Clara Pereira<sup>1</sup>, André M. Pereira<sup>2</sup>, Cristina Freire<sup>1</sup>, Tânia V. Pinto<sup>1</sup>,  
Rui S. Costa<sup>1,2</sup> and Joana S. Teixeira<sup>1,2</sup>

<sup>1</sup>REQUIMTE/LAQV, Chemistry and Biochemistry Department, Faculty of Sciences, University of Porto, Porto, Portugal, <sup>2</sup>IFIMUP, Institute of Physics for Advanced Materials, Nanotechnology and Photonics, Physics and Astronomy Department, Faculty of Sciences, University of Porto, Porto, Portugal

### 21.1 Nanotechnology on textiles

In recent decades, the industry has been facing a new paradigm due to the obligation to constantly innovate on the way of manufacturing its products, boosted by the necessity to continuously create new functionalities. Among the different industrial sectors that are following this trend, the textile and clothing industry has been witnessing a major revolution, driven by market and consumer demand for innovative and trendy high-value-added products [1,2].

Nanotechnology has played a major role in the design of high-performance (multi)functional and smart textiles, creating new market opportunities for a myriad of applications ranging from healthcare, sports and protection to fashion, military, transportation, and IoT (Internet of Things; see Fig. 21.1) [1–5]. *Functional textiles* are those that besides their traditional aesthetic and decorative properties exhibit additional functionalities, while *smart textiles* are those that can sense and respond to external stimuli, namely mechanical, thermal, magnetic, chemical, electrical, optical, and physiological.

The nanoscale modification of textile substrates allows improving the performance or imparting new high-value-added functionalities to fabrics,

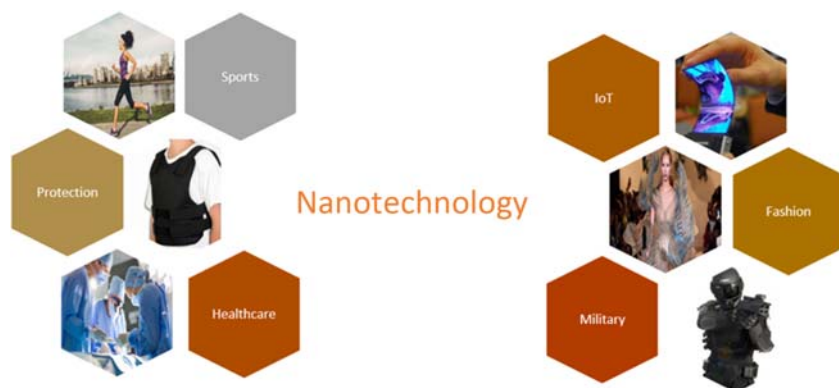


**FIGURE 21.1** Applications of nanotechnology on textiles.

while preserving their aesthetic properties (e.g., appearance, feel, breathability), lightness, flexibility, and comfort [1,2,4–6]. Moreover, the washing fastness and mechanical properties (mechanical strength, wear, and abrasion resistance) can be improved.

Several types of functional nanomaterials with fine-tuned properties have been incorporated on textiles at several stages of their production, ranging from 0D and 1D to 2D nanomaterials (nanoparticles, nanotubes, and plate-like materials), during fiber spinning, during yarn formation, or at the finishing/coating step [2,3,5,7]. In particular, hybrid silica nanoparticles (NPs), titanium dioxide, noble metal NPs, transition metal oxides, and carbon-based nanomaterials are remarkable building blocks, due to their outstanding electrical, thermal, chemical, magnetic, and/or optical characteristics and to the possibility of engineering their surface properties [1,2,4,5,8]. In this context, a new generation of groundbreaking textile and clothing products with innovative and multiple functionalities have emerged, such as (super)hydro/oleophobicity, fire retardancy, self-cleaning, radiation protection, antimicrobial properties, anti-static, thermochromism, and photochromism.

More recently, the birth of wearable technology and IoT marked the dawn of a new era in the textiles and clothing industry, with advanced intelligent technologies being introduced on garments, such as communication devices, flexible/wearable sensors for healthcare and safety, energy-harvesting and storage components (e.g., batteries, supercapacitors, solar cells), lighting systems, etc. [1,9,10]. The global market of smart textiles is growing at an unprecedented pace, being expected to reach USD 5.3 billion by 2024, at a compound annual growth rate (CAGR) of 26.2% [11].

Although the fusion of nanotechnology and textiles seems to offer many advances and advantages for mankind, nanoengineered textile products also created a global awareness on their potential environmental impact and human health risks [1,12,13]. For instance, today textiles and apparel represent ~10%

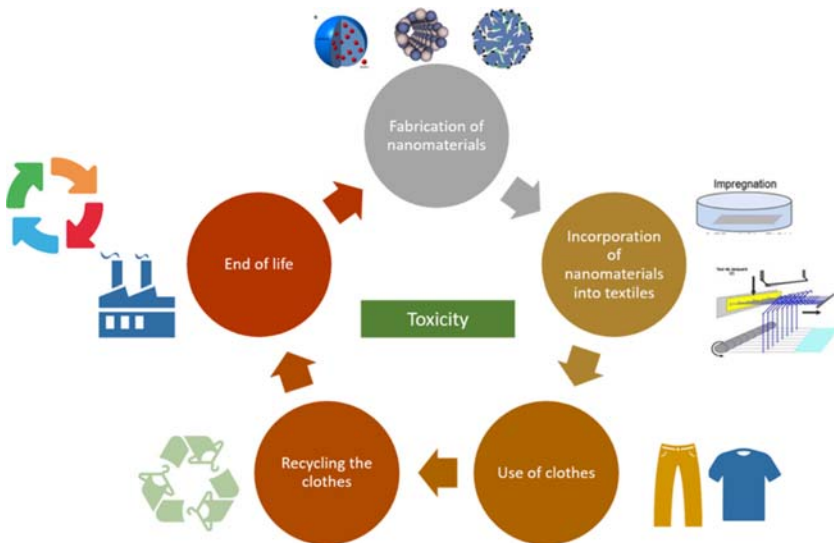


**FIGURE 21.2** Life cycle of nanoengineered textiles.

of the total carbon emissions, with 17% – 20% of industrial water pollution originating from textile industry dyeing and finishing agents [1]. In this sense, it has become mandatory for textile manufacturers to ensure that the new nano-textile products will not have adverse effects on human health nor on the environment during all stages of their life, starting from their production, to their use and end of life (disposal) (Fig. 21.2). In this context, the life cycle assessment and risk analysis need to be critically performed, including nanotoxicity and the effects of uncontrolled release of nanomaterials from fabrics upon washing, with the aim of producing safer products with reduced carbon footprint. The nanomaterials leached from textiles during laundering may no longer exist in the pristine and intact form, but form agglomerates, and suffer oxidation, ionization, or other degradation phenomena [14,15].

This chapter gives an overview of the significant progress on functional nanomaterials with engineered properties and their incorporation on textile fabrics and fibers through scalable processes used in the textile industry, highlighting the role of nanotechnology to boost the design of innovative high-performance textile and clothing products. It will start with an introduction to the conventional and advanced processes for the incorporation of functional nanomaterials on fabrics and fibers. Afterward, the different types of nanomaterials that can be incorporated on textiles will be presented, as well as the processes used for their tailored fabrication and functionalization, with special emphasis on those that are scalable, cost-effective, and ecosustainable. For each family of nanomaterials, the most recent advances in nanoengineered textiles will be reviewed, namely those with superamphiphobic, antimicrobial, self-cleaning, antistatic, drug

release, radiation protection, photochromic, and thermochromic properties. Moreover, the emerging generation of smart textiles with sensing, energy-harvesting, and storage functionalities will be highlighted as part of the new paradigm of electronic textiles. Finally, future trends and prospects to further develop advanced nanomaterials with fine-tuned properties for the next generation of functional and smart textiles will be presented.

## 21.2 Nanoengineered textiles: functionalization processes

As previously mentioned, in the textile industry there are two routes to incorporate functional and smart nanomaterials on textiles: (1) at the finishing/coating stage on a ready-made fabric (top-down approach) by impregnation/dyeing, spray coating, or printing technologies; or (2) during the fiber production (bottom-up approach), fabricating the fiber from the scratch by spinning processes (Fig. 21.3).

The application of nanomaterials by finishing/coating of preexisting fabrics/fibers can be accomplished by dyeing, coating, lamination, or by printing the surface of traditional textiles [16]. These strategies can be more easily embraced by textile manufacturers than fiber spinning, since they use well-established and simpler processes already implemented in the traditional textile industry, are more cost-effective, and minimize production time and infrastructure/machinery adaptation. On the other hand, fiber spinning processes offer greater flexibility for the textile industry since they can yield multicomponent fibers with more versatile geometries. Nevertheless, the development of scalable fine-tuned nanoengineered fibers is still at an embryonic state since it still requires adjustments to boost the implementation on high production lines.

### 21.2.1 Conventional processes

#### 21.2.1.1 Textile dyeing

*Conventional dyeing* continues to be one of the most viable options to be implemented by the textile industry for the design and development of

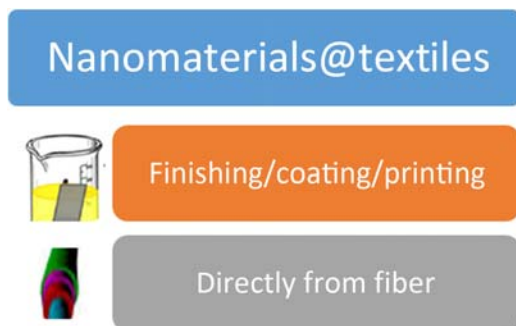


**FIGURE 21.3** Strategies for nanotechnology incorporation on textiles.

nanoengineered clothing. It takes advantage of the traditional dyeing machinery, replacing the dye bath by a dispersion containing the nanomaterial. Two strategies are typically implemented depending on the type of textile substrate (fiber composition, fiber construction, wetting/swelling capacity, etc.) and nanomaterial–substrate affinity: *exhaustion* and *padding*.

In the case of *exhaustion* (batch dyeing), the textile substrate is in repeated contact with the nanomaterial dispersion bath (dye liquor) during the whole dyeing process [17–19]. During the process, the nanomaterial is transferred from the aqueous bath to the fabric, followed by gradual adsorption onto the fabric surface and finally diffusion into the fiber interior. Absorption (overall process of adsorption and diffusion) and desorption phenomena occur until an equilibrium stage is reached. This process is performed in a winch, jigger, or jet dyeing machine and requires precise control of the dyeing conditions, namely the exhaustion temperature and time, pH, nanomaterial concentration, and addition of auxiliary agents [19]. Finally, the resulting functional fabric is washed and dried.

On the other hand, in the *padding process* (semicontinuous or continuous) the substrate is immersed in the nanomaterial dispersion (dipping) and then squeezed by passing between a pair of rollers to force the nanomaterial to penetrate within the fabric and remove the excess solution (Fig. 21.4) [17,19]. A padding mangle is used for both dip and pad stages, which allows controlling the rollers pressure and the speed at which the fabric is passed through the padder. Afterward, the fabric is dried to remove the solvent (typically water) and cured (heating at a certain temperature higher than the drying temperature) to promote the fixation of the nanomaterial. Each section of the fabric only encounters the nanomaterial liquor once, thus requiring uniform padding across the whole fabric area. This process is the most

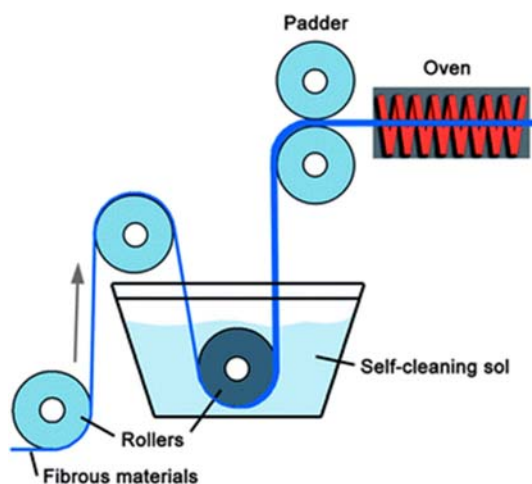


**FIGURE 21.4** Schematic representation of the textile padding process. Reproduced from Tung WS, Daoud WA. Self-cleaning fibers via nanotechnology: a virtual reality. *J Mater Chem* 2011;21:7858–69 [20] with permission from The Royal Society of Chemistry (RSC).

common finishing route since it is faster, simpler, and more cost-effective than exhaustion, allowing the functionalization of larger fabric portions [21].

### 21.2.1.2 Coating and lamination

Coating and lamination processes are widely used in the textile industry to impart value to technical textiles. They have been used to improve and/or modify the chemical and physical properties and the appearance of the textile fabrics, through the incorporation of nanomaterials and polymers [22].

The *coating process* consists of the application of a layer of a polymeric solution directly to one or both sides of the fabric substrate. The coated fabric is then heated to promote the polymerization and improve the polymer adhesion to the fabric (curing process) [22]. The functional nanomaterials are added to the polymer solution to create a paste that is then used as the coating layer. The study of the rheological properties of the doped polymer solution is required to unveil the maximum quantity of nanomaterial that can be added without compromising the polymer matrix properties. There are several conventional methods to apply a polymeric coating to textiles substrates, such as *direct (knife or spread) coating*, *dip coating*, *foam coating*, *transfer coating*, *calender coating*, and *hot-melt extrusion coating* [21,22].

The *direct coating* is the simplest and oldest coating method, where a polymeric solution is applied to the fabric and then is spread with the help of a knife blade, followed by a dry and curing process (Fig. 21.5A). The polymeric solution should be viscous, in order to prevent it from soaking through the fabric, and the knife blade can have different shapes and be angled to improve the contact with the substrate, determining the coating thickness [21,22].

*Dip coating*, also known as the impregnation method, is used to produce a thin and uniform coating onto flat or cylindrical substrates (e.g., fibers). This method consists of dipping the textile substrate onto the coating bath (low viscosity polymer solution) and then forcing it to pass through a nip roll system to remove the excess material (Fig. 21.5B). After the impregnation step, the resulting fabric is dried/cured in order to improve the adhesion between the incorporated material and the substrate [21].

In *foam coating*, a coating material, such as a polymer emulsion, is converted into foam by adding a foaming agent and other suitable additives, and is then used to coat one side of the fabric [21,23]. This method is used for fabrics with open structures that cannot be directly coated, such as floor and wall coverings, blackout curtains, curtain linings and carpets [22].

*Calender coating* involves the fabric passing through a set of heated rollers in various configurations (three vertical rolls, three inclined rolls, inverted L, L-type, flat Z or inclined Z or S; Fig. 21.5C), which rotate in opposite directions in order to squeeze the polymeric solution and smooth it into films with uniform and controlled thickness (by adjusting the space between the rolls). Normally, this process is used to produce a continuous

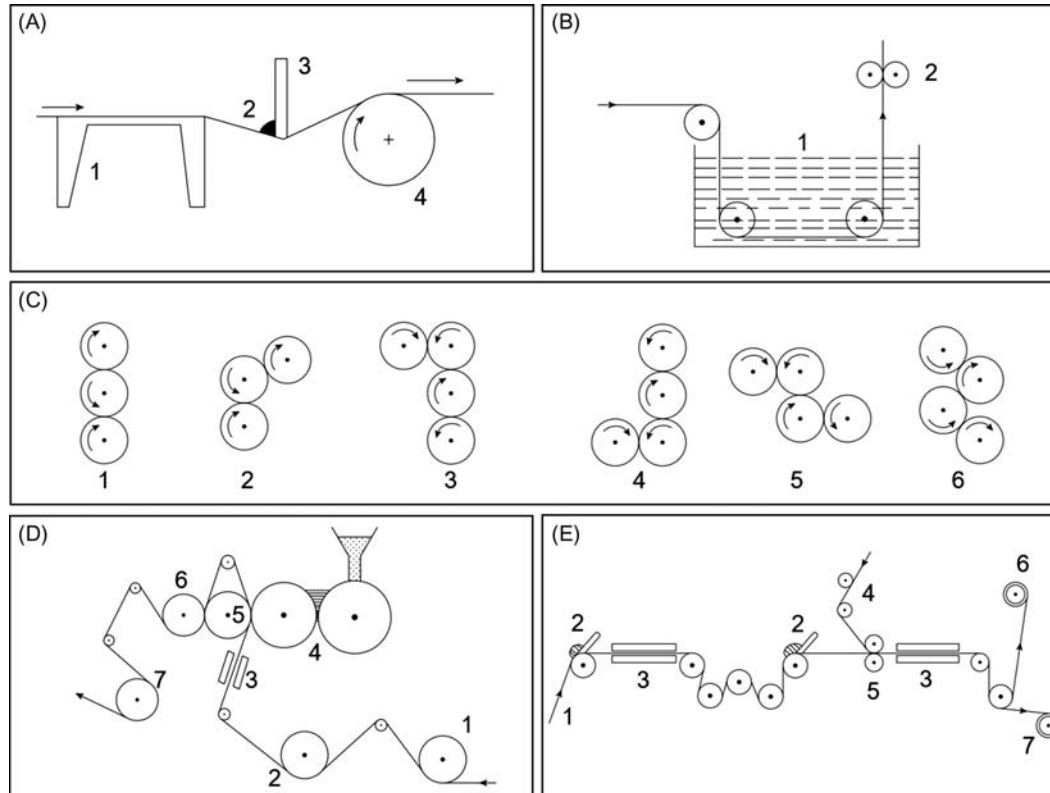


**FIGURE 21.5** Different coating processes: (A) direct coating: 1—support channel, 2—coating ink, 3—coating knife, and 4—support roll; (B) dip coating: 1—dipping tank, 2—squeeze rolls system; (C) calender coating configurations: 1—three vertical rolls, 2—three inclined rolls, 3—inverted L, 4—L-type, 5—flat Z, 6—inclined Z or S; (D) hot-melt extrusion coating (Zimmer coater): 1—fabric roll, 2—substrate preheat roll, 3—infrared heaters, 4—melt rolls, 5—backup rolls, 6—embossing roll, 7—cooling roll; and (E) transfer coating: 1—release paper, 2—coating head, 3—oven, 4—textile substrate, 5—laminating nip rolls, 6—coated fabric take-off roll and 7—release paper wind roll. Adapted from Joshi M, Butola BS. Application technologies for coating, lamination and finishing of technical textiles. In: Gulrajani ML, editor. *Adv. Dye. Finish. Tech. Text.* Elsevier; 2013. p. 355–411 [21] with permission from Elsevier.



film of polyvinyl chloride (PVC) or rubber from bulk material, which can then be put in contact with the fabric in order to adhere to its surface [21].

The *hot-melt extrusion coating* is similar to the calender coating. In this process, the material to be coated is obtained from granules of thermoplastic polymers, such as PVC, polyolefins, or polyurethane, which are added into the nip between the moving heated rollers. During this process, the polymer is melted and then directly applied to coat the substrate (Fig. 21.5D). There are two different configurations: two melt rollers and three melt rollers [22].

The *transfer coating* process is normally used for open and stretchy knitted fabrics that cannot be directly coated since they cannot be distorted under tension to form a flat surface. This method includes four steps: [21,22] in the first step, a transfer paper is coated with a polymeric solution, which forms the *top layer*, and then is dried to evaporate the solvent; in the second step, the second layer (called *base layer*) is coated into the fabric with an adhesive (to join both layers); in the third step, the *top layer* (coated transfer paper) is assembled with the base layer (coated fabric) and the system is dried to evaporate the solvent and bond both layers; and finally, in the fourth step, the transfer paper is removed (Fig. 21.5E).

Some of these processes have been evolving to satisfy the new generation of functional and smart textiles, namely to impart to the textile features such as water repellency, electrical conductivity, flame retardancy, radiation protection, or antibacterial properties [22].

Similarly to the coating process, *lamination* is used to impart particular features to the fabrics. A laminated textile can be described as a combined textile, composed of two or more layers of textile fabrics and component layers bonded together via an adhesive material, heat and pressure, or by the inherent adhesion properties of one of the component layers. Normally, the component layers are composed of polymers [22]. Lamination is an alternative to coating processes when it is difficult to formulate a resin or paste from the polymeric material and/or the polymeric material has low affinity to the substrate. Lamination allows producing functional textiles by a separated process: firstly, the polymer film is prepared and then it is laminated onto the fabric [21,22]. The lamination process comprises several methods, such as flame lamination, heat lamination, hot-melt lamination, and film lamination [21,22,24]. For instance, flame lamination is generally used in the automotive sector to laminate the car seat fabrics with polyurethane foam, since it is a fast, cost-effective, and single-step process that produces a triple laminated fabric [22,24]. In this process, one side of the polyurethane foam is melted and immediately covered by one of the fabrics that will be laminated. The same process is repeated on the other side of the foam, and finally the three layers are fed into the flame lamination machine, giving rise to a single product (Fig. 21.6) [22]. However, the main challenge is to preserve the original features of the textile, namely the appearance, handling, flexibility, and durability [21].

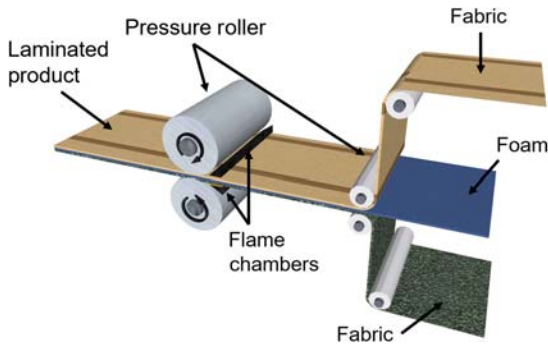


**FIGURE 21.6** Flame lamination process.

## 21.2.2 Advanced processes

### 21.2.2.1 Screen-printing

In the printing sector, there is a plethora of technologies to print a variety of patterns into textiles. The *printing processes* are commonly classified into two main groups: (1) *contact printing*, such as gravure printing, offset printing, flexography printing, micro/nano printing, pad printing, and roll-to-roll printing; and (2) *noncontact printing*, such as screen-printing, inkjet printing, and slot-die printing [25]. Printing processes differ from coating and lamination since the former allow designing tailored patterns, while the latter confer a continuous coating layer on the fabric surface [25].

Among all printing techniques, *screen-printing* is often preferred because it presents high reproducibility and versatility, which allows producing thick layers ( $5\text{--}25\text{ }\mu\text{m}$ ) with very well-defined patterns from inks or pastes, and with very low ink losses during the printing process. Moreover, screen-printing is recognized not only as a high-resolution-art printing technique, but also as an industrial process with advantages such as being scalable, low cost and of adding simplicity, affordability, speed, and adaptability to the fabrication process [25–29]. Furthermore, it can be used on a wide range of substrates, such as textiles, ceramics, glass, polyethylene, polypropylene, paper, metal, and wood [26,27]. In this technique, a design is imposed on a screen of fine mesh, containing “black” areas coated with an impermeable substance (emulsion). Then, the ink is forced through the mesh onto the printing substrate by moving a squeegee across the mesh (Fig. 21.7) [27,29]. The screen-printing process can be divided into two main steps: (1) production of the desired pattern in the screen mesh, and (2) printing of the pattern in the substrate. In the first step, the screen mesh is filled with an emulsion in order to produce a “mask” with the desired pattern. The mask has “white” and “black” areas, which allow and avoid, respectively, the ink to pass through the screen mesh to the substrate. In the second step, the screen mesh is placed over and close to the substrate, but not in direct contact, in order to avoid pulling away the screen mesh in an uncontrolled manner after printing

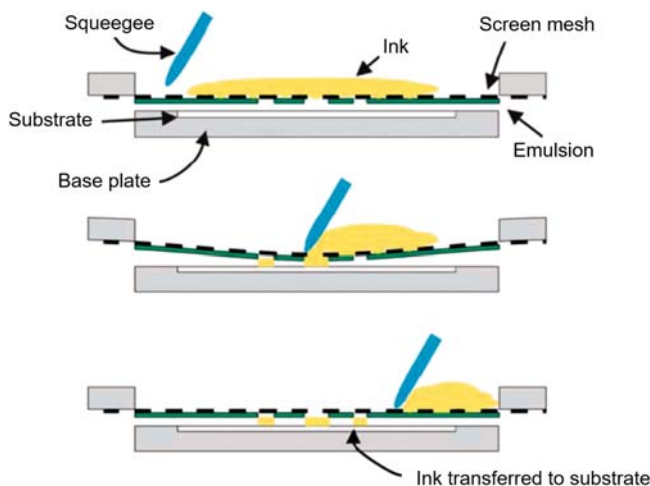


**FIGURE 21.7** Illustration of the screen-printing process. Adapted from Ahmed MU, Hossain MM, Safavieh M, Wong YL, Rahman IA, Zourob M, et al. Towards the development of smart and low cost point-of-care biosensors based on screen printed electrodes. *Crit Rev Biotechnol* 2015;36:1–11 [29] with permission from Taylor & Francis.

and spoiling the printed pattern. Finally, the squeegee is forced to enter in contact with the screen mesh, previously filled with ink, putting it in contact with the substrate. Afterward, the squeegee is moved linearly (in a predefined angle) in order to force the coating ink through the holes of the mesh onto the substrate, thus reproducing the desired pattern [27,29].

The screen-printing process can be performed using three different methods (Fig. 21.8): (1) *flat-to-flat method*: both the screen mesh and the substrate are flat; the ink is transferred through the mesh onto the substrate forced by the squeegee; (2) *screen-printing on a curve surface*: the screen mesh is flat, while the substrate is attached to a rotating cylinder; (3) *round-to-round method*: the screen mesh is cylindrical, while the substrate is attached to a moving flat plate that is in contact with a rotating cylinder (press cylinder); in this method, all components are moving synchronously and the ink is transferred from inside of the cylindrical screen mesh onto the substrate [28,30].

Each method has its own advantages. For instance, in the *flat-to-flat method* it is easier to optimize materials and processing steps, making it a good option for small laboratory systems. On the other hand, the other two methods are recommended when it is necessary to produce patterns at a larger scale (continuous processing system), since the rotating systems can achieve relatively higher printing speeds than the flat system. However, the rotary screens are more expensive and harder to clean than the flat ones [25,30].

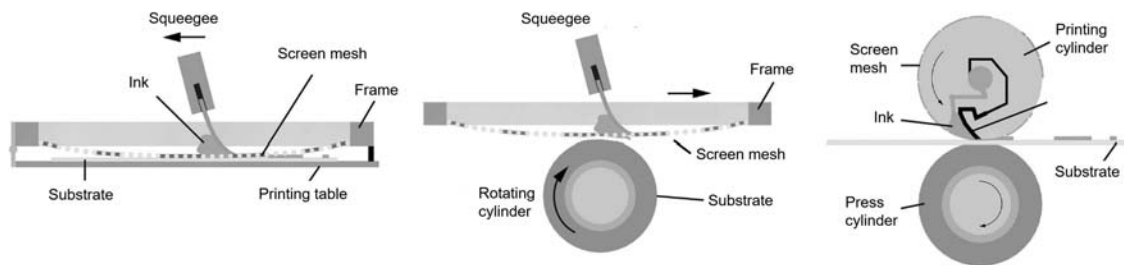


**FIGURE 21.8** Illustration of the different types of screen-printing methods. Adapted from Novaković D, Kašiković N, Vladić G, Pál M, *Screen printing*. In: Joanna Izdebska ST, editor. *Print. Polym. Fundam. Appl. William Andrew Inc.*; 2016. p. 247–61 [28] with permission from Elsevier.

Today, screen-printing is widely used by both academia and industry (Fig. 21.9), being one of the most important printing techniques for large-scale applications, not only for simple tasks such as printing images, texts, or conductive patterns on textiles, but also for more complex applications, such as for the production of flexible and lightweight electronics (printed electronics), including electrical circuits, organic light-emitting devices, solar cells, energy storage devices, (bio)sensors, or even microfluidic systems [26–28,31–33].

### 21.2.2.2 Lithography

The escalating growth of wearable technologies and miniaturization of electronic devices require the production of small-sized devices (at nanoscale) that are difficult to produce using traditional textile processes. For instance, the maximum resolution of screen-printing is around 5  $\mu\text{m}$  and so, to improve it, alternative techniques are required, such as *lithography*. The word lithography originates from the Greek language, where *lithos* means stones, and *graphia* means write, meaning literally writing in the stones [34]. In general, the stones are the substrates and the desired patterns are written using a highly sensitive polymer. Lithography consists of the fabrication of 3D micro/nanostructures (<10 nm to 500  $\mu\text{m}$ ) through extrusion of a 2D pattern by a process called patterning. In general, the patterning process involves four steps: [34,35] (1) deposition of a uniform film of a sensitive material (such as a light-sensitive polymer) on a substrate; (2) lithographic creation of a positive (or negative) pattern using a mask (with the desired pattern) into the previously deposited film; (3) etching process to remove the exposed (or unexposed) areas of the sensitive material, resulting in a patterned layer; and (4) construction of the device by filling the pattern with nanomaterial.

Several deposition techniques can be used to construct the structure of the desired device, such as *sputtering*, *pulsed laser deposition*, or *evaporation*, which belong to the *physical vapor deposition* family (top-down approach), or *chemical deposition* techniques, such as *molecular beam epitaxy*, *atomic layer deposition*, or *chemical vapor deposition* (bottom-up methodology) [35,36]. These techniques can create devices with thicknesses ranging from a few angstroms to micrometer size.

On the other hand, etching, which is a selective process of materials removal, can be performed. It is based on the transformation of a solid material into a liquid or gas in order to be able to remove it. Usually etching can be performed by two different routes: *dry etching* and *wet etching*. In dry etching, the promoting reaction agent, called etchant, is in the form of gas or plasma, whereas wet etching is characterized by using an etchant in the liquid state. Depending on how the material is removed, the etching process can be classified as *isotropic*, if the removed material is equal in all



**FIGURE 21.9** Examples of laboratorial (left) and industrial (right) screen-printing apparatus. *Reproduced from Krebs FC. Fabrication and processing of polymer solar cells: a review of printing and coating techniques. Sol Energy Mater Sol Cell 2009;93:394–412 [27] with permission from Elsevier.*

directions, or *anisotropic*, if there is a preferred direction of removal of the material [34,35].

The production of nanosized devices or structures has great significance for both scientific and technological applications and largely depends on the use of nanolithography techniques, since it requires high resolution during the production process. *Nanolithography* can be subdivided into several techniques, including *ion beam lithography*, *electron beam lithography*, *colloidal lithography*, *copolymer lithography*, *scanning probe lithography*, and *photolithography* [35–37].

In *electron and ion beam lithography* a desired pattern is written on the polymeric resist layer by one or more scanning beams of electrons or ions. Both techniques are capable of producing  $<10$  nm size structures [36,37]. However, the manufacturing speed of these processes is too slow to be used in industrial production (it can take more than 24 h to produce a pattern with  $1\text{ cm}^2$ ) [38]. Moreover, these techniques require high beam intensity (high-energy intensity), which can lead to irreparable damage to delicate substrates, such as textiles.

*Copolymer and colloidal lithography* are based on the self-assembly of macromolecules on a substrate, allowing the fabrication of a wide range of planar patterns. The main difference between both techniques is the type of compound that is used to produce the pattern, copolymer, and colloidal crystals, respectively. The patterns are then transferred to the substrate by processes such as etching, deposition, or stamping [35,37,39].

In *scanning probe lithography*, a scanning probe is used to draw a pattern into the substrate by an additive or subtractive process of adding or removing molecules, proteins, or polymers through mechanical, diffusive, electrical, or thermal processes [37,40]. This technique allows drawing patterns with higher resolution (10 nm) but with slower writing of  $10\text{ }\mu\text{m}^2/\text{h}$ , limiting its throughput for industrial applications [40].

*Photolithography* using mask aligner is the most commonly used nanolithography process to fabricate small-sized devices and structures [36]. In this technique, a substrate (typically, glass or silicon) is coated with a photoresist layer. The photoresist is then exposed to light using a mask with white and black regions (photomask) that has the desired pattern. For that purpose, it is possible to select two types of photoresists: *positive photoresist* and *negative photoresist*. In the case of a positive photoresist, after light exposure, the chemical structure of the exposed areas changes, becoming soluble when immersed in an appropriate solvent. In contrast, in the case of a negative photoresist, the exposed areas become insoluble when immersed in a solvent appropriate for negative photoresists. Then, the desired pattern is obtained after an etching step, which removes the chemically changed photoresist areas. Although it does not allow reaching the high resolution of beam-based lithography, photolithography uses low-energy intensity (amount of energy needed to write the desired pattern into the photoresist), being

suitable for soft substrates (plastic, paper, or textile). Photolithography is applicable at both laboratorial and industrial scales, but the throughput and resolution are very different. At a laboratorial scale, the instrumentation cost can be two orders of magnitude lower when compared with industrial scale, because no expensive optics nor automatization machinery are required to produce microstructures with reasonable resolution (in the order of micrometers). On the other hand, at an industrial level, there is a need to produce microstructures with fast throughput and high resolution (in the order of nanometers), requiring expensive instrumentation. However, with sophisticated technology and optimized setups, it is possible to produce more than 100 wafers per hour, which makes the production cost of each pattern more cost-effective [36–38].

When lithographic processes emerged, they were preferentially used for rigid substrates. However, with the continuous evolution of technologies and instrumentation, they offer great potentialities for being used to produce nanostructures directly on textiles. Moreover, lithographic techniques have been successfully applied to print patterns on flexible and easily damageable substrates, such as flexible plastics and polymers [41,42]. Table 21.1 summarizes the basic working principles, the fabrication specifications (simple or multiple structures), the maximum resolution, and the throughput of the different nanolithography processes [37].

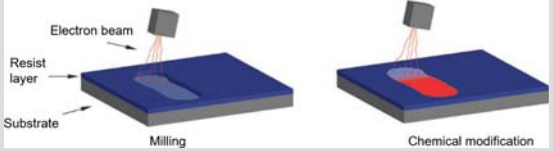
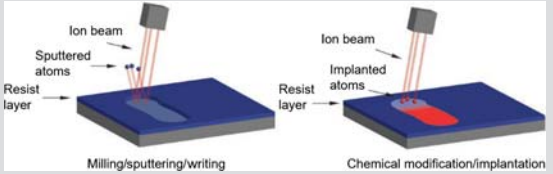
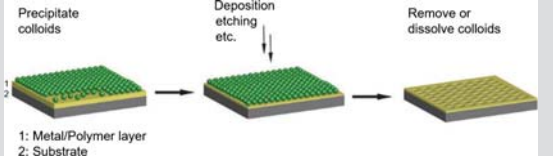
### 21.2.2.3 3D printing

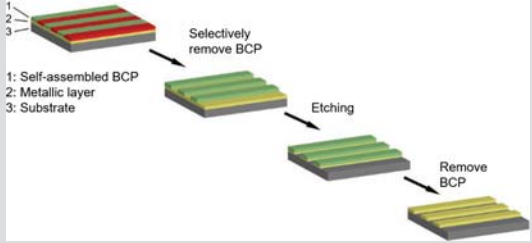
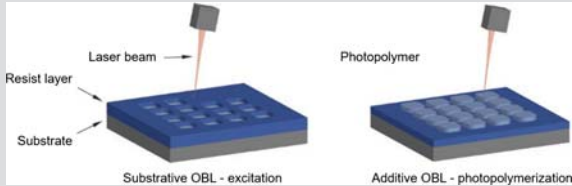
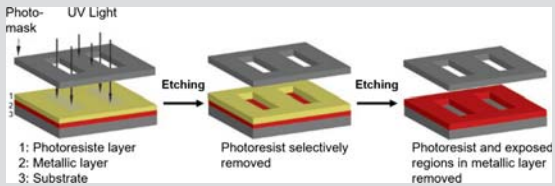
The emerging trend in printing technologies for the textile sector is *3D printing*. Usually known as an additive manufacturing technology [43], 3D printing allows producing 3D structures on substrates starting from a raw material, such as polymers, composites, metals, ceramics, sand, glass, nylon, or wax [44,45]. 3D printing is a cost-effective and versatile process for the development and production of customized structures, since it requires low amount of raw materials, reduces the labor costs by eliminating many labor-intensive processes, and decreases the number of human errors during the manufacturing process [44,46,47]. The technology behind 3D printing is related to the direct manufacturing of 3D structures from digital computer-aided design (CAD) files [46]. 3D printing can be made by different methods, such as *fused deposition modeling*, *selective laser sintering*, and *stereolithography*, which differ in the way each layer is deposited and on the type of materials that are used.

The most commonly used and cost-effective process is *fused deposition modeling*, where an extrudable material is melted through a nozzle and deposited in a layer-by-layer manner to fabricate the 3D structure [44]. The *selective laser sintering* creates a 3D structure from a powder material by the incidence of a laser. Normally, this process uses high-power lasers (such as CO<sub>2</sub> laser) to increase the temperature to a value above the powder melting

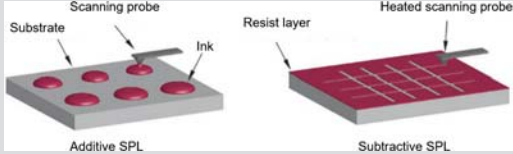


**TABLE 21.1** Summary of fabrication methods, production complexity, resolution, and throughput of the different nanolithography processes

Fabrication method	Production complexity	Resolution	Throughput
Electron beam lithography (EBL)	Simple structures	4 nm	Low
			
Ion beam lithography (IBL)	Simple structures	8 nm	Low
			
Colloidal lithography	Simple structures	<10 nm	Medium
 <p>1: Metal/Polymer layer 2: Substrate</p>			

<p>Block copolymer lithography (BCP)</p>  <p>1: Self-assembled BCP 2: Metallic layer 3: Substrate</p> <p>Selectively remove BCP</p> <p>Etching</p> <p>Remove BCP</p>	Simple structures	10–450 nm	Medium
<p>Optical beam lithography (OBL)</p>  <p>Resist layer</p> <p>Substrate</p> <p>Laser beam</p> <p>Substrative OBL - excitation</p> <p>Photopolymer</p> <p>Additive OBL - photopolymerization</p>	Simple structures	52 nm	Low
<p>Photolithography</p>  <p>Photo-mask</p> <p>UV Light</p> <p>Etching</p> <p>Etching</p> <p>1: Photoresist layer 2: Metallic layer 3: Substrate</p> <p>Photoresist selectively removed</p> <p>Photoresist and exposed regions in metallic layer removed</p>	Multiple structures	<37 nm and potentially <10 nm	Very high
(Continued)			

**TABLE 21.1** (Continued)

Fabrication method	Production complexity	Resolution	Throughput
Scanning probe lithography (SPL)	Multiple structures	Up to 500 $\mu\text{m}$	Low
			

Source: Adapted from van Assenbergh P, Meinders E, Geraedts J, Dodou D. Nanostructure and microstructure fabrication: from desired properties to suitable processes. Small 2018; 14:1801989 [37] with permission from John Wiley & Sons.

point, fusing it with strong adhesiveness into the final product [44,45]. Finally, *stereolithography* uses UV light to cure a photopolymer resin, in order to create 3D objects by a chemical process called photosolidification [44–46]. Photosolidification consists of the polymerization of monomers through the absorption of visible or UV light. The polymerization only occurs in the exposed regions, making it possible to remove unreacted monomer from unexposed regions [44,46].

Cellulose materials, such as wood or cotton, have emerged as engineered substrates for 3D printing due to their remarkable properties such as sustainability, hydrophilicity, biocompatibility, biodegradability, and nontoxicity [44]. In this sense, cellulose materials combined with other polymers, such as polyacrylamide, polyethylene glycols, gelatin, agarose, alginate, collagen, and chitosan [48], have already started to be used for several applications including medicine, biological devices, electronics, energy storage, and textile applications [44,48–50]. For instance, Tenhunen et al. reported the surface tailoring and design-driven prototyping of fabrics based on cellulose materials by direct-writing 3D printing [49]. The cellulose derivative materials were printed on three types of cellulose fabrics—woven cotton, knitted cotton, and woven viscose—in order to impart different functionalities to textile-based prototypes, namely refractiveness and thermoresponsiveness (Fig. 21.10 I). To produce the refractive prototypes, the authors mixed refractive glass beads with cellulose acetate, which acted as a binder, to attach the active components to the textile, and then printed the resulting mixture on the cellulose fabrics (Fig. 21.10 I). The thermoresponsive prototypes were obtained by printing the cellulose fabrics with a paste containing a thermochromic powder and acetoxypopyl cellulose (Fig. 21.10 II). Finally, by embedding a conductive metal wire into the thermochromic paste, the authors developed indicator cellulose fabrics that changed their color when an electrical current passed through them due to the dissipated heat arising from the electrical resistance of the wire (Fig. 21.10 III).

Similarly, Beecroft developed a weft knitted textile based on nylon powder by selective laser sintering [51]. The 3D printed textile exhibited the natural features of the knitted textile such as flexibility, strength, and stretchability, being a good alternative solution to technical textiles. The combination of 3D printing with cellulose materials thus opens new horizons on the development of all-customized e-textiles without requiring complex manufacturing processes.

#### 21.2.2.4 Fiber spinning

The *fiber spinning technologies* for fiber and yarn manufacturing present some significant advantages relative to conventional dyeing and coating processes, such as: lower water and energy consumption (related to dyeing and washing off steps); minimal or nonexistent wastewater effluents; fewer pigments/fillers and chemical agents (in contrast to the high quantity of pigments/dyes and

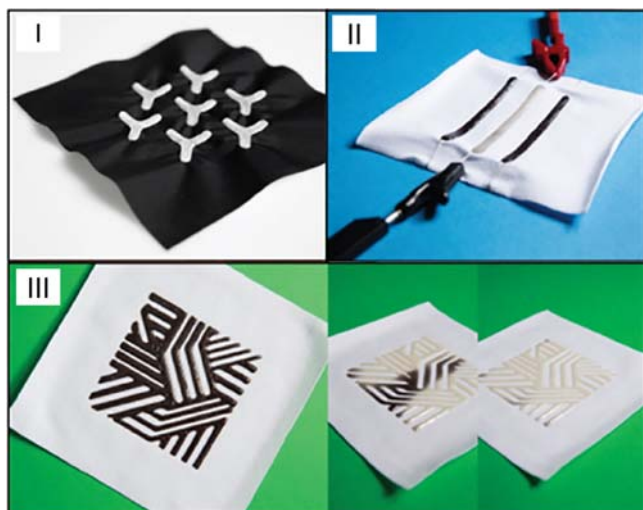


**FIGURE 21.10** Several prototypes produced by direct 3D printing based on cellulose materials: (I) refractive fabric based on refractive glass beads mixed with cellulose acetate (CA); (II) and (III) thermoresponsive structures printed on cellulose fabric based on a mixture of thermochromic pigment and acetoxypropyl cellulose. *Adapted from Tenhunen T-M, Moslemian O, Kammiovirta K, Harlin A, Kääriäinen P, Österberg M, et al. Surface tailoring and design-driven prototyping of fabrics with 3D-printing: an all-cellulose approach. Mater Des 2018;140:409–19 [49] with permission from Elsevier.*

auxiliaries required in conventional dyeing and printing due to poor dye fixation); and good washing fastness [52,53]. Nevertheless, they still pose limitations for high-throughput applications in terms of costs and of ensuring good dispersion of the nanofillers within the polymer matrix and interfacial interaction. In several cases the nanomaterial surface needs to be functionalized with suitable organic groups or a compatibilizing agent needs to be used [5].

Fibers can be classified as monocomponent or multicomponent. Multicomponent fibers combine at least two polymers with distinct properties and/or chemical composition. The polymers are extruded together, and their position along the fiber length depends on factors such as the geometry of spinneret holes and the intrinsic properties of the polymers (e.g., viscosity and molecular weight). In the case of bicomponent fibers (containing two polymer components), depending on the type of geometry of the cross-section, they can be classified as side-by-side, core sheath (concentric, eccentric; and trilobal), “islands in a sea,” among other configurations (Fig. 21.11). The core-sheath is the most common configuration, in which the polymer used as core provides the desired physical characteristics, while the polymer in the sheath imparts a specific functionality to the filament [54]. The fiber manufacturing technologies can be used to produce multicomponent fibers with tailored cross-sections and surface functionalities by combining different polymers

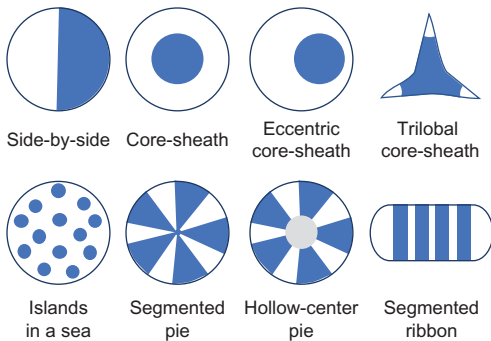


**FIGURE 21.11** Types of bicomponent fibers.

and/or additives [55]. Fillers such as carbon nanomaterials (e.g., carbon black, carbon nanotubes, and graphene), metal/metal oxide NPs (e.g., silver and iron oxide), silica NPs, biologically active molecules, among others, can be added during the spinning process to produce high-performance fibers with new structures and functionalities (e.g., antibacterial [56], electrical conductivity [57,58], radar/infrared camouflage [59], photochromism [60,61], tissue engineering [62], drug delivery [62], and flame retardancy [63]) for particular applications. After the fiber/yarn production using functional or smart nanomaterials, several techniques can be used to convert them into a textile structure, such as knitting, weaving, embroidering, sewing or spinning knitting, weaving, embroidering, or sewing [26].

Spinning technologies can be classified as *melt spinning* and *solution spinning* (e.g., *dry spinning*, *wet spinning*, and *gel spinning*). In *melt spinning*, a thermoplastic polymer is heated to a melt state, extruded into fibers, and quenched. Most commercial synthetic fibers, including nylon, polyester, and polypropylene, are produced by *melt spinning*, which is a relatively simple and cost-effective technique when compared with *solution spinning*. Nevertheless, for polymers without a stable melt phase, the spinning from a solution is required. In *solution spinning*, the polymer is dissolved in a solvent to form a spinnable dope that is extruded into fibers, followed by solvent removal; examples of solvent spun fibers include Kevlar, Nomex, Lycra, and Lyocell [64,65]. The *solution spinning* comprises two processes: (1) *dry spinning*—uses solvents with high volatility (high vapor pressure) and the fiber formation occurs by solvent evaporation during the spinning process; and (2) *wet spinning*—when the polymer is soluble in solvents with low volatility (low vapor pressure), the fibers are spun into a nonsolvent bath to remove the solvent and to coagulate. Nevertheless, there are also several variations of these processes.

#### 21.2.2.4.1 Melt spinning

*Melt spinning* has been used since the late 1950s because it provides an effective way of combining two or more polymers to produce multicomponent

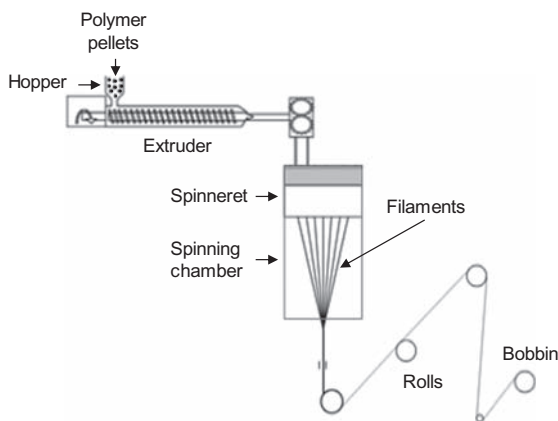


**FIGURE 21.12** Schematic representation of a typical melt spinning process unit.

fibers, in which each component plays an important role on defining the features of the final product [66]. A schematic representation of a melt spinning unit is shown in Fig. 21.12.

Typically, the melt spinning process requires a constant mass flow rate of the molten polymer, which is maintained by a metering or a spinning pump generally positioned inside the spinning head [64]. The polymer pellets are introduced through a hopper into the extruder, in which it is melted (e.g., polypropylene melts around 170 °C, while nylon and polyester melt at temperatures above 250 °C) [67] and transported to a flow pump. Then, the molten polymer is channeled into a spinneret consisting of several individual capillary holes with defined cross-sectional shapes and sizes. Afterward, the long continuous filaments extruded through the spinneret holes are cooled-off, solidified, drawn, and collected on a winder [68]. Melt spinning is considered an economical and environmentally friendly process due to its high productivity, ability to easily spin multicomponent fibers with different cross-sectional shapes, and absence of additional toxic solvents [63,69]. It is used to produce polyamide (nylon), polyethylene terephthalate (polyester), and polypropylene fibers, all of which are widely used commodity textiles for apparel and upholstery applications [70]. The nonuniformity of the fiber diameter, the thermal decomposition of the molten polymer during extrusion due to oxidation, and the use of only thermoplastic polymers are the main drawbacks [69,70].

#### 21.2.2.4.2 Solution spinning

Apparel synthetic fibers are mainly manufactured by melt spinning. However, there are many solvent spun fibers used for high-end applications, such as Kevlar, Nomex, Lycra, Lyocell, and Rayon, in which their unique properties justify their elevated cost [65]. Among the *solution spinning* technologies, the *dry spinning process* is employed when the polymer is

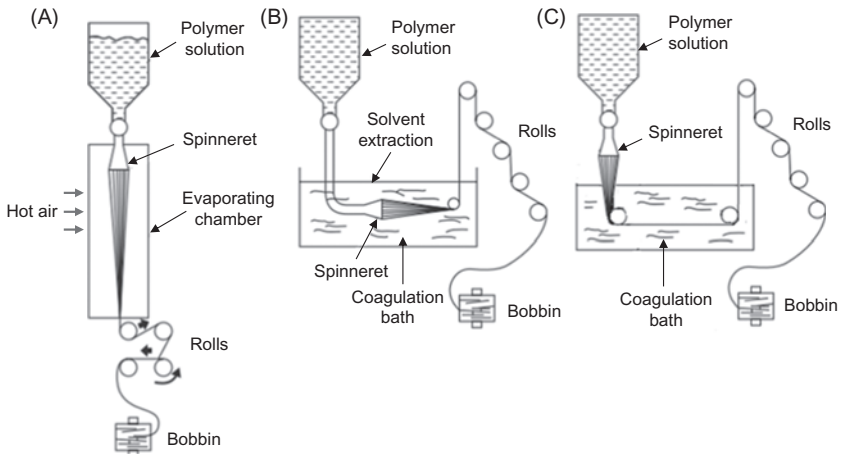


**FIGURE 21.13** Schematic representation of solution spinning process units: (A) dry spinning, (B) wet spinning, and (C) dry-jet wet spinning. Adapted from Imura Y, Hogan RMC, Jaffe M. Dry spinning of synthetic polymer fibers. In: Zhang D, editor. *Adv. Filam. Yarn Spinn. Text. Polym.* 1st ed. Cambridge: Elsevier B.V.; 2014. p. 187–202 [71] with permission from Elsevier.

susceptible to thermal degradation, cannot form thermally stable or viscous melts, or when particular surface features of the filament are necessary. This process is used to produce fibers such as secondary cellulose acetate, cellulose triacetate, acrylics (e.g., Orlon), Spandex-type polyurethane elastomeric fibers (e.g., Lycra), and PVC (e.g., Rhovyl and Teviron) [71]. A schematic representation of a dry spinning unit is depicted in Fig. 21.13A. A dope (i.e., a solution consisting of a polymer dissolved in a volatile organic solvent such as *N,N*-dimethylformamide is usually used in dry spinning) [64] is filtered, deaired, preheated, and then pumped through the fine holes of the spinneret into a heated column or chamber. The resulting fine dope streams face a flow of hot air that promotes instantaneous evaporation of the solvent from the surface, resulting in immediate filament formation with a solid skin. As the filaments pass through the evaporating chamber, the solvent is increasingly removed from the interior of the filaments, thereby continually solidifying and strengthening them. Subsequently, the filaments are drawn by rotating rolls (or godets) and put on bobbins.

In a typical *wet spinning process*, the dope is extruded through a multiple hole spinneret immersed in a coagulation bath containing a nonsolvent [55]. The spinning solution undergoes spinodal decomposition and phase separation into polymer-rich and polymer-poor regions and ultimately into a solid phase. The structure and properties of the fibers are highly controlled by polymer–solvent interactions. Additionally, the phase separation essentially depends on the solvent to nonsolvent relative diffusion rates [55,72]. After passing through the coagulation bath, the solid filaments are submitted to a



series of operations such as orientational drawing, drying, crimping, and annealing. A schematic representation of a wet spinning unit is shown in Fig. 21.13B. The linear speed of the fiber is very slow in comparison to the speeds achieved in melt spinning; as a result, the manufacturing productivity is performed using multiple spinnerets with several thousand holes [55]. The filaments from many spinnerets are often combined to form a single-fiber tow bundle. In general, viscose rayon, acrylic, Spandex-type elastomeric fibers, polyvinyl alcohol, and aromatic polyamides are produced by wet spinning [64,70].

The *dry-jet wet spinning* is an alternative method to wet spinning, and is used for some polymers that, when extruded directly into the bath, lead to the formation of voids (micro- or macrovoids) that negatively affect the final properties of the fibers due to the solvent being drawn out of the liquid too quickly. The major technical difference lies in the existence of a gap between the end of the spinneret and the coagulating bath, as can be seen in Fig. 21.13C. It is used, in particular, for processing some types of aramid fibers [70].

Recent development of another type of solution spinning—*gel spinning*—has resulted in commercialization of several high-performance polyethylene-based fibers (e.g., Spectra and Dyneema) [64]. Briefly, a dope consisting of ultrahigh molecular weight polyethylene dissolved in a solvent is channeled into an extrusion tank (usually filled with water) through a multihole spinneret. As the dope is cooled and part of the solvent is extracted, gel-like filaments are formed in a type of network arrangement. Afterward, the as-spun filaments are transferred to an oven and slowly drawn. The resulting fibers are then wound on packages [65].

Although solution spinning allows manufacturing fibers with properties that cannot be achieved through melt spinning, there are many disadvantages of using this process. For instance, the spin speed in a solvent spun system is lower than that obtained in melt spinning, the equipment and the process analysis are more complex, and the use and recovery of organic solvents for large-scale manufacturing increase the production cost and can cause potential environmental pollution [65].

#### 21.2.2.4.3 Electrospinning

Another widely used spinning technology for fiber production is *electrospinning*. This technique is based on the principle of electrostatic instabilities in liquids or the distortion of a drop by the application of electric charge [73]. A schematic representation of an electrospinning unit is illustrated in Fig. 21.14A.

In a typical procedure, the polymer solution (in the case of *solution electrospinning*) or melt (in the case of *melt electrospinning*) is introduced in a syringe equipped with a piston and a capillary acting as electrode, and

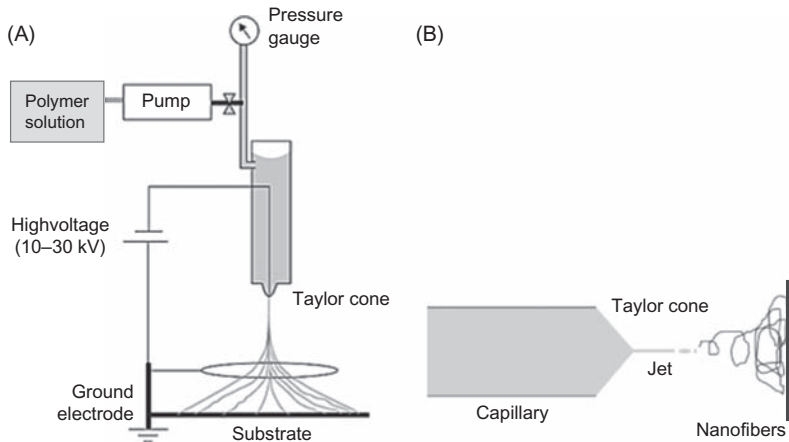


**FIGURE 21.14** Schematic representation of (A) electrospinning process unit and (B) Taylor cone. Adapted from Ni QQ, Jin X, Xia H, Liu F, *Electrospinning, processing and characterization of polymer-based nano-composite fibers*. In: Zhang D, editor. *Adv. Filam. Yarn Spinn. Text. Polym.* 1st ed. Cambridge: Elsevier B.V.; 2014. p. 128–48 [74] with permission from Elsevier.

pushed through a pump with a defined flow rate [64]. The spinneret connected to the voltage source applies a high voltage (usually in the range of 10–30 kV) to the polymer [73], resulting in the formation of a polymer drop at the end of the spinneret that changes its shape from hemispherical to conical (Taylor cone), illustrated in Fig. 21.14B. At a defined voltage, the surface tension of the polymer cone at the tip of the spinneret starts to elongate and stretch, forming a charged liquid jet. The solvent evaporates as the jet travels through the air, leaving behind ultrafine polymeric fibers that gather an electrically grounded target. The jet often follows a bending or a spiral track, resulting from the interaction between the external electric field and the surface charge of the jet [64]. Many distinct polymers have been used in solution or molten state to produce nanofibers by electrospinning: for instance, synthetic (e.g., polyesters, polyamides, polyurethanes, and polycarbonates), natural (e.g., chitosan, silk, collagen, gelatin, and elastin), and synthetic biodegradable polymers (e.g., poly(lactic acid), poly(glycolic acid), and poly(lactide-co-glycolide)) [8,75].

The electrospinning process exhibits several advantages relative to solution spinning technologies, namely its simplicity and cost-effectiveness. Additionally, it allows good control of fiber diameter (ranging from tens of nanometers to a few micrometers), morphology, and functionality [54,76]. However, the major drawbacks of this process are the extremely low production rates, difficult solvent recovery, and toxicity. This process has been employed in liquid filtration (wastewater treatment and desalination), energy production (e.g., photovoltaic devices), energy storage (e.g., as battery separators), protective textiles, and biomedicine [69,75,77–80].

## 21.3 Functional nanomaterials@textiles: from production to textile applications

### 21.3.1 Functional silica nanoparticles

#### 21.3.1.1 Production processes

In recent decades, silica NPs have received increased attention as supporting matrices or as building blocks, opening exciting opportunities for the design of innovative (bio)functionalized nanomaterials for a wide range of areas, including medicine [81–85], biology [86], food and nutrition [87], chemistry [88], environmental science [89,90], and toxicology [91]. Nanosized silica represents a promising alternative to its bulk counterpart, exhibiting attractive physical and chemical features, namely good colloidal stability in several solvents, high chemical, thermal, and UV stability, large surface area-to-volume ratio, and high concentration of surface silanol groups [92]. Additionally, an extensive number of functional groups, (bio)molecules, or metal/metal oxide NPs can be assembled on its surface, encapsulated within or incorporated both inside and onto the surface through different chemical routes, in order to build multifunctional nanosystems with synergistic properties when compared with those of the individual components [84,93–95].

Remarkable progress has been achieved in the processes of  $\text{SiO}_2$  NPs fabrication with precisely controlled physicochemical properties. Several methods have been reported, such as *flame spray pyrolysis* [96], *chemical vapor deposition* [97], and *wet-chemistry methodologies* like *sol–gel* [98–100], *microemulsion* [101,102], *hydrothermal* [103] and *solvothermal* methods [104].

In particular, research has been mostly focused on the *sol–gel process*, since it is straightforward, scalable, easily controllable, and time and energy saving [105]. This process, also known as the Stöber process, was first introduced by Stöber in 1968 to synthesize monodisperse silica particles with diameters ranging from 50 nm to 200  $\mu\text{m}$ . It consists of controlled hydrolysis and condensation of a silica precursor (e.g., tetraethylorthosilicate, TEOS) in a mixture of alcohol and water, using ammonia as catalyst (Fig. 21.15A [98]). Since then, many contemporary research works describing the synthesis of  $\text{SiO}_2$  NPs evolved from that method. For instance, the addition of structure-directing agents during the synthesis process, such as surfactants (e.g., dodecyl- and hexadecyltrimethylammonium salts like cetyltrimethylammonium bromide, CTAB), polymers (often a nonionic diblock or triblock copolymer, such as Pluronic P65, P123, and F127, conjugated with cationic surfactants and swelling agents, such as 1,3,5-trimethylbenzene), and other additives can lead to the formation of an ordered porous network, thus forming mesoporous  $\text{SiO}_2$  NPs with a broad range of morphologies and pore sizes (Fig. 21.15B). For instance, Bein et al. reported a one-pot strategy for the synthesis of mesoporous  $\text{SiO}_2$  NPs with small sizes (40 – 150 nm), narrow particle size distribution, large specific surface areas, and high

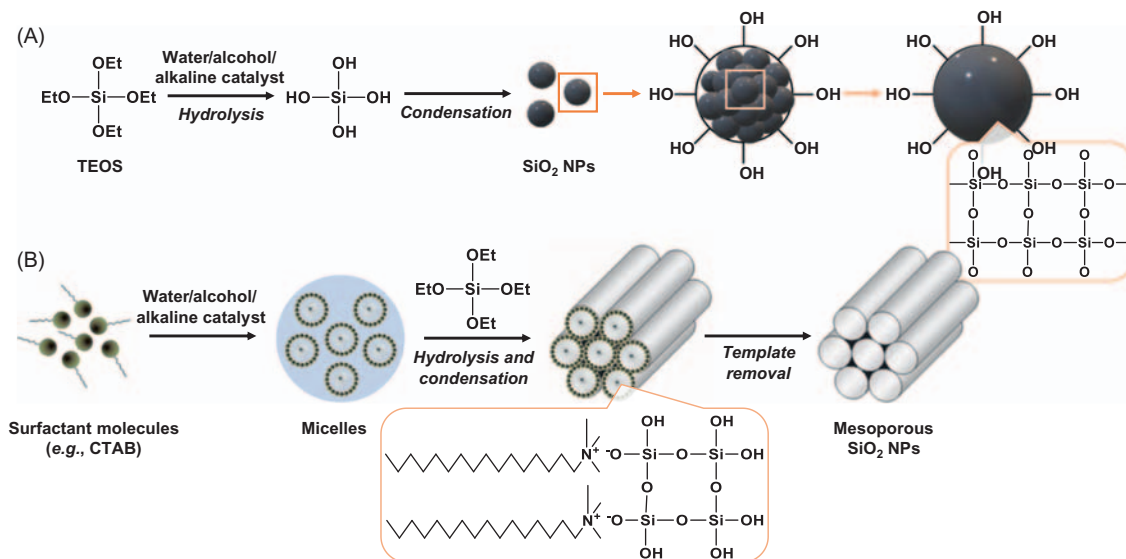


**FIGURE 21.15** Schematic representation (not drawn to scale) of the synthesis of: (A) nonporous  $\text{SiO}_2$  NPs by the Stöber method, and (B) mesoporous  $\text{SiO}_2$  NPs by a modified Stöber method with addition of a structure-directing agent. Adapted from Yang P, Gai S, Lin J. Functionalized mesoporous silica materials for controlled drug delivery. *Chem Soc Rev* 2012;41:3679–98 [106] with permission from RSC.

colloidal stability [100,107,108]. In their approach, a polyalcohol base, triethanolamine, was used during the sol–gel process, which acted as alkaline agent, as complexing agent for silica precursors, and as encapsulating agent for the resulting mesoporous particles, thus controlling the alkoxides hydrolysis/condensation rates and limiting the particle growth and aggregation. Besides the type of alkaline agent, the fine-tuning of other reaction parameters, such as the type/concentration of silica precursor, structure-directing agent, pH, solvent, temperature, reaction time, aging time, and stirring rate allows the precise adjustment of the particle size, morphology (e.g., spheres, hollow spheres, fibers, tubules, gyroids, and many hierarchical structures), and pore structure, in the case of mesoporous silica NPs (e.g., hexagonal, wormhole-like) [109].

An alternative synthetic approach to preparing SiO<sub>2</sub> NPs was developed by Arriagada and Osseo-Asare in the early 1990s involving the ammonia-catalyzed polymerization of TEOS in a *reverse phase*, or *water-in-oil microemulsion* [101,102]. In this process, nanometer-size monodispersed water droplets are stabilized by surfactant molecules dissolved in organic solvents (e.g., cyclohexane, *n*-pentane, *n*-hexane, *n*-heptane, *n*-decane, and *n*-hexadecane) to form spheroidal aggregates called reverse micelles. The silica precursor undergoes hydrolysis/condensation inside the droplets that act as nanoreactors, providing a suitable environment for controlled nucleation and growth. The size and shape of the aqueous core can be tailored by varying the water:surfactant molar ratio. This method produces highly monodisperse spherical particles with sizes smaller than 100 nm and with improved control over particle size/size distribution relative to the sol–gel method, does not require extreme conditions of temperature and pressure, and allows easy encapsulation of guest molecules and metal/metal oxide NPs (e.g., Au, Fe<sub>3</sub>O<sub>4</sub>, etc.) [83,110,111]; nevertheless, it involves higher costs and the removal of the surfactants is tedious and time-consuming [88]. Yokoi et al. reported a greener alternative method for the synthesis of uniform nanosized spheres (12 nm) formed in the emulsion system containing TEOS, water, and basic amino acids (lysine) under weakly basic conditions [112].

The *hydrothermal method* is one of the most common and effective synthetic routes to fabricate different types of nanomaterials with a variety of morphologies. In this method, the reactions are conducted in a specially sealed container or high-pressure autoclave, usually a Teflon-lined autoclave, under subcritical or supercritical conditions, using water as solvent; in the case of nonaqueous solvents the process is referred to as *solvothermal method* [113]. Hydrothermal/solvothermal process is of particular importance to produce ultrafine and pure inorganic crystals with uniform nanosize distributions, at temperatures substantially below those required by solid-state reactions, and without requiring postannealing treatments. In addition, the crystallographic phase, particle size, shape, and functionalization of the nanomaterial can be tailored by varying the reaction parameters, such as temperature

and/or pressure, pH, reaction time, solvent, reagent concentrations, and use of selected additives (chemical species added to the reaction medium to control the nucleation and growth processes and, consequently, to govern the particle size, morphology, and dispersion degree).

An emerging area that has recently arisen consists of waste recycling to produce novel high-value-added products, within the new paradigms of circular economy and sustainable development. In particular, with the escalating increase of worldwide population, adding value to agroindustrial solid wastes produced at a large scale, while reducing the contamination of the environment, is a challenge for green chemistry. Recently, SiO<sub>2</sub> NPs have been produced from *agroindustrial byproducts*, such as rice husk [114,115], sugarcane [115–117], and bamboo [115]. For example, Peres et al. obtained high-purity SiO<sub>2</sub> NPs (98.8%) with particle size of 93 nm from rice husk using an alternative microwave process [114]. Rovani et al. used sugarcane ash to produce nanosized silica with particle size <20 nm, >99% purity, and nondefined form [118].

### 21.3.1.2 Functionalization

The surface chemistry of SiO<sub>2</sub> NPs is governed by the reactivity of their silanol groups (Si–OH) [119,120], offering the possibility of introducing a great variety of functionalities in the material and, consequently, fine-tuning the nanomaterials properties. The SiO<sub>2</sub> NPs surface can be easily modified via physical adsorption, electrostatic interactions, or covalent bonding through silane chemistry.

The most relevant strategies to achieve covalent functionalization of SiO<sub>2</sub> NPs are through *cocondensation* and *postsynthetic* grafting [84,99]. The *cocondensation*, also termed *direct* or *one-pot synthesis*, involves the simultaneous synthesis and functionalization of SiO<sub>2</sub> NPs typically by sol–gel chemistry, illustrated in Fig. 21.16A for mesoporous SiO<sub>2</sub> NPs. This can be accomplished by hydrolysis and condensation between a tetraalkoxysilane [(RO)<sub>4</sub>Si] and a bifunctional organotrialkoxysilane [(R'O)<sub>3</sub>SiR, in which R is an organic functional group and R' an alkoxy group] [99]. This route is straightforward to control the degree of surface functionalization and a homogeneous distribution of the desired functional groups is usually obtained even when a high concentration of about 10 mol% silane is used [120–122]. Bein et al. developed a straightforward cocondensation method to prepare mesoporous SiO<sub>2</sub> NPs with different surface properties in an alkaline aqueous medium, by introducing organosilanes with different functional groups, such as vinyl-, benzyl-, or phenyltriethoxysilanes, or by generating surface charges through the functionalization with chargeable groups, like amines and thiols, during the formation of the SiO<sub>2</sub> NPs [100,122]. In addition, since it is a simple one-step procedure, it minimizes possible contaminations or mass losses that can occur more easily in complicated, multistep

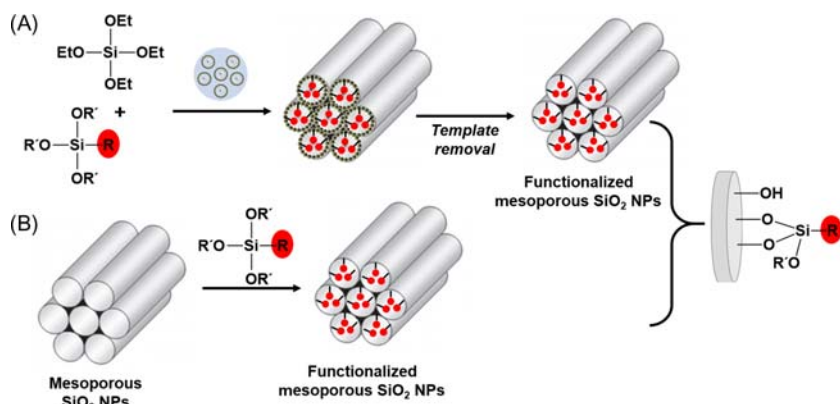


**FIGURE 21.16** Schematic representation (not drawn to scale) of the functionalization of ordered mesoporous  $\text{SiO}_2$  NPs with a bifunctional organotrialkoxysilane  $(\text{R}'\text{O})_3\text{SiR}$  containing an organic functional R group through: (A) cocondensation and (B) postgrafting. The structure-directing agent is represented in (A) by the blue micelle on top of the first arrow.

postsynthetic functionalization methods [123]. An eventual drawback of this methodology is the decrease of the degree of mesoscopic order of the resulting nanomaterial upon the increase of the concentration of  $(\text{R}'\text{O})_3\text{SiR}$  in the reaction mixture [120,121]. In the case of mesoporous  $\text{SiO}_2$  NPs produced in the presence of a structure-directing agent, the increase of the organosilane: alkoxysilane ratio during the synthesis can lead to a reduction of the pore diameter, pore volume, and specific surface area [120]. Moreover, the removal of the surfactant is usually performed by solvent extraction processes (e.g., acid extraction for anionic surfactants) instead of calcination, in order to preserve the structural integrity of the as-synthesized functional  $\text{SiO}_2$  NPs, and prevent particle aggregation [120–122]. New alternatives, such as the use of a reversible temperature-sensitive polymer template (poly (*N*-isopropylacrylamide)) that can be removed and recycled only by temperature regulation, have been reported [124].

The *postsynthetic* functionalization, also referred to as *postgrafting*, allows introducing the functional groups after the formation of the silica network; in the case of mesoporous  $\text{SiO}_2$  NPs, this can be performed either before or after the removal of the structure-directing agent [120,121]. Organo-functionalization is mostly carried out by silylation, in which the surface free ( $\equiv\text{Si}-\text{OH}$ ) and geminal [ $=\text{Si}(\text{OH})_2$ ] silanol groups act as suitable anchoring points for organotrialkoxysilanes (or, less frequently, organotrichlorosilanes), illustrated in Fig. 21.16B for mesoporous  $\text{SiO}_2$  NPs [119]. Through this route, specific parts of the silica surface can be modified (e.g., external surface, pore surface, and pore entrances), promoting good functionalization degrees without compromising the mesoscopic order [121]. Nevertheless, the distribution and concentration of the functional groups are

affected by the reactivity of the  $(R'O)_3SiR$  moieties and by their accessibility to surface silanols, being limited by diffusion and steric factors [120]. A promising strategy consists of combining both cocondensation and grafting approaches to achieve a selective functionalization, in which more than one type of functional groups can be introduced. For instance, to restrict the functionalization to the external surface of mesoporous  $SiO_2$  NPs, the modification can be performed prior to the extraction of the structure-directing agent; after removing the structure-directing agent, the protected silanol groups in the pore surface can be further functionalized [120].

The silylation of  $SiO_2$  NPs with charged functional groups, such as positively charged amine-containing (e.g., 3-aminopropyltriethoxysilane [125] and dimethyloctadecyl(3-(trimethoxysilyl)propyl)ammonium chloride) [126], negative (e.g., 3-(trihydroxysilyl)propyl methylphosphonate) [127], or zwitterion organosilanes (e.g., 3-(dimethyl(3-(trimethoxysilyl)propyl)ammonio)propane-1-sulfonate) [128], by cocondensation or postgrafting can result in tailored charged surfaces [83].

$SiO_2$  NPs can also be functionalized with positively charged species through electrostatic interactions due to the presence of negatively charged silanolate ( $Si-O^-$ ) groups that result from silanol groups deprotonation at pH values above the isoelectric point (pH 2–3). Moreover, the incorporation of carboxylic groups onto the  $SiO_2$  surface is a very effective route to promote attractive electrostatic interactions with positively charged species (e.g., cationic metals and hydrophilic drugs) [129,130]. Besides electrostatic interactions, hydrogen bonding and physical adsorption are important weak noncovalent interactions to immobilize species into the channels of mesoporous silica materials, such as therapeutic drugs [106].

Multifunctional  $SiO_2$  NPs with more complex architectures, such as core-shell, raspberry, and hollow, have been proposed for advanced applications. In particular, core-shell structures have received great attention for biomedical applications as “nanocarriers” for the transport of therapeutic drugs, antibiotics, and fluorescent dyes to cells. The decoration of the inner and outer surface of the NPs with specific species, such as tracking markers (e.g., fluorescent dyes, superparamagnetic iron oxide NPs, and quantum dots), spacers (e.g., polyethylene glycol and biocompatible polymers), gatekeepers (e.g., proteins, superparamagnetic iron oxide NPs, and gold NPs), targeting ligands (e.g., antibodies), and supported lipid bilayers [84,131], can impart important features for successful drug delivery (Fig. 21.17). Metal NPs (e.g., palladium, copper, iron, gold), quantum dots, superparamagnetic metal oxide NPs, among others, have been encapsulated in core-shell silica NPs to confer catalytic, imaging, and biological capabilities [84,132]. Oils, fragrances, and insect repellents, such as silicone oil, *Eucalyptus globulus* L., *Citrus limon* L., tetradecane, limonene, benzyl salicylate, and citronella oil, as well as fungicides (e.g., prochloraz) have also been encapsulated within silica capsules [133–136]. These functional systems can be incorporated in fabrics, for the



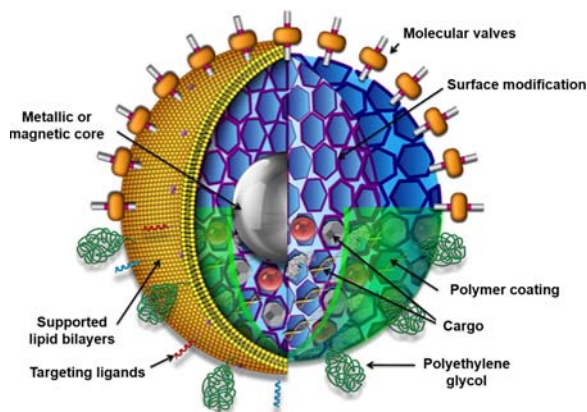


**FIGURE 21.17** Schematic illustration of a multifunctional mesoporous core-shell  $\text{SiO}_2$  NP illustrating the versatility of surface modifications and types of coating layers. *Reproduced from Tarn D, Ashley CE, Xue M, Carnes EC, Zink JJ, Brinker CJ. Mesoporous silica nanoparticle nanocarriers: biofunctionality and biocompatibility. Acc Chem Res 2013;46:792–801 [131] with permission from The American Chemical Society (ACS).*

production of antimicrobial, insect repellent, and cosmetotextiles. In all cases, the silica shell protects the encapsulated guest molecules/NPs from degradation and environmental conditions.

Compared to  $\text{SiO}_2$  NPs with smooth surfaces, raspberry-like NPs have a unique hierarchical structure, which results in a surface with high roughness and low surface energy [137]. This well-defined surface geometry may also exhibit liquid-repellent properties; therefore, many studies have been devoted to the fabrication of superhydrophobic surfaces applying raspberry-like  $\text{SiO}_2$  particles, namely for self-cleaning coatings [137–140].

Hollow mesoporous  $\text{SiO}_2$  NPs have been used in diverse applications, including catalysis and drug release, due to their highly permeable mesoporous shell and inner cavity that allows the encapsulation of guest molecules with diverse functionalities [109,141]. The “core-templating method” is frequently used for their synthesis via *sol–gel method* or *layer-by-layer assembly*. Many soft (e.g., micelles, microemulsion droplets, and vesicular structures) and hard templates (e.g., carbon NPs, polymers such as polystyrene and polymethylmethacrylate, and metal/metal oxide/semiconductor NPs such as gold, silver,  $\text{Fe}_3\text{O}_4$ , CdS, ZnS) are used to form the core [109], followed by silica coating using a silica precursor in different concentrations to obtain a shell with the desired thickness. The template removal is then performed through solvent extraction or calcination at moderate temperatures, or by acid or base etching, depending on the nature of the core.

More recently, silica NPs have evolved into a third generation of more complex multilevel structures (hierarchical structures) that include: (1) hollow mesoporous spheres, (2) core-in-(hollow porous shell) spheres,

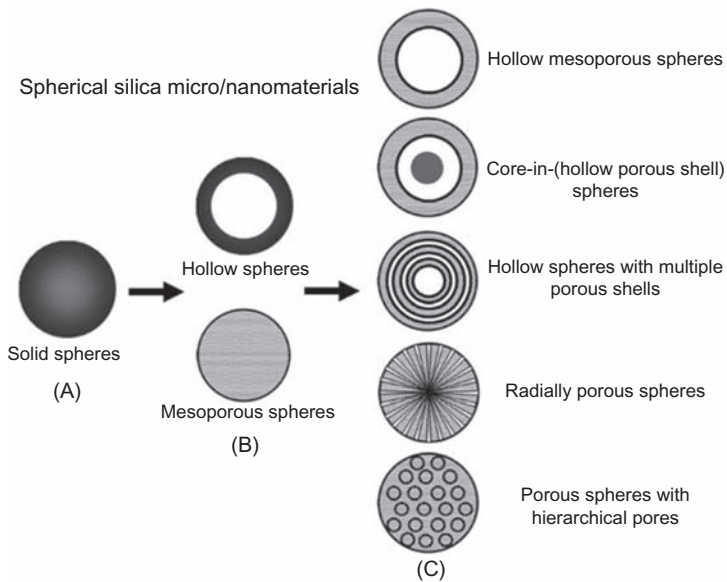


**FIGURE 21.18** Structural evolution of  $\text{SiO}_2$  NPs: (A) solid  $\text{SiO}_2$  NPs with one-level structure; (B) hollow and mesoporous  $\text{SiO}_2$  NPs with two-level structures; (C)  $\text{SiO}_2$  NPs with multilevel (hierarchical) structures, including hollow mesoporous spheres, core-in-(hollow porous shell) spheres, hollow spheres with multiple porous shells, and hierarchical porous spheres. Hierarchical porous structures include radially porous spheres and porous spheres with ordered (e.g., hexagonal order or radial orientation) or nonordered (e.g., worm-like pores) hierarchical pores. Reproduced from Du X, He J. *Spherical silica micro/nanomaterials with hierarchical structures: synthesis and applications*. *Nanoscale* 2011;3:3984–4002 [142] with permission from RSC.

(3) hollow spheres with multiple porous shells, and (4) hierarchically porous spheres with radial pores or hierarchical pores (Fig. 21.18) [142]. These complex nanostructures have tremendous interest for a myriad of applications, namely as drug carriers, in functional coatings (superhydrophilicity or superhydrophobicity, antireflection, antifogging properties, etc.), in photovoltaic cells, etc. [142].

### 21.3.1.3 Nanosilica-coated textiles: applications

The nanoscale modification of textiles with  $\text{SiO}_2$  NPs has been reported as a promising approach to produce textiles with water/oil repellency [143–149], flame retardancy [150], UV protection [151,152], antibacterial [151–153], among other properties. Furthermore,  $\text{SiO}_2$  NPs containing direct organic [154,155] or chromic dyes (e.g., fluorescent [156], photochromic [151,157–160], and thermochromic [161]) have been applied on textiles to improve the dye photostability and washing fastness [6,162].

New approaches for the design of superamphiphobic textiles that confer both superhydrophobicity and superoleophobicity protection are focused on the surface functionalization of SiO<sub>2</sub> NPs with nonfluorinated alkylsilanes or fluorosilanes. Pereira et al. reported the synthesis of superhydrophobic colloidal mesoporous SiO<sub>2</sub> NPs functionalized with tridecafluorooctyl-triethoxysilane (42–45 nm particle size), and the synthesis and simultaneous incorporation of those hybrid SiO<sub>2</sub> NPs onto cotton textiles through a scalable, efficient, and less time-consuming one-pot cocondensation route [145]. The enhanced surface roughness imparted by the mesoporous SiO<sub>2</sub> NPs and the reduction of the surface free energy induced by the hydro/oleophobic organosilane were responsible for the enhanced water repellence properties. In addition, the fabric functionalized with the SiO<sub>2</sub> NPs containing the highest loading of fluorocarbon groups was superamphiphobic.

Regarding flame retardancy, Carosio and coworkers developed thin films of colloidal silica deposited on cotton fibers via layer-by-layer process (LbL) [163]. Negatively charged SiO<sub>2</sub> NPs (8 and 27 nm) were assembled with either positively charged silica (12 nm) or cationic polyethylenimine (PEI); each coating was evaluated at 10 and 20 bilayers. The treatment of the cotton fabric with an aqueous NaOH solution (pH 10) prior to the LbL assembly increased the negative charge of the substrate and resulted on improved deposition and flame-retardant behavior. All coated fabrics retained their weave structure after being exposed to a vertical flame test, while the uncoated cotton was destroyed. The coated fabrics exhibited a 20% lower peak heat release rate than the uncoated control (227 vs 285 W/g). Coatings consisting of 8 nm size SiO<sub>2</sub> NPs resulted in better flame retardancy properties relative to those made with larger particles (27 nm).

Hashemikia et al. produced a cotton fabric with antibacterial and anti-inflammatory drug delivery properties. Mesoporous SiO<sub>2</sub> NPs (SBA-15 type) functionalized with (3-aminopropyl)triethoxysilane by postgrafting were used as carrier for the anti-inflammatory drug betamethasone sodium phosphate [164]. The cotton fabrics were then immersed in a bath containing the drug-loaded SiO<sub>2</sub> NPs followed by padding, with a wet pick-up of 100%. Afterward, the SiO<sub>2</sub>-loaded fabrics were treated with polysiloxane reactive softener and/or chitosan followed by curing. The chitosan-treated fabrics exhibited excellent antibacterial properties against *Escherichia coli* and *Staphylococcus aureus* preserving the activity after five washing cycles.

Gomes patented the production of cellulosic fibers with insect repellency through the incorporation of functionalized SiO<sub>2</sub> NPs by the pad-fix process [165]. To achieve that goal, an insect repellent compound, ethyl-3-(*N*-*n*-butyl-*N*-acetyl)aminopropionate, was firstly reacted with an epoxysilane coupling agent, 3-glycidylpropylmethoxysilane. SiO<sub>2</sub> NPs were then synthesized by cocondensation between TEOS (or sodium silicate) and the as-modified epoxysilane (sol–gel method). The epoxysilane allowed not only to covalently

bond the insect repellent compound to the  $\text{SiO}_2$  NPs, but also to anchor the nanomaterial to the cellulosic fibers through the epoxy groups.

Active textiles (e.g., light-responsive, thermo-responsive, pH-responsive, etc.) are an interesting class of smart textiles that can sense or detect a stimulus sent by the environment or by the user's body (e.g., light, temperature, pH, etc.) transforming it into a signal (e.g., color change). For instance, Pinto et al. produced efficient light-responsive cotton fabrics through the incorporation of photochromic  $\text{SiO}_2$  NPs functionalized with silylated and nonsilylated naphthopyran derivatives (via postgrafting) by screen-printing [157]. The nanocoated fabrics revealed high color contrast (color difference,  $\Delta E^* = 27.0\text{--}57.4$ ); good coloration/decoloration kinetics (coloring in 1 min under UV/sunlight irradiation, and fading in only 2 min); diversified photo-generated color pallet (yellow, orange, pink, and purple); and low residual coloration (Fig. 21.19A). In addition, the functional fabrics showed high photostability, resistance to photodegradation, and washing fastness for up to five washing cycles. The photochromic nanomaterials were also incorporated

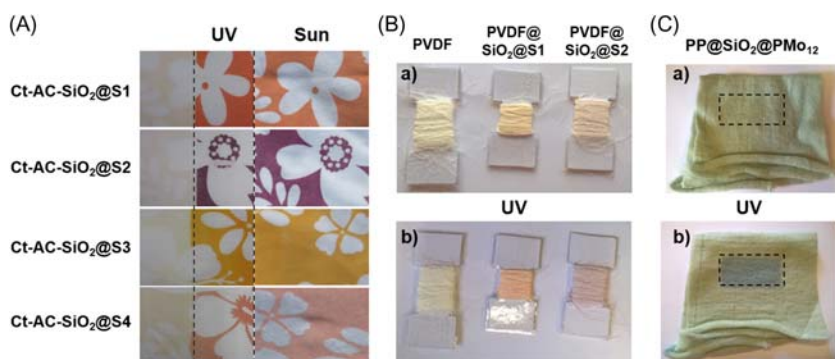


**FIGURE 21.19** Photographs of: (A) cotton fabrics (Ct) coated with a screen-printing acrylic paste (AC) containing photochromic  $\text{SiO}_2$  NPs functionalized with silylated naphthopyran derivatives ( $\text{SiO}_2\text{@S1}$ ,  $\text{SiO}_2\text{@S2}$ ,  $\text{SiO}_2\text{@S3}$ , and  $\text{SiO}_2\text{@S4}$ ) before (uncolored region) and after (colored region) UV ( $\lambda = 365$  nm) and sunlight irradiation for 1 min at room temperature; (B) PVDF fibers doped with  $\text{SiO}_2\text{@S1}$  and  $\text{SiO}_2\text{@S2}$  (PVDF@ $\text{SiO}_2\text{@S1}$  and PVDF@ $\text{SiO}_2\text{@S2}$ ) prepared by dry-jet wet spinning (a) before and (b) after UV ( $\lambda = 365$  nm) irradiation for 1 min at room temperature; (C) PP mesh doped with  $\text{SiO}_2$  NPs functionalized with Keggin-type  $\text{PMo}_{12}$  (PP@ $\text{SiO}_2\text{@PMo}_{12}$ ) fabricated via melt spinning (a) before and (b) after UV ( $\lambda = 254$  nm) irradiation during 7 h at room temperature. Adapted from Pinto T V, Costa P, Sousa C M, Sousa C A D, Pereira C, Silva C J S M et al. Screen-printed photochromic textiles through new inks based on  $\text{SiO}_2\text{@naphthopyran}$  nanoparticles. *ACS Appl Mater Interfaces* 2016; 8:28935–28945 [157] with permission from ACS and from Pinto T V, Cardoso N, Costa P, Sousa C M, Durães N, Silva C, et al. Light driven PVDF fibers based on photochromic nanosilica@naphthopyran fabricated by wet spinning. *Appl Surf Sci* 2019; 470: 951–958 [61] and Pinto T V, Fernandes D M, Guedes A, Cardoso N, Durães N F, Silva C, et al. Photochromic polypropylene fibers based on UV-responsive silica@phosphomolybdate nanoparticles through melt spinning technology. *Chem Eng J* 2018; 350: 856–866 [60] with permission from Elsevier.

within polyvinylidene fluoride (PVDF) fibers by dry-jet wet spinning (Fig. 21.19B), revealing fast coloration kinetics and good color contrast ( $\Delta E^* = 7.2\text{--}15.1$ ) [61]. Later on, the same group fabricated photochromic polypropylene (PP) fibers based on UV-responsive  $\text{SiO}_2$ @phosphomolybdate NPs through melt spinning technology [60]. The photochromic hybrid nanomaterial was prepared by immobilization of a negatively charged Keggin-type phosphomolybdate ( $\text{PMo}_{12}\text{O}_{40}$ ) onto positively charged amine-functionalized  $\text{SiO}_2$  NPs through electrostatic interactions. Afterward, bicomponent core-sheath-type fibers were prepared via melt spinning, using PP doped with 5 wt.% of the hybrid silica NPs ( $\text{SiO}_2$ @ $\text{PMo}_{12}\text{O}_{40}$ ) as sheath and pristine PP as the core of the filaments. The resulting doped fibers presented good mechanical properties, which allowed the knitting of a photoresponsive mesh (Fig. 21.19C). Although the photochromic performance of the inorganic Keggin-type phosphomolybdates was not comparable to that of photochromic organic molecules (naphthopyrans), presenting slower coloration/decoulation kinetics (coloring in 1 h under UV irradiation and fading during several days), the  $\text{SiO}_2$ @ $\text{PMo}_{12}\text{O}_{40}$  NPs exhibited remarkable thermal stability and robustness to up to  $T \sim 180^\circ\text{C}$ , without any decomposition or loss of their photochromic performance.

Ribeiro et al. prepared thermochromic cotton fabrics through the incorporation of thermochromic dye-functionalized  $\text{SiO}_2$  NPs by exhaustion dyeing method [161]. The thermochromic  $\text{SiO}_2$  NPs were prepared by cocondensation of TEOS and dimethyloctadecyl[3-(trimethoxysilyl)propyl]ammonium chloride with a thermochromic dye added into the reaction medium before introducing the silica precursors. The dyed cotton changed from pink to white coloration when heated above room temperature.

Ayazi-Yazdi et al. produced a cotton fabric with multifunctional properties—antibacterial activity against *E. coli* and *S. aureus*, hydrophobicity, photochromism, and UV blocking properties—and good washing fastness, maintaining its performance after 10 washing cycles [151]. To achieve that goal, the cotton fabrics were immersed on a  $\text{SiO}_2$  NPs/spirooxazine ethanolic solution for 24 h at room temperature followed by curing ( $110^\circ\text{C}$  for 10 min). Afterward, the fabrics were treated with triethoxyoctylsilane to impart hydrophobicity; the static water contact angle was  $141.2^\circ$ . The photochromic fabrics changed their color from colorless to blue upon sunlight irradiation (5 min) with good color contrast ( $\Delta E^* = 10.1\text{--}33.4$ ). In addition, they exhibited strong antibacterial activity, with a bacteria reduction of 99.99%.

Hendrick et al. produced nonwoven cellulose acetate fibers doped with fluorescent core-shell  $\text{SiO}_2$  NPs (Cornell dots, C dots) by electrospinning for anticounterfeiting and pH-sensing applications [156]. Two types of C dots were used: one consisting of fluorescent dye-containing silica core surrounded by a silica shell, which exhibited fluorescence at  $\lambda = 572$  nm when excited by an external light source at  $\lambda = 541$  nm; and the other type

containing both a fluorescent core and a pH-sensitive shell, which exhibited fluorescence at  $\lambda = 572$  and  $\lambda = 518$  nm when exposed to an external light source at  $\lambda = 488$  nm. Both C dot-containing fibers were white under ambient light, fluorescing at their respective wavelengths. The fluorescence intensity at  $\lambda = 541$  nm increased with the increase of the pH. Moreover, the mechanical properties of the electrospun fibers were not negatively affected by C dot addition, even though the final loading constituted nearly one-third of the weight of the fibers.

## 21.3.2 Functional TiO<sub>2</sub> nanoparticles

### 21.3.2.1 Production processes

Titanium dioxide (TiO<sub>2</sub>) is one of the most important and widely studied photocatalysts due to its singular and attractive photocatalytic activity (with highly oxidizing photogenerated holes and highly reducing photogenerated electrons), chemical stability, nontoxicity, and moderate cost [166,167]. In recent years, it has gained particular interest for photoelectrocatalysis (e.g., dye-sensitized solar cells, water splitting for hydrogen production, and degradation of organic pollutants) [167–169]; functional coatings (e.g., self-cleaning, superhydrophilicity, UV blocking and antimicrobial activity) [170,171]; and energy storage applications (e.g., supercapacitors and Li-ion batteries) [172,173].

TiO<sub>2</sub> can occur in mainly three crystalline polymorphs: rutile (tetragonal, two coordinated Ti), anatase (tetragonal, four coordinated Ti), and brookite (orthorhombic, eight coordinated Ti) [169,170,174–176]. Under ambient conditions, the rutile phase is the thermodynamically stable phase of TiO<sub>2</sub>. Anatase and brookite are thermodynamically metastable, but can be easily transformed into the rutile phase when treated at high temperatures [169,174–176]. Among the polymorphs, anatase shows the highest photocatalytic activity, producing active species under UV irradiation and triggering a series of reduction and oxidation reactions [169]. Furthermore, nanostructured TiO<sub>2</sub> materials offer improvements for most of the abovementioned applications due to the large active surface area, namely leading to an enhancement of catalytic reaction rates, an increase of the electrical double layer capacity, an increase of the charge/discharge rate of Li-ion batteries, the tuning of the optical reflectivity and absorbance [177], among other.

Sulfate and chloride processes have been traditionally employed for large-scale production of TiO<sub>2</sub> pigment particles (e.g., anatase and rutile crystalline phases in the sulfate process, and rutile phase in the chloride process) from titanium mineral concentrates [176]. From an economical and environmental point of view, the continuous chloride process is more favorable than the batch sulfate process. Many strategies have been developed for the synthesis of nanostructured TiO<sub>2</sub>, including *hydrothermal sol-gel*

*method, chemical vapor deposition, physical vapor deposition, solvothermal method electrochemical approaches* (e.g., anodization process), *water-in-oil (W/O) and oil-in-water (O/W) microemulsion*, and *green synthesis* (e.g., biosynthesis and phytosynthesis) [169,176]. The crystal phase, particle size, and shape are strongly affected by the synthesis route and experimental conditions, such as the type of  $\text{TiO}_2$  precursor (typically titanium(IV) chloride, titanium(IV) sulfate, or titanium(IV) alkoxides such as titanium(IV) isopropoxide, titanium(IV) isobutoxide, and titanium(IV) ethoxide), surfactant or peptizing agent, solvent, temperature, and reaction time. Among these synthetic routes, the sol–gel and hydrothermal method processes are the most successful ones due to their ability to control the morphology, particle size, and crystallinity of the final nanomaterials [176]. Several types of  $\text{TiO}_2$  nanostructures (e.g., nanoparticles, nanowhiskers, nanofibers, nanospindles, nanocuboids, nanowires, nanotubes, and nanobelts) have been successfully synthesized by these methods.

For instance, Sugimoto et al. proposed a new *sol–gel procedure* for the preparation of uniform anatase  $\text{TiO}_2$  NPs with different sizes and shapes through the phase transformation of a  $\text{Ti}(\text{OH})_4$  gel matrix (titanium(IV) isopropoxide used as precursor) in the presence of shape controllers [178–180]. In this system, ammonia and two amines (triethanolamine and diethylenetriamine) were used as shape controllers, yielding ellipsoidal particles due to their specific adsorption onto the crystal planes parallel to the *c*-axis of the tetragonal system. On the other hand, the addition of sodium oleate and stearate as shape controllers produced cuboidal particles with sharp-edged cubes. Similar shape control was achieved with primary amines, such as ethylenediamine, trimethylenediamine, and triethylenetetramine. However, secondary and tertiary amines acted as complexing agents to promote the growth of ellipsoidal particles with lower aspect ratio, rather than as shape controllers. Moreover, if no ammonia was added to the reaction medium, the mean size and aspect ratio of the anatase particles were drastically reduced to the nano-size range (5–30 nm and  $\sim 3.2$  nm, respectively). Finally, the introduction of an inert electrolyte, such as  $\text{NaClO}_4$ , retarded or, in some cases, inhibited the nucleation of anatase.

Kotsokechagia et al. reported a two-step nonaqueous sol–gel strategy involving (1) the prealkoxylation of titanium(IV) chloride in ethanol, followed by (2) its nonhydrolytic decomposition and formation of anatase  $\text{TiO}_2$  NPs in benzyl alcohol [181]. This approach combined the benefits of nonaqueous synthetic processes (good control over crystallinity and size) with those of surface functionalization in water medium, allowing the incorporation of a wider variety of functional groups onto the NPs. Based on this route, Frantz et al. recently obtained anatase nanocrystals with 4 nm diameter, which were readily dispersible in various polar solvents, allowing the easy preparation of colloidal dispersions in water, isopropyl alcohol, dimethyl sulfoxide, and ethanol [177].



Concerning the fabrication of nanocrystalline  $\text{TiO}_2$  through the *hydrothermal method*, in 1988, Oguri et al. reported the preparation of spherical polycrystalline anatase particles by hydrothermally processing amorphous hydrous  $\text{TiO}_2$  synthesized by controlled hydrolysis and polymerization of titanium(IV) ethoxide in ethanol [182]. Later on, this method was extended to the fabrication of erbium-doped  $\text{TiO}_2$  NPs ( $\sim 30$  nm) [183]. To achieve that goal, the authors synthesized anatase NPs through a sol–gel process, using titanium(IV) isopropoxide as precursor, followed by peptization with tetramethylammonium hydroxide, dropwise addition of erbium(III) nitrate pentahydrate, and finally hydrothermal method treatment. The morphology of the  $\text{TiO}_2$  NPs changed from rod-like to triangular as the amount of Er increased from 1 to 3 mol%.

Cheng et al. developed a hydrothermal method to prepare uniform nanosized rutile and anatase particles from aqueous titanium(IV) chloride at different pH values [184]. The acidic conditions favored rutile NP formation, while the basic conditions led to pure anatase phase. Furthermore, higher temperatures benefited more highly dispersed products and mineralizers, such as tin(IV) chloride, while sodium chloride tended to reduce the average grain size, and ammonium chloride led to particle agglomeration. Dinh et al. obtained nanostructured  $\text{TiO}_2$  with different shapes (e.g., rhombic, truncated rhombic, spherical, truncated and elongated rhombic, dog-bone, and bar) through that route (Fig. 21.20) [185]. In their approach, titanium(IV) butoxide was chosen as titanium source due to its low hydrolysis rate. In particular, the presence of an alkyl group slowed down the diffusion and polymerization processes, leading to the formation of  $\text{TiO}_2$  nanocrystals with controlled morphology. Moreover, the presence of an appropriate amount of water vapor combined with two distinct capping surfactants (oleic acid and oleylamine) played an important role in the control of the size and morphology of  $\text{TiO}_2$  nanostructures.

*Coprecipitation*, also known as the wet chemical solution method, is a common approach to produce  $\text{TiO}_2$  micro- and nanostructures, such as nanorods and NPs [166]. It consists of the precipitation of titanium hydroxide by the addition of an alkaline solution (e.g., NaOH,  $\text{NH}_4\text{OH}$ ,  $\text{NH}_3$ , or urea) to a titanium precursor, such as titanium(III) chloride, or titanium(IV) chloride, followed by thermal treatment to crystallize the oxide [186].

*Chemical vapor deposition (CVD)* and *physical vapor deposition (PVD)* processes involve the deposition of atoms or molecules by the reduction or decomposition of a chemical vapor species (precursor gas) onto the substrate surface. In the CVD process, the deposited material chemically reacts with the substrate, while in PVD processes, the deposited molecules and substrate are still distinct [187]. The groups of Wu and Chen synthesized well-aligned rutile and anatase  $\text{TiO}_2$  nanostructures (nanorods and nanocrystals) through metal organic chemical vapor deposition (MOCVD) on fused silica or sapphire substrates using titanium(IV) acetylacetonate and titanium(IV) isopropoxide as  $\text{TiO}_2$  precursor, respectively [188,189].



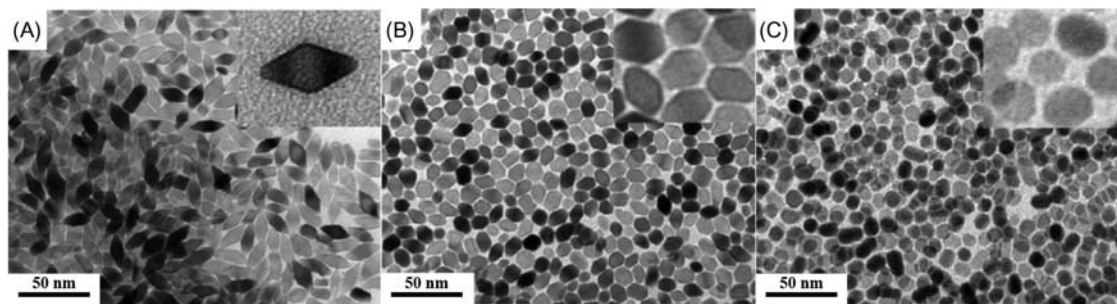


**FIGURE 21.20** TEM images of nanostructured  $\text{TiO}_2$  with: (A) rhombic shape, (B) truncated rhombic shape, and (C) spherical shape. The insets show the corresponding high-magnification images. Adapted from Dinh C-T, Nguyen T-D, Kleitz F, Do T-O. Shape-controlled synthesis of highly crystalline titania nanocrystals. *ACS Nano* 2009;3:3737–43 [185] with permission from ACS.

### 21.3.2.2 Functionalization/doping

Extensive research on the surface modification of TiO<sub>2</sub> nanostructures either by organic/inorganic surface coating or by adding dopants has been carried out. Surface functionalization with organic species has been preferred since it can impart a diversity of functional groups to the TiO<sub>2</sub> surface, such as hydroxyl, aldehyde, and carboxylic groups [166]. (Bio)sensors [190] and drug release systems [191] based on TiO<sub>2</sub> nanostructures have been recently designed through surface functionalization and immobilization of specific biomolecules [192]. As example, alkoxysilanes, such as (3-aminopropyl) triethoxysilane, have been used as linkers because they can be selectively photodegraded to prompt the controlled release of proteins, enzymes, and bioactive molecules [192]. Moreover, TiO<sub>2</sub> NPs surface has been modified with (3-aminopropyl)trimethoxysilane, phenyltrimethoxysilane, and (3-isocyanatopropyl)trimethoxysilane in order to improve the affinity of TiO<sub>2</sub> to fabrics [193,194].

The addition of dopants, such as nonmetals (e.g., C, N, S, I) [167,195–198], noble metals (e.g., Pt, Ag, Au, Pd) [167,198,199], transition metal cations (e.g., Cu, Fe, Co, Ni) [167,198,200,201], or rare-earth elements (e.g., La, Ce, Er, Pr, Gd, Nd, Sm) [183,202], into the TiO<sub>2</sub> lattice has been carried out, especially for sustainable energy generation, environmental pollution treatment and, more recently, functional textiles. The inclusion of a dopant modifies the electronic structure of TiO<sub>2</sub>, lowering its band gap either by increasing the valence band energy and/or by decreasing the conduction band energy, thus extending its optical absorption into the visible region. Furthermore, the combination of TiO<sub>2</sub> with carbon (nano)materials (e.g., activated carbon, carbon nanotubes, fullerenes, graphene) [197,203–205] is being increasingly investigated as a means to increase the photocatalytic activity. Many methods have been developed to produce doped or functionalized TiO<sub>2</sub> NPs, including *sol–gel* [198,203,206,207], *hydrothermal method* [195,198,203,207], *deposition processes* (including physical vapor deposition, chemical vapor deposition, and electrophoretic deposition) [198,203], *anodization* [198], *ball milling* [200,203], and *chemical reduction* [201]. Fig. 21.21 summarizes the different synthetic routes used for the preparation of N-doped TiO<sub>2</sub> [208].

### 21.3.2.3 Nano-TiO<sub>2</sub>-coated textiles: applications

During the past years, many efforts have been made to incorporate TiO<sub>2</sub> NPs onto textile fabrics in order to impart multifunctional properties such as self-cleaning [209–211], superhydrophilicity [212], antibacterial and antifungal activity [209,210], UV protection [210], and flame retardancy [213].

For instance, Yu et al. fabricated a photocatalyzed self-cleaning cotton fabric based on the incorporation of commercial anatase TiO<sub>2</sub> NPs (5 – 10 nm) [214]. The authors developed a new strategy to covalently



**FIGURE 21.21** Schematic diagram illustrating the different synthetic routes for the preparation of N-doped TiO<sub>2</sub>.

immobilize TiO<sub>2</sub> NPs onto the cotton fabric surface using a vinyl monomer (maleic anhydride) to form a graft chain network. First, TiO<sub>2</sub> NPs were functionalized by an esterification reaction with maleic anhydride; second, the functionalized TiO<sub>2</sub> NPs and 2-hydroxyethyl acrylate were cografed onto cotton fabric under  $\gamma$ -ray irradiation. The functionalized cotton fabrics showed photocatalyzed self-cleaning activity under UV irradiation (355 nm, 0.2 mW/cm<sup>2</sup>) after 48 h ( $\lambda = 355$  nm), and the covalent bonds between the TiO<sub>2</sub> NPs and the cotton fabrics bridged by the poly(2-hydroxyethyl acrylate) graft chains were strong enough to endure 30 accelerated laundering cycles (which was equivalent to 150 commercial or domestic launderings).

Emami et al. reported the fabrication of nylon-6 fabric with self-cleaning and antibacterial properties through corona discharge pretreatment and coating with commercial TiO<sub>2</sub> P25 NPs ( $\sim 21$  nm) by the pad-dry-cure method [215]. The self-cleaning property was evaluated by discoloration of methylene blue dye, ketchup, tea, and coffee stains from the corona/TiO<sub>2</sub> treated fabric. The methylene blue stain was almost completely removed from the treated nylon after 24 h under UV (Fig. 21.22;  $\Delta E^* = 32.87$  vs 15.3 for the untreated fabric) and daylight irradiation. Also, effective discolorations were observed for tea and coffee stains from the treated fabric after 24 h under daylight. Antibacterial activity against *Bacillus subtilis* and *E. coli* bacteria were observed for the corona/TiO<sub>2</sub> treated fabric. In addition, the corona pretreatment allowed preserving the TiO<sub>2</sub> NPs leaching from the surface of the nylon fabric after five washing cycles.

Karimi et al. reported the preparation of cotton fabrics with multifunctional properties—self-cleaning, electrical conductivity, UV blocking, and antimicrobial activity—through the incorporation of graphene oxide/TiO<sub>2</sub> nanocomposites by dip-drying technique [210]. Graphene oxide/TiO<sub>2</sub> P25 nanocomposites were prepared by mixing and sonication (60 min at 50 °C) in water. Different amounts of graphene oxide (0.04, 0.08, 0.12, 0.2, and 0.4 wt.%) and TiO<sub>2</sub> (0.1, 0.5 and 1 wt.%) were tested. Cotton fabrics were immersed into the resulting suspensions, heated for 1 h at 80 °C, and then dried at 100 °C during 15 min. The graphene oxide/TiO<sub>2</sub> nanocomposite-coated cotton fabrics showed photocatalytic self-cleaning activity under sunlight irradiation after four consecutive days; the increase of the concentration

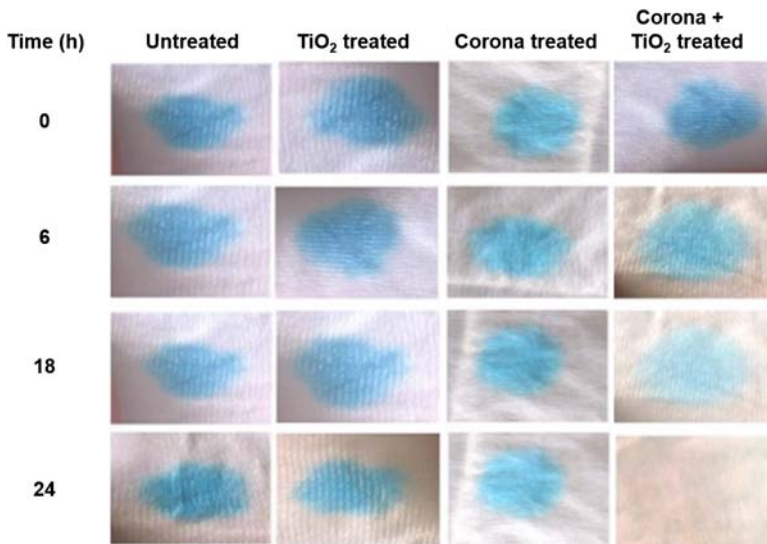


**FIGURE 21.22** Discoloration of methylene blue stains on nylon-6 fabrics before and after treatment with TiO<sub>2</sub>, corona, and corona + TiO<sub>2</sub> under UV irradiation (from 0 to 24 h). Reproduced from Emami F, Shekariz S, Shariatinia Z, Moridi Mahdieh Z. Self-cleaning properties of nylon 6 fabrics treated with corona and TiO<sub>2</sub> nanoparticles under both ultraviolet and daylight irradiations. *Fibers Polym* 2018;19:1014–23 [215] with permission from Springer Nature.

of graphene oxide/TiO<sub>2</sub> improved the degradation of methylene blue. In particular, the photoactivity efficiency of the treated cotton fabric containing 0.4 wt.% of graphene oxide and 1 wt.% of TiO<sub>2</sub> was 89.87%. Additionally, the electrical resistance of the coated fabrics significantly decreased with the irradiation time: for instance, the electrical resistance of the treated cotton fabric containing 0.4 wt.% of graphene oxide and 1 wt.% of TiO<sub>2</sub> decreased from 2 G  $\Omega$ /square to 303 k $\Omega$ /square after 3 days of sunlight irradiation. The finished cotton fabrics demonstrated strong antimicrobial activity of 99% against *S. aureus* and *E. coli*, and UV blocking activity after being incubated for 24 h at 37 °C.

Kowalczyk et al. reported the preparation of a multifunctional thin-coating textile finishing with antibacterial and antifungal activity, self-cleaning, and UV protection using hybrid Al<sub>2</sub>O<sub>3</sub>/SiO<sub>2</sub> sol modified with commercial Ag/Cu NPs (97.5%/2.5%, ~100 nm) and TiO<sub>2</sub> P25 NPs (~21 nm) [216]. The hybrid Al<sub>2</sub>O<sub>3</sub>/SiO<sub>2</sub> sol was prepared by mixing two separately synthesized sols, Al<sub>2</sub>O<sub>3</sub> and SiO<sub>2</sub>. Ag/Cu (0.2%) and TiO<sub>2</sub> (1%) NPs were separately dispersed in a small quantity of the Al<sub>2</sub>O<sub>3</sub>/SiO<sub>2</sub> hybrid sol during 1 h and then mixed together for another hour. The resulting material was deposited on polyester/cotton woven fabrics through the padding method. The modified fabrics revealed good bioactive properties against

*E. coli* and *S. aureus* bacteria (83%–92% reduction) and *Candida albicans* and *Aspergillus niger* fungi (87%–93% reduction), as well as photocatalytic self-cleaning capabilities ( $\Delta E^* \sim 11.6$  after being exposed to UV light for 112 vs  $\sim 4.0$  h for the unmodified fabric) and high UV protection (ultraviolet protection factor, UPF  $> 50$ , while the unmodified fabric presented a UPF  $< 40$ ). Furthermore, the modified woven fabrics exhibited high resistance to abrasion due to the presence of Ag/Cu and TiO<sub>2</sub> P25, despite the increased roughness conferred by the coating, and consequent increase of the abrasion coefficient.

### 21.3.3 Noble metal nanoparticles

#### 21.3.3.1 Production processes

Noble metal NPs, such as Au and Ag, are attracting huge interest on the scientific and industrial communities due to their electrical, chemical and optical properties. Several methods can be used for their preparation, such as *chemical reduction*, *hydrothermal method*, *pyrolysis*, *polyol*, *sol–gel*, or even *biological processes* (Fig. 21.23) [217,218]. Several of these fabrication methods are similar or slightly modified from those used to prepare other types of nanomaterials, such as nanosilica, nano-TiO<sub>2</sub>, metal oxides, among others.

*Chemical reduction* is one of the most used methods for the synthesis of noble metal NPs due to its simplicity and high product yield. This method consists of solubilizing a metal salt (e.g., hydrogen tetrachloroaurate(III)

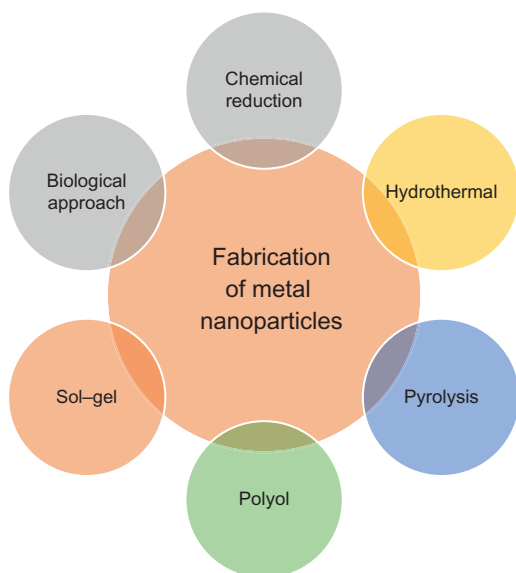


**FIGURE 21.23** Typical bottom-up methods for the fabrication of noble metal NPs.

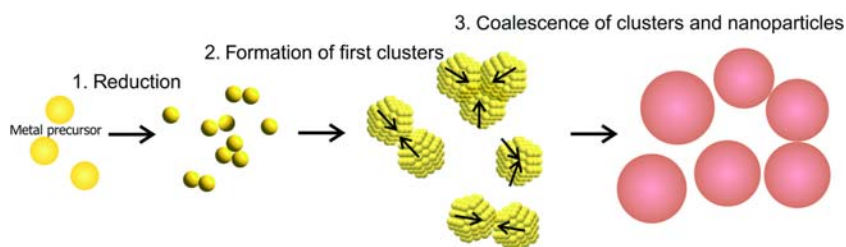


**FIGURE 21.24** Illustration of the chemical reduction process for the synthesis of metal NPs. Reproduced from Polte J. *Fundamental growth principles of colloidal metal nanoparticles—a new perspective*. *CrystEngComm* 2015;17:6809–30 [219] with permission from RSC.

( $\text{HAuCl}_4$ ), silver(I) nitrate ( $\text{AgNO}_3$ ), molybdenum(III) chloride ( $\text{MoCl}_3$ ) on a proper solvent (such as, water and ethylene glycol) and then adding a small quantity of a relatively strong reducing agent (such as, sodium borohydride ( $\text{NaBH}_4$ ), hydrazine ( $\text{N}_2\text{H}_4$ ), sodium citrate ( $\text{Na}_3\text{C}_6\text{H}_5\text{O}_7$ ), and  $\text{NaOH}$ ). The goal of the reducing agent is to reduce the metal cations to the corresponding metals, initiating homogeneous nucleation of seeds in the reaction medium, followed by their growth (Fig. 21.24) [220].

Several types of metal NPs have been prepared by this method, namely gold NPs, which have been extensively produced since at least 1857, when the first documented solution-phase synthesis of colloidal gold by reducing gold(III) ( $\text{HAuCl}_4$ ) with phosphorous in an aqueous medium was published [221]. Along the years, several improvements have been performed to this method. One of the major breakthroughs was reported by Brust in 1994, also called the Brust–Schiffrin method [222]. The novelty was related with the addition of thiol ligands during the synthesis process, which strongly bound to gold. The first step consisted of the transference of gold salt from an aqueous phase to an organic solvent (e.g., toluene) mediated by a phase transfer agent (e.g., tetrabutylammonium bromide) followed by the addition of an organic thiol solution. At the end, a strong reducing agent was added (e.g., sodium borohydride), producing Au NPs capped with a thiolate shell. The major advantages of this method are the ease of synthesis, thermal stability of the produced NPs, reduced degree of NP dispersion, and control of size.

Similarly to gold, a one-step chemical reduction process is widely used to produce Ag NPs. The simplest method to obtain silver NPs is through reduction of silver(I) nitrate ( $\text{AgNO}_3$ ) in ethanol in the presence of a surfactant [223]. This process can be extended to the synthesis of other metals, such as Pt [224], Cu [225], Ni [226], etc.

The *hydrothermal method process* is also simple and has been widely used for the synthesis of different types of metal NPs [227,228]. For example, Zou et al. produced silver NPs of  $\sim 10$  nm diameter using  $\text{AgNO}_3$  and polyvinylpyrrolidone (PVP) [229].  $\text{NH}_3$  was added into an aqueous  $\text{AgNO}_3$  solution, dropwise, until a clear colorless solution was obtained, and then the

resulting solution was mixed with an aqueous solution of PVP. The mixture was then introduced into a Teflon autoclave for 36 h at different temperatures ranging from 100 °C to 240 °C. It can also be highlighted the work reported by Yin et al. that synthesized  $\sim 3$  nm thickness triangular-shaped Ru nanoplates using  $\text{RuCl}_3 \cdot \text{H}_2\text{O}$  and  $\text{HCHO}$  (40 wt.%) at 160 °C for 4 h [230]. The authors were able to tailor the particle size by changing the Ru salt or the solvent concentration. The versatility of this method for the synthesis of other types of NPs was demonstrated by changing the Ru precursor to  $\text{AgNO}_3$ , leading to triangular-shaped Ag nanoplates with sharp and curved corners in the presence of PVP at 160 °C for 6 h [231].

In the *pyrolysis* process the metal precursor is solubilized and heated under specific conditions to evaporate the solvent and form the metallic NPs. Several examples of metal and metal alloy NPs were produced through this method, such as Au [232], Ag, FePt [233], etc. One of the most commonly used methods is *spray pyrolysis* in which the precursor solution undergoes aerosol process that atomizes the solution and heats the droplets to produce solid particles [234]. The shape and the size of the prepared NPs can be tailored by adjusting the composition of the precursor solution and the furnace heat. Lee et al. synthesized dispersed Ag NPs with sizes of 6 and 8.59 nm (depending on the synthesis temperature) using PVP matrix and  $\text{AgNO}_3$  without adding any reducing agent [235]. One of the main advantages of this method is that it allows obtaining dense, shell-structured and hollow NPs.

*Polyol synthesis* is a well-known and commonly used method to synthesize a wide range of metallic nanostructures with different sizes and shapes. It is based on the use of liquid polyols with high boiling temperature (allowing a broad temperature range from room temperature to the boiling temperature characteristic of the solvent). In this case, propylene glycol, 1,2-propylene glycol, or 1,5-pentanediol are commonly used reducing agents, which reduce metal ions present in the solution. Temperature and metal precursor concentration are very important parameters to control the final reaction product properties [236]. Fiévet and coauthors were the first to use the term “polyol process” or “polyol synthesis.” Ag NPs were one of the first nanomaterials produced by this method. Besides Au and Ag, several metal NPs were produced such as Co, Ni, Cu, and Pt, and then extended to further metals, intermetallics, and alloys ( $\text{Re}$ ,  $\text{Rh}$ ,  $\text{Au}$ ,  $\text{Ru}$ ,  $\text{Sn}$ ,  $\text{Co}_x\text{Cu}_{1-x}$ ,  $\text{Co}_{20}\text{Ni}_{80}$ ,  $\text{FeNi}$ , or  $\text{FeCoNi}$ ) [237,238].

The *sol–gel method* is another approach that provides an alternative and usual way for the synthesis of nanomaterials. This process engages a colloidal suspension, called *sol*, and gelation of the sol to form a network in a continuous liquid phase, called *gel*. Three reactions occur and describe the sol–gel process: (1) hydrolysis reaction, (2) alcohol condensation process, and (3) water condensation process. Several metallic NPs have been precipitated in sol–gel-derived matrices. For instance, sol–gel doped silica films were prepared by dipping, starting from an acid-catalyzed solution of TEOS



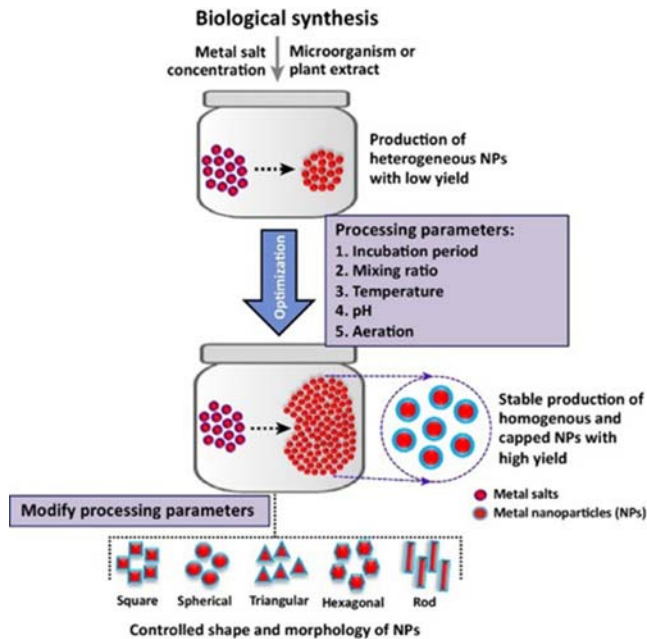


**FIGURE 21.25** Biological approach to the synthesis of metal NPs. Reproduced from Singh P, Kim Y-J, Zhang D, Yang D-C. Biological synthesis of nanoparticles from plants and microorganisms. *Trends Biotechnol* 2016;34:588–99 [244] with permission from Elsevier.

doped with Au, Ag, Pt, and Pd colloids [239]. For instance, Renteria et al. synthesized Ag NPs through this method by introducing  $\text{AgNO}_3$  in the sol–gel precursor solution. Then, the silver cations were thermally reduced in air at 800 °C. At the end, the diameter of the silver particles was found to be about 10 nm [239].

Finally, *living microorganisms*, such as bacteria, fungi, and plants, have great potential for the synthesis of metal NPs (Au, Ag, CdS, Zr, Ti, etc.) [240–243]. This process is environmentally friendly since it uses microorganisms, with the advantage of providing control over particle size and size distribution (Fig. 21.25).

### 21.3.3.2 Metal nanoparticle-coated textiles: applications

Noble metal NPs have been immobilized on textile substrates as colorants for high fashion textiles and with protection purposes. In particular, gold and silver NPs exhibit remarkable optical properties (from the localized surface plasmon resonance (SPR)), resulting in a diversified palette of colors depending on their size and shape [245–247]. Moreover, they exhibit significant chemical stability, namely to UV light exposure and when in contact with the skin. In this context, they can be used as dyeing agents for textile



coloration, replacing conventional dyes and improving the washing fastness and color resistance under UV and sunlight irradiation. Nevertheless, the color stability under UV light is only preserved if there is no variation on particle size because of particle agglomeration. Besides the aesthetic properties, they can endow new functionalities to textiles, namely antimicrobial, UV protection, electrical conductivity, and electromagnetic shielding [4,8,245].

The functionalization of textile substrates with gold and silver NPs (among other metals) can be performed by four different strategies: (1) impregnation of textile fabrics in a colloidal dispersion of the metal NPs; (2) in situ synthesis of the metal NPs in the presence of the textile fabric; (3) incorporation of metal NPs in polymer matrixes followed by fiber spinning; and (4) textile printing with noble metal inks [247].

Concerning strategy (1), Tang and coauthors fabricated anisotropic silver NPs with different morphologies and, consequently, with tunable colors (blue, red, and yellow) by mixing an aqueous solution of  $\text{AgNO}_3$ , trisodium citrate, PVP, and hydrogen peroxide, at room temperature, and adding  $\text{NaBH}_4$  as reducing agent [248]. Moreover, by mixing silver NPs with blue, red, and yellow colors in different ratios, the color palette could be significantly widen (Fig. 21.26). Silk fibers were then successfully coated with the resulting Ag NPs due to Ag strong adsorption ability, presenting a broad color palette (Fig. 21.26) and significant antibacterial properties against *E. coli*. The coloration process presented advantages over the traditional silk

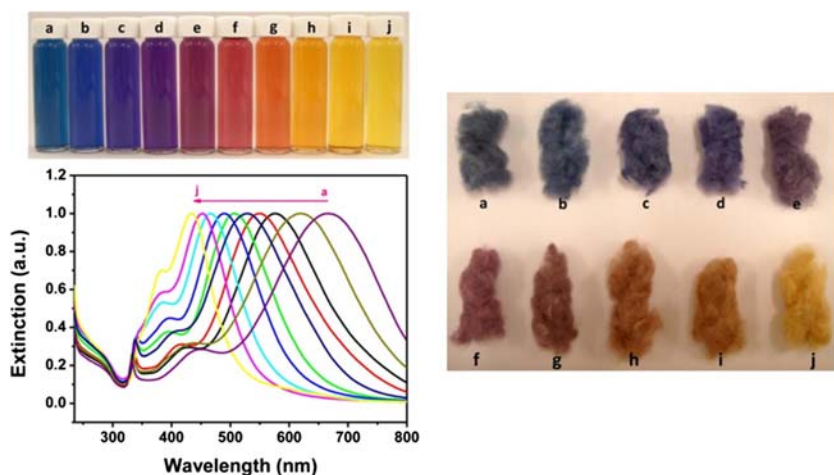


**FIGURE 21.26** Left: Photograph of colloidal dispersions of silver NPs with different particle size and corresponding UV-Vis spectra; Right: Photograph of silk fibers colored by the corresponding silver NP dispersions. *Reproduced from Tang B, Li J, Hou X, Afrin T, Sun L, Wang X. Colorful and antibacterial silk fiber from anisotropic silver nanoparticles. Ind Eng Chem Res 2013;52:4556–63 [248] with permission from ACS.*

dyeing method since it was performed at room temperature and required a shorter time ( $<10$  min), thus reducing energy consumption. The authors suggested that the coloration of the fibers was due to electrostatic interactions between the positively charged fibers surface and the negatively charged silver NPs at pH 4. Finally, upon the coating of the resulting silver-treated silk fibers with polydimethylsiloxane, the color fastness upon washing could be improved.

Gold NPs have also been used as functional building blocks to impart multifunctionality to textile fabrics. For instance, Zheng et al. fabricated gold nanorods with different length-to-diameter aspect ratios, and consequently, with different colors through the seed-mediated growth method followed by anisotropic oxidation [249]. Colloidal dispersions were prepared by dispersing the resulting gold NPs in an aqueous CTAB solution. Cotton and silk fabrics were then efficiently dyed with the resulting nanogold colloidal dispersions, most probably by electrostatic interactions between the negatively charged fabric surfaces (at pH  $\sim 8$ ) and the positively charged gold nanorods, exhibiting a wide variety of colors, ranging from brownish red through green to purplish red, due to the distinct longitudinal plasmon wavelength of the deposited Au nanorods. The coated cotton and silk fabrics also presented UV blocking in both UVA and UVB regions, with UPF values of 41.3 and 32.1, respectively, vs 6.3 and 8.6 for the uncoated counterparts. Additionally, they presented antibacterial properties against *S. aureus* and *E. coli*. Finally, washing fastness to laundering tests and color fastness to dry cleaning tests were performed, revealing that the gold-coated cotton fabrics were commercially acceptable, while the silk-based ones were not.

In the case of strategy (2), typically the main procedure consists on adapting the chemical reaction method (see Section 21.3.3.1). For instance, gold NPs have been in situ synthesized and simultaneously incorporated on silk fabrics by immersion of silk substrates onto aqueous  $\text{HAuCl}_4$  solutions with different concentrations at room temperature during 30 min, to promote the adsorption of chloroaurate ions, followed by heating to  $85^\circ\text{C}$  for 60 min, silk fabric removal, rinsing with deionized water, and finally drying at room temperature [250]. Remarkably, no reducing agent was required, just heating. The authors proposed that the reduction of gold(III) to gold(0) was probably induced by tyrosine groups on silk fibers upon heating. The silk samples with low gold content were coated with gold nanospheres and presented a red color, while those with higher loading contained gold nanoplates and exhibited a brown coloration. The resulting samples presented excellent UVA and UVB protection with UPF values  $4 \times -7 \times$  higher than that of the parent silk, high antibacterial activity against *E. coli*, and improved thermal conductivity. Moreover, they presented good color fastness to washing (after the first washing cycle and upon seven washing cycles) and light irradiation. Later on, the same authors extended the strategy to the coloration of bamboo pulp fabrics with both gold and silver NPs (heating at  $80^\circ\text{C}$  for 60 min)

[251]. In the case of silver coating, an alkaline agent was required during the in situ process (NaOH; pH 10). More recently, a knitted cotton fabric was dyed with gold NPs (heating at 85 °C during 90 min, acidic conditions) [252]. In all cases, the incorporation of the noble metal NPs endowed the fabrics with multifunctional properties, namely excellent UV protection and antimicrobial properties. Moreover, in the case of the cotton fabric functionalized with gold NPs, it also acted as surface-enhanced Raman scattering (SERS) substrate for dyes analysis on the fabric, thus enhancing the Raman signals of the dyes, and presented catalytic activity in the reduction of 4-nitrophenol using  $\text{NaBH}_4$  as reducing agent.

Wool fibers have also been coated with noble metal NPs to impart coloration and multifunctionality. For instance, the group of Johnston proposed a robust in situ strategy to color merino wool fibers with gold and silver NPs of different sizes and, consequently, different colors [253,254]. In the case of gold NPs coating, it occurred through adsorption of Au(III) cations onto the wool fiber surface, followed by their reduction to Au(0) and binding to the sulfur groups from cysteine amino acids of keratin proteins from wool, preventing their leaching upon washing and rubbing [253]. The incorporation of gold endowed the fabric with stability to UV light, in contrast to organic colorants. In the case of silver NPs, their in situ synthesis in the presence of wool was achieved through reduction of Ag(I) cations to Ag(0) by trisodium citrate, followed by the chemical binding of the resulting NPs to the amino acids (nitrogen- and sulfur-containing groups) of the keratin proteins on the wool surface via the trisodium citrate which acted as linking agent [254]. The resulting multifunctional fibers presented antimicrobial activity against *S. aureus* microbes and antistatic properties (electrical conductivity:  $3.2 \times 10^{-5}$ – $4.0 \times 10^{-5}$  vs  $< 10^{-10}$  S/cm), and durability to washing (24 h) and rubbing.

Noble metal nanoclusters have also been incorporated on textile substrates to impart luminescent properties [255,256]. Zhang and coauthors reported an environmentally friendly and cost-effective in situ strategy to coat natural silk fiber and fabric with luminescent gold nanoclusters composed of tens to hundreds of Au atoms, at 80 °C, using  $\text{HAuCl}_4$  as gold precursor, in the presence of both silk and NaOH [256]. The proteins at the surface of the silk acted both as reducing agent and stabilizer of the as-synthesized luminescent gold nanoclusters. The resulting coated samples presented good optical properties, namely a relatively long wavelength fluorescence (red), high quantum yield (8%), long fluorescence lifetime (322 vs 0.3 ns for silk), high photostability, and comparable in vitro biosafety to that of the parent silk (incubation tests with A549 cancer cells and contact with animal skin—abdomen of nude mice). Additionally, they presented improved mechanical properties and UV light protection in comparison with the pristine silk (UVA light transmission: 50.0% vs 66.4%; UVB light transmission: 7.7% vs 18.8%).

Another potential application of metallic NPs is in electromagnetic shielding, namely for blocking a wide range of frequencies, from a few kHz

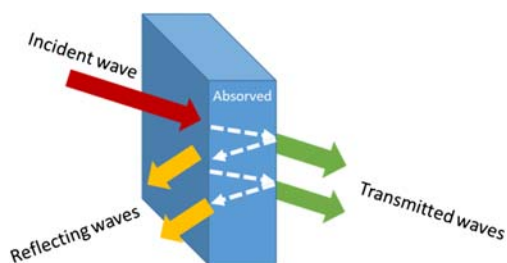


**FIGURE 21.27** Electromagnetic shielding mechanism.

for beacon to up to 110 GHz (W band) for satellite communications, astronomy, defense, and security applications. The fundamentals of electromagnetic shielding are based on the effect that occurs when an electromagnetic wave strikes a material. The material will offer a barrier toward the propagation of the electromagnetic wave, which will lead to reflection, absorption, and multiple internal reflections (Fig. 21.27). Consequently, this mechanism will depend on the wave nature and characteristics of the material [257]. The reflection generally occurs at the interfaces, arising from the difference on the impedance between air and the interacting material. This component is the main mechanism that takes place in highly conducting materials (e.g., metals, carbon materials) due to high charge carrier concentration. Another effect is absorption, that involves interaction between the electric/magnetic dipoles of the material and the incident electromagnetic radiation. Materials with high permittivity or high permeability are the most appropriate [258]. In this way, the design of tailored nanomaterials with improved properties can promote better control of the efficiency of electromagnetic shielding.

On metallic NPs, scarce studies have been performed to test this property. It can be highlighted the use of composite nanofibers of Au NPs on a charged polymer skeleton made of poly(pyridobisimidazole)-grafted-poly(dimethyl diallyl ammonium chloride) (PIPD-g-PDDA), by Li et al., which led to a shielding effectiveness of over  $-64.9$  dB in the frequency range of 250 MHz–1.5 GHz for a thickness of 20  $\mu\text{m}$  [259]. A promising result was achieved by Kardarian et al. that proposed a process based on the in situ synthesis of silver NPs at the textile fiber surface, followed by their sintering, to obtain highly conductive fabrics. A sheet resistance of 5.2  $\Omega/\text{sq}$  and a shielding effectiveness of 19.2 dB were achieved (tests performed in the frequency range of 100 kHz to 6 GHz) [260].

### 21.3.4 Transition metal oxide nanoparticles

#### 21.3.4.1 Production processes

In recent decades, interest in transition metal oxide NPs has been increasing due to their remarkable physicochemical properties and great variety of morphologies and crystalline structures. They are important building blocks

for the development of advanced technologies for chemical and biosensing, biolabeling, photonics, environmental remediation, targeted drug delivery, theragnostics, information technologies, fuel cells, electromagnetic shielding, ecofriendly catalysis, among others [218,261–263].

The unusual properties of transition metal oxides are clearly due to the unique nature of their outer *d*-electrons. For instance, they can present ferroelastic properties (e.g.,  $\text{Gd}(\text{MoO}_4)_3$ ), highly isolating behavior (e.g.,  $\text{BaTiO}_3$ ), antiferromagnetism (e.g.,  $\text{LaCrO}_3$ ), ferroelectric properties (e.g.,  $\text{BaTiO}_3$  and  $\text{KNbO}_3$ ), and photocatalytic properties (e.g.,  $\text{Cu}_2\text{O}$ ) [263–265].

Transition metal oxides can be classified as binary,  $\text{A}_x\text{O}_y$ , and ternary,  $\text{A}_x\text{B}_y\text{O}_z$ , whether they are composed of two or three distinct chemical elements, respectively, where A and B are different transition metal cations. Binary systems, such as  $\text{MnO}_2$  and  $\text{Fe}_2\text{O}_3$ , are attractive candidates for different applications, including catalysis, sustainable hydrogen production, energy storage, electronic, and magnetic devices [266,267]. On the other hand, ternary metal oxide nanostructures, such as  $\text{BaTiO}_3$  and  $\text{MnCo}_2\text{O}_4$ , present tunable chemical, structural, electronic, and optical properties due to the presence of different transition metal cations within the same structure, promoting a broader range of technological applications, namely in transistors and transducers, computing devices, energy storage, and infrared sensors [268,269].

Among the different classes of transition metal oxides, transition metal ferrite ( $\text{MFe}_2\text{O}_4$ ) NPs represent one of the most studied systems due to their natural abundance, biocompatibility (e.g.,  $\text{Fe}_3\text{O}_4$ , as well as  $\text{ZnFe}_2\text{O}_4$  and  $\text{NiFe}_2\text{O}_4$  at low concentrations), high chemical stability, high surface-to-volume ratio, and magnetic properties, combined with facile synthesis processes that enable industrial scalability [270–272].

The family of metal ferrites can be classified according to the type of structure in spinel- (e.g.,  $\text{MFe}_2\text{O}_4$ ), hexagonal- (e.g.,  $\text{MFe}_{12}\text{O}_{19}$ ) and garnet-type (e.g.,  $\text{M}_3\text{Fe}_5\text{O}_{12}$ ) [267].

Spinel-type nanoferrites, such as magnetite ( $\text{Fe}_3\text{O}_4$ ), maghemite ( $\gamma\text{-Fe}_2\text{O}_3$ ), hematite ( $\alpha\text{-Fe}_2\text{O}_3$ ), manganese(II) ferrite ( $\text{MnFe}_2\text{O}_4$ ), nickel(II) ferrite ( $\text{NiFe}_2\text{O}_4$ ), copper(II) ferrite ( $\text{CuFe}_2\text{O}_4$ ), and zinc(II) ferrite ( $\text{ZnFe}_2\text{O}_4$ ), present a vast importance arising from their versatile chemical composition and magnetic properties [267]. In particular, they can be easily separated from the reaction medium by magnetic separation and recycled/reused, being the perfect match between time (with fast separation processes) and environmental friendliness (with reduced waste disposal and energy consumption) [273,274]. The spinel structure is constituted by a compact cubic arrangement of oxygen atoms, with M(II) and Fe(III) cations occupying different crystallographic positions and presenting tetrahedral and octahedral coordination with oxygen atoms. Depending on the occupation of M(II) and Fe(III) cations between the octahedral and tetrahedral positions, spinel materials can be classified as normal spinel (e.g.,  $\text{ZnFe}_2\text{O}_4$  in the bulk state),

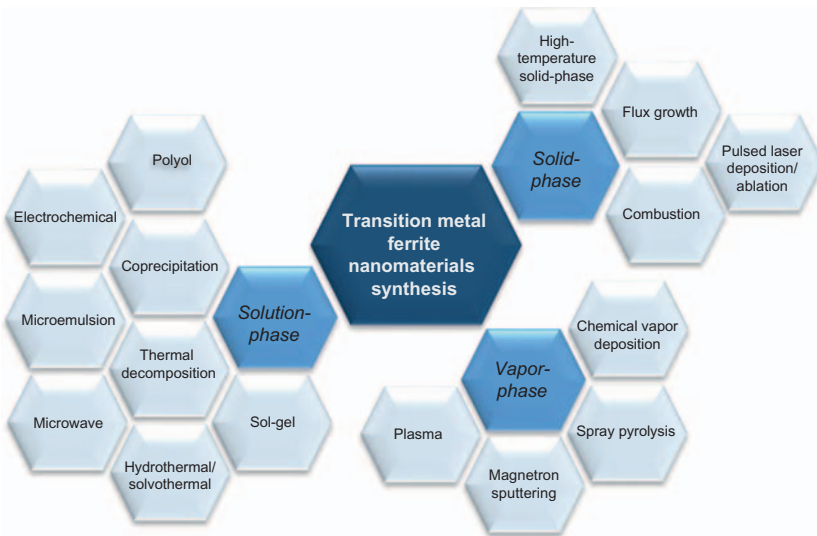


**FIGURE 21.28** Different methods for the synthesis of transition metal ferrite NPs.

inverted spinel (e.g.,  $\text{NiFe}_2\text{O}_4$ ) and partially inverse spinel (e.g.,  $\text{CuFe}_2\text{O}_4$ ) [275–277].

Transition metal ferrite NPs can be produced by several methods that can be divided into three important groups (Fig. 21.28): (1) *solid-phase methods*—high-temperature solid-phase, flux growth, solid-phase combustion, and pulsed laser deposition/ablation; (2) *solution-phase methods*—such as coprecipitation, thermal decomposition, sol–gel, hydrothermal/solvothermal method, microemulsion, microwave, electrochemical, and polyol; and (3) *vapor-phase methods*—chemical vapor deposition, spray pyrolysis, magnetron sputtering, and plasma method [275,278,279]. Solid-state methods present great potentialities for large-scale industrial applications. However, they require high-temperature annealing and typically lead to significant particle aggregation arising from uncontrolled nucleation and growth processes.

*Liquid-phase processes* revolutionized the nanotechnology world since they allow producing engineered nanomaterials with custom-made properties and controlled and uniform particle size [280]. Among the different wet-chemical methods, the most common are *coprecipitation*, *sol–gel*, *microwave-assisted method*, *reverse microemulsion*, *solvothermal method*, and *polyol method*.

The *coprecipitation method* consists of mixing aqueous solutions of  $\text{M(II)}$  and  $\text{Fe(III)}$  salts in the presence of an alkaline agent, which leads to the formation of a precipitate (Fig. 21.29) [281]. It was first proposed by Massart in 1981 [282] and, since then, it has evolved by changing the type/concentration of metal salts, pH, temperature, and the type/concentration of base

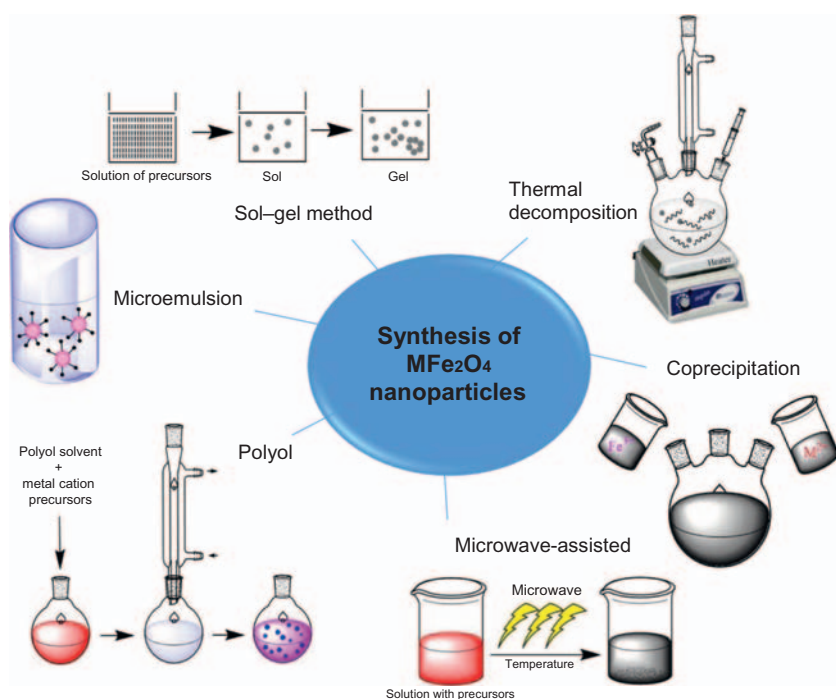


**FIGURE 21.29** Schematic representation of the different methods to synthesize  $MFe_2O_4$  NPs.

[270]. The nature of the salts includes perchlorates, chlorides, sulfates, and nitrates. Several types of alkaline agents have been used, namely  $NH_3$ ,  $NaOH$  and, more recently, alkanolamines [281]. Coprecipitation is an environmentally friendly and fast process based on the use of cost-effective reagents, aqueous solvents, and gentle reaction conditions. Moreover, it leads to high yields of nanomaterials, boosting technological transfer to industrial applications. Nevertheless, it presents some disadvantages, such as the difficult control of the particle size and shape, crystallinity, and magnetic properties [270]. These issues have been tackled by several research groups. For instance, Pereira et al. prepared superparamagnetic  $MFe_2O_4$  ( $M(II) = Mn, Fe, Co$ ) NPs with reduced particle size and improved saturation magnetization by changing the coprecipitation agent from  $NaOH$  to monoisopropanolamine and diisopropanolamine [281].

In the *sol-gel method* a metal alkoxide solution undergoes hydrolysis and condensation, leading to a nanosol, which then undergoes further condensation and polymerization into a gel (Fig. 21.29). Afterward, a thermal treatment is required in order for the metal oxide to acquire a crystalline structure [283]. The advantages of this method include a good control of the particle size, size distribution, microstructure, and chemical composition.



Moreover, it allows obtaining nanomaterials with different structures depending on the experimental conditions. The main limitations are the purity of the final product and the necessity of thermal treatment to obtain high crystallinity [284]. Several parameters influence the kinetics of the hydrolysis and condensation reactions, and consequently, the structure and properties of the final gel, such as the solvent type (normally water or ethylene glycol), temperature (for monophasic transition metal ferrites: up to 1000 °C; for solid-state synthesis: 1400 °C–1800 °C), nature and/or concentration of the salt precursors, pH, and stirring rate [270,284,285]. For instance, maghemite NPs embedded in an inert temperature-resistant silica matrix were prepared by direct heating of the gels at 400 °C [286]. The particle size could be tuned by changing the heating temperature and the iron salt concentration.

In *microwave-assisted synthesis*, the microwave radiation is absorbed by solvents with high dielectric constants (such as water) producing uniform heat in the reaction mixture, which induces a uniform nucleation (Fig. 21.29) [261]. Metal salts such as  $\text{Fe}(\text{NO}_3)_3$  and  $\text{Ba}(\text{NO}_3)_2$ , among others, have been used as metal precursors [287]. The temperature used in the synthesis needs to be tuned depending on the desired ferrite (e.g., to obtain  $\text{MnZnFe}_2\text{O}_4$  it is possible to use a temperature of  $\sim 100$  °C) [288]. This method requires lower energy and time to obtain NPs with better quality control than the processes that use conventional heating [288].

The *microemulsion method* can also be used to prepare ferrite NPs by mixing an aqueous phase containing the metal precursors with an organic phase comprising the organic solvents and stabilizing tensioactive agents (Fig. 21.29) [270,289]. The most appealing advantages of this method are the fine-tuning of the particle size, the possibility of fabricating a variety of ferrite NPs by changing the type/concentration of surfactant, cosurfactant, oil:water:surfactant ratio, etc. Additionally, it requires low temperatures and can be scaled up to an industrial level [270,290]. Nevertheless, the major disadvantages are the requirement of a large amount of organic solvents, the poor crystallinity of the resulting nanoferrites and, in some cases, higher particle polydispersion.

*Thermal decomposition* is an endothermic process based on the decomposition of organometallic precursors (such as metal acetylacetonates, metal cupferronates, metal alkoxides, metal carbonyls, and metal halides) in high-boiling point organic solvents (e.g., 1-octadecene, 1-eicosene, and *N*-methyl-2-pyrrolidone) containing stabilizing surfactants (such as fatty acids and aliphatic amines; Fig. 21.29) [270,273]. This process allows good control over size and shape, leading to a high level of particle monodispersion [270]. However, it requires high temperatures, time-consuming reactions, and toxic/expensive solvents/reagents, introducing major drawbacks toward industrial implementation and ecosustainable technological applications [273]. Verma and Pravarthana were able to prepare  $\text{CoFe}_2\text{O}_4$  and  $\text{Fe}_3\text{O}_4$  NPs at a relatively lower boiling temperature of  $\sim 200$  °C, using *N*-methyl 2-pyrrolidone as



solvent [291]. The solvent presented high stability at room temperature, low volatility, and low flammability.

The *polyol method* is another versatile chemical method used to prepare ferrite NPs. Briefly, a solution containing the polyol solvent and the metal precursors (metal complex or metal salt) is heated and stirred, leading to the formation of an intermediate, which is then reduced to form nuclei and, subsequently, the metal oxide NPs (Fig. 21.29). Smaller particles can be produced through an increase of the temperature and by seeding the reaction medium with foreign NPs (heterogeneous nucleation) [271]. The liquid polyol (e.g., ethylene glycol) plays a triple role, as solvent, reducing agent, and stabilizer of the resulting NPs, controlling the particle growth and preventing particle aggregation [270]. For example, water-dispersible superparamagnetic  $\text{Fe}_3\text{O}_4$  NPs with sizes in the range of 3–6 nm were prepared by polyol method using diethylene glycol as solvent [292].

Regardless of the synthesis process, it can be performed in the presence of a chelating agent, such as carboxylate, citric, gluconic, and oleic acid, or of a coating agent such as polymers (dextran, carboxymethylated dextran, carboxydextran, starch, arabinogalactan, glycosaminoglycan, sulfonated styrene – divinylbenzene, polyethylene glycol (PEG), polyvinyl alcohol (PVA), poloxamers, and polyoxamines) to improve the stability of the nanomaterial and prevent particle aggregation in the dispersion medium [293]. Alternatively, the chelating or coating agent can be added after the synthesis of the nanomaterial.

To obtain spinel nanoferrites with fine-tuned properties, the fabrication process is critical. In particular, for industrial applications, the preparation processes should be simple, environmentally friendly, and produce the nanomaterials in high yields. In this sense, coprecipitation has been one of the preferential processes, albeit the lower control over the particle size/size distribution. Nevertheless, the quest for low-temperature and faster processes for the design of these nanomaterials has been an ongoing challenge [284].

Hexagonal nanoferrites, also known as hexaferrites, can present different types of structures (Fig. 21.30), such as M, W, X, Y, Z, and U. Their formation involves a cumbersome process with complex mechanisms, and requires high temperatures (above 1000 °C), resulting in larger particle size [294]. This type of ferrites presents several magnetoelectric/multiferroic applications, such as for microwave shielding devices, resonators over a wide frequency range (15–110 GHz), high-density magnetic recording, tunable microwave multiferroic devices, and compact and lightweight magnetic field sensors [295].

Several methods have been reported for the synthesis of hexagonal ferrites, such as *standard ceramic techniques* (preferred for M-hexaferrites, such as those of  $\text{MFe}_{12}\text{O}_{19}$ -type), *coprecipitation* (e.g., M-type  $\text{BaFe}_{12}\text{O}_{19}$ ), *salt-melt method* (e.g.,  $\text{SrFe}_{12}\text{O}_{19}$ ), *ion-exchange* (e.g.,  $\text{K}_{0.8}\text{Ba}_{0.6}\text{Fe}_{10.5}\text{Co}_{0.25}\text{O}_{17}$ ), *sol–gel* (e.g.,  $\text{Co}_2\text{Fe}_{12}\text{O}_{19}$ ), *citrate precursor method* (e.g., Z-type  $\text{BaFe}_{12}\text{O}_{19}$ ), and

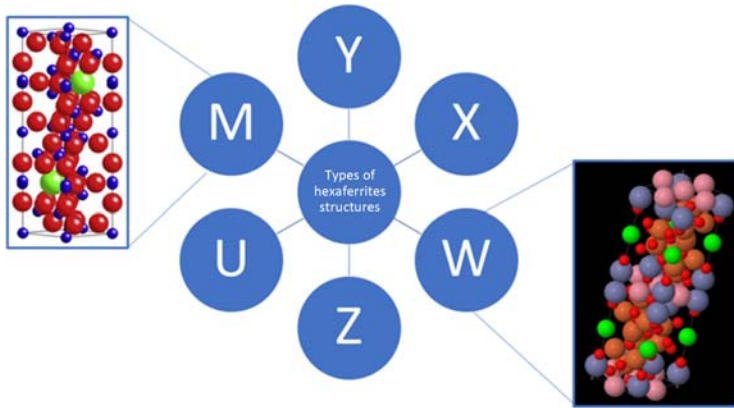


FIGURE 21.30 Types of hexaferrite structures.

*hydrothermal method* (e.g., M-type  $\text{BaFe}_{12}\text{O}_{19}$ ) [294,296,297]. They can also be synthesized by *glass crystallization* (e.g., W-type barium hexaferrite particles), *combustion* (e.g.,  $\text{PbFe}_{12}\text{O}_{19}$ ), *self-propagating high-temperature synthesis*, *spray drying*, and *microemulsion* (e.g., M-type  $\text{BaFe}_{12}\text{O}_{19}$ ) [294,298]. All of these methods can be applied in different areas, such as density magnetic recording applications, 3G and 4G communications, and multilayer chip inductors [299].

In industry, the most common hexagonal ferrites are those of M-type produced through the *standard ceramic method*. This method is a simple solid-state process based on the direct reaction between metal oxides and carbonate precursor powders at high temperatures (in the range of  $500\text{ }^{\circ}\text{C}$ – $2000\text{ }^{\circ}\text{C}$ ) [300]. However, in order to obtain high yields of nanomaterials, it requires high-energy consumption and great availability of raw materials; nevertheless, this process requires low reaction times ( $\sim 3\text{ h}$  depending on the reaction) [300].

Regardless of the type of transition metal oxide nanomaterial, in terms of scalability for industrial applications, in general the most suitable processes for their production are coprecipitation, sol–gel, reverse microemulsion, thermal decomposition, solvothermal method, microwave-assisted, and flow synthesis [261].

In order to stabilize transition metal oxide NPs within a liquid medium and thus obtain stable colloidal dispersions, for instance to produce inks, they can be functionalized with suitable organic molecules or coated with polymers or inorganic layers. The encapsulating layers also protect the NPs against degradation. In the case of functionalization/stabilization with organic molecules (capping agents), this includes carboxylates (e.g., citric acid, gluconic acid, oleic acid, and lauric acid), alkanesulfonic and alkane-phosphonic acids (e.g., dodecylphosphonic and hexadecylphosphonic acid),

alkyl phosphates (e.g., dihexadecyl phosphate), and alkylamines (e.g., oleylamine) [284,293]. In the case of coating strategies, inorganic layers include silica, carbon, and gold, while the organic layers are natural or synthetic polymers, such as dextran, chitosan, alginate, and polyethylene glycol [270,284,293].

Finally, for practical applications, the surface of transition metal oxide NPs often needs to be functionalized with suitable bifunctional tethering agents to ensure the robust bonding to the target substrate and prevent particle leaching. The selection of the tethering agent often relies on organosilanes, namely those containing amine, carboxylic acids and thiol groups, and phosphonates [270,293].

#### 21.3.4.2 *Applications of metal oxide nanoparticles on textiles*

Metal/metal oxide NPs have been incorporated on textiles to impart radiation protection properties. For instance, in the medical field, health professionals and patients are daily exposed to ionizing radiations, such as X-rays, through diagnostic examinations and therapeutic procedures. Prolonged or accumulated dosage of high-energy electromagnetic radiation is hazardous, resulting in serious long-term health problems (e.g., carcinogenesis, cell mutations) [301,302]. Traditionally, heavy metal elements, such as Pb, W, Bi, PbO, Pb<sub>3</sub>O<sub>4</sub>, or composites of these materials, have been used in protective clothing against direct or scattered X-rays [302,303]. Among these metals, lead is the most widely and effective material used as radiation shield due to its high mass density, atomic number and availability. However, conventional Pb-based personal protective clothing (e.g., aprons, gloves, gonadal shields, and thyroid collars) are heavy and uncomfortable for prolonged interventional radiology procedures. In addition, lead is extremely toxic, making its manufacture and disposal restricted or, in some cases, prohibited. Consequently, significant research efforts have been focused on the design of lightweight, cost-effective, flexible, and durable Pb-free shielding coatings for protective X-rays garments. In this regard, Pb-free composite shielding systems consisting of metals (e.g., W, Bi, Sn, Cu, Sb) [304–307], their oxides (e.g., Bi<sub>2</sub>O<sub>3</sub>, BaTiO<sub>3</sub>, CuO) [304,308–312], or salts (e.g., BaSO<sub>4</sub>) [305,308–310,313] with similar absorbing or blocking X-ray properties to those of Pb embedded in polymeric matrices (e.g., poly(vinyl chloride) [311,313,314] and methyl vinyl silicone rubber [304,305,307]) have been developed. According to the personal protection standards, a protective clothing and/or equipment against X-rays for medical applications should have an attenuation equal or higher than 90%, which means a protective equivalent of no less than 0.25 mm lead for X-rays with energy up to 100 kV [315].

Cotton [305,307], polyester [309,311], nylon [311,314], and cellulose fibers (viscose) [308,316] with X-ray shielding properties have been produced through coating [305,307,309,311,314], Lyocell [308], and wet

spinning [316] processes. For instance, Aral et al. reported the fabrication of flexible Pb-free X-ray shielding woven cotton fabrics through their coating with a blend of metal powder (W, Bi, Sn, and Cu) and silicone rubber (SR) in different ratios using a knife over roll coater [307]. The sample based on W-Sn (60 wt.% of W and 10 wt.% of Sn) reached higher attenuation levels than those based on W-Cu (60 wt.% of W and 10 wt.% of Cu) or with only W (60 wt.%), for similar coating thicknesses, meaning that the addition of 10 wt.% of metal powder (Sn or Cu) in the coating blend resulted in better radiation attenuation performance. Moreover, the increase of W content from 60 wt.% to 81 wt.% resulted in higher X-ray shielding performance for the same coating thickness, while the lower silicone rubber amount in the coating led to thinner and lighter fabrics with equal protection level. For instance, in order to obtain 90% protection level, a coating with 1.73 mm thickness was needed for the blend with 60 wt.% of W, whereas for the coating containing 81% of W, a thickness of only 0.69 mm could be estimated for the same level of X-ray shielding. In addition, the coated fabrics showed good resistance to repetitive folding, although the increase of W amount in the coating resulted in stiffer fabrics.

Currently lead-free aprons for medical and military protection X-ray are already commercially available, provided by XENOLITE, Rothband, Infab Corporation, Radiation Shield Technologies, among other (Fig. 21.31).

Nanosized materials are attractive for radiological protection applications especially on the design of lightweight and Pb-free clothing [317,318]. The size effects (nanoparticles vs microparticles) on X-ray attenuation properties of CuO embedded in bee wax were reported by Botelho et al. [317]. The

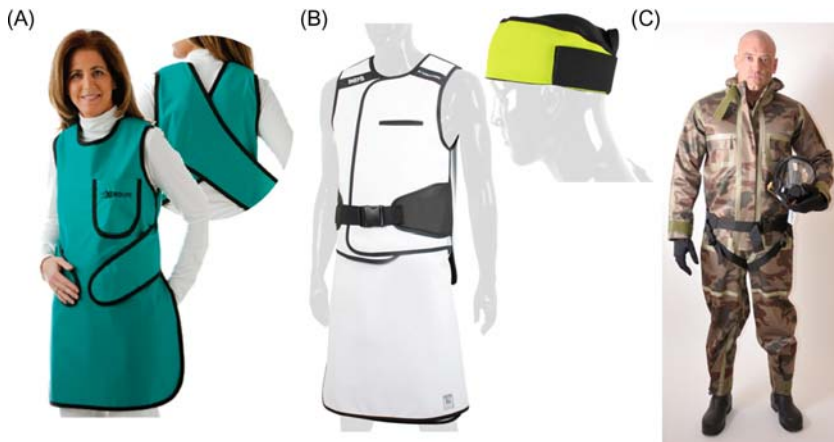


**FIGURE 21.31** Lead-free garments for medical and military personal X-ray protection: (A) Apron from XENOLITE (<https://www.xenoliteXray.com>); (B) Lumbar vest and skirt, and thinking cap from Infab Corporation (<https://www.infabcorp.com>); (C) Demron full body suit from Radiation Shield Technologies (<https://www.radshield.com>).

CuO NPs ( $\sim 13.4$  nm) showed enhanced attenuation characteristics at low X-ray energies (26 kV and 30 kV) when compared to microparticles ( $\sim 56$   $\mu\text{m}$ ). Recently, a composite consisting of Bi NPs (5 nm; produced using bismuth(III) nitrate, cellulose nanofibers, and  $\text{NaBH}_4$ ) dispersed in polydimethylsiloxane was reported by Li et al. [319]. For comparison, the authors also prepared a polymer composite film containing bismuth microparticles (5  $\mu\text{m}$ ). The attenuation ratio of the composite film containing 8.0 wt.% of Bi NPs reached 96.6% at 60 kV, when compared with the polydimethylsiloxane film with similar thickness (5 mm). Moreover, a  $4 \times$  reduction of the total mass of Bi (equal to 2.0 wt.%) was observed for the composite containing Bi NPs relative to the composite film incorporating Bi microparticles.

Carbon-based polymeric composites (e.g., based on single-wall carbon nanotubes, multiwall carbon nanotubes, graphene oxide, highly oriented pyrolytic graphite, and fullerenes) [302,320–322] have shown interesting X-ray shielding properties. For instance, a polyvinylidene fluoride/graphene oxide nanocomposite film with 0.1 mm thickness and containing 1.88 wt.% of graphene oxide attenuated 82.9% and 48.5% of X-ray beams with energies of 6.9 and 8.1 keV, respectively [322]. Nevertheless, research still needs to be extended not only to other nanomaterials with high atomic number, but also to those that confer protection at higher X-ray energies and within a broader X-ray energy range (e.g., the diagnostic X-rays range from 40 to 150 kV) [303], in order to understand and explore the singular properties offered by nanomaterials. Moreover, the rational design of composites containing precisely tuned combinations of metal/metal oxides, carbon-based nanomaterials, and other components is still lacking.

On electromagnetic shielding, iron oxides ( $\text{Fe}_x\text{O}_y$ ) and transition metal ferrites (hexagonal or spinel-like) have been used as absorbers of radiofrequency (RF) and microwave radiation due to their high magnetic permeability. For instance, recently, superparamagnetic magnetite NPs were in situ fabricated on flexible polyester fabric and using poly(3,4-ethylenedioxythiophene) (PEDOT) [323]. The authors achieved an electrical resistivity lower than  $1000 \Omega \cdot \text{cm}$ , leading to a shielding effectiveness of up to 13–17 dB by reflection.

### 21.3.5 Functional carbon-based nanomaterials

#### 21.3.5.1 Functionalization

Carbon nanomaterials are commonly chosen for scientific and technological applications due to the wide variety of physicochemical properties that can be imparted through their functionalization or doping [324]. There is great interest in carbon nanotubes (CNTs) and graphene. CNTs, either single-walled (a single sheet of graphene rolled over itself) or multiwalled (several

sheets of graphene rolled over themselves), exhibit a unique 1D hollow tubular structure, high aspect ratio (length/diameter), low density, large specific surface area, high electrical conductivity, and excellent thermal and chemical stabilities [324]. Graphene, on the other hand, is a single atom-thick sheet with a hexagonal arrangement of  $sp^2$ -bonded carbon atoms. Monolayer is the purest form identified but graphene has the particularity of exhibiting different properties with the increase of the number of layers [325]. It is not only the thinnest and strongest material of all materials that are known but is also considered harder than diamond. Moreover, the combination of properties such as high strength, flexibility, and easy chemical modification makes it one of the most explored and studied materials in the world [326,327].

For industrial applications, similarly to other classes of nanomaterials, the limitation when selecting the type of carbon nanomaterial can be its high cost, especially when high quality is required. The progressive reduction on the production costs of CNTs makes them highly appealing for several technological applications, namely sensors, capacitors, membranes, electrodes, catalysts, and translators [328].

Different strategies have been developed to functionalize carbon nanomaterials surface in order to fine-tune their intrinsic characteristics, including surface oxidation, grafting of organic groups or macromolecules, polymer wrapping, alkali activation, sulfonation, and halogenation (Fig. 21.32) [330–333].

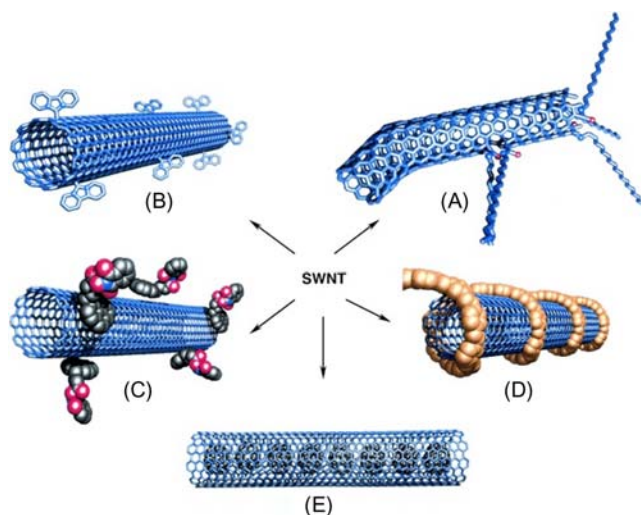


**FIGURE 21.32** Different methods to functionalize carbon materials (exemplified for SWCNTs): (A) defect-group functionalization; (B) covalent sidewall functionalization; (C) non-covalent exohedral functionalization with surfactants; (D) noncovalent exohedral functionalization with polymers; (E) endohedral functionalization. *Reproduced from Hirsch A. Functionalization of single-walled carbon nanotubes. Angew Chem Int Ed* 2002;41:1853–9 [329] with permission from John Wiley & Sons.

*Surface oxidation* is a controlled process to introduce oxygen-containing groups on the surface of carbon nanomaterials, such as ketone, phenol, lactone, carboxyl, and ether groups [331]. These oxygen-containing functionalities can confer hydrophilicity to the nanomaterial or act as anchorage sites for chemical grafting of organic or inorganic species by covalent, noncovalent, or electrostatic interactions. More recently, this strategy has been used to tailor the electrochemical performance of CNTs for sensing, electrocatalysis, and energy applications, since oxygen-containing groups can lower the activation energy and facilitate electronic transfer on the surface. Nevertheless, careful control of the type and amount of oxygen-based functionalities needs to be carried out since excessive oxidation may cause deleterious effects to the carbon nanomaterial structure and result in the deterioration of carrier mobility, electrical/thermal conductivity, and mechanical properties [331].

Oxidative treatments can be performed by different routes in order to introduce different types of functional groups on the carbon nanomaterial surface: (1) in the liquid phase using strong acids (e.g.,  $\text{HNO}_3$ ) or nonacidic oxidants (e.g.,  $\text{H}_2\text{O}_2$ ) to incorporate acidic oxygen-based groups; (2) in the gas phase, namely with  $\text{O}_2$  and  $\text{O}_3$ , to introduce neutral and basic groups, or with  $\text{NH}_3$  to impart basic oxygen-containing groups [334]. Moreover, the amount of oxygen-containing groups can be tuned by controlling the oxidizing conditions, namely the temperature, acid concentration, reaction time, and sonication/heating conditions [331,335]. This type of treatment is useful for the removal of amorphous carbon and impurities with metallic properties [334]. The most widely used oxidants for this process have been nitric acid and sulfuric acid (either concentrated or diluted) [336]. Alternatively, mixtures of  $\text{H}_2\text{SO}_4\text{--HNO}_3$  and  $\text{H}_2\text{SO}_4\text{--H}_2\text{O}_2$  can be used, with a stronger oxidizing effect. Nonacidic oxidants, such as  $\text{H}_2\text{O}_2$  or  $\text{KMnO}_4$ , have also been used for the oxidation of CNTs, but the degree of functionalization has been limited. In the case of graphene, the chemical oxidation of graphite with strong oxidant agents (e.g.,  $\text{HNO}_3$  or  $\text{KMnO}_4$ ) by the Hummers method [337] has rapidly evolved into a representative chemical modification method. This process yields graphite oxide, which can then be converted into graphene oxide by exfoliation [335].

*Grafting of organic groups or macromolecules* is a postgrafting method used to modify the surface of carbon nanomaterials when they already present surface functionalities, that can be further substituted by organic groups [331]. An example of this process is the reaction of thionyl chloride with carbon nanomaterial containing surface carboxylic groups to form acyl chloride groups.

*Polymer wrapping* consists of the noncovalent modification of carbon nanomaterials with polymers, such as polystyrene sulfonate, chitosan, among others. This strategy allows preserving the intrinsic backbone of the carbon nanomaterial without compromising its electronic structure [338]. Moreover,



it is considered a promising solution to overcome the problem of carbon nanomaterial dispersion in liquid medium and its strong tendency to aggregate.

Conventional *ball milling* (mechanochemical synthesis) is a traditional powder-processing technique, which is normally used for reducing particle size and for mixing different materials [339]. It presents a special interest for industrial applications due to its versatility, low cost, and ecofriendliness [333]. This process is considered as a promising method to tailor carbon nanomaterials structure. For instance, in the case of CNTs, it allows adjusting their length, opening the closed ends, and increasing their specific surface area [340]. In the case of graphene, it can be used both for its fabrication and chemical functionalization/doping [341]. In most ball milling apparatus, there are two possible routes responsible for the exfoliation and fragmentation effects: (1) through the shear force, which is considered an excellent mechanical route for exfoliation; and (2) through the collisions executed by the balls during the rolling process, which cause fragmentation effects. In the case of graphene, in order to obtain high-quality large-size flakes, the second effect should be minimized since it can lead to fragmentation of large flakes or even cause the destruction of its structure [342].

*Alkali activation* is a method used to tailor the textural properties of carbon materials, namely the surface area and pore volume, via heating (between 600 °C and 800 °C under a nitrogen flow) with alkali or CO<sub>2</sub> [331].

*Halogenation* consists of the modification of the carbon nanomaterial surface with halogens (e.g., fluorine, chlorine, bromine, iodine, and astatine) accompanied by a significant variation of its physicochemical properties [335]. The most common halogen used is fluorine, namely to produce hydrophobic surfaces, and the treatment can be performed at different temperatures, ranging from room temperature to 350 °C [331,335]. Halogenation with bromine is performed through direct treatment with bromine at high temperatures (e.g., 200 °C) over Lewis acid catalysts, and can generate grafting groups on the carbon nanomaterial surface for nucleophilic substitution with alcohols, amines, anilines, and thiols [331].

*Physical adsorption, electrostatic and noncovalent interactions* (including  $\pi$ - $\pi$ , van der Waals, hydrogen bonding, and hydrophobic-hydrophilic interactions) are alternative methods for the functionalization of carbon nanomaterial surface [332]. Regardless of the type of functionalization process, it can be performed by two main strategies: (1) *direct synthesis*—functionalization during the synthesis of the nanomaterial; (2) *posttreatment*—modification of the nanomaterial after its synthesis [333].

### 21.3.5.2 Heteroatom doping

Besides the functionalization of carbon nanomaterials surface, recently, there has been an increasing interest in tailoring their whole structure to endow



new or improved electromagnetic, physicochemical, optical, and structural properties through a process named *heteroatom doping*. *Heteroatom doping* is a process where carbon atoms in the graphitic structure are replaced by other atoms with similar atomic size and higher or lower electronegativity than carbon [343].

This process can be classified as *n*-doping or *p*-doping depending on the charge carriers: (1) *n*-doping in carbon materials consists of the substitution of carbon atoms by electron-rich atoms, such as nitrogen and oxygen; (2) *p*-doping is based on the replacement of carbon atoms by an electron-deficient nature atom, such as boron, where the atom can catch an additional outer electron leaving a hole in the valence band in the other atom [344].

Among the different heteroatoms, nitrogen and boron atoms have been the most frequently used to tailor carbon nanomaterials properties, namely of graphene and CNTs [345]. In the specific case of CNTs, in situ doping can lead to different types of structures depending on the type of heteroatom: in situ boron doping may cause an increase of the overall length, preventing tube closure for the zigzag geometry, and resulting in a knee-like structure; in situ sulfur doping originates a branch-type structure characterized by the presence of ramifications; in situ nitrogen doping normally originates shorter tubes with smaller diameter, leading to corrugated or bamboo-like structures (Fig. 21.33) [333]. Phosphorus and fluorine are other types of doping atoms but have been relatively less investigated.

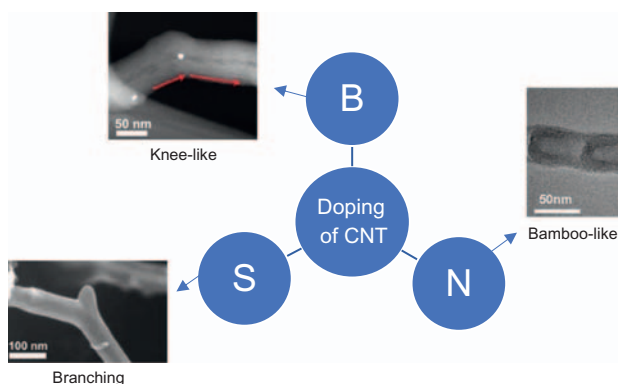


**FIGURE 21.33** Types of atoms used during the in situ doping of CNTs and resulting structures. TEM images adapted from Ozhukil Kollath V, Arjmand M, Egberts P, Sundararaj U, Karan K. Quantitative analysis of nanoscale electrical properties of CNT/PVDF nanocomposites by current sensing AFM. *RSC Adv* 2017;7:32564–73 [346]; Elías AL, Perea-López N, Rajukumar LP, McCreary A, López-Urías F, Terrones H, et al. Three-dimensional nanotube networks and a new horizon of applications. In: Schulz MJ, Shanov V, (John) Yin Z, editors. *Nanotub. Superfiber Mater.* 1st ed. Waltham: Elsevier Inc.; 2014. p. 457–93 [347]; Hashim DP, Narayanan NT, Romo-Herrera JM, Cullen DA, Hahn MG, Lezzi P, et al. Covalently bonded three-dimensional carbon nanotube solids via boron induced nanojunctions. *Sci Rep* 2012;2:363–71 [348] with permission from RSC, Elsevier and Springer Nature, respectively.

More recently, the codoping of carbon nanomaterials with two or more distinct heteroatoms, namely N/P, B/N, and B/P, emerged as a promising strategy to fine-tune their (electro)chemical properties due to the synergistic effect between the different functionalities [349].

In all cases, the selection of the type and amount of doping agent and the thermal treatment conditions are crucial parameters that should be carefully controlled in order to prevent structural deterioration, namely the number of defects on the surface of the carbon material, and introduce the desired type of functional groups [350]. Several methods have been developed to dope carbon nanomaterials, namely *chemical vapor deposition*, *plasma treatment*, *arc discharge*, *solvothermal method*, *pyrolysis*, and *ball milling*. Similarly to the functionalization strategies, heteroatoms can be incorporated in the graphitic lattice either during the material fabrication (in situ routes) or afterward by postsynthetic treatments [349,350]. For instance, in the case of nitrogen doping by the in situ route, a nitrogen-rich carbon precursor (e.g., melamine, polyaniline, cyanamide, polyacrylonitrile, biomass, metal-organic frameworks, and organic polymers) is carbonized [349–351], followed by steam activation. On the other hand, in the postsynthetic route, the nitrogen doping can be performed by impregnation of undoped porous carbon nanomaterials with nitrogen-containing compounds (e.g., urea, amines) followed by thermal treatment and plasma treatment, among others [349,350].

Figs. 21.34 and 21.35 summarize the advantages and disadvantages of the different methods for heteroatom doping of graphene and CNTs, respectively.

Concerning the best process for N-doping, in general the thermal and hydrothermal methods lead to a relatively high N content (in the range of 2.12–8.15 at%) in graphene or CNTs and to a high concentration of graphitic nitrogen (in the range of 8.6–22.6 at%) [333]. In the case of B-doping, the CVD method can incorporate a higher B amount than the thermal and hydrothermal method processes (0.5–19 at% vs 0.82–3.26 at%) [333].

### 21.3.5.3 Hybrid carbon-metal/metal oxide nanomaterials

The combination of carbon nanomaterials and NPs has led to the generation of novel multifunctional hybrid systems. The conjugation of distinct building blocks with complementary physicochemical characteristics in a unique material creates new functionalities on the resulting hybrid with synergistic properties [273]. In particular, transition metal oxide and ferrite NPs have been increasingly used for the design of advanced hybrid carbon nanomaterials, namely  $\text{RuO}_x$ ,  $\text{NiO}_x$ ,  $\text{CoO}_x$ ,  $\text{FeO}_x$ ,  $\text{MnO}_x$ , and spinel-type  $\text{MFe}_2\text{O}_4$  (where M = 2d transition metal cation, such as Fe, Mn, Co, Ni, Cu). These carbon– $\text{MFe}_2\text{O}_4$  and carbon– $\text{MO}_x$  hybrids present great potentialities for a wide range of applications, including energy harvesting and storage (working as electrode materials in supercapacitors and batteries), electromagnetic

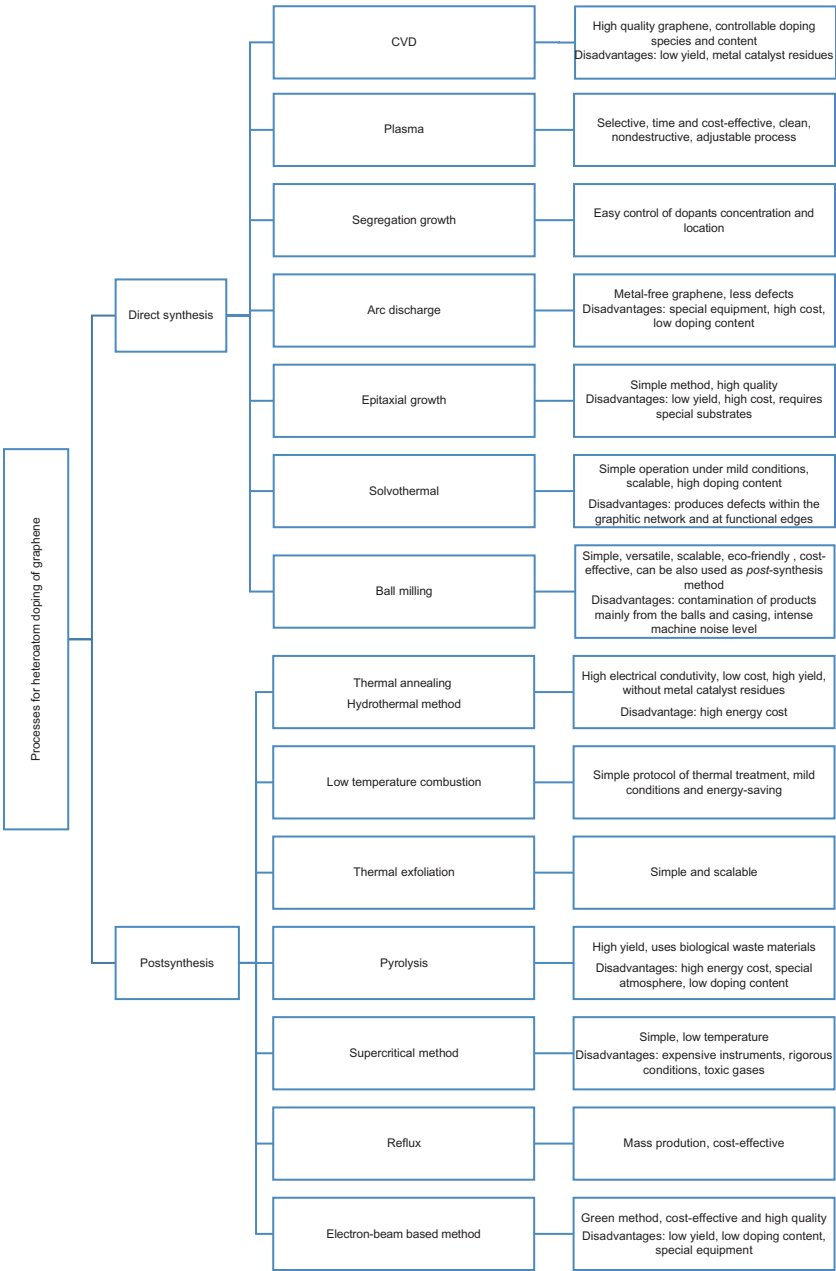


**FIGURE 21.34** Advantages and disadvantages of the different methods for heteroatom doping of graphene [333].

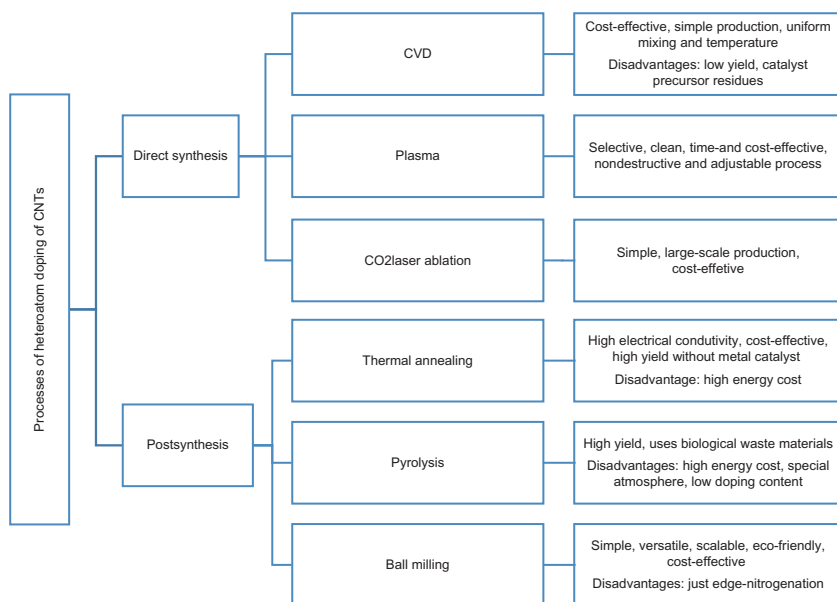


**FIGURE 21.35** Advantages and disadvantages of the different methods for heteroatom doping of CNTs [333].

shielding, electronics, functional and smart textiles, ecosustainable catalysis, wastewater treatment, among others, due to the new or synergistically enhanced properties arising from the combination of the intrinsic features of the carbon matrix (electrical conductivity, large surface area, high thermal and chemical stability, and high adsorption capacity) and those of the metal oxide/ferrite NPs (rich chemical composition, redox properties, magnetic properties, electronic structure, optical properties, etc.) [273,352–355].

The preparation of carbon-metal oxide/ferrite nanohybrids can be achieved by *in situ* strategies or by *postgrafting* of presynthesized NPs. The former consists of the synthesis of the metal oxide/ferrite NPs in the presence of the carbon support, with simultaneous grafting to its surface, while the latter is based on the attachment of preformed metal oxide/ferrite NPs to the carbon nanomaterial via linking agents through covalent grafting, noncovalent or electrostatic interactions [356–358]. Fig. 21.36 summarizes the different types of strategies for the hybridization (in situ and ex situ) of carbon nanomaterials with different building blocks (e.g., polymers, metal oxide/ferrite NPs).

In general, *in situ* strategies present more advantages than the postsynthesis methods: they can provide a stronger contact between the NPs and the carbon nanomaterial, guaranteeing a better control over the amount of grafted NPs and their distribution along the carbon support. Moreover, the physicochemical properties of the hybrids can be fine-tuned for each target

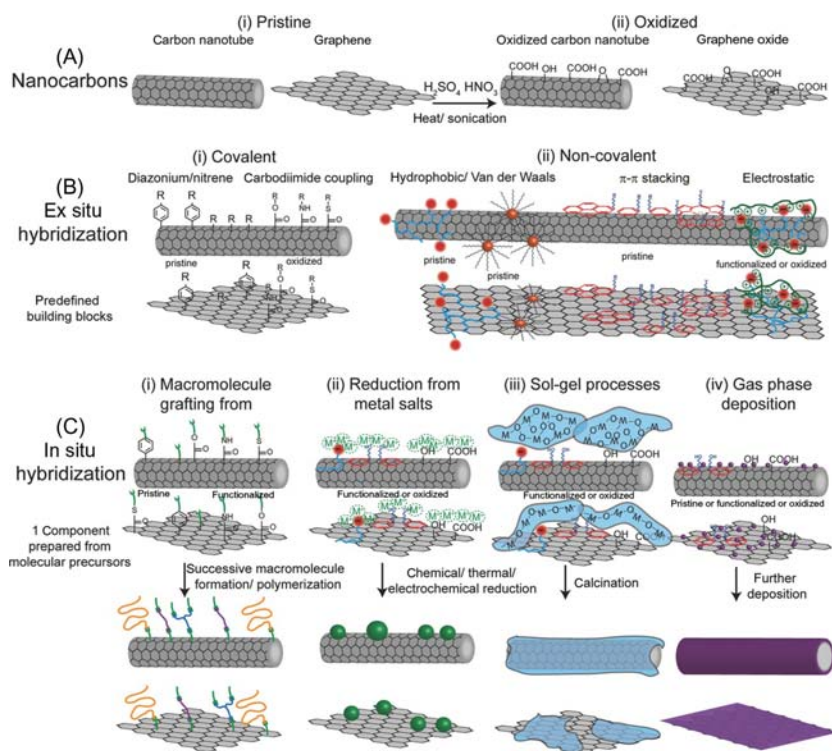


**FIGURE 21.36** Strategies for hybridization of carbon nanomaterials: (A) Nature of the carbon nanomaterial - (i) pristine and (ii) oxidized; (B) Ex situ postgrafting hybridization of pristine and oxidized nanocarbon based on (i) covalent bonding or (ii) noncovalent interactions; (C) In situ synthesis of the hybrid nanomaterial by (i) grafting from molecular precursors with subsequent macromolecule formation and/or polymerization, (ii) chemical reduction from metal salts (for metal/metal oxide NPs immobilization), (iii) sol-gel process (for semiconducting thin films or NPs); and (iv) gas-phase deposition (for thin metallic or semiconducting films). *Reproduced from Shearer C.J, Cherevan A, Eder D. Application and future challenges of functional nanocarbon hybrids. Adv Mater 2014;26:2295–2318 [358] with permission from John Wiley & Sons.*

application [357]. Among the in situ strategies, several methods have been developed and improved, namely *incipient wetness impregnation*, *deposition precipitation*, *hydrothermal/solvothermal method*, *polyol*, and *thermal decomposition*. The latter is considered the most efficient method for the selective nucleation and growth of the metal oxide/ferrite NPs, leading to a more uniform distribution throughout the support surface [273]. Nevertheless, this process often requires hazardous/toxic solvents/reagents and high reaction temperatures, which are still major limitations for industrial and ecofriendly applications.

Wang and Dai developed a new two-step route for the fabrication of strongly coupled inorganic/nanocarbon hybrid materials under milder conditions for the immobilization of metal oxide, hydroxide, or sulfide NPs on

CNTs and graphene bearing oxygen or nitrogen-containing functional groups. The process involved the *selective hydrolysis* of metal salt precursors on the carbon nanomaterial in solution under mild conditions, followed by *hydrothermal/solvothermal method treatment* or *gas-phase annealing* [356].

*Coprecipitation* has also been reported as an alternative strategy due to the use of cost-effective reagents, aqueous solvents, mild reaction conditions, and possibility of obtaining nanomaterials in high yields [273]. However, this method often leads to nanoparticle aggregation, uneven distribution throughout the support, and free NP growth in the reaction medium. Very recently, our group proposed a new ecosustainable and less time-consuming one-pot in situ coprecipitation route (Fig. 21.37) for the covalent immobilization of superparamagnetic  $\text{MFe}_2\text{O}_4$  NPs ( $\text{M(II)} = \text{Mn, Fe, Co}$ ) with sizes of 3.2–5.4 nm on the surface of bamboo-like nitrogen-doped CNTs, that overcame the limitations of conventional coprecipitation [273]. The use of CNTs bearing nitrogen-containing functionalities as supporting matrix combined with an alkaline coprecipitation agent with chelating properties (monoisopropanolamine) toward transition metal cations, under aqueous conditions and low temperatures, allowed the precise control of particle nucleation and growth rates, and lead to the selective formation and simultaneous grafting of the NPs to the carbon surface. Moreover, the process prevented particle aggregation and formation of free NPs in the reaction medium. Finally, no thermal annealing or hydrothermal method treatment was needed to impart crystallinity to the grafted ferrite NPs.

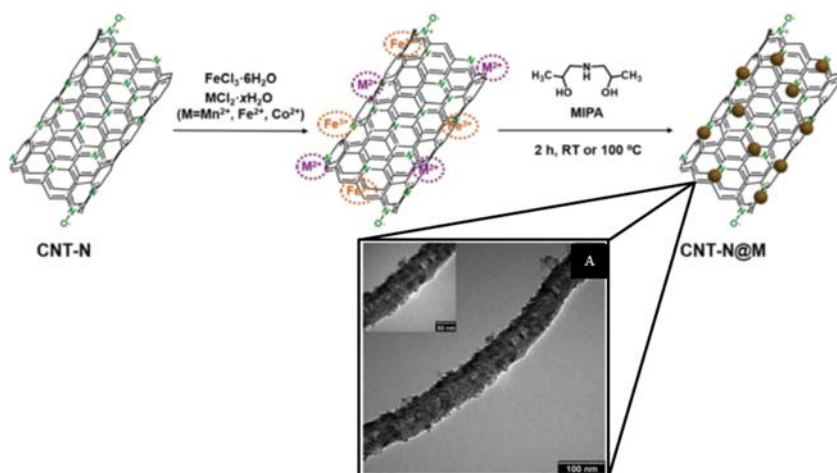


**FIGURE 21.37** Mechanism of one-pot in situ coprecipitation method for the fabrication of hybrid N-doped CNT/ferrite magnetic nanomaterial (CNT–N@M) and TEM micrographs of the resulting hybrid. Adapted from Pereira C, Costa RS, Lopes L, Bachiller-Baeza B, Rodríguez-Ramos I, Guerrero-Ruiz A, et al. Multifunctional mixed valence N-doped CNT@MFe<sub>2</sub>O<sub>4</sub> hybrid nanomaterials: from engineered one-pot coprecipitation to application in energy storage paper supercapacitors. *Nanoscale* 2018;10:12820–40 [273] with permission from RSC.

Hence, the development of ecofriendly and cost-effective routes that allow the precise control of the size and distribution of grafted metal/metal oxide NPs throughout carbon materials surface, while at the same time ensuring the robust chemical bonding and preventing free particle growth continues to be a challenging milestone [273].

#### 21.3.5.4 *Applications of carbon-based nanomaterials on textiles*

Natural fabrics exhibit low thermal and electrical conductivity and reduced resilience/tenacity, which limits their applicability [5,359]. Carbon-based nanomaterials present an excellent synergy between physical and chemical properties, such as lightness, large surface area, high adsorption ability, high thermal and electrical conductivity, and high tensile strength. In this sense, their incorporation on textiles plays an important role in tuning the fabric properties, increasing the scope of potential industrial applications [360]. The advantageous properties of carbon-based nanomaterials have been widely investigated in several areas of textile engineering, to impart desired functionalities into fabrics, such as high mechanical resilience [1], water/oil repellency [361,362], antistatic properties [5,363], fire retardancy [364–367], electromagnetic shielding [368,369], and antimicrobial properties [370–372].

Hydrophobicity is essential in the textile industry for the fabrication of waterproof, self-cleaning, and stain-resistance fabrics [1,2,197]. For instance, Liu et al. reported the functionalization of cotton substrates with multiwalled carbon nanotubes (MWCNTs) to impart superhydrophobicity [366]. The authors showed that hydrophilic cotton fabrics, after the deposition of both pristine MWCNTs and poly-butylacrylate modified MWCNTs via dip-dry-cure finishing method, exhibited a superhydrophobic effect, with water contact angles higher than 150 degrees (Fig. 21.38A). Both types of MWCNTs could lead to the artificial formation of a lotus-like leaf into the textile surface at the nanoscale level.

Carbon nanomaterials can also be combined with clay particles [374] or with hydrate aluminum silicate NPs (flakes) [375], polymers [365], and metal oxides [367] to fabricate flame-retardant or UV-light protective fabrics. For instance, Kim and Davis developed a flame-retardant coating for polyurethane foam (PUF), which is usually used on upholstery textiles, based on MWCNTs functionalized with polyethylenimine (MWCNT–PEI) through direct amination [365]. The authors coated the surface of PUF through an LbL assembly, with trilayers composed of polyacrylic acid, MWCNT–PEI and polyethyleneimine (PAA/MWCNT–PEI/PEI) containing 51 wt.% of MWCNTs. The flammability of PUF was reduced by 35% with four coating trilayers.

Yazhini et al. developed a flame-retardant fabric based on polypyrrole-zinc oxide-singlewalled carbon nanotube (ppy/ZnO/SWCNT) composite. The composite was prepared by sol–gel method and then coated on cotton fabric



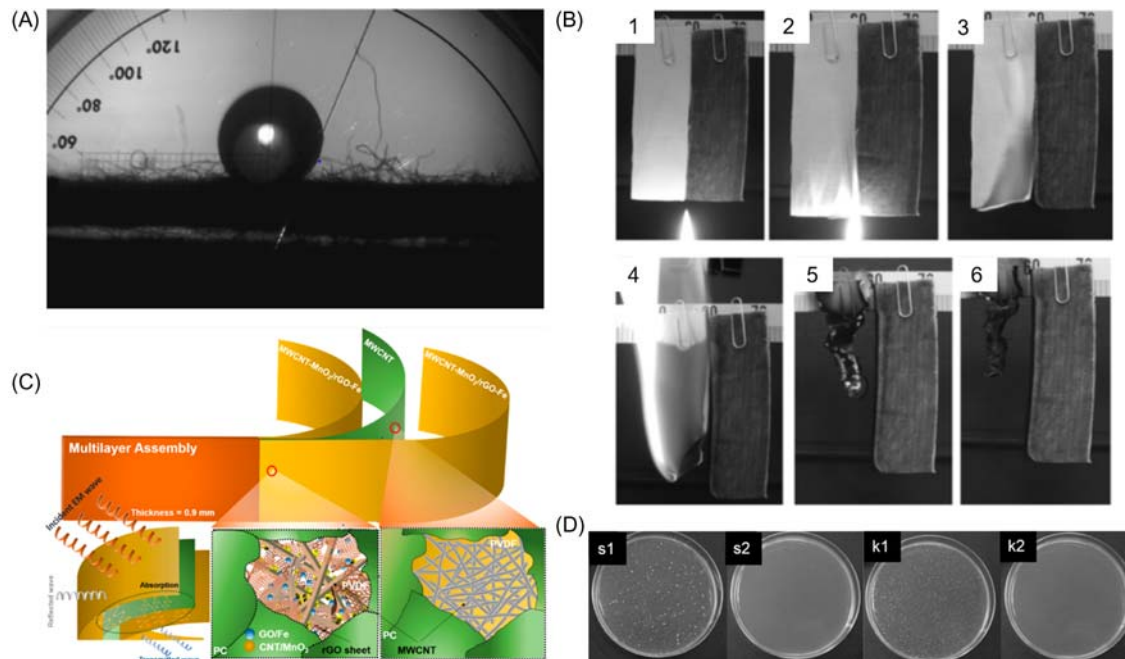


**FIGURE 21.38** Carbon-based nanomaterials applied on fabrics: (A) Hydrophobic textiles based on CNTs. (B) Flame retardancy tests on pristine cotton fabric (left) and cotton coated with CNTs–PBA (right) during six different periods (1–6). (C) Schematic representation of the electromagnetic shielding mechanism of a multilayer structure composed of two outer layers of PVDF containing MnO<sub>2</sub> doped MWCNT and Fe<sub>3</sub>O<sub>4</sub> doped graphene oxide, and an intermediate layer of polycarbonate/PVDF and MWCNTs. (D) Antibacterial tests on textiles coated with carbon films using two different cultures (*Staphylococcus aureus* (s) and *Klebsiella pneumoniae* (k)) before (s1 and k1) and after (s2 and k2) an incubation period of 18 h. (A) Reproduced from Liu Y, Wang X, Qi K, Xin JH. Functionalization of cotton with carbon nanotubes. *J Mater Chem* 2008;18:3454–60 [366] with permission from RSC. (B) Adapted from Liu Y, Wang X, Qi K, Xin JH. Functionalization of cotton with carbon nanotubes. *J Mater Chem* 2008;18:3454–60 [366] with permission from RSC. (C) Reproduced from Biswas S, Arief I, Panja SS, Bose S. Absorption-dominated electromagnetic wave suppressor derived from ferrite-doped cross-linked graphene framework and conducting carbon. *ACS Appl Mater Interfaces* 2017;9:3030–39 [373] with permission from ACS. (D) Adapted from Kitahara N, Sato T, Isogawa H, Ohgoe Y, Masuko S, Shizuku F, et al. Antibacterial property of DLC film coated on textile material. *Diam Relat Mater* 2010;19:690–4[371] with permission from Elsevier.



through a pad-dry-cure process [367]. The cotton fabric was previously modified with a cross-linking agent (1,2,3,4-butane tetracarboxylic acid, BTCA) using sodium hypophosphite (SHP) as catalyst. The authors showed that the cotton substrate coated with ppy/ZnO/SWCNT composite did not burn and just charred at the edge during the burning process, while the pristine cotton sample burnt to ashes completely. Moreover, the resulting functional fabric showed good stability after 10 washing cycles using tap water.

Liu et al. grafted poly(butyl acrylate) on MWCNTs (MWCNTs–PBA) and then coated cotton fabrics with the resulting material through a common dip-dry-cure process to reduce the textile flammability [366]. The untreated cotton completely burnt within  $\sim 25$  s, while the cotton fabric coated with 5 wt.% MWCNTs–PBA did not burn at all (Fig. 21.38B).

Nanotechnology has a great role on the enhancement of antistatic properties of synthetic fibers (such as nylon or polyester), which can present high static charge accumulation due to their low water absorption properties [5]. The antistatic properties can be imparted to textiles by coating processes [1], or during the fiber fabrication by fiber spinning processes, such as melt [376], dry [376], and wet [377] spinning or even conjugate spinning [363,378]. For instance, Hu et al. produced antistatic and biocompatible core-sheath and segmented-pie fibers based on a mixture of carbon black particles/polybutylene terephthalate (CB/PBT) and polyethylene terephthalate (PET), on a ratio of 30:70 wt.%, by a conjugate spinning process [363]. In the core-sheath configuration, the core was composed of CB/PBT, while the sheath was constituted by PET, and the fibers where in contact with each other through the sheath side. On the other hand, in the segmented-pie configuration, CB/PBT and PET were disposed radially in alternated segments. The authors then prepared an antistatic woven fabric through the combination of commercial PET yarns with antistatic draw-textured yarns (DTYs) produced from the antistatic core-sheath fibers (ACSF) and antistatic segmented-pie fibers (ASPF). The resulting fabric exhibited high mechanical strength and elongation, as well as low electrical resistance of  $1.2 \times 10^6 \Omega/\text{sq}$  (nonconductive synthetic fabrics typically exhibit an electrical resistance of  $10^9$ – $10^{12} \Omega/\text{cm}$ ) even after being washed 20 times. The authors also produced antistatic glove fingertips from blended yarns containing commercial acrylic yarns and DTYs of ACSF, demonstrating their applicability on capacitive touchscreens of wearable electronics.

Conductive textiles are essential to produce smart clothing because they can be used as electrically conductive substrates for electronic devices [1,58]. In particular, conductive textiles based on carbon nanomaterials, such as CNTs [379] and graphene [380], show excellent electrical and thermal properties, transparency, and mechanical flexibility. For instance, Hu et al. produced conductive textiles through the incorporation of singlewalled carbon nanotubes (SWCNTs) by dip-dry process. The resulting textiles presented high electrical conductivity of 125 S/cm and a sheet resistance lower

than  $1 \Omega/\text{sq}$ , maintaining the flexibility and stretchability characteristics of the parent cotton fabric [379].

Another textile feature with great importance for several applications is electromagnetic shielding, namely for electronics, aerospace, medical, or military devices/textiles. For instance, electromagnetic shielding is important to reduce electromagnetic interference arising from electronic devices or set-ups that transmit, process, or use electrical energy and to increase the society security avoiding, for instance, unauthorized surveillance and electromagnetic forms of spying [368,369]. Carbon-based nanomaterials, such as carbon black, CNTs, carbon nanofibers (CNFs), and graphene, are promising materials for electromagnetic shielding, simultaneously acting by reflection and absorption of the electromagnetic radiation.

Zhao et al. developed poly(ethylene terephthalate) (PET)-spunbond nonwoven fabrics with electromagnetic shielding properties using composites with different arrangements of continuous carbon fibers (CCF) [368]. The PET-spunbond nonwoven fabric was composed of several layers, with each layer being composed of grid-type carbon fibers. In order to prepare each layer, first CCF filament bundles were laid parallel and positioned with the same distance (array spacing) along the warp direction and then glued by an acrylic adhesive on PET-spunbond nonwoven fabric; in the second step, the CCF filament bundles were laid parallel along the weft direction and again positioned with equal distances; finally, another piece of PET-spunbond nonwoven was added to the top of the laid carbon fibers. The electromagnetic shielding properties of the fabric composed of a multilayer composite containing three layers with array spacing of 12 mm and overlapped angles of  $0-0-45$  degrees were evaluated in the frequency range of 30 MHz–1.5 GHz, exhibiting a shielding effectiveness of 60.49 dB at 1.0 GHz.

Zou and coauthors coated cotton substrates with MWCNTs by the impregnation method and studied the effect of two different surfactants for prior dispersion of the MWCNTs: Nafion and sodium dodecylbenzenesulfonate [381]. A shielding effectiveness of 11.48 dB was obtained in the frequency range of 8–12 GHz. More recently, a cotton substrate was coated with graphene by the LbL self-assembly process [382]. The resulting functional textile, besides presenting high electrical conductivity ( $1.67 \times 10^3 \text{ S/m}$ ), showed a maximum attenuation value of 30.04 dB when tested between 30 MHz and 6 GHz.

However, the most promising strategy to overcome the limitations associated with each type of material, namely the ability to attenuate RF from 2 to 18 GHz, consists of the development of multifunctional hybrid or composite materials consisting of one component with electrical properties and another with magnetic properties, in order to promote synergistic effects between both components, and thus maximize the absorption properties over a wider frequency range [369]. Recently, promising results were obtained for carbon composites combined with magnetic or dielectric nanomaterials ( $\text{ZnO}$ ,  $\text{BaTiO}_3$ ,  $\text{Al}_2\text{O}_3$ ) dispersed in polymeric matrices [383]. For example, a

polycarbonate and poly(styrene-*co*-acrylonitrile) polymer matrix containing MWCNTs (3 wt.%) and nickel (5–8 nm) magnetic NPs immobilized on partially reduced graphene sheets (10 wt.%) was prepared. A total shielding efficiency of –48 dB at 18 GHz was obtained for a thickness of 5 mm, corresponding to >99.99% total attenuation, with 91.1% of the incident radiation being absorbed [384]. In another study, the same authors developed a multi-layer structure consisting of two outer layers of PVDF containing  $\alpha$ -MnO<sub>2</sub> doped MWCNT (dielectric and antiferromagnetic nanomaterial) and graphene oxide doped with Fe<sub>3</sub>O<sub>4</sub> magnetic NPs (3 wt.%), and an intermediate layer of polycarbonate and PVDF containing MWCNTs (3 wt.%) (Fig. 21.38C) [373]. The resulting composite material with a thickness of 0.9 mm had a shielding efficiency of –57 dB at 18 GHz, corresponding to >99.999% total attenuation, with 92% of the radiation being absorbed. The outer layers acted as radiation absorption agents, while the intermediate layer acted as radiation reflector. Cao and coauthors compared the performance of a composite of MWCNTs and Fe<sub>3</sub>O<sub>4</sub> dispersed in paraffin (20 wt.%) before and after coating with a polyaniline conductive polymer [385]. The best results were obtained for the uncoated composite, with a total attenuation of 75 dB for a thickness of 3 mm in the range of 7–18 GHz.

In the medical field, carbon nanomaterials have been used as antibacterial agents. They can present antibacterial properties, which are greatly dependent on the type of surface functionalities and dispersion degree in the biological medium [370]. Zhao et al. developed antibacterial cotton fabrics based on graphene oxide by adsorption, radiation-induced cross-linking, and chemical cross-linking [372]. The sample prepared by adsorption (cotton–GO), through deposition of an aqueous dispersion of GO on the cotton substrate by vacuum filtration, presented the best performance when considering the simplicity of the fabrication process and the washing fastness. In particular, it inactivated 99.2% of bacteria in less than 4 h when tested with two different colonies (*E. coli* and *B. subtilis*). Furthermore, it exhibited the best inactivation efficiency (above 90%) after 100 laundering cycles and safety, without causing skin irritation when animal (rabbit) skin irritation tests were performed. In another work, Kitahara et al. coated cotton textiles with carbon-based films with 100 nm thickness by plasma-based ion implantation [371]. Antibacterial tests were then performed on the resulting functional textiles using two different cultures (*S. aureus* (s) and *Klebsiella pneumoniae* (k)). In both tests, no active bacteria were observed after an incubation period of 18 h (Fig. 21.38D).

### 21.3.5.5 Emerging applications

The current wave of wearable technologies and the new world of the Internet of Things combined with the continuous development of nanotechnology opened the doors to a new generation of innovative smart textiles for

emerging applications, namely for energy storage, energy harvesting and sensing [1,58,386]. In a few years, the idea of wearing a self-powered and multifunctional suit will be a reality due to the continuous efforts made by both scientific and industrial communities.

Among all the aforementioned carbon nanomaterials properties [360,387], their high electron mobility, high current density, ion adsorption ability, and easy assembly into multiscaled structures make them excellent building blocks for sensors, such as strain, temperature, and humidity sensors, or even for electronic devices such as supercapacitors, batteries, and micro/nanogenerators [1,218,360,387,388]. For instance, Zhao and coauthors developed a multistimulus sensitive smart environmental responder (SER) based on graphene fibers (GFs) [389]. The SER was composed of a GF coated with graphitic carbon nitride (GCN) by electrochemical deposition twisted with another GF, forming double-helix core-sheath graphene fibers (Fig. 21.39A). The resulting fibriform SER could detect small temperature changes ( $\Delta T = 4\text{ }^{\circ}\text{C}$ ), slight forces (0.05 N for press and 0.3 N for pull) and relatively low moisture fluctuations (relative humidity of 3%). Based on SER ability to detect external stimulus, the authors constructed a wearable and flexible multifunctional respiratory sensor to monitor human breath.

CNT films have also been widely explored to fabricate flexible textile-based sensors to detect and to monitor human motion [386,390,392–394]. For instance, Ryu et al. fabricated a wearable and stretchable strain sensor based on aligned dry-spun CNT fibers [393]. The CNT fibers were directly dry-spun on the surface of a prestretched (at strain of 100%) flexible elastic substrate (Ecoflex) forming van der Waals interactions. Finally, to enable the CNT fibers to behave as a sensitive strain sensor, they were coated with an Ecoflex thin film, in order to trigger a constant decrease of the conductive pathways and contact areas between the CNTs. The authors used conductive electrodes, attached to the strain sensor with clamps, and connected to wires by silver paste, to measure the relative variation of resistance with strain. Afterward, the CNT-based sensor was attached to a fabric garment using Ecoflex glue and used to monitor the elbow motion, presenting an extremely high stretchability of 900%, without losing its high sensitivity, responsiveness, and durability. Furthermore, Zhong et al. developed a stretchable self-powered fiber-based strain sensor (AFSS) [390]. The AFSS was produced by twinning two pretreated cotton threads, one coated with CNTs (CCT) and the other coated with both polytetrafluoroethylene (PTFE) and CNT (PCCT), to form a double-helix structure fiber. The resulting fiber was coiled around a silicone fiber. The AFSS exhibited excellent stability and sensitivity, measuring the amount of transferred charges (electrostatic effect), and could detect the stretch strain for up to 25% due to its helix structure and high stretchability of the silicone fiber. Moreover, the self-powered strain sensor enabled detecting finger motion states by measuring the quantity of charges, which varied linearly with the stimulated strain (Fig. 21.39B).

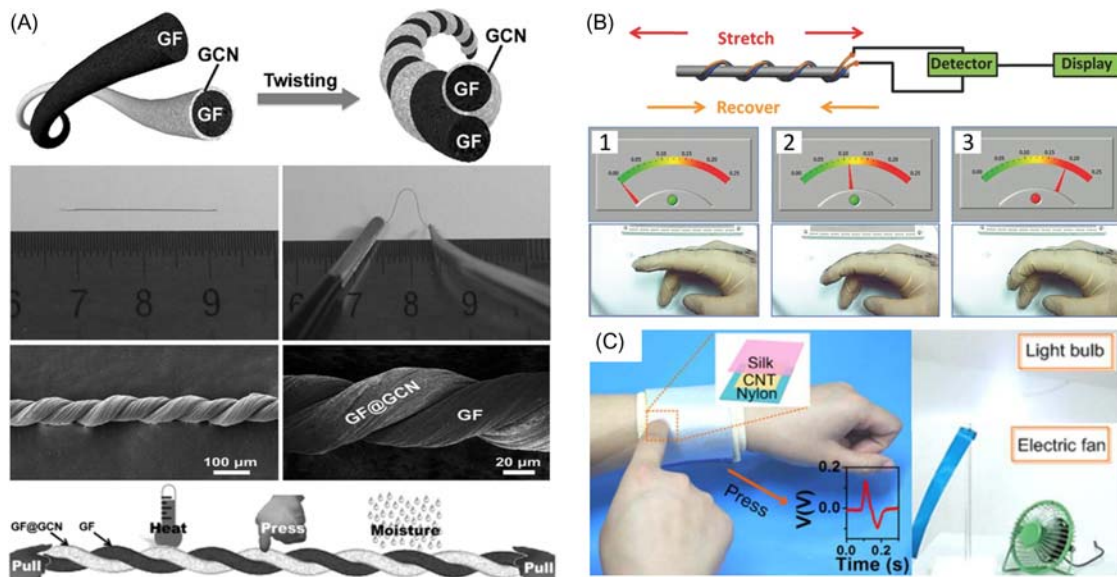


**FIGURE 21.39** Emerging applications of carbon-based textiles: (A) Temperature, pressure and humidity sensor fabricated from inter-twining fibers based on graphene (GF) and GF coated with graphitic carbon nitride (GF@GCN), respectively; (B) Illustration of a finger motion detector fiber sensor and the detecting results when the fingers do not move (1), move with smaller (2), and larger (3) angular amplitude; (C) Self-powered touch/gesture triboelectric sensor based on screenprinted CNTs used to control a lightbulb and an electric fan. (A) Adapted from Zhao F, Zhao Y, Cheng H, Qu L. A graphene fibriform resporator for sensing heat, humidity, and mechanical changes. *Angew Chem Int Ed* 2015;54:14951–5 [389] with permission from John Wiley & Sons; (B) adapted from Zhong J, Zhong Q, Hu Q, Wu N, Li W, Wang B, et al. Stretchable self-powered fiber-based strain sensor. *Adv Funct Mater* 2015;25:1798–1803 [390] with permission from John Wiley & Sons; and (C) adapted from Cao R, Pu X, Du X, Yang W, Wang J, Guo H, et al. Screen-printed washable electronic textiles as self-powered touch/gesture tribo-sensors for intelligent human–machine interaction. *ACS Nano* 2018;12:5190–6 [391] with permission from ACS.

Carbon-based systems have also gained significant interest for both energy harvesting and storage [218]. Due to the high importance for wearable technologies, energy harvesting systems have been widely explored through different types of energy conversion mechanisms based on piezoelectricity, thermoelectricity, triboelectricity, or photovoltaic phenomena [388,395–398]. In this field, Wang's group has been one of the major drivers in the development of energy harvesting systems [391,399–403]. For instance, his group developed a washable self-powered touch/gesture triboelectric textile sensor for intelligent human–machine interaction, taking advantage of the interaction between the CNTs and the textile fibers [391]. The sensor electrodes were produced by coating several fabrics (silk, nylon, flax, cotton, wool, leather, and velvet) with CNTs through the screenprinting process. The sensor produced using nylon as substrate generated maximum open-circuit voltage and short-circuit current values of  $\sim 7$  V and  $\sim 88$  nA, respectively, under relatively humidity of 10%. Moreover, it presented an output voltage of  $\sim 12$  V when submitted to a pressure of 650 kPa. The device showed excellent stability under harsh mechanical deformation and even after washing. Finally, when incorporated into clothes, it could serve as remote control system for wireless applications such as lightbulb, electric fan, or microwave oven (Fig. 21.39C). Ryan et al. fabricated a textile-based thermoelectric device composed of MWCNT:PVP coated n-type yarns and PEDOT:poly(styrenesulfonate) (PSS) dyed p-type yarns [404]. The n-type yarns were produced by coating PET yarns with PVP solution through a manual dripping process, followed by coating with MWCNTs through the same process. The p-type yarns were fabricated by submerging silk or cotton yarns in PEDOT:PSS aqueous dispersion twice, followed by a drying step at  $130^\circ\text{C}$  for 30 min [405]. The resulting silk-based thermoelectric device composed of 38 n-p elements generated an output voltage of 143 mV when applying a temperature gradient of  $116^\circ\text{C}$  and a maximum power of 7.1 nW at a temperature gradient of  $80^\circ\text{C}$ .

In the context of energy storage, carbon nanomaterials are important active electrode components to increase the overall performance of both supercapacitors and batteries due to their excellent electrical conductivity, high surface area, and mechanical strength. Moreover, they can be used as substrate or combined with active electrode (nano)materials with pseudocapacitive features, such as transition metal oxides and conductive polymers [387,388,406,407]. The first flexible textile SC based on carbon nanomaterials was produced by Hu et al. consisting of two cotton fabrics coated with SWCNTs through a simple dip-dry process, which acted as electrodes, separated by a liquid electrolyte (2 M aqueous  $\text{Li}_2\text{SO}_4$ ) (Fig. 21.40A) [379]. The textile electrodes presented a high electrical conductivity of 125 S/cm and a sheet resistance of  $1\ \Omega/\text{sq}$ , maintaining the flexibility and stretchability features of the pristine fabric. The porous structure of the textile allowed the incorporation of high SWCNTs loading and easy access of the electrolyte



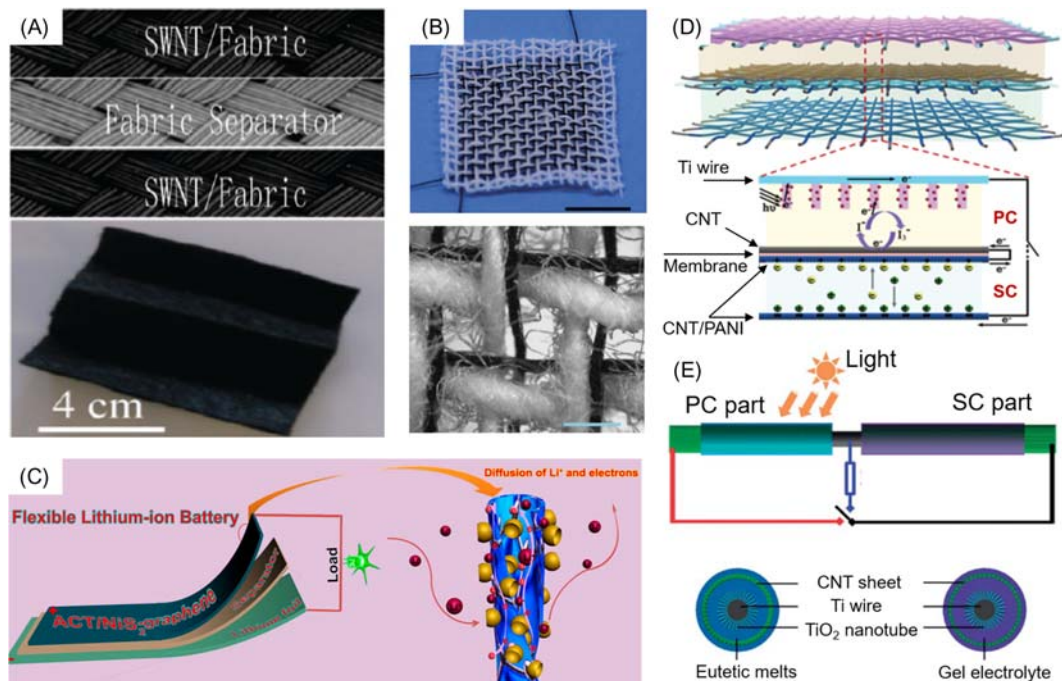


**FIGURE 21.40** (A) SWCNT textile-based SC. (B) Cowoven cloth composed by cotton yarns and two rGO + CNT/CMC coaxial fibers. (C) Electrochemical performance of assembled textile battery composed by ACT/NiS<sub>2</sub>/GFN as cathode and lithium foil as anode. (D) Self-powered device combining a flexible SC based on aligned MWCNT/PANI composite combined with a photovoltaic cell. (E) Coaxial energy fiber integrating a dye-sensitized solar cell and a SC based on Ti wire/TiO<sub>2</sub> nanotubes/CNT sheet composite. (A) Adapted from Hu L, Pasta M, La Mantia F, Cui L, Jeong S, Deshazer HD, et al. Stretchable, porous, and conductive energy textiles. *Nano Lett* 2010;10:708–14 [379] with permission from ACS. (B) Adapted from Kou L, Huang T, Zheng B, Han Y, Zhao X, Gopalsamy K, et al. Coaxial wet-spun yarn supercapacitors for high-energy density and safe wearable electronics. *Nat Commun* 2014;5:3754 [408] with permission from Springer Nature. (C) Adapted from Gao Z, Song N, Zhang Y, Li X. Cotton-textile-enabled, flexible lithium-ion batteries with enhanced capacity and extended lifespan. *Nano Lett* 2015;15:8194–203 [409] with permission from ACS. (D) Adapted from Pan S, Lin H, Deng J, Chen P, Chen X, Yang Z, et al. Novel wearable energy devices based on aligned carbon nanotube fiber textiles. *Adv Energy Mater* 2015;5:1401438 [410] with permission from John Wiley & Sons. (E) Adapted from Chen X, Sun H, Yang Z, Guan G, Zhang Z, Qiu L, et al. A novel “energy fiber” by coaxially integrating dye-sensitized solar cell and electrochemical capacitor. *J Mater Chem A* 2014;2:1897–902 [411] with permission from RSC.

ions to the electrodes surface, resulting on an improvement of the overall performance of the SC, with a specific capacitance of  $\sim 60 \text{ F/g}$  at a current density of  $1 \text{ mA/cm}^2$ . Furthermore, the textile-based SC exhibited an energy density of  $20 \text{ Wh/kg}$  at a power density of  $10 \text{ kW/kg}$  and excellent cycling stability, with a capacitance retention of up to 98% over 130,000 charge/discharge cycles. In another example, Abdelkader et al. fabricated a solid-state reduced graphene oxide (rGO)-based textile SC by screenprinting a cotton substrate [412]. The SC electrodes were prepared with the configuration of 5-interdigital finger pattern. The screenprinting paste was produced by mixing an aqueous solution of graphene oxide (GO) ( $5 \text{ mg/mL}$ ) with acrylate thickening agent to adjust the viscosity to be  $>1 \text{ Pa.s}$ . The GO screenprinted on cotton was then reduced by an electrochemical method. Finally, the electrodes were coated with a solid-gel electrolyte ( $\text{H}_2\text{SO}_4/\text{PVA}$ ) and assembled in a sandwich-type configuration to form the textile-based SC. The screenprinted SC showed a specific capacitance of  $257 \text{ F/g}$  at  $1 \text{ mA/cm}^2$  and maintained  $\sim 96\%$  of the initial value when tested under bending conditions. Moreover, it exhibited excellent stability, maintaining 97% of the original capacitance after 10,000 charge/discharge cycles.

An alternative to multilayer (sandwich)- and planar-type energy storage devices are fiber/yarn-type devices, since they present design versatility, high flexibility, and good compatibility with other fiber-based electronics systems (energy harvesting devices and sensors) [388,413,414]. Kou et al. produced a two-ply yarn SC based on polyelectrolyte-wrapped CNT/graphene core-sheath fiber electrodes. The core-sheath fibers were prepared by coaxial wet spinning, using sodium carboxymethyl cellulose polyelectrolyte (CMC) as sheath and CNTs, rGO, or their mixture as core [408]. The CMC polyelectrolyte prevented short circuits between intertwined fiber electrodes due to its electrically insulating properties, while enabling electrolyte ions diffusion due to its ionic conductivity. rGO@CMC, CNT@CMC, and rGO + CNT@CMC coaxial fibers were thus prepared following the same procedure. All fiber-based SCs were fabricated by twisting two identical coaxial fibers together (one acting as negative electrode and the other as positive electrode) and then coating them with a solid-gel electrolyte ( $\text{H}_3\text{PO}_4/\text{PVA}$ ) by dip coating. The rGO + CNT@CMC fiber SC exhibited higher areal capacitance ( $177 \text{ mF cm}^{-2}$  at  $0.1 \text{ mA/cm}$ ) than CNT@CMC and RGO@CMC based ones ( $127$  and  $47 \text{ mF/cm}^2$  at  $0.1 \text{ mA/cm}^2$ , respectively). Moreover, it afforded an areal energy density of  $3.84 \mu\text{Wh/cm}^2$  and a power density of  $0.02 \text{ mW/cm}^2$  at  $0.1 \text{ mA/cm}^2$ , and high capacitance retention of 75% at  $1 \text{ mA/cm}^2$ . The authors then produced a cowoven cloth using cotton yarns and two coaxial fibers (Fig. 21.40B). The fibers presented sufficient flexibility to produce the cloth without any fracture (attested by optical microscopic image).

Similarly, Zhu and coworkers fabricated a solid-state flexible fiber-shaped SC based on hierarchical  $\text{MnO}_2$  nanowire/rGO by wet spinning



followed by chemical reduction [415]. First, hybrid  $\text{MnO}_2/\text{GO}$  fibers were produced by injecting an aqueous mixture of  $\text{MnO}_2$  nanowires, previously prepared by hydrothermal method, and an aqueous solution of GO, in a weight ratio of 40:60, into a rotating coagulation bath (acetic bath). The GO on the  $\text{MnO}_2/\text{GO}$  fibers was then reduced to rGO by rolling the fibers onto a drum, followed by drying at  $60^\circ\text{C}$ , and addition to a hydrazine solution in a Teflon vessel sealed and kept at  $85^\circ\text{C}$  for 24 h. The fiber-based SC was then produced by coating rGO and  $\text{MnO}_2/\text{rGO}$  fibers with a solid-gel electrolyte ( $\text{H}_3\text{PO}_4/\text{PVA}$ ) and then twisting them together. The hybrid SC exhibited a high volumetric capacitance of  $66.1\text{ F/cm}^3$ , excellent cycling stability with capacitance retention of 96% over 10,000 cycles and energy and power densities of  $5.8\text{ mWh/cm}^3$  and  $0.51\text{ W/cm}^3$  at  $0.12\text{ A/cm}^3$ , respectively.

Carbon nanomaterials are also important to improve the performance of lithium-ion batteries that suffer from fast capacitance decay, poor cycling life, and lower coulombic efficiency than SCs [409,416]. Nevertheless, they present higher energy density than SCs, being more oriented for applications demanding high energy storage capability, while SCs are more suitable for applications that require high power [417]. For instance, Li and coworkers improved the capacitance and the cycling stability of a textile-based lithium-ion battery by fabricating an anode of lithium foil assembled with a cathode based on porous activated cotton textile (ACT). The cathode was prepared by dipping a cotton fabric into 1 M NaF solution followed by annealing at  $120^\circ\text{C}$  for 3 h. Then, the porous ACT was embedded with  $\text{NiS}_2$  nanobowls and wrapped with graphene sheets (GFN) through a two-step heat treatment method [409]. The assembled textile battery (Fig. 21.40C) was composed of ACT/ $\text{NiS}_2$ /GFN composite as cathode, lithium foil as anode, Celgard 2400 as separator, and a liquid electrolyte (1 M  $\text{LiPF}_6$  in ethylene carbonate + dimethyl carbonate + diethyl carbonate electrolyte, in 1:1:1 v/v/v). The textile-based device exhibited a high initial discharge capacitance of  $\sim 1710\text{ mAh/g}$  at 0.01 C, a very good rate performance and maintained a reversible capacitance of  $\sim 1016\text{ mAh/g}$  at 0.1 C after 400 cycles.

The new generation of wearable devices combine both energy production and storage features, being the so-called self-powered devices [410,418,419]. Pan and coauthors developed a self-powered textile device combining a flexible SC based on aligned MWCNT/polyaniline (PANI) fibers and a photovoltaic cell (PC) (Fig. 21.40D) [410]. The fiber electrodes were fabricated starting from a spinnable MWCNT array, which was converted into aligned CNT sheets, stacked into a thicker film, and then twisted into aligned CNT fibers that were woven into textiles, followed by electrochemical deposition of PANI (MWCNT/PANI). The MWCNT/PANI fabrics were then coated with  $\text{H}_3\text{PO}_4/\text{PVA}$  solid-gel electrolyte, resulting in a textile SC with a specific capacitance of  $272.7\text{ F/g}$ . The SC maintained 96.4% of the initial specific capacitance value after bending for 200 cycles. The PC cell was produced by assembling a textile-based Ti wire fabricated by electrochemical

anodization with a MWCNT fiber textile separated by a gel electrolyte. The electrolyte was produced by mixing poly(vinylidene fluoride-*co*-hexafluoropropene) (10 wt.%) and 3-methoxypropionitrile solution containing 0.1 M LiI, 0.05 M I<sub>2</sub>, 0.5 M 4-*tert*-butylpyridine, and 0.5 M 1-propyl-2,3-dimethylimidazolium iodide. Finally, both PC and SC were stacked in a multilayer configuration to fabricate the self-powered device. The device enabled converting solar energy into electrical energy besides storing it, reaching a photoelectric conversion of 2.1% and a storage efficiency of 60.3%. Similarly, Chen et al. developed a self-powered fiber which coaxially integrated both a dye-based solar cell and a SC (Fig. 21.40E) [411]. The coaxial-type SC was composed of vertically aligned TiO<sub>2</sub> nanotubes grown on Ti wires by electrochemical anodization as core, and an external layer of CNT sheets synthesized by chemical vapor deposition, separated by H<sub>3</sub>PO<sub>4</sub>/PVA solid-gel electrolyte. On the other hand, the coaxial-type PC consisted of CNT sheet wrapped onto TiO<sub>2</sub> nanotube-modified Ti wire and coated with a solid-state electrolyte composed of a mixture of 1-ethyl-3-methylimidazolium iodide (EMII), 1-propyl-3-methylimidazolium iodide (PMII) and iodine. The resulting self-powered fiber was inserted into a transparent fluorinated ethylene propylene tube and showed a photovoltaic conversion efficiency of 2.73%, and an energy storage efficiency of 75.7%, reaching a specific capacitance of 3.32 mF/cm<sup>2</sup> and a power density of 0.27 mW/cm<sup>2</sup> at a current of 50  $\mu$ A.

## 21.4 Future trends and prospects

The unceasing and ever-growing demand of customers for trendy clothing and accessories with improved aesthetics, innovative functionalities and connectivity boosted the market of functional and smart textiles. The conjugation of nanotechnology with textiles has been a challenge for scientists, engineers, designers, and textile manufacturers. In recent decades, we have witnessed the exciting creation of advanced multifunctional textile fabrics and fibers through the incorporation of high-performance nanomaterials, including nanosilicas, titanium dioxide, metal/metal oxide NPs, carbon nanomaterials, and, more recently, of multifunctional hybrid nanomaterials and nanocomposites.

The first strategy to introduce nanotechnology to textiles used traditional finishing and coating processes already implemented in the textile industry. However, since the early beginnings, the challenges faced in this fusion led to the search for new production routes, creating new opportunities for the development of high-tech processes, namely fiber spinning (multicomponent fibers), printing technologies (in particular, 3D printing) and, more recently, high-tech technologies, such as lithography. Nevertheless, scalability, cost-effectiveness, ecosustainability, time and energy savings are prime factors that need to be considered at all stages of engineered products design. In particular, the high cost of nanomaterial fabrication and batch-to-batch quality reproducibility upon scale-up still hamper their commercialization. In many

cases, a balance between enhanced performance vs manufacturing cost needs to be reached.

Besides more conventional functionalities imparted on textiles by nanotechnology, such as water/oil repellence, antimicrobial and antistatic properties, more advanced features have emerged, including drug release, chromism (photo-, thermo-, electro-, and halochromism), and electromagnetic radiation protection. Recently, with the advent of electronic textiles, sensing, energy harvesting and storage became new target properties. In particular, in the era of IoT, the integration of electronics, sensors, antennas, batteries/supercapacitors, solar cells, and other energy harvesting components on textiles became a reality, initially by coupling external modules, but now transitioning to flexible components directly integrated on the fabric/fiber itself (intelligent and wearable electronics).

The introduction of nanotechnology on textiles created a global awareness by consumers on its potential impact on human health and the environment. Thus, the life cycle assessment and toxicity evaluation of released nanomaterials are mandatory at all stages of the product manufacturing and life, starting from the production of the nanomaterials themselves, to their incorporation on textiles, their eventual release upon washing/handling, the use of the resulting textile product by the consumers and, ultimately, its disposal. Nevertheless, the nanometer dimensions of the materials create new barriers for their detection and treatment when released from textiles, and thus new methodologies still need to be developed.

Finally, the escalating concern about waste management worldwide grounded in the paradigms of circular economy and sustainable development is leading to a reinvention of the textile industry toward a new generation of recycled textiles with reduced carbon footprint. This revolution is also extended to the fabrication of nanomaterials from bio- and industrial waste.

Despite the advances achieved so far on nanoengineered textiles, the rapid evolution on miniaturized electronics and integrated multifunctionalities is shaping the future of textiles. New and exciting opportunities are thus envisioned in the upcoming years.

## Acknowledgments

This work was funded by ERDF – European Regional Development Fund through COMPETE 2020 – Operacional Programme for Competitiveness and Internationalisation (POCI), and by Portuguese funds through Fundação para a Ciência e a Tecnologia (FCT)/MEC under Program PT2020 in the framework of the projects PTDC/CTM-TEX/31271/2017, UID/QUI/50006/2019, and UID/NAN/50024/2019. C.P., T.V.P. and J.S.T. thank FCT for FCT Investigator contract IF/01080/2015, Research contract PTDC/CTM-TEX/31271/2017, and PhD grant SFRH/BD/145513/2019, respectively. R.S.C. acknowledges the grant funding from the European Union's Horizon 2020 Research and Innovation Programme under grant agreement No. 863307.

## References

- [1] Yetisen AK, Qu H, Manbachi A, Butt H, Dokmeci MR, Hinestroza JP, et al. Nanotechnology in textiles. *ACS Nano* 2016;10:3042–68.
- [2] Sawhney APS, Condon B, Singh KV, Pang SS, Li G, Hui D. Modern Applications of nanotechnology in textiles. *Text Res J* 2008;78:731–9.
- [3] Mishra R, Militky J. Nanotechnology in textiles: theory and application. 1st ed. Cambridge: Woodhead Publishing Ltd; 2018.
- [4] Riaz S, Ashraf M, Hussain T, Hussain MT, Rehman A, Javid A, et al. Functional finishing and coloration of textiles with nanomaterials. *Color Technol* 2018;134:327–46.
- [5] Joshi M, Bhattacharyya A. Nanotechnology—a new route to high-performance functional textiles. *Text Prog* 2011;43:155–233.
- [6] Mahltig B, Haufe H, Böttcher H. Functionalisation of textiles by inorganic sol–gel coatings. *J Mater Chem* 2005;15:4385–98.
- [7] Schindler WD, Hauser PJ, editors. Chemical finishing of textiles. 1st ed. Cambridge: Woodhead Publishing Ltd; 2004.
- [8] Rivero PJ, Urrutia A, Goicoechea J, Arregui FJ. Nanomaterials for functional textiles and fibers. *Nanoscale Res Lett* 2015;10:1–22.
- [9] Weng W, Chen P, He S, Sun X, Peng H. Smart electronic textiles. *Angew Chem Int Ed* 2016;55:6140–69.
- [10] Ghahremani Honarvar M, Latifi M. Overview of wearable electronics and smart textiles. *J Text Inst* 2017;108:631–52.
- [11] Smart Clothing Market worth \$5.3 billion by 2024, Mark. Res. Rep. Smart Clothing Market by Textile Type, Product Type, End-User Industry, and Geography — Global Forecast to 2024. <<https://www.marketsandmarkets.com/PressReleases/smart-clothing.asp>>; 2019 [accessed 28.02.20].
- [12] Som C, Wick P, Krug H, Nowack B. Environmental and health effects of nanomaterials in nanotextiles and façade coatings. *Env Int* 2011;37:1131–42.
- [13] Rovira J, Domingo JL. Human health risks due to exposure to inorganic and organic chemicals from textiles: a review. *Env Res* 2019;168:62–9.
- [14] Hussain CM, Mishra AK, editors. Nanotechnology in environmental science. 1st ed. Weinheim, Germany: Wiley-VCH Verlag GmbH & Co. KGaA; 2018.
- [15] Hussain CM, Kharisov B, editors. Advanced environmental analysis: application of nanomaterials. Cambridge: Royal Society of Chemistry; 2016.
- [16] Syduzzaman M, Patwary SU. Smart textiles and nano-technology: a general overview. *J Text Sci Eng* 2015;05:1–7.
- [17] Broadbent AD. An introduction to dyes and dyeing. *Basic Princ. Text. Color*. Yorkshire: Society of Dyers and Colourists; 2001. p. 174–98.
- [18] Holme I. Coloration of technical textiles. In: Horrocks AR, Anand SC, editors. *Handb. Tech. Text*. 1st ed. Cambridge: Woodhead Publishing Ltd and CRC Press LLC; 2000. p. 187–222.
- [19] Choudhury AKR. Introduction to finishing. *Princ. Text. Finish*. Cambridge: Elsevier Ltd; 2017. p. 1–20.
- [20] Tung WS, Daoud WA. Self-cleaning fibers via nanotechnology: a virtual reality. *J Mater Chem* 2011;21:7858–69.
- [21] Joshi M, Butola BS. Application technologies for coating, lamination and finishing of technical textiles. In: Gulrajani ML, editor. *Adv. Dye. Finish. Tech. Text*. Elsevier; 2013. p. 355–411.

- [22] Singha K. A review on coating & lamination in textiles: processes and applications. *Am J Polym Sci* 2012;2:39–49.
- [23] Sen AK. Coated textiles - principles and applications. 2nd ed. Boca Raton: CRC Press; 2007.
- [24] Fung W. Coated and laminated textiles. Cambridge: CRC Press; 2002.
- [25] Khan S, Lorenzelli L, Dahiya RS. Technologies for printing sensors and electronics over large flexible substrates: a review. *IEEE Sens J* 2015;15:3164–85.
- [26] Stoppa M, Chiolerio A. Wearable electronics and smart textiles: a critical review. *Sensors* 2014;14:11957–92.
- [27] Krebs FC. Fabrication and processing of polymer solar cells: a review of printing and coating techniques. *Sol Energy Mater Sol Cell* 2009;93:394–412.
- [28] Novaković D, Kašiković N, Vladić G, Pál M. Screen printing. In: Joanna Izdebska ST, editor. *Print. Polym. Fundam. Appl.* William Andrew Inc.; 2016. p. 247–61.
- [29] Ahmed MU, Hossain MM, Safavieh M, Wong YL, Rahman IA, Zourob M, et al. Toward the development of smart and low cost point-of-care biosensors based on screen printed electrodes. *Crit Rev Biotechnol* 2015;36:1–11.
- [30] Kipphan H, editor. *Handbook of print media: technologies and production methods.* Berlin, Heidelberg: Springer; 2001.
- [31] McCann J, Bryson D, editors. *Smart clothes and wearable technology.* Boca Raton: CRC Press; 2009.
- [32] Dixon C, Lamanna J, Wheeler AR. Printed microfluidics. *Adv Funct Mater* 2017;27:1604824.
- [33] Bandonkar AJ, Jia W, Wang J. Tattoo-based wearable electrochemical devices: a review. *Electroanalysis* 2015;27:562–72.
- [34] Introduction to semiconductor lithography. In: Mack C, editor. *Fundam. Princ. Opt. Lithogr. Sci. Microfabr..* 1st ed. Chichester: John Wiley & Sons; 2008.
- [35] Geissler M, Xia Y. Patterning: principles and some new developments. *Adv Mater* 2004;16:1249–69.
- [36] Liddle JA, Gallatin GM. Nanomanufacturing: a perspective. *ACS Nano* 2016;10:2995–3014.
- [37] van Assenbergh P, Meinders E, Geraedts J, Dodou D. Nanostructure and microstructure fabrication: from desired properties to suitable processes. *Small* 2018;14:1801989.
- [38] Gates BD, Xu Q, Stewart M, Ryan D, Willson CG, Whitesides GM. New approaches to nanofabrication: molding, printing, and other techniques. *Chem Rev* 2005;105:1171–96.
- [39] Ai B, Möhwald H, Wang D, Zhang G. Advanced colloidal lithography beyond surface patterning. *Adv Mater Interfaces* 2017;4:1600271.
- [40] Garcia R, Knoll AW, Riedo E. Advanced scanning probe lithography. *Nat Nanotechnol* 2014;9:577–87.
- [41] Liao W, Hsu SL-C, Chu S-Y, Kau P-C. Imprint lithography for flexible transparent plastic substrates. *Microelectron Eng* 2004;75:145–8.
- [42] Simon D, Ware T, Marcotte R, Lund BR, Smith DW, Di Prima M, et al. A comparison of polymer substrates for photolithographic processing of flexible bioelectronics. *Biomed Microdevices* 2013;15:925–39.
- [43] Gibson I, Rosen D, Stucker B. *Additive manufacturing technologies.* New York: Springer; 2015.
- [44] Wang Q, Sun J, Yao Q, Ji C, Liu J, Zhu Q. 3D printing with cellulose materials. *Cellulose* 2018;25:4275–301.
- [45] Vanderploeg A, Lee S-E, Mamp M. The application of 3D printing technology in the fashion industry. *Int J Fash Des Technol Educ* 2017;10:170–9.

- [46] Hashemi Sanatgar R, Campagne C, Nierstrasz V. Investigation of the adhesion properties of direct 3D printing of polymers and nanocomposites on textiles: effect of FDM printing process parameters. *Appl Surf Sci* 2017;403:551–63.
- [47] Valtas A, Sun D. 3D printing for garments production: an exploratory study. *J Fash Technol Text Eng* 2016;04.
- [48] Piras CC, Fernández-Prieto S, De Borggraeve WM. Nanocellulosic materials as bioinks for 3D bioprinting. *Biomater Sci* 2017;5:1988–92.
- [49] Tenhunen T-M, Moslemian O, Kammiovirta K, Harlin A, Kääriäinen P, Österberg M, et al. Surface tailoring and design-driven prototyping of fabrics with 3D-printing: an all-cellulose approach. *Mater Des* 2018;140:409–19.
- [50] Ligon SC, Liska R, Stampfl J, Gurr M, Mülhaupt R. Polymers for 3D printing and customized additive manufacturing. *Chem Rev* 2017;117:10212–90.
- [51] Beecroft M. 3D printing of weft knitted textile based structures by selective laser sintering of nylon powder. *IOP Conf Ser Mater Sci Eng* 2016;137:012017.
- [52] Babu BR, Parande AK, Raghu S, Kumar TP. Cotton textile processing: waste generation and effluent treatment. *J Cotton Sci* 2007;11:141–53.
- [53] Terinte N, Manda BMK, Taylor J, Schuster KC, Patel MK. Environmental assessment of coloured fabrics and opportunities for value creation: spin-dyeing versus conventional dyeing of modal fabrics. *J Clean Prod* 2014;72:127–38.
- [54] Naeimirad M, Zadhoush A, Kotek R, Esmaeely Neisiany R, Nouri Khorasani S, Ramakrishna S. Recent advances in core/shell bicomponent fibers and nanofibers: a review. *J Appl Polym Sci* 2018;135:46265.
- [55] Lewin M. *Handbook of fiber chemistry*. 3rd ed. Boca Raton: CRC Press; 2006.
- [56] Yeo SY, Jeong SH. Preparation and characterization of polypropylene/silver nanocomposite fibers. *Polym Int* 2003;52:1053–7.
- [57] Nilsson E, Oxfall H, Wandelt W, Rychwalski R, Hagström B. Melt spinning of conductive textile fibers with hybridized graphite nanoplatelets and carbon black filler. *J Appl Polym Sci* 2013;130:2579–87.
- [58] Lund A, van der Velden NM, Persson N-K, Hamed MM, Müller C. Electrically conducting fibres for e-textiles: an open playground for conjugated polymers and carbon nanomaterials. *Mater Sci Eng R: Rep* 2018;126:1–29.
- [59] Yu B, Qi L, Ye J, Sun H. The research of radar absorbing property of bicomponent fibers with infrared camouflage. *J Polym Res* 2007;14:107–13.
- [60] Pinto TV, Fernandes DM, Guedes A, Cardoso N, Durães NF, Silva C, et al. Photochromic polypropylene fibers based on UV-responsive silica@phosphomolybdate nanoparticles through melt spinning technology. *Chem Eng J* 2018;350:856–66.
- [61] Pinto TV, Cardoso N, Costa P, Sousa CM, Durães N, Silva C, et al. Light driven PVDF fibers based on photochromic nanosilica@naphthopyran fabricated by wet spinning. *Appl Surf Sci* 2019;470:951–8.
- [62] Elahi MF, Lu W. Core-shell fibers for biomedical applications-a review. *J Bioeng Biomed Sci* 2013;3:1–14.
- [63] Kiliaris P, Papaspyrides CD. Polymer/layered silicate (clay) nanocomposites: an overview of flame retardancy. *Prog Polym Sci* 2010;35:902–58.
- [64] Zhang D, editor. *Advances in filament yarn spinning of textiles and polymers*. 1st ed. Cambridge: Woodhead Publishing Limited; 2014.
- [65] Hagewood J. Technologies for the manufacture of synthetic polymer fibers. In: Zhang D, editor. *Adv. Filam. Yarn Spinn. Text. Polym..* 1st ed. Cambridge: Elsevier B.V.; 2014. p. 48–71.

- [66] Bhat G, Kandagor V. Synthetic polymer fibers and their processing requirements. In: Zhang D, editor. *Adv. Filam. Yarn Spinn. Text. Polym.*. 1st ed. Cambridge: Elsevier B.V.; 2014. p. 3–30.
- [67] Moody V, Needles HL. Major fibers and their properties. *Tufted Carpet*. 1st ed. NY: William Andrew Publishing; 2004. p. 35–59.
- [68] Rawal A, Mukhopadhyay S. Melt spinning of synthetic polymeric filaments. In: Zhang D, editor. *Adv. Filam. Yarn Spinn. Text. Polym.*. 1st ed. Cambridge: Elsevier B.V.; 2014. p. 75–99.
- [69] Persano L, Camposeo A, Tekmen C, Pisignano D. Industrial upscaling of electrospinning and applications of polymer nanofibers: a review. *Macromol Mater Eng* 2013;298:504–20.
- [70] Mather RR, Wardman RH. *The chemistry of textile fibres*. 2nd ed. Cambridge: The Royal Society of Chemistry; 2015.
- [71] Imura Y, Hogan RMC, Jaffe M. Dry spinning of synthetic polymer fibers. In: Zhang D, editor. *Adv. Filam. Yarn Spinn. Text. Polym.*. 1st ed. Cambridge: Elsevier B.V.; 2014. p. 187–202.
- [72] Bottino A, Camera-Roda G, Capannelli G, Munari S. The formation of microporous polyvinylidene difluoride membranes by phase separation. *J Memb Sci* 1991;57:1–20.
- [73] Nayak R. *Polypropylene nanofibers*. 1st ed. Cham: Springer International Publishing; 2017.
- [74] Ni QQ, Jin X, Xia H, Liu F. Electrospinning, processing and characterization of polymer-based nano-composite fibers. In: Zhang D, editor. *Adv. Filam. Yarn Spinn. Text. Polym.*. 1st ed. Cambridge: Elsevier B.V.; 2014. p. 128–48.
- [75] Góra A, Sahay R, Thavasi V, Ramakrishna S. Melt-electrospun fibers for advances in biomedical engineering, clean energy, filtration, and separation. *Polym Rev* 2011;51:265–87.
- [76] Fang J, Zhang L, Sutton D, Wang X, Lin T. Needleless melt-electrospinning of polypropylene nanofibres. *J Nanomater* 2012;2012:1–9.
- [77] Venugopal J, Ramakrishna S. Applications of polymer nanofibers in biomedicine and biotechnology. *Appl Biochem Biotechnol* 2005;125:147–58.
- [78] Lee S, Kay Obendorf S. Developing protective textile materials as barriers to liquid penetration using melt-electrospinning. *J Appl Polym Sci* 2006;102:3430–7.
- [79] Mirjalili M, Zohoori S. Review for application of electrospinning and electrospun nanofibers technology in textile industry. *J Nanostructure Chem* 2016;6:207–13.
- [80] Lee S, Obendorf SK. Use of electrospun nanofiber web for protective textile materials as barriers to liquid penetration. *Text Res J* 2007;77:696–702.
- [81] Knopp D, Tang D, Niessner R. Review: bioanalytical applications of biomolecule-functionalized nanometer-sized doped silica particles. *Anal Chim Acta* 2009;647:14–30.
- [82] Bae SW, Tan W, Hong J-I. Fluorescent dye-doped silica nanoparticles: new tools for bioapplications. *Chem Commun* 2012;48:2270–82.
- [83] Tang L, Cheng J. Nonporous silica nanoparticles for nanomedicine application. *Nano Today* 2013;8:290–312.
- [84] Argyo C, Weiss V, Bräuchle C, Bein T. Multifunctional mesoporous silica nanoparticles as a universal platform for drug delivery. *Chem Mater* 2014;26:435–51.
- [85] Du X, Li X, Xiong L, Zhang X, Kleitz F, Qiao SZ. Mesoporous silica nanoparticles with organo-bridged silsesquioxane framework as innovative platforms for bioimaging and therapeutic agent delivery. *Biomaterials* 2016;91:90–127.
- [86] Tang L, Zheng Y, Chen S, Wang L, Wang H. Flexible X-ray radiation protection membrane PVA/Pb(NO<sub>3</sub>)<sub>2</sub> microcapsule composites supported by bacterial cellulose. *J Appl Polym Sci* 2016;133:43120.



- [87] Kasaai MR. Nanosized particles of silica and its derivatives for applications in various branches of food and nutrition sectors. *J Nanotechnol* 2015;2015:1–6.
- [88] Sharma RK, Sharma S, Dutta S, Zboril R, Gawande MB. Silica-nanosphere-based organic–inorganic hybrid nanomaterials: synthesis, functionalization and applications in catalysis. *Green Chem* 2015;17:3207–30.
- [89] Bapat G, Labade C, Chaudhari A, Zinjarde S. Silica nanoparticle based techniques for extraction, detection, and degradation of pesticides. *Adv Colloid Interface Sci* 2016;237:1–14.
- [90] Rawtani D, Khatri N, Tyagi S, Pandey G. Nanotechnology-based recent approaches for sensing and remediation of pesticides. *J Env Manag* 2018;206:749–62.
- [91] Barik TK, Kamaraju R, Gowswami A. Silica nanoparticle: a potential new insecticide for mosquito vector control. *Parasitol Res* 2012;111:1075–83.
- [92] Piao Y, Burns A, Kim J, Wiesner U, Hyeon T. Designed fabrication of silica-based nanostructured particle systems for nanomedicine applications. *Adv Funct Mater* 2008;18:3745–58.
- [93] Ogawa M. Mesoporous silica layer: preparation and opportunity. *Chem Rec* 2017;17:217–32.
- [94] Liu J, Liu T, Pan J, Liu S, Lu QM. Advances in multicompartment mesoporous silica micro/nanoparticles for theranostic applications. *Annu Rev Chem Biomol Eng* 2018;9:389–411.
- [95] Hanske C, Sanz-Ortiz MN, Liz-Marzán LM. Silica-coated plasmonic metal nanoparticles in action. *Adv Mater* 2018;30:1707003.
- [96] Wang Y, Zhang L, Hu Y, Li C. In situ surface functionalization of hydrophilic silica nanoparticles via flame spray process. *J Mater Sci Technol* 2015;31:901–6.
- [97] Rezaei S, Manoucheri I, Moradian R, Pourabbas B. One-step chemical vapor deposition and modification of silica nanoparticles at the lowest possible temperature and superhydrophobic surface fabrication. *Chem Eng J* 2014;252:11–16.
- [98] Stöber W, Fink A, Bohn E. Controlled growth of monodisperse silica spheres in the micron size range. *J Colloid Interface Sci* 1968;26:62–9.
- [99] Trewyn BG, Slowing II, Giri S, Chen H, Lin VS-Y. Synthesis and functionalization of a mesoporous silica nanoparticle based on the sol–gel process and applications in controlled release. *Acc Chem Res* 2007;40:846–53.
- [100] Kobler J, Möller K, Bein T. Colloidal suspensions of functionalized mesoporous silica nanoparticles. *ACS Nano* 2008;2:791–9.
- [101] Arriagada FJ, Osseo-Asare K. Phase and dispersion stability effects in the synthesis of silica nanoparticles in a non-ionic reverse microemulsion. *Colloids Surf* 1992;69:105–15.
- [102] Arriagada FJ, Osseo-Asare K. Synthesis of nanometer-sized silica by controlled hydrolysis in reverse micellar systems. In: Bergna H, editor. *Colloid Chem. Silica*. 1st ed. Washington: American Chemical Society; 1994. p. 113–28.
- [103] Gu L, Zhang A, Hou K, Dai C, Zhang S, Liu M, et al. One-pot hydrothermal synthesis of mesoporous silica nanoparticles using formaldehyde as growth suppressant. *Microporous Mesoporous Mater* 2012;152:9–15.
- [104] Chandra S, Beaune G, Shirahata N, Winnik FM. A one-pot synthesis of water soluble highly fluorescent silica nanoparticles. *J Mater Chem B* 2017;5:1363–70.
- [105] Ciriminna R, Fidalgo A, Pandarus V, Béland F, Ilharco LM, Pagliaro M. The sol–gel route to advanced silica-based materials and recent applications. *Chem Rev* 2013;113:6592–620.



- [106] Yang P, Gai S, Lin J. Functionalized mesoporous silica materials for controlled drug delivery. *Chem Soc Rev* 2012;41:3679–98.
- [107] Möller K, Kobler J, Bein T. Colloidal suspensions of nanometer-sized mesoporous silica. *Adv Funct Mater* 2007;17:605–12.
- [108] Möller K, Kobler J, Bein T. Colloidal suspensions of mercapto-functionalized nanosized mesoporous silica. *J Mater Chem* 2007;17:624–31.
- [109] Wu S-H, Mou C-Y, Lin H-P. Synthesis of mesoporous silica nanoparticles. *Chem Soc Rev* 2013;42:3862–75.
- [110] Vivero-Escoto JL, Huang Y-T. Inorganic-organic hybrid nanomaterials for therapeutic and diagnostic imaging applications. *Int J Mol Sci* 2011;12:3888–927.
- [111] Guerrero-Martínez A, Pérez-Juste J, Liz-Marzán LM. Recent progress on silica coating of nanoparticles and related nanomaterials. *Adv Mater* 2010;22:1182–95.
- [112] Yokoi T, Wakabayashi J, Otsuka Y, Fan W, Iwama M, Watanabe R, et al. Mechanism of formation of uniform-sized silica nanospheres catalyzed by basic amino acids. *Chem Mater* 2009;21:3719–29.
- [113] Cushing BL, Kolesnichenko VL, O'Connor CJ. Recent advances in the liquid-phase syntheses of inorganic nanoparticles. *Chem Rev* 2004;104:3893–946.
- [114] Peres EC, Slaviero JC, Cunha AM, Hosseini-Bandegharai A, Dotto GL. Microwave synthesis of silica nanoparticles and its application for methylene blue adsorption. *J Env Chem Eng* 2018;6:649–59.
- [115] Vaibhav V, Vijayalakshmi U, Roopan SM. Agricultural waste as a source for the production of silica nanoparticles. *Spectrochim Acta Part A Mol Biomol Spectrosc* 2015;139: 515–20.
- [116] Boza AF, Kupfer VL, Oliveira AR, Radovanovic E, Rinaldi AW, Meneguín JG, et al. Synthesis of  $\alpha$ -aminophosphonates using a mesoporous silica catalyst produced from sugarcane bagasse ash. *RSC Adv* 2016;6:23981–6.
- [117] Arumugam A, Ponnusami V. Synthesis of SBA-15 from low cost silica precursor obtained from sugarcane leaf ash and its application as a support matrix for lipase in bio-diesel production. *J Sol-Gel Sci Technol* 2013;67:244–50.
- [118] Rovani S, Santos JJ, Corio P, Fungaro DA. Highly pure silica nanoparticles with high adsorption capacity obtained from sugarcane waste ash. *ACS Omega* 2018;3:2618–27.
- [119] Corma A, García H. Silica-bound homogenous catalysts as recoverable and reusable catalysts in organic synthesis. *Adv Synth Catal* 2006;348:1391–412.
- [120] Hoffmann F, Cornelius M, Morell J, Fröba M. Silica-based mesoporous organic–inorganic hybrid materials. *Angew Chem Int Ed* 2006;45:3216–51.
- [121] Brühwiler D. Postsynthetic functionalization of mesoporous silica. *Nanoscale* 2010;2:887–92.
- [122] Möller K, Bein T. Talented mesoporous silica nanoparticles. *Chem Mater* 2017;29: 371–88.
- [123] Cashin VB, Eldridge DS, Yu A, Zhao D. Surface functionalization and manipulation of mesoporous silica adsorbents for improved removal of pollutants: a review. *Env Sci Water Res Technol* 2018;4:110–28.
- [124] Du B, Cao Z, Li Z, Mei A, Zhang X, Nie J, et al. One-pot preparation of hollow silica spheres by using thermosensitive poly(N-isopropylacrylamide) as a reversible template. *Langmuir* 2009;25:12367–73.
- [125] Kardys AY, Bharali DJ, Mousa SA. Amino-functionalized silica nanoparticles: in vitro evaluation for targeted delivery and therapy of pancreatic cancer. *J Nanotechnol* 2013;2013:1–8.

- [126] Pinto TV, Fernandes DM, Pereira C, Guedes A, Blanco G, Pintado JM, et al. Lanthano phosphomolybdate-decorated silica nanoparticles: novel hybrid materials with photochromic properties. *Dalton Trans* 2015;44:4582–93.
- [127] Nam Y, Lee D, Cho E-B. Role of phosphate-modified mesoporous silica nanoparticles for altering biomimetic metal-induced aggregation process of pluronic F127 block copolymer. *Mater Lett* 2013;110:176–9.
- [128] Estephan ZG, Jaber JA, Schlenoff JB. Zwitterion-stabilized silica nanoparticles: toward nonstick nano. *Langmuir* 2010;26:16884–9.
- [129] Yang C, Zibrowius B, Schüth F. A novel synthetic route for negatively charged ordered mesoporous silica SBA-15. *Chem Commun* 2003;3:1772–3.
- [130] Colilla M, González B, Vallet-Regí M. Mesoporous silicananoparticles for the design of smart delivery nanodevices. *Biomater Sci* 2013;1:114–34.
- [131] Tarn D, Ashley CE, Xue M, Carnes EC, Zink JJ, Brinker CJ. Mesoporous silica nanoparticle nanocarriers: biofunctionality and biocompatibility. *Acc Chem Res* 2013;46:792–801.
- [132] Gawande MB, Goswami A, Asefa T, Guo H, Biradar AV, Peng D-L, et al. Core–shell nanoparticles: synthesis and applications in catalysis and electrocatalysis. *Chem Soc Rev* 2015;44:7540–90.
- [133] Pang H, Zhou S, Wu L, Chen M, Gu G. Fabrication of silicone oil microcapsules with silica shell by miniemulsion method. *Colloids Surf A Physicochem Eng Asp* 2010;364:42–8.
- [134] Radulova GM, Slavova TG, Kralchevsky PA, Basheva ES, Marinova KG, Danov KD. Encapsulation of oils and fragrances by core-in-shell structures from silica particles, polymers and surfactants: the brick-and-mortar concept. *Colloids Surf A: Physicochem Eng Asp* 2018;559:351–64.
- [135] Zhang W, He S, Liu Y, Geng Q, Ding G, Guo M, et al. Preparation and characterization of novel functionalized prochloraz microcapsules using silica–alginate– elements as controlled release carrier materials. *ACS Appl Mater Interfaces* 2014;6:11783–90.
- [136] Sousa FL, Santos M, Rocha SM, Trindade T. Encapsulation of essential oils in SiO<sub>2</sub> microcapsules and release behaviour of volatile compounds. *J Microencapsul* 2014;31:627–35.
- [137] Zhao Z-B, Zhang D-M, Meng Y-F, Tai L, Jiang Y. One-pot fabrication of fluoride-silica@silica raspberry-like nanoparticles for superhydrophobic coating. *Ceram Int* 2016;42:14601–8.
- [138] Liu S, Latthe SS, Yang H, Liu B, Xing R. Raspberry-like superhydrophobic silica coatings with self-cleaning properties. *Ceram Int* 2015;41:11719–25.
- [139] Hwang HS, Lee SB, Park I. Fabrication of raspberry-like superhydrophobic hollow silica particles. *Mater Lett* 2010;64:2159–62.
- [140] Yu M, Wang Q, Zhang M, Deng Q, Chen D. Facile fabrication of raspberry-like composite microspheres for the construction of superhydrophobic films and applications in highly efficient oil–water separation. *RSC Adv* 2017;7:39471–9.
- [141] Fang X, Zhao X, Fang W, Chen C, Zheng N. Self-templating synthesis of hollow mesoporous silica and their applications in catalysis and drug delivery. *Nanoscale* 2013;5:2205–18.
- [142] Du X, He J. Spherical silica micro/nanomaterials with hierarchical structures: synthesis and applications. *Nanoscale*. 2011;3:3984–4002.
- [143] Yu M, Gu G, Meng W-D, Qing F-L. Superhydrophobic cotton fabric coating based on a complex layer of silica nanoparticles and perfluorooctylated quaternary ammonium silane coupling agent. *Appl Surf Sci* 2007;253:3669–73.

- [144] Bae GY, Min BG, Jeong YG, Lee SC, Jang JH, Koo GH. Superhydrophobicity of cotton fabrics treated with silica nanoparticles and water-repellent agent. *J Colloid Interface Sci* 2009;337:170–5.
- [145] Pereira C, Alves C, Monteiro A, Magén C, Pereira AM, Ibarra A, et al. Designing novel hybrid materials by one-pot co-condensation: from hydrophobic mesoporous silica nanoparticles to superamphiphobic cotton textiles. *ACS Appl Mater Interfaces* 2011;3:2289–99.
- [146] Jeong SA, Kang TJ. Superhydrophobic and transparent surfaces on cotton fabrics coated with silica nanoparticles for hierarchical roughness. *Text Res J* 2017;87:552–60.
- [147] Teli MD, Annaldewar BN. Superhydrophobic and ultraviolet protective nylon fabrics by modified nano silica coating. *J Text Inst* 2017;108:460–6.
- [148] Mohamed AL, El-Sheikh MA, Waly AI. Enhancement of flame retardancy and water repellency properties of cotton fabrics using silanol based nano composites. *Carbohydr Polym* 2014;102:727–37.
- [149] Aslanidou D, Karapanagiotis I, Panayiotou C. Superhydrophobic, superoleophobic coatings for the protection of silk textiles. *Prog Org Coat* 2016;97:44–52.
- [150] Carosio F, Laufer G, Alongi J, Camino G, Grunlan JC. Layer-by-layer assembly of silica-based flame retardant thin film on PET fabric. *Polym Degrad Stab* 2011;96:745–50.
- [151] Ayazi-Yazdi S, Karimi L, Mirjalili M, Karimnejad M. Fabrication of photochromic, hydrophobic, antibacterial, and ultraviolet-blocking cotton fabric using silica nanoparticles functionalized with a photochromic dye. *J Text Inst* 2017;108:856–63.
- [152] El-Naggar ME, Hassabo AG, Mohamed AL, Shaheen TI. Surface modification of SiO<sub>2</sub> coated ZnO nanoparticles for multifunctional cotton fabrics. *J Colloid Interface Sci* 2017;498:413–22.
- [153] El-Gabry LK, Allam OG, Hakeim OA. Surface functionalization of viscose and polyester fabrics toward antibacterial and coloration properties. *Carbohydr Polym* 2013;92:353–9.
- [154] Juan D, Li Z, Shuilin C. Wash fastness of dyed fabric treated by the sol-gel process. *Color Technol* 2005;121:29–36.
- [155] Mahltig B, Textor T. Combination of silica sol and dyes on textiles. *J Sol-Gel Sci Technol* 2006;39:111–18.
- [156] Hendrick E, Frey M, Herz E, Wiesner U. Cellulose acetate fibers with fluorescing nanoparticles for anti-counterfeiting and ph-sensing applications. *J Eng Fiber Fabr* 2010;5:21–30.
- [157] Pinto TV, Costa P, Sousa CM, Sousa CAD, Pereira C, Silva CJSM, et al. Screen-printed photochromic textiles through new inks based on SiO<sub>2</sub> @naphthopyran nanoparticles. *ACS Appl Mater Interfaces* 2016;8:28935–45.
- [158] Lin T, Wang X. Nano related research in fibres and textiles. *Int J Nanotechnol* 2009;6:579–98.
- [159] Cheng T, Lin T, Brady R, Wang X. Fast response photochromic textiles from hybrid silica surface coating. *Fibers Polym* 2008;9:301–6.
- [160] Cheng T, Lin T, Brady R, Wang X. Photochromic fabrics with improved durability and photochromic performance. *Fibers Polym* 2008;9:521–6.
- [161] Ribeiro LS, Pinto T, Monteiro A, Soares OSGP, Pereira C, Freire C, et al. Silica nanoparticles functionalized with a thermochromic dye for textile applications. *J Mater Sci* 2013;48:5085–92.
- [162] Mahltig B, Textor T. *Nanosols and textiles*. 1st ed. Singapore: World Scientific Publishing Co. Pte. Ltd.; 2008.

- [163] Laufer G, Carosio F, Martinez R, Camino G, Grunlan JC. Growth and fire resistance of colloidal silica-polyelectrolyte thin film assemblies. *J Colloid Interface Sci* 2011;356:69–77.
- [164] Hashemikia S, Hemmatinejad N, Ahmadi E, Montazer M. Antibacterial and anti-inflammatory drug delivery properties on cotton fabric using betamethasone-loaded mesoporous silica particles stabilized with chitosan and silicone softener. *Drug Deliv* 2016;23:2946–55.
- [165] Nayolor da Rocha Gomes JI. Compounds and reactive nanoparticles of silica with insect repellent activity on textile substrate and other materials and respective process of preparation and binding. WO/2014/200378; 2014.
- [166] Verma R, Gangwar J, Srivastava AK. Multiphase TiO<sub>2</sub> nanostructures: a review of efficient synthesis, growth mechanism, probing capabilities, and applications in bio-safety and health. *RSC Adv* 2017;7:44199–224.
- [167] Ni M, Leung MKH, Leung DYC, Sumathy K. A review and recent developments in photocatalytic water-splitting using TiO<sub>2</sub> for hydrogen production. *Renew Sustain Energy Rev* 2007;11:401–25.
- [168] Grätzel M. Dye-sensitized solar cells. *J Photochem Photobiol C Photochem Rev* 2003;4:145–53.
- [169] Jing L, Zhou W, Tian G, Fu H. Surface tuning for oxide-based nanomaterials as efficient photocatalysts. *Chem Soc Rev* 2013;42:9509–49.
- [170] Montazer M, Pakdel E. Functionality of nano titanium dioxide on textiles with future aspects: focus on wool. *J Photochem Photobiol C Photochem Rev* 2011;12:293–303.
- [171] Radetić M. Functionalization of textile materials with TiO<sub>2</sub> nanoparticles. *J Photochem Photobiol C Photochem Rev* 2013;16:62–76.
- [172] Zhu G-N, Wang Y-G, Xia Y-Y. Ti-based compounds as anode materials for Li-ion batteries. *Energy Env Sci* 2012;5:6652–67.
- [173] Zhou H, Zhang Y. Electrochemically self-doped TiO<sub>2</sub> nanotube arrays for supercapacitors. *J Phys Chem C* 2014;118:5626–36.
- [174] Wang X, Li Z, Shi J, Yu Y. One-dimensional titanium dioxide nanomaterials: nanowires, nanorods, and nanobelts. *Chem Rev* 2014;114:9346–84.
- [175] Rahimi N, Pax RA, Gray EM. Review of functional titanium oxides. I: TiO<sub>2</sub> and its modifications. *Prog Solid State Chem* 2016;44:86–105.
- [176] Khataee A, Mansoori GA. Nanostructured titanium dioxide materials. 1st ed. Singapore: World Scientific Publishing Co. Pte. Ltd; 2011.
- [177] Frantz C, Lauria A, Manzano CV, Guerra-Núñez C, Niederberger M, Storrer C, et al. Nonaqueous sol–gel synthesis of anatase nanoparticles and their electrophoretic deposition in porous alumina. *Langmuir* 2017;33:12404–18.
- [178] Sugimoto T, Zhou X. Synthesis of uniform anatase TiO<sub>2</sub> nanoparticles by the gel–sol method: 2. Adsorption of OH<sup>−</sup> ions to Ti(OH)<sub>4</sub> gel and TiO<sub>2</sub> particles. *J Colloid Interface Sci* 2002;252:347–53.
- [179] Sugimoto T, Zhou X, Muramatsu A. Synthesis of uniform anatase TiO<sub>2</sub> nanoparticles by gel–sol method: 3. Formation process and size control. *J Colloid Interface Sci* 2003;259:43–52.
- [180] Kanie K, Sugimoto T. Shape control of anatase TiO<sub>2</sub> nanoparticles by amino acids in a gel–sol system. *Chem Commun* 2004;4:1584–5.
- [181] Kotskechagia T, Cellesi F, Thomas A, Niederberger M, Tirelli N. Preparation of ligand-free TiO<sub>2</sub> (anatase) nanoparticles through a nonaqueous process and their surface functionalization. *Langmuir* 2008;24:6988–97.

- [182] Oguri Y, Riman RE, Bowen HK. Processing of anatase prepared from hydrothermally treated alkoxy-derived hydrous titania. *J Mater Sci* 1988;23:2897–904.
- [183] Jeon S, Braun PV. Hydrothermal synthesis of Er-doped luminescent TiO<sub>2</sub> nanoparticles. *Chem Mater* 2003;15:1256–63.
- [184] Cheng H, Ma J, Zhao Z, Qi L. Hydrothermal preparation of uniform nanosize rutile and anatase particles. *Chem Mater* 1995;7:663–71.
- [185] Dinh C-T, Nguyen T-D, Kleitz F, Do T-O. Shape-controlled synthesis of highly crystalline titania nanocrystals. *ACS Nano* 2009;3:3737–43.
- [186] Carp O, Huisman CL, Reller A. Photoinduced reactivity of titanium dioxide. *Prog Solid State Chem* 2004;32:33–177.
- [187] Chen X, Mao SS. Titanium dioxide nanomaterials: synthesis, properties, modifications, and applications. *Chem Rev* 2007;107:2891–959.
- [188] Wu J-J, Yu C-C. Aligned TiO<sub>2</sub> nanorods and nanowalls. *J Phys Chem B* 2004;108:3377–9.
- [189] Chen CA, Chen YM, Korotcov A, Huang YS, Tsai DS, Tiong KK. Growth and characterization of well-aligned densely-packed rutile TiO<sub>2</sub> nanocrystals on sapphire substrates via metal-organic chemical vapor deposition. *Nanotechnology* 2008;19:075611.
- [190] Rajh T, Dimitrijevic NM, Bissonnette M, Koritarov T, Konda V. Titanium dioxide in the service of the biomedical revolution. *Chem Rev* 2014;114:10177–216.
- [191] Song Y-Y, Hildebrand H, Schmuki P. Photoinduced release of active proteins from TiO<sub>2</sub> surfaces. *Electrochem Commun* 2009;11:1429–33.
- [192] Meroni D, Lo Presti L, Di Liberto G, Ceotto M, Acres RG, Prince KC, et al. A close look at the structure of the TiO<sub>2</sub>-APTES interface in hybrid nanomaterials and its degradation pathway: an experimental and theoretical study. *J Phys Chem C* 2017;121:430–40.
- [193] Chen Q, Yakovlev NL. Adsorption and interaction of organosilanes on TiO<sub>2</sub> nanoparticles. *Appl Surf Sci* 2010;257:1395–400.
- [194] Zhao J, Milanova M, Warmoeskerken MMCG, Dutschk V. Surface modification of TiO<sub>2</sub> nanoparticles with silane coupling agents. *Colloids Surf A: Physicochem Eng Asp* 2012;413:273–9.
- [195] Abdelraheem WHM, Patil MK, Nadagouda MN, Dionysiou DD. Hydrothermal synthesis of photoactive nitrogen- and boron- codoped TiO<sub>2</sub> nanoparticles for the treatment of bisphenol A in wastewater: synthesis, photocatalytic activity, degradation byproducts and reaction pathways. *Appl Catal B: Env* 2019;241:598–611.
- [196] Katoueizadeh E, Zebarjad SM, Janghorban K. Investigation of mechanical characteristics of functionalized cotton textiles by N-doped TiO<sub>2</sub> nanoparticles. *Mater Chem Phys* 2018;218:239–45.
- [197] Stan MS, Badea MA, Pircalabioru GG, Chifiriuc MC, Diamandescu L, Dumitrescu I, et al. Designing cotton fibers impregnated with photocatalytic graphene oxide/Fe, N-doped TiO<sub>2</sub> particles as prospective industrial self-cleaning and biocompatible textiles. *Mater Sci Eng C* 2019;94:318–32.
- [198] Shen S, Chen J, Wang M, Sheng X, Chen X, Feng X, et al. Titanium dioxide nanostructures for photoelectrochemical applications. *Prog Mater Sci* 2018;98:299–385.
- [199] Mishra A, Butola BS. Deposition of Ag doped TiO<sub>2</sub> on cotton fabric for wash durable UV protective and antibacterial properties at very low silver concentration. *Cellulose* 2017;24:3555–71.
- [200] Park HS, Kim DH, Kim SJ, Lee KS. The photocatalytic activity of 2.5wt% Cu-doped TiO<sub>2</sub> nano powders synthesized by mechanical alloying. *J Alloy Compd* 2006;415:51–5.

- [201] Obregón S, Muñoz-Batista MJ, Fernández-García M, Kubacka A, Colón G. Cu–TiO<sub>2</sub> systems for the photocatalytic H<sub>2</sub> production: influence of structural and surface support features. *Appl Catal B: Env* 2015;179:468–78.
- [202] Saqib NU, Adnan R, Shah I. A mini-review on rare earth metal-doped TiO<sub>2</sub> for photocatalytic remediation of wastewater. *Env Sci Pollut Res* 2016;23:15941–51.
- [203] Leary R, Westwood A. Carbonaceous nanomaterials for the enhancement of TiO<sub>2</sub> photocatalysis. *Carbon* 2011;49:741–72.
- [204] Yang M, Zhang N, Xu Y. Synthesis of fullerene–, carbon nanotube–, and graphene–TiO<sub>2</sub> nanocomposite photocatalysts for selective oxidation: a comparative study. *ACS Appl Mater Interfaces* 2013;5:1156–64.
- [205] Martins AC, Cazetta AL, Pezoti O, Souza JRB, Zhang T, Pilau EJ, et al. Sol-gel synthesis of new TiO<sub>2</sub>/activated carbon photocatalyst and its application for degradation of tetracycline. *Ceram Int* 2017;43:4411–18.
- [206] Rabhi S, Belkacemi H, Bououdina M, Kerrami A, Ait Brahem L, Sakher E. Effect of Ag doping of TiO<sub>2</sub> nanoparticles on anatase-rutile phase transformation and excellent photo-degradation of amlodipine besylate. *Mater Lett* 2019;236:640–3.
- [207] Margan P, Haghighi M. Hydrothermal-assisted sol–gel synthesis of Cd-doped TiO<sub>2</sub> nanophotocatalyst for removal of acid orange from wastewater. *J Sol-Gel Sci Technol* 2017;81:556–69.
- [208] Ansari SA, Khan MM, Ansari MO, Cho MH. Nitrogen-doped titanium dioxide (N-doped TiO<sub>2</sub>) for visible light photocatalysis. *N J Chem* 2016;40:3000–9.
- [209] Karimi L, Yazdanshenas ME, Khajavi R, Rashidi A, Mirjalili M. Using graphene/TiO<sub>2</sub> nanocomposite as a new route for preparation of electroconductive, self-cleaning, antibacterial and antifungal cotton fabric without toxicity. *Cellulose* 2014;21:3813–27.
- [210] Karimi L, Yazdanshenas ME, Khajavi R, Rashidi A, Mirjalili M. Functional finishing of cotton fabrics using graphene oxide nanosheets decorated with titanium dioxide nanoparticles. *J Text Inst* 2016;107:1122–34.
- [211] Tung WS, Daoud WA. Effect of wettability and silicone surface modification on the self-cleaning functionalization of wool. *J Appl Polym Sci* 2009;112:235–43.
- [212] Li M, Deng T, Liu S, Zhang F, Zhang G. Superhydrophilic surface modification of fabric via coating with nano-TiO<sub>2</sub> by UV and alkaline treatment. *Appl Surf Sci* 2014;297:147–52.
- [213] Cardoso GV, Di Salvo Mello LR, Zanatta P, Cava S, Raubach CW, Moreira ML. Physico-chemical description of titanium dioxide–cellulose nanocomposite formation by microwave radiation with high thermal stability. *Cellulose* 2018;25:2331–41.
- [214] Yu M, Wang Z, Liu H, Xie S, Wu J, Jiang H, et al. Laundering durability of photocatalyzed self-cleaning cotton fabric with TiO<sub>2</sub> nanoparticles covalently immobilized. *ACS Appl Mater Interfaces* 2013;5:3697–703.
- [215] Emami F, Shekarriz S, Shariatinia Z, Moridi Mahdiah Z. Self-cleaning properties of nylon 6 fabrics treated with corona and TiO<sub>2</sub> nanoparticles under both ultraviolet and daylight irradiations. *Fibers Polym* 2018;19:1014–23.
- [216] Kowalczyk D, Brzeziński S, Kamińska I. Multifunctional nanocoating finishing of polyester/cotton woven fabric by the sol-gel method. *Text Res J* 2018;88:946–56.
- [217] Foss C, Feldheim D. Metal nanoparticles: synthesis, characterization, and applications. 1st ed. New York: CRC Press; 2001.
- [218] Hussain CM, editor. Handbook of nanomaterials for industrial applications. 1st ed. Cambridge: Elsevier; 2018. Available from: <https://doi.org/10.1016/C2016-0-04427-3>.
- [219] Polte J. Fundamental growth principles of colloidal metal nanoparticles—a new perspective. *CrystEngComm*. 2015;17:6809–30.

- [220] Arvizo RR, Bhattacharyya S, Kudgus RA, Giri K, Bhattacharya R, Mukherjee P. Intrinsic therapeutic applications of noble metal nanoparticles: past, present and future. *Chem Soc Rev*, 41. 2012. p. 2943–70.
- [221] Cepero González M, Padial Ruz R, Rojas Ruiz FJ, Romero Sánchez D, De La Cruz Márquez JC. The bakerian lecture: experimental relations of gold (and other metals) to light. *Philos Trans R Soc Lond* 1857;147:145–81.
- [222] Brust M, Walker M, Bethell D, Schiffrin DJ, Whyman R. Synthesis of thiol-derivatised gold nanoparticles in a two-phase Liquid–Liquid system. *J Chem Soc, Chem Commun* 1994;801–2.
- [223] Frattini A, Pellegrini N, Nicastro D, de Sanctis O. Effect of amine groups in the synthesis of Ag nanoparticles using aminosilanes. *Mater Chem Phys* 2005;94:148–52.
- [224] Herricks T, Chen J, Xia Y. Polyol synthesis of platinum nanoparticles: control of morphology with sodium nitrate. *Nano Lett* 2004;4:2367–71.
- [225] Gawande MB, Goswami A, Felpin F-X, Asefa T, Huang X, Silva R, et al. Cu and Cu-based nanoparticles: synthesis and applications in catalysis. *Chem Rev* 2016;116:3722–811.
- [226] Winnischofer H, Rocha TCR, Nunes WC, Socolovsky LM, Knobel M, Zanchet D. Chemical synthesis and structural characterization of highly disordered Ni colloidal nanoparticles. *ACS Nano* 2008;2:1313–19.
- [227] Wang C, Hu Y, Lieber CM, Sun S. Ultrathin Au nanowires and their transport properties. *J Am Chem Soc* 2008;130:8902–3.
- [228] Tian B, Xie P, Kempa TJ, Bell DC, Lieber CM. Single-crystalline kinked semiconductor nanowire superstructures. *Nat Nanotechnol* 2009;4:824–9.
- [229] Zou J, Xu Y, Hou B, Wu D, Sun Y. Controlled growth of silver nanoparticles in a hydrothermal process. *China Particuol* 2007;5:206–12.
- [230] Yin A-X, Liu W-C, Ke J, Zhu W, Gu J, Zhang Y-W, et al. Ru nanocrystals with shape-dependent surface-enhanced Raman spectra and catalytic properties: controlled synthesis and DFT calculations. *J Am Chem Soc* 2012;134:20479–89.
- [231] Yang Y, Zhong X-L, Zhang Q, Blackstad LG, Fu Z-W, Li Z-Y, et al. The role of etching in the formation of Ag nanoplates with straight, curved and wavy edges and comparison of their SERS properties. *Small* 2014;10:1430–7.
- [232] Majerič P, Jenko D, Friedrich B, Rudolf R. Formation mechanisms for gold nanoparticles in a redesigned Ultrasonic Spray Pyrolysis. *Adv Powder Technol* 2017;28:876–83.
- [233] Serga V, Maiorov M, Cvetkovs A, Krumina A, Popov AI. Fabrication and characterization of magnetic FePt nanoparticles prepared by extraction–pyrolysis method. *Chemija* 2018;29:109–14.
- [234] Kim JH. PhD Thesis, Generation of size-monodisperse metal nanoparticles by spray pyrolysis. College Park: University of Maryland; 2003.
- [235] Lee KH, Rah SC, Kim S-G. Formation of monodisperse silver nanoparticles in poly(vinylpyrrolidone) matrix using spray pyrolysis. *J Sol-Gel Sci Technol* 2008;45:187–93.
- [236] Dong H, Chen Y-C, Feldmann C. Polyol synthesis of nanoparticles: status and options regarding metals, oxides, chalcogenides, and non-metal elements. *Green Chem* 2015;17:4107–32.
- [237] Viau G, Ravel F, Acher O, Fiévet-Vincent F, Fiévet F. Preparation and microwave characterization of spherical and monodisperse Co<sub>20</sub>Ni<sub>80</sub> particles. *J Appl Phys* 1994;76:6570–2.
- [238] Viau G, Fiévet-Vincent F, Fiévet F. Monodisperse iron-based particles: precipitation in liquid polyols. *J Mater Chem* 1996;6:1047–53.

- [239] Renteria VM, Campero A, Garcia JM. Thermochromic properties of silver colloids embedded in SiO<sub>2</sub> gels. *J Sol-Gel Sci Technol* 1998;13:663–6.
- [240] Bansal V, Rautaray D, Ahmad A, Sastry M. Biosynthesis of zirconia nanoparticles using the fungus *Fusarium oxysporum*. *J Mater Chem* 2004;14:3303–5.
- [241] Armendariz V, Herrera I, Peralta-videa JR, Jose-yacaman M, Troiani H, Santiago P, et al. Size controlled gold nanoparticle formation by *Avena sativa* biomass: use of plants in nanobiotechnology. *J Nanopart Res* 2004;6:377–82.
- [242] Bansal V, Poddar P, Ahmad A, Sastry M. Room-temperature biosynthesis of ferroelectric barium titanate nanoparticles. *J Am Chem Soc* 2006;128:11958–63.
- [243] Gericke M, Pinches A. Biological synthesis of metal nanoparticles. *Hydrometallurgy* 2006;83:132–40.
- [244] Singh P, Kim Y-J, Zhang D, Yang D-C. Biological synthesis of nanoparticles from plants and microorganisms. *Trends Biotechnol* 2016;34:588–99.
- [245] Kang H, Buchman JT, Rodriguez RS, Ring HL, He J, Bantz KC, et al. Stabilization of silver and gold nanoparticles: preservation and improvement of plasmonic functionalities. *Chem Rev* 2019;119:664–99.
- [246] Motl NE, Smith AF, DeSantis CJ, Skrabalak SE. Engineering plasmonic metal colloids through composition and structural design. *Chem Soc Rev* 2014;43:3823–34.
- [247] Elmaaty TA, El-Nagare K, Raouf S, Abdelfattah K, El-Kadi S, Abdelaziz E. One-step green approach for functional printing and finishing of textiles using silver and gold NPs. *RSC Adv* 2018;8:25546–57.
- [248] Tang B, Li J, Hou X, Afrin T, Sun L, Wang X. Colorful and antibacterial silk fiber from anisotropic silver nanoparticles. *Ind Eng Chem Res* 2013;52:4556–63.
- [249] Zheng Y, Xiao M, Jiang S, Ding F, Wang J. Coating fabrics with gold nanorods for colouring, UV-protection, and antibacterial functions. *Nanoscale* 2013;5:788–95.
- [250] Tang B, Sun L, Kaur J, Yu Y, Wang X. In-situ synthesis of gold nanoparticles for multifunctionalization of silk fabrics. *Dye Pigm* 2014;103:183–90.
- [251] Tang B, Sun L, Li J, Kaur J, Zhu H, Qin S, et al. Functionalization of bamboo pulp fabrics with noble metal nanoparticles. *Dye Pigm* 2015;113:289–98.
- [252] Tang B, Lin X, Zou F, Fan Y, Li D, Zhou J, et al. In situ synthesis of gold nanoparticles on cotton fabric for multifunctional applications. *Cellulose* 2017;24:4547–60.
- [253] Johnston JH, Lucas KA. Nanogold synthesis in wool fibres: novel colourants. *Gold Bull* 2011;44:85–9.
- [254] Kelly FM, Johnston JH. Colored and functional silver nanoparticle – wool fiber composites. *ACS Appl Mater Interfaces* 2011;3:1083–92.
- [255] Wang X, Gao W, Xu S, Xu W. Luminescent fibers: in situ synthesis of silver nanoclusters on silk via ultraviolet light-induced reduction and their antibacterial activity. *Chem Eng J* 2012;210:585–9.
- [256] Zhang P, Lan J, Wang Y, Xiong ZH, Huang CZ. Luminescent golden silk and fabric through in situ chemically coating pristine-silk with gold nanoclusters. *Biomaterials* 2015;36:26–32.
- [257] Panigrahi R, Srivastava SK. Tollen's reagent assisted synthesis of hollow polyaniline microsphere/Ag nanocomposite and its applications in sugar sensing and electromagnetic shielding. *Mater Res Bull* 2015;64:33–41.
- [258] Chung DDL. Materials for electromagnetic interference shielding. *J Mater Eng Perform* 2000;9:350–4.



- [259] Li J, Liu H, Guo J, Hu Z, Wang Z, Wang B, et al. Flexible, conductive, porous, fibrillar polymer–gold nanocomposites with enhanced electromagnetic interference shielding and mechanical properties. *J Mater Chem C* 2017;5:1095–105.
- [260] Kardarian K, Busani T, Osório I, Domingos H, Igreja R, Franco R, et al. Sintering of nanoscale silver coated textiles, a new approach to attain conductive fabrics for electromagnetic shielding. *Mater Chem Phys* 2014;147:815–22.
- [261] Kikam AV, Prasad BLV, Kulkarni AA. Wet Chemical Synthesis of Metal Oxide Nanoparticles: A Review. *CrystEngComm* 2018;20:5091–107.
- [262] Liu Y, Chen T, Wu C, Qiu L, Hu R, Li J, et al. Facile surface functionalization of hydrophobic magnetic nanoparticles. *J Am Chem Soc* 2014;136:12552–5.
- [263] Salunkhe RR, Kaneti YV, Yamauchi Y. Metal–organic framework-derived nanoporous metal oxides toward supercapacitor applications: progress and prospects. *ACS Nano* 2017;11:5293–308.
- [264] Yang X, Wang Y, Xiong H, Xia Y. Interfacial synthesis of porous  $\text{MnO}_2$  and its application in electrochemical capacitor. *Electrochim Acta* 2007;53:752–7.
- [265] Pal J, Pal T. Faceted metal and metal oxide nanoparticles: design, fabrication and catalysis. *Nanoscale* 2015;7:14159–90.
- [266] Zhang Y, Li L, Su H, Huang W, Dong X. Binary metal oxide: advanced energy storage materials in supercapacitors. *J Mater Chem A* 2015;3:43–59.
- [267] Darr JA, Zhang J, Makwana NM, Weng X. Continuous hydrothermal synthesis of inorganic nanoparticles: applications and future directions. *Chem Rev* 2017;117:11125–238.
- [268] Chen D, Wang Q, Wang R, Shen G. Ternary oxide nanostructured materials for supercapacitors: a review. *J Mater Chem A* 2015;3:10158–73.
- [269] Mao Y, Park T-J, Wong SS. Synthesis of classes of ternary metal oxide nanostructures. *Chem Commun* 2005;5721–35.
- [270] Cruz IF, Freire C, Araújo JP, Pereira C, Pereira AM. Multifunctional ferrite nanoparticles: from current trends toward the future. In: El-Gendy AA, Barandiarán JM, Hadimani RL, editors. *Magn. Nanostructured Mater. From Lab to Fab*. 1st ed. Elsevier; 2018. p. 59–116.
- [271] Wu W, Wu Z, Yu T, Jiang C, Kim W-S. Recent progress on magnetic iron oxide nanoparticles: synthesis, surface functional strategies and biomedical applications. *Sci Technol Adv Mater* 2015;16:023501.
- [272] Reddy LH, Arias JL, Nicolas J, Couvreur P. Magnetic nanoparticles: design and characterization, toxicity and biocompatibility, pharmaceutical and biomedical applications. *Chem Rev* 2012;112:5818–78.
- [273] Pereira C, Costa RS, Lopes L, Bachiller-Baeza B, Rodríguez-Ramos I, Guerrero-Ruiz A, et al. Multifunctional mixed valence N-doped  $\text{CNT}@\text{MFe}_2\text{O}_4$  hybrid nanomaterials: from engineered one-pot coprecipitation to application in energy storage paper supercapacitors. *Nanoscale* 2018;10:12820–40.
- [274] Wang D, Astruc D. Fast-growing field of magnetically recyclable nanocatalysts. *Chem Rev* 2014;114:6949–85.
- [275] Zhao Q, Yan Z, Chen C, Chen J. Spinels: controlled preparation, oxygen reduction/evolution reaction application, and beyond. *Chem Rev* 2017;117:10121–211.
- [276] Anandan S, Selvamani T, Prasad GG, Asiri AM, Wu JJ. Magnetic and catalytic properties of inverse spinel  $\text{CuFe}_2\text{O}_4$  nanoparticles. *J Magn Magn Mater* 2017;432:437–43.
- [277] Nam D-H, Bushuyev OS, Li J, De Luna P, Seifitokaldani A, Dinh C-T, et al. Metal–organic frameworks mediate Cu coordination for selective  $\text{CO}_2$  electroreduction. *J Am Chem Soc* 2018;140:11378–86.

- [278] Sun S, Zeng H, Robinson DB, Raoux S, Rice PM, Wang SX, et al. Monodisperse  $MFe_2O_4$  ( $M = Fe, Co, Mn$ ) nanoparticles. *J Am Chem Soc* 2004;126:273–9.
- [279] Yi DK, Lee SS, Papaefthymiou GC, Ying JY. Nanoparticle architectures templated by  $SiO_2/Fe_2O_3$  nanocomposites. *Chem Mater* 2006;18:614–19.
- [280] Nguyen T-D. From formation mechanisms to synthetic methods toward shape-controlled oxide nanoparticles. *Nanoscale* 2013;5:9455–82.
- [281] Pereira C, Pereira AM, Fernandes C, Rocha M, Mendes R, Fernández-García MP, et al. Superparamagnetic  $MFe_2O_4$  ( $M = Fe, Co, Mn$ ) nanoparticles: tuning the particle size and magnetic properties through a novel one-step coprecipitation route. *Chem Mater* 2012;24:1496–504.
- [282] Massart R. Preparation of aqueous magnetic liquids in alkaline and acidic media. *IEEE Trans Magn* 1981;17:1247–8.
- [283] Rao BG, Mukherjee D, Reddy BM. Novel approaches for preparation of nanoparticles. In: Grumezescu AM, Ficaí D, editors. *Nanostructures Nov. Ther.*. 1st ed. Cambridge: Elsevier; 2017. p. 1–36.
- [284] Laurent S, Forge D, Port M, Roch A, Robic C, Vander Elst L, et al. Magnetic iron oxide nanoparticles: synthesis, stabilization, vectorization, physicochemical characterizations, and biological applications. *Chem Rev* 2008;108:2064–110.
- [285] Sutka A, Mezinskis G. Sol-gel auto-combustion synthesis of spinel-type ferrite nanomaterials. *Front Mater Sci* 2012;6:128–41.
- [286] del Monte F, Morales MP, Levy D, Fernandez A, Ocaña M, Roig A, et al. Formation of  $\gamma\text{-Fe}_2O_3$  isolated nanoparticles in a silica matrix. *Langmuir* 1997;13:3627–34.
- [287] Junliang L, Yanwei Z, Cuijing G, Wei Z, Xiwei Y. One-step synthesis of barium hexaferrite nano-powders via microwave-assisted sol-gel auto combustion. *J Eur Ceram Soc* 2010;30:993–7.
- [288] Zhenyu L, Guangliang X, Yalin Z. Microwave assisted low temperature synthesis of MnZn ferrite nanoparticles. *Nanoscale Res Lett* 2007;2:40–3.
- [289] Tatarchuk T, Bououdina M, Judith Vijaya J, John Kennedy L. In: Fesenko O, Yatsenko L, editors. *Spinel ferrite nanoparticles: synthesis, crystal structure, properties, and perspective applications*. Cham: Springer International Publishing; 2017. p. 305–25.
- [290] Kefeni KK, Msagati TAM, Mamba BB. Ferrite nanoparticles: synthesis, characterisation and applications in electronic device. *Mater Sci Eng B* 2017;215:37–55.
- [291] Verma S, Pravarthana D. One-pot synthesis of highly monodispersed ferrite nanocrystals: surface characterization and magnetic properties. *Langmuir* 2011;27:13189–97.
- [292] Hu F, MacRenaris KW, Waters EA, Liang T, Schultz-Sikma EA, Eckermann AL, et al. Ultrasmall, water-soluble magnetite nanoparticles with high relaxivity for magnetic resonance imaging. *J Phys Chem C* 2009;113:20855–60.
- [293] Gupta AK, Gupta M. Synthesis and surface engineering of iron oxide nanoparticles for biomedical applications. *Biomaterials* 2005;26:3995–4021.
- [294] Pullar RC. Hexagonal ferrites: a review of the synthesis, properties and applications of hexaferrite ceramics. *Prog Mater Sci* 2012;57:1191–334.
- [295] Palneedi H, Annapureddy V, Priya S, Ryu J. Status and perspectives of multiferroic magnetoelectric composite materials and applications. *Actuators* 2016;5:9.
- [296] Ataie A, Heshmati-Manesh S, Kazempour H. Synthesis of barium hexaferrite by the co-precipitation method using acetate precursor. *J Mater Sci* 2002;37:2125–8.
- [297] Rashid AU, Southern P, Darr JA, Awan S, Manzoor S. Strontium hexaferrite ( $SrFe_{12}O_{19}$ ) based composites for hyperthermia applications. *J Magn Magn Mater* 2013;344:134–9.

- [298] Xu P, Han X, Wang M. Synthesis and magnetic properties of  $\text{BaFe}_{12}\text{O}_{19}$  hexaferrite nanoparticles by a reverse microemulsion technique. *J Phys Chem C* 2007;111:5866–70.
- [299] Chatterjee A, Das D, Pradhan SK, Chakravorty D. Synthesis of nanocrystalline nickel-zinc ferrite by the sol-gel method. *J Magn Magn Mater* 1993;127:214–18.
- [300] Singh VP, Jasrotia R, Kumar R, Raizada P, Thakur S, Batoo KM, et al. A current review on the synthesis and magnetic properties of M-Type hexaferrites material. *World J Condens Matter Phys* 2018;08:36–61.
- [301] Rantanen J. Radiation carcinogenesis. *J Toxicol Env Health* 1980;6:971–6.
- [302] Nambiar S, Yeow JTW. Polymer-composite materials for radiation protection. *ACS Appl Mater Interfaces* 2012;4:5717–26.
- [303] Nambiar S, Osei EK, Yeow JTW. Polymer nanocomposite-based shielding against diagnostic X-rays. *J Appl Polym Sci* 2013;127:4939–46.
- [304] Chai H, Tang X, Ni M, Chen F, Zhang Y, Chen D, et al. Preparation and properties of novel, flexible, lead-free X-ray-shielding materials containing tungsten and bismuth(III) oxide. *J Appl Polym Sci* 2016;133:43012–17.
- [305] Aral N, Banu Nergis F, Candan C. An alternative X-ray shielding material based on coated textiles. *Text Res J* 2016;86:803–11.
- [306] Çetin H, Yurt A, Yüksel SH. The absorption properties of lead-free garments for use in radiation protection. *Radiat Prot Dosimetry* 2016;173:345–50.
- [307] Aral N, Nergis FB, Candan C. The X-ray attenuation and the flexural properties of lead-free coated fabrics. *J Ind Text* 2017;47:252–68.
- [308] Günther K, Giebing C, Askani A, Leisegang T, Krieg M, Kyosev Y, et al. Cellulose/inorganic-composite fibers for producing textile fabrics of high X-ray absorption properties. *Mater Chem Phys* 2015;167:125–35.
- [309] Pulford S, Fergusson M. A textile platform for non-lead radiation shielding apparel. *J Text Inst* 2016;107:1610–16.
- [310] Mahltig B, Günther K, Askani A, Bohnet F, Brinkert N, Kyosev Y, et al. X-ray-protective organic/inorganic fiber—along the textile chain from fiber production to clothing application. *J Text Inst* 2017;108:1975–84.
- [311] Maghrabi HA, Vijayan A, Deb P, Wang L. Bismuth oxide-coated fabrics for X-ray shielding. *Text Res J* 2016;86:649–58.
- [312] Botelho MZ, Künzel R, Okuno E, Levenhagen RS, Basegio T, Bergmann CP. X-ray transmission through nanostructured and microstructured  $\text{CuO}$  materials. *Appl Radiat Isot* 2011;69:527–30.
- [313] Singh AK, Singh RK, Sharma B, Tyagi AK. Characterization and biocompatibility studies of lead free X-ray shielding polymer composite for healthcare application. *Radiat Phys Chem* 2017;138:9–15.
- [314] Maghrabi HA, Vijayan A, Mohaddes F, Deb P, Wang L. Evaluation of X-ray radiation shielding performance of barium sulphate-coated fabrics. *Fibers Polym* 2016;17: 2047–54.
- [315] Benzon HT. Fluoroscopy and radiation safety. In: Benzon HT, Raja SN, Fishman SM, Liu SS, Cohen SP, editors. *Essentials pain med.* 4th ed. Philadelphia: Elsevier; 2018. p. 703–14.
- [316] Qu L, Tian M, Zhang X, Guo X, Zhu S, Han G, et al. Barium sulfate/regenerated cellulose composite fiber with X-ray radiation resistance. *J Ind Text* 2015;45:352–67.
- [317] Botelho MZ, Kunzel R, Okuno E, Levenhagen RS, Basegio T, Bergmann CP. X-ray transmission through nanostructured and microstructured tin oxide materials. *Appl Radiat Isot* 2011;69:527–30.

- [318] Cho J, Kim M. Performance analysis of low-level radiation shielding sheet with diamagnetic nanoparticles. *J Magn* 2015;20:103–9.
- [319] Li Q, Wei Q, Zheng W, Zheng Y, Okosi N, Wang Z, et al. Enhanced radiation shielding with conformal light-weight nanoparticle-polymer composite. *ACS Appl Mater Interfaces* 2018;10:35510–15.
- [320] Pastore R, Micheli D, Marchetti M, Angelini E. X-ray attenuation properties of carbon nanotubes filled composite materials. 2016 IEEE Metrol. Aerosp. IEEE; 2016. p. 619–23.
- [321] Fujimori T, Tsuruoka S, Fugetsu B, Maruyama S, Tanioka A, Terrones M, et al. Enhanced X-ray shielding effects of carbon nanotubes. *Mater Express* 2011;1:273–8.
- [322] Viegas J, Silva LA, Batista AMS, Furtado CA, Nascimento JP, Faria LO. Increased X-ray attenuation efficiency of graphene-based nanocomposite. *Ind Eng Chem Res* 2017;56:11782–90.
- [323] Sedighi A, Montazer M, Mazinani S. Fabrication of electrically conductive superparamagnetic fabric with microwave attenuation, antibacterial properties and UV protection using PEDOT/magnetite nanoparticles. *Mater Des* 2018;160:34–47.
- [324] Jeon I, Wook D, Ashok N, Baek J-B. Functionalization of carbon nanotubes. In: Yellampalli S, editor. *Carbon nanotubes-polymer nanocomposites*. InTechOpen; 2011. Available from: <https://doi.org/10.5772/18396>.
- [325] Li Z, Liu Z, Sun H, Gao C. Superstructured assembly of nanocarbons: fullerenes, nanotubes, and graphene. *Chem Rev* 2015;115:7046–117.
- [326] Geim AK, Novoselov KS. The rise of graphene. *Nat Mater* 2007;6:183–91.
- [327] Vicarelli L, Heerema SJ, Dekker C, Zandbergen HW. Controlling defects in graphene for optimizing the electrical properties of graphene nanodevices. *ACS Nano* 2015;9:3428–35.
- [328] Datsyuk V, Kalyva M, Papagelis K, Parthenios J, Tasis D, Siokou A, et al. Chemical oxidation of multiwalled carbon nanotubes. *Carbon* 2008;46:833–40.
- [329] Hirsch A. Functionalization of single-walled carbon nanotubes. *Angew Chem Int Ed* 2002;41:1853–9.
- [330] Richter H, Hernadi K, Caudano R, Fonseca A, Migeon H-N, Nagy JB, et al. Formation of nanotubes in low pressure hydrocarbon flames. *Carbon* 1996;34:427–9.
- [331] Yan Y, Miao J, Yang Z, Xiao F-X, Bin Yang H, Liu B, et al. Carbon nanotube catalysts: recent advances in synthesis, characterization and applications. *Chem Soc Rev* 2015;44:3295–346.
- [332] Freire C, Pereira C, Rebelo S. Green oxidation catalysis with metal complexes: from bulk to nano recyclable hybrid catalysts. *Catalysis* 2012;116–203.
- [333] Chen X, Oh W-D, Lim T-T. Graphene- and CNTs-based carbocatalysts in persulfates activation: material design and catalytic mechanisms. *Chem Eng J* 2018;354:941–76.
- [334] Wepasnick KA, Smith BA, Schrote KE, Wilson HK, Diegelmann SR, Fairbrother DH. Surface and structural characterization of multi-walled carbon nanotubes following different oxidative treatments. *Carbon* 2011;49:24–36.
- [335] Stein A, Wang Z, Fierke MA. Functionalization of porous carbon materials with designed pore architecture. *Adv Mater* 2009;21:265–93.
- [336] Maiti UN, Lee WJ, Lee JM, Oh Y, Kim JY, Kim JE, et al. 25th anniversary article: chemically modified/doped carbon nanotubes & graphene for optimized nanostructures & nanodevices. *Adv Mater* 2014;26:40–67.
- [337] Hummers WS, Offeman RE. Preparation of graphitic oxide. *J Am Chem Soc* 1958;80:1339.

- [338] Ding C, Hashida T. High performance anode-supported solid oxide fuel cell based on thin-film electrolyte and nanostructured cathode. *Energy Env Sci* 2010;3:1729–31.
- [339] Chen Y. Solid-state formation of carbon nanotubes. In: Dai L, editor. *Carbon Nanotechnol.* 1st ed. Kidlington: Elsevier; 2006. p. 53–80.
- [340] Soares OSGP, Rocha RP, Gonçalves AG, Figueiredo JL, Órfão JJM, Pereira MFR. Easy method to prepare N-doped carbon nanotubes by ball milling. *Carbon* 2015;91:114–21.
- [341] León V, Quintana M, Herrero MA, Fierro JLG, La Hoz AD, Prato M, et al. Few-layer graphenes from ball-milling of graphite with melamine. *Chem Commun* 2011;47:10936–8.
- [342] Yi M, Shen Z. A review on mechanical exfoliation for the scalable production of graphene. *J Mater Chem A* 2015;3:11700–15.
- [343] Hu C, Liu D, Xiao Y, Dai L. Functionalization of graphene materials by heteroatom-doping for energy conversion and storage. *Prog Nat Sci Mater Int* 2018;28:121–32.
- [344] Wang X, Sun G, Routh P, Kim D-H, Huang W, Chen P. Heteroatom-doped graphene materials: syntheses, properties and applications. *Chem Soc Rev* 2014;43:7067–98.
- [345] Sumpter BG, Meunier V, Romo-Herrera JM, Cruz-Silva E, Cullen DA, Terrones H, et al. Nitrogen-mediated carbon nanotube growth: diameter reduction, metallicity, bundle dispersability, and bamboo-like structure formation. *ACS Nano* 2007;1:369–75.
- [346] Ozhukil Kollath V, Arjmand M, Egberts P, Sundararaj U, Karan K. Quantitative analysis of nanoscale electrical properties of CNT/PVDF nanocomposites by current sensing AFM. *RSC Adv* 2017;7:32564–73.
- [347] Elías AL, Perea-López N, Rajukumar LP, McCreary A, López-Urías F, Terrones H, et al. Three-dimensional nanotube networks and a new horizon of applications. In: Schulz MJ, Shanov V, Yin Z (John), editors. *Nanotub. Superfiber Mater.* 1st ed. Waltham: Elsevier Inc.; 2014. p. 457–93.
- [348] Hashim DP, Narayanan NT, Romo-Herrera JM, Cullen DA, Hahm MG, Lezzi P, et al. Covalently bonded three-dimensional carbon nanotube solids via boron induced nano-junctions. *Sci Rep* 2012;2:363–71.
- [349] Pereira C, Pereira AM. Functional carbon-based nanomaterials for energy storage: towards smart textile supercapacitors. *Bol Grup Esp Carbón* 2016;40:42–8.
- [350] Inagaki M, Toyoda M, Soneda Y, Morishita T. Nitrogen-doped carbon materials. *Carbon* 2018;132:104–40.
- [351] Deng Y, Xie Y, Zou K, Ji X. Review on recent advances in nitrogen-doped carbons: preparations and applications in supercapacitors. *J Mater Chem A* 2016;4:1144–73.
- [352] Clancy AJ, Bayazit MK, Hodge SA, Skipper NT, Howard CA, Shaffer MSP. Charged carbon nanomaterials: redox chemistries of fullerenes, carbon nanotubes, and graphenes. *Chem Rev* 2018;118:7363–408.
- [353] Dyke CA, Tour JM. Covalent functionalization of single-walled carbon nanotubes for materials applications. *J Phys Chem A* 2004;108:11151–9.
- [354] Bai S, Shen X, Zhong X, Liu Y, Zhu G, Xu X, et al. One-pot solvothermal preparation of magnetic reduced graphene oxide-ferrite hybrids for organic dye removal. *Carbon* 2012;50:2337–46.
- [355] Xu H, Anlage SM, Hu L, Gruner G. Microwave shielding of transparent and conducting single-walled carbon nanotube films. *Appl Phys Lett* 2007;90:183119.
- [356] Wang H, Dai H. Strongly coupled inorganic–nano-carbon hybrid materials for energy storage. *Chem Soc Rev* 2013;42:3088–113.
- [357] Eder D. Carbon nanotube–inorganic hybrids. *Chem Rev* 2010;110:1348–85.
- [358] Shearer CJ, Cherevan A, Eder D. Application and future challenges of functional nano-carbon hybrids. *Adv Mater* 2014;26:2295–318.

- [359] Akin DE. Industrial applications of natural fibres. Chichester: John Wiley & Sons, Ltd; 2010.
- [360] Nasir S, Hussein M, Zainal Z, Yusof N. Carbon-based nanomaterials/allotropes: a glimpse of their synthesis, properties and some applications. *Materials* 2018;11:295.
- [361] Ramaratnam K, Tsyalkovsky V, Klep V, Luzinov I. Ultrahydrophobic textile surface via decorating fibers with monolayer of reactive nanoparticles and non-fluorinated polymer. *Chem Commun* 2007;4510–12.
- [362] Liu Y, Tang J, Wang R, Lu H, Li L, Kong Y, et al. Artificial lotus leaf structures from assembling carbon nanotubes and their applications in hydrophobic textiles. *J Mater Chem* 2007;17:1071–8.
- [363] Hu C-C, Chang S-S, Liang N-Y. Fabrication of antistatic fibers with core/sheath and segmented-pie configurations. *J Ind Text* 2018;47:569–86.
- [364] Wesolek D, Gieparda W. Single- and multiwalled carbon nanotubes with phosphorus based flame retardants for textiles. *J Nanomater* 2014;2014:1–6.
- [365] Kim YS, Davis R. Multi-walled carbon nanotube layer-by-layer coatings with a trilayer structure to reduce foam flammability. *Thin Solid Films* 2014;550:184–9.
- [366] Liu Y, Wang X, Qi K, Xin JH. Functionalization of cotton with carbon nanotubes. *J Mater Chem* 2008;18:3454–60.
- [367] Bharathi Yazhini K, Gurumallesh Prabu H. Study on flame-retardant and UV-protection properties of cotton fabric functionalized with ppy–ZnO–CNT nanocomposite. *RSC Adv* 2015;5:49062–9.
- [368] Zhao X, Fu J, Wang H. The electromagnetic interference shielding performance of continuous carbon fiber composites with different arrangements. *J Ind Text* 2016;46:45–58.
- [369] Jagatheesan K, Ramasamy A, Das A, Basu A. Fabrics and their composites for electromagnetic shielding applications. *Text Prog* 2015;47:87–161.
- [370] Xin Q, Shah H, Nawaz A, Xie W, Akram MZ, Batool A, et al. Antibacterial Carbon-Based Nanomaterials. *Adv Mater* 2018;1804838:1804838.
- [371] Kitahara N, Sato T, Isogawa H, Ohgoe Y, Masuko S, Shizuku F, et al. Antibacterial property of DLC film coated on textile material. *Diam Relat Mater* 2010;19:690–4.
- [372] Zhao J, Deng B, Lv M, Li J, Zhang Y, Jiang H, et al. Graphene oxide-based antibacterial cotton fabrics. *Adv Healthc Mater* 2013;2:1259–66.
- [373] Biswas S, Arief I, Panja SS, Bose S. Absorption-dominated electromagnetic wave suppressor derived from ferrite-doped cross-linked graphene framework and conducting carbon. *ACS Appl Mater Interfaces* 2017;9:3030–9.
- [374] Hapuarachchi TD, Peijs T, Bilotti E. Thermal degradation and flammability behavior of polypropylene/clay/carbon nanotube composite systems. *Polym Adv Technol* 2013;24:331–8.
- [375] Martins MSS, Scharrel B, Magalhães FD, Pereira CMC. The effect of traditional flame retardants, nanoclays and carbon nanotubes in the fire performance of epoxy resin composites. *Fire Mater* 2017;41:111–30.
- [376] Lv P, Zhao Y, Liu F, Li G, Dai X, Ji X, et al. Fabrication of polyaniline/polyimide composite fibers with electrically conductive properties. *Appl Surf Sci* 2016;367:335–41.
- [377] Gao Q, Ma H, Bao W, Gao C, Ge M. Polyacrylonitrile/electroconductive TiO<sub>2</sub> nanoparticles composite fibers via wet-spinning. *Fibers Polym* 2016;17:1048–54.
- [378] Deopura B, Alagirusamy R, Joshi M, Gupta B. Polyesters and polyamides. Cambridge: Woodhead Publishing Ltd; 2008.
- [379] Hu L, Pasta M, La Mantia F, Cui L, Jeong S, Deshazer HD, et al. Stretchable, porous, and conductive energy textiles. *Nano Lett* 2010;10:708–14.

- [380] Neves AIS, Rodrigues DP, De Sanctis A, Alonso ET, Pereira MS, Amaral VS, et al. Towards conductive textiles: coating polymeric fibres with graphene. *Sci Rep* 2017;7:4250.
- [381] Zou L, Yao L, Ma Y, Li X, Sailimujiang S, Qiu Y. Comparison of polyelectrolyte and sodium dodecyl benzene sulfonate as dispersants for multiwalled carbon nanotubes on cotton fabrics for electromagnetic interference shielding. *J Appl Polym Sci* 2014;131:40588.
- [382] Tian M, Du M, Qu L, Chen S, Zhu S, Han G. Electromagnetic interference shielding cotton fabrics with high electrical conductivity and electrical heating behavior: via layer-by-layer self-assembly route. *RSC Adv* 2017;7:42641–52.
- [383] Singh SK, Akhtar MJ, Kar KK. Impact of  $\text{Al}_2\text{O}_3$ ,  $\text{TiO}_2$ ,  $\text{ZnO}$  and  $\text{BaTiO}_3$  on the microwave absorption properties of exfoliated graphite/epoxy composites at X-band frequencies. *Compos Part B: Eng* 2019;167:135–46.
- [384] Pawar SP, Gandhi M, Saraf C, Bose S. Exceptional microwave absorption in soft polymeric nanocomposites facilitated by engineered nanostructures. *J Mater Chem C* 2016;4:4954–66.
- [385] Cao M-S, Yang J, Song W-L, Zhang D-Q, Wen B, Jin H-B, et al. Ferroferric oxide/multiwalled carbon nanotube vs polyaniline/ferroferric oxide/multiwalled carbon nanotube multiheterostructures for highly effective microwave absorption. *ACS Appl Mater Interfaces* 2012;4:6949–56.
- [386] Heo JS, Eom J, Kim Y, Park SK. Recent progress of textile-based wearable electronics: a comprehensive review of materials, devices, and applications. *Small* 2017;14:1703034.
- [387] Jian M, Wang C, Wang Q, Wang H, Xia K, Yin Z, et al. Advanced carbon materials for flexible and wearable sensors. *Sci China Mater* 2017;60:1026–62.
- [388] Dubal DP, Chodankar NR, Kim D-H, Gomez-Romero P. Towards flexible solid-state supercapacitors for smart and wearable electronics. *Chem Soc Rev* 2018;47:2065–129.
- [389] Zhao F, Zhao Y, Cheng H, Qu L, Graphene A. Fibriform resporor for sensing heat, humidity, and mechanical changes. *Angew Chem Int Ed* 2015;54:14951–5.
- [390] Zhong J, Zhong Q, Hu Q, Wu N, Li W, Wang B, et al. Stretchable self-powered fiber-based strain sensor. *Adv Funct Mater* 2015;25:1798–803.
- [391] Cao R, Pu X, Du X, Yang W, Wang J, Guo H, et al. Screen-printed washable electronic textiles as self-powered touch/gesture tribo-sensors for intelligent human–machine interaction. *ACS Nano* 2018;12:5190–6.
- [392] Vu C, Kim J. Human motion recognition by textile sensors based on machine learning algorithms. *Sensors* 2018;18:3109.
- [393] Ryu S, Lee P, Chou JB, Xu R, Zhao R, Hart AJ, et al. Extremely elastic wearable carbon nanotube fiber strain sensor for monitoring of human motion. *ACS Nano* 2015;9:5929–36.
- [394] Choi C, Lee JM, Kim SH, Kim SJ, Di J, Baughman RH. Twistable and stretchable sandwich structured fiber for wearable sensors and supercapacitors. *Nano Lett* 2016;16:7677–84.
- [395] Kaushik V, Lee J, Hong J, Lee S, Lee S, Seo J, et al. Textile-based electronic components for energy applications: principles, problems, and perspective. *Nanomaterials* 2015;5:1493–531.
- [396] Gowthaman S, Chidambaram GS, Rao DBG, Subramya HV, Chandrasekhar U. A review on energy harvesting using 3D printed fabrics for wearable electronics. *J Inst Eng Ser C* 2018;99:435–47.
- [397] Wang ZL, Wu W. Nanotechnology-enabled energy harvesting for self-powered micro-/nanosystems. *Angew Chem Int Ed* 2012;51:11700–21.



- [398] Khan U, Kim S-W. Triboelectric nanogenerators for blue energy harvesting. *ACS Nano* 2016;10:6429–32.
- [399] Yu A, Jiang P, Lin Wang Z. Nanogenerator as self-powered vibration sensor. *Nano Energy* 2012;1:418–23.
- [400] Zhu G, Bai P, Chen J, Lin Wang Z. Power-generating shoe insole based on triboelectric nanogenerators for self-powered consumer electronics. *Nano Energy* 2013;2:688–92.
- [401] Pu X, Li L, Liu M, Jiang C, Du C, Zhao Z, et al. Wearable self-charging power textile based on flexible yarn supercapacitors and fabric nanogenerators. *Adv Mater* 2016;28:98–105.
- [402] Wu W, Bai S, Yuan M, Qin Y, Wang ZL, Jing T. Lead zirconate titanate nanowire textile nanogenerator for wearable energy-harvesting and self-powered devices. *ACS Nano* 2012;6:6231–5.
- [403] Dong K, Wang Y-C, Deng J, Dai Y, Zhang SL, Zou H, et al. A highly stretchable and washable all-yarn-based self-charging knitting power textile composed of fiber triboelectric nanogenerators and supercapacitors. *ACS Nano* 2017;11:9490–9.
- [404] Ryan JD, Lund A, Hofmann AI, Kroon R, Sarabia-Riquelme R, Weisenberger MC, et al. All-organic textile thermoelectrics with carbon-nanotube-coated n-type yarns. *ACS Appl Energy Mater* 2018;1:2934–41.
- [405] Ryan JD, Mengistie DA, Gabriellson R, Lund A, Müller C. Machine-washable PEDOT: PSS dyed silk yarns for electronic textiles. *ACS Appl Mater Interfaces* 2017;9:9045–50.
- [406] Lv T, Yao Y, Li N, Chen T. Wearable fiber-shaped energy conversion and storage devices based on aligned carbon nanotubes. *Nano Today* 2016;11:644–60.
- [407] Molina J. Graphene-based fabrics and their applications: a review. *RSC Adv* 2016;6: 68261–91.
- [408] Kou L, Huang T, Zheng B, Han Y, Zhao X, Gopalsamy K, et al. Coaxial wet-spun yarn supercapacitors for high-energy density and safe wearable electronics. *Nat Commun* 2014;5:3754.
- [409] Gao Z, Song N, Zhang Y, Li X. Cotton-textile-enabled, flexible lithium-ion batteries with enhanced capacity and extended lifespan. *Nano Lett* 2015;15:8194–203.
- [410] Pan S, Lin H, Deng J, Chen P, Chen X, Yang Z, et al. Novel wearable energy devices based on aligned carbon nanotube fiber textiles. *Adv Energy Mater* 2015;5:1401438.
- [411] Chen X, Sun H, Yang Z, Guan G, Zhang Z, Qiu L, et al. A novel “energy fiber” by coaxially integrating dye-sensitized solar cell and electrochemical capacitor. *J Mater Chem A* 2014;2:1897–902.
- [412] Abdelkader AM, Karim N, Vallés C, Afroj S, Novoselov KS, Yeates SG. Ultraflexible and robust graphene supercapacitors printed on textiles for wearable electronics applications. *2D Mater* 2017;4:035016.
- [413] Sun J, Huang Y, Fu C, Wang Z, Huang Y, Zhu M, et al. High-performance stretchable yarn supercapacitor based on PPy@CNTs@urethane elastic fiber core spun yarn. *Nano Energy* 2016;27:230–7.
- [414] Choi C, Sim HJ, Spinks GM, Lepró X, Baughman RH, Kim SJ. Elastomeric and dynamic MnO<sub>2</sub>/CNT core-shell structure coiled yarn supercapacitor. *Adv Energy Mater* 2016;6:1–8.
- [415] Ma W, Chen S, Yang S, Chen W, Cheng Y, Guo Y, et al. Hierarchical MnO<sub>2</sub> nanowire/graphene hybrid fibers with excellent electrochemical performance for flexible solid-state supercapacitors. *J Power Sources* 2016;306:481–8.
- [416] Gao Z, Zhang Y, Song N, Li X. Towards flexible lithium-sulfur battery from natural cotton textile. *Electrochim Acta* 2017;246:507–16.



- [417] Gulzar U, Goriparti S, Miele E, Li T, Maidecchi G, Toma A, et al. Next-generation textiles: from embedded supercapacitors to lithium ion batteries. *J Mater Chem A* 2016;4: 16771–800.
- [418] Karim N, Afroj S, Tan S, He P, Fernando A, Carr C, et al. Scalable production of graphene-based wearable E-textiles. *ACS Nano* 2017;11:12266–75.
- [419] Wen Z, Yeh M-H, Guo H, Wang J, Zi Y, Xu W, et al. Self-powered textile for wearable electronics by hybridizing fiber-shaped nanogenerators, solar cells, and supercapacitors. *Sci Adv* 2016;2 e1600097–e1600097.

## Section 8

# **Functionalized nanomaterial in cosmetics industry**

This page intentionally left blank

# Functional nanomaterials for the cosmetics industry

Suman Singh\*, Satish Kumar Pandey\* and Neelam Vishwakarma

*CSIR - Central Scientific Instruments Organisation, Chandigarh, India*

## 22.1 Introduction

In the 20th century, the concept of nanomaterials, namely materials with particles less than 100 nm ( $1 \times 10^{-9}$  m) in size in at least one direction, was introduced. Nanomaterials have a number of advantages over conventional materials due to their smaller dimensions [1]. Because of their physicochemical properties, these new materials have found many applications. Like almost every area in research and market today, ranging from healthcare to window shields to military-grade equipment and quantum-sized devices, the cosmetic industry has also benefitted from advancements of nanotechnology. The scope of nanotechnology increased manifolds in this industry due to the advanced properties of nanoparticles that enable enhancing performance, solubility, transparency, and absorption of cosmetics.

Technically, the word ‘cosmetics’ refers to the products that amplify the appearance of the skin, intensify the cleansing, and promote skin beauty. Although, the use of ‘cosmetics’ word backs to the time of Egyptians around 4000 BCE, but this term was first coined in 1961 by the founding members of US Society of Cosmetic Chemists, Raymond Reed.

The technology of using nanoparticles also dates back to early 1960s once the use of liposome technology was introduced to moisturizers and skin creams. Not only the optical properties of the products were enhanced using liposomes, but the solubility and absorption. Nanoparticles are already being used in several cosmetics like sunscreens, lotion, anti-aging creams, haircare products, etc. Even though nanotechnology has been present in the cosmetic industry for some time now, it surely holds a brighter future with tons for new research work going on for nanocosmetics. Cosmetic companies are using nanotechnology to downscale existing ingredients for improving deep

---

\* Contributed equally

skin penetration, sustained absorption in skin, UV protection, higher stability and final quality of product, etc. Submicron emulsions, liposomes, microspheres, as well as nanospheres made of biodegradable polymers are already used in medicine, especially for skin-related diseases [2–4]. While nanotechnology is more commonly being used in industries including cosmetics, regulations need to be developed to determine toxicity since nanoparticles can enter the human body. Nanotechnology has promising potential but its benefits must outweigh the risks to human health and the environment. This chapter highlights various nanotechnologies used for the delivery of nanocosmeceuticals as well as their advantages and disadvantages.

## **22.2 Cosmetics: performance enhancement using nanotechnology**

The main strategy behind converting regular materials into nanosized formulations is to:

1. Formulate nanoparticulate products that can penetrate deeper into the skin layers (e.g., antiaging creams). For cosmetic products, particles in the range of nanometers are believed to be absorbed easily into the skin and help in repairing skin damage more efficiently.
2. Make fragrances that can last longer and perform better.
3. Formulate sunscreens with physical blockers having better dispersibility and transparency.
4. Optimize the manufacturing conditions for skincare and hair formulations.

## **22.3 Nanocosmetics: types and applications**

For the purpose of cosmetics, the European Commission has defined nanomaterials very explicitly in Article 2(k) of its new cosmetic regulations (EC/1223/2009), which was published on December 22, 2009 in the Official Journal of the European Union [5]. According to this document, the term “nanomaterials” means “an insoluble or biopersistent and intentionally manufactured material with one or more external dimension or an internal structure, on the scale from 1 to 100 nm.” These materials are further classified into “insoluble nanomaterials” and “labile nanomaterials.”

## **22.4 Classification of nanocosmetics on the basis of formulation technologies**

With benefits such as skin hydration, bioavailability, stability, and controlled occlusion, nanolipidic carriers (NLCs) have been widely exploited as a potential cosmetic delivery agents. In addition, a variety of encapsulation

techniques have been proposed for delivering these cosmetic components into the skin. Other novel materials and technologies like nanocrystals, nanoemulsions, fullerenes, and dendrimers are also being investigated for application in the cosmetic industry. Numerous patents have been filed for their application in cosmetics [6]. Some of the different types of nanotechnology-based delivery systems are discussed as follows.

#### 22.4.1 Vesicular delivery systems

This category comprises structures beyond liposomes and niosomes [7]. Liposomes may be defined as structures having a hydrophobic lipid bilayer surrounding the aqueous core created by the extrusion of the phospholipids. The lipid bilayer of liposomes can fuse with other bilayers, such as the cell membrane, and help in transport of the core therapeutic material. This makes it a very useful delivery system for drugs and cosmetically useful active ingredients [8]. Liposomes vary in size from 15 nm to several micrometers depending on variable factors and can either be unilamellar or multilamellar in nature. Liposomes that have vesicles in the range of nanometers are called nanoliposomes. Recently, newer types of liposomes, called transferosomes, have been developed. These typically lie in the range of 200–300 nm and are more elastic than liposomes. These have been shown to penetrate the skin with better efficiency than liposomes. These self-assembled lipid droplets have potential applications in cosmetics and drug delivery due to their spontaneous penetration of the stratum corneum through intracellular or transcellular routes, finding their way to commercial cosmetics.

#### 22.4.2 Nanoemulsions

These are transparent metastable dispersions with droplets of one liquid within another and possessing unique tactile and textural properties. Their structure can be manipulated based on the method of preparation to give products with distinct characteristics (e.g., water-like fluids or gels). Nanoemulsions possess distinct advantages over large-scale emulsions. They are transparent or translucent systems and have a larger surface area due to their reduced dimensions [9]. Researchers have already established that the smaller the size of the oil globule in an emulsion, the higher the stability and the better the suitability to load active ingredients. It is therefore necessary to understand the various processes of nanoemulsification. Kabri et al. [10] formulated and characterized nanoemulsions and concluded that homogenization is the best method to achieve the desired size of nanoemulsion droplet. The components of nanoemulsions are generally recognized as safe (GRAS) ingredients that can break down to safe components and are therefore considered as relatively safe systems. A popular cosmetic item, Korre's Red Vine Hair sunscreen, makes use of these nanoemulsions.

### 22.4.3 Solid lipid nanoparticles

Popularly known as SLNs, solid-lipid nanoparticles are nanometer-sized lipid droplets, with a solid lipid matrix that are stabilized by surfactants. These nanoparticles have the potential to protect the encapsulated agents against degradation [11]. Researchers have shown that compounds like coenzyme Q10 and retinol can remain stable in SLNs over long periods. Thus these agents can be used for the controlled delivery of cosmetic agents over a prolonged period of time. In addition, they have been shown to improve the penetration of active moieties into the stratum corneum.

### 22.4.4 Nanostructured lipid carriers

These second-generation lipid particles are formulated by mixing a predefined fixed ratio of solid lipids with liquid lipids [12,13] and were developed as alternative carrier systems to emulsions, liposomes, and polymeric nanoparticles. They are popularly known as NLCs and are distorted in structure. These distortions or imperfections create several spaces to accommodate the active compound in carrier molecules. They possess a high occlusion factor, high loading capacity, and high level of skin adherence properties. In addition, their long-term stability makes them superior to SLNs for use in cosmetics [14,15]. They prevent dehydration by forming a thin film on the surface due to the adherence of particles on the outer skin layers. It has also been found that the release profile of the active compounds can be manipulated by changing the matrix structure of the nanoparticles. Nanobeads and nanopearls are a few examples of NLCs which are used in the cosmetic industry.

### 22.4.5 Nanosponges and microsponges

These are highly cross-linked, polymeric, porous systems and are free flowing and non-gritty in texture. These properties make them a drug-delivery system of choice for dermatological and cosmetic products [16]. They have very high entrapment efficiency and release drugs/actives in a diffusion controlled manner [17]. They can be prepared by methods like liquid–liquid suspension polymerization, quasiemulsion solvent diffusion method, etc. The size and entrapment efficiency depends on factors such as drug solubility, the nature of the polymer, the volatility of the porogen, the polymer cross-linking agent, the type and concentration of the plasticizer, temperature, and the speed of the emulsification process [18].

### 22.4.6 Nanocrystals

Typically in the size range of 10–400 nm, these aggregates exhibit physical and chemical properties intermediate between bulk solids and molecules.

Several hundreds to tens of thousands of atoms are aggregated into a cluster to form nanocrystals. Their unique properties such as bond gap, charge conductivity, crystalline structure, and melting temperature can be tailored by controlling their size and surface area. These nanocrystals can then easily be converted into a topical formulation by dispersing into water (i.e., nanosuspensions) first.

#### **22.4.7 Nanocapsules**

These are based on encapsulation technology and can carry drug payloads for local action or targeted drug delivery. Depending on the nature of the material to be incorporated, different types of nanocapsules can be formulated [19]. Companies like Exlica Ltd. and MiCapt are exploring various materials to be utilized as nanocapsule shells (e.g., polymer microbeads, silica nanoshells, microbial cell walls).

#### **22.4.8 Nanopigments**

Silver and gold are the two most important metals whose incorporation in the nanocolloidal range has a wide spectrum of activity. Gold and silver nanopigments have been prepared to give new colored pigments for lipsticks and have been found to be safe and with enhanced pigment dispersion. For example, in the case of gold, if the structural dimensions are reduced to few hundreds of nanometers, it begins to exhibit red color instead of its natural appearance of yellow color [20]. Similarly, in the case of silver, nanoparticles show yellow color and not the gray—silver color. Since gold and silver, unlike conventional pigments, have no toxicity, have strong disinfecting abilities and high stabilities, they have potential in the cosmetics and personal care industries. Titanium dioxide and zinc oxide are the two metal oxides used as physical sun-blocking agents in sunscreens. Their presence in the formulation gives skin a white color. Reducing the particle size to the nanorange not only improves spreadability but also provides transparency to the product. Reducing the particle size to the nanoscale can lead to the manufacture of sun-blocking agents that are transparent. Many other pigments and nanoparticles also used in cosmetics.

#### **22.4.9 Dendrimers**

Dendrimers and hyperbranched polymers have been widely explored in the cosmetic industry. Dendrimers can be considered as unimolecular, monodisperse, and micellar nanostructures. They have a well-defined regularly branched symmetrical structure with a high density of functional end groups on their periphery, which offer distinct advantages for their formulations in cases where thin films are required, such as in nail enamel and mascara.



### 22.4.10 Cubosomes

Defined as self-assembled liquid crystalline nanoparticles of a particular surfactant with a certain ratio of water with a microstructure cubosomes, offer distinct and interesting properties [21]. They have the potential to be incorporated as high drug and cosmeceuticals payloads due to their large internal surface area, cubic crystalline structures, relatively simple preparation method, biodegradability of lipids, the ability of encapsulating hydrophobic, hydrophilic, and amphiphilic substances, and high stability. These advantages, in addition to their low cost, make them attractive for applications in the cosmetic industry.

## 22.5 Nanocosmetics: some popular categories

There are several products in the cosmetics industry that are enhanced by nanoparticles. Ranging from antiaging creams to toothpaste, UV protection to perfumes and nail polishes, nanocosmetics have proven to be safer alternatives for the chemical products used before with better performance and fewer side effects. Some of the available nanotechnology-based cosmetics are discussed here.

### 22.5.1 Toothpastes

Theramed SOS Sensitive Toothpaste with Nanit (Henkel KGaA) uses a unique nanotechnology-based dentin repair technology to build a protective film from materials similar to the tooth itself. An interdisciplinary team of researchers from Sustech Dermstadt and Henkel have developed an innovative substance comprised of calcium phosphate nanoparticles and proteins (the same components present in natural teeth). The claim made for the product is that, after its first use, the product reduces the sensitivity of the nerves to pain and continued use reduces the sensitivity of the teeth to pain caused by either hot, cold, sweet, or sour conditions. Silver products such as toothpastes, soap, and toothbrushes are manufactured in South Korea under the name “Nanosystem” silver products. All these products are made from colloidal silver that, due to its enormous surface area, acts as a very potent microbicide [22]. Other nanoscaled materials used in the toothpaste are nano-hydroxyapatite (nano-HA) and nano-sized titanium oxide, which is used as whitener. Nano-HA is a calcium compound and is similar to that found naturally in teeth and bones. It helps to prevent tooth pain associated with sensitivity and protects teeth from decay and cavities.

### 22.5.2 Hair cosmetics

Hair dyes/colorants and growth-promoting preparations have utilized nanotechnology to their benefit (e.g., a shampoo containing Proxiphen-N,

for alopecia/baldness (<http://www.onlyhairloss.com>). Hair preparations containing silver nanoparticle colloids (0.1–500 ppm of nanosilver colloid with particle size below 200 nm) are now available for the treatment of bacteria-caused hair depilation.

### 22.5.3 Antiaging creams

Since nanoparticles can penetrate deep into the skin, drugs like vitamin E, retinol, etc., are expected to perform better as antiaging agents. For example, it has been reported that *Chantecaille* (a nanogold-containing energizing cream) contains nanoparticles of 24-carat gold bound to silk microfibers, which as a natural protein claims to act as an effective moisturizing, antioxidant, and antiinflammatory preparation [23,24]. With the help of nanotechnology these elements are expected to reach the cellular level where they can help in fast healing.

### 22.5.4 Sunscreen creams

Reducing the particle size of sun-blocking agents, like titanium dioxide and zinc oxide, has made it possible to combine extremely effective protection with a clear and natural finish.

### 22.5.5 Lipsticks

Lipsticks are colored cosmetics that use dyes and pigments to achieve the desired color. However, these pigments can be toxic. It has been reported that nanogold exhibits red color and nanosilver gives a yellow color. Hence gold and silver nanopigments have been prepared and added to lipsticks to give new colored pigments [25]. They have been reported to be safe and have good pigment dispersion.

## 22.6 Nanotechnology for UV protection

Sunscreens containing zinc oxide (ZnO) and titanium dioxide (TiO<sub>2</sub>) particles have been widely used for many years. These agents act as UV filters and are thus beneficial in skin protection against the harmful rays of the sun. Sunscreens used till date appear white as these particles reflect visible light when applied on the skin due to their micrometer size. The result is thicker, sticky paste that is difficult to administer and undesirable to consumers. To overcome this problem, recently, these oxides (ZnO and TiO<sub>2</sub>) have been formulated as nanoparticles wherein they retain the UV filtration and absorption properties while eliminating the white chalky appearance of traditional sunscreens [26]. These nanoparticle sunscreens are more stable, do not need frequent reapplication, and reduce allergic reactions. Another advantage is

that, at the nanoscale, ZnO and TiO<sub>2</sub> feel “lighter on the skin” according to Megan Osmond–McLeod, a researcher at Australia’s Commonwealth Scientific and Industrial Research Organization (CSIRO) [27]. In addition, products containing ZnO or TiO<sub>2</sub> nanoparticles are transparent, less smelly, less greasy, and more absorbable by the skin, thereby increasing the aesthetic appeal of the product.

Products from renowned companies like Boots, Avon, The Body Shop, L’Oréal, Nivea, and Unilever now use these nanoparticles in formulations of sunscreens and moisturizers. Over the last decade, these UV protection systems have undergone a number of modifications to increase their efficacy and stability. The addition of 1% manganese in a standard formula containing TiO<sub>2</sub> has led to the development of *Optisol*, a UV absorption system by Oxonica. Similarly, dispersing nanoparticles of carnauba wax in addition to TiO<sub>2</sub> nanoparticles significantly enhances the sun protection factor (SPF) [28]. Dedicated facilities have cropped up to provide particles with specified characteristics. Nanophase technologies provide polymeric nanocrystals of ZnO with size less than 35 nm to companies including BASF for personal care applications. Various other nanoparticles have also been developed for UV protection. Sol–gel technologies make use of silica nanoshells to encapsulate a variety of cosmetic ingredients. UV Pearls<sup>TM</sup> contain these silica shells with UV filters to block UV rays when applied on the top surface of the skin. These products additionally provide improved photostability and reduced filter uptake by the skin.

## 22.7 Formulation and manufacturing aspects

Nanoparticles require sophisticated and specialized equipment to be formulated. Special types of instrumentation and methods are also needed to characterize their various aspects such as size, stability, and solubility in different solutions/formulations.

The particles should be characterized for size and size distribution, aggregation and agglomeration characteristics, surface chemistry (zeta potential/surface charge, surface coating, functionalization, and catalytical activity); morphology (shape, surface area, surface topology, and crystallinity); solubility; density; stability; porosity; etc. Although a wide range of analytical techniques are available for measurement of the physicochemical properties of materials, many of these methods have not been validated for the evaluation of nanomaterials in cosmetic products. It is now the call of the day that appropriate analytical methods suitable for the specific nanomaterial and the cosmetic product formulation should be chosen and the results obtained from such tests must be appropriately interpreted and reported for adequate characterization of the material.

## 22.8 Guidance documents on nanomaterials in cosmetics

Nanotechnology made its first commercial impact in 2000 and since then it has revolutionized the world. Food, pharmaceuticals, and cosmetics are no exception. The safety concerns raised by many have finally gotten the attention the drug regulatory bodies all over the world. An initiative has been taken to define their size and classify these materials based on their altered physico-chemical properties and biological interaction. After the recommendations of its Task Force in 2007, the US Food and Drug Administration (FDA) published a guidance document (No. FDA-2011-D-D0489) under the title of Guidance for Industry: Safety of Nanomaterials in Cosmetic Products [29].

## 22.9 Safety assurance

Cosmetics are not regulated as stringently as pharmaceuticals by any drug regulatory agency across the globe. The safety profiling of any new cosmetic product to be launched in the market is actually the responsibility of the manufacturer itself. With the interfacing of new technologies, like herbal technology, biotechnology, and nanotechnology with cosmetic products, the job of regulatory bodies has become more difficult. Initially, none of the agencies realized that nanomaterials would be entirely different in their properties, as compared to their larger or traditional material forms. But with the concerns of social sciences groups, some research laboratories, in particular after the initiative taken by the Royal Society of Sciences, UK, it was inevitable that nanomaterials would be treated as new entities. The FDA (USA), EMEA (EU) followed by Health Canada (Canada), TGA, and NICNAS (Australia) created initiatives in the direction of defining, classifying, and designing regulations for the industry. The nanomaterials used in the cosmetics industry differ from nanomaterials used by other industries in various aspects, which primarily include their shape and molecular structures followed by their mode of use and specific interactions with the living world and the environment. These nanomaterials are now being extensively used in sunscreen creams, fairness creams, antiaging formulations, hand and body lotions, colored makeup, lipsticks, toothpastes, hair cosmetics, and so on. Active ingredients, such as vitamins like ascorbic acid, vitamins A and K, and other delicate essential oils, which may become oxidized in air, are protected inside the lipoidal wall of nanosized vesicular systems, such as liposomes, niosomes, and phytosomes. Nanopigments added in cosmetics may be metallic or nonmetallic. SLNs and nanolipid carrier structures are nonmetallic nanoparticles of various actives that are used for dermatological benefits. Concerns of these particles entering body circulation and any probable toxic effects raised several concerns. Following which, FDA came out with- Guidance for Industry: Safety of Nanomaterials in Cosmetic Products

(FDA-2011-D-0489), which came in effect from June 27, 2014. This document reflects FDA's thinking on safety assessments. Some more issues which FDA recently tried to address are:

- Whether a material or end-product is engineered to have at least one external dimension, or an internal or surface structure, in the nanoscale range (approximately 1–100 nm).
- Whether a material or end-product is so engineered that it exhibits novel properties or phenomena, be it physical, chemical, or biological properties, which can actually be attributed to its minute dimensions.

As it is the guidelines of the drug agency of the United States as well as many more countries, cosmetics and cosmetic ingredients (excluding color additives) are exempted from premarket approval and therefore it is the responsibility of the cosmetic manufacturers to ensure that their product is not misbranded or adulterated [Section 201(b) of Federal Food, Drug, and Cosmetic Act-US Code 361 and 362]. These guidelines are applicable for the safety potentiation of cosmetic products irrespective of the fact that they contain nanomaterials or conventionally manufactured ingredients. However, it may be noted that a larger-scale material differs from the same material at the nanoscale with the same chemical composition in physicochemical properties, behaviors, and/or effects, especially the biological interactions. Needless to say, conventional testing methods that have been used to evaluate the safety of cosmetic ingredients and finished products thus far may not be applicable to nanomaterials due to their unique properties and behavior. Therefore the FDA has started toxicity evaluations for the safety assessment of nanomaterials in cosmetics products. For this purpose a diverse range of physical and chemical properties of nanomaterials as well as of impurities, if present, are considered. Similar to any conventional cosmetic ingredient, the nanomaterial should be fully described, including the name of the nanomaterials, Chemical Abstract Service (CAS) number, structural formula, elemental and molecular composition, etc.

## 22.10 Impurity profiling

The impurities expected in a cosmetic product containing nanomaterials cannot be assumed to be the same as those found with conventional materials. Nanoscale impurities may arise from the changed manufacturing process, use of different solvents, different temperature conditions, or the use of different starting materials or even additional agents like surface modifiers or dispersing agents.

## 22.11 Evaluation of nanomaterial toxicology

The types of tests that can be carried out to assess toxicology varies from material to material since these tests are based on many factors including the

ingredient's chemical structure, composition, physicochemical properties, intended use, degree of exposure, etc. As the nanomaterials are new and no prior safety data exists, it is important to address both acute and chronic toxicity of nanomaterials, along with evaluation of possible ingredient–ingredient interactions or ingredient–packaging interactions. The FDA guidance in this regard is that initially, the traditional method such as animal testing (Draize rabbit test) etc., should be applied and if obligatory, they may be modified in respect to factors like solubility, agglomeration, aggregation of particles, etc. Some traditional *in vitro* and *in vivo* test methods may be ignored at the time of testing insoluble or partially soluble nanomaterials. The suitability of traditional toxicity testing methods is also affected by agglomeration and aggregation of particles. The responsibility to ensure that the adopted methods appropriately reflect the range of free particles and any aggregates or agglomerates found in the cosmetic product lies with the formulation manufacturers. Toxicological testing should be conducted on both (i.e., individually on the free nanoparticles as well as their agglomerates or aggregates).

Since the nanomaterials possess very high surface energy, there might be increased chances of either interaction of nanomaterials with the testing medium or adsorption onto surfaces of various substances such as proteins. This will require necessary adjustments to existing evaluation methods. In situations where traditional toxicity–testing methods cannot be satisfactorily modified, the FDA does not restrict development of new methods to adequately assess the toxicity of the nanomaterial in cosmetics products.

The use of nanotechnology in cosmetics will also require certain modifications in nomenclature as well as dose metrics. The conventional dose metrics currently being used for toxicological testing of manufactured chemicals (e.g., mg/kg, mg/L) may not be appropriate for nanomaterials due to their large surface area per particle mass or volume. The FDA has also suggested that evaluations of nanomaterials should encompass alternative metrics such as “weight/volume concentration,” “particle number concentration,” and “surface area” until some appropriate and more relevant parameters for dose metrics are proposed and accepted.

## 22.12 Toxicity testing

The Cosmetic, Toiletry and Fragrance Association (CTFA), as well as the Organization for Economic Cooperation and Development (OECD), has introduced guidelines for toxicity testing based on the toxicological profile of the ingredient and its routes of exposure. For example, if a cosmetic product is intended to be used on sun-exposed skin [30], then some of the recommended toxicological tests that should be performed are skin irritation and skin sensitization test, ocular irritation test, phototoxicity testing, and a test for mutagenicity and genotoxicity. Traditional tests like acute toxicity,

repeated dose toxicity (21–28 days), and subchronic toxicity (90 days) should be done in the routine manner. These guidelines are subject to change due to the fast rate of advancement in this area. Researchers are therefore expected to follow the latest guidelines.

In vivo toxicity testing, when performed additionally, is useful in obtaining information on translocation, biodistribution, accumulation, and clearance of these materials from the organs. For evaluation of the dermal route of administration, the test substances should be applied directly to the skin and, for the oral route, test substances should be given either by gavage or in the diet. The dose metrics (mass, volume, and number of particles) are important criteria for in vivo studies.

In addition, the surface area, number of particles, and mass concentration in the study design should be considered by the manufacturer in the study design of in vivo toxicity testing. Animals were once primarily used in toxicity testing of new chemicals but some of the validated nonanimal alternative testing methods that already exist can be optimized for specific nanomaterials. The Interagency Coordinating Committee on the Validation of Alternative Methods (ICCVAM) and the European Centre for the Validation of Alternative Methods (ECVAM) are the primary two bodies working in this direction. Some of the alternative materials and methods include the availability of reconstructed human skins such as EPISkin and EPIDerm (for skin irritation and corrosion testing) and 3T3 NRPT–3T3 fibroblasts neutral red uptake phototoxicity testing (for phototoxicity testing, applicable to UV-absorbing substances). To carry out dermal absorption studies human/pig skin is recommended, while ocular irritation potential is assessed through Bovine Corneal Opacity and Permeability (BCOP) and the Isolated Chicken Eye (ICE).

## 22.13 Conclusions

In the last two decades, nanotechnology has been widely used and is beneficial in the field of biomedical application dermatology and cosmetics. Because of the increase in use of cosmeceuticals, conventional delivery systems are being replaced with novel delivery systems. Novel nanocarriers currently being used are liposomes, niosomes, NLC, SLNs, gold nanoparticles, nanoemulsion, and nanosomes. These novel delivery systems have remarkable potential in achieving controlled penetration, better stability, biocompatibility, and prolonged action. Nearly all the major cosmetics manufacturers use nanotechnology in their various products with investments of millions of dollars. Cosmetics giant Estee Lauder entered the NanoMarket in 2006 with a range of products containing “NanoParticles.” L’Oreal, the world’s largest cosmetics company, is devoting about \$600 million dollars of its \$17 billion dollar revenues to nanopatents, and ranks number 6 in nanotech patent holders in the United States.

However, there are concerns regarding the toxicity and safety of nanomaterials. Studies on the safety profiles of nanomaterials for cosmetics applications are required. Nanoproducts should be fabricated to ensure safety and performance of these cosmetics. Regulations are also need to ensure adequate testing is done on new nanomaterials and their applications.

## Acknowledgment

The authors acknowledge the support of Director, CSIR–CSIO for his constant encouragement. NV acknowledges the JRF fellowship from Council of Scientific and Industrial Research (CSIR), New Delhi, for project HCP-0012. SP acknowledges the financial support received from CSIR, New Delhi Pool Scientist.

## References

- [1] Rao CNR, Nthony AM, Cheetham K. The chemistry of nanomaterials: synthesis, properties and applications. Wiley VCH; 2004. p. 761.
- [2] Boonme P, Rojas-Gutierrez PA, Andreani T, Rosmaninho A, Weichers JW, Souto EB. Use of nanotechnology in the development of cosmeceuticals for skin health. Nutrigenomics: application to the development of nutraceuticals & cosmeceuticals. New York, NY: Nova Science Publishers; 2012. p. 215.
- [3] Bangale MS, Mitkare S, Gattani SG, Sakarkar DM. Recent nanotechnological aspects in cosmetics and dermatological preparations. *Int J Pharm Pharm Sci* 2012;4(2).
- [4] Andreani T, Doktorovova S, Lopes CM, Souto EB. Nanobiotechnology approaches for targeted delivery of pharmaceuticals and cosmetics ingredients. *Int J Nanotechnol* 2010;8(1-2):66–83.
- [5] Mildau G, Huber B. The new EC cosmetics regulation 1223/2009—contents and first explanations. *SOFW-J* 2010;3:40–59.
- [6] Lens M. Use of fullerenes in cosmetics. *Recent Pat Biotechnol* 2009;3(2):118–23.
- [7] Anchal Sankhyan PDP. Recent trends in niosome as vesicular drug delivery system. *J Appl Pharm Sci* 2012;2(6):20–32.
- [8] Zhou Z. Liposome formulation of fullerene-based molecular diagnostic and therapeutic agents. *Pharmaceutics* 2013;5(4):525.
- [9] Thakur N, Garg G, Sharma PK, Kumar N. Nanoemulsions: a review on various pharmaceutical applications. *Glob J Pharmacol* 2012;6(3):222–5.
- [10] Kabri T-h, et al. Physico-chemical characterization of nano-emulsions in cosmetic matrix enriched on omega-3. *J Nanobiotechnol* 2011;9(1):41.
- [11] Wissing S, Lippacher A, Muller R. Investigations on the occlusive properties of solid lipid nanoparticles (SLN). *J Cosmet Sci* 2001;52(5):313–24.
- [12] Naseri N, Valizadeh H, Zakeri-Milani P. Solid lipid nanoparticles and nanostructured lipid carriers: structure, preparation and application. *Adv Pharm Bull* 2015;5(3):305–13.
- [13] Müller RH, Radtke M, Wissing SA. Solid lipid nanoparticles (SLN) and nanostructured lipid carriers (NLC) in cosmetic and dermatological preparations. *Adv Drug Deliv Rev* 2002;54:S131–55.
- [14] Gaba B, et al. Nanostructured lipid carrier system for topical delivery of terbinafine hydrochloride. *Bull Faculty Pharm Cairo Univ* 2015;53(2):147–59.



- [15] Pardeike J, Hommoss A, Müller RH. Lipid nanoparticles (SLN, NLC) in cosmetic and pharmaceutical dermal products. *Int J Pharm* 2009;366(1):170–84.
- [16] Vishal Yadav PJ, Dombé S, Bodhe A, Salunkhe P. Formulation and evaluation of micro-sponge gel for topical delivery of antifungal drug. *Int J Appl Pharm* 2017;9(4).
- [17] Nanda S. Microsponges and nanosponges: emerging drug delivery systems for dermatological benefits. *Nanotechnology: novel perspectives and prospects*. New Delhi: McGraw Hill Education Pvt. Ltd.; 2015.
- [18] Patel EK, Oswal R. Nanosponge and microsponges: a novel drug delivery system. *Int J Res Pharm Chem* 2012;2:237–44.
- [19] Tadros TF. Future developments in cosmetic formulations. *Int J Cosmetic Sci* 1992;14(3):93–111.
- [20] Patricia Marchi-Lemann (Paris), A.C.C.I.R., Myriam Mellul (L'Hay-les-Roses) *Cosmetic compositions comprising nanopigments*, US, Editor. 1999, L'Oreal (Paris).
- [21] Garg G, Saraf S, Saraf S. Cubosomes: an overview. *Biol Pharm Bull* 2007;30(2):350–3.
- [22] Dakal TC, et al. Mechanistic basis of antimicrobial actions of silver nanoparticles. *Front Microbiol* 2016;7(1831).
- [23] Nanda S, Nanda A, Singh B. Federal perspectives of nanostructured systems: an update. *Nano structured drug delivery systems*. USA: M/s Studium Press, LLC; 2015.
- [24] Nanda S, Khurana RK, Dhiman S, Sandhu PS, Singh B. *Nano cosmetics: fundamental, safety and regulatory aspects*. In: Sing KK, Singh B, Rekhi GS, editors. *Nanobiomedicine*, Vol. 2. Houston, USA: Studium Press; 2015.
- [25] *Nanotechnology in cosmetics analysed*. [Last accessed on 2010]. Available from: <http://www.personalcaresmagazine.com/Story.aspx?Story=7419>
- [26] Singh P, Nanda A. Enhanced sun protection of nano-sized metal oxide particles over conventional metal oxide particles: an in vitro comparative study. *Int J Cosmet Sci* 2014;36(3):273–83.
- [27] <https://www.theguardian.com/science/small-world/2014/mar/13/nanotechnology-sun-screen-skin-cancer>
- [28] Neseem D. Formulation of sunscreens with enhancement sun protection factor response based on solid lipid nanoparticles. *International journal of cosmetic science* 2011;33(1):70–9.
- [29] <http://www.fda.gov>.
- [30] Tran TD, Salmon R. Potential photocarcinogenic effects of nanoparticle sunscreen. *Australas J Dermatol* 2010;37:185–7.

# Naturally derived pyroxene nanomaterials: an ore for wide applications

Gerardo Vitale, Ghada Nafie, Afif Hethnawi and Nashaat N. Nassar

*Department of Chemical and Petroleum Engineering, University of Calgary, Calgary, Alberta, Canada*

## 23.1 Introduction

Nanomaterials are the foundation of the development of nanotechnologies and several reviews describing their preparation and uses can be found in the literature [1–11]. Due to their small size (i.e., below 100 nm in at least one dimension) and concomitant large surface area per unit volume holding particular atomic sites, nanomaterials exhibit novel properties not found in the bulk materials of similar compositions. Fig. 23.1 shows a simplistic schematic representation in 2D illustrating why the nanomaterial has different surface properties than the bulk material and thus different behavior. The “infinite” bulk material has very few surface atoms of the type “2” (flat top-uncoordinated) and “3” (corner uncoordinated) as compared with atoms of the type “1” (complete coordination), which are the bulk. In this simple example, if the bulk material can be cut into very small pieces to produce materials in the nanorange, then it will be possible to increase the number of the atoms of type “3” present, which should be more prone to adsorption and reaction to get stabilized. This increase of uncoordinated or nonsaturated atoms on the surface or edges is responsible for the different behavior of nanomaterials when compared with bulk materials of the same chemistry, even within different sizes of the nanomaterials. The smaller the nanomaterials the more uncoordinated atoms with different structural arrangements on the surface will be formed. The increase of uncoordinated atoms on the surface makes variations in the structure that are not seen in the atoms belonging to the bulk because of the increase of the surface-to-volume ratio in the nanomaterials. Surface restructuring or modifying can occur making the atoms in the surface exhibit a distinct environment or organization that is

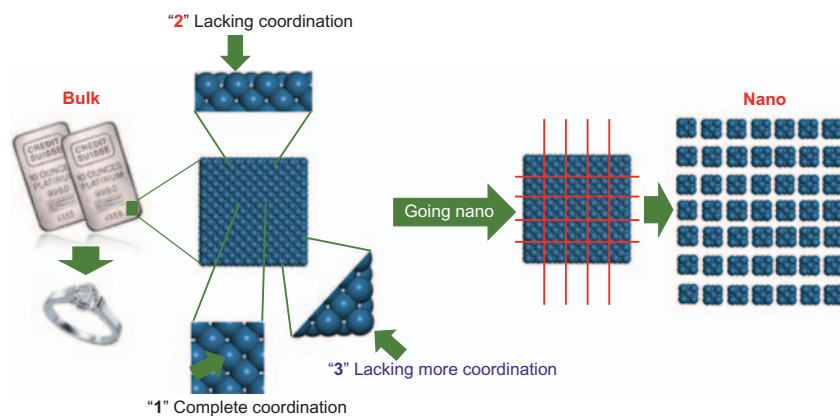


**FIGURE 23.1** Simplistic schematic 2D representation of the difference between the surfaces of a nanomaterial and a bulk material. There is an increase in the type “3” atoms as the particle gets smaller.

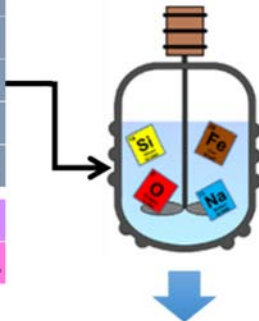
different from the bulk and thus more prone to adsorb or react with other compounds. Nanomaterials of silicates or oxides types tend to dissociate water molecules on their surface and get their surfaces enriched with hydroxyl groups that could be detected very easily by infrared, XPS, TGA, or NMR techniques.

Fig. 23.2 shows that in principle it is possible to produce nanomaterials with combinations of the elements from the Periodic Table. However, for real industrial applications that deal with large quantities of raw or produced feedstocks, it is necessary to produce nanomaterials that can be commercially sourced. This limits the selection of the elements in order to prepare naturally derived nanomaterials, by avoiding selecting precious and rare elements. Therefore the sustainability and feasibility of many present and future technologies depend on the ability to develop novel naturally derived materials that can be manufactured with the most abundant chemical elements on earth [12,13]. This also includes the production of nanomaterials for applications dealing with commodity feedstocks and products requiring large quantities of nanomaterials.

Many nanomaterials are produced with rare metals and/or expensive ones that are not suitable for large-scale production for the treatment of commodity feedstocks like those in the oil and gas industry or wastewater treatment applications. For these reasons, more environmentally friendly and inexpensive practical materials must be produced for these type of applications. Large quantities of such materials will be required and thus an economically feasible synthesis method must be developed. Tailor-made mineral-like nanomaterials compatible with the environment must be considered as well. For example, iron–silicate materials meet these requirements, and can be easily produced at the commercial scale.

## The “ingredients”

Periodic table of elements																		18 VIIA																				
1 IA H Hydrogen 1.008																	19 IIA K Potassium 39.098	20 IIA Ca Calcium 40.078	36 VIA Se Selenium 78.96	54 Xenon 131.29	72 Hf Hafnium 178.49	90 Th Thorium 232.04	108 Pt Platinum 200.58	126 Xe Xenon 254.04														
2 IIA He Helium 4.003																	35 Br Bromine 79.904	53 I Iodine 126.905	71 Ta Tantalum 180.948	89 Ac Actinium 227	107 Ir Iridium 223.03	125 Te Tellurium 127.6	143 Ce Cerium 140.12	161 Er Erbium 167.26	179 Tm Thulium 168.934	197 Ho Holmium 164.930	215 Tl Thallium 204.38	233 Fr Francium 223	251 Uu Ununpentium 262									
3 IIIA Li Lithium 6.941	4 IIIA Be Beryllium 9.0122																	37 Rb Rubidium 85.468	55 Cs Cesium 132.91	73 Hf Hafnium 178.49	91 Th Thorium 232.04	109 Pt Platinum 200.58	127 I Iodine 126.905	145 Pr Praseodymium 140.908	163 Tm Thulium 168.934	181 Lu Lutetium 174.967	209 Tl Thallium 204.38	227 Fr Francium 223	253 Uu Ununpentium 262									
11 Na Sodium 22.990	12 Mg Magnesium 24.305	13 Al Aluminum 26.982	14 Si Silicon 28.086	15 P Phosphorus 30.974	16 S Sulfur 32.06	17 Cl Chlorine 35.453	18 Ar Argon 39.948											38 Sr Strontium 87.62	56 Ba Barium 137.33	74 Ta Tantalum 180.948	92 U Uranium 238.03	110 Hg Mercury 200.59	128 Xe Xenon 254.04	146 Ce Cerium 140.12	164 Er Erbium 167.26	182 Lu Lutetium 174.967	210 Pb Lead 207.2	228 Ac Actinium 227	254 Uu Ununpentium 262									
19 K Potassium 39.098	20 Ca Calcium 40.078	21 Sc Scandium 44.956	22 Ti Titanium 47.88	23 V Vanadium 50.942	24 Cr Chromium 51.996	25 Mn Manganese 54.938	26 Fe Iron 55.845	27 Co Cobalt 58.933	28 Ni Nickel 58.69	29 Cu Copper 63.546	30 Zn Zinc 65.38	31 Ga Gallium 69.723	32 Ge Germanium 72.64	33 As Arsenic 74.922	34 Se Selenium 78.96	35 Br Bromine 79.904	36 Kr Krypton 83.798																					
37 Rb Rubidium 85.468	38 Sr Strontium 87.62	39 Y Yttrium 88.906	40 Zr Zirconium 91.224	41 Nb Niobium 92.906	42 Mo Molybdenum 95.94	43 Tc Technetium 98.906	44 Ru Ruthenium 101.07	45 Rh Rhodium 102.91	46 Pd Palladium 106.42	47 Ag Silver 107.87	48 Cd Cadmium 112.41	49 In Indium 114.82	50 Sn Tin 118.71	51 Sb Antimony 121.76	52 Te Tellurium 127.6	53 I Iodine 126.9	54 Xe Xenon 131.29																					
55 Cs Cesium 132.91	56 Ba Barium 137.33	57-71 Lanthanide Series	72 Hf Hafnium 178.49	73 Ta Tantalum 180.948	74 W Tungsten 183.84	75 Re Rhenium 186.21	76 Os Osmium 190.23	77 Ir Iridium 223.03	78 Pt Platinum 200.58	79 Au Gold 196.967	80 Hg Mercury 200.59	81 Tl Thallium 204.38	82 Pb Lead 207.2	83 Bi Bismuth 208.98	84 Po Polonium 209	85 At Astatine 210	86 Rn Radon 222																					
87 Fr Francium 223	88-103 Actinide Series	104 Rf Rutherfordium 261	105 Db Dubnium 262	106 Sg Seaborgium 266	107 Bh Bohrium 264	108 Mt Meitnerium 268	109 Ds Darmstadtium 271	110 Dt Darmstadtium 273	111 Nh Nihonium 284	112 Fl Flerovium 289	113 Mc Moscovium 288	114 Lv Livermorium 293	115 Ts Tennessine 289	116 Og Oganesson 294	117 Uu Ununseptium 294	118 Uu Ununseptium 294	119 Uu Ununseptium 294																					
																		139 La Lanthanum 138.905	141 Ce Cerium 140.12	143 Pr Praseodymium 140.908	145 Nd Neodymium 144.24	147 Pm Promethium 144.913	149 Sm Samarium 150.36	151 Eu Europium 151.964	153 Gd Gadolinium 157.25	155 Tb Terbium 158.925	157 Dy Dysprosium 162.50	159 Ho Holmium 164.930	161 Er Erbium 167.26	163 Tm Thulium 168.934	165 Yb Ytterbium 173.05	167 Lu Lutetium 174.967						
																		89 Ac Actinium 227	91 Th Thorium 232.04	93 Pa Protactinium 231.04	95 U Uranium 238.03	97 Np Neptunium 237	99 Pu Plutonium 244	101 Am Americium 243	103 Cm Curium 247	105 Bk Berkelium 247	107 Cf Californium 251	109 Es Einsteinium 252	111 Fm Fermium 257	113 Md Mendelevium 258	115 No Nobelium 259	117 Lr Lawrencium 262						
																		Alkal Metal	Alkali Metal	Transi tion Metal	Semi Metal	Nonmet al	Basic Metal	Halogen	Noble Gas	Lanthanide	Actinide											



## Possibility of producing large quantities of nanomaterials by hydrothermal synthesis

**FIGURE 23.2** Importance of the selection of low-cost and naturally derived abundant elements from the Periodic Table to produce large quantities of nanomaterials.

This chapter focuses exclusively on iron–silicate-based nanomaterial nanoparticles as potential adsorbents for water and wastewater treatment and catalysts for enhancing heavy oil quality and decomposing heavy organic waste. The chapter is aimed at providing a summary of information related to pyroxenes as naturally derived nanomaterials for energy and environmental applications as alternatives to conventional adsorbents and catalysts such as activated carbon, zeolite, activated alumina, etc. In particular, we discuss (1) hydrothermal synthesis of nanomaterials and its mechanism following the Avrami–Erofe’ev crystallization kinetic model, (2) the main preparation procedure for pyroxene nanomaterials, (3) the typical preparation procedure of Aegirine, (4) surface and structural modifications by metal doping and incorporations, (5) polymer grafting, and (6) polymer functionalization. The chapter also presents various factors and experimental conditions affecting the synthesis of aegirine nanomaterials. Finally, example applications of surface-structural modified aegirine nanomaterials as adsorbent and catalyst are presented.

## **23.2 Synthesis of iron–silicate-based nanomaterials by the hydrothermal method**

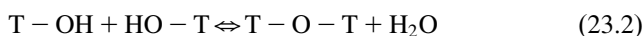
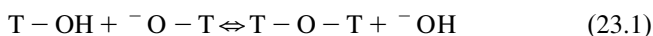
The selection of hydrothermal methods for producing iron silicate-based nanomaterials may allow obtaining large quantities at reasonable cost if the synthesis method can be scaled up to the already existing facilities where hydrothermal synthetic zeolites are produced. Hydrothermal methods are traditionally used to obtain meta-stable microporous and mesoporous materials, which include aluminosilicates, aluminophosphates, and metal-silicate variants [14,15]. This type of soft chemistry has been explored to prepare non-microporous oxide materials [16,17]. This synthetic approach appears to be a highly attractive option to produce materials because it is easily reproducible, good for obtaining homogeneous mixtures, allows the easy addition of other dopants, and can be easily scaled up as there are commercial facilities available to produce large quantities of such materials. A particular advantage of hydrothermal over precipitation/calcination methods is the operating temperatures required for formation of the desired materials. Generally, the usual temperatures for hydrothermal methods are below 473K, and thus compounds that may decompose at elevated temperatures (like organic acids) can now be utilized under hydrothermal conditions.

### **23.2.1 Hydrothermal synthesis mechanism**

The mechanism for the synthesis of materials under hydrothermal conditions is not unique, but is complex due to the nature of the reactant mixture and the conditions employed in the synthesis. It involves several steps that depend on many factors and are challenging to obtain experimentally.

However, because of the successful preparation under hydrothermal conditions of naturally occurring zeolites and nonnaturally zeotype counterparts and their commercial applications, most synthesis mechanisms proposed in the literature are related to these types of zeolitic materials [18–36]. However, the latest proposed mechanism called the “solution-mediated model” by Cundy and Cox [36] is more universal than previous methods and is applicable not only to zeolite and zeolite-like materials but to other nonmicroporous solids prepared in similar conditions, such as the one synthesized and presented in this chapter. For this reason, a description of this method is provided for understanding the formation of the iron–silicate pyroxene aegirine under the studied hydrothermal conditions of preparation.

Even though the complexity of the processes involved in the hydrothermal synthesis of zeolite and zeolite-like materials may discourage an attempt to understand the mechanism of formation, it is important to realize that the T–O–T bond-making and bond-breaking reactions (where T is Si, Al, Fe, etc.) are the predominant key reactions, as illustrated here:



These reactions establish the equilibration between solid and solution components, which are fundamental to the ordering process of hydrothermal synthesis. In general, the following sequence is observed during the hydrothermal crystallization of zeolite and zeolite-like materials: induction period, nucleation, and crystal growth.

### 23.2.1.1 *The induction period*

The induction period is the time ( $t$ ) between the start of the reaction and the point at which the crystalline product is first detected. Therefore this time depends on the moment chosen for  $t=0$  (usually the time at which the desired working temperature is reached in the mixture), and the method of analysis selected to detect the product (X-ray diffraction tends to be used the most). During this period, the initial reactants begin to interact forming a primary heterogeneous amorphous phase, which evolves to a more organized and homogeneous secondary amorphous phase (equilibrated intermediate). In this state, the relationship between the solid and solution present in the intermediate secondary amorphous phase approaches equilibrium and a characteristic distribution of ions is established.

### 23.2.1.2 *Nucleation*

The changes in the amorphous phase involve an increase in structural ordering but without the establishment of the periodic lattice itself. In order to form the lattice, a discreet nucleation event has to occur. In this step,

statistical selection of the reconstructed areas reaches a critical nuclear size and degree of order such that a periodic structure is able to propagate.

### 23.2.1.3 Crystal growth

Crystal growth occurs through an in situ, localized construction process from small mobile species ordered by the participating cations in the mixture. As the process continues, the crystals grow until no more secondary amorphous reactants are present. At this point the crystal growth ends and equilibrium between the crystal surface and the solution is achieved.

Fig. 23.3 shows an adaptation of the solution-mediated model mechanism for hydrothermal synthesis developed by Cundy and Cox [36], which can be applied to the preparation of the nanoiron–silicate pyroxene aegirine. Key features from the model are summarized as follows: after preparation of the

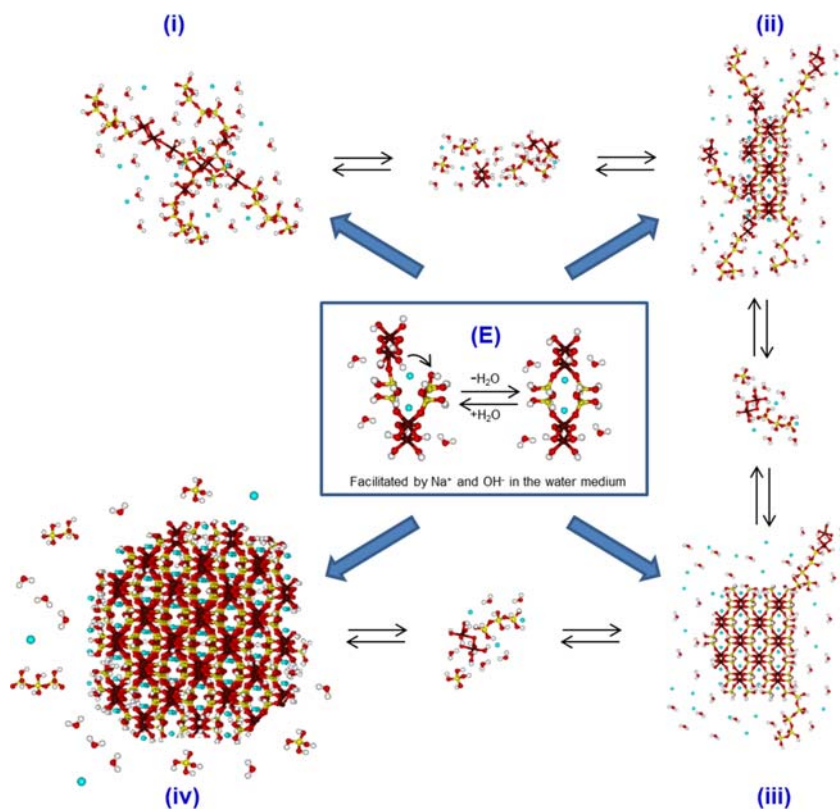


**FIGURE 23.3** Solution-mediated model mechanism for hydrothermal synthesis of nanoaegirine, after Cundy and Cox [36]. Permissions related to the material excerpted were obtained from the authors.

gel, domains of amorphous material (labeled as “i” in Fig. 23.3) equilibrate with solution species (anions and cations) to develop elements with local order (“ii” in Fig. 23.3) and increase in surface areas. With the increase in the temperature over time, equilibration reactions (T–O–T bond-making and bond-breaking) lead to areas of sufficient order for a periodic structure to become established, and thus instantaneous nucleation occurs (“iii” in Fig. 23.3) and a maximum in surface area is reached. The same equilibration process allows the nascent crystal to grow by consuming domains, which decreases the surface area of the precursor gel (“iv” in Fig. 23.3). The self-assembly process is mediated by the associated solvated cations, which act as coordinated centers (templates) for the construction of the framework (“E” in Fig. 23.3). As the spherical domains reach a certain size, the dissolution–reconstruction of the surface of the particles reaches equilibrium and all the iron is consumed to produce the crystals, leaving the excess silica in the solution.

### 23.2.2 Avrami–Erofe’ev crystallization kinetic model

Hydrothermal crystallization isotherms of different materials (like zeolites, zeotypes, and oxides) have sigmoidal shaped, or “S-shaped,” curves [37–43] when the crystallization fraction ( $\alpha$ ) is plotted against time (these plots are frequently called  $\alpha$ -time curves). This type of crystallization process can be analyzed by using the kinetic model proposed by Avrami [44–46] and Erofe’ev [47], which is written as:

$$\alpha = 1 - \exp[(-k(t - t_0))^n] \quad (23.3)$$

or

$$[-\ln(1 - \alpha)]^{1/n} = k(t - t_0) \quad (23.4)$$

where  $\alpha$  is the extent of reaction or crystallization fraction (usually measured with X-ray diffraction),  $k$  is the rate constant,  $n$  is the Avrami–Erofe’ev order of reaction,  $t_0$  is the time where crystallization begins (end of induction period), and  $t$  is the elapsed time.

This model assumes that “germ nuclei” of the new phase are distributed randomly within the original reacting phase. After a nucleation event occurs, grains grow throughout the old phase until the transformation is complete. The sigmoidal shape of these types of kinetic plots may then be analyzed by breaking the curve up into different regions: (1) an induction period, (2) an acceleration region, (3) a deceleration region, and (4) completion of reaction. Fig. 23.4 shows an illustration of the regions described above.

The induction period tends to be dominated by nucleation events and is considered to be terminated by the development of stable nuclei. The acceleration region tends to be dominated by the growth of nuclei until a maximum rate of reaction is reached. The deceleration region occurs because the



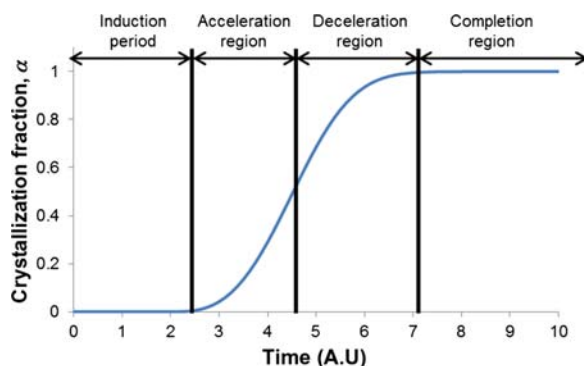


**FIGURE 23.4**  $\alpha$ -time plot summarizing the characteristic behavior observed for isothermal crystallization of solids. Permissions related to the material excerpted were obtained from the authors.

continued expansion of nuclei is no longer possible due to impingement and consumption of reactants. This process continues until the completion of the reaction [48].

The linearization of Eq. (23.5) is known as the Sharp and Hancock method [49], and it is employed to extract kinetic data from the  $\alpha$ -time plot:

$$\ln[-\ln(1-\alpha)] = n\ln(k) + n\ln(t-t_0) \quad (23.5)$$

Therefore by plotting  $\ln[-\ln(1-\alpha)]$  against  $\ln(t-t_0)$ , it is possible to explore the order of reaction rate law. The Avrami–Erofe’ev exponent  $n$  is extracted from the slope of the best-fit-line and the kinetic constant  $k$  can be obtained from the intercept ( $n\ln(k)$ ).

The Avrami–Erofe’ev exponent  $n$  can give further details on crystallization because it is a compounded term with two components,  $\beta$  and  $\lambda$ .  $\beta$  is the number of steps involved in nucleus formation, and its values are frequently 1 or 0. When  $\beta = 1$ , it corresponds to a very slow nucleation rate. When  $\beta = 0$  it corresponds to instantaneous nucleation.  $\lambda$  is the number of dimensions in which the nuclei grow:  $\lambda = 3$  for spheres or hemispheres, 2 for discs or cylinders, and 1 for linear development [48].

Values of  $n$  between 1 and 2 are typically observed for crystals growing preferentially in one dimension with needle-like morphology. Values of  $n$  between 2 and 3 are typically observed for crystals growing in two dimensions with plate- or disk-like morphology. Values of  $n$  between 3 and 4 are typically observed for crystals growing in three dimensions with spherical-like morphology. Fig. 23.5 shows the typical shapes that the  $\alpha$ -time plots acquire depending on the value of  $n$ , which may suggest the morphology of the crystalline particles.

The rate constants for this type of isothermal processes exhibit Arrhenius-type behavior, thus activation energy,  $E_a$ , and preexponential

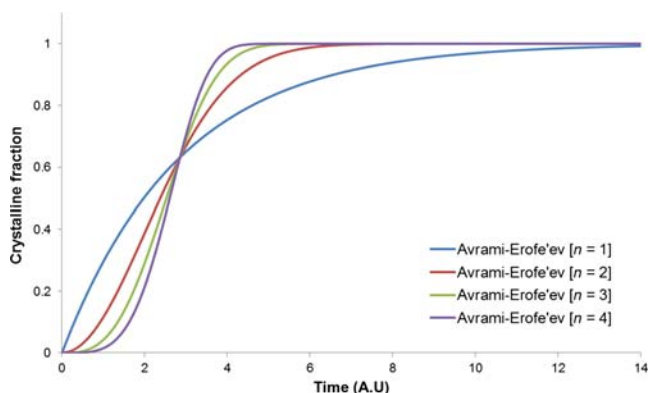


**FIGURE 23.5** Typical  $\alpha$ -time plots showing the characteristic shape depending on the value of the Avrami–Erofe'ev exponent  $n$ . Permissions related to the material excerpted were obtained from the authors.

factor,  $\nu$ , as described in the Arrhenius Eq. (23.6), can be determined from the slope and intercept of the best-fit-line of  $\ln(k)$  against  $1/T$ , respectively:

$$\ln(k) = \ln(\nu) - (E_a/RT) \quad (23.6)$$

### 23.2.3 Synthesis of iron–silicate materials

Preparations under hydrothermal conditions of some types of iron–silicate materials for use as catalysts or adsorbents are described in open [50–56] and patent [57–63] literature. It is very important to point out that the conventional preparation methods of iron–silicates materials described in these references succeeded only if organic structure guiding compounds (“organic templates”) were added to the synthesis mixture. In general, tetraalkylammonium compounds, tertiary and secondary amines, alcohols, ethers, and heterocyclic compounds are used as organic templates in those synthesis methods. It appears that iron does not play a structural directing role in these cases as the structure formation is guided strictly by the used organic template. The hydrothermal synthesis routes used so far only produce synthetic iron–silicate materials with the same framework structure of some of the synthetic microporous aluminosilicate counterparts. In addition, the large sizes of the organic molecules typically found in heavy oils and bitumen cannot enter the pore network of these iron–silicate materials. Thus the advantageous property of zeolitic materials—their high microporous area—is not used, making them inappropriate for the intended application.

All these known methods of producing iron–silicate materials have a series of drawbacks if it is desired to produce them at commercial scale for the intended applications. For instance, the organic templates used are toxic

and also easily flammable. Thus, since the synthesis must be carried out under hydrothermal conditions and at high pressure in autoclaves, a release of these organic templates into the atmosphere can never be completely prevented.

In addition, the use of organic templates increases the cost of production of the material because organic templates are expensive. Also, the effluent from the production of the iron silicate contains toxic materials, which require expensive and careful disposal in order to prevent contamination of the environment. The iron silicates obtained by those methods typically have organic molecules inside the channels and cavities of the produced materials. Hence, to be useful as catalysts or adsorbents, this organic material must be removed from the lattice. The removal of the organic template is typically carried out by combustion at high temperatures, which introduces an additional step, making the final product costly. The removal of the organic template can also cause damage to the lattice structure of the iron–silicate material obtained, thus diminishing its catalytic and adsorption properties. This also contributes to the production of greenhouse gases.

Currently, there is another research area that focuses on the development of ordered mesoporous materials for cracking of heavy fractions [64,65]. This trend has one disadvantage in the present application (i.e., the production of ordered mesoporous materials is too expensive for the given use, and also, many of the problems described earlier for the synthesis of crystalline iron–silicate materials using organic aid agents apply to the ordered mesoporous as well).

Searching for other types of iron–silicate preparation, we find mostly references in mineralogical and geoscience literature where several iron–silicate materials are prepared under nonhydrothermal conditions by thoroughly mixing appropriate proportions of the reactants and finally heating the mixtures at high temperatures and pressures, being the desired crystalline materials formed by solid state reactions or by growing from the melt after careful cooling. This type of preparation is not cost effective and is designed to obtain appropriate single crystals for further studies. However, some of the materials prepared by those synthesis methods have not been tested for any catalysis or adsorption applications, as far as these authors know, making them attractive to produce novel catalysts or adsorbents. One of the materials prepared in such way is the iron–silicate pyroxene mineral known as aegirine.

#### 23.2.4 Pyroxenes

The term pyroxene refers to a group of minerals and synthetic materials with similar crystal structure, which include important components of the earth's crust and mantle, lunar and martian rocks, and meteorites [66–70]. Pyroxenes are chain silicates having the general formula  $M2MIT_2O_6$ , and

depending on the earth's region, can comprise up to about 25% of the earth's volume deep down to 400 km [71], where they are produced under severe naturally occurring conditions of pressure and temperature [72,73]. Besides the naturally rich variety of minerals, there are a series of synthetic pyroxenes, which may or may not have the same chemical composition as the natural minerals. The five- to eight-coordinated *M2* cation site can be occupied by elements like Na, K, Li, Ca, Ba,  $\text{Fe}^{2+}$ , Mg, and Sr while the six-coordinated *M1* site can be occupied by elements like Mg, Mn,  $\text{Fe}^{2+}$ ,  $\text{Fe}^{3+}$ , Al, Cr, Ga, Zn,  $\text{Ti}^{3+}$ , V, Sc, Cu, Co, Ni, or In. The four-coordinated tetrahedral site, T, is preferentially occupied by Si. However, minor amounts of other elements like Al,  $\text{Fe}^{3+}$ , Ti, and others can be found in naturally occurring materials [66,67].

Any pyroxene belongs to either the orthorhombic (cell parameters  $a \neq b \neq c$ ;  $\alpha = \beta = \gamma = 90^\circ$ ) or monoclinic (cell parameters  $a \neq b \neq c$ ;  $\alpha = \gamma = 90^\circ$ ,  $\beta \neq 90^\circ$ ) crystal systems. There are two types of orthorhombic pyroxene: the orthopyroxene that crystallizes in the space group *Pbca*, which are found in nature, and the orthopyroxene that crystallizes in the space group *Pbcn*, which are prepared synthetically. Clinopyroxenes are the pyroxenes that crystallize in the monoclinic space groups *C2/c*, *P2<sub>1</sub>/c*, and *P2<sub>1</sub>/n*, depending on their chemical composition and genetic history [66].

The well-known characteristic structural feature of the pyroxenes is the chain of linked  $\text{SiO}_4$  tetrahedra, shown in Fig. 23.6. The dimensional characteristic of this chain allows it to fit by sharing oxygen atoms with chains of octahedra of different cations.

Fig. 23.7 shows an idealized pyroxene structure along the directions [010], [99], and [001] showing the tetrahedral and octahedral chains. As mentioned above, there are two kinds of cation sites, the one labeled *M1* and the one labeled *M2* [66]. Site *M1*, which contains atoms like Mg, Mn,  $\text{Fe}^{2+}$ ,  $\text{Fe}^{3+}$ , Al, Cr, Ga, Zn,  $\text{Ti}^{3+}$ , V, Sc, Cu, Co, Ni, or In (green octahedra in Fig. 23.7), is more or less regularly coordinated by an octahedron of oxygen atoms. However, the *M2* site, which is occupied by Na, K, Li, Ca, Ba,  $\text{Fe}^{2+}$ , Mg, and/or Sr (purple atoms in Fig. 23.7), have different coordination numbers according to the atom present (e.g., sixfold for Mg, and eightfold for Ca and Na). It should be noted that whereas the oxygen atoms coordinating *M1* are all oxygen atoms linked to one silicon atom of the pyroxene chains, the

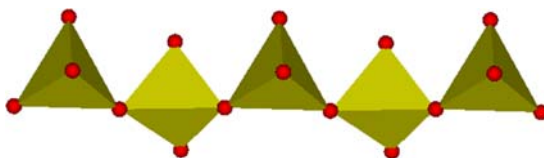


**FIGURE 23.6** Part of a pyroxene-type chain of  $\text{SiO}_4$  tetrahedra (red atoms represent oxygen). Permissions related to the material excerpted were obtained from the authors.

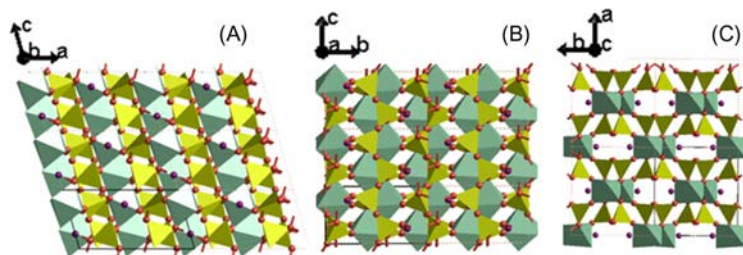


**FIGURE 23.7** Monoclinic pyroxene structure showing the tetrahedral (yellow) and octahedral (green) chain layers. (A) Structural drawing looking down in the [010] direction; (B) looking down in the [100] direction; and (C) looking down in the [001] direction. Purple atoms represent the  $M2$  cations and the  $M1$  cations are grouped in the green octahedra. The black box represents the unit cell. *Permissions related to the material excerpted were obtained from the authors.*

$M2$  atom is coordinated partly by oxygens, which are bonded to two silicon atoms. It can be seen from Fig. 23.7 that the pyroxene structure can also be regarded as made up of “layers” of tetrahedral alternating with “layers” of polyhedra with sixfold or higher coordination.

#### 23.2.4.1 Synthesis of pyroxenes

Geologists prepare pure synthetic counterparts of the naturally occurring pyroxenes minerals using high temperatures (up to about 2173K) and high pressures (up to about 10 GPa), which resemble the conditions where those materials were formed in nature. Conventionally, pyroxenes are produced by the mixture of oxides, hydroxides, and carbonates in stoichiometric ratios and heating them up to high temperatures and pressures. For instance, the preparation of single crystals of the synthetic pyroxene material  $\text{CaNiSi}_2\text{O}_6$  was carried out by solid-state reaction using a belt type high-pressure apparatus. The starting material was a mixture of  $\text{CaSiO}_3$  (the mineral Wollastonite),  $\text{NiO}$ , and  $\text{SiO}_2$  in stoichiometric ratio to produce the desired pyroxene. The mixture was then heated at 1773K at 6 GPa for 20 h to obtain several single crystals of the material [74].

Another example is the preparation of synthetic counterparts of the naturally occurring hedenbergite ( $\text{CaFeSi}_2\text{O}_6$ ) and petedunnite ( $\text{CaZnSi}_2\text{O}_6$ ) minerals and their solid solutions [75]. In this study, the syntheses were conducted preparing mixtures of the following reactants:  $\text{SiO}_2$ ,  $\text{CaCO}_3$ ,  $\text{Fe}_2\text{O}_3$ , Fe, FeO, and ZnO. All the oxides were annealed at high temperature. The precursors were prepared by sintering oxides in the appropriate portions to prepare the hedenbergite, petedunnite, or mixtures of them. Preparation temperatures ranged from 1098K up to 1473K, the pressure ranged from 0.5 up to 2.5 GPa, and synthesis times were from 22 up to 153 h. Some pyroxenes can be prepared at high temperature and at atmospheric pressure, pyroxenes like the synthetic counterpart of the mineral called Kosmochlor,  $\text{NaCrSi}_2\text{O}_6$ ,

was crystallized from a powdered Na-Cr silicate glass in a muffle furnace at 1073K for 96 h [76].

Most of the studies found in literature dealing with the pyroxenes are related to the compressibility behavior of them, and the way these materials are able to propagate seismic waves. Other studies show how they can be used as “indicators” of the pressure and temperature that were present during their formation. However, from a practical point of view, a less severe methodology of preparation should be found if important quantities of these materials are needed, and an understanding of their formation in these low-severity conditions of preparation must be addressed.

#### 23.2.4.2 *The pyroxene aegirine*

Aegirine has the ideal formula  $\text{NaFeSi}_2\text{O}_6$  (before 1989, the name acmite was accepted as synonymous with aegirine, but this has been discredited) [66]. The earliest reference to this material dates from 1835 in a note from Berzelius where the name aegirine was suggested in honor of Aegir the Scandinavian sea god [77]. The structure of aegirine [78], similar to the one depicted in Fig. 23.7, has iron in single zig-zag chains of edge-sharing octahedral *M1* sites and sodium in the eightfold coordinated *M2* sites. The direct Fe–Fe distance within the chains is 0.319 nm whereas the separation of chains is 0.655 nm in the *ab* plane, although the shortest Fe–Fe distance between chains is 0.618 nm [78].

The preparation of synthetic aegirine materials by geologists is usually carried out at high temperatures or at high temperatures and pressures to be able to produce good-quality crystals suitable for their characterization under different conditions and to understand the compressibility behavior of this type of material [79–92].

#### 23.2.4.3 *Typical preparation procedure of aegirine*

Aegirine can be prepared by the mixture of oxides on dry heating as other pyroxenes or it can be prepared under high-temperature hydrothermal conditions ( $> 573\text{K}$ ) and pressures. As an example of the dry preparation at atmospheric pressure, the synthesis of aegirine carried out at the US Bureau of Mines is described [79]. The material is synthesized by reaction of a stoichiometric mixture of  $\text{Na}_2\text{CO}_3$ ,  $\text{Fe}_2\text{O}_3$ , and silicic acid. The reactants are thoroughly blended by grinding before the initial heat treatment in order to optimize the homogeneity of the mixture. The mixture is heated in a platinum dish at 1093K for 30 minutes. The product is ground and thoroughly blended without dusting or loss of reactants and then is heated again at 1093K for 24 h. Next, it is heated again at 1143K for 5 days, and at 1173K for 68 h, with grinding and blending after each heating step. The final product is aegirine with a very small trace of hematite.

Examples of the preparation of aegirine under high-temperature hydrothermal methods are reported by Redhammer et al. [80,81]. In these procedures the gels are prepared starting from  $\text{Na}_2\text{CO}_3$ ,  $\text{Fe}(\text{NO}_3)_3 \cdot 9\text{H}_2\text{O}$ , and  $\text{C}_8\text{H}_{20}\text{O}_4\text{Si}$ . The gels are then heated at different temperatures (from 573K up to 973K) at 400 MPa from 96 to 476 h. Single crystals of aegirine together with quartz crystals are obtained in most of the experiments. Only at 973K and at 400 MPa with 144 h of crystallization is pure aegirine obtained.

#### 23.2.4.4 Low-temperature hydrothermal synthesis of aegirine

Looking further into the open and patented literature, there are two references worth mentioning. Riman and Cho [91] described a method for coating ferrous materials in which the material is placed into a reactor containing a water solution mixture of silica, sodium hydroxide, and glycol (an organic aid), heating them for several hours between 453 and 513K at autogenous pressure to produce a coating of aegirine on the surface of the ferrous material (the authors used the name acmite).

These authors claimed a corrosion-resistant workpiece characterized by being entirely and uniformly coated with an aegirine passivation coating formed by heating the workpiece in an aqueous treatment bath comprising  $\text{NaOH}$ ,  $\text{SiO}_2$ , and a water-soluble glycol (organic aid) at a temperature above 453K, until said passivation coating is formed. The aegirine in this case seems to be a film of several microns thick attached to the surface of the ferrous material, covering it completely to protect it from corrosion.

The second reference worth describing is the one that presents the possibility of preparing aegirine at low temperature by hydrothermal methods [92]. The method of preparation requires several steps that are not cost effective for commercial purposes and require long crystallization times (4 weeks) using as reactants:  $\text{SiO}_2 \cdot \text{Na}_2\text{O} \cdot 5\text{H}_2\text{O}$  and  $\text{FeCl}_2 \cdot 4\text{H}_2\text{O}$ . Syntheses were performed at 348, 363, 373, 383, 398, 423, and 473K, under equilibrium water pressure for 4 weeks. The authors claim that aegirine was synthesized only at 473K, but the product is not a pure material and is instead a mixture with a 2:1 phyllosilicate clay material. Below 473K aegirine is not produced; only 2:1 phyllosilicate materials are obtained. It is important to quote the authors comment on page 88 of the article [92]: “From our data, it appears that it is impossible, or very difficult, to synthesize aegirine hydrothermally below 473K” ... “Thus 473K appears as the lowest synthesis temperature for aegirine.” This statement has previously been suggested in an older work [90], which indicated that the lower temperature to form aegirine is between 473 and 523K.

#### 23.2.4.5 Hydrothermal synthesis of nanocrystalline aegirine

The original approach that may be useful for the preparation of nanocrystals aegirine in the sense of obtaining a cost-effective product with good yields is

the combination of high concentrations of sodium hydroxide with high density gels. In this way, the growth of the crystals can be controlled by the polymerization–depolymerization of the iron–silicate species and the availability of the iron because of the hydroxide formation. In the case of sodium-rich aluminosilicate gels to obtain zeolite A it is possible to obtain small crystals following a similar approach [93].

Preliminary experiments carried out in the development of this work indicated not only that aegirine can be obtained by hydrothermal methods below 473K but that it can also be obtained in pure form in less than 72 h (like many commercial zeolitic materials). The intention of this research was to produce the material as nanocrystals, so it is important to note that nucleation occurs more readily than crystal growth. Normally, this can be accomplished through lower synthesis temperatures, but this implies prolonged synthesis times and low yields, which are not suitable for a cost-effective product.

The preparation of nanocrystals of some zeolites with these methods, using clear solutions (not visible gel particles), also requires the help of organic aids [94–97]. For instance, silicalite I and ZSM-5 require TPAOH (tetra propyl ammonium hydroxide), faujasite and zeolite A require TMAOH (tetra methyl ammonium hydroxide), beta requires TEAOH (tetra ethyl ammonium hydroxide), making the production of these materials in large scales prohibitive. Another way to obtain nanocrystals of zeolitic materials is by the use of “space-confined synthesis” [98–100] in which the gel is introduced in the cavities of a suitable “container” and the crystallization is carried on inside the cavities. The confined space of the “container” allows the growth of the crystals until they fill the void space, then, elimination of the “container” produces the nanocrystals. Compounds like carbon black, starch, and polymer hydrogels are used as confinement additives and normally calcination steps are required to obtain the final product. This method is thus not suitable to produce large quantities of aegirine in a cost-efficient way.

#### 23.2.4.6 *Modifications to the pyroxene aegirine*

Aegirine has the formula  $\text{NaFeSi}_2\text{O}_6$ . Hence, the Si/Fe and Na/Fe ratios are fixed. However, by adding other components to the crystallization gel these ratios can be modified and thus new properties can be incorporated to the prepared material.

##### 23.2.4.6.1 **Structural isomorphous modification for the bulk and surface**

Ni-doped aegirine to produce selective active sites for hydrogenation of olefins is an example of this isomorphous modification. As described previously, the properties of aegirine can be modified by replacing any of the main elements conforming its structure: Fe, Si, and/or Na. The great advantage of doing this is that any element incorporated can be atomically very



well dispersed within the framework of the pyroxene and thus a new set of tailor-made nanomaterials can be produced. The atoms on the surface of nanoaegirine materials behave very differently from the atoms in bulk and thus can catalyze desired reactions. A very recent example of this selective application can be found in reference [101] where Sebakhy et al. showed that the incorporation of nickel in the structure of the nanopyroxene aegirine produced very selective and stable metallic nickel sites on the surface that were able to preferentially hydrogenate 1-octene in a mixture of 1-octene/toluene. Even further, the nanopowder was processed producing extrudates that were able to be placed in a bed reactor of a Pilot Test Unit to test the selective hydrogenation of the olefins presented in a catalytic naphtha feedstock that was employed. The novel catalyst not only produced the expected selective hydrogenation of the olefins in the feedstock but also did not show signs of deactivation even though the feed contained about 4 wt% sulfur, which is well known to poison nickel catalysts. Thus the small metallic nickel sites were protected from sulfur poisoning by their arrangement on the structure but at the same time were active for the selective hydrogenation of olefins over aromatic molecules. The results of the used feedstock together with the ones for the model molecules experiments and the characterization carried out on the materials indicated that the Ni-doped nanoaegirine material is a promising catalyst for the possible replacement of noble metals for hydrogenation reactions. It seems that the metallic nickel single or double sites were produced on the surface of the material; a double nickel site is depicted in Fig. 23.8. This concept of single or double metallic sites on the surface of

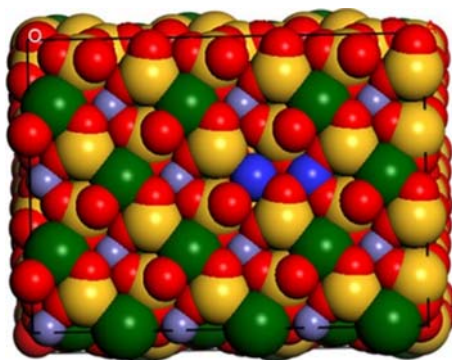


**FIGURE 23.8** Corey–Pauling–Koltun (CPK) space filled surface representation of the surface (001) of aegirine after isomorphous substitution of nickel atoms in one Fe and one Na centers producing a double metallic nickel center. Dark blue atoms represent nickel, yellow atoms represent silicon, red atoms represent oxygen, green atoms represent sodium, and light blue atoms represent iron. *Reprinted (adapted) with permission from Sebakhy KO, Vitale G, Pereira-Almao PR, Dispersed Ni-doped aegirine nanocatalysts for the selective hydrogenation of olefinic molecules. ACS Appl Nano Mater 2018, 1, 11, 6269–6280; doi.org/10.1021/acsanm.8b01472. Copyright 2018 American Chemical Society.*

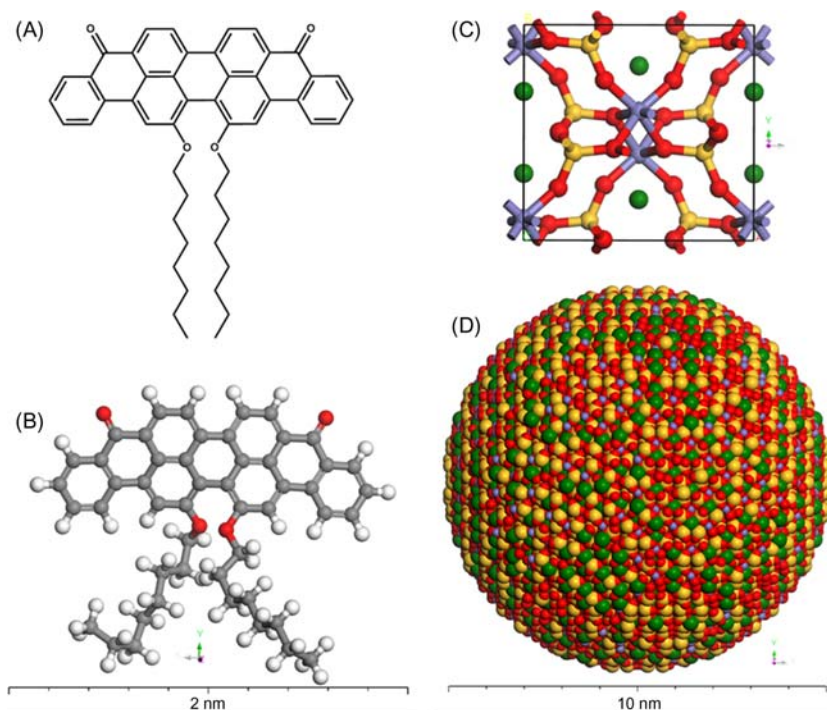


**FIGURE 23.9** Chemical structure of (A) VO-79 drawn with ChemDraw V14.0, (B) 3D ball and stick molecular structure of V79 optimized with BIOVIA Forcite module [24]. (C) Ball and stick aegirine unit cell structure drawn with BIOVIA Builder module. (D) CPK structure of a 10 nm nanoaegirine particle drawn with the BIOVIA nanostructure module [24]. Green atoms represent sodium, red atoms represent oxygen, blue atoms represent iron, yellow atoms represent silicon, grey atoms represent carbon, and white atoms represent hydrogen. *Permissions related to the material excerpted were obtained from the Royal Society of Chemistry (RSC) and further permission should be directed to the RSC; Hmoudah M, Nassar NN, Vitale G, El-Qanni A. Effect of nanosized and surface-structural-modified nano-pyroxene on adsorption of violanthrone-79, RSC Adv 2016;6:64482-64493.*

prepared materials [102,103] is leading to the possible substitution of homogeneous catalysts by heterogeneous catalyst, which has many practical advantages and in which metal-doped nanoaegirine materials can play an important role in future endeavors in catalysis.

Another example is the structural incorporation of zirconium (Zr) and cerium (Ce) while Zr and Ce were individually doped in the structure of aegirine nanoparticles by isomorphous substitution of Fe and Si. The doping of Ce and Zr showed a significant change in the crystalline domain size of the nanoparticles. This had an effect on the adsorption of Violanthrone-79 (V79) molecules as shown in Fig. 23.9. Both of them were able to successfully adsorb V79 [104].

#### 23.2.4.6.2 Structural isomorphous modification for the surface only

The surface of nanoaegirine can be modified by ion exchange (a property not present in naturally occurring pyroxene samples). This cannot be extended to the bulk due to the lack of porosity. Aegirine has the ideal formula  $\text{NaFeSi}_2\text{O}_6$  and thus the Si/Fe and Na/Fe ratios are fixed. However, this ratio can be modified by altering the central atoms (Fe or Si) with other elements by adding their procurers under controlled preparation methods [104]. The potential for structural modification of aegirine results from having outstanding superficial ion exchange properties, allowing for partially or totally surface modification by introducing a Bronsted acid site or univalent/divalent ions [105]. Making such modifications while the produced aegirine is small (nanosize) is favorable for catalytic and adsorptive applications [105]. In a recent study, our group investigated the effect of nanosized and surface-structural—modified nanopyroxene on adsorptive removal of a model molecule of V79. In that work, different nanosizes of aegirine have been hydrothermally synthesized at various conditions following several modifications steps, and the synthesized materials were investigated for removing the V79 in batch processes. To form small sizes of aegirine, small crystals were produced from the hydrothermal crystallization method for the desired treating time. These small crystals were nucleated and used as seeds to produce larger particle sizes via crystal growth with a seeding technique [104]. In the batch adsorption process, the adsorbed amount of V79 molecules for the small size nanocrystals was the highest among the different particle sizes. Functionalization, on the other hand, was used for structural modifications as following: ion exchanging, wet impregnation, and isomorphous substitution. Accordingly, aegirine surface was functionalized with hydrogen (H), calcium (Ca), and nickel (Ni). H and Ca ions were used for altering the original cation on the surface (sodium). Nickel, at low mass percentage (3 wt%), was impregnated on aegirine surface under wet conditions. As a result, functionalization with ion exchange and wet impregnation led to a slight change in the crystalline domain sizes of the nanoparticles compared with the unmodified ones. The protonated nanoparticles and the ion-exchanged nanoparticles with Ca and H doubled the adsorption capacity under the batch process [104] (Fig. 23.10).

#### 23.2.4.6.3 Structural surface modification by polymer grafting

There are several surface modification and functionalization techniques such as grafting [106–109]. Grafting involves modifying surface functionalities by bonding a preferred end functionalized polymer, which redefines the surface properties. One or more polymers can be added to the same substrate while still providing precise localization of the chain of the polymer at the surface.

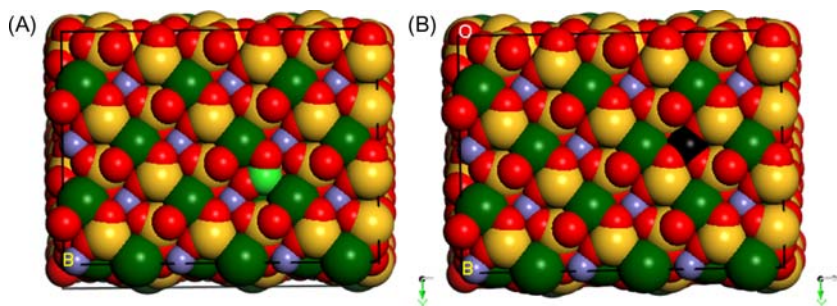


**FIGURE 23.10** CPK (001) optimized surface structures of aegirine drawn with the BIOVIA Builder module. (A) surface (001) with zirconium replacing a silicon atom and (B) surface (001) with cerium replacing an iron atom. Dark green atoms represent sodium, bright green atoms represent zirconium, red atoms represent oxygen, blue atoms represent iron, black atoms represent cerium, and yellow atoms represent silicon. *Permissions related to the material excerpted were obtained from the Royal Society of Chemistry (RSC) and further permission should be directed to the RSC; Hmoudah M, Nassar NN, Vitale G, El-Qanni A. Effect of nanosized and surface-structural-modified nano-pyroxene on adsorption of violanthrone-79, RSC Adv 2016;6:64482-64493.*

Bonding between the substrate and the polymer are key in the strength and duration of the grafting. Interactions formed as a result of physisorption techniques form fragile polymer bonding and are considered weak bonds presenting short-term adhesion. Chemisorption techniques on the other hand, provide strong covalent bonding, which is most desirable due to its strong long-term adhesion [110]. Grafting also depends on how active the surface of the substrate is; highly active surfaces will be a strong predicament to the polymer. If the surface cannot perform a chemical reaction due to its nature, activation agents are usually utilized to increase the reactivity of the surface by introducing effective active species such as coupling agents, chlorite, epoxychloropropane, acids, organic isocyanat, and many more.

**23.2.4.6.3.1 Coupling agents** Silane coupling agents are found to be most effective when dealing with aegirine and a polymer that are different in nature (i.e., organic and inorganic material). They greatly improve the mechanical strength of the composite material and form strong adhesion to the surfaces. They act as a bridge that binds reactive functional groups from both ends to the organic and inorganic materials as shown in Fig. 23.11.

There are different silane groups available but certain factors must be considered when selecting a silane for an inorganic substrate surface modification. These factors include the hydroxyl group concentration on the surface of the aegirine, which contributes to the maximization of the grafting. The more accessible the active sites, the more the silanes react with them and hence the grafting is maximized. Another factor is the physical and chemical properties of the interphase region, which can promote or detract the

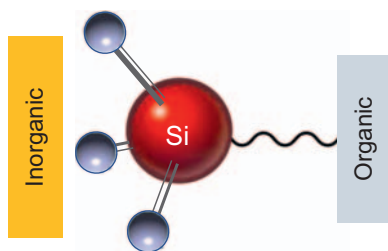


**FIGURE 23.11** Schematic of an individual molecule of a silane coupling agent with two types of reactive groups at each end—one to react with organic and the other with inorganic.

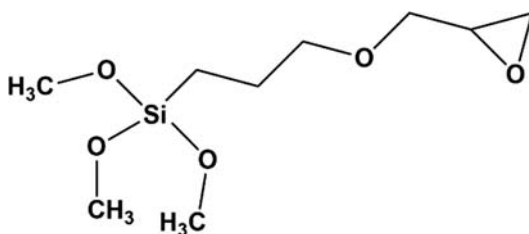


**FIGURE 23.12** The (3-Glycidyloxypropyl) trimethoxysilane organic-inorganic hybrid chemical structure.

grafting. Usually silanes containing three alkoxy groups are used for grafting due to their high coverage maximizing the anchoring to the organic material on the other side. (3-Glycidyloxypropyl) trimethoxysilane (3GT) is among the most commonly used organic-inorganic hybrid material as well as a grafting agent to functionalize silica-based surfaces [111]. 3GT is an organically modified alkoxide whose organic group contains an epoxide ring and the inorganic group contains methoxy groups as shown in Fig. 23.12 [112]. The epoxide ring opens presenting a large variety of possible reaction pathways and side reactions, but particular important to this research is opening the ring and bonding with polymers [111].

**23.2.4.6.3.2 Polymers** The choice of polymer is highly dependent on the application and on the contaminants of interest. In the case of aegirine, grafting depends primarily on the reaction between the inorganic nanoparticle surface hydroxyl groups and the monomer of choice. Monomers are chosen due to their affinity in the removal of the desired contaminant from the wastewater.

**23.2.4.6.3.2.1  $\beta$ -Cyclodextrin**  $\beta$ -cyclodextrin ( $\beta$ -CD) natural monomer is a cyclic oligosaccharides consisting of ( $\alpha$ 1,4)-linked- $\alpha$ -D-glucopyranose units and their numerous derivatives [113]. It contains large numbers of primary and secondary hydroxyls sitting on hydrophilic shells contained in

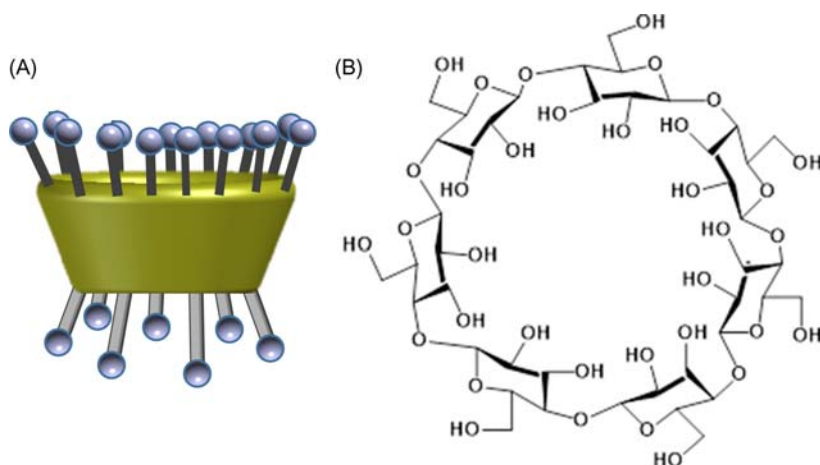


**FIGURE 23.13**  $\beta$ -CD monomer (A) schematic representation and (B) chemical structure.

**TABLE 23.1** Physical and chemical properties of  $\beta$ -CD monomer.

Property	$\beta$ -CD monomer
MW	1135
Diameter of the cavity ( $\text{\AA}$ )	8.0
Volume of the cavity ( $\text{\AA}^3$ )	346
Solubility in water at 25°C (g/100 mL)	1.85

lipophilic cone-shaped cavities (lined with hydrogen atoms and bridged with glucosidic oxygen atoms) as shown in Fig. 23.13. That makes it an ideal candidate for the inclusion of suitably sized organic guest species [110,114]. They are known for their low toxicity and the fact that they do not provoke an immune response in humans [115]. Therefore they are widely used as carriers for drug delivery applications and in the food industry [116–118].

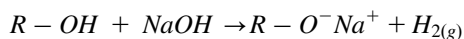
$\beta$ -CD has been shown to remove organic micropollutants from aqueous solution including aromatic model compounds similar in structure to naphthenic acids [119]. The physical and chemical properties of  $\beta$ -CD monomer are listed in Table 23.1 [120].

Polymers can be integrated with silica-based materials using four main principles: oligosaccharide impregnation, polymerization, sol–gel processes, or chemical grafting. Chemical grafting of  $\beta$ -CD forms a strong covalent bond that prevents leaching of the cyclodextrins from the aegirine surface [121].



**23.2.4.6.3.3 Preparation of  $\beta$ -cyclodextrins grafted nanoaegirines** Two steps are involved in grafting the nanoaegirine, after the hydrothermal preparation of nanoaegirine with the surface-enriched in hydroxyl groups as described before; chemical bonding of the bridge compound to the surface of the nanoaegirine and nucleophilic attack from the ionized  $\beta$ -CD to the bridge anchoring it to the nanoparticle [122]. Grafting the nanoaegirine (nano-AE) with  $\beta$ -CD monomer is accomplished via the inorganic-organic hybrid—3-Glycidyloxypropyl trimethoxysilane (3GT) by a two-step reaction—between the inorganic nanoparticles and the hybrid bridge and between the hybrid bridge and the organic polymer [116,121]. As 3GT is highly sensitive to water in which it will react with it causing the opening of the epoxy ring, the synthesis must be performed in a dry environment [121,123]. The calculated amount of 3GT is added to dried toluene percolated through molecular sieves desiccants and added dropwise. During a 3 h period, covalent bonding of methoxy oxygen occurs, thus anchoring the 3GT to the nano-AE [121].

To anchor the  $\beta$ -CD monomer to the epoxy ring of the 3GT, dried  $\beta$ -CD monomer is dissolved in dried N, N-DimethylFormamide or DMF. This is an important consideration for an aprotic reagent [124]. To activate the hydroxyls on the surface of the monomer, sodium hydride is added to the mixture as the basic catalyst (later filtered) for some time to allow it to react with the  $\beta$ -CD monomer in DMF under dry conditions. The  $\beta$ -CD monomer is exposed to sodium hydride (NaH) where the hydride reacts with the hydrogen from the hydroxyl present in the monomer forming  $H_2$  gas and leaving an alkoxide like ion as per the following reaction [125]:



A reflux system is set up with a mixture of dried DMF,  $\beta$ -CD slurry after filtration, and previously anchored bridge on the nano-AE and heated to 423K for 2 h under agitation (300 rpm) to react. At this point, activated  $O^-$  from the  $\beta$ -CD hydroxyls conducts a nucleophilic attack opening the epoxy ring and bonding to it. The presence of the ethoxide functional group triggers the nucleophilic attack over the epoxy ring from the bridge, as shown in Fig. 23.14. When the nucleophilic attack takes place, it opens the epoxy ring.

The monomer is then anchored through oxygen to the bridge, thereafter filtered, washed with DMF, toluene, and methanol and placed under vacuum at 333K [123].

**23.2.4.6.3.3.1 Interaction of epoxy hybrid with the aegirine surface** The three alkoxy silane coupling agent is used to graft the surface of the aegirine by reacting the silanol groups to the hydroxyl groups on the surface. There are three possibilities for the anchoring of the bridge molecules to the surface of the aegirine: the formation of one, two, or three bonds with the surface through one, two, or three methoxy groups. As previously mentioned, the distribution of hydroxyl groups as well as the topography of

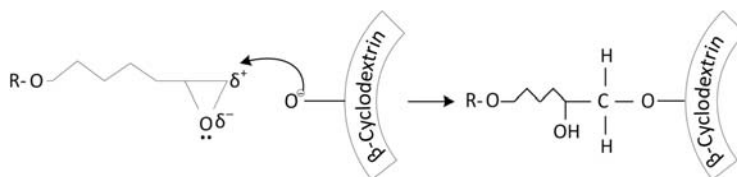


**FIGURE 23.14** Schematic representation of the nucleophilic substitution between the  $\beta$ -CD monomer and the epoxy group at the end tail of the 3GT. *Permissions related to the material excerpted were obtained from ACS and further permission should be directed to the ACS; Nafie G, Vitale G, Carbognani Ortega L, Nassar NN. Nanopyroxene grafting with  $\beta$ -cyclodextrin monomer for wastewater applications. ACS Appl Mater Interfaces 2017;9:42393–42407. <https://pubs.acs.org/doi/abs/10.1021%2Facsami.7b13677>.*

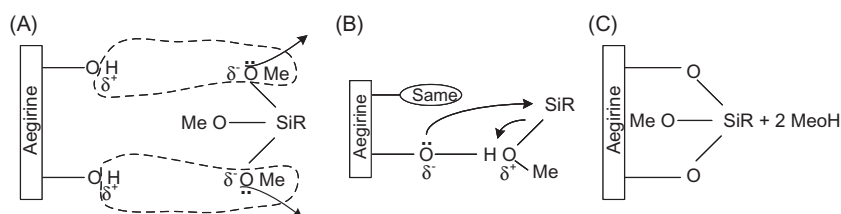


**FIGURE 23.15** Direct exchange chemical reaction with the substrate. (A) shows the electro-negativity of the nano-AE and methoxy on the 3GT, (B) reaction between the  $\ddot{O}$  and Si with methanol as the leaving group, and (C) bonding of the 3GT to the nano-AE. *Permissions related to the material excerpted were obtained from ACS and further permission should be directed to the ACS; Nafie G, Vitale G, Carbognani Ortega L, Nassar NN. Nanopyroxene grafting with  $\beta$ -cyclodextrin monomer for wastewater applications. ACS Appl Mater Interfaces 2017;9:42393–42407. <https://pubs.acs.org/doi/abs/10.1021%2Facsami.7b13677>.*

the surface will influence the number of bonds that can be formed by the reacted 3GT molecule. The structural geometric optimization shows that anchoring by forming three bonds with the surface requires three  $-\text{OH}$  groups very close to each other; however, this arrangement implies some physical constraints because of the three formed bonds, which impedes the stabilization of the 3GT molecule anchored in this way on the surface. On the other hand, if only a few silanol groups are present on the surface, the only possibility for anchoring the reacted 3GT molecule is by forming only one bond. However, the analysis of the used nanopyroxene indicates a critical number of hydroxyl groups on its surface suggesting that there are enough hydroxyl groups to bond two of them to each methoxylated 3GT molecule; thus each 3GT molecule bonds to two hydroxyl groups on the surface of the silica.

The methoxy group on the 3GT reacts with the surface of the nano-AE as shown schematically in Fig. 23.15 [126]. Reflux heating helps accelerate the reaction as the reactivity is lower than the condensation reaction of silanols [126].



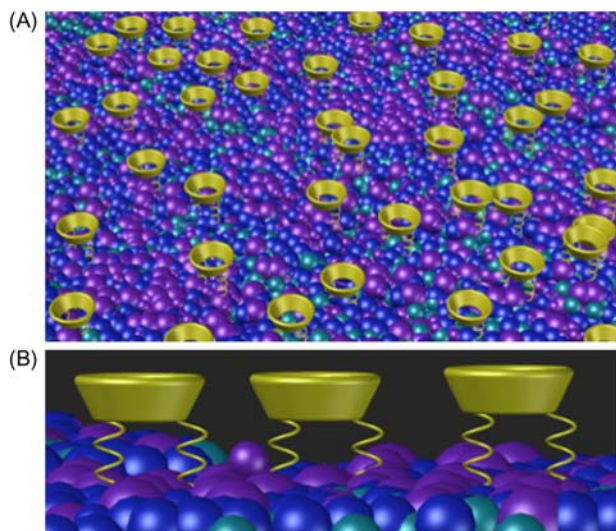


**FIGURE 23.16** Top and side views of  $\beta$ -CD molecule bonded to two hydrolyzed 3GT molecules anchored to two hydroxyls groups onto the silica surface.

**23.2.4.6.3.3.2 Interaction of  $\beta$ -CD with the aegirine surface** As reported previously, the  $\beta$ -CD molecule will bond to the 3GT molecule through its  $-\text{CH}_2\text{-OH}$  groups [117,121,125]. This is particularly true since these groups are easily activated to form alkoxy groups performing the nucleophilic attack to the epoxy ring present in the 3GT molecule already anchored onto the surface of the nanopyroxene. There are seven of these groups present in each  $\beta$ -CD molecule. However, it is not desirable to anchor all of them to the surface as this will impose physical and chemical constraints to the possibility of the  $\beta$ -CD molecule for trapping and forming inclusion complexes with small or large molecules. Fig. 23.16 shows the top and side views of the geometrically optimized composite material (Fig. 23.16A), and also, illustrates the composite material expanded to show how the surface will look with several anchored  $\beta$ -CD molecules (Fig. 23.16B).

#### **23.2.4.6.3.4 Applications of $\beta$ -CD grafted nanopyroxene in wastewater treatment**

**23.2.4.6.3.4.1 Oil extraction wastewater-organic contaminant removal** Tailing ponds contain naphthenic acids (NA), which are formed as a result of the oil sand's reaction with caustic (NaOH) releasing those carboxylic surfactants. NA is the primary source of toxicity in oil sand process-affected water (OSPW) [127–129] as per Environment Canada and is severely toxic to mammals [130]. NA influences the aquatic microorganisms' community even

at as low concentrations as 6–20 mg/L (tailing ponds contain typically between 80 and 100 mg/L of NA) [131]. Naturally occurring NA in rivers is generally below 1 mg/L, but in tailing ponds it can get as high as 110 mg/L [132]. The removal of NA from OSPW has been challenging due to its high solubility in water, which in turn makes it resistant to the conventional oil water separation processes [133,134].

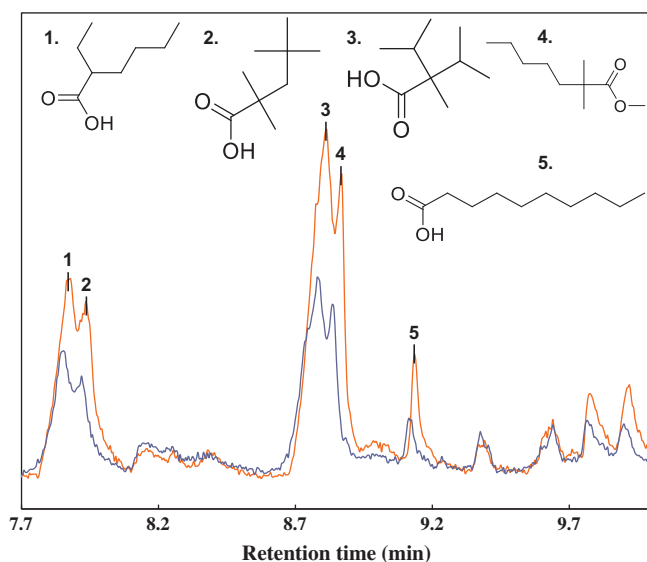
**23.2.4.6.3.4.1.1 Naphthenic acid model molecules**—Naphthenic acid molecules were chosen to study the interaction with the  $\beta$ -CD molecule attached to the hydroxylated silica surface through the 3GT molecule with different sizes, shapes, and morphologies. The small-size molecules enter inside the cavity of the  $\beta$ -CD molecule inducing some change on the conformation of the anchored  $\beta$ -CD molecule. They move closer to the silica surface then inside the cavity. Based on the molecular arrangement, some take longer than others to enter the cavity but they all eventually enter within a considerably fast time and stabilize inside. The carboxylic groups of the molecules tend to be stabilized toward the side of the  $\beta$ -CD molecule having the 14 hydroxyl groups. However, the larger molecules are attracted by the  $\beta$ -CD molecule but do not enter the cavity of the  $\beta$ -CD molecule. The interaction with the  $\beta$ -CD molecule is through the carboxyl groups but only with the hydrophilic surface of the  $\beta$ -CD molecule containing the 14 hydroxyl groups. They are attracted by the  $\beta$ -CD molecule then move around the upper part of the cup keeping the hydroxyl groups close to the mouth of the  $\beta$ -CD molecule upper part but never enter inside the cup. In this case, they can form clusters around the top of the cup.

Therefore the sizes, shapes, and morphologies of the naphthenic molecules do indeed impact their interactions with the anchored  $\beta$ -CD molecule revealing the importance of the fundamental understanding of the design of the nanotrap adsorbents.

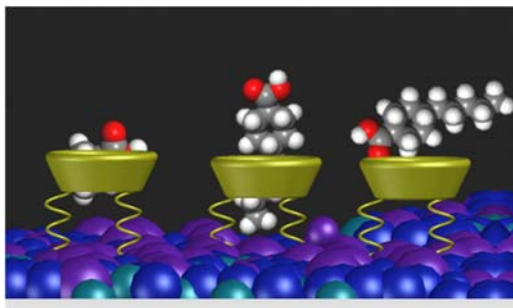
**23.2.4.6.3.4.1.2 Interaction of  $\beta$ -CD with naphthenic acids**—As shown before and in the literature,  $\beta$ -CD molecule can form inclusion complexes with organic molecules trapped inside its cavity [122,135–141]. A great variety of guest molecules can be trapped into the annular structure of  $\beta$ -CD forming nanosized host–guest inclusion complexes. It has been found that a benzoic acid molecule can be trapped inside each  $\beta$ -CD molecule protruding its  $-\text{COOH}$  group outside the part of the cone having the  $-\text{CH}_2-\text{OH}$  groups [141].

Fig. 23.17 shows the GC–MS chromatogram of a commercial naphthenic acid wastewater sample before and after being exposed to  $\beta$ -CD grafted nanopyroxene. It is estimated that 50% of the NA was captured as observed in Fig. 23.17. However, the removal capacity differs based on the structure, size, and conformation of the compound being removed.

The driving forces for the removal of the organic compounds with  $\beta$ -CD monomer grafted nanopyroxenes are mainly the solubility of the NA whose carbon backbones are lipophilic and expected to selectively partition over



**FIGURE 23.17** GC–MS chromatogram of commercial naphthenic acid wastewater sample before (orange) and after (blue).



**FIGURE 23.18** Schematic of the interaction possibilities for the removal of naphthenic acids from wastewater.

the cyclodextrin grafted moiety of the synthesized nanoparticles, H-bonding, polarity, and host–guest inclusion depending on the size of the compound being adsorbed [121]. It is not necessary to have one  $\beta$ -CD for each NA molecule present in the wastewater sample to remove it all. This is because the removal is not only caused by the inclusion complex but also the attraction on the outside of the  $\beta$ -CD forming clusters of the NA species as shown in Fig. 23.18.

When the molecule is small, the carboxyl group interacts with the fourteen -OH groups of  $\beta$ -CD and enters the cavity. If the molecule is larger than

the cavity of the  $\beta$ -CD, it is likely that the alkyl chain will protrude outside of the  $\beta$ -CD. Some molecules have a small end that allows them to partially enter the cavity leaving the large group outside. Grafting using a bridge produces a configuration that allows for the physical space for various molecules to enter the cavity, partially or fully, before being hammered by the surface of the nanoaegirine. Alternatively, clusters of the contaminants can form by interacting with the hydroxyls sitting on the top of the cup. In fact, more than one naphthenic acid molecule can be trapped inside each  $\beta$ -CD monomer grafted to the nanoaegirine or by forming a cluster around the naphthenic acids.

**23.2.4.6.3.4.2 Removal of pharmaceutical active compounds from water**  $\beta$ -CD grafted nanopyroxene can provide an application for pharmaceutical wastewater treatment removing contaminants from the wastewater in a similar mechanism as the one described previously for the removal of organic contaminants.

The levels of pharmaceutically active compounds (PhACs) have been increasing drastically in the last few years to many micrograms per liter [142]. The most commonly PhACs found in wastewater are metformin, carbamazepine, acetaminophen, diclofenac, sulfamethoxazole, trimethoprim, and erythromycin [143,144]. Among those contaminants metformin is the most commonly prescribed pharmaceutical worldwide as it is an antidiabetic drug treating more than 360 million people [145]. The compound is not fully metabolized in humans where about 70% is excreted unchanged in urine while the rest is excreted in feces [146]. Metformin is a compound that has different ionic species with different equilibrium concentrations at different pH. Similar to the behavior of NA,  $\beta$ -CD is a great candidate for the removal of metformin. Fig. 23.19 shows the simulated removal of metformin from water using  $\beta$ -CD nanopyroxene.

**23.2.4.6.3.4.3 Enhanced settling of fine particles** Extraction of bitumen from the oil sand results in fluids called tailings, which are discharged into tailing ponds [147]. These tailings or OSPW are defined as the extraction water, surface water in tailing ponds, water in the pores of sludge or tailings, water contained in the sand depositing at the bottom of the pond, and seepage water generated, collected, and returned via engineering means to the tailing ponds [148]. Fig. 23.20 shows the typical layers formed in tailing ponds made up of water, sands, clays, solids (suspended and settled), residual hydrocarbons, organic compounds, and inorganic salts [149]. As clearly shown, the coarse sand settles at the very bottom of the pond, and the middle layers consist of fine and mature tailings that contain suspended fine solids believed to be in the nanoparticle range [150]. The top layer is the recyclable water that goes back to be used in the oil sand extraction processing reducing the demand for freshwater from rivers [151]. Without the introduction of a material to assist with the settling process of these fine clays, it is estimated to take thousands of years to settle [152].

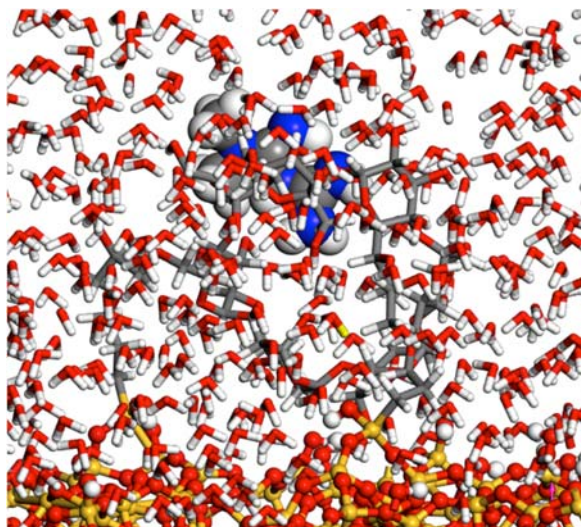


**FIGURE 23.19** Top view of the optimized metformin (CPK representation) trapped inside the  $\beta$ -cyclodextrin molecule bonded to *two* hydrolyzed (3-Glycidyloxypropyl)trimethoxysilane molecules, where each are anchored to two hydroxyls groups onto the silica surface. Geometry optimization and dynamic simulation carried out with the module Forcite and the COMPASS forcefield within BIOVIA Materials Studio 2017.

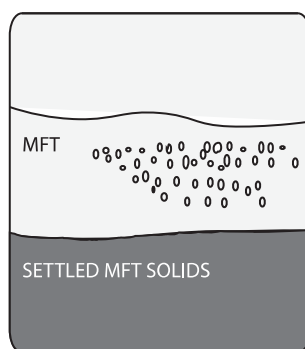


**FIGURE 23.20** Tailing pond layers formed upon discharge.

Grafting nanoaegirine presents an opportunity for enhanced fine particle settling in wastewater. Fine particles are suspended because they have a layer of hydrocarbons surrounding the colloids impeding their ability to aggregate and settle. Grafted nanopyroxene can be applied to the water to destabilize the suspended particles by interacting and breaking the bonds between the organic species and the particles. Removing the hydrocarbons layer will release the fine particles freeing them up to settle, consequently enhancing

settling in produced wastewater. Ongoing work is carried out by our group with published results expected.

#### 23.2.4.6.4 Ionic surface modification of nanoaegirine and its application in adsorptive removal of contaminants from wastewater

Nanoaegirine has also been functionalized with polyethylenimine for the removal of total organic carbon (TOC) from wastewater. Branched polyethylenimine (PEI) is a cationic organic polymer with a lot of branched amino groups on the surface, with a high level of buffering capacity in a broad pH range inside the wastewater solution [153–156]. Thus it has been used as functionalizing agents for magnetic nanoparticles (MNPs) to remove the TOC from sewage wastewater as well as various heavy metals from their aqueous solutions. Hethnawi et al. [157] has used PEI as a functionalizing agent for nanoaegirine at mild conditions without the need for primary surface modifications. Fig. 23.21 shows a pictorial representation of the cationic polymer, nanoaegirine particle, and their electrostatic interaction after functionalization [157]. In an aqueous solution, aegirine imparts negatively

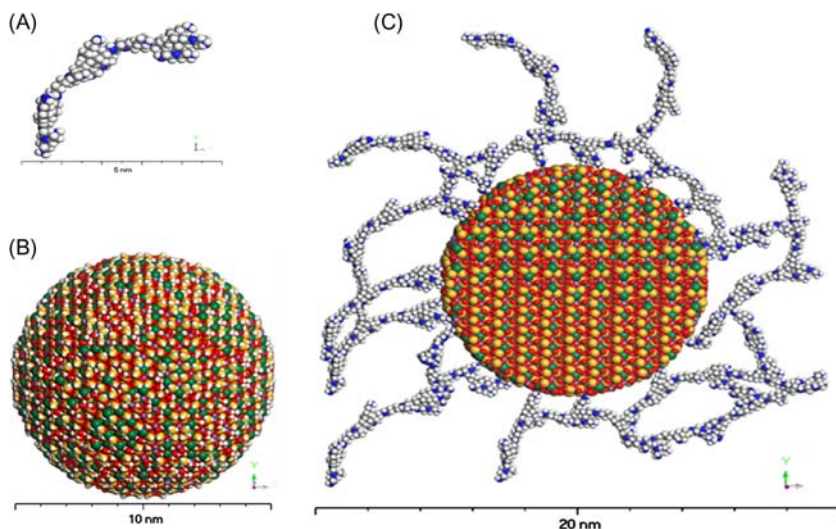


**FIGURE 23.21** CPK representation of (A) possible conformation of a PEI polymer chain; (B) a 10-nm spherical nanoparticle of the pyroxene aegirine; and (C) cross-sectional pictorial representation of the interaction of the PEI polymer with the surface of a 10-nm nanoparticle of the pyroxene aegirine. Red spheres represent oxygen atoms, yellow spheres represent silicon atoms, green spheres represent sodium atoms, light purple spheres represent iron atoms, white spheres represent hydrogen atoms, grey spheres represent carbon atoms, and blue spheres represent nitrogen atoms. Permissions related to the material excerpted were obtained from Elsevier and further permission should be directed to Elsevier; Hethnawi A, Nassar NN, Vitale G. Preparation and characterization of polyethylenimine-functionalized pyroxene nanoparticles and its application in wastewater treatment, *Colloids Surf A: Physicochem Eng Asp* 2017; 525:20–30.



charged iron atoms and can exchange the sodium ions with a cationic moiety of PEI. Accordingly, PEI-functionalized aegirine is formed with a long chain of polymeric structure of amino groups that produce interacting sites or pockets to capture various organic matters. These interacting sites can interact with various organic molecules via (1) hydrogen bonding, (2) electrostatic interactions, and (3) host–guest interactions in the formed cavities within the PEI polymer anchored on the anionic surface of the nanopyroxene material through metal coordination, hydrophobic forces, van der Waals forces, and/or pi–pi interactions. Effectiveness of capturing organic pollutants (effluent of textile industry) was tested for the functionalized nanoparticles with PEI in batch, continuous, and field-scale experiments.

**23.2.4.6.4.1 Batch adsorptive removal of the TOC from industrial effluent** Fig. 23.22 compares the batch adsorptive removal of PEI-functionalized aegirine (PEI–APs) with the nonfunctionalized aegirine (APs), magnetic nanoparticles (MNP), PEI-functionalized magnetic nanoparticles (PEI–MNP), and activated carbon (AC). It also includes fitting the adsorption equilibrium data with the Sips model (blue line), which considers the heterogeneity of different adsorbent surfaces and the interaction between the adsorbed molecules. As shown, the highest capacity for adsorption is

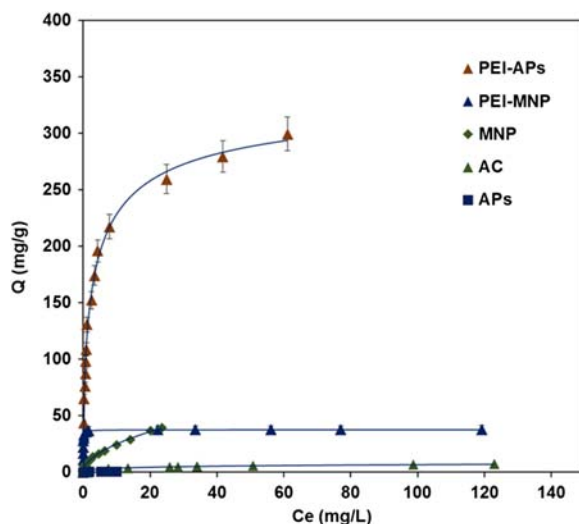


**FIGURE 23.22** Adsorption isotherms of industrial textile wastewater onto different adsorbents. Adsorbent dose: 10 g/L; shaking rate: 200 rpm; pH: 8;  $T$ : 298K. The symbols are experimental data, and the solid lines are fitting the data with Sips model. *Permissions related to the material excerpted were obtained from Elsevier and further permission should be directed to Elsevier; Hethnawi A, Nassar NN, Vitale G. Preparation and characterization of polyethylenimine-functionalized pyroxene nanoparticles and its application in wastewater treatment, Colloids Surf A: Physicochem Eng Asp 2017; 525:20–30.*

obtained for the functionalized nanoaegirine (340 mg/g), compared with the other adsorbents (<50 mg/g) [157]. AC has a very low capacity for adsorption due to its nonuniform pore structure, and these pores are in microranges, providing low adsorption efficiency in adsorbing the large molecules. On the other hand, MNP, even after PEI functionalization, has low effectiveness in batch adsorption compared with that for PEI-APs, indicating that the particular surface characteristics are important in performance. In addition, functionalizing MNP surface, opposed to APs, requires a primary surface coating before the end-grafting with PEI at well-monitored conditions. This primary surface coating limits utilizing such nanoparticle type in real water and wastewater treatment processes.

**23.2.4.6.4.2 Continuous adsorptive removal of TOC at in a fixed-bed column** In continuous adsorption, the removal of wastewater in terms of TOC was tested compared with the aforementioned adsorbents inside a fixed-bed column that operates under the effects of various operational parameters. The nanoadsorbents inside the column should not be directly employed in massive amounts. This might cause pressure drop buildup, especially at high initial concentration of pollutants. For that reason, the nanoadsorbents are embedded into supporting material at very low mass fraction such as diatomite (D). Diatomite (D) is a commercial filter aid that has a low adsorptive capacity, but is attractive for wastewater applications since it has abundant, low cost, and tunable properties. However, it has large particle size and low effectiveness in removal of many dissolved pollutants (i.e., TOC). Supporting it with nanoadsorbents that have a high adsorptive removal of the dissolved TOC can improve its performance in filtration of both dissolved and suspended pollutants. Fig. 23.23 shows a pictorial representation for supporting or embedding PEI-APs into hydroxylated Diatomite (D) surface.

Fig. 23.24 shows the experimental breakthrough curves obtained for Diatomite (D) before and after embedding low mass percentages (5 wt%) of the aforementioned nanoadsorbents as well as the AC at the same operational parameters. The removal efficiency for the organic pollutants is indicated by the achieved breakthrough times for every adsorbent, such that the highest removal efficiency is obtained for the highest breakthrough time. Embedding the Diatomite (D) with PEI-APs, as can be seen, has very high breakthrough time compared with the other adsorbents, resulting in the best removal efficacy.

**23.2.4.6.4.3 Continuous adsorption in a field test experiments using rotary drum filter** Rotary drum filter (RDF) is a conventional filtration method applied to remove the suspended solids and TOC from industrial effluents [160]. As shown in Fig. 23.25, RDF consists of a drum rotating in a tub of wastewater to be filtered. The drum is precoated with a filter aid,



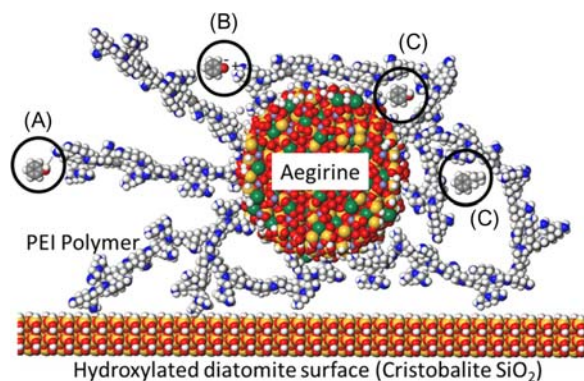


**FIGURE 23.23** Schematic representation of the possible supramolecular interactions (noncovalent interactions in water) of the pollutant molecules with the developed adsorbent for their removal: (A) hydrogen bonding interactions, (B) electrostatic interactions, and (C) host–guest interactions in the formed cavities within the PEI polymer anchored on the anionic surface of the nanopyroxene material through metal coordination, hydrophobic forces, van der Waals forces, and/or pi–pi interactions. Permissions related to the material excerpted were obtained from Elsevier and further permission should be directed to Elsevier; Hethnawi A, Manasrah AD, Vitale G, Nassar NN. Fixed-bed column studies of total organic carbon removal from industrial wastewater by use of diatomite decorated with polyethylenimine-functionalized pyroxene nanoparticles. *J Colloid Interface Sci* 2018;513:28–42 [158].

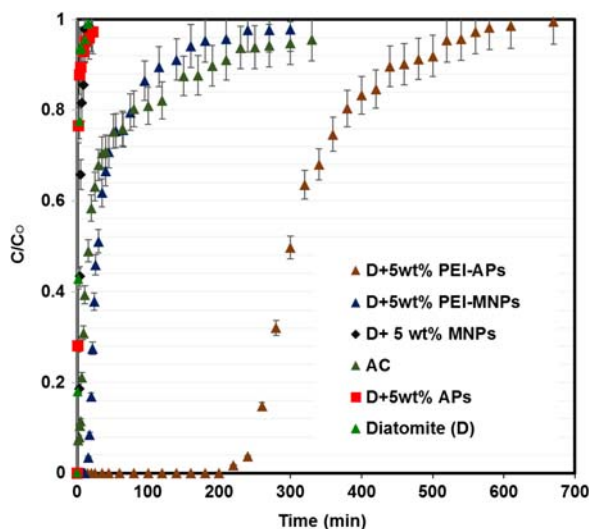


**FIGURE 23.24** Experimental breakthrough curve (BTC) of fixed-bed column for different nanoparticle types embedded on Diatomite (D) at 5 wt%, temperature of 298K, and pH of 8 for the removal of textile effluent at flow rate, influent concentration, and bed depth of 0.8 mL/min, 49 mg/L, and 7.5 cm, respectively. Permissions related to the material excerpted were obtained from Elsevier and further permission should be directed to Elsevier; Hethnawi A, Nassar NN, Manasrah AD, Vitale G. Polyethylenimine-functionalized pyroxene nanoparticles embedded on diatomite for adsorptive removal of dye from textile wastewater in a fixed-bed column. *Chem Eng J* 2017;320:389–404 [159].

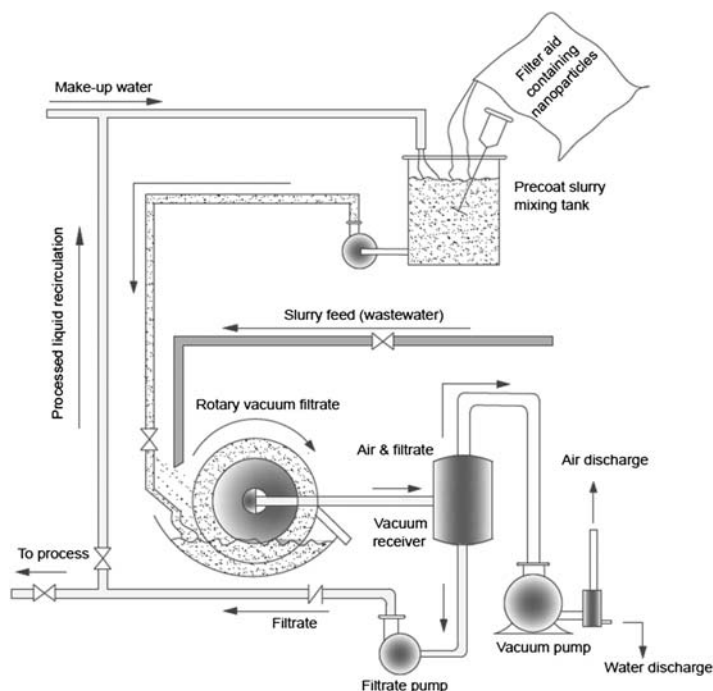


**FIGURE 23.25** Schematic diagram for the rotary drum filter (RDF).

typically Diatomite (D). After applying the precoat, the wastewater is sent to the tub below the drum, which rotates through the wastewater liquid, applying a vacuum. The vacuum sucks the wastewater onto the drum's precoated surface, separating it into liquid and solid portions. The vacuum sucks the liquid portion through the filter media to the internal part of the drum, resulting in a filtrated liquid that is pumped away. Contaminants, on the other hand, adhere to the precoated surface. The drum then automatically passes a knife through the adhered contaminants and part of the filter media (Diatomite (D)), revealing a fresh surface media. Although RDF is effective in some types of wastewater, it is inefficient, especially when the wastewater contains a high level of dissolved TOC. This is because the employed Diatomite (D) has a very weak adsorption capacity but excellent absorption power. It is therefore widely used as a filter aid in the filtration of suspended solids, but is ineffective in the adsorption of the dissolved pollutants. As a result, an improvement in the filtration efficiency of Diatomite (D) is needed.

This is frequently accomplished by etching the Diatomite (D) with a stronger acid or base to modify its adsorption efficiency. Unfortunately, using strong acids or bases is environmentally unsafe and their action is

corrosive to the RDF. Thus there is a need for innovative and integrated technology to be used with the conventional processes to overcome these problems. Modifying the Diatomite (D) with PEI-functionalized aegirine by embedding <5 wt% of nanoparticles with it can contribute to improving the removal of suspended solids and also increasing the adsorption capacity of the TOC when applied in RDF process. An industrial-level RDF field-tests of this proposed technique that aims at exploring the possibility of utilizing such nanoparticle type in a continuous mode has been reported [161]. Thus two experiments were performed to test the TOC removal performance before and after embedding low mass fraction of the functionalized nanoparticles. The first experiment used Diatomite as its own following the typically adapted method. The second experiment was accomplished by embedding 1 wt% of the PEI-functionalized nanoaegirine. Fig. 23.26A represents the obtained breakthrough curve of the standalone Diatomite (D), while Fig. 23.26B shows that of PEI-APs. Both figures also include photographs of selected samples, which shows the gradual changing in the color from colorless to dark as the time increases. As can be seen, in the absence of nanoparticles, very low efficiency in the TOC removal was obtained as indicated from the rapid change in color from colorless to dark. In the presence of nanoparticle 1 wt% of APs, however, more efficient TOC removal was achieved as indicated by the gradual changing of the color from colorless to dark.

### 23.3 Conclusions

Nanoparticles are being developed and manufactured very rapidly at lab scale, but not yet at the commercial level as they are costly to produce. Despite the fact that nanoparticles have numerous advantages compared with conventional particles and their bulk counterparts, they face a number of challenges for scaling up. Thus innovation of naturally derived nanoparticle-based materials with moderate preparation conditions is of paramount importance. This chapter summarized the work related to the synthesis of nanoaegirine, a naturally derived based material, using mild operating temperature and pressure to make it a cost-effective process for scaling up. The synthesis and preparation techniques for iron silicate-based aegirine were briefly introduced and discussed. Various factors and operating conditions affecting surface and structural modifications have been addressed as well. Grafting and functionalizing nanoaegirine with different polymers to improve its interactions with different contaminants present in water were reviewed. Examples of the use of surface and structural modified nanoaegirine were illustrated that showed that modified nanoaegirine can be effectively employed as adsorbent and catalyst for energy and environmental applications. Polymer-grafted and functionalized nanoaegirine has been employed successfully for

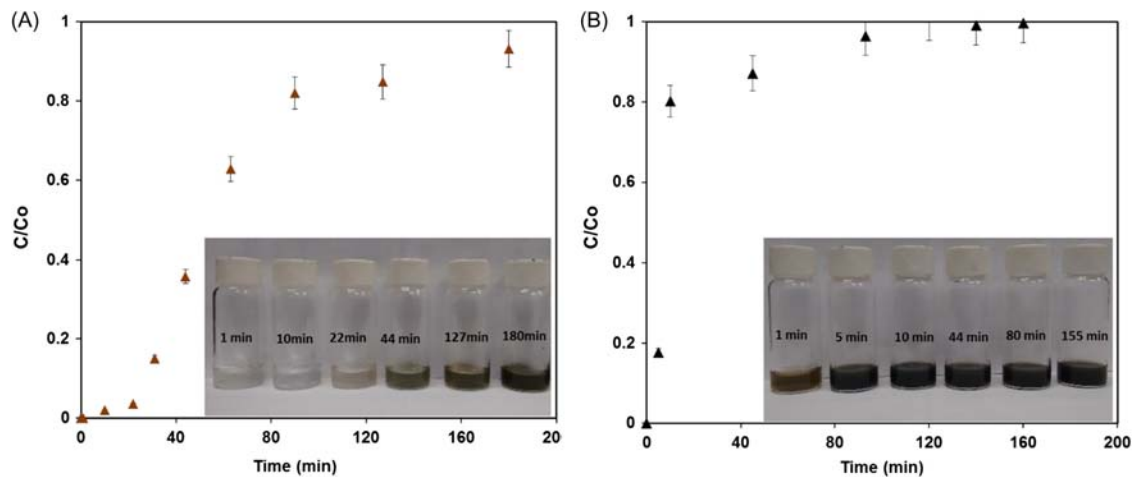


**FIGURE 23.26** Breakthrough curves (BTCs) and images of selected samples for adsorption of TOC by (A) standalone Diatomite (D), and (B) 1 wt.% PEI-APs embedded into Diatomite (D). The symbols represent experimental data. *Permissions related to the material excerpted were obtained from the authors; Hethnawi AJ. Poly(ethylenimine)-functionalized pyroxene nanoparticles embedded on diatomite for removal of total organic carbon from industrial wastewater: batch and fixed-bed studies, MSc Thesis, Department of Chemical and Petroleum Engineering, University of Calgary, 2017 [161].*

removing contaminants from different industrial effluents like pharmaceuticals, textiles, and oil sand tailing.

As can be seen, nanoaegirine is an alternate, cost-effective, and environmentally friendly adsorbent or catalyst for commonly used expensive materials like granular and powder-activated carbons and zeolite-based catalysts. Further, due to its naturally derived properties and easily tunable surface functionalities, nanoaegirine is suitable for in situ application and site-specific targeting of certain contaminants, where recovery and regeneration of the spent adsorbent or catalysts are not necessary. Furthermore, aegirine is earth abundant, naturally occurring, cost-effective, and environmentally friendly and could maximize the sustainability of adsorption/catalysis processes for saving energy and reducing the environmental footprint of industry.

## References

- [1] Prieto G, Tuysuz H, Duyckaerts N, Knossalla J, Wang GH, Schuth F. Hollow nano- and microstructures as catalysts. *Chem Rev* 2016;116:14056–119.
- [2] Zhang A, Lieber CM. Nano-bioelectronics. *Chem Rev* 2016;116:215–57.
- [3] Varma A, Mukasyan AS, Rogachev AS, Manukyan KV. Solution combustion synthesis of nanoscale materials. *Chem Rev* 2016;116:14493–586.
- [4] Cheng L, Wang C, Feng L, Yang K, Liu Z. Functional nanomaterials for phototherapies of cancer. *Chem Rev* 2014;114:10869–939.
- [5] Dang S, Zhu Q-L, Xu Q. Nanomaterials derived from metal–organic frameworks. *Nat Rev Mater* 2017;3:17075.
- [6] Jain A, Ranjan S, Dasgupta N, Ramalingam C. Nanomaterials in food and agriculture: an overview on their safety concerns and regulatory issues. *Crit Rev food Sci Nutr* 2018;58:297–317.
- [7] Chen Y, Fan Z, Zhang Z, Niu W, Li C, Yang N, et al. Two-dimensional metal nanomaterials: synthesis, properties, and applications. *Chem Rev* 2018;118:6409–55.
- [8] Khan A, Wen Y, Huq T, Ni Y. Cellulosic nanomaterials in food and nutraceutical applications: a review. *J Agric Food Chem* 2018;66:8–19.
- [9] Ghosal K, Sarkar K. Biomedical applications of graphene nanomaterials and beyond. *ACS Biomater Sci Eng* 2018;4:2653–703.
- [10] Hussain CM. Nanotechnology in environmental science. Wiley, Wiley Online Library; 2018.
- [11] Chaudhery Mustansar BK. Hussain, advanced environmental analysis-application of nanomaterials. Royal Society of Chemistry (RSC); 2017.
- [12] Krohns S, Lunkenheimer P, Meissner S, Reller A, Gleich B, Rathgeber A, et al. The route to resource-efficient novel materials. *Nat Mater* 2011;10:899–901.
- [13] Nakamura E, Sato K. Managing the scarcity of chemical elements. *Nat Mater* 2011;10:158.
- [14] Feng S, Xu R. New materials in hydrothermal synthesis. *Acc Chem Res* 2001;34:239–47.
- [15] Cheetham AK, Férey G, Loiseau T. Open-framework inorganic materials. *Angew Chem Int Ed* 1999;38:3268–92.
- [16] Whittingham MS, Guo J-D, Chen R, Chirayil T, Janaauer G, Zavalij P. The hydrothermal synthesis of new oxide materials. *Solid State Ion* 1995;75:257–68.

- [17] Whittingham MS. Hydrothermal synthesis of transition metal oxides under mild conditions. *Curr Opin Solid State Mater Sci* 1996;1:227–32.
- [18] Barrer RM, Baynham JW, Bultitude FW, Meier WM. Hydrothermal chemistry of the silicates. Part VIII. Low-temperature crystal growth of aluminosilicates, and of some gallium and germanium analogues. *J Chem Soc (Resumed)* 1959;195–208.
- [19] Breck DW. Zeolite molecular sieves: structure, chemistry and use. New York: John Wiley & Sons Inc; 1974.
- [20] Breck DW. Crystalline molecular sieves. *J Chem Educ* 1964;41:678.
- [21] Kerr GT. Chemistry of crystalline aluminosilicates. I. Factors affecting the formation of zeolite A. *J Phys Chem* 1966;70:1047–50.
- [22] Kerr GT. Crystallization of sodium zeolite A. *Zeolites* 1989;9:451.
- [23] Derouane EG, Determerrie S, Gabelica Z, Blom N. Synthesis and characterization of ZSM-5 type zeolites I. Physico-chemical properties of precursors and intermediates. *Appl Catal* 1981;1:201–24.
- [24] Gabelica Z, Derouane EG, Blom N. Synthesis and characterization of pentasil type zeolites: II. Structure-directing effect of the organic base or cation. *Appl Catal* 1983;5:109–17.
- [25] Gabelica Z, Blom N, Derouane EG. Synthesis and characterization of zsm-5 type zeolites: III. A critical evaluation of the role of alkali and ammonium cations. *Appl Catal* 1983;5:227–48.
- [26] Chang CD, Bell AT. Studies on the mechanism of ZSM-5 formation. *Catal Lett* 1991;8:305–16.
- [27] Burkett SL, Davis ME. Mechanism of structure direction in the synthesis of Si-ZSM-5: an investigation by intermolecular  $1\text{H}$ - $29\text{Si}$  CP MAS NMR. *J Phys Chem* 1994;98:4647–53.
- [28] Burkett SL, Davis ME. Mechanisms of structure direction in the synthesis of pure-silica zeolites. 1. Synthesis of TPA/Si-ZSM-5. *Chem Mater* 1995;7:920–8.
- [29] Burkett SL, Davis ME. Mechanism of structure direction in the synthesis of pure-silica zeolites. 2. Hydrophobic hydration and structural specificity. *Chem Mater* 1995;7:1453–63.
- [30] Ravishankar R, Kirschhock C, Schoeman BJ, Vanoppen P, Grobet PJ, Storck S, et al. Physicochemical characterization of silicalite-1 nanophas material. *J Phys Chem B* 1998;102:2633–9.
- [31] Ravishankar R, Kirschhock CEA, Knops-Gerrits P-P, Feijen EJP, Grobet PJ, Vanoppen P, et al. Characterization of nanosized material extracted from clear suspensions for MFI zeolite synthesis. *J Phys Chem B* 1999;103:4960–4.
- [32] Kirschhock CEA, Ravishankar R, Verspeurt F, Grobet PJ, Jacobs PA, Martens JA. Identification of precursor species in the formation of MFI zeolite in the TPAOH – TEOS –  $\text{H}_2\text{O}$  system. *J Phys Chem B* 1999;103:4965–71.
- [33] Kirschhock CEA, Ravishankar R, Loooveren LV, Jacobs PA, Martens JA. Mechanism of transformation of precursors into nanoslabs in the early stages of MFI and MEL zeolite formation from TPAOH – TEOS –  $\text{H}_2\text{O}$  and TBAOH – TEOS –  $\text{H}_2\text{O}$  mixtures. *J Phys Chem B* 1999;103:4972–8.
- [34] Kirschhock CEA, Ravishankar R, Jacobs PA, Martens JA. Aggregation mechanism of nanoslabs with zeolite MFI-type structure. *J Phys Chem B* 1999;103:11021–7.
- [35] Kirschhock CEA, Buschmann V, Kremer S, Ravishankar R, Houssin CJY, Mojet BL, et al. Zeosil nanoslabs: building blocks in  $\text{nPr}_4\text{N}^+$ -mediated synthesis of MFI zeolite. *Angew Chem Int Ed* 2001;40:2637–40.
- [36] Cundy CS, Cox PA. The hydrothermal synthesis of zeolites: precursors, intermediates and reaction mechanism. *Microporous Mesoporous Mater* 2005;82:1–78.

- [37] Francis RJ, O'Brien S, Fogg AM, Halasyamani PS, O'Hare D, Loiseau T, et al. Time-resolved in-situ energy and angular dispersive X-ray diffraction studies of the formation of the microporous gallophosphate ULM-5 under hydrothermal conditions. *J Am Chem Soc* 1999;121:1002–15.
- [38] Norquist AJ, O'Hare D. Kinetic and mechanistic investigations of hydrothermal transformations in zinc phosphates. *J Am Chem Soc* 2004;126:6673–9.
- [39] Grandjean D, Beale AM, Petukhov AV, Weckhuysen BM. Unraveling the crystallization mechanism of CoAPO-5 molecular sieves under hydrothermal conditions. *J Am Chem Soc* 2005;127:14454–65.
- [40] Walton RI, Millange F, Smith RI, Hansen TC, O'Hare D. Real time observation of the hydrothermal crystallization of barium titanate using in situ neutron powder diffraction. *J Am Chem Soc* 2001;123:12547–55.
- [41] Norby P. Hydrothermal conversion of zeolites: an in situ synchrotron X-ray powder diffraction study. *J Am Chem Soc* 1997;119:5215–21.
- [42] Beale AM, Sankar G. In situ study of the formation of crystalline bismuth molybdate materials under hydrothermal conditions. *Chem Mater* 2003;15:146–53.
- [43] McIntyre LJ, Prior TJ, Fogg AM. Observation and isolation of layered and framework ytterbium hydroxide phases using in situ energy-dispersive X-ray diffraction. *Chem Mater* 2010;22:2635–45.
- [44] Avrami M. Kinetics of phase change. I: general theory. *J Chem Phys* 1939;7:1103–12.
- [45] Avrami M. Kinetics of phase change. II Transformation-time relations for random distribution of nuclei. *J Chem Phys* 1940;8:212–24.
- [46] Avrami M. Granulation, phase change, and microstructure kinetics of phase change. III. *J Chem Phys* 1941;9:177–84.
- [47] Erofe'ev B. Generalized equation of chemical kinetics and its application in reactions involving solids. *Compt Rend Acad Sci USSR* 1946;52 51 1-514 111.
- [48] Bamford TC, Comprehensive CH. Chap. 3 Chemical kinetics series 22: reactions in the solid state. Amsterdam: Elsevier; 1980. p. 41–113.
- [49] Hancock JD, Sharp JH. Method of comparing solid-state kinetic data and its application to the decomposition of kaolinite, brucite, and  $\text{BaCO}_3$ . *J Am Ceram Soc* 1972;55:74–7.
- [50] Szostak R, Thomas TL. Preparation of ferrisilicate ZSM-5 molecular sieves. *J Catal* 1986;100:555–7.
- [51] Wu P, Lin H, Komatsu T, Yashima T. Synthesis of ferrisilicate with the MCM-22 structure. *Chem Commun* 1997;663–4.
- [52] Fan W, Li R, Zhong B, Du H, Roduner E. Hydrothermal synthesis of ferrisilicates with ZSM-48 structure from precipitated gels. *Microporous Mesoporous Mater* 1998;25:95–101.
- [53] Raj A, Sivasanker S, Lazar K. Studies on the stability of  $\text{Fe}^{3+}$  ions in the ferrisilicate analog of zeolite beta. *J Catal* 1994;147:207–13.
- [54] Kumar R, Thangaraj A, Bhat RN, Ratnasamy P. Synthesis of iron-silicate analogs of zeolite beta. *Zeolites* 1990;10:85–9.
- [55] Chandwadkar AJ, Bhat RN, Ratnasamy P. Synthesis of iron-silicate analogs of zeolite mordenite. *Zeolites* 1991;11:42–7.
- [56] Singh AP. Comparison of iron and aluminum silicates with the TON topology. *Zeolites* 1992;12:858–61.
- [57] Kumar R, Reddy KR, Ratnasamy P. Process for the preparation of novel molecular sieves, June 15, 1993.

- [58] Nair V, Szostak R. Ferrisilicate molecular sieve, U.S. Patent 5,077,026, December 31, 1991.
- [59] Patarin J, Guth J-L, Kesler, H, Coudurier G, Raatz F. Process for the synthesis of zeolites of the ferrisilicate type, products so obtained. U.S. Patent 5, 013,537, May 7, 1991.
- [60] Nair VS, Szostak, R. Ferrisilicate molecular sieve and use as a catalyst. U.S. Patent 4,952,385A, August 28, 1990.
- [61] Desmond MJ, Pepera MA, Callahan JL. Synthesis of molecular sieving metallosilicates using silica-transition metal oxide sols. U.S. Patent 4,705,675, November 10, 1987.
- [62] Desmond MJ, Pesa FA. Synthesis of molecular sieving metallosilicates using heteropoly-metallates. Canadian Patent CA1249564A, January 14, 1986.
- [63] Boersma MAM, Nanne JM, Post MFM. Process for the preparation of crystalline silicates. U.S. Patent 4,337,176, June 29, 1982.
- [64] Byambajav E, Ohtsuka Y. Cracking behavior of asphaltene in the presence of iron catalysts supported on mesoporous molecular sieve with different pore diameters. *Fuel* 2003;82:1571–7.
- [65] Tan Q, Fan Y, Liu H, Song T, Shi G, Shen B, et al. Bimodal micro-mesoporous aluminosilicates for heavy oil cracking: porosity tuning and catalytic properties. *AIChE J* 2008;54:1850–9.
- [66] Morimoto N. Nomenclature of pyroxenes. *Mineral J* 1989;14:198–221.
- [67] Cameron JJP M. Structural and chemical variations in pyroxenes. *Am Miner* 1981;66:1–50.
- [68] Thompson RM, Downs RT, Redhammer GJ. Model pyroxenes III: volume of C2/c pyroxenes at mantle P, T, and x. *Am Mineral* 2005;90(11-12):1840–51.
- [69] Wang A, Jolliff BL, Haskin LA, Kuebler KE, Viskupic KM. Characterization and comparison of structural and compositional features of planetary quadrilateral pyroxenes by Raman spectroscopy. *Am Mineral* 2001;86(7-8):790–806.
- [70] McSween Jr. HY. What we have learned about Mars from SNC meteorites. *Meteoritics* 1994;29:757–79 (ISSN 0026-1114).
- [71] Maaloe SA, Aoki KI. The major element composition of the mantle estimated from the composition of iherzolites. *Contrib Miner Pet* 1977;63:161–73.
- [72] Zussman J. The crystal chemistry of pyroxenes and amphiboles. *Earth Sci Rev* 1968;4:39–67.
- [73] Kogarko LNW, Williams CT, Woolley AR. Compositional evolution and cryptic variation in pyroxenes of the peralkaline Lovozero intrusion, Kola Peninsula, Russia, 70 (2006) pp. 347-359.
- [74] Nestola F, Ballaran TB, Tribaudino M, Ohashi H. Compressional behaviour of CaNiSi<sub>2</sub>O<sub>6</sub> clinopyroxene: bulk modulus systematic and cation type in clinopyroxenes. *Phys Chem Miner* 2005;32:222–7.
- [75] Heuer M, Huber AL, Bromiley GD, Fehr KT, Bente K. Characterization of synthetic hedenbergite (CaFeSi<sub>2</sub>O<sub>6</sub>)-petedunnite (CaZnSi<sub>2</sub>O<sub>6</sub>) solid solution series by X-ray single crystal diffraction. *Phys Chem Miner* 2005;32:552–63.
- [76] Origlieri MJ, Downs RT, Thompson RM, Pommier CJ, Denton MB, Harlow GE. High-pressure crystal structure of kosmochlor, NaCrSi<sub>2</sub>O<sub>6</sub>, and systematics of anisotropic compression in pyroxenes. *Am Mineral* 2003;88:1025–32.
- [77] Berzelius J. Note on Aegirine - Neues Jahrbuch für Mineralogie, Geognosie, Geologie und Petrefaktenkunde, 1835:184–185.
- [78] Appleman DE, Clark JR, Papike JJ. Crystal-chemical characterization of clinopyroxenes based on eight new structure refinements. *Miner Soc Am Spec Pap* 1969;2:31–50.



- [79] Bennington K, Brown RR. Thermodynamic properties of synthetic acmite ( $\text{NaFe}^{3+}\text{Si}_2\text{O}_6$ ), US Dept. of the Interior, Bureau of Mines1, 981.
- [80] Redhammer GJ, Amthauer G, Roth G, Tippelt G, Lottermoser W. Single-crystal X-ray diffraction and temperature dependent  $^{57}\text{Fe}$  Mössbauer spectroscopy on the hedenbergite-aegirine ( $\text{Ca, Na}(\text{Fe}^{2+}, \text{Fe}^{3+})\text{Si}_2\text{O}_6$  solid solution. *Am Mineral* 2006;91:1271–1292.
- [81] Redhammer GNJ, Amthauer G, Lottermoser W, Treutmann W. Synthesis and structural properties of clinopyroxenes of the hedenbergite  $\text{CaFe}^{2+}\text{Si}_2\text{O}_6$ –aegirine  $\text{NaFe}^{3+}\text{Si}_2\text{O}_6$  solid-solution series. *Eur J Mineral* 2000;12:105–20.
- [82] El-Shennawi AWA, Mandour MA, Morsi MM, Abdel-Hameed SA. Monopyroxenic basalt-based glass-ceramics. *J Am Ceram Soc* 1999;82:1181–6.
- [83] Nestola F, Ballaran TB, Liebske C, Bruno M, Tribaudino M. High-pressure behaviour along the jadeite  $\text{NaAlSi}_2\text{O}_6$ –aegirine  $\text{NaFeSi}_2\text{O}_6$  solid solution up to 10 GPa. *Phys Chem Miner* 2006;33:417–25.
- [84] Nolan J, Edgar A. An X-ray investigation of synthetic pyroxenes in the system acmite-diopside-water at 1000 kg/cm<sup>2</sup> water-vapour pressure. *Miner Mag* 1963;33:625–34.
- [85] Bailey D, Schairer J. The system  $\text{Na}_2\text{O} - \text{Al}_2\text{O}_3 - \text{Fe}_2\text{O}_3 - \text{SiO}_2$  at 1 atmosphere, and the petrogenesis of alkaline rocks. *J Petrol* 1966;7:114–70.
- [86] Yagi K. The system acmite-diopside and its bearing on the stability relations of natural pyroxenes of the acmite-hedenbergite-diopside series. *Am Mineral J Earth Planet Mater* 1966;51:976–1000.
- [87] Kopp OC, Harris LA. Synthesis of grunerite and other phases in the system  $\text{SiO}_2$ – $\text{NaOH}$ – $\text{Fe}$ – $\text{H}_2\text{O}$ . *Am Mineral J Earth Planet Mater* 1967;52:1681–8.
- [88] Nolan J. Physical properties of synthetic and natural pyroxenes in the system diopside–hedenbergite–acmite. *Mineral Mag* 1969;37:216–29.
- [89] Dollase W, Gustafson W.  $^{57}\text{Fe}$  Moessbauer spectral analysis of the sodic clinopyroxenes. *Am Mineral* 1982;67:311–27.
- [90] Christophe-Michel-Levy MB. *Soc Franc Min* 1954;LXXVII:1328–9.
- [91] Riman RE, Cho S-B. Inorganic conversion coatings for ferrous substrates, Google Patents, 2001.
- [92] Decarreau A, Petit S, Vieillard P, Dabert N. Hydrothermal synthesis of aegirine at 200 °C. *Eur J Mineral* 2004;16:85–90.
- [93] Itani L, Liu Y, Zhang W, Bozhilov KN, Delmotte L, Valtchev V. Investigation of the physicochemical changes preceding zeolite nucleation in a sodium-rich aluminosilicate gel. *J Am Chem Soc* 2009;131:10127–39.
- [94] Larsen SC. Nanocrystalline zeolites and zeolite structures: synthesis, characterization, and applications. *J Phys Chem C* 2007;111:18464–74.
- [95] Morales-Pacheco P, Alvarez-Ramirez F, Del Angel P, Bucio L, Domínguez JM. Synthesis and structural properties of zeolytic nanocrystals I. MFI type zeolites. *J Phys Chem C* 2007;111:2368–78.
- [96] Lartus O, Mintova S, Bein T. Environmental syntheses of nanosized zeolites with high yield and monomodal particle size distribution. *Microporous Mesoporous Mater* 2006;96:405–12.
- [97] Liu Y, Pinnavaia TJ. Aluminosilicate nanoparticles for catalytic hydrocarbon cracking. *J Am Chem Soc* 2003;125:2376–7.
- [98] Madsen C, Madsen C, Jacobsen CJH. Nanosized zeolite crystals—convenient control of crystal size distribution by confined space synthesis. *Chem Commun* 1999;673–4.
- [99] Shi BWZMZ. Synthesis of nanosized NaY zeolite by confined space method. *Chin Chem Lett* 2002;13:385–8.

- [100] Wang H, Holmberg BA, Yan Y. Synthesis of template-free zeolite nanocrystals by using in situ thermoreversible polymer hydrogels. *J Am Chem Soc* 2003;125:9928–9.
- [101] Sebakhy KO, Vitale G, Pereira-Almao PR. Dispersed Ni-doped aegirine nanocatalysts for the selective hydrogenation of olefinic molecules. *ACS Appl Nano Mater* 2018;.
- [102] Tian S, Wang Z, Gong W, Chen W, Feng Q, Xu Q, et al. Temperature-controlled selectivity of hydrogenation and hydrodeoxygenation in the conversion of biomass molecule by the Ru1/mpg-C3N4 catalyst. *J Am Chem Soc* 2018;140:11161–4.
- [103] Han Y, Wang Z, Xu R, Zhang W, Chen W, Zheng L, et al. Ordered porous nitrogen-doped carbon matrix with atomically dispersed cobalt sites as an efficient catalyst for dehydrogenation and transfer hydrogenation of N-heterocycles. *Angew Chem* 2018;130:11432–6.
- [104] Hmoudah M, Nassar NN, Vitale G, El-Qanni A. Effect of nanosized and surface-structural-modified nano-pyroxene on adsorption of violanthrone-79. *RSC Adv* 2016;6:64482–93.
- [105] Vitale G. Iron silicate nano-crystals as potential catalysts or adsorbents for heavy hydrocarbons upgrading. *Univ Calg* 2013;305.
- [106] Minko S. Grafting on solid surfaces: “grafting to” and “grafting from” methods. In: Stamm M, editor. *Polymer surfaces and interfaces: characterization, modification and applications*. Berlin, Heidelberg: Springer Berlin Heidelberg; 2008. p. 215–34.
- [107] Vansant EF, Van Der Voort P, Vrancken KC. *Characterization and chemical modification of the silica surface*. Elsevier Science; 1995.
- [108] Jal PK, Patel S, Mishra BK. Chemical modification of silica surface by immobilization of functional groups for extractive concentration of metal ions. *Talanta* 2004;62:1005–28.
- [109] Kango S, Kalia S, Celli A, Njuguna J, Habibi Y, Kumar R. Surface modification of inorganic nanoparticles for development of organic–inorganic nanocomposites—a review. *Prog Polym Sci* 2013;38:1232–61.
- [110] Mévellec V, Roussel S, Tessier L, Chancelon J, Mayne-L’Hermite M, Deniau G, et al. Grafting polymers on surfaces: a new powerful and versatile diazonium salt-based one-step process in aqueous media. *Chem Mater* 2007;19:6323–30.
- [111] Innocenzi P, Figus C, Kidchob T, Valentini M, Alonso B, Takahashi M. Sol-gel reactions of 3-glycidoxypropyltrimethoxysilane in a highly basic aqueous solution. *Dalton Trans* 2009;9146–52.
- [112] Innocenzi P, Brusatin G, Guglielmi M, Bertani R. New synthetic route to (3-glycidoxypropyl)trimethoxysilane-based hybrid organic – inorganic materials. *Chem Mater* 1999;11:1672–9.
- [113] Cheng J, Khin KT, Jensen GS, Liu A, Davis ME. Synthesis of linear, beta-cyclodextrin-based polymers and their camptothecin conjugates. *Bioconjug Chem* 2003;14:1007–17.
- [114] Schwartz A, Bar R. Cyclodextrin-enhanced degradation of toluene and p-toluic acid by *Pseudomonas putida*. *Appl Environ microbiol* 1995;61:2727–31.
- [115] Uekama K, Hirayama F, Irie T. Cyclodextrin drug carrier systems. *Chem Rev* 1998;98:2045–76.
- [116] Jacobsen PA, Nielsen JL, Juhl MV, Theilgaard N, Larsen KL. Grafting cyclodextrins to calcium phosphate ceramics for biomedical applications. *J Incl Phenom Macrocycl Chem* 2012;72:173–81.
- [117] Lv Y, Mei D, Pan X, Tan T. Preparation of novel  $\beta$ -cyclodextrin functionalized monolith and its application in chiral separation. *J Chromatogr B* 2010;878:2461–4.

- [118] Gibbs F, Selim Kermasha, Inteaz Alli, Catherine N, Mulligan B. Encapsulation in the food industry: a review. *Int J Food Sci Nutr* 1999;50:213–24.
- [119] Alsaiee A, Smith BJ, Xiao L, Ling Y, Helbling D, Dichtel WR. Rapid removal of organic micropollutants from water by a porous  $\beta$ -cyclodextrin polymer. *Nature* 2016;529:190–4.
- [120] Hegde RP. Drug-cyclodextrin inclusion compounds. studies of the formulation of pharmaceutical products containing cyclodextrins, 1985.
- [121] Ponchel A, Abramson S, Quartararo J, Bormann D, Barbaux Y, Monflier E. Cyclodextrin silica-based materials: advanced characterizations and study of their complexing behavior by diffuse reflectance UV–Vis spectroscopy. *Microporous Mesoporous Mater* 2004;75:261–72.
- [122] Nafie G, Vitale G, Carbognani Ortega L, Nassar NN. Nanopyroxene grafting with  $\beta$ -cyclodextrin monomer for wastewater applications. *ACS Appl Mater Interfaces* 2017;9:42393–407. Available from: <https://pubs.acs.org/doi/abs/10.1021%2Facsami.7b13677>.
- [123] Armstrong DW. Bonded phase material for chromatographic separations. In U. Patents (Ed.) Google Patents, Google Patents, US Patents, 1985.
- [124] Yu J-G, Huang K-L, Liu S-Q, Tang J-C. Preparation and characterization of soluble methyl- $\beta$ -cyclodextrin functionalized single-walled carbon nanotubes. *Phys E Low-Dimensional Syst Nanostruct* 2008;40:689–92.
- [125] Armstrong DW. Bonded phase material for chromatographic separations. Google Patents, 1985.
- [126] Ishida H. Controlled interphases in glass fiber and particulate reinforced polymers: structure of silane coupling agents in solutions and on substrates. The interfacial interactions in polymeric composites. Springer; 1993. p. 169–99.
- [127] Mohseni P, Hahn NA, Frank RA, Hewitt LM, Hajibabaei M, Van Der Kraak G. Naphthenic acid mixtures from oil sands process-affected water enhance differentiation of mouse embryonic stem cells and affect development of the heart. *Environ Sci Technol* 2015;49:10165–72.
- [128] Leung SS, MacKinnon MD, Smith REH. The ecological effects of naphthenic acids and salts on phytoplankton from the Athabasca oil sands region. *Aquat Toxicol* 2003;62:11–26.
- [129] Headley JV, Peru KM, Barrow MP. Advances in mass spectrometric characterization of naphthenic acids fraction compounds in oil sands environmental samples and crude oil—a review. *Mass Spectrometry Rev* 2016;35:311–28.
- [130] Rogers VV, Liber K, MacKinnon MD. Isolation and characterization of naphthenic acids from Athabasca oil sands tailings pond water. *Chemosphere* 2002;48:519–27.
- [131] Leung SS, MacKinnon MD, Smith RE. The ecological effects of naphthenic acids and salts on phytoplankton from the Athabasca oil sands region. *Aquat Toxicol (Amsterdam, Neth)* 2003;62:11–26.
- [132] Allen EW. Process water treatment in Canada's oil sands industry: I. Target pollutants and treatment objectives. *J Environ Eng Sci* 2008;7:123–38.
- [133] Quagraine EK, Peterson HG, Headley JV. In situ bioremediation of naphthenic acids contaminated tailing pond waters in the athabasca oil sands region--demonstrated field studies and plausible options: a review, *Journal of environmental science and health. Part A, Toxic/Hazardous Substances Environ Eng* 2005;40:685–722.
- [134] Islam MS, Zhang Y, McPhedran KN, Liu Y, El-Din MG. Mechanistic investigation of industrial wastewater naphthenic acids removal using granular activated carbon (GAC) biofilm based processes. *Sci Total Environ* 2016;541:238–46.

- [135] Li D-X, Chen C-L, Liu B-L, Liu Y-S. Molecular simulation of  $\beta$ -cyclodextrin inclusion complex with 2-phenylethyl alcohol. *Mol Simul* 2009;35:199–204.
- [136] Gerloczy A, Fonagy A, Szejtli J. Reduction of residual toluene content in beta-cyclodextrin through preparing inclusion complexes. *Starch-Stärke* 1983;35:320–2.
- [137] Roik N, Belyakova L. IR spectroscopy, X-ray diffraction and thermal analysis studies of solid “ $\beta$ -cyclodextrin—para-aminobenzoic acid” inclusion complex. *Phys Chem Solid State* 2011;12:168–73.
- [138] Salvatierra D, Jaime C, Virgili A, Sánchez-Ferrando F. Determination of the inclusion geometry for the  $\beta$ -cyclodextrin/benzoic acid complex by NMR and molecular modeling. *J Org Chem* 1996;61:9578–81.
- [139] Pop MM, Goubitz K, Borodi G, Bogdan M, De Ridder DJ, Peschar R, et al. Crystal structure of the inclusion complex of  $\beta$ -cyclodextrin with mefenamic acid from high-resolution synchrotron powder-diffraction data in combination with molecular-mechanics calculations. *Acta Crystallogr Sect B: Struct Sci* 2002;58:1036–43.
- [140] Hamilton JA, Chen L. Crystal structure of an inclusion complex of beta-cyclodextrin with racemic fenoprofen: direct evidence for chiral recognition. *J Am Chem Soc* 1988;110:5833–41.
- [141] Aree T, Chaichit N, Engkakul C. Polymorphism in  $\beta$ -cyclodextrin—benzoic acid inclusion complex: a kinetically controlled crystal growth according to the Ostwald’s rule. *Carbohydr Res* 2008;343:2451–8.
- [142] Cai Z, Dwivedi AD, Lee W-N, Zhao X, Liu W, Sillanpää M, et al. Application of nanotechnologies for removing pharmaceutically active compounds from water: development and future trends. *Environ Sci Nano* 2018;5:27–47.
- [143] Kim M, Guerra P, Shah A, Parsa M, Alaee M, Smyth SA. Removal of pharmaceuticals and personal care products in a membrane bioreactor wastewater treatment plant. *Water Sci Technol: A J Int Assoc Water Pollut Res* 2014;69:2221–9.
- [144] Guo Y, Qi P, Liu Y. A Review on Advanced Treatment of Pharmaceutical Wastewater, IOP Conference Series: Earth and Environmental Science. IOP Publishing; 2017. p. 012025.
- [145] Scheurer M, Michel A, Brauch H-J, Ruck W, Sacher F. Occurrence and fate of the anti-diabetic drug metformin and its metabolite guanilurea in the environment and during drinking water treatment. *Water Res* 2012;46:4790–802.
- [146] Pentikainen PJ, Neuvonen PJ, Penttilä A. Pharmacokinetics of metformin after intravenous and oral administration to man. *Eur J Clin pharmacol* 1979;16:195–202.
- [147] Rosa L, Davis KF, Rulli MC, D’Odorico P. Environmental consequences of oil production from oil sands. *Earths Future* 2017;5:158–70.
- [148] MacKinnon M, Kampala G, Marsh B, Fedorak P, Guigard S. Indicators for Assessing Transport of Oil Sands Process-Affected Waters, 297. Iahs Publication; 2005. p. 71.
- [149] Headley JV, McMartin DW. A review of the occurrence and fate of naphthenic acids in aquatic environments. *J Environ Sci Health, Part A* 2004;39:1989–2010.
- [150] Majid A, Argue S, Boyko V, Pleizier G, L’Ecuyer P, Tunney J, et al. Characterization of sol–gel-derived nano-particles separated from oil sands fine tailings. *Colloids Surf A: Physicochem Eng Asp* 2003;224:33–44.
- [151] Masliyah J, Zhou ZJ, Xu Z, Czarnecki J, Hamza H. Understanding water-based bitumen extraction from athabasca oil sands. *Can J Chem Eng* 2004;82:628–54.
- [152] Mikula RK, Kasperski KL, Burns RD, MacKinnon MD. The nature and fate of oil sands fine tailings. In: Laurier L. Schramm (Ed.), *Suspensions: fundamentals and applications in the petroleum industry*, Advance in Chemistry Series 1996;251:677–723.

- [153] Lakshmanan R, Sanchez-Dominguez M, Matutes-Aquino JA, Wennmalm S, Kuttuva Rajarao G. Removal of total organic carbon from sewage wastewater using poly (ethyleneimine)-functionalized magnetic nanoparticles. *Langmuir* 2014;30:1036–44.
- [154] Boussif O, Lezoualc'h F, Zanta MA, Mergny MD, Scherman D, Demeneix B, et al. A versatile vector for gene and oligonucleotide transfer into cells in culture and in vivo: polyethylenimine. *Proc Natl Acad Sci* 1995;92:7297–301.
- [155] Kim WJ, Chang C-W, Lee M, Kim SW. Efficient siRNA delivery using water soluble lipopolymer for anti-angiogenic gene therapy. *J Controlled Rel* 2007;118:357–63.
- [156] Mai H Le Thi, Tran Thi D, Tran Mau D, Nguyen Huu D, Dang Mau C. Preparation and characterization of magnetic nanoparticles coated with polyethylene glycol. *J Phys Conf Ser* 2009;187:012048.
- [157] Hethnawi A, Nassar NN, Vitale G. Preparation and characterization of polyethylenimine-functionalized pyroxene nanoparticles and its application in wastewater treatment. *Colloids Surf A: Physicochem Eng Asp* 2017;525:20–30.
- [158] Hethnawi A, Manasrah AD, Vitale G, Nassar NN. Fixed-bed column studies of total organic carbon removal from industrial wastewater by use of diatomite decorated with polyethylenimine-functionalized pyroxene nanoparticles. *J Colloid Interface Sci* 2018;513:28–42.
- [159] Hethnawi A, Nassar NN, Manasrah AD, Vitale G. Polyethylenimine-functionalized pyroxene nanoparticles embedded on Diatomite for adsorptive removal of dye from textile wastewater in a fixed-bed column. *Chem Eng J* 2017;320:389–404.
- [160] Haug G. Aspects of rotary vacuum filter designs and performance. *Fluid Part Sep J* 2000;13:44–59.
- [161] Hethnawi AJ. Poly(ethylenimine)-Functionalized Pyroxene Nanoparticles Embedded on Diatomite for Removal of Total Organic Carbon from Industrial Wastewater: Batch and Fixed-bed studies, MSc Thesis. Department of Chemical and Petroleum Engineering, University of Calgary; 2017.

## Chapter 24

# Nanomaterial-based cosmeceuticals

**Pravin Shende, Drashti Patel and Anjali Takke**

*Shobhaben Pratapbhai Patel School of Pharmacy and Technology Management, SVKM's NMIMS, Mumbai, India*

### 24.1 Introduction

Nanotechnology is currently one of the fastest growing scientific fields and is used in various applications in food items, electronic devices, cosmetics and pharmaceuticals, and in personal care [1]. Cosmeceuticals have been expanded range of products which include personal care products like skin care, hair care in photoaging, hyperpigmentation, wrinkles, and hair damage. The global cosmeceutical market is expected to reach a value of USD 80.36 billion by 2023 [2]. Nanomaterials in cosmetics have extensive potential because of their small size, surface area, and effective transport in skin layers [3]. Nanomaterials provide various advantages in cosmetics such as improved stability, controlled release, better UV protection, site-specific targeting and enhanced skin penetration and hydration of active materials [3,4]. Some of the advantages of nanocosmeceuticals are shown in Fig. 24.1.

Nanomaterial-based products include nanoemulsions, liposomes, niosomes, solid-lipid nanoparticles (SLNs), nanopigments, and fullerenes. Nanomaterials are extensively used in the preparation of moisturizing creams, antiaging creams, hair shampoos, conditioners, and skin-whitening creams [5]. However, there are some noted disadvantages associated with nanomaterial-based cosmetics. For example, the antibacterial effect of nanomaterials can interfere with the healthy bacterial system in the environment. Currently regulatory authorities have no stringent regulations for the safety of nanocosmeceuticals.

### 24.2 Nanomaterials in cosmeceuticals

Various nanomaterials are used in cosmeceuticals as depicted in Fig. 24.2.

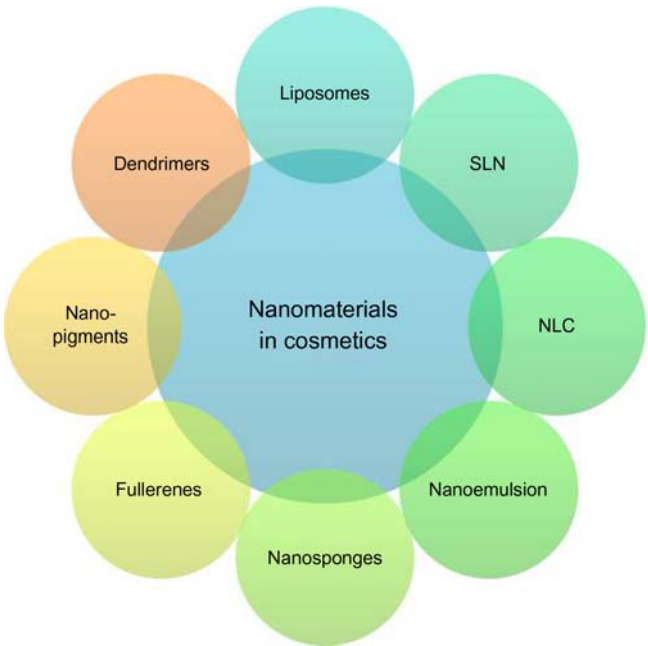


FIGURE 24.1 Types of nanomaterials used in cosmetics.

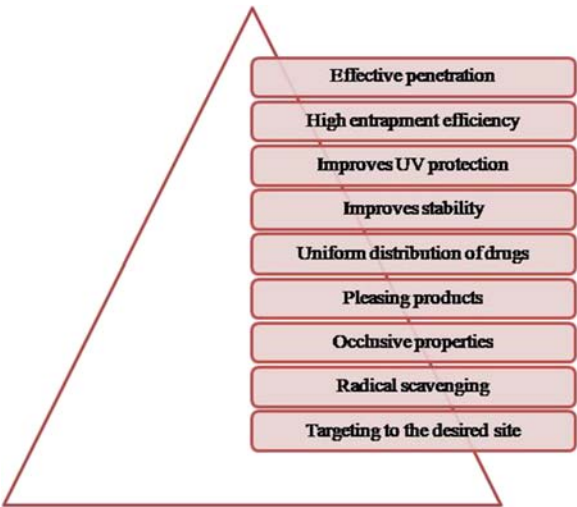


FIGURE 24.2 Advantages of nanomaterials used in cosmetics.

### 24.2.1 Liposomes

Liposomes are vesicular structures ranging from 15 nm up to several  $\mu\text{m}$  with an aqueous core surrounded by a lipid bilayer and have shown wide applications in cosmetic drug delivery systems [6]. The liposomes used in cosmetics can be categorized based on composition and indications, such as transfersomes, niosomes, ultrasomes, ethosomes, phytosomes, etc. [7]. In 1986, Dior launched “Capture,” an antiaging cream, the first liposomal cosmetic product on the market [8]. Liposome-containing products are widely used because they are nontoxic, biodegradable, and biocompatible [9]. Topical creams contain lipids like cholesterol, ceramides, and phospholipids as biological lipids that are found in normal skin tissue [10]. They are also easy to incorporate into liposomes and can improve skin hydration and texture and impart softness and smoothness to the skin. Liposomes are preferred for delivery of vitamins and other molecules to regenerate the epidermis as they facilitate a continuous supply to cells over a sustained period of time. They are used as functionalized carriers in the delivery of active components, increase solubility and stability of formulation, enhance targeted site delivery, reduce potential toxicity, and are cost effective [11]. Amber extract is sometimes incorporated into liposomes to allow programmed release of the active ingredient [12].

### 24.2.2 Nanoemulsions

Nanoemulsions are submicron size, ranging from 50 to 1000 nm and considered as ultrafine emulsions in which an oil phase and water phase are combined with a surfactant [13]. They are known for applications in personal care products as potential vehicles for the controlled delivery of cosmetics. They are mostly used in cosmetics like deodorants, sunscreens, and shampoos [14,15]. Nanoemulsions containing andiroba and copaiba oils can repel mosquitoes for a period of 30 min as compared to diethyltoluamide (commercial product) on topical application [16]. On topical application of nanoemulsions composed of rice bran seed oil the relative hydration and the oiliness of skin is increased and normal pH values of the skin are maintained. Hence these nanoemulsions can be considered as alternative treatments for skin diseases such as atopic dermatitis and psoriasis [17,18].

### 24.2.3 Solid-lipid nanoparticles

SLNs are submicron, colloidal carriers whose size range from 50 to 100 nm that are formed by the sol–gel method and are comprised of phospholipid, dispersed water, or an aqueous solution of surfactants. SLNs exhibit low toxicity, enhance efficacy as penetration via skin pathways is increased, and small size leads to increased contact area [19]. Shah et al. developed SLN-



based tretinoin (TRE) gel, which improves topical delivery of TRE as compared to existing conventional TRE formulations [7]. Hydrogel formulations (Carbopol 943, xanthum gum, chitosan, and hydroxyethyl 4000) lipid nano-carriers exhibit good physical stability. It was found by Wissing et al. that SLNs can act as UV blocker and can improve UV protection. SLNs are advantageous for dermal application of cosmetics and pharmaceuticals products because they can increase skin hydration, modify release, increase occlusive properties, and have better targeting effects [20].

#### 24.2.4 Nanostructured lipid carriers

Factors such as high occlusion, increased level of skin adhesion, long-term stability, and high loading of nanostructured lipid carriers (NLCs) (second generation of lipid particles) make nanostructured lipid carriers superior to SLNs in cosmetic products. As compared to microparticles, lipid nanoparticles help to increase the penetration capabilities of active components. Lipid nanoparticles appear white, rather than yellowish, which increases the aesthetic appeal of the product [21]. In 2005, the first product containing lipid nanoparticles was available on the market called Nanorepair cream and lotion by Dr. Rimpler GmbH, Germany, which offered increased skin penetration.

The second product developed with CLR is an active-loaded NLC concentrate, in which the particles are prepared with a mixture of black currant seed oil, coenzyme Q10, and carnauba wax [21]. In June 2006, Dr. Rimpler GmbH launched a third product called NanoVital, which is primarily intended to be used as a night cream. NLC loaded with kukui oil from the Hawaiiin islands is used in the skin care for the sensitive skin of infants and babies [22].

#### 24.2.5 Dendrimers

Dendrimers are a new class of macromolecular components, micellar nanostructures, monodisperse, unimolecular around 20 nm in size and can be used in various applications such as skin care, nail care and hair care [6]. A patented dendrimer cosmetic product formulated using carbosiloxane claimed to provide resistance to water and sebum, increase tactile sensation and increase bioadhesion to skin and/or hair [22]. A complex of dendrimer containing free amino groups and keratolytic or antiacne agents is cosmetically acceptable in formulations used for the treatment of acne vulgaris. US patent 6,001,342 described the composition of dendrimers containing polyamidoamines (Starburst, Starpharma) in antiperspirant deodorant to help reduce underarm odor. Dendrimer-containing formulations show self-tanning activity and improved efficacy when applied to skin [23].

### 24.2.6 Nanosponges and microsponges

These are highly cross-linked, polymeric, porous systems that are nongritty and free-flowing in nature. These properties have been exploited for drug-delivery systems in cosmetics and for dermatological applications. The release of drug in a diffusion controlled manner with a very high entrapment efficacy [24]. The size and entrapment efficiency depend on various factors like the nature of the polymer, drug solubility, type and concentration of the plasticizer, and speed and temperature of the emulsification process. Sunscreens prepared by nanosponges produce better protection against sunburns with minimal irritancy and sensitivity [25]. For example, microsponges containing benzoyl peroxide are more effective, less sensitive, and produces less skin irritation. Microsponges also offer great advantages over other formulations with respect to mutagenic and irritancy of the drug, and thus have a lot of potential for developing novel formulations for topical disease [26].

### 24.2.7 Fullerenes

Carbon fullerenes have potent scavenging capacities against radical oxygen species and are used for their skin rejuvenation properties in cosmeceutical formulations. They are not soluble in aqueous solutions due to their hydrophobic nature, which limits their applications, but surface modification and surfactants increase the ability of fullerenes to solubilize in water and thus be used in pharmaceuticals [27]. Chirico et al. examined the protection ability of carboxyfullerenes for normal human keratinocytes from UVB-induced apoptosis and results indicate that carboxyfullerenes penetrate human keratinocytes and act by scavenging free radicals and by protecting cells from apoptosis by using confocal laser microscopy and transmission electron microscopy [28]. They are used antiaging products as they exhibit antioxidative properties. For example, fullerene-C60 (LipoFullerene) is used as an active ingredient due to its antiwrinkle efficacy [29].

### 24.2.8 Niosomes

Niosomes are nonionic, bilayer vesicles that are developed by using self-assembly of hydrated nonionic surfactants with or without corporation of lipophilic compounds and possess high entrapment efficacy, suitable for both hydrophobic as well hydrophilic drugs, good chemical stability, increase penetration as well as economic to produce on large scale [30]. The diameter of the vesicles range from 100 nm to 2  $\mu$ m in diameter, they can be multilamellar or unilamellar phase vesicles in an aqueous solution enclosed by membrane organized as bilayer. Niosomes are advantageous for dermal application, as they enhance residence time of API, reduce the barrier resistance of horny layer in stratum corneum and also reduce systemic absorption

[11]. Niosomes are better carriers of resveratrol and showed high delivery of resveratrol in deeper layers of the skin compared to liposomes [31]. Niosomal benzyl peroxide incorporated into HPMC gel results into good drug skin retention, sustain release and reduced toxicity of the drug with improved drug permeation [32]. Niosomal gallidermin gel showed more chemical stability than gallidermin aqueous gel, for efficient topical localization and good skin permeation without any threat to systemic circulation [30].

### 24.2.9 Nanopigments

Gold and silver nanoparticles are considered as valuable pigments in cosmetic products as they are inert, nontoxic, highly stable as well as biocompatible. Gold and silver are used due to their known antibacterial and antifungal action. They are incorporated into various products like perfumes, creams such as antiaging products, and in face packs or mask. Ointments containing  $\text{AgNO}_3$  can be used for skin infection and inflammation caused by wounds [13]. Nanopigments containing gold and silver nanoparticles provide new colored pigments for lipsticks and have been to be safe and show good pigment dispersion [23].  $\text{ZnO}$  and  $\text{TiO}_2$  are widely used in sunscreens as they are known to reflect and scatter UV light and protect skin against various adverse effects of UV light, including melanoma (skin cancer). Carbon black (cosmetic colorant) when used in nano-form alters the strength and opacity of color [33]. Various nanomaterials along with their advantages are shown in Fig. 24.3.

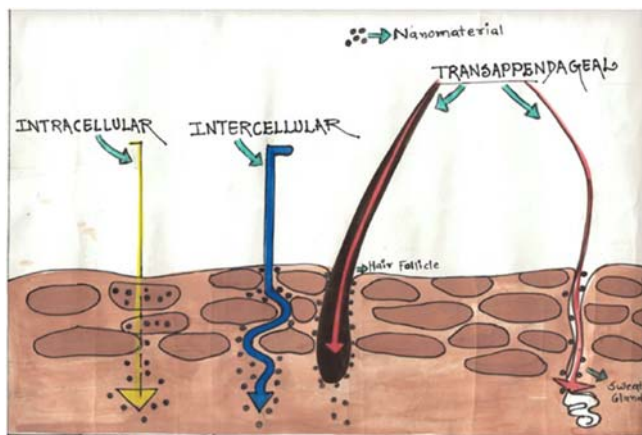


FIGURE 24.3 Penetration routes of nanomaterials throughout the skin.

## 24.3 Classification of nanocosmeceuticals

### 24.3.1 Skin care

A cosmetic formulation such as lotion or cream applied to the skin whose main purpose to counter dryness, protect and lubricant the skin. Some level of moisture content is present in the skin layers but moisturizers are applied to prevent the skin from dryness [34]. Moisturizers containing nanomaterials such as liposomes, SLNs, and nanoemulsions are widely used for enhancing the skin penetration [4]. Skin is the soft outer tissue that is covered with a hydrolipid film that provides a natural defense against pathogenic organisms [13]. Skin cleansers containing nanoparticles increase skin penetration, efficacy of active ingredients and provide skin protection.

### 24.3.2 Antiaging products

Antiaging creams usually contain specific antiaging ingredient like hydroxy acids, retinol, tea extract, coenzyme Q10, grapeseed, vitamin C, or some in combination to reduce fine lines and pores [35]. They are also used to lift and tighten skin in aging. Products with protein and silica are used to fill the mesoporous structure that lifts and tightens the skin. Nanopeeling Renovator Microdermablazing and VitActive Activator nanoemulsion are complementary antiaging products: the first one works by a mechanical process of exfoliation which contains Xylitol and Vitamin C microcrystals and the second one VitActive Activator nanoemulsion, which imparts skin hydration [35].

### 24.3.3 Hair care

Hair follicle and shaft targeting, increased the quantity of incorporated active ingredients are achieved by nanocosmeceuticals which improves hair care. Hair follicle, shaft targeting, and increased quantity of active ingredient are achieved by intrinsic properties and unique size of nanoparticles [15]. Nanoparticles moisturize hair cuticles by forming a protective film as well increasing residence time in hair follicles. Sericin combined with nanoparticles can be used in hair cosmeceuticals because they adhere to the hair surface easily and treat damaged cuticles [36,37].

### 24.3.4 Lip care

Incorporation of different nanomaterials into lipsticks and lip gloss help soften the lips by preventing transdermal water loss and also prevent pigments from migrating from the lips and to maintain color for longer periods of time. Lip volumizer containing liposomes increases lip volume, hydrates and outlines the lips, and fills wrinkles in the lip contour [4].

### 24.3.5 Nail care

Nail care is important because it prevents nail problems, such as fungi and ingrown toenails. Cosmeceuticals containing functionalized nanomaterials in nail care are advantageous since they improve toughness [38]. Metal oxide or silver nanoparticles containing antifungal medicaments are used to prevent fungal infections [38,39]. The nanocosmeceuticals available on the market today are listed in Tables 24.1 and 24.2 along with patent data.

## 24.4 Penetration of nanoparticles

The penetration of nanoparticles through the skin, their biodistribution, rate of excretion, and toxicity are determined by the characteristic of nanoparticles (e.g., shape, size, surface charge) [4]. Some of the proposed benefits of incorporating nanoparticles in cosmetics are unique texture, increased efficiency and protection of active ingredient [58]. There are three ways nanomaterials penetrate the skin: intercellularly, intracellularly, and transappendagally. In the intercellular route, the nanomaterials diffuse across lipid bilayers and the matrix of corneocytes; the intracellular route comprises of aqueous areas surrounded by polar lipids that creates microchannels, the transappendageal route employs through sweat glands or hair follicles [38]. Lipid bilayers within the intercellular spaces, matrix of corneocytes, and high levels of proteins below the stratum corneum can affect the passive transport of nanomaterials through the stratum corneum as shown in Fig. 24.3.

## 24.5 Toxicity of nanocosmeceuticals

Despite their immense potential, some researchers have noted the toxicity of nanocosmeceuticals in organisms and the environment. Nanoparticles from various cosmeceuticals are applied on the skin show toxic effects after reaching to the bloodstream [59]. Pulmonary administration of ultrafine particles of  $\text{TiO}_2$  results in lung injury. The exposure of  $\text{TiO}_2$  nanoparticles in pregnant mice has resulted in brain damage of the male offspring. The trace of  $\text{TiO}_2$  observed in offspring and after certain time reduce sperm production in male offspring and lead to brain damage [60]. The toxicity of nanoparticles is caused by the generation of free radicals, which leads to oxidative stress and cell toxicity. When nanoparticles are inhaled, absorbed through the skin, or accidentally orally consumed skin, pulmonary tract, brain, and other organ (via blood) damage can result [61].

## 24.6 Safety of nanocosmeceuticals

Dermal exposure has raised concerns about the safety and toxicity of nanomaterials that are present in many cosmetic products such as skin care

**TABLE 24.1** Nanocosmeceuticals available on the market.

Product name	Manufacturer	Use	Type of nanomaterial
Hydra Zen Cream	Lancome	Moisturizer	Nanocapsules
Ferndale Nouriva	Ferndale Laboratories	Moisturizer	Nanoparticles
Nano In Hand and Nail Moisturizing Serum and Foot Moisturizing Serum	Nano-Infinity Nanotech	Moisturizer	Nanoparticles
Lip Tender	Kara Vita	Lip moisturizer	Lyphazomes
Primordiale Optimum Lip	Lancome	Lip treatment	Nanocapsules
Sircuit Skin	Sircuit Skin Cosmeceuticals	Antiaging	Fullerenes
Nanosphere Plus	DermaSwiss	Antiaging	Nanosphere
Nano Gold Firming Treatment	Chantecaille	Antiaging	Nanoparticles
ZelensFullere C-60 Night Cream	Zelens	Antiaging	Fullerene
Lancome Soleil Soft-Touch Antiwrinkle Sun Cream SPF 15	L'Oreal	Antiaging	Nanocapsules
Neova	ProCyte Corporation	Antiaging	Nanocapsules
Clearly It! Complexion Mist	Kara Vita	Antiacne	Nanosphere
Celazome	Celazome New Zealand Limited	Antiacne	Lyphazome
Soleil Instant Cooling Sun Spritz SPF 15	Lancome	Sun protection spray	Nanocapsule
DS Laboratories Spectral DNC	DS Laboratories	Hair loss treatment	Nanosomes
DS Laboratories Hydroviton. CR Liquid Normalizing Soap	DS Laboratories	Body wash/cleanser	Nanosomes
Boscia (Cleansing oil)	Fancil International	Facial cleanser	Nanotechnology

*(Continued)*

**TABLE 24.1 (Continued)**

Product name	Manufacturer	Use	Type of nanomaterial
Cosil Nano Beauty Soap	Natural Korea	Cleanser	Nanoparticles
Eye Tender	Kara Vita	Antiwrinkle	Nanosphere
Revitalift Double Lifting	L’Oreal	Antiwrinkle	Nanosomes
Eye Contour Nanolift	Euoko	Antiwrinkle	Nanocapsules
Revitalift Antiwrinkle and Firming Face and Neck Contour Cream	L’Oreal	Antiwrinkle	Nanosomes
LifePak Nano	Pharmanex	Antiaging	Nanotechnology
Nanorama–Nano Gold Mask Pack	LEXON Nano Tech	Antiacne	Nanoparticles
Nano-in Foot Deodorant Powder/Spray	Nano-Infinity Nanotech Co., Ltd.	Antimicrobial	Nanoparticles
Nano-in Deep Cleaning for make-up removal and exfoliation	Nano-Infinity Nanotech Co., Ltd.	Cleanser	Nanoparticles

products, hair products and sunscreens etc. applied to skin [62]. Some nanoparticles may also be concerned about contaminated solvents, side products, organics and endotoxins for toxicity. Studies have shown that nanoparticles can go deeper than bigger particles. The change in the physicochemical characteristics of nanomaterials in the final product and impurities present in nanomaterials also need to be considered [63]. The properties of nanomaterials may change during storage and handling making it difficult to predict their reactivity and risk. In the case of developing new cosmetics, safety, efficacy, stability, and aesthetic appeal of the formulations should be taken into consideration [64,65].

### 24.7 Regulations of nanocosmeceuticals

Cosmeceuticals are the products that are the combination of pharmaceuticals and cosmetics. In the last 10 years, there have been unanswered challenges

**TABLE 24.2** Patent data on nanocosmeceuticals.

Type of nanomaterial	Patent number	Publication date	Patent description	Inventor
Nanoemulsion	EP1264595A1	11/12/2002	Nanoemulsion by using lecithin and tocopheryl derivatives for application to the skin	Yoo, Byung Hee Paldal-ku, Kyunggi-do et al.
	[40]			
Nanopigments	US005658555A	19/8/1997	Sunscreen/cosmetic compositions for enhanced photoprotection including nanopigments of metal oxides	Jean-Marc Ascione, Delphine Allard
	[41]			
Nanoemulsion	US20150335538	9/1/2018	Cosmetic composition in the form of nano- or microemulsion for cleansing and conditioning the keratin fibers	Anne-Laure Bernard, Jinglan Li
	[42]			
Nanocapsules	DE10008306A1	6/9/2001	Use of nanocapsules in detergents, cleansing agents and in cosmetic products	Wolf Eisfeld, Ute Krupp
	[43]			
Nanoparticles	DE10333029A1	17/2/2005	Use of nanoparticulate UV protectant delivery system in cosmetic, sunscreens and other protective use	Bernd Hirth
	[44]			
Nanoparticles	DE10351611A1	11/8/2005	Use of silver nanoparticulate delivery system in antimicrobial pharmaceutical or cosmetic formulations	Christoph Cichos et al.
	[45]			
Nanoemulsion	US8980293B2	17/3/2015	Cosmetic composition containing vitamin A stabilized by nanoemulsification by porous polymer beads	Sang-Ho Jeong et al.
	[46]			

*(Continued)*



**TABLE 24.2 (Continued)**

Type of nanomaterial	Patent number	Publication date	Patent description	Inventor
Lipidic nanoparticles	US20160271024A1	20/3/2018	Conditioning shampoo cosmetic compositions by lipidic nanoparticles	Juliana Bucchi Alencastre Moroz et al.
	[47]			
Nanocarriers or nanopolymers	US20150223451A1	13/8/2015	Nanocarrier or nanopolymers composed of musk-derived bioactive compounds	Shaker A. Mousa, Amna Saddiq
	[48]			
Nanodispersions	US20120093896A1	22/7/2008	Use of nanodispersions to protect, ascorbic acid or vitamin C a water soluble ingredient in cosmetic end formulations	Sebastien Mongiat et al.
	[49]			
Metal oxide nanoparticles	US 20130022655 A1	24/1/2013	Metal oxide nanocomposite particles for UV protection	Bernd Sachweh et al.
	[50]			
Nanoparticles	US 8449868 B2	28/5/2013	Cationic nanoparticles provides conditioning properties to hair-care and skin-care products	John Jennings et al.
	[51]			
Nanocrystals	EP 2099420A1	16/9/2009	Cosmetic formulations containing nanocrystals for topical use	Rolf Petersen
	[52]			
Gold or silver nanoparticles	EP1909745A1	16/4/2008	Cosmetic nano-pigment composition containing gold or silver nanoparticles	Bong Hyun Jung, Yong Taik Lim, Jin Kyeong Kim, Jin Young Jeong, Tai Hwan Ha
	[53]			

Nanoparticles	EP2229142A1	27/12/2007	Gel system containing nanoparticles and macroscopic particles effective to blurrfine lines and wrinkles	Prithwiraj Maitra et al.
	<a href="#">[54]</a>			
Nanoparticles	EP 1239823B1	16/6/2004	Nanoscale active antidandruff ingredients having a particle for the production of hair-cosmetic preparations	Achim Ansmann et al.
	<a href="#">[55]</a>			
Nanopowder	US2005022683OA1	13/10/2005	The topical application comprises nanopearl powder	Harvard Fang
	<a href="#">[56]</a>			
Magnetic nanoparticles	US8637055B2	28/01/2014	A novel and cost-effective cosmetic compositions comprising magnetic particles	Zeev Maor, Michael RoyZ
	<a href="#">[57]</a>			

for regulators of nanocosmeceuticals procedure by FDA for approval of the final product. European regulators require cosmetic manufacturers to report any nanoparticle present in products marketed within the European Union. The FDA has the authority to prohibit the manufacturing and sale of a product or ban certain ingredients, warning labels and even category of cosmetics require different type of license from state food and drug administration, this way FDA regulate these products [66]. Scientific committee on consumer products (SCCP) has raised interest over the safety of nanomaterials used in cosmetic products. The Environment Protection Agency (EPA) needs research underway at other US government agencies, and the recommendation of the OECD (Organisation for Economic Cooperation and Development) works on manufactured nanomaterials and the European Commission's (EC) Scientific Committee on Consumer Products (SCCP) expressed their role on the use of insoluble nanoparticles in topically applied cosmetic products [67,68].

## 24.8 Conclusions and future perspectives

The demand in the cosmetic market is increasing day by day around the world and new cosmetics products are being developed by various companies. A number of different nanomaterials are now routinely incorporated into many cosmetics and personal care products. Nevertheless, more studies are needed to determine toxicity and other factors such as encapsulation and triggered release mechanism observed for the delivery of cosmetic ingredients present in nanomaterials.

## References

- [1] Melo A, Amadeu MS, Lancellotti M, De Hollanda LM, Machado D. The role of nanomaterials in cosmetics: national and international legislative aspects. *Quim Nova* 2015;38:599–603.
- [2] Global Cosmeceuticals Market 2018-2023 by demand, various products, production cost, top regions, worldwide consumption - Reuters; 2018.
- [3] Gianeti MD, Maia Campos PMBG. Efficacy evaluation of a multifunctional cosmetic formulation: the benefits of a combination of active antioxidant substances. *Molecules* 2014;19:18268–82.
- [4] Kaul S, Gulati N, Verma D, Mukherjee S, Nagaich U. Role of nanotechnology in cosmeceuticals: a review of recent advances. *J Pharm* 2018;2018:3420204.
- [5] Chaudhri N, Soni GC, Prajapati SK. Nanotechnology: an advance tool for nano-cosmetics preparation. *Int J Pharma Res Rev* 2015;4:28–40.
- [6] Raj S, Jose S, Sumod US, Sabitha M. Nanotechnology in cosmetics: opportunities and challenges. *J Pharm Bioallied Sci* 2012;4:186–93.
- [7] Shah KA, Date AA, Joshi MD, Patravale VB. Solid lipid nanoparticles (SLN) of tretinoin: potential in topical delivery. *Int J Pharm* 2007;345:163–71.

- [8] Müller-Goymann CC. Physicochemical characterization of colloidal drug delivery systems such as reverse micelles, vesicles, liquid crystals and nanoparticles for topical administration. *Eur J Pharm Biopharm* 2004;58:343–56.
- [9] Tiwari G, Tiwari R, Sriwastawa B, Bhati L, Pandey S, Pandey P, et al. Drug delivery systems: an updated review. *Int J Pharm Investig* 2012;2:2–11.
- [10] Feingold KR. Thematic review series: skin lipids the role of epidermal lipids in cutaneous permeability barrier homeostasis. *J Lipid Res* 2007;48:2531–46.
- [11] Vinardell MP, Mitjans M. Nanocarriers for delivery of antioxidants on the skin. *Cosmetics* 2015;2:342–54.
- [12] Cauchard, JH, Bonte, F, Archambault, JC. Cosmetic composition containing an amber extract. US 2008/0181974 A1; 2008.
- [13] Srinivas K. The current role of nanomaterials in cosmetics Available Online [Www.Jocpr.Com](http://www.jocpr.com) *J Chem Pharm Res.* 2016;8:906–14.
- [14] Doke SY. Applications of nanotechnology in pharmaceuticals. *Int J Pharm Sci Rev Res* 2016;37:49–62.
- [15] Gavazzoni Dias MFR. Hair cosmetics: an overview. *Int. J. Trichol.* 2015;7:2–15.
- [16] da Rocha-Filho PA. Nanoemulsions as a vehicle for drugs and cosmetics. *Nanosci Technol Open Access* 2013;1.
- [17] Bernardi DS, Pereira TA, Maciel NR, Bortoloto J, Viera GS, Oliveira GC, et al. Formation and stability of oil-in-water nanoemulsions containing rice bran oil: in vitro and in vivo assessments. *J Nanobiotechnol* 2011;9:44.
- [18] Azeem A, Rizwan M, Ahmad FJ, Iqbal Z, Khar RK, Aqil M, et al. Nanoemulsion components screening and selection: a technical note. *AAPS PharmSciTech* 2009;10:69–76.
- [19] Ekambaram P, Abdul A, Sathali H, Priyanka K. Solid lipid nanoparticles: a review. *Sci Rev Chem Commun J* 2012;2:80–102.
- [20] Wissing SA, Müller RH. The influence of solid lipid nanoparticles on skin hydration and viscoelasticity--in vivo study. *Eur J Pharm Biopharm* 2003;56:67–72.
- [21] Müller RH, Petersen RD, Hommoss A, Pardeike J. Nanostructured lipid carriers (NLC) in cosmetic dermal products. *Adv Drug Deliv Rev* 2007;59:522–30.
- [22] Dragicevic N, Maibach HI. Percutaneous penetration enhancers chemical methods in penetration enhancement *Nanocarriers* 2016;162–83.
- [23] Lohani A, Verma A, Joshi H, Yadav N, Karki N. Nanotechnology-based cosmeceuticals. *ISRN Dermatol* 2014;2014:843687.
- [24] Kaur G, Aggarwal G, Harikumar SL. Nanosponge: new colloidal drug delivery system for topical delivery. *Indo Glob J Pharm Sci* 2015;5:53–7.
- [25] Bhowmik H, Venkatesh DN, Kuila A, Kumar KH. Nanosponges: a review. *Int J App Pharm* 2018;10:1–5.
- [26] Kaity S, Maiti S, Ghosh AK, Pal D, Ghosh A, Banerjee S. Microsponges: a novel strategy for drug delivery system. *J Adv Pharm Technol Res* 2010;1:283–90.
- [27] Lens M. Use of fullerenes in cosmetics. *Recent Pat Biotechnol* 2009;3:118–23.
- [28] Yapar EA. Nanomaterials and cosmetics. *J Pharm Inst Univ* 2012;42:43–70.
- [29] Kato S, Taira H, Aoshima H, Saitoh Y, Miwa N. Clinical evaluation of fullerene-C60 dissolved in squalane for anti-wrinkle cosmetics. *J Nanosci Nanotechnol* 2010;10:6769–74.
- [30] Arul Jothy M, Shanmuganathan S, Nagalakshmi. An overview on niosome as carrier in dermal drug delivery. *J Pharm Sci Res* 2015;7:923–7.
- [31] Muzzalupo R, Tavano L. Niosomal drug delivery for transdermal targeting: recent advances. *Res Rep Transdermal Drug Deliv* 2015;4:23.

- [32] Vyas J, Vyas P, Raval D, Paghdar P. Development of topical niosomal gel of benzoyl peroxide. *ISRN Nanotechnol* 2011;2011:1–6.
- [33] Cornier J, Keck CM, Van de Voorde M. Nanocosmetics: From Ideas to Products. 2019;16–26.
- [34] Chung BH, Lim YT, Kim K, Jeong Y, Ha H. Cosmetic pigment composition containing gold or silver nano-particles. EP1909745A; 2008.
- [35] Sharma B, Sharma A. Future prospect of nanotechnology in development of anti-ageing formulations. *Int J Pharm Pharm Sci* 2012;4:57–66.
- [36] Raj S, Jose S, Sumod US, Sabitha M. Nanotechnology in cosmetics: Opportunities and challenges. *J Pharm Bioallied Sci.* 2012;4:186–93.
- [37] Justo GZ, Shishido SM, Machado D, da Silva RA, Ferreira Andrade CV, Santana MH, Dieamant GDC, Marcelino AG, Nogueira C, Polezel MA, Rossan MR, et al. Sericin cationic nanoparticles for application in products for hair and dyed hair. WO 2010146415; 2010.
- [38] Katz LM. Nanotechnology and applications in cosmetics: general overview. 2007;193–200.
- [39] Palit S, Hussain CM. Engineered nanomaterial for industrial use. *Handb Nanomater Ind Appl* 2018;3–12.
- [40] Yoo BH., Use of tocopherol derivatives for stabilizing nano-sized emulsion particles containing lecithin and their external application to the skin. EP1264595A1; 2002.
- [41] Ascione J-M, Allard D. Photoprotective/cosmetic compositions comprising synergistic admixture of sunscreen compounds/nanopigments. US005658555A; 1997.
- [42] Bernard A-L, Li J. Cosmetic composition. US20150335538; 2018.
- [43] Eisfeld W, Krupp U. Micro- and nano-capsules with cationic charges on surface are used in laundry and other detergents, skin cleansers, shampoos and skin and hair cosmetics. DE10008306A1; 2001.
- [44] Hirthe B, John S, Pflücker F, Sängner H. Nanoparticulate UV protectants used in cosmetic, sunscreen, dermatological or other protective uses (e.g. as textile or packaging coatings) comprise a metal oxide with a silicon dioxide coating. DE10333029A1; 2005.
- [45] Cichos C, Cichos I, Peter J, Guggenbichler. Liquid phase containing pure nano-particulate silver, useful in antimicrobial pharmaceutical or cosmetic preparations, obtained by eluting silver from (in)organic solid precursor with (in)organic liquid phase. DE10351611A1; 2005.
- [46] Jeong S-H, Son J-H, Jang S-J, Kim Y-J, Cheon J-W. Cosmetic composition containing retinol stabilized by porous polymer beads and nanoemulsion. US8980293B2; 2015.
- [47] Alencastre Moroz JB, Da Silva FL, Ferreira Adami DS, De Oliveira PMS, Caroline C, Raffin RP, et al. A nanostructured conditioning cosmetic composition, the use thereof in cosmetic preparations, and a conditioning shampoo. US20160271024A1; 2018.
- [48] Mousa SA, Saddiq A. Nanoformulation of musk-derived bioactive ingredients for nanocosmetic applications. US20150223451A1; 2015.
- [49] Mongiat S, Grumelard J, Baschong W, Herzog B. Use of nanodispersions to protect water-soluble ingredients in cosmetic end formulations. US20120093896A1; 2008.
- [50] Sachweh B, Koban W, Wohlleben W, Peukert W, Taylor RK, Distaso M. Metal oxide nanocomposites for UV protection. US 20130022655 A1; 2013.
- [51] Jennings J, Hüglin D, Mao J, Mühlebach A. Preparation of cationic nanoparticles and personal care compositions comprising said nanoparticles. US 8449868 B2; 2013.
- [52] Petersen R. Nanocrystals for use in topical cosmetic formulations and method of production thereof. EP 2099420A1; 2009.

- [53] Maitra P, Brown SE, Glynn JR, Rothouse J, Brahms JC, Fair MJ. Gel technology suitable for use in cosmetic compositions. EP2229142A1; 2007.
- [54] Maitra P, Carlo S, Ranade A. Nanoparticle compositions providing enhanced color for cosmetic formulations. EP2229142A1; 2007.
- [55] Ansmann A, Brüning S, Eggers A. Use of nanoscale deodorants. EP 1239823B1; 2004.
- [56] Fang H. Nano pearl cream. US2005022683OA1; 2005.
- [57] Maor Z, Royz M. Cosmetic compositions containing small magnetic particles. US8637055B2; 2014.
- [58] Contado C. Nanomaterials in consumer products: a challenging analytical problem. *Front. Chem.* 2015;3:48.
- [59] Jatana S, Callahan LM, Pentland AP, DeLouise LA. Impact of cosmetic lotions on nanoparticle penetration through ex vivo C57BL/6 hairless mouse and human skin: a comparison study. *Cosmetics* 2016;3.
- [60] Miralles P, Church TL, Harris AT. Toxicity, uptake, and translocation of engineered nanomaterial in vascular plants. *Environ Sci Technol* 2012;46:9224–39.
- [61] Jia X, Wang S, Zhou L, Sun L. The potential liver, brain, and embryo toxicity of titanium dioxide nanoparticles on mice. *Nanoscale Res Lett* 2017;12:478.
- [62] Patrick L. Lead toxicity part II: the role of free radical damage and the use of antioxidants in the pathology and treatment of lead toxicity. *Altern Med Rev* 2006;11:114–27.
- [63] Guix M, Carbonell C. Nanoparticles for cosmetics: how safe is safe? *Contrib Sci* 2008;4:213–17.
- [64] Kaul S, Gulati N, Verma D, Mukherjee S, Nagaich U. Role of Nanotechnology in Cosmeceuticals: A Review of Recent Advances. *J Pharm (Cairo)* 2018;27:3420204.
- [65] Hussain CM, Hussain CG. Future of industrial development and nanomaterials: (concluding notes). *Handb Nanomater Ind Appl* 2018;1073–6.
- [66] Oberdörster G, Oberdörster E, Oberdörster J. Nanotoxicology: an emerging discipline evolving from studies of ultrafine particles. *Environ Health Perspect* 2005;113:823–39.
- [67] Gupta S, Bansal R, Gupta S, Jindal N, Jindal A. Nanocarriers and nanoparticles for skin care and dermatological treatments. *Indian Dermatol Online J* 2013;4:267–72.
- [68] Furukawa F, Doi Y, Suguro M, Morita O, Kuwahara H, Masunaga T, et al. Lack of skin carcinogenicity of topically applied titanium dioxide nanoparticles in the mouse. *Food Chem Toxicol* 2011;49:744–9.

## Further reading

- Ajazzuddin M, Jeswani G, Jha A. Nanocosmetics: past, present and future trends. *Recent Patents Nanomed* 2015;5:3–11.
- Gigliobianco MR, Casadidio C, Censi R, Di Martino P. Nanocrystals of poorly soluble drugs: drug bioavailability and physicochemical stability. *Pharmaceutics* 2018;10.
- Spar E, Millecamps D, Isoir M, Burnier V, Larsson Å, Cabane B. Controlling the hydration of the skin though the application of occluding barrier creams. *J R Soc Interface* 2013;10:20120788.

This page intentionally left blank

## Section 9

# **Functionalized nanomaterials for aerospace, vehicle and sports industry**



This page intentionally left blank

# Functionalized nanomaterials for the aerospace, vehicle, and sports industries

Sadaf Abbasi<sup>1</sup>, M.H. Peerzada<sup>2</sup>, Sabzoi Nizamuddin<sup>1</sup> and Nabisab Mujawar Mubarak<sup>3</sup>

<sup>1</sup>*School of Engineering, RMIT University, Melbourne, VIC, Australia,* <sup>2</sup>*School of Engineering, Swinburne University, Melbourne, VIC, Australia,* <sup>3</sup>*Department of Chemical Engineering, Faculty of Engineering and Science, Curtin University, Sarawak, Malaysia*

## 25.1 Introduction

Generally, fiber-reinforced composites (FRCs) have been used to make aerospace parts with high strength: weight and modulus: weight ratios when related with metals. However, in recent decades, researchers have focused on nanomaterial-based composites, because of their high mechanical and multifunctional properties. Current research on nanomaterials for the aerospace, automotive, and sport industries is based on inorganic clay technology Carbon nanotube (CNTs), CNFs, single-walled CNTs (SWCNTs), multi-walled CNTs (MWCNTs), nanoclays, and nanocomposites. However, more research is needed in this area to better understand these materials and their properties [1]. The main disadvantage is the mechanical reinforcement using the nanoparticles in the polymers, which can be addressed through the degree of dispersion, impregnation in the matrix, and interfacial adhesion, which is still a challenging task. Thus their chemical, physical, and morphological properties must be studied. This chapter discusses nanomaterials used in the aerospace, automotive, and sports industries, along with their morphology properties.

## 25.2 Types of nanomaterials

### 25.2.1 Nanocomposites (polymer and carbon nanotubes/nanocomposite fibers, manufacturing process, morphology, and properties)

A nanocomposite is a matrix containing dispersed nanoparticles that enhance the properties of the end-product. Nanocomposites have received the attention of various field experts because of their unique thermal, conductive, and mechanical properties. In conventional composite material, two or more materials are combined to produce a hybrid material with the properties. However, if composite materials has the nanosize particle in the solution then it is defined as a “nanocomposite.” Nanosize particles have a large surface area that enables more contact with surrounding materials and thus more reactivity leading to a stronger material with lighter weight (Fig. 25.1).

The different categories of nanoparticles (shown in Table 25.1) are based on the functional properties require in composite plate. For example, lamellar nanoparticles are preferred for mechanical properties whereas fibrillar nanoparticles are selected for strength and rigidity.

Nanosize materials have been used in thermoplastics and thermosets as shown in Fig. 25.2. They have several advantages over conventional particles including high aspect ratio, electrical conductivity, resistance strength against gases and water, mechanical properties, chemical resistance, flame retardancy, and thermal stability.

### 25.2.2 Carbon nanotubes

CNTs are used in polymer composites due to their excellent thermal, mechanical, and electrical properties [2–4]. CNTs are basically cylinders, created from one sheet of graphene (SWCNT) or several sheets of graphene

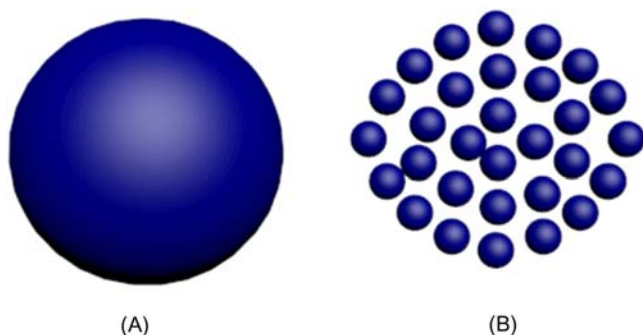


**FIGURE 25.1** (A) Conventional macroparticle and (B) nanoparticle with increased surface area.

**TABLE 25.1** Overview of different categories of nanoparticles.

Categories of matrix	Categories according to shape	Categories according to dimension
<ul style="list-style-type: none"><li>• Metallic nanocomposites</li><li>• Ceramic nanocomposites</li><li>• Polymer nanocomposites</li></ul>	<ul style="list-style-type: none"><li>• Spherical</li><li>• Lamellar</li><li>• Fibrillar</li><li>• Tubular</li></ul>	<ul style="list-style-type: none"><li>• One dimension (platelets)</li><li>• Two dimensions (fibers/whiskers)</li><li>• Three dimensions (nearly spherical particles)</li></ul>

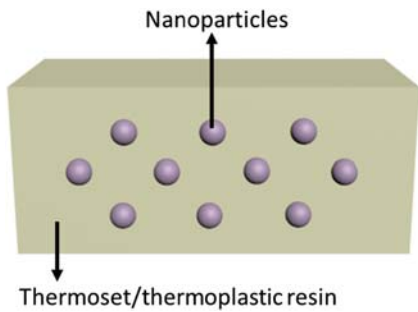


**FIGURE 25.2** Schematic diagram of nanoparticles mixed with matrix.

(MWCNTs). Due to their relatively small size, wetting process is quite challenging process. In nanocomposite material, the adhesion between constituents in the polymer composites is crucial. Since fiber is stiffer than matrix it takes higher force to deform. Thus it is important to have proper adhesion between the matrix, CNT, and fiber to create the desired properties in the end-product. Several studies have been carried out to understand the failure mechanism of CNT/polymer composites [5,6]. Latex technology, laminating layer by layer [7], and solid-state shear pulverization are reported to be the most effective techniques to disperse CNTs into polymer composites. Generally, CNTs are synthesized in the following three ways.

*25.2.2.1 Laser ablation*

Laser ablation is a thermal or nonthermal process used to release source material such as atoms/molecules, ions, and solids to synthesize CNT, fullerenes, and metals. As the laser is targeted at a certain angle, the atoms/molecules move with velocity to a specific location. The material produced by this technique consists of single-walled nanotubes. The size and dimeter of

CNTs can be varied by changing the growth temperature and other parameters. This is a low-cost manufacturing technique and can be used to synthesize the complex composition of nanoparticles.

#### 25.2.2.2 *Arc discharge*

This is the easiest way to produce CNTs, but it requires further purification. The process involves arc vaporization of two carbon rods usually placed in an enclosure filled with inert gas at low pressure. A direct current of 50–100 A creates discharge, resulting the form a small rod-shaped producing CNTs.

#### 25.2.2.3 *Chemical vapor deposition*

This is a traditional method used for producing various carbon material includings carbon fibers, filaments, and mass production of CNTs with high yield and controllability and low cost. However, the produced CNTs contain contaminants that need to be removed by a thermal or chemical process.

### 25.2.3 Carbon nanotube composite membranes

Mixing two additives in solution is the conventional method used to change the characteristics of composite material. Blending nanoparticles is an alternative approach to developing processes and enhancing composite properties, particularly physiochemical and mechanical. CNTs are prime material for improving the antibacterial, porosity, electrical, and thermal properties. These properties can be benefited in composite material by incorporating the CNT's into a matrix (polymer/ceramics/metals). High surface area, high aspect ratio, and high axis strength make CNTs an ideal additive for reinforcing the nanocomposite membranes [8]. Recent applications of CNTs in the form of Bucky tube include self-heating hybrid composites, EMI shielding, fire-retardant coating, super capacitance, strain sensing, gas sensing, and water purification [9–18]. CNT membranes can be classified in different ways, but are generally categorized into two broad classes: (1) freestanding CNT membranes and (2) mixed (nanocomposites) CNT membranes.

#### 25.2.4 Nanoclay

Nanoclay polymer composite, formally known as Bakelite, has been used since the 1900s. It attracted the attention of the research community when the Toyota Research Group reported that adding nanoclay into nylon increases its yield and tensile strength [19,20]. Clay varies in composition and purity and these properties have a direct influence on the final properties of nanoclay composites. While clays are classified by structure such as allophane, kaolinite, and vermiculite they can also be classified into three main

categories: (1) 1:1 type, (2) 2:1 type, and (3) layered silicic acids. Similarly, polymer–clay nanocomposites are grouped into three classes (see Table 25.2).

Type 1: In this type, clays are used as conventional fillers. Tactoids (clay particles) are dispersed in the polymer resin; these are known as conventional composites.

Type 2: In this type, layers of clay are separated and randomly distributed in polymer resin; these are known as exfoliated nanocomposites.

Type 3: In this type, each clay layer is surrounded by polymer chains and space is created in between them, but the layers still have a well-defined relationship; these are known as intercalated nanocomposites.

#### 25.2.4.1 Preparation method of polymer–clay nanocomposites

The effective penetration of polymer into clay is dependent on the right selection of modified clay. There are three main preparation methods of polymer–clay nanocomposites.

##### 25.2.4.1.1 Intercalation of polymer from solution

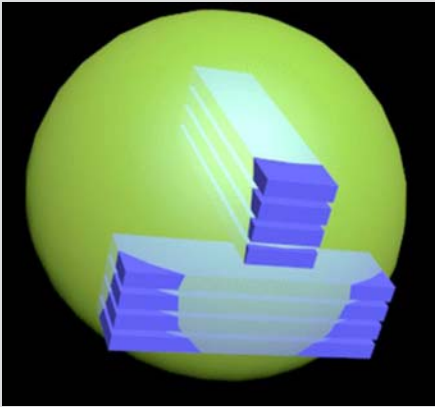
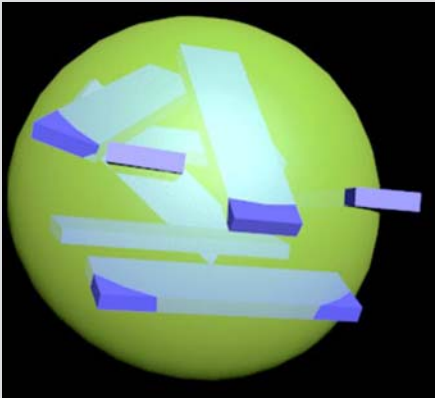
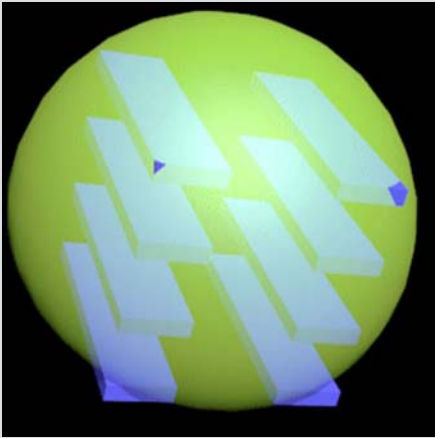
This method involves unusual physical chemistry and can enhance the mechanical [21,22] and physical properties of several processes. This process allows the choice of solvent comprising soluble polymer and swellable silicate layers. A solvent such as toluene, water or chloroform, or toluene swells the clay. Once the polymer and silicate solution are mixed, the polymer chains intercalate and displace the absorbed solvent. After removing the solvent from silicate galleries, polymer–clay nanocomposites appear in the form of intercalated structures.

##### 25.2.4.1.2 In situ intercalative polymerization method

In this method the incorporation of monomer molecules adjusts into pores of host structures. The monomers intercalate into clay minerals. The clay travels along their galleries while heat/radiation started and subsequently leading to polymerization in between the clay layers, which is often known as *in situ* polymerization.

##### 25.2.4.1.3 Melt intercalation method

This method involves the heating and then cooling processes (annealing) of a blend of polymer and clay. The polymer chains disperse between silicate layers during annealing. As a result, a range of nanocomposites with structure of exfoliated are created. However, it is mainly dependant on the penetration of polymer chains into interlayer spaces.

TABLE 25.2 Types of polymer–clay nanocomposites.		
S. no.	Types of polymer–clay nanocomposites	Schematic representation
1.	Conventional composites	
2.	Exfoliated nanocomposites	
3.	Intercalated nanocomposites	

### 25.2.5 Graphene nanoplatelets

Nanoplatelets are one nanoscale dimension nanoparticles comprising stacks of platelet-shaped graphene sheets. It is possible to add hydrogen or covalent bonding capability on the edges of platelets through functionalization at sites. While due to pure graphite composition, the nanoplatelets are excellent thermal and electrical conductors, the unique size and morphology of graphene nanoplatelets determines the mechanical and barrier properties of the composite. Graphene nanoplatelets have been used with different matrices such as epoxy, polyimide, nylon 6, nylon 6,6, vinyl esters, polypropylene, biodegradable polymers, and others to improve the wide range of properties (e.g., modulus, impact, thermal and electrical conductivities). Graphene nanoplatelets can be produced by different ways but common methods include chemical exfoliation and dry exfoliation with plasma. Ball milling is one of the most promising methods for edge functionalization, a simple and efficient way to produce graphene nanoparticles. In this method, graphite powders are mixed with chemicals (containing dry ice, such as sulfur trioxide or melamine) in a sealed jar. During high-speed ball milling, strong shear forces are generated to crack the graphite bonds leading to exfoliation of graphene nanoplates with grain size  $<1\ \mu\text{m}$ . Graphene nanoplatelets can be used in a wide range of applications due to their improved thermal conductivity and stability, flame retardancy, toughness, stiffness, and electrical conductivity.

### 25.2.6 Graphene

Graphene is a promising semimetal comprising sheets of pure carbon atoms. It is a basic unit of carbon material and makes different forms such as wrapped into 0D fullerenes, curled into 1D CNTs and stacked into 3D graphite. This material is impermeable to gases, stronger than steel, has a high surface area with a theoretical value of  $2630\ \text{m}^2/\text{g}$ , is almost transparent, has good foldability, and is an excellent conductor of electrical properties even after bending. Graphene is synthesized by top-down (destruction) and bottom-up (construction) methods [23]. Graphene has been used in different applications including batteries, supercapacitors, electrodes, conductive inks, polymer composites, and sensors. First process breaks the stacked layer of graphite to produce single graphene sheets, whereas the second process synthesizes graphene sheet from alternative sources containing carbon. The graphite layers are stacked together by Van der Waals forces. Consequently, it is an easy task to break these layers in the top-down method but challenging to separate them efficiently and without damage. As graphite is a natural and finite material bottom-up methods with a high level of graphitization should be used to produce a high-quality material. Although through this process, large area graphene films can be produced yet higher level of



defects observed in bottom-up method as compared to top-bottom methods that need to be addressed as well.

### 25.2.7 Nanofibers

Nanofibers have gained attention because they are lightweight, small in diameter compared to conventional fibers, and possess unique characteristics such as large surface area-to-volume ratio, superior mechanical properties, and the ability to improve the mechanical, electrical, and thermal properties of polymer matrix composites. There is significant impact noted in wide range of material such as natural polymers, synthetic polymers, carbon-based materials, semiconducting materials, and composite materials. Carbon nanofibers (CNFs) are one of the most rapidly evolving areas of composite material. The dimensions of CNFs vary—70–200 nm in diameter and length  $<1\ \mu\text{m}$  to several milometers. The common shape of stacked graphene sheets for internal structure of CFN are the cones or cups. The carbon nanofibers with high purity are manufactured by a catalytic chemical vapor deposition process in enough quantities and low cost. The incorporation of CNFs into polymer addresses the potential solution to many existing issues in composite applications. It provides the effective shielding from electromagnetic interference (EMI), enhance the various properties, improve the processability and recyclability of thermoplastic matrix nanocomposites, and have excellent surface finish. The nanofibers are used in several application including the capturing the individual cancer cells, therapeutic drug delivery, lithium ion battery electrodes, and sensors.

## 25.3 Properties of functional nanomaterials

Nanomaterials are the new innovative materials that exhibit improved properties such as more flexibility, stronger, lighter and also characterize high sensibility, intelligence, and multifunctionality. Therefore the development of new nanomaterials and enhancing their properties has become the prime reason of interest in recent years. The use of these nanomaterials and its applications are giving a cheap and mass producible method of creating new products. Nanomaterials having higher energy efficiency, specific strength, stiffness, damage tolerance, ductility, and stability in extreme environments are mainly used in aerospace, automobiles and sport applications. Carbon fiber composites with the addition of nanoparticles can considerably improve the composite properties. In addition to the improved intrinsic properties of composites, control of the degree of dispersion of the nanofillers in composites is still an issue for functional nanocomposite materials. Various attempts have been made in the uniform distribution of the nanoparticles, size of nanoparticles, concentration, and interfacial properties of nanocomposite material for specific applications.

Mechanical properties are required in the manufacturing of the structural materials like wing panels of aeroplane, which requires high fracture toughness, stability. In addition to mechanical properties, the materials used in the structural applications might be essential to have some more important properties such as lower density to reduce the fuel consumption and increase the speed in the racing bicycles and cars. Nanomaterials are often used for their corrosion resistance properties for the durability of structural materials. Multifunctionality is a relatively new concept for a structural material to be able to serve multiple functions. Multifunctional properties are also prime properties in high-temperature and high thermal conductive materials. Damage sensing is one of the examples of nonstructural function. Damage sensing, which is normally called structural health monitoring, is useful to sense damage and prevent hazards. This technique is attained by embedding sensors in the structure. These sensors increase detectability but can decrease the mechanical properties of the material.

High strength, high modulus, high ductility, high fracture toughness properties, and high capacity to absorb vibration are the fundamental mechanical properties for structural material. Other mechanical properties such as fatigue, creep, scratch, and wear resistance are also parallelly important properties. Structural materials are mainly divided in to three categories: metal-based, cement-based, and polymer-based. Polymer-based materials also include carbon and ceramic-based materials, which are mostly used in the aerospace, automotive and sports industry. Among the polymer-based categories polymer nanocomposites plays dominant role among the applications of high strength and low-density materials. Polymer nanocomposites consist of a polymer or copolymer with nanomaterials, nanofillers nanoclays, or graphene dispersed in the polymer matrix. These nanomaterials can be manufacture in different shapes (e.g., in the shape of fibers, spheroids, and platelets).

### 25.3.1 Aerospace material properties

Polymer nanocomposites have been studied by numerous researchers [24–31]. It has been proved that nanofillers can be able to give functional properties. Table 25.3 lists some important nanomaterials along with their functional properties mostly for use in the aerospace industry. In this part of the chapter the possible functional properties for aerospace applications are discussed.

#### 25.3.1.1 Weight reduction

Weight reduction is a big concern in the aerospace industry. With weight reduction more payload capacity, supplies, and power system can be achieved. Weight reduction not only provides the above advantages but can also reduce fuel consumption and lower carbon and gas emissions.

**TABLE 25.3** Nanomaterials and their functional properties used in aerospace applications.

Nanomaterials	Functional properties
CuO, ZnO, TiO <sub>2</sub>	Antimicrobial property
Nanoclays, graphene	Gas barrier, corrosion resistance
CNTs, graphene, SnO <sub>2</sub>	Electrical conductivity
Nanoclays	Fire retardancy
Nanoclays, ZrO <sub>2</sub>	Heat stability
SiO <sub>2</sub> , CaSiO <sub>3</sub> , CNTs, clay	Impact resistance
Al <sub>2</sub> O <sub>3</sub> , SiO <sub>2</sub> , ZrO <sub>2</sub>	Scratch resistance

The aerospace industry is maximizing the use of lightweight composites to minimize fuel consumption. A Boeing 787 is made up of around 50% of composite materials, which is 7% more than the Boeing 777. In conventional composite material it is important to have a fully densified matrix but voids in the composite material can lead to loss in mechanical defects and premature failure and degradation of the composite parts. It has been predicted that adding nanoparticles can reduce the voids to nanopores, resulting in matrices that can withstand mechanical loads and provide better durability. NASA has been working to increase multifunctional insulation properties with the help of structural polymer nanoaerogels.

The density of nanoporous polymers is about 0.2 g/cm<sup>3</sup>, which is around 1/5th of a full dense polymer. Researchers have made different attempts to improve the mechanical properties of insulated material, and believe that the improvement can be achieved by adding nanofillers such as CNTs, nanoclays, and graphene. The addition of nanofillers can strengthen nanopore walls and improve the mechanical properties of the structural materials. Replacing conventional carbon fibers with CNT fibers results in high tensile strength, which can reduce the weight of the composite panel.

### 25.3.1.2 Ultimate strength and stiffness

Carbon nanocomposites have higher modulus and tensile strength than normal carbon composites. Siegel et al. reported that fracture toughness for a 10 vol.% multiwalled carbon nanotube composite increased by 24% from 3.4 to 4.2 MPa/m<sup>2</sup> [32]. Whereas with addition of 0.5 vol.% nanotubes in CNT–polystyrene composites, the elastic stiffness and tensile strength increased about 42% and 25%, respectively [33]. Researchers have manufactured short fiber composite to show that 10 wt.% of carbon fibers (which is

about 5 vol.%) would be essential to accomplish similar growth in elastic modulus as achieved with 1 wt.% of CNTs [34].

#### 25.3.1.3 Thermal and fire resistance properties

Thermal and fire resistance are essential properties, particularly for the design of next-generation aerospace materials with increased multifunctionality and durability. In many cases, such as in electric aircraft, military appliances, and most sensing systems, improved thermal stability and fire resistance of materials are fundamentally required. Potential applications include microprocessors and power electronics in military applications.

Nanoclays are well-known materials with thermal and fire resistance [35–44]. Nanoclays act as heat resistors, and can increase the overall thermal resistance of the system and give assistance in the making of char during thermal decomposition. Fire properties are not affected by the addition of nanoclays. However, combining aluminium hydroxide and organophosphorous flame retardants can increase fire retardancy [45,46].

While nanoclays are effective materials for thermal and fire resistance other nanomaterials such as CNTs have shown greater improvement in fire retardancy [41,47–50]. CNTs can increase the glass-transition temperature and melting and thermal decomposition temperatures due to the constraints effect on the polymer segments and chains. The use of CNTs is increasing rapidly in thermal management materials [51–54].

#### 25.3.1.4 Field emission and optical properties

Field emissions using CNTs are ideal for high-voltage, low-current electrical power applications such as field emission electric propulsion, small electrodynamic tethers, and microion thrusters. CNT-based field emissions are suitable for microsatellites, which can reduce the mass, volume, and power requirements for small satellites and satellite subsystems [55–58]. Research on electronic devices has focused primarily on the use of SWCNTs and MWCNTs as field emission electron sources for flat-panel displays, lamps, and gas discharge tubes providing surge protection and X-ray and microwave generators. EMI shielding has also shown increased importance in the fields of electronics and communication, especially in space and military applications, due to the widespread use of packed, highly sensitive electronic devices. Researchers have also used MWCNTs with improved specific stiffness and strength for radar technology [55].

#### 25.3.1.5 Age and durability performance

Extreme environments such as UV radiation and high/low temperature can cause physical, chemical, and mechanical changes in any material. These changes reduce the lifetime and restrict the further use of these

materials. This degradation in polymers includes biodegradation, oxidation, photolytic, and pyrolysis [59].

Due to their chemical morphology, most polymers are susceptible to destructive effects. Even though organic UV absorbers have extensive applicability, due to their pure organic structures, they have disadvantages such as volatility and migration, which not only affect performance but also lead to environmental pollution [60]. Functional nanomaterials are used as UV absorbers, such as nano-ZnO and nano-CeO<sub>2</sub>. These materials have more chemical and thermal stability, are nontoxic and odorless, and have a wide range of wavelength for the UV shielding [60].

#### 25.3.1.6 *Impact resistivity and energy absorption*

Low- and high-velocity impact damage on composite materials weakens the structure and may cause flaws such as delamination, matrix cracks, fiber debonding, and fire damage. These damages can change the mechanical properties of composite structures, leading to possible catastrophic failure. Many studies have shown that the damage energy absorption capability can be increased by adding nanoscale fillers in the matrix. Rigid nanosized particles such as SiO<sub>2</sub>, TiO<sub>2</sub>, CaSiO<sub>3</sub>, Al<sub>2</sub>O<sub>3</sub>, CNTs, and clay nanoplatelets have been used to enhance the impact strength of composite.

A significant increase in the impact strength of polymer composites has been achieved with the addition of amino-functionalized MWCNTs or SWCNTs. By adding these nanofillers, the sensitivity of fiber-reinforced polymers (FRPs) to intrinsic damage (i.e., delamination, matrix cracking, and fatigue) and their negligible multifunctionality need a substantial effort to improve their performance to meet spacecraft application standards. Today, however, there are many questions surrounding the combination of nanoparticles, such as CNTs and CNFs, in FRPs regarding manufacturing methodology and structural integrity. Number of researchers have used clay nanoplatelets into epoxy when the clay nanoplatelets are not fully exfoliated and intercalated clay nanoplatelets are present to improve the fracture toughness properties. Nanostructured composites have eight times' higher tensile strength and energy dissipation than normal composites. This can achieve greater damping with reduced and lighter structural design. The number of CNT walls and their size also play an important role in stress concentration in the composite. It has been observed that short and round particles are strongest. However, longer fibers are flexible and may give better results in damping. A single CNT acts like a nanoscale spring and a crack-holding material in composites. This holding capacity can increase when CNTs are dispersed. Orientation and geometry (waviness) of CNT particles may affect the mechanisms of energy dissipation and fracture mechanics.

### 25.3.1.7 *Tribological and anticorrosive coatings*

Nanocoatings are a key trend in the materials of aircraft to increase the robustness of metals. Due to high chemical reactivity of magnesium alloy, they corrode easily. Coatings are used to prevent this corrosion, but many of these coating agents contain chromium complexes that are highly pollutant and harmful to the environment. Novel nanocoatings include silicon and boron oxides and cobalt/phosphorous nanocrystals [61,62]. Nanocoatings are also now being used on turbine blades and other mechanical parts that must resist higher temperatures and where friction wear is used. Tribological coatings can significantly lower the friction coefficient and improve resistance to wear, which significantly improves the efficiency of engines. Many nanostructured and nanoscale coating materials have been recommended as possible friction-modifying agents, such as carbides, nitrides, metals, and various ceramics.

## 25.3.2 **Automotive material properties**

Nanocomposites are an emerging class of polymeric materials with excellent mechanical properties, enhanced modulus and dimensional stability, improved scratch and mar resistance, higher thermal properties, and improved impact resistance. These properties make them fit to replace metals in automotive applications [63]. Cost and performance are also stringent demands of polymeric nanocomposites in the automotive field. In this section some of the important automotive material properties are discussed. These properties need to be improved and managed to make nanocomposites viable alternative materials for vehicle parts and systems.

### 25.3.2.1 *Modulus and dimensional stability*

Polymer nanocomposites and their properties have been studied by various researchers [64–67]. One of the studies describes the modulus in terms of volume fraction, aspect ratio, particle size, and maximum filler fraction. This model proposes that stiffness of the composite can be maximized by using smaller filler size and by maintaining the toughness of the material. Due to the increased surface-to-volume ratio, adhesion of fillers can be achieved. Conventional fillers like glass fibers limit the modulus but using surface-coated fillers can improve the modulus of composite. This can enhance the stress transfer between fiber and matrix. In nanocomposites the matrix and nanoparticles are interactive between the interfaces and create very large surface area, which promotes higher dispersion and makes possible large increases in modulus and tensile strength along with a decrease in the coefficient of linear thermal expansion, which is an important factor in the dimensional stability of any vehicle part.

### 25.3.2.2 *Higher heat-distortion temperature*

Automotive parts like interior or engine are prone to high and elevated temperatures. To withstand these temperatures fillers such as talc, calcium carbonate, or nanofillers are proposed to increase the temperature-resistant properties. Fillers are making joints between the crystallites and amorphous region and make it soft above its glass-transition temperature. However, nanofiller are not imparting many property losses of conventional fillers because of the smaller size which creates less stress concentration [68].

### 25.3.2.3 *Improved scratch resistance and mar resistance*

Maintenance of surface quality is important in many automotive applications. Scratch and mar resistance are enhanced when modulus is improved [69]. As discussed previously, adding nanofillers can improve the modulus, which decreases the scratch and mar resistance because of the delamination and void formation from displaced filler particles. Due to the smaller particle size nanofillers are less vulnerable to void formation. Nanoparticles have fewer stress concentration, which decreases the potential for damage. In addition, when nanosized particles are displaced, the subsequent voids decrease, thus scattering less light. This reduces the amount of whitening created by particles that are displaced.

### 25.3.2.4 *Toughness and rheological properties*

The addition of filler in the polymer can increase the modulus, but it can also reduce the toughness and result in poor rheological properties. Recent advances at Dow in constrained geometry polyolefin polymerization catalysis (Insite Technology: trademark of The Dow Chemical Company) have afforded polyolefin elastomers with exceptional physical and mechanical properties because of the narrow comonomer and molecular weight distributions [70]. This unique molecular structure results in many improved rheological properties, such as enhanced shear thinning, melt elasticity, and improved polymer melt processability.

Strengthening of the polymer/filler interface is critical to properly managing stress transfer during deformation. Most approaches to this problem involve the use of other polymers or low-molecular-weight additives that have some affinity for both the filler and the matrix polymer. A more rational methodology would involve the use of in situ compatibilization, whereby either the nanofiller or the matrix polymer is chemically designed to actually react with the other and form covalent bonds with it during the compounding process. This approach has a number of obvious costs and process advantages associated with it compared to other approaches, which may involve various pretreatment/compatibilization steps prior to actual compounding. The rheological behavior of nanoreinforced polymers is also crucial to its success in the real world. Nanocomposite materials must be processable on

**TABLE 25.4** Nanocomposites, benefits and applications.

Products	Key benefits	Applications
Polyolefin nanocomposites	Less brittle, lighter, more easily recycled, improved flame retardancy, very good impact properties	Heavy-duty electrical enclosures, door frames, seat brackets, instrumental panels
Nylon nanocomposites	Improved modulus, strength, heat-distortion temperature, barrier properties	Engine cover, fuel line, fuel hoses, fuel valves, fuel tanks
Nanoclays	Improved flexural and tensile strength, barrier properties, and flame retardancy of polymer matrix	Additives and reinforcements
Carbon nanotubes	Higher electrical and thermal properties, low coefficient of thermal expansion	Electrostatic painting, EMI shielding, additives, and reinforcements
Elastomeric nanocomposites (butyl, ethylene propylene diene monomer, natural rubber/ clay)	Reduced weight, higher durability, reduced rolling resistance, high barrier coatings	Tires

existing injection-molding equipment with minimal deviation from current practices. In theory, if the dispersion/compatibility issue discussed above is managed properly, the impact on rheology due to the presence of the filler will be minimal. However, other molecular architecture approaches to the design of the matrix polymer can also be applied if needed (Table 25.4).

**25.3.3 Sport material properties**

Nanotechnology has been used in the sports industry, such as in stadium floor coverings where it can influence performance and increase durability and cleanliness [71–73]. The use of various functional nanomaterials including carbon-nanomaterials in sports [74]. The incorporation of nano-material improves the properties of sports material such as mechanical, physical, compressible recovery, elasticity, durability, antflaming, anti-static, and other properties. The following are the main properties of sport materials.



### 25.3.3.1 *Waterproof resistance*

Waterproof breathable fabrics are used for sports clothing to protect against moisture but also extreme wind, rain, and loss of body heat. Waterproof fabrics do not allow water to penetrate into the fabric but allow air to diffuse water vapors through the fibers. There are different classes of breathable fabrics such as dense interlaced fabric, microporous membrane, and coated and smart breathable fabrics [75]. Nanotechnology has created new opportunities for the development of waterproof breathable fabrics. A typical waterproof fabric, ideal for swimmers, is produced with polyester and coated with nanosilicate that can prevent continuous penetration of water for more than 2 months. Another example is a sport shoe called “LSMZ” manufactured with nanomembrane [71,76]. Electrospinning extrudes nanofibers collected on drum or suitable platform to collect ultrathin web exhibiting high surface area, flexibility, desired porous that are suitable for sportswear. Laminating the number of nanowebs with different construction, web density, and fibers makes it a unique fabric with multifunctional properties such as higher resistance to water and moisture vapor penetration and air permeability. In addition to this, mixing metal vapors into nanowebs enhances the thermal comfort property.

### 25.3.3.2 *Antibacterial*

Apart from hospitals, antibacterial material is in demand in the sports industry for athlete health care. During sports a huge amount of sweating is produced that generates bacteria and then unpleasant odors. One common bacterium that causes infection is *Staphylococcus aureus*. Antibacterial fabric prevents microorganisms from infecting the human body as well as damaging the material. Previously, chitosan fibers were used as an antibacterial and moisture controlling material [77,78].

Today functional nanomaterials are being used to enhance antimicrobial properties either in the finishing method or during the spinning process through the mixing of nanoparticles into fibers. Silver nanoparticles are extensively used for sports clothing and shoes. Additionally, some researchers have studied the use of organic metals, organic silicones, and zinc oxide nanoparticles for antibacterial sportswear [79,80]. The efficiency of the antibacterial property is dependent on particle size and surface area.

### 25.3.3.3 *Ultraviolet protection*

In the outdoors, sports players are exposed to ultraviolet (UV) radiation. Nanoparticles added into sportswear minimize the risks associated with UV radiation. Some UV-protective materials such as  $\text{Al}_2\text{O}_3$ ,  $\text{SiO}_2$ , and  $\text{TiO}_2$  have exhibited promising results due to absorbing UV light instead of reflecting or scattering it. In addition to this, they are cheaper, readily available, and chemically stable. It has been observed that proper diffusion of

nanoparticles can improve the efficiency of these materials. A nanofiber (functional zinc oxide polyurethane) was spun to collect nanoweb with anti-UV and antimicrobial properties and is suitable for the sports industry.

#### 25.3.3.4 *Self-cleaning*

Nanotechnology is used in many applications in sport technology. One successful application is sport clothing and tents with self-cleaning ability. The photocatalytic nanoparticles ( $\text{TiO}_2$  and  $\text{ZnO}$ ) were incorporated to produce fabrics with hydrophobic surface with self-cleaning activity [81,82]. Such fabrics could be used for sportswear [83,84]. Under exposure to light, the nanoparticles have photocatalytic activity with energy greater than their band gap and produce electron pairs that further can be transferred to generate radicals (e.g., hydroperoxyl, hydroxyl). These radicals are oxidizing agents (bleaching agents) and provide self-cleaning and stain removal properties. The company Schoeller Textile AG introduced a product called “Nanosphere” for producing self-cleaning fabrics suitable for tents and sportswear [85].

#### 25.3.3.5 *Protection from extreme weather (heat/cold)*

During any physical activity, either light or heavy, the body’s temperature is constantly changing and thus sportswear with insulation against heat/cold is needed for activities such as skiing, snowboarding, diving, mountain climbing, and cycling. Thermo-regulated smart textiles with the use of phase change materials (PCMs) are used to manufacture sportswear that can maintain body temperature. PCMs can be categorized into two classes: (1) paraffin (nonadecane and octadecane) and (2) nonparaffin (fatty acids, alcohols, and glycolic acids).

PCMs are filled into microcapsules or nanocapsules. The PCM nanocapsules give better results than microcapsules due to their smaller particle size and higher rate of heat transfer. The shells used for capsules consist of materials such as polymethacrylate, urea formaldehyde, and polystyrene. The PCMs can be applied on the surface of the textile material during the finishing process or can be added in the fiber formation stage (spinning process) [86–88]. Recent techniques for manufacturing PCM nanofibers include composite electrospinning and coaxial electrospinning. The PCMs fused into this type of fiber can stabilize body heat, for example, by absorbing body heat while playing or releasing energy when required.

#### 25.3.3.6 *Multifunctional properties*

Multifunctional fabric protects the human body from different environments such as hot, cold, rain, and microorganisms and can be used in various sports including mountain climbing, skiing, football, cricket, and canoeing. Nanomaterials added in fabric for sportswear provide multifunctional

**TABLE 25.5** Properties of sportswear and shoes incorporated with nanotechnology.

Properties	Clothing types
UV protection	Outdoor sports
Self-cleaning	Mountaineering tents
Antibacterial	All types of sportswear and shoes
Waterproofing	Swimsuit, diving, canoeing, and sport shoes
Enhanced blood circulation and recovery muscles	Therapeutic knee bands, elbow bands, back belts
E-textiles	Mountaineering, running, and fencing clothing, referee gadgets
Protection from heat and cold	Skiing, snowboard, diving, mountaineering, canoeing, and cycling clothes
Comfort	All types of sportswear

properties for shoes and clothing. Some of the properties of these materials are listed in [Table 25.5](#).

## 25.4 Applications of functional nanomaterials

### 25.4.1 Aerospace applications

Lightweight is the main requirement in aircraft, rotorcraft, missile, and unmanned aerial vehicles. Along with this property increased speed, maneuverability, visual and thermal signature is also important. Researchers have examined many new advanced materials and systems that can incorporate these functionalities. CNTs meet all these requirements, mainly in weight reduction by replacement of current airframe material and wiring that minimize fuel consumption.

Wiring is another area of aeronautics that directly reduces weight and fuel. Generally, copper wires are used in aeroplanes that contribute significant weight (e.g., the length of wire in a Boeing 747 is 135 miles with a weight of 4000 lbs). It is believed that wire, namely 1553B made of CNTs, can save 69% weight and avoid overheating, vibration fatigue, and premature failure.

#### 25.4.1.1 Carbon nanofiber-incorporated three-phase carbon/epoxy composites

The properties of fabric/epoxy composites mainly depend on both fabric and matrix properties. To enhance these properties researchers have attempted to

manufacture high-performance carbon/epoxy composites. For instance, blending of rubber enhances the toughness of epoxy composites, but it also decreases thermomechanical properties and strength. Carbon nanoparticles can give better matrix properties because they provide a large interfacial area. One of the novel research three-phase composites was done by M. Joshi et al. [89,90]. In this research, epoxy composites were fabricated using nanofillers with carbon fibers. An ultrasonic technique (with high stirring speed) was used to disperse the nanofillers uniformly into matrix, achieving high fracture toughness and high tensile strength. The strong interface between carbon fiber and epoxy resin caused the improvement in mechanical properties. The addition of carbon nanofillers in epoxy composites caused the improvement of thermal and electrical conductivities due to the inherent properties of carbon nanofillers.

#### 25.4.1.2 *Nanostructured alloys for aerospace components*

Nanotechnology has shown promise in many applications in the automotive and aerospace industries. Nanostructured alloys are emerging in manufacturing engines in aerospace systems. Tensile strength and ultrahigh yield are the main advantages of nanostructured alloys. However, there are some disadvantages such as:

1. processing to achieve the necessary ultrafine grain sizes is poorly reproducible
2. Important mechanical properties like ductility and fatigue and fracture are inferior to those of conventional structural alloys
3. High manufacturing costs [91].

#### 25.4.1.3 *Carbon nanocomposites for EM shielding*

CNTs and graphene are perfect nanoscale fillers for metals, ceramics, and polymer composites not only due to their high mechanical, thermal, and electrical properties but also due to their ultrahigh surface area. Nanofillers could be used as a matrix modifier for improving electrical and thermal conductivities. EMI shielding is one of the most important factors for carbon FRP components. One study [92] showed that conductive interconnected CNTs and iron nanoparticles increase the EMI shielding effectiveness at a much higher rate than other shielding materials. CNTs have improved properties, which makes this material suitable for EMI shielding materials.

#### 25.4.1.4 *Nanomaterials for propellant materials*

Aluminium is a major ingredient in the manufacture of propellants. It has been proven that metallic nanoparticles have unique combustion properties (e.g., very fast ignition with shorter combustion times). Aluminium nanoparticles have been used to improve the ballistic properties of propellers. These

aluminium nanoparticles are coated with protective oxide layer(s) to decrease/avoid aggregation, agglomeration, and inadvertent ignition.

#### 25.4.1.5 *Electrodeposited coatings*

Hard chromium electroplating is the process of applying coating on the parts of aircraft to avoid corrosion and for wear protection. However, this process has some disadvantages such as the fact that the process contains an electrolytic bath having hexavalent chromium, which is a highly carcinogenic material. Nickel alloys are conventional electroplating alternatives [93], but these alloys are not environmentally friendly. These problems have encouraged researchers to come up with better solutions for protective coatings.

Researchers have found the nanocrystalline coatings of CO-based alloys are Co–P, Co–W, Co–Ni–Fe, Co–W–Fe, and CO-based nanocomposites such as Co–P, Co–W, Co–Ni–Fe, Co–W–Fe, and Co–P–SiC, Co–Ni–YZA, Co–W–Al<sub>2</sub>O<sub>3</sub>, respectively. These coatings have better mechanical and corrosive properties than chromium alloys [94,95].

#### 25.4.1.6 *Polymer-based solid lubricant coatings*

In recent years, different attempts have been made in the invention of solid lubricant coatings for an extensive series of industrial applications. These coatings are now available in nanostructure and/or -composite forms and offer better performance and durability even under very severe conditions. Adding these nanofillers in the polymer matrix can provide better mechanical and tribological properties along with the abrasion resistance [96]. Different types of nanosized filler materials such as MoS<sub>2</sub>, graphite, Al<sub>2</sub>O<sub>3</sub>, ZnO, TiO<sub>2</sub>, and so on have been used for the manufacture of polymer nanocomposites [97,98]. The effect of nanofillers depends on the optimized use of filler volume and on particle size.

Nanostructured solid lubricant has a wide variety of applications in the aerospace industry, in space systems, satellites, and launch vehicles [99,100]. These applications include foil air bearings, satellite components, gears, pumps, slip rings, solar arrays, reaction wheels, journal bearings, ball bearings, gimbal bearings, cams, space telescope mounts, etc. Table 25.6 shows the main applications of nanostructures solid lubricant coatings.

### 25.4.2 **Automotive applications**

The automotive industry uses metals, fillers, and plastics to meet the requirements of specific applications. Cost and performance are the major drivers for selecting the proper material for specific applications. Many attempts have been made to enhance the properties of conventional materials, such as using alternative metals and alloys and reinforcing fillers structural plastics, but all these methods have limitations. For example, structural plastics

**TABLE 25.6** Nanostructured solid lubricant coatings and their applications.

Coating system	Applications
MoS <sub>2</sub> /Au	Switches, potentiometers slip rings
TiN/In	Dry machining of carbon steel C35
Ti–C:H	Drilling of JIS SKH51 high-speed steel
MoST	Ejector pins for plastic molds, coining dies, Punching and piercing, low friction coatings
Korolon	
DLC	High-temperature foil bearing
Graphite-iC	Ball bearings for space application
	Dry drilling of automotive Al–Si alloy

require postforming surface modifications and have longer processing times and higher cost. However, nanomaterials have are being increasingly used in many applications in the automotive industry due to their enhanced performance and cost effectiveness. Nanomaterials are used in many applications, some of which are discussed in the following.

25.4.2.1 *Car bodies*

Strength is the main requirement for making the body of cars safe for passengers. Indeed, it is important to manufacture nanostructured material that can not only provide high strength but also give high intensity of impact during any accident. Nanostructured materials can also reduce the weight of the car, which leads to fuel efficiency.

25.4.2.2 *Nanocoatings/paints*

Conventionally metallic or nonmetallic paints were used to paint automotive parts. However, today nanobased paints migrate the silicon particles to the outer surface of the coating and generate a thin, hard, glass-like surface, which is three times more scratch resistant than conventional paints. Today, car paints with self-healing and dirt-repellent properties are being used in cars.

25.4.2.3 *Nanomaterials for car chassis*

The primary concern for the automotive industry is reducing weight and increasing fuel efficiency, which can reduce the CO<sub>2</sub> and exhaust emission. Nanotechnology offers better solutions to these problems. Nanomaterials are lighter and more resistant and have better mechanical properties. Nanobased

thermoplastic materials are giving promising reduction in weight compared with conventional steel chassis parts up to 40%.

#### 25.4.2.4 *Tires*

Automobile tires were the first product to draw attention of researchers for using nanomaterials. Carbon black was the first nanomaterial used in automotive tires as a pigment and reinforcing agent. Tires need to be manufactured with material with good grip and low rolling resistance. Nanoreinforcing fillers can improve grip, abrasion resistance, resistance to initial wear and tear, and tear propagation properties. Three products are mainly used to improve the properties of natural rubber: soot, silica, and organosilane. These materials are used in nanoscale and produce cross-linking between rubber molecules giving better properties.

#### 25.4.2.5 *Nanovarnishes for scratch resistance*

Nanovarnishes are extensively used for scratch resistivity and also for maintaining paint brilliance longer. In conventional varnishes, binders and cross-linking agents are used, but nanovarnishes use organic binders that give high elasticity and high strength. The tightly packed nanostructure makes these paints and varnishes scratch resistant.

#### 25.4.2.6 *Nanolayer for windscreens, mirrors, and reflectors*

Polymer glass is used in place of conventional mineral glass, reducing not only the weight of the car but providing better scratch and impact resistance. Polymer glass is coated with a very thin layer of paint made of very hard aluminium oxide nanoparticles. These nanoparticles are added during the hardening process of glass.

#### 25.4.2.7 *Improved fuel injection system*

Improving fuel efficiency is a major concern in the automobile industry. Controlling the pressure and precise times of injection can minimize the use of fuel and also provide better combustion. Direct injection pumps are the part through which fuel is sprayed to the combustion chamber. Piezo ceramic materials are famous for achieving higher fuel economy, reduced pollution and noise. Lead zirkone titanate (a nanocrystalline piezoelectric material) is used to regulate distance for injectors. These piezoelectric injectors can provide several finely closed injections per combustion cycle at around 1600 bar injection pressure.

### 25.4.3 **Sports industry applications**

CNTs are extensively used in the sport industry for different applications. As discussed above CNTs are electrically conductive, have good thermal

conductivity, and are much lighter than conventional metals, making them ideal for use in sport products. Sporting goods made of CNTs have higher strength and reduced weight compared to conventional products [101–106]. There are a variety of applications of nanomaterials, some of which are discussed below.

#### 25.4.3.1 *Nanomaterials in sport clothing and shoes*

Nanomaterials including nanofibers, nanocomposite fibers, and nanofinishes are providing multipurpose properties to the sports clothing industry. Many companies are using nanomaterials to make sports fabrics more comfortable, air permeable, wind and water resistant, with self-cleaning properties, etc. For example, “SoleFresh” socks can eliminate foot odor. These socks are treated with silver nanoparticles made by JR Nanotech. The nanoparticles have the ability to be easily absorbed on the surface of textile fabrics, without damaging the fabric breathability and fabric feel, due to their high specific area. One of the best nanowaterproof fabrics is manufactured by the Institute of Physical Chemistry University of Zurich. This fabric is manufactured with polyester fibers and coated with fibrillar silicate. This coating prevents rain drops from penetrating into the fabric. Furthermore, there is an air gap of fibrillar silicate that makes sure the water does not come into contact with the polyester fibers. This fabric has a tendency to prevent water penetration for 2 months. This fabric is best suited for swimsuits or scuba diving suits. There are number of benefits of nanotechnology in the sports industry for example, sports clothing (increased wicking), mountaineer (protection from cold and rain), and extreme climates (breathable and temperature regulating clothing).

Nanotechnology is also showing promise in the sports shoe industry with antislip footwear soles. Nanofunctional shoes designed by Chen et al. [73] have the ability to repel water and have antibacterial properties. These shoes are made of nanomembrane that consists of nanocomposite  $\text{TiO}_2$  and  $\text{ZnO}$  material, fluoronate surfactant, and perfluoroalkyl, which gives the shoes a Lotus effect. These nanoparticles have good chemical and thermal stability.

#### 25.4.3.2 *Nanomaterials in tennis rackets*

Today nanorackets are famous among tennis players because of their low weight, higher flexibility, durability, and hand feel. Nanorackets are made up of filling  $\text{SiO}_2$  into the holes of carbon fiber compound materials, which gives the tennis racket a smooth structure and making it stronger. Apacs badminton racket company developed a lightweight and high-speed racket namely Apacs Feather Weight-500 using graphite. This racket is extremely fast due to its lightness and weighs only 63 grams. The company YONEX has improved the impact resistance, elasticity,



and hand feel by successful penetration of nanofullerene particles into gaps between carbon atoms.

#### 25.4.3.3 *Nanomaterials in sports stadiums and gymnasiums*

Stadiums and gymnasiums should be clean, dry, and have the ability to withstand harsh weather for not only players but for the service life of stadiums and gymnasiums. Nanomaterials were used in the National Sports Stadium in China in the floor, wall, glass, and acoustic panels. Transparent nanomembranes have been used to cover stone floors and walls. Because of the low surface tension of membranes, they prevent water in leakage and make it easy to clean. Further, these transparent nanomembranes maintain the floor and walls tactile sensation and respiration. The humidity can be transferred to outside the walls and floors, which can prevent walls from stains and spots generated by the humidity. Nanopaints are applied on the walls to prevent the effects of harsh weather and also for self-cleaning, anti-dust adhesion, anti-UV light, and color protection. The glass roof of the Nation Gymnasium in China is coated with nano-TiO<sub>2</sub> defensive liquid, which gives the glass a more slippery surface and helps water to slide down from the roof easily.

#### 25.4.3.4 *Application of nanomaterials in running tracks*

Traditional plastic running tracks are made of polyurethane, which provides good intensity, elasticity, antiaging, hardness, and durability properties. Mixing of nanopowder in polyurethane can improve these properties. Nanopolyurathane can provide improved physical and mechanical properties along with environmental friendliness and excellent rebound resilience and compressible recoverability [107].

#### 25.4.3.5 *Nanomaterials in golf shafts*

Generally two types of materials are used to create golf shafts: steel and graphite. Golf shafts made with graphite are lighter than metal shafts. The common characteristics required for golf shafts are torque, weight, recommended swing speed range, and shaft tip diameter. Nanocomposites can enable golf shafts to increase distance of shots with accuracy. They also help players by reducing stiffness, bending, and torsional rigidity. These properties lead to better product quality.

### 25.5 Benefits and challenges

The key benefits of nanomaterials are their high mechanical, electrical, thermal, barrier, and chemical properties. Nanomaterials have better tensile strength, higher thermal conductivity, and improved heat deflection temperature, flame

retardancy, etc. These properties can be achieved by 3–5 wt% of nanomaterials such as nanoclays, CNTs, and nanofibers. However, there are some limitations:

- *Processing*

Compatibility, dispersion, and exfoliation between nanomaterials and polymer matrices are still challenges. There are some plastic matrices that are compatible with nanoclays, nanotubes, and nanofibers as intercalations of clays with the precursor of a polymer.

- *High cost and lead time*

The most obvious problem for nanomaterials is their high cost. The cost of high-quality CNTs are about \$1000/g [108]. However, the price of CNTs has drastically dropped in the past few years due to several attempts at mass production of CNTs. It is believed that the synthesis methods for manufacturing CNTs will increase in the future. Commercialization of nanomaterials for end-use products may have a high lead time due to stringent approval processes by regulatory agencies.

- *Oxidative/thermal instability of nanoclays*

Organoclays are commonly used nanomaterials that are thermally unstable due to the exchange of metal cations in clay galleries with organic ammonium salts and easily degrade at temperatures lower than 170°C.

### 25.5.1 Biological safety problems caused by nanomaterials

Nanomaterials have numerous advantages but also have biological safety problems for the following reasons:

1. Reducing the particle size can lead to changes in magnitude performance (e.g., an inert material can change to a catalyst and stable material can be burn).
2. Small-size nanoparticles can accumulate thousands of atoms on the surface and generate high surface energy with high reactivity, making them extremely unstable and easily combined with other atoms.
3. Ultrafine nanosized particles in the air can generate high deposition in the human respiratory system. Because of the smaller size it is difficult to remove its deposition and also, they can easily travel to the lung tissue organs thought breathing. They may then pass through the blood–brain barrier and blood–ocular barrier and cause damage.
4. High distribution of these ultrafine particles in the air can harm humans as well as animals and marine life. They can come into contact through breathing, skin, and injection and result in damage to cells, lungs, liver, kidney, and brain tissues.

Along with the above challenges, some critical challenges for nanomanufacturing include:

1. Controlling the assembly of 3D heterogeneous systems
2. Make them environmentally friendly and fit for human health
3. Manufacturing different nanostructures in high-rate/high-volume applications without reducing the inherent properties
4. Ensuring the long-term reliability of nanostructures

These problems and challenges can be overcome by doing more research on nanomaterials. Also, it is required to characterize advanced instrumentation and new approaches for producing nanomaterials with improved functional properties.

## 25.6 Conclusion

The automotive, aerospace, and sport industries are deeply influenced by nanotechnology. It is believed that in the next few years the use of nanomaterials in these industries will be increased due to their excellent physical, chemical, and multifunctional properties. These materials have the ability to improve the overall properties of conventional materials. Nanomaterials have unique mechanical, physical, and processing properties, which makes them fit for applications in the automotive and aerospace industries. For example, the increased surface area of metal nanoparticles can enhance the reactivity of the catalyst and reduce gas emissions. Nanomaterials can also be used to create highly efficient nanolayers for electronic components, engine control systems, airbags, and antilock brake systems. The current challenge is to produce nanomaterials at a reasonable cost, with high reliability and superior performance to replace metals and/or existing polymeric-filled composites.

Nanotechnology has become popular in the sports industries due to its ability to improve product performance. However, nanobased equipment may be harmful to users and thus more research is needed to develop safer, environmentally friendly nanoproducts.

## References

- [1] Hussain CM. Handbook of nanomaterials for industrial applications. Elsevier; 2018.
- [2] Gupta TK, Kumar S. 4 - Fabrication of carbon nanotube/polymer nanocomposites. In: Rafiee R, editor. Carbon nanotube-reinforced polymers. Elsevier; 2018. p. 61–81.
- [3] Spitalsky Z, et al. Carbon nanotube–polymer composites: chemistry, processing, mechanical and electrical properties. *Prog Polym Sci* 2010;35(3):357–401.
- [4] Thostenson ET, Ren Z, Chou T-W. Advances in the science and technology of carbon nanotubes and their composites: a review. *Compos Sci Technol* 2001;61(13):1899–912.
- [5] Qian D, et al. Load transfer and deformation mechanisms in carbon nanotube-polystyrene composites. *Appl Phys Lett* 2000;76(20):2868–70.

- [6] Assouline E, et al. Nucleation ability of multiwall carbon nanotubes in polypropylene composites. *J Polym Sci Part B: Polym Phys* 2003;41(5):520–7.
- [7] Arif AM, et al. Molecular design of strong single-wall carbon nanotube/polyelectrolyte multilayer composites. *Nat Mater* 2002;1(3):190.
- [8] Daraei P, et al. Fabrication of PES nanofiltration membrane by simultaneous use of multi-walled carbon nanotube and surface graft polymerization method: comparison of MWCNT and PAA modified MWCNT. *Sep Purif Technol* 2013;104:32–44.
- [9] Dumée LF, et al. Characterization and evaluation of carbon nanotube Bucky-Paper membranes for direct contact membrane distillation. *J Membr Sci* 2010;351(1):36–43.
- [10] Slobodian P, et al. Multi-wall carbon nanotube networks as potential resistive gas sensors for organic vapor detection. *Carbon* 2011;49(7):2499–507.
- [11] Benlikaya R, Slobodian P, Riha P. Enhanced strain-dependent electrical resistance of polyurethane composites with embedded oxidized multiwalled carbon nanotube networks. *J Nanomater* 2013;2013.
- [12] Rein MD, Breuer O, Wagner HD. Sensors and sensitivity: carbon nanotube buckypaper films as strain sensing devices. *Compos Sci Technol* 2011;71(3):373–81.
- [13] Kang I, et al. A carbon nanotube strain sensor for structural health monitoring. *Smart Mater Struct* 2006;15(3):737–48.
- [14] Zheng C, et al. Ionic liquid coated single-walled carbon nanotube buckypaper as supercapacitor electrode. *Particuology* 2013;11(4):409–14.
- [15] Zhu W, et al. Buckypaper-based catalytic electrodes for improving platinum utilization and PEMFC's performance. *Electrochim Acta* 2010;55(7):2555–60.
- [16] Fu X, et al. Carbon nanotube buckypaper to improve fire retardancy of high-temperature/high-performance polymer composites. *Nanotechnology* 2010;21(23):235701.
- [17] Park JG, et al. Electromagnetic interference shielding properties of carbon nanotube buckypaper composites. *Nanotechnology* 2009;20(41):415702.
- [18] Chu H, et al. Self-heating fiber reinforced polymer composite using meso/macropore carbon nanotube paper and its application in deicing. *Carbon* 2013;66(C).
- [19] Kojima Y, et al. Mechanical properties of nylon 6-clay hybrid. *J Mater Res* 2011;8(5):1185–9.
- [20] Usuki A, et al. Synthesis of nylon 6-clay hybrid. *J Mater Res* 2011;8(5):1179–84.
- [21] Lan T, Pinnavaia T. Clay-reinforced epoxy nanocomposites. *Chem Mat* 1994;6(12):2216–19.
- [22] Cui L, Tarte N, Woo S. Effects of modified clay on the morphology and properties of PMMA/clay nanocomposites synthesized by in situ polymerization. *Macromolecules* 2008;41(12):4268–74.
- [23] Edwards RS, Coleman KS. Graphene synthesis: relationship to applications. *Nanoscale* 2012;5(1):38–51.
- [24] Ramanathan T, et al. Functionalized graphene sheets for polymer nanocomposites. *Nat Nanotechnol* 2008;3:327.
- [25] Moniruzzaman M, Winey KI. Polymer nanocomposites containing carbon nanotubes. *Macromolecules* 2006;39(16):5194–205.
- [26] Giannelis EP. Polymer-layered silicate nanocomposites: synthesis, properties and applications. *Appl Organomet Chem* 1998;12(10–11):675–80.
- [27] Potts JR, et al. Graphene-based polymer nanocomposites. *Polymer* 2011;52(1):5–25.
- [28] Kim H, Abdala AA, Macosko CW. Graphene/polymer nanocomposites. *Macromolecules* 2010;43(16):6515–30.

- [29] Podsiadlo P, et al. Ultrastrong and stiff layered polymer nanocomposites. *Science* 2007;318(5847):80.
- [30] Du F, et al. Nanotube networks in polymer nanocomposites: rheology and electrical conductivity. *Macromolecules* 2004;37(24):9048–55.
- [31] Jordan J, et al. Experimental trends in polymer nanocomposites—a review. *Mater Sci Eng: A* 2005;393(1):1–11.
- [32] Siegel R, et al. Mechanical behavior of polymer and ceramic matrix nanocomposites. *Scr Mater* 2001;44(8-9):2061–4.
- [33] Poulin P, Vigolo B, Launois P. Films and fibers of oriented single wall nanotubes. *Carbon* 2002;40(10):1741–9.
- [34] Tibbetts GG, McHugh JJ. Mechanical properties of vapor-grown carbon fiber composites with thermoplastic matrices. *J Mater Res* 2011;14(7):2871–80.
- [35] Leszczyńska A, et al. Polymer/montmorillonite nanocomposites with improved thermal properties: part I. Factors influencing thermal stability and mechanisms of thermal stability improvement. *Thermochim Acta* 2007;453(2):75–96.
- [36] Hwu JM, et al. The characterization of organic modified clay and clay-filled PMMA nanocomposite. *J Appl Polym Sci* 2002;83(8):1702–10.
- [37] Laoutid F, et al. New prospects in flame retardant polymer materials: from fundamentals to nanocomposites. *Mater Sci Eng R: Rep* 2009;63(3):100–25.
- [38] Hapuarachchi TD, Peijs T. Multiwalled carbon nanotubes and sepiolite nanoclays as flame retardants for polylactide and its natural fibre reinforced composites. *Compos Part A: Appl Sci Manuf* 2010;41(8):954–63.
- [39] Chattopadhyay DK, Webster DC. Thermal stability and flame retardancy of polyurethanes. *Prog Polym Sci* 2009;34(10):1068–133.
- [40] Wang Z-y, Han E-h, Ke W. Fire-resistant effect of nanoclay on intumescent nanocomposite coatings. *J Appl Polym Sci* 2007;103(3):1681–9.
- [41] Isitman NA, Gunduz HO, Kaynak C. Nanoclay synergy in flame retarded/glass fibre reinforced polyamide 6. *Polym Degrad Stab* 2009;94(12):2241–50.
- [42] Awad WH, et al. Material properties of nanoclay PVC composites. *Polymer* 2009;50(8):1857–67.
- [43] Schmidt D, Shah D, Giannelis EP. New advances in polymer/layered silicate nanocomposites. *Curr Opin Solid State Mater Sci* 2002;6(3):205–12.
- [44] Vyazovkin S, et al. Kinetics of the thermal and thermo-oxidative degradation of a polystyrene–clay nanocomposite. *Macromol Rapid Commun* 2004;25(3):498–503.
- [45] Liang S, Neisius NM, Gaan S. Recent developments in flame retardant polymeric coatings. *Prog Org Coat* 2013;76(11):1642–65.
- [46] Hull TR, Witkowski A, Hollingbery L. Fire retardant action of mineral fillers. *Polym Degrad Stab* 2011;96(8):1462–9.
- [47] Kashiwagi T, et al. Nanoparticle networks reduce the flammability of polymer nanocomposites. *Nat Mater* 2005;4:928.
- [48] Isitman NA, Kaynak C. Nanoclay and carbon nanotubes as potential synergists of an organophosphorus flame-retardant in poly(methyl methacrylate). *Polym Degrad Stab* 2010;95(9):1523–32.
- [49] Scharrel B, et al. Fire behaviour of polyamide 6/multiwall carbon nanotube nanocomposites. *Eur Polym J* 2005;41(5):1061–70.
- [50] Xiang F, et al. Carbon nanotube buckypaper to improve fire retardancy of high-temperature/high-performance polymer composites. *Nanotechnology* 2010;21(23):235701.

- [51] Sarvar F, Whalley DC, Conway PP. Thermal interface materials - A Review of the state of the art in 2006 1st electronic systemintegration technology conference; 2006.
- [52] Kreupl F, et al. Carbon nanotubes in interconnect applications. *Microelect Eng* 2002;64(1):399–408.
- [53] Chai Y, et al. Carbon nanotube/copper composites for via filling and thermal management. In: *Proceedings of 57th electronic components and technology conference (ECTC'07)*; 2007.
- [54] Zhao Y, et al. Interfacial energy and strength of multiwalled-carbon-nanotube-based dry adhesive. *J Vac Sci Technol B: Microelectron Nanometer Struct Proc Measurement Phenom* 2006;24(1):331–5.
- [55] Lee S-E, Kang J-H, Kim C-G. Fabrication and design of multi-layered radar absorbing structures of MWNT-filled glass/epoxy plain-weave composites. *Compos Struct* 2006;76(4):397–405.
- [56] Baughman RH. Conducting polymer artificial muscles. *Synth Met* 1996;78(3):339–53.
- [57] Mirfakhrai T, Madden JDW, Baughman RH. Polymer artificial muscles. *Mater Today* 2007;10(4):30–8.
- [58] Li D, Xia Y. Welding and patterning in a flash. *Nat Mater* 2004;3:753.
- [59] Pieliowski K, Njuguna J. Thermal degradation of polymeric materials. iSmithers Rapra Publishing; 2005.
- [60] Wang H, et al. Effects of additives on weather-resistance properties of polyurethane films exposed to ultraviolet radiation and ozone atmosphere. *J Nanomater* 2014;2014:1.
- [61] Voevodin AA, O'Neill JP, Zabinski JS. Nanocomposite tribological coatings for aerospace applications. *Surf Coat Technol* 1999;116-119:36–45.
- [62] Edward Anand E, Natarajan S. Preparation and characterisation of nanocrystalline cobalt–phosphorus coatings reinforced with carbon nanotubes. *Surf Eng* 2014;30(10):716–21.
- [63] Garcés JM, et al. Polymeric nanocomposites for automotive applications. *Adv Mater* 2000;12(23):1835–9.
- [64] Nguyen QT, Baird DG. Preparation of polymer–clay nanocomposites and their properties. *Adv Polym Technol* 2006;25(4):270–85.
- [65] Park CI, et al. The fabrication of syndiotactic polystyrene/organophilic clay nanocomposites and their properties. *Polymer* 2001;42(17):7465–75.
- [66] Azizi Samir MAS, Alloin F, Dufresne A. Review of recent research into cellulosic whiskers, their properties and their application in nanocomposite field. *Biomacromolecules* 2005;6(2):612–26.
- [67] Huang Z-M, et al. A review on polymer nanofibers by electrospinning and their applications in nanocomposites. *Compos Sci Technol* 2003;63(15):2223–53.
- [68] Bhattacharya M. Polymer nanocomposites-A comparison between carbon nanotubes, graphene, and clay as nanofillers. *Mater (Basel, Switz)* 2016;9(4):262.
- [69] Brostow W, et al. Improvement of scratch and wear resistance of polymers by fillers including nanofillers. *Nanomaterials* 2017;7(3):66.
- [70] Chum PS, Swogger KW. Olefin polymer technologies—history and recent progress at The Dow Chemical Company. *Prog Polym Sci* 2008;33(8):797–819.
- [71] Harifi T, Montazer M. Application of nanotechnology in sports clothing and flooring for enhanced sport activities, performance, efficiency and comfort: a review. *J Ind Text* 2015;46(5):1147–69.
- [72] Gong ZG. Nanotechnology application in sports. *Adv Mater Res* 2013;662:186–9.

- [73] Kai Y. Study of biosafety of nanomaterials in sports engineering. *Appl Mech Mater* 2013;340:348–52.
- [74] Patra JK, Gouda S. Application of nanotechnology in textile engineering: an overview. *J Eng Technol Res* 2013;5(5):104–11.
- [75] Mukhopadhyay A, Vinay Kumar M. A review on designing the waterproof breathable fabrics part I: fundamental principles and designing aspects of breathable fabrics. *J Ind Text* 2008;37(3):225–62.
- [76] Zhao HE, Shen F. The applied research of nanophase materials in sports engineering. *Advanced materials research. Trans Tech Publ*; 2012.
- [77] Kong M, et al. Antimicrobial properties of chitosan and mode of action: a state of the art review. *Int J Food Microbiol* 2010;144(1):51–63.
- [78] Heine E, et al. Antimicrobial functionalisation of textile materials. Multifunctional barriers for flexible structure. *Springer*; 2007. p. 23–38.
- [79] Pulit-Prociak J, et al. Functionalization of textiles with silver and zinc oxide nanoparticles. *Appl Surf Sci* 2016;385:543–53.
- [80] Jacobson HW, Scholla MH, Wigfall AW. Antimicrobial particles of silver and barium sulfate or zinc oxide. 1997, Google Patents.
- [81] Benedix R, et al. Application of titanium dioxide photocatalysis to create self-cleaning building materials. *Lacer* 2000;5:157–68.
- [82] Parkin IP, Palgrave RG. Self-cleaning coatings. *J Mater Chem* 2005;15(17):1689–95.
- [83] Meilert KT, Laub D, Kiwi J. Photocatalytic self-cleaning of modified cotton textiles by TiO<sub>2</sub> clusters attached by chemical spacers. *J Mol Catal A: Chem* 2005;237(1):101–8.
- [84] Bozzi A, Yuranova T, Kiwi J. Self-cleaning of wool-polyamide and polyester textiles by TiO<sub>2</sub>-rutile modification under daylight irradiation at ambient temperature. *J Photochem Photobiol A: Chem* 2005;172(1):27–34.
- [85] Holme I. Innovative technologies for high performance textiles. *Coloration Technol* 2007;123(2):59–73.
- [86] Dastjerdi R, Montazer M. A review on the application of inorganic nano-structured materials in the modification of textiles: focus on anti-microbial properties. *Colloids Surf B: Biointerfaces* 2010;79(1):5–18.
- [87] Mondal S. Phase change materials for smart textiles – an overview. *Appl Therm Eng* 2008;28(11):1536–50.
- [88] Nelson G. Application of microencapsulation in textiles. *Int J Pharm* 2002;242(1):55–62.
- [89] Rana S, Alagirusamy R, Joshi M. Mechanical behavior of carbon nanofibre-reinforced epoxy composites. *J Appl Polym Sci* 2010;118(4):2276–83.
- [90] Rana S, Alagirusamy R, Joshi M. Development of carbon nanofibre incorporated three phase carbon/epoxy composites with enhanced mechanical, electrical and thermal properties. *Compos Part A: Appl Sci Manuf* 2011;42(5):439–45.
- [91] Prasad NE, Wanhil RJ. *Aerospace materials and material technologies.*, vol. 3. Springer; 2017.
- [92] Wu ZP, et al. Electromagnetic interference shielding of carbon nanotube macrofilms. *Scr Materialia* 2011;64(9):809–12.
- [93] Sudagar J, Lian J, Sha W. Electroless nickel, alloy, composite and nano coatings – a critical review. *J Alloy Compd* 2013;571:183–204.
- [94] Weng F, et al. Microstructures and wear properties of laser cladding Co-based composite coatings on Ti–6Al–4V. *Mater Des* 2015;80:174–81.
- [95] Shi L, et al. Electrodeposition and characterization of Ni–Co–carbon nanotubes composite coatings. *Surface Coatings Technol* 2006;200(16):4870–5.

- [96] Upová M, et al. Effect of nanofillers dispersion in polymer matrices: a review. *Sci Adv Mater* 2011;3(1):1–25.
- [97] Yang HG, Zeng HC. Synthetic architectures of  $\text{TiO}_2/\text{H}_2\text{Ti}_5\text{O}_{11} \cdot \text{H}_2\text{O}$ ,  $\text{ZnO}/\text{H}_2\text{Ti}_5\text{O}_{11} \cdot \text{H}_2\text{O}$ ,  $\text{ZnO}/\text{TiO}_2/\text{H}_2\text{Ti}_5\text{O}_{11} \cdot \text{H}_2\text{O}$ , and  $\text{ZnO}/\text{TiO}_2$  nanocomposites. *J Am Chem Soc* 2005;127(1):270–8.
- [98] Xiao F-X. Construction of highly ordered  $\text{ZnO}-\text{TiO}_2$  nanotube arrays ( $\text{ZnO}/\text{TNTs}$ ) heterostructure for photocatalytic application. *ACS Appl Mater Interfaces* 2012;4(12):7055–63.
- [99] Abad MD. Nanostructured lubricant systems for tribological applications; 2010.
- [100] Hilton MR, Fleischauer PD. Applications of solid lubricant films in spacecraft. *Surf Coat Technol* 1992;54-55:435–41.
- [101] Esawi AMK, Farag MM. Carbon nanotube reinforced composites: potential and current challenges. *Mater Des* 2007;28(9):2394–401.
- [102] Breuer O, Sundararaj U. Big returns from small fibers: a review of polymer/carbon nanotube composites. *Polym Compos* 2004;25(6):630–45.
- [103] Ajayan PM, Tour JM. Nanotube composites. *Nature* 2007;447:1066.
- [104] De Volder MFL, et al. Carbon nanotubes: present and future commercial applications. *Science* 2013;339(6119):535–9.
- [105] Byrne MT, Gun'ko YK. Recent advances in research on carbon nanotube–polymer composites. *Adv Mater* 2010;22(15):1672–88.
- [106] Bal S, Samal SS. Carbon nanotube reinforced polymer composites—a state of the art. *Bull Mater Sci* 2007;30(4):379.
- [107] Tang M, Yang L, Zhou H. Applications and safety of nanotechnology and nanomaterials in sports. London: Springer London; 2013.
- [108] Zhou Y, Azumi R. Carbon nanotube based transparent conductive films: progress, challenges, and perspectives. *Sci Technol Adv Mater* 2016;17(1):493–516.



This page intentionally left blank

## Section 10

# **Functionalized nanomaterial in construction industry**

This page intentionally left blank

# Nanomaterials for enhancement of thermal energy storage in building applications

Teng Xiong and Kwok Wei Shah

*Department of Building, School of Design and Environment, National University of Singapore, Singapore, Singapore*

## 26.1 Introduction

Energy shortage is a critical issue facing economic growth and social progress. The global energy demand, according to International Energy Agency (IEA)'s report, will expand by 40% between today and 2040 due to the rapid population growth and urbanization [1]. As one of the major energy consumers, buildings are responsible for about 30% of the final energy consumption. A majority of the energy use in building sector is associated with the heavy demand for heating and cooling to keep a comfortable indoor thermal environment. On the other hand, the upsurge in building energy use and its negative impacts on global climate change should not be overlooked, since fossil fuels still account for nearly 80% of the current energy mix [2]. The burning of fossil fuels releases greenhouse gases, leading to critical environmental problems, such as air pollution, global warming, and land degradation. In this context, countless efforts have been made to decarbonize the building sector over the past decades [3,4]. The key initiatives are focused on implementing clean energy policies, integrating renewable energy technologies, developing energy-efficient materials, and increasing public awareness of energy sustainability [5]. In the long run, the rapid depletion of fossil fuels will compel the energy mix to be shifted toward the wide adoption of sustainable energy sources including solar energy [6,7], hydro energy [8], wind energy [9,10], geothermal energy [11], etc. However, most of these renewable sources are intermittent, which is hard to ensure a round-the-clock energy supply [12]. Thermal energy storage (TES) solutions could be used to

store the surplus energy collected from the renewable energy sources and release it during the peak hours, thus improving system efficiency and energy flexibility.

TES in the form of passive and active systems can be applied as a newly integrated or retrofitted element in buildings to improve energy efficiency. In some climate regions, TES strategy was found to be effective in improving the building indoor environment. For example, stone walls and roofs with large thermal inertia are able to attenuate the daily room temperature oscillation, reduce the energy consumption of air conditioning and shift the peak load [13]. Active TES solutions can improve the reliability of domestic solar water-heating systems by balancing the time mismatch between energy supply and demand [14]. In addition, TES as a new strategy has been implemented to recover waste heat from power plant, both passively [3] and actively [15]. The captured waste heat can be reused by district energy systems to provide a cleaner way for heating in buildings. Other energy management solutions include using water, packed bed, heating oil, or molten salt ( $40\% \text{KNO}_3 + 60\% \text{NaNO}_3$ ) as the TES medium in concentrated solar power [16] or nuclear power plants [17]. In brief, the main role of TES is to reduce the unwanted loss of thermal energy and bridge the demand–supply gap caused by time difference or geographic difference.

The major TES technologies can be broadly divided into sensible heat, latent heat, and thermochemical systems. Lizana et al. [18] compare and discuss the advantages, disadvantages, and challenges of the three TES methods for building applications. The authors conclude that latent heat thermal energy storage (LHTES) systems using phase change materials (PCMs) offers an effective way to improve both indoor thermal environment and building energy efficiency. PCMs are substances that release or absorb a large amount of latent heat while changing their physical state, usually from solid to liquid, and vice versa [19]. In comparison to other methods, PCMs are distinguished by their unique properties such as higher TES density, isothermal phase transition, and low space requirement [20]. In addition, PCMs have a broad range of phase transition temperature, providing excellent versatility for various applications. Studies have shown that PCMs could reduce air-conditioning energy use by about 10%–30% in different climatic conditions in the United States [21]. PCMs have also been used for thermal management of building-integrated photovoltaic (BIPV) system [22], lithium-ion battery [23] and electronic device [24]. Alva et al. [25] pointed out that molten salt-based PCMs can function as both heat transfer fluid (HTF) and TES materials in the high temperature thermal systems due to their high decomposition temperature. In particular, molten salts have been used as the primary coolant in nuclear reactors with the advantages of no high pressure requirements and solid–liquid interface [17]. In recent years, commercial PCM products have been designed to deliver high performance and usability along the value chain in end applications.

Depending on the material nature, PCMs can be either organic, inorganic, or eutectic mixtures. Organic PCMs consist of hydrocarbon-based paraffin wax, while inorganic PCMs include metals, metal alloys, and hydrated salts. Eutectic PCMs are compositions of two or more PCMs (e.g., fatty acids and hydrate salts) with eutectic mass ratio, each of which melts and freezes at the same eutectic temperature and is able to decrease the degree of supercooling [26]. Typical shortcomings of pure PCMs include supercooling, leakage, flammability, toxicity, phase separation, corrosion, volume expansion, thermal degradation after a large number of thermal cycles, and low thermal conductivity [27,28]. Some of the drawbacks can be effectively resolved by technologies such as adding nucleating agents [29], encapsulation [30,31], and form-stable PCM [32]. However, the intrinsic low thermal conductivity remains the most significant concern since it leads to poor responsiveness to fast thermal changes occurring in melt-freeze cycles and overall decreased storage capacity. For example, paraffins usually have low thermal conductivity values varying between 0.1 and 0.4 W/m K. PCM such as n-octadecane in solid state has poor thermal conductivity of 0.35 W/m K, compared to 0.149 W/m K in liquid state [33]. Because of this downside, the real-life applications of PCM technologies are being developed slower than expected.

Heat transfer enhancement has been a key focus of PCM-based TES system research. A majority of past works have focused on extending surface area to get a higher heat gain (heat flux) from the HTF. Despite the fact that charging and discharging rates can be improved, the following problems may occur:

- The additional complexity reduces the amount of PCM in the system, while largely increasing the final costs and system weight. In some studies, the increased charging or discharging rate is partially due to the reduced PCM loading (latent heat storage capacity), whereas the improvement in energy and exergy efficiency may be limited.
- The presence of supporting surface such as fins may hamper the natural convection, which plays an important role in promoting melting heat transfer [34].
- PCM is self-insulating material, which is because the solid PCM crust covering the heat exchanger surface grows as an “insulation” layer throughout the solidification process [35]. This can reduce the quality (outlet temperature of HTF) and quantity (duration of high-grade thermal energy supply) of the retrieved thermal energy even if a larger heat transfer surface is mounted. Thus it is more important to improve the thermal performance of PCM itself rather than the heat transfer area of system.
- Extending the surface area may not be suitable for some passive building applications. In passive systems, the weight of each PCM capsule is strictly controlled to ensure an effective TES density without affecting the envelope’s bearing capacity. The extended surface will create a trade-off between TES performance and system weight.

Thermal conductivity enhancement of PCMs is critical to their applications since pure PCMs cannot satisfy the stringent requirement for a quick charging–discharging rate. One strategy is to impregnate the pure PCMs into metallic and graphite foams with excellent thermal conductivity, high porosity, and continuous structure [27]. Nevertheless, the fabrication of metallic and carbon foams is time consuming and costly. For example, high temperature and pressure are needed for the pyrolysis of hydrocarbon to form graphite foam and a blowing agent is added to control the porosity during the foaming process [36]. Moreover, vacuum impregnation is needed to guarantee the loading ratio of PCM in the porous foam [28]. With the growing advancements in the field of nanomaterials, a novel promising strategy to enhance the thermal conductivity of pure PCM arises by dispersing thermally conductive nanostructures with dimension of  $\sim 100$  nm. The generally used ultrasmall nanostructures include nanocarbons (carbon, graphene, graphite), nanometals (Cu, Ag, Al) and nanometal oxides (CuO,  $\text{Al}_2\text{O}_3$ , MgO,  $\text{TiO}_2$ ,  $\text{SiO}_2$ ,  $\text{Fe}_2\text{O}_3$ ), which can be synthesized in diverse morphologies, such as nanoparticles, nanospheres, nanoflakes, nanoplatelets, nanotubes, nanorods, nanosheets, etc. [37]. The resulting mixture of pure PCM and nanostructures is known as nanoenhanced PCM (NePCM), which enables the LHTES technologies to be more versatile, feasible, and efficient for both passive and active applications thanks to the improved thermal properties.

To evaluate system performance, numerical modeling using computational dynamics fluid (CFD) technique is used by researchers to solve the complex heat transfer problems in PCM systems and evaluate key design parameters. The numerical solutions also provide a more thorough understanding of the related phase change behaviors, while reducing the time duration and costs for experimental test rigs [38]. Leong et al. [39] noted that in addition to thermal conductivity, adding nanostructures to base PCM will also alter other important thermophysical properties, such as latent heat, specific heat, supercooling degree, melting point, density, and viscosity. For this reason, numerical simulation can be used to examine the influence of these changed properties on TES performance. This can greatly facilitate the system design, analysis, and optimization. Furthermore, it is important to compare innovative NePCMs with other traditional heat transfer enhancement techniques, both technically and economically, to evaluate their potential contributions to TES enhancement.

In this chapter, we provide a comprehensive summary of advancements in NePCM, involving both TES material preparation and system performance analysis. In the following sections, we focus on nanometals, nanometal oxides, and nanocarbons which have been widely used to develop NePCMs with unique thermal properties. Insights are given into their thermal conductivity enhancement and the heat transfer behavior of NePCMs. Several state-of-the-art building applications using NePCMs are also reported to highlight the improved thermal and energy performance. Further discussion focuses on

the benefits and limitations of suspending nanostructures with different concentrations, morphologies, and dimensions into pure PCMs. We also look at the knowledge gap in current technology and the outlook for future research is also discussed. The work is helpful for researchers and designers to select the proper nanostructures and methods to enhance PCMs.

## 26.2 Nanometal enhancer

Metals are well known for their thermally conductive property. For example, silver has the highest thermal conductivity value of 429 W/(m K), followed by copper of 398 W/(m K) and gold of 315 W/(m K). However, silver is prone to oxidation and gold is rare and exorbitant. Hence, copper with its abundant reserves, low cost, high melting point and moderate corrosion rate has been frequently used to enhance the poor thermal conductivity of PCMs. In addition, copper is also a very effective metal for reducing the energy loss during heat transfer [40].

### 26.2.1 Preparation of nanometal-enhanced PCMs

Al-Shannaq et al. [33] used nanothick Ag shells to enhance thermal conductivity ( $k$  value) of PCM by 1168%. Pure PCM is microencapsulated to prevent PCM leakage when changing from solid to liquid state. However, the poor  $k$  value of the microencapsulated shell hinders their heat transfer and energy storage performance. To improve the  $k$  value of microencapsulated PCM, a novel technique of covering microcapsules using a layer of metallic shell by surface activating with dopamine and performing electroless plating (Fig. 26.1) was developed. Increasing the uncoated PCM diameter from 2.4 to 26.9  $\mu\text{m}$  improves its  $k$  value from 0.062 to 0.189 W/m K. The measured

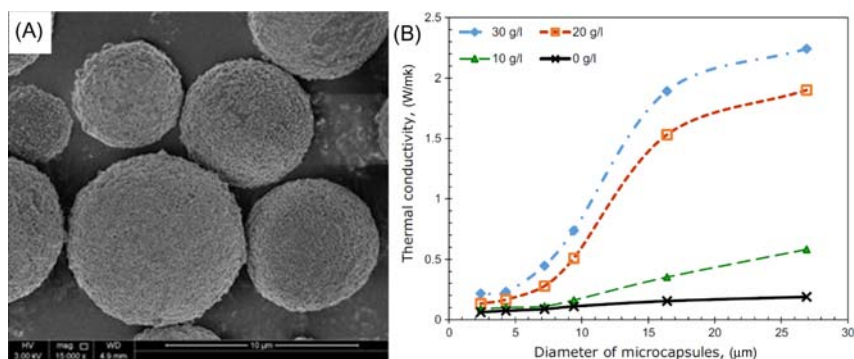


**FIGURE 26.1** (A) Scanning electron microscopy (SEM) image of Ag-coated PCM microcapsules with shell Ag-coverage of 70.4 wt.%. Silver nitrate of 20 g/L concentration was utilized. (B) Uncoated PCM mean microcapsule diameter and different silver nitrate concentration and its effect on their thermal conductivity [33].



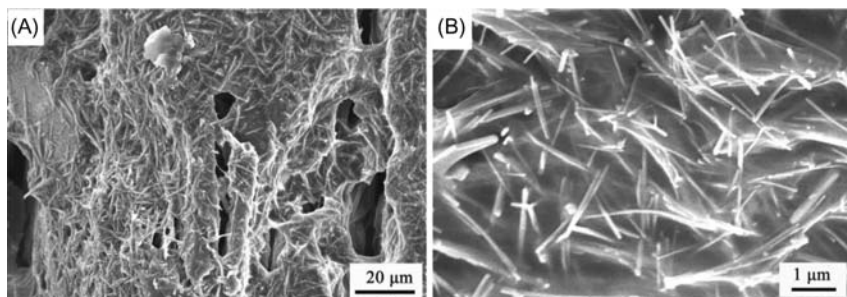


**FIGURE 26.2** SEM images of polyethylene glycol (PEG)–Ag/EVM ss-CPCM containing 19.3 wt.% of AgNWs with a scale bar of (A) 20  $\mu\text{m}$  and (B) 1  $\mu\text{m}$  [41].

thermal conductivity of metal-coated PCM capsules increased greatly from 0.189 to 2.41 W/m K, (about 1168% enhancement) when particle size is fixed at 26.9  $\mu\text{m}$ . This thermal conductivity enhancement is dependent on the amount of silver-coated shell area on the PCM microsphere surface, with fast improvement when continuous pathways for thermal conduction are formed.

Deng et al. [41] fabricated novel shape-stabilized composite PCMs (ss-CPCMs) by impregnating polyethylene glycol (PG)-wrapped silver nanowires (AgNWs) into the pores of expanded vermiculite (EVM). In these composites, polyethylene glycol (PEG), AgNWs, and EVM were used as the base PCM, thermal conductivity enhancer, and shape stabilizer, respectively. The polyol method was used to prepare the AgNWs with a length of 5–20  $\mu\text{m}$  and a diameter of 50–100 nm. AgNWs wrapped by PEG were well-dispersed and enwrapped inside the pores and surfaces of EVM (Fig. 26.2). It was found that the maximum encapsulation capacity of PEG in all cases with good shape stability was 66.1 wt.%. The EVM also reduced the supercooling degree of PEG by about 7°C, since it serves as nucleation to promote the crystallization of PEG (Fig. 26.3A). The  $k$  value of AgNW (19.3 wt.%)–enhanced composite PCM reached 0.68 W/m K, which was almost 11.3 times higher than that of the pure PEG (Fig. 26.3B).

Copper nanowires (CuNWs), with their high thermal conductivities and aspect ratio, have been used to develop NePCMs. Shah et al. [42] prepared CuNWs by disproportionation of a Cu + precursor in octadecyl amine (ODA). After purification, reddish nanostructures were obtained, and their structures were verified by transmission electron microscopy (TEM) and X-ray diffraction (XRD), as shown in Fig. 26.4. The prepared CuNWs were incorporated into a hydrated  $\text{CaCl}_2 \cdot 6\text{H}_2\text{O}$  salt-based PCM and the corresponding thermal conductivities at different concentrations of CuNWs were measured. The results showed that 0.02 wt.% of CuNWs increased the  $k$  value by more than 20%, although it should be noted that the effect of diminishing returns is also observed past 0.08 wt.% of CuNWs (Fig. 26.5).

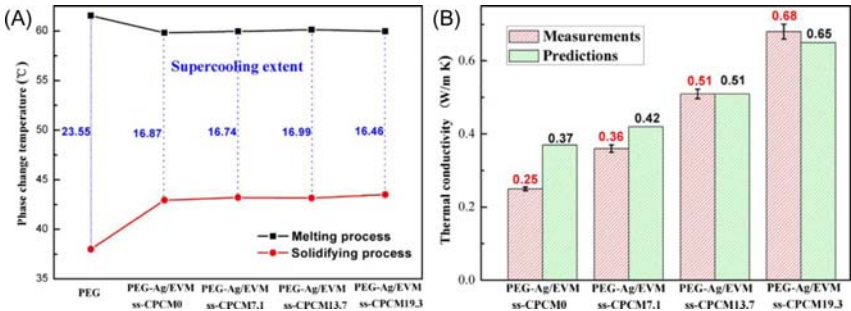


**FIGURE 26.3** (A) Supercooling extent of PEG and PEG–Ag/EVM ss-CPCMs with different concentrations of AgNWs and (B) measured and predicted thermal conductivities of PEG–Ag/EVM ss-CPCMs at 20°C [41].

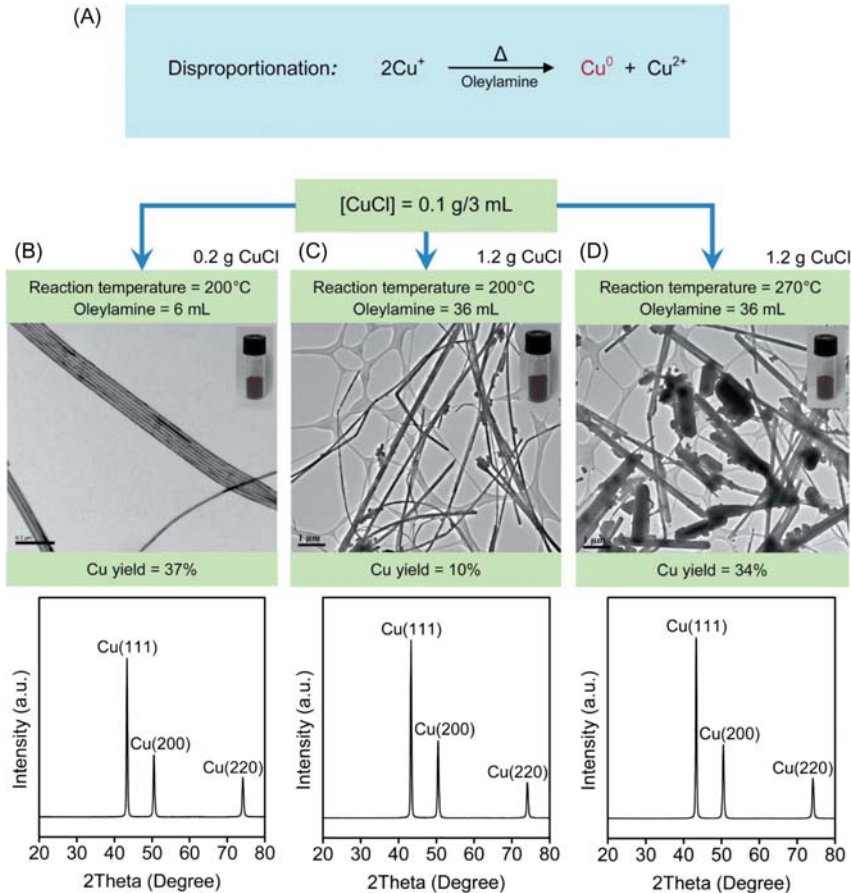


**FIGURE 26.4** (A) Reaction formula for producing CuNWs. (B–D) Yield, morphology, and XRD pattern of the CuNWs prepared under different conditions. Insets show the reddish CuNW products after purification [42].

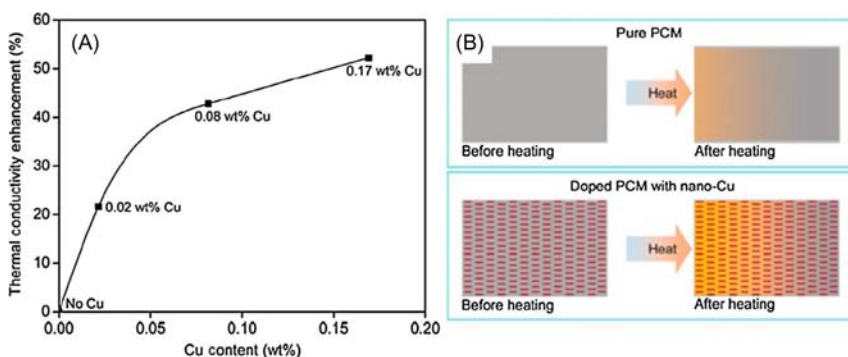


**FIGURE 26.5** (A) Thermal conductivity enhancement of PCM (B). Schematic diagram of heat transfer and dissipation in the pure PCM versus CuNW-doped PCM upon heating [42].

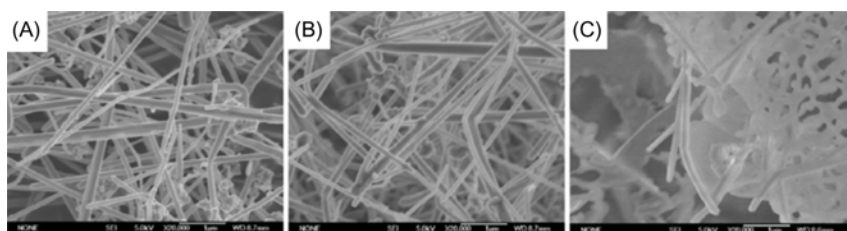


**FIGURE 26.6** SEM images of CuNWs (A), NePCM with 58.9 wt.% (B), and 1.32 wt.% (C) of CuNWs [43].

Similarly, Zeng et al. [43] synthesized ultralong CuNWs and dispersed them into tetradecanol (TD) as the base PCM. The SEM image (Fig. 26.6) shows that the TD-based PCM was absorbed within the sponge-like structure of CuNWs. The differential scanning calorimetry (DSC) results showed that the endothermic peak of the composite PCM was sharper than that of TD due to the improved  $k$  value of CuNWs (Fig. 26.7A). In addition, the enthalpy changes ( $\Delta H$ ) of the composite PCMs were calculated and found to be linear (Fig. 26.7B). Thermogravimetry (TG) tests showed that the pure TD underwent a single-step weight loss, corresponding to the evaporation of TD during the heating process. The composite PCMs lost weight slower than that of TD due to the absorption of TD in the voids of CuNWs (Fig. 26.7C). The thermal conductivity measurements of the composite PCMs showed that a relatively linear relationship between the  $k$  value and loading of CuNWs existed. The composite PCM containing 11.9 vol.% of CuNWs showed a  $k$  value of 2.86 W/m K, which was almost nine times higher than that of TD only (0.32 W/m/K) (Fig. 26.7D).

Copper nanoparticles (CuNPs) is another widely used nanocopper structure. For example, Molefi et al. [44] used CuNPs to improve the  $k$  value of

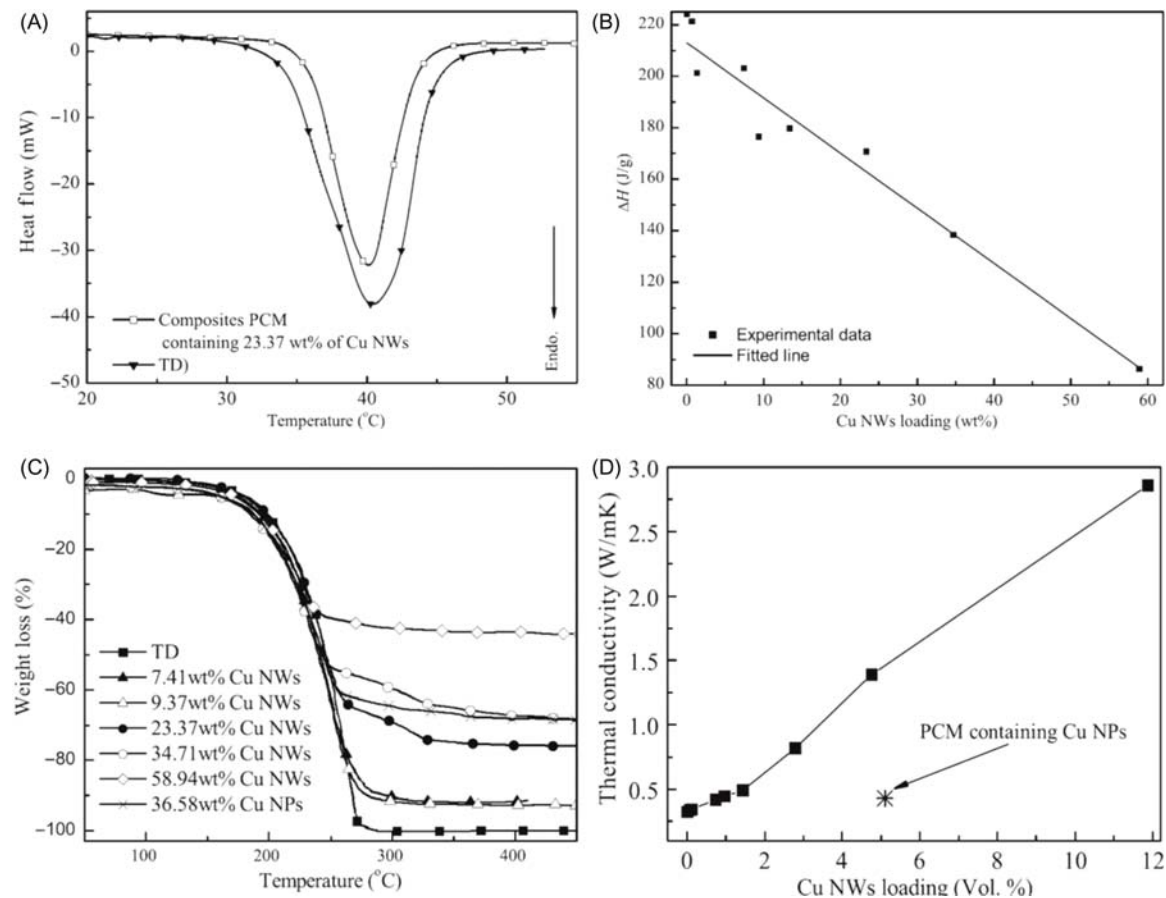


**FIGURE 26.7** (A) DSC curves, (B) phase change enthalpy ( $\Delta H$ ) with different loadings of CuNWs, and (C) TG curves of TD and the NePCMs. (D) Thermal conductivity of the NePCMs [43].

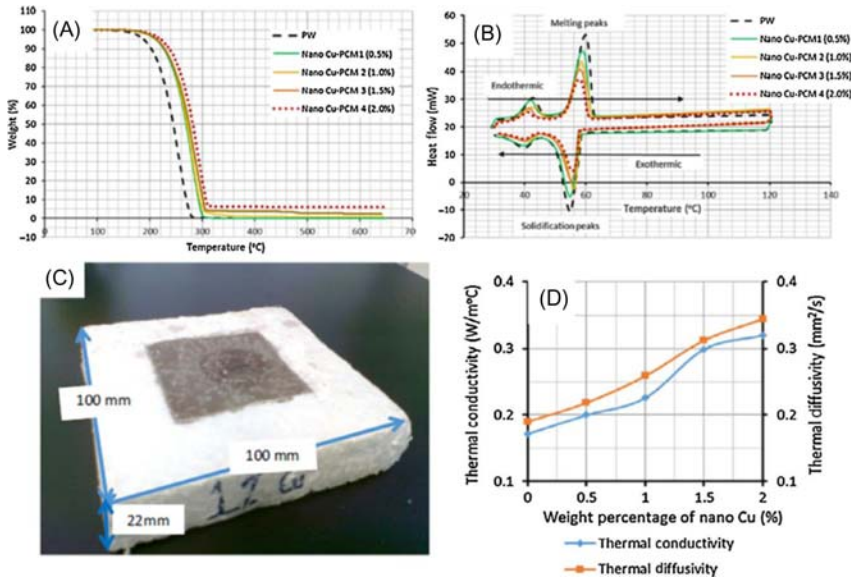


**FIGURE 26.8** (A) DSC, (B) TGA, (C) sample images of Cu–PCM nanocomposites, and (D) thermal conductivity and thermal diffusivity change due to the addition of CuNPs at various percentages [45].

paraffin by 70%. Molefi reported the near-linear increases to the  $k$  value with increasing content of CuNPs. The soft paraffin wax was mixed with low-, medium-, and high-molecular-weight polyethylene. The paraffin mixture was then blended with CuNPs to enhance the  $k$  value of the base polyethylene PCM. The CuNPs with an average particle size of 30  $\mu\text{m}$  enhanced the  $k$  value of PCM by about 70%. The authors noted that the CuNPs could improve the  $k$  value without negatively impacting other thermophysical properties such as crystalline nature, while being able to stay thermally stable and maintain its mechanical strength.

Lin et al. [45] reported the dispersion of 20 nm CuNPs into paraffin wax to fabricate Cu–PCM nanocomposites. The microstructure of the paraffin wax samples was formed by a stack of layers as shown in Fig. 26.8. All prepared samples demonstrated the same thermal degradation trend as observed by thermogravimetric analysis (TGA) measurements (Fig. 26.8A). In comparison to pure paraffin wax, the starting and ending of thermal degradation temperature of composite PCMs shifted higher with a wider temperature range of weight loss, indicating there were physical bonds between CuNPs and paraffin wax. In addition, the added CuNPs lowered the melting temperature while increasing the solidification temperature of pure paraffin wax. DSC results showed that CuNPs also reduced the degree of supercooling due to the improved nucleation of paraffin wax (Fig. 26.8B). The  $k$  value of the

NePCMs increased in a nonlinear fashion (Fig. 26.8D) by 14%, 23.9%, 42.5%, and 46.3% when 0.5 wt.%, 1.0 wt.%, 1.5 wt.%, and 2.0 wt.% of 20 nm CuNPs was added to the pure paraffin wax, respectively.

## 26.2.2 Melting process

By using the enthalpy–porosity method, numerical simulation of melting in a horizontally orientated concentric annulus was carried out by Darzi et al. [46]. The authors compared the benefits of adding nanocopper particles (diameter of 80 nm) to n-eicosane and using inner tubes with different shapes as shown in Fig. 26.9. User-defined functions (UDFs) were used to input the NePCM thermophysical properties based on the Brinkman, thermal dispersion, and mixture models. Quantitatively, the inclusion of 4 wt.% and 2 wt.% of nanocopper particles shortened the charging time by 46% and 25%, respectively. The authors pointed out that nanoparticles did not improve the ratio of convective and conductive heat transfer at the bottom region. Namely, the presence of nanocopper did not attenuate the heat accumulation in the upper section. Under the same operating condition, adding 4 wt.% of nanocopper particles showed a higher heat transfer efficiency than mounting four fins.

A similar study of an annulus system was conducted by Jourabian et al. [47] to discuss the combinations of varying the inner tube position and copper nanoparticles percentages (0%, 2%, and 4%). The effective thermal conductivity of water–nanocopper PCM was determined by a semiempirical correlation [48]. In their study, an enthalpy-based lattice Boltzmann (LB) technique with a double distribution function (DDF) model was applied for solving the temperature and velocity fields. The best thermal enhancement scheme was found to be mounting the inner tube at the bottom with doping 4% of nanocopper. The enhancement is due to the shrinkage of the heat conduction-dominated region, and more regions were subject to convection melting. The authors also indicated that the augmentation of NePCM viscosity could weaken the convective heat transfer. Jourabian et al. [49] also drew similar results in another melting study for square cavity system.

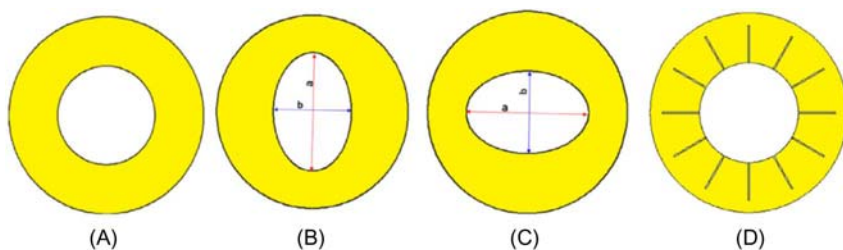


**FIGURE 26.9** (A) Circular tube (CT), (B) vertical-oriented elliptical tube (VOE), (C) horizontal-oriented elliptical tube (HOE), and (D) finned circular tube (FCT) [46].



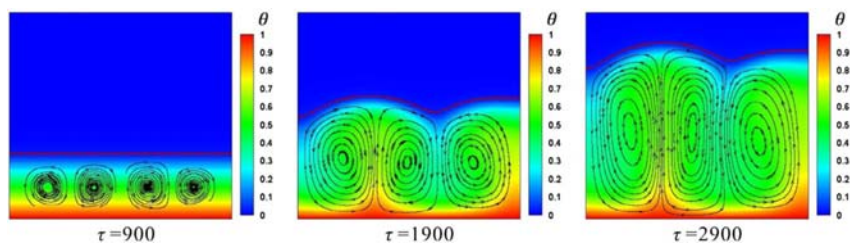


**FIGURE 26.10** Streamlines, temperature fields, and formations of solid–liquid interface at different dimensionless times in the case of  $\phi = 0.1$  and  $Gr = 5.0 \times 10^4$  [50].

Feng et al. [50] developed an innovative LB method to solve the convection melting of nanocopper/water in a bottom-heated rectangular cavity. The authors defined density evolution and temperature evolution functions to model the fluid flow and heat transfer. The novel LB method performed remarkable calculation efficiency using an implicit scheme to avoid iteration steps for the temperature field. The results showed that the mixture exhibited better heat transfer efficiency than the pure ice. Increasing the loading of nanocopper from 0 to 0.05 and 0.10, the melting time for achieving a liquid fraction of 0.7 was lowered by 9.1% and 16.9% for Grashof ( $Gr$ ) number of  $5.0 \times 10^4$  and 6.5% and 17.2% for  $Gr$  number of  $2.5 \times 10^5$ . Interestingly, in the case of high particle percentage and  $Gr$  number, an asymmetric solid–liquid interface formed as shown in Fig. 26.10. The authors noted that it was due to the asymmetric distribution of the convection cells.

### 26.2.3 Solidification process

Khodadadi and Hosseinzadeh [51] first reported on the enhanced freezing process of water by adding nano-Cu particles with an average diameter of 10 nm. Their numerical methodology was later employed in a body of studies based on effective medium theory. The results showed that the freezing time of water was shortened from 3000 to 1400 s by the presence of 20 wt.% nanocopper particle. However, the authors did not consider the sedimentation and homogeneous dispersion of nanometals at such high loading. In fact, nanometals are heavier than water and thus can sediment and change their physical properties, causing the thermal conductivity and viscosity in different regions to vary. Therefore numerical results based on effective medium theory might not be reliable. On the other hand, the thermal capacity of nanometal is very small, which means a high particle loading regime will heavily reduce the latent heat of nano-PCM.

Several simulation-based studies have compared different heat transfer enhancement strategies for improving the solidification rate of NePCMs. The freezing process of water in a vertical wavy enclosure (Fig. 26.11) was numerically modeled by Abdollahzadeh and Esmailpour [52] to analyze the contributions of surface waviness and suspension of nanocopper. The

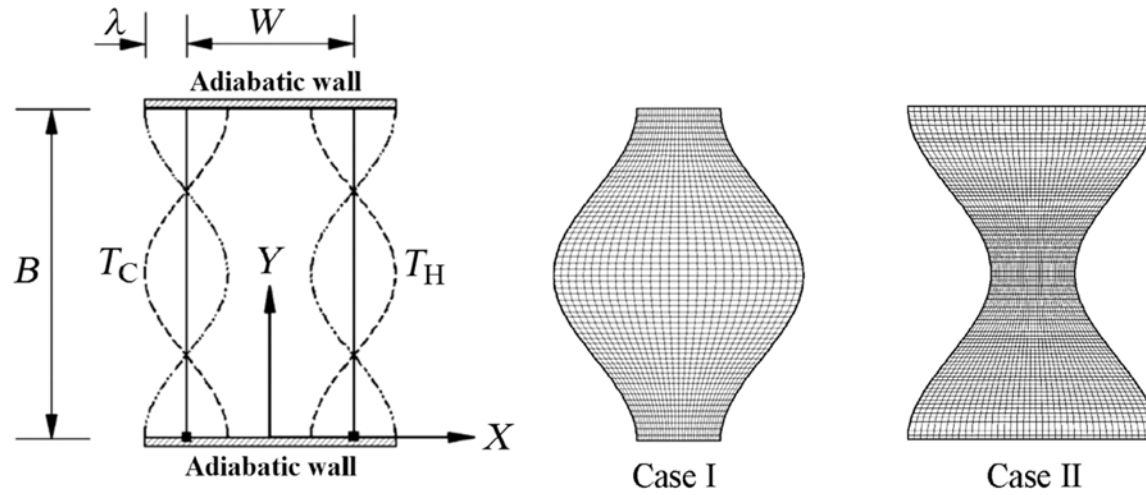


**FIGURE 26.11** Schematic diagram of the vertically placed wavy enclosure housing nano-PCM [52].



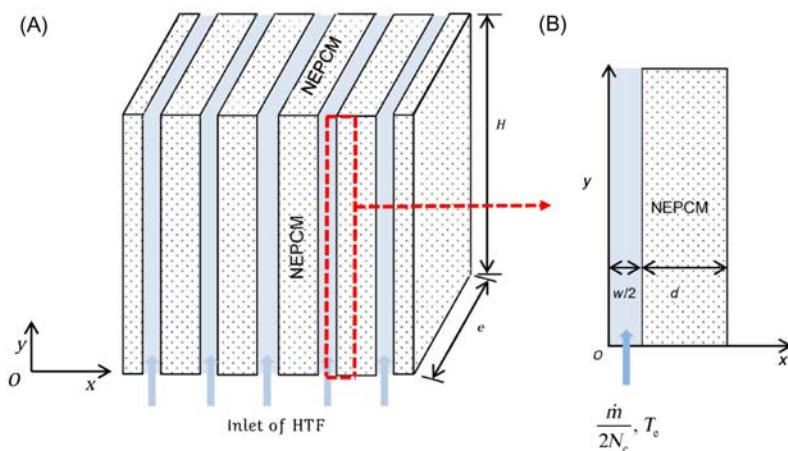


FIGURE 26.12 (A) LHTES consists of PCM slabs and (B) computational domain [56].

Brinkman model and thermal dispersion model were respectively employed for the effective dynamic viscosity and thermal conductivity of the mixtures. Using the enthalpy–porosity method, numerical results indicated that the addition of nanocopper shortened the freezing time, whereas a better option without affecting the effective TES capacity could be applying an optimized surface waviness. The authors stated that the surface waviness did not reduce the latent heat capacity which is the advantage over nano dispersion. Similar study and results can be found in Ref. [53].

Modularized PCM slab is another good option to increase the contact surface between PCM and HTF. Elbahjaoui and Qarnia [54] numerically studied the solidification process of nanocopper/n-octadecane in a LHTES unit consisting of PCM slabs (Fig. 26.12) using the enthalpy–porosity method. The effects of varying the particle loading, aspect ratio of the slab, and the dimensionless HTF temperature were explored. An improvement of 26.9% was achieved for the solidification in the case of volume fraction of 8%, aspect ratio of 6, and dimensionless HTF temperature of 1.1.

### 26.2.4 Practical applications

Lin et al. [57] designed a flat-plate solar collector (Fig. 26.13A) integrated with built-in TES. In their experiment, 1 wt.% 20 nm–CuNPs/paraffin wax nanocomposite was used and the temperature of the absorber plate at the inclination angle of 10 degrees were measured for three operational cases, namely without PCM (case 1), with PCM (case 2), and with NePCM (case 3). As shown in Fig. 26.9B and C, in cases 2 and 3, part of the solar radiation was collected to the PCM and NePCM, causing them to melt. The results showed that the  $k$  value of the NePCM was enhanced by 24%

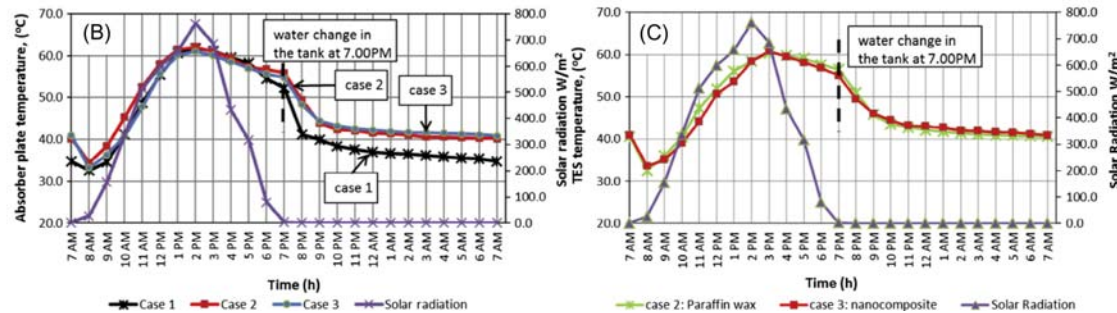
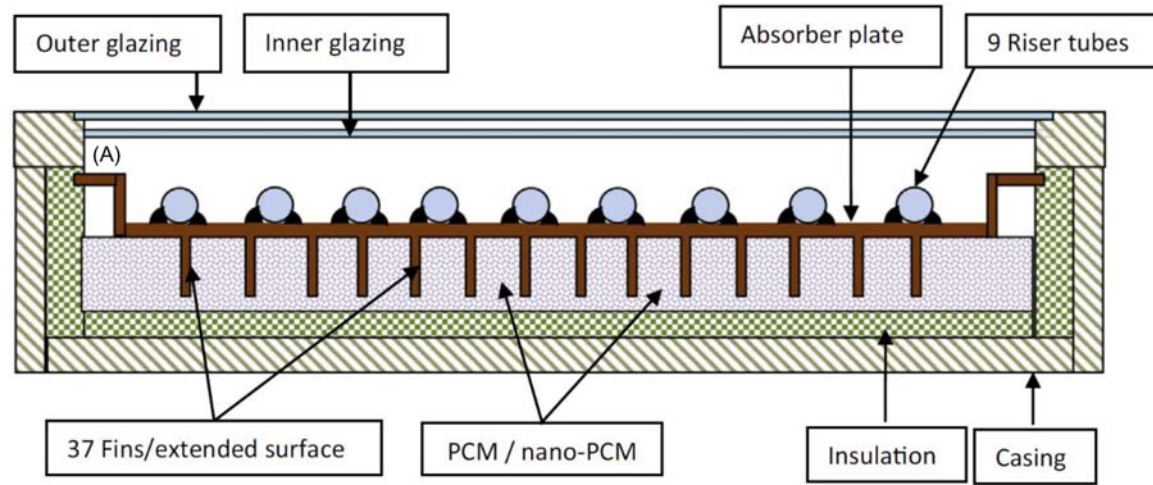


**FIGURE 26.13** (A) Schematic diagram of the solar-TES integrated collector. (B) Absorber plate and temperatures at the 10 degrees inclination angle for three operational cases. (C) TES temperatures at 10 degrees inclination angle, in the case of using PCM and the NePCM [55].

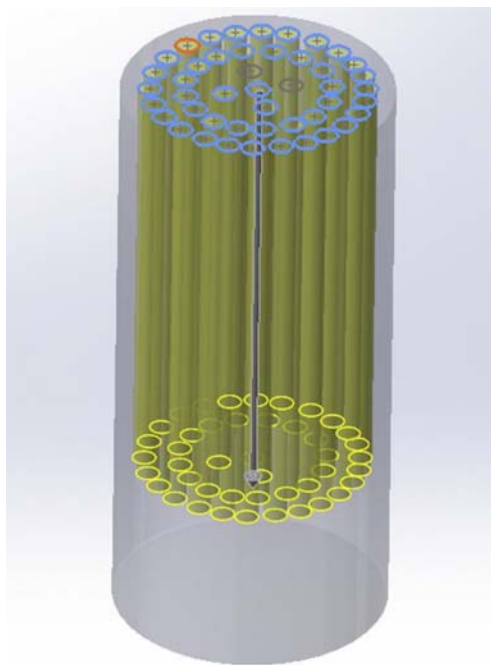


**FIGURE 26.14** Schematic diagram of the hot water tank integrated with NePCM [56].

compared to the pure paraffin wax. The best efficiency of the plate solar collector was improved by 6.9% and 8.4% when the integrated TES was filled with paraffin wax and NePCM nanocomposite, respectively.

Nabavitabatabayi et al. [56] developed a hot water tank integrated with CuNP-enhanced PCM, as shown in Fig. 26.14. The study aimed to test the improved power demand shifting ability by comparing the NePCM water tank with the pure PCM water tank. A 3D mathematical model was developed to thoroughly investigate the effects of three design and operation parameters (nanoparticle fraction, amount of PCM, mass flow rate) on the thermal performance of the NePCM water tank overcharging and discharging processes. As shown in Fig. 26.15, the solidification time is 103 min for the pure PCM case, and it can be reduced to 64 min for the NePCM case. Quantitatively, a reduction of 60% can be achieved at 10 vol.% of nanoparticles. Due to the high thermal inertia of the NePCM, the hot water tank could keep the temperature from plummeting over the discharging process. The calculations also indicated that the NePCM could shift the power demand by 2 h compared to the pure PCM.

### 26.3 Nanometal oxide enhancer

Nanostructured metal oxides including  $\text{Al}_2\text{O}_3$  and CuO are another attractive strategy to enhance pure PCMs. Since metal oxides possess relatively low

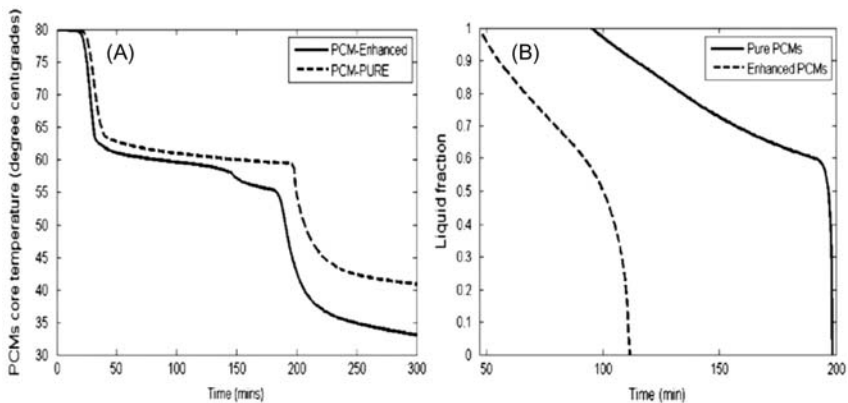


**FIGURE 26.15** (A) PCM core temperature and (B) liquid fraction during discharging process (pure PCM and 10 vol.% copper nanoparticle–enhanced PCM) [56].

thermal conductivity ( $\sim 40$  W/m K), their loadings are usually higher than nanocarbons and nanometals. Suspending metallic and metal oxide particles in base fluid to form a hybrid nanofluid has also been widely applied to combine the thermophysical properties of individual particles.

### 26.3.1 Preparation of nanometal oxide-enhanced PCMs

Babapoor et al. [57] used  $\text{Al}_2\text{O}_3$ ,  $\text{Fe}_2\text{O}_3$ ,  $\text{ZnO}$ , and  $\text{SiO}_2$  NPs to enhance the  $k$  value of paraffin wax by as much as 144%, 144%, 110%, and 110%, respectively. In this study, different NPs were tested, namely silica ( $\sim 20$  nm), alumina ( $\sim 20$  nm), iron oxide ( $\sim 20$  nm), and zinc oxide ( $> 50$  nm). They were added as thermal conductivity enhancers to fabricate NePCMs by blending paraffin with nanoparticles and surfactant. The highest enhancement sample was doped with  $\text{Al}_2\text{O}_3$  NPs with the greatest increase in  $k$  value of 0.919 W/m K. For  $\text{Al}_2\text{O}_3$  NPs, the enhancement factor was about 120%, 141.2%, and 144% at 4, 6, and 8 wt.% concentration, respectively. For  $\text{Fe}_2\text{O}_3$  NPs, the enhancement factor was about 80%, 135%, and 144% at 4, 6, and 8 wt.% concentration, respectively. For  $\text{ZnO}$  NPs, the enhancement factor was about 85%, 100%, and 110% at 4, 6, and 8 wt.% concentration, respectively. For  $\text{SiO}_2$  NPs, the enhancement factor was about 78%, 110%, and 110% at 4, 6, and 8 wt.% concentration, respectively. Experiments revealed that the  $k$  value of NePCMs were greatly improved by higher dosage of conductive NPs. In conclusion,  $\text{Al}_2\text{O}_3$  and  $\text{Fe}_2\text{O}_3$  NPs exhibited the most significant effect on improving paraffin-based PCM and its thermophysical properties.

Sharma et al. [58] utilized nano- $\text{TiO}_2$  to enhance the  $k$  value by up to 80%. The TES performance of synthesized PCM composites made of palmitic acid (PA) dispersed with  $\text{TiO}_2$  NPs (Fig. 26.16) were studied. The  $\text{TiO}_2$

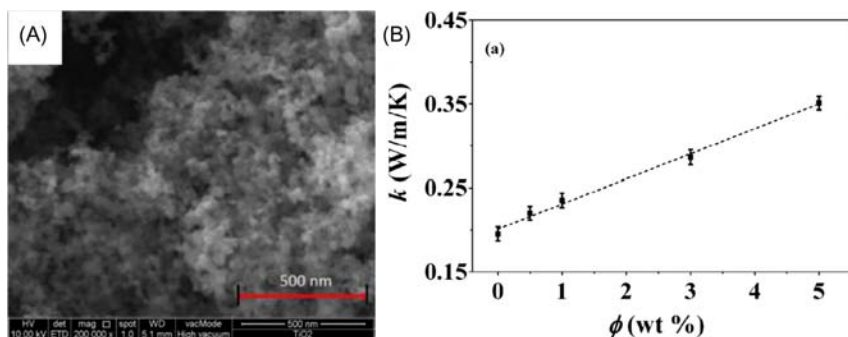


**FIGURE 26.16** (A) SEM of TiO<sub>2</sub>. (B) Thermal conductivity of PA with increasing TiO<sub>2</sub> dosages [58].

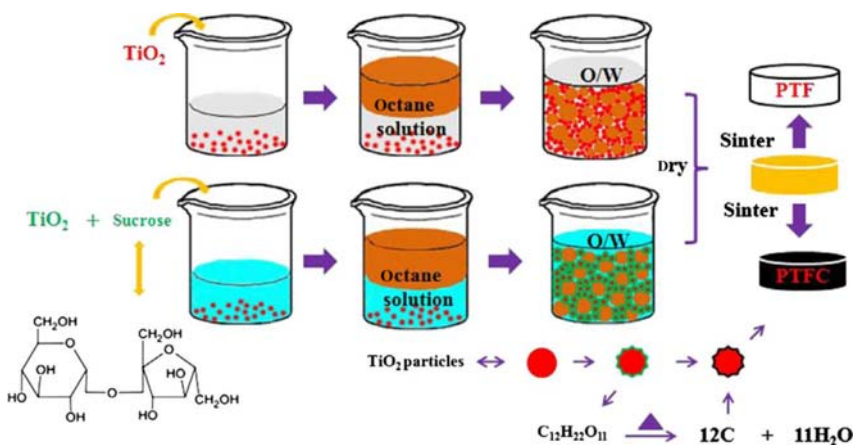


**FIGURE 26.17** Schematic diagram of the preparation of paraffin/PTF (PTFP) and paraffin/PTFC (PTFCP) composite PCMs by particle-stabilized emulsion method [59].

NPs were mixed into neat PCM and the  $k$  value of PA was enhanced by 12.7%, 20.6%, 46.6%, and 80% for TiO<sub>2</sub> percentages of 0.5, 1, 3, and 5 wt. %, respectively. The authors pointed out that the curvilinear characteristic of thermal enhancement was largely due to the aggregation of NPs caused by the excessive dosage of TiO<sub>2</sub> in the PCM.

Li et al. [59] used TiO<sub>2</sub> NPs foam to enhance the  $k$  value by 43.8% and TiO<sub>2</sub> NPs with a nanocarbon shell layer to enhance thermal conductivity by 404%. The porous TiO<sub>2</sub> foams (PTFs) were prepared by microemulsion technique (Fig. 26.17). This templating technique uses octane as microemulsifier and TiO<sub>2</sub> as particle stabilizer. TiO<sub>2</sub> was nanosized  $\sim 23$  nm and made of 80% anatase and 20% rutile phase. For dispersing agent, polyacrylic acid-ammonium salt was added and for surface modifier, propyl gallate (C<sub>10</sub>H<sub>12</sub>O<sub>5</sub>), which is amphiphilic small molecule, was added. PTFs have a

porous structure with 3D continuous connected holes. Paraffin wax was able to fully absorb into the porous structure without requiring any addition of surfactant. Sucrose was absorbed into the porous structure and burnt off at 1200°C to create a thin carbon-based film forming 2 nm thin carbon nanolayer. The pure PTF and carbon-based PTF nanocomposites exhibited  $k$  values of 0.302 and 1.059 W/m K, respectively. Both were more conductive compared to pure paraffin. The result of adding 25 wt.% of TiO<sub>2</sub> to pure PCM was a  $k$  value of 0.302 W/m K, which is an enhancement of 0.092 W/m K. The addition of TiO<sub>2</sub> was able to improve  $k$  value of pure PCM. The  $k$  value of paraffin absorbed into the TiO<sub>2</sub> foam structure lined with carbon nanofilm was 1.059 W/m K, representing a 5.04-fold increment of the  $k$  value compared to pure paraffin. The large enhancement is caused by carbon matrix adhered onto the TiO<sub>2</sub>-NP surfaces. This novel hybrid nanoparticle TiO<sub>2</sub>-formed porous foam with inner-lining carbon nanofilms is an excellent nanostructure for enhancing PCM for industrial purposes.

### 26.3.2 Melting process

Instead of using prediction models, Ghalambaz et al. [60] applied a linearized equation based on experimental data to determine the correlation between effective properties of nanofluids and hybrid particle loading. The governing equations were solved by user-defined MATLAB subroutines based on the enthalpy–porosity theory. The melting of hybrid nano-PCMs occurred in a square cavity heating from its left wall. The authors particularly analyzed the variation of solid–liquid interface in the cases of four different dimensionless variables (conductivity, viscosity) = (0,0), (5,18), (18,18), and (18,5)) to find the best composition of hybrid nanoparticles. Numerical results showed that the best thermal performance was achieved by dispersing 2 wt.% Ag–MgO hybrid nanoparticles. The same authors also simulated the melting of Ag–MgO/water in a square cavity enclosure heating by its inner tube [61]. A similar study was carried out by Elsayed [62], in which binary and triple mixtures of metallic and metal oxide hybrid nanoparticles were added to enhance the melting of neopentyl-glycol in a cylinder heated from the outer surface. The results showed that the best heat storage performance for the solid-to-solid PCM was attained by the composition of 6% Al, 3% SiO<sub>2</sub>, and 3% TiO<sub>2</sub>.

Another strategy is to fill the NePCM into porous media. A scale analysis by Hossain et al. [63] first reported on the melting behavior of nano-CuO enhanced cyclohexane in porous aluminum foam. Using the local thermal equilibrium (LTE) assumption and neglecting the convective motion in the porous metal foam, the phase change problem was solved using the AHC method. The authors found that the nano-PCM melted faster in the porous medium with lower porosity. Similarly, a hybrid metal foam/nano-Al<sub>2</sub>O<sub>3</sub> combination was examined by Mahdi and Nsofor [64], which remarkably



enhanced the melting of paraffin RT82 in a triplex-tube heat exchanger. The authors modified the enthalpy–porosity equations using a local thermal non-equilibrium (LTNE) assumption to describe the fluid motion and heat transfer of nano-PCM in the porous copper foam. They considered the convection of molten PCM, non-Darcy effect, Brownian motion of nanoparticles, and temperature-dependency of thermophysical properties. By adding nano- $\text{Al}_2\text{O}_3$  in nonporous cases, the melting time was shortened by 16.7%, 17.9%, and 19.7% for the volume fraction of 1%, 3%, and 5%, respectively. A much faster melting was observed for porosity of 0.95 (18 min) compared to 0.98 (120 min). In the lower porosity case the total volume occupied by the foam increased, as well as the total heat transfer area. The melting rate could be significantly expedited using metal foam with only a small amount of storage capacity lost. However, it should be noted that in the above studies [65,66], the convection contribution was critically weakened by the presence of porous metal foam. On this basis, the selection of the foam porosity and the particle loading should be considered to maintain the convective heat transfer.

It is beneficial to optimize the geometrical structure to further improve the nano-PCM system. Recently, Huo and Rao [67] applied a separate plate to weaken the undesirable heat accumulation in a cavity's upper region. The Vajjha's model, Maxwell–Garnetts model, and other mixture models were used for calculating the effective properties of  $\text{Al}_2\text{O}_3$ –paraffin mixture. A total-enthalpy-based LB method was employed to discretize the governing equations. For all given Rayleigh numbers and nanoparticle percentages, a middle-located plate showed the fastest melting rate. In particular, the melting time was shortened by over 10% for dimensionless plate height of 0.5 and volume fraction of 3%. The temperature standard deviation could be diminished by the separate plate, indicating the reduction of heat accumulation in the upper region. However, when the dimensionless plate height is less than 0.3, the heat accumulation will slow down the melting rate. With the same objective, a study by Elbahjaoui and Qarnia [68] optimized the combinations of alumina particle loading, Reynolds number, Rayleigh number, and the aspect ratio of NePCM slab. The results showed that the increase in these parameters, particularly the Reynolds and Rayleigh numbers, could improve the melting process.

Among various encapsulation methods, cylindrical systems have received widespread interest due to their ease of manufacturing and maintenance. Given different inclination angles, a comparative study by Pahamli et al. [69] identified that the vertical shell-and-tube cylinder achieved the fastest melting rate with dispersing 4% of nano-CuO in the paraffin RT50. Alomair et al. [70] experimentally and numerically investigated the influence of particle percentage and cylinder height on the melting behavior of coconut oil. Nano-CuO/coconut oil mixture was successfully prepared with little sedimentation. Based on their measurements, piecewise linear treatment was

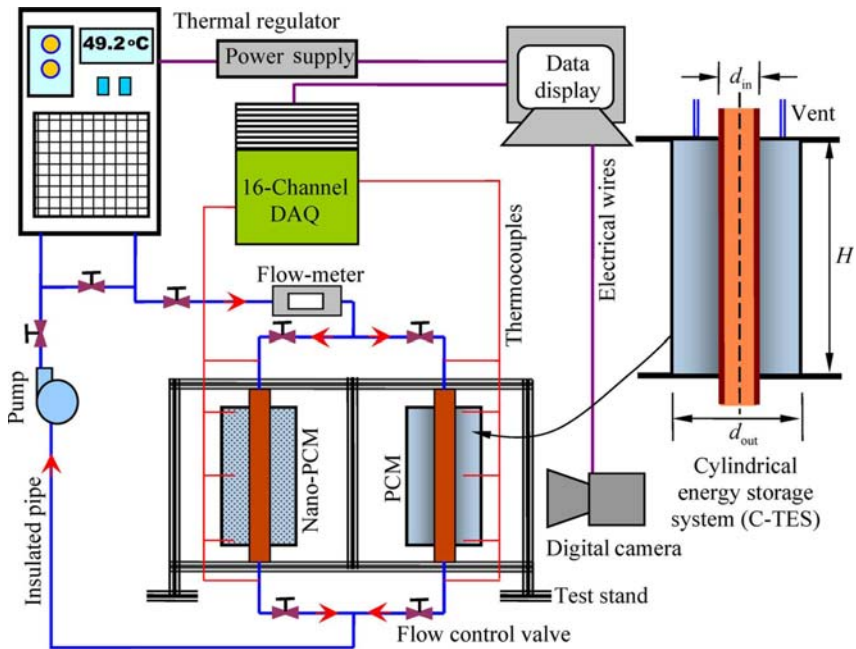


**FIGURE 26.18** Experimental test rig installed for visualization and validation [73].

applied for the transition of the mixture's density, thermal conductivity, and heat capacity within solid and liquid state. Visualization equipment was used for validation, as shown in Fig. 26.18. Both numerical and experimental results showed an improved melting rate in the nano-PCM. Later, the visualization showed that a small portion of gradually diminished solid PCM/nano-PCM remained at the bottom region for a prolonged time. Similar findings were obtained in Refs. [71,72]. These results again show that the nanoenhancers alone is not enough to diminish the heat accumulation in the upper region for a system with high aspect ratio. Thus other techniques are needed to support nano-PCM.

### 26.3.3 Solidification process

Recently, a triplex-tube heat exchanger filled with nano  $\text{Al}_2\text{O}_3$ -enhanced paraffin (RT82) was modeled by Mahdi and Nsofor [74]. Based on the enthalpy–porosity method and effective medium theory, the solidification process of NePCM at two HTF temperatures (65°C and 70°C) were investigated, respectively. For numerical accuracy, the authors developed UDF schemes to input the temperature-dependent thermophysical properties to CFD code. The dispersion of different nanoenhancers did not show much difference at the initial stage, but the solidification rate increased with the percentage of



nanoparticles and elapse of time when heat conduction dominated the heat transfer regime. A total time savings of  $\sim 20\%$  was achieved by dispersing alumina nanoparticles with a volume fraction of 8% at both  $65^\circ\text{C}$  and  $70^\circ\text{C}$ .

Later on, Mahdi and Nsofor [75] used open-celled copper foam to further promote the solidification rate of the same system studied in Refs. [64,71]. Three cases were simulated including nano- $\text{Al}_2\text{O}_3/\text{RT82}$ , metal foam alone, and metal foam with nano- $\text{Al}_2\text{O}_3/\text{RT82}$  combination. The authors first compared the accuracy of the LTE model to the LTNE model previously used in a melting study [64], and found a slight difference. This was due to the small temperature differences between the nano-PCM and metal foam during the natural conduction-dominated solidification. Based on an LTE-modified enthalpy–porosity technique, the numerical results showed that compared to the pure PCM, the complete solidification time was reduced by 19.6% (nano-PCM with loading of 5 vol.%), 74.7% (porous nano-PCM with loading of 5 vol.% and porosity of 0.98), and 96.5% (porous nano-PCM with loading of 5 vol.% and porosity of 0.95), respectively.

For the same system, Mahdi and Nsofor [73] improved the solidification of paraffin RT82 using a hybrid strategy of immersing fins and dispersing nano- $\text{Al}_2\text{O}_3$ . The combinations of using different fin arrays mounted on the inner tube and outer tube and varying the particle percentage were intensively analyzed, with considering the volume usage (ratio of occupied volume by nanoenhancers or fins to the total volume of PCM) in each technique. ANSYS FLUENT 17.0 was used for problem solving. Their results indicated that the solidification process was greatly improved using the hybrid strategy. However, for the same volume usage, better heat transfer efficiency was obtained using mounting fins alone. The 2D models established in Refs. [74,71–73] are shown in Fig. 26.19. These works have provided notable examples of using different numerical methods to compare the different heat transfer enhancement strategies and evaluate the individual contributions at system level.

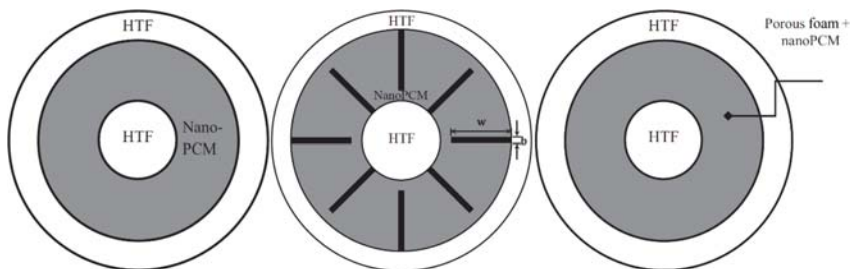


**FIGURE 26.19** 2D triplex-tube heat exchanger with: (left) nano-PCM [71], (middle) fins and nano-PCM [73], and (right) porous foam and nano-PCM [64,72].

### 26.3.4 Practical applications

Traditional glazed windows are characterized by high solar heat gain with small thermal inertia. To improve the thermal and energy performance of double-glazed windows, Li et al. [74] filled the cavity between the glass panels with a NePCM layer consisting of  $\text{Al}_2\text{O}_3$  NPs and paraffin wax. The effects of particle loading and diameter size on the temperature difference between the internal glass surface and indoor air and heat gain were numerically investigated for different seasons including summer, autumn, and winter. The authors adopted the Vajjha model to calculate the effective thermal conductivity values for four cases including A (1 vol.%, 10 nm), B (1 vol.%, 100 nm), C (10 vol.%, 10 nm), and D (10 vol.%, 100 nm). For the numerical method, the enthalpy-based energy equation was adopted for the NePCM layer with the addition of a radiative source term. The radiative source term is related to layer thickness, solar radiation, solar transmittance, and absorptance. For easy analysis, the NePCM layer was divided into phase 1 and phase 2 by ignoring the thermal convection of NePCM, as shown in Fig. 26.20. The numerical results showed that the minimal heat gain was obtained at the particle concentration of 1 vol.% and diameter of 100 nm. Comparison between the four cases indicated that heat gain could be reduced by up to 1.5%, 2.0%, and 4.0% for summer, autumn, and winter, respectively. However, the authors did not address its use for reducing the heat gain in autumn and winter.

Later, Li et al. [75] numerically investigated the thermal and optical performance of window units filled with different NePCMs. Following the same methodology used in Ref. [74], the effects of Cu, CuO, and  $\text{Al}_2\text{O}_3$  nanoparticles together with different particle concentrations (0.1–10 vol.%) and diameters (5–25 nm) were tested. The results for optical performance indicated that the improvement was nearly the same regardless of the particle types,

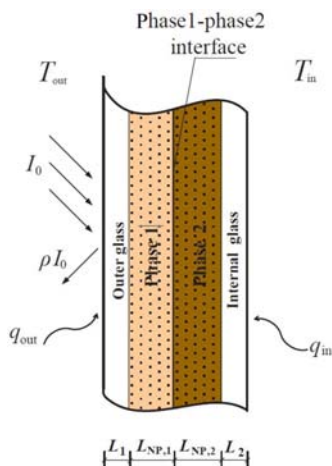


**FIGURE 26.20** Numerical model of a double-glazed window housing NePCM [74].

but the impact of particle concentration and dimension were slightly higher. As for thermal performance, the authors drew similar conclusions as reported in Ref. [74].

### 26.4 Nanocarbon enhancer

Carbon nanostructures, such as carbon nanotube (CNT), carbon nanofiber, graphite, and graphene, have been positively used to enhance base material due to their excellent thermal conductivity (2000–3500 W/m K). Since the synthesis of carbon nanostructures is becoming more and more affordable, many studies are focused on using carbon as thermal conductivity enhancer.

#### 26.4.1 Preparation of nanocarbon-enhanced PCMs

Ji et al. [76] used ultrathin graphite foams (UGF) to enhance the  $k$  value of PCM by 1700%. Ji demonstrated that blending  $\sim 1.2$  vol.% connected ultrathin graphite foams (UGFs) in a PCM can increase the  $k$  value by 18-folds (i.e., 1700% enhancement). There is no observable variation in the specific heat of fusion or melting temperature. Graphite foams are made up of ultrathin graphite connected strips, and the connected strips have a  $k$  value higher than metals and carbon foams in solid state, giving better thermal properties and heat response. The UGFs and paraffin are connected with each other (Fig. 26.21). The foam-interconnected graphite strips have dimensions ranging from a few hundred nanometers to a few micrometers thick. Thus its  $k$  value is unaffected by phonon scattering at the interboundary surfaces of graphite and PCM. Interfacial phonon scattering can significantly decrease the basal plane  $k$  value multilayered graphene. It is possible to elucidate and estimate the  $k$  value enhancement in the graphite foam–paraffin composites using single-phase mixture models.

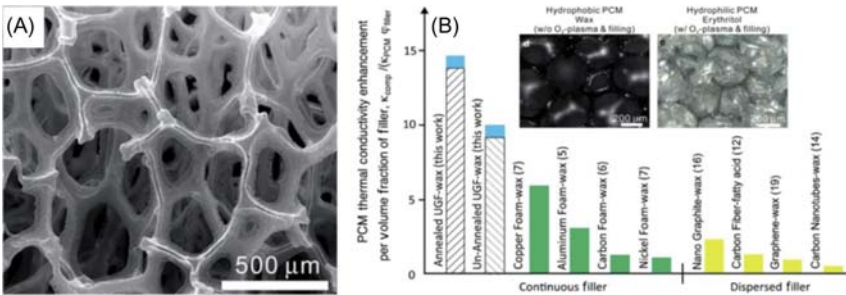


**FIGURE 26.21** (A) SEM photo of ultrathin graphite foams without PCM after etching of nickel template. (B) Thermal conductivity enhancement for graphite–paraffin wax and various nanofillers with different volume fractions. All PCMs have  $k$  values ranging from 0.17 to 0.31 W/m K. (inset) Differential interference contrast images of PCM [76].

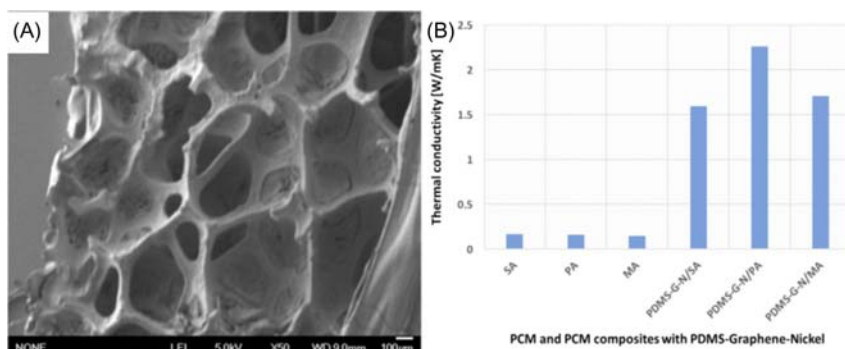


**FIGURE 26.22** (A) SEM image of the morphology of micropores of PA-PDMS-G-NF. (B) Thermal conductivity values of n-carboxylic acids PCM (SA, PA, MA) and PDMS-Graphene-Nickel (PDMS-G-NF) foam composites [77].

Liang et al. [77] used superoleophilic graphene nanosheets combined with porous nickel Ni foam to enhance thermal conductivity of PCM by 1300%. Graphene-covered nickel foam modified by polydimethylsiloxane (PDMS-G-NF) was synthesized by layering graphene nanosheets on the surface of porous Ni foam to form graphene-nickel foam G-NF. The porous support G-NF is further surface modified by using siloxane PDMS to fabricate shape-stable PCM composite (Fig. 26.22). The micropores in the PCM composite matrix were soaked in palmitic acid (PA). The  $k$  value of NePCM reached  $\sim 2.262$  W/m K with PCM loading of  $\sim 59.02$  wt.%, which is 14 times higher than the pure PA (0.162 W/m K). This showed that PDMS-modified graphene-nickel porous foams can significantly enhance the  $k$  values of organic PCM acids.

Chen et al. [78] used CNT foam to the  $k$  value of PCM by 500%. A sponge-like CNT network acts as a permeable support matrix to absorb PCM. This CNT-based PCM can improve latent heat storage capacity and is able to conduct electricity and heat efficiently. The PCM composite can convert electrical energy to heat and absorb light energy. The PCM composite is made of soft-flexible CNT-based porous material filled with paraffin (Fig. 26.23). The deformable support matrix has high thermal conductivity in melting and solidification processes. The CNT matrix has a strong effect on the thermal properties of the PCM, since CNTs have a very high  $k$  value of 3000 W/m K. While neat paraffin wax as PCM has very poor conductivity, ranging from 0.16 to 0.20 W/m K, the use of CNT-based sponges composite can increase the  $k$  values to 1.2 W/m K with 80 wt.% paraffin.

### 26.4.2 Melting process

Das et al. [79] explored the melting behavior in a vertical shell-and-tube system using the enthalpy-porosity technique. In their study, alkane n-

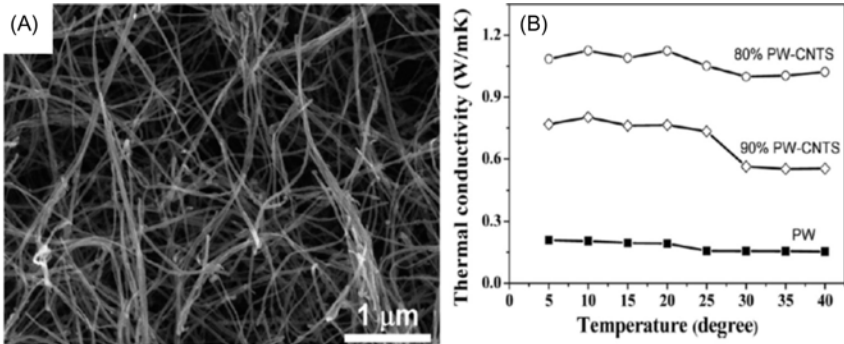


**FIGURE 26.23** (A) SEM image of the interior of CNT porous foam revealing a sponge-like microstructure. (B) Thermal conductivities of paraffin wax with 10 and 20 wt.% loadings of CNT foams, namely 80 and 90 wt.% paraffin [78].

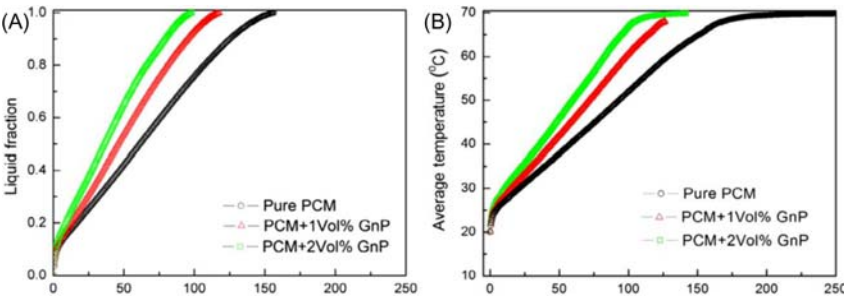


**FIGURE 26.24** (A) average liquid fraction and (B) average temperature profile of NePCMs with different percentages of graphene nanoplatelets [82].

eicosane/graphene nanosheets was used as the NePCM. The K–D and N–B models were used to calculate the effective dynamic viscosity and thermal conductivity of nanocomposites, respectively. An aspect ratio of  $10^{-3}$  (length of  $1\mu\text{m}$ , thickness of  $10\text{ nm}$ ) was assumed for the shape of graphene nanoplatelets (GnP). The authors reported that by increasing the volume fraction to 3%, natural convection was damped by the increased viscosity of the molten NePCM. As shown in Fig. 26.24, the melting time was significantly lowered by 41%, at GnP loading of 2 vol.% and HTF inlet temperature of  $70^\circ\text{C}$ . The same authors [80,81] further compared different nanomorphologies and system orientations using the same numerical solution. The conductive nanoenhancers were spherical (nanodiamond, ND), 1D (single-walled carbon nanotube, SWCNT), and 2D (GnP) nanostructures. A low percentage regime (1 vol.%) was adopted to maintain a moderate increase in the dynamic

viscosity. For the horizontal system, the melting time was reduced by 2%, 27%, and 40% for ND, SWCNT, and GnP, respectively [80]. For the vertical system, the melting time was shortened by 1%, 15%, and 25% for ND, SWCNT, and GnP, respectively [81].

Kant et al. [82] numerically analyzed the melting of graphene nanoparticle promoted PCM in a square cavity heating from the left vertical wall. COMSOL 5.0 was employed to solve the governing equations with adding a source term to mimic the Darcy flow in porous media, thus making it a hybrid of the AHC method and enthalpy–porosity method. Three kinds of PCMs (capric Acid,  $\text{CaCl}_2 \cdot 6\text{H}_2\text{O}$ , and n-octadecane) were enhanced by graphene nanoparticles with volume fractions of 1%, 3%, and 5%. The authors applied the Brinkman’s model, Vajjha’s model for the effective dynamic viscosity, and thermal conductivity, respectively. However, these models may not be able to reflect the actual properties as discussed before. The melting rate was accelerated in all cases, but it was note that the increased viscosity also weakened the efficiency of convective heat transfer. On this basis, in this study the degraded convection was not strong enough to outweigh the contribution of improved thermal conductivity. The numerical solution might be useful in selecting the optimal particle loading for large LHTES systems such as PCM tank, with both considering the contributions of conduction and convection.

It has been reported that the effective thermal conductivity of GnP mixture nonlinearly increases with the GnP loading, which is due to the interaction between GnP and their high aspect ratio and thermal conductivity [83]. Singh et al. [84] adopted this theory to calculate the effective thermal conductivity of GnP/sugar alcohol–PCM for medium temperature ( $160^\circ\text{C}$ – $200^\circ\text{C}$ ) TES applications. Based on the enthalpy–porosity approach, a 2D shell-and-tube model was established to analyze the combinations of varying the fin height and the GnP loading for the melting process. It was reported that 44% and 47% reduction in the melting time was achieved for fin heights of 0.5(R-r) and 0.75 (R-r), respectively. The small growth rate was due to the depression of the convection currents, and an aspect ratio of 0.5 (R-r) was the optimum fin size from an economical point of view. Additionally, the 3% GnP case could almost achieve the same melting time as the 0.5 (R-r) case, as shown in Fig. 26.25. The results can be used to find the optimum set of heat transfer enhancement strategies, both considering the costs of mounting fins and doping GnP for a given system.

### 26.4.3 Solidification process

A pioneering study by Fan et al. [85] simulated the unidirectional solidification process of GnP-enhanced dodecanol mixture. Instead of using the existing prediction models, they measured the thermophysical properties of NePCM at different weight fractions of GnP. The relative solidification rates

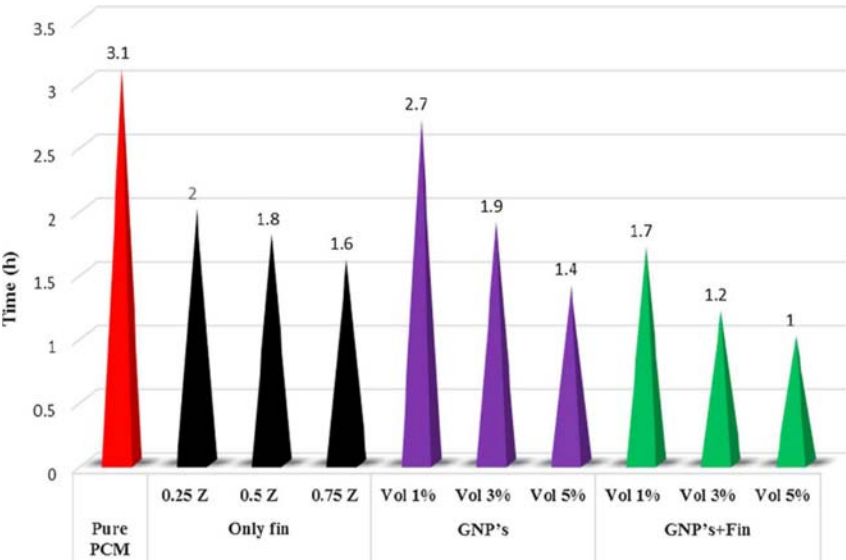


FIGURE 26.25 Total melting time using different sets of thermal enhancement methods [84].

were quantitatively compared, showing an expedited solidification rate of 34% at the highest GnP percentage of 1.0 wt.%. Since the simulation was based on effective medium theory, interactions between the nanoenhancers, sedimentation, and morphological instability were ignored. Experimental studies are needed to verify the numerical results. A work by Sathishkumar et al. [86] investigated the freezing process of GnP/water in a sphere. The best thermal conductivity enhancement of 56% (ice) and 11.7% (water) was obtained by adding 1.2 wt.% GnP. The highly conductive GnP reduced the supercooling degree and shortened the solidification time by 25%.

Recently, Singh et al. [87] numerically analyzed the solidification of GnP–PCM in a finned shell-and-tube system. The fin’s aspect ratio was optimized in a previous melting study [84]. The authors first measured the specific heat and dynamic viscosity of the base PCM (binary eutectic salt  $\text{LiNO}_3/\text{KCl}$ ) within the working temperature, and then calculated the effective properties using Vajjha’s model, Chu’s model [83], and other effective mixture models. The thermophysical properties of NePCM were treated as temperature-dependent polynomials in the enthalpy–porosity equations. Fig. 26.9 shows that the solidification time was shortened by 26.2% in the case of finned PCM, and was reduced by 49% in the presence of 5% GnP (Fig. 26.26). Additionally, decreasing the Stefan number (inlet temperature of HTF) and increasing the Reynolds number (flow rate of HTF) also expedited the solidification rate. A potential follow-up study could focus on the economic benefits of individual or combined techniques.



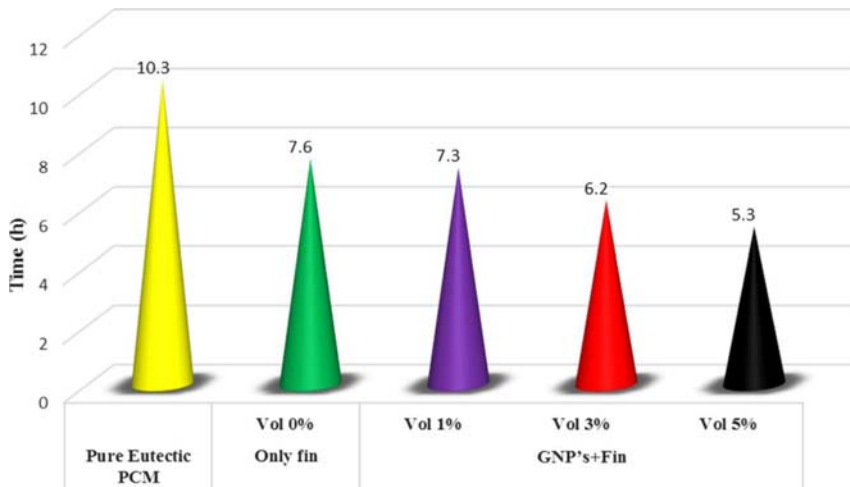


FIGURE 26.26 Solidification time for pure PCM, finned PCM, and finned NePCM [87].

#### 26.4.4 Practical applications

Sayyar et al. [88] prepared shape-stable NePCM consists of 69.8 wt.% of fatty acids, 22.2 wt.% of palmitic acid, and 8.0 wt.% of graphite nanosheets and integrated it into a gypsum wallboard. The authors built two test cells to compare the thermal performance of NePCM-integrated wallboard with commercial drywall panels. Experimental results showed the use of nano-PCM wallboard produced larger peak load-shifting ability with smaller interior temperature oscillation. To evaluate the energy savings for cooling and heating, a numerical model was established based on Fourier's law. Boundary conditions were based on the measured temperature values of the exterior and interior wall surface by experiments. Computed heat flux showed that the cooling and heating energy demands were reduced by 75.5% and 83.1%, respectively. In this study, the outdoor environment was simulated by periodically varying the temperature of exterior wall surface.

A similar experimental and numerical work was carried out by Biswas et al. [89] to evaluate the energy-saving benefits of a novel NePCM-incorporated gypsum wallboard. Following the procedure described in Ref. [88], a shape-stable nano-PCM was prepared by mixing 8 wt.% of expanded graphite (interconnected) nanosheets with 92 wt.% of n-heptadecane. The authors experimentally compared the heat gains of the NePCM wallboard with a regular wallboard under natural exposure conditions for three typical hot days, as shown in Fig. 26.27. To evaluate the annual energy saving, a COMSOL-based 2D numerical model was established. The numerical results for a south-oriented wall showed the highest annual reduction in wall heat gains with an indoor temperature set point of 22°C. The annual heat gains and cooling electricity consumption could be reduced by 24.65% and



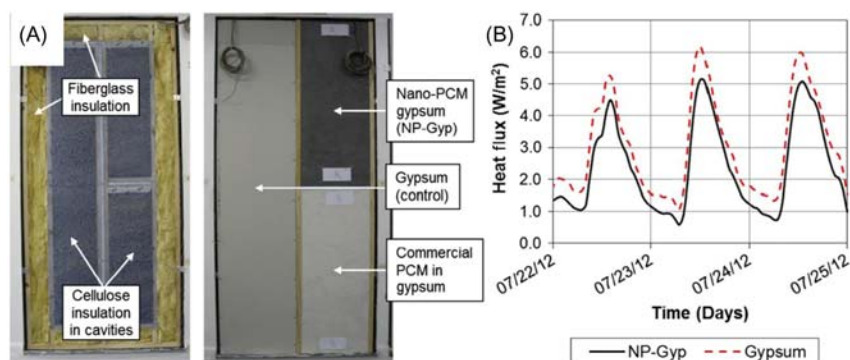


**FIGURE 26.27** (A) Test wall using NePCM wallboard and regular wallboard and (B) experimental results of heat gains through the two wallboards [89].

21.90% using the NePCM wallboard. The authors also investigated the influence of indoor cooling set points and found that 21°C (about the center of the melting range) could better reduce the heat gains and shift the peak cooling load during peak summer days. In this study, the exterior boundary condition was based on TMY3 weather data including hourly values of outdoor temperatures, solar radiation, and exterior surface convective heat transfer coefficients.

## 26.5 Conclusions

The great advancements achieved in nanotechnology play a key role in many modern industries [90]. The fundamental properties of a bulk material can dramatically change when its dimensions are reduced to the nanoscale [91]. Nanostructures have attracted great attention in the thermal enhancement of base material, particularly PCMs for TES applications. This chapter provided a framework for recent studies of NePCM and system performance of TES using NePCM. The important influence of nanostructure type, concentration, morphology, and dimension on the thermal conductivity enhancement and heat transfer behavior of NePCM were discussed thoroughly. Important conclusions are as follows:

1. Continuous interconnected nanofillers generally have greater thermal conductivity enhancement than discontinuous disconnected nanofillers. Essentially matrix foam macrostructures with nanosized walls or struts have higher contact surface area, and greater aspect ratios, leading to greater thermal conductivities and thermally better performance than nanofibers and nanoparticles, as PCM enhancers.
2. Carbon-based nanoenhancers have greater thermal conductivity compared to metal-based and metal oxide-based materials. Higher surface affinity

between organic PCM and its carbon nanofillers reduces phonon scatterings at interfacial surfaces and improves the uniform interpenetration.

3. Carbon-based nanomaterials generally have a smaller mass density difference from the organic PCM materials compared to heavier metals or metal oxides. Hence, organic PCM composites have better dispersibility and homogeneity within mediums.
4. PCM composites have generally a higher thermal conductivity as well as greater enhancement effect in liquid state compared to solid state. Nanofibers or nanoparticles group can easily separate when the composite is melting, whereas the big agglomerated clusters and group packings cannot separate and disperse completely in solid.
5. Results have shown that GnP can provide better heat transfer enhancement for both melting and solidification processes, compared to the metallic and metal oxide nanoenhancers. This can be attributed to its high thermal conductivity, high aspect ratio, large interface contact area, and the low thermal contact resistance with the base material.
6. The melting rate of NePCM increases with the concentration of nanoenhancers, but this result is built on the premise that the concentration is within a certain range. Once the concentration exceeds the threshold, the augmentation of viscosity will degrade the convection efficiency and in turn offset the improved conduction contribution.
7. The solidification rate increases with the concentration of nanoenhancers, which is due to the conduction-dominated heat transfer mechanism in the solidification process. To select the optimum concentration for given system, both the loss in TES density and impact on melting process are needed to be considered.

NePCM as a novel composite LHTES material should be analyzed by more researchers in the future. We envision that the influence of nanoenhancer type, morphology and size, and concentration will remain the aims of numerical studies of NePCM. In particular, one key point is to find out the optimum concentration for given systems. Most studies do not consider the impact of sedimentation of nanoparticles in the case of high particle concentration regime. Experimental works should be considered to test the homogeneity and stability of NePCM before simulation. More importantly, efforts are still needed to standardize the current prediction models for NePCM in three states. Empirical and semiempirical formulas are very useful for numerical simulation. Two-dimensional simulations are mostly applied, but sometimes 2D models are unable to provide the value of the HTF outlet temperature (e.g., the longitudinally finned shell-and-tube system [73]). For an active system, the variation of HTF outlet temperature is critical for evaluating the matching performance between the end-user and LHTES system. Therefore more studies are needed to examine the influence of nanoenhancers on the HTF outlet temperature. The system performance should not be

judged solely on the melting and solidification rates but also on the total energy and exergy stored. Hence, the influence of dispersing nanostructures on energy and exergy efficiencies of the system is worthy of research effort.

## References

- [1] IE Agency. World Energy Outlook 2018, International Energy Agency; 2018.
- [2] Kumar L, Hasanuzzaman M, Rahim NA. Global advancement of solar thermal energy technologies for industrial process heat and its future prospects: a review. *Energy Convers Manag* 2019;195:885–908.
- [3] Royo P, Acevedo L, Ferreira VJ, García-Armingol T, López-Sabirón AM, Ferreira G. High-temperature PCM-based thermal energy storage for industrial furnaces installed in energy-intensive industries. *Energy* 2019;173:1030–40.
- [4] Ma Z, Lin W, Soheli MI. Nano-enhanced phase change materials for improved building performance. *Renew Sustain Energy Rev* 2016;58:1256–68.
- [5] Napp TA, Gambhir A, Hills TP, Florin N, Fennell PS. A review of the technologies, economics and policy instruments for decarbonising energy-intensive manufacturing industries. *Renew Sustain Energy Rev* 2014;30:616–40.
- [6] Huang J, Fan J, Furbo S. Feasibility study on solar district heating in China. *Renew Sustain Energy Rev* 2019;108:53–64.
- [7] Liu J, Chen X, Cao S, Yang H. Overview on hybrid solar photovoltaic-electrical energy storage technologies for power supply to buildings. *Energy Convers Manag* 2019;187:103–21.
- [8] Rehman S, Al-Hadhrami LM, Alam MM. Pumped hydro energy storage system: a technological review. *Renew Sustain Energy Rev* 2015;44:586–98.
- [9] Poompavai T, Kowsalya M. Control and energy management strategies applied for solar photovoltaic and wind energy fed water pumping system: a review. *Renew Sustain Energy Rev* 2019;107:108–22.
- [10] Sahu BK. Wind energy developments and policies in China: a short review. *Renew Sustain Energy Rev* 2018;81:1393–405.
- [11] Li K, Liu C, Jiang S, Chen Y. Review on hybrid geothermal and solar power systems. *J Clean Prod* 2020;250:119481.
- [12] Nazir H, Batool M, Osorio FJ Bolivar, Isaza-Ruiz M, Xu X, Vignarooban K, et al. Recent developments in phase change materials for energy storage applications: a review. *Int J Heat Mass Transf* 2019;129:491–523.
- [13] Hughes BR, Chaudhry HN, Ghani SA. A review of sustainable cooling technologies in buildings. *Renew Sustain Energy Rev* 2011;15(6):3112–20.
- [14] Kasaeian A, bahrani L, Pourfayaz F, Khodabandeh E, Yan W-M. Experimental studies on the applications of PCMs and nano-PCMs in buildings: a critical review. *Energy Build* 2017;154:96–112.
- [15] Li D, Wang J, Ding Y, Yao H, Huang Y. Dynamic thermal management for industrial waste heat recovery based on phase change material thermal storage. *Appl Energy* 2019;236:1168–82.
- [16] Pelay U, Luo L, Fan Y, Stitou D, Rood M. Thermal energy storage systems for concentrated solar power plants. *Renew Sustain Energy Rev* 2017;79:82–100.
- [17] Edwards J, Bindra H, Sabharwal P. Exergy analysis of thermal energy storage options with nuclear power plants. *Ann Nucl Energy* 2016;96:104–11.

- [18] Lizana J, Chacartegui R, Barrios-Padura A, Valverde JM. Advances in thermal energy storage materials and their applications toward zero energy buildings: a critical review. *Appl Energy* 2017;203:219–39.
- [19] Lin Y, Alva G, Fang G. Review on thermal performances and applications of thermal energy storage systems with inorganic phase change materials. *Energy* 2018;165:685–708.
- [20] Mahdi JM, Lohrasbi S, Ganji DD, Nsofor EC. Accelerated melting of PCM in energy storage systems via novel configuration of fins in the triplex-tube heat exchanger. *Int J Heat Mass Transf* 2018;124:663–76.
- [21] Akeiber H, Nejat P, Majid MZA, Wahid MA, Jomehzadeh F, Zeynali Famileh I, et al. A review on phase change material (PCM) for sustainable passive cooling in building envelopes. *Renew Sustain Energy Rev* 2016;60:1470–97.
- [22] Singh P, Khanna S, Becerra V, Newar S, Sharma V, Mallick TK, et al. Power improvement of finned solar photovoltaic phase change material system. *Energy* 2020;193:116735.
- [23] Hekmat S, Molaeimanesh GR. Hybrid thermal management of a Li-ion battery module with phase change material and cooling water pipes: An experimental investigation. *Appl Therm Eng* 2020;166:114759.
- [24] Huang Z, Xie N, Zheng X, Gao X, Fang X, Fang Y, et al. Experimental and numerical study on thermal performance of Wood's alloy/expanded graphite composite phase change material for temperature control of electronic devices. *Int J Therm Sci* 2019;135:375–85.
- [25] Alva G, Lin Y, Fang G. An overview of thermal energy storage systems. *Energy* 2018;144:341–78.
- [26] Ma Y, Sun S, Li J, Tang G. Preparation and thermal reliabilities of microencapsulated phase change materials with binary cores and acrylate-based polymer shells. *Thermochim Acta* 2014;588:38–46.
- [27] Tao YB, He Y-L. A review of phase change material and performance enhancement method for latent heat storage system. *Renew Sustain Energy Rev* 2018;93:245–59.
- [28] Zhang P, Xiao X, Ma ZW. A review of the composite phase change materials: fabrication, characterization, mathematical modeling and application to performance enhancement. *Appl Energy* 2016;165:472–510.
- [29] Zahir MH, Mohamed SA, Saidur R, Al-Sulaiman FA. Supercooling of phase-change materials and the techniques used to mitigate the phenomenon. *Appl Energy* 2019;240:793–817.
- [30] Arconada N, Arribas L, Lucio B, González-Aguilar J, Romero M. Macroencapsulation of sodium chloride as phase change materials for thermal energy storage. *Sol Energy* 2018;167:1–9.
- [31] Jamekhorshid A, Sadrameli SM, Farid M. A review of microencapsulation methods of phase change materials (PCMs) as a thermal energy storage (TES) medium. *Renew Sustain Energy Rev* 2014;31:531–42.
- [32] Lv P, Liu C, Rao Z. Review on clay mineral-based form-stable phase change materials: preparation, characterization and applications. *Renew Sustain Energy Rev* 2017;68:707–26.
- [33] Al-Shannaq R, Kurdi J, Al-Muhtaseb S, Farid M. Innovative method of metal coating of microcapsules containing phase change materials. *Sol Energy* 2016;129:54–64.
- [34] Wang Y, Yang X, Xiong T, Li W, Shah KW. Performance evaluation approach for solar heat storage systems using phase change material. *Energy Build* 2017;155:115–27.
- [35] Liu S, Li Y, Zhang Y. Mathematical solutions and numerical models employed for the investigations of PCMs' phase transformations. *Renew Sustain Energy Rev* 2014;33:659–74.
- [36] Kim J-H, Jeong E, Lee Y-S. Preparation and characterization of graphite foams. *J Ind Eng Chem* 2015;32:21–33.

- [37] Shah KW. A review on enhancement of phase change materials - a nanomaterials perspective. *Energy Build* 2018;175:57–68.
- [38] de Gracia A, Cabeza LF. Numerical simulation of a PCM packed bed system: a review. *Renew Sustain Energy Rev* 2017;69:1055–63.
- [39] Leong KY, Abdul Rahman MR, Gurusathan BA. Nano-enhanced phase change materials: a review of thermo-physical properties, applications and challenges. *J Energy Storage* 2019;21:18–31.
- [40] Shah KW, Lu Y. Morphology, large scale synthesis and building applications of copper nanomaterials. *Constr and Build Mater* 2018;180:544–78.
- [41] Deng Y, Li J, Qian T, Guan W, Li Y, Yin X. Thermal conductivity enhancement of polyethylene glycol/expanded vermiculite shape-stabilized composite phase change materials with silver nanowire for thermal energy storage. *Chem Eng J* 2016;295:427–35.
- [42] Sreethawong T, Shah KW, Zhang S-Y, Ye E, Lim SH, Maheswaran U, et al. Optimized production of copper nanostructures with high yields for efficient use as thermal conductivity-enhancing PCM dopant. *J Mater Chem A* 2014;2(10).
- [43] Zeng J-L, Zhu F-R, Yu S-B, Zhu L, Cao Z, Sun L-X, et al. Effects of copper nanowires on the properties of an organic phase change material. *Sol Energy Mater Sol Cell* 2012;105:174–8.
- [44] Molefi JA, Luyt AS, Krupa I. Investigation of thermally conducting phase-change materials based on polyethylene/wax blends filled with copper particles. *J Appl Polym Sci* 2010;116(3):1766–74.
- [45] Lin SC, Al-Kayiem HH. Evaluation of copper nanoparticles – paraffin wax compositions for solar thermal energy storage. *Sol Energy* 2016;132:267–78.
- [46] Rabienataj Darzi AA, Jourabian M, Farhadi M. Melting and solidification of PCM enhanced by radial conductive fins and nanoparticles in cylindrical annulus. *Energy Convers Manag* 2016;118:253–63.
- [47] Jourabian M, Farhadi M, Rabienataj Darzi AA. Outward melting of ice enhanced by Cu nanoparticles inside cylindrical horizontal annulus: lattice Boltzmann approach. *Appl Math Model* 2013;37(20-21):8813–25.
- [48] Patel HE, Sundararajan T, Pradeep T, Dasgupta A, Dasgupta N, Das SK. A micro-convection model for thermal conductivity of nanofluids. *Pramana* 2005;65(5):863–9.
- [49] Jourabian M, Farhadi M, Sedighi K. On the expedited melting of phase change material (PCM) through dispersion of nanoparticles in the thermal storage unit. *Comput Math Appl* 2014;67(7):1358–72.
- [50] Feng Y, Li H, Li L, Bu L, Wang T. Numerical investigation on the melting of nanoparticle-enhanced phase change materials (NEPCM) in a bottom-heated rectangular cavity using lattice Boltzmann method. *Int J Heat Mass Transf* 2015;81:415–25.
- [51] Khodadadi JM, Hosseinzadeh SF. Nanoparticle-enhanced phase change materials (NEPCM) with great potential for improved thermal energy storage. *Int Commun Heat Mass Transf* 2007;34(5):534–43.
- [52] Abdollahzadeh M, Esmailpour M. Enhancement of phase change material (PCM) based latent heat storage system with nano fluid and wavy surface. *Int J Heat Mass Transf* 2015;80:376–85.
- [53] Kashani S, Ranjbar AA, Abdollahzadeh M, Sebt S. Solidification of nano-enhanced phase change material (NEPCM) in a wavy cavity. *Heat Mass Transf* 2012;48(7):1155–66.
- [54] Elbahjaoui R, El Qarnia H. Thermal analysis of nanoparticle-enhanced phase change material solidification in a rectangular latent heat storage unit including natural convection. *Energy Build* 2017;153:1–17.

- [55] Al-Kayiem HH, Lin SC. Performance evaluation of a solar water heater integrated with a PCM nanocomposite TES at various inclinations. *Sol Energy* 2014;109:82–92.
- [56] Nabavitatabayy M, Haghighat F, Moreau A, Sra P. Numerical analysis of a thermally enhanced domestic hot water tank. *Appl Energy* 2014;129:253–60.
- [57] Babapoor A, Karimi G. Thermal properties measurement and heat storage analysis of paraffinnanoparticles composites phase change material: comparison and optimization. *Appl Therm Eng* 2015;90:945–51.
- [58] Sharma RK, Ganesan P, Tyagi VV, Metselaar HSC, Sandaran SC. Thermal properties and heat storage analysis of palmitic acid-TiO<sub>2</sub> composite as nano-enhanced organic phase change material (NEOPCM). *Appl Therm Eng* 2016;99:1254–62.
- [59] Li Y, Li J, Deng Y, Guan W, Wang X, Qian T. Preparation of paraffin/porous TiO<sub>2</sub> foams with enhanced thermal conductivity as PCM, by covering the TiO<sub>2</sub> surface with a carbon layer. *Appl Energy* 2016;171:37–45.
- [60] Ghalambaz M, Doostani A, Chamkha AJ, Ismael MA. Melting of nanoparticles-enhanced phase-change materials in an enclosure: effect of hybrid nanoparticles. *Int J Mech Sci* 2017;134:85–97.
- [61] Chamkha AJ, Doostanidezfuli A, Izadpanahi E, Ghalambaz M. Phase-change heat transfer of single/hybrid nanoparticles-enhanced phase-change materials over a heated horizontal cylinder confined in a square cavity. *Adv Powder Technol* 2017;28(2):385–97.
- [62] Elsayed AO. Numerical study on performance enhancement of solid–solid phase change materials by using multi-nanoparticles mixtures. *J Energy Storage* 2015;4:106–12.
- [63] Hossain R, Mahmud S, Dutta A, Pop I. Energy storage system based on nanoparticle-enhanced phase change material inside porous medium. *Int J Therm Sci* 2015;91:49–58.
- [64] Mahdi JM, Nsofor EC. Melting enhancement in triplex-tube latent heat energy storage system using nanoparticles-metal foam combination. *Appl Energy* 2017;191:22–34.
- [65] Huo Y, Rao Z. Lattice Boltzmann investigation on phase change of nanoparticle-enhanced phase change material in a cavity with separate plate. *Energy Convers Manag* 2017;154:420–9.
- [66] Elbahjaoui R, El Qarnia H. Transient behavior analysis of the melting of nanoparticle-enhanced phase change material inside a rectangular latent heat storage unit. *Appl Therm Eng* 2017;112:720–38.
- [67] Pahamli Y, Hosseini MJ, Ranjbar AA, Bahrampoury R. Effect of nanoparticle dispersion and inclination angle on melting of PCM in a shell and tube heat exchanger. *J Taiwan Inst Chem Eng* 2017;81:316–34.
- [68] Alomair M, Alomair Y, Tasnim S, Mahmud S, Abdullah H. Analyses of bio-based nano-PCM filled concentric cylindrical energy storage system in vertical orientation. *J Energy Storage* 2018;20:380–94.
- [69] Ebadi S, Humaira Tasnim S, Abbas Aliabadi A, Mahmud S. Geometry and nanoparticle loading effects on the bio-based nano-PCM filled cylindrical thermal energy storage system. *Appl Therm Eng* 2018;141:724–40.
- [70] Ebadi S, Tasnim SH, Aliabadi AA, Mahmud S. Melting of nano-PCM inside a cylindrical thermal energy storage system: numerical study with experimental verification. *Energy Convers Manag* 2018;166:241–59.
- [71] Mahdi JM, Nsofor EC. Solidification of a PCM with nanoparticles in triplex-tube thermal energy storage system. *Appl Therm Eng* 2016;108:596–604.
- [72] Mahdi JM, Nsofor EC. Solidification enhancement in a triplex-tube latent heat energy storage system using nanoparticles-metal foam combination. *Energy* 2017;126:501–12.
- [73] Mahdi JM, Nsofor EC. Solidification enhancement of PCM in a triplex-tube thermal energy storage system with nanoparticles and fins. *Appl Energy* 2018;211:975–86.

- [74] Li D, Wu Y, Liu C, Zhang G, Arıcı M. Energy investigation of glazed windows containing nano-PCM in different seasons. *Energy Convers Manag* 2018;172:119–28.
- [75] Li D, Wu Y, Liu C, Zhang G, Arıcı M. Numerical investigation of thermal and optical performance of window units filled with nanoparticle enhanced PCM. *Int J Heat Mass Transf* 2018;125:1321–32.
- [76] Ji H, Sellan DP, Pettes MT, Kong X, Ji J, Shi L, et al. Enhanced thermal conductivity of phase change materials with ultrathin-graphite foams for thermal energy storage. *Energy Environ Sci* 2014;7(3):1185–92.
- [77] Liang W, Zhang G, Sun H, Chen P, Zhu Z, Li A. Graphene–nickel/*n*-carboxylic acids composites as form-stable phase change materials for thermal energy storage. *Sol Energy Mater Sol Cell* 2015;132:425–30.
- [78] Chen L, Zou R, Xia W, Liu Z, Shang Y, Zhu J, et al. Electro- and photodriven phase change composites based on wax-infiltrated carbon nanotube sponges. *ACS Nano* 2012;6(12):10884–92.
- [79] Das N, Takata Y, Kohno M, Harish S. Melting of graphene based phase change nanocomposites in vertical latent heat thermal energy storage unit. *Appl Therm Eng* 2016;107:101–13.
- [80] Das N, Kohno M, Takata Y, Patil DV, Harish S. Enhanced melting behavior of carbon based phase change nanocomposites in horizontally oriented latent heat thermal energy storage system. *Appl Therm Eng* 2017;125:880–90.
- [81] Das N, Takata Y, Kohno M, Harish S. Effect of carbon nano inclusion dimensionality on the melting of phase change nanocomposites in vertical shell-tube thermal energy storage unit. *Int J Heat Mass Transf* 2017;113:423–31.
- [82] Kant K, Shukla A, Sharma A, Henry Biwole P. Heat transfer study of phase change materials with graphene nano particle for thermal energy storage. *Sol Energy* 2017;146:453–63.
- [83] Chu K, Jia C-c, Li W-s. Effective thermal conductivity of graphene-based composites. *Appl Phys Lett* 2012;101(12).
- [84] Singh RP, Kaushik SC, Rakshit D. Melting phenomenon in a finned thermal storage system with graphene nano-plates for medium temperature applications. *Energy Convers Manag* 2018;163:86–99.
- [85] Fan L-W, Zhu Z-Q, Liu M-J. A similarity solution to unidirectional solidification of nano-enhanced phase change materials (NePCM) considering the mushy region effect. *Int J Heat Mass Transf* 2015;58:478–81.
- [86] Sathishkumar A, Kumaresan V, Velraj R. Solidification characteristics of water based graphene nanofluid PCM in a spherical capsule for cool thermal energy storage applications. *Int J Refrig* 2016;66:73–83.
- [87] Singh RP, Kaushik SC, Rakshit D. Solidification behavior of binary eutectic phase change material in a vertical finned thermal storage system dispersed with graphene nano-plates. *Energy Convers Manag* 2018;171:825–38.
- [88] Sayyar M, Weerasiri RR, Soroushian P, Lu J. Experimental and numerical study of shape-stable phase-change nanocomposite toward energy-efficient building constructions. *Energy Build* 2014;75:249–55.
- [89] Biswas K, Lu J, Soroushian P, Shrestha S. Combined experimental and numerical evaluation of a prototype nano-PCM enhanced wallboard. *Appl Energy* 2014;131:517–29.
- [90] Hussain CM. Preface. In: Hussain CM, editor. *Handbook of nanomaterials for industrial applications*. Elsevier; 2018. p. xxxi–xxxii.
- [91] Shah KW, Xiong T. Multifunctional metallic nanowires in advanced building applications. *Materials* 2019;12(11):1731.

# Application of functionalized nanomaterials in asphalt road construction materials

Henglong Zhang<sup>1</sup>, Chongzheng Zhu<sup>1</sup>, Chuanwen Wei<sup>1</sup>, Haihui Duan<sup>1</sup> and Jianying Yu<sup>2</sup>

<sup>1</sup>Key Laboratory for Green & Advanced Civil Engineering Materials and Application Technology of Hunan Province, College of Civil Engineering, Hunan University, Changsha, P.R. China, <sup>2</sup>State Key Laboratory of Silicate Materials for Architectures, Wuhan University of Technology, Wuhan, P.R. China

## 27.1 Introduction

Asphalt has been widely used in many aspects of infrastructure construction, such as pavement, waterproofing, shock absorption and protective coatings, etc. It has been used, in particular, for pavement construction due to its excellent road performance, such as driving comfort and safety, low noises levels, fast construction and easy maintenance, etc. However, as an organic viscoelastic material, asphalt is prone to flow at high temperature and become brittle at low temperature, which in turn cause high-temperature rutting and low-temperature cracking of pavement. Asphalt is also vulnerable to aging under heat, sunlight, oxygen, or a combination of these factors, further contributing to asphalt pavement deterioration and limiting its applications [1–3]. Therefore for certain applications asphalt properties need to be improved. For a long time, various modification methods have been used to improve asphalt properties, such as acid modification, mineral filler modification, and polymer modification, etc. [4,5]. Recently, with the development of nanotechnology, different kinds of nanomaterials have been increasingly applied in industries because of their unique characteristics [6]. In the field of road engineering, various inorganic nanomaterials have been used to modify asphalt, especially for layered silicates and inorganic nanoparticles [7–10]. Layered silicates are readily available and low in cost, consisting of layers of tetrahedral silicate and octahedral hydroxide sheets. They mainly include montmorillonite, vermiculite, and rectorite. Indeed, the addition of



layered silicates with tiny amounts (usually less than 5 wt.%) and its ultimate dispersion as 1 nm-thick nanolayers in a polymer matrix allow many properties, such as stiffness, fluid, gas barrier properties, etc., to be increased. However, the interlayers of layered silicate are hydrophilic, and the interlayer spacing is small. This makes the polymer chain insertion into its interlayers difficult. To increase the ease of insertion, layered silicate needs to be functionalized, which is commonly exchanged with organic cations, particularly alkylammonium ions, making the layered silicate lipophilic, and enlarging the interlayer spacing. Inorganic nanoparticles mainly include nano-ZnO, nano-TiO<sub>2</sub>, and nano-SiO<sub>2</sub>. The addition of inorganic nanoparticles can improve the high- or low-temperature performance and photooxidative aging resistance of asphalt. However, inorganic nanoparticles have huge surface area and extreme high surface energy and are easy to agglomerate, which not only make uniform dispersion more difficult, but also may make their nanometer effect lost. In order to avoid the agglomeration, the functionalization of inorganic nanoparticles is also an effective way, namely surface modification by silane coupling agent. After surface modification, the inorganic nanoparticles are easier to disperse in asphalt and the compatibility between them can be improved.

This chapter includes three sections: First, applications of organic layered silicates in asphalt are discussed; secondly, applications of surface modification inorganic nanoparticles in asphalt; and lastly, applications of multidimensional nanomaterials composed of zero-dimensional surface modification inorganic nanoparticles and two-dimensional organic layered silicates in asphalt. The chapter also discusses likely future trends in applications of functionalize nanomaterials in asphalt road construction materials.

## **27.2 Application of organic layered silicate in asphalt**

### **27.2.1 Preparation of organic layered silicates and modified asphalts**

#### *27.2.1.1 Preparation of organic layered silicates*

A 500 mL round-bottom, three-necked flask with a mechanical stirrer, thermometer, and condenser with a drying tube is used as a reactor. Layered silicate (10 g) [e.g., expanded vermiculite (EVMT), rectorite (REC), or montmorillonite (MMT)] is gradually dissolved in 200 mL of deionized water and stirred for 30 min. Then a certain amount of intercalated agent [e.g., cetyltrimethyl ammonium bromide (CTAB) or octadecyl dimethyl benzyl ammonium chloride (ODBA)] is added to the solution. The resulting suspension is vigorously stirred for 10 h. The treated layered silicate (LS) is repeatedly washed with deionized water. The filtrate is titrated with 0.1N AgNO<sub>3</sub> until no precipitate of AgBr or AgCl is formed. This ensures the complete removal of bromine or chloride ions. The filter cake is then placed

in a vacuum oven at 80°C for 24 h for drying. The dried cake is ground to obtain the OLS [e.g., organic EVMT (OEVTM), organic REC (OREC), or organic MMT (OMMT)] with particle sizes of 300 mesh [11–13].

### 27.2.1.2 Preparation of layered silicate or organic layered silicate-modified asphalts

The LS- or OLS-modified asphalt is prepared as follows: asphalt is heated to 150°C ± 5°C in an oil-bath heating container until it flows fully. Then appropriate amounts of LS or OLS are added slowly at a low mixing speed. The mixture is sheared at 5000 rpm for 60 min using a high shear mixer. The base asphalt is also treated using the same process for preferable comparison with the LS- or OLS-modified asphalts [11–13].

## 27.2.2 X-ray diffraction analysis of organic layered silicates

### 27.2.2.1 X-ray diffraction analysis of organic layered silicates

The XRD patterns of LS and OLS are shown in Fig. 27.1. The interlayer spacing of LS and OLS is calculated according to the Bragg equation ( $\lambda = 2d\sin\theta$ ), which is given in Table 27.1. The basal spacing ( $d_{001}$ ) of MMT, REC, and EVMT are 1.53, 2.25, and 1.42 nm, respectively, while the  $d_{001}$  values of OMMT, OREC, and OEVTM are 2.31, 4.37, and 5.33 nm, respectively. It can be seen that all the data values of OLS are higher than that of LS, which indicates that the intercalated agent (ODBA) molecules intercalate into the galleries of the LS. Compared with OREC and OMMT, OEVTM shows the highest  $d_{001}$  values as well as increased interlayer spacing. This implies that the galleries of EVMT are more easily expended by the intercalated agent (ODBA) in comparison with MMT and REC.

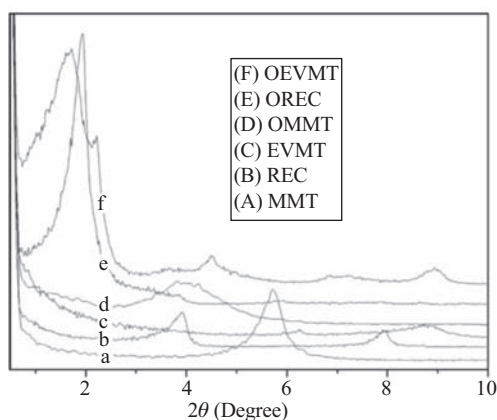
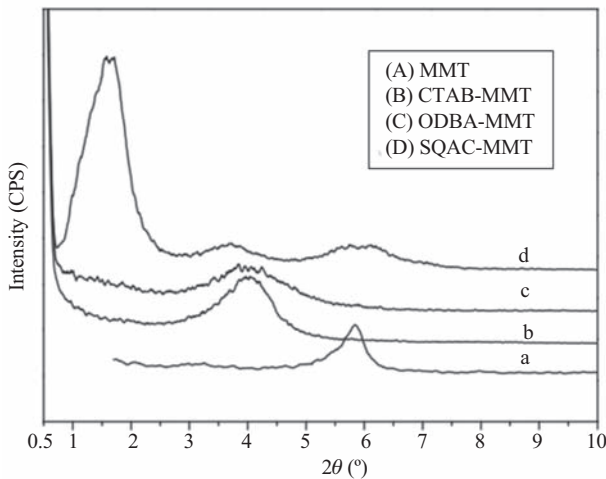


FIGURE 27.1 XRD patterns of LS and OLS [15].

**TABLE 27.1** Interlayer spacing of LS and OLS [15].

Samples	$2\theta$ (degrees)	$d_{001}$ (nm)	$d_{001}$ variation after organic modification (nm)
MMT	5.76	1.53	—
OMMT	3.81	2.31	0.78
REC	3.92	2.25	—
OREC	2.02	4.37	2.12
EVMT	6.23	1.42	—
OEVMT	1.66	5.33	3.91



**FIGURE 27.2** XRD patterns of MMT and OMMT with different intercalated agents [16].

The relatively higher  $d_{001}$  can contribute to the good interactions between EVMT and asphalt [14,15].

The XRD patterns of MMT and OMMT with different intercalated agents [e.g., CTAB, ODBA, or star quaternary alkylammonium chloride modifier (SQAC)] are shown in Fig. 27.2. The interlayer spacing is given in Table 27.2. The  $d_{001}$  values of MMT, CTAB–MMT, ODBA–MMT, and SQAC–MMT are 1.53, 2.20, 2.31, and 5.87 nm, respectively. The  $d_{001}$  values for the OMMTs are greater than that for the MMT, which indicates that a cationic-exchange reaction occurs between the MMT and organic intercalated agents, and that the galleries in the MMT are filled with

**TABLE 27.2** Interlayer spacing of MMT and OMMT with different intercalated agents [16].

Samples	$2\theta$ (degrees)	$d_{001}$ (nm)
MMT	5.76	1.53
CTAB–MMT	3.99	2.20
ODBA–MMT	3.81	2.31
SQAC–MMT	1.51	5.87

molecules containing organic cations. The  $d_{001}$  value of the ODBA–MMT is slightly higher than that of CTAB–MMT, which may be attributed to the different chain structures of the intercalated agents (i.e., ODBA contains an alkyl chain and a benzyl chain that can efficiently increase the interlayer spacing of the MMT, and CTAB contains only an alkyl chain). The SQAC–MMT shows the largest  $d_{001}$  value, up to 5.87 nm, which is due to the complicated molecular chain structure of SQAC, which has two long alkyl chains [16].

### 27.2.2.2 XRD analysis of separated organic layered silicates from modified asphalt

The XRD patterns of EVMT-, OEVT-, OEVT-modified asphalt and separated OEVT from OEVT-modified asphalt are shown in Fig. 27.3, and the interlayer spacing is given in Table 27.3. It can be observed that the diffraction peak of OEVT after compounding with asphalt disappears, which implies either the formation of an intercalated nanocomposite with a basal spacing larger than 17.60 nm, the formation of an exfoliated nanostructure, or a very disorganized structure of the silicate platelets. In an effort to determine the exact microstructure of OEVT-modified asphalt, a dissolving–filtrating procedure is performed as follows: first, OEVT-modified asphalt is dissolved in trichloroethylene, then the OEVT is filtered from this solution. After that, the separated OEVT is characterized by XRD. The XRD pattern of separated OEVT is shown in Fig. 27.3D. As can be seen separated OEVT shows an obvious diffraction peak in XRD curve, with a corresponding  $d_{001}$  value of 4.82 nm. This implies that not all OEVT are peeled off, and that there are still some regular layered structures of OEVT in modified asphalt. Moreover, this  $d_{001}$  value is lower than that of OEVT, which can be attributed to the existing organic compounds in the EVMT interlayers. The asphalt molecules intercalated into the interlayers of OEVT are dissolved by trichloroethylene, which contributes to the decreased  $d_{001}$  value of the separated OEVT. The above discussion indicates that OEVT-modified asphalt forms a semiexfoliated nanostructure [12].

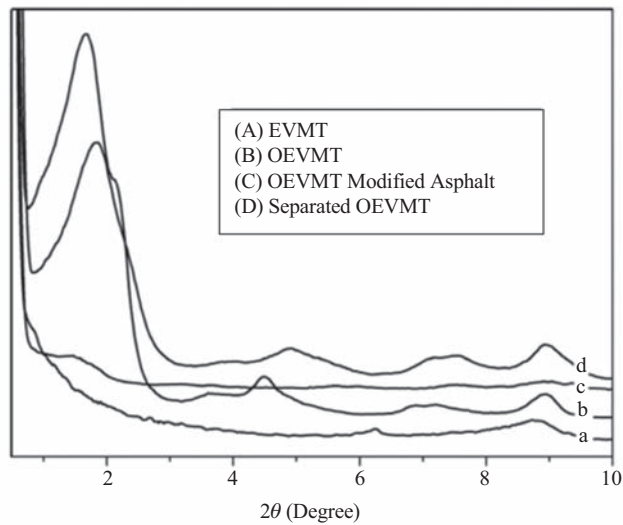


**FIGURE 27.3** XRD patterns of EVMT-, OEVT-, OEVT-modified asphalt and separated OEVT from modified asphalt [12].

**TABLE 27.3** Interlayer spacing of EVMT-, OEVT-, OEVT-modified asphalt and separated OEVT from modified asphalt [12].

Samples	$2\theta$ (degrees)	$d_{001}$ (nm)	$d_{001}$ variation (nm)
EVMT	6.23	1.42	—
OEVT	1.66	5.33	3.91
OEVT in modified asphalt	—	> 17.60	—
Separated OEVT from modified asphalt	1.83	4.82	3.40

### 27.2.2.3 Microstructure of organic layered silicate-modified asphalts

Similar to polymer/layered silicate nanocomposites, LS- and OLS-modified asphalts have three structure types, namely phase-separated microstructure, intercalated nanostructure, and exfoliated nanostructure, as shown in Fig. 27.4 [11,13,17].

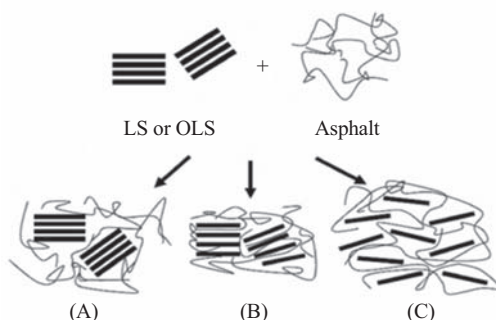


**FIGURE 27.4** Schematic of structures of LS- and OLS-modified asphalts: (A) phase separated (microcomposite); (B) intercalated (nanocomposite); and (C) exfoliated (nanocomposite) [11,13].

The phase-separated microstructure means that LS and asphalt is separated, and that LS remains intact, as shown in Fig. 27.4A. In general, LS-modified asphalt forms a phase-separated structure. This is because LS layers are hydrophilic and the spaces between them are small, which makes the intercalation and peeling of layers harder. Thus it is not easy that the lipophilic asphalt chains enter into the gallery space between silicate layers, which cause the compatibility between LS and asphalt is very weak [17].

The intercalated nanostructures correspond to well-ordered multilayered structures where the asphalt chains are inserted into the gallery space between silicate layers, while the exfoliated nanostructures correspond to delaminating structures where the individual silicate layers are no longer close enough to interact with the gallery, as shown in Fig. 27.4B and Fig. 27.4C, respectively. OLS-modified asphalt usually forms an intercalated nanostructure or exfoliated nanostructure, which mainly depends on the types of LS and organic intercalated agent. For example, ODBA–REC-modified asphalt forms an intercalated nanostructure, whereas CTAB–REC-modified asphalt forms an exfoliated nanostructure [11]. Compared to the intercalated nanostructure, the exfoliated nanostructure is more stable.

### 27.2.3 Fourier transform infrared spectroscopy analysis of organic layered silicate and organic layered silicate-modified asphalts

#### 27.2.3.1 Fourier transform infrared spectroscopy analysis of organic layered silicates

FTIR spectra of MMT and OMMT with hexadecyl dimethyl benzyl ammonium chloride (HDBA) are shown in Fig. 27.5. In the spectra of OMMT, except for the peaks in MMT, the presence of new peaks at 2925 and 2851  $\text{cm}^{-1}$  is seen. These are caused by C–H ( $-\text{CH}_2$ ,  $-\text{CH}_3$ ) stretching and bending absorptions in the organic intercalation agent. The disappearing peak at 1636  $\text{cm}^{-1}$  (belonging to bending vibrations of O–H) illustrates the disappearance of inorganic water that exists in the silicate layers in MMT,

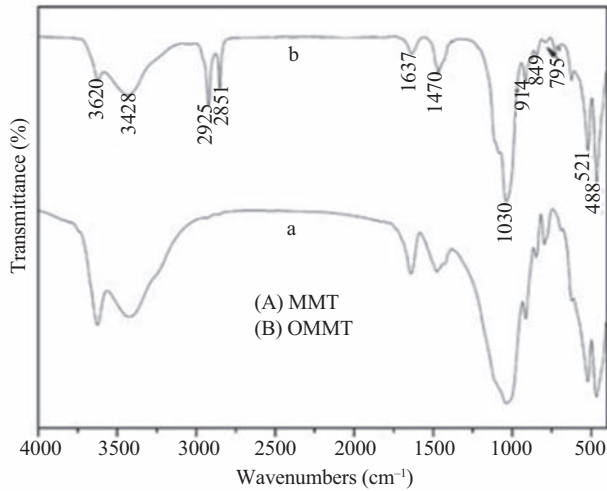


**FIGURE 27.5** FTIR spectra of MMT and OMMT [17].

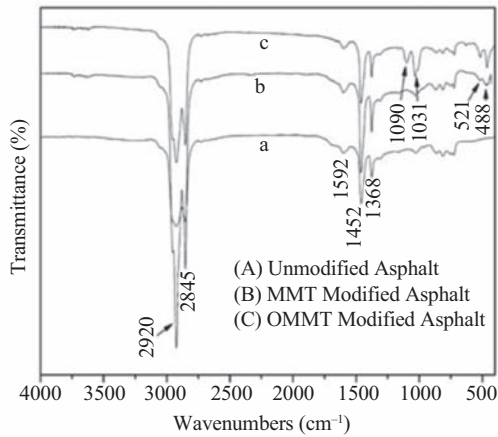


**FIGURE 27.6** FTIR spectra of MMT and OMMT-modified asphalts [17].

which in turn indicates that the organic intercalated agents are intercalated in the layers of MMT [17].

### 27.2.3.2 Fourier transform infrared spectroscopy analysis of organic layered silicate-modified asphalts

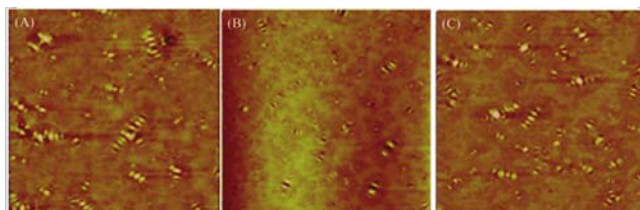
The FTIR spectra of MMT and OMMT (HDBA–MMT)-modified asphalts are shown in Fig. 27.6. New peaks appear with the introduction of OMMT. The peak at  $1031\text{ cm}^{-1}$  due to the stretching vibrations of Si–O, and the

peaks at  $521$  and  $488\text{ cm}^{-1}$  from the bending vibrations of Si—O—Al and Si—O—Si bonds in the OMMT structure. It can be seen that the peak at  $1031\text{ cm}^{-1}$  in OMMT is split into two peaks,  $1090$  and  $1031\text{ cm}^{-1}$ , which can be attributed to the increase of interlayer spacing of OMMT. This in turn implies that asphalt molecules are intercalated into the layers of OMMT during the melt blending process. However, the peaks identifying MMT are not exhibited in MMT-modified asphalt (e.g., the peak at  $1031\text{ cm}^{-1}$ ). This is because MMT is not dispersed homogeneously in asphalt due to the poor compatibility between the MMT and asphalt, which contributes the small amount of MMT in the FTIR analysis sample [17].

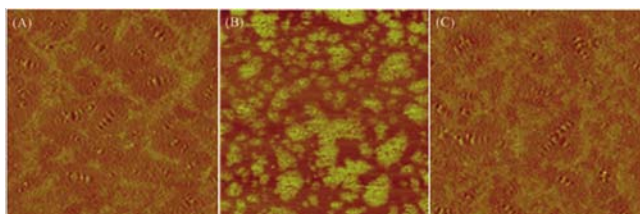
#### 27.2.4 Atomic force microscopy analysis of organic layered silicate-modified asphalts

Fig. 27.7A shows a typical topographic AFM image of asphalt, where the dispersed domains (the dark-looking regions) show a succession of pale and dark lines, which are often called “bee-like” structures. The “bee-like” appearance is attributed to the microcrystalline waxes ( $> C_{40}$ ) and/or the highly aromatics and long alkyl chain asphaltene (denoted waxy molecules) found in asphaltene [17].

The topographic images of unmodified asphalt, MMT-modified asphalt and OMMT (HDBA—MMT)-modified asphalt are shown in Fig. 27.7. The corresponding phase images of unmodified asphalt, MMT-modified asphalt and OMMT-modified asphalt are shown in Fig. 27.8. After MMT modification, the contrast between the matrix and the dispersed domains increases.



**FIGURE 27.7** Topographic image of (A) unmodified asphalt, (B) MMT-modified asphalt, and (C) OMMT-modified asphalt on a scale of  $15 \times 15\text{ }\mu\text{m}$ . The color contrast covers a height variation of  $\sim 120\text{ nm}$  [17].



**FIGURE 27.8** Phase image of (A) unmodified bitumen, (B) MMT-modified bitumen, and (C) OMMT-modified bitumen on a scale of  $15 \times 15\text{ }\mu\text{m}$  [17].



This is because MMT and OMMT interact in a different way with the dispersed domains and the matrix in asphalt during the melt blending process. AFM image arises from changes in composition and stiffness across a sample surface. The greater the contrast between the domains in the friction image, the greater the difference in stiffness and composition. In MMT-modified asphalt, the phase contrast (Fig. 27.8B) is inverted relative to unmodified asphalt (Fig. 27.8A). This indicates a change in the tip–sample interactions, which are affected by the sample modulus, and hydrophilic/hydrophobic interactions between the tip and the sample. In the dark-looking regions in Fig. 27.8B, the stiffness is increased with the introduction of MMT, so the stiffness in these areas is relatively higher than that of the other parts. As a result, the phase contrasts are inverted [17].

However, after OMMT modification, OMMT-modified asphalt shows a similar phase image as unmodified asphalt except with increased phase contrast due to the good compatibility between the OMMT and asphalt. This is because MMT is modified by organic intercalated agents. The dispersed domains containing “bee-like” structures are the aromatic compounds, and the organic intercalated agents contain a benzyl chain. Based on the principle of similarity, OMMT shows a better interaction with the dispersed domains in comparison with the matrix in asphalt. Hence, the stiffness of the dispersed domains is increased [17].

### 27.2.5 Compatibility analysis between organic layered silicate and asphalt

A high-temperature storage stability test is used to estimate the compatibility between OLS and asphalt. The experimental system consists of a tube (25.4 mm in diameter and 140 mm in height), vertically placed in an oven, at 163°C for 48 h, followed by cooling down to room temperature and being cut into three equal sections. The softening points of the upper and lower parts materials are then determined. If the difference between the softening points of the top and the bottom sections ( $\Delta S$ ) is very small, the sample is considered to have good compatibility. Otherwise, it is designated as unstable.

The high-temperature storage stabilities of REC- and OREC-modified asphalts are shown in Fig. 27.9. It can be seen that REC and OREC show good compatibility with asphalt. The  $\Delta S$  for the modified asphalts are all lower than 1.5°C. After organic modification, the  $\Delta S$  is decreased from 1.1°C to 0.8°C in CTAB–REC-modified asphalt. Compared with CTAB–REC, the  $\Delta S$  are further reduced to 0.5°C in ODBA–REC-modified asphalt since the benzyl chain in ODBA increases the adsorption effect of asphalt molecules on individual REC layers, which contributes to the good compatibility between the ODBA–REC and asphalt [11].

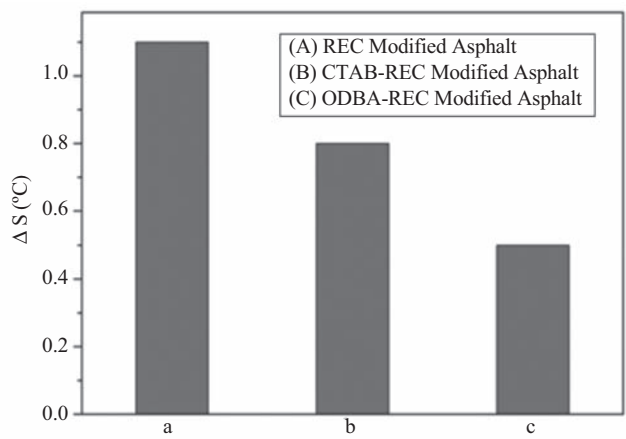


FIGURE 27.9 High-temperature storage stabilities of REC- and OREC-modified asphalts [11].

TABLE 27.4 Effect of REC and OREC on the physical properties of asphalt [11].				
Samples	Penetration/ 0.1 mm	Softening point (°C)	Ductility/ (10°C, cm)	Viscosity/ (60°C, Pa·s)
Unmodified asphalt	60	50.5	11.5	292
REC-modified asphalt	61	51.9	9.5	315
ODBA–REC-modified asphalt	62	52.1	10.1	325
CTBA–REC-modified asphalt	63	52.3	10.5	340

27.2.6 Physical properties of organic layered silicate-modified asphalts

The effects of REC and OREC on the physical properties of the asphalt are shown in Table 27.4. Compared with the unmodified asphalt, the softening point, penetration, and viscosity of the REC- and OREC-modified asphalt are increased, whereas the ductility at 10°C is decreased in varying degrees. However, the ductility at 10°C of the OREC-modified asphalts is higher than that of the REC-modified asphalt. This indicates that organic modification of REC prevents the decreasing of ductility. The OREC-modified asphalts show higher increases in softening point and viscosity because of the induction of

organic intercalated agents. Compared with ODBA–REC-modified asphalt, the softening point and viscosity of CTAB–REC-modified asphalt is further increased, which may be attributed to the formation of an exfoliated structure in the modified asphalt. The individual silicate layers with high aspect ratios in the exfoliated structure greatly obstruct the movement of asphalt molecule [11].

## 27.2.7 Antiaging properties of organic layered silicate-modified asphalts

### 27.2.7.1 Physical properties

Generally, the aging degree of the asphalt binder can be evaluated by physical aging indexes (e.g., viscosity aging index VAI, softening point increment SPI, ductility retention ratio DRR, and penetration retention ratio PRR). These aging indexes are calculated by the formulas (27.1)–(27.4). The higher the value of VAI and SPI, the deeper the degree of asphalt aging, while the DRR and PRR are reversed.

$$\text{VAI} = (\text{Aged viscosity} - \text{Unaged viscosity}) / \text{Unaged viscosity} \times 100 \quad (27.1)$$

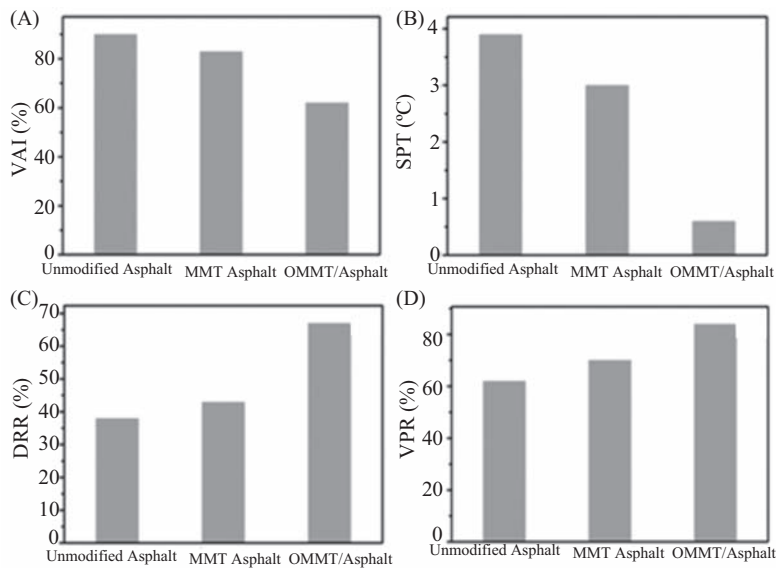
$$\text{SPI} = \text{Aged softening point} - \text{Unaged softening point} \quad (27.2)$$

$$\text{DRR} = \text{Aged ductility} / \text{Unaged ductility} \times 100 \quad (27.3)$$

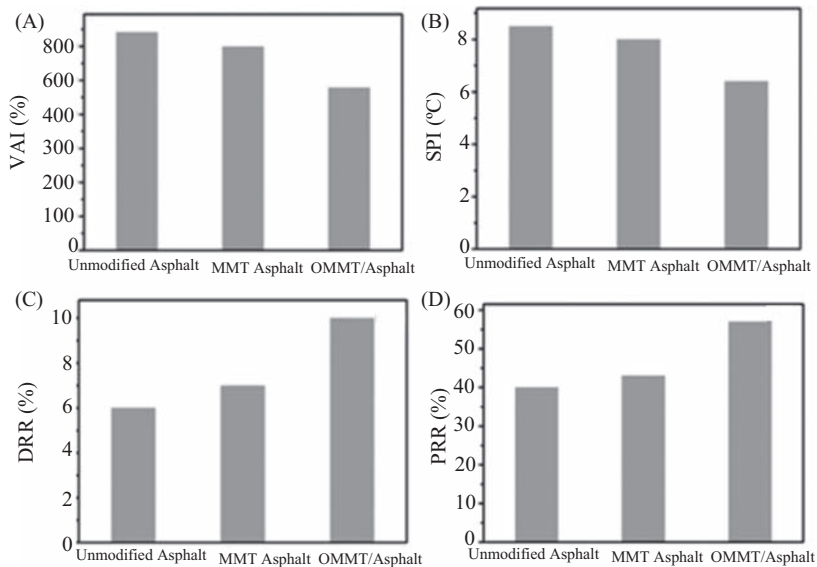
$$\text{PRR} = \text{Aged penetration} / \text{Unaged penetration} \times 100 \quad (27.4)$$

Fig. 27.10A–D and 27.11A–D show the physical aging indexes of MMT and OMMT (ODBA–MMT)-modified asphalts after thin film oven test (TFOT) and pressure aging vessel (PAV) aging, respectively. As can be seen, VAI and SPI values of MMT and OMMT-modified asphalts are lower than that of the unmodified asphalt, while DRR and PRR are higher than that of the unmodified asphalt, especially for the OMMT-modified asphalt, which indicates the good short-term and long-term thermal oxidation aging resistance of OMMT-modified asphalt. This is because the asphalt molecules are intercalated into the interlayer of OMMT, and then the intercalated structure shows good barrier properties to oxygen during aging and reduces the oxidation of asphalt. However, for MMT-modified asphalt, MMT shows poor interactions with asphalt by forming a phase-separated structure [18].

The VAI values of LS and OLS (ODBA–LS)-modified asphalts before and after TFOT and PAV aging are shown in Table 27.5. It can be seen that the VAI values of the binders are increased after both TFOT and PAV aging, indicating the hardening of the binders during the aging process. However, the VAI values are decreased with the introduction of LS. In addition, these values are further decreased for OLS-modified asphalts. This implies the good thermal oxidation aging resistance of LS- and OLS-modified asphalts. As should be obvious, the influence of LS and OLS on the aging properties



**FIGURE 27.10** (A) VAI, (B) SPI, (C) DRR, and (D) PRR of MMT- and OMMT-modified asphalts after TFOT aging [18].



**FIGURE 27.11** (A) VAI, (B) SPI, (C) DRR, and (D) PRR of MMT- and OMMT-modified asphalts after PAV aging [18].

**TABLE 27.5** VAI of LSs and OLSs-modified asphalts after TFOT and PAV aging [15].

Sample	VAI (%)	
	TFOT aging	PAV aging
Unmodified asphalt	88	832
Asphalt/MMT	76	780
Asphalt/OMMT	70	760
Asphalt/REC	70	732
Asphalt/OREC	65	703
Asphalt/EVMT	54	659
Asphalt/OEVMT	49	590

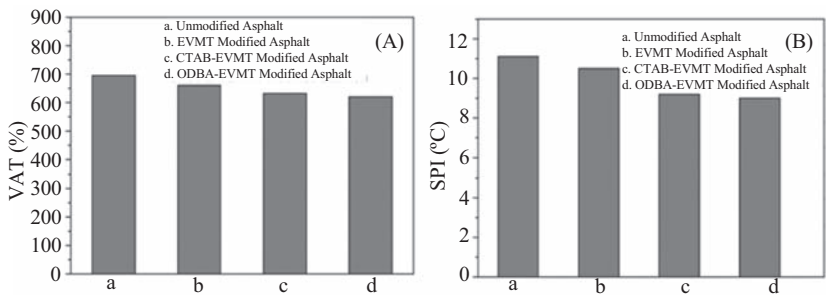


**FIGURE 27.12** (A) VAI and (B) SPI of EVMT- and OEVMT-modified asphalts after UV aging [19].

of asphalt depends on the microstructures of the modified asphalts. OEVMT-modified asphalt with exfoliated nanostructure has the lowest VAI values after TFOT and PAV aging. Compared with MMT-modified asphalt, REC-modified asphalt with intercalated nanostructure shows relatively lower VAI values, similar to the results after organic modification of REC [15].

Like other polymers, asphalt molecules are easy to reach to its excited states that are easily oxidized in the presence of oxygen by the influence of the ultraviolet (UV) radiation. The influence of UV aging on VAI and SPI of EVMT- and OEVMT-modified asphalts is shown in Fig. 27.12A and B, respectively. As can be seen, after UV aging, the VAI and SPI values of the asphalt are decreased to some extent after modification. In addition, the decreased degree of OEVMT-modified asphalts relative to unmodified asphalt is more obvious than that of EVMT-modified asphalt. This is because the diffusion of oxygen in the asphalt

matrix is encumbered by EVMT and OEVMT silicate layers. As a result, the UV aging resistance of asphalt is improved. However, the improved aging resistance of the binders after thermooxidative aging (e.g., PAV aging) is more obvious than that after UV aging [19].

### 27.2.7.2 Atomic force microscopy

The topographic images of unmodified asphalt, MMT-modified asphalt, and OMMT (HDBA–MMT)-modified asphalt after UV aging are shown in Fig. 27.13. The corresponding phase images of unmodified asphalt, MMT-modified asphalt, and OMMT-modified asphalt after UV aging are shown in Fig. 27.14. Compared with unaged samples (as seen in Figs. 27.7 and 27.8), the contrast between the matrix and the dispersed domains in the aged samples is significantly decreased. In particular, for the unmodified asphalt, the boundary between the matrix and the dispersed domains disappears. This implies a great association of the dispersed domains in the asphalt appears during UV aging, which can be explained by the fact that oxidation leads to a decrease of the difference in chemical properties between the dispersed domains and the matrix. Before aging, the domains can disperse in the matrix steadily, but after aging, they cannot. Consequently, the difference in stiffness between the two phases is reduced. There is also a single-phase trend of the asphalt during UV aging (Fig. 27.14A). Based on the contrast changes between the dispersed phase and the matrix, it is reasonable to assume that the stiffness of the matrix in asphalt is increased, which leads to hardening of the asphalt [17].

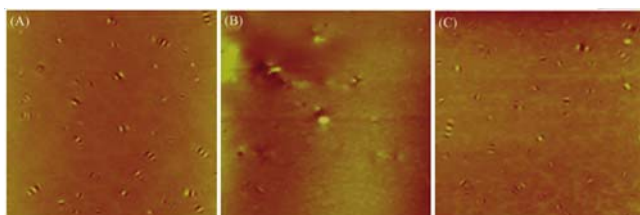


**FIGURE 27.13** Topographic image of (A) unmodified asphalt, (B) MMT-modified asphalt, and (C) OMMT-modified asphalt after UV aging on a scale of  $15 \times 15 \mu\text{m}$ . The color contrast covers a height variation of  $\sim 120 \text{ nm}$  [17].

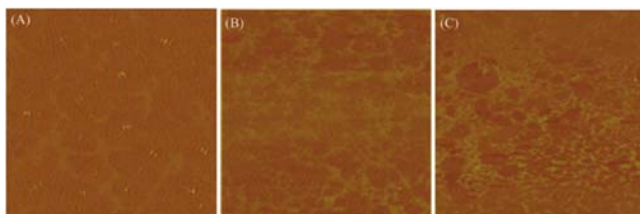


**FIGURE 27.14** Phase image of (A) unmodified bitumen, (B) MMT-modified bitumen, and (C) OMMT-modified bitumen after UV aging on a scale of  $15 \times 15 \mu\text{m}$  [17].

Compared with unmodified asphalt, the contrast between the matrix and the dispersed domains in MMT-modified asphalt is still obvious after UV aging (Fig. 27.13B and C). Moreover, there are still two phases in MMT-modified asphalt (Fig. 27.14B and C). It can be observed that association of the asphalt molecules in the dispersed domains due to various chemical and physical interactions is prevented and the single-phase trend of the asphalt is also obstructed by the introduction of MMT. In contrast with MMT-modified asphalt, the phase contrast between the matrix and the dispersed domains in OMMT-modified asphalt is more obvious after UV aging. This indicates that the association interactions and single-phase trend of the asphalt during UV aging can be further prevented after organic modification of MMT, indicating the good aging resistance of OMMT-modified asphalt [17].

## 27.3 Application of surface modification inorganic nanoparticles in asphalt

### 27.3.1 Preparation of SMINs and surface modification inorganic nanoparticles-modified asphalts

#### 27.3.1.1 Preparation of surface modification inorganic nanoparticles

Silane coupling agents [e.g.,  $\gamma$ -methacryloxypropyl trimethoxy silane (MTS), 3-aminopropyltriethoxysilane (APTS), and  $\gamma$ -(2, 3-epoxypropoxy) propyltrimethoxy-silane (EPTMS)] are used to modify the inorganic nanoparticles (e.g., nano-ZnO, nano-SiO<sub>2</sub>, and nano-TiO<sub>2</sub>) surface. First, inorganic nanoparticles (INs) are mixed into the ethanol water solution containing the silane coupling agent. By using a paddle agitator, the pH value of the suspension is controlled at 6.0 using acetic acid (95 wt.%). Then the suspension is stirred for 5 h. After that, ethanol water solution is removed by a filtration process. The treated IN is repeatedly washed by acetone. The washed inorganic nanoparticle is then placed in a vacuum oven to dry at 120°C for 4 h [10,20,21].

#### 27.3.1.2 Preparation of surface modification inorganic nanoparticle-modified asphalts

Asphalt is heated to 150°C  $\pm$  5°C in an oil-bath heating container until it flows fully. Then a certain amount of IN or SMIN is added into asphalt, and the mixture is blended at 5000 rpm for 60 min by using a high shear mixer. After that, the mixture is blended using a paddle agitator at a rotation speed of 2000 rpm for about 90 min to produce modified asphalt. The same process is also performed on the base asphalt in order to compare it with the modified asphalt.

### 27.3.2 UV–visible absorbance and reflectance spectra analysis of INs

UV–visible diffuse reflectance spectra of the INs are obtained from dry-pressed disk samples with a UV–visible spectrometer (UV2550, Shimadzu, Japan).  $\text{BaSO}_4$  is used as a reflectance standard in the UV–visible diffuse reflectance experiments.

Fig. 27.15 shows the UV–visible absorbance and reflectance spectra of INs. As can be seen, nano- $\text{SiO}_2$  has good reflecting for UV–visible light (200–800 nm); the average reflectance is more than 50%. The average reflectance is near 100% for UV-A (315–400 nm) and UV-B (300–315 nm). Compared with nano- $\text{SiO}_2$ , nano- $\text{TiO}_2$  and nano- $\text{ZnO}$  show good absorbing properties for UV-A and UV-B. Furthermore, nano- $\text{ZnO}$  shows better absorbing properties than nano- $\text{TiO}_2$ . The highest absorbance of nano- $\text{ZnO}$  is near 1.4, while the highest absorbance of nano- $\text{TiO}_2$  is 1.2 [22].

### 27.3.3 Fourier transform infrared spectroscopy analysis of surface modification inorganic nanoparticles

The FTIR spectra of INs before and after surface modification by 3-aminopropyltriethoxysilane (APTS) are shown in Fig. 27.16. As shown in Fig. 27.16A, the broad peak at  $3451\text{ cm}^{-1}$  is caused by asymmetrical stretching vibration of  $-\text{OH}$  and the peak at  $1636\text{ cm}^{-1}$  is caused by bending vibration of  $\text{H}-\text{O}-\text{H}$  due to the physical and chemical water in nano- $\text{SiO}_2$ . The peaks at  $1096\text{ cm}^{-1}$  result from asymmetrical stretching vibration of  $\text{Si}-\text{O}-\text{Si}$ . In the spectra of surface-modified nano- $\text{SiO}_2$ . Except for the peaks in untreated nano- $\text{SiO}_2$ , the new peaks at 2926, 2855, and  $1468\text{ cm}^{-1}$  appear, which are caused by asymmetrical stretching vibration, symmetrical stretching vibration, and bending vibration of  $\text{C}-\text{H}$  ( $-\text{CH}_2-$ ) in the APTS, respectively. In Fig. 27.16B, the peaks at 3436 and  $668\text{ cm}^{-1}$  are caused by the stretching vibration of  $-\text{OH}$  and the vibration of  $\text{Ti}-\text{O}-\text{Ti}$  in nano-

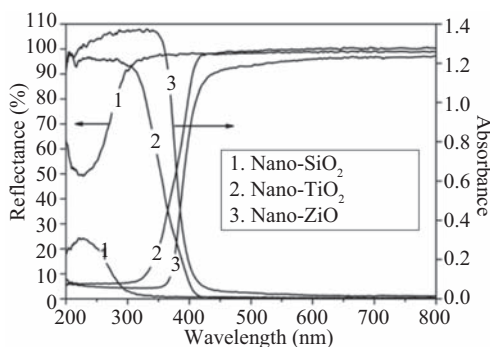
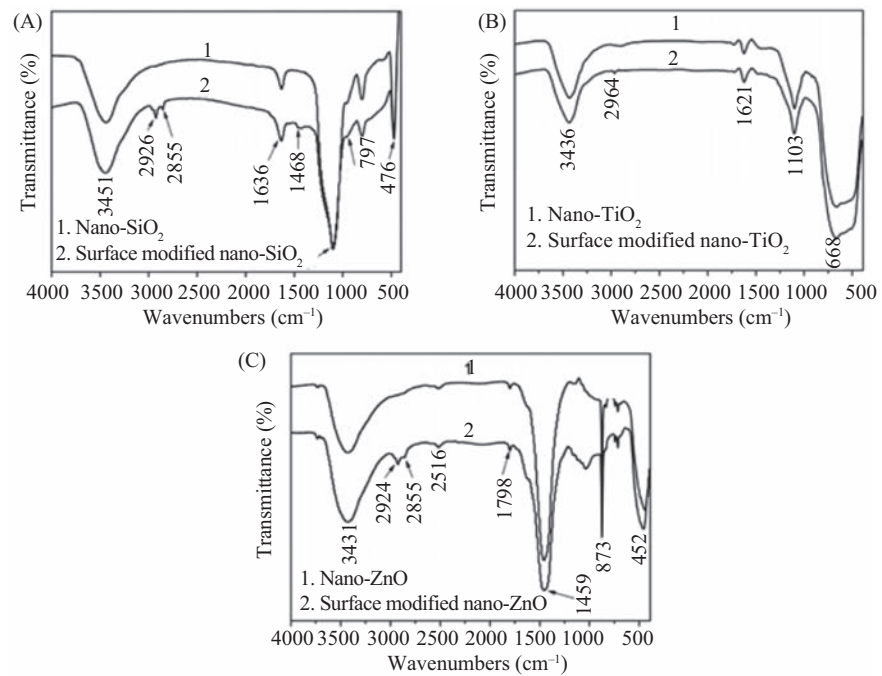
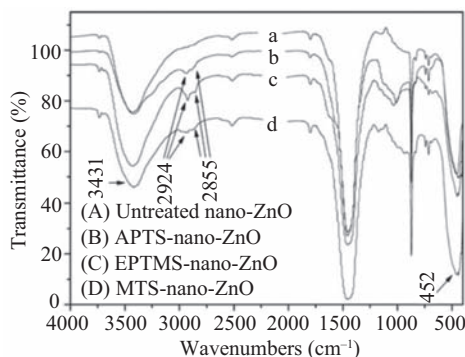


FIGURE 27.15 UV–visible absorbance and reflectance spectra of INs [22].





**FIGURE 27.16** FTIR spectra of INs and SMINs [22].



**FIGURE 27.17** FTIR spectra of nano-ZnO and surface-modified nano-ZnOs [20].

TiO<sub>2</sub>, respectively. Compared with untreated nano-TiO<sub>2</sub>, the new peaks at 2964 cm<sup>-1</sup> appear in surface-modified nano-TiO<sub>2</sub>, which are caused by the asymmetrical stretching vibration of C—H (—CH<sub>3</sub>) in the APTS. In Fig. 27.16C, similar to nano-SiO<sub>2</sub> and nano-TiO<sub>2</sub>, except for the peaks in untreated nano-ZnO, the new peaks at 2924 and 2855 cm<sup>-1</sup> in surface-modified nano-ZnO are indicated, which are caused by the C—H (—CH<sub>2</sub>—) asymmetrical stretching vibration and symmetrical stretching vibration in the APTS. All of the previous discussion indicates that APTS is successfully bound on the surface of three INs in the form of a chemical bond [22].

The FTIR spectra of nano-ZnO before and after surface modification by MTS, APTS, and EPTMS are shown in Fig. 27.17. The peaks at 3431 and 452 cm<sup>-1</sup> are caused by the stretching of —OH and Zn—O in nano-ZnO, respectively. In the spectra of MTS-nano-ZnO, APTS-nano-ZnO, and EPTMS-nano-ZnO, except for the peaks in nano-ZnO, the presence of new peaks at 2924 and 2855 cm<sup>-1</sup> is indicated. These peaks are caused by C—H (—CH<sub>2</sub>, —CH<sub>3</sub>) stretching and bending absorptions in the MTS, APTS, or EPTMS. This indicates that MTS, APTS, or EPTMS is successfully bound on the surface of nano-ZnO [20].

#### 27.3.4 Atomic force microscopy of surface modification inorganic nanoparticle-modified asphalts

The phase images of unmodified asphalt, nano-ZnO-modified asphalt, and EPTMS-nano-ZnO-modified asphalt are shown in Fig. 27.18. As can be seen the unmodified asphalt shows two separate domains, a homogeneous matrix and the dispersed domains (the dark-looking region) in that matrix. The dispersed domains show a succession of pale and dark lines, which are often called “bee-like” structures. After nano-ZnO modification, the dimension of “bee-like” structures is obviously decreased. The maximum dimension of “bee-like” structures is decreased from 3.047 to 2.109 μm. The average size

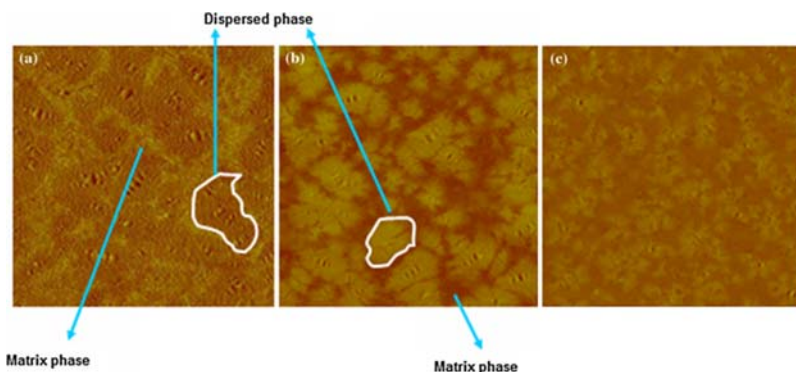


**FIGURE 27.18** Phase images of (A) unmodified asphalt, (B) asphalt/nano-ZnO, and (C) asphalt/EPTMS-nano-ZnO on a scale of  $15 \times 15 \mu\text{m}$  [10].

of particles in “bee-like” structures is also decreased. The appearance of the “bee-like” structures is attributed to the crystallization of the microcrystalline waxes ( $>C_{40}$ ) and/or waxy molecules contained in the asphaltenes, indicating that the crystal morphology is changed with the introduction of nano-ZnO. Compared with nano-ZnO-modified asphalt, the dimension of “bee-like” structures is further decreased in PTMS-nano-ZnO-modified asphalt. Moreover, the “bee-like” structures disperse in the asphalt more homogeneously. This can be explained as follows: during cooling from high to ambient temperature, the crystallization of microcrystalline waxes ( $>C_{40}$ ) and waxy molecules in asphalt occurs. Nano-ZnO particles dispersed in asphalt act as nucleating agents during the crystallization process, which contributes to the heterogeneous nucleation crystallization of asphaltenes. For nano-ZnO, its dispersion in asphalt is not homogeneous, which leads to the relatively large size of crystallization products (“bee-like” structures). However, EPTMS-nano-ZnO disperses in asphalt more homogeneously than nano-ZnO. There are more heterogeneous nucleation crystallization points in the asphalt. As a result, the dimension of crystals is further decreased and its dispersion in asphalt is more homogeneous [10].

### 27.3.5 Compatibility analysis of surface modification inorganic nanoparticle and asphalt

High-temperature storage stability test can be used to evaluate the compatibility of nano-ZnO and asphalt. If the difference between the softening points of the top and the bottom sections ( $\Delta S$ ) is very small, the sample is considered to have good high-temperature storage stability, indicating good compatibility between nano-ZnO and asphalt. As shown in Fig. 27.19, the  $\Delta S$  is  $1.3^\circ\text{C}$  for untreated nano-ZnO-modified asphalt. After surface modification,

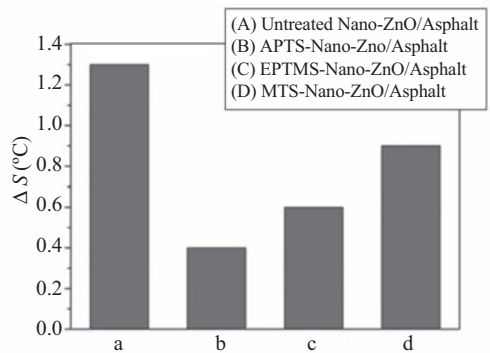


FIGURE 27.19 High-temperature storage stability of the nano-ZnO-modified asphalts [20].

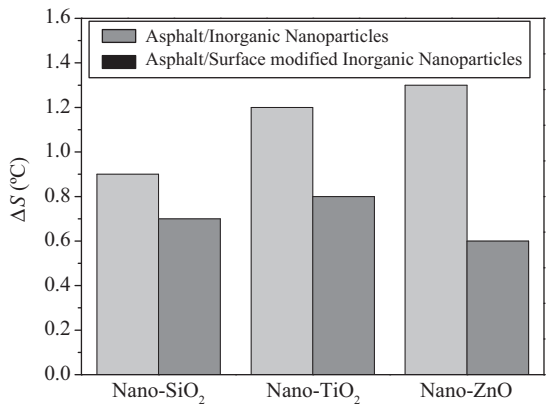


FIGURE 27.20 Influence of surface modification on compatibility between INs and asphalt [23].

the  $\Delta S$  is decreased obviously. this indicates that the compatibility between nano-ZnO and asphalt is improved by its surface modification. However, the influence of surface modification on the high-temperature stability of nano-ZnO-modified asphalt depends on the surface modifiers.

The  $\Delta S$  for APTS- and EPTMS-nano-ZnO-modified asphalts is lower than that of MTS-nano-ZnO-modified asphalt. Compared with EPTMS-nano-ZnO-modified asphalt, the  $\Delta S$  for APTS-nano-ZnO-modified asphalt is further decreased [20].

The  $\Delta S$  is shown for different IN-modified asphalt in Fig. 27.20. Before surface modification, the  $\Delta S$  of nano-SiO<sub>2</sub>, nano-TiO<sub>2</sub>, and nano-ZnO-modified asphalt are 0.9°C, 1.2°C, and 1.3°C, respectively, which indicates that the compatibility between nano-SiO<sub>2</sub> and asphalt is better than that between nano-TiO<sub>2</sub> or nano-ZnO and asphalt. After surface modification (silane coupling agent is EPTMS), the compatibility between INs and asphalt

is improved obviously compared with before surface modification. Especially for nano-ZnO, after surface modification, the  $\Delta S$  is decreased obviously to only 0.6°C, indicating that the compatibility between nano-ZnO and asphalt is better than that between nano-SiO<sub>2</sub> or nano-TiO<sub>2</sub> and asphalt after surface modification [23].

27.3.6 Physical properties of surface modification inorganic nanoparticle-modified asphalts

The effects of different INs before and after surface modification on penetration, softening point, viscosity (60°C), and ductility (10°C) are shown in Figs. 27.21–27.24, respectively. As shown in Fig. 27.21, before surface

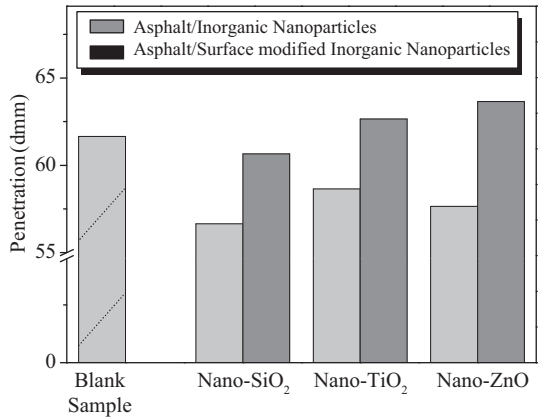


FIGURE 27.21 Effect of INs and SMINs on penetration of asphalt [23].

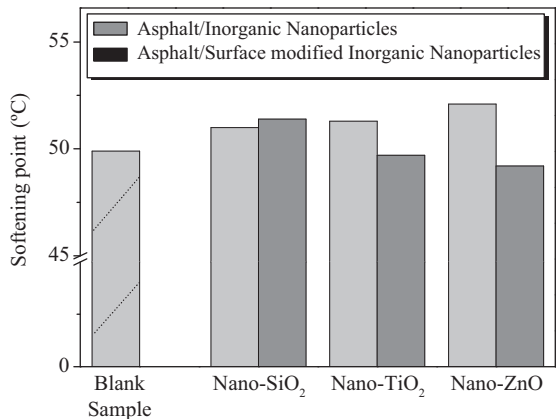


FIGURE 27.22 Effect of INs and SMINs on softening point of asphalt [23].

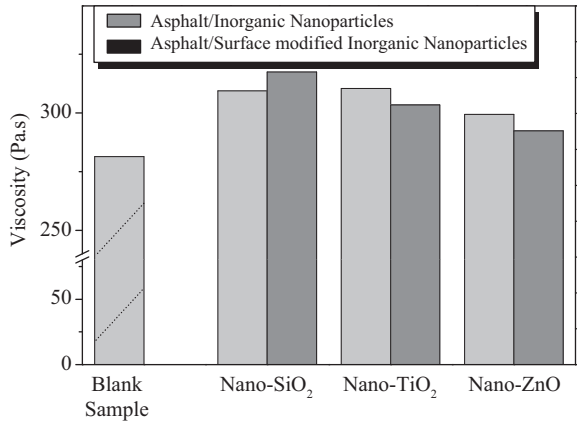


FIGURE 27.23 Effect of INs and SMINs on viscosity of asphalt [23].

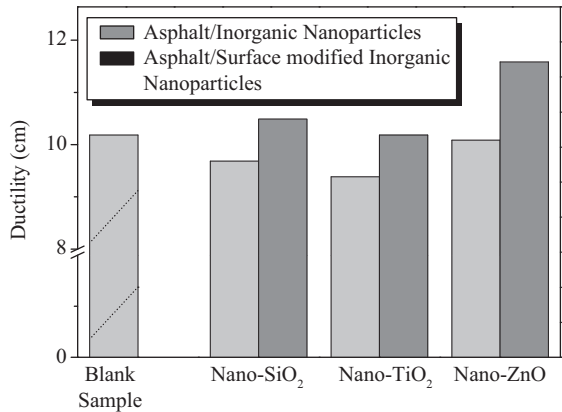


FIGURE 27.24 Effect of INs and SMINs on ductility of asphalt [23].

modification, the penetration is decreased about 4~6 dmm with the addition of INs. However, after surface modification (silane coupling agent is EPTMS), the penetration is increased obviously compared with before surface modification, especially for nano-ZnO. This is because INs without surface modification show agglomeration phenomena in the asphalt, which limits the movement of the molecular chains of the asphalt and increases the consistency of the asphalt under 25°C test temperature condition. However, surface modification can enhance the dispersion degree of INs in asphalt, then with the addition of INs, can increase the distance between asphalt molecules, reduce the intermolecular forces, and make the movement of molecular chains of the asphalt easier. Impact energy can be consumed

through the relaxation of molecular chains of asphalt when the standard needle free falls and penetrates into asphalt. Consequently, the penetration is increased [23].

As shown in Fig. 27.22, after adding INs, the softening point of IN-modified asphalt is increased to some extent, but different INs have different influence on the softening point of asphalt. The relationship of the softening points of three IN-modified asphalt is  $\text{nano-ZnO} > \text{nano-TiO}_2 > \text{nano-SiO}_2$ . Compared with  $\text{nano-TiO}_2$  and  $\text{nano-SiO}_2$ , the softening point increment of  $\text{nano-ZnO}$ -modified asphalt relative to blank sample is maximum, which is  $2.1^\circ\text{C}$ . This is because INs added in asphalt present agglomeration phenomena, which limits the movement of the molecular segments of asphalt. In the process of temperature programming, the softening point shows some lag, as is shown by the increasing softening point. However, it can be seen that the softening point of  $\text{nano-SiO}_2$ -modified asphalt has little change before and after surface modification, while the softening points of  $\text{nano-ZnO}$ -modified asphalt and  $\text{nano-TiO}_2$ -modified asphalt are decreased obviously before and after surface modification. Especially for  $\text{nano-ZnO}$ -modified asphalt, the softening point is decreased by  $2.9^\circ\text{C}$ , which is closed to that of blank sample. This is because surface modification improves dispersion between INs and asphalt. INs added in asphalt weaken the intermolecular forces. As temperature increases, the movement ability of molecular chains of asphalt with SMINs is stronger than the movement ability of molecular chains of asphalt with no surface-modified INs, and the softening point is reduced accordingly. From the above discusses, the effect of surface modification on the dispersion  $\text{nano-ZnO}$  in asphalt is the most obvious of the three INs, followed by  $\text{nano-TiO}_2$ , and  $\text{nano-SiO}_2$  is the weakest [23].

As shown in Fig. 27.23, compared with the blank sample, the viscosities of modified asphalt with INs before and after surface modification are different. The viscosity ranking of three IN-modified asphalts is  $\text{nano-SiO}_2 > \text{nano-TiO}_2 > \text{nano-ZnO}$ . Compared with  $\text{nano-TiO}_2$  and  $\text{nano-ZnO}$ , the  $\text{nano-SiO}_2$ -modified asphalts have higher viscosity, and the asphalt with surface-modified  $\text{nano-SiO}_2$  has the highest viscosity, increased by  $36 \text{ Pa} \cdot \text{s}$  compared with the blank sample. This indicates that the surface modification of  $\text{nano-SiO}_2$  further enhances the viscosity of the modified asphalt. In contrast to  $\text{nano-SiO}_2$ , the viscosity of the modified asphalt with surface-modified  $\text{nano-TiO}_2$  or  $\text{nano-ZnO}$  is lower than that of modified asphalt with no surface-modified  $\text{nano-TiO}_2$  or  $\text{nano-ZnO}$ . The viscosity characterizes the flow and deformation capacity of asphalt under specific test condition ( $60^\circ\text{C}$ ). Because INs without surface modification added in asphalt present the agglomeration phenomena, which limits the movement of molecule chains of the asphalt and obstructs the flow and deformation of asphalt. All the above illustrates that surface modification improves the compatibility between INs and asphalt and the dispersion degree of INs in asphalt. Particularly for  $\text{nano-TiO}_2$  and  $\text{nano-ZnO}$ , INs added in asphalt weaken

intermolecular forces. The movement ability of molecular chains of modified asphalt with SMINs is stronger than that of modified asphalt with no surface-modified INs, and the flow and deformation capacity of modified asphalt are strengthened accordingly, thus decreasing their viscosity [23].

As shown in Fig. 27.24, compared with the blank sample, INs without surface modification added to asphalt make the ductility decrease to some extent, and the effect of nano-ZnO is minimum. However, the ductility of asphalt with SMINs increases compared with that of asphalt with nonsurface-modified INs, and all measured ductility values of asphalt with SMINs are bigger than that of the blank sample. This indicates that SMINs can enhance the plastic deformability of asphalt, especially for asphalt with surfaced-modified nano-ZnO [23].

27.3.7 Antiaging properties of surface modification inorganic nanoparticle-modified asphalts

27.3.7.1 Physical properties

The VAI and SPI values of asphalt with different INs after UV aging are shown in Fig. 27.25, respectively. As can be seen, all INs added in asphalt can reduce the VAI and SPI values of asphalt after UV aging. In particular, for nano-ZnO, the VAI and SPI values relative to the blank sample are reduced by 39% and 0.8°C, respectively. According to the UV-Vis absorbance spectra of the three types of INs, as shown in Fig. 27.15, the longest absorption wavelength of nano-TiO<sub>2</sub> in the UV-Vis absorbance spectra is 300 nm, while the longest absorption wavelength of nano-ZnO is 370 nm. It can be seen the absorption range of nano-ZnO to UV light far exceeds the absorption range of nano-TiO<sub>2</sub>. For nano-SiO<sub>2</sub>, the shield effect on UV light

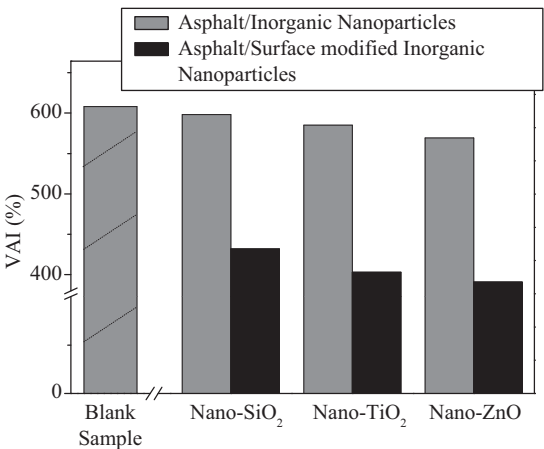
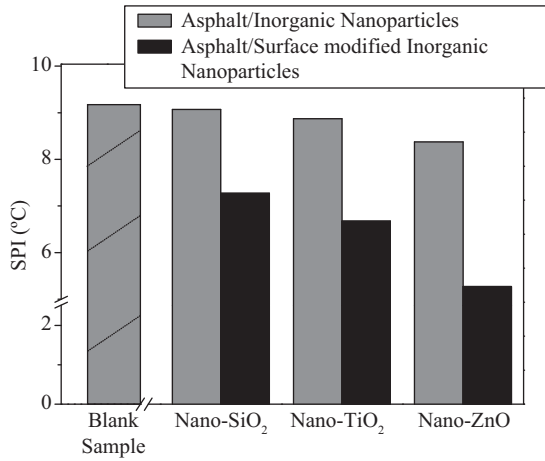


FIGURE 27.25 VAI of INs and SMIN-modified asphalts after UV aging [23].





**FIGURE 27.26** SPI of INs and SMIN-modified asphalts after UV aging [23].

is mainly based on the reflection effect. This indicates that the absorption effect of INs on UV is more effective than the reflection effect of INs on UV radiation and thus provides more UV aging resistance for asphalt [23].

After surface modification, the VAI and SPI values of three IN-modified asphalts relative to the blank sample or asphalt with no surface-modified INs are obviously decreased. Thus surface modification significantly improves the effect of INs on the UV aging resistance of asphalt. This is because surface modification improves the dispersion INs in asphalt, then relatively uniform dispersed INs have an more obvious effect on shielding UV radiation and can effectively inhibit the effect of UV aging process on hardening of asphalt. Compared with nano-SiO<sub>2</sub> and nano-TiO<sub>2</sub>, the VAI and SPI values of asphalt with surface-modified nano-ZnO are decreased by 217% and 3.9°C, indicating that the effect of surface-modified nano-ZnO on UV aging resistance of asphalt is better than that of surface-modified nano-SiO<sub>2</sub> and nano-TiO<sub>2</sub>. This is due to the fact that the dispersion of surface-modified nano-ZnO in asphalt is more homogeneous than surface-modified nano-SiO<sub>2</sub> or surface-modified nano-TiO<sub>2</sub>. Consequently, surface-modified nano-ZnO can better shield UV radiation, thus making it good for UV aging resistance [23].

Fig. 27.27 shows the VAI values of OEVMT (SQAC–EVMT) and APTS-nano-ZnO-modified asphalts after PAV and UV aging. As can be seen, the VAI values of asphalt decrease from 901% to 553% after modification by OEVMT, indicating good thermooxidative aging resistance. Oxidation of the asphalt is prevented due to the barrier properties of the EVMT layers that form an exfoliated nanostructure. However, nano-ZnO-modified asphalt shows similar VAI values as unmodified asphalt after PAV aging, indicating that nano-ZnO has little influence on the thermooxidative aging properties of asphalt [24].

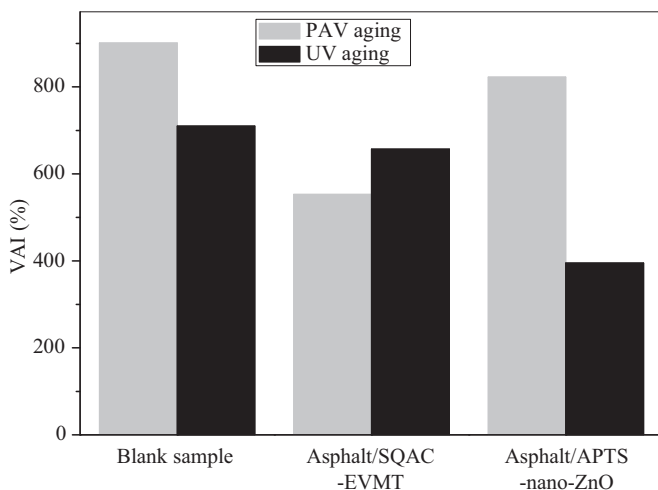


**FIGURE 27.27** VAI of OLS- and SMIN-modified asphalts after PAV and UV aging [24].

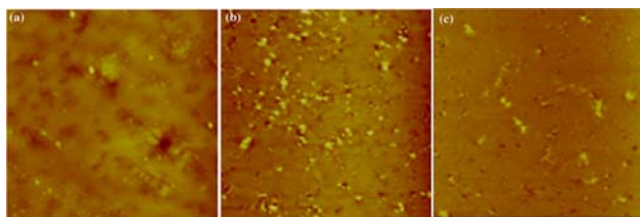


**FIGURE 27.28** Topographic images of (A) unmodified asphalt, (B) asphalt/nano-ZnO, and (C) asphalt/EPTMS-nano-ZnO after UV aging on a scale of  $15 \times 15 \mu\text{m}$  [10].

In addition, as shown in Fig. 27.27 the OEVMT-modified asphalt has similar VAI values as unmodified asphalt, indicating that OEVMT has little effect on the UV aging resistance of asphalt. However, the VAI values of asphalt decrease from 710% to 395% with the addition of nano-ZnO, indicating the good UV aging resistance of nano-ZnO-modified asphalt. Nano-ZnO has good absorbance of UV light (the highest absorbance value reaches 1.4). The influence of UV radiation on asphalt molecules can be effectively reduced during UV aging, which contributes to the improved UV aging resistance of nano-ZnO-modified asphalt [24].

### 27.3.7.2 Atomic force microscopy

The topographic images of unmodified asphalt, nano-ZnO-modified asphalt, and EPTMS-nano-ZnO-modified asphalt after UV aging are shown in Fig. 27.28. The corresponding phase images of unmodified asphalt, nano-ZnO-modified asphalt, and EPTMS-560-nano-ZnO-modified asphalt after UV aging are shown in Fig. 27.29, respectively. As shown in Fig. 27.30A, the “bee-like” structures disappear and the surface of the unmodified asphalt

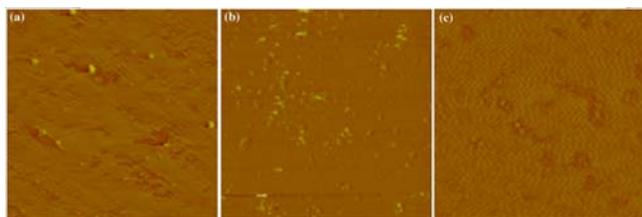


**FIGURE 27.29** Phase images of (A) unmodified asphalt, (B) asphalt/nano-ZnO, and (C) asphalt/EPTMS-nano-ZnO after UV aging on a scale of  $15 \times 15 \mu\text{m}$  [10].

becomes very rough after UV aging. In Fig. 27.31A, there is only one phase for unmodified asphalt after UV aging, showing there is a single-phase trend of unmodified asphalt during UV aging. However, the surface of nano-ZnO-modified asphalt after UV aging is relatively smooth, and the “bee-like” structures are still obvious (Fig. 27.28B). In addition, there are still two phases in EPTMS-nano-ZnO-modified asphalt after UV aging (Fig. 27.29C), implying that the single-phase trend of asphalt is prevented by EPTMS-nano-ZnO during UV aging [10].

## 27.4 Applications of multidimensional nanomaterials in asphalt

### 27.4.1 Preparation of multidimensional nanomaterials-modified asphalts

Three types of base asphalts (called 70#, 90#, and 110#) from different origins are adopted. 70#, 90#, and 110# asphalts are 60/80, 80/100, and 100/120 penetration-grade asphalt, respectively. The MN contains EPTMS-nano-ZnO and CTAB–OEVMT. MN-modified asphalt is prepared with the following procedure: asphalt is first heated to  $150 \pm 5^\circ\text{C}$  in an oil-bath heating container until it flows fully. Then MN containing 1% EPTMS-nano-ZnO + 3% CTAB–OEVMT by weight of asphalt is interfused into the asphalt. The mixture is sheared at 4000 r/min for 1 h using a high-speed shear apparatus. Subsequently, it is stirred at 2000 rpm for 1.5 h using a paddle agitator. The blank sample is obtained using the same process [25].

### 27.4.2 Physical properties of multidimensional nanomaterials-modified asphalts

Effects of MN on softening point, penetration ( $25^\circ\text{C}$ ), viscosity ( $60^\circ\text{C}$ ), and ductility ( $15^\circ\text{C}$ ) are shown in Fig. 27.30A–D, respectively. As shown in Fig. 27.30A, the addition of MN enhances softening point of the three asphalts. Furthermore, the softening point increment of 70# and 90# asphalt are  $2.5^\circ\text{C}$  and  $2.4^\circ\text{C}$ , separately, while that of 110# asphalt is more obvious about  $2.8^\circ\text{C}$ . This show that MN can effectively improve the

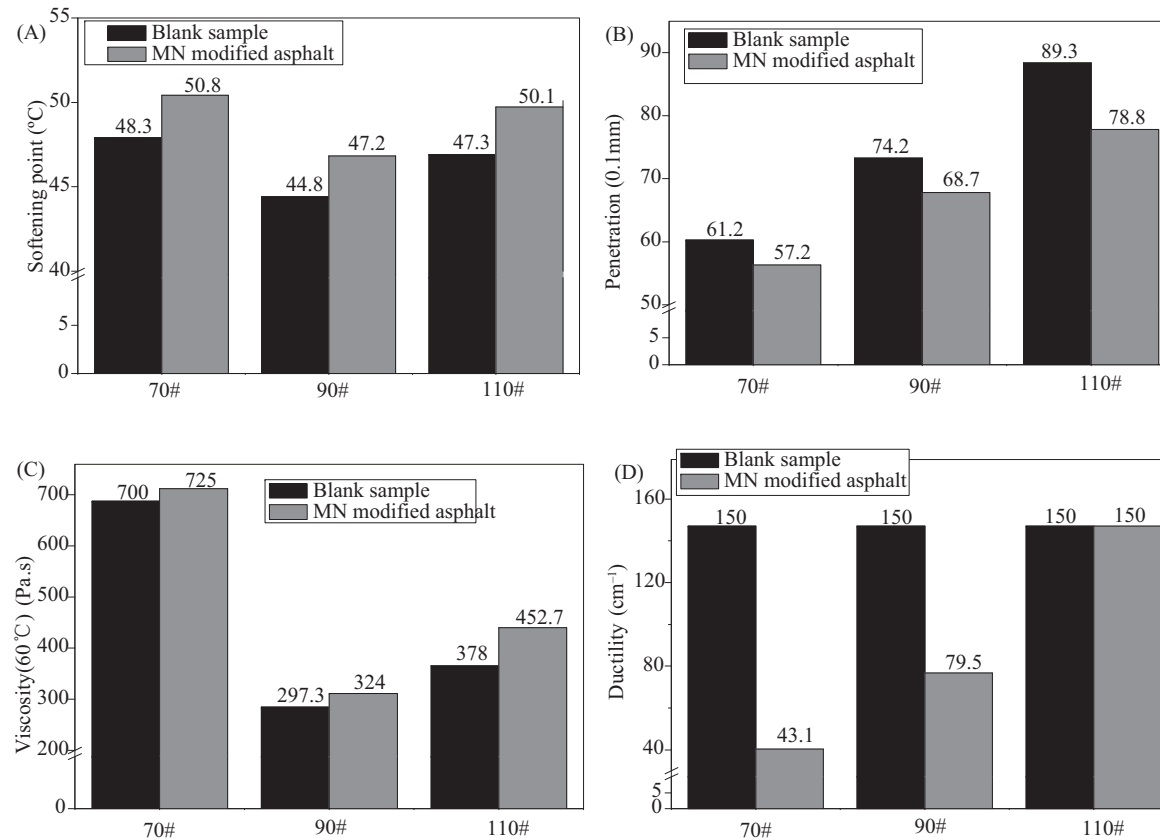


**FIGURE 27.30** Effect of MN on the physical properties of different asphalts [26].

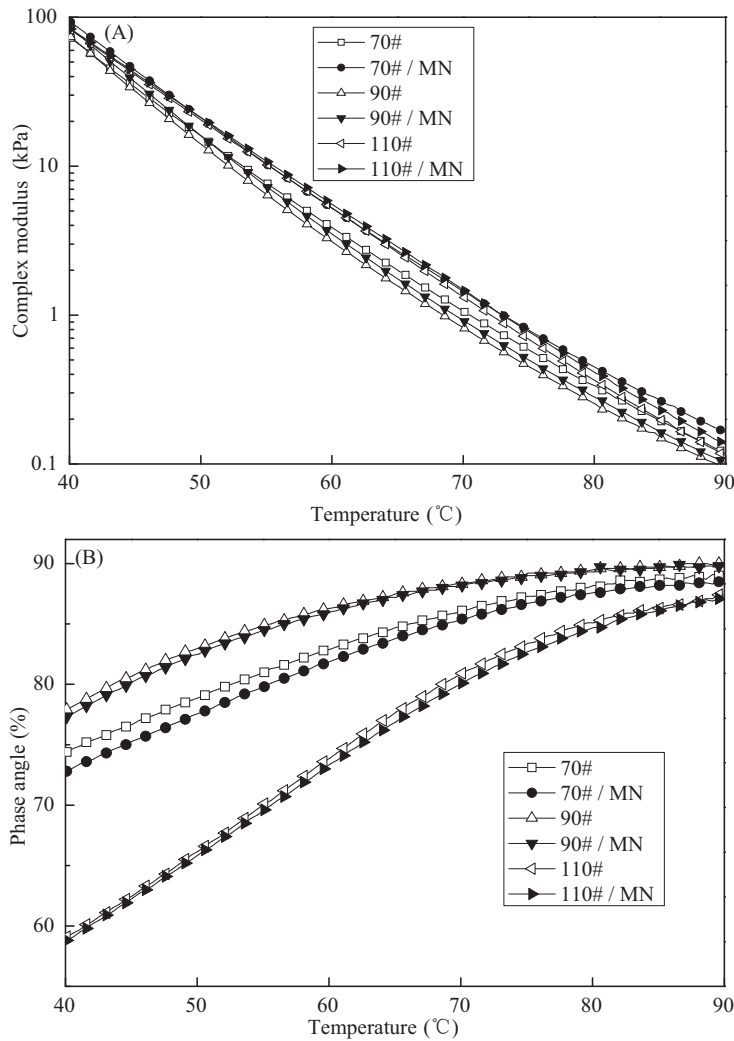


**FIGURE 27.31** Effect of MN on the rheological properties of different asphalts [27].

high-temperature stability of different asphalts. Moreover, the improvement in 110# asphalt is more obvious than for 70# and 90# asphalt.

Fig. 27.30B shows that the penetration of MN-modified asphalt is smaller than that of the blank sample. The ranking of the penetration decrement of the three types of asphalt before and after modification with MN is  $70\# < 90\# < 110\#$ , and the values are 4.0, 5.7, and 10.5 dmm, respectively. It implies that the consistencies of three asphalts increase after adding MN and the increment of 110# asphalt consistency is the greatest.

As seen in Fig. 27.30C, the viscosities of the three asphalts are enhanced by adding MN. The ranking of viscosity increment for three asphalts before and after modification with MN is 70# < 90# < 110#, and the increments are 25.0, 26.7, and 74.7 Pa·s, respectively. This indicates that the addition of MN can reduce the flow and deformation capacity of asphalt (the reduction for 110# asphalt is the most obvious).

As shown in Fig. 27.30D, the influence of MN on the ductility values of the three asphalts is different. In terms of the 70# and 90# asphalt, the ductility declines to some extent after adding MN. The ductility of 70# asphalt drops from 150.0 to 43.1 cm and that of 90# asphalt drops from 150.0 to 79.5 cm. With regard to 110# asphalt, the ductility is unchanged and the value still exceeds 150 cm after introducing MN. The conclusion drawn from Fig. 27.30D is that MN can reduce the plastic deformation ability of 70# and 90# asphalts, but it has no obvious influence on 110# asphalt [26].

### 27.4.3 Rheological properties of multidimensional nanomaterials-modified asphalts

The complex modulus ( $G^*$ ) and phase angle ( $\delta$ ) are usually used to characterize the dynamic shear rheological properties of asphalt.  $G^*$  is related to the ability to resist shear deformation of asphalt material, while  $\delta$  is generally used to evaluate the ratio between elastic and viscous response during the shearing process. The  $G^*$  and  $\delta$  of all binders at whole scanning temperature region (40°C–90°C) before aging are shown in Fig. 27.31. As can be seen, the addition of MN slightly augments the  $G^*$  and drops the  $\delta$  of the three types of asphalts. Thus MN introduced in these base asphalts can enhance the shear deformation resistance and elastic behavior, while decreasing the viscous behavior due to the movement of asphalt molecules being hindered by adding MN, leading to the hardness of these asphalts [27].

### 27.4.4 Antiaging properties of multidimensional nanomaterials-modified asphalts

#### 27.4.4.1 Physical properties

The changes in the physical properties of the three asphalts with or without MN before and after TFOT aging are shown in Fig. 27.32. As can be seen in Fig. 27.32A, the SPI of the three modified asphalts declines significantly compared to the corresponding blank sample. Additionally, the decrease amplitude of the SPI for 110# asphalt before and after modification with MN is more than that to 70# and 90# asphalt. The decreased value of 110# asphalt before and after modification with MN is 6.6°C, while that of 70# and 90# asphalts are 3.5°C.

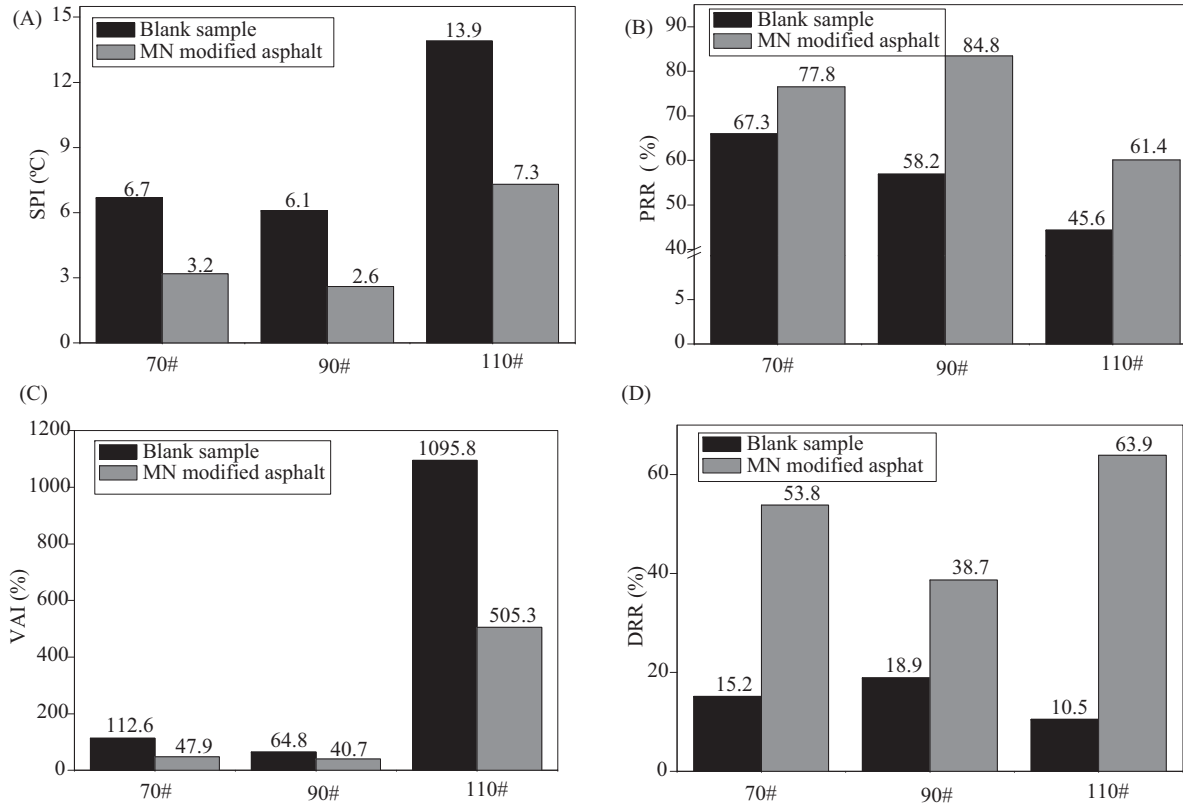


FIGURE 27.32 Effect of MN on the physical properties of different asphalts after TFOT aging [26].

As described in Fig. 27.32B, the PRR of the three asphalts after TFOT aging are obviously enhanced with the introduction of MN. The ranking of enhanced value for three asphalts before and after modification with MN is 90# > 110# > 70# and the values are 26.6%, 15.8%, and 10.5%, respectively.

From Fig. 27.32C, it can be seen that the VAI of the three asphalts after TFOT aging remarkably declines with the addition of MN. The declined amplitude ranking is 110# > 70# > 90# and the values are 590.5%, 64.7%, and 24.1%, respectively. Finally, as presented in Fig. 27.32D, the DRR of the three asphalts after TFOT aging increases by adding MN. Moreover, the increased amplitude for the three asphalts is 110# > 70# > 90#, which are 53.4%, 38.6%, and 19.8%, respectively.

In summary, MN can significantly improve the physical properties of the three asphalts after TFOT aging. This indicates that short-term thermal-oxidative aging resistance of the three asphalts is improved, which is attributed to the exfoliated microstructure formed between OEVMT and asphalt can prevent light components from volatilizing and oxygen from infiltrating during the aging process. At the same time, nano-ZnO scatters in asphalt can also retard the aging process to a certain extent. These physical indexes suggest that improvement in 110# asphalt is more significant than in 70# and 90# asphalts due to the differences in the chemical compositions of the three types of asphalt. Moreover, it is worth noting that TFOT aging has the greatest influence on the physical properties of the 110# blank sample [26].

The effect of MN on the physical properties of different asphalts after PAV aging is shown in Fig. 27.33. As seen in Fig. 27.33A and B, after introducing MN, the SPI and VAI values of the three asphalts decline. Comparison of SPI decrement for three asphalts before and after modification with MN, the ranking is 70# > 90# > 110#, the values are 6.1°C, 4.5°C, and 4.2°C, respectively. Additionally, comparison of VAI dropped value to three asphalts, it can be found that 110# > 70# > 90# and the values are 1188.3%, 956.8%, and 558.8%, respectively. This shows that the resistance of the three asphalts to long-term thermal-oxidative aging is improved significantly. Moreover, it can be seen that the influence of PAV aging on the physical properties of the 110# blank sample is greater than for the 70# and 90# blank samples [26].

It can be seen in Fig. 27.34 that the SPI and VAI values of the three asphalts after UV aging remarkably decrease with the addition of MN. Moreover, as presented in Fig. 27.34A, the ranking of SPI decrement for three asphalts before and after modification with MN after UV aging is 90# > 70# > 110#, and that the values are 3.7°C, 2.4°C, and 2.2°C, respectively. In addition, as shown in Fig. 27.34B, the VAI dropped value to three asphalts after UV aging is 110# > 90# > 70# and the values are 590.9%, 92.5%, and 88.8%, respectively. These results suggest that MN can effectively improve UV aging resistance due to the ability of nano-ZnO to reflect



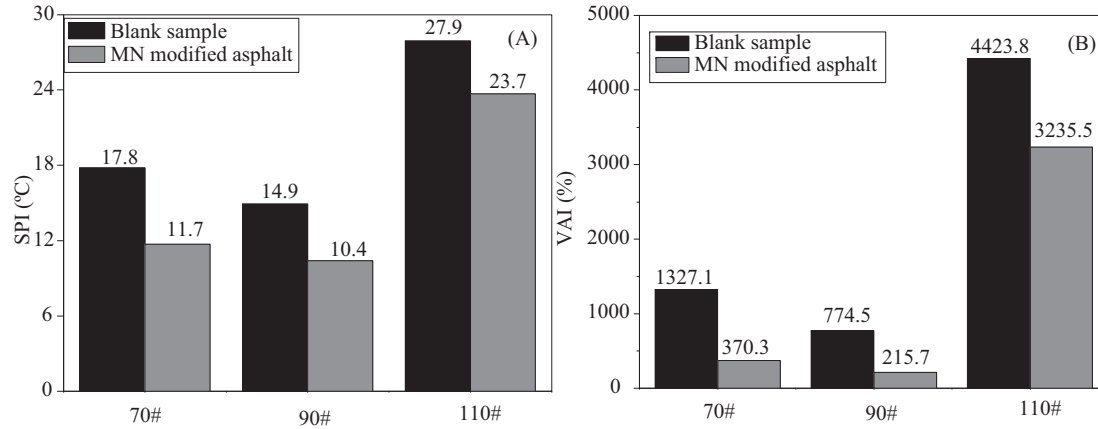


**FIGURE 27.33** Effect of MN on the physical properties of different asphalts after PAV aging [26].

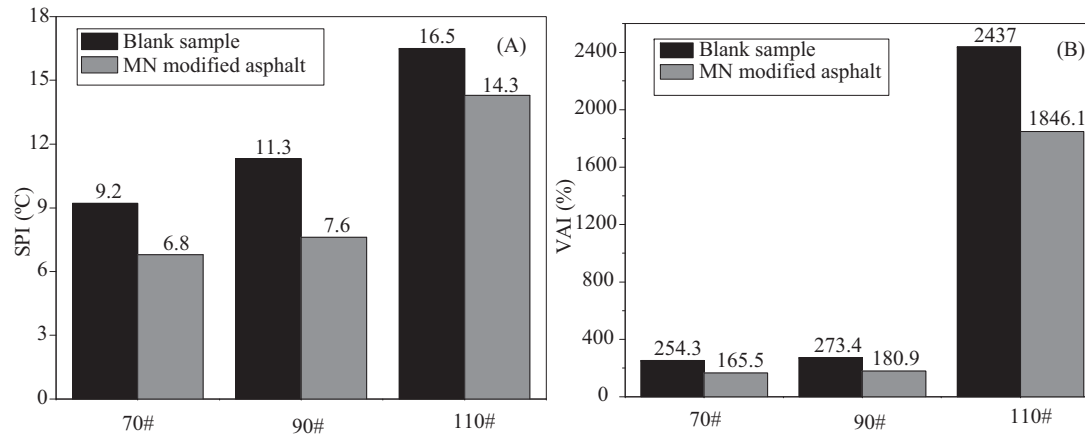


**FIGURE 27.34** Effect of MN on the physical properties of different asphalts after UV aging [26].

and absorb UV rays and weaken the damage of UV rays. The influence of UV aging on the physical properties of the 110# blank sample is the most significant [26].

27.4.4.2 Rheological properties

The effect of MN on the dynamical shear rheological properties of asphalts after TFOT aging is shown in Fig. 27.35. As can be seen, the MN-modified asphalts show lower  $G^*$  and higher  $\delta$  than the corresponding blank samples. Thus MN results in improvement of the short-term thermal oxidation aging resistance of these asphalts due to the exfoliated nanostructures formed in the OEVMT/asphalt compound. This nanostructure can effectively increase the average path length of the oxygen molecule penetration and the light

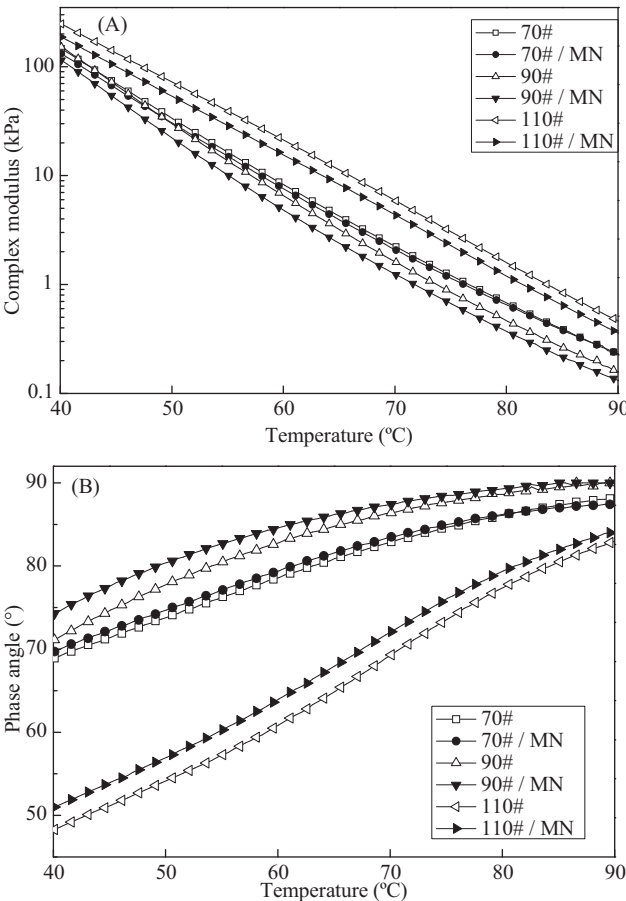
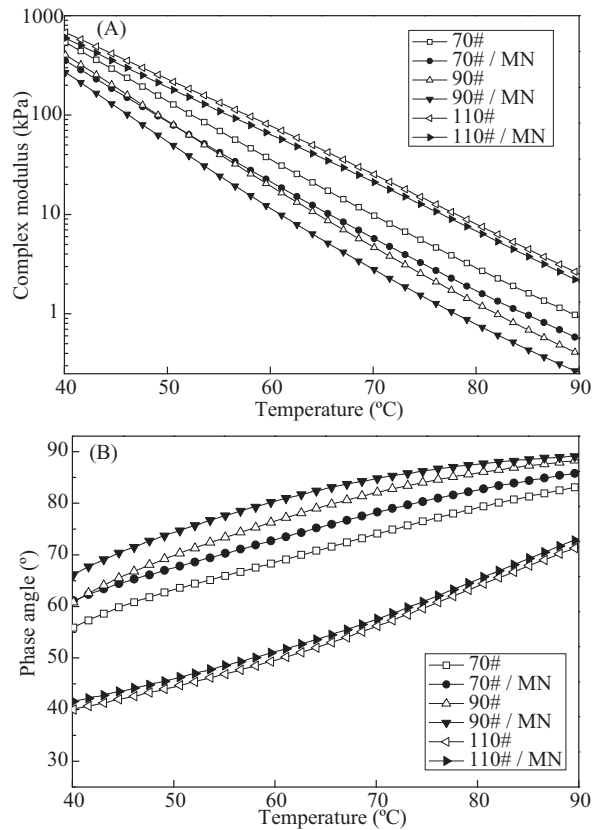


FIGURE 27.35 Effect of MN on the rheological properties of different asphalts after TFOT aging [27].



**FIGURE 27.36** Effect of MN on the rheological properties of different asphalts after PAV aging [27].

component volatilization during thermal oxidation aging. Accordingly, the oxidation rate of asphalt is reduced significantly [27].

The influence of MN on the dynamic shear rheological properties of asphalts after PAV aging is illustrated in Fig. 27.36. Adding MN leads to a decrease in  $G^*$  and an increase in  $\delta$  of the three types of asphalts after PAV aging. The results demonstrate that the MN can significantly reduce the long-term thermal oxidation aging of asphalt. This reason is the same as the explanation in TFOT aging.

Fig. 27.37 compares the modified asphalts and unmodified asphalts, and the decrease in  $G^*$  and increase in  $\delta$  of the asphalts containing MN after UV aging can be seen. This suggests that the resistance of asphalt to photooxidation aging is enhanced by the introduction of MN since nano-ZnO has good absorbance of UV light. The highest absorbance value is 1.4, which means that UV radiation can be effectively absorbed by nano-ZnO during UV

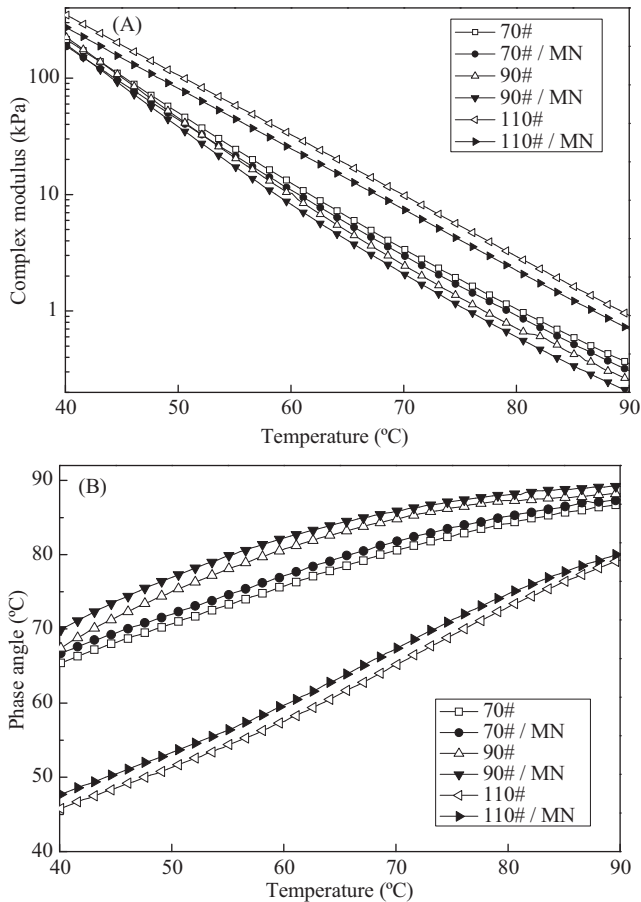


**FIGURE 27.37** Effect of MN on the rheological properties of different asphalts after UV aging [27].

aging. Consequently, the influence of UV radiation on asphalt molecules can be weakened [27].

#### 27.4.4.3 Fourier transform infrared spectroscopy

The aging of asphalt is an oxidation process that can cause oxygen-containing functional groups (e.g., carbonyl) to increase. In this research, carbonyl index ( $I_{C=O}$ ) is used to assess the oxidation of asphalt undergoing aging, as follows:

$$I_{C=O} = \frac{\text{Area of carbonyl centered around } 1698 \text{ cm}^{-1}}{\text{Area of CH}_3 \text{ umbrella vibration centered around } 1376 \text{ cm}^{-1}} \quad (27.5)$$

The infrared spectrums of asphalts with or without MN after TFOT aging are shown in Fig. 27.38, and the corresponding  $I_{C=O}$  is listed in Table 27.6.

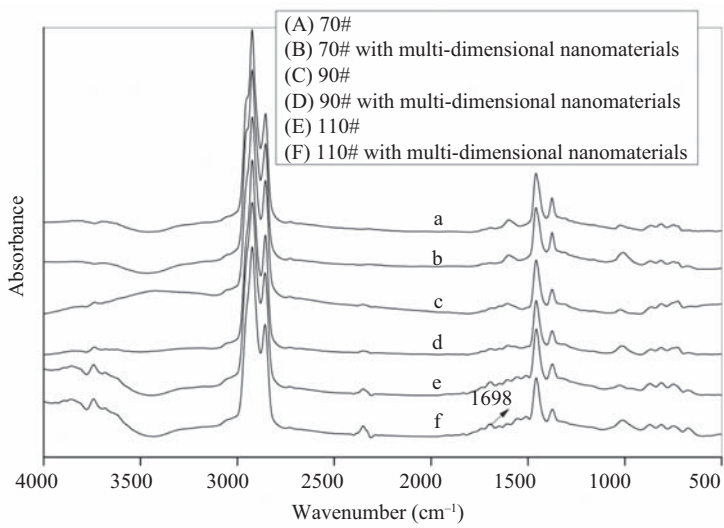
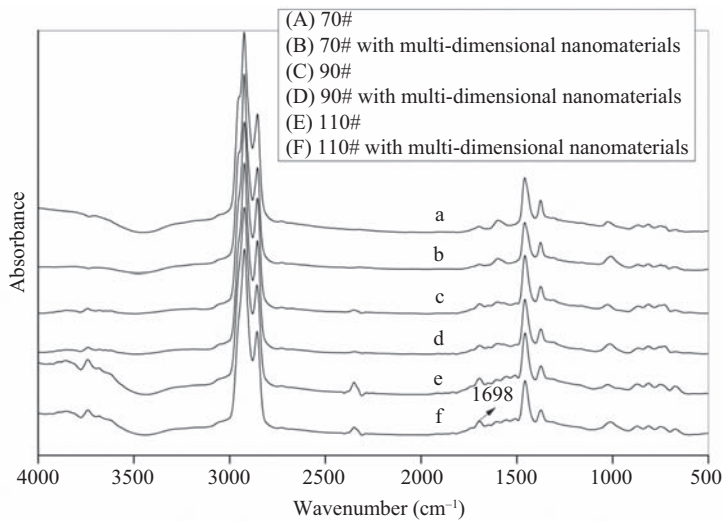


FIGURE 27.38 FTIR of asphalts with or without MN after TFOT aging [25].

**TABLE 27.6**  $I_{C=O}$  of asphalts with or without MN before and after TFOT aging [25].

Samples	Unaged	TFOT aging	Increment
70#	0.037	0.073	0.036
70#/MN	0.032	0.051	0.019
90#	0.065	0.100	0.035
90#/MN	0.124	0.154	0.030
110#	0.224	0.321	0.097
110#/MN	0.231	0.306	0.075

As seen in Table 27.6, after TFOT aging, it is obvious that the  $I_{C=O}$  of all binders increases at different degrees. However, the increased amplitude of the asphalts with MN is lower than that of the corresponding blank samples, illustrating that the introduction of MN can prevent carbonyl formation in asphalts undergoing TFOT aging. This is because the exfoliated nanostructure formed between the asphalt and OEVMt can increase the average path length of the oxygen molecule infiltration in the process of thermal-oxidative aging. Moreover, by comparing the three types of asphalt, it can be seen that the ranking of decrement values of the  $I_{C=O}$  increment of modified asphalt relative to that of unmodified asphalt is 110# > 70# > 90#, namely 0.022,



**FIGURE 27.39** FTIR of asphalts with or without MN after PAV aging [25].

**TABLE 27.7**  $I_{C=O}$  of asphalts with or without MN before and after PAV aging [25].

Samples	Unaged	PAV aging	Increment
70#	0.037	0.172	0.135
70#/MN	0.032	0.135	0.103
90#	0.065	0.284	0.219
90#/MN	0.124	0.270	0.146
110#	0.224	0.571	0.347
110#/MN	0.231	0.536	0.305

0.017, and 0.005, respectively. This show that MN has the best effect in inhibiting carbonyl formation for the 110# asphalt, followed by the 70# asphalt and finally the 90# asphalt [25].

The FTIR of asphalts with or without MN after PAV aging is shown in Fig. 27.39, and the corresponding  $I_{C=O}$  is listed in Table 27.7. After PAV aging, the  $I_{C=O}$  values of the three asphalts further increase. Nonetheless, the  $I_{C=O}$  values of the three types of asphalt are decreased by adding MN. Furthermore, the ranking of three asphalts is 90# > 110# > 70#, that is, 0.073, 0.042, and 0.032, respectively. This indicates that the addition of MN can also effectively prevent carbonyl formation in asphalts undergoing long-

term thermal-oxidative aging. The effect for the 90# asphalt is the most obvious [25].

The FTIR of all binders after UV aging is presented in Fig. 27.40, and the calculated results for  $I_{C=O}$  are listed in Table 27.8. As can be seen in Table 27.8, the interfusion of MN can effectively decrease the  $I_{C=O}$  value of asphalts after UV aging, indicating that the carbonyl formation in asphalts is suppressed. Furthermore, the decrement value ranking of the three asphalts before and after modification with MN is 90# > 110# > 70#, namely 0.042, 0.027, and 0.004, respectively. This also shows that MN can inhibit carbonyl

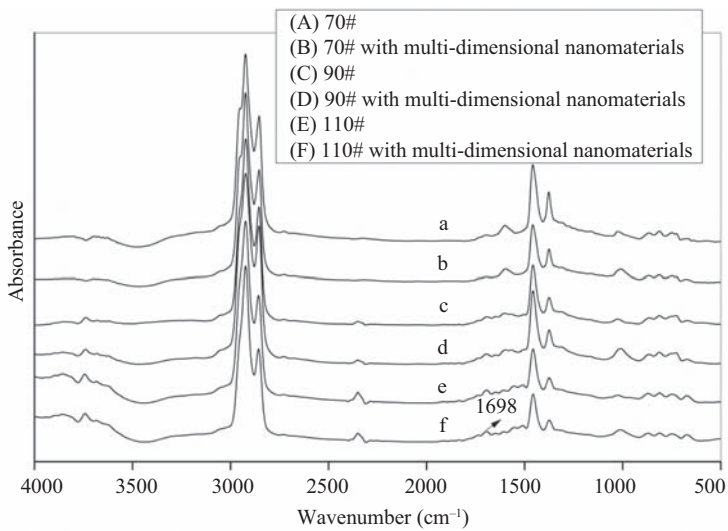


FIGURE 27.40 FTIR of asphalts with or without MN after UV aging [25].

TABLE 27.8  $I_{C=O}$  of asphalts with or without MN before and after UV aging [25].

Samples	Unaged	UV aging	Increment
70#	0.037	0.080	0.043
70#/MN	0.032	0.071	0.039
90#	0.065	0.189	0.125
90#/MN	0.124	0.207	0.083
110#	0.224	0.431	0.207
110#/MN	0.231	0.411	0.180



formation of asphalts in the process of photooxidation aging. The effect for the 90# asphalt is the most obvious [25].

## 27.5 Future trends in research of functionalized nanomaterial-modified asphalt

From the above discussion it is clear that functionalized nanomaterials (e.g., OLS, SMIN, and MN) can improve the various properties of base asphalt, such as physical properties, rheological properties, and aging resistance of asphalt. However, more research on functionalized nanomaterial-modified asphalt is still needed because of the following:

1. Current studies only relate to base asphalt, and the effects of functionalized nanomaterials on other asphalts, such as SBS, SBR, EVA, PE, and crumb rubber-modified asphalts, are unknown. Therefore it is necessary to apply functionalized nanomaterials to these asphalts in the future.
2. The presented studies mostly focus on the asphalt binders and less attention has been paid to asphalt mixtures. Research on asphalt mixtures containing functionalized nanomaterials will contribute to the better understanding of the interactions between functionalized nanomaterials and asphalt, which will also help understand the properties of asphalt mixtures containing functionalized nanomaterials.

## References

- [1] Zhu CZ, Zhang HL, Huang LQ, Wei CW. Long-term performance and microstructure of asphalt emulsion cold recycled mixture with different gradations. *J Clean Prod* 2019;215:944–51.
- [2] Zhang HL, Chen ZH, Xu GQ, Shi CJ. Evaluation of aging behaviors of asphalt binders through different rheological indices. *Fuel*. 2018;221:78–88.
- [3] Zhang DM, Zhang HL, Shi CJ. Investigation of aging performance of SBS modified asphalt with various aging methods. *Constr Build Mater* 2017;145:445–51.
- [4] Chen ZH, Zhang HL, Shi CJ, Wei CW. Rheological performance investigation and sustainability evaluation of asphalt binder with thermochromic powders under solar radiation. *Sol Energy Mater Sol Cell* 2019;191:175–82.
- [5] Zhang HL, Chen ZH, Xu GQ, Shi CJ. Physical, rheological and chemical characterization of aging behaviors of thermochromic asphalt binder. *Fuel*. 2018;211:850–8.
- [6] Hussain CM. *Handbook of nanomaterials for industrial applications*. Elsevier; 2018.
- [7] Yu JY, Wang L, Zeng X, Wu SP, Li B. Effect of montmorillonite on properties of styrene–butadiene–styrene copolymer modified bitumen. *Polym Eng Sci* 2007;47(9):1289–95.
- [8] Yu JY, Feng PC, Zhang HL, Wu SP. Effect of organo-montmorillonite on aging properties of asphalt. *Constr Build Mater* 2009;23(7):2636–40.
- [9] Yu JY, Zeng X, Wu SP, Wang L, Liu G. Preparation and properties of montmorillonite modified asphalts. *Mater Sci Eng A* 2007;447(1-2):233–8.

- [10] Zhang HL, Zhu CZ, Yu JY, Tan BY, Shi CJ. Effect of nano-zinc oxide on ultraviolet aging properties of bitumen with 60/80 penetration grade. *Mater Struct* 2014;48(10):3249–57.
- [11] Zhang HL, Zhu CZ, Yan KZ, Yu JY. Effect of rectorite and its organic modification on properties of bitumen. *J Mater Civ Eng* 2014;27(8) C4014002-1-5.
- [12] Zhang HL, Xu HB, Wang XL, Yu JY. Microstructures and thermal aging mechanism of expanded vermiculite modified bitumen. *Constr Build Mater* 2013;47:919–26.
- [13] Zhang HL, Zhang DM, Zhu CZ. Properties of bitumen containing various amounts of organic montmorillonite. *J Mater Civ Eng* 2015;27(11):04015010.
- [14] Zhang HL, Shi CJ, Han J, Yu JY. Effect of organic layered silicates on flame retardancy and aging properties of bitumen. *Constr Build Mater* 2013;40:1151–5.
- [15] Zhang HL, Tan BY, Xu HB, Yan KZ. Microstructures and thermal aging properties of layered silicate modified bitumens. *Pet Sci Technol* 2014;32(14):1697–703.
- [16] Yu JY, Wang X, Hu L, Tao YY. Effect of various organomodified montmorillonites on the properties of montmorillonite bitumen nanocomposites. *J Mater Civ Eng* 2010;22(8):788–93.
- [17] Zhang HL, Yu JY, Xue LH, Li ZC. Effect of montmorillonite organic modification on microstructures and ultraviolet aging properties of bitumen. *J Microsc* 2011;244(1):85–92.
- [18] Zhang HL, Yu JY, Kuang DL. The effect of sodium and organic montmorillonites on the thermal aging properties of bitumen. *Pet Sci Technol* 2013;31(20):2074–81.
- [19] Zhang HL, Yu JY, Kuang DL. Effect of expanded vermiculite on aging properties of bitumen. *Constr Build Mater* 2012;26(1):244–8.
- [20] Liu HY, Zhang HL, Hao PW, Zhu CZ. The effect of surface modifiers on ultraviolet aging properties of nano-zinc oxide modified bitumen. *Pet Sci Technol* 2014;33(1):72–8.
- [21] Liu CH, Zhang HL, Li S, Zhu CZ. The effect of surface-modified nano-titania on the ultraviolet aging properties of bitumen. *Pet Sci Technol* 2014;32(24):2995–3001.
- [22] Zhang HL, Zhang DM. Effect of different inorganic nanoparticles on physical and ultraviolet aging properties of bitumen. *J Mater Civ Eng* 2015;27(12):04015049.
- [23] Zhang HL, Zhu CZ, Yu JY, Shi CJ, Zhang DM. Influence of surface modification on physical and ultraviolet aging resistance of bitumen containing inorganic nanoparticles. *Constr Build Mater* 2015;98:735–40.
- [24] Zhang HB, Zhang HL, Ke NX, Huang JH, Zhu CZ. The effect of different nanomaterials on the long-term aging properties of bitumen. *Pet Sci Technol* 2015;33(4):388–96.
- [25] Zhu CZ, Zhang HL, Xu GQ, Wu CW. Investigation of the aging behaviors of multi-dimensional nanomaterials modified different bitumens by Fourier transform infrared spectroscopy. *Constr Build Mater* 2018;167:536–42.
- [26] Zhang HL, Zhao B, Zhu CZ, Chen ZH. Physical and aging properties of different bitumens with multi-scale nanomaterials. *Pet Sci Technol* 2017;35(13):1389–95.
- [27] Zhu CZ, Zhang HL, Shi CJ, Li S. Effect of nano-zinc oxide and organic expanded vermiculite on rheological properties of different bitumens before and after aging. *Constr Build Mater* 2017;146:30–7.

This page intentionally left blank

## Section 11

# **Functionalized nanomaterial in wood & paper-related applications**

This page intentionally left blank

# Functional rubber—clay nanotube composites with sustained release of protective agents

Ye Fu<sup>1,2</sup>, Liquan Zhang<sup>2</sup> and Yuri Lvov<sup>3</sup>

<sup>1</sup>School of Materials Science and Mechanical Engineering, Beijing Technology and Business University, Beijing, P.R. China, <sup>2</sup>State Key Laboratory of Organic-Inorganic Composites, Beijing University of Chemical Technology, Beijing, P.R. China, <sup>3</sup>Institute for Micromanufacturing, Louisiana Tech University, Ruston, LA, United States

## 28.1 Introduction

Halloysite tubes are an economically viable aluminosilicate clay with a hollow cylindrical structure 50–70 nm in diameter, with 10–15 nm lumen and c. 1  $\mu\text{m}$  in length. The surface of halloysite is comprised of  $\text{SiO}_2$  and its internal lumen is  $\text{Al}_2\text{O}_3$ , which may be considered as a rolled sheet of kaolin containing 15–20 internal layers. The tighter wall packing with layer periodicity shifting from 1.0 to 0.7 nm can be achieved by the removal of hydrated water via processing a raw halloysite (mined as white stones resembling chalk) with milling and heating to 110°C–120°C. Halloysite is available in thousands of tons at a few dollars per kilogram from companies in the United States, New Zealand, China, and Turkey. It is possible to load the lumen of these clay nanotubes with chemical inhibitors such as anticorrosion, flame-retardant, and antimicrobial agents and make halloysite a functional filler for polymers [1–6]. The halloysite inner-loading capacity is 15–20 wt.%. The loaded agents release from the tubes in hours to days if these nanotubes are dispersed in solutions and much longer time, from months to years, if halloysite is embedded in a polymeric matrix [7–12]. By slow release from halloysite, the chemical agents protect rubber from degradation and unwanted reactions during the curing processes. The concentration of antioxidants in rubber–halloysite formulations can be increased up to 4–5 wt.% without causing damaging “blooming” defects. All these make

halloysite an accessible nanocontainer for loading protective chemicals functionalized with long-lasting sustained release.

Nanocomposites may combine the mechanical properties of a substrate with the properties of nanoparticles to possess properties that are not available to the respective components alone [13,14]. Rubber composites with fibrillar and tubular nanoclays have attracted a lot of attention due to their significant reinforcing effects [7,15–17]. Compared with conventional spherical fillers, for fibrillar and tubular clay we need less filler. Another important advantage of tubule halloysite as compared with platy clays like montmorillonite, kaolin, and bentonite, which are stacked in larger crystallites, is that it does not need exfoliation, which is an energy-consuming and expensive process [3,18]. Halloysite can be not only easily dispersed in water or polar polymers, but also be well dispersed in low polar polymers (even in melted polypropylene). Under the strong shearing force of the blending process, surface-silanized halloysite forms good, even dispersions in bulk rubber [19,20]. Tight interfacial bonding and fine dispersions of the clay are crucial factors for the best performance of the rubber–halloysite composites [21]. After endowing these tubular nanofillers with different functions, they can be used for elastomer reinforcement exhibiting synergy in the physical/chemical properties of the matrix and filling materials.

We present in this chapter recent studies on tubule clay-based functional rubber nanocomposites with special properties focus on halloysites as containers for loading and sustained and controlled release of antioxidant, antifouling, anticorrosion, and flame-retardant. Comparative study of these composites with and without halloysite encapsulated are presented, revealing its application on functional rubber composites.

## 28.2 Encapsulation and sustained release of chemical agents

### 28.2.1 Halloysite structure

Halloysite is a white mineral formed in volcanic zones (Fig. 28.1), and is similar to rolled kaolinite with additional water between the adjacent layers [16,22]. The most widely used is which achieved by removing hydrated water. Dried halloysite is a roll of 15–20 aluminosilicate sheets with packing periodicity of 0.72 nm and with hollow lumens (Fig. 28.1B). Dimensions of the halloysite tubes vary depending on the deposit, but their outside diameter is in the range of 50–70 nm and the diameter of the internal lumen is 10–15 nm [7,16]. The surface of halloysite is comprised of silicon-dioxide tetrahedrons and its internal lumen is aluminum-oxide octahedrons. The monoclinic unit cell of the halloysite crystalline structure is shown in Fig. 28.1D.

The average hydrodynamic size of individual halloysite tubes obtained from light scattering and reflect orientation/size averaging corresponds

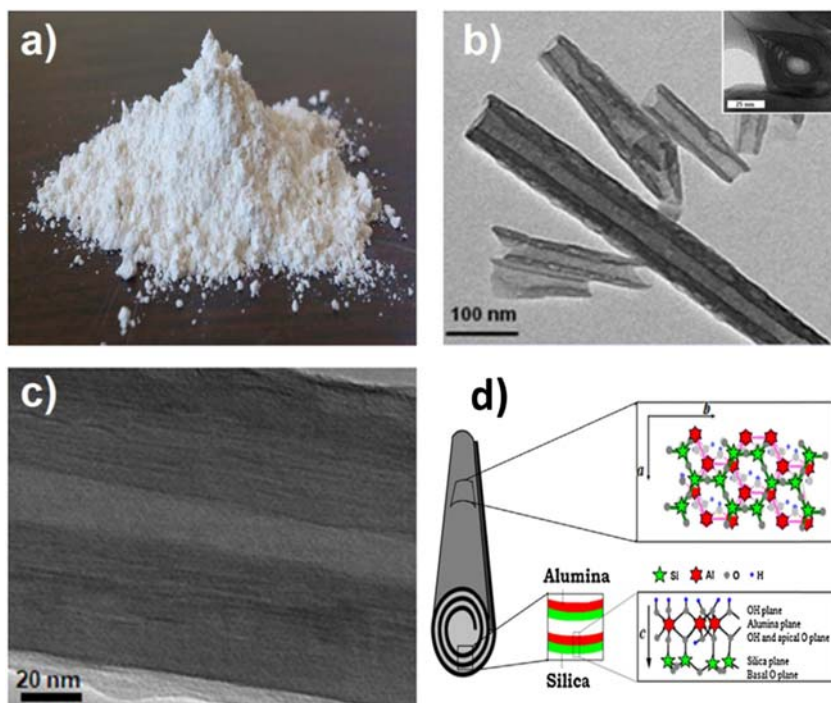


**FIGURE 28.1** Halloysite images: (A) powdered clay, (B, C) TEM of halloysite including tube cross-section, (D) halloysite crystal structure—tubular morphology, side and top view where  $a$ ,  $b$ ,  $c$  are crystalline directions [7,23].

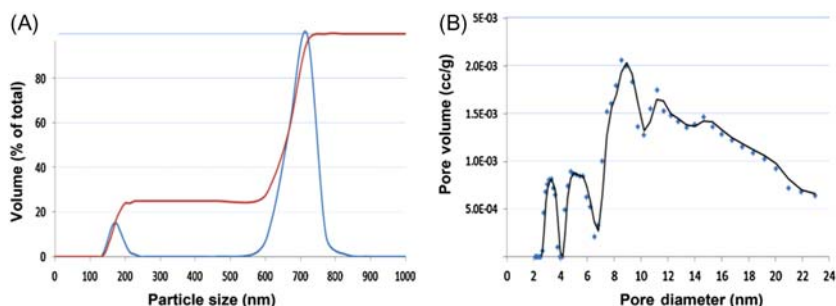


**FIGURE 28.2** Bimodal particle size (A) and pore volume distribution (B) of halloysite [7].

to 300–400 nm, which results in good dispersion of single nanotubes. (Fig. 28.2A). Halloysite tubes have porosity distribution extended up to 30 nm, with most pores less than 10 nm. Their specific surface area is in the range of 50–150 m<sup>2</sup>/g (depending on natural deposit and processing) and cation exchange capability ranges from 0.1 to 0.7 mol/kg [16,22].



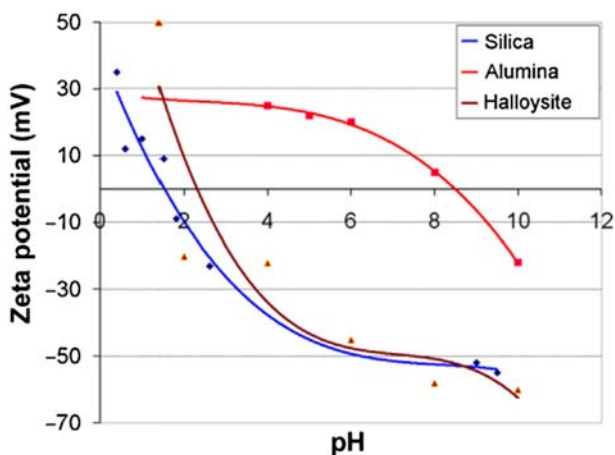


**FIGURE 28.3** Zeta potential for halloysite nanotubes, silica, and alumina nanoparticles (compounds of similar size and surface chemistry) [8].

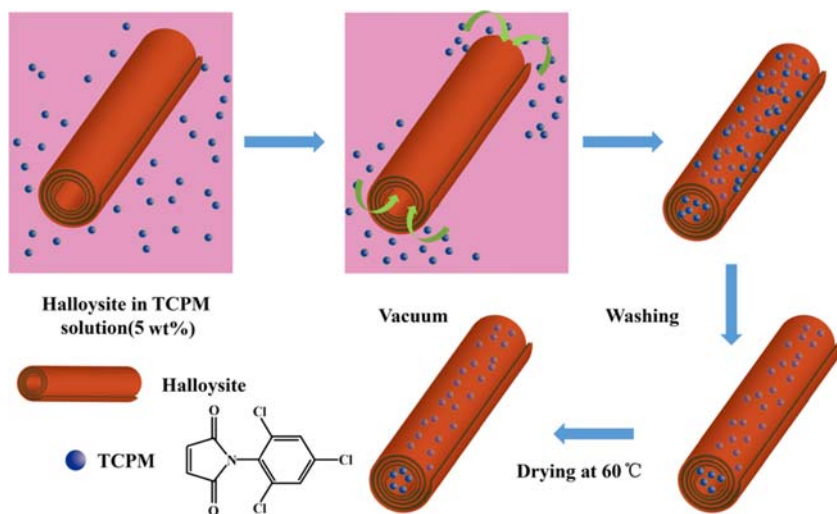
Salts (potassium, ammonium, and cesium acetates) and small organic compounds such as urea, formaldehyde, glycerol, and dimethylsulfoxide can intercalate in the wall multilayers of halloysite, which can be demonstrated with the XRD data [22,24,25]. When halloysite dehydrates, strong hydrogen bonds are formed between its wall layers, which leads to the disablement of intercalate capability and the encapsulation of chemical agents into the lumens [16,26].

As shown in Fig. 28.3, the outer silica and inner alumina surfaces of halloysite tubes lead to different surface chemistry, which gives different ionization properties and surface charge evident from the zeta potentials of c.  $-30$  mV in water. The positive charge of alumina (up to pH 8.5) and negative silica (above pH 2.5) allows for the selective loading of negatively charged molecules inside the halloysite lumen.

### 28.2.2 Lumen loading

Halloysite can be loaded with various substances including inorganic salts, organic molecules, polymers, and biologically active substances (such as drugs, enzymes, and DNA) via different methods including adsorption to the external and internal walls of the tubes, intercalation, and loading into lumens [1,4,22,24,27–29]. Among these methods, loading into 15-nm diameter lumens is achieved by sucking concentrated chemical solution (or melt) accompanied by condensation/crystallization of the chemicals [30,31]. Laplace's equation estimates the capillary pressure in 15-nm halloysite lumen to be about 180 atm in water, which is sufficiently high for pulling solution into the empty tube lumen.

Halloysite can work as container for loading functional chemical agents with sustained release in solutions or polymer matrix. The halloysite lumen loading is achieved by mixing halloysite powder with highly concentrated chemical agent solutions with low viscosity and that can wet halloysite walls (acetone is often used). The mixture is placed in a vacuum chamber for 10–30 min, then at atmospheric pressure for 5–15 min. This vacuum cycle is repeated 2–3 times, which removes air from the halloysite lumens. Once the vacuum is broken, the solution enters into the tubes accompanied by condensation/crystallization of the chemicals. The loaded halloysite is washed with deionized (DI) water to remove any unloaded chemicals/antioxidant, followed by being placed in a vacuum oven for drying. The dried halloysite is milled to a fine powder for doping into polymer matrix. Typically, a successful halloysite lumen encapsulation reaches 10–12 wt.%, which is close to the theoretical estimation for the 10 nm inner and 50 nm outer diameter tubes with a density of  $2.53 \text{ g/cm}^3$ , while the chemicals are close to  $1.1 \text{ g/cm}^3$ . By this method, chemical agents including antioxidant, flame-retardant, anticorrosion, and antifoulant/antimicrobials can be loaded into halloysite [32–34] (Scheme 28.1).



**SCHEME 28.1** Loading halloysite nanotubes with antifoulant TCPM [32].

### 28.2.3 Sustain release of chemical agents

The release rates of chemicals loaded into halloysite lumens is much lower than direct dissolution of these compounds in water [1,31]. The release speed is affected by the viscosity of the medium and the tube's opening diameter and affinity with chemicals. The kinetics of antioxidant release in

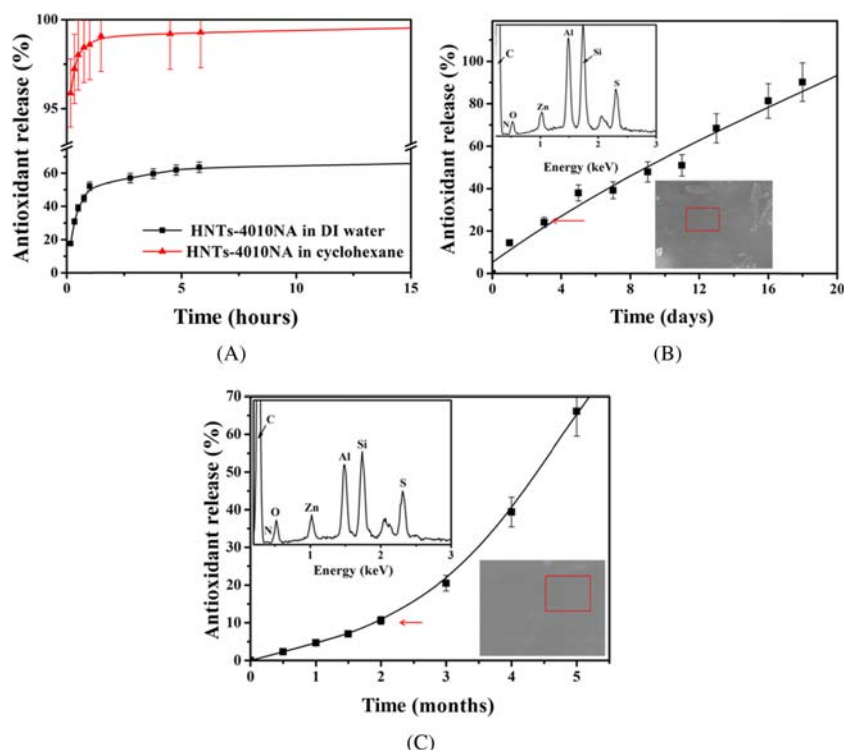


**FIGURE 28.4** Antioxidant 4010NA release from (A) loaded halloysite in water and cyclohexane and halloysite–rubber composite at (B) 90°C and (C) 25°C. The inset images are the SEM images and the EDS spectra of the selected area [34].

cyclohexane is much faster than in water (3 and 6 h), which is attributed to its higher solubility in cyclohexane (Fig. 28.4A). The antioxidant release burst at the initial stage is acceptable for the rubber protection initiation. The release in styrene–butadiene rubber is drastically slowed down as the halloysite openings are clogged with the cross-linked rubber. The release kinetics of antioxidant from halloysite in rubber composite at 90° and room temperature (25°) demonstrate slow and sustained release. (Fig. 28.4B and C) [34].

Extrapolation shows that 90% release will take 9 months [34]. In water, about 50 wt.% of *N*-(2,4,6-trichlorophenyl) maleimide (TCPM) releases from halloysite lumens within 24 h, while more than 90 wt.% releases in cyclohexane at the same time. The release kinetic of antifoulant TCPM from ethylene-vinyl acetate copolymer (EVA) polymer matrix with halloysite encapsulated allowed for maleimide release into the polymer matrix and its further migration to the composite surface. The release rate of EVA/TCPM with direct admixture of the inhibitor was almost five times faster than that for halloysite formulation, EVA/HNT–TCPM (Fig. 28.5B). Analytical

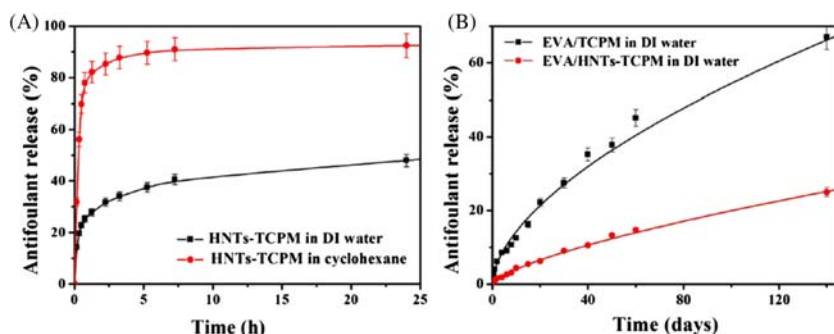


**FIGURE 28.5** Antifoulant TCPM release from (A) halloysite in DI water and cyclohexane and (B) EVA composite doped with antifoulant TCPM-loaded halloysite in DI water as compared to the control sample containing no halloysite (upper curve) [32].

extrapolation shows that a 50% release in the EVA/HNT–TCPM composite will take 12 months, while no-encapsulation EVA/TCPM formulation (direct maleimide admixing) allowed for only 3 months’ supply [32].

## 28.3 Functional halloysite rubber nanocomposites

### 28.3.1 Aging resistant halloysite SBR (styrene – butadiene rubber) materials

#### 28.3.1.1 Morphology and properties of the SBR/HNT composites

The morphology of SBR/HNT composites is shown in Fig. 28.6. The dispersion of halloysite modified with silane is excellent (Fig. 28.6B–D) and is not possible without such treatment. In the inset images, it can be seen that the shape of nanotubes embedded into rubber matrix is preserved. Note that with halloysite density of  $2.53 \text{ g/cm}^3$ , 27 wt.% filling corresponds to c. 13 vol.%, which is evident from the visual SEM image. The TEM images of ultrathin sections show good halloysite tube dispersion in rubber matrix. Such excellent dispersion of single clay particles was obtained without any additional exfoliation processing of this tubular clay.

The effect of antioxidant and HNTs on vulcanization and cross-linking density is described in Fig. 28.7 and Table 28.1. Three controlled samples, pure SBR rubber (SBR#1), SBR rubber with 27 wt.% of empty halloysite filler (SBR#2), and SBR rubber without halloysite admixed with 1.0 wt.% of 4010NA antioxidant (SBR#3), were not able to provide slow nanopore-controlled 4010NA release. Two designed functional materials contained SBR filled with antioxidant-loaded halloysite (SBR#4) and the same material but with 1.0 wt.% of free antioxidant added (SBR#5). Therefore in SBR#4 nanocomposite we had 2.2 wt.% of nanotube-encapsulated antioxidant and in SBR#5 we had 2.2 wt.% of encapsulated 4010NA providing sustained

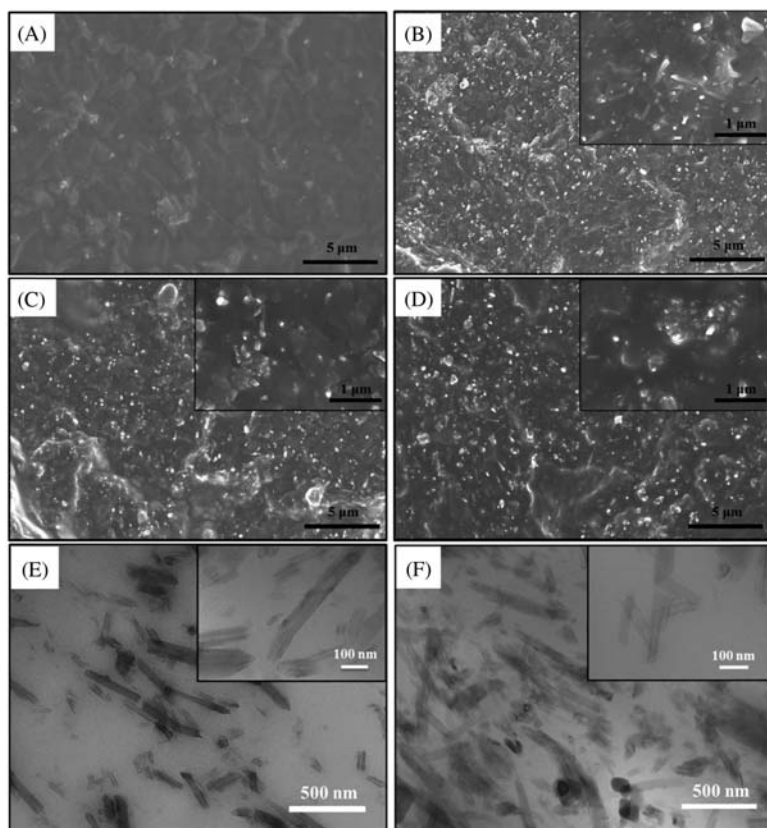


**FIGURE 28.6** SEM images of SBR/HNT composites with different formulas: (A) SBR#1 pure rubber, (B) SBR#2 pristine halloysite composites, (C) SBR#4 with 4010NA-loaded halloysite, and (D) SBR#5 with loaded halloysite plus admixed free antioxidant. TEM images of © SBR#2 and (F) SBR#5 ultrathin section surface [34].

release plus 1.0 wt.% of 4010NA nonencapsulated antioxidant (blooming concentration threshold). With this formulation we tripled the amount of antioxidant agent dispersed in the rubber without blooming defects. In the target functional formulations (SBR#4 and SBR#5), the optimum curing time ( $T_{90}$ ) was reduced to 4–5 min. The inclusion of halloysite led to significant increase in the torque and curing rate index (CRI) of the vulcanization and an increase in cross-link density, which can be attributed to the silanized surface taking a part of the cross-links and silane working as antireversion agent. Cross-linking density was enhanced 4%–5% with halloysite filling. The cross-linking density of the composite with antioxidant (SBR#3, 4, 5) was slightly lower than the one without antioxidant because of its reacting with the free radicals; another reason could be the plasticization of antioxidant.

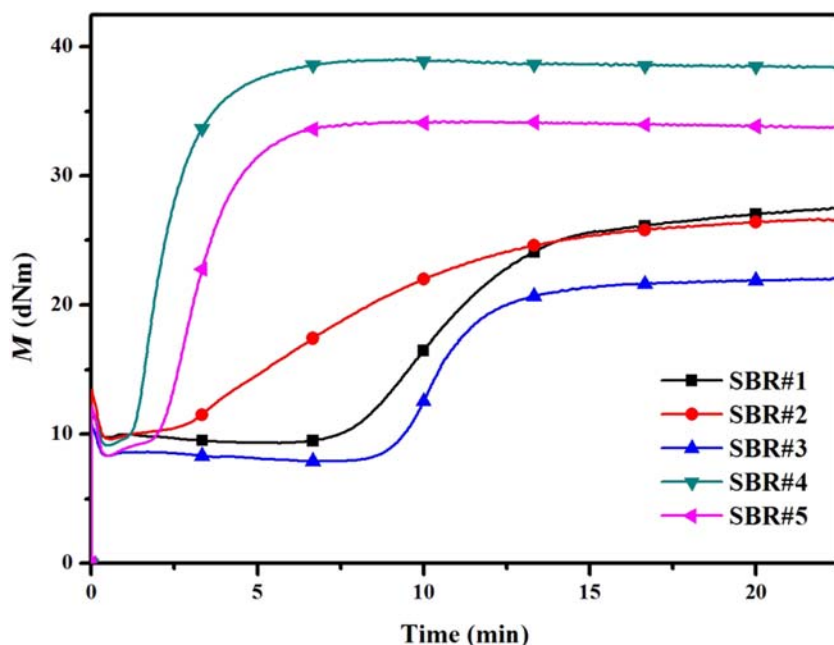


FIGURE 28.7 Vulcanization curves of the SBR/HNT compounds [34].

**TABLE 28.1** Cross-linking density of SBR/HNT–1040NA nanocomposites [34].

Sample code	SBR#1	SBR#2	SBR#3	SBR#4	SBR#5
Cross-linking density/ $10^{-5} \text{mol} \cdot \text{cm}^{-3}$	$14.96 \pm 0.36$	$15.61 \pm 0.47$	$14.35 \pm 0.11$	$13.51 \pm 0.17$	$14.69 \pm 0.20$

### 28.3.1.2 Aging performance of SBR/HNT nanocomposite

The aging resistance of SBR/HNTs was studied by comparing the mechanical properties before and after thermal-oxidative aging. Fig. 28.8 shows the mechanical properties of SBR/HNT nanocomposites before and after aging at 90°C and 120°C for 24, 72, and 168 h.

Compared with the SBR#1, the higher cross-linking density of the composite filled with pristine halloysite (SBR#2) leads to higher tensile strength, almost two times higher. The hardness increases after the filling of halloysite, which is attributed to its nanoreinforcement. The lower cross-linking density of the composite with antioxidant (SBR#3 compared with SBR#1,

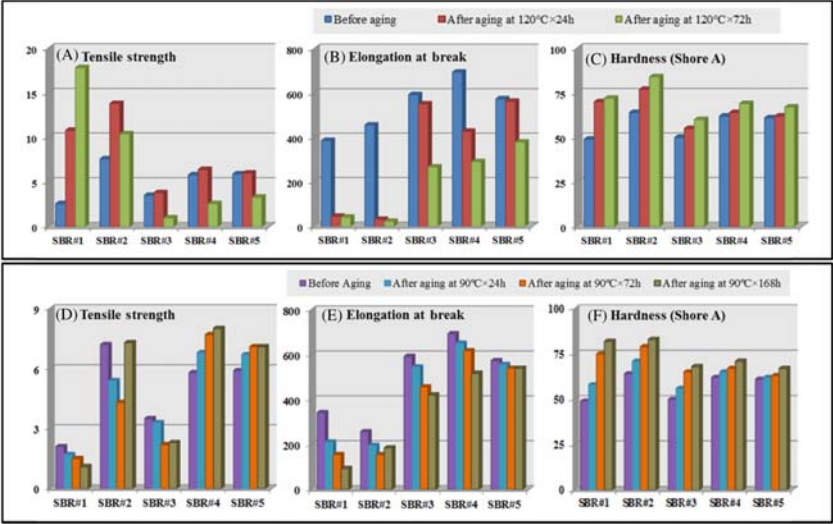


**FIGURE 28.8** Mechanical properties of SBR/HNT composites before and after aging at (A–C) 120°C and (D–F) 90°C (experimental error 5%) [34].

SBR#4 compared with SBR#2, and SBR#4 compared with SBR#5) leads to higher elongation at break and lower hardness.

After aging for 24 h at 120°C, the elongation at break of SBR#1 and with pristine halloysite filler (SBR#2) decreases significantly. Meanwhile, the retention rate of elongation at break of SBR#3 with the addition of antioxidant is at least 45% after aging for 72 h and the retention rate is 42% with the addition of HNT–4010NA (SBR#4). The elongation at break is more or less the same even after aging for 168 h at 90°C for the composite with the addition of both halloysite-encapsulated antioxidant and free antioxidant (our best sample was SBR#5). This SBR#5 formulation demonstrates much better mechanical properties as compared with direct loading of free antioxidant into rubber. The increase of hardness after aging is attributed to the further cross-linking of SBR, which leads to the loss of elasticity. SBR#5 containing 2.2 wt.% of encapsulated plus 1.0 wt.% of free antioxidant gave the least increase in hardness after 168 h aging, indicating good aging protection due to sustained release of the antioxidant.

The enhanced mechanical properties of SBR/HNT composite demonstrate that HNTs–4010NA can not only be used as reinforcing filler but can also improve the aging resistance of this designed nanomaterial. Particularly good results were seen at 168 h aging at 90°C when rubber without antioxidant became brittle and decreased 73% in elongation break, but sample SBR#5 with halloysite-encapsulated antioxidant demonstrated only a 2% decrease in elongation break without losing tensile strength and elasticity (Fig. 28.8E).



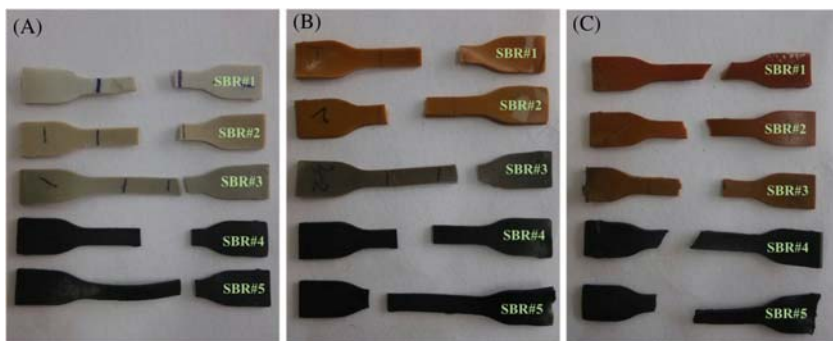


**FIGURE 28.9** Images of tensile fracture dogbone-shaped rubber–halloysite nanocomposite samples: (A) before aging, (B) after aging for 24 h, and (C) 168 h at 120°C [34].

During aging, formation and degradation of cross-links occur at the same time. If the formation is faster, the cross-linking density of the composite will increase and the hardness will increase too, leading to a decrease in the elasticity. The cross-linking density of the SBR sample without filler or antioxidant (SBR#1) decreases with the aging time extended and then increases. This is because at the initial stage the cross-links perform mild thermal degradation rather than further curing, which is the typical aging performance of polybutadiene (there is 76.5% of butadiene in the SBR we used). Thus the tensile strength and elongation at break decrease, while the hardness increases. The changes in the cross-linking density of SBR with antioxidant (SBR#3, SBR#4, and SBR#5) were due to the free radical reaction with antioxidant instead of polymer molecules, which slows down further curing.

Images of tensile fracture dogbone-shaped samples before and after aging at 120°C are shown in Fig. 28.9. Without antioxidant, SBR#1 and SBR#2 turn yellow after 24 h aging and the color gets darker with longer aging time. For the SBR#3 sample, the gray color gets darker at the beginning of aging and finally turns to light brown at 168 h when the antioxidant is exhausted.

The color retention of the designed samples SBR#4 and SBR#5 with tube-encapsulated 4010NA indicates that sustained release of the antioxidant allows for long-lasting rubber protection while avoiding the blooming, which otherwise would be inevitable at such high antioxidant content (3.2 wt.%). After aging for 24 h, the permanent set at break of SBR#5 was the same with SBR#3 but the elongation at break of SBR#5 was much larger. This indicates that the presence of 4010NA-loaded halloysite improved the sample elasticity.

### 28.3.1.3 Blooming test of SBR/HNT nanocomposite as compared with direct antioxidant addition

The control sample for blooming test was prepared with the addition of 27 wt.% of empty halloysite plus 3.2 wt.% free antioxidant, making its



composition similar to the best sample SBR#5 but without antioxidant-loaded halloysite.

Keeping samples at 90°C speeds up the blooming process. The blooming amount of antioxidant was analyzed with the nitrogen amount on the sample surface measured with XPS. The wide scan spectra after normalization show much larger blooming of antioxidant on the surface of the control sample than for the SBR#5 nanocomposite (Fig. 28.10). Quantitative analysis indicates the nitrogen amount on the surface of the control sample increases from 3.3 to 13.7 at% after aging for 7 days then decreases to 12.0 at% in 15 days, while the nitrogen amount on the surface of SBR#5 increases from 3.0 to 8.4 at% after aging for 7 days then decreases to 4.8 wt.% in 15 days. The results present the combined impact of the blooming and the antioxidant loss due to oxygen reaction and the vapor of antioxidant. The half-life of antioxidant is 3.5 days at 90°C calculated with TGA data.

The SEM images of samples after the blooming test at 90°C for 15 days are shown in Fig. 28.10. The aggregates of antioxidant (“bloom”) on the control sample surface can be observed as well as the “clean” not blooming surface of the SBR#5 halloysite composite sample. The nitrogen amount of the

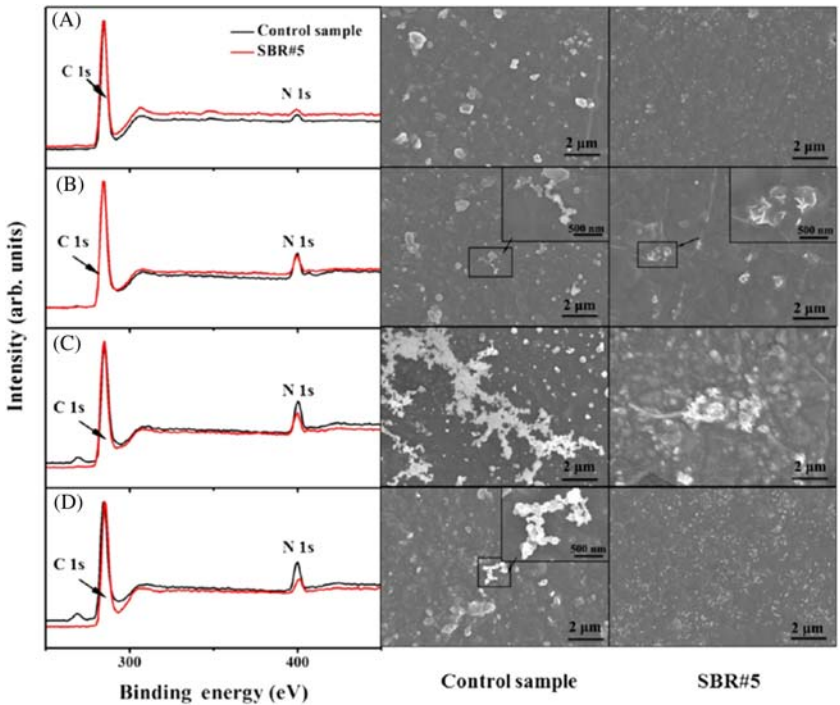


**FIGURE 28.10** XPS wide scan spectra and the SEM images of the control samples and SBR # 5 (A) before aging, and after aging for (B) 3 days, (C) 7 days, and (D) 15 days [34].

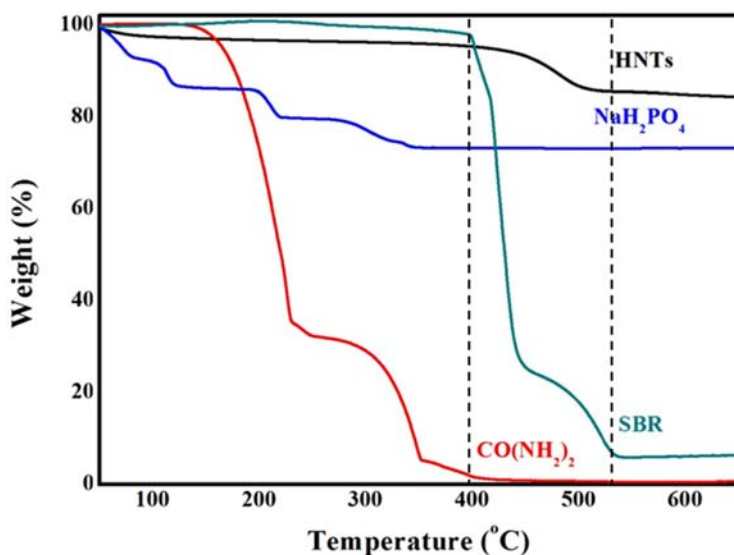


FIGURE 28.11 TGA curves of SBR, halloysite, urea, and sodium dihydrogen phosphate.

aggregates is about 4 wt.% measured with EDS, which demonstrates the aggregates are antioxidant because there is no nitrogen except other than the antioxidant. Thus the amount of antioxidant in the composite formulation without blooming was dramatically increased using loaded halloysite, while rubber with the same amount of free antioxidant caused severe blooming.

### 28.3.2 Flame-retardant halloysite rubber composites

In air atmosphere, styrene–butadiene rubber begins its rapid decomposition when heated to 400°C. Halloysite loses crystal water during the pyrolysis processing from 400°C to 550°C. In SBR/HNT composites, if ignited, the decomposition of halloysite and the evaporation of water can take away a lot of heat. The release of water vapor can dilute and cool flammable gases. Additionally, formation of inorganic barrier layers of halloysite on composite surface insulates bulk rubber from contact with oxygen in air. Urea and dihydrogen phosphate decompose below 400°C (i.e., before the decomposition of SBR during the combustion process). This decomposition helps the flame retardancy by producing carbon dioxide and ammonia, thus blocking oxygen. All the components matched with the thermal decomposition of styrene–butadiene rubber, which explain the rationality of the design of the halloysite flame-retardant system (Fig. 28.11).

#### 28.3.2.1 Mechanical property of SBR/HNTs

The tensile property and hardness of SBR filled with different amount of halloysite are shown in Table 28.2. SBR is loaded with halloysite, sodium

**TABLE 28.2** The mechanical properties of SBR/HNT composites<sup>a</sup>.

	HNTs (phr)	HNT–P (phr)	HNT–N (phr)	HNT–P/N (phr)	Ts (MPa)	Eb (%)	Ts at 300% (MPa)	Hardness (Shore A)
SBR	—	—	—	—	1.5	209	—	49
SBR-1	40	—	—	—	3.5	458	2.6	62
SBR-2	100	—	—	—	6.7	628	3.9	76
SBR-3	150	—	—	—	8.7	693	4.3	79
SBR-4	200	—	—	—	10.6	647	7.0	83
SBR-5	—	—	—	40	2.9	350	2.6	61
SBR-6	—	—	—	100	4.4	450	3.4	75
SBR-7	—	—	—	150	5.8	493	3.9	80
SBR-8	—	—	—	200	5.7	598	3.3	83
SBR-9	—	29	11	—	2.9	367	2.5	61
SBR-10	—	73	27	—	4.5	411	3.5	76
SBR-11	—	109.5	40.5	—	5.5	574	3.7	80
SBR-12	—	146	54	—	6.5	524	4.6	85

<sup>a</sup>phr (parts per hundred rubber).

dihydrogen phosphate-loaded halloysite (HNT–P), urea loaded halloysite (HNT–N), and urea and sodium dihydrogen phosphate-loaded halloysite (HNT–P&N). The tensile strength, breaking elongation, and hardness of SBR gradually increase with the increase of the proportion of halloysite, due to the reinforcement of the nanotubes of the rubber matrix. The less increasement of tensile strength and elongation at break of SBR with the addition of halloysite encapsulated with flame-retardant is due to a certain amount of flame-retardant (urea and sodium dihydrogen phosphate) inevitably being absorbed on the outer surface of the nanotubes even after washing, which affects the filler–rubber interaction and reduces the mechanical performance of composites. The hardness of SBR with the same proportion of halloysite with and without encapsulation are basically the same.

The morphology of the tensile failure section of SBR/HNTs is shown in Fig. 28.12, from which the increase of roughness with the content of halloysite can be observed. Halloysite can bear the tension and disperse the stress. The interaction between halloysite and SBR matrix leads to the obvious tracks of shear deformation. With the increase amount of halloysite, these small cracks along the tortuous path on the fracture surface become more homogeneous. This shows that the reinforcement of halloysite to SBR increases with the amount of clay nanotubes.

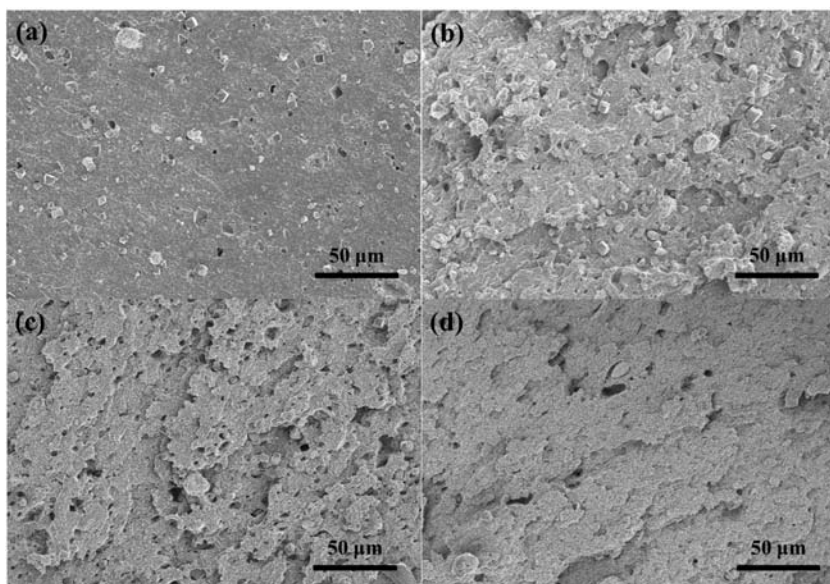


**FIGURE 28.12** SEM images of the tensile failure section of SBR/HNT composites with different halloysite addition amount: (A) 40 phr, (B) 100 phr, (C) 150 phr, and (D) 200 phr.

**TABLE 28.3** The flame-retardant properties of SBR/HNT composites.

	HNTs	HNT–P	HNT–N	HNT–P/N	LOI (%)	Smoke Production (mg/g)	Extinguish Time (s)	Combustion Condition
SBR	—	—	—	—	20.5	9.9	—	Melting drips
SBR-1	40	—	—	—	21.8	1.6	—	Melting drips
SBR-2	100	—	—	—	23.7	1.0	56	Carbonization
SBR-3	150	—	—	—	25.2	0.6	36	
SBR-4	200	—	—	—	27.6	0.4	29	
SBR-5	—	—	—	40	22.3	1.8	—	Melting drips
SBR-6	—	—	—	100	23.9	1.3	52	Carbonization Spark spatter
SBR-7	—	—	—	150	25.2	0.9	33	
SBR-8	—	—	—	200	28.2	0.5	17	
SBR-9	—	29	11	—	22.3	2.4	—	Melting drips
SBR-10	—	73	27	—	24.4	1.5	49	Carbonization
SBR-11	—	109.5	40.5	—	25.8	1.0	34	
SBR-12	—	146	54	—	28.2	0.5	21	

### 28.3.2.2 Flame-retardant performance of SBR/HNT composites

In order to investigate the flame-retardant properties of SBR/HNTs, the limiting oxygen index (LOI), vertical burning test, smoke production (SL), and thermogravimetric analysis of SBR doped with different amount of halloysite were studied. Table 28.3 shows the LOI, smoke production, time to self-extinguishing, and combustion condition of the SBR/HNT composite.

The LOI and smoke production of SBR rubber composites loaded with different amounts of halloysite, halloysite encapsulated with urea, and sodium dihydrogen phosphate were analyzed. The limiting oxygen index of styrene–butadiene rubber without halloysite is 20.5, which is a flammable material with a large amount of smoke. The LOI of SBR is significantly improved with the increasing addition amount of halloysite, which can reach the highest to 27.6 (as a refractory material) with 200 phr clay nanotubes. The flame-retardant performance of SBR is greatly enhanced with the decreased smoke production to about 5% and without melting and dropping during combustion. The LOI of SBR has been significantly improved with the addition of halloysite, due to the highly endothermic halloysite pyrolysis processing during which crystal water is lost. In SBR/HNT composites, if ignited, the decomposition of halloysite and the evaporation of water can take away a lot of heat. The release of water vapor can dilute and cool flammable gases. The significant decrease in smoke production is mainly due to the highly adsorption action of halloysite caused by its specific porous tubular structure, which absorbs the smoke generated during combustion. Smoke and toxic gases at the scene of a fire is the biggest threat to escape and rescue. It is very important to control the smoke of rubber in combustion. The LOI of SBR was enhanced to 28.2 with 200 phr of halloysite-encapsulated urea and sodium dihydrogen phosphate, and the smoke amount was extremely low. During the combustion process, urea was decomposed into ammonia gas and carbon dioxide gas, which led to the expansion of specimens. The bubbles burst and produce sound and splash. Compared to rubber with pristine halloysite, the increased LOI of rubber composited with halloysite encapsulated with urea and sodium dihydrogen phosphate (HNTs–P, HNTs–N, and HNTs–P&N) indicates synergy of these salts and halloysite on the flame-retardant performance of the rubber composite.

The TGA curve of SBR filled with halloysite (HNTs), halloysite loaded with both urea and sodium dihydrogen phosphate inside (HNT–P&N), halloysite loaded with urea (HNT–N), and halloysite loaded with sodium dihydrogen phosphate (HNT–P) in the air atmosphere is shown in Fig. 28.13. The major degradation step of SBR starts at 270°C, which is elevated to 400°C with the addition of halloysite. A significant reduction in the rate of decomposition in the presence of the unmodified clay at the major degradation step was obtained. SBR loses 2.5% weight at 408°C, and after enlarging

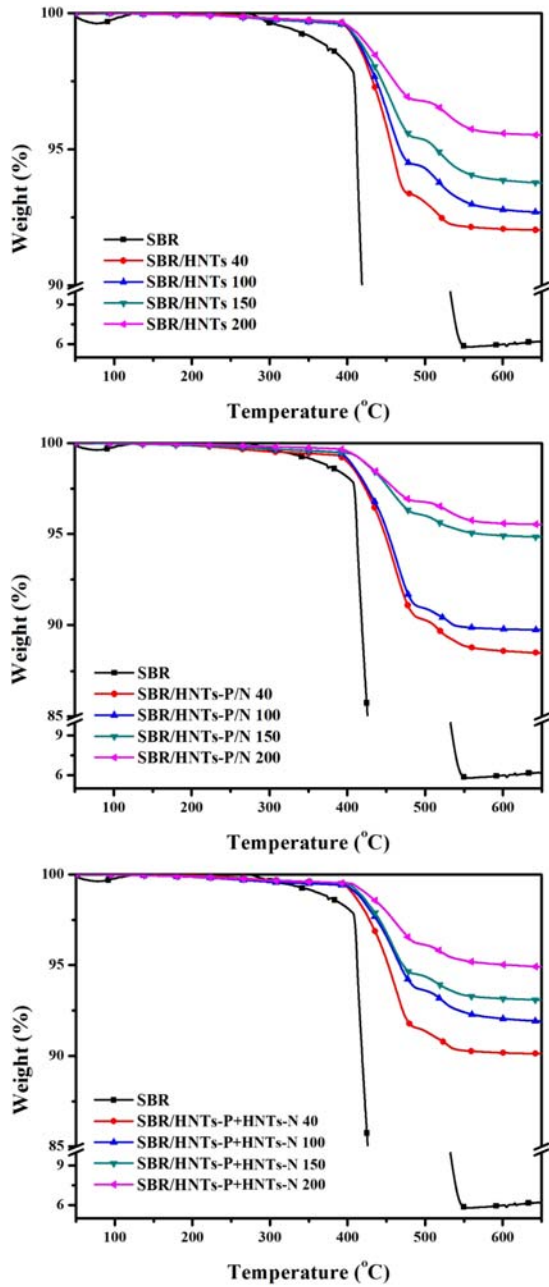


**FIGURE 28.13** TGA curves of SBR filled with halloysite(HNTs), halloysite loaded with both urea and sodium dihydrogen phosphate inside (HNT–P&N), halloysite loaded with urea (HNT–N) and halloysite loaded with sodium dihydrogen phosphate (HNT–P).

**TABLE 28.4** The combustion characteristics of SBR/HNT composites.

	HRR (kW/m <sup>2</sup> )	THR (kJ/m <sup>2</sup> )	SEA (m <sup>2</sup> /kg)	EHC (MJ/kg)	MLR (g/s)	toxicity index
SBR	404.7	111.3	1157	33.0	0.11	0.037
SBR-1	248.3	93.1	774	30.7	0.07	0.046
SBR-5	270.1	100.0	706	31.0	0.08	0.047
SBR-9	341.2	90.4	635	20.8	0.13	0.051

the amount of halloysite to 200 phr, SBR composite loses 2.5% weight at 461°C. The temperature was 432°C, 423°C, and 428°C for SBR composite formulated by doping with 40 phr halloysite, 40 phr HNT–P&N, and 29 phr HNT–P plus 11 phr HNT–N (total 40 phr) lost 2.5% weight. Including urea and sodium dihydrogen phosphate causes the decomposition temperature reduction of SBR composites, mainly because the decomposition temperature of urea and sodium dihydrogen phosphate is lower. The above results indicate that the thermal decomposition temperature of SBR can be significantly increased with the addition of halloysite.

The combustion characteristics of SBR composited with 40 phr halloysite (SBR-1), 40 phr HNT–P&N (SBR-5), and 29 phr HNT–P plus 11 phr HNT–N (SBR-9) are shown in Table 28.4. The maximum heat release rate (HRR) of SBR filled with halloysite is significantly reduced, which indicates its effect on slow thermal release in the combustion process and avoiding intense combustion. The total heat release (THR) and effective heat combustion (EHC) of SBR composites with HNT–P and HNT–N decreased. The mass loss rate (MLR) of SBR composite was significantly reduced after formulating with halloysite. The toxicity index refers to the ratio of carbon monoxide release and carbon dioxide release during combustion. The presence of halloysite and flame-retardant salt slightly increased the toxicity index. The amount of smoke produced during the combustion process can be explained by the specific extinction area (SEA), the higher of which indicates the larger smoke amount. In accordance with the LOI results, composite with halloysite can decrease smoke production. A lower smoke amount can be achieved by using halloysite-loaded flame retardants as functional fillers. Thus the flame-retardant properties can be significantly improved by compositing SBR with halloysite-loaded flame retardants.

Photos of the combustion products are shown in Fig. 28.14. After being burned, a carbon layer forms on the surface of SBR/HNTs composite, which covers the rubber surface to prevent further burning of the material and



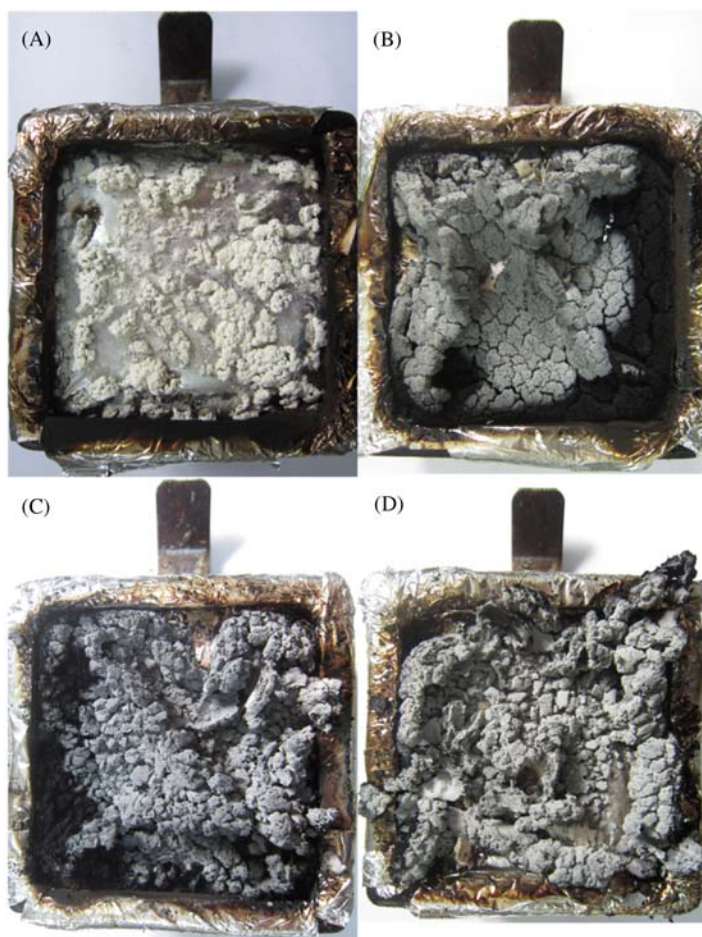


**FIGURE 28.14** Images of combustion products of (A) SBR, (B) SBR filled with 40 phr halloysite, (C) SBR filled with 40 phr halloysite loaded with both urea and sodium dihydrogen phosphate (HNT-P&N), (D) SBR filled with 11 phr halloysite loaded with urea (HNT-N), and 29 phr halloysite loaded with sodium dihydrogen phosphate (HNT-P).

reduce the burning rate. Many bubble holes can be seen on the SBR-HNT composite combustion products, the inflation of which is obvious, and is mainly due to the inflammable gas of carbon dioxide and ammonia thermal decomposed from urea, which can prevent oxygen supplement. The thermal conductivity of bubble holes caused by the inflammable gas escaped from rubber composite combustion products is obviously lower than that of rubber matrix. This can improve the flame-retardant properties of styrene-butadiene rubber composites.

### 28.3.2.3 Antiblooming property of halloysite-encapsulated flame retardants in SBR composite

The antiblooming property of halloysite-encapsulated flame retardants in SBR composite can be studied by comparing the surface of SBR composited with 146 phr HNT–P and 54 phr HNT–N (SBR-12) and SBR doped with 167.6 phr halloysite, 18.2 phr urea and 14.2 phr sodium dihydrogen phosphate (control). The composition of the control SBR sample is similar to the SBR-12 but without flame-retardant loading. The surface of SBR-12 is clean and smooth, free from frost, bubble holes, and other defects. The control sample shows a lot of bubble holes and obvious “blooming”. During the process of rubber composites, urea and sodium dihydrogen phosphate thermal decomposes and forms gas because of the heat produced by the strong shear force. The large amount of halloysite used in the composite (200 phr) increases the hardness of the compound, which makes the shear heating higher. Urea and sodium dihydrogen phosphate also decompose in the curing process as the temperature of vulcanization is 125°C. The gas that does escape in time leaves bubble holes in the rubber matrix, as shown in Fig. 28.15B. The results show that halloysite nanotubes can act as the nanometer containers so that the flame-retardant with internal loading will not decompose during the rubber processing and solve the “blooming” problem of small-molecule flame retardants.

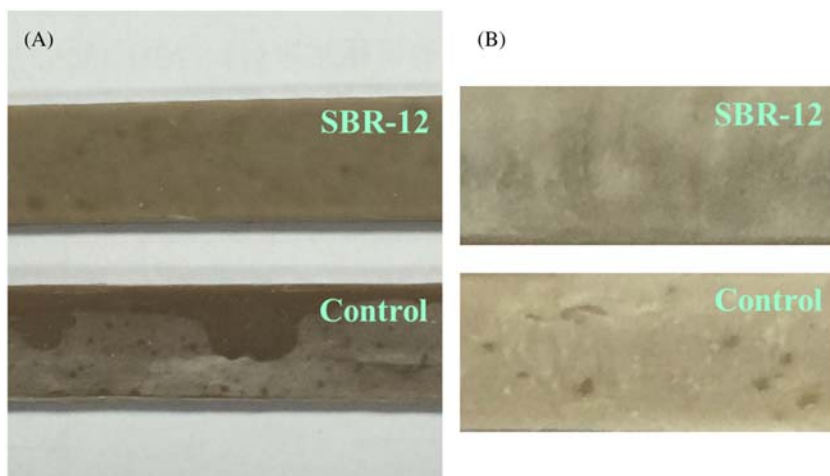


**FIGURE 28.15** Images of SBR-12 filled with HNT–P/N and SBR control sample filled with HNTs and free flame-retardant.

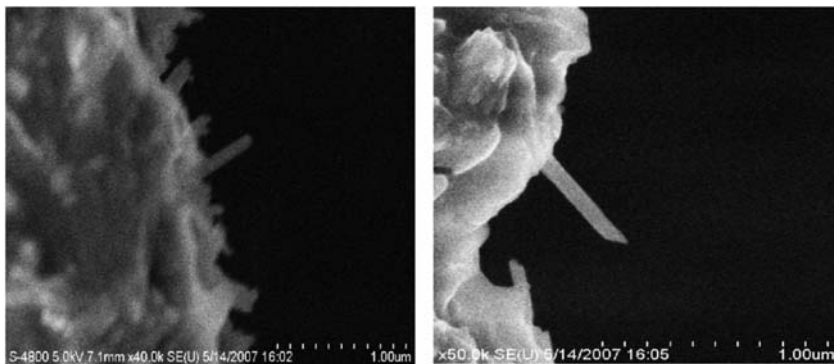


**FIGURE 28.16** SEM micrographs of a paint scratch containing 5 wt.% of halloysite nanotubes [4].

### 28.3.3 Anticorrosion halloysite elastomer composite coatings

#### 28.3.3.1 Halloysite elastomer nanocomposite coating

In Fig. 28.16, SEM micrographs of halloysite nanotubes in a scratched paint layer are shown. Nanotubes are exposed to the external environment at a paint scratch or cracks. Benzotriazole-loaded halloysite will start enhanced release of the inhibitor when a crack occurs, protecting the metal underneath from corrosion process development.

Halloysite is readily mixed with a variety of metal protective coatings (paints), which is an important advantage of this nanomaterial. Water-contact angles for halloysite pressed in the tablet were found to be as low as  $10 \pm 3$  degrees, but the material was still mixing well with paint. Surprisingly, for the paint droplet, the contact angle was even less, c. 3 degrees. The paint droplets spontaneously spread over a halloysite tablet, which is an indication of the good wettability of the halloysite tablet by paint. The presence of undisclosed surfactant additives in the paint may be the reason for this good wettability. Another reason could be due to specific chemical interactions between halloysite surface OH groups and paint hydrocarbon molecules. This interaction could be analogous to the interaction between water molecules and hydrocarbon chains as was described in various publications [35,36], where polar OH groups interact with the local charges of the CH groups formed because of the electronegativity difference between carbon and hydrogen atoms.

Addition of nanotubes into industrial oil-based paint significantly improved the strain–stress characteristics of the coating and its adhesivity (Fig. 28.17). A three-fold increase in paint tensile strength was observed with addition of 5 wt.% halloysite (0.7 MPa for pure paint versus 1.9 MPa for 5 wt.% halloysite-loaded paint). Halloysite filler also increases the hardness of the paint. Elastic modulus values of the dry paint samples were

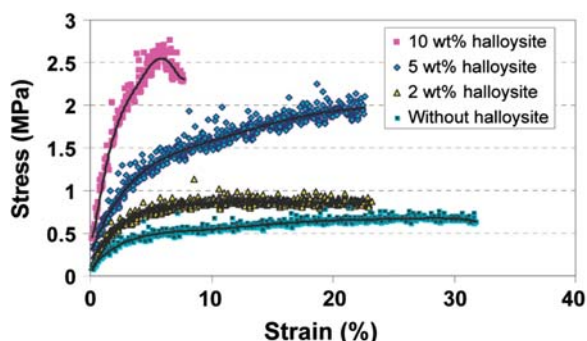


FIGURE 28.17 Stress–strain relationship of industrial oil-based blue paint [4].

16.3 MPa for a layer of pure paint and 23.1, 34.6, and 69.3 MPa for 2, 5, and 10 wt.% composites of halloysite with paint, respectively. However, paint films became brittle with more than 10 wt.% halloysite loading. These data correspond to results on halloysite clay/polymer bulk composites. For example, incorporation of 5–13 wt.% of halloysite in polypropylene resulted in a 30%–50% strength increase [37,38]. Therefore for optimal cover strength halloysite addition into paint should be below 10 wt.%.

### 28.3.3.2 Enhanced corrosion protection with benzotriazole-loaded halloysite

The initial stages of corrosion development in metal coatings and the self-healing ability of the halloysite-doped film were analyzed by the scanning vibrating electrode technique on 2024-Al alloy (taken as a substrate), which contains 4 wt.% copper. Alloy plates were coated by a dip-coating procedure with a  $\text{ZrO}_x$ – $\text{SiO}_x$  sol–gel layer and artificially scratched in a similar way. Both samples with and without inhibitor-loaded halloysites were immersed in corrosion solution, and corrosion development was observed over 24 h as maps of the corrosion current.

Anodic corrosion activity on the aluminum alloy coated by a simple sol–gel layer was high and rapidly increased within several hours (Fig. 28.18) in the scratched area. This indicates a fast pitting corrosion process taking place at the artificially introduced defect. In the case of alumina coated with sol–gel-containing halloysite tubes filled with benzotriazole, the rate of corrosion at the defect points is strongly slowed down in the first moment of corrosion and almost no corrosion current (both cathodic and anodic) was developed. In comparison to the pure sol–gel coating, the maximum current density in this case was six times smaller (c.  $3 \mu\text{A}/\text{cm}^2$  for inhibitor-containing sol–gel and  $18 \mu\text{A}/\text{cm}^2$  for pure sol–gel after 24 h of immersion), which indicates a very strong anticorrosion self-healing effect caused by controlled release of the inhibitor from the halloysite nanotubes in the cracked area.

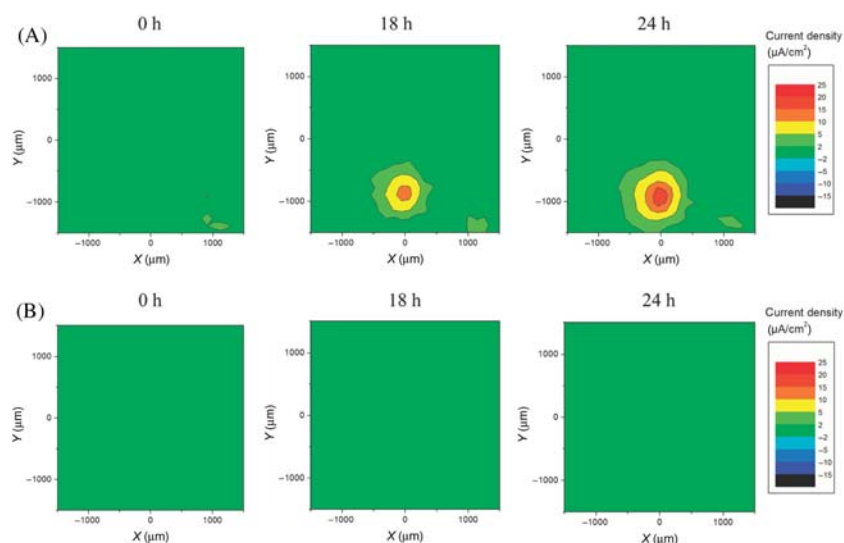


**FIGURE 28.18** Corrosion current densities of 2024-Al alloy coated with (A) pure sol-gel and (B) sol-gel particles containing halloysite loaded with benzotriazole [4].

Scratched copper strips coated with industrial oil-based paint with or without loaded halloysite were studied. Both of these strips were exposed to a highly corrosive environment simulating seawater for 10 days. Images show that paint containing benzotriazole-loaded nanotubes effectively slowed down copper corrosion, because no evidence of rust is visible in the scratched area. Elemental analysis of the reacted corrosive solution also demonstrated that 128 ppm of Cu(II) ions was dissolved for the sample B, whereas no copper was detected for sample A with halloysite-loaded coating. This result is an indication that entrapment of benzotriazole into paint using halloysite nanocontainers is efficient for metal corrosion inhibition, especially when the scratched surface is exposed to a highly corrosive liquid such as seawater. However, a longer release rate for benzotriazole may be needed for applications, which was reached with tube stopper formation, as described in the following section (Fig. 28.19).

### 28.3.4 Marine antifouling halloysite-rubber composites

#### 28.3.4.1 Morphology and properties of the EVA/HNT nanocomposites

The dispersion of clay nanotubes in the polymer matrix has a decisive impact on the final properties of the composite. We obtained the composites with uniformly distributed halloysite as shown in Fig. 28.20. The addition of anti-foulant TCPM has no adverse influence on the dispersion of halloysite tubes.



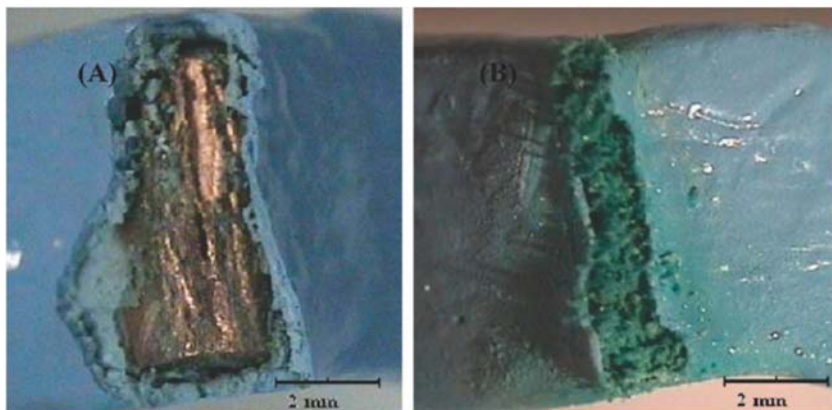


**FIGURE 28.19** Images of scratched copper strips painted with oil-based blue paint (A) containing halloysite nanotubes loaded with benzotriazole and (B) without these tubes, after exposure to a corrosive environment for 10 days [4].

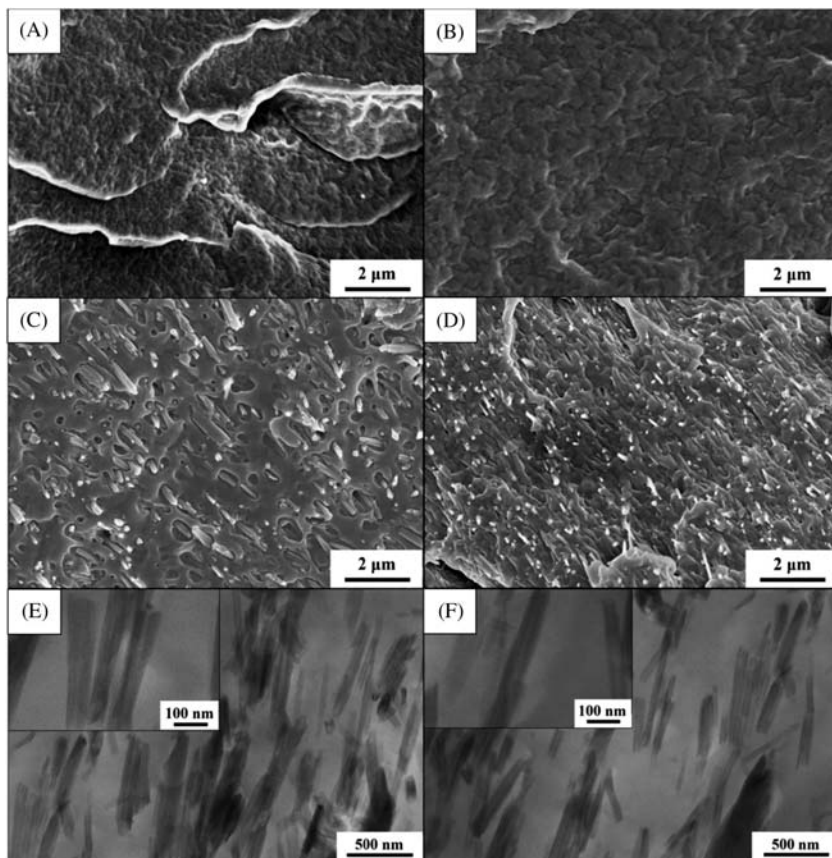


**FIGURE 28.20** SEM images of EVA/HNT composites with different formulas: (A) pure EVA#1, (B) EVA#2 composited with pristine halloysite, (C) EVA#3 doped with antifoulant TCPM, and (D) EVA#4 composited with TCPM-loaded halloysite. TEM images of (E) EVA#2 and (F) EVA#4. Halloysite consists of 12.4 vol.% of the composite [32].

The TEM images of the composite doped with pristine halloysite EVA#2 (Fig. 28.20E) and TCPM-loaded halloysite EVA#4 (Fig. 28.20F) show uniform dispersion of halloysite without aggregation. Such excellent dispersion of single clay particles is obtained without any additional exfoliation processing of this tubular clay. One can estimate from the images that the amount of the tubes in the polymer matrix corresponds to the formulation of 28.6 wt.% = 12.4 vol.% added halloysite.

The orientation of the halloysite nanotubes in the EVA matrix observed in TEM images reveals the anisotropic properties of EVA/HNT nanocomposites. We assume that the tube orientation was induced by shared force during the composite film formation. The alignment of halloysite in the melted EVA during squeezing for the pate formation produces the tubes' orientation. A similar halloysite orientation assisted by the Margoni flow was observed at the edges of drying halloysite droplets [39,40]. This nanotube's orientation phenomenon opens possibilities for formation of the plates with anisotropic strength and better coating smoothness.

The orientation of halloysite nanotubes in EVA matrix resulted in the anisotropic tensile property of EVA/HNT composite sheets (Fig. 28.21A). The tensile strength and elongation at break along the halloysite alignment direction are much higher than those in the perpendicular direction. The elastic modulus along the alignment direction is  $0.79 \pm 0.02$  MPa, and it is 1.5 times larger than the perpendicular value of  $0.54 \pm 0.02$  Mpa. The higher yield strength and more significant hardening shown in the stress–strain curve along the alignment direction of halloysite may be attributed to the macromolecules' orientation along the nanotubes. Another strengthening mechanism may be related to the clay nanotubes bridging the polymer breaks/gaps appearing during a sample elongation. These two mechanisms are also discussed in Refs. [41,42].

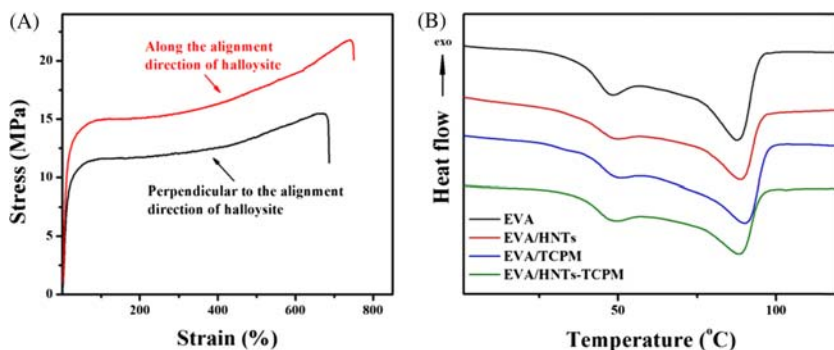


**FIGURE 28.21** (A) The tensile profile of EVA with the inclusion of halloysite nanotubes in two perpendicular directions, and (B) DSC curves of EVA composite: pure EVA, EVA composited with pristine halloysite (EVA/HNT), EVA doped with antifoulant TCPM (EVA/TCPM), and EVA composited with TCPM-loaded halloysite (EVA/HNT–TCPM) [32].

The DSC curves of the nanocomposites are shown in Fig. 28.6B. The inclusion of halloysite and antifoulant TCPM makes the full width at half-maximum of fusion peaks get wider. The crystallinity can be calculated with the equation:

$$w_c = \frac{\Delta H_m}{\Delta H_m^0} \times \frac{1}{w_E} \quad (28.1)$$

in which  $w_c$  is the crystallinity,  $\Delta H_m$  is the fusion enthalpy of EVA/HNT nanocomposites,  $\Delta H_m^0$  is the fusion enthalpy of 100% crystalline polyethylene,  $H_m^0 = 293$  mJ/mg, and  $w_E$  is the EVA content in the nanocomposites. The crystallinity of pure EVA is  $24.7 \pm 0.4$  wt.%, while the inclusion of halloysite improves it to  $31.1 \pm 0.4$  wt.%, which indicates that clay nanotubes have a significant influence on the crystallization of EVA. Halloysite nanotubes may act as crystallization nucleation sites inducing the polymer crystallization along their orientation direction. The orientation of clay nanotubes in polymeric matrix improves the composite film surface strength and smoothness as it was demonstrated for sand-resistant halloysite–epoxy solar battery coatings. Aligning these nanotubes along the water flow direction in marine coating may be also helpful.

#### 28.3.4.2 Antifouling test of EVA/HNT nanocomposites

To analyze the antifouling property of EVA/HNT, the cultured marine *Vibrio natriegens* on the EVA/HNT composite surfaces were fixed with ethanol followed by SEM monitoring. The images of EVA/HNTs were incubated in the bacterial suspension ( $OD_{600\text{ nm}} = 1.0$ ) at  $30^\circ\text{C}$  for 3 days before and after shaking at 150 r/min in 100 mL of artificial seawater (replaced every 5 days) for 60 days. A few bacteria were found on the surface of EVA (pure or loaded with antifoulant; Fig. 28.22A and E). Bacteria attached first on the surface of EVA with empty halloysite, and *V. natriegens* even formed a biofilm on the surface (Fig. 28.22B). The bacteria and halloysite can be well differentiated with their sizes: the clay tube diameter is 50 nm and *V. natriegens* is more than 700 nm; therefore these large ellipsoidal particles on the surface are bacteria. The halloysite inclusion increases the surface roughness, which leads to better proliferation of bacteria.

After exposing/shaking in artificial seawater for 60 days, the amount of bacteria attached on the surface of EVA directly doped with TCPM increases significantly, while there were no bacteria on the surface of EVA composites with TCPM encapsulated in halloysite (Fig. 28.22E and F).

The amount of *V. natriegens* adsorbed on the plate of EVA doped with TCPM after exposing in artificial seawater for 60 days was estimated as c.  $1.7 \times 10^8$  (with 20 SEM images analyzed), while only 20–50 bacteria were detected on the EVA with TCPM–halloysite surface. The bacteria adsorbed on the sample surface were observed with SEM, and the amount of



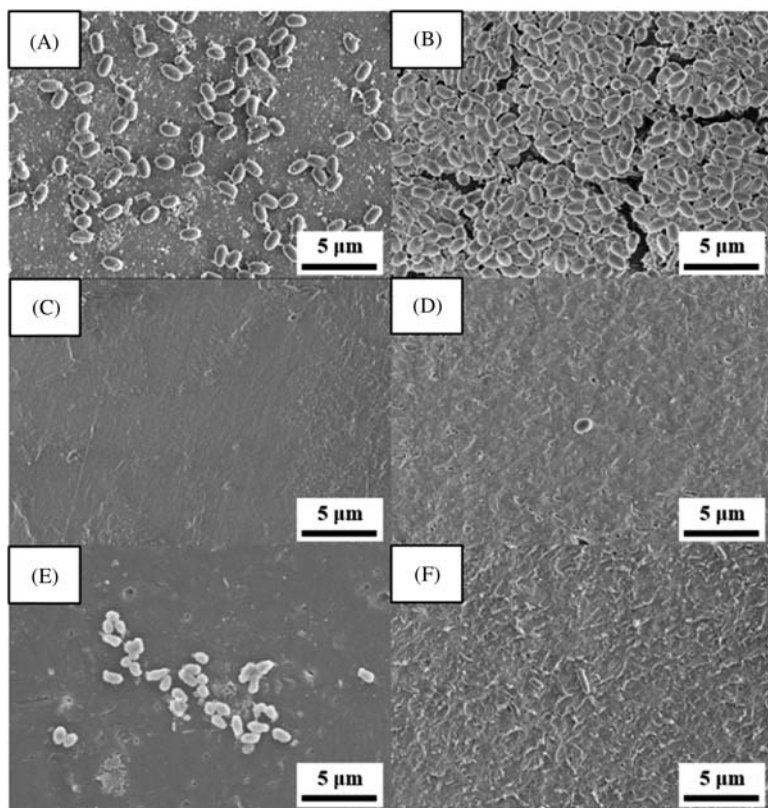


**FIGURE 28.22** SEM images of EVA/HNT composites with different formulas: (A) pure EVA#1, (B) EVA#2 composited with pristine halloysite, (C) EVA#3 doped with antifoulant TCPM, and (D) EVA#4 composited with TCPM-loaded halloysite. TEM images of (E) EVA#2 and (F) EVA#4. Halloysite consists of 12.4 vol% of the composite [32].

these bacteria was calculated. The total amount of the EVA-loaded TCPM was the same ( $3.0 \pm 0.1$  wt.%) in both formulations. This result clearly demonstrates excellent antibacterial protection with the halloysite formulation. The sustained release of antifoulant from halloysite nanotubes slowed the TCPM diffusion into the external environment and prolonged its action time, significantly improving the antifouling property of the composite. This result was further confirmed by the marine antifouling panels tests (blank plate and coated with halloysite formulation) exposed in shallow sea submergence. After soaking in the Sanya Bay, South China Sea, for 1 year, a  $35 \times 25$  cm<sup>2</sup> flat panel coated with halloysite-encapsulated TCPM remained clean, while on the control uncoated panel many marine microorganisms colonies (spots) were observed.

## 28.4 Conclusions

Natural clay nanotubes are used as containers for loading and for slow sustained release of chemical agents to prevent them from busting into rubber matrix. The encapsulation of antioxidant into halloysite allows its concentration of 3.2 wt.% (which otherwise would cause rubber defects) without any indication of surface blooming. After doping the tube-encapsulated antioxidant into bulk styrene – butadiene rubber (SBR), its release was extended to more than 9 months (66 wt.% was released in the first 5 months). After the incubation at 90°C for 7 days, the SBR with antioxidant-loaded halloysite composite showed well-retained mechanical properties. Therefore we conclude that antioxidant-functionalized halloysite improves the SBR composite aging resistance without blooming.

A long-acting antifouling ethylene-vinyl acetate (EVA) copolymer composite was prepared with the N-(2,4,6-trichlorophenyl) maleimide (TCPM) using halloysite clay as tubule nanocontainer to encapsulate TCPM and extend its release time to more than a year. Encapsulating the antifoulant agent in the nanotubes at 3 wt.% allowed for its release over 12 months, resulting in much longer protection as compared to TCPM directly admixed into the copolymer. Very few bacteria were attached on the composite with halloysite–TCPM after exposure in seawater for 2 months while control sample was completely covered with microorganisms.

Halloysite loaded with anticorrosion agents like benzotriazole, hydroxyquinoline, and then doped to elastomers provided long-lasting anticorrosion protection. Halloysite nanotube additions also provide fire retardancy and smoke suppression, which is attributed to the bound water and the highly porous surface of this nanoclay. The halloysite containers prevent loaded flame-retardant chemicals from degradation during the blending and curing processes. The addition of 10 wt.% halloysite loaded with sodium dihydrogen phosphate increases the limiting oxygen index (LOI) of the rubber from 20 to 28, while decreasing smoke production by 95%.

In conclusion, halloysite clay nanotubes are abundantly available, environmentally safe, and inexpensive natural material allowing for functional rubber–ceramic composites with enhanced properties, and its usage may be scaled up for industrial production.

## References

- [1] Veerabadran NG, Price RR, Lvov YM. Clay nanotubes for encapsulation and sustained release of drugs. *Nano* 2007;2(02):115–20.
- [2] Abdullayev E, Lvov Y. Halloysite clay nanotubes as a ceramic “skeleton” for functional biopolymer composites with sustained drug release. *J Mater Chem B* 2013;1(23):2894–903.
- [3] Jing H, et al. Internally modified halloysite nanotubes as inorganic nanocontainers for a flame retardant. *Chem Lett* 2013;42(2):121–3.

- [4] Abdullayev E, et al. Halloysite tubes as nanocontainers for anticorrosion coating with benzotriazole. *ACS Appl Mater Interfaces* 2009;1(7):1437–43.
- [5] Yuan P, et al. Organosilane functionalization of halloysite nanotubes for enhanced loading and controlled release. *Nanotechnology* 2012;23(37):375705.
- [6] Song K, et al. Spray-coated halloysite-epoxy composites: a means to create mechanically robust, vertically aligned nanotube composites. *ACS Appl Mater Interfaces* 2016;8(31):20396.
- [7] Lvov Y, Abdullayev E. Functional polymer–clay nanotube composites with sustained release of chemical agents. *Prog Polym Sci* 2013;38(10):1690–719.
- [8] Vergaro V, et al. Cytocompatibility and uptake of halloysite clay nanotubes. *Biomacromolecules* 2010;11(3):820–6.
- [9] Fakhru'llina GI, et al. Toxicity of halloysite clay nanotubes in vivo: a *Caenorhabditis elegans* study. *Environ Sci Nano* 2014.
- [10] Melo JDD, et al. Encapsulation of solvent into halloysite nanotubes to promote self-healing ability in polymers. *Adv Composite Mater* 2014;1–13 (ahead-of-print).
- [11] Fix D, et al. Application of Inhibitor-Loaded Halloysite Nanotubes in Active Anti-Corrosive Coatings. *Adv Funct Mater* 2009;19(11):1720–7.
- [12] Yuri L, et al. Halloysite Clay Nanotubes for Loading and Sustained Release of Functional Compounds. *Adv Mater* 2015.
- [13] Hussain CM. Handbook of nanomaterials for industrial applications. Elsevier; 2018.
- [14] Hussain CM, Mishra AK. New polymer nanocomposites for environmental remediation. Elsevier; 2018.
- [15] Du M, Guo B, Jia D. Newly emerging applications of halloysite nanotubes: a review. *Polym Int* 2010;59(5):574–82.
- [16] Lvov YM, et al. Halloysite clay nanotubes for controlled release of protective agents. *Acs Nano* 2008;2(5):814–20.
- [17] Fu Y, et al. Highly conductive one-dimensional nanofibers: silvered electrospun silica nanofibers via poly(dopamine) functionalization. *ACS Appl Mater Interfaces* 2014;6(7):5105–12.
- [18] Zhao Y, et al. Phase change heat insulation based on wax-clay nanotube composites. *Adv Eng Mater* 2014;16(11):1391–9.
- [19] Carli LN, et al. The effects of silane coupling agents on the properties of PHBV/halloysite nanocomposites. *Appl Clay Sci* 2014;87:311–19.
- [20] Raman VS, et al. Reinforcement of solution styrene butadiene rubber by silane functionalized halloysite nanotubes. *J Macromol Sci, Part A* 2013;50(11):1091–106.
- [21] Guo B, et al. Styrene-butadiene rubber/halloysite nanotubes nanocomposites modified by sorbic acid. *Appl Surf Sci* 2009;255(16):7329–36.
- [22] Joussein E, et al. Halloysite clay minerals — a review. *Clay Miner* 2005;40(4):383–426.
- [23] Abdullayev E, et al. Natural tubule clay template synthesis of silver nanorods for antibacterial composite coating. *Acs Appl Mater Interfaces* 2011;3(3):4040–6.
- [24] Carr RM, Chaikum N, Patterson N. Intercalation of salts in halloysite. *Clays Clay Miner* 1978;26(2):144–52.
- [25] Liu M, et al. Properties of halloysite nanotube–epoxy resin hybrids and the interfacial reactions in the systems. *Nanotechnology* 2007;18(45):455703.
- [26] Levis S, Deasy P. Characterisation of halloysite for use as a microtubular drug delivery system. *Int J Pharmaceutics* 2002;243(1):125–34.
- [27] Zhao M, Liu P. Adsorption behavior of methylene blue on halloysite nanotubes. *Microporous Mesoporous Mater* 2008;112(1–3):419–24.

- [28] Luo P, et al. Study on the adsorption of Neutral Red from aqueous solution onto halloysite nanotubes. *Water Res* 2010;44(5):1489–97.
- [29] Abdullayev E, Lvov Y. Halloysite clay nanotubes for controlled release of protective agents. *J Nanosci Nanotechnol* 2011;11(11):10007–26.
- [30] Price RR, Gaber BP, Lvov Y. In-vitro release characteristics of tetracycline HCl, khellin and nicotinamide adenine dinucleotide from halloysite; a cylindrical mineral. *J Microencapsul* 2008;18(6):713–22.
- [31] Wenbo W, et al. Clay nanotube/poly(methyl methacrylate) bone cement composites with sustained antibiotic release. *Macromol Mater Eng* 2012;297(7):645–53.
- [32] Fu Y, et al. antifouling thermoplastic composites with maleimide encapsulated in clay nanotubes. *ACS Appl Mater Interfaces* 2017;9(35):30083–91.
- [33] Fu Y, et al. Antioxidant sustained release from carbon nanotubes for preparation of highly aging resistant rubber. *Chem Eng J* 2017.
- [34] Fu Y, et al. Highly aging-resistant elastomers doped with antioxidant-loaded clay nanotubes. *ACS Appl Mater Interfaces* 2015;7(15):8156–65.
- [35] Shinoda K, Kobayashi M, Yamaguchi N. Effect of “Iceberg” formation of water on the enthalpy and entropy of solution of paraffin chain compounds: the effect of temperature on the critical micelle concentration of lithium perfluorooctane sulfonate. *J Phys Chem* 1987;91(20):5292–4.
- [36] Horvath AL. Halogenated hydrocarbons: solubility-miscibility with water. Dekker; 1982. p. 37–55.
- [37] Choi JH, Lee HY, Kim JC. Release behavior of freeze-dried alginate beads containing poly(N-isopropylacrylamide) copolymers. *J Appl Polym Sci* 2010;110(1):117–23.
- [38] Liu M, et al. Interactions between halloysite nanotubes and 2,5-bis(2-benzoxazolyl) thiophene and their effects on reinforcement of polypropylene/halloysite nanocomposites. *Nanotechnology* 2008;19(20):205709.
- [39] Liu M, et al. Self-assembling halloysite nanotubes into concentric ring patterns in a sphere-on-flat geometry. *Langmuir* 2016;33(12).
- [40] Zhao Y, et al. Orientation of charged clay nanotubes in evaporating droplet meniscus. *J Colloid Interface Sci* 2015;440:68–77.
- [41] Ye Y, et al. High impact strength epoxy nanocomposites with natural nanotubes. *Polymer* 2007;48(21):6426–33.
- [42] Tao D, et al. Chain orientation in poly(glycolic acid)/halloysite nanotube hybrid electro-spun fibers. *Pol Sci* 2015;60:284–91.

This page intentionally left blank

## Section 12

# **Environmental, Legal, Health and Safety Issues of Functionalized Nanomaterials**

This page intentionally left blank

# Handbook of surface-functionalized nanomaterials: safety and legal aspects

Neil John Hunt

*Risk Assessment Services Yordas Group, Lancaster, United Kingdom*

### 29.1 Introduction

The unique properties of nanomaterials have resulted in an increasing amount of research into their use in novel or improved technologies [1–3], such as the use of functionalized carbon allotrope nanomaterials in pollution abatement [4] or in improved analytical techniques for environmental samples [5]. This is leading to an increasing volume of nanomaterials or nano-enabled products being placed on the market for use by industry and the general public [6]. Their small size, high surface area-to-mass ratio, and unique properties have led to concern that nanomaterials might have new or increased hazard properties [7]. Significant research has aimed at investigating these hazard properties but there is no evidence of unique toxicological mechanisms applicable to all nanomaterials. However, nanoforms of some substances may display a different toxicity profile when compared to their bulk forms. This has been linked to a number of phenomena including:

- The mechanisms for cell uptake of particles are different than ionic forms [8].
- Nanosized particles can cross biological barriers that larger particles or molecules cannot [9].
- As most chemistry/biology occurs on the surface of a particle, the high surface area-to-mass ratio of nanomaterials may lead to increased reactivity.
- The small size of a nanomaterial can lead to some surface atoms being in a strained conformation resulting in greater reactivity [10].

As many of the physical and chemical properties of a nanomaterial can depend on the properties of the surface, surface modification of a



nanomaterial can be used to tune its properties to optimize their technological use. However, changing the surface properties of a nanomaterial may also change its biological and physical properties, including toxicology, toxicokinetics and environmental fate.

## **29.2 Different types of surface modification**

The term surface modification can be used to describe a number of different types of functionalization of the pure core nanomaterial.

### **29.2.1 Covalent bonds with core substance**

Some substances contain functionality that can react with other reagents to form a covalent bond resulting in new functionality on the surface of the particle. This can be regarded as modification at a specific point on the surface rather than application of a formal layer. The type and degree of functionalization can be controlled by the reaction conditions and stoichiometry of the reaction.

Once this simple functionality is established, it is relatively easy to tune the surface chemistry by reaction of the functional groups with other reagents using standard synthetic chemistry methods. This can change the charge, reactivity, hydrophobicity, agglomeration characteristics, and other properties of the nanomaterial.

### **29.2.2 Doping of particles**

Another approach to changing the properties of a nanomaterial is to intentionally dope the nanomaterial with another substance. This may be done during the synthesis of the nanomaterial where the doping substance is entrained within the entirety of the particle. Alternatively a small amount of doping can be applied to the surface of an existing particle without creating a formal coating. Although the former example is not a formal surface modification, some of the doping substance will be present at the surface of the particle and could alter the behavior of the nanomaterial when compared to a pristine substance [11,12]. It should be noted that unintentional doping of nanomaterials with impurities from the manufacturing process can also change the toxicology of a nanomaterial [13].

### **29.2.3 Intentional adsorption of substance onto surface**

An alternative approach to surface functionalization of the nanomaterial is to use intermolecular forces, such as electrostatic and van der Waals attraction, to coat a nanoparticle with a different substance by adsorption. The strength of this adsorption can vary depending on the properties of the particle and

the reagent. A nanoparticle will have three types of electric potential, surface, Stern, and zeta potential that can be regarded as a measure of the charge on the surface [14]. The magnitude of the charge and the properties of the coating reagent can determine the strength of the adsorption and the rate of degradation/substitution of the coating substance [15].

#### 29.2.4 Adsorption of natural substances in biological or environmental systems

Thus far we have only considered surface modification of the nanomaterial from a planned, synthetic point of view. However, once a nanomaterial departs from a controlled laboratory or manufacturing situation and enters a biological or environmental media, it will become coated with substances in the environment or itself agglomerate with other particles [6,16]. There is a growing belief that the whole complex of particle and adsorbed substances should be treated as the entity that drives the toxicology, toxicokinetics, and environmental fate of the substance rather than the nanomaterial in isolation [17]. The risk assessment for these structures becomes yet more complex as the nanomaterial moves between different environments because the composition of this natural coating is likely to change. For example, as the nanomaterial passes through the body it will be exposed to different proteins in different parts of the body [18]. In the environment, changes to pH, salinity, and natural organic material (NOM) can all change the natural coating of the nanomaterial [19]. Changes to the surface functionality of a nanomaterial can change how the nanomaterial interacts with these natural systems. It should be noted that toxic substances can also adsorb onto the surface of a nanomaterial and be transported across biological barriers where the nonadsorbed substance cannot. This could lead to an adverse effect even if the core substance itself is not toxic.

#### 29.2.5 Degradation of layers

The surface functionality of the nanomaterial can be degraded on exposure to the environment or other biological systems. The substance adsorbed onto a surface can be replaced by natural substances if the natural substance has a greater affinity for the core nanomaterial or if it is present at high concentration. In addition the surface functionality can be changed or degraded by the same mechanisms that degrade bulk substances such as biodegradation, hydrolysis, or photolysis [20]. These mechanisms can also change the nature of coatings bound to the nanomaterial by formal covalent bonds, either changing or removing the surface functionality [21]. The complexity of these interactions with biological systems can make the hazard and risk assessment of surface-functionalized nanomaterials difficult as multiple entities need to

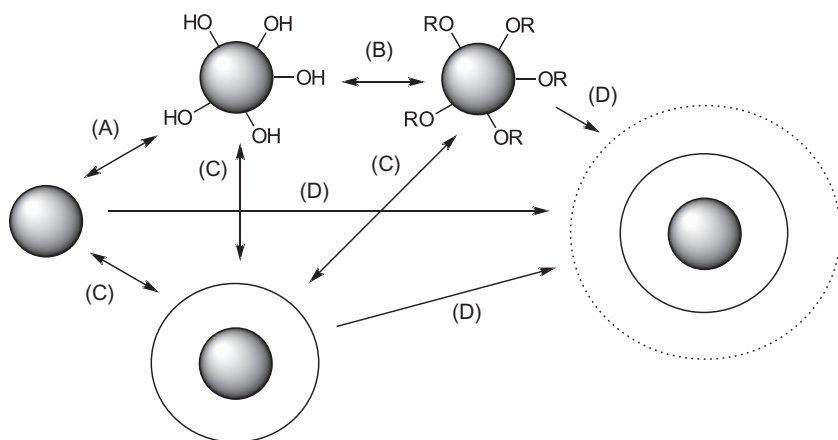


**FIGURE 29.1** Different methods to surface functionalize a nanomaterial. (A) Formation of covalent bonds with atoms on the surface (shown as oxygen but may be other elements). (B) Further functionalization on surface modification. (C) Adsorption of an intentionally added substance using electrostatic, van der Waals, or other forces. (D) Adsorption of biological or environmental substances after release of nanomaterial. The covalent bond formation and adsorption of substances are shown as reversible because degradation pathways may remove a coating to expose the core substance.

be considered rather than just one entity as would be the case with a mono-constituent organic substance (Fig. 29.1).

### 29.3 Effect of surface on biological mechanisms

In the research on hazard assessment of nanomaterials there is much more *in vitro* data than *in vivo* data. In addition, there have been difficulties in predicting *in vivo* outcomes from the *in vitro* studies. Some researchers have highlighted problems with the identification and characterization of the nanomaterial, which may help explain this issue:

- Poor physical and chemical characterization of the nanomaterial [1].
- The pristine nanomaterial might not be the appropriate substance for the *in vitro* test [19,22].
- Poorly designed experiments, such as failing to account for chelation or assay interference [23].

The suggested mechanisms for toxicity in biological and environmental situations are many and varied. A nonexhaustive list of the more commonly suggested mechanisms is as follows:

- Generation of ROS (either by the surface or by dissolved ions) [24].
- Disruption of cell membranes [25].
- Transport of toxic adsorbed substances across biological barriers [26].

- Agglomeration of particles onto biological surfaces preventing growth or molting (ecotoxicology) [27].
- Removal of nutrients available for uptake [23].

Some researchers have postulated that a change in surface functionalization can trigger an entirely different mechanism [6]. Additionally, it is increasingly apparent that the synthesized nanomaterial cannot be treated in isolation when predicting any adverse outcome.

### 29.3.1 Impact of Adsorption of substances from the media—protein corona and natural organic matter

As a nanomaterial is exposed to a biological system, proteins and other substances in the body will adsorb on the surface of the particle. The composition and behavior of this “protein corona” will depend on the surface properties of the nanomaterial and where in the body that particle is. It is this complex of particle and corona that interacts with cells and other biological systems to define its toxicokinetics. The protein corona can be divided into the hard corona that lies adjacent to the surface of the nanoparticle and the soft corona that consists of additional proteins that interact with the surface of the hard corona. Proteins in the hard corona are strongly bound and may not be replaced quickly when the nanomaterial moves to a new biological environment, whereas the proteins in the soft corona are weakly bound and will rapidly exchange in a new environment [16,28] (Fig. 29.2).

The effect of surface functionalization may also have a similar impact on ecotoxicology and environmental fate. Instead of the protein corona formed in the body, the substance present in the environment will adsorb on the surface of a nanoparticle. When looking at aqueous compartments, NOM, which is the byproduct of decomposition of natural matter and algal metabolic reactions, can include humic acids, fulvic acids, proteins, and carbohydrates [6,20]. The exact composition will depend on the characteristics of the watershed, the season, short- and long-term meteorology, and human and animal activity. How NOM adsorbs onto the nanoparticle can depend on the surface functionalization of the nanomaterial, the characteristics and concentration of NOM, pH, and salinity of the water [29]. Both synthetic and natural coating may cause changes in the agglomeration behavior (both with itself and natural colloids) and the rate of dissolution of the nanomaterial [30,31]. In order to predict *in vivo* results from *in vitro* and *in silico* studies, it may be necessary to also take into account the protein corona or ecocorona as changes in the corona might trigger a new adverse outcome pathway (AOP) or alter the outcome of the existing AOP. This could lead to a change in severity of the adverse effect or even trigger a different adverse effect [14].

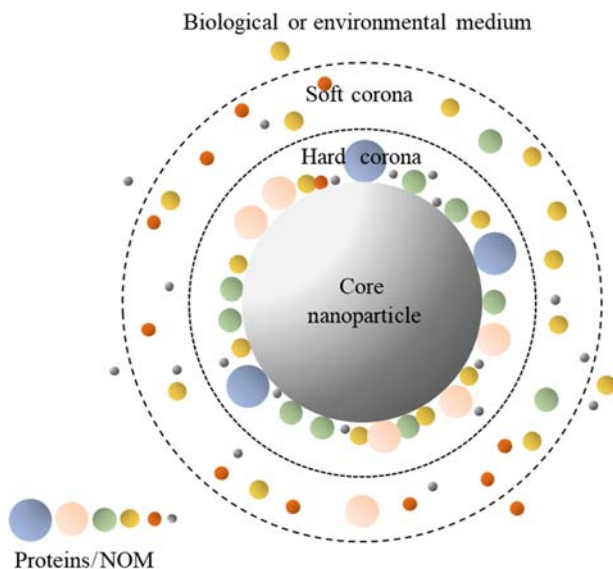


**FIGURE 29.2** The hard corona of proteins or NOM is tightly adsorbed to the nanoparticle and will not exchange rapidly. The surrounding soft corona can rapidly exchange with substances in the surrounding medium. It will rapidly change if the structure is introduced to a different medium. The whole structure is likely to impact on biological mechanisms.

### 29.3.2 Adverse outcome pathway

The adverse outcome pathway (AOP) concept is an attempt to link molecular and cellular interactions of a substance with the apical adverse endpoint. It is intended to predict the potential impact of simple interactions on the molecular scale through increasingly complex biological systems to the whole organism (Fig. 29.3).

The effect of surface functionalization on the formation of protein corona in the body is a molecular interaction that may or not place the nanomaterial on an established AOP, meaning that correctly designed *in vitro* studies could more accurately predict *in vivo* outcomes. Different surface functionalization of the same core nanomaterial could place it on a different AOP giving a different toxicological profile [32]. It must be noted that the AOP has some shortcomings that should be taken into account if the effect of surface functionalization on the toxicology of a nanomaterial is to be thoroughly explored [33,34]:

- The AOP starts from the final adverse outcome and works back to the molecular interactions that triggered it. The molecular interactions can be the starting point of a number of different AOPs.
- The AOP does not take into account toxicokinetics, so it must be considered that the AOP can be interrupted by other factors, preventing the final adverse outcome.

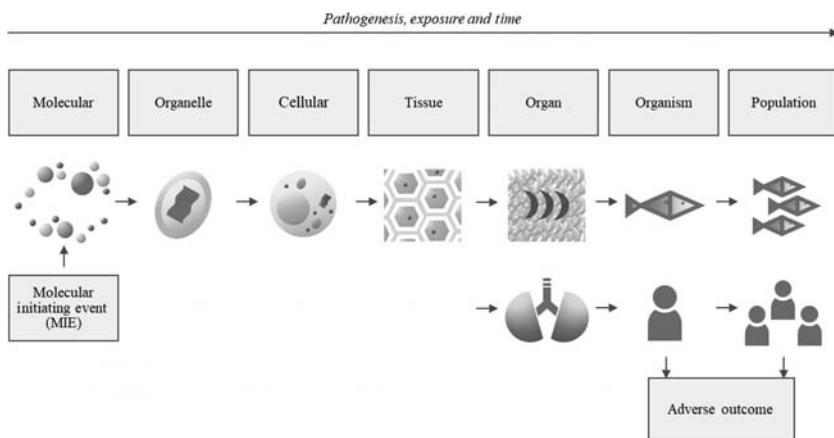


**FIGURE 29.3** A summary of the adverse outcome pathway showing the link between molecular interaction and the adverse outcome.

- The AOP is focused on an adverse outcome. It may also be important to identify pathways that lead to a nonadverse outcome or compensatory mechanisms that interrupt an AOP [34].

It is hoped that the AOP concept can be used to help with the grouping of different nanoforms of the same substance to reduce the need for extensive testing. For example, if it is shown that all nanoforms of a substance that display a negative surface charge on their surface have similar protein corona and hence the same AOP applies it would not be necessary to perform *in vivo* studies on every new nanoform with a novel coating as long as physical characterization shows it has a negative surface charge [35].

The AOP concept is equally relevant to understanding and predicting ecotoxicology as it is to human toxicology [36]. In complex environmental systems, it is not necessarily the form of the substance released that triggers adverse effects. A number of studies have linked the ecotoxicity of nanomaterials to metallic ions released during dissolution. This means that nanomaterials might have a lower acute toxicity than their ionic equivalent, but there are still concerns over accumulation of nanomaterials slowly releasing toxic ions over an extended period of time, although studies have shown that particulate effects should still be considered and that there are different response mechanisms to the particulate and ionic forms [37–39]. This also means that sedimentation of nanomaterials is not necessarily a removal mechanism when considering toxicity to the aqueous compartment [40].

Surface functionalization of a nanomaterial can change the ecotoxicity and environmental fate in a number of ways including:

- Surface coating can slow the rate of dissolution of the core nanomaterial, reducing acute toxicity [41].

- Increasing the hydrophilicity of the surface can improve the dispersion of a nanomaterial, meaning it is more likely to remain suspended in the aqueous compartment rather than flocculating into the sediment compartment and lead to higher bioaccumulation. It may also be more susceptible to transport away from the release site but be less likely to demonstrate high local accumulation [42].
- May change the probability of accumulation on biological surfaces such as gills, which has been highlighted as being part of a potential AOP for aquatic organisms [32].

### 29.3.3 Physical impacts

The previous section discussed the impacts of surface functionalization on the interaction of the nanomaterial with biological systems. However, the surface functionalization can also change the physical behavior of the nanomaterial, which will impact on the exposure of an organism to the nanomaterial. Nanomaterials are often surface functionalized to allow improved dispersion in media. Without the treatment, the pristine nanomaterial might agglomerate into large masses, meaning that the desired functionality is lost or the substance cannot be easily handled. However, this stabilization of the nanomaterial as its primary particle or small, weak agglomerates can also increase the potential for exposure to the substance, such as by increasing dustiness and hence exposure via inhalation.

## 29.4 Substance-specific examples

There are some examples of where surface functionalization has resulted in a change to the toxicological, ecotoxicological, or environmental fate of the substance. It is not an exhaustive review and there is a much larger body of research available for those interested in exploring this further.

## 29.5 Allotropes of carbon

Many carbon allotropes consist of an aromatic matrix of fused six-membered rings. These can be in 2D planes (graphene, reduced graphene oxide, and graphene oxide), elongated tubes (MWCNT, SWCNT), or polyhedrons (fullerenes). The allotropes can be functionalized by oxidation or substitution with other heteroatoms with a variety of functionalization and subsequent reaction can develop this functionality further. The surface of carbon allotropes can also be modified by adsorption of a new substance. Unmodified carbon allotropes are extremely hydrophobic and rapidly agglomerate in suspension, making them difficult to handle. This can be reduced by modification of the surface with oxygen or other heteroatoms, but this functionalization can also change the behavior of carbon allotropes in

biological and environmental systems. MWCNTs have been shown to trigger an adverse response by oxidative stress [43] leading to an inflammatory response [44]. Changing the degree of oxidation on the nanotubes has been shown to change the level and mechanism of interaction with cells in the lungs [13,45] and liver [43,46], possibly due to a change in the protein corona formed in biological media [47]. This has been seen to lead to both a reduction [46,47], and an increase [44] in cytotoxicity in *in vitro* studies, indicating that different cells can display different responses. The cytotoxicity of MWCNT has been reduced by coating with polyethylene glycol (PEG) [45] or carbon dots [48], and *in vivo* fibrotic response was reduced by functionalization with aluminum oxide [13]. Adverse effects have been seen to increase after coating with polyetherimide [13] and with metallic impurities arising from the manufacturing process [49].

Coating of SWCNTs with arginine [50] or albumin [51] has reduced the cytotoxicity when compared with untreated tubes. Graphene, reduced graphene oxide, and graphene oxide differ by the oxygen content of the substance. A study investigating the cytotoxicity of lung cells and lung inflammation in mice indicated that cytotoxicity and inflammation increases with lower oxygen content and yet further with hydrolysis of carbon–oxygen bonds. This was associated with increasing levels of carbon radicals in the substance after hydrolysis [52]. A similar increase in cytotoxicity was noted after hydrogenation, although this was linked to increased adsorption of micronutrients [53]. Fullerenes and carbon black have also shown reduced *in vitro* cytotoxicity with oxidation [54] and coating with albumin [55], although other authors have shown an increase in cytotoxicity in different cells with oxidation [56] and *in vivo* studies have shown no adverse effects [54].

In environmental media, changes in surface modification alter the interaction with NOM and degree of agglomeration [57,58]. It has been seen that increasing the stability of MWCNT colloidal suspensions increases toxicity to invertebrates [59].

## 29.6 Polymeric nanomaterials

The surface of organic polymeric nanoparticles can be functionalized to change the surface charge. Although the unmodified nanomaterials do not show strong adverse activity, some changes have been seen after modification. Modification of nanocellulose can slightly reduce, slightly increase, or leave cytotoxicity unchanged in biological [60,61] and environmental scenarios [62]. *In vivo* studies with functionalized polystyrene have shown a correlation between surface charge and biomarkers for lung inflammation [63], whereas modification to give polyurethane nanoparticles a negative charge reduced the production of inflammatory markers [64].



## 29.7 Quantum dots

Quantum dots are semiconductor nanomaterials that have unique optical properties that are used in various types of electrical equipment. Quantum dots may be a single semiconductor, often containing toxic elements such as cadmium or selenium, or core/shell structures where the core is coated with a different semiconductor such as zinc sulphide. The quantum dots may then be coated with organic ligands to tune their physical properties. Toxicity of quantum dots is postulated to be due to oxidative stress from release of toxic ions from the core of the quantum dot. The application of layers onto the core is thought to reduce toxicity by reducing the release of these toxic ions [65]. In vitro studies have shown that quantum dots with a positively charged surface have a stronger interaction with cells [66], but it is not clear whether this results in increased toxicity as it is difficult to extrapolate in vivo toxicity from in vitro results [67–69]. Other studies into modification of the surface ligands have shown that changing chirality [70] or carbon chain length [71] can alter the toxicity of quantum dots. Investigations using zebrafish embryos indicate that the toxicological mechanism of quantum dots in the environment can occur via interaction of the particles with the chorion resulting in negatively charged surfaces having greater toxicity [72] and via release of toxic ions from the core meaning that weathered quantum dots have higher toxicity than the pristine precursors [73].

## 29.8 Inorganic elements and oxides

Gold nanomaterials have received a great deal of attention in the medical arena as either anticancer treatments or as a tool to transport drugs into cells. Much research has focused on the cytotoxicity, cell uptake, and biodistribution of the nanoparticles. In vitro studies have indicated that gold nanomaterials with a positive surface charge have a greater uptake in cells than other gold species, potentially due to electrostatic attraction with negatively charged cells [74]. Other research has highlighted the importance of changes to the protein corona with changes to surface functionalization [75–77] and that gold nanoparticles with different surface charge may use different cell uptake mechanisms [78,79]. These complex interactions have meant that it is difficult to predict in vivo outcomes from in vitro studies [80,81]. The shape of gold nanomaterials can be directed by the addition of surfactants such as cetyltrimethylammonium bromide. It has been seen that the presence of these surfactants on the gold nanoparticle surface can lead to increased toxicity [82]. Changes to the surfactant used [83] or the manufacturing process to remove residues [84] have reduced the toxicity of the nanomaterial. In environmental media, the effect of surface functionalization and charge appears to differ between target organisms [27,85] and concentration [86], meaning that grouping for prediction of ecotoxicity could be difficult for functionalized gold nanomaterials.

Silver nanomaterials are antimicrobial and could have a wide range of uses in materials. The most common surface modifications are application of neutral polyvinylpyrrolidone (PVP) or negatively charged citrate coatings. As with other nanomaterials, it is difficult to predict *in vivo* results from *in vitro* studies [87], but Alessandrini [88] has shown that citrate-coated silver nanomaterials display a greater allergic response in the lungs than AgNP coated with PVP. Fears over the release of silver nanomaterials from these materials into the environment have meant that a great deal of research has investigated the effect of surface functionalization on ecotoxicity. The mechanism for ecotoxicity is commonly believed to be due to release of toxic silver ions, although additional mechanisms have been suggested [89]. Therefore ecotoxicity of surface-functionalized silver nanomaterials has been linked to the rate of release of silver ions and the availability of the nanomaterial (greater with increased suspension stability). Coating has reduced toxicity when compared to uncoated silver nanoparticles [90], but the relative toxicity of coated nanoparticles depends on the target organism [42,91,92], NOM content in water [93,94], salinity [31,94], and soil type [95].

Inhalation exposure to silica has been linked to severe outcomes to health (silicosis), with the inflammatory response being linked to production of reactive oxygen species (ROS). Silica can have Si—OH (silanol) groups on the surface that can then react to covalently bond the functionalizing agent, but it is also possible to adsorb a coating onto the silica nanomaterial. The presence of free silanol groups have been linked with causing the production of ROS so coating usually reduces toxicity [96–99]. Interestingly the manufacturing conditions of silica nanomaterials can influence the silanol concentration on the surface and a lower concentration is linked to increased cytotoxicity [100]. This appears to contradict the previous statement, but it is thought that high silanol concentration leads to increased hydrogen bonding between silanol groups making them less likely to generate ROS when compared to isolated silanol groups. As with other nanomaterials, changing the surface functionalization changes the protein corona which impacts on lung fibrosis [101], cell uptake [102], and transfer of the nanomaterial from mother to fetus [103].

Titanium dioxide has also been linked to adverse effects from inhalation exposure, meaning that it has been proposed to classify the substance as Carcinogen 2 (by inhalation) in the EU. Coating titanium dioxide can either increase or decrease cytotoxicity and pulmonary toxicity depending on the identity of the coating substance. Titanium dioxide coated with aluminum oxide or other hydrophilic substances increases toxicity whereas coating with hydrophobic coatings such as silanes reduces toxicity [104,105]. Interestingly the opposite effect appears to apply to ecotoxicology [106,107]. Doping of the nanomaterial with other metals (e.g., silver, gold, palladium) has increased cytotoxicity [108,109]. In their opinion on the proposal for harmonized classification of titanium dioxide, the Risk Assessment Committee proposed a note stating, “If the substance is to be placed on the market as

fibres (with diameter  $<3\ \mu\text{m}$ , length  $>5\ \mu\text{m}$  and aspect ratio  $\geq 3:1$ ) or particles of the substance fulfilling the WHO fibre criteria or asparticles with modified surface chemistry, their hazardous properties must be evaluated in accordance with Title II of this Regulation, to assess whether a higher category (Carc. 1B or 1A) and/or additional routes of exposure (oral or dermal) should be applied,” which recognizes the potential impact of modification of a surface on toxicity [110].

Zinc oxide nanomaterials are used in sun protection products. Although untreated zinc oxide nanoparticles have displayed low *in vivo* toxicity, *in vitro* studies have shown some cytotoxicity associated with release of zinc ions. The release of zinc ions was also linked to toxicity in the environment. Studies with coated zinc oxide nanoparticles have indicated that coating with silica can reduce cytotoxicity, supporting this hypothesis [111], but changing the degree of hydroxylation can also change the degree of cytotoxicity indicating that other mechanisms may also be occurring [112]. Changing the hydrophobicity of the coating of zinc oxide has different effects on ecotoxicity depending on the target organism [113,114], indicating that different mechanisms may be in effect, but doping with other metals may increase toxicity [115,116].

## 29.9 Regulatory and legal issues that impact surface-functionalized nanomaterials

The use of chemicals is governed by a myriad of different regulations across the globe. Some regulations are based on the chemical, physical, or biological characteristics of the substance whereas others are defined by the use of the substance. In almost all regions, nanomaterials are regarded as a form of the chemical substance and hence fall under the remit of the regulations that apply to all other forms of a chemical substance. The unique properties of nanomaterials mean that there is an international drive to develop nanospecific testing protocols [117] [Organisation for Economic Co-operation and Development (OECD)]. There are very few if any regulations that apply specifically to nanomaterials. If surface-modified nanomaterials are considered in a regulation, it is usually as a member of a group of forms defined by the chemical composition of the core particle. Probably the most detailed regulation that explicitly discusses nanomaterials is the REACH [Registration, Evaluation, Authorisation and Restriction of Chemicals, (EC) No 1907/2006] Regulation in force in the EU and European Economic Area (EEA) [118].

### 29.10 Current REACH situation with nanomaterials

REACH came into force in the EEA in 2007 and it was immediately recognized that, although the regulations could be applied to nanomaterials, some of the requirements within the regulation would need to be amended for nanomaterials. Three projects were initiated to identify the necessary

modifications and allow the production of guidance documents to allow industry to register nanomaterials. Project members were experts drawn from regulatory, industrial, and nongovernmental organizations across the EEA and were expected to reach a consensus on the conclusions of the projects. These projects were the REACH Implementation Projects on Nanomaterials (RIP-oN), with RIP-oN 1 covering Substance Identification [119], RIP-oN 2 focusing on Information Requirements [120], and RIP-oN 3 assessing exposure assessment and hazard/risk characterization [121]. RIP-oN 2 and RIP-oN 3 were able to arrive at a common position outlined in the project reports. However, no consensus was arrived at for the RIP-oN 1 project. One of the key areas of disagreement was how surface-treated nanomaterials should be approached under the REACH regulations. The industry position was that surface-treated substances were clearly covered by FAQ (Frequently Asked Question)<sup>1</sup> 6.3.8, whereby the surface modification was only a minor proportion of the substance as a whole so the surface-modified substance should not be regarded as a new substance or as a mixture. Other members of the project team did not agree with this position and insisted that the high surface area-to-mass ratio of nanomaterials meant that the surface modification now made up a significant proportion of the substance and that the properties of the nanomaterial may often be governed by the chemistry of the surface rather than the core of the nanomaterial. Therefore it should be regarded as a key identifier for the identity of the substance.

The document produced by the European Chemical Agency (ECHA) to support registrants “Guidance for identification and naming of substances under REACH and CLP” states that surface modification may be used as an additional identifier for a registered substance, but it is up to the registrant to decide if it is relevant to their product or not [122].

## 29.11 Board of appeal review

The REACH regulation requires that an evaluation process should occur for some registered substances to assess whether additional regulatory or technical measures should be put in place to adequately control the risk arising from the use of the substance. The evaluation process consists of two types of evaluation:

- Dossier evaluation—Performed by ECHA to ensure that all the information requirements stated in REACH are included in an individual registrant’s dossier (Articles 40–43).

---

1. A Frequently Asked Question (FAQ) is a question that has been raised repeatedly to the individual member states and has required a response from the Competent Authorities for REACH and CLP (CARACAL) group to clarify the regulation. A FAQ response can be viewed as lying behind only the legal text of the regulation in terms of precedence if there appear to be contradictions in the official documentation associated with the regulation.

- Substance evaluation—Performed by a Member State Competent Authority to ensure that sufficient information of high enough quality is contained in the dossier to be able to identify the hazard and risk associated with the use of the substance and that suitable risk management measures have been identified to control the risk (Articles 44–48).

The outcome of an evaluation may require the registrant to generate more information by commissioning additional studies. If the registrant does not agree with the conclusions of the evaluation, either based on technical or scientific arguments, they can lodge an appeal with the Board of Appeal. The Board is an independent group of legal and scientific experts who will reach a binding conclusion on the appeal.

There have been three successful or partially successful appeals made to the Board of Appeal covering surface-treated nanomaterials by registrants that may have influenced a change in the REACH regulation in 2020 (Table 29.1).

A common feature of the original evaluation decisions reached by ECHA was that there was insufficient information contained in the registration dossier to allow a decision to be reached on the hazard and risk of the substance, especially whether the data held in within the registration dossier was applicable to the substances being placed on the market. As we have seen, the nature of the surface of a nanomaterial may impact on its toxicity and exposure behavior. Without information on surface treatment for either the tested substance or the substance placed on the market, it was very difficult for ECHA to reach a conclusion to the evaluation. In order to overcome this impasse, a number of changes to REACH, including the requirement to provide information on surface treatment, have been proposed and are expected to come into force in early 2020.

## 29.12 Amendments to the annexes of REACH (2019)

### 29.12.1 Concepts of nanoforms and similar sets of nanoforms

In order to acknowledge that the toxicity, exposure, and fate of a nanomaterial may be dependent on more parameters than simply the chemical composition of the core of the particle, the concept of nanoforms of the same substance was formally included in REACH in 2019 [127]. The amendment states that, “The term ‘nanoform’ should be used for the purposes of Regulation (EC) No 1907/2006 to identify any form of a substance or a distinct substance that fulfills the definition of nanomaterial.” A new nanoform is manufactured if a product is placed on the market that intentionally differs from another product by any physical or chemical parameter. However, unintentional interbatch variability does not result in the formation of a new nanoform. Although it is expected that each nanoform placed on the market should be assessed to demonstrate that their associated hazards and risks are

**TABLE 29.1** A summary of the Board of Appeal decisions that have directly referred to nanomaterials.

Substance/case number	Summary of original evaluation decision	Summary of basis of appeal	Decision of board of appeal
Titanium dioxide/A-011–2014 [123] <sup>a</sup>	Further particle characterization was required, including identification of surface treatment, for each grade of the substance placed on the market.	The REACH registration allows registrants to define how their substance is defined and it is not an obligation to define the substance beyond its chemical composition.	Appeal upheld and the requested for further information was annulled.
Synthetic Amorphous Silica (SAS) A-015–2015 [124] <sup>a</sup>	Although four types of SAS were discussed in the dossier, no mention of nanoforms of SAS were included. It was suspected that some grades would be nanomaterials. Additional particle characterization for each grade should be added to the dossier. Subchronic toxicity studies by inhalation on four grades of pyrogenic SAS differentiated by specific surface area and surface treatment are required.	Further testing should be based on a justified concern regarding hazard or risk. It was believed that the additional information was required only because nanoforms existed without evidence that this would lead to increased hazard/risk.	The request for additional physicochemical properties on individual forms of SAS was annulled.
			The request for subchronic inhalation toxicity data on four forms of pyrogenic SAS was upheld.
Silicic acid, sodium aluminum salt A-010–2015 [125], A-011–2015 [126]	Further information on the composition of different nanoforms/grades of the substance was requested including information on surface treatment.	The terms nanoform and grade are not clearly defined in the regulations and there is no requirement to provide this information for different products meeting the description of nanomaterial in REACH	Appeal upheld

<sup>a</sup>It should be noted that similar decisions have been reached for different appellants who registered the same substance.

known and controlled, there are some approaches defined that will reduce the amount of new testing required, thus meeting the requirement of REACH to minimize animal testing. If different nanoforms within a single dossier can be demonstrated to have a similar hazard and risk profile across all endpoints stipulated within REACH, then only one set of data is required for this set of similar nanoforms. In addition, for individual endpoints, grouping of nanoforms and read-across to data-rich nanoforms is encouraged to fulfill the obligations for data-poor nanoforms. Both grouping and establishing the set of similar nanoforms will require strong scientific justification based on comprehensive knowledge of the physical and chemical properties of each nanoform and how these impact on the biological pathways that might lead to toxic effects.

After publication of the proposed amendments to the regulation, comments were invited from other interested parties. The Nanotechnology Industries Association (NIA) highlighted that it may not always be clear how to define the boundary between one nanoform and another (or two groups of nanomaterials and another) [128]. For example, it is straightforward to differentiate between coated and uncoated nanoforms but for surface-treated nanomaterials where there is a continuum of the surface-treatment parameter (e.g., degree of oxygenation of a MWCNT) it may be more difficult to define where one nanoform stops and the next one starts. The European Chemical Industry Council (CEFIC) commented that the definition of a nanoform would need to be improved before the revised regulation is put into place [129]. The Center for Environmental Law (CIEL) highlighted an uncertainty regarding requirements for environmental fate and ecotoxicology. “Similarly, the absence of specific requirements to distinguish nanoforms depending on their surface treatment and assess them separately (despite Subsection 2.4.3 of guidance note that includes ‘Description of surface functionalization or treatment and identification of each agent including IUPAC name and CAS or EC number’) is a serious gap that should be addressed in future versions.” [130]. The proposed new regulations also appear to place requirements on downstream users to communicate changes in nanoforms during their use to the registrant in order for these changes to be included in the risk assessment in the registration dossier by stating that, “A use may modify the nanoforms of the substance, potentially changing one nanoform into another form or generating a new nanoform. Downstream users should provide this information up the supply chain to ensure that the use is adequately covered by the registration dossier of the manufacturer or importer, or alternatively cover the specific use in their own chemical safety report.”

In December 2018, the amendments were formally introduced into EU law [131]. These changes require that any registration dossiers should be updated by January 1, 2020 to reflect the amendments. In addition to the introduction of the terms *nanoform* and *set of similar nanoforms* to the regulation, the amendments also recognize that some of the endpoints previously

in Annexes VII–X of REACH would need to be satisfied using different techniques to those used for other forms. For example, as the behavior in solution/suspension of nanomaterials in water is a kinetic phenomenon, the thermodynamic endpoint partition coefficient is not relevant, so the dispersion behavior in water is needed instead.

Changes to the surface functionalization of a nanomaterial are explicitly stated to result in a new nanoform, with the registrant being expected to give details of either the new functionality and/or the reagents used to give the surface functionalization. However, if different methods of functionalization produce nanoforms that can be shown to have similar hazard and risk profiles across all endpoints, they can be regarded as belonging to a set of similar nanoforms and would only require one set of endpoint data. As a hypothetical example, if it can be scientifically justified to state that any nanoform of a given substance that has a negative surface charge has a similar hazard profile, then all nanoforms with varying degrees of carboxylate or alkoxide functionality could be regarded as falling within one set of similar nanoforms and thus only require one set of endpoint data in the substance registration dossier.

There are a number of issues with the amended regulation that will require further clarification in updated guidance document, that at the time of writing, have not been published. These include:

- What is the precise definition of *similar*?
- What degree of scientific justification will be needed by the regulators to define the boundaries of both *a set of similar nanoforms* and for grouping?

### 29.12.2 Complexity of risk assessment for nanomaterials (looking at surface modification)

The amendment to REACH requires a risk assessment of different nanoforms, both as manufactured nanoforms or new nanoforms formed during their service life, that may lead to significantly increased complexity when compared to a nonnano form of a substance.

A risk assessment for an organic, monoconstituent substance is outlined in Fig. 29.4 (upper). An assessment of the life cycle of the substance will identify all the uses of the substance, and hence all potential exposures to the substance, both human and environmental. Once the routes of exposure are identified, corresponding hazard data needs to be collated to calculate the risk associated with the uses of the substance. The exposure assessment will investigate both direct exposure to humans (workers and consumers, based on the characteristics of the activity, containment, and risk management measures) and exposure to the environment including indirect exposure to humans via the environment (based on release, partitioning between



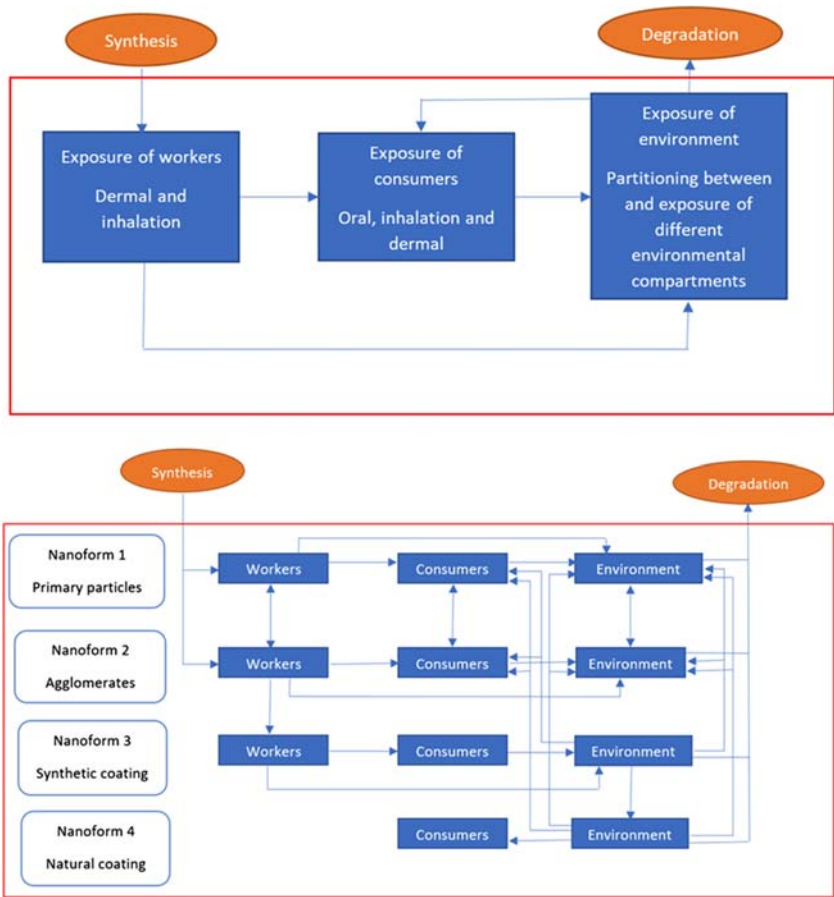


**FIGURE 29.4** Upper, risk assessment across the life cycle of a “bulk” substance. Lower, risk assessment network across the life cycle of a nanomaterial that can exist as four distinct nanoforms with different hazard profiles (note neither network includes degradation products to reduce complexity).

environmental compartments and rates of degradation). This process is simplified by the hazard of such a substance being an intrinsic property of the substance, meaning the same hazard data can be applied throughout the risk assessment. It has been shown that conversion to a new nanoform of the same substance can change the toxicological/ecotoxicological properties of the substance. This means that the complexity of the risk assessment of a nanomaterial can be significantly greater than other forms of a substance (see Fig. 29.4, lower). For a surface-treated substance, knowledge of the degree of modification and rate of degradation or changes to the surface modification through the lifespan of the nanomaterial will be required.

In addition, how these changes affect other parameters such as degree of agglomeration/aggregation, solubility, and surface charge would need to be considered.

It is clear that if testing on all nanoforms of a substance manufactured and all the forms it might convert to through its life cycle were mandated, the overall cost would be prohibitive to the development of nanotechnology and the animal testing requirements would be ethically difficult to justify. This issue has already been confronted in the risk assessment of “bulk” substances within REACH, meaning that the use of *in silico*, *in vitro*, grouping, categorization, and read-across are all encouraged if they are scientifically justified [132].

### 29.12.3 Use of grouping for the risk assessment of nanomaterials

The use of existing information to inform an assessor of the hazard, exposure, and risk parameters of a novel substance is a well-established method to avoid excessive and expensive testing. There are a number of approaches that can be used for the prediction of properties.

- Category approach—Identification of group of substances that have similar structures, composition, or a common mechanism of toxicity. The category approach can use one set of experimental data that is applied to the whole category. Alternatively if there is a correlation between two parameters within a category, it is possible to predict the value of one of these parameters for a data-poor member if the other parameter is known, which is known as a Quantitative Structure Activity Relationship (QSAR). Both these approaches have been used for the REACH registration of a number of the oil-sourced hydrocarbon substances that are defined by their manufacturing method but have a similar chemical composition.
- Analogue approach—Often known as read-across, this is the application of data from a data-rich substance to a structurally similar, data-poor substance.

Any type of grouping must be scientifically justified to be used for REACH registrations. Although structural similarities, such as common functional groups, are often used to define a category, the basis for the category will be based on knowledge of the toxicological mechanism for hazard endpoints. An analogous approach can be used to predict ecotoxicological and environmental fate data. Grouping is also used for the exposure part of a risk assessment, with the grouping being based on both the activity and simple physical properties of the substance.

It has been seen that there is the potential for multiple nanoforms of the same substance to be formed and that REACH may soon require each nanoform to be assessed within a registration dossier. To avoid costly

**TABLE 29.2** Four groups of different nanomaterials postulated by DF4 nanogrouping [134].

Group definition	Potential toxicological mechanism	Examples
Soluble nanomaterials	Ion-based mechanisms	ZnO, CuO
Biopersistent high aspect ratio nanomaterials	Frustrated phagocytosis	MWCNT
Passive nanomaterials	Rapid metabolism or clearance mechanisms	Low surface carbon black, hematite
Active nanomaterials	Oxidative stress from surface reactivity	Graphene, graphite nanoplatelets, TiO <sub>2</sub> , CeO <sub>2</sub>

and complex testing programs, the use of groupings for nanomaterials could be a useful strategy. Unfortunately, the shortage of information around the toxicological mechanisms of nanomaterials means that grouping of nanomaterials is in its infancy. Arts et al. developed the DF4 nanoGrouping decision framework that identified four different groups of nanomaterials that can be supported by common toxicological mechanisms [133]. Interestingly different forms of amorphous silica were placed in different groups if the surface functionalization was changed [134] (Table 29.2).

A number of EU-funded projects have investigated the use of grouping to reduce the need for testing or to develop predictive models (nano-QSARs). It is hoped that the recently started GRACIOUS project will pull together these approaches, identify and fill technical gaps and produce a holistic tool that will allow grouping of all types of nanoforms for all aspects of risk assessment, including ecotoxicology (<https://www.h2020gracious.eu>).

The grouping of surface-treated nanomaterials can be done in a number of ways:

- Grouping of surface-treated nanoforms with untreated nanoforms
- Grouping of nanoforms with different surface treatment but similar physical properties (e.g., surface charge)
- Grouping of surface-treated nanoforms with the bulk forms of the substance
- Grouping of nanoforms of different substances with the same surface treatment
- Definition of ranges of surface functionalization that display the same or predictable properties (e.g., degree of oxygenation of carbon-based nanomaterials) (Fig. 29.5).

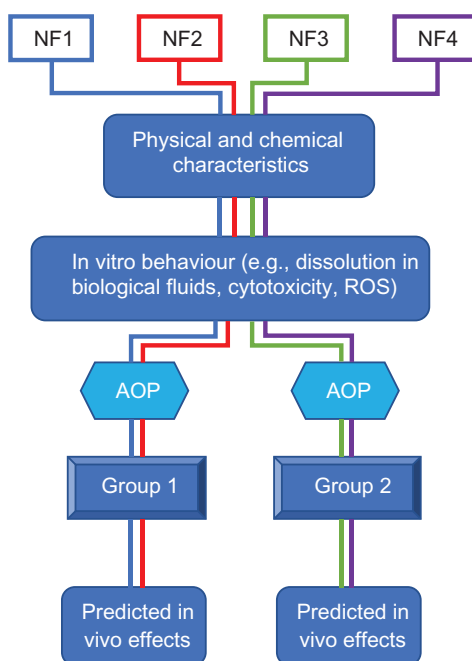


**FIGURE 29.5** The physical and chemical characteristics of the distinct nanoforms can be used to postulate groups. In vitro studies may then be used to confirm these groups by identifying potential common AOPs. In vivo properties can then be predicted without the need to perform excessive animal studies.

## 29.13 Other EU regulations

A number of other EU regulations of chemicals refer to nanomaterials, but many do not specifically refer to surface-treated nanomaterials or nanoforms. However, the structure of these regulations can be used to predict the probable requirements for a surface-treated nanomaterial.

### 29.13.1 Biocidal Products Regulation

The biocidal products regulation (BPR) requires that the active substance (i.e., the component of a product that has biocidal properties) is approved and that biocidal products (i.e., formulations placed on the market) are authorized [135]. Both active substance approval and biocidal product approval require chemical characterization using validated analytical protocols, efficacy testing, and human/environmental risk assessment. The regulation requires that if an active substance can exist as both bulk and a nanomaterial, separate active substance approvals are needed [Article 4(4)]. The concept of different nanoforms are not currently included in the regulation, so it is not immediately obvious whether a surface-treated nanomaterial would require

an additional active substance approval if a different nanoform had already been approved. However, nanosilver is currently being evaluated so the outcome of this evaluation will give a clearer idea of the regulator's approach to different nanoforms [136].

One requirement that registrants need to fulfill is technical equivalence with the substance used to generate the efficacy and toxicological data in the original substance approval dossier. If a nontreated substance was used for the active substance approval dossier, it might be difficult to prove technical equivalence if the surface-treated nanoform was used as the active substance in the biocidal product. The best chance of using the existing approval would be to prove that surface treatment of the nanomaterial had no effect on the toxicity and environmental fate, perhaps if surface treatment is only required to improve the stability of the biocidal product.

### 29.13.2 Cosmetics regulation

Regulation (EC) No 1223/2009 on cosmetic products has specific requirements for ingredients that are nanomaterials unless their function in the product is as a colorant, a UV-filter or a preservative under Article 16 [137]. In addition to the standard notification required for all cosmetic products, the responsible person for a cosmetic product containing a nanomaterial must notify the Commission 6 months before the product is placed on the market unless it is in conformity with the requirements of Annex III. The notification should include "the specification of the nanomaterial including size of particles, physical and chemical properties," "the toxicological profile of the nanomaterial" and "reasonable foreseeable exposure conditions" [Article 16 (3)]. The SCCS will give its opinion on the safety of the nanomaterial and the product within 6 months, possibly after requesting further information from the responsible person. The commission will also keep a catalog of nanomaterials used in cosmetics in the EU [138].

The regulation does not explicitly mention surface-treated nanomaterials, although it can be inferred that the chemical characteristics of the substance would include surface treatment. Moreover, the catalog of nanomaterials used in cosmetic markets does include separate entries for hydrated silica, silica, silica dimethicone silylate, silica dimethyl silylate, and silica silylate, all of which could be viewed as surface-functionalized silica. However, these substances do have separate CAS numbers and as such could be viewed as different substances as opposed to different nanoforms of the same substance. The entries for titanium dioxide and zinc oxide do not contain information on surface treatment, so it is not possible to ascertain whether different entries are distinguished by different surface treatments. It is reasonable to assume that if the surface treatment of a nanomaterial results in a change to the toxicological profile of the nanomaterial, a new or updated notification would need to be submitted to the Commission.

### 29.13.3 Medical devices

There are two regulations that cover medical devices in the EU, Regulation (EU) 2017/745 on medical devices [139] and Regulation (EU) 2017/746 on in vitro diagnostic medical devices [140]. Only the former explicitly discusses nanomaterials in its wording. If a nanomaterial is present in a medical device, the level of risk assessment required will depend on the potential for release of the nanomaterial and hence internal exposure. If there is a negligible chance of exposure the device would be defined as a class IIa device, a low chance of exposure would result in classification as class IIB and a medium or high chance of exposure would define the device as class III. The different device classes have differing degrees of risk assessment and reporting obligations under the regulation. There is no reference to different nanoforms of a substance, so if the nanomaterial is changed from a nonsurface-treated nanomaterial to a treated nanomaterial it would be advisable to seek regulatory advice regarding the requirements for a change in a medical device.

### 29.13.4 Various food and food contact materials

Food contact materials are regulated by an overarching regulation on materials and articles intended to come into contact with food [REGULATION (EC) No. 1935/2004] [141] and other regulations that cover specific types of material. The overarching regulation does not refer to nanomaterials or nanoforms but the regulation specifically covering plastic materials and articles intended to come into contact with food [REGULATION (EU) No 10/2011] [142] does acknowledge that “New technologies engineer substances in particle size that exhibit chemical and physical properties that significantly differ from those at a larger scale, for example, nanoparticles. These different properties may lead to different toxicological properties and therefore these substances should be assessed on a case-by-case basis by the Authority as regards their risk until more information is known about such new technology. Therefore it should be made clear that authorisations based on the risk assessment of the conventional particle size of a substance do not cover engineered nanoparticles (Paragraph 23).” This means that a Union Authorisation granted to a bulk form of a substance does not apply to the same substance in its nanoform so a separate Authorisation would be required. The regulation does not refer to different nanoforms of the same substance. However it should be noted that the description of a nanoform of one substance granted Union Authorisation, titanium nitride, does give a detailed description of its physical parameters. In addition, “titanium dioxide, coated with a copolymer of n-octyltrichlorosilane and [aminotris(methylenephosphonic acid), penta sodium salt]” has a separate authorization to titanium dioxide. Although there is no explicit description in the regulation of how to handle surface-treated

nanomaterials, these positions could give an indication of the intention of the regulation. However, this may need to be tested legally in a similar fashion as has occurred for REACH.

The European Food Safety Authority (EFSA) recently published a draft guidance document for public consultation for “The risk assessment of the application of nanoscience and nanotechnologies in the food and feed chain: Part 1, Human and Animal Health” [143]. This guidance document is intended to cover any regulation referring to food (novel foods, food/feed additives, biocides, pesticides, and food contact materials). It suggests that each nanomaterial should be characterized for its size, shape aspect ratio, surface functionalization, and other relevant parameters and that if changes to these parameters results in a change to toxicity (primarily oral toxicity) or toxicokinetics a separate risk assessment should be performed. The guidance document does not recommend whether these assessments should be done as part of a separate authorization or as an extension of an existing dossier.

### 29.13.5 National notification requirements in the EU

There are no common notification requirements for nanomaterial or nano-enabled products across the whole EU but some individual nations do have obligations.

**France:** If a party imports, manufactures, or distributes a nanomaterial in quantities over 100 g per year, as pure substance, a mixture or in an article with an intended release of the substance, a notification must be made. This notification must include a range of particle characteristics including information on surface coating [144].

**Belgium:** If a party places a substance intentionally manufactured as a nanomaterial on the market, as the substance or as part of a mixture for professional use, in quantities greater than 100 g per year a notification must be made. Along with other physical and chemical parameters, a qualitative description of surface coating must be included [145].

**Denmark:** If a party places a mixture or article on the market that contains an intentionally manufactured nanomaterial that can be expected to be released during its normal use, a notification must be made. This notification must include, among other physicochemical parameters, information on surface treatment or coating. There a number of exemptions to the requirement to notify, including the product being covered by other regulation and the primary use of the substance being as a pigment [146].

**Sweden:** As part of the chemical products registry, any manufacturer or importer of a chemical product in quantities over 100 kg p.a., that contains an intentionally manufactured nanomaterial, needed to submit a notification by February 2019. The notification should include information on any coating. There are exemptions to having to provide this information for any

nanomaterial used as a pigment or for companies with an annual turnover of less than 5 million SEK [147].

Norway: As part of the Norwegian Chemical Products register, if the chemical or the mixture contains a chemical present as a nanomaterial, this should be highlighted in the notification. There is no requirement to give any detail on surface treatment or coating [148].

## 29.14 Other national regulations that impact nanomaterials

United States: The overarching regulation that applies to the import, manufacture, and placing on the market of chemical substances and mixtures is the Toxic Substances Control Act (TSCA) [149], which was amended in 2016 by the Frank R. Lautenberg Chemical Safety for the 21st Century Act (LCSA) (US Congress, [150]). The Act places substances into two groups that define the obligations of the manufacturer, processor, or importer of the substance;

- New Chemical Substances
- Existing Chemical Substances

A party wishing to place a New Chemical Substance in commerce should submit a Pre-Manufacture Notice (PMN) to the Environmental Protection Agency (EPA) 90 days before starting manufacture, import, or processing. A New Chemical Substance is one that is not on the TSCA inventory [151].

For Existing Chemical Substances the data requirements are generally lower, but information can be requested by the EPA for specific chemicals or groups of chemicals. A specific reporting and recordkeeping rule has been produced for substances manufactured or processed on a nanoscale [152]. An affected party should include a range of physicochemical parameters, use, exposure, and risk management practices and available human and environmental health and safety information. Information on surface treatment and surface coating is specified as one of the key physicochemical parameters required. Although the rule does not refer to the term nanof orm, it does require that information on separate discrete forms be included. One of the definitions of a discrete form is where “A reportable chemical substance that is coated with another chemical substance or mixture at the end of manufacturing or processing has a coating that consists of a different chemical substance or mixture” [153].

Canada: The Canadian chemical regulation does not currently make an explicit reference to nanomaterials. However, as an acknowledgment to increasing concerns, it has issued a Notice requiring all applicable persons to submit information on specified chemicals that exist as a nanomaterial. The notice did not specify that information on surface treatment must be included, although it did request “the study title(s) of any unpublished or published data or studies on the substance with regard to physical-chemical



properties.” This information will be used to prioritize regulatory requirements based on hazards and patterns of exposure to the nanomaterial [154].

**Australia:** The regulation applicable to industrial chemicals in Australia requires a different approach to be taken for existing and new chemicals. If the chemical is not on the Australian Inventory of Chemical Substances (AICS) a notification must be made to the National Industrial Chemicals Notification and Assessment Scheme (NICNAS). The data requirements for this notification does include information on the surface chemistry of the substance including coatings and modifications of nanomaterials. In addition some exemptions and self-assessment options available to the bulk form are not available to the nanomaterial [155]. Nanomaterials that are existing chemical substances do not require notification and assessment, but if new health risks become apparent further assessment may be started. The development of additional regulatory requirements for nanomaterials has been deferred until the review of NICNAS has been completed [156].

**Taiwan:** Industrial chemicals are regulated by the Toxic Chemical Substance Control Act (TCSCA) in Taiwan. As with many other national regulations, chemicals are divided into existing and new chemicals, depending on whether they appear on the Taiwan Chemical Substance Inventory (TCSI) [157]. Existing chemical registrations only need to detail registrant and substance identity and usage information so no information specifically relating to a nanomaterial is needed. However, for a new substance registration, a substance that exist as a nanomaterial must have included a number of “nanometer specifications” including surface properties in its registration. It is not clear from the guidance document whether surface properties includes surface treatment or coating information. Additionally, the guidance document for the regulation specifies that where a chemical substance is surface treated, both the surface substance and the core substance should be identified separately to assess their individual regulatory obligations [158]. It is hoped that future guidance from the regulators will clarify the obligations for a surface-treated nanomaterial. In addition, it is not clear whether a nanoform of an existing substance would be regarded as the existing substance description or whether it should be treated as a new substance, or whether two different nanoforms of a new substance would require two separate new substance registrations or be contained within one overarching registration.

**Rest of the world:** There are voluntary and obligatory notification schemes in place in many countries for nanomaterials in certain products. For example, nanomaterial ingredients of cosmetic products placed on the market in Russia must be registered with Rospotrebnadzor including information on surface modification [159] and the recent update to the Chemical Ordinance in Switzerland requires notification of nanomaterials with a high aspect ratio [160].

## 29.15 Conclusion

The nature of the surface of a nanomaterial pays an intrinsic role in all aspects of toxicity, biodistribution, environmental fate, and ecotoxicity. The surface can be modified to give a nanomaterial important technological advantages but care must be taken to ensure this does not also increase the hazard, exposure, and risk of the substance, so a “safe-by-design” approach to research is advised. The European Union REACH regulations have the most detailed requirements for surface-functionalized nanomaterials and the requirements are likely to increase in the future. However, if surface functionalization changes the toxicity of the nanomaterial, other national regulatory requirements may be required.

## References

- [1] Baer DR, Engelhard MH, Johnson GE, Laskin J, Lai J, Mueller K, et al. Surface characterization of nanomaterials and nanoparticles: important needs and challenging opportunities. *J Vac Sci Technol A* 2013;31(5):50820. Available from: <https://doi.org/10.1116/1.4818423>.
- [2] Shin S, Song I, Um S. Role of physicochemical properties in nanoparticle toxicity. *Nanomater (Basel)* 2015;5(3):1351 Retrieved from <<http://www.mdpi.com/2079-4991/5/3/1351>>.
- [3] Hussain CM. In: Hussain CM, editor. *Handbook of nanomaterials for industrial applications*. 1st ed. Amsterdam: Elsevier; 2018.
- [4] Mehdi H, Bhattachayya KG. Functionalized nanomaterials for pollution abatement. In: Hussain CM, Mishra AK, editors. *Nanotechnology in environmental science*. Weinheim: Wiley-VCH; 2018. p. 599–649.
- [5] Hussain CM, Kharisov B. *Advanced environmental analysis. Applications of nanomaterials*, 2016.
- [6] Pulido-Reyes G, Leganes F, Fernández-Piñas F, Rosal R. Bio-nano interface and environment: a critical review. *Environ Toxicol Chem* 2017;36(12):3181–93. Available from: <https://doi.org/10.1002/etc.3924>.
- [7] Roduner E. Size matters: why nanomaterials are different. *Chem Soc Rev* 2006;35(7):583–92. Available from: <https://doi.org/10.1039/B502142C>.
- [8] Barua S, Mitragotri S. Challenges associated with penetration of nanoparticles across cell and tissue barriers: a review of current status and future prospects. *Nano Today* 2014;9(2):223–43. Available from: <https://doi.org/10.1016/j.nantod.2014.04.008>.
- [9] Busquets MA, Espargaró A, Sabaté R, Estelrich J. Magnetic nanoparticles cross the blood-brain barrier: when physics rises to a challenge. *Nanomaterials* 2015;5(4):2231–48. Available from: <https://doi.org/10.3390/nano5042231>.
- [10] Klaessig FC. Dissolution as a paradigm in regulating nanomaterials. *Environ Sci Nano* 2018;5(5):1070–7. Available from: <https://doi.org/10.1039/C7EN01130J>.
- [11] Tong T, Zhang J, Tian B, Chen F, He D. Preparation of Fe<sup>3+</sup>-doped TiO<sub>2</sub> catalysts by controlled hydrolysis of titanium alkoxide and study on their photocatalytic activity for methyl orange degradation. *J Hazard Mater* 2008;155(3):572–9. Available from: <https://doi.org/10.1016/j.jhazmat.2007.11.106>.

- [12] Deng L, Wang S, Liu D, Zhu B, Huang W, Wu S, et al. Synthesis, characterization of Fe-doped TiO<sub>2</sub> nanotubes with high photocatalytic activity. *Catal Lett* 2009;129(3):513–18. Available from: <https://doi.org/10.1007/s10562-008-9834-5>.
- [13] Sharma M, Nikota J, Halappanavar S, Castranova V, Rothen-Rutishauser B, Clippinger AJ. Predicting pulmonary fibrosis in humans after exposure to multi-walled carbon nanotubes (MWCNTs). *Arch Toxicol* 2016;90(7):1605–22. Available from: <https://doi.org/10.1007/s00204-016-1742-7>.
- [14] Forest V, Pourchez J. Preferential binding of positive nanoparticles on cell membranes is due to electrostatic interactions: a too simplistic explanation that does not take into account the nanoparticle protein corona. *Mater Sci Eng C* 2017;70:889–96. Available from: <https://doi.org/10.1016/j.msec.2016.09.016>.
- [15] Neouze M-A, Schubert U J M f C-C M. Surface modification and functionalization of metal and metal oxide nanoparticles by organic ligands. *Monatsh Chem* 2008;139(3):183–95. Available from: <https://doi.org/10.1007/s00706-007-0775-2>.
- [16] Shannahan J. The biocorona: a challenge for the biomedical application of nanoparticles. *Nanotechnol Rev* 2017;6(4):345–53. Available from: <https://doi.org/10.1515/ntrev-2016-0098>.
- [17] Jain P, Pawar RS, Pandey RS, Madan J, Pawar S, Lakshmi PK, et al. In-vitro in-vivo correlation (IVIVC) in nanomedicine: is protein corona the missing link? *Biotechnol Adv* 2017;35(7):889–904. Available from: <https://doi.org/10.1016/j.biotechadv.2017.08.003>.
- [18] Lundqvist M, Stigler J, Cedervall T, Berggård T, Flanagan MB, Lynch I, et al. The evolution of the protein corona around nanoparticles: a test study. *ACS Nano* 2011;5(9):7503–9. Available from: <https://doi.org/10.1021/nn202458g>.
- [19] Lowry GV, Gregory KB, Apte SC, Lead JR. Transformations of nanomaterials in the environment. *Environ Sci Technol* 2012;46:6893–9.
- [20] Bundschuh M, Filser J, Luderwald S, McKee MS, Metreveli G, Schaumann GE, et al. Nanoparticles in the environment: where do we come from, where do we go to? *Environ Sci Eur* 2018;30(1):6. Available from: <https://doi.org/10.1186/s12302-018-0132-6>.
- [21] Mitrano DM, Motellier S, Clavaguera S, Nowack B. Review of nanomaterial aging and transformations through the life cycle of nano-enhanced products. *Environ Int* 2015;77:132–47. Available from: <https://doi.org/10.1016/j.envint.2015.01.013>.
- [22] Teunenbroek TV, Baker J, Dijkzeul AJP, Toxicology F. Towards a more effective and efficient governance and regulation of nanomaterials. Part *Fibre Toxicol* 2017;14(1):54. Available from: <https://doi.org/10.1186/s12989-017-0235-z>.
- [23] Petersen EJ, Henry TB, Zhao J, MacCuspie RI, Kirschling TL, Dobrovolskaia MA, et al. Identification and avoidance of potential artifacts and misinterpretations in nanomaterial ecotoxicity measurements. *Environ Sci Technol* 2014;48(8):4226–46. Available from: <https://doi.org/10.1021/es4052999>.
- [24] Fu PP, Xia Q, Hwang H-M, Ray PC, Yu H. Mechanisms of nanotoxicity: generation of reactive oxygen species. *J Food Drug Anal* 2014;22(1):64–75. Available from: <https://doi.org/10.1016/j.jfda.2014.01.005>.
- [25] Slavin YN, Asnis J, Häfeli UO, Bach H. Metal nanoparticles: understanding the mechanisms behind antibacterial activity. *J Nanobiotechnol* 2017;15:1–20. Available from: <https://doi.org/10.1186/s12951-017-0308-z>.
- [26] Lindner K, Webering S, Stroebele M, Bockhorn H, Hansen T, König P, et al. Low dose carbon black nanoparticle exposure does not aggravate allergic airway inflammation in mice irrespective of the presence of surface polycyclic aromatic hydrocarbons. *Nanomaterials (Basel)* 2018;8(4). Available from: <https://doi.org/10.3390/nano8040213>.

- [27] Nasser F, Davis A, Valsami-Jones E, Lynch I. Shape and charge of gold nanomaterials influence survivorship, oxidative stress and moulting of *Daphnia magna*. *Nanomaterials* (Basel) 2016;6(12):222 Retrieved from <<http://www.mdpi.com/2079-4991/6/12/222>>.
- [28] Saptarshi SR, Duschl A, Lopata AL. Interaction of nanoparticles with proteins: relation to bio-reactivity of the nanoparticle J. J. o. N.J Nanobiotechnol. 2013;11(1):26. Available from: <https://doi.org/10.1186/1477-3155-11-26>.
- [29] Peng C, Zhang W, Gao H, Li Y, Tong X, Li K, et al. Behavior and potential impacts of metal-based engineered nanoparticles in aquatic environments. *Nanomaterials* (Basel) 2017;7(1):21 Retrieved from <<http://www.mdpi.com/2079-4991/7/1/21>>.
- [30] Liu J, Legros S, Ma G, Veinot JG, von der Kammer F, Hofmann T. Influence of surface functionalization and particle size on the aggregation kinetics of engineered nanoparticles. *Chemosphere* 2012;87(8):918–24. Available from: <https://doi.org/10.1016/j.chemosphere.2012.01.045>.
- [31] Tejamaya M, Römer I, Merrifield RC, Lead JR. Stability of citrate, PVP, and PEG coated silver nanoparticles in ecotoxicology media. *Environ Sci Technol* 2012;46(13):7011–17. Available from: <https://doi.org/10.1021/es2038596>.
- [32] Gerloff K, Landesmann B, Worth A, Munn S, Palosaari T, Whelan M. The Adverse Outcome Pathway approach in nanotoxicology. *Computat Toxicol* 2017;1:3–11. Available from: <https://doi.org/10.1016/j.comtox.2016.07.001>.
- [33] Vinken M, Knapen D, Vergauwen L, Hengstler JG, Angrish M, Whelan M J A o T. Adverse outcome pathways: a concise introduction for toxicologists. *Arch Toxicol* 2017;91(11):3697–707. Available from: <https://doi.org/10.1007/s00204-017-2020-z>.
- [34] Leist M, Ghallab A, Graepel R, Marchan R, Hassan R, Bennekou SH, et al. Adverse outcome pathways: opportunities, limitations and open questions. *Arch Toxicol* 2017;91(11):3477–505. Available from: <https://doi.org/10.1007/s00204-017-2045-3>.
- [35] Park MV, Catalan J, Ferraz N, Cabellos J, Vanhauhen R, Vazquez-Campos S, et al. Development of a systematic method to assess similarity between nanomaterials for human hazard evaluation purposes - lessons learnt. *Nanotoxicology* 2018;12(7):652–76. Available from: <https://doi.org/10.1080/17435390.2018.1465142>.
- [36] Fay KA, Villeneuve DL, LaLone CA, Song Y, Tollefsen KE, Ankley GT. Practical approaches to adverse outcome pathway development and weight-of-evidence evaluation as illustrated by ecotoxicological case studies. *Environ Toxicol Chem* 2017;36(6):1429–49. Available from: <https://doi.org/10.1002/etc.3770>.
- [37] Ribeiro MJ, Maria VL, Scott-Fordsmund JJ, Amorim MJB. Oxidative stress mechanisms caused by Ag nanoparticles (NM300K) are different from those of AgNO<sub>3</sub>: effects in the soil invertebrate *Enchytraeus crypticus*. *Int J Environ Res Public Health* 2015;12:9589–602.
- [38] Hayashi Y, Heckmann L-H, Simonsen V, Scott-Fordsmand JJ. Time-course profiling of molecular stress responses to silver nanoparticles in the earthworm *Eisenia fetida*. *Ecotoxicol Environ Saf* 2013;98:219–26.
- [39] Li L, Wu H, Peijnenburg WJGM, van Gestel CAM. Both released silver ions and particulate Ag contribute to the toxicity of AgNPs to earthworm *Eisenia fetida*. *Nanotoxicology* 2015;9(6):792–801.
- [40] Mudunkotuwa IA, Grassian VH. The devil is in the details (or the surface): impact of surface structure and surface energetics on understanding the behavior of nanomaterials in the environment. *J Env Monit* 2011;13(5):1135–44. Available from: <https://doi.org/10.1039/c1em00002k>.

- [41] Furtado LM, Bundschuh M, Metcalfe CD. Monitoring the Fate and Transformation of Silver Nanoparticles in Natural Waters J. B. o. E. C., & ToxicologyChem Med 2016;97 (4):449–55. Available from: <https://doi.org/10.1007/s00128-016-1888-2>.
- [42] Hou J, Zhou Y, Wang C, Li S, Wang X. Toxic effects and molecular mechanism of different types of silver nanoparticles to the aquatic crustacean *Daphnia magna*. Env Sci Technol 2017;51(21):12868–78. Available from: <https://doi.org/10.1021/acs.est.7b03918>.
- [43] Henderson WM, Bouchard D, Chang X, Al-Abed SR, Teng Q. Biomarker analysis of liver cells exposed to surfactant-wrapped and oxidized multi-walled carbon nanotubes (MWCNTs). Sci Total Env 2016;565:777–86. Available from: <https://doi.org/10.1016/j.scitotenv.2016.05.025>.
- [44] Figarol A, Pourchez J, Boudard D, Forest V, Akono C, Tulliani JM, et al. In vitro toxicity of carbon nanotubes, nano-graphite and carbon black, similar impacts of acid functionalization. Toxicol Vitro 2015;30(1 Pt B):476–85. Available from: <https://doi.org/10.1016/j.tiv.2015.09.014>.
- [45] Bhattacharya K, Mukherjee SP, Gallud A, Burkert SC, Bistarelli S, Bellucci S, et al. Biological interactions of carbon-based nanomaterials: from coronation to degradation. Nanomed Nanotechnol Biol Med 2016;12(2):333–51. Available from: <https://doi.org/10.1016/j.nano.2015.11.011>.
- [46] Jain S, Thakare VS, Das M, Godugu C, Jain AK, Mathur R, et al. Toxicity of multiwalled carbon nanotubes with end defects critically depends on their functionalization density. Chem Res Toxicol 2011;24(11):2028–39. Available from: <https://doi.org/10.1021/tx2003728>.
- [47] Allegri M, Perivoliotis DK, Bianchi MG, Chiu M, Pagliaro A, Koklioti MA, et al. Toxicity determinants of multi-walled carbon nanotubes: the relationship between functionalization and agglomeration. Toxicol Rep 2016;3:230–43. Available from: <https://doi.org/10.1016/j.toxrep.2016.01.011>.
- [48] Mandani S, Majee P, Sharma B, Sarma D, Thakur N, Nayak D, et al. Carbon dots as nanodispersants for multiwalled carbon nanotubes: reduced cytotoxicity and metal nanoparticle functionalization. Langmuir 2017;33(31):7622–32. Available from: <https://doi.org/10.1021/acs.langmuir.7b00557>.
- [49] Yan L, Zhao F, Li S, Hu Z, Zhao Y. Low-toxic and safe nanomaterials by surface-chemical design, carbon nanotubes, fullerenes, metallofullerenes, and graphenes. Nanoscale 2011;3(2):362–82. Available from: <https://doi.org/10.1039/c0nr00647e>.
- [50] Charbgo F, Behmanesh M, Nikkhah M. Enhanced reduction of single-wall carbon nanotube cytotoxicity in vitro: applying a novel method of arginine functionalization. Biotechnol Appl Biochem 2015;62(5):598–605. Available from: <https://doi.org/10.1002/bab.1311>.
- [51] Liu Y, Ren L, Yan D, Zhong W. Mechanistic study on the reduction of SWCNT-induced cytotoxicity by albumin coating. Part Part Syst Charact 2014;31(12):1244–51. Available from: <https://doi.org/10.1002/ppsc.201400145>.
- [52] Abbaszadegan A, Gholami A, Abbaszadegan S, Aleyasin ZS, Ghahramani Y, Dorostkar S, et al. The effects of different ionic liquid coatings and the length of alkyl chain on antimicrobial and cytotoxic properties of silver nanoparticles. Iran Endod J 2017;12 (4):481–7. Available from: <https://doi.org/10.22037/iej.v12i4.17905>.
- [53] Chng EL, Sofer Z, Pumera M. Cytotoxicity profile of highly hydrogenated graphene. Chemistry 2014;20(21):6366–73. Available from: <https://doi.org/10.1002/chem.201304911>.
- [54] Sayes CM, Marchione AA, Reed KL, Warheit DB. Comparative pulmonary toxicity assessments of C60 water suspensions in rats: few differences in fullerene toxicity in vivo

- in contrast to in vitro profiles. *Nano Lett* 2007;7(8):2399–406. Available from: <https://doi.org/10.1021/nl0710710>.
- [55] Wu H, Chen M, Shang M, Li X, Mu K, Fan S, et al. Insights into the binding behavior of bovine serum albumin to black carbon nanoparticles and induced cytotoxicity. *Spectrochim Acta A Mol Biomol Spectrosc* 2018;200:51–7. Available from: <https://doi.org/10.1016/j.saa.2018.04.010>.
- [56] Kamat JP, Devasagayam TP, Priyadarsini KI, Mohan H. Reactive oxygen species mediated membrane damage induced by fullerene derivatives and its possible biological implications. *Toxicology* 2000;155(1-3):55–61.
- [57] Boncel S, Kyziol-Komosinska J, Krzyzewska I, Czupiol J. Interactions of carbon nanotubes with aqueous/aquatic media containing organic/inorganic contaminants and selected organisms of aquatic ecosystems—a review. *Chemosphere* 2015;136:211–21. Available from: <https://doi.org/10.1016/j.chemosphere.2015.04.095>.
- [58] Kennedy AJ, Hull MS, Steevens JA, Dontsova KM, Chappell MA, Gunter JC, et al. Factors influencing the partitioning and toxicity of nanotubes in the aquatic environment. *Env Toxicol Chem* 2008;27(9):1932–41.
- [59] Cerrillo C, Barandika G, Igarua A, Areitioaurtena O, Uranga N, Mendoza G. Colloidal stability and ecotoxicity of multiwalled carbon nanotubes: influence of select organic matters. *Cellulose* 2016;35(1):74–83. Available from: <https://doi.org/10.1002/etc.3172>.
- [60] Yanamala N, Kisin ER, Menas AL, Farcas MT, Khaliullin TO, Vogel UB, et al. In vitro toxicity evaluation of lignin(un)coated cellulose based nanomaterials on human A549 and THP-1 cells. *Biomacromolecules* 2016;17(11):3464–73. Available from: <https://doi.org/10.1021/acs.biomac.6b00756>.
- [61] Lopes VR, Sanchez-Martinez C, Stromme M, Ferraz N. In vitro biological responses to nanofibrillated cellulose by human dermal, lung and immune cells: surface chemistry aspect. *Part Fibre Toxicol* 2017;14(1):1. Available from: <https://doi.org/10.1186/s12989-016-0182-0>.
- [62] Harper BJ, Clendaniel A, Sinche F, Way D, Hughes M, Schardt J, et al. Impacts of chemical modification on the toxicity of diverse nanocellulose materials to developing zebrafish. *Cellulose* 2016;23(3):1763–75. Available from: <https://doi.org/10.1007/s10570-016-0947-5>.
- [63] Kim J, Chankeshwara SV, Thielbeer F, Jeong J, Donaldson K, Bradley M, et al. Surface charge determines the lung inflammogenicity: a study with polystyrene nanoparticles. *Nanotoxicology* 2016;10(1):94–101. Available from: <https://doi.org/10.3109/17435390.2015.1022887>.
- [64] Huang YJ, Hung KC, Hung HS, Hsu SH. Modulation of macrophage phenotype by biodegradable polyurethane nanoparticles: possible relation between macrophage polarization and immune response of nanoparticles. *ACS Appl Mater Interfaces* 2018;10(23):19436–48. Available from: <https://doi.org/10.1021/acsami.8b04718>.
- [65] Breus VV, Pietuch A, Tarantola M, Basché T, Janshoff A. The effect of surface charge on nonspecific uptake and cytotoxicity of CdSe/ZnS core/shell quantum dots. *Beilstein J Nanotechnol* 2015;6:281–92. Available from: <https://doi.org/10.3762/bjnano.6.26>.
- [66] Chang S, Kang B, Liu X, Dai Y, Chen D. The combined influence of surface modification, size distribution, and interaction time on the cytotoxicity of CdTe quantum dots in PANC-1 cells. *Acta Biochim Biophys Sin (Shanghai)* 2012;44(3):241–8. Available from: <https://doi.org/10.1093/abbs/gmr126>.
- [67] Speranskaya ES, Sevrin C, De Saeger S, Hens Z, Goryacheva IY, Grandfils C. Synthesis of hydrophilic CuInS<sub>2</sub>/ZnS quantum dots with different polymeric shells and study of their

- cytotoxicity and hemocompatibility. *ACS Appl Mater Interfaces* 2016;8(12):7613–22. Available from: <https://doi.org/10.1021/acsami.5b11258>.
- [68] de Carvalho SM, Mansur AAP, Mansur HS, Guedes M, Lobato ZIP, Leite MF. In vitro and in vivo assessment of nanotoxicity of CdS quantum dot/aminopolysaccharide bionanconjugates. *Mater Sci Eng C Mater Biol Appl* 2017;71:412–24. Available from: <https://doi.org/10.1016/j.msec.2016.10.023>.
- [69] Hoshino A, Hanada S, Yamamoto K. Toxicity of nanocrystal quantum dots: the relevance of surface modifications. *Arch Toxicol* 2011;85(7):707–20. Available from: <https://doi.org/10.1007/s00204-011-0695-0>.
- [70] Kuznetsova VA, Visheratina AK, Ryan A, Martynenko IV, Loudon A, Maguire CM, et al. Enantioselective cytotoxicity of ZnS:Mn quantum dots in A549 cells. *Chirality* 2017;29(8):403–8. Available from: <https://doi.org/10.1002/chir.22713>.
- [71] Xiang X, Wu C, Zhang BR, Gao T, Zhao J, Ma L, et al. The relationship between the length of surface ligand and effects of CdTe quantum dots on the physiological functions of isolated mitochondria. *Chemosphere* 2017;184:1108–16. Available from: <https://doi.org/10.1016/j.chemosphere.2017.06.091>.
- [72] Rotomskis R, Jurgelene Z, Stankevicius M, Stankeviciute M, Kazlauskienė N, Jokšas K, et al. Interaction of carboxylated CdSe/ZnS quantum dots with fish embryos: towards understanding of nanoparticles toxicity. *Sci Total Env* 2018;635:1280–91. Available from: <https://doi.org/10.1016/j.scitotenv.2018.04.206>.
- [73] Wicinski PN, Metz KM, King Heiden TC, Louis KM, Mangham AN, Hamers RJ, et al. Toxicity of oxidatively degraded quantum dots to developing zebrafish (*Danio rerio*). *Environ Sci Technol* 2013;47(16):9132–9. Available from: <https://doi.org/10.1021/es304987r>.
- [74] Freese C, Gibson MI, Klok HA, Unger RE, Kirkpatrick CJ. Size- and coating-dependent uptake of polymer-coated gold nanoparticles in primary human dermal microvascular endothelial cells. *Biomacromolecules* 2012;13(5):1533–43. Available from: <https://doi.org/10.1021/bm300248u>.
- [75] Braun NJ, DeBrosse MC, Hussain SM, Comfort KK. Modification of the protein coronan nanoparticle complex by physiological factors. *Mater Sci Eng C Mater Biol Appl* 2016;64:34–42. Available from: <https://doi.org/10.1016/j.msec.2016.03.059>.
- [76] Fraga S, Brandao A, Soares ME, Morais T, Duarte JA, Pereira L, et al. Short- and long-term distribution and toxicity of gold nanoparticles in the rat after a single-dose intravenous administration. *Nanomedicine* 2014;10(8):1757–66. Available from: <https://doi.org/10.1016/j.nano.2014.06.005>.
- [77] Kah JCY, Grabinski C, Untener E, Garrett C, Chen J, Zhu D, et al. Protein coronas on gold nanorods passivated with amphiphilic ligands affect cytotoxicity and cellular response to Penicillin/Streptomycin. *ACS Nano* 2014;8(5):4608–20. Available from: <https://doi.org/10.1021/nn5002886>.
- [78] Quan X, Peng C, Zhao D, Li L, Fan J, Zhou J. Molecular understanding of the penetration of functionalized gold nanoparticles into asymmetric membranes. *Langmuir* 2017;33(1):361–71. Available from: <https://doi.org/10.1021/acs.langmuir.6b02937>.
- [79] Grzincic EM, Yang JA, Drnevich J, Falagan-Lotsch P, Murphy CJ. Global transcriptomic analysis of model human cell lines exposed to surface-modified gold nanoparticles: the effect of surface chemistry. *Nanoscale* 2015;7(4):1349–62. Available from: <https://doi.org/10.1039/C4NR05166A>.
- [80] Parveen A, Malashetty VB, Mantripragada B, Yalagatti MS, Abbaraju V, Deshpande R. Bio-functionalized gold nanoparticles: benign effect in Sprague-Dawley rats by



- intravenous administration. Saudi J Biol Sci 2017;24(8):1925–32. Available from: <https://doi.org/10.1016/j.sjbs.2017.11.041>.
- [81] Brun E, Sicard-Roselli CJCN. Could nanoparticle corona characterization help for biological consequence prediction? Cancer Nanotechnol 2014;5(1):7. Available from: <https://doi.org/10.1186/s12645-014-0007-5>.
- [82] Alkilany AM, Nagaria PK, Wyatt MD, Murphy CJ. Cation exchange on the surface of gold nanorods with a polymerizable surfactant: polymerization, stability, and toxicity evaluation. Langmuir 2010;26(12):9328–33. Available from: <https://doi.org/10.1021/la100253k>.
- [83] Allen JM, Xu J, Blahove M, Canonico-May SA, Santaloci TJ, Braselton ME, et al. Synthesis of less toxic gold nanorods by using dodecylethyldimethylammonium bromide as an alternative growth-directing surfactant. J Colloid Interface Sci 2017;505:1172–6. Available from: <https://doi.org/10.1016/j.jcis.2017.06.101>.
- [84] Harper B, Sinche F, Ho Wu R, Gowrishankar M, Marquart G, Mackiewicz M, et al. The impact of surface ligands and synthesis method on the toxicity of glutathione-coated gold nanoparticles. Nanomaterials (Basel) 2014;4(2):355 Retrieved from <<http://www.mdpi.com/2079-4991/4/2/355>>.
- [85] Feng ZV, Gunsolus IL, Qiu TA, Hurley KR, Nyberg LH, Frew H, et al. Impacts of gold nanoparticle charge and ligand type on surface binding and toxicity to Gram-negative and Gram-positive bacteria. Chem Sci 2015;6(9):5186–96. Available from: <https://doi.org/10.1039/C5SC00792E>.
- [86] Wray AT, Klaine SJ. Modeling the influence of physicochemical properties on gold nanoparticle uptake and elimination by *Daphnia magna*. Environ Toxicol Chem 2015;34(4):860–72. Available from: <https://doi.org/10.1002/etc.2881>.
- [87] Breitrner EK, Burns KE, Hussain SM, Comfort KK. Implementation of physiological fluids to provide insight into the characterization, fate, and biological interactions of silver nanoparticles. Nanotechnology 2018;29(25):254001. Available from: <https://doi.org/10.1088/1361-6528/aabb9d>.
- [88] Alessandrini F, Vennemann A, Gschwendtner S, Neumann A, Rothballer M, Seher T, et al. Pro-inflammatory versus immunomodulatory effects of silver nanoparticles in the lung: the critical role of dose, size and surface modification. Nanomaterials (Basel) 2017;7(10):300 Retrieved from <<http://www.mdpi.com/2079-4991/7/10/300>>.
- [89] Hu Y, Chen X, Yang K, Lin D. Distinct toxicity of silver nanoparticles and silver nitrate to *Daphnia magna* in M4 medium and surface water. Sci Total Env 2018;618:838–46. Available from: <https://doi.org/10.1016/j.scitotenv.2017.08.222>.
- [90] Nix CE, Harper BJ, Conner CG, Richter AP, Velev OD, Harper SL. Toxicological assessment of a lignin core nanoparticle doped with silver as an alternative to conventional silver core nanoparticles. Antibiotics (Basel) 2018;7(2). Available from: <https://doi.org/10.3390/antibiotics7020040>.
- [91] Kim KT, Tanguay RL. The role of chorion on toxicity of silver nanoparticles in the embryonic zebrafish assay. Env Health Toxicol 2014;29:e2014021. Available from: <https://doi.org/10.5620/eh.t.e2014021>.
- [92] Pereira SPP, Jesus F, Aguiar S, de Oliveira R, Fernandes M, Ranville J, et al. Phytotoxicity of silver nanoparticles to *Lemna minor*: surface coating and exposure period-related effects. Sci Total Env 2018;618:1389–99. Available from: <https://doi.org/10.1016/j.scitotenv.2017.09.275>.
- [93] Caceres-Velez PR, Fascinelli ML, Sousa MH, Grisolia CK, Yate L, de Souza PEN, et al. Humic acid attenuation of silver nanoparticle toxicity by ion complexation and the formation of a Ag(3+) coating. J Hazard Mater 2018;353:173–81. Available from: <https://doi.org/10.1016/j.jhazmat.2018.04.019>.



- [94] Wang X, Fan W, Dong Z, Liang D, Zhou T. Interactions of natural organic matter on the surface of PVP-capped silver nanoparticle under different aqueous environment. *Water Res* 2018;138:224–33. Available from: <https://doi.org/10.1016/j.watres.2018.03.048>.
- [95] Shoults-Wilson WA, Reinsch BC, Tsyusko OV, Bertsch PM, Lowry GV, Unrine JM. Role of particle size and soil type in toxicity of silver nanoparticles to earthworms. *Soil Sci Soc Am J* 2011;75(2):365–77.
- [96] Marzaioli V, Aguilar-Pimentel JA, Weichenmeier I, Luxenhofer G, Wiemann M, Landsiedel R, et al. Surface modifications of silica nanoparticles are crucial for their inert versus proinflammatory and immunomodulatory properties. *Int J Nanomed* 2014;9:2815–32. Available from: <https://doi.org/10.2147/ijn.S57396>.
- [97] Marzaioli V, Gross CJ, Weichenmeier I, Schmidt-Weber CB, Gutermuth J, Gross O, et al. Specific surface modifications of silica nanoparticles diminish inflammasome activation and in vivo expression of selected inflammatory genes. *Nanomaterials (Basel)* 2017;7(11). Available from: <https://doi.org/10.3390/nano7110355>.
- [98] Nabeshi H, Yoshikawa T, Arimori A, Yoshida T, Tochigi S, Hirai T, et al. Effect of surface properties of silica nanoparticles on their cytotoxicity and cellular distribution in murine macrophages. *Nanoscale Res Lett* 2011;6(1):93. Available from: <https://doi.org/10.1186/1556-276x-6-93>.
- [99] Yoshida T, Yoshioka Y, Matsuyama K, Nakazato Y, Tochigi S, Hirai T, et al. Surface modification of amorphous nanosilica particles suppresses nanosilica-induced cytotoxicity, ROS generation, and DNA damage in various mammalian cells. *Biochem Biophys Res Commun* 2012;427(4):748–52. Available from: <https://doi.org/10.1016/j.bbrc.2012.09.132>.
- [100] Spyrogianni A, Herrmann IK, Keevend K, Pratsinis SE, Wegner K. The silanol content and in vitro cytolytic activity of flame-made silica. *J Colloid Interface Sci* 2017;507:95–106. Available from: <https://doi.org/10.1016/j.jcis.2017.07.096>.
- [101] Wang X, Sun B, Liu S, Xia T. Structure activity relationships of engineered nanomaterials in inducing NLRP3 inflammasome activation and chronic lung fibrosis. *NanoImpact* 2017;6:99–108. Available from: <https://doi.org/10.1016/j.impact.2016.08.002>.
- [102] Kurtz-Chalot A, Villiers C, Pourchez J, Boudard D, Martini M, Marche PN, et al. Impact of silica nanoparticle surface chemistry on protein corona formation and consequential interactions with biological cells. *Mater Sci Eng C Mater Biol Appl* 2017;75:16–24. Available from: <https://doi.org/10.1016/j.msec.2017.02.028>.
- [103] Pietroiusti A, Vecchione L, Malvindi MA, Aru C, Massimiani M, Camaioni A, et al. Relevance to investigate different stages of pregnancy to highlight toxic effects of nanoparticles: the example of silica. *Toxicol Appl Pharmacol* 2018;342:60–8. Available from: <https://doi.org/10.1016/j.taap.2018.01.026>.
- [104] Hashizume N, Oshima Y, Nakai M, Kobayashi T, Sasaki T, Kawaguchi K, et al. Categorization of nano-structured titanium dioxide according to physicochemical characteristics and pulmonary toxicity. *Toxicol Rep* 2016;3:490–500. Available from: <https://doi.org/10.1016/j.toxrep.2016.05.005>.
- [105] Wang J, Fan Y. Lung injury induced by TiO<sub>2</sub> nanoparticles depends on their structural features: size, shape, crystal phases, and surface coating. *Int J Mol Sci* 2014;15(12):22258 Retrieved from <<http://www.mdpi.com/1422-0067/15/12/22258>>.
- [106] Wallis LK, Diamond SA, Ma H, Hoff DJ, Al-Abed SR, Li S. Chronic TiO<sub>2</sub> nanoparticle exposure to a benthic organism, *Hyalella azteca*: impact of solar UV radiation and material surface coatings on toxicity. *Sci Total Env* 2014;499:356–62. Available from: <https://doi.org/10.1016/j.scitotenv.2014.08.068>.

- [107] Hurel C, Bignon C, Said-Mohamed C, Amigoni S, Devers T, Guittard F. Functionalized and grafted TiO<sub>2</sub>, CeO<sub>2</sub>, and SiO<sub>2</sub> nanoparticles-ecotoxicity on *Daphnia magna* and relevance of ecofriendly polymeric networks. *Env Sci Pollut Res Int* 2018;25(21):21216–23. Available from: <https://doi.org/10.1007/s11356-018-2251-4>.
- [108] Mikolajczyk A, Sizochenko N, Mulkiewicz E, Malankowska A, Nischk M, Jurczak P, et al. Evaluating the toxicity of TiO<sub>2</sub>-based nanoparticles to Chinese hamster ovary cells and *Escherichia coli*: a complementary experimental and computational approach. *Beilstein J Nanotechnol* 2017;8:2171–80. Available from: <https://doi.org/10.3762/bjnano.8.216>.
- [109] Ahamed M, Khan MAM, Akhtar MJ, Alhadlaq HA, Alshamsan A. Ag-doping regulates the cytotoxicity of TiO<sub>2</sub> nanoparticles via oxidative stress in human cancer cells. *Sci Rep* 2017;7(1):17662. Available from: <https://doi.org/10.1038/s41598-017-17559-9>.
- [110] Committee for Risk Assessment. Opinion proposing harmonised classification and labelling at EU level of Titanium dioxide, Retrieved from <<https://echa.europa.eu/documents/10162/682fac9f-5b01-86d3-2f70-3d40277a53c2>>; 2017.
- [111] Chia SL, Leong DT. Reducing ZnO nanoparticles toxicity through silica coating. *Heliyon* 2016;2(10):e00177. Available from: <https://doi.org/10.1016/j.heliyon.2016.e00177>.
- [112] Punnoose A, Dodge K, Rasmussen JW, Chess J, Wingett D, Anders C. Cytotoxicity of ZnO nanoparticles can be tailored by modifying their surface structure: a green chemistry approach for safer nanomaterials. *ACS Sustain Chem Eng* 2014;2(7):1666–73. Available from: <https://doi.org/10.1021/sc500140x>.
- [113] Yung MMN, Fougères P-A, Leung YH, Liu F, Djurišić AB, Giesy JP, et al. Physicochemical characteristics and toxicity of surface-modified zinc oxide nanoparticles to freshwater and marine microalgae. *Sci Rep* 2017;7(1):15909. Available from: <https://doi.org/10.1038/s41598-017-15988-0>.
- [114] Zhou Z, Son J, Harper B, Zhou Z, Harper S. Influence of surface chemical properties on the toxicity of engineered zinc oxide nanoparticles to embryonic zebrafish. *Beilstein J Nanotechnol* 2015;6:1568–79. Available from: <https://doi.org/10.3762/bjnano.6.160>.
- [115] Mukherjee A, Sun Y, Morelius E, Niu G, et al. Differential toxicity of bare and hybrid zno nanoparticles in green pea (*Pisum sativum L.*): a life cycle study. *Front Plant Sci* 2016;6(1242). Available from: <https://doi.org/10.3389/fpls.2015.01242>.
- [116] Azevedo SL, Holz T, Rodrigues J, Monteiro T, Costa FM, Soares A, et al. A mixture toxicity approach to predict the toxicity of Ag decorated ZnO nanomaterials. *Sci Total Env* 2017;579:337–44. Available from: <https://doi.org/10.1016/j.scitotenv.2016.11.095>.
- [117] Organisation for Economic Co-operation and Development (OECD). Testing programme of manufactured nanomaterials. Retrieved from <<http://www.oecd.org/chemicalsafety/nanosafety/testing-programme-manufactured-nanomaterials.htm>>.
- [118] European Parliament Council of the European Union. REGULATION (EC) No 1907/2006 OF THE EUROPEAN PARLIAMENT AND OF THE COUNCIL of 18 December 2006 concerning the Registration, Evaluation, Authorisation and Restriction of Chemicals (REACH), establishing a European Chemicals Agency, amending Directive 1999/45/EC and repealing Council Regulation (EEC) No 793/93 and Commission Regulation (EC) No 1488/94 as well as Council Directive 76/769/EEC and Commission Directives 91/155/EEC, 93/67/EEC, 93/105/EC and 2000/21/EC; 2006.
- [119] European Commission. REACH Implementation Project Substance Identification of Nanomaterials (RIP-oN 1); 2011.

- [120] Hankin SM, Peters SAK, Poland CA, Foss Hansen S, Holmqvist J, Ross BL, et al. Specific advice on fulfilling information requirements for nanomaterials under REACH (RIP-oN 2) – Final Project Report; 2011.
- [121] Aitken RA, Bassan A, Friedrichs S, Hankin SM, Hansen SF, Holmqvist J, et al. Specific Advice on exposure assessment and hazard/risk characterisation for nanomaterials under REACH (RIP-oN 3) – Final Project Report, 2011.
- [122] European Chemical Agency. Guidance for identification and naming of substances under REACH and CLP, 2017. Retrieved from <[https://echa.europa.eu/documents/10162/23036412/substance\\_id\\_en.pdf/ee696bad-49f6-4fec-b8b7-2c3706113c7d](https://echa.europa.eu/documents/10162/23036412/substance_id_en.pdf/ee696bad-49f6-4fec-b8b7-2c3706113c7d)>.
- [123] European Chemicals Agency. Decision of the Board of Appeal of the European Chemicals Agency 2 March 2017 (Dossier evaluation – Compliance check – Substance identity – Nanomaterials – Nanoforms). Case number A-011-2014, 2017a.
- [124] European Chemicals Agency. Decision of the Board Of Appeal of the European Chemicals Agency, 30 June 2017, (Substance evaluation – Nanomaterials – Potential risk – ‘Forms’ of a nanomaterial – Proportionality – Error of assessment – Article 25 – Legal certainty). Case number A-015-2015; 2017b.
- [125] European Chemicals Agency. Decision of the Board of Appeal of the European Chemicals Agency, 12 October 2016, (Compliance check – Nanomaterials – Request for information – Legal certainty). Case number A-010-2015; 2016a.
- [126] European Chemicals Agency. Decision of the Board of Appeal of the European Chemicals Agency, 12 October 2016, (Compliance check – Nanomaterials – Request for information – Legal certainty). Case number A-011-2015; 2016b.
- [127] European Commission. Amending Regulation (EC) No 1907/2006 of the European Parliament and of the Council on the Registration, Evaluation, Authorisation and Restriction of Chemicals (REACH) as regards Annexes I, III, VI, VII, VIII, IX, X, XI, and XII to address nanoforms of substances (Annex) (draft); 2017.
- [128] Nanotechnology Industries Association. NIA Position on Draft Commission Regulation (EU) XXX amending Regulation (EC) No 1907/2006 (REACH) as regards Annexes I, III, VI, VII, VIII, IX, X, XI and XII to address nanoforms of substances [Press release]; 2017.
- [129] European Chemical Industry Council (CEFIC). Cefic Feedback on the Amendments of the Annexes to REACH for registration of nanomaterials [Press release]; 2017.
- [130] Center for International Environmental Law (CIEL). [Press release]; 2017.
- [131] European Commission. COMMISSION REGULATION (EU) 2018/1881 of 3 December 2018 amending Regulation (EC) No 1907/2006 of the European Parliament and of the Council on the Registration, Evaluation, Authorisation and Restriction of Chemicals (REACH) as regards Annexes I, III, VI, VII, VIII, IX, X, XI, and XII to address nanoforms of substances; 2018.
- [132] European Chemicals Agency. Guidance on information requirements and chemical safety assessment Chapter R.6: QSARs and grouping of chemicals. Retrieved from <[https://echa.europa.eu/documents/10162/13632/information\\_requirements\\_r6\\_en.pdf/77f49f81-b76d-40ab-8513-4f3a533b6ac9](https://echa.europa.eu/documents/10162/13632/information_requirements_r6_en.pdf/77f49f81-b76d-40ab-8513-4f3a533b6ac9)>; 2008.
- [133] Arts JH, Hadi M, Irfan MA, Keene AM, Kreiling R, Lyon D, et al. A decision-making framework for the grouping and testing of nanomaterials (DF4nanoGrouping). Regul Toxicol Pharmacol 2015;71(2 Suppl). Available from: <https://doi.org/10.1016/j.yrtph.2015.03.007> S1-27.
- [134] Arts JH, Irfan MA, Keene AM, Kreiling R, Lyon D, Maier M, et al. Case studies putting the decision-making framework for the grouping and testing of nanomaterials

- (DF4nanoGrouping) into practice. Regul Toxicol Pharmacol 2016;76:234–61. Available from: <https://doi.org/10.1016/j.yrtph.2015.11.020>.
- [135] European Parliament Council of the European Union. REGULATION (EU) No 528/2012 OF THE EUROPEAN PARLIAMENT AND OF THE COUNCIL of 22 May 2012 concerning the making available on the market and use of biocidal products, 2012.
  - [136] European Chemical Agency. List of notifications. Prepared as of 19 October 2018, 2018. Retrieved from <[https://echa.europa.eu/documents/10162/23907025/list\\_of\\_notification-s\\_en.pdf/e39a07ea-52dd-4562-a8e5-eab6be898312](https://echa.europa.eu/documents/10162/23907025/list_of_notification-s_en.pdf/e39a07ea-52dd-4562-a8e5-eab6be898312)>.
  - [137] European Parliament Council of the European Union. Regulation (EC) No 1223/2009 of the European Parliament and of the Council of 30 November 2009 on cosmetic products; 2009.
  - [138] European Commission. Catalogue of nanomaterials used in cosmetic products placed on the market. Retrieved from <[file:///C:/Users/n.hunt/Downloads/nanocatalogue\\_06\\_2017\\_en%20\(2\).pdf](file:///C:/Users/n.hunt/Downloads/nanocatalogue_06_2017_en%20(2).pdf)>; 2017c.
  - [139] European Parliament Council of the European Union. REGULATION (EU) 2017/745 OF THE EUROPEAN PARLIAMENT AND OF THE COUNCIL of 5 April 2017 on medical devices, amending Directive 2001/83/EC, Regulation (EC) No 178/2002 and Regulation (EC) No 1223/2009 and repealing Council Directives 90/385/EEC and 93/42/EEC; 2017a.
  - [140] European Parliament Council of the European Union. REGULATION (EU) 2017/746 OF THE EUROPEAN PARLIAMENT AND OF THE COUNCIL of 5 April 2017 on in vitro diagnostic medical devices and repealing Directive 98/79/EC and Commission Decision 2010/227/EU; 2017b.
  - [141] European Parliament Council of the European Union. REGULATION (EC) No 1935/2004 OF THE EUROPEAN PARLIAMENT AND OF THE COUNCIL of 27 October 2004 on materials and articles intended to come into contact with food and repealing Directives 80/590/EEC and 89/109/EEC; 2004.
  - [142] European Parliament Council of the European Union. COMMISSION REGULATION (EU) No 10/2011 of 14 January 2011 on plastic materials and articles intended to come into contact with food; 2011.
  - [143] Hardy A, Benford D, Halldorsson T, Jeger MJ, Knutsen HK, More S, et al. DRAFT for public consultation: guidance on risk assessment of the application of nanoscience and nanotechnologies in the food and feed chain: part 1, human and animal health. EFSA J 2018.
  - [144] Grall J-Y, Rousseau L, Michel L, Combexelle J-D, Dehaumont P. Ministerial Order of 6 August 2012 on the content and the conditions for the presentation of the annual declaration on substances at nanoscale, in application of articles R. 523-12 and R. 523-13 of the Environment code; 2013.
  - [145] Federal Public Service Health Food Chain Safety and Environment. Royal Decree amending the Royal Decree of May 27th 2014 concerning the placing on the market of substances produced in nanoparticulate state; 2014.
  - [146] Sorensen G, Fischer CH, Ingerslev F, Bom K, Johansen V. Guideline for the Danish Inventory of Nanoproducts. Retrieved from Copenhagen; 2014.
  - [147] Swedish Chemicals Agency (KEMI). Compulsory declaration for nanomaterial. Retrieved from <<https://www.kemi.se/en/products-register/compulsory-declaration-for-nanomaterial>>; 2018.

- [148] Norwegian Environment Agency. What Chemicals Must Be Reported? Retrieved from <<http://www.miljodirektoratet.no/en/Areas-of-activity1/Chemicals/The-Product-Register/What-Chemicals-Must-Be-Reported/>>; 2015.
- [149] Ontario, & United States. Toxic substances control act (TSCA) chemical substance inventory; 1979.
- [150] Frank R. Lautenberg Chemical Safety for the 21st Century Act, H2576-60 Stat; 2016.
- [151] United States Environmental Protection Agency. TSCA Chemical Substance Inventory. Retrieved from <<https://www.epa.gov/tsca-inventory>>; 2018.
- [152] United States Environmental Protection Agency. Working Guidance on EPA's Section 8 (a) Information Gathering Rule on Nanomaterials in Commerce. Retrieved from <[https://www.epa.gov/sites/production/files/2017-08/documents/august\\_2017guidance.8-7-2017\\_002.pdf](https://www.epa.gov/sites/production/files/2017-08/documents/august_2017guidance.8-7-2017_002.pdf)>; 2017b.
- [153] United States Environmental Protection Agency. CHEMICAL SUBSTANCES MANUFACTURED OR PROCESSED AT THE NANOSCALE., 40 CFR § 704.20. Retrieved from <<https://www.gpo.gov/fdsys/pkg/CFR-2017-title40-vol33/pdf/CFR-2017-title40-vol33-sec704-20.pdf>>; 2017a.
- [154] Government of Canada. Notice with respect to certain nanomaterials in Canadian commerce. Can Gaz 2015;149(30) Retrieved from <<http://gazette.gc.ca/rp-pr/p1/2015/2015-07-25/html/notice-avis-eng.html#n1>>.
- [155] Australian Government Department of Health. Data requirements for notification of new industrial nanomaterials. Guidance on providing additional data requirements. Retrieved from <<https://www.nicnas.gov.au/notify-your-chemical/data-requirements-for-new-chemical-notifications/data-requirements-for-notification-of-new-industrial-nanomaterials>>; 2018a.
- [156] Australian Government Department of Health. Nanomaterials that are 'existing chemicals'. Retrieved from <<https://www.nicnas.gov.au/chemical-information/Topics-of-interest2/subjects/nanomaterials-nanotechnology/nicnas-national-and-international-cooperation-in-nanomaterials>>; 2018b.
- [157] Occupational Safety and Health Administration. Taiwan Chemical Substance Inventory (TCSI). Retrieved from <[https://csnn.osha.gov.tw/content/home/Substance\\_Home.aspx](https://csnn.osha.gov.tw/content/home/Substance_Home.aspx)>; 2018.
- [158] Chemical Watch. CW + AsiaHub Taiwan. Guidance for New and Existing Chemical Substances Registration; 2015.
- [159] TECHNICAL Regulations of the customs union TR CU 009/2011 on safety of perfumery and cosmetic products; 2015.
- [160] The Federal Council Joint Chemical Notification Body. Ordonnance sur la protection contre les substances et les préparations dangereuses. Retrieved from <[https://www.anmeldestelle.admin.ch/dam/chem/fr/dokumente/aenderung-chemv-2018.pdf.download.pdf/Revisionsentwurf\\_ChemV\\_f.pdf](https://www.anmeldestelle.admin.ch/dam/chem/fr/dokumente/aenderung-chemv-2018.pdf.download.pdf/Revisionsentwurf_ChemV_f.pdf)>; 2015.

## Chapter 30

# Functional nanomaterials: selected legal and regulatory issues

Md. Ershadul Karim<sup>1,2</sup>

<sup>1</sup>*Faculty of Law, University of Malaya, Kuala Lumpur, Malaysia,* <sup>2</sup>*Bangladesh Supreme Court, Dhaka, Bangladesh*

### 30.1 Introduction

Natural nanomaterials are abundant in the environment and even though the inhabitants of ancient civilizations in Rome, Greece, China, India, etc., used to know the techniques to exploit and apply some of the nanoparticles in different products to achieve different purposes, the deliberate and purposeful use of engineered nanomaterials (ENMs) in different consumer and industrial products is a trend of the 21st century. Nanotechnology<sup>1</sup> is the catalyst and the key enabling technology in the age of “Fourth Industrial Revolution” [1,2], though there are some theoretical debates about whether there is anything that can be considered as the “Fourth Industrial Revolution.” This debate should not undermine the potentials and prospects of nanotechnologies and engineered or manmade or functional nanomaterials.

With the active participation of stakeholders from different disciplines, countries across the world have joined the race to take the lead of the trillion-dollar market of the ENMs after the enactment of the 21st Century Nanotechnology Research and Development Act, 2003 in the United States. More than a hundred countries around the world have a specific program of nanotechnology research and development. Various magical applications of nanomaterials are already available and found on supermarket shelves. Realizing the prospects of ENMs and nanotechnologies, the EU Commission

---

1. In this chapter, the terms “nanotechnology” and “nanotechnologies” are used interchangeably. Although the word “nanotechnology” is widely used in published literature, scientists are of the opinion that there is no such thing as “nanotechnology” as there is no single technology that can be addressed like this and rather the word “nanotechnologies” should be used.

has been considering this as one of the six “key enabling technologies” alongside advanced materials, biotechnology, etc. Nevertheless, due to the exceptional and unique behavior of engineered nanoparticles (ENPs), at the nanoscale especially between 1 and 3 nm, there arise some legal and regulatory concerns since scientific research findings frequently report that some ENMs may have adverse effects on the environment and human health.

Functional nanomaterials are very promising and have various intended applications. Being nanoscale materials, it is believed that they will have to face similar human health and environmental concerns and challenges. In this context, this chapter aims to cover and review some of the human health and environmental concerns of ENMs shared from recent studies. Subsequently, it will highlight some of the legal and regulatory concerns and some of the possible challenges faced by regulators in terms of implementing relevant legal provisions. This chapter will also provide an overview of recent developments as to how the international and municipal communities have been working to overcome these challenges. Some suggestions and recommendations will be shared at the end of the chapter. The issue of occupational health and safety, which is very serious, will be covered in the next chapter.

## 30.2 Functional nanomaterials: an overview

The use of nanomaterials to improve different characteristics of various industrial and consumer products is not new [3]. Apart from their historical applications in different civilizations, nanomaterials were added to rubber to make tires last long and enhance their grip on the ground as far back as the end of the 19th century. But general interest in nanomaterials gained momentum only at the end of the 20th century when scientists developed techniques to control the production methods (i.e., properties, size, characteristics, etc.) and when they were successful to produce these on a larger scale [4].

Nanomaterials, substances in the nanoscale (i.e., between 1 and 100 nm), are ubiquitous in nature and thus scientists have been exploring different shapes and sources of nanomaterials from different natural things such as animals, trees, etc. [5]. So far, scientific literature has confirmed that natural nanomaterials are not harmful to human health and thus they remain free from regulatory concerns. Accidental or unintentional nanomaterials have been by ancient civilizations for centuries. Currently the main legal and regulatory concern is over industrial, intentional, manmade, or engineered nanomaterials (i.e., nanomaterials that are intentionally produced for specific performance). Industrial nanomaterials are produced in huge quantities [6]. Nanomaterials are intensively used in industrial and consumer products due to their beneficial characteristics in improving the products efficiently [7].

Functional nanomaterials are nanometer-scale compounds whose properties have been altered or augmented for a specific application. They can be

prepared with various physical, chemical, electric, and magnetic properties. They are different from natural and accidental nanomaterials. Functional nanomaterials play a particularly important role in two areas: lab-on-a-chip technology, which promises to assist in real-time monitoring of human health; and research into clean renewable energy technologies, which is encouraged to exploit to reduce greenhouse gases responsible for global warming leading to climate change [8].

### 30.3 Functionalized nanomaterials: applications, human health, and environmental concerns

Nanotechnology, or nanotechnologies, can be exploited for various purposes [9,10] and as a result can be described as a “general purpose technology,” “transformative technology,” “key enabling technology,” etc. Nanotechnologies have the potential to be used in agriculture [11–13], industrial wastewater treatment and water purification [14], biomedical applications [15,16], in removing pharmaceutically active compounds from water [17], and in pharmacological applications [18]. The nanomaterial-membrane coupling system can remove waterborne pathogenic viruses that threaten human health [19]. Thus these systems can be used to achieve various goals listed in the UN Sustainable Development Goals.

With all these applications, ENMs can induce reproductive and developmental toxicity that may cause microbial community variations in the environment and change biodiversity [20]. Sensitivity and exposure time have an impact on adverse effects of nanomaterials in the environment and biodiversity [20]. A German Federal Ministry of Education and Research funded project found that nanomaterials such as cerium oxide and barium sulfate frequently processed in various products can be exposed to human and other organisms. Even low doses of long-term exposure have adverse effects on lung and lung tissue [7]. Silver nanomaterials were found to have a detrimental effect on memory and cognitive coordination processes [21], have toxic effects on aquatic organisms [22], and can induce neurodevelopmental toxicity [23].

Nanomaterials found in the human environment have potential toxicological effects [24]. A recent study confirmed that ZnO–NPs are toxic to oyster larvae under seawater conditions [25]. Nanomaterials may enter the human body in a number of ways and then may move to the whole body through blood circulation [26]. Inhaled gold nanoparticle can enter the blood within 15 min and can be there for at least 3 months and thus can contribute to cardiovascular disease [27]. Silica nanoparticles have effects on cardiovascular, dermal, respiratory, neural, hepatic, genetic, immune, reproductive, and renal systems [28]. Some ENMs may impact on plant growth, seed germination, cell viability, and reduce microbial biodiversity [29].



Consumers can be exposed to nanoparticles from products such as enabled toner-based printing equipment [30], where nanomaterials are incorporated into toner formulations and become airborne during printing [30]. Silver nanoparticles, popular for their antimicrobial properties, and used in commercial toothbrushes can be exposed to the consumers and be released to the environment [31]. A study on online databases of nano-enabled consumer and personal care products revealed that up to 90% of all nanoenabled personal care products involve intentional or unintentional dermal exposure [32].

Long-term exposure effects of silver NPs was also tested and it was revealed that long-term exposure of AgNPs at environmentally relevant concentrations induced adverse effects on the soil microbiome, significantly decreased the microbial biomass, an abundance of total soil bacteria, and the soil microbes responsible for nitrogen cycling [33]. Nevertheless, the benefits and opportunities promised by nanotechnologies outweigh the risks [34]. The toxicity or beneficial use of nanomaterials depend on their concentration, size, shape, ultrasonication, etc. [35]. Thus it is possible that these nanomaterials can be made safe for the consumers.

It is a matter of great concern that while companies are busy exploiting nanomaterials, they are reluctant to share information on the quantity of nanomaterials they produce. For policymakers, it is crucial to know the quantity of nanomaterials produced for environmental risk assessment [6]. Therefore various countries have introduced the reporting mechanism that was initially voluntary. However, some of these countries made it compulsory later on as the voluntary calls were not responded adequately.

### 30.4 Functionalized nanomaterials: legal and regulatory aspects

The relationship between regulation and innovation is complicated and paradoxical. To some, regulations are an obstacle to innovation and for others products are being produced on such a fast scale that regulators are incapable of catching up. To some, regulations are an obstacle to innovation and for others, products using emerging technologies are being produced on such a fast scale that it is hard for the regulators to pinpoint the issues that need to be addressed [36].

Legal and regulatory aspects of ENMs have been reported in the literature [37–39]. Different factors such as the specific effects of ENMs on human health and the environment and the absence of uniform and widely recognized testing guidelines to assist in risk assessment and management, etc., prevent regulators from reaching binding regulations, with some exceptions.

Regulators and policymakers in developed countries, considering the nanoenabled product's cradle-to-grave life cycle, have already identified

several legal and regulatory concerns regarding ENMs, which are also relevant for functionalized nanomaterials [40]. They have assessed the adequacy of existing municipal legal provisions and concluded that existing laws on chemical, environment, occupational health and safety, consumer protection, and product liability, etc., are relevant in the discussion of legal and regulatory concerns about ENMs. Initially, the regulators of some of the developed countries believed that the existing legal frameworks were enough, with some required modifications only; but gradually, it is apparent that an increasing number of regulators have been introducing some regulatory tools such as guidelines on the reporting about ENMs manufacturing or import, etc. While such initiatives are necessary to regulate ENMs within the national boundary, due to the nature of ENMs, some extraterritorial impacts of ENMs or nanoenabled products are expected and should be seriously considered. Unfortunately, there are no direct and specific international law provisions in this regard and only some broad and general provisions can be found in international law instruments that can be used [41].

More than 30 definitions of ENMs are available in the literature. These definitions were adopted to serve different purposes. It appears that the definition of nanomaterials is one of the main regulatory concerns and challenges. In these existing definitions, there are several ill-defined terms and thus future applications of nanomaterials may face legal uncertainties [42]. While this issue may not be that serious to the scientific community, the regulatory bodies, both international standard-setting organizations and governmental bodies, need more clarity [3] as there is a lack of reliable scientific data. Hence, the sharing of more data by the scientific community is desired.

### 30.5 Functionalized nanomaterials: highlights of legal and regulatory initiatives

In terms of regulation of nanomaterials, empirical data shows that not governments but private actors started the process of regulation by way of self-risk-management strategies since there were scientific uncertainties and lack of scientific and technical knowledge [43]. Subsequently, public bodies joined in the move. In this section, the initiatives taken by the European Union (EU) and the United States in regulating ENMs and nanoenabled products are discussed.

The EU can be seen as leading in the regulation of nanomaterials. Already there are both general and product-specific community legislation in place and nanomaterials are regulated within the scope of this legislation [44]. A number of community laws such as Registration, Evaluation, Authorisation, and Restriction of Chemicals (REACH) Regulation 1907/2006, Regulation concerning the making available on the market and use of biocidal products (Biocidal products regulation 528/2012), Cosmetic Products Regulation 1223/2009, Novel Food Regulation 2015/2283, Food

Additives Regulation 1333/2008, Plastic Food Contact Materials Regulation 10/2011, Active and Intelligent Food Contact Materials Regulation 450/2009, Provision of Food Information to Consumers Regulation 1169/2011, and Medical Devices Regulation Proposal COM (2012) 542 contain provisions on the definition of nanomaterials or nanoform substances, approval process, safety assessment, labeling, etc. In some cases, guidance notes/guidelines to comply with the regulatory requirements have also been published [44].

In May 2017, the ECHA, as the administrator of REACH, published a document titled “How to prepare registration dossiers that cover nanoforms: best practices” containing the best practices or recommendations to assist users to comply with the obligations under REACH. In December 2018, the EC adopted several amendments in the REACH Annexes to clarify the information requirements for ENMs. EFSA issued the new Guidance on risk assessment of the application of nanoscience and nanotechnologies in the food and feed chain in May 2018.

Researchers have reported that the application of REACH is complex, time consuming, and expensive [45]. Therefore the European Chemical Agency (ECHA) developed the “Recommendations for nanomaterials applicable to the Guidance on QSARs and Grouping” and “Read-Across Assessment Framework.” A group of scientists successfully applied these 19 different types of multiwalled carbon nanomaterials focusing on their genotoxicity [46].

Due to the membership of the EU, some of the member states have also started enforcing stricter regulatory measures. European countries such as France, Belgium, Denmark, and Sweden have already developed product registers. However, even with the success of these measures, manufacturers can still move to other countries with more lenient regulatory frameworks.

In the United States, the Environmental Protection Agency (EPA) is the main regulatory authority responsible for ensuring that ENMs do not cause unreasonable risk to human health and the environment. The EPA has issued an information-gathering rule effective from August 14, 2017 under section 8 (1) of the Toxic Substances Control Act, 1976. Under this new rule, manufacturers and importers of nanoscale chemicals need to inform the EPA about the specific chemical identity, production volume, methods of manufacture, processing, use, exposure and release information, and available health and safety data. EPA has also issued a Working Guidance on Information Gathering Rule on Nanomaterials in Commerce.<sup>2</sup>

Once nanomaterials are used in various products, they come under the regulatory control of the FDA, which has historically created product-

---

2. The US Environmental Protection Agency, Control of Nanoscale Materials under the Toxic Substances Control Act, available at <https://www.epa.gov/reviewing-new-chemicals-under-toxic-substances-control-act-tsca/control-nanoscale-materials-under>.

specific science-based regulatory policy. Based on the product-specific statutory legal standards, the FDA takes an adaptive and flexible approach to regulating nanoenabled products but does not determine whether nanotechnology is safe or not. The FDA mainly tries to understand the interactions of ENMs with biological systems, adequacy of testing approaches for assessing safety, effectiveness, and quality of the product during the premarket and postmarket level. While there are premarket requirements, the FDA encourages consultation to reduce unintended harm to human and animal health. Most notably, the FDA imposes obligations on the industry to ensure that their products meet all legal requirements including safety standards.

It is relevant to share here that the FDA has also issued a number of Guidelines such as (1) Final Guidance for Industry—Considering Whether an FDA-Regulated Product Involves the Application of Nanotechnology, (2) Final Guidance for Industry—Safety of Nanomaterials in Cosmetic Products, (3) Final Guidance for Industry—Assessing the Effects of Significant Manufacturing Process Changes, Including Emerging Technologies, on the Safety and Regulatory Status of Food Ingredients and Food Contact Substances, Including Food Ingredients that are Color Additives, and (4) Final Guidance for Industry—Use of Nanomaterials in Food for Animals. The organization is in the process of developing another Guidance for Industry—Drug Products, Including Biological Products, that Contain Nanomaterials.<sup>3</sup> Manufacturers and business entities working with ENMs and functional nanomaterials must use this guidance to avoid adverse legal and regulatory consequences.

Various international organizations such as the Organisation for Economic Co-operation and Development (OECD), European Union have also been working to ensure the safety of engineered nanomaterials. After 7 years of research, the OECD's Working Party on Manufactured Nanomaterials finally published its findings on the testing program for ENMs and disclosed that the Test Guidelines used for regular chemical substances are, in most cases, suitable for use with manufactured nanomaterials. However, some researchers, after in-depth analysis of the OECD research findings, did not agree since the dossier contained an incomplete portfolio of ENM ecotoxicological evaluations making it difficult to draw substantive conclusions. A follow-up program and more research are suggested [47].

## 30.6 Discussion

The legal and regulatory challenges and uncertainties on the effects and risks of ENMs on human health and the environment highlighted above have an impact on the exploitation of the full potentials of ENMs [45]. Already a

---

3. The FDA's Approach to Regulation of Nanotechnology Products, <https://www.fda.gov/ScienceResearch/SpecialTopics/Nanotechnology/ucm301114.htm>.

number of new tools have been proposed or are in the stage of near completion that can be used for regulatory risk assessment of nanomaterials [48]. A tiered risk assessment approach is recommended. Even though authoritative bodies like the OECD and the SSCI of Europe have confirmed that existing risk assessment methods are adequate for now, no organization has actually excluded the need to continue the risk assessment. Therefore risk assessment should be a continuous process where rigorous toxicological research can guide effective risk assessment and management [12].

Development of databases on nanomaterials and/or product registrations could help the development of nanomaterial regulation. In various countries, the majority of them are from Europe, have already developed such databases with important relevant information that can be used and considered by the stakeholders.

Lack of consistent data is a challenge for regulators and thus may result in regulations with unintended consequences. It has been reported that after the EU accepted the definition of nanomaterials, some conventional materials widely used for commercial purposes for years such as cement, rubber, and even green tea were technically classified as nanomaterials [9]. Some nanomaterials are in use for decades, like the use of rubber in tires, nanoscale ingredients in cosmetics without any reported adverse incident [9].

Nanomaterials should be categorized based on their properties and toxicity instead of size as this approach may facilitate toxicological risk assessment [49]. The unique characteristics of nanomaterials pose regulatory challenges and therefore a multidisciplinary team of professionals having expertise in different stages of the life cycle should be involved in policy-making [50,51].

For the registration of nanomaterials, blockchain technology can be considered as this technology, considered a decentralized and distributed ledger, promises reliability, accountability, and transparency.

Under the 2011 European Regulation Concerning the Provision of Food Information to Consumers, any ingredient containing nanomaterials must be labeled as such, with the name if the materials followed by the word “nano”. Several professional bodies such as the Soil Association of the United Kingdom, Biological Farmers of Australia, and the General Standard Board of Canada have already banned the use of ENMs in food [3]. The 5-year Swiss National Research Programme concluded that whenever a new nanomaterial is identified or a new application of an established nanomaterial is attempted, a risk reassessment is essential to guarantee safety [34].

Safe and sustainable development of nanotechnologies, or safety-by-design ENMs, is the latest approach to designing nanomaterials and nanoenabled or nanoenhanced products where relevant available information on potential adverse effects on human health and biodiversity is taken into account [52]. In this approach, researchers and manufacturers consider known toxicity and redesign ENMs, including functional nanomaterials, by

redesigning the detrimental characteristics. Some guidelines for the redesign of safer NPs have already been introduced [53].

Awareness campaigns have potential impacts on the sustainable and responsible development of nanotechnologies [54]. Funding should be allocated and spent judiciously to conduct research on nanotoxicity. Various non-EU countries have been regulating nanomaterials using guidance [37] and global leader South Korea has started to regulate ENMs.

### 30.7 Conclusion

ENMs can be seen as part of the Fourth Industrial Revolution. This chapter has attempted to share an overview of the legal and regulatory issues, concerns, and challenges associated with ENMs and functional nanomaterials and the need for regulation. As discussed only some developed countries have introduced some form of regulation, and most developing countries have not.

Good manufacturing practices should be encouraged, but some researchers believe existing legal frameworks provide significant hurdles to innovative chemical design [55]. State-based regulatory systems or command and control regulatory systems are getting popularity in the EU and the US [56]. A hybrid governance framework involving both public and private governance mechanisms (i.e., responsible innovation, risk management, and guidelines/industry standards) may be able to address human health, safety, and environmental risk assessment issues [57]. It is time to work on harmonization of regulations on nanomaterials and nanoenabled products.

An anticipatory and principle-based approach of regulation, coupled with strict implementation of precautionary principles, by way of development of a product database or product register, may be an appropriate option for regulators to ensure safe and sustainable development of ENMs and functional nanomaterials.

### References

- [1] Dai L. From conventional technology to carbon nanotechnology: the fourth industrial revolution and the discoveries of C60, carbon nanotube and nano diamond. In: Dai L, editor. *Carbon nanotechnology*. Elsevier; 2006. p. 3–11.
- [2] Schwab K. *The fourth industrial revolution*. New York: Crown Business; 2017.
- [3] Jeevanandam J, et al. Review on nanoparticles and nanostructured materials: history, sources, toxicity and regulations. *Beilstein J Nanotechnol* 2018;9:1050–74.
- [4] Wohlleben W, et al. *Safety of nanomaterials along their lifecycle: release, exposure, and human hazards*. CRC Press; 2014.
- [5] Hochella MF, Spencer MG, Jones KL. Nanotechnology: nature's gift or scientists' brain-child? *Environ Sci Nano* 2015;2(2):114–19.
- [6] Piccinno F, et al. Industrial production quantities and uses of ten engineered nanomaterials in Europe and the world. *J Nanopart Res* 2012;14(9):1109.

- [7] Schwotzer D, et al. Effects from a 90-day inhalation toxicity study with cerium oxide and barium sulfate nanoparticles in rats. *Part Fibre Toxicol* 2017;14(1):23.
- [8] Crutchley RJ. Preface to functional nanomaterials. *Coord Chem Rev* 2016;320–321:1.
- [9] Koltsov D, Koltsov I. Application of nanomaterials to industry: how are nanomaterials used and what drives future applications? *Metrology and standardization of nanotechnology*. Wiley-VCH Verlag GmbH & Co. KGaA; 2017. p. 465–84.
- [10] Koodali RT. Nanoparticles: from fundamentals to applications. In: Kent JA, Bommaraju TV, Barnicki SD, editors. *Handbook of industrial chemistry and biotechnology*. Cham: Springer International Publishing; 2017. p. 1673–93.
- [11] Concha-Guerrero SI, Brito EM, Caretta CA. Impact of the nanomaterials on soil bacterial biodiversity. *Nanotechnology*. Springer; 2017. p. 173–90.
- [12] Iavicoli I, et al. Nanotechnology in agriculture: opportunities, toxicological implications, and occupational risks. *Toxicol Appl Pharmacol* 2017;329:96–111.
- [13] Parisi C, Vigani M, Rodríguez-Cerezo E. Agricultural nanotechnologies: what are the current possibilities? *Nano Today* 2015;10(2):124–7.
- [14] Palit S. Nanomaterials for industrial wastewater treatment and water purification. In: Martínez LMT, Kharissova OV, Kharisov BI, editors. *Handbook of ecomaterials*. Cham: Springer International Publishing; 2017. p. 1–41.
- [15] Silva M, Alves NM, Paiva MC. Graphene-polymer nanocomposites for biomedical applications. *Polym Adv Technol* 2017;.
- [16] Foo ME, Gopinath SC. Feasibility of graphene in biomedical applications. *Biomed Pharmacother* 2017;94:354–61.
- [17] Cai Z, et al. Application of nanotechnologies for removing pharmaceutically active compounds from water: development and future trends. *Environ Sci Nano* 2017;.
- [18] Sharma D, Shrivastava R, Bisht GS. Nanomaterial in diverse biological applications. *Metabolic engineering for bioactive compounds*. Springer; 2017. p. 293–317.
- [19] Cheng R, et al. Removal of waterborne pathogen by nanomaterial-membrane coupling system. *J Nanosci Nanotechnol* 2018;18(2):1027–33.
- [20] Chen M, Qin X, Zeng G. Biodiversity change behind wide applications of nanomaterials? *Nano Today* 2017;.
- [21] Węsierska M, et al. Silver ions are responsible for memory impairment induced by oral administration of silver nanoparticles. *Toxicol Lett* 2018;290:133–44.
- [22] Klingelfus T, et al. Acute and long-term effects of trophic exposure to silver nanospheres in the central nervous system of a neotropical fish *Hoplias intermedius*. *NeuroToxicology* 2017;63(Suppl. C):146–54.
- [23] Yamada S, Yamazaki D, Kanda Y. Silver nanoparticles inhibit neural induction in human induced pluripotent stem cells. *Nanotoxicology* 2018;1–11.
- [24] Sardoiwala MN, Kaundal B, Choudhury SR. Toxic impact of nanomaterials on microbes, plants and animals. *Environ Chem Lett* 2017;.
- [25] Noventa S, Rowe D, Galloway T. Mitigating effect of organic matter on the in vivo toxicity of metal oxide nanoparticles in the marine environment. *Environ Sci Nano* 2018;.
- [26] Sahu SC, Hayes AW. Toxicity of nanomaterials found in human environment. *Toxicol Res Application* 2017;1. p. 2397847317726352.
- [27] Miller MR, et al. Inhaled nanoparticles accumulate at sites of vascular disease. *ACS Nano* 2017;11(5):4542–52.
- [28] Mohammadi P, et al. The toxicology of silica nanoparticles: a review. *Toxicol Environ Chem* 2018;1–32.

- [29] Chen M, et al. Toxicity of carbon nanomaterials to plants, animals and microbes: recent progress from 2015-present. *Chemosphere* 2018;206:255–64.
- [30] Pirela SV, et al. Nanoparticle exposures from nano-enabled toner-based printing equipment and human health: state of science and future research needs. *Crit Rev Toxicol* 2017;47(8):678–704.
- [31] Mackevica A, Olsson ME, Hansen SF. The release of silver nanoparticles from commercial toothbrushes. *J Hazard Mater* 2017;322:270–5.
- [32] Adawi HI, et al. Nano-enabled personal care products: current developments in consumer safety. *NanoImpact* 2018;11:170–9.
- [33] Grün A-L, et al. Long-term effects of environmentally relevant concentrations of silver nanoparticles on microbial biomass, enzyme activity, and functional genes involved in the nitrogen cycle of loamy soil. *J Environ Sci* 2018;69:12–22.
- [34] Aebi U, Gehr P. Swiss national research programme “opportunities and risks of nanomaterials” (NRP 64): key findings. *J Nanobiotechnol* 2017;15.
- [35] Shweta KV, et al. 16 Plants and carbon nanotubes (CNTs) interface: present status and future prospects. *Nanotechnol Food Environ Paradig* 2017;317.
- [36] Sayre PG, Steinhäuser KG, van Teunenbroek T. Methods and data for regulatory risk assessment of nanomaterials: questions for an expert consultation. *NanoImpact* 2017;8 (Suppl. C):20–7.
- [37] Amenta V, et al. Regulatory aspects of nanotechnology in the agri/feed/food sector in EU and non-EU countries. *Regulatory Toxicol Pharmacol* 2015;73(1):463–76.
- [38] Karim ME, Munir AB. Nanotechnology and international environmental law: a preliminary assessment. *Adv Environ Anal* 2016;348–80.
- [39] Karim ME, et al. Too enthusiastic to care for safety: present status and recent developments of nanosafety in ASEAN countries. *Tech. Forecasting Social Change* 2015;92:168–181.
- [40] Karim M, Munir ABJAB. Nanotechnology in Asia: a preliminary assessment of the existing legal framework. *Nanotechnol Asia Prelim Assess Existing Leg Framew* 2015;.
- [41] Karim ME, et al. Polymer nanocomposites and related legal issues: an overview. *New polymer nanocomposites for environmental remediation*. Elsevier; 2018. p. 679–98.
- [42] Miernicki M, et al. Legal and practical challenges in classifying nanomaterials according to regulatory definitions. *Nat Nanotechnol* 2019;14(3):208–16.
- [43] Snir R. Trends in global nanotechnology regulation: the public-private interplay. *Vanderbilt J Entertain Technol Law* 2014;17:107.
- [44] Rauscher H, Rasmussen K, Sokull-Klüttgen B. Regulatory aspects of nanomaterials in the EU. *Chem Ing Technik* 2017;89(3):224–31.
- [45] Van Teunenbroek T, et al. Towards a more effective and efficient governance and regulation of nanomaterials. 2017;14(1):54.
- [46] Aschberger K, et al. Grouping of multi-walled carbon nanotubes to read-across genotoxicity: a case study to evaluate the applicability of regulatory guidance. *Comput Toxicol* 2019;9:22–35.
- [47] Hansen SF, et al. A critical analysis of the environmental dossiers from the OECD sponsorship programme for the testing of manufactured nanomaterials. 2017;4(2):282–91.
- [48] Steinhäuser KG, Sayre PG. Reliability of methods and data for regulatory assessment of nanomaterial risks. *NanoImpact* 2017;7(Suppl. C):66–74.
- [49] Bierkandt FS, et al. The impact of nanomaterial characteristics on inhalation toxicity. 2018;7(3):321–46.



- [50] Ribeiro AR, et al. Challenges on the toxicological predictions of engineered nanoparticles. *NanoImpact* 2017;8(Suppl. C):59–72.
- [51] Beaudrie CE, et al. Scientists versus regulators: precaution, novelty & regulatory oversight as predictors of perceived risks of engineered nanomaterials. 2014;9(9):e106365.
- [52] Schwarz-Plaschg C, Kallhoff A, Eisenberger I. *Making nanomaterials safer by design?* Springer; 2017.
- [53] Bastús NG, Puentes V. Nanosafety: toward safer nanoparticles by design. *Curr Med Chem* 2018;25(35):4587–601.
- [54] de Melo NF, Fraceto LF, Grillo R. Heightening awareness for graduate students of the potential impacts of nanomaterials on human health and the environment using a theoretical–practical approach. *J Chem Educ* 2017;.
- [55] Stark WJ, et al. Industrial applications of nanoparticles. *Chem Soc Rev* 2015;44(16):5793–805.
- [56] Justo-Hanani R, Dayan T. The role of the state in regulatory policy for nanomaterials risk: analyzing the expansion of state-centric rulemaking in EU and US chemicals policies. *Res Policy* 2014;43(1):169–78.
- [57] Hemphill TA. Regulating nanomaterials: a case for hybrid governance. *Bull Sci, Technol Soc* 2016;36(4):219–28.

# Functional nanomaterials: selected occupational health and safety concerns

Md. Ershadul Karim<sup>1,2</sup>

<sup>1</sup>*Faculty of Law, University of Malaya, Kuala Lumpur, Malaysia,* <sup>2</sup>*Bangladesh Supreme Court, Dhaka, Bangladesh*

### 31.1 Introduction

In spite of apparent limitless potentials due to the presence of multidimensional exciting characteristics, the findings of various published scientific research has confirmed over the last few years that human being and environmental components can be exposed to manmade engineered nanomaterials (ENMs) during their cradle-to-grave life cycle [1–4]. Moreover, even though the long-term effects of these ENMs has yet to be confirmed, manufacturers of ENMs are found to be too enthusiastic to harness the benefits of these ENMs. However, after the enactment of the 21st Century Nanotechnology Research and Development Act, 2003 by the United States, the issue of Occupational Health and Safety (OHS) related to the workers and researchers who handle ENMs started to get the attention of the stakeholders within their general research agenda on nanorisk and safety. After more than 17 years, the regulators of some developed countries have started to treat the OHS issues of the workers and researchers of this sector with better care. Some of these regulators have conducted studies using different methodologies, and subsequently, have either suggested the improvement of existing guidelines and standards on OHS or issued new guiding documents in this regard.

Recent studies have confirmed that the ENMs work better in a functionalized form where the functional group can be added on to the surface of the ENMs. Functionalized nanomaterials can be developed in a different manner than ENMs due to the presence of different mechanical, absorption, optical, or chemical properties. These nanomaterials are expected to address the drawbacks and limitations of ENMs [5] and to play an important role in

developing safe ENMs that help ensure better OHS of workers, employees, researchers, etc. The issue of OHS in the nanotechnology industries has been addressed by many researchers [6,7], although there are limited research findings in relation to functionalized nanomaterials. However, there are some new developments as will be discussed in this chapter. While various chapters of this book have covered technical aspects of functionalized nanomaterials this chapter will be an attempt to discuss OHS issues from a legal point of view in the context of ENMs. With this aim in mind, this chapter is divided into six parts including an introduction and conclusion. Part 2 will provide some highlights of the findings from scientific literature regarding OHS issues in the ENM context, including some of the challenges faced by regulators in terms of implementing relevant municipal OSH provisions. Part 4 will discuss some of the initiatives taken by various stakeholders such as governmental bodies and universities. We will further share how some international and municipal communities have been working to overcome these challenges and offer our own suggestions.

### 31.2 ENMs and OHS concerns

The OHS and exposure of engineered nanoparticles (ENPs) have been considered on a limited scale in the scientific literature. Instead, most research has focused on the exciting features and characteristics of ENMs. Several countries such as South Korea [8], France [9], the United States [10,11], Spain [12], and the Netherlands [13], etc., have already conducted national survey "on exposure and occupational health and safety aspects of nanomaterials". In some instances, international surveys were also conducted [14]. Researchers have also evaluated the OHS practices in some countries [15].

As some studies have indicated about the possibility of adverse consequences on human health due to ENP exposure and if the cradle-to-grave product life cycle is considered, workers and researchers will be found as the primary victims. The issue of protection of workers and researchers who handle ENMs should be treated seriously as some ENMs (e.g., carbon nanotubes (CNT)) have a similar shape as asbestos [16]. Research has also shown that some ENMs have serious potential impacts on human health and the environment [17] even when these materials are embedded in consumer goods [18–21]. Functional nanomaterials (e.g., TiO<sub>2</sub> used in medical applications) can also pose serious health risks and therefore it has been suggested to avoid the use of such materials in healthcare settings [22]. Not only workers working in labs or manufacturing plants are at risk [23], even agricultural workers who come in contact with pesticides can also be exposed to ENMs [24]. ENMs inhaled by a pregnant woman can influence fetal health [25,26] and can produce psychological deficits [27]. Moreover, inhaled nano-TiO<sub>2</sub> can cause significant epigenetic and transcription changes in a pregnant

woman's fetus and can have a similar lung burden after working almost 1.5 years [28].

The countries leading in ENM research and development have municipal legal frameworks in place regarding OHS. However, it has been reported that investors, both public and private, are not serious about allocating money to consider the human health and environmental implications of ENMs [29]. While no conclusive proof has been confirmed thus far, news of the death of two workers and illness in five others handling nanomaterials in two Chinese paint factories can be considered as concerning evidence. In the United States, a 26-year-old female chemist was reported to develop nickel sensitization when she working with nickel nanoparticle powder without using personal protective equipment [30]. These incidents have alerted stakeholders to seriously consider the OHS issues of workers and researchers [31,32]. As a result, various regulators from developed countries have started to assess and evaluate existing municipal legal frameworks to determine their effectiveness.

### **31.3 ENMs and OHS laws: an overview**

It is neither possible nor desirable to survey the municipal OHS-related laws of all the countries in the world. Instead, this part will discuss the legal provisions in place to protect workers and researchers in their occupational settings. For example, within the European Union (EU), a good number of community laws contain provisions to protect and ensure the OHS of workers. The list of such laws include: (1) the Directive on the introduction of measures to encourage improvements in the safety and health of workers at work, 1989 (Directive 89/391/EEC of 12 June 1989); (2) the Directive on the Protection of the Health and Safety of Workers from the risks related to chemical agents at work (Directive 98/24/EC of 7 April 1998); (3) the Directive on the protection of workers from the risks related to exposure to carcinogens or mutagens at work (Directive 2004/37/EC of 29 April 2004); (4) the Regulation on the Registration, Evaluation, Authorisation and Restriction of Chemicals (Regulation No. 1907/2006 of 18 December 2006); (5) the Regulation on classification, labelling and packaging of substances and mixtures on the classification, labelling and packaging of substances and mixtures (Regulation No. 1272/2008 of 16 December 2008), etc. Similar kinds of legal provisions can be found in the context of many other countries and these include provisions on safe handling and control, assessment of exposure, hazard and risk, use of Safety Data Sheet (SDS) or Material Safety Data Sheet (MSDS), personal protective equipment (PPE), etc. Moreover, available legal instruments also include provisions through which regulators can frame a code of conduct for stakeholders.

Labeled SDS or MSDS, an important hazard communication tool regarding the manufacturing, storage, transportation, etc., related activities

regarding chemicals, plays an important role in making workers and researchers aware of the chemical substances they have been handling [33,34]. These allow the workers and researchers to use various techniques and instruments to monitor ENMs in the workplace [35].

It is a matter of great concern that MSDS or SDS is not usually available for ENMs [8], rather these contain information on bulk substances and thus are not adequate or enough to serve the same purpose for ENMs. Of the 110,000 synthetic chemicals produced in industrial quantities, it was found that adequate hazard assessment data are available only for around 6000 hazardous chemicals and occupational exposure limits have been set for only 500–600 hazardous chemicals [36]. SDSs are not updated as there is no mandatory requirement that the term “nanomaterial” be included in the SDSs [8,33].

In a very recent study, by using one criterion, it was found that out of 67 MSDS, only 28.4% were reliable, whereas 35.8% were found to be reliable with restrictions, and 35.8% were found to be unreliable. In the same research, using another criterion, only 3% MSDS were found as satisfactory, 17.9% were in need of improvement, and 79% were in need of significant improvement [37]. Even though MSDS has evidentiary value [29], it is unfortunate that the situation has not been improved significantly; these findings are similar to those from previous research findings [33,34] conducted a few years ago. Most of the SDSs did not include sufficient information on the safety of nanomaterials, such as their toxicity and physicochemical properties. The reasons for this lack of information in the nanomaterial SDSs can mainly be attributed to (1) a lack of toxicity and physicochemical property information on nanomaterials; (2) unawareness of the effectiveness of conventional exposure controls, such as local exhaust ventilation and encapsulation, and PPE, in protecting against nanomaterial exposure; (3) a lack of information on emergency and firefighting measures; and (4) a lack of knowledge on how existing regulations apply to nanomaterials [34].

Moreover, in most developed countries, though provisions on PPE can be found regarding the handling of hazardous materials, these are neither adequate to protect the workers and researchers handling ENMs as these are not designed specifically for ENMs, nor are these strictly implemented. The unique behavior of these substances at nanoscale, the long-term health effects of ENMs, and the claim by the authoritative bodies that the existing provisions on bulk substance are applicable for ENMs may be identified as possible reasons for this. Fortunately, various regulators have changed their views and have issued authoritative guidance documents in this regard. For example, the International Organization for Standardization (ISO), as a supplement to ISO 11014:2009 on the preparation of SDSs, has issued a technical report with a guideline on the development of SDS for manufactured nanomaterials (MNs) and for chemical products containing MNs. The Swiss State Secretariat for Economic Affairs has published Version 3.0 of the

“Safety data sheet (SDS): Guidelines for synthetic nanomaterials” in November 2016 [38]. The innovative part of this initiative is that it has also included the relevant legal requirements that other countries can consider if they plan to develop something similar.

### **31.4 Initiatives taken by the stakeholders**

Relevant stakeholders have taken a good number of initiatives to protect workers and researchers due to the prediction that ENMs may have adverse health consequences. In 2008, the European Commission recommended a voluntary Code of Conduct for responsible nanosciences and nanotechnologies (N & N) research. The Code provides that the Member States, N&N research funding bodies, and organizations should encourage N&N research where, inter alia, a priority should be given to research that will protect the public and the environment, consumers, or workers.

Trade unions, as the representative voice of workers, are in a better position to play an influential role in the protection of interests of the workers [39]. Unfortunately, in the case of nanotechnologies, the trade unions of developed economies such as the United States and Australia still do not consider this issue as serious, let alone the discussion in the other parts of the world, where the unions are busy addressing other problems [40]. For example, the European Trade Union Confederation (ETUC) adopted resolutions on nanotechnologies and nanomaterials in 2008 and 2010. Unfortunately, nothing much has been done in recent years to update these resolutions. Recently the ETUC has opined that the decision of European regulators to set up an observatory of nanomaterials instead of a register will not be able to protect workers from the possible health risks of ENMs as the observatory will work like an observer only. The European Trade Union Institute (ETUI), the independent training and research center of ETUC, has made five proposals on the regulatory governance of nanomaterials and these include making nano-related information public and visible, priorities nano-forms, mandatory safety datasheets, have the nano ID and cross-fertilization of national registries.<sup>1</sup> The Dutch trade union has also joined in by conducting a study [41]. Trade unions should take initiatives to educate workers about the adverse effects of nanomaterials and should not rely on management in relation to various risks [42].

Different international organizations such as the ILO, World Health Organization (WHO), and European Agency for Safety and Health and Work have also been working to study the safety aspects of ENMs. In 2017, the

---

1. Aida Ponce Del Castillo, Proposals on the regulatory governance of nanomaterials, Stakeholder Dialogue European Union Observatory for Nanomaterials EUON March 9th, 2018, [https://euon.echa.europa.eu/documents/23168237/23875831/090318\\_euon\\_aida\\_etui\\_en.pdf/d9dce65-702d-b814-69b3-8a83f19ac39a](https://euon.echa.europa.eu/documents/23168237/23875831/090318_euon_aida_etui_en.pdf/d9dce65-702d-b814-69b3-8a83f19ac39a)

WHO issued Guidelines on Protecting Workers from Potential Risks of Manufactured Nanomaterials [43]. These guidelines were developed based on the precautionary principle and hierarchy of control measures (i.e., preference of measures like the use of personal protective equipment having closer relation to the root of the problem; grouping of nanomaterials by toxicity, fibrous characteristics and granular biopersistence; education and training of workers on nanomaterials; and involvement of workers in every aspect of assessment and control).<sup>2</sup> Similarly, the European Agency for Safety and Health at Work (EU–OSHA) published an info sheet with an overview of how to deal with manufactured nanomaterials in the workplace.<sup>3</sup> Earlier in January 2016, the National Institute for Occupational Safety and Health (NIOSH) in the United States issued a draft on the health effects of occupational exposure of silver nanomaterials. This was revised in October 2018 with a recommended exposure limit for silver nanoparticles during the production or use of nanomaterials.

## 31.5 Evaluation

More than a hundred countries around the world have a specific program on nanotechnology research and development. Though there are concerns that some of the nanomaterials used in huge volumes in consumer products have adverse effects on the environment and human health, companies have been increasing the use of ENMs in their products since some of these consumer products such as cosmetics have been for a long without any significant health effects. The workers and researchers working with ENMs will be the initial victims in case these are found to have any adverse effects. As a result, regulators from different countries have started to make the issue of OHS and nanosafety a priority and published material-specific or workplace-specific guidelines to protect workers from possible adverse effects of ENMs. For example, the Organisation for Economic Co-operation and Development’s Working Party on Manufactured Nanomaterials has recently published dossiers on certain nanomaterials and revealed that the test guidelines used for regular chemical substances are, in most of the cases, suitable for use on nanomaterials. However, some researchers are not convinced, and do not agree with the findings of the Working Party and have appealed for more research [44].

Popular ENMs such as CNTs have similarities to asbestos, which was also considered as a magic fiber when first introduced. However, the

---

2. WHO guidelines on protecting workers from potential risks of manufactured nanomaterials, <https://apps.who.int/iris/bitstream/handle/10665/259671/9789241550048-eng.pdf>

3. European Agency for Safety and Health at Work, Manufactured nanomaterials in the workplace, 2018, <https://osha.europa.eu/en/tools-and-publications/publications/manufactured-nanomaterials-workplace>

devastating effects of asbestos were later identified and many companies went bankrupt later after paying compensation injured workers. For the last couple of years, CNTs have been suggested as possible cancer-causing agents [45–48]. This was confirmed very recently [49]. If we take the late lessons of the early warnings given in the case of asbestos, workers will be the first victims if ENMs are found to have adverse effects.

Nanomaterials have limitless potential and can be used in almost every sector of human life. However, the success of exploiting these miracle materials will only be possible if their safety, both occupational and consumer, can be ensured. Responsible development of nanotechnology requires protection of workers at all stages of the technological life cycle [50]. As ENMs can become airborne to the environment when mixed in solution by sonication or in water containing natural organic matter, laboratory workers are at increased risk of exposure to ENMs [51]. Workers may also be exposed to nanometal oxides with industrial wastewater treatment processes [52]. In workplaces that handle nanomaterials, workers have been reported to have respiratory occupational disease [8], allergic dermatitis, and sneezing [15]. Workers are exposed to nanomaterials frequently due to handling tasks [53].

With the increased production of nanomaterials, the chances of occupational risks are increasing [54]. Potential risks relating to workers' health who can be potentially exposed to industrial nanomaterials is not a concern or point of interest to manufacturers [13]. The OSHA practice in industries handling nanomaterials should not be taken lightly. Even a few years ago, workplace monitoring and nano-specific waste disposal were not seriously considered [55]. Registries for nanomaterial workers including issues such as funding, potential for legal risks, access to data, confidentiality of business information, privacy, and worker expectations should be considered [56]. A recent study found that 1 out of 6 international semiconductor industrial companies maintain lists of employees working with nanomaterials but the practice of medical follow-up was not well established [57].

Lack of sufficient data should not be considered as evidence of the safety of ENMs [58]. Even though so far there is no clear confirmed case of harm from ENMs, if we take into account the history of asbestos we know that it may take around 20 years from campaigning against asbestos to start of death with the effects continuing for 40 years [59]. This may also happen in the case of ENMs. Therefore it is important to use engineering safeguards and follow personal protection strategies [60]. Identification and adoption of effect control technologies is another important step that should be adopted to save workers from the risk of exposure to ENMs [61].

Protection of workers through an insurance policy can also be considered actively though the insurers considered that the benefits of nanotechnology will outweigh the risks. It may be due to the fact that insurers perception depends on past experience and there was no reported major incident happened. The situation may be changed dramatically as it was changed in case of terrorism risks after the 9/11 [62].



Legally, workers have the right to know what materials they have been handling, their associated risks and safety aspects, and the employers are under an obligation to provide them proper training. In a recent survey among construction industry workers, only 13% of respondents knew that nanomaterials were used in construction materials [63]. The WHO has identified things that should be included in the training of workers [64], and similar kind of documents can be found in the context of laboratories issued by government agencies or universities.<sup>4</sup> Training of workers can include modules on types of nanomaterials, uses at work, risks, presence in the workplace, exposure, and experience sharing [65].

Various developed countries have taken some initiatives. France has decided to implement an epidemiological surveillance tool of workers likely to be exposed to ENMs [66]. An innovative approach is suggested for the management of nanomaterials in the research environment [32]. However, there were no studies published regarding exposure assessment between January 2000 and January 2015 in low- and middle-income countries [53].

Switzerland adopted new disclosure rules for synthetic nanomaterials at the beginning of 2018. In August, 2018, Safe Work Australia issued national guidelines on the classification of hazardous chemicals to assist manufacturers and importers of substances, mixtures, and articles having duties under the municipal laws to classify them. Moreover, the guidelines provide advice on, inter alia, nanomaterials where it is recommended to prepare and label an appropriate MSDS if the health hazards of ENPs are not completely characterized.

In February 2018, the NIOSH released a poster titled “Controlling Health Hazards When Working with Nanomaterials: Questions to Ask Before You Start” with a visual tool containing information for those who work with ENMs and how to prevent exposure. The poster aims to educate workers on different control and PPE options before start of work involving ENMs.

## 31.6 Conclusion

According to the ILO, it was anticipated that by 2020 approximately 20% of all goods manufactured globally will use nanotechnologies to some extent [36]. Therefore more and more workers and researchers will be in contact with ENMs and ENPs. In the absence of ENM-specific legal and regulatory instruments, existing ones on hazardous substances should be strictly followed and implemented to avoid serious legal consequences. At the XXI World Congress on Safety and Health at Work held in Singapore in

---

4. Deutsche Gesetzliche Unfallversicherung e.V. (DGUV), Nanomaterials in the Laboratory Tips and Handling Information, March 2015, <http://publikationen.dguv.de/dguv/pdf/10002/213-854.pdf>; USA OSHA, Working Safely with Nanomaterials, [https://www.osha.gov/Publications/OSHA\\_FS-3634.pdf](https://www.osha.gov/Publications/OSHA_FS-3634.pdf).

September, 2017, the European Agency for Safety and Health at Work together with the ILO presented new estimates of the cost of poor OHS where it was revealed that worldwide work-related injury and illness result in the loss of 3.9% of GDP, at an annual cost of roughly €2680 billion.<sup>5</sup> Moreover, 2.78 million workers continue to die each year from work-related injuries and illnesses and 2.4 million of these deaths can be attributed to work-related diseases alone.<sup>6</sup> As mentioned earlier, many successful companies dealing with asbestos were declared bankrupt after settling asbestos-related injury, medical cost, and loss of income claims, etc. Similar events should not be repeated in the case of ENMs.

## References

- [1] Semenzin E, et al. Controlling the risks of nano-enabled products through the life cycle: The case of nano copper oxide paint for wood protection and nano-pigments used in the automotive industry. *Environ Inter* 2019;131:104901.
- [2] Cucurachi S, Rocha CFB. Life-cycle assessment of engineered nanomaterials. *Nanotechnology in eco-efficient construction*. Elsevier; 2019. p. 815–46.
- [3] Wu F, et al. Life cycle impact of titanium dioxide nanoparticle synthesis through physical, chemical, and biological routes. *Environ. Sci. Technol* 2019;53(8):4078–87.
- [4] Jafarizadeh-Malmiri H, et al. Potential hazards of nanoparticles. *Nanobiotechnology in food: concepts, applications and perspectives*. Springer; 2019. p. 115–35.
- [5] Darwish M, Mohammadi A. Functionalized Nanomaterial for Environmental Techniques. In: Hussain CM, Mishra AK, editors. *Nanotechnology in environmental science*. John Wiley & Sons, Inc; 2018. p. 315–50.
- [6] Simeone FC, et al. Assessing occupational risk in designs of production processes of nano-materials. *NanoImpact* 2019;14:100149.
- [7] Graczyk H, Riediker M. Occupational exposure to inhaled nanoparticles: are young workers being left in the dust? *J Occup Health* 2019;.
- [8] Kim J, Yu JJ. National survey of workplaces handling and manufacturing nanomaterials, exposure to and health effects of nanomaterials, and evaluation of nanomaterial safety data sheets. *BioMed Res Int* 2016;2016 pp. 8389129–8389129.
- [9] Canu IG, et al. French registry of workers handling engineered nanomaterials as an instrument of integrated system for surveillance and research. *Journal of Physics: Conference Series*. IOP Publishing; 2013.
- [10] Schubauer-Berigan MK, et al. Engineered carbonaceous nanomaterials manufacturers in the United States: workforce size, characteristics, and feasibility of epidemiologic studies. *J Occup Environ Med* 2011;53:S62–7.
- [11] Schubauer-Berigan MK, et al. Association of pulmonary, cardiovascular, and hematologic metrics with carbon nanotube and nanofiber exposure among U.S. workers: a cross-sectional study. *Part Fibre Toxicol* 2018;15(1):22.

---

5. European Agency for Safety and Health at Work, Work-related accidents and injuries cost EU €476 billion a year according to new global estimates, Press release, 4 September, 2017.

6. International Labour Organization, World Congress on Safety and Health in Singapore, ILO head calls for global coalition on safety and health at work, Press release, 4 September, 2017.

- [12] Díaz-Soler BM, López-Alonso M, Martínez-Aires MD. Nanosafety practices: results from a national survey at research facilities. *J Nanopart Res* 2017;19(5):169.
- [13] Bekker C, et al. Industrial production and professional application of manufactured nanomaterials-enabled end products in Dutch industries: potential for exposure. *Ann Occup Hyg* 2012;57(3):314–27.
- [14] Conti JA, et al. Health and safety practices in the nanomaterials workplace: results from an international survey. ACS Publications; 2008.
- [15] Gulumian M, et al. Systematic review of screening and surveillance programs to protect workers from nanomaterials. *PLoS one* 2016;11(11):e0166071.
- [16] Lynch I. Far-reaching effects from carbon nanotubes. *Nat. Nanotechnol* 2019;14:639–40. Available from: <https://doi.org/10.1038/s41565-019-0477-z>.
- [17] Schulte PA, et al. Current state of knowledge on the health effects of engineered nanomaterials in workers: a systematic review of human studies and epidemiological investigations. *Scand J Work Environ Health* 2019;45(3):217–38.
- [18] Mackevica A, Olsson ME, Hansen SF. The release of silver nanoparticles from commercial toothbrushes. *J Hazard Mater* 2017;322:270–5.
- [19] Mackevica A, Olsson ME, Hansen SF. Silver nanoparticle release from commercially available plastic food containers into food simulants. *J Nanopart Res* 2016;18(1):5.
- [20] Limpitprakan P, et al. Release of silver nanoparticles from fabrics during the course of sequential washing. *Environ Sci Pollut Res Int* 2016;23(22):22810–18.
- [21] Tulve NS, et al. Characterization of silver nanoparticles in selected consumer products and its relevance for predicting children's potential exposures. *Int J Hyg Environ Health* 2015;218(3):345–57.
- [22] Bressot C, et al. Assessment of functional nanomaterials in medical applications: can time mend public and occupational health risks related to the products' fate? *J Toxicol Environ Health, Part A* 2018;1–17.
- [23] Filon FL, et al. Occupational dermal exposure to nanoparticles and nano-enabled products: Part I—Factors affecting skin absorption. *Int J Hyg Environ Health* 2016;219(6):536–44.
- [24] Iavicoli I, et al. Nanotechnology in agriculture: Opportunities, toxicological implications, and occupational risks. *Toxicol Appl Pharmacology* 2017;329:96–111.
- [25] Stapleton PA, et al. Maternal engineered nanomaterial exposure and fetal microvascular function: does the Barker hypothesis apply? *Am J Obstet Gynecol* 2013;209(3):227.e1–227.e11.
- [26] Stapleton PA, et al. Microvascular and mitochondrial dysfunction in the female F1 generation after gestational TiO<sub>2</sub> nanoparticle exposure. *Nanotoxicology* 2015;9(8):941–51.
- [27] Engler-Chiurazzi EB, et al. Impacts of prenatal nanomaterial exposure on male adult Sprague-Dawley rat behavior and cognition. *J Toxicol Environ Health, Part A* 2016;79(11):447–52.
- [28] Stapleton PA, et al. Maternal engineered nanomaterial inhalation during gestation alters the fetal transcriptome. *Part fibre Toxicol* 2018;15(1) pp. 3–3.
- [29] Karim ME, et al. Too enthusiastic to care for safety: Present status and recent developments of nanosafety in ASEAN countries. *Technol Forecast Soc Chang* 2015;92:168–81.
- [30] Journeay WS, Goldman RH. Occupational handling of nickel nanoparticles: a case report. *Am J Ind Med* 2014;57(9):1073–6.
- [31] Song Y, Li X, Du X. Exposure to nanoparticles is related to pleural effusion, pulmonary fibrosis and granuloma. *Eur respiratory J* 2009;.
- [32] Groso A, et al. Management of nanomaterials safety in research environment. *Part Fibre Toxicol* 2010;7(1):1.

- [33] Eastlake A, et al. A critical evaluation of material safety data sheets (MSDSs) for engineered nanomaterials. *J Chem Health Saf* 2012;19(5):1–8.
- [34] Lee JH, et al. Evaluation of information in nanomaterial safety data sheets and development of international standard for guidance on preparation of nanomaterial safety data sheets. *Nanotoxicology* 2012;7(3):338–45.
- [35] Ferrante R, et al. 30 - Measurement techniques of exposure to nanomaterials in workplaces. In: Pacheco-Torgal F, et al., editors. *Nanotechnology in eco-efficient construction*. 2nd ed Woodhead Publishing; 2019. p. 785–813.
- [36] Office IL. Labour protection in a transforming world of work A recurrent discussion on the strategic objective of social protection (labour protection) in Report VI. Geneva: International Labour Organization; 2015.
- [37] Hodson L, et al. An evaluation of engineered nanomaterial safety data sheets for safety and health information post implementation of the revised hazard communication standard. *J Chem Health Saf* 2019;26(2):12–18.
- [38] (SECO), S.S.f.E.A., Safety data Sheet (SDS): Guidelines for Synthetic Nanomaterials. 2016.
- [39] van Broekhuizen P, Reijnders L. Building blocks for a precautionary approach to the use of nanomaterials: positions taken by trade unions and environmental NGOs in the European nanotechnologies debate. *Risk Anal Int J* 2011;31(10):1646–57.
- [40] Invernizzi N. Union perspectives on the risks and implications of nanotechnology. Little by little; expansions of nanoscience and emerging technologies. Heidelberg: IOS Press; 2012. p. 195–215.
- [41] van Broekhuizen P, Dorbeck-Jung B. Exposure limit values for nanomaterials—capacity and willingness of users to apply a precautionary approach. *J Occup Environ Hyg* 2013;10(1):46–53.
- [42] Foladori G, Zayago Lau E. The role of organized workers in the regulation of nanotechnologies. In: Cozzens SE, Wetmore J, editors. *Nanotechnology and the challenges of equity, equality and development*. Dordrecht: Springer Netherlands; 2011. p. 181–98.
- [43] Organization, W.H., Guidelines on Protecting Workers from Potential Risks of Manufactured Nanomaterials. 2017: Geneva.
- [44] Hansen SF, et al. A critical analysis of the environmental dossiers from the OECD sponsorship programme for the testing of manufactured nanomaterials. *Environ Sci Nano* 2017;4(2):282–91.
- [45] Kane AB, Hurt RH. Nanotoxicology: the asbestos analogy revisited. *Nat Nanotechnol* 2008;3(7):378.
- [46] Pacurari M, Castranova V, Vallyathan V. Single-and multi-wall carbon nanotubes versus asbestos: are the carbon nanotubes a new health risk to humans? *J Toxicol Environ Health, Part A* 2010;73(5-6):378–95.
- [47] Poland CA, et al. Carbon nanotubes introduced into the abdominal cavity of mice show asbestos-like pathogenicity in a pilot study. *Nat Nanotechnol* 2008;3(7):423.
- [48] Ryman-Rasmussen JP, et al. Inhaled carbon nanotubes reach the subpleural tissue in mice. *Nat Nanotechnol* 2009;4(11):747.
- [49] Chernova T, et al. Long-fiber carbon Nanotubes replicate asbestos-induced Mesothelioma with disruption of the tumor suppressor gene Cdkn2a (Ink4a/Arf). *Curr Biol* 2017;27(21):3302–3314.e6.
- [50] Schulte PA, et al. Taking stock of the occupational safety and health challenges of nanotechnology: 2000–2015. *J Nanopart Res* 2016;18(6):159.

- [51] Johnson DR, et al. Potential for occupational exposure to engineered carbon-based nano-materials in environmental laboratory studies. *Environ health Perspect* 2010;118(1):49.
- [52] Brenner SA, et al. Occupational exposure to airborne nanomaterials: an assessment of worker exposure to aerosolized metal oxide nanoparticles in semiconductor wastewater treatment. *J Occup Environ Hyg* 2015;12(7):469–81.
- [53] Debia M, et al. A systematic review of reported exposure to engineered nanomaterials. *Ann Occup Hyg* 2016;60(8):916–35.
- [54] Stebounova LV, et al. Health and safety implications of occupational exposure to engineered nanomaterials. *Wiley Interdiscip Rev Nanomed Nanobiotechnol* 2012;4(3):310–21.
- [55] Conti J, et al. Health and safety practices in the nanomaterials workplace: results from an international survey. *Environ Sci Technol* 2008;42(9):3155–62.
- [56] Schulte P, et al. Exposure registries: overview and utility for nanomaterial workers. *J Occup Environ medicine/Am Coll Occup Environ Med* 2011;53(Suppl. 6):S42.
- [57] Vandebroek E, Hons L. 896 Working with engineered nanomaterials: what's the occupational physician's role? *BMJ Publishing Group Ltd*; 2018.
- [58] Bianchi MG, et al. Evaluation of potential engineered nanomaterials impacts on human health: from risk for workers to impact on consumers. *Exposure to Engineered Nanomaterials in the Environment*. Elsevier; 2019. p. 263–87.
- [59] Mullins S, Gatof J. Chapter 3 - are we willing to heed the lessons of the past? Nanomaterials and Australia's asbestos legacy. In: Hull MS, Bowman DM, editors. *Nanotechnology environmental health and safety*. 2nd ed Oxford: William Andrew Publishing; 2014. p. 25–52.
- [60] Ding Y, et al. Airborne engineered nanomaterials in the workplace—a review of release and worker exposure during nanomaterial production and handling processes. *J Hazard Mater* 2017;322(Part A):17–28.
- [61] Heitbrink WA, Lo L-M, Dunn KH. Exposure controls for nanomaterials at three manufacturing sites. *J Occup Environ Hyg* 2015;12(1):16–28.
- [62] Baublyte L, et al. Insurance market perception of nanotechnology and nanomaterials risks. *The Geneva Association*; 2014. p. 54.
- [63] Lippy B, West G. 1682d Improving awareness of nanomaterials among u.s. construction workers. *Occup Environ Med* 2018;75(Suppl. 2) pp. A71–A71.
- [64] Von Mering Y, Schmacher C, Organization WH. Development of a systematic evidence review for the WHO guideline on protecting workers from potential risks of manufactured nanomaterials: what training should be provided to workers who are at risk from exposure to the specific nanomaterials or groups of nanomaterials? *World Health Organization*; 2017.
- [65] Castillo APD. Training for workers and safety representatives on manufactured nanomaterials. *N Solutions J Environ Occup Health Policy* 2019;29(1):36–52.
- [66] Boutou-Kempf O, et al. Development of a French epidemiological surveillance system of workers producing or handling engineered nanomaterials in the workplace. *J Occup Environ Med/Am Coll Occup Environ Med* 2011;53(Suppl. 6):S103.

# Index

*Note:* Page numbers followed by “f” and “t” refer to figures and tables, respectively.

## A

- Abraxane, 547–548, 547t
- Acetic acid, 142–144
- Acetone, 142
- Aciclovir, 564t
- Acid-activated montmorillonite, 45–46
- Acid-functionalized MWCNTs, 41
- Actinidia deliciosa* var. *deliciosa*, 250–252
- Activated carbon (AC), 479–480, 483, 512–513
- Activated cotton textile (ACT), 690
- Active organic ingredients (AOI), 231
- Active pharmaceutical ingredient (API), 220–221
- Active polysaccharides, 146–147
- O*-Acylisourea, 447
- Additive manufacturing technology. *See* 3D printing
- Adsorbents, regeneration of, 319–320
- Adsorptive mixed-matrix membranes for heavy-metal removal, 40–47
- Adverse outcome pathway (AOP), 949–952
- Aegirine, 740, 743, 745
  - low-temperature hydrothermal synthesis of, 744
  - nanocrystalline aegirine, hydrothermal synthesis of, 744–745
  - typical preparation procedure of, 743–744
- Aegirine surface
  - interaction of epoxy hybrid with, 752–753
  - interaction of  $\beta$ -CD with, 754
- Aerospace applications of functional nanomaterials, 812–814
  - carbon nanocomposites for EM shielding, 813
  - carbon nanofiber-incorporated three-phase carbon/epoxy composites, 812–813
  - electrodeposited coatings, 814
  - nanostructured alloys for aerospace components, 813
  - polymer-based solid lubricant coatings, 814
  - propellant materials, nanomaterials for, 813–814
- Aerospace material properties of functional nanomaterials, 803–807
  - age and durability performance, 805–806
  - field emission and optical properties, 805
  - impact resistivity and energy absorption, 806
  - thermal and fire resistance properties, 805
  - tribological and anticorrosive coatings, 807
  - ultimate strength and stiffness, 804–805
  - weight reduction, 803–804
- Agaricus bisporus* L., 152
- Agglomeration, 404–405
- Aggregation of nanoparticles, 479–480
- Aging resistant halloysite SBR (styrene–butadiene rubber) materials, 917–923
  - aging performance of SBR/HNT nanocomposite, 919–921
  - blooming test of SBR/HNT nanocomposite as compared with direct antioxidant addition, 921–923
  - morphology and properties of the SBR/HNT composites, 917–918
- Agriculture and agroindustry, 248–252
  - impact of functionalized nanomaterials in, 248–250
  - impact of surface modified, labeled, and conjugated nanomaterials in, 250–252
- Agroindustrial byproducts, 639
- Air pollution, 427
  - remediation, 514–515
- Albumin NPs, 541–542
- Aldrin, 364
- Alginate (ALG), 238–239, 541, 545
- Alginate albumin, 545–546
- Alginic acid (AA), 18–22
- Alizarin red S (ARS), 359–360, 480–483

- Alkali activation, 673  
 Alkali etching, 427–428  
 Alkaline fuel cells, 288–290  
 Alkoxysilanes, 651  
 Allicin-loaded locust bean gum nanoparticles, 144  
*Allium cepa*, 249–252  
*Allium fistulosum*, 250–252  
 Allotropes of carbon, 952–953  
*Aloe vera*, 565*t*, 567*t*  
 $\alpha$ -lactalbumin ( $\alpha$ -LA), 136–137  
 $\alpha$ -lipoic acid, 549–550  
 $\alpha$ -melanocyte stimulating hormone ( $\alpha$ -MSH), 546  
 D- $\alpha$ -tocopheryl polyethylene glycol 1000 succinate (TPGS), 192  
 Aluminium, 813–814  
 Alzheimer's disease (AD), 549  
*Amaranthus gangeticus*, 351–352  
 AMD-CNT-incorporated MMMs, 17–18  
 Amidation, 447  
 Amido-oxime-polyacrylonitrile (AOPAN–NFs), 587  
 Amines, 333  
 3-(2-(2-Aminoethylamino) ethylamino) propyltrimethoxysilane (NHNH2-PTMS), 212–213  
 Amino-functionalized silica, 213  
 3-Aminophenol, 355  
 3-Aminopropyltriethoxysilane (APTES), 31, 39–40, 213, 418–419, 427–428, 641, 644, 881–883  
 (3-Aminopropyl)trimethoxysilane, 210–212, 651  
 Ammonium persulfate (APS), 310–311  
 Amyotrophic lateral sclerosis (ALS), 549  
 Aniline, 330–331  
 Anionic pollutants, adsorption of, 311–315  
   arsenic, adsorption of, 313–314  
   Cr(VI), adsorption of, 314–315  
   fluoride, adsorption of, 312–313  
 Anions, 312  
 Anisotropic etching process, 622–624  
 Anthracene and dyes, 352  
 Anthracycline, 198–199  
 Antiaging creams, 723  
 Antiaging products, 781  
 Antibacterial drugs, 513–514, 810  
 Antibodies, 543  
 Antibody-conjugated Au nanorods, 467–468  
 Antibody-directed PLGA nanoparticles, 194–195  
 Anticorrosion halloysite elastomer composite coatings, 932–934  
   enhanced corrosion protection with benzotriazole-loaded halloysite, 933–934  
   halloysite elastomer nanocomposite coating, 932–933  
 Antifouling, 26–27, 32  
 Antimony, 287–288  
 Antioxidant activity (AA), 527–528  
 Antioxidants, 527–528  
 Antistatic core-sheath fibers (ACSF), 682  
 Antistatic segmented-pie fibers (ASPF), 682  
 Aptamer, 467–468  
 Aquatic ecosystem, 509–510  
*Arabidopsis*, 250–252  
*Arabidopsis thaliana*, 250–252, 409  
 Arc discharge, 798  
 Aromatic amines, 327–329, 333  
 Aromatic phenols, 333  
 Arrhenius-type behavior, 738–739  
 Arsenic, adsorption of, 313–314  
 Arsenic groundwater contamination, 12  
 Arsenite, 313  
 Ascorbic acid (AA), 276  
*Aspergillus niger*, 653–654  
 Astaxanthin, 549–550  
 Atomic force microscopy analysis of organic layered silicate-modified asphalts, 873–874  
*Aureobasidium pullulans*, 147  
 Australian Inventory of Chemical Substances (AICS), 970  
 Automotive applications of functional nanomaterials, 814–816  
   car bodies, 815  
   improved fuel injection system, 816  
   nanocoatings/paints, 815  
   nanolayer for windscreens, mirrors, and reflectors, 816  
   nanomaterials for car chassis, 815–816  
   scratch resistance, nanovarnishes for, 816  
   tires, 816  
 Automotive material properties of functional nanomaterials, 807–809  
   higher heat-distortion temperature, 808  
   improved scratch resistance and mar resistance, 808  
   modulus and dimensional stability, 807  
   toughness and rheological properties, 808–809

Avrami–Erofe'ev crystallization kinetic model, 737–739  
 Avrami–Erofe'ev exponent, 738  
 4-Azidoaniline hydrochloride, 447–449  
 Azo dyes, 327–329, 333  
 Azophloxine dye nanocomposite, 467–468

## B

*Bacillus* spores, 467–468  
*Bacillus subtilis*, 405, 407, 454, 652, 684  
 Bakelite. *See* Nanoclay polymer composite  
 Ball milling, 801  
 Batch adsorptive removal of the TOC from industrial effluent, 760–761  
 Battery design, role of functionalized nanomaterials in, 285–287  
 “Bee-like” structures, 873, 883–884  
 Benzene, 514  
 Benzidine, 327–329, 333  
 Benzoquinones, 353–354  
 Benzotriazole, 934  
 Benzotriazole-loaded halloysite, enhanced corrosion protection with, 933–934  
 Beta-(1–4)-2-acetarnido-2-deoxy-D-glucopynnosic structural units (GlcNAc), 168–169  
*N*-β-(aminoethyl)-γ-aminopropyltrimethoxy silane (AEAPTMS), 427–428  
 β-cyclodextrin, 510, 750–751  
 β-cyclodextrins grafted nanopyroxenes, preparation of, 752–754  
   interaction of epoxy hybrid with the aegirine surface, 752–753  
   interaction of β-CD with the aegirine surface, 754  
 Betamethasone sodium phosphate, 644  
 Bicomponent core-sheath-type fibers, 645–646  
 Bicomponent fibers, types of, 631f  
 Bifunctional electrocatalysts, 96–100  
   intermetallic nonnoble nanocatalysts, 98–100  
   noble metal nanocatalysts, 96  
   nonnoble metal nanocatalysts, 96–98  
 Bilayer, 156  
 Bimetallic oxides (BMOs), 355  
 Bimetallic Pd/Fe NPs, 515–516  
 Biocidal products regulation (BPR), 965–966  
 Biodegradable and biocompatible polymers, 245–246  
 Biological safety problems caused by nanomaterials, 819–820  
 Biomarkers and biomolecules, 466–467  
 Biomedical and agriculture industries, functionalized nanomaterials for, 231  
   functionalized carbon-based materials for biomedical and pharmaceutical applications, 236–241  
   functionalized magnetic nanoparticles for biomedical applications, 243–245  
   functionalized metal nanoparticles for biomedical applications, 241–242  
   functionalized polymer-based nanomaterials for biomedical and pharmaceutical applications, 245–248  
   impact of functionalized nanomaterials in agriculture, 248–250  
   impact of surface modified, labeled, and conjugated nanomaterials in agriculture, 250–252  
   strategies for functionalization of nanomaterials, 232–236  
 Biomedical-related applications of functionalized nanomaterials, 205  
   biopharmaceutical sector, functionalized nanoparticles in, 206–208  
   functionalized nanoparticles as drug delivery systems, 220–221, 222f  
   future trends, 221–223  
   immobilization of functionalized nanomaterials in membranes, 217–220  
   types and synthesis procedures of functionalized nanomaterials, 208–217  
     carbon nanomaterials, 215–217  
     metal-based nanoparticles (metal-NPs), 208–211  
     silica nanoparticles, 211–214  
 Bionanocomposites, 173–174  
 Biopharmaceutical sector, functionalized nanoparticles in, 206–208  
 Biopolymer-based nanodelivery systems, fabrication methods of, 134–162  
   coacervation, 147–156  
   layer-by-layer (LbL) deposition  
     nanotube formation through, 159–162  
     spherical particle formation through, 156–159  
   nanoprecipitation/desolvation  
     of carbohydrates, 142–147  
     of proteins, 134–142  
 Biopolymer-based nanomaterials, 178  
   applications of, 173–177



Biopolymer-based nanomaterials (*Continued*)  
 cellulose, 174  
 chitosan and zein, 176–177  
 starch, 175  
 for food, nutrition, and healthcare sectors,  
   167  
   cellulose, 174  
   chitosan and zein, 176–177  
   future perspectives, 178  
   preparation of biopolymer-based  
     nanomaterials, 173  
   properties and functions of biopolymers,  
     170–172  
   properties and functions of  
     nanomaterials, 172  
   safety and toxicity of biopolymer-based  
     nanomaterials, 173  
   starch, 175  
   preparation of, 173  
   safety and toxicity of, 173  
 Biopolymer NPs, 554–555  
 Biopolymers, 583–584  
   properties and functions of, 170–172  
 (Bio)sensors, 651  
 Biotechnological method (BTM), 121–124  
 Biotin–streptavidin chemistry, 453–454  
 Bisphenol A (BPA), 333  
   degradation of, by FNMs, 366–371  
 Blood–brain barrier (BBB), 185, 188  
 Board of Appeal, 957–958  
 Bovine Corneal Opacity and Permeability  
   (BCOP), 728  
 Bovine serum albumin (BSA), 17–18,  
   134–135, 151  
 Bragg equation, 867–868  
*Brassica napus*, 250–252  
*Brassica oleracea*, 249  
*Brassica oleracea* var. capitata, 250–252  
 Br-functionalized CNTs, 332  
 Brinkman's model, 840–842, 855  
 Bronsted acid, 748  
 Brust–Schiffrin method, 655  
 1,2,3,4-Butane tetracarboxylic acid (BTCA),  
   680–682  
 Bydureon, 185–186

## C

Caelyx, 547*t*  
*Caenorhabditis elegans*, 409  
 Caffeine, 549–550  
 Calcium peroxide NPs, 515–516  
 Calcium phosphate NPs (CPNs), 515–516

Calender coating, 616–618  
*Camellia sinensis*, 567*t*  
 Camptothecin (CPT), 240–241  
 CaNanoLab, 221  
 Cancer, 552  
 Cancer cells, 245  
*Candida albicans*, 653–654  
 Cannabidiol (CBD), 546  
 Cannabinoids, 546  
 Capping approaches, 454–457  
 Carbocatalysis, 118–119  
 Carbocatalyst, 118–119  
 Car bodies, 815  
 Carbohydrates, nanoprecipitation/desolvation  
   of, 142–147  
 Carbon, allotropes of, 952–953  
 Carbonaceous nanomaterials, 271  
 Carbon-based functionalized materials, 334  
 Carbon-based materials, 236–238  
   for biomedical and pharmaceutical  
     applications, 236–241  
 Carbon-based nanocomposites, 480–486,  
   496–497  
 Carbon-based nanomaterials, 334–346, 444,  
   612, 683  
   applications, on textiles, 680–684  
   mixed-matrix membranes incorporated  
     with, 16–26, 19*t*  
     carbon nanotubes, 17–24  
     graphene oxide, 24–26  
 Carbon-based NPs, 466  
 Carbon-based polymeric composites, 670  
 Carbon-based systems, 687  
 Carbon black, 683, 953  
 Carbon black particles/polybutylene  
   terephthalate (CB/PBT), 682  
 Carbon dots (CDs), 236, 435–436, 444–445,  
   461–462  
 Carbon-metal oxide/ferrite nanohybrids, 677  
 Carbon nanocomposites for EM shielding, 813  
 Carbon nanofiber-incorporated three-phase  
   carbon/epoxy composites, 812–813  
 Carbon nanofibers (CNFs), 288, 683, 802  
 Carbon nanohorns (CNH), 207  
 Carbon nanomaterials, 9–10, 207, 215–217,  
   670–671, 680, 690  
 Carbon nanoparticles (CNPs), 424  
 Carbon nanostructures, 852  
 Carbon nanotube composite membranes, 798  
 Carbon nanotubes (CNT), 17–24, 207,  
   236–240, 248–249, 270, 279, 280*f*,  
   438–439, 444, 483, 484*t*, 496, 560,

- 670–672, 683, 685, 687, 796–798, 805, 809*t*, 813
- arc discharge, 798
- chemical vapor deposition, 798
- CNT-protein bioconjugates, 216–217
- laser ablation, 797–798
- Carbon quantum dots (CQDs), 16–17
- Carboxyl functionalized NPs, 512–513
- Carboxylic-functionalized GO, 314
- Carboxymethyl cellulose polyelectrolyte (CMC), 689
- Car chassis, nanomaterials for, 815–816
- Cardiovascular diseases, 550–551
- Carnitine, 550–551
- Carotenoids, 552
- Casein nanoparticles, 137–138
- Catalyst dose, effect of
  - on the photodegradation of Rhodamine-B dye, 74–75
- Catalysts, 288–290
- Catalytic degradation of organic pollutants, 496
- Catalytic oxidation, 495–496
- Catechol-terminated thiol, 460–461
- Cationic pollutants, adsorption of, 315–318
- Cbfa-1* gene, 197–198
- CD44, 543
- Cd doped ZnONPs, 514–515
- CdTe QDs, 464
- Cell target ligands coupled on the surface of PLGA nanoparticles, 193–194
- Cellular organisms, 405–408
- Cellulose, 144–146, 168–171, 174
- Cellulose acetate (CA)-dope solution, 30
- Cellulose-based nanomaterials, 173
- Cellulose materials, 629
- Cellulose nanocrystals (CNCs), 173–174
- Center for Environmental Law (CIEL), 960
- CeO<sub>2</sub>/CdO binary metal oxide nanostructure, 56–57
- CeO<sub>2</sub>/CdO heterogeneous catalyst
  - degradation of Rhodamine-B using, 69–71
  - photocatalytic degradation of Rhodamine-B dye using, 71–72
  - visible light–induced decomposition of Rhodamine-B using, 72
- CeO<sub>2</sub>/CdO nanostructures, structural investigation of, 57–58
- Cerium, 747
- Cerium oxide NPs, 510–511
- Cetyltrimethyl ammonium bromide (CTAB), 211–212, 276, 866–867
- Chantecaille*, 723
- Chattonella marina*, 407
- Chemical agents, 912–917
  - halloysite structure, 912–914, 913*f*
  - lumen loading, 914–915
  - sustain release of, 915–917
- Chemical composition, classification of
  - nanomaterials according to, 271–272
- Chemically modified graphenes (CMGs), 116–117
- Chemical methods, 274–276
- Chemical reduction, 654–655
- Chemical reduction method (CRM), 121–124
- Chemical sensor applications, 435
  - engineering aspects for functionalization of NMs, 446–457
    - capping approaches, 454–457
    - covalent conjugation, 446–450
    - self-assembly, 450–454
  - future perspectives, 468–469
  - general characteristics of NMs for, 437–446
    - morphology, 438–440
    - optical property, 440–442
    - toxicity and biocompatibility, 442–446
  - sensing applications, 457–468
    - biomarkers and biomolecules, 466–467
    - metal ions, 459–462
    - microorganisms, 467–468
  - pH, 458–459
  - simple molecules and organic pollutants, 462–466
- Chemical vapor deposition (CVD), 649, 798
- Chemoprevention, 552
- Chitin, 168–169
- Chitosan, 142–144, 151–152, 156–158, 168–169, 171, 173, 176–177, 192–193, 195, 238–239, 541, 544–546
- Chitosan coacervates, 149–151
- Chitosan-folate conjugated MWCNT, 238–239
- Chitosan functionalized NPs, 513–514
- Chitosan-to-WPI mass ratio, 151–152
- Chlamydomonas reinhardtii*, 407
- Chloroanilines, 327–329
- Chlorophenol- 2,4-dichlorophenol (2,4-DCP), 515–516
- 3-Chloropropyltriethoxysilane (CI-PTES), 212–214
- 3-Chloropropyltrimethoxysilane, 418–419
- Chromium, 311–312, 314–315

- Chrysene, 371  
 Chu's model, 856  
 Cinnamaldehyde, 153–154  
 Citrate-coated nAg, 409  
*Citrullus lanatus*, 250–252  
*Citrus reticulata*, 250–252  
 Clay-based materials, 426  
 Clay supported TiO<sub>2</sub> photocatalyst, 514–515  
 Clinopyroxenes, 741  
 Clotrimazole, 564*t*  
 CNMs, 334–347  
 Co<sub>3</sub>O<sub>4</sub> NPs, 94–95  
 Coacervates, 153–154  
 Coacervation, 147–156  
 Coating process, 616  
 Cobalt-doped nickel sulfide, 288  
 Cocondensation, 639–641  
 Coenzyme Q10, 549–550  
 Colloidal dispersions, 659  
 Colloidal lithography, 624  
 Color Index, 330–331  
 Commonwealth Scientific and Industrial Research Organization (CSIRO), 723–724  
 Composite functional NFs, 584–585  
 Computational dynamics fluid (CFD) technique, 832  
 Computer-aided design (CAD) files, 625  
 COMSOL 5.0, 855  
 Conductive textiles, 682–683  
 Contact printing, 619  
 Continuous adsorptive removal of TOC at in a fixed-bed column, 761  
 Continuous carbon fibers (CCF), 683  
 Conventional antibiotics, 513–514  
 Conventional ball milling, 673  
 Conventional composites, 799  
 Conventional dyeing, 614–615  
 Conventional-polymeric membranes, 15  
 Copolymer and colloidal lithography, 624  
 Copolymer lithography, 624  
 Copolymers of lactic and glycolic acid (PLGA), 540–542, 546  
 Copper ion-exchanged nanotubes (Cu-TNT), 30  
 Copper nanoparticles (CuNPs), 836–838  
 Copper nanowires (CuNWs), 834  
 Copper oxide NPs, 407  
 Copper strips, 934  
 Coprecipitation method, 649, 663–664, 679  
 CoQ10, 550–551  
 Core-binding factor alpha-1 (Cbfa-1) siRNA, 197–198  
 Core-shell lycopene/oligomerized epigallocatechin-3-*O*-gallate/chitosan NPs, 546  
 Core-shell nanomaterials, 271  
 Core-templating method, 642  
 Corey–Pauling–Koltun (CPK), 746*f*, 749*f*, 759*f*  
*Coriandrum sativum*, 565*t*  
 Cornell dots (C dots), 646–647  
 Corona, 949  
 Cosmeceuticals, nanomaterials in, 775–780  
   dendrimers, 778  
   fullerenes, 779  
   future perspectives, 788  
   liposomes, 777  
   nanocosmeceuticals  
     regulations of, 784–788  
     safety of, 782–784  
     toxicity of, 782  
   nanocosmeceuticals, classification of, 781–782  
     antiaging products, 781  
     hair care, 781  
     lip care, 781  
     nail care, 782  
     skin care, 781  
   nanoemulsions, 777  
   nanoparticles, penetration of, 782  
   nanopigments, 780  
   nanosponges and microsponges, 779  
   nanostructured lipid carriers (NLCs), 778  
   niosomes, 779–780  
   solid-lipid nanoparticles (SLNs), 777–778  
 Cosmetic, Toiletry and Fragrance Association (CTFA), 727–728  
 Cosmetics industry, functional nanomaterials for, 715  
   classification of nanocosmetics on the basis of formulation technologies, 718–722  
   cubosomes, 722  
   dendrimers, 721  
   nanocapsules, 721  
   nanocrystals, 720–721  
   nanoemulsions, 719  
   nanopigments, 721  
   nanosponges and microsponges, 720  
   nanostructured lipid carriers (NLCs), 720  
   solid lipid nanoparticles (SLNs), 720  
   vesicular delivery systems, 719

- evaluation of nanomaterial toxicology, 726–727
  - formulation and manufacturing aspects, 723–724
  - guidance documents on nanomaterials in cosmetics, 725
  - impurity profiling, 726
  - nanocosmetics, 718
  - nanocosmetics, 722–723
    - antiaging creams, 723
    - hair cosmetics, 722–723
    - lipsticks, 723
    - sunscreen creams, 723
    - toothpastes, 722
  - nanotechnology, performance enhancement using, 718
  - nanotechnology for UV protection, 723
  - safety assurance, 725–726
  - toxicity testing, 727–728
  - Cosmetics regulation, 966
  - Coulomb interactions, 72
  - Coupling agents, 749–750
  - Covalent bonds with core substance, 946
  - Covalent conjugation, 446–450
  - Covalent functionalization, 216, 232–234, 334–347
  - Cr(VI), adsorption of, 314–315
  - Cremophor EL, 547–548
  - Cross-linked cellulose (CLC), 170–171
  - Crystal growth, 736–737
  - Crystal violet (CV), 510
  - Cubosomes, 722
  - Cucumis sativus*, 249–252
  - Cucurbita mixta* cv. *White cushaw*, 250–252
  - Curcuma longa*, 567*t*
  - Curcumin (CCM), 136, 140–141, 156–158, 213, 545, 549–550, 552
  - Curie point, 273
  - Cyclosporin A, 564*t*
  - Cysteamine (Cyst), 209–210
  - L-Cysteine (L-Cys), 407, 462–463
  - Cysteine-arginine-glycine-aspartic acid-lysine (CRGDK) peptide, 247–248
- D**
- Damage sensing, 803
  - Daphnia magna*, 400, 409
  - Daucus carota*, 249
  - Debye–Scherer’s formula, 58
  - Decyltrimethylammonium bromide (DeTAB), 419–420
  - Degradation pathways, 355
  - Degrees of esterification (DE), 155
  - Dendrimers, 721, 778
  - Dengue envelope (DENV3E) proteins, 239–240
  - Density functional theory (DFT) calculations, 282–283
  - Dermatological nanoproducts, 559, 563*t*
  - Desolvation. *See* Nanoprecipitation technique
  - Dexamethasone, 559
  - Dextran, 541
  - Dextran sulfate, 156–158
  - Diabetes, 552–553
  - Diatomite, 761–764
  - Dichlorodiphenyltrichloroethane (DDT), 464
  - 1,2-Didecanoylphosphatidylcholine (DDPC), 192
  - Diethylenetriaminepentacetic acid (DTPA), 515–516
  - Differential scanning calorimetry (DSC), 836
  - Diffuse reflectance Fourier transform infrared spectroscopy (DRFT-IRS), 113–114
  - Diffuse reflectance spectroscopy (DRS) studies, 61–64, 63*f*
  - Dihydrolipoic acid (DHLA), 407
  - 3,3’-Diindolylmethane (DIM), 240–241
  - Dimension, classification of nanomaterials based on, 270–271
    - one-dimensional nanostructures, 271
    - three-dimensional nanostructures, 270
    - two-dimensional nanostructures, 270–271
    - zero-dimensional nanostructures, 271
  - 3-(Dimethyl(3-(trimethoxysilyl)propyl) ammonio) propane-1-sulfonate, 641
  - N, N*-Dimethylformamide, 632–633, 752
  - Dimethyloctadecyl(3-(trimethoxysilyl)propyl) ammonium chloride, 641, 646
  - 3-(4,5-Dimethylthiazol-2-yl)–2,5-diphenyl-tetrazolium bromide (MTT) assay, 442–443
  - 1,2-Di-*O*-octadecenyl-3-trimethylammonium propane (DOTMA), 195, 199
  - 1,2-Dipalmitoylphosphatidylcholine (DPPC), 192
  - Dip coating, 616
  - Direct coating, 616
  - Direct functionalization, 334–348
    - covalent functionalization, 334–347
    - heteroatoms doping, functionalization by, 347
    - immobilization, functionalization by, 348
    - inorganic functionalization, 347
    - noncovalent functionalization, 347

Direct methanol fuel cells, 288–290  
 Direct/one-pot synthesis. *See* Cocondensation  
 Dissolution, 402–404  
   influence of engineered coatings on, 402–403  
   influence of macromolecules coatings on, 403–404  
 Dithiocarbamate, 510–511  
 Dithiothreitol, 140–141  
 Dithranol, 564*t*  
 Docetaxel (Dtxl)-encapsulated PLGA nanoparticles, 191  
 Docosahexaenoic acid (DHA), 550–551  
 Dodecyltrimethylammonium bromide (DTAB), 211–212  
 Dopamine, 466  
 Doping of particles, 946  
 Double distribution function (DDF) model, 839  
 Double-wall carbon nanotubes (DWCNTs), 248–249  
 Doxil, 547, 547*t*  
 Doxorubicin (Dox), 238–239, 247–248  
 Doxorubicin, 137–138  
 Doxorubicin hydrochloride (DOX), 213  
 Draw-textured yarns (DTYs), 682  
*Drosophila melanogaster*, 409  
 Drug delivery systems (DDS), 206–207, 221, 537  
   functionalized nanoparticles as, 220–221, 222*t*  
 Drug delivery technology, 544  
 Drug/deoxy nucleic acid (DNA), 176  
 Drug-to-polymer ratios, 147  
 Dry etching, 622–624  
 Dry-jet wet spinning, 634  
 Dry spinning process, 631–633  
 Ductility retention ratio (DRR), 876  
 Dyes, 509–510

## E

EDTA-functionalized magnetic GO, 311, 318  
 EGCG (epigallocatechin-3-gallate), 550–551  
 EIA (environmental impact assessment), 121–124  
 Eicosapentaenoic acid (EPA), 550–551  
 Elastomeric nanocomposites, 809*t*  
 Electrical industry, application of functionalized nanomaterials in, 281–282  
 Electrical transformers, 281

Electrocatalysts, functionalized nanomaterials as, 86  
 Electrochemical double layer supercapacitors (EDLS), 287  
 Electrodeposited coatings, 814  
 Electromagnetic interference (EMI), 281, 802  
 Electromagnetic shielding, 661*f*, 683  
 Electron and ion beam lithography, 624  
 Electron beam lithography, 624  
 Electronic property of nanomaterials, 273  
 Electronics and electrical and energy industries, functionalized nanomaterials for, 267  
   chemical composition, classification of nanomaterials according to, 271–272  
   dimension, classification of nanomaterials based on, 270–271  
     one-dimensional nanostructures, 271  
     three-dimensional nanostructures, 270  
     two-dimensional nanostructures, 270–271  
     zero-dimensional nanostructures, 271  
   energy applications, 282–290  
     battery design, role of functionalized nanomaterials in, 285–287  
     fuel cells, role of functionalized nanomaterials in, 288–290  
     hydrogen evolution reaction, role of functionalized nanomaterials in, 284–285  
     oxygen evolution reaction, role of functionalized nanomaterials in, 282–284  
     supercapacitors, role of functionalized nanomaterials in, 287–288  
   functionalization of nanomaterials, 274–278  
     chemical methods, 274–276  
     grafting of synthetic polymers, 277–278  
     ligand exchange process, 276–277  
     miscellaneous methods, 278  
   industrial applications, 278–290  
     electrical industry, application of functionalized nanomaterials in, 281–282  
     electronics industry, applications of functionalized nanomaterials in, 278–281  
   properties of nanomaterials, 272–273  
     electronic property, 273  
     magnetic property, 273  
     mechanical property, 273

- optical property, 273
- structural property, 272–273
- thermal property, 272
- Electronics industry, applications of
  - functionalized nanomaterials in, 278–281
- Electrospinning, 581, 582*f*, 634–635, 635*f*
  - of polymer blends, 584–585
- Electrospun NFs, polymers used in, 583–584
- Electrospun porous NFs, 584
- Electrostatic interaction, 405–407, 409
- Emeraldine salt (ES), 94
- Emulsion–diffusion technique, 187
- Endothelial cells (ECs), 587
- Endrin, 364
- Energy and environmental sectors, 5–6
- Energy and environmental sustainability, scientific vision of, 11
- Energy storage, 428–429
- Engineered coatings, influence of
  - on dissolution, 402–403
- Engineered nanomaterial coatings, 405–409
  - cellular organisms, 405–408
  - invertebrates and vertebrates, 409
- Engineered nanomaterials (ENMs), 4–5, 7, 399–400, 404, 409–410, 983, 995–999
  - molecular approaches to toxicity of, 409–410
- Engineered nanoparticles (ENPs), 983–984, 996
- Enhanced permeation and retention (EPR)
  - effect, 188
- ENMs, 332
- Enthalpy–porosity method, 839–842, 853–855
- Environmental degradation, 118
- Environmental industry, applications of
  - functionalized halloysite nanotubes in, 421–429
  - energy storage, 428–429
  - heavy metal remediation, 426–427
  - pesticide sensing and remediation, 422–425
  - remediation of toxic dyes, 425–426
  - separation of harmful gases, 427–428
- Environmental Protection Agency (EPA), 969, 988
- Environmental protection and industrial ecology, recent research in, 11
- Environmental remediation, 118, 505
  - application of nanographene in, 118*f*
  - functionalized nanomaterial, implementation of
    - air pollution remediation, 514–515
    - soil pollution remediation, 515–516
    - water pollution remediation, 509–514
- Environmental sustainability, scientific vision of, 11
- Environment Industry, defined, 7
- Environment Protection Agency (EPA), 784–788
- Epigallocatechin-3-*O*-gallate/chitosan NPs, 546
- Epirubicin (Epi), 198–199
- Epirubicin (Epi)-loaded PLGA nanoparticles, 193
- Epoxysilane, 644–645
- Ergosterol, 152
- Eruca sativa*, 250–252
- Escherichia coli*, 25–26, 142–144, 176, 206, 405–407, 410, 444–445, 467–468, 644, 646, 652–654, 659–660, 684
- Ethanol, 141–142
- Ethosomes, 561
- 1-Ethyl-3-(3-dimethylaminopropyl) carbodiimide (EDC), 216–217, 447
- 1-Ethyl-3-(3-dimethylaminopropyl) carbodiimide hydrochloride, 194
- 1-Ethyl-3-methylimidazolium iodide (EMII), 690–691
- 2-Ethyl-4-methylimidazole, 213–214
- Ethyl-3-(*N*-nbutyl-*N*-acetyl)aminopropionate, 644–645
- Ethylenediamine (EDA), 30, 648
- Ethylenediaminetetraacetic acid (EDTA), 41–42
- Ethylene-vinyl acetate copolymer (EVA)
  - polymer matrix, 916–917
- Eupenicillium shearii*, 424
- European Agency for Safety and Health at Work (EU–OSHA), 999–1000
- European Centre for the Validation of Alternative Methods (ECVAM), 728
- European Chemical Agency (ECHA), 957, 988
- European Chemical Industry Council (CEFIC), 960
- European Food Safety Authority (EFSA), 968
- European Trade Union Confederation (ETUC), 999
- European Trade Union Institute (ETUI), 999
- Eutectic PCMs, 831
- Exfoliated nanocomposites, 799

Exhaustion, 615

Expression vectors, 195–196

Extracellular matrix (ECM) components, 197–198

## F

Fabrication methods of biopolymer-based nanodelivery systems, 134–162

coacervation, 147–156

layer-by-layer (LbL) deposition, 156–162  
nanotube formation through, 159–162  
spherical particle formation through, 156–159

nanoprecipitation/desolvation, 134–147  
of carbohydrates, 142–147  
of proteins, 134–142

Fabrication of nanomaterials, 505–506

Ferrite NPs, 663, 663*f*

Fiber-reinforced composites (FRCs), 795

Fiber-reinforced polymers (FRPs), 806

Fiber-spinning technologies, 629–635  
electrospinning, 634–635, 635*f*  
melt spinning, 631–632  
solution spinning, 632–634

Field-effect-transistors (FETs), 279–280

Field emission and optical properties, 805

Field emission scanning electron microscopy (FESEM) studies, 59–61

Fine particles, enhanced settling of, 757–759

Fin's aspect ratio, 856

Flame lamination process, 618, 619*f*

Flame-retardant halloysite rubber composites, 923–931

antiblooming property of halloysite-encapsulated flame retardants in SBR composite, 931

flame-retardant performance of SBR/HNT composites, 927–930

mechanical property of SBR/HNTs, 923–926

Flash nanoprecipitation technique (FNP), 139–140

Flat-to-flat method, 620

Flavonoids, 550–551

Fluconazole, 564*r*

Fluorescein-isothiocyanate-dextran, 141–142

Fluoride, 311–312

adsorption of, 312–313

Fluorine, 674

Fluorine-doped tin oxide (FTO), 100

Flux recovery rate (FRR), 22–23, 25, 27

FNMs

degradation of BPA by, 371

degradation of PAHs by, 371

degradation of phenols by, 366–371  
green synthesis in, 349

importance of green synthesis in, 351–356

FNPs, working mechanism of, 350–351

Foam coating, 616

Foam-interconnected graphite strips, 852

Folate (FA), 543

Food, 5

Food and Drug Administration (FDA), 173

Food and food contact materials, 967–968

Food supplements, nanoproducts in,

548–555

cancer, 552

cardiovascular diseases, 550–551

diabetes, 552–553

and its clinical usage, 549

nanotechnology and food supplements, 553–555, 556*r*

neurodegenerative diseases, 549–550

Formononectin (FMN), 238–239

Förster resonance energy transfer (FRET), 460–461

Fossil fuels, 83

Fourier transform infrared spectroscopy, 58–59, 902–906

of organic layered silicate-modified asphalts, 872–873

of organic layered silicates, 871–872

of surface modification inorganic nanoparticles, 881–883

Fourth Industrial Revolution, 983

Freundlich model, 318, 425

Fuel cells, 6

role of functionalized nanomaterials in, 288–290

Fuel injection system, 816

Fullerene C<sub>60</sub>, 560

Fullerenes, 270, 560, 779, 953

Fulvic acid (FA), 403

Functional carbon-based nanomaterials

(fCBNMs), 248–249, 670–691

applications of carbon-based nanomaterials on textiles, 680–684

emerging applications, 684–691

functionalization, 670–673

heteroatom doping, 673–675

hybrid carbon-metal/metal oxide nanomaterials, 675–680

Functional halloysite rubber nanocomposites, 917–938

- aging resistant halloysite SBR (styrene–butadiene rubber) materials, 917–923
- aging performance of SBR/HNT nanocomposite, 919–921
- blooming test of SBR/HNT nanocomposite as compared with direct antioxidant addition, 921–923
- morphology and properties of the SBR/HNT composites, 917–918
- anticorrosion halloysite elastomer composite coatings, 932–934
- enhanced corrosion protection with benzotriazole-loaded halloysite, 933–934
- halloysite elastomer nanocomposite coating, 932–933
- flame-retardant halloysite rubber composites, 923–931
- antiblooming property of halloysite-encapsulated flame retardants in SBR composite, 931
- flame-retardant performance of SBR/HNT composites, 927–930
- mechanical property of SBR/HNTs, 923–926
- marine antifouling halloysite–rubber composites, 934–938
- antifouling test of EVA/HNT nanocomposites, 937–938
- morphology and properties of the EVA/HNT nanocomposites, 934–937
- Functionalization of nanomaterials, 274–278
  - chemical methods, 274–276
  - grafting of synthetic polymers, 277–278
  - ligand exchange process, 276–277
  - miscellaneous methods, 278
- Functionalization of nanomaterials for
  - industrial applications, 1
  - current research on nanomaterials, 6–7
  - environmental protection and industrial ecology, recent research in, 11
  - functionalized nanomaterials, 4–5
  - future perspectives, 12
  - future research trends in nanotechnology and nanomaterials, 12
  - groundwater remediation and nanotechnology, 12
  - integrated water resource management and human factor engineering, 11–12
  - nanotrends in industrial development, 4
  - potential of nanomaterials, 4
  - recent scientific research, 8–11
  - scientific vision of energy and environmental sustainability, 11
  - use of functionalized nanomaterials in industry, 5–6
  - energy and environmental sectors, 5–6
  - engineered nanomaterials, applications of, 6
  - food, 5
- Functionalized carbon-based materials for biomedical and pharmaceutical applications, 236–241
- Functionalized CNTs (f-CNTs), 22–23
- Functionalized graphene-based catalysts, 115*f*
- Functionalized halloysite nanotubes, 417, 424–425
  - applications in environmental industry, 421–429
  - energy storage, 428–429
  - harmful gases, separation of, 427–428
  - heavy metal remediation, 426–427
  - pesticide sensing and remediation, 422–425
  - toxic dyes, remediation of, 425–426
- functionalization techniques for halloysite nanotubes, 418–421
- future prospects, 429
- Functionalized magnetic nanoparticles for biomedical applications, 243–245
- Functionalized metal-based nanoelectrocatalysts for water splitting, 83
- bifunctional electrocatalysts, 96–100
- intermetallic nonnoble nanocatalysts, 98–100
- noble metal nanocatalysts, 96
- nonnoble metal nanocatalysts, 96–98
- electrocatalysts, functionalized nanomaterials as, 86
- functionalized nanoelectrocatalysts for HER, 88–92
  - nonnoble metal carbides and oxides, 90
  - nonnoble metal dichalcogenides and phosphides, 90–92
  - other transition metal nanostructures, 92
  - Pt-based HER catalysts, 88–89
- hydrogen evolution reaction (HER) process, 85*f*, 86–87
- oxygen evolution reaction (OER) catalysts, 92–96
  - noble-metal nanocatalysts, 92–93
  - nonnoble metal nanocatalysts, 94–96



- Functionalized metal-based
    - nanoelectrocatalysts for water splitting (*Continued*)
      - oxygen evolution reaction (OER) process, 88
      - water electrolysis, fundamentals of, 84–86
  - Functionalized metal nanoparticles for biomedical applications, 241–242
  - Functionalized multiwall CNTs, 41, 94
  - Functionalized nanoelectrocatalysts for HER, 88–92
    - nonnoble metal carbides and oxides, 90
    - nonnoble metal dichalcogenides and phosphides, 90–92
    - Pt-based HER catalysts, 88–89
    - transition metal nanostructures, 92
  - Functionalized nanographene, 114–119
    - catalytic applications, 117–119
    - catalytic properties, 116–117
  - Functionalized nanomaterial-modified asphalt, future trends in research of, 906
  - Functionalized nanomaterials, 4–5, 331–332, 467–468, 510, 512–513
  - Functionalized polymer-based nanomaterials for biomedical and pharmaceutical applications, 245–248
  - Functionalized with MNPs (fMNPs), 248–249
  - Functionalizing carboxylic CNTs, 18–22
  - Functionally active nanomaterials, 10–11
  - Functional nanofibers, 579, 584–590
    - composite functional NFs, 584–585
    - electrospinning, 581, 582*f*
    - electrospun NFs, polymers used in, 583–584
    - fabrication of structural functional, 584
    - fabrication steps, 582–583
    - future trends, 590–597
    - inorganic NFs production with different styles and various functions, 585
    - molecular imprinting, 589–590
    - polymer NFs, surface modification and functionalization of, 586–589
      - using biotechnology, 589
      - using chemical technologies, 587
      - using nanotechnologies, 587–589
      - using physical technologies, 587
    - potential applications, 590
    - and their potential applications, 591*t*
  - Functional rubber–clay nanotube composites with sustained release of protective agents, 909
    - chemical agents, 912–917
      - halloysite structure, 912–914, 913*f*
      - lumen loading, 914–915
      - sustain release of, 915–917
  - Functional silica nanoparticles, 636–647
    - functionalization, 639–643
    - nanosilica-coated textiles, 643–647
    - production processes, 636–639
  - Functional textiles, 611
  - Functional TiO<sub>2</sub> nanoparticles, 647–654
    - functionalization/doping, 651
    - nano-TiO<sub>2</sub>-coated textiles: applications, 651–654
    - production processes, 647–650
  - Fused deposition modeling, 625–629
- ## G
- Garlic extracts, 550–551
  - Gelatin, 153–154, 541–542, 545–546
  - Gelatin nanoparticles, 141–142, 545
  - Gelatin-to-high methyl pectin particles, 153–154
  - Gelatin-to-low methoxyl pectin particles, 153–154
  - Gelatin-to-pectin ratios, 153–154
  - Gel spinning, 634
  - Generally recognized as safe (GRAS) ingredients, 719
  - Gentamicin, 207
  - Geobacter metallireducens*, 515–516
  - Geobacter sulfurreducens*, 351–352
  - GI tract, 553–554
  - Gliadin, 140–141
  - Glucose, 428–429
  - Glucosinolates, 552
  - Glutamate dehydrogenase (GDH), 213
  - Glutaraldehyde, 450
  - 3-Glycidoxypropyltriethoxysilane (Gly-PTES), 212–213
  - 3-Glycidoxypropyltriethoxysilane-iminodiacetic acid (IDA), 213
  - (3-Glycidylloxypropyl) trimethoxysilane (GPTMS), 213, 749–750, 752
  - (3-Glycidylloxypropyl) trimethoxysilane organic-inorganic hybrid chemical structure, 750*f*
  - 3-Glycidylpropylmethoxysilane, 644–645
  - Gold, 721
  - Gold colloid nanoparticles, 210–211
  - Gold nanomaterials, 232–234, 954

- Gold nanoparticles (AuNPs), 208, 210–211, 232, 241–242, 438*f*, 440, 542, 655, 659, 780
- Gold-NPs-modified electrode, 209–210
- Golf shafts, nanomaterials in, 818
- Good solvent, 134
- Gossypium hirsutum*, 250–252
- Grafting, 234, 640–641
- Grafting nanoaegirine, 758–759
- Granular AC (GAC), 483
- Grapheme, 236–238
- Graphene, 111–113, 215, 236, 271, 301–302, 486, 496, 670–671, 683, 801–802, 813
- Graphene-based catalysts, 119
- Graphene-based nanocatalysts, 117–118
- Graphene-based nanomaterials, 117–120, 124
- health and safety concerns of, 121*f*
- for pollutant removal, 487*f*
- Graphene-based products market, 119–120
- Graphene fibers (GFs), 685
- Graphene/grapheme oxide, 240
- Graphene-multiwalled carbon nanotube (G-MWCNT) hybrid, 286
- Graphene nanoplatelets (GnP), 801, 853–855
- Graphene nanosheets (GNS), 117–118
- Graphene oxide (GO), 16–17, 24–26, 117–120, 207, 240–241, 486, 687–689
- and magnesium oxide (MgO) nanohybrid (GO–MgO), 308
- preparation functionalized with iron oxide nanoadsorbents, 303–306
- Graphene oxide functionalization with metal oxide nanomaterials, 297
- inorganic pollutants removal from water using metal oxide-functionalized GO–nanosubstrates, 311–320
- adsorbents, regeneration of, 319–320
- adsorption isotherms, kinetics, and thermodynamics, 318–319
- anionic pollutants, adsorption of, 311–315
- cationic pollutants, adsorption of, 315–318
- preparation of GO, 306–309
- functionalized with iron oxide nanoadsorbents, 303–306
- using modified Hummer's method, 302, 302*f*
- surface modified GO metal oxides composite nanoadsorbents, preparation of, 310–311
- Graphene oxide/TiO<sub>2</sub> nanocomposite-coated cotton fabrics, 652–653
- Graphene quantum dots (GQDs), 444, 446–447
- Graphene sheets (GFN), 690
- Graphite foams, 852
- Graphite powder, 302
- Graphitic carbon nitrite (GCN), 685
- Green catalyst, 114–116
- Green materials, 4
- Green revolution, 5
- Green synthesis, 355
- in FNMs, 349, 351–356
- Groundwater remediation and nanotechnology, 12
- Gymnasiums, nanomaterials in, 818
- ## H
- Hair care, 781
- Hair cosmetics, 722–723
- Hair follicles, 559
- Halloysite elastomer nanocomposite coating, 932–933
- Halloysite nanotubes (HNTs), 31, 46, 418–419, 421–424, 426–427, 429
- functionalization techniques for, 418–421
- structure of, 418*f*
- Halloysite structure, 912–914, 913*f*
- Halloysite tubes, 911–912
- Halogenation, 673
- Harmful gases, separation of, 427–428
- Health products, nanotechnology in, 539*f*
- Heat transfer enhancement, 831–832
- Heat transfer fluid (HTF), 830
- Heavy metal remediation, 426–427
- Heavy-metal removal, adsorptive mixed-matrix membranes for, 40–47
- Heck coupling reaction, 351–352
- HeLa cells, 440
- Hematite, 303
- Heteroatom doping, 673–675
- of CNTs, 677*f*
- of graphene, 676*f*
- Heteroatoms doping, functionalization by, 347
- Hexaferrites, 666
- structures, 667*f*
- Hexagonal nanoferrites, 666
- Hexamethylenetetramine (HMTA), 30
- Heyrovsky step, 86
- Highly branched dendrimers, 271
- High-resolution transmission electron microscopy (HRTEM) studies, 61, 62*f*
- Holospheres, 271

Honeycomb lattice, 112–113  
*Hordeum vulgare*, 250–252  
 Hot-melt extrusion coating, 618  
 HPMC gel, 779–780  
 Huang's group, 147–149  
 Human factor engineering, 11–12  
 Human mesenchymal stem cells (hMSCs), 198  
 Human serum albumin (HSA), 161–162  
 Humic acid (HA), 403  
 Hummers' method, 121–124  
   preparation of GO using, 302, 302*f*  
 Huntington's disease (HD), 549  
 Hyaluronic acid (HA), 543  
 Hybrid carbon-metal/metal oxide nanomaterials, 675–680  
 Hybrid NPs, 512–513  
 Hybrid silica nanoparticles (NPs), 612  
 Hydrated ferric oxide (HFO) NPs, 489–491  
   HFO-201, 489–493  
 Hydrated manganese dioxide (HMO), 493  
   HMO-001, 493  
 Hydrogel, 559  
 Hydrogen evolution reaction (HER) process, 83–84, 85*f*, 86–87, 96, 282  
   polarization curves, 283*f*  
   role of functionalized nanomaterials in, 284–285  
 Hydrogen trititanate nanotubes (pTNT), 30  
 Hydrolysis-susceptible NPs, 561  
 Hydrophilic coatings, 221  
 Hydrophilicity, 16, 23–24, 27–29, 33  
 Hydrophilic substances, 561  
 Hydrophobicity, 680  
 Hydrophobic nanoparticle, 146–147  
 Hydrothermal crystallization isotherms, 737  
 Hydrothermal method, 55–56, 638–639, 649, 655–656  
 Hydrothermal/solvothermal process, 638–639  
 Hydrothermal synthesis mechanism, 734–737  
   crystal growth, 736–737  
   induction period, 735  
   nucleation, 735–736  
 Hfrous zirconium oxide (HZO), 491–493  
   HZO-201, 491–493  
 2-Hydroxyethyl acrylate, 651–652  
 2-Hydroxy groups of cellulose, 168–169  
 Hydroxypropyl- $\beta$ -Cyclodextrin (HP- $\beta$ -CD), 238–239  
 Hyperglycemia, 553  
 Hyperthermia drugs, 242

## I

Imidazole, 213–214  
 Immobilization, functionalization by, 348  
 Immobilization of functionalized nanomaterials in membranes, 217–220  
 Implementation of functionalized nanomaterial  
   air pollution remediation, 514–515  
   soil pollution remediation, 515–516  
   water pollution remediation, 509–514  
 Impregnation method. *See* Dip coating  
 Incidental nanoparticles, 4  
 Indirect or postsynthetic functionalization (grafting), 348–349  
   polymer coating, 349  
 Indomethacin, 147  
 Induction period, 735  
 Industrial applications, 278–290  
   electrical industry, application of functionalized nanomaterials in, 281–282  
   electronics industry, applications of functionalized nanomaterials in, 278–281  
 Industrial ecology, recent research in, 11  
 Industrial wastewater treatment, 6–7  
 Infab Corporation, 669  
 Inorganic elements and oxides, 954–956  
 Inorganic functionalization, 347  
 Inorganic NPs, 538  
 Inorganic pollutants, 299–301  
 Inorganic pollutants removal from water using metal oxide-functionalized GO–nanosubstrates, 311–320  
   adsorption isotherms, kinetics, and thermodynamics, 318–319  
   anionic pollutants, adsorption of, 311–315  
   adsorption of arsenic, 313–314  
   adsorption of Cr(VI), 314–315  
   adsorption of fluoride, 312–313  
   cationic pollutants, adsorption of, 315–318  
   regeneration of adsorbents, 319–320  
 In situ intercalative polymerization method, 799  
 Insoluble nanomaterials, 718  
 Insulin, 544–545, 552–553  
 Integrated water resource management and human factor engineering, 11–12  
 Intentional adsorption of substance onto surface, 946–947

- Interagency Coordinating Committee on the Validation of Alternative Methods (ICCVAM), 728
- Intercalated nanocomposites, 799
- Interfacial deposition. *See* Nanoprecipitation technique
- Intermetallic nonnoble nanocatalysts, 98–100
- International Council of Harmonization (ICH), 538
- International Organization for Standardization (ISO), 998–999
- Invertebrates and vertebrates, 409
- Iodine, 690–691
- Ion beam lithography, 624
- Ionic liquids (ILs), 213–214
- Ionizable groups, 541–542
- Iresine herbstii*, 565*t*
- Iron oxide nanoadsorbents, preparation of GO functionalized with, 303–306
- Iron oxide NPs (IONP), 446, 543
- Iron–silicate-based nanomaterial nanoparticles, 734
- Iron–silicate-based nanomaterials synthesis by hydrothermal method, 734–764
- Avrami–Erofe'ev crystallization kinetic model, 737–739
- hydrothermal synthesis mechanism, 734–737
- crystal growth, 736–737
- induction period, 735
- nucleation, 735–736
- pyroxenes, 740–764
- hydrothermal synthesis of nanocrystalline aegirine, 744–745
- low-temperature hydrothermal synthesis of aegirine, 744
- modifications to the pyroxene aegirine, 745–764
- pyroxene aegirine, 743
- synthesis of, 742–743
- typical preparation procedure of aegirine, 743–744
- synthesis of iron–silicate materials, 739–740
- Iron–silicate materials, synthesis of, 739–740
- Irradiation time, effect of
- on the photodegradation of Rhodamine-B dye, 74
- (3-Isocyanatopropyl) trimethoxysilane, 651
- Isoflavones, 550–551
- Isolated Chicken Eye (ICE), 728
- Isothermal titration calorimetry (ITC), 149, 151
- Isotropic etching process, 622–624
- ## K
- Kafirin nanoparticles, 135–136, 156–158
- Keggin-type phosphomolybdates, 645–646
- Klebsiella pneumoniae*, 684
- Korre's Red Vine Hair sunscreen, 719
- Kosmochlor, 742–743
- Krebs Cycle, 186
- ## L
- Labile nanomaterials, 718
- Lactate dehydrogenase (LDH), 213
- Lactic acid, 187
- Lactuca sativa*, 249
- Lamination, 616–618
- Langmuir adsorption isotherm model, 425
- Langmuir adsorption mechanism, 353–354
- Langmuir isotherm model, 312
- Langmuir model, 314, 318
- Lanthanum carbonate NPs, 467
- Laplace's equation, 914
- Laser ablation, 797–798
- Latent heat thermal energy storage (LHTES) systems, 830, 859–860
- Lavandula stoechas* ssp, 567*t*
- Layer-by-layer (LbL) assembly, 209, 644, 680
- Layer-by-layer (LbL) deposition, 156–162, 588–589
- nanotube formation through, 159–162
- spherical particle formation through, 156–159
- Layer by layer (LbL) technique, 214
- Layered double hydroxides (LDH), 86
- Layered silicate/organic layered silicate-modified asphalts, preparation of, 867
- Layers, degradation of, 947–948
- Lectins, 193–194
- Legal and regulatory issues, 983
- functional nanomaterials, 984–985
- applications, human health, and environmental concerns, 985–986
- legal and regulatory aspects, 986–987
- legal and regulatory initiatives, highlights of, 987–989
- Lemna minor*, 250–252
- Lidocaine hydrochloride, 564*t*
- Lifecycle assessment (LCA), 121–124
- Ligand exchange process, 276–277

- Lime essential oil-loaded chitosan nanoparticles, 142–144
- Limiting oxygen index (LOI), 927
- Lindane, 364
- Linear discriminate analysis (LDA), 461–462
- Lip care, 781
- Lipid-based nanoparticles (lipid NPs), 538–540, 560
- Lipid–drug conjugates (LDCs), 538
- Lipid NPs, 538
- Lipid–polymer hybrid nanoparticles (LPNs), 199
- Lipids, 545–546
- Lipoic acid, 553
- Lipophilic bioactive molecules, 554
- Lipophilic substances, 561
- Liposomes, 538–540, 561–562, 777  
defined, 719
- Lipsticks, 723
- Liquid hourly space velocity (LHSV), 493–495
- Liquid lipid NPs (LLNs), 554
- Liquid-phase processes, 663
- Listeria monocytogenes*, 142–144
- Lithium-ion batteries (LIBs), 285–286
- Lithography, 622–625
- Living microorganisms, 657
- Local thermal equilibrium (LTE), 847–848
- Local thermal nonequilibrium (LTNE), 847–848
- Lolium perenne* L., 250–252
- Loosely bound (LB) proteins, 24–25
- L-sulforaphane isothiocyanate, 549–550
- Lumen loading, 914–915
- Lutein, 567*t*
- Luteinizing hormone-releasing hormone (LH–RH) receptor, 185–186
- Lycopene, 546, 550–552
- Lycopersicon esculentum*, 249
- M**
- Macromolecules coatings, influence of  
on dissolution, 403–404
- Maghemite, 303
- Magnesium oxide NPs, 446
- Magnetic and functionalized NPs, 512*f*
- Magnetic graphene hybrids, 303–304
- Magnetic iron oxide nanoparticles, 304–305
- Magnetic nanoparticles (MNPs), 236,  
759–760  
for biomedical applications, 243–245  
functionalization of, 236
- Magnetic property of nanomaterials, 273
- Magnetic resonance imaging (MRI), 243
- Magnetite, 303
- Magnetite NPs, 512–513
- Magneto-fluorescent carbon QDs, 238–239
- Maltodextrin, 146–147
- Maltodextrin nanoparticles, 146–147
- Manganese dioxide/iron oxide/graphene-based  
magnetic nanocomposites, 305
- Manufactured nanomaterials (MNs), 998–999
- Marine antifouling halloysite–rubber  
composites, 934–938  
antifouling test of EVA/HNT  
nanocomposites, 937–938  
morphology and properties of the EVA/  
HNT nanocomposites, 934–937
- Marquibo, 547, 547*t*
- Material Safety Data Sheet (MSDS), 997–998
- Maxwell–Garnetts model, 848
- MCM-41, 39
- Mechanical property of nanomaterials, 273
- Medicago sativa*, 250–252
- Medical devices, 967
- Medicines, nanotechnology in, 528–548  
approved nanopharmaceuticals containing  
natural products, 546–548  
lipid-based nanoparticles (lipid NPs),  
538–540  
metallic NPs, 542–543  
natural products, examples of NPs made  
from, 544–545  
natural products encapsulated in NPs,  
545–546  
polymeric nanoparticles, 540–542  
targeting and sustained release, 543–544
- Melt intercalation method, 799–800
- Melt spinning, 631–632
- Membrane-based technology, 15
- Membranes, immobilization of functionalized  
nanomaterials in, 217–220
- Mercaptoacetic acid (MMA), 407
- 2-Mercaptoethanol, 140–141
- Mercaptopropionic acid (MPA), 209–210,  
400
- Mercaptopropyltriethoxysilane, 418–419
- 3-Mercaptopropyltriethoxysilane (SH-PTES),  
212–213
- 3-Mercaptopropyl trimethoxysilane, 428–429
- Mercaptosuccinic acid, 460–461
- Mesoporous silica, 36–39
- Mesoporous silica nanoparticles (MSN),  
211–213

- Mesoporous SiO<sub>2</sub> NPs, 644  
 Messenger RNA (mRNA), 195–196  
 Metal-based nanoparticles (metal-NPs), 208–211  
 Metal ferrites, 306  
 Metal hexacyanoferrate nanoparticles, 353  
 Metal ions, 459–462  
 Metallic carrier systems, 207  
 Metallic nanomaterials, 271, 446  
 Metallic NPs, 542–543  
 Metal/metal oxide nanoparticle, 271, 668  
 Metal nanoparticles, 210, 241–242, 641–642, 654–661, 654*f*  
     for biomedical applications, 241–242  
     -coated textiles, 657–661  
     production processes, 654–657  
 Metal–organic frameworks (MOFs), 33–36, 455–456  
 Metal-oxide nanoparticle, 44–45, 486–489  
     on textiles, 668–670  
 Metal oxides, 301–302, 315  
 Metal oxides functionalized GO  
     nanocomposites, preparation of, 302–311  
     functionalization of GO with metal oxides  
         nanomaterials, 303–309  
         preparation of GO functionalized with  
         iron oxide nanoadsorbents, 303–306  
         preparation of GO functionalized with  
         other metal oxide nanoadsorbents,  
         306–309  
     preparation of GO using modified  
         Hummer's method, 302, 302*f*  
     preparation of surface modified GO metal  
     oxides composite nanoadsorbents,  
     310–311  
 Metal oxides nanomaterials, functionalization  
     of GO with, 303–309  
     GO preparation functionalized with iron  
     oxide nanoadsorbents, 303–306  
 Metal powder, 668–669  
 Metformin, 757  
 3-Methacryloxypropyl trimethoxysilane, 275,  
     275*f*  
 Methanol, 141–144  
 Method-based functionalization of  
     nanographene, 114  
 Methotrexane, 564*t*  
 Methotrexate, 564*t*  
 3-Methoxypropionitrile, 690–691  
 Methylene blue, 144–146  
 Methylene blue stain, 652  
 1-Methylimidazole, 213–214  
 Methyl orange (MO), 480–483  
 2'-*O*-Methyl-RNA-chitosan-PLGA  
     nanoparticles, 196–197  
*N*-(Methylsulfonic acid), 144  
 Methyltriethoxysilane (Me-TES), 212–213  
 Microemulsion method, 665  
 Microorganisms, 467–468  
 Microporous UF membranes, 47  
 Micro-Raman spectroscopy, 64, 65*f*  
 Microsponges, 779  
 Microwave-assisted synthesis, 665  
 Microwave radiation, 670  
 Minoxidil, 564*t*  
 Mixed-matrix membranes (MMMs), 16,  
     427–428  
     adsorptive mixed-matrix membranes for  
     heavy-metal removal, 40–47  
 AMD-CNT-incorporated MMMs, 17–18  
 incorporated with carbon-based  
     nanomaterials, 16–26, 19*t*  
     carbon nanotubes (CNTs), 17–24  
     graphene oxide (GO), 24–26  
 incorporated with other nanomaterials,  
     33–40  
 incorporated with titania-based  
     nanomaterials, 26–33  
 Mn-modulated cobalt selenide nanosheets  
     (CoMnSe<sub>2</sub>), 95  
 Mo-based electrocatalysts, 90  
 Moisturizer, 781  
 Molecular imprinting, 589–590  
 Molecularly imprinted polymers (MIPs), 457  
 Monoclonal antibodies (mAb), 194  
 Monocrotophos, 365–366  
 Montmorillonite (MMT) clay particles,  
     281–282  
*Morinda tinctoria*, 352  
 Mucilage-to-caseinate ratio, 155  
 Mucin 1 (MUC1) aptamer, 198–199  
 Multidimensional nanomaterials-modified  
     asphalts, 892–906  
     antiaging properties of, 895–906  
         Fourier transform infrared spectroscopy,  
         902–906  
         physical properties, 895–900  
         rheological properties, 900–902  
     physical properties of, 892–895  
     preparation of, 892  
     rheological properties of, 895  
 Multifunctional mesoporous core-shell SiO<sub>2</sub>  
     NP, 642*f*

- Multifunctional SiO<sub>2</sub> NPs, 641–642
- Multiple sclerosis (MS), 549
- Multistep postsynthetic functionalization methods, 639–640
- Multiwalled-carbon nanotubes (MWCNTs), 16–18, 41–42, 238–240, 248–249, 464, 680, 683, 805, 952–953
- MWCNT/polyaniline (PANI) fibers, 690–691
- MWCNTs functionalized with polyethylenimine (MWCNT–PEI), 680
- Multiwalled nanotubes (MWNTs), 332
- Myocet, 547*t*
- N**
- Nafion, 683
- Nail care, 782
- Nanoaegirine, ionic surface modification of, 759–764
- batch adsorptive removal of the TOC from industrial effluent, 760–761
- continuous adsorption in a field test experiments using rotary drum filter, 761–764
- continuous adsorptive removal of TOC at in a fixed-bed column, 761
- Nanocapsules, 721
- Nanocarbon enhancer, 852–858
- melting process, 853–855
- practical applications, 857–858
- preparation of nanocarbon-enhanced PCMs, 852–853
- solidification process, 855–856
- Nanocarriers, 537, 641–642
- Nanocatalysts, 495–496
- intermetallic nonnoble, 98–100
- noble-metal, 92–93, 96
- nonnoble metal, 94–98
- Nanocellulose, 174
- Nanoclay polymer composite, 798–800
- polymer–clay nanocomposites, preparation method of, 799–800
- in situ intercalative polymerization method, 799
- intercalation of polymer from solution, 799
- melt intercalation method, 799–800
- Nanoclays, 805, 809*t*
- Nanocoatings/paints, 815
- Nanocomposite adsorbents, 480–493
- carbon-based nanocomposites, 480–486
- polymer-based nanocomposites, 486–493
- Nanocomposite catalysts, 495–497
- Nanocomposite membranes for water purification, 493–495
- Nanocomposites, 272, 796, 912
- Nanocosmeceuticals
- classification of, 781–782
- antiaging products, 781
- hair care, 781
- lip care, 781
- nail care, 782
- skin care, 781
- regulations of, 784–788
- safety of, 782–784
- toxicity of, 782
- Nanocosmetics, 718, 722–723
- antiaging creams, 723
- hair cosmetics, 722–723
- lipsticks, 723
- sunscreen creams, 723
- toothpastes, 722
- Nanocosmetics, classification of on the basis of formulation technologies, 718–722
- cubosomes, 722
- dendrimers, 721
- nanocapsules, 721
- nanocrystals, 720–721
- nanoemulsions, 719
- nanopigments, 721
- nanosponges and microsponges, 720
- nanostructured lipid carriers (NLCs), 720
- solid lipid nanoparticles (SLNs), 720
- vesicular delivery systems, 719
- Nanocrystalline aegirine, hydrothermal synthesis of, 744–745
- Nanocrystals, 720–721
- Nanoemulsions, 719, 777
- Nanoencapsulation, 142–144
- Nanoengineered textiles, 611
- active textiles, 645–646
- functional carbon-based nanomaterials, 670–691
- applications of carbon-based nanomaterials on textiles, 680–684
- emerging applications, 684–691
- functionalization, 670–673
- heteroatom doping, 673–675
- hybrid carbon-metal/metal oxide nanomaterials, 675–680
- functionalization processes, 614–635
- advanced processes, 619–635

- conventional processes, 614–618
- functional silica nanoparticles, 636–647
  - functionalization, 639–643
  - nanosilica-coated textiles: applications, 643–647
  - production processes, 636–639
- functional TiO<sub>2</sub> nanoparticles, 647–654
  - functionalization/doping, 651
  - nano-TiO<sub>2</sub>-coated textiles: applications, 651–654
  - production processes, 647–650
- future trends and prospects, 691–692
- life cycle of, 613*f*
- nanotechnology on textiles, 611–614, 612*f*
- noble metal nanoparticles, 654–661, 654*f*
  - metal nanoparticle-coated textiles: applications, 657–661
  - production processes, 654–657
- transition metal oxide nanoparticles, 661–670
  - applications of metal oxide nanoparticles on textiles, 668–670
  - production processes, 661–668
- Nanoengineering, 3, 528
- Nanoenhanced PCM (NePCM), 832–833, 844, 858–860
- Nanofibers, 802
- Nanofibrillated cellulose (NFC), 174
- Nanoform, 958–961
- Nanofunctionalization of water-splitting electrocatalysts, 102
- Nanogels, 554–555
- Nanographene, 111–114, 112*f*, 119–124
  - applications, 114
  - biocompatibility, 121–124
  - characterization tools, 113–114
  - chemistry of, 112–113
  - functionalization of, 114
  - industrial issues, 119–120
  - interest in, 112
  - sustainability, 124
  - synthetic methods, 113
  - toxicity, 120
- Nanographene functionalization, 115*f*, 124
- Nano-hydroxyapatite (nano-HA), 722
- Nanolipidic carriers (NLCs), 718–719
- Nanolithography, 624
- Nanomaterial Registry, 221
- Nanomaterials, defined, 718
- Nanomedicine, 528
- Nanometal enhancer, 833–844
  - melting process, 839–840
  - practical applications, 842–844
  - preparation of nanometal-enhanced PCMs, 833–839
  - solidification process, 840–842
- Nanometal oxide enhancer, 844–852
  - melting process, 847–849
  - practical applications, 851–852
  - preparation of nanometal oxide-enhanced PCMs, 845–847
  - solidification process, 849–850
- Nanometer-size monodispersed water droplets, 638
- Nanopaints, 818
- Nanoparticles (NPs), 172, 537
- Nanopeeling Renovator Microdermoblazing and VitActive Activator nanoemulsion, 781
- Nanopharmaceuticals, 528, 538
  - containing natural products, 546–548
- Nanopigments, 721, 725–726, 780
- Nanoplatelets, 801
- Nanoprecipitated chitosan nanoparticles, 144
- Nanoprecipitation technique, 134, 140–144, 187
- Nanoproducts in food supplements, 548–555
  - cancer, 552
  - cardiovascular diseases, 550–551
  - diabetes, 552–553
  - food supplement and its clinical usage, 549
  - nanotechnology and food supplements, 553–555, 556*t*
  - neurodegenerative diseases, 549–550
- Nanopyroxene aegirine, 745–747
- Nanosilica-coated textiles, 643–647
- Nanosized materials, 669–670
- Nano-sized titanium oxide, 722
- Nanosphere, 811
- Nanosponges, 779
- Nanosponges and microsponges, 720
- Nanostructured lipid carriers (NLCs), 538, 540, 720, 778
- Nanostructured solid lubricant, 814
- Nanotechnology, 3, 8–10, 269–270, 479–480, 682
  - and food supplements, 553–555, 556*t*
  - future research trends in nanotechnology and nanomaterials, 12
  - in health products, 539*f*
  - in medicines, 528–548
    - approved nanopharmaceuticals containing natural products, 546–548



Nanotechnology (*Continued*)

- examples of NPs made from natural products, 544–545
- lipid-based nanoparticles (lipid NPs), 538–540
- metallic NPs, 542–543
- natural products encapsulated in NPs, 545–546
- polymeric nanoparticles, 540–542
- targeting and sustained release, 543–544
- performance enhancement using, 718
- for UV protection, 723
- Nanotechnology Industries Association (NIA), 960
- Nano-TiO<sub>2</sub>-coated textiles: applications, 651–654
- Nanotrends in industrial development, 4
- Nanotube formation through layer-by-layer deposition, 159–162
- Nanozero-valent iron (nZVI), 332, 334–346
- 1,8-Naphthalimide derivative, 459
- Naphthenic acid model molecules, 755
- Naphthenic acids (NA), 754–755
- Naphthol Green B dye, 425
- National Industrial Chemicals Notification and Assessment Scheme (NICNAS), 970
- National Institute for Occupational Safety and Health (NIOSH), 999–1000
- National notification requirements in the EU, 968–969
  - Belgium, 968
  - Denmark, 968
  - France, 968
  - Norway, 969
  - Sweden, 968–969
- Natural-based consumer health nanoproducts, 525
  - nanoproducts in food supplements, 548–555
    - cancer, 552
    - cardiovascular diseases, 550–551
    - diabetes, 552–553
    - food supplement and its clinical usage, 549
    - nanotechnology and food supplements, 553–555, 556*t*
    - neurodegenerative diseases, 549–550
  - nanotechnology in medicines, 528–548
    - approved nanopharmaceuticals containing natural products, 546–548
    - examples of NPs made from natural products, 544–545
    - lipid-based nanoparticles (lipid NPs), 538–540
    - metallic NPs, 542–543
    - natural products encapsulated in NPs, 545–546
    - polymeric nanoparticles, 540–542
    - targeting and sustained release, 543–544
    - natural products, nanotechnology, and skin, 555–564
- Natural hydrophilic polymers, 540–541
- Natural inorganic nanomaterials, 4
- Naturally derived pyroxene nanomaterials, 731
  - Avrami–Erofe'ev crystallization kinetic model, 737–739
  - hydrothermal synthesis mechanism, 734–737
    - crystal growth, 736–737
    - induction period, 735
    - nucleation, 735–736
  - hydrothermal synthesis of nanocrystalline aegirine, 744–745
  - low-temperature hydrothermal synthesis of aegirine, 744
  - pyroxene aegirine, 743
  - pyroxene aegirine, modifications to, 745–764
    - nanoaegirine, ionic surface modification of, 759–764
    - structural isomorphous modification for the bulk and surface, 745–747
    - structural isomorphous modification for the surface only, 748
    - structural surface modification by polymer grafting, 748–759
  - synthesis of iron–silicate materials, 739–740
  - synthesis of pyroxenes, 742–743
  - typical preparation procedure of aegirine, 743–744
- Natural materials, 173–174
- Natural organic material (NOM), 949
- Natural organic matters (NOMs), 24–25, 400
- Natural polymers, 133–134
- Natural products
  - approved nanopharmaceuticals containing, 546–548
  - encapsulated in NPs, 545–546
  - examples of NPs made from, 544–545
  - Natural substances, adsorption of in biological or environmental systems, 947
- N-doping, 674–675

Negative photoresist, 624–625  
 Nernstian potential, 87  
 Neurodegenerative diseases, 549–550  
*N*-hydroxysuccinimide (NHS), 213, 447  
 Nickel, 745–748  
*Nicotiana tabacum*, 250–252  
*Nicotiana tabacum* cv petite Havana, 250–252  
*Nicotiana xanthi*, 250–252  
 Ni-doped aegirine, 745–747  
 Niosomal gallidermin gel, 779–780  
 Niosomes, 561, 779–780  
   -based formulations, 561  
 Nitric acid, 216  
 Nitrogen-doped TiO<sub>2</sub> nanotubes (N-TNT), 30  
 Nitrogen-doped ultrathin Mo<sub>2</sub>C nanosheets, 90  
 Nitrogen-rich emeraldine salt (ES), 94  
 NM functionalization, methods of, 334  
 Noble-metal nanocatalysts, 92–93, 96  
 Noble metal nanoclusters, 660  
 Noble metal nanoparticles, 271, 612, 654–661, 654f  
   metal nanoparticle-coated textiles, 657–661  
   production processes, 654–657  
 Noble metals, 330–331  
 Noncontact printing, 619  
 Noncovalent functionalization, 234, 347  
 Noncovalent functionalization of PLGA nanoparticles, 189–195  
   antibody-directed PLGA nanoparticles, 194–195  
   cell target ligands coupled on the surface of PLGA nanoparticles, 193–194  
   PEGylated PLGA nanoparticle, 190–191  
   polyelectrolyte–PLGA nanoparticles, 192–193  
   surfactant PLGA nanoparticles, 191–192  
 Noncovalent surface functionalization, 216–217  
 Noncovalent surface modification, 189–190  
 Nonmetal nanomaterials, 236  
 Nonnoble metal carbides and oxides, 90  
 Nonnoble metal dichalcogenides and phosphides, 90–92  
 Nonnoble metal nanocatalysts, 94–98  
 Nonwoven cellulose acetate fibers, 646–647  
 Norwegian Chemical Products, 969  
 Nucleation, 735–736  
 Nucleic acid-functionalized PLGA, 195–200  
 Nylon nanocomposites, 809t

## O

Occupational Health and Safety (OHS), 995  
   engineered nanomaterials (ENMs), 996–999  
   evaluation, 1000–1002  
   stakeholders, initiatives taken by, 999–1000  
 Octadecyl amine (ODA), 834  
 Octadecyl dimethyl benzyl ammonium chloride (ODBA), 866–867  
 OECD (Organisation for Economic Cooperation and Development), 784–788  
 Oil extraction wastewater-organic contaminant removal, 754–757  
   interaction of  $\beta$ -CD with naphthenic acids, 755–757  
   naphthenic acid model molecules, 755  
 Oil sand process-affected water (OSPW), 754–755, 757  
 Oil–water–oil emulsion (o/w/o), 188  
*Olea europaea*, 565t  
 Oleic acid (OA), 276  
 Oleylamine (OAm), 276  
 Oligonucleotides, 241–242  
 Olsen's group, 147–149  
 Omega-3 fatty acid, 550–551  
 One-dimensional nanostructures, 271  
 One-pot synthesis. *See* Cocondensation  
 Open reading frame (ORF), 197  
 Optical property of nanomaterials, 273  
*Optisol*, 724  
 Organic armor, 276  
 Organic contaminants (OCs), 299–301, 359–360  
   necessity of functionalization of NMs for remediation of, 350  
 Organic dyes, 356–364  
   degradation of pesticides by functionalized NMs, 362–364  
 Organic EVMT (OEVMT), 866–867, 902–904  
 Organic layered silicate in asphalt, 866–880  
   compatibility analysis between organic layered silicate and asphalt, 874  
   Fourier transform infrared spectroscopy analysis of, 871–872  
   preparation of, 866–867  
   X-ray diffraction analysis of organic layered silicates, 867–869  
 Organic layered silicate-modified asphalts  
   antiaging properties of, 876–880

- Organic layered silicate-modified asphalts  
     (*Continued*)  
         atomic force microscopy, 879–880  
         physical properties, 876–879  
         atomic force microscopy analysis of,  
             873–874  
         Fourier transform infrared spectroscopy  
             analysis of, 872–873  
         microstructure of, 870–871  
         physical properties of, 875–876  
         preparation of, 867  
         XRD analysis of, 869
- Organic layered silicates, X-ray diffraction  
     analysis of, 867–871  
     microstructure of organic layered silicate-  
         modified asphalts, 870–871  
     X-ray diffraction analysis of organic  
         layered silicates, 867–869  
     XRD analysis of separated organic layered  
         silicates from modified asphalt, 869
- Organic MMT (OMMT), 866–869, 874
- Organic NPs, 538
- Organic pollutants, 509–510  
     catalytic degradation of, 496  
     simple molecules and, 462–466
- Organic pollutants remediation by potential  
     functionalized nanomaterials, 327  
     degradation of OP pesticides by FNMs,  
         365–371  
         degradation of PAHs by FNMs, 371  
         degradation of phenols and BPA by  
             FNMs, 366–371  
     direct functionalization, 334–348  
         covalent functionalization, 334–347  
         functionalization by heteroatoms doping,  
             347  
         functionalization by immobilization, 348  
         inorganic functionalization, 347  
         noncovalent functionalization, 347  
     future perspectives, 377  
     green synthesis in FNMs, 349  
     importance of green synthesis in FNMs,  
         351–356  
     indirect/postsynthetic functionalization  
         (grafting), 348–349  
         polymer coating, 349  
     necessity of functionalization of NMs for  
         remediation of organic contaminants,  
             350  
     organic dyes, 356–364  
         degradation of pesticides by  
             functionalized NMs, 362–364  
         toxicity and functionalized nanoparticles,  
             371–377  
         working mechanism of FNPs, 350–351
- Organic REC (OREC), 866–867
- Organization for Economic Cooperation and  
     Development (OECD), 7, 727–728
- Organofullerenes, 560
- Organofunctionalization, 640–641
- Organophosphorus (OP) pesticides,  
     degradation of, 365–371  
     degradation of PAHs by FNMs, 371  
     degradation of phenols and BPA by FNMs,  
         366–371
- Organosilanes, 418–419
- Organotrialkoxysilanes, 640–641
- Orthopyroxene, 741
- Orthorhombic pyroxene, 741
- Oryza sativa*, 250–252
- Ovalbumin (OVA), 136–137, 564*t*
- (1,3)-Oxazine ring, 459
- Oxygen-containing functional groups, 486
- Oxygen evolution reaction (OER), 83–84, 88,  
     92–96, 282–283  
     noble-metal nanocatalysts, 92–93  
     nonnoble metal nanocatalysts, 94–96  
     polarization curves, 283*f*
- Oxygen evolution reaction, role of  
     functionalized nanomaterials in,  
         282–284
- Oxygen groups, 216
- Oxygen reduction reaction (ORR), 290
- ## P
- P. phosphoreum*, 407
- Paclitaxel, 564*t*
- Paclitaxel-loaded chitosan NPs, 544–545
- Paclitaxel-protein bound NP formulation,  
     547–548
- Padding process, 615–616
- Pad-dry-cure method, 652
- Palladium (Pd) NPs, 465–466
- Palmitic acid (PA), 845–846
- Palm-mill effluent (POME) treatment, 18
- Paraffin, 852
- Paraoxon, 464
- Parkinson's disease (PD), 549
- Parvifloron D (PvD), 546
- Pathogenic bacteria, 509–510
- p*-doping, 674
- Pectin, 153–154, 552
- PEGylated PLGA nanoparticle, 190–191
- PEGylation, 208–209

- Penetration retention ratio (PRR), 876
- Pentachlorophenol (PCP), 515–516
- 1,5-Pentanediol, 656
- 1*H*, 1*H*, 2*H*, 2*H*-Perfluorooctyltriethoxysilane (FTES), 29–30
- Personal protective equipment (PPE), 997
- Pesticides, 327–329, 333, 509–510  
degradation of, by functionalized NMs, 362–364  
sensing and remediation, 422–425
- pH levels, 458–459
- Pharmaceutical active compounds removal from water, 757
- Pharmaceutically active compounds (PhACs), 757
- Phase change materials (PCMs), 811, 830
- pH effect on the photodegradation of Rhodamine-B dye, 73–74
- Phenanthrene, 371
- Phenolic compounds, 509–510
- Phenols, 327–329, 333
- Phenols and BPA, degradation of by FNMs, 366–371
- Phenyltriethoxysilane (Ph-TES), 212
- Phenyltrimethoxysilane, 651
- Phosphoric acid fuel cells, 288–290
- Phosphorus, 674
- Photocatalytic degradation (PCD), 56–57, 75–76
- Photocatalytic oxidation, 495–496
- Photocatalytic oxygen evolution reaction, 53  
CeO<sub>2</sub>/CdO nanostructures, structural investigation of, 57–58  
degradation of Rhodamine-B using CeO<sub>2</sub>/CdO heterogeneous catalyst, 69–71  
diffuse reflectance spectroscopy (DRS) studies, 61–64, 63*f*  
effect of catalyst dose on photodegradation of Rhodamine-B dye, 74–75  
effect of initial concentration of Rhodamine-B dye, 75–76  
effect of irradiation time on photodegradation of Rhodamine-B dye, 74  
effect of pH on the photodegradation of Rhodamine-B dye, 73–74  
field emission scanning electron microscopy (FESEM) studies, 59–61  
Fourier transform infrared spectroscopy, 58–59  
high-resolution transmission electron microscopy (HRTEM) studies, 61, 62*f*  
micro-Raman spectroscopy, 64, 65*f*  
photocatalysis, mechanism of, 77–78  
photocatalytic activity, 69  
photocatalytic degradation of Rhodamine-B dye using CeO<sub>2</sub>/CdO heterogeneous catalyst, 71–72  
photoluminescence (PL) spectra, 64–67, 66*f*  
removal of Rhodamine-B from urban wastewater, 76  
thermogravimetric (TG) analysis, 68–69  
visible light–induced decomposition of Rhodamine-B using CeO<sub>2</sub>/CdO heterogeneous catalyst, 72  
X-ray photoelectron spectroscopy (XPS) studies, 67–68, 67*f*
- Photochromic hybrid nanomaterial, 645–646
- Photochromic nanomaterials, 645–646
- Photolithography, 624–625
- Photoluminescence (PL) spectra, 64–67, 66*f*
- Photothermal therapy (PTT), 242
- Photovoltaic solar cells, 6
- Physcomitrella patens*, 409
- Physical vapor deposition (PVD), 587, 649
- Phytochemicals, 536*t*
- Phytoestrogens, 552–553
- Phytosomes, 561–562
- Phytosterols, 550–551
- $\pi$ -bonds, 112–113
- Piezo ceramic materials, 816
- Pilot Test Unit, 745–747
- Pimephales promelas*, 409–410
- Pinus roxburghii*, 515–516
- Piperine–pro–nanolipospheres (PPNs), 546
- Pistacia integerrima*, 565*t*
- Pisum sativum*, 250–252
- Plasmid DNA (pDNA), 195–196  
pDNA–PEI–PLGA nanocomplexes, 198
- Plasmonic properties of NPs, 232
- Plectranthus amboinicus*, 565*t*
- PMEL34, 564*t*
- Podophyllotoxin, 564*t*
- Pollutant remediation, 417
- Pollutant treatment, 507*t*
- Poloxamer 188, 141–142
- Poloxamer 407, 141–142
- Poly(3,4-ethylenedioxythiophene) (PEDOT), 670
- Poly(D,L-lactide-co-glycolide) (PLGA) nanoparticles, 185–186, 186*f*  
active targeting by surface functionalization of, 188–189

- Poly(D,L-lactide-*co*-glycolide) (PLGA) nanoparticles (*Continued*)
- noncovalent functionalization of PLGA nanoparticles, 189–195
    - antibody-directed PLGA nanoparticles, 194–195
    - cell target ligands coupled on the surface of PLGA nanoparticles, 193–194
    - PEGylated PLGA nanoparticle, 190–191
    - polyelectrolyte–PLGA nanoparticles, 192–193
    - surfactant PLGA nanoparticles, 191–192
  - nucleic acid-functionalized PLGA, 195–200
  - production techniques, 187–188
  - structure and properties of, 186–187
- Poly( $\epsilon$ -caprolactone) (PCL), 540–541
- Poly(ethylene glycol) (PEG), 346
- Poly(ethylene terephthalate) (PET)-spunbond nonwoven fabrics, 683
- Poly(propylene glycol) (PPG), 191–192
- Poly(pyridobisimidazole)-grafted-poly (dimethyl diallyl ammonium chloride) (PIPD-*g*-PDDA), 661
- Poly(sulfobetaine methacrylate) (PSBMA), 36
- Poly(vinyl alcohol) (PVA), 18–22, 187–188
- Poly(vinylidene fluoride-*co*-hexafluoropropene), 690–691
- Poly(vinylpyrrolidone) (PVP), 187–188
- Poly-3-aminobenzenesulfonic, 249
- Polyacrylic acid (PAA) surface coating, 41
- Polyallylamine hydrochloride (PAH), 214, 400
  - degradation of, by FNMs, 371
- Polyaniline (PANI), 43
- Polyanion, 214
- Polyaspartate (PAA), 452–453
- Poly-butylacrylate modified MWCNTs, 680
- Poly butylene adipate, 419
- Polychlorinated biphenyls (PCBs), 512–513, 515–516
- Polycyclic aromatic hydrocarbons (PAHs), 327, 329–330
- Polydimethylsiloxane (PDMS), 279–280, 280*f*
- Polydispersity index (PI), 197
- Poly-D-lysine (PDL), 151
- Polydopamine (PDA) nanoparticles, 46
- Polyelectrolyte–PLGA nanoparticles, 192–193
- Polyetherimide (PEI) membrane, 30
- Polyethersulfone (PES), 22–23
- Polyethylene glycol (PEG), 444, 543–544
- Polyethyleneimine (PEI), 195, 419
  - PEI–PLGA nanoparticles, 197–198
- Polyethylene oxide (PEO), 26–27
- Polyethylene terephthalate (PET), 682
- Polyethylenimine (PEI), 161–162, 444, 452–453, 644, 759–760
- Polygonum Hydropiper*, 352
- Poly(lactic acid) (PLA), 540–541
- Polymer-based nanocomposites, 486–493
- Polymer-based solid lubricant coatings, 814
- Polymer–clay nanocomposites, preparation method of, 799–800
  - in situ intercalative polymerization method, 799
  - intercalation of polymer from solution, 799
  - melt intercalation method, 799–800
- Polymer coating, 349, 543–544
- Polymer glass, 816
- Polymer grafting, structural surface modification by, 748–759
  - applications of  $\beta$ -CD grafted nanopyroxene in wastewater treatment, 754–759
  - enhanced settling of fine particles, 757–759
  - oil extraction wastewater-organic contaminant removal, 754–757
  - removal of pharmaceutical active compounds from water, 757
  - $\beta$ -cyclodextrins grafted nanopyroxenes, preparation of, 752–754
  - interaction of epoxy hybrid with the aegirine surface, 752–753
  - interaction of  $\beta$ -CD with the aegirine surface, 754
  - coupling agents, 749–750
  - polymers, 750–751
    - $\beta$ -cyclodextrin, 750–751
- Polymeric micelles (PMs), 246–248
- Polymeric nanomaterials, 953
- Polymeric nanoparticles, 540–542, 559
  - encapsulating bioactive drugs in, 133
- Polymeric resin, 281
- Polymer/nanocomposite NFs, 584–585
- Polymer nanocomposites, 172
- Polymer NFs, surface modification and functionalization of, 586–589
  - using biotechnology, 589
  - using chemical technologies, 587
  - using nanotechnologies, 587–589
  - using physical technologies, 587
- Polymer NPs, 562

- Polymers, 479–480, 750–751  
 $\beta$ -cyclodextrin, 750–751  
 used in electrospun NFs, 583–584  
 wrapping, 672–673
- Polymethyl methacrylate, 419
- Polyolefin nanocomposites, 809*t*
- Polyol method, 666
- Polyol process, 656
- Polyol synthesis, 656
- Polyoxyethylated castor oil, 547–548
- Polyphenols, 353–354, 419–421
- Polypropylene (PP), 645–646
- Polypropylene oxide (PPO), 26–27
- Polypyrrole-zinc oxide-single-walled carbon nanotube (ppy/ZnO/SWCNT) composite, 680–682
- Polysaccharide, 146–147
- Polysorbate 20, 141–142
- Polysorbate 80, 141–142
- Polystyrene sulfonate (PSS), 214
- Polystyrene-supported nanocomposites, 490*t*
- Polysulfone (PSF) membrane, 18–22
- Polysulfone (PSf) microporous substrate, 493–495
- Polytetrafluoroethylene (PTFE), 685
- Polyurethane foam (PUF), 680
- Polyvinyl alcohol (PVA), 276
- Polyvinyl chloride (PVC), 616–618
- Polyvinylidene difluoride (PVDF) membrane, 17–18, 25–26, 645–646  
 c-PVDF membranes, 39  
 g-PVDF membranes, 39
- Polyvinylidene fluoride-co-hexafluoropropylene (PVDF-HFP) electrospun membranes, 29–30
- Polyvinyl pyrrolidone (PVP), 276, 655–656, 955
- Porous nanocomposites for water treatment, 479  
 nanocomposite adsorbents, 480–493  
 carbon-based nanocomposites, 480–486  
 polymer-based nanocomposites, 486–493  
 nanocomposite catalysts, 495–497  
 nanocomposite membranes for water purification, 493–495
- Porous TiO<sub>2</sub> foams (PTFs), 846–847
- Positive photoresist, 624–625
- Postgrafting, 641. *See also* Postsynthetic functionalization methods
- Postsynthetic functionalization methods, 639–641
- Postsynthetic grafting, 639–640
- Potential of nanomaterials, 4
- Pre-Manufacture Notice (PMN), 969
- Pressure aging vessel (PAV), 876
- Printing processes, 619
- Pristine kafirin nanoparticles, 135–136
- Pristine maltodextrin nanoparticles, 146–147
- Production of inorganic NFs with different styles and various functions, 585
- Propellant materials, nanomaterials for, 813–814
- Properties and functions of nanomaterials, 172
- Properties of nanomaterials, 272–273  
 electronic property, 273  
 magnetic property, 273  
 mechanical property, 273  
 optical property, 273  
 structural property, 272–273  
 thermal property, 272
- 1-Propyl-3-methylimidazolium iodide (PMII), 690–691
- Propylene glycol, 656
- Prosopis cineraria*, 351–352
- Prostaglandins, 550–551
- Prostate-specific membrane antigen (PSMA), 191
- Protein corona, 949
- Protein functionalized carbon nanomaterials, 9–10
- Protein NPs, 541–542
- Proteins, nanoprecipitation/desolvation of, 134–142
- Protein utilization, 133–134
- Proton exchange membrane fuel cells, 288–290
- Pseudomonas aeruginosa*, 513–514
- Psidium guajava*, 351–352
- Psoralen, 564*t*
- Psyllium, 553
- Pt-based HER catalysts, 88–89
- Pullulan, 147
- Pullulan-g-poly(*N*-isopropylacrylamide), 147
- Pyrolysis process, 655–656
- Pyroxene, 745–747
- Pyroxene aegirine, 743
- Pyroxene aegirine, modifications to, 745–764  
 ionic surface modification of nanoaegirine, 759–764  
 batch adsorptive removal of the TOC from industrial effluent, 760–761

- Pyroxene aegirine, modifications to  
     (*Continued*)  
         continuous adsorption in a field test  
         experiments using rotary drum filter,  
         761–764  
         continuous adsorptive removal of TOC at  
         in a fixed-bed column, 761  
     structural isomorphous modification  
     for the bulk and surface, 745–747  
     for the surface only, 748  
     structural surface modification by polymer  
     grafting, 748–759  
         applications of  $\beta$ -CD grafted  
         nanopyroxene in wastewater treatment,  
         754–759  
          $\beta$ -cyclodextrins grafted nanopyroxenes,  
         preparation of, 752–754  
         coupling agents, 749–750  
         polymers, 750–751  
 Pyroxenes, 740–764  
     hydrothermal synthesis of nanocrystalline  
     aegirine, 744–745  
     low-temperature hydrothermal synthesis of  
     aegirine, 744  
     modifications to the pyroxene aegirine,  
     745–764  
         ionic surface modification of  
         nanoaegirine, 759–764  
         structural isomorphous modification for  
         the bulk and surface, 745–747  
         structural isomorphous modification for  
         the surface only, 748  
         structural surface modification by  
         polymer grafting, 748–759  
     pyroxene aegirine, 743  
     synthesis of, 742–743  
     typical preparation procedure of aegirine,  
     743–744
- Q**  
 Quantitative Structure Activity Relationship  
 (QSAR), 963  
 Quantum dots (QDs), 271–272, 407,  
 438–439, 441*f*, 443–444, 453–454,  
 459, 954  
 Quantum size effect (QSE), 61–64  
 Quercetin, 546  
*Quercus macdougalii*, 250–252  
 Quinalphos, 365–366
- R**  
 Radiation Shield Technologies, 669  
 Radiofrequency (RF), 670  
*Ralstonia solanacearum*, 513–514  
 Raman spectroscopy, 113–114  
*Raphanus sativus*, 250–252  
 Rare earth metal oxides, 55–56  
 Raspberry-like NPs, 642  
 Rayleigh numbers, 848  
 REACH regulation, 956–957  
 Reactive oxygen species (ROS), 72, 407, 549,  
 955  
 Recent scientific research in the field of  
 functionalized nanomaterials, 8–11  
 Redox reactions, 117–118  
 Reduced graphene oxide (rGO), 120,  
 286–287, 486, 689  
 Reduced graphene oxide-based (rGO) textile  
 SC, 687–689  
 Registration, Evaluation, Authorisation, and  
 Restriction of Chemicals (REACH)  
 Regulation, 987–988  
 Reinforced fillers, 173–174  
 Renewable biopolymers, 168  
 Research on nanomaterials, 6–7  
 Resveratrol, 545–546, 550–551, 567*t*  
 Reticulo-endothelial system (RES), 188  
 Retinol, 564*t*  
 Reverse micelles, 638  
 Reverse transcription polymerase chain  
 reaction (RT–PCR), 197–198  
 Reynolds number, 848, 856  
 Rhodamine-B (RhB) dye, 56–57  
     effect of catalyst dose on the  
     photodegradation of, 74–75  
     effect of initial concentration of, 75–76  
     effect of irradiation time on the  
     photodegradation of, 74  
     effect of pH on the photodegradation of,  
     73–74  
     visible light–induced decomposition of,  
     using  $\text{CeO}_2/\text{CdO}$  heterogeneous  
     catalyst, 72  
 Rhodamine-B, degradation of  
     using  $\text{CeO}_2/\text{CdO}$  heterogeneous catalyst,  
     69–71  
 Rhodamine-B dye, photocatalytic degradation  
 of  
     using  $\text{CeO}_2/\text{CdO}$  heterogeneous catalyst,  
     71–72  
*Ricinus communis*, 250–252  
 Rose Bengal, 424–425  
*Rosmarinus officinalis*, 567*t*  
 Rotary drum filter (RDF), 761–764, 763*f*

- continuous adsorption in a field test
  - experiments using, 761–764
- Rothband, 669
- Round-to-round method, 620
- Royal Society of Sciences, 725–726
- Running tracks, application of nanomaterials in, 818
- RuO<sub>2</sub>-based electrocatalysts, 96
- Ruta graveolens*, 351–352
- S**
- Sabatier principle, 87
- Saccharomyces cerevisiae*, 352
- Safety Data Sheet (SDS), 997–998
- Salmonella typhi*, 176
- Salmonella typhimurium*, 467–468
- Sambucus nigra*, 565*t*
- Saponin, 353–354, 552
- Scanning probe lithography, 624
- Scanning tunneling microscopy (STM), 113–114
- Schiff base, 514–515
- Scientific Committee on Consumer Products (SCCP), 784–788
- Scientific research in the field of
  - functionalized nanomaterials, 8–11
- Scratch resistance, nanovarnishes for, 816
- Screenprinting, 619–622, 620*f*
- Selective laser sintering, 625–629
- Selenium, 549–550
- Selenoprotein P, 549–550
- Self-assembled monolayer (SAMs), 209–210
- Self-assembly, 450–454
- Self-cleaning, 811
- Self-fabricated GO-embedded membrane, 24
- Sensing applications, 457–468
  - biomarkers and biomolecules, 466–467
  - metal ions, 459–462
  - microorganisms, 467–468
  - pH, 458–459
  - simple molecules and organic pollutants, 462–466
- Sensor electrodes, 687
- Sertraline hydrochloride, 564*t*
- Shape-stabilized composite PCMs (ss-CPCMs), 834
- Sharp and Hancock method, 738
- Shewanella oneidensis*, 351–352, 400, 405–407
- Shigella dysenteriae*, 142–144
- Ship in the bottle polymerization, 799
- $\sigma$ -bonds, 112–113
- Silane coupling agents, 749, 880
- Silica-based nanomaterials, 8
- Silica-based NMs, functionalization of, 346–347
- Silica-coated maghemite, 515–516
- Silica-coated magnetite NPs, 510
- Silica-coated metal-NPs, 210–211
- Silica nanoparticles (Si-NPs), 211–214, 286–287, 479–480, 636, 642–643
  - functional, 636–647
  - functionalization, 639–643
  - nanosilica-coated textiles, 643–647
  - production processes, 636–639
- Silicates, 479–480
- Silicon alkoxides, 212
- Silicone rubber (SR), 668–669
- Silver, 721
- Silver-coated starch, 175
- Silver nanoparticles, 208, 242, 351–352, 542, 780, 810
- Silylation of SiO<sub>2</sub> NPs, 641
- Single-walled carbon nanotubes (SWCNTs), 16–17, 236–239, 248–249, 682–683, 687–689, 805, 952–953
- Sintered activated carbon (SAC), 483
- SiO<sub>2</sub> NPs, 636–646, 643*f*
  - silylation of, 641
- Sips model, 760–761
- Sitophilus* species, 250
- Size-controlled copper nanoparticles, 279
- Size effect, 272
- Skimmia laureola*, 513–514
- Skin care, 781
- Small interfering RNAs (siRNAs), 195–196
- Smart drug delivery systems, 231
- Smart textiles, 611
- SNLs, 540
- Sodium alginate, 149–151
- Sodium carboxymethyl cellulose
  - polyelectrolyte, 689
- Sodium dodecanoate, 419–420
- Sodium dodecylbenzenesulfonate, 683
- Sodium dodecyl sulfate (SDS), 191–192, 402–403
- Sodium hypophosphite (SHP), 680–682
- Sodium-ion batteries (SIBs), 285–286
- Sodium lignosulfonate (SLS), 22–23
- Sodium nitrate, 302
- Softening point increment (SPI), 876, 878–879, 889–890
- Soil pollution remediation, 515–516
- Solanum lycopersicum*, 249–252



- Solar-light-driven thermocatalysis, 515f
- Sol–gel method, 587–588, 636–638, 656–657, 664–665, 680–682, 724
- Solid lipid nanoparticles (SLNs), 158, 538, 554, 560–561, 720, 725–726, 777–778
- Solid-oxide fuel cells, 288–290
- Solid-phase methods, 663
- Solid-state methods, 663
- Solution-mediated model, 734–735
- Solution-phase methods, 663
- Solution spinning, 631–634
- Solvent, 134
- Solvent displacement. *See* Nanoprecipitation technique
- Solvent-to-nonsolvent ratio, 146–147
- Soy, 550–551
- $SP_2$  hybridization, 112–113
- Space-confined synthesis, 745
- Specific extinction area (SEA), 929
- Spherical nanoparticles, 144–146
- Spherical particle formation through layer-by-layer deposition, 156–159
- Spherical polycrystalline anatase particles, 649
- Spinel nanoferrites, 666
- Spinel-type nanoferrites, 662–663
- Spinning technologies, 631
- Spirodela polyrhiza*, 250–252
- Sport material properties of functional nanomaterials, 809–812
- antibacterial, 810
  - extreme weather (heat/cold), protection from, 811
  - multifunctional properties, 811–812
  - self-cleaning, 811
  - ultraviolet protection, 810–811
  - waterproof resistance, 810
- Sports industry applications of functional nanomaterials, 816–818
- golf shafts, nanomaterials in, 818
  - running tracks, application of nanomaterials in, 818
  - sport clothing and shoes, nanomaterials in, 817
  - sports stadiums and gymnasiums, nanomaterials in, 818
  - tennis rackets, nanomaterials in, 817–818
- Sports stadiums and gymnasiums, nanomaterials in, 818
- Stadiums, nanomaterials in, 818
- Stakeholders, initiatives taken by, 999–1000
- Standard ceramic method, 667
- Staphylococcus aureus*, 142–144, 176, 513–514, 644, 646, 652–654, 659, 684, 810
- Starch, 168, 171, 175
- Starch nanoparticles, 142
- Stefan number, 856
- Stereolithography, 625–629
- Strategies for functionalization of nanomaterials, 232–236
- Stratum corneum*, 555, 559, 561–562
- Streptavidin, 453–454
- Stretchable self-powered fiber-based strain sensor (AFSS), 685
- Strontium titanate NPs, 510–511
- Structural isomorphous modification
- for the bulk and surface, 745–747
  - for the surface only, 748
- Structural property of nanomaterials, 272–273
- Stöber process, 210–211, 636–638
- Sulfate and chloride processes, 647–648
- Sulforaphane, 550–551
- Sulfosuccinimidyl 4-(*N*-maleimidomethyl) cyclohexane-1-carboxylate (sulfo-SMCC), 449
- Sulfuric acid, 302
- Sun protection factor (SPF), 724
- Sunscreen creams, 723
- Sunscreens, 723–724
- Supercapacitors, role of functionalized nanomaterials in, 287–288
- Superoleophilic graphene nanosheets, 853
- Superparamagnetic IONPs (SPIONPs), 543
- Superparamagnetic iron oxide (SPIO), 175
- Superparamagnetic iron oxide nanoparticles (SPION), 175, 244
- Superparamagnetic property of nanomaterials, 273
- Surface coatings on engineered nanomaterials for environmental systems, 399
- agglomeration, 404–405
  - dissolution, 402–404
    - influence of engineered coatings on dissolution, 402–403
    - influence of macromolecules coatings on dissolution, 403–404
  - engineered nanomaterial coatings, 405–409
    - cellular organisms, 405–408
    - invertebrates and vertebrates, 409
  - engineered nanomaterials, molecular approaches to toxicity of, 409–410

- Surface enhanced Raman scattering (SERS), 458, 659–660
  - Surface functionalization, 562, 651
  - Surface functionalization of PLGA nanoparticles, 188–189
  - Surface-functionalized MWNTs, 40–41
  - Surface functionalized nanomaterials, 943
    - allotropes of carbon, 952–953
    - biological mechanisms, effect of surface on, 948–952
    - adsorption of substances from media—protein corona and natural organic matter, 949
    - adverse outcome pathway (AOP), 950–952
    - physical impacts, 952
  - Board of Appeal review, 957–958
  - current REACH situation with nanomaterials, 956–957
  - different types of surface modification, 946–948
    - adsorption of natural substances in biological or environmental systems, 947
    - covalent bonds with core substance, 946
    - degradation of layers, 947–948
    - doping of particles, 946
    - intentional adsorption of substance onto surface, 946–947
  - EU regulations, 965–969
    - biocidal products regulation (BPR), 965–966
    - cosmetics regulation, 966
    - food and food contact materials, 967–968
    - medical devices, 967
    - inorganic elements and oxides, 954–956
    - national notification requirements in the EU, 968–969
      - Belgium, 968
      - Denmark, 968
      - France, 968
      - Norway, 969
      - Sweden, 968–969
    - national regulations that impact nanomaterials, 969–970
      - Australia, 970
      - Canada, 969–970
      - Taiwan, 970
      - United States, 969
  - polymeric nanomaterials, 953
  - quantum dots, 954
  - REACH (2019), amendments to the annexes of, 958–964
    - complexity of risk assessment for nanomaterials, 961–963
    - concepts of nanoforms and similar sets of nanoforms, 958–961
    - use of grouping for the risk assessment of nanomaterials, 963–964
  - regulatory and legal issues that impact surface-functionalized nanomaterials, 956
    - substance-specific examples, 952
  - Surface-functionalized nanotubes, 425
  - Surface modification inorganic nanoparticle-modified asphalts, 880–892
    - antiaging properties of, 889–892
    - atomic force microscopy, 891–892
    - physical properties, 889–891
    - atomic force microscopy of, 883–884
    - physical properties of, 886–889
    - preparation of, 880
    - UV–visible absorbance and reflectance spectra analysis of INs, 881
  - Surface modification inorganic nanoparticles and asphalt
    - compatibility analysis of, 884–886
    - Fourier transform infrared spectroscopy analysis of, 881–883
    - preparation of, 880
  - Surface oxidation, 216, 672
  - Surface-plasmon-resonant (SPR) effect, 442, 458
  - Surfactant PLGA nanoparticles, 191–192
  - Surfactants, 211–212
  - Sustainability, 11
  - Synthesized nanocomposites, 512–513
  - Synthesized nanographene- and graphene-based nanocatalysts, 113–114
  - Synthetic dyes, 333
  - Synthetic polymers, 133, 540–541
    - grafting of, 277–278
  - Synthetic wastewater (SW), 18–22
  - Systems engineering, 11–12
- ## T
- Tafel equation, 84–85
  - Tafel step, 86
  - Taiwan Chemical Substance Inventory (TCSI), 970
  - Tamoxifen-loaded chitosan NPs, 544–545
  - Tannins, 552
  - Taxol, 547*t*

- Taylor cone, 634–635, 635*f*  
 Teflon-lined stainless-steel autoclave, 306–308  
 Tennis rackets, nanomaterials in, 817–818  
 Ternary magnetic composite polypyrrole-modified rGO–Fe<sub>3</sub>O<sub>4</sub> nanoparticles, 310–311  
 Testosterone, 564*t*  
 Tetrabutyl titanate (TBT), 26–27  
 Tetradecanol (TD), 836  
 Tetraethoxysilane (TEOS), 211  
 Tetraethylenepentamine (TEPA), 30  
 Tetraethylorthosilicate (TEOS), 636–638, 644–646  
 Δ9-Tetrahydrocannabinol (THC), 546  
 Tetrakis(5-hexyn-oxy) Fe(II) phthalocyanine, 447–449  
 Tetraoctylammonium bromide, 655  
 Textile dyeing, 614–616  
 Textiles, nanoengineered. *See* Nanoengineered textiles  
 Thermal and fire resistance properties, 805  
 Thermal conductivity enhancement of PCMs, 832  
 Thermal decomposition, 665–666  
 Thermal energy storage (TES), 827, 829–830  
   nanocarbon enhancer, 852–858  
     melting process, 853–855  
     practical applications, 857–858  
     preparation of nanocarbon-enhanced PCMs, 852–853  
     solidification process, 855–856  
   nanometal enhancer, 833–844  
     melting process, 839–840  
     practical applications, 842–844  
     preparation of nanometal-enhanced PCMs, 833–839  
     solidification process, 840–842  
   nanometal oxide enhancer, 844–852  
     melting process, 847–849  
     practical applications, 851–852  
     preparation of nanometal oxide-enhanced PCMs, 845–847  
     solidification process, 849–850  
 Thermal property of nanomaterials, 272  
 Thermogravimetric (TG) analysis, 68–69, 153–154  
   measurements, 838–839  
 Thermogravimetry (TG) tests, 836  
 Thin film nanocomposite (TFN) membrane, 493–495  
 Thin film oven test (TFOT), 876, 902–904  
 Thiol functionalization, 209  
 Three-dimensional nanostructures, 270  
 3D printed textile, 629  
 3D printing, 625–629  
 Tightly bound (TB) proteins, 24–25  
 TiO<sub>2</sub> nanoparticles, 651–652  
   functional, 647–654  
     functionalization/doping, 651  
     nano-TiO<sub>2</sub>-coated textiles: applications, 651–654  
     production processes, 647–650  
 Tires, 816  
 Tirrell's group, 147–149  
 Titania-based nanomaterials, mixed-matrix membranes incorporated with, 26–33  
 Titania nanotubes (TNTs), 30  
   TNTs-SO<sub>3</sub>H, 32  
 Titanium(IV) butoxide, 649  
 Titanium(IV) chloride, 648  
 Titanium (IV) isopropoxide (TIP) solution, 31  
 Titanium dioxide, 424–425, 612, 647, 721, 723–724, 955–956  
 Titanium-dioxide halloysite nanotube (TiO<sub>2</sub>-HNTs) composites, 31  
 Toluene, 655  
 Toluidine, 327–329  
 Toothpastes, 722  
 Total organic carbon (TOC), 759–760, 763–764  
 Toxic Chemical Substance Control Act (TCSCA), 970  
 Toxic dyes, remediation of, 425–426  
 Toxicity testing, 727–728  
 Toxic Substances Control Act (TSCA), 969, 988  
 Toyota Research Group, 798–799  
 Transdermal drug delivery, 559  
 Transfer coating process, 618  
 Transfersomes, 719  
 Transfersomes, 561  
 Transitional metal oxide (TMO), 56  
 Transition metal dichalcogenide crystals, 90–91  
 Transition metal oxide nanoparticles, 661–670  
   applications of metal oxide nanoparticles on textiles, 668–670  
   production processes, 661–668  
 Transition metal oxide NPs, 667–668  
 Transition metal oxides, 612, 662  
 Transition metal phosphides, 90  
 Transmembrane pressure (TMP), 24

Transmission electron microscopy (TEM),  
542, 834  
Tribological and anticorrosive coatings, 807  
1,1,1-Trichloro-2,2-bis(chlorophenyl)acetic  
acid, 464  
*N*-(2,4,6-Trichlorophenyl) maleimide (TCPM),  
916–917  
Triethylenetetramine, 648  
3-(Trihydroxysilyl)propyl methylphosphonate,  
641  
Trimethylenediamine, 648  
Trinitrotoluene (TNT), 464–465  
Trioctylphosphine (TOP), 276  
Trioctylphosphine oxide/trioctylphosphine  
(TOPO/TOP), 276  
Trisodium citrate, 402–403  
*Triticum aestivum*, 250–252  
TritonX-100, 141–142  
Tween 80, 402–403  
Tween 80 emulsifier, 146–147  
Tween 80-stabilized emulsions, 135–136  
Two-dimensional nanostructures, 270–271

## U

Ultimate strength and stiffness, 804–805  
Ultrasonication method (USM), 121–124  
Ultrathin graphite foams (UGF), 852  
Ultraviolet (UV) radiation, 878–879  
UV protection, 724, 810–811  
nanotechnology for, 723  
UV–visible absorbance and reflectance  
spectra analysis of INs, 881  
Uncapped PLGA, 187  
Urban wastewater, removal of Rhodamine-B  
from, 76  
User-defined functions (UDFs), 839

## V

Vajjha's model, 848, 851, 855–856  
Vanadium-doped NiS<sub>2</sub> nanosheets, 98  
Vapor-phase methods, 663  
Vesicular delivery systems, 719  
*Vibrio natriegens*, 937–938  
Vincristine, 547  
Viscosity aging index (VAI), 876–879,  
889–890  
Visible light–induced decomposition of  
Rhodamine-B using CeO<sub>2</sub>/CdO  
heterogeneous catalyst (Ce<sub>2</sub>/Cd<sub>1</sub>), 72  
Vitamin D<sub>3</sub>, 176–177  
Vitamin E, 549–550  
Volatile organic compounds (VOCs), 514  
Volmer step, 86

## W

Wang's group, 687  
Wastewater treatment, applications of  $\beta$ -CD  
grafted nanopyroxene in, 754–759  
enhanced settling of fine particles,  
757–759  
oil extraction wastewater-organic  
contaminant removal, 754–757  
interaction of  $\beta$ -CD with naphthenic  
acids, 755–757  
naphthenic acid model molecules, 755  
removal of pharmaceutical active  
compounds from water, 757  
Water channel protein (WCP), 249–250  
Water electrolysis, 84–86, 84f  
Water flux, 22–23, 29–31  
Water–oil–water emulsion (w/o/w), 188  
Water pollution, 299–301, 510–511  
remediation, 509–514  
Waterproof resistance, 810  
Water-soluble carbodiimides (EDC), 213  
Water-splitting electrocatalysts,  
nanofunctionalization of, 102  
Water treatment  
applications of nanocomposite membranes  
in, 494t  
porous nanocomposites for. *See* Porous  
nanocomposites for water treatment  
Wearable technology, 612  
Weight reduction, 803–804  
Western Blot, 197–198  
Wet chemical solution method.  
*See* Coprecipitation method  
Wet etching, 622–624  
Wet-spinning process, 631, 633–634  
Whey protein isolate (WPI), 151–152  
Whey protein nanoparticles, 138–139  
Wool fibers, 660

## X

XENOLITE, 669  
X-ray absorption fine structure (XRAFS)  
analysis, 113–114  
X-ray absorption near edge structure  
(XRANES) analysis, 113–114  
X-ray diffraction (XRD), 57–58, 113–114,  
834  
X-ray diffraction analysis of organic layered  
silicates, 867–871  
microstructure of organic layered silicate-  
modified asphalts, 870–871  
X-ray diffraction analysis of organic  
layered silicates, 867–869

X-ray diffraction analysis of organic layered silicates (*Continued*)

XRD analysis of separated organic layered silicates from modified asphalt, 869

X-ray photoelectron spectroscopy (XPS), 67–68, 67*f*, 113–114

## Y

YONEX, 817–818

## Z

*Zea mays*, 250–252

Zein, 169, 171–173, 176–177

Zein/chitosan colloid particles (ZCCPs), 176–177

Zein-chitosan core–shell NPs, 176–177

Zeolites, 46, 745

Zeolitic imidazolate framework-8 (ZIF-8), 36  
hZIF-8, 36

Zero-dimensional nanostructures, 271

Zeta potentials of coacervates, 153–154

Zinc oxide (ZnO) NPs, 514–515, 956

Zinc oxide, 359–360, 721, 723–724

Zirconium, 747

Zirconium oxide nanoparticles, 40

Zoladex, 185–186

Zwitterion organosilanes, 641

# HANDBOOK OF FUNCTIONALIZED NANOMATERIALS FOR INDUSTRIAL APPLICATIONS

Edited by Chaudhery Mustansar Hussain, PhD

Functionalized nanomaterials have extremely useful properties, which can outperform their conventional counterparts because of their superior chemical, physical, and mechanical properties and exceptional formability. They are being used for the development and innovation in a range of industrial sectors. However, the use of functionalized nanomaterials is still in its infancy in many industrial settings. Functionalized nanomaterials have the potential to create cheaper and more effective consumer products and industrial processes. However, they also could have adverse effects on the environment, human health, and safety, and their sustainability is questionable, if used incorrectly. This book discusses the opportunities and challenges of using functionalized nanomaterials in a variety of major industrial sectors.

*Handbook of Functionalized Nanomaterials for Industrial Applications* provides a concise summary of the major applications of functionalized nanomaterials in industry today. It covers the enhancements in industrial techniques and processes, due to functionalized nanomaterials, showing how they substantially improve the performance of existing procedures, and how they can deliver exciting consumer products more cheaply. Emphasis is given to greener approaches, leading to more sustainable products and devices. The legal, economical, and toxicity aspects of functionalized nanomaterials are also discussed in detail.

## Key Features

- Highlights established industrial applications of functionalized nanomaterials and discusses their future potential for a range of industrial sectors.
- Discusses how functionalized nanomaterials are being used to create new types of commercial products and devices.
- Assesses the challenges of using functionalized nanomaterials in industry, setting out major safety and regulatory challenges.

## About the authors

**Chaudhery Mustansar Hussain**, PhD is an Adjunct Professor, Academic Advisor, and Lab Director in the Department of Chemistry & Environmental Sciences at the New Jersey Institute of Technology (NJIT), Newark, NJ, United States. His research is focused on the application of nanotechnology and advanced materials, in environment, analytical chemistry, and various industries. He is the author of numerous papers in peer-reviewed journals and is a prolific author and editor of numerous (more than 25) scientific monographs and handbooks in his research areas, published with Elsevier, The Royal Society of Chemistry, Springer, John Wiley & Sons, CRC Press, etc.



ELSEVIER

[elsevier.com/books-and-journals](http://elsevier.com/books-and-journals)

Material Science

ISBN 978-0-12-816787-8



9 780128 167878